Durham University

Durham E-Theses

Synthesis and applications of N- and S-substituted 1,2,4-triazolium salts as stable radical and carbene precursors

MATTHEW STEPHEN SMITH

How to cite:

SMITH, MATTHEW STEPHEN (2024) Synthesis and applications of N- and S-substituted 1,2,4-triazolium salts as stable radical and carbene precursors. Doctoral thesis, Durham University.

Use policy

The full-text may be used and/or reproduced, and given to third parties in any format or medium, without prior permission or charge, for personal research or study, educational, or not-for-profit purposes provided that:

- a full bibliographic reference is made to the original source
- a https://etheses.durham.ac.uk/id/eprint/15527/ is made to the metadata record in Durham E-Theses
- the full-text is not changed in any way

The full-text must not be sold in any format or medium without the formal permission of the copyright holders.

Please consult the full Durham E-Theses policy for further details.

Academic Support Office, The Palatine Centre, Durham University, Stockton Road, Durham, DH1 3LE
e-mail: e-theses.admin@durham.ac.uk Tel: +44 0191 334 6107
https://etheses.durham.ac.uk

Synthesis and applications of *N*- and *S*-substituted 1,2,4-triazolium salts as stable radical and carbene precursors

Matthew Stephen Smith

A thesis submitted in partial fulfilment of the requirements for the degree of Doctor of Philosophy





Department of Chemistry
Durham University

Centre for Cancer
Newcastle University

2024

Declaration

The work described in this thesis was carried out at the Department of Chemistry at Durham University under the supervision of Prof. AnnMarie O'Donoghue, and the Centre for Cancer at Newcastle University under the supervision of Prof. Ian Hickson, between October 2019 and February 2024. The material within has not been previously submitted for a degree at these universities or at any other university. All work has been carried out by the author unless otherwise indicated.

M. S. Smith

Copyright

The copyright of this thesis rests with the author. No extracts should be published without prior consent, and the information from it should be acknowledged. Figures reproduced or adapted from literature are used under permission / licence of the respective journal – further information is available upon request from the author.

Publications and presentation of research

The following list of publications are partly or entirely a result of work detailed within this thesis.

1. P. Quinn, M. S. Smith, J. Zhu, D. R. W. Hodgson and A. C. O'Donoghue, *Catalysts*, 2021, **11**, 1055.
2. M. S. Smith, A. C. O'Donoghue and D. S. Yufit, *CSD Communications*, 2022, DOI: 10.5517/ccdc.csd.cc2cztls.
3. M. S. Smith, A. C. O'Donoghue and D. S. Yufit, *CSD Communications*, 2022, DOI: 10.5517/ccdc.csd.cc2cztmt.
4. J. Murray, M. S. Smith, D. S. Yufit, T. M. Richardson, M. A. Fox, V. Chechik and A. C. O'Donoghue, *manuscript in preparation*. Stable Blatter Radicals from an Unexplored C(3)-Anilino Triazolium Scaffold: Synthesis and Mechanistic Role of Zwitterion-Carbene Tautomerisation.

The research detailed within this thesis has been presented, in part, at the following events.

1. *Nitron Derivatives to Blatter Radicals: Novel Anticancer Prodrugs and Mechanistic Probes*, 3 minute flash presentation, MoSMed Annual Symposium, 8th January 2020, Newcastle University, UK.
2. *Nitron Derivatives to Blatter Radicals: Novel Anticancer Prodrugs and Mechanistic Probes*, Poster presentation and 3 minute flash presentation, MoSMed Annual Symposium, 15th and 16th December 2020, online only.
3. *From Stable Carbenes to Blatter-type Radicals*, 1 hour talk, Research Spotlight (seminar series, Durham University Chemistry Society), 9th March 2022, Durham University, UK.
4. *From Stable Carbenes to Blatter-type Radicals*, 15 minute talk, Department of Chemistry Gala Symposium, 22nd and 23rd June 2022, Durham University, UK.
5. *Nitron Derivatives to Blatter Radicals: Novel Anticancer Prodrugs and Mechanistic Probes*, 15 minute talk, MoSMed Annual Symposium, 12th and 13th July 2022, Durham University, UK.
6. *From Bench-stable Carbenes to Blatter-type Radicals,* Poster presentation and 1 minute flash presentation, RSC Organic Chemistry Poster Symposium, 5th December 2022, Royal Society of Chemistry, Burlington House, London, UK.
7. *From Bench-stable Carbenes to Blatter-type Radicals*, poster presentation, European Symposium on Organic Reactivity, 19th – 22nd September, Amsterdam, The Netherlands.
8. *From Bench-stable Carbenes to Blatter-type Radicals*, 15 minute talk, 51st Ontario-Quebec Physical-Organic Mini Symposium, 3rd – 5th November 2023, Queens University, Kingston, Ontario, Canada.

9. *Synthesis and Mechanistic Evaluation of S-triazolium Organocatalysts*, poster presentation, 51st Ontario-Quebec Physical-Organic Mini Symposium, 3rd – 5th November 2023, Queens University, Kingston, Ontario, Canada.
10. *1,2,4-Triazolium Ions as Organocatalyst and Bench-Stable Radical Precursors*, 1 hour talk, BCOOL Seminar, 7th November 2023, State University of New York at Buffalo, Buffalo, New York, USA.
11. *1,2,4-Triazolium Ions as Organocatalyst and Bench-Stable Radical Precursors*, 1 hour talk, invited seminar, 17th November 2023, Georgia Institute of Technology, Atlanta, Georgia, USA.

Abstract

1,2,4-Triazolium salts, and the triazolylidine NHC generated from deprotonation at the pre-carbenic site, have shown a broad range of applications within the literature. Herein we report the synthesis of 1,2,4-triazolium salts with C(3)-N-Ar and C(3)-S-Ar substitution, enabling studies into the rearrangement to stable Blatter radicals, organocatalysis, and antiproliferative activity against cancer cell lines.

Nitron is a 1,2,4-triazolium salt with a C(3)-N anilino substituent, which enables a tautomerisation between the C(3)-N and C(5) positions. As a result, Nitron partially exists in a carbenic tautomer at levels too low for NMR observation. The work herein continues from our initial report whereby Nitron can undergo an unusual rearrangement to stable Blatter radicals, a species of growing interest particularly within the fields of photochemistry, magnetochemistry and organic electronics. The synthesis of Nitron is revisited to enhance the scope and yields compared to the published route. The analogues of Nitron are explored within the transformation to Blatter radical, allowing for the isolation of 16 new radicals. Evaluation of the propensity of Nitron analogues to undergo transformation to Blatter radical, including computational and kinetic analysis, has allowed the role of the carbenic tautomer of Nitron in Blatter radical formation to be investigated. The potential organocatalytic activity of Blatter radicals in oxidative coupling is also explored.

S-triazolium salts, with a C(3)-S-Ar substituent, are scarcely described within the literature. This work describes the development of a high-yielding synthetic methodology enabling 26 novel salts to be synthesized. The route consists of a Ullmann coupling to a *S*-triazole, followed by *N*-alkylation. The selectivity of this alkylation step is explored computationally and through isolation of both *S*-triazolium salt isomers. The use of azolium-derived carbenes for organocatalysis, in particular the carbene obtained by deprotonation of 1,2,4-triazolium salts, is a continually growing field. We report studies on the H/D exchange of *S*-triazolium salts isolated in this work, which shows an acidifying effect of the sulfur atom on C(5)-H. The collection of single-crystal XRD data allows for the development of structural relationships to the rate of C(5)-H/D exchange, enabling the approximation of second-order rate constants for the exchange process from XRD data only. Initial investigations into the organocatalytic activity of *S*-triazolium salts in the benzoin and Stetter reaction are also described.

Blatter radicals have been implicated in the mechanism of action of the experimental anticancer prodrug Tirapazamine, a benzotriazine-1,4-dioxide that exhibits enhanced activity under hypoxic conditions. Within this work Tirapazamine is synthesized, with the synthetic route explored towards the development of benzotriazine-1,4-dioxide analogues. Based on literature reports, 3-amino-1,2,4-benzotriazine is investigated in the synthesis of Blatter radicals by the addition of organolithium

reagents. This work has discovered an intriguing transformation of the benzotriazine scaffold under literature conditions, which has been explored through reaction with organolithium and Grignard reagents.

The compounds isolated in this work are further explored in tissue culture assays to evaluate their antiproliferative activity. Blatter radicals are seen to show promising cytotoxic activity against 2 cancer cell lines, with the potential of Nitron analogues as a prodrug form of the Blatter radical explored through prolonged incubation assays. Blatter radicals are also described within the literature as scavengers of reactive oxygen species – initial work herein provides the foundation for the development of antioxidant nanoparticles containing Blatter radicals.

Acknowledgements

This work would not have been possible without the support and guidance of my supervisor, AnnMarie O'Donoghue, who throughout COVID lockdowns and long hours in the lab has encouraged me to develop as a researcher. I must also thank Ian Hickson who allowed me to undertake tissue culture assays and appreciate the biological testing of compounds as a chemist.

Within the lab I have been fortunate to work with lots of great scientists and generally great people. In particular I would like to thank Jacob Murray for his support over the years and suggestions on the Blatter radical project, Josh Rawlinson for his support and help with proof-reading, Jiayun (Estelle) Zhu for being a great Post-Doc who was always willing to help, and Will Brittain for support on the bioconjugation work. I'd also like to thank the Sandford and Cobb groups for their support throughout the project. As part of my biological testing work, I would like to thank Suzanne Kyle for her support teaching me to undertake my own tissue culture assays and more broadly everyone in the lab who were always willing to help.

Within the wider department in Durham, I would like to thank Juan Aguilar-Malavia and Eric Hughes for supporting me to learn manual NMR spectroscopy. I'd also like to thank Peter Stokes and David Parker of the mass spectrometry service, along with Dimitrii Yufit and Toby Blundell for X-ray crystallography.

The MoSMed CDT has provided me with a lot of great training and support over the years, and I would like to thank everyone in the CDT for supporting this work. I would also like to thank EPSRC for financially supporting this work.

Last but not least I would like to thank my family and particularly my parents who have supported me not just over the last four years, but throughout my academic journey to allow me to get to this position.

Table of contents

Declaration i
Copyright i
Publications and presentation of research ii
Abstract iv
Acknowledgements vi
Table of contents vii
Abbreviations x

1 – Research Foundations 1

1.0 – Foreword 2
1.1 – Stable Organic Radicals 3
1.2 – Carbenes 10
1.3 – Conclusions 14
1.4 – Summary and aims of the project 15

2 – The syntheses of Nitron analogues 19

2.0 – Foreword 20
2.1 – Chapter contributions 20
2.2 – Introduction 21
2.3 – Synthesis and properties of Nitron analogues 34
2.4 – Sulfur-substituted 1,2,4-triazolium salts from 1,2,4-triazoles 57
2.5 – Bioconjugation of 1,2,4-triazolium salts to peptide and peptidomimetic scaffolds 86
2.6 – Conclusions 98

3 – Synthesis and reactions of Blatter radicals 99

3.0 – Foreword 100
3.1 – Chapter contributions 100
3.2 – Introduction 101
3.3 – Synthesis of Blatter radicals from 1,2,4-triazolium salts 117
3.4 – Late-stage modification of Blatter radicals 142
3.5 – The organocatalytic applications of Blatter radicals 147
3.6 – Bioconjugation of Blatter radicals 154
3.7 – Conclusions 156

4 – The syntheses of 1,2,4-benzotriazines and their related N-oxides 157

4.0 – Foreword 158
4.1 – Chapter contributions 158
4.2 – Introduction 159
4.3 – Synthesis of 1,2,4-benzotriazines 162

4.4 – Further reactions from 1,2,4-benzotriazine-1-oxide 167
4.5 – Reaction of 1,2,4-benzotriazines with organometallic reagents 169
4.6 – Conclusions 178

5 – Kinetic studies of 1,2,4-triazolium salts in organocatalysis 179

5.0 – Foreword 180
5.1 – Chapter contributions 180
5.2 – Introduction 181
5.3 – Evaluation of NHC carbon acidity using H/D-exchange 187
5.4 – Determination of first and second order rate constants for C^5-H/D exchange 194
5.5 – XRD structure to activity relationships 201
5.6 – Estimation of C^5-H pK_a values 211
5.7 – Initial organocatalytic evaluation 213
5.8 – Conclusions 216

6 – The evaluation of antiproliferative and antioxidant activity of Blatter radicals, 1,2,4-triazolium salts and related species 217

6.0 – Foreword 218
6.1 – Chapter contributions 218
6.2 – Introduction 219
6.3 – Evaluation of antiproliferative and cytotoxic activity 229
6.4 – Blatter radicals as reactive oxygen species scavengers 244
6.5 – Conclusions 246

7 – Conclusions and future work 247

7.1 – Conclusions 248
7.2 – Future work 252

8 – Experimental 259

8.1 – General experimental information – chemistry work 260
8.2 – Syntheses from Chapter 2 267
8.3 – Syntheses from Chapter 3 311
8.4 – Syntheses from Chapter 4 325
8.5 – Syntheses from Chapter 5 333
8.6 – General experimental information – biology work 334
8.7 – SRB assay methodology 335
8.8 – Determination of Error 337

Appendix A - Crystallographic information 341

A-1 – XRD data from Chapter 2 342
A-2 – XRD data from Chapter 3 364

A-3 – XRD data from Chapter 4 367

Appendix B - Supplementary information for Chapter 2 371

B-1 – XRD structural parameters for Nitron analogues 372
B-2 – Zwitterion – carbene tautomerisation calculations 378
B-3 – Calculation of $F_{carbene}$ 504
B-4 – Attempted *S*-triazole arylation by Cu-diamine catalysis 506

Appendix C - Supplementary information for Chapter 3 507

C-1 – Potential isomerisation of 181b during hydrolysis 508
C-2 – NMR spectroscopy of Blatter radicals 510
C-3 – Blatter radical formation studies by ^{1}H NMR 511

Appendix D - Supplementary information for Chapter 5 521

D-1 – Detailed description of H/D-exchange experiments 522
D-2 – H/D-exchange results 525
D-3 – *S*-triazolium organocatalytic activity 566

Appendix E - Supplementary information for Chapter 6 569

E-1 – SRB assay results overview 570
E-2 – SRB assay graphs 574

Bibliography 615

Abbreviations

ABS – Arndt benzotriazine synthesis
Ac – acetyl
Ad – 1-adamantyl
ADC – antibody-drug conjugate
AIBN – azobisisobutyronitrile
a_{iso} – anisotropic electron-nuclear hyperfine coupling constant
Akt – protein kinase B
Ar – aryl
ArM – Artificial metalloenzyme
at – acquisition time
BAC – bis(amino)cyclopropenylidine
BAC-H – bis(amino)cyclopropenium
BAC-Phos – bis(amino)cyclopropenium phosphonates
Bn – benzyl
Boc – *tert*-butoxycarbonyl
BR – Blatter radical
BTO – benzotriazine 1,4-di-*N*-oxide
BTZ – benzotriazine
CDI – carbonyldimidazole
CoRC – covalent radical catalysis
CPZ – chlorpromazine
CT – computed tomography
CuAAC – copper-catalysed azide-alkyne cycloaddition
CV – cyclic voltammetry
CYPOR – NADPH-cytochrome P450 oxidoreductase
d – day
$\mathbf{d_1}$ – relaxation delay
DCC – *N*, *N'*-dicyclohexylcarbodiimide
DCM – dichloromethane
DFT – density functional theory
DIC – *N*, *N'*-diisopropylcarbodiimide
DIPEA – *N, N'*-diisopropylethylamine
DMAP – 4-dimethylaminopyridine
DMEDA – *N*, *N'*-dimethylethylenediamine
DMEM – Dulbecco's modified eagle medium
DMF – dimethylformamide
DMF-DMA – dimethylformamide dimethyl acetal
DMS – dimethyl sulfate
DMSO – dimethylsulfoxide
DNA – deoxyribonucleic acid
DNP – dynamic nuclear polarization
Dppf – 1,1'-Bis(diphenylphosphino)ferrocene
DSB – double-strand break
DSC – differential scanning calorimetry
$\mathbf{DSPE\text{-}PEG_{1000}}$ – 1,2-distearoyl-sn-glycero-3-phosphoethanol-amine-*N*-[methoxy-(polyethylene glycol)-1000]
E – applied potential
$\mathbf{E_{1/2}}$ – half-wave potential
ECP – effective core potential
EDC – 1-ethyl-3-(3-dimethylaminopropyl)carbodiimide
EDG – electron-donating group
EDTA – ethylenediaminetetraacetic acid
ee – enantiomeric excess
EPR – electron paramagnetic resonance (spectroscopy)
Equiv. – equivalent(s)
ERK – extracellular regulated kinase
ES+ – positive electrospray ionisation
EsNuEl – Estimating Nucleophilicity and Electrophilicity (web application)
EWG – electron-withdrawing group
Fab – fragment antigen binding
Fc – fragment crystallisable
FID – free induction decay
FRET – Förster resonance energy transfer
g – gyromagnetic ratio
GC – gas chromatography
GC-MS – gas chromatography-mass spectrometry
$\mathbf{GI_{50}}$ – half-maximal growth inhibition
h – hour
HAD – hypoxia-activated drug
HAP – hypoxia-activated prodrug
HIF – hypoxia-inducible factor
HMBC – heteronuclear multiple bond correlation
HOBt – Hydroxybenzotriazole
HOMO – highest occupied molecular orbital
HPC – high-performance computing
HRMS – high resolution mass spectrometry
I – ionic strength
ip – isophthalic acid
IPA – isopropyl alcohol
IS – internal standard
JMP – John's Macintosh program
KDAC – lysine deacetylase
LADH – liver alcohol dehydrogenase
LC-MS – liquid chromatography-mass spectrometry
LC-MS-MS – liquid chromatography-mass spectrometry-mass spectrometry
LLE – liquid-liquid extraction
mAb – monoclonal antibody
MAPK – mitogen-activated protein kinase

MCA – methyl cation affinity
mCPBA – *meta*-chloroperbenzoic acid
MDR1 – multidrug resistance 1
Mes – mesityl (2,4,6-trimethylphenyl)
MeTHF – 2-methyltetrahydrofuran
MOF – metal-organic framework
MRI – magnetic resonance imaging
Mtb – *Mycobacterium tuberculosis*
mTOR – mammalian target of rapamycin
MTSSL – (1-oxyl-2,2,5,5-tetramethylpyrroline-3-methyl)methanethiosulfonate
MTT – 3-[4,5-dimethylthiazol-2-yl]-2,5 diphenyl tetrazolium bromide
MW – microwave
NADPH – nicotinamide adenine dinucleotide phosphate (reduced form)
NASA – North American Space Agency
NBS – *N*-bromosuccinimide
NCL – Native chemical ligation
NCS – *N*-chlorosuccinimide
NHC – *N*-heterocyclic carbene
NIS – *N*-iodosuccinimide
NMR – nuclear magnetic resonance (spectroscopy)
NOE – nuclear Overhauser effect
NOS – nitric oxide synthases
NP – nanoparticle
NQO – NADPH : Quinone acceptor oxidoreductase
o-DNP – Overhauser dynamic nuclear polarisation
OD – optical density
PA – polarising agent
PBS – phosphate-buffered saline
PCM – polarised continuum model
PDI – polydispersity index
PEG – poly(ethylene glycol)
PELDOR – pulsed electron-electron double resonance
PET – positron emission tomography
PFP – pentafluoropyridine
PhAC – pharmaceutically active compound
PI3K – phosphatidylinositol-3-kinase
pO_2 – oxygen partial pressure
PSYCHE – pure shift yielded by chirp excitation (NMR)
PyBOP – benzotriazol-1-yloxytripyrrolidinophosphonium hexafluorophosphate
QdNO – quinoxaline-1,4-di-*N*-oxide
qNMR – quantitative nuclear magnetic resonance (spectroscopy)
RNR – ribonucleotide reductase
ROMP – ring-opening metathesis polymerisation
ROS – reactive oxygen species
RP-LC – reverse phase liquid chromatography
RPMI – Roswell park memorial institute (growth medium)
SARS-CoV-2 – severe acute respiratory syndrome coronavirus 2
SCC – squamous cell carcinoma
SCGE – single cell gel electrophoresis
SDSL – site-directed spin labelling
SFRP – stable free radical polymerisation
S_NAr – nucleophilic aromatic substitution
SOMO – singly occupied molecular orbital
SPPS – solid-phase peptide synthesis
SPR – surface plasmon resonance
SRB – sulforhodamine B
SSB – single strand break
STING – stimulator of interferon genes
TBD – triazabutadiene
TCA – trichloroacetic acid
TEMPO – 2,2,6,6-tetramethylpiperidine
TEMPOL – 4-hydroxy-2,2,6,6-tetramethylpiperidin-1-oxyl
TFA – trifluoracetic acid
TFP – tetrafluoropyrid-4-yl
TGA – thermogravimetric analysis
THF – tetrahydrofuran
TLC – thin layer chromatography
TMACl – tetramethylammonium chloride
TME – tumour microenvironment
Topo – topoisomerase
TPM – triphenylmethyl radical
TPZ – Tirapazamine
t_R – repetition time
Trx – thioredoxin
TrxR – thioredoxin reductase
Ts – tosyl (*p*-toluenesulfonyl)
UV – ultraviolet
VEGFA – vascular endothelial growth factor A
XRD – X-ray diffraction
ZIF – zeolite imidazole framework

1 – Research Foundations

1.0 – Foreword

This thesis focusses on the synthesis and applications of Blatter-type radicals, a class of stable organic radicals, prepared from 1,2,4-triazolium precursors structurally akin to an *N*-substituted 1,2,4-triazolium salt. The work presented within also investigates the synthesis, properties and applications of *N*-substituted and novel *S*-substituted 1,2,4-triazolium salts, neither of which have been explored within the literature.

Preparation of *N*- and *S*-substituted 1,2,4-triazolium salts (Chapter 2), and the rearrangement of the *N*-substituted salts to persistent *N*-centred Blatter-type radicals (Chapter 3) are discussed. The synthesis of 1,2,4-benzotriazines, and their intriguing ring-contraction using organometallic reagents, is the subject of Chapter 4. The acid-base properties of carbenes generated from 1,2,4-triazolium salt precursors, and their potential as organocatalysts, are investigated in Chapter 5. A preliminary investigation of the anti-cancer properties of compounds synthesized within this work through cytotoxicity assays (Chapter 6) are also investigated. Further details on the aims of this work can be found at the end of this chapter. This introductory chapter briefly explores the chemical nature of stable carbenes and organic radicals, which underpins all work within this thesis.

1.1 – Stable Organic Radicals

The unusual electronic structure of radicals leads to a range of interesting properties, most notably their enhanced reactivity over closed-shell species. Whilst radicals are in many cases highly reactive, stabilisation can give rise to species with significantly longer half-lives. The first report of a stabilised radical by Gomberg, the triphenylmethyl radical (TPM, **1**), has initiated a field that has seen continual growth since 1900 (**Figure 1**).[1] Driving this growth is the variety of applications in which open-shell systems have shown promise – photochemistry, magnetochemistry, catalysis and medicinal chemistry, to name a few. The development of metal-free magnetic materials and molecule-based electronics and optoelectronics are areas receiving particular focus.[2, 3]

A variety of scaffolds have developed since Gomberg's discovery including phenoxyl (**2**), nitroxide (**3**), verdazyl (**4**), phenalenyl (**5**), boron-stabilised TPM (**6**), bis(triarylamine) (**7**) and dithiazoyl radicals (**8**).[2-4] Chapter 4 discusses a class of stable organic radicals with rapidly growing interest, the 1,2,4-benzotriazinyl (Blatter) radical (BR, **9**).

Radical character arises from the presence of a singly occupied molecular orbital (SOMO). The tendency to form closed-shell species from the SOMO, through processes such as dimerization and disproportionation, results in radicals being highly reactive in the majority of cases.[4] Tuning the stability of organic radicals is key to enable implementation, as their commonly transient nature explains their relative rarity within organic chemistry and industry.[2, 5] Stable organic radicals arise through a combination of kinetic and thermodynamic stabilisation (steric and electronic effects, respectively) which can be achieved through covalent and non-covalent means.[5] Considering **1**, **6** and **7**, kinetic stabilisation protects the radical centre from attack and limits the ability of the radical centre to attack. In the case of **1**, dimerization and reaction with oxygen are still very fast,[4, 6] and so functionalisation of the phenyl rings (**Figure 2**) is necessary to prolong half-life. Polychlorinated trityl radical (**10**) has increased kinetic stabilisation through limiting C$^{\bullet}$-Ar rotation, with the barrier to rotation around 23 kcal mol^{-1}.[4] Polychlorinated trityl radicals and their analogues have shown promise for implementation in magnetic networks, dynamic nuclear polarisation (DNP) and as oximetric probes.[7] The Finland trityl radical (**11**), developed by Nycomed Innovations for Overhauser magnetic resonance imaging (OMRI), has shown good aqueous solubility and *in vivo* stability.[8-11] Recent work with Finland trityl radical analogues has shown improvements in hydrophilicity,[12] alongside possible applications within futile redox cycling.[13]

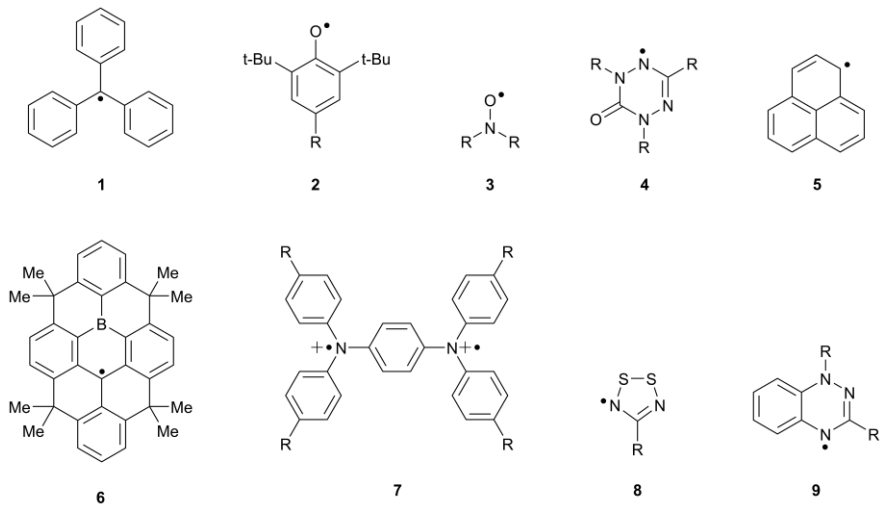


Figure 1 – Examples of persistent organic radicals: triphenylmethyl or trityl radical (**1**), the first reported stable radical; phenoxyl (**2**); nitroxide (**3**); verdazyl (**4**); phenalenyl (**5**); boron-stabilised TPM (**6**); bis(triarylamine) (**7**); dithiazoyl (**8**); and 1,2,4-benzotriazinyl (**9**), also referred to as Blatter radical.

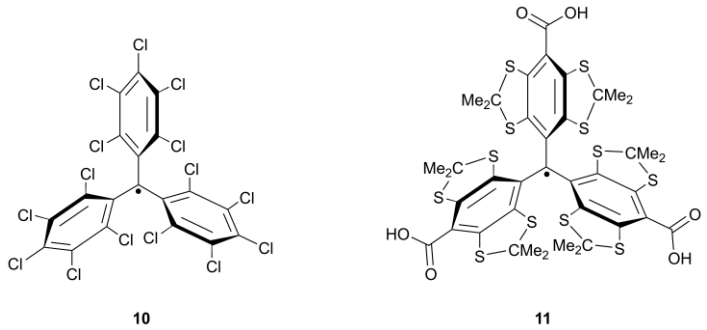


Figure 2 – Analogues of trityl radical **1**. The (polychloro)trityl radical **10** which exhibits interesting electrochemical and magnetic properties, and the Finland trityl radical **11** developed for OMRI.

Thermodynamic stabilisation occurs due to the presence of electron-donating groups (EDGs) and electron-withdrawing groups (EWGs). Interaction of the radical SOMO with an empty antibonding orbital (**Figure 3a**) or an occupied non-bonding orbital (**Figure 3b**) both lead to a stabilising effect.[14] Thermodynamic stabilisation can also result from the delocalisation of radical character, with a common example of this being **5** for which dimerization is mostly suppressed.[5] Thermodynamic stabilisation is best achieved through a combination of EDGs and EWGs, as this allows for a greater level of delocalisation illustrated through the existence of a larger number of resonance forms – this is known as the captodative effect.[14] An example of a radical exhibiting the captodative effect is the (4-(dimethylamino)phenyl)dicyanomethyl radical (**12**, **Figure 4**) which has recently been used to support the solvent-dependent behaviour key to the existence of the captodative effect.[15]

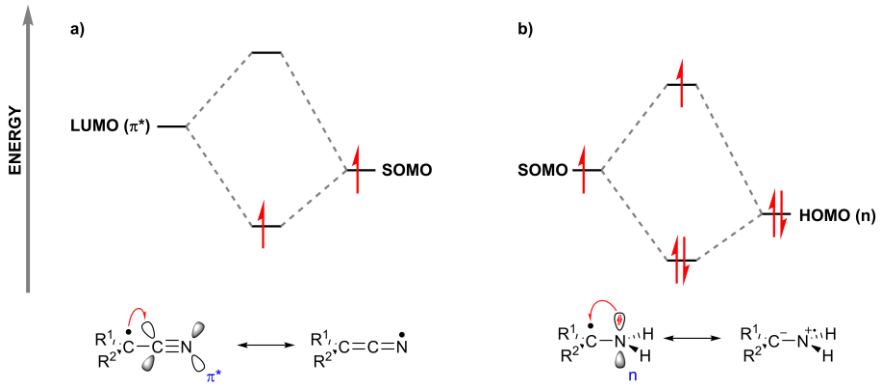


Figure 3 – A stepwise perturbational approach to describe the electronic stabilisation of radicals. **a)** Electron-withdrawing groups such as the π antibonding orbital of the cyano group lower SOMO energy. **b)** Interaction of a low energy HOMO, such as the non-bonding lone pair of an amino group, leads to an overall reduction in electron energy.

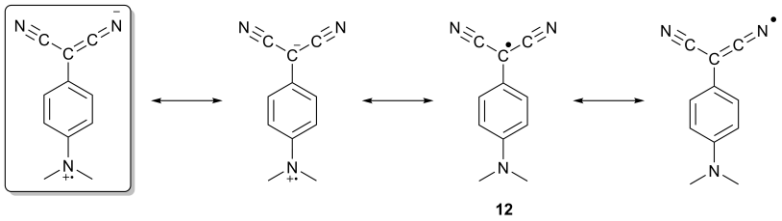
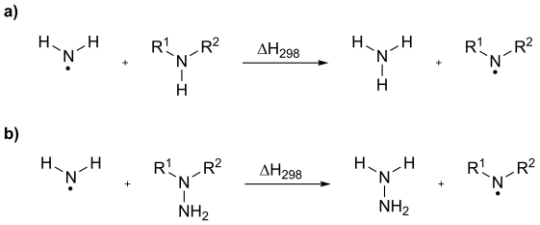


Figure 4 – Resonance forms of the radical **12**, which shows the captodative effect. The structure shown boxed is possible as a result of the captodative effect, with enhanced charge separation.

With sufficient stabilisation, radicals can be described as 'persistent' – this term is reserved for radicals with half-lives significantly longer than the methyl radical.[16] Radical persistence can be quantified by the radical stabilisation energy (RSE), the enthalpy of the isodesmic process illustrated in **Scheme 1** when considering nitrogen-centred radicals.[17] The H-abstraction shown in **Scheme 1a** is commonly used to determine RSE as it directly relates to the fundamental hydrogen transfer process, however this does not consider the possible substituent effects through homolytic fission of the polarised N-H bond – N-N homolytic fission shown in **Scheme 1b** considers bond dipole and thus more accurately quantifies substituent effects on radical centres.[18, 19] For carbon-centred, oxygen-centred and sulfur-centred radicals, the reference radicals are methyl, hydroxyl and thiyl radicals respectively.[18] The hydrazino radical for example, with half-life of ~ 33 h in the atmosphere at sea-level, has an RSE of −84 (± 5) kcal mol^{-1} compared to the aminyl-ammonia pair.[17, 20]



Scheme 1 – **a)** The reference aminyl-ammonia pair used to define RSE for *N*-centred radicals. **b)** Improved methodology to determine RSE, considering non-polar bond formation.

Characterisation of radicals by nuclear magnetic resonance (NMR) spectroscopy is complicated by the presence of unpaired electrons, as coupling of the unpaired electron's magnetic moment to that of the observed nucleus results in rapid nuclear relaxation and broad spectral lines.[21] Experimental techniques to characterise radicals by solution-state NMR are available; however, they must use rapid, high power pulse sequences to achieve optimal results.[22] The NMR spectra of radicals can also be predicted through density functional theory (DFT) calculations, providing parameters that can aid experimental acquisition.[21]

Alternative techniques that are specific to paramagnetic species can also be utilised, one of which is electron paramagnetic resonance (EPR) spectroscopy. EPR spectroscopy, like NMR spectroscopy, probes the interaction of magnetic dipoles within the molecule using an applied magnetic field and electromagnetic radiation. The techniques differ on the dipole of interest; NMR spectroscopy investigates nuclear spin states whilst EPR spectroscopy investigates the splitting of electronic spin states. EPR therefore relies on the presence of an electron magnetic dipole moment, which is only seen in open shell species as a result of the magnetic dipole from the unpaired electrons.[23]

Similar to chemical shift in NMR spectroscopy, the interaction of the unpaired electron(s) with the applied magnetic field is described by a *g* value; this value is also independent of instrument frequency, however, unlike chemical shift, it describes the intrinsic resonance position rather than being given relative to a reference compound. The most useful source of information from an EPR spectrum is the electron-nuclear hyperfine interaction between the unpaired electron and the surrounding nuclei. This interaction consists of an isotropic part (a_{iso}), concerning the probability of finding the electron spins at the position of a particular nucleus (a through-bond interaction), and an anisotropic part which describes dipole-dipole interactions – this is only detected in the solid state. Knowledge relating to a_{iso} allows mapping of spin delocalisation onto a molecular structure, useful in the persistent radical field as a means of identifying stabilising atoms in the molecule. The spectral outputs are rarely explainable through measurement of peak positions and hyperfine couplings, and usually require simulations to retrieve the desired information.[23]

Figure 5 shows the EPR spectrum of the verdazyl radical dimer (**13**). It consists of a nonet, with intensity 1:4:10:16:19:16:10:4:1 resulting from the coupling of each unpaired electron to two pairs of equivalent nitrogen atoms. All four nitrogen atoms within the verdazyl scaffold contribute to the stabilisation of **13**.[24, 25]

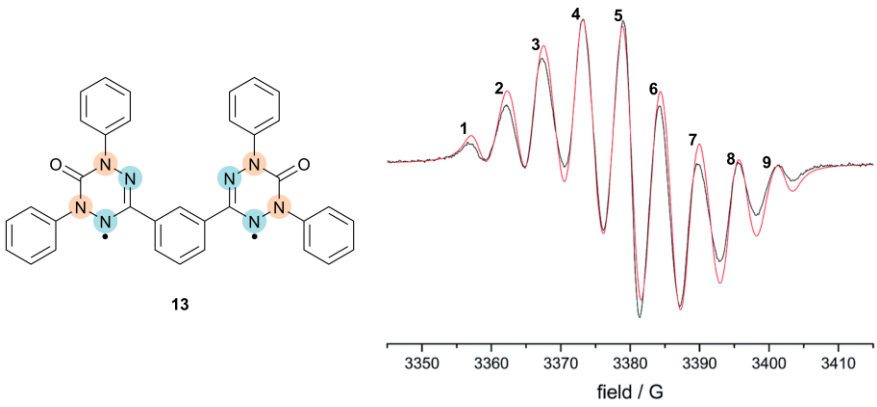


Figure 5 – Structure and EPR spectrum of verdazyl radical **13**. The nonet splitting observed results from each unpaired electron coupling to the two pairs of equivalent nitrogen atoms (highlighted). Black line = experimental data, red line = simulated fit. Adapted with permission from: D. Matuschek, S. Eusterwiemann, L. Stegemann, C. Doerenkamp, B. Wibbeling, C. G. Daniliuc, N. L. Doltsinis, C. A. Strassert, H. Eckert and A. Studer, *Chem. Sci.*, 2015, **6**, *4712*. Copyright 2015 © The Royal Society of Chemistry.

Another method of analysis available is cyclic voltammetry (CV), a powerful technique popular in the fields of catalysis and radical chemistry alongside being adapted for *in vivo* use in neurochemical dynamics.[26, 27] CV provides information on the oxidation and reduction processes of molecular species, including electron transfer-initiated chemical reactions and the one-electron process to obtain the corresponding anion and cation of persistent radicals.[26] An applied potential (E) is provided to a degassed solution of the analyte, with the current passed through solution recorded to give rise to voltammograms such as that shown in **Figure 6**.[4, 26] The shape of each couple arises from changes in local species concentration surrounding the working electrode: increasing current as the electrochemical process occurs; peak maxima, where the current is diffusion-limited; decrease in current as the diffusion layer of oxidised/reduced species grows in thickness; and then reversal of the process following the switch in potential scanning. The shape for the whole voltammogram is characteristic for the majority of persistent radicals, with two reversible processes consistent with oxidation and reduction of the radical. The midpoint between the two peaks in the couple is the point at which concentrations of the two species are equal and thus $E = E_{1/2}$, where $E_{1/2}$ is the half-wave potential. The difference in potential between the two peaks in the couple relates to the barrier to electron transfer, whilst the difference in $E_{1/2}$ values for the two couples quantifies the potential window useful in determining capability of the material to act as a battery.[26]

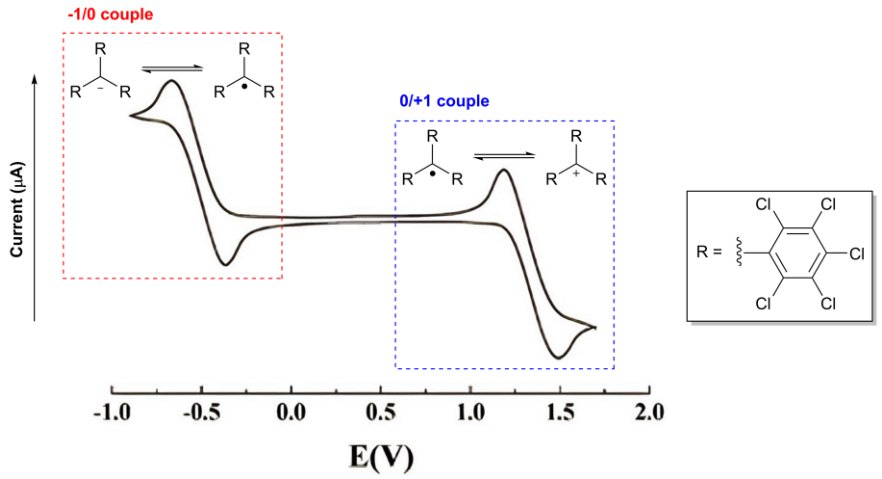


Figure 6 – The CV spectrum of (polychloro)trityl radical **10**, showing the two single-electron oxidation and reduction processes – the closed cycle indicates full reversibility of the two processes. Adapted with permission from: I. Ratera and J. Veciana, *Chem. Soc. Rev.*, 2012, **41**, *303*. Copyright 2012 © The Royal Society of Chemistry.

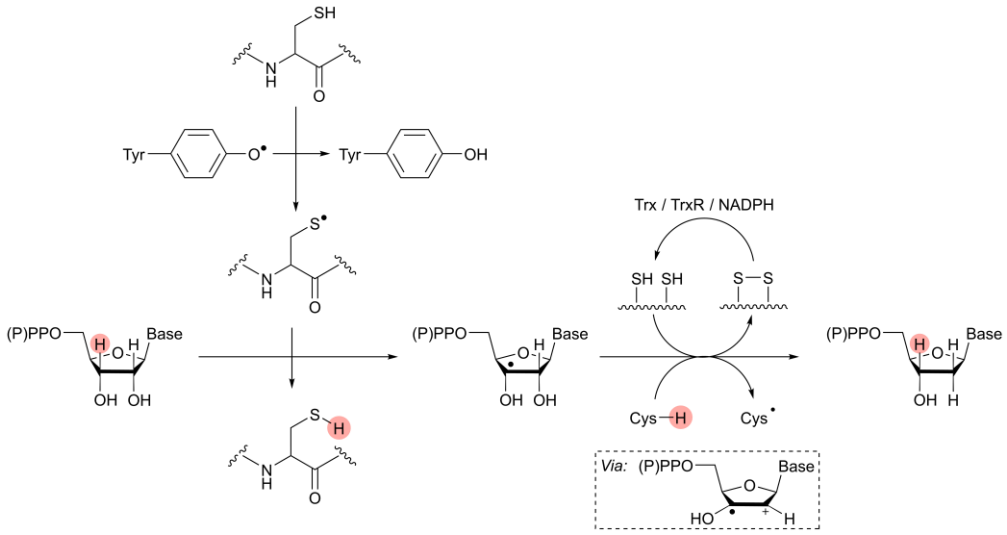
1.1.1 – Radicals within biology and medicinal chemistry

Within the general population radicals are normally portrayed as highly reactive species linked with death, decreased vascular permeability through lipid peroxidation, and the effects of aging.[28, 29] Radicals can damage a range of cellular components *via* processes including the depolymerisation of polysaccharides, the generation of atherosclerotic plaques, deoxyribonucleic acid (DNA) strand scission and the inactivation of some enzymes.[28, 30] Whilst these negative impacts are important to consider, describing all radicals in this manner ignores the key role radicals play within the body – superoxide anion radicals ($O_2^{\bullet-}$) have a key role in the assembly of enzymatic metal clusters whilst $NO^{\bullet}$ is a signalling agent that is generated from nitric oxide synthase and activates soluble guanylate cyclase, leading to a variety of biological functions such as vasodilation.[29, 31]

Ribonucleotide reductases (RNRs), containing the first identified stable protein radical in the form of a tyrosyl residue within RNR from *E Coli*,[32] are essential for the conversion of nucleoside triphosphates into deoxynucleotides. They are key in regulating DNA replication and cell survival. The action of RNR is initiated by a thiyl radical from cysteine, generated from the identified tyrosyl radical, which reduces the nucleoside through *H*-abstraction and a reduction process resulting in formation of a disulfide bond (**Scheme 2**). The cysteinyl radical is regenerated in this process, whilst the disulfide is recycled by thioredoxin (Trx), thioredoxin reductase (TrxR) and the reduced form of nicotinamide adenine dinucleotide phosphate (NADPH).[29]

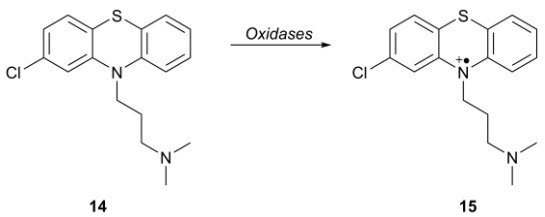
As part of phagocytosis, leukocytes and macrophages transform large amounts of oxygen into $O_2^{\bullet-}$ using NADPH oxidase – this process is called the respiratory burst. The superoxide anion radicals are converted into hydrogen peroxide, hydroxyl radicals and potentially singlet oxygen to destroy invading microorganisms. This cytotoxicity is further enhanced upon complexation with

myeloperoxidase, also released into the phagocytic vacuole, which can generate hypochlorous acid amongst other oxidised halide species.[30]



Scheme 2 – The mechanism of action of type I RNRs; wavy lines represent the rest of the protein structure. Cysteinyl radicals abstract the 3' hydrogen atom from the sugar generating a carbon-centred radical intermediate. Protonation by cysteine gives a radical cation through loss of water (dashed box). Transfer of 'H$^-$' from the cysteine pair leads to the disulfide, and finally the transfer of H• from the other cysteine gives the deoxynucleotide.

Pharmaceuticals can also implement open shell systems, normally generated through *in vivo* activation of a closed shell prodrug form.[33, 34] One example of a drug acting through an activated radical form is chlorpromazine (CPZ, **14**, **Scheme 3**), a sedative and antipsychotic medication that has a body cooling effect and is also used to control excitement and agitation.[35, 36] Piette and coworkers[35, 36] showed that oxidised salts of **14** ($CPZ^{+\bullet}$, **15**) show signals by EPR, and must therefore exist as radical cations. Gooley and coworkers[34] illustrated that the pharmacological effect of **14** depends, at least in part, on this free radical form through observation of enhanced sedative and body cooling effects in mice upon formation of a charge transfer complex with sulfur dioxide as an electron acceptor. *In vivo* oxidation of **14** to **15** is made possible implementing one of a variety of microsomal oxidases throughout the lung, liver and gut wall.[37-39] The biological roles of persistent organic radicals are further reviewed in section 7.2.



Scheme 3 – The *in vivo* oxidation of chlorpromazine (**CPZ**) into the activated radical cation form ($\mathbf{CPZ^{+\bullet}}$). This process is made possible by a variety of microsomal oxidases located within the lung, liver and gut wall as verified by animal studies.[37-39]

1.2 – Carbenes

Carbenes are electron-deficient, divalent carbon species with a neutral charge. Two of the valence electrons of carbon exist within bonds (two pairs of electrons in molecular orbitals), with the other two as non-bonding electrons that can exist in various electronic arrangements differing based on geometry and multiplicity (**Figure 7**). Bonding about the carbon atom can be either linear or bent, which leads to alterations in orbital hybridisation. Linear carbenes are less common and arise from an sp-hybridised centre, leading to two degenerate p-orbitals; the bent geometry leads to two sp^2-hybridised atomic orbitals that form two sigma orbitals, leaving the p_y unhybridized orbital (now referred to as p_π). For linear carbenes, Hund's rule of maximum spin multiplicity is followed – the most stable electronic configuration arises from same spin electrons in the degenerate p-orbitals to give triplet carbenes; the same is not always the case with bent carbenes. Spin pairing of the non-bonding electrons leads to singlet carbenes which can exist as ambiphiles with pairing in the same σ or p_π orbital ($^1A_1$) or in the excited state with single occupation of both orbitals ($^1B_1$). Occupation of both orbitals with parallel-spin electrons gives rise to triplet carbenes ($^3B_1$), generally regarded as diradicals.[40]

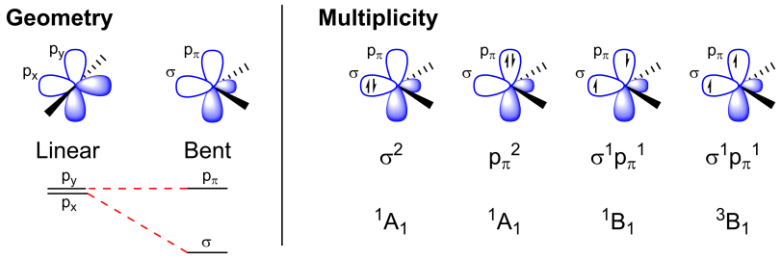


Figure 7 – The different electronic arrangements of carbenes, arising from alterations in geometry about carbon or spin multiplicity. Relative orbital energies of the two geometries are also shown.

The preference for singlet or triplet carbene is dictated by the σ-p_π orbital energy gap, with values greater than 2 eV likely to lead to singlet carbenes and less than 1.5 eV to triplet carbenes.[41] This energy gap can be altered by the electronic nature of the substituents through altering stability of the σ orbital; electron-withdrawing substituents stabilise this orbital and thus favour singlet carbenes whilst electron-donating substituents favour triplet carbenes through σ orbital destabilisation. Inductive effects only dictate the ground-state multiplicity of the minority of carbenes and mesomeric effects are usually more significant.[40] Pauling[42] realised the importance of both inductive and mesomeric effects in carbene stability in 1980, considering *ab initio* calculations upon a variety of singlet carbenes. He identified the need for carbene centre electroneutrality that can be achieved using π-donor and π-acceptor substituents (denoted X and Z respectively) in three different ways (**Figure 8**). (X,X)-carbenes show p_π destabilisation through interaction with the substituent lone pair, increasing the σ-p_π gap and favouring the singlet state. They are predicted to be bent singlets due to the presence of a nonsymmetric lone pair combination. (Z,Z)-carbenes show interaction of the

carbene lone pair with the substituent vacant p-orbitals, interrupting (p_x,p_y) degeneracy and leading to a linear singlet carbene with a two-electron three center π-system. The final possibility is a (X,Z)-carbene, with the X substituent interacting with the p_y orbital and Z with the p_x orbital. Both interactions favour the singlet state, with p_x stabilisation and p_y destabilisation, and the resulting allene-like system is quasi-linear.[40]

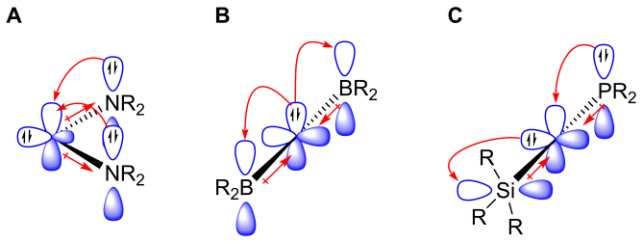
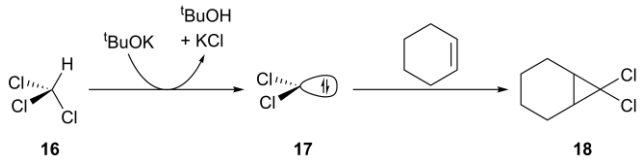


Figure 8 – Electronic effects present within stabilised singlet carbenes. **A)** diaminocarbene, an example of a (X,X)-carbene, with two π-donor and σ-acceptor substituents. **B)** diborylcarbene, an example of a (Z,Z)-carbene, with two π-acceptor and σ-donor substituents **C)** phosphinosilylcarbene, an example of a (X,Z)-carbene, with a π-donor and π-acceptor substituent.

Steric effects also impact carbene stability through crowding and, in cases where electronic effects are negligible, impact multiplicity. By introduction of steric bulk about the carbene centre the bond angle tends towards linearity, which as shown in **Figure 7** reduces the frontier orbital gap and favours triplet carbenes.[40]

The earliest report of an attempted carbene synthesis is that of Dumas and Péligot,[43, 44] who postulated the methanol dehydration in sulfuric acid and phosphorous pentoxide to give methylene. Geuther[45, 46] implemented a similar logic to successfully generate dichlorocarbene from chloroform and potassium ethoxide *in situ*. It was not until the work of Doering,[47] roughly 90 years later, that carbenes were implemented within organic synthesis (**Scheme 4**) – the reaction of generated dichlorocarbene (**17**) with cyclohexene to give bicycloheptane **18**. Carbenes were however still seen as short-lived molecules, and work towards bench-stable carbenes would facilitate their utilisation in a wider range of transformations.[44]



Scheme 4 – The first synthetic utilisation of a carbene. Dichlorocarbene (**17**) is generated from chloroform (**16**) in cyclohexene, giving 7,7-dichlorobicyclo[4.1.0]heptane **18**.

1.2.1 – Stable carbenes

As highlighted earlier, work towards stabilised singlet and triplet carbenes relies on opposing substitution pattern designs. Work in the area of stabilising triplet carbenes (**Figure 9**) is beyond the scope of this thesis, but the methodologies used mirror those in persistent radical development.

Zimmermann and Paskovich[48] were the first to attempt synthesis of a stable triplet carbene – they obtained 3 tetraarylethylene analogues with evidence of the sterically crowded diarylmethylene intermediates **19a-c**. Tomioka *et al*[49] later implemented a large bis(9-anthryl) conjugated system, stabilised by the 10-phenyl substitution, to access triplet carbene **20** with half-life of 19 minutes. Recent work by Nakajo *et al*[50] has integrated fluorene carbenes into a zinc-isophthalic acid metal-organic framework (MOF) (**21**), increasing the thermal stability and reactivity, the latter a result of the porous structure. These examples represent the 3 current approaches to stable triplet carbene preparation.

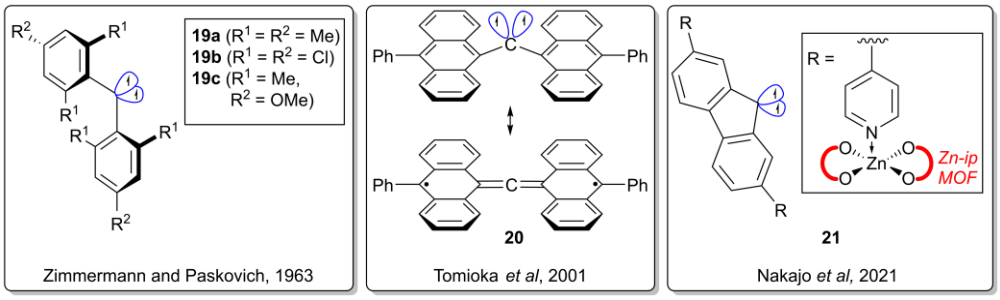
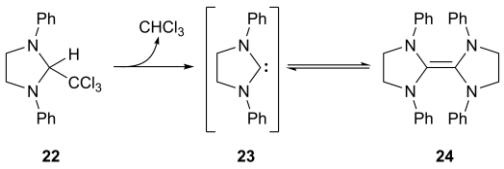
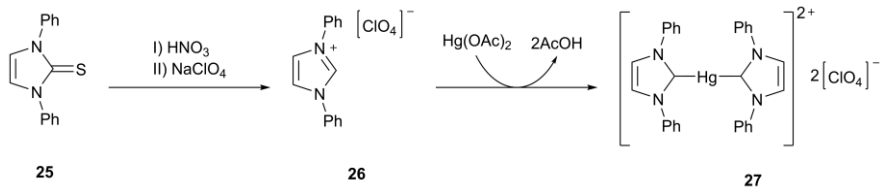


Figure 9 – Work towards stabilised triplet carbenes, including that of Zimmermann and Paskovich on kinetic stabilisation through steric crowding; Tomioka *et al* on thermodynamic stabilisation with a bis(9-(10-phenyl)anthryl)carbene; and Nakajo *et al* on metal-organic framework fixation. ip = isophthalic acid.

Wanzlick and coworkers[51, 52] identified the effectiveness of amino substituents in stabilising singlet carbenes in the early 1960s (**Scheme 5**), and although only the dimer **24** was isolated, evidence for **23** was seen in high temperature molecular weight determination and a series of reactions with electrophiles.[53] Several years later Wanzlick and Schönherr[54] undertook the first direct synthesis of a metal-carbene complex (**Scheme 6**), preparing the carbenoid *in situ* by desulfurization of a thiourea.

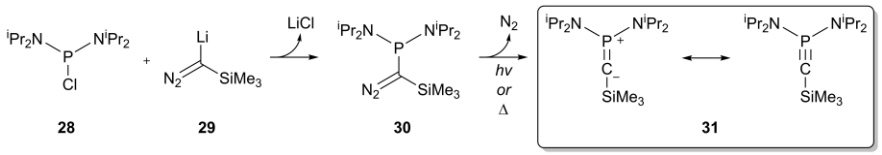


Scheme 5 – Attempted preparation of 1,3-diphenylimidazolidin-2-ylidine **23** by thermal elimination of chloroform from **22**. Only the dimeric olefin product **24** was isolated.



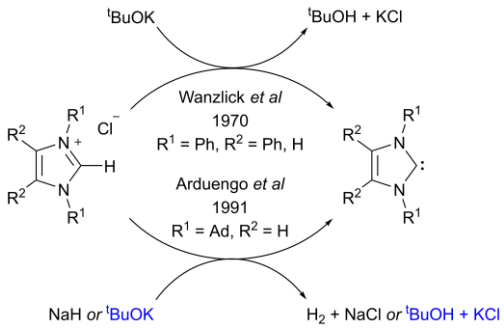
Scheme 6 – The first direct synthesis of a metal-carbene complex, undertaken by Wanzlick and coworkers. Thiourea **25** is desulfurized with nitric acid to give the imidazolium nitrate, which is converted into **26** using sodium perchlorate. Reaction with mercury(II) acetate allows for preparation of the carbene complex **27**.

The first stable carbene was prepared by Bertrand *et al*,[55] a phosphinosilyl (X,Z)-carbene (**31**) obtained from reaction of phosphine **28** with (diazo(trimethylsilyl)methyl)lithium (**29**) and subsequent loss of nitrogen gas (**Scheme 7**). The phosphinoacetylene resonance form of **31** accounts for the observed stability, which is supported to exist by ^{31}P $^{1}J(PC)$ and $^{2}J(PSi)$ NMR coupling constants.



Scheme 7 – Synthesis of the first stable carbene by Bertrand *et al*. **28** reacts with **29** to give the diazo derivative **30**. Photolysis or flash thermolysis of **30** affords the carbene **31**.

The preparation of carbenes from azolium salts is an alternative route first demonstrated by Wanzlick *et al*[56] in 1970, whereby imidazolium salts were deprotonated by potassium *tert*-butoxide to afford the corresponding imidazolylidene species, however these were not isolated (**Scheme 8**). This technique was successfully implemented over 20 years later by Arduengo and coworkers[57] to isolate the thermally stable 1,3-di(1-adamantyl)imidazolylidene species.



Scheme 8 – Overview of the syntheses by Wanzlick *et al*, and Arduengo and coworkers, to afford imidazolylidene species from deprotonation of the corresponding imidazolium salt. Ad = adamantyl.

The imidazolylidene species shown within this section are part of a wider range of singlet carbenes known as *N*-heterocyclic carbenes (NHCs), which are commonly generated *in situ* from C(2)/C(3)-H deprotonation of the corresponding heterocyclic azolium salt. **Figure 10** highlights a selection of other NHC precursors. A range of asymmetric NHC organocatalysts are documented with the literature, such as the pyrrolidino-fused triazolium **32**. The amino-substituted 1,2,4-triazolium salt Nitron (**33a**) displays unusual characteristics relating to the existence of the carbene tautomer *in situ*,[58, 59] **33a** was the only example of this scaffold present within the literature before work within our group. Bis(amino)cyclopropeniums (BAC-Hs, e.g. **34**) are a comparatively newer class of NHC-related compounds showing interesting orthogonal behaviour.[40, 60] Other types of NHC precursor beyond the scope of this thesis include diamidocarbenes (e.g. **35**), which show behaviour similar to non-resonant carbenes and enhanced electrophilicity,[61] and abnormal NHCs (e.g. **36**) resulting from protection of the preferred deprotonation site.[62] Our group are interested in the organocatalytic

applications of NHCs, particularly fundamental physical organic properties and the mechanisms underpinning their reactivity.[63-66]

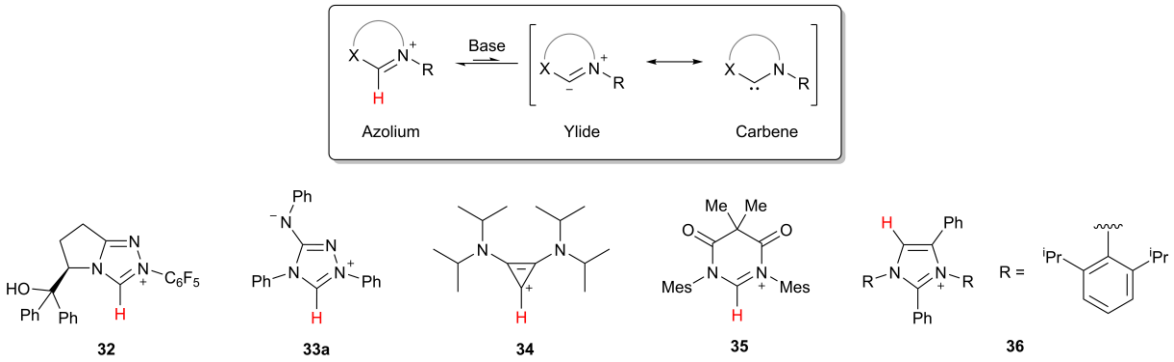


Figure 10 – Top: The generation of carbene, through an ylide resonance form, by base-deprotonation of the azolium ion at C-H. Bottom: Examples of NHC precursors, with acidic sites highlighted. Mes = mesityl (2,4,6-trimethylphenyl).

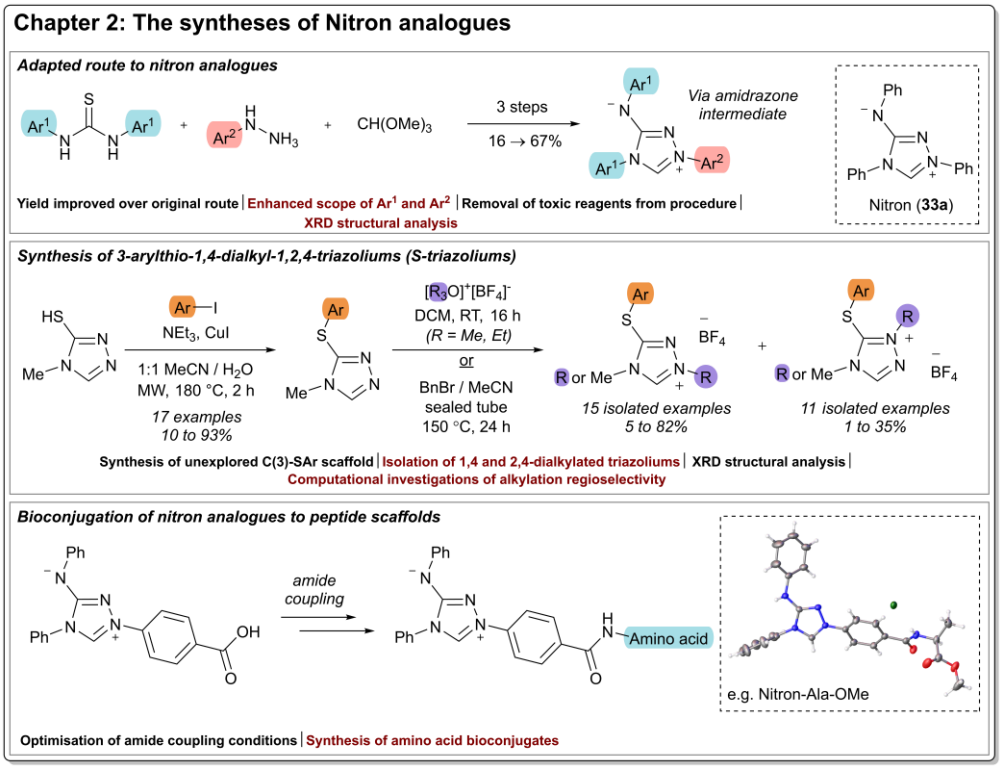
1.3 – Conclusions

This section discusses the synthesis and properties for two broad classes of compound explored within this work – stable organic radicals and carbenes. Both classes of compound have varied applications, and therefore have gained widespread appeal.

1.4 – Summary and aims of the project

This thesis is broadly split into synthetic aspects (Chapter 2-4), mechanistic and NMR kinetic experiments (Chapter 5) and biological analysis through cell-based assays in Chapter 6.

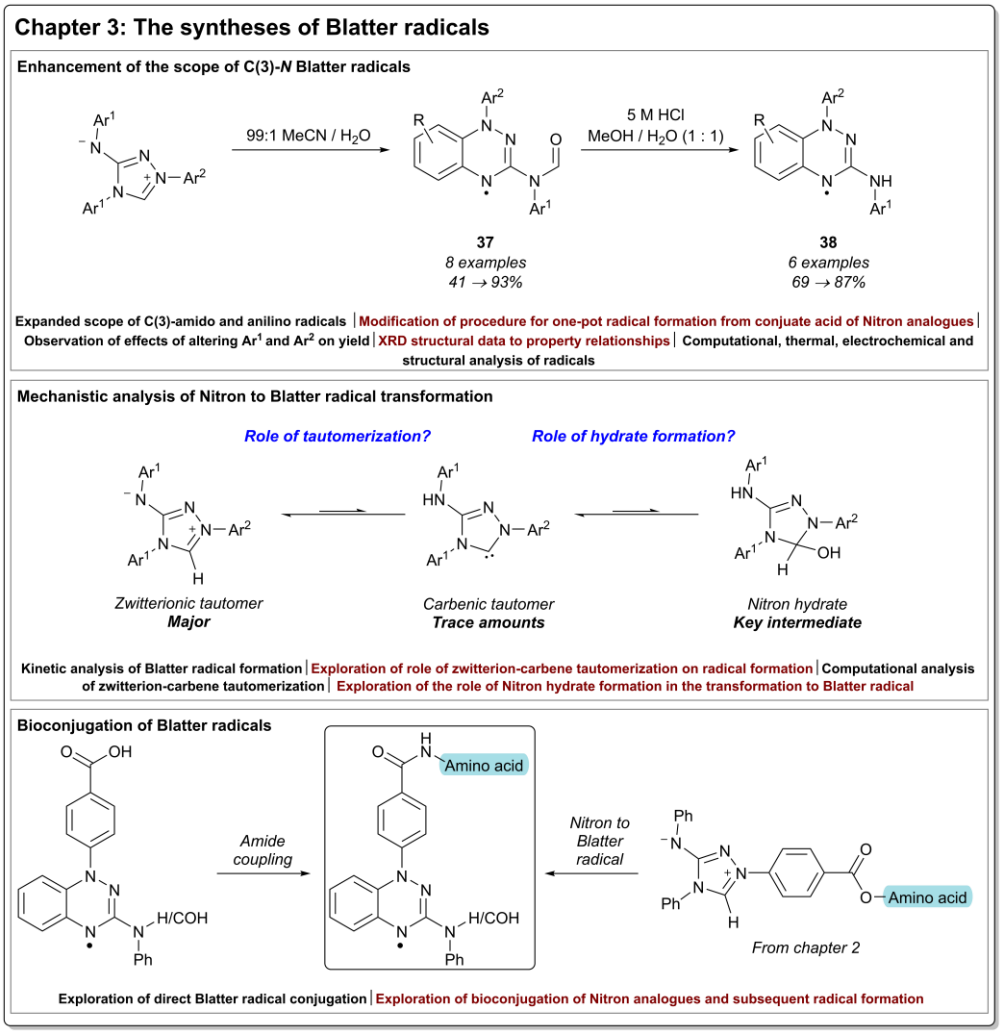
Chapter 2 explores the synthetic routes to 1,2,4-triazolium ions, all bearing structural similarity to the commercially available reagent Nitron (**33a**, **Scheme 9**) for which we recently published an unusual rearrangement to a series of persistent radicals termed Blatter radicals.[59] The first section explores the route historically used in the synthesis of Nitron[67] and how this may be adapted to improve yield, scope and reduce use of toxic reagents. The sulfur-derivatisation of the 1,2,4-triazolium scaffold is then explored. Finally, with interest in the development of enzyme mimic scaffolds and derivatization of the nitron scaffold for medicinal applications, the bioconjugation of 1,2,4-triazolium scaffolds to amino acids is explored.



Scheme 9 – Overview of research results presented and discussed in Chapter 2.

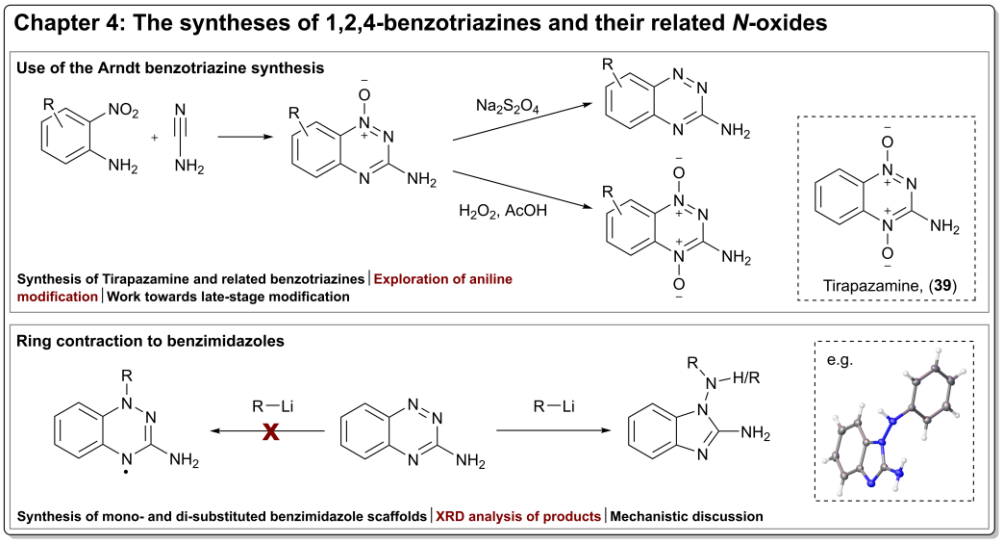
Chapter 3 explores the conversion of Nitron and the new analogues (Chapter 2) to bench-stable *N*-centred Blatter radicals (**37**) and (**38**) with C(3)-N substitution, first reported by our group in 2017 (**Scheme 10**).[59] Prior to this work, only the parent Nitron (**33a**) had been synthesized. With the adapted route discussed in Chapter 2, the impact of altering the *N*-aryl substituents on the reaction to form radicals has been explored. Existence of a carbenic tautomer of nitron was proposed relatively recently,[58] this work aimed to further explore the relationship between tautomerisation ability and the propensity to form Blatter radicals. Finally, accessing Blatter radicals conjugated to amino acids

are of interest for the development of spin probes and the potential to improve pharmacokinetics of the radical – initial studies towards the bioconjugation of Blatter radicals is explored in Chapter 3.



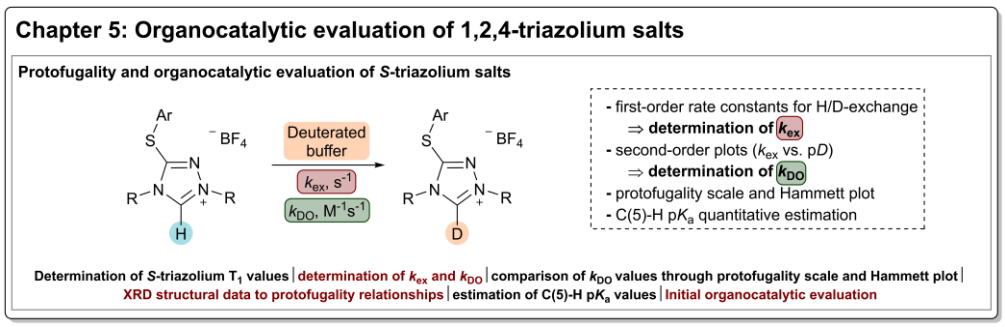
Scheme 10 – Overview of research results presented and discussed in Chapter 3.

Chapter 4 explores the synthesis of experimental anticancer prodrug Tirapazamine (**39**), and more broadly the series of 1,2,4-benzotriazine scaffolds that can be accessed using this route (**Scheme 11**).[68] In contrast to previous reports relating to the synthesis of Blatter radicals,[69, 70] the reaction of 3-amino-1,2,4-benzotriazine with organometallic reagents is found to form a variety of scaffolds including ring contraction to 1,2-diaminobenzimidazoles. The route to these benzimidazole scaffolds is explored in Chapter 4.



Scheme 11 – Overview of research results presented and discussed in Chapter 4

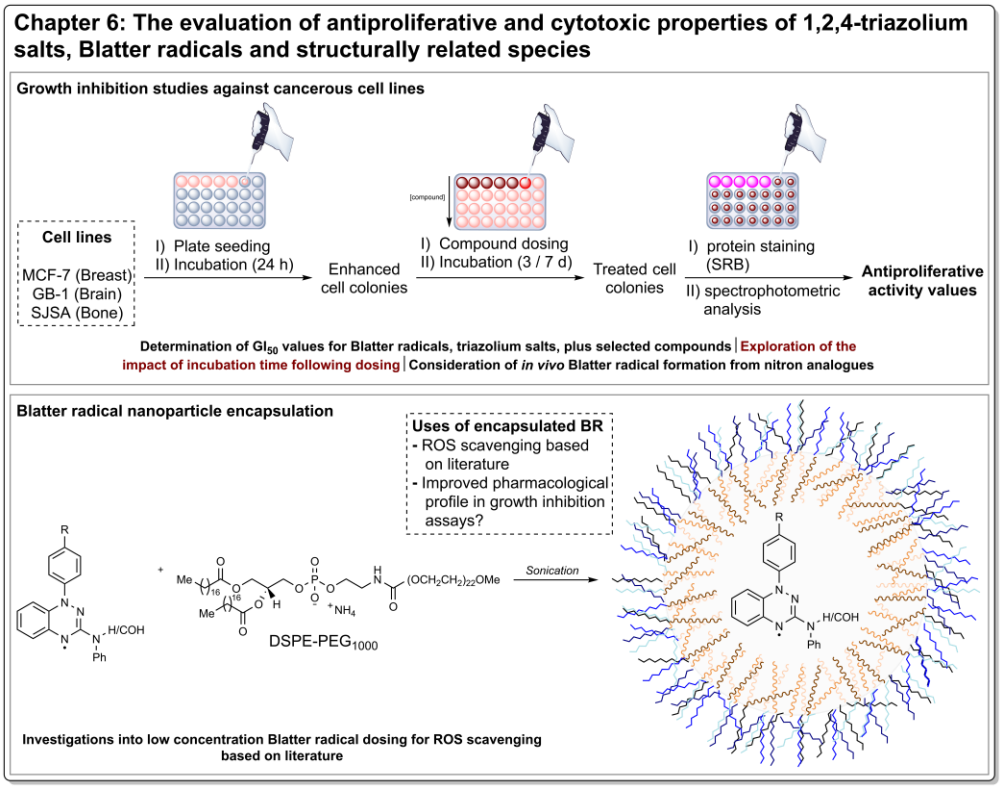
Chapter 5 explores the properties of 1,2,4-triazolium salts of relevance to organocatalytic application utilising potential as NHC catalysts (**Scheme 12**). The sulfur-derivatized triazolium salts explored within Chapter 2 are investigated for their protofugality (rate of proton transfer to common base), using ^{1}H NMR H/D-exchange studies, with some initial organocatalytic evaluation also undertaken – the potential for greener organocatalytic transformations within aqueous and semi-aqueous media is considered. The potential for organocatalysis using nitron derivatives, with consideration of their inherent instability in neutral or alkaline solution, is also explored.



Scheme 12 – Overview of research results presented and discussed in Chapter 5.

Chapter 6 starts with a review of the literature regarding the biological applications of persistent radicals, including the use of hypoxia-activated prodrugs (HAPs) as selective cytotoxic agents. The chapter then explores new results of the biological activity of Blatter radicals based on the anticancer activity of the HAP TPZ (**39**), for which the benzotriazinyl scaffold has been implicated as an active species under hypoxic conditions (**Scheme 13**). Related scaffolds are also explored, most notably the Nitron precursors to blatter radicals, with the aim to explore the possibility of Nitron being a prodrug form of the Blatter radical. The end of Chapter 6 discusses initial work based on literature[71] where Blatter radicals are encapsulated in poly(ethylene glycol) (PEG) based amphiphilic polymers to give

nanoparticles; the formed nanoparticles show enhanced water solubility and show promise as scavengers of reactive oxygen species (ROS).



Scheme 13 – Overview of research results presented and discussed in Chapter 6.

2 – The syntheses of Nitron analogues

2.0 – Foreword

The 1,2,4-triazolium salt Nitron (**33a**) has been known for over 100 years,[72] and within this time has been implemented in a number of applications: gravimetric analysis of predominantly nitrate salts;[72, 73] nitrate-responsive chemical sensors;[74, 75] metal ligands;[58] anchoring to metal surfaces;[76] and stabilisers for inks.[77, 78] Nitron is an anilino substituted 1,2,4-triazolium ion with zero overall charge. Surprisingly, only one published route to Nitron exists[67] involving the use of toxic and carcinogenic reagents. Furthermore, with studies showing the existence of a carbenic tautomer of Nitron,[58] enhancing the synthetic scope may allow for studies of the NHC properties of Nitron. Prior to our work, no analogues of Nitron were reported in the literature. Using the unmodified literature synthesis,[67] we recently reported four alkyl-substituted analogues of Nitron.[59]

Section 2.2 presents a brief overview of the general applications of 1,2,4-triazolium salts and the synthetic routes that can be used to access them. The exploration of routes to further Nitron analogues herein starts with the adapted version of the route to Nitron in Section 2.3. To extend the synthetic scope, the development of sulfur-derivatized 1,2,4-triazolium salts is explored in Section 2.4. Initial work towards bioconjugation of Nitron analogues to amino acid scaffolds is detailed in Section 2.5.

2.1 – Chapter contributions

The work presented in this chapter was undertaken in collaboration with the individuals listed below, with their contributions to this work noted. All other work detailed in this chapter was undertaken by the present author.

Katherine Deck (former O'Donoghue group 4th year MChem student): investigations into *N*-terminal bioconjugation strategies for Nitron analogues; synthesis of Nitron esters.

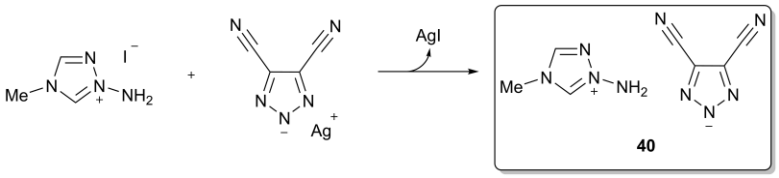
Jacob Murray (former O'Donoghue group PhD student): development of improved route to Nitron analogues; synthesis of 9 analogues of Nitron, with structural characterisation by XRD; collection of pK_a values for the C(5)-H and C(3)-NH positions of Nitron analogues.

2.2 – Introduction

2.2.1 – General applications of 1,2,4-triazolium salts

The 1,2,4-triazolium scaffold is a key moiety in a variety of fields due to high heteroatom content enabling effective H-bonding and solubility in polar solvents. The introduction of the 1,2,4-triazolium moiety into drug candidates has been shown to improve specificity, efficacy and aqueous solubility.[79]

One of the major areas of interest for 1,2,4-triazolium salts is their application as ionic liquids,[80] which have applications in chemical biology,[81] synthesis[82] and electrochemistry.[83] Work has allowed for the development of triazolium-triazolide ionic liquids (**40**, **Scheme 14**) that are a safer alternative to those bearing halogenated counterions, with high conductivity and lower viscosity than other ionic liquids.[80] Poly(ionic liquids) (PILs) of 1,2,4-triazolium salts show interesting physiochemical properties that are of interest broadly within materials chemistry – examples include their ability to form hydrogen bonding networks, access to polycarbenic scaffolds and metal binding.[84] Mixed imidazolium and 1,2,4-triazolium PILs have been shown to enable generation of porous membranes.[85]

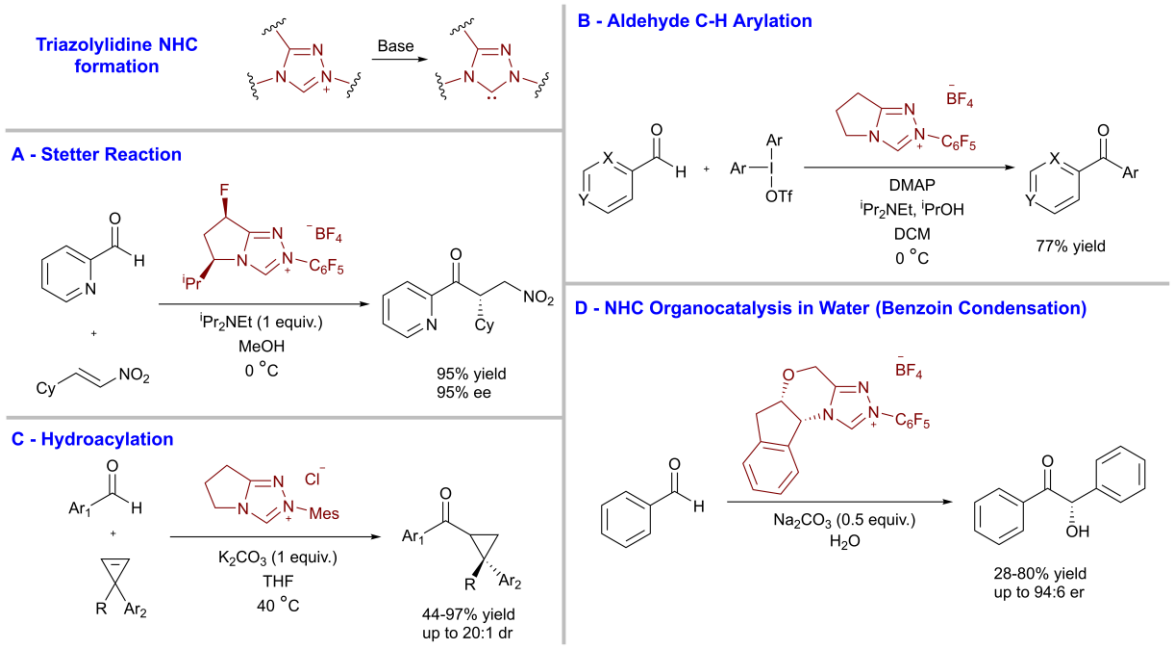


Scheme 14 – Preparation of a triazolium-triazolide ionic liquid by Savateev and coworkers.[80]

There have also been multiple reports of 1,2,4-triazolium salts possessing activity as anticancer, antibacterial and antifungal agents.[86] The medicinal applications of 1,2,4-triazolium salts will be discussed in detail in Chapter 7.

1,2,4-Triazolium salts are commonly used within carbenic organocatalysis. The active form of the catalyst is a triazolylidine *N*-heterocyclic carbene (NHC) formed *in situ* by deprotonation (**Scheme 15**). 1,2,4-Triazolium salt organocatalysts have been shown to catalyse a variety of transformations. The 1,4-addition of aldehydes to α, β-unsaturated systems, the Stetter reaction, can be catalysed by pentafluorophenyl-substituted triazolium salts (**Scheme 15A**).[87] Aldehyde C-H arylation to ketones[88] and hydroacylation[89, 90] have also been reported (**Scheme 15B**, **C**). Recently, interest has moved to organocatalysis within aqueous and semi-aqueous conditions,[91] with an initial focus on the NHC-organocatalysed benzoin condensation (**Scheme 15D**)[92] and Stetter reaction.[93] Asymmetric organocatalysis has also been made possible through introduction of chirality to the catalyst[87, 92] or as a result of the structure of the transition state.[89, 90] Additional to the transformations shown in

Scheme 15, the application of triazolium NHCs as proton-transfer catalysts in the polymerisation of dimethylacrylates has also been illustrated.[94]



Scheme 15 – **A**) Rovis and co-workers[87] reported the triazolium-catalysed enantioselective Stetter reaction. **B**) Gaunt and co-workers[88] reported the triazolium-catalysed C-H arylation of aldehydes. **C**) Glorius and co-workers[89, 90] illustrated the potential for diastereoselective hydroacylation of cyclopropenes. **D**) A key catalytic example to this work, reported by Zhong and co-workers,[92] is the enantioselective benzoin condensation in water.

Metal complexes containing triazolium-derived NHCs are of growing interest given the easy preparation of the NHC ligand, the strong metal-NHC bond and the property tuning possible by altering the NHC scaffold.[95, 96] The major application of these complexes is within catalysis of a wide range of transformations, such as transfer hydrogenation[97] and hydrosilylation[98] with iridium complexes being particularly prevalent. The development of 'smart' NHC ligands has also been illustrated, where the NHC can mediate catalytic activity as a result of external stimuli such as redox processes, pH, light, changes in coordination and changes in the reaction conditions. Multifunctional NHC ligands have also been reported, whereby groups upon the NHC ligand participate in the catalytic process – this can be through interactions with the substrate, or interactions with the metal centre to initiate catalytic steps.[96] Metal NHC complexes have also been implemented as medicinal agents against a variety of targets such as cancer and cystic fibrosis.[99-102]

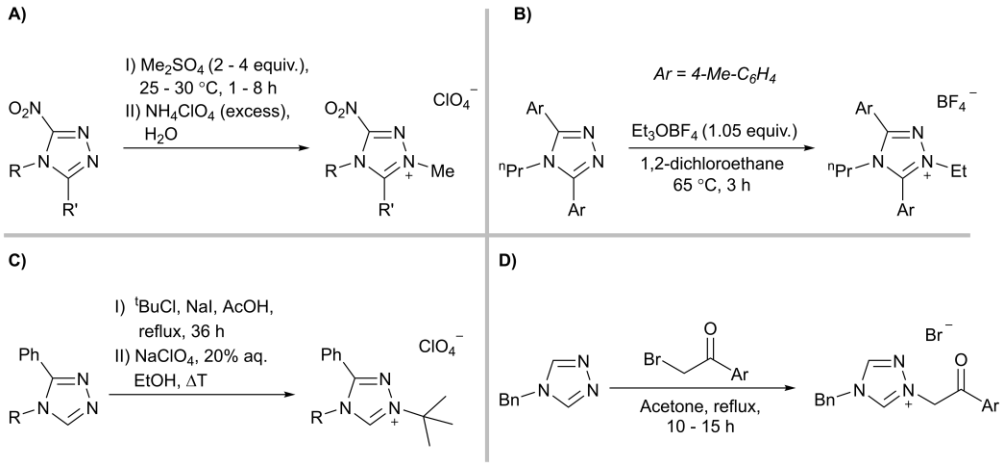
2.2.2 – Synthesis of 1,2,4-triazolium salts

The following section provides a brief overview of the synthetic methods used to prepare 1,2,4-triazolium salts, focussing on those relevant to this work.

2.2.2.1 – Preparation of 1,2,4-triazolium salts from triazole precursors

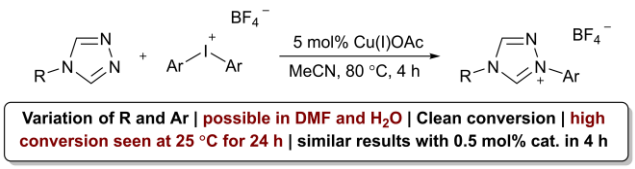
Given the numerous routes for the synthesis of neutral 1,2,4-triazole containing scaffolds,[103-105] the generation of 1,2,4-triazolium salts by reaction upon the diverse triazole scaffolds previously reported can be a straightforward method to rapidly generate a library of compounds. The diverse range of methods to synthesize triazole scaffolds[103-105] is generally beyond the scope of this thesis, though methods key to the work within this thesis are included.

Alkylation of 1,2,4-triazoles can be undertaken using a series of alkyl halides under forcing conditions. Sheikov[106] illustrated the ability to methylate 1,2,4-triazoles using dimethyl sulfate (DMS) (**Scheme 16A**). Carlsen[107] introduced an ethyl group through reaction with triethyloxonium tetrafluoroborate, however requiring higher temperatures, as part of studies into the thermal rearrangement of alkyl substituents on 1,2,4-triazoles (**Scheme 16B**). Růžička[108] showed the reaction of *tert*-butyl chloride, under reflux in acetic acid and the presence of NaI, to give high yields of the corresponding triazolium salts (**Scheme 16C**). Finally, Ivanov[109] introduced 2-oxo-2-arylethyl groups by reaction with the alkyl bromide, reacting these with substituted azirines to generate pyrrole rings (**Scheme 16D**).



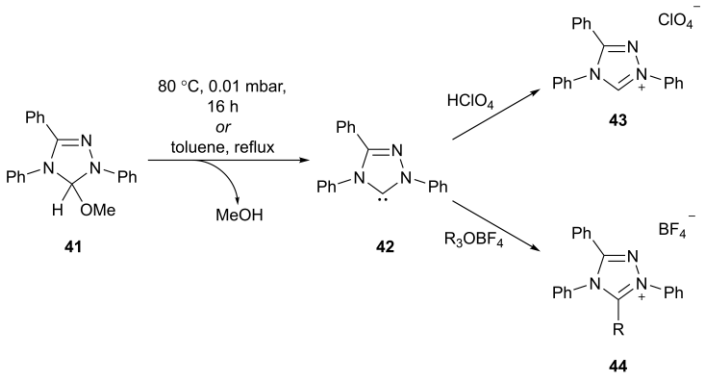
Scheme 16 – Synthesis of 1,2,4-triazolium salts by *N*-alkylation.

Given the generally lower reactivity of arylating agents *versus* the alkylating counterparts, addition of an aryl group onto 1,2,4-triazoles is particularly challenging. Diaryliodonium salts have however been successfully implemented in the arylation of 1,2,4-triazoles (**Scheme 17**); the Cu-catalysed process is possible under mild conditions, tolerates the presence of water, and proceeds without the formation of byproduct.[110]



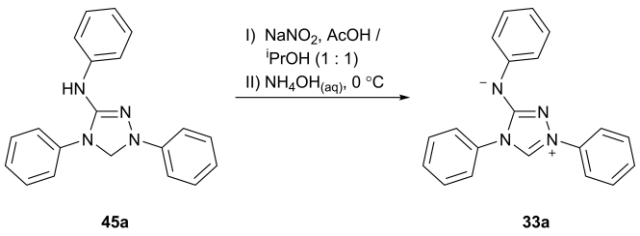
Scheme 17 – The synthesis of 1,2,4-triazolium salts using diaryliodonium salts.

Through thermal decomposition of a 5-methoxy-1,5-dihydrotriazole (**41**), Teles[111] illustrated the ability to generate the corresponding triazolylidine species **42** *in situ* (**Scheme 18**). The resultant carbene can be easily protonated with perchloric acid, or alkylated with trialkyloxonium salts, to generate triazolium salts **43** and **44** in yields greater than 90%.



Scheme 18 – Triazolium salt preparation is possible through thermal decomposition of the corresponding 5-methoxy-1,5-dihydro-1,2,4-triazole (**41**) to the corresponding carbene (**42**), followed by formal addition of a proton or alkyl cation to give the corresponding triazolium salt.[111]

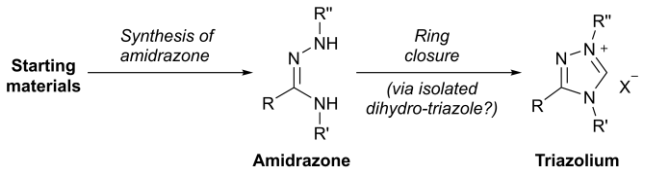
1,2,4-Triazolium salts may also be obtained *via* oxidation of the corresponding 1,5-dihydro-1,2,4-triazole. For the literature synthesis of Nitron (**33a**) by Kriven'ko and Morozova,[67] the final step involves oxidation of dihydro-1,2,4-triazole **45a** using sodium nitrite (**Scheme 19**).[67]



Scheme 19 – Access to 1,2,4-triazolium salts (**33a**) by oxidation of the corresponding 1,5-dihydrotriazole species (**45a**) within a mixture of acetic acid and isopropanol.[67]

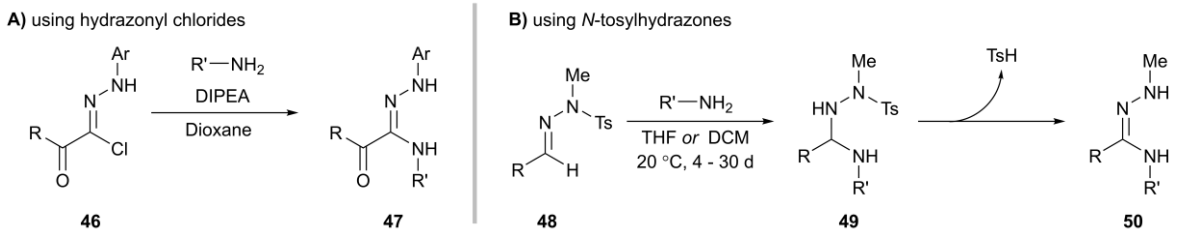
2.2.2.2 – Synthesis of 1,2,4-triazolium salts via amidrazone intermediates

Another route to 1,2,4-triazolium salts considers the synthesis of amidrazones, and their ring closure to triazolium salts (**Scheme 20**). For each step there are several possibilities, and so this section will illustrate the potential scope of the route.



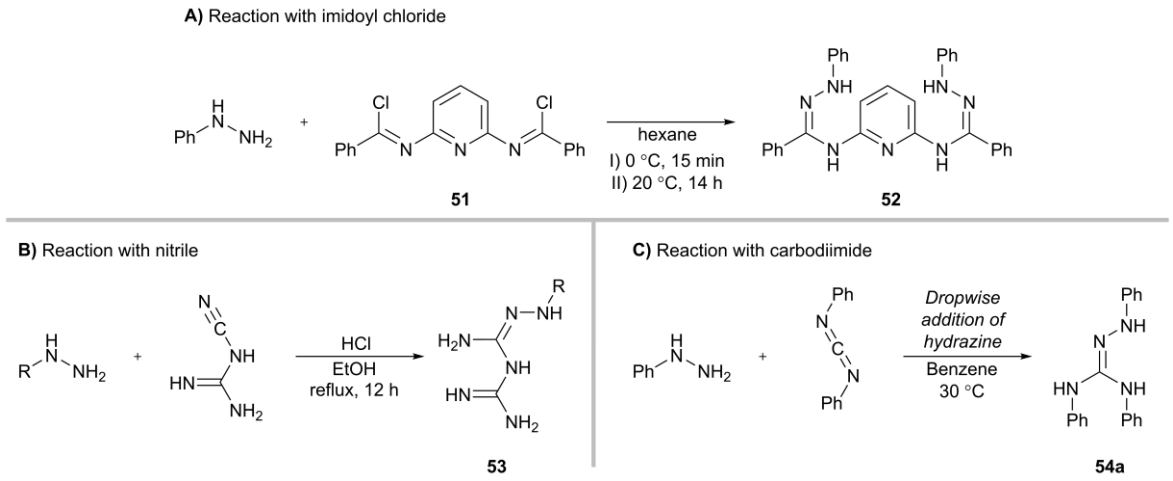
Scheme 20 – General route for the synthesis of 1,2,4-triazolium salts *via* an amidrazone intermediate. The route to the amidrazone, and how the amidrazone can be cyclised to the triazolium salt, must be considered.

Given the reactivity exhibited by amidrazones,[112, 113] they are not commercially available on synthetic scales, however their synthesis is relatively straightforward and so this route has not been impeded by their instability. One possibility is to react primary amines with activated hydrazone species, such as hydrazonyl chlorides (**46**) which were used by Belskaya[114] and Fershtat[115] (**Scheme 21A**) or *N*-tosylhydrazones (**48**) used by Novikov[116] (**Scheme 21B**). These routes benefit from the wide variety of primary amines that are commercially available, however require synthesis of the activated hydrazones which can pose a significant issue.



Scheme 21 – **A)** Hydrazonyl chloride **46**, synthesized using the Japp-Klingemann reaction,[117] can be used to prepare amidrazones **47**. **B)** *N*-methyl-*N*-tosylhydrazone **48** can be used to prepare dihydroamidrazone **49**, which can eliminate TsH to give **50**.

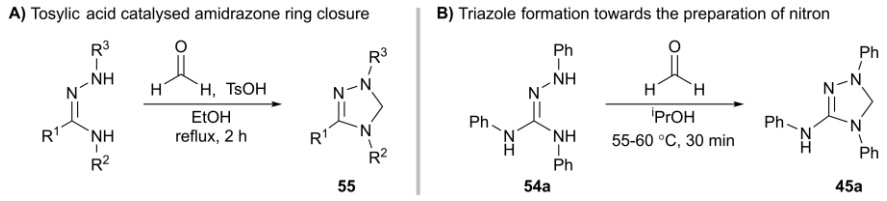
The other main route to amidrazones involves the reaction of hydrazines with activated imines, nitriles or carbodiimides. Hydrazines are more limited in terms of commercial availability, and are prone to N-N cleavage to give the amine. The activated imines or nitriles are easier to access than activated hydrazones as imidoyl chloride precursors can be obtained from the corresponding amide through reaction with thionyl chloride.[118] Schreiner[118] used imidoyl chloride **51** to synthesize bis(amidrazone) species **52** as an intermediate to an acridine analogue (**Scheme 22A**). Aly[119] demonstrated the synthesis of amidrazone **53** from reaction of hydrazines with cyanoguanidine under acidic conditions (**Scheme 22B**). Finally, in the synthesis of Nitron (**33a**), Kriven'ko and Morozova[67] show the generation of anilinoamidrazone **54a** through reaction of carbodiimide with hydrazine (**Scheme 22C**).



Scheme 22 – **A)** Imidoyl chloride **51** readily reacts with hydrazines in high yields to give **52**. **B)** The reaction of activated nitriles, such as cyanoguanidine, with hydrazines can allow access to amidrazones **53**. **C)** As part of the literature synthesis of Nitron (**33a**), carbodiimide is reacted with dropwise addition of hydrazine to give the desired amidrazone **54a**.

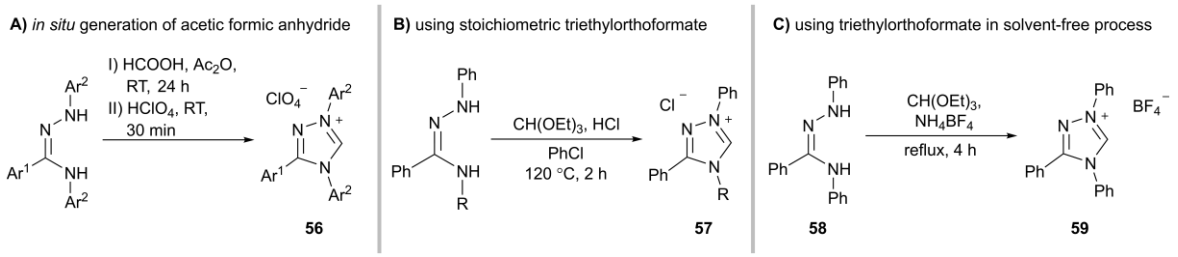
Other methods to form amidrazones have been reported, such as from amides and imidates, and have been reviewed.[112, 120]

One of the routes to 1,2,4-triazolium species from amidrazones involves cyclisation to the dihydro-1,2,4-triazole. Nuhn[121] illustrated the ability to form dihydrotriazoles (**55**) by reaction of amidrazones with formaldehyde, using catalytic tosylic acid (**Scheme 23A**). As part of the synthesis of Nitron, Kriven'ko and Morozova[67] used a similar method to generate dihydrotriazole (**45a**) (**Scheme 23B**) from amidrazone **54a**, however found that the procedure was possible without addition of tosylic acid. The dihydro-1,2,4-triazole can subsequently be oxidised to the triazolium salt.



Scheme 23 –**A)** Amidrazones have been shown to undergo ring closure catalysed by tosylic acid. **B)** As part of Nitron synthesis, 3-anilinoamidrazone ring closure was shown by heating with formaldehyde in isopropanol.

Alternatively, amidrazone may be cyclised in a single synthetic step to the triazolium salt. Chen[94] achieved this through *in situ* generation of acetic formic anhydride (**Scheme 24A**) with the formation of the perchlorate salt **56** by treatment with perchloric acid. Berkessel[122] used triethylorthoformate (8 equivalents) to undertake the same transformation to **57** under acidic conditions (**Scheme 24B**), however Grubbs[123] has undertaken this transformation solvent free by using triethylorthoformate with ammonium tetrafluoroborate to access **59** (**Scheme 24C**) from triphenylamidrazone **58**. In all cases a dihydrotriazole intermediate is generated, however, it immediately undergoes the necessary loss of water / ethanol to form the triazolium salt unlike the previously discussed methods.



Scheme 24 –**A)** Acetic formic anhydride allows for the generation of triazolium **56**. **B)** Triethyl orthoformate can cyclise amidrazones to give **57**. **C)** Amidrazone **58** ring closure and formation of **59** can be undertaken in neat triethyl orthoformate and ammonium tetrafluoroborate.

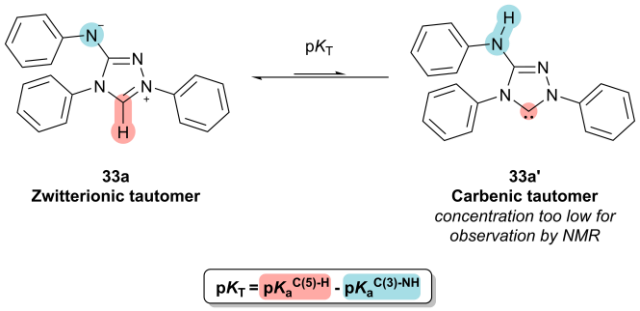
2.2.3 – Properties, applications and synthesis of *N*-functionalised 1,2,4-triazolium salts

The 1,2,4-triazolium salt Nitron (**33a**) is a mesomeric betaine traditionally used in the gravimetric and spectrophotometric detection of nitrate and perchlorate salts,[72, 124] with more recent work investigating potential applications by the North American Space Agency (NASA) as a chemical sensor for atmospheric nitrogen oxides.[75] Both nitrates and perchlorates are common by-products resulting from human activity: nitrogen oxides are used on the kiloton scale annually as nitrate salts in fertilizers, and are present in automobile exhaust gases; perchlorates are used in solid rocket propellants (including fireworks), disinfectants and bleach. Through these uses, aided by their high aqueous solubility and the processes within the nitrogen fixation cycle, both nitrate and perchlorate salts pervade soil, groundwater, rivers and the atmosphere.[125] Nitron forms insoluble salts with a variety of anions, such as halides and chromate, which may aid quantification of these species. Nitrates, perchlorates and picrates give rise to highly insoluble Nitron salts applicable for gravimetric analysis.[126]

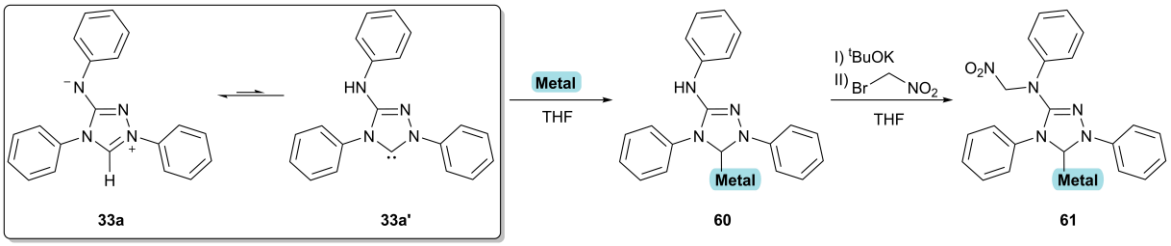
The potential of Nitron to form an NHC through C(5)-H deprotonation underpins a variety of metal-catalysed and organocatalytic applications. Work by Siemeling *et al*[58] proposed Nitron zwitterion **33a** is in equilibrium with a carbenic form **33a'** arising from tautomerisation (**Scheme 25**) although levels are too low for detection by NMR. Recent work within our group has quantitatively estimated the pK_a value of the C(5)-H position (~17.1 to ~18.1) and determined the pK_a of the C(3)-NH position experimentally (8.85 – 10.4) to enable estimation of the tautomerisation constant pK_T and the relative concentrations of both tautomers *in situ*.[127]

Self-assembled monolayers of Nitron scaffolds upon gold and platinum have been shown to act as nucleophilic handles for alkyl halides through the C(3)-NH position, with thermal stability up to 200 °C and no displacement by thiol ligands (**Scheme 26**).[76] A range of Nitron metal complexes have also been synthesized where the triazolium exhibits a strong *trans*-influence (**Figure 11**).[58, 128] Iridium complexes of Nitron also demonstrate catalytic activity in the hydrosilylation of benzaldehyde, transfer hydrogenation to reduce acetophenone, dehydrogenation of formic acid and

dehydrocoupling of alcohols and hydrosilanes. To our knowledge, the Nitron-derived carbene has not been implemented as an organocatalyst within the literature. Also key to the work within this thesis is that no analogues of the Nitron scaffold have been explored for their possible applications within the literature, potentially due to the lack of insight towards Nitron synthesis.



Scheme 25 – Nitron can undergo tautomerisation to generate low levels of carbene *in situ* – evidence for this tautomerisation is the observation of Nitron undergoing reactions typical of a nucleophilic carbene and also acting as a metal ligand providing a strong *trans*-effect.



Scheme 26 – A THF solution of Nitron (**33a / 33a'**) added to Au- and Pt-coated Si wafers overnight gave Nitron decorated metal surfaces **60**. The Nitron-derived units could be used as a handle for S_N2 chemistry shown by reaction with bromonitromethane (**61**).

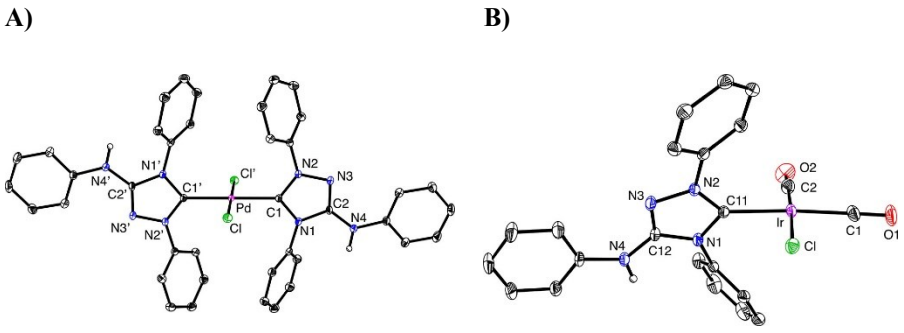
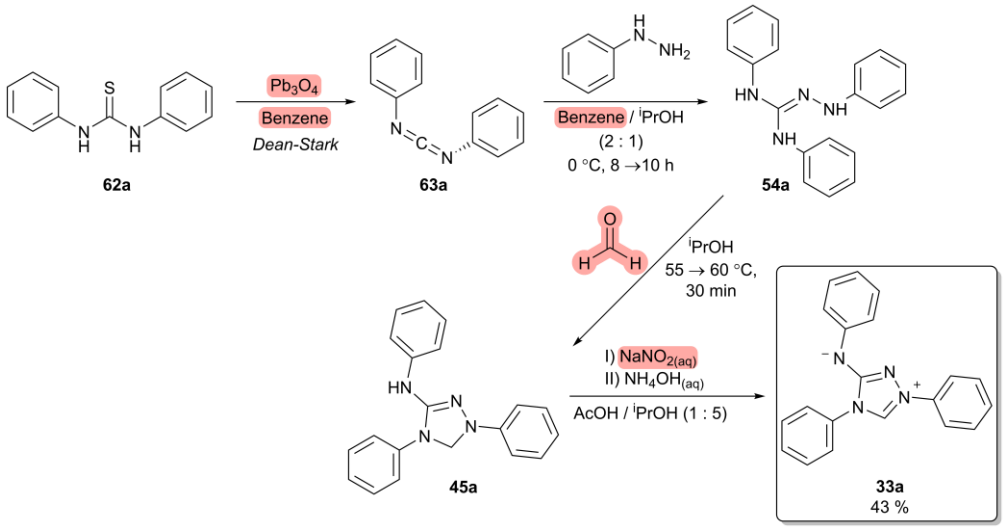


Figure 11 – Crystal structures of Nitron-metal complexes. **A)** The crystal structure of the square-planar *trans*-[$PdCl_2$(Nitron)$_2$] complex. **B)** The crystal structure of the square-planar *cis*-[$IrCl(CO)_2$(Nitron)] complex. Hydrogen atoms are omitted on carbon for clarity. Reprinted with permission from P. J. Quinlivan, A. Loo, D. G. Shlian, J. Martinez and G. Parkin, *Organometallics*, 2021, **40**, 166-183. Copyright © 2023 American Chemical Society.

The literature route to synthesize Nitron, inspired by the original synthesis by Busch,[124] is shown in **Scheme 27**. The thiourea **62a** is desulfurized to carbodiimide **63a** and reacted with phenylhydrazine to give the C(3)-anilino amidrazone **54a**. Ring closure with formaldehyde, oxidation with sodium nitrite and treatment with ammonium hydroxide solution gives the desired Nitron product **33a** in respectable yield.[67] This is an improvement on the ≤ 20% yield achieved with Busch's original

synthesis,[124] however with the need for more environmentally friendly processes and the interest in developing this chemistry for pharmaceutical applications it is of great importance to replace highly toxic reagents. There are also synthetic challenges within this procedure that should be addressed to enable a wider range of Nitron analogues to be isolated. The desulfurization step to give **63a** uses lead(II,IV) oxide which is suspected to damage fertility and is very toxic to aquatic life presenting bioaccumulation concerns.[129] Lead has no known biological role within humans and has been linked to developmental and neurological issues.[130] Lead-based reagents are also difficult to dispose of due to the strict protocols to prevent their release into the environment. The desulfurization step along with the C(3)-anilino amidrazone formation uses benzene, a well-known carcinogen with well-established links to leukaemia and links to decreased DNA repair capacity;[131] usage of benzene in consumer products is no longer permitted due to the related risks.[132] The ring closure with formaldehyde to the 1,2,4-triazole in step 3 could benefit from recent work whereby the formation of the 1,2,4-triazolium can be undertaken in a single, higher-yielding step from the amidrazone.[122, 123, 133] This adapted route is also of interest as the oxidation of 1,2,4-triazole with sodium nitrite in the final step is overly harsh and readily leads to decomposition of the formed product, such as through over-oxidation.



Scheme 27 – The route to Nitron (**33a**) developed by Kriven'ko and Morozova. Reagents that require replacing in efforts to improve yield and reduce toxicity are highlighted in pink.

2.2.4 – Synthesis and applications of *S*-substituted triazolium salts.

Whilst sulfur is encountered within the substituents of 1,2,4-triazolium salts and other heterocycles,[134] the introduction of sulfur substituents directly attached to the 1,2,4-triazolium heterocycle (referred to within the limited literature and by our group as *S*-triazolium salts)[135] is uncommon. For this reason investigations of the impact of sulfur substitution on applications of triazolium salts is limited. The properties of NHCs, such as biological activity and coordination chemistry, are shown to be significantly impacted by altering the substituents upon the heterocycle.[96,

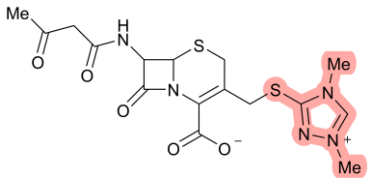
[136, 137] Given the diffuse electron density due to the size of sulfur in comparison to common carbon, nitrogen and oxygen substituents, the altered ability to donate electron density will impact the properties of the NHCs that can be generated from 1,2,4-triazolium salts.

S-triazolium salts (**64**) have seen application through the carbene **64'** that can be generated by deprotonation in base. Reaction of **64'** (*S*-triazolylidine) with primary alkyl halides generates a series of triazolium salts (**65**) that can be reduced and hydrolysed to give aldehydes that are one carbon longer than the starting alkyl chain (**Scheme 28**).[135, 138] A similar method is used in the generation of truncated and branched aldehydes from carboxylic acids by generation of **65** through ring closure of the carboxylic acid with amidrazone.[139-141] The sulfur-substituted triazolium has also been used as part of a larger scaffold; a *S*-triazolium bound to a cephalosporin scaffold has been synthesized (**66**), and shows good antimicrobial activity against *S. aureus*.[142]



64 64' 65

Scheme 28 – The reaction of alkyl halide with the carbene **64'** generated from **64** gives access to a series of alkyl-substituted *S*-triazolium salts **65** that can be reduced to the 1,2,4-triazole and hydrolysed to gain access to aldehydes of chain length one carbon greater than the starting alkyl halide, plus a thioamidrazone species.

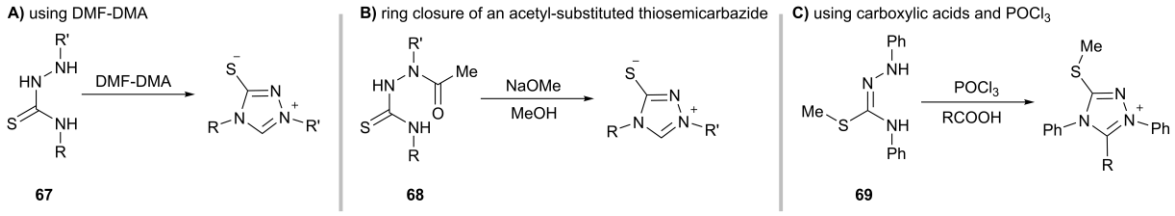


66

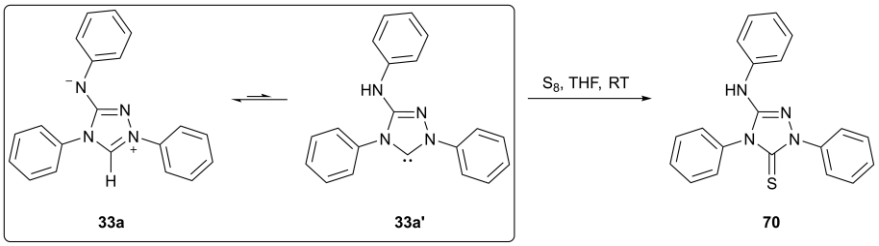
S-triazolium salts are traditionally synthesized using ring closure of the corresponding sulfur-substituted amidrazone (or thiosemicarbazide, when sulfur does not bear further substitution). The thiosemicarbazide starting material is synthesized by the reaction of hydrazine with isothiocyanates, then substitution upon sulfur with alkyl or aryl groups gives the sulfur-substituted amidrazone. *N*,*N*-dimethylformamide dimethyl acetal (DMF-DMA) has been shown to cyclise thiocarbazides (**67**) to give the corresponding triazolium thiolate in generally good yields (**Scheme 29A**).[143] Using a thiosemicarbazide bearing an *N*-acetyl substituent (**68**), cyclisation is possible using sodium methoxide (**Scheme 29B**).[144] *S*-substituted amidrazones (**69**) can also undergo cyclisation by reaction with carboxylic acids in the presence of phosphoryl chloride (**Scheme 29C**).[141]

1,2,4-Triazole thiones can also be generated by the reaction of triazolylidine species with elemental sulfur. The zinc active site of liver alcohol dehydrogenase (LADH) has been modelled using a pincer ligand incorporating two 1,2,4-triazole thiones which chelate through sulfur – this ligand is synthesized from the corresponding triazole through reaction with acetate base followed by S_8.[145]

Given the existence of a carbenic tautomer, the generation of the corresponding thione of Nitron (**70**) can be achieved using elemental sulfur alone without the need for additional base (**Scheme 30**) – this trapping of the carbene **33a'** was initial evidence of the previously unknown tautomerization occurring *in situ*.[58] A similar procedure has been used to trap the carbenic tautomer of a series of 1-(2-hydroxyphenyl)-1,2,4-triazolium salts.[146]



Scheme 29 – The synthesis of *S*-triazolium salts from amidrazone-like intermediates.



Scheme 30 – Nitron can undergo reaction with elemental sulfur to give the corresponding 1,2,4-triazole thione, which is typical of nucleophilic carbenes. This indicated the presence of a carbenic tautomer of Nitron.

2.2.5 – Towards bioconjugation to triazolium scaffolds for bio- and organocatalysis

Bioconjugation describes a series of techniques that enable the covalent binding of payloads such as pharmaceutically active compounds (PhACs), immobilisation supports, or structural probes to biomolecules such as proteins or exogenous moieties present upon cells.[147, 148] The benefits bioconjugation can provide can be generally summarised as either gaining a greater understanding of the function of biomolecules and the chemical basis of life, or the property enhancement of agents or biomolecules in biological systems. The bioconjugation of triazolium ions to peptides or proteins could enable enhanced drug delivery or alternatively a novel biocatalyst for catalysis in sustainable aqueous conditions.

Pharmaceutical research is moving towards the use of carrier systems that can enhance their pharmacokinetics. Of particular interest in drug carrier systems are those that can provide a targeting ability for the desired site, and protein bioconjugates present an appealing option that have highly customisable structures and advantageous properties over other drug delivery systems.[149]

There are three classes of peptide bioconjugation in regard to the site of covalent bond formation to the payload (**Figure 12**). The classical methodologies of bioconjugation explore addition to the *N*-

terminus, commonly achieved through transamination, native chemical ligation (NCL)[150] and reaction with ketenes. Bioconjugation upon the R-group of amino acids, referred to as 'in-chain conjugation', is the most popular class of peptide bioconjugation given the range of chemistry that is known for the derivatization of amines, thiols and phenols.[147] The final method is *C*-terminal conjugation, for which methods are scarce on account of the lack of selectivity *versus* carboxylate-containing R groups. Thioester generation underpins most *C*-terminal conjugation techniques, most notably NCL.

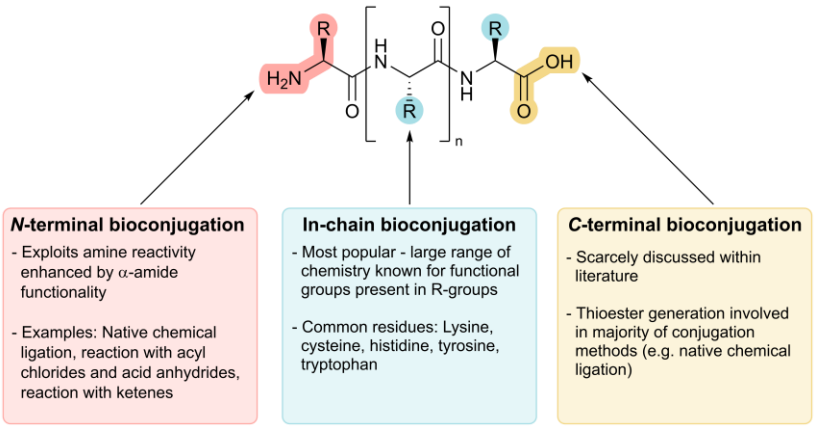


Figure 12 – A summary of the three classes of bioconjugation. *N*-terminal bioconjugation and in-chain bioconjugation constitute the vast majority of methodologies given the ability to selectively target these positions or for the range of chemistry known to modify these functional groups. *C*-terminal bioconjugation is mostly for amino acid thioester substrates, such as NCL.

The high level of specificity of enzymes is one of the major challenges for their application within synthesis, and coupled with the challenges of synthesizing such complex molecules[150] has promoted research into the development of artificial enzymes that can promote new-to-nature reactions. One of most common techniques to generate artificial enzymes is to functionalise natural enzymes with catalytic units that can enable new binding properties (increasing catalytic promiscuity) or provide novel activity for an alternative reaction (**Figure 13A**). A key strategy as part of this is to modify the metal cofactors that underpin the function of many enzymes; the properties of the generated artificial metalloenzymes (ArMs) are dependent on the nature of the modified metal cofactor. The development of artificial enzymes can also be undertaken from the opposite direction; modifying a protein with a large hydrophobic core and no catalytic activity such that a catalytic domain is developed (**Figure 13B**).[151] The ultimate goal in artificial enzyme development is to synthesize from scratch a highly optimised scaffold that provides the level of substrate specificity and selectivity of functional group required for the process (**Figure 13C**). Such an approach relies on significant knowledge about the reaction mechanism and also protein folding such that protein optimisation places the required catalytic residues in the correct orientation and close within the active site. Computational descriptions of metal-binding proteins have accurately described their tertiary and quaternary structure, and can be used to direct modification to enhance catalytic performance.[151]

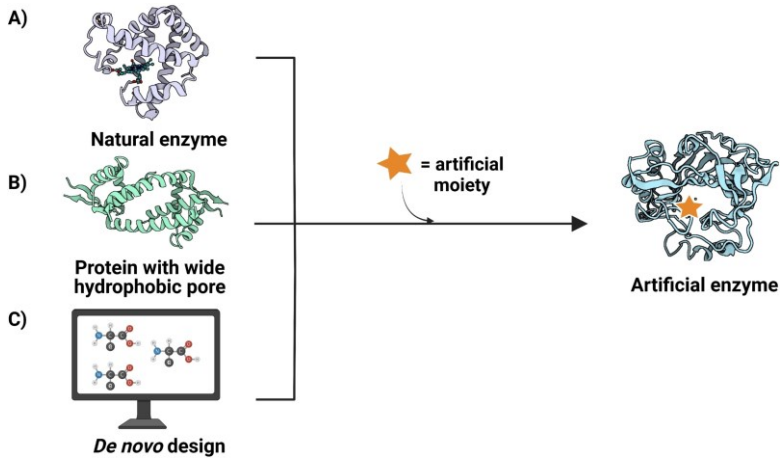
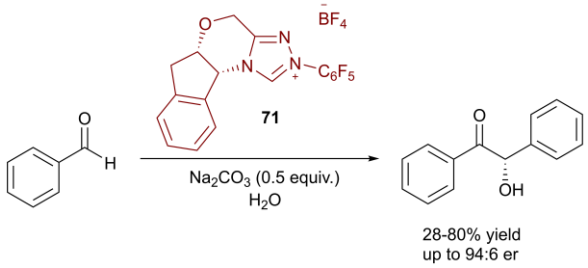


Figure 13 – The three approaches available for the design of artificial enzymes. **A** – natural enzymes can undergo functionalisation to tailor their catalytic activity. **B** – an artificial moiety(s) can be introduced into a protein that previously showed no catalytic activity. **C** – *De novo* design of artificial enzymes is the ultimate goal, by developing methodologies to synthesize enzymes that do not show the issues with stability, solubility and yield commonly observed in current methodologies. Reprinted with permission from: S. Hanreich, E. Bonandi and I. Drienovská, *ChemBioChem*, **24(6)**, e202200566. Copyright © 2022 Chemistry Europe.

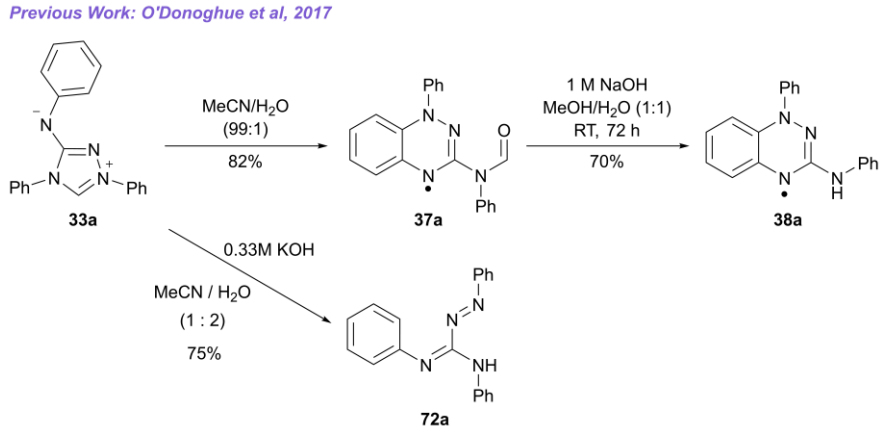
The only known examples within the literature of NHCs within artificial enzymes involve the development of metalloenzyme active site mimics with NHCs as ligands to zinc[145] and copper.[152] The growing interest in organocatalytic reactions of NHCs within water has illustrated that the NHC alone can display catalytic activity within aqueous conditions. Artificial enzymes containing NHC organocatalytic groups are therefore seen to be possible. Zhong *et al*[92] illustrated the ability to undertake benzoin condensations with 1,2,4-triazolium salts (**71**) within water (**Scheme 31**), showing good enantioselectivity and high yields in some cases. Several other triazolylidine catalysed transformations have also been undertaken in partially aqueous media, such as the asymmetric hydration of α-halogenated aldehydes,[153] and oxidation of aldehydes to esters.[154]



Scheme 31 – 1,2,4-triazolium-derived NHCs have been used to undertake asymmetric benzoin condensations with good enantioselectivity by Zhong *et al*.

2.3 – Synthesis and properties of Nitron analogues

Our group's initial interest in Nitron stemmed from the lack of organocatalytic applications and our general interest in the mechanistic evaluation of 1,2,4-triazolium derived carbenes as organocatalysts. It was however found that under catalytically relevant conditions Nitron (**33a**) undergoes ring opening to yield a 1,2,4-benzotriazinyl radical termed Blatter radical (BR, **37a**) as the major product, with traces of a triazabutadiene species (**72**) that could be obtained in high yields with the addition of potassium hydroxide (**Scheme 32**). The C(3)-anilino BR **38a** could be also obtained from acid- or base-catalysed hydrolysis of **37a**.[59] Four analogues of Nitron were synthesized using the traditional synthetic route[67] and also underwent the transformation to Blatter radical, however to explore this transformation further it was necessary to develop a more contemporary route that addresses the concerns discussed earlier. Conversely, with a greater understanding of the transformation of Nitron to BR, it may be possible to suppress triazolium ring-opening to give potentially useful scaffolds for organocatalysis.



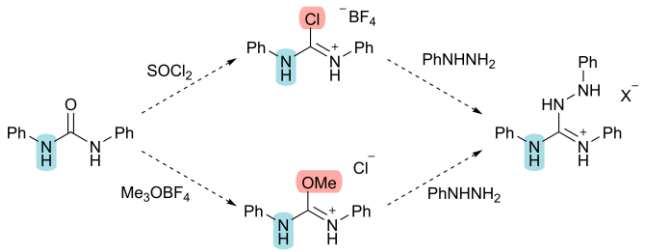
Scheme 32 – Within wet acetonitrile, Nitron (**33a**) can give the C(3)-amido BR **37a** in high yield. This BR can then undergo hydrolysis to give the C(3)-anilino BR **38a**. Triazabutadiene **72a** identified in trace amounts within the formation of **37a** can be prepared using dilute KOH.

This section presents work by Jacob Murray and myself to develop an improved synthetic strategy to Nitron, thereby allowing access to a greater range of analogues. The work towards a contemporary synthetic route to Nitron is mainly that of Murray[127] within our group, however as the synthesis of Nitron analogues with this route was a collaborative effort a summarised version of the work is provided below including independent observations by the present author. For a more detailed discussion, the reader is directed to the work of Murray.[127]

2.3.1 – The desulfurization of 1,3-diarylthiourea

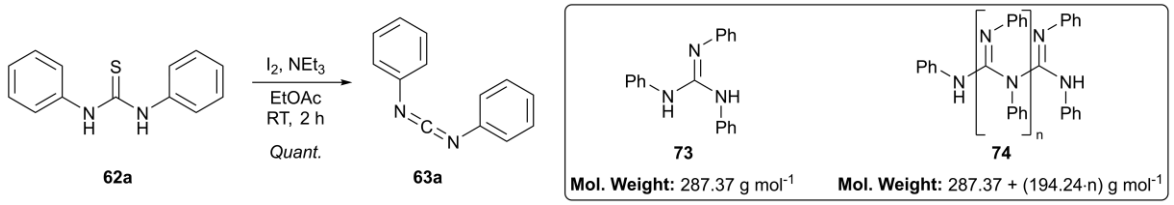
The synthesis of 1,2,4-triazolium salts from amidrazone precursors is common within the literature as discussed earlier. Typically this synthesis starts with activation of an amide by *O*-methylation or chlorination followed by reaction with a hydrazine to give the amidrazone.[155-157] The challenge

presented by Nitron is that the additional exocyclic anilino group requires use of urea or thiourea starting materials in place of the commonly used amides to access the C(3)-anilino functionalised amidrazone. Attempts by Murray to generate an equivalent activated carbonyl species using trimethyloxonium tetrafluoroborate or thionyl chloride were ineffective (**Scheme 33**), and so improvement of the carbodiimide formation by Kriven'ko and Morozova (**Scheme 27**) was deemed the most promising route to access anilinoamidrazones.[127]



Scheme 33 – The reaction of urea with thionyl chloride and trimethyloxonium tetrafluoroborate theoretically gives activated carbonyl derivatives with good leaving groups highlighted in pink – such reactions are typical of the synthesis of 1,2,4-triazolium salts from amides. In both cases the reaction failed to proceed, suggesting that the extra nitrogen of the urea (highlighted in blue) complicates the reactivity.

Using iodine and triethylamine, following the work of Patel *et al*,[158] the desulfurization of 1,3-diphenylthiourea (**62a**) to **63a** was found to occur with quantitative yield (**Scheme 34**). Residual iodine could be easily removed using an aqueous thiosulfate extraction, with limited urea formation if undertaken efficiently.[127] The resultant oil was found by liquid chromatography-mass spectrometry (LC-MS) to contain the aniline adduct **73** and related polymeric by-product **74** – carbodiimides with pendant aromatic groups have previously been reported to be susceptible to polymerisation.[159] The polymer was found to be insoluble in hexane, and so filtration through a celite plug enabled isolation of the desired carbodiimide in high yield.[127]

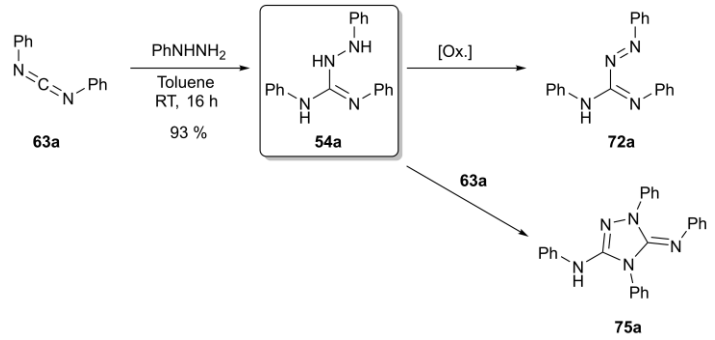


Scheme 34 – Desulfurization of thiourea **62a** to give carbodiimide **63a**. Unlike the traditional synthesis,[67] the heavy metal oxidant is replaced with iodine and the carbodiimide product can be isolated.

2.3.2 – The reaction of carbodiimide with arylhydrazines

The onward reaction of **63a** with arylhydrazines to give the desired anilinoamidrazones (**54a**) was not significantly changed from the work of Kriven'ko and Morozova (**Scheme 27**),[67] with the only change in reagents being the use of toluene instead of the benzene / isopropanol solvent mixture previously employed (**Scheme 35**).[127] The reaction conditions used were altered to account for the oxidative instability of anilinoamidrazones upon exposure to air;[113, 160] the reaction was carried out

under argon with the solvent stringently degassed. Although triazabutadiene **72a**, the product of oxidation, can undergo the ring closure, their significantly diminished reactivity (imine-like instead of amine-like) means a low yield of the desired 1,2,4-triazolium.[127] The slow addition of carbodiimide to the degassed hydrazine mixture is also important to prevent further reaction to the N^5-adduct **75a**[127] – this scaffold has been previously reported[113, 161, 162] in the late 1800s and early 1900s but has not reported in the literature since then.



Scheme 35 – The reaction of carbodiimide **63a** with phenylhydrazine gave the desired C(3)-anilino amidrazone intermediate **54a** in high yields with a straightforward isolation procedure. Care must be taken with the reaction setup to supress by-product formation that can drastically affect yield.

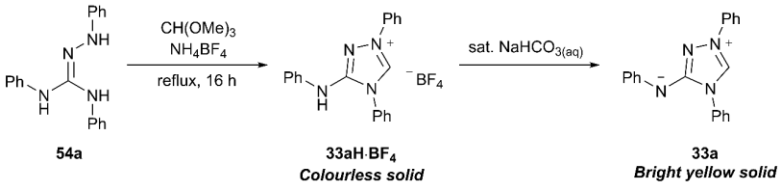
2.3.3 – The ring closure of C(3)-anilino amidrazones to 1,2,4-triazolium salts

Multiple methods exist to undertake the ring-closure of amidrazones to 1,2,4-triazolium heterocycles as presented in Section 2.2.[133, 163] Since the publication of Kriven'ko and Morozova's route to Nitron,[67] conditions for the high yielding one-step ring closure and oxidation to the corresponding triazolium have been published.[94, 122, 123] These conditions can replace the traditional two-step procedure *via* an isolable 1,2,4-triazole intermediate that requires harsh oxidants to give the desired product.[67]

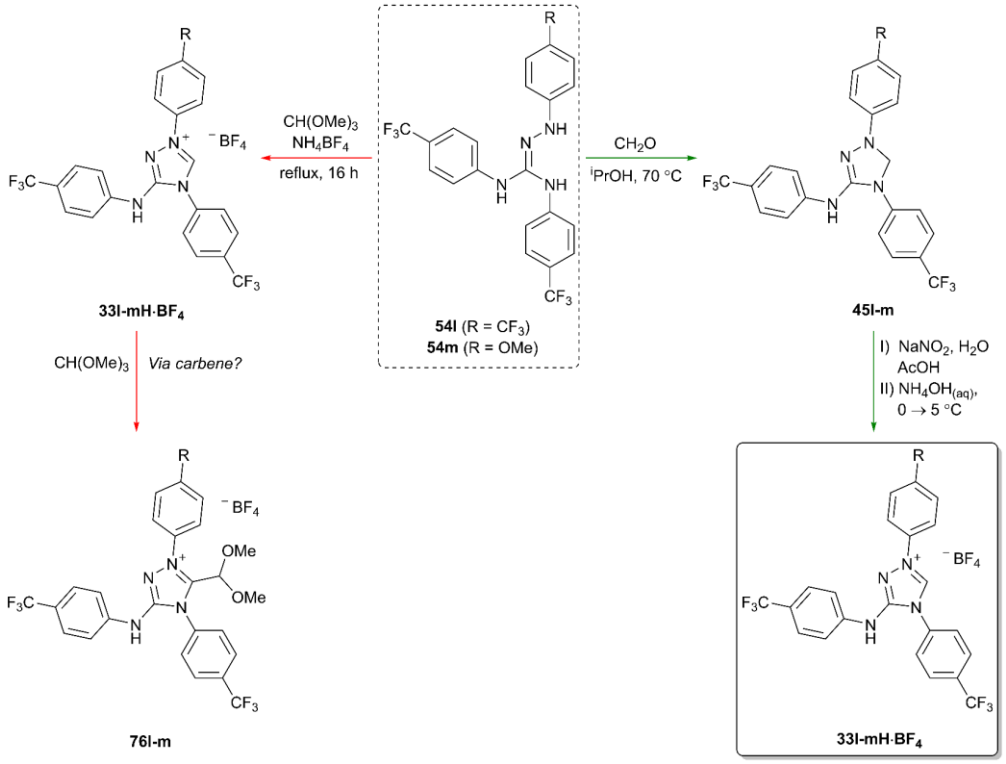
Initial work by Murray[127] showed that the use of trimethyl orthoformate in the presence of the weak acid ammonium tetrafluoroborate allows for the formation of the desired triazolium as a protonated tetrafluoroborate salt (**33aH·BF$_4$**) that precipitates upon cooling (**Scheme 36**). The zwitterionic form **33a** can be obtained using an aqueous bicarbonate wash – the immediate colour change of the colourless tetrafluoroborate salt solution to the characteristic bright yellow solution of the zwitterion is indicative of this process.[127]

Further investigations on Nitron analogues bearing electron-withdrawing groups on the three phenyl rings reveal further reaction can occur with trimethyl orthoformate (**Scheme 37**). Highly acidic Nitron analogues **33lH·BF$_4$** and **33mH·BF$_4$**, presumably *via* the triazolylidine species, can react to give the dimethoxymethyl substituted byproduct **76l** and **76m** which have not been previously reported for 1,2,4-triazolium salts. To avoid this issue, a modified version of the two-step procedure detailed in Kriven'ko and Morozova's route[67] was used in these cases. The acetic acid / isopropanol

mixture at 65 °C was swapped for use of acetic acid only at room temperature. Kriven'ko and Morozova's synthetic route has the downside of commonly leading to over-oxidation of the triazolium to a triazol-3-one species, and the occurrence of other side reactions, due to the harsh oxidation conditions used. The use of these modified conditions gave clean, quantitative conversion to **33lH·BF$_4$** and **33mH·BF$_4$**.[127]



Scheme 36 – The ring closure of anilinoamidrazone **54a** can be achieved using trimethyl orthoformate with ammonium tetrafluoroborate. The resulting colourless tetrafluoroborate salt **33aH·BF$_4$** can be converted to the bright yellow zwitterion **33a** by treating with concentrated bicarbonate solution.

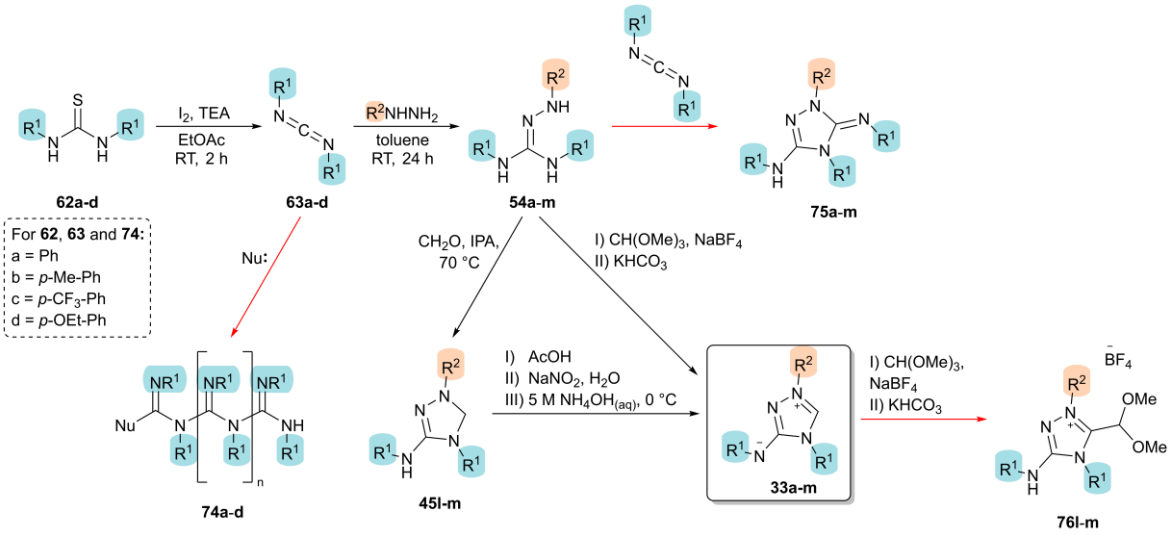


Scheme 37 – The ring closure of anilinoamidrazones bearing electron withdrawing groups with trimethyl orthoformate (red arrows) leads to acidic triazolium salts, which can undergo further reaction with trimethyl orthoformate to give the dimethoxymethyl byproduct. Using an adapted version of the ring closure method used in Kriven'ko and Morozova's Nitron synthesis (green arrows), the triazolium salts can be formed *via* the corresponding 1,2,4-triazole.

2.3.4 – Exploring the synthetic scope of the new synthetic strategy

Scheme 38 summarises the synthetic route developed by Murray[127] to gain access to Nitron in higher yield (65%, *versus* 43% reported by Kriven'ko and Morozova[67]), using reagents posing fewer hazards than the previously employed lead oxide and benzene, and reducing the pathway from four synthetic steps to three. Variation of the thiourea and arylhydrazine starting materials enabled the

generation of Nitron analogues, which are detailed in **Table 1** including the previous work of Murray.[127] In many cases, due to compound instability, the hydrazine used was commercially available as a hydrochloride salt and so the anilinoamidrazone-forming step used triethylamine to liberate the neutral hydrazine. The resultant ammonium salts were easily removed from the anilinoamidrazone intermediate with a bicarbonate wash in almost all cases. The Nitron analogues were also isolated as the protonated tetrafluoroborate salt in most cases (denoted **33a-mH·BF_4**).



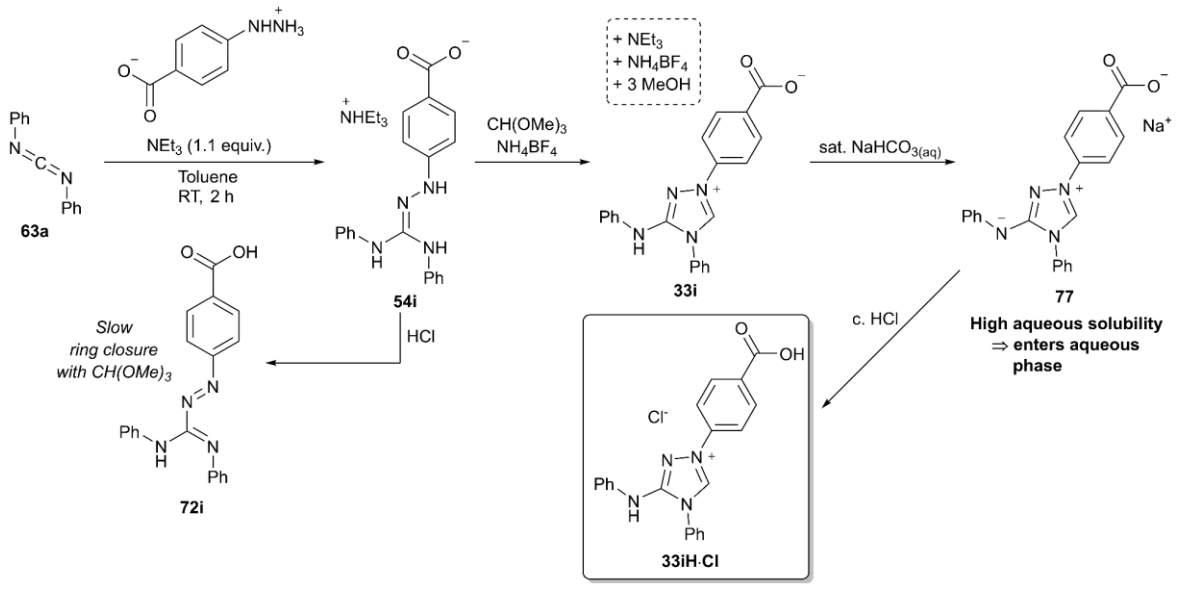
Scheme 38 – Summary of the complete synthetic pathway implemented to obtain Nitron analogues from thiourea, arylhydrazine and either trimethyl orthoformate or formaldehyde. The red arrows show the byproducts within the route, apart from the triazabutadiene **72a-m** for which ring closure to the desired triazolium may occur slowly.

Table 1 – Summary of the Nitron analogues synthesized using the updated route. The analogues synthesized by J. Murray[127] are also included as they are investigated within work detailed later in this thesis. Bn = benzyl.

Analogue	R^1	R^2	Yield – 54 (%) [a]	Yield – 33 (%) [b]
33a[c]	Ph	Ph	93	64
33b[c]	*p*-Me-C_6H_4	Ph	45	7
33c[c]	*p*-CF_3-C_6H_4	Ph	45	40
33d[c]	*p*-OEt-C_6H_4	Ph	41	34
33e[c]	Ph	*p*-F-C_6H_4	78	51
33f	Ph	*p*-Br-C_6H_4	90	24
33g	Ph	*p*-I-C_6H_4	- [d]	67
33h[c]	Ph	*p*-OMe-C_6H_4	54	31
33i	Ph	*p*-COOH-C_6H_4	98	50
33j[c]	Ph	*p*-CN-C_6H_4	38	21
33k	Ph	Bn	- [d]	12
33l[c]	*p*-CF_3-C_6H_4	*p*-CF_3-C_6H_4	- [d]	30
33m[c]	*p*-CF_3-C_6H_4	*p*-OMe-C_6H_4	- [d]	86

[a] Overall yield of first 2 steps. [b] Overall yield of full process. [c] Synthesized by J. Murray. [d] Carried forward to next step without purification

33i, one of the new analogues presented as part of this work with a *p*-COOH substituent, introduces an additional complexity to the isolation of the anilinoamidrazone (**Scheme 39**). The hydrazine in this case exists predominantly as a zwitterionic form and so also requires base deprotonation to react with carbodiimide, however treatment with acid to protonate the carboxylate group gives a highly unstable species that readily undergoes oxidation to the corresponding triazabutadiene **72i**. The anilinoamidrazone was therefore carried forward to the ring closure as an ammonium carboxylate salt, giving the triazolium **33i** in a mixture of amine and ammonium salts. The triazolium, upon removal of trimethyl orthoformate *in vacuo* and resuspension in dichloromethane, was extracted with bicarbonate as the highly charged zwitterionic carboxylate salt **77** and then precipitated by treatment with concentrated hydrochloric acid. This method was preferable over reverse-phase liquid chromatography (RP-LC) of crude **33i**, which was also successful in isolating the triazolium, due to the ability to easily undertake multigram synthesis in higher yields. In agreement with Murray's work,[127] it was found that isolation as the *N*-protonated salt gave enhanced yields and stability.



Scheme 39 – Overview of the isolation procedure for **33iH·Cl**.

The use of electron-donating aryl R^1 groups, as may be predicted, was found by Murray to slow formation of anilinoamidrazone and give rise to significant amounts of the corresponding N^5-adduct. Decreased oxidative stability of the anilinoamidrazone was also observed when R^1 is an electron-donating aryl ring, resulting from the increase in energy of the highest occupied molecular orbital (HOMO). The use of highly electron withdrawing substituents upon R^2 was also found to give greater yields of the N^5-adduct, as expected due to the slow reaction to give the C(3)-anilino amidrazone intermediate.[127] The new analogues presented in this work show variation upon R^2, and further support these conclusions when considering aryl groups for R^1 and R^2 – **54f** and **54g** (σ_p = 0.23 and 0.18, respectively, for the bromo and iodo substituents on R^2)[164] readily undergo N^5-adduct formation

whilst **54i** (σ_p = 0.00 for the carboxylate substituent on R^2)[164] showed only traces of the N^5-adduct by LC-MS under these conditions.

54k, being the only example to date where an alkyl carbon is directly attached to the triazolium salt core (R^2 = Bn), gives mostly N^5-adduct formation – analysis of the crude reaction mixture by LC-MS suggested small amounts of the C(3)-anilino amidrazone and triazabutadiene were present *in situ* in comparison to the N^5-adduct. The outcome is proposed to result from the loss of delocalisation of the non-bonding electrons upon the nitrogen bonded to R^2 (**Figure 14**) and the electron-donating nature of benzyl over phenyl (σ_I = −0.04 and 0.12, respectively).[164] **53k** is significantly more nucleophilic than the triaryl analogues and so reaction with carbodiimide outcompetes the reaction of benzylhydrazine with carbodiimide. Given that benzylhydrazine is commercially available as the dihydrochloride salt, and thus addition of base is necessary to facilitate the C(3)-anilino amidrazone formation, the use of excess equivalents of base may exacerbate the formation of undesired N^5-adduct – studies using 2.2, 2 and 1.5 equivalents of triethylamine do not show a significant change in the reaction outcome. Low yields of the corresponding 1,2,4-triazolium **33k** were generally obtained as a result of the high levels of N^5-adduct formation.

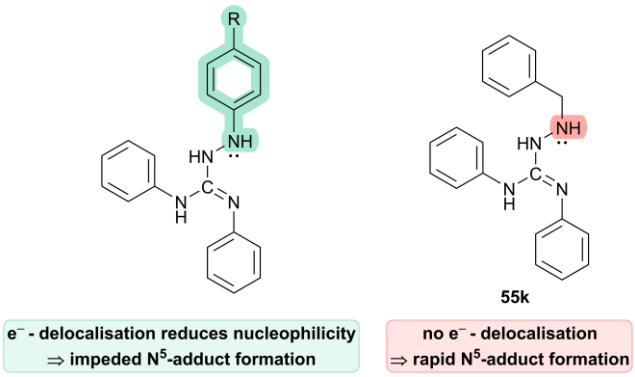


Figure 14 – The proposed role of delocalisation on anilinoamidrazone stability.

Characterisation of the Nitron analogues was possible by NMR spectroscopy and mass spectrometry in all cases. Where possible, X-ray diffraction (XRD) crystal structures were also obtained (**Figure 15**). Suitable crystals were formed by slow evaporation of methanol from the solution at room temperature of the protonated Nitron salt with tetrafluoroborate or chloride counterion. Detailed crystallographic information can be found in Appendix A. The N(1)-Ar and C(3)-NHPh groups are close to planarity, indicating a stabilising effect of these two aryl groups by conjugation. Conversely the N(4)-Ph group has a dihedral angle of 64.3 ± 0.4° and −49.8 ± 0.3° for **33fH·BF$_4$** and **33iH·BF$_4$**, respectively, in relation to the C^3-N^4 bond. This out-of-plane arrangement can be attributed to the steric clash with the C(3)-NHPh group. As can be expected, the N(1)-Ar bond is shorter than the N(4)-Ph for **33fH·BF$_4$** (1.434 ± 0.004 Å *versus* 1.449 ± 0.004 Å) and **33iH·BF$_4$** (1.427 ± 0.003 Å *versus* 1.441 ± 0.002 Å) due to the cationic N(1) nitrogen atom drawing greater electron density from

the aryl ring than the neutral N(4) nitrogen atom. A more detailed structural analysis will be undertaken in Section 2.3.6.

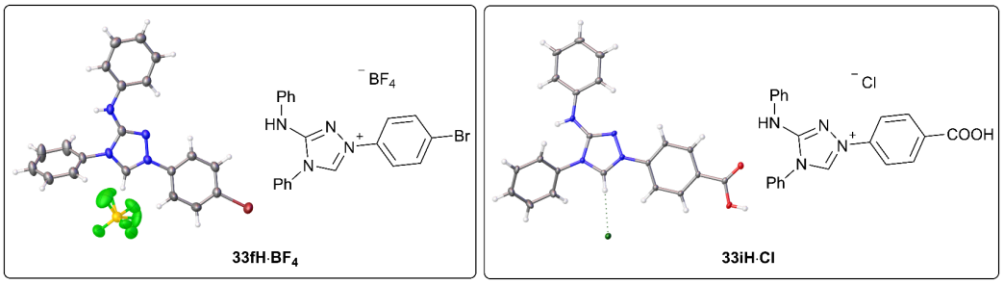
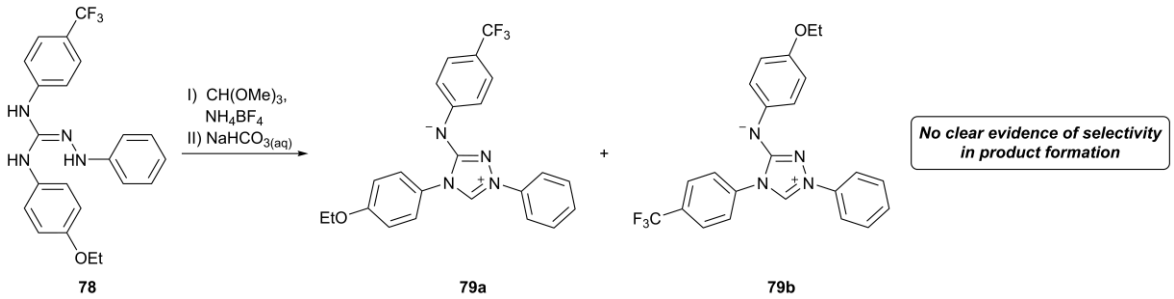


Figure 15 – Crystal structures of protonated Nitron analogues synthesized during this work, determined by single crystal XRD. Detailed crystallographic information can be found in Appendix A.

2.3.5 – Late-stage modification of the Nitron scaffold

The more contemporary synthetic route to Nitron discussed above enables variation of the substituents upon the thiourea and aryl hydrazine to give a diverse range of analogues, however the method becomes significantly more complicated with the use of unsymmetrical thioureas (**Scheme 40**). Murray[127] found that the ring closure of anilinoamidrazones derived from unsymmetrical thioureas (**78**) does not show a clear selectivity for the 1,2,4-triazolium formed. A complex mixture of **79a** and **79b**, alongside the two possible N^5-adducts, were formed and was not able to be separated to determine the absolute selectivity.

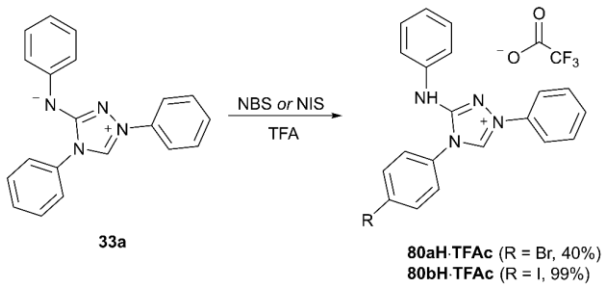


Scheme 40 – The ring closure of unsymmetrical C(3)-anilino amidrazone **78** was found by Murray[127] to give a complex mixture of **79a** and **79b**.

The development of a high yielding, selective transformation of Nitron post-cyclisation may enable the isolation of analogues that vary at either C(3)-NHAr or N(4)-Ar, alongside N(1)-Ar variation by use of different hydrazines in the earlier reported synthesis. Additionally, given that Nitron is a commercially available reagent, late-stage modification could enable straightforward generation of analogues in comparison to undertaking the synthetic route from thiourea.

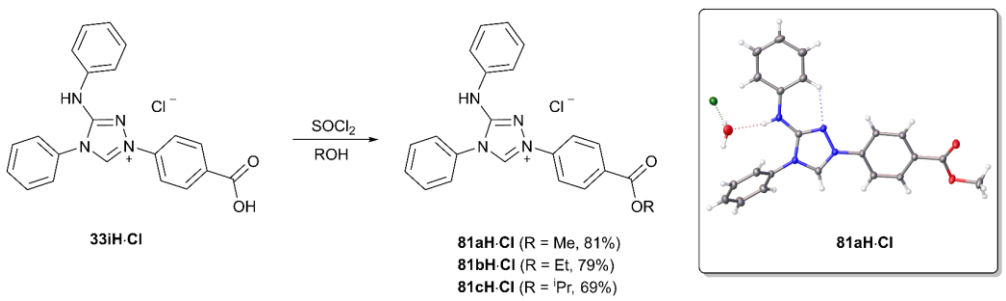
The electrophilic halogenation of Nitron, using the procedure of Brittain and Cobb,[165] gave good to excellent yields with generation of a single isomer (**Scheme 41**). Nitron was dissolved in trifluoroacetic acid (TFA) followed by the addition of either *N*-bromosuccinimide (NBS) or *N*-

iodosuccinimide (NIS). After stirring for 2 h both analogues were easily purified – **80aH·TFAc** by precipitation from ethanol upon the addition of water, and **80b-TFAc** by trituration of the crude product oil by diethyl ether. Analysis by ^{1}H NMR spectroscopy, including comparison to the data obtained for isomers **33f** and **33g**, supported halogenation of the *para*-position of either the C(3)-NHAr or N(4)-Ar ring. XRD analysis of **80aH·TFAc** or **80bH·TFAc** was unsuccessful, including after swapping the counteranion to chloride with HCl addition to the zwitterionic form or to tetrafluoroborate by stirring in a solution of ammonium tetrafluoroborate overnight. The location of the halogen substituent was indirectly determined by XRD analysis of a radical derivative, which will be discussed in Chapter 3.3. The halogen may be useful as an electrophilic handle for further reactions with nucleophiles or within metal-catalysed cross-coupling reactions.



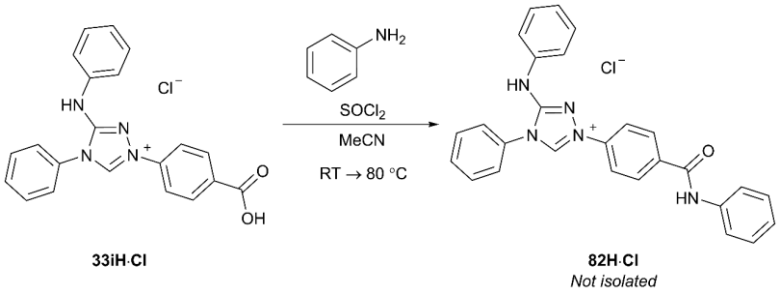
Scheme 41 – The electrophilic halogenation of Nitron.

The carboxyl-functionalised Nitron **33iH·Cl** may be a useful nucleophilic handle, and so reactions upon this position were explored to guide further studies in this area. This work was undertaken in collaboration with a 4th year MChem student, Katherine Deck, under my supervision. Using thionyl chloride, stirring within a series of alcohol solvents, the generation of the corresponding alkyl esters (**81a-cH·Cl**) was straightforward and high yielding (**Scheme 42**) – increased temperatures and reaction times were necessary moving from methanol to isopropanol. This reaction illustrates the potential to synthesize a range of Nitron analogues through generation of the corresponding acyl chloride and reaction with a range of nucleophiles. The XRD crystal structure of **81aH·Cl** was obtained in independent work by the present author – the previously discussed near-planarity of N(1)-Ar and C(3)-NHPh, out-of-plane N(4)-Ph, and shorter N(1)-Ar bond *versus* N(4)-Ar, was observed.



Scheme 42 – The reaction of Nitron analogue **33iH·Cl** with thionyl chloride in alcoholic solvents effectively generated a series of Nitron esters. XRD analysis of the methyl ester **81aH·Cl** was possible (see box) – see Appendix A for detailed crystallographic information.

Within independent work by the present author, exploration of amide **82H·Cl** preparation was also undertaken. The reaction of aniline with **33iH·Cl** in the presence of thionyl chloride (**Scheme 43**) showed partial conversion; with the addition of 4 equivalents of aniline LC-MS data indicated the presence of unreacted acyl chloride through generation of **81aH·Cl** with methanol used as the chromatographic eluent. The reaction was heated to 80 °C which seemingly led to a drastic increase in conversion based on LC-MS data, however the reaction was stopped due to the appearance of byproducts indicating ring-opening of the triazolium ring. Purification of the mixture by RP-LC was non-trivial and isolation of the *N*-phenyl amide **82H·Cl** was not possible.



Scheme 43 – The reaction of the acyl chloride form of **33iH·Cl**, generated *in situ*, with aniline leads to partial conversion to the corresponding amide **82H·Cl**. The isolation of **82H·Cl** was not possible by RP-LC.

The generation of amide bonds with **33iH·Cl** will be explored in Section 2.5.1 in the context of bioconjugation to peptide and peptidomimetic scaffolds. One of the compounds that will be discussed is the synthesis of the Nitron-alanyl-OMe hydrochloride salt **83H·Cl** for which XRD analysis has been possible (**Figure 16**). This data will be used in the *in crystallo* structural analysis of Nitron analogues in Section 2.3.6, with discussion of the synthesis provided in Section 2.5.1.

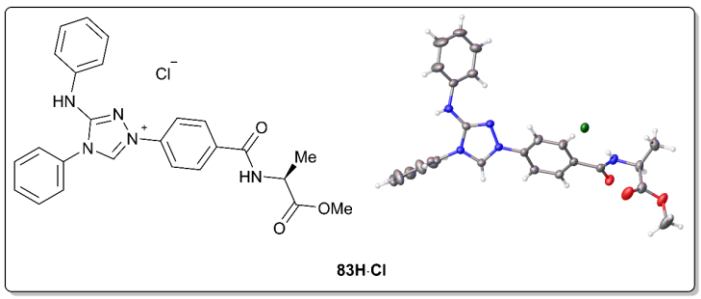


Figure 16 – Crystal structure of the Nitron-alanyl-OMe hydrochloride salt **83H·Cl**, obtained by single crystal XRD and highlighted due to the use of this data in the structural analysis of Section 2.3.6. See Appendix A for detailed crystallographic information.

2.3.6 – Structural analysis of the Nitron scaffold by *in crystallo* techniques

With 19 new Nitron analogues isolated within the project, including XRD characterisation in many cases, structural analysis can be undertaken to quantify the structural effects of substituents. This analysis will use the XRD data highlighted above, and also that obtained by Murray.[127] The definition of structural elements of Nitron will refer to the general structure given in **Figure 17** – data for the

meta- and *para*-carbons of each aryl ring are not considered. The positions C^7, C^{11} and C^{14} are defined as the *ortho*-position on the left hand side when looking down the N^1-C^6, N^9-C^{10} and N^4-C^{13} bonds respectively (in other words, the position that best agrees with **Figure 17** when looking at the Nitron scaffold in the shown orientation). Bond lengths, bond angles and dihedral angles are denoted L, A and D respectively.

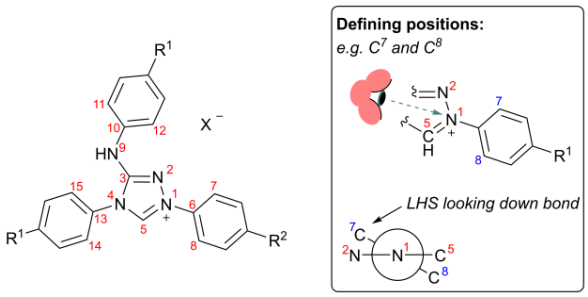


Figure 17 – The numbering of positions to be used in the structural analysis of protonated Nitron analogues, with a graphical representation of how positions about the three aryl rings are defined.

In this analysis, two general assumptions are made. The first is that the counterion does not significantly affect the structure of the triazolium salt in the crystal form, such that all triazolium salts can be compared irrespective of the location and structure of the counterion within the unit cell. The counterion will have a role in the packing of the triazolium in the crystal form, however given the size of the counterion relative to the Nitron analogue it is assumed that the impact will be small enough to still enable qualitative analysis of trends in the XRD data. The second is that the dihedral angles can be considered as deviation from planarity in either direction of the highly conjugated molecule, such that analysis can use the modulus of the dihedral angle; this assumption is deemed fair based on the modulus of the dihedral angles having similar values (or, in the cases of highly variable dihedral angles, showing similar levels of variation) across the library of Nitron analogues.

Selected data relating to Nitron analogues is provided in **Table 2**, with the full dataset provided in Appendix B-1. To link the XRD data to the structure of the Nitron analogue, σ_p values are used from literature[164] with the assumption that the CONH-Ala-OMe group of **83H·Cl** can be described with the σ_p value determined for the CONHMe group (+0.36). Structural analysis does not include **33m** as it is the only example where R^1 is altered, furthermore it is also the only zwitterionic triazolium in the dataset – comparisons in the data for **33m** and that generally obtained for protonated Nitron salts will instead be made.

Table 2 – Selected structural data of Nitron analogues obtained from single crystal XRD analysis.

Analogue	33aH·BF_4	33eH·BF_4	33fH·BF_4	33hH·BF_4	33iH·Cl	33jH·BF_4	81aH·Cl	83H·Cl	33m[a]
R^1 (σ_p) [b]	H (0)	H (0)	H (0)	H (0)	H (0)	H (0)	H (0)	H (0)	CF_3 (+0.54)
R^2 (σ_p) [b]	H (0)	F (+0.06)	Br (+0.23)	OMe (−0.27)	COOH (+0.45)	CN (+0.66)	COOMe (+0.45)	CONH-Ala-OMe (+0.36) [c]	OMe (−0.27)
L ($N^1 – C^6$) (Å)	1.433 (± 0.002)	1.432 (± 0.002)	1.434 (± 0.004)	1.433 (± 0.002)	1.427 (± 0.003)	1.431 (± 0.001)	1.426 (± 0.002)	1.430 (± 0.003)	1.430 (± 0.004)
L (N^4-C^{13}) (Å)	1.444 (± 0.002)	1.446 (± 0.002)	1.449 (± 0.004)	1.439 (± 0.002)	1.441 (± 0.002)	1.446 (± 0.002)	1.439 (± 0.002)	1.446 (± 0.003)	1.427 (± 0.003)
L (C^3-N^9) (Å)	1.347 (± 0.002)	1.355 (± 0.002)	1.342 (± 0.004)	1.347 (± 0.002)	1.345 (± 0.002)	1.343 (± 0.002)	1.348 (± 0.002)	1.359 (± 0.003)	1.313 (± 0.004)
A (N^1-C^5-N^4) (°)	107.6 (± 0.1)	107.2 (± 0.2)	107.5 (± 0.2)	107.3 (± 0.1)	107.3 (± 0.1)	107.1 (± 0.1)	106.7 (± 0.1)	106.8 (± 0.2)	108.8 (± 0.2)
D (C^5-N^1-C^6-C^8) (°)	−5.2 (± 0.2)	−8.9 (± 0.3)	−7.5 (± 0.4)	−5.2 (± 0.2)	+16.8 (± 0.3)	−4.8 (± 0.2)	+19.6 (± 0.2)	34.4 (± 0.3)	−3.7 (± 0.4)
D (C^5-N^4-C^{13}-C^{14}) (°)	−59.2 (± 0.2)	−72.9 (± 0.2)	+62.7 (± 0.4)	+55.9 (± 0.2)	−50.6 (± 0.3)	−74.4 (± 0.17)	−66.4 (± 0.19)	−77.8 (± 0.3)	+35.5 (± 0.4)
D (N^2-C^3-N^9-C^{10}) (°)	+2.1 (± 0.2)	−19.0 (± 0.3)	−2.2 (± 0.5)	0.0 (± 0.2)	−14.7 (± 0.4)	−2.0 (± 0.2)	−8.5 (± 0.2)	+18.3 (± 0.4)	−5.9 (± 0.5)

[a] Compound crystallised as zwitterion. [b] Values taken from literature.[164] [c] σ_p value corresponding to CONHMe used.

Comparison of L(N^1-C^6) *versus* L(N^4-C^{13}) shows the former is always shorter, with the variation in bond lengths increased as the substituent becomes more electron withdrawing and σ_p becomes more positive (**Figure 18A –** the propagation of errors to give the error bars shown is described in Chapter 8.8.1). The shorter N^1-C^6 bond is a result of greater electron density from the aryl ring being donated into the bond to the electron poor cationic N^1 nitrogen than aryl donation to the bond to N^4. Note that L(N^1-C^5) is consistently shorter than L(N^4-C^5), showing that the C-N double bond preferentially lies between N^1 and C^5 and thus that the cationic character is mostly upon N^1 – data shown in Appendix B-1. With more electron-withdrawing substituents upon N^1-Ar this electron donation is reduced and the bond length increases to a value closer to the N^4-Ar bond. Considering **33m**, introduction of an electron-withdrawing substituent upon N^4-Ar decreases the bond length *versus* **33hH·BF$_4$** such that L(N^4-C^{13}) is less than L(N^1-C^6). No clear trend is seen between L(C^3-N^9) and σ_p, however there is a significant drop in length considering the zwitterionic **33m** *versus* the protonated triazolium salts. Donation of the negative charge upon the anionic nitrogen of **33m** leads to an increase in bond order between C^3 and N^9, and in the full dataset shown in Appendix B-1 it can be seen that the bond length of N^2-C^3 is increased *versus* the protonated Nitron salts.

Bond angles about the carbenic position of the triazolium, described in this work as A(N^1-C^5-N^4), have recently been correlated with the acidity of a library of fused ring 1,2,4-triazolium salts typical to those used in NHC organocatalysis – a decrease in this angle aligns with increased acidity.[166] A small change is seen in the data for Nitron analogues, however there is a weak correlation in agreement with decreased angle as σ_p becomes more positive (or as more electron withdrawing groups are introduced to the Nitron scaffold (**Figure 18B**). The data appears to form two parallel lines of decreasing bond angle, suggesting a binary situation that leads to two outcomes in the crystallisation of Nitron analogues – the outcome does not appear to be linked to the counterion used, location of the counterion in the unit cell, space group or crystallisation solvent. The orientation of the adjacent N^1-Ar ring is proposed to account for this difference, with a plot of A(N^1-C^5-N^4)/D(N^5-N^1-C^6-C^8) against σ_p (**Figure 18C –** propagation of error described in Chapter 8.8.1) showing a significantly improved fit with the removal of an anomalous dataset corresponding to **33jH·BF$_4$.** With the increase in dihedral angle of the N^1-Ar ring, upon which the varying substituent is located, there is a switch from the substituent being able to exhibit inductive and resonance effects to just the inductive effects due to decreased π(Ar)-π^*(N^1-C^5) orbital overlap. By division of the substituent effect (σ_p) by the dihedral angle, which can be considered to inversely correlate with the effectiveness of the substituent on changing the properties of the triazolium ring, an 'effective substituent effect' can be obtained. **33jH·BF$_4$** has the smallest value for D(N^5-N^1-C^6-C^8) in the library, which will be explored further below, and due to this the datapoint is far above the regression line for the linear fit. A decrease in bond angle is seen upon addition of CF_3 groups to R^2 (**33m** *versus* **33hH·BF$_4$**) to give a more acidic triazolium salt – this is consistent with the literature.

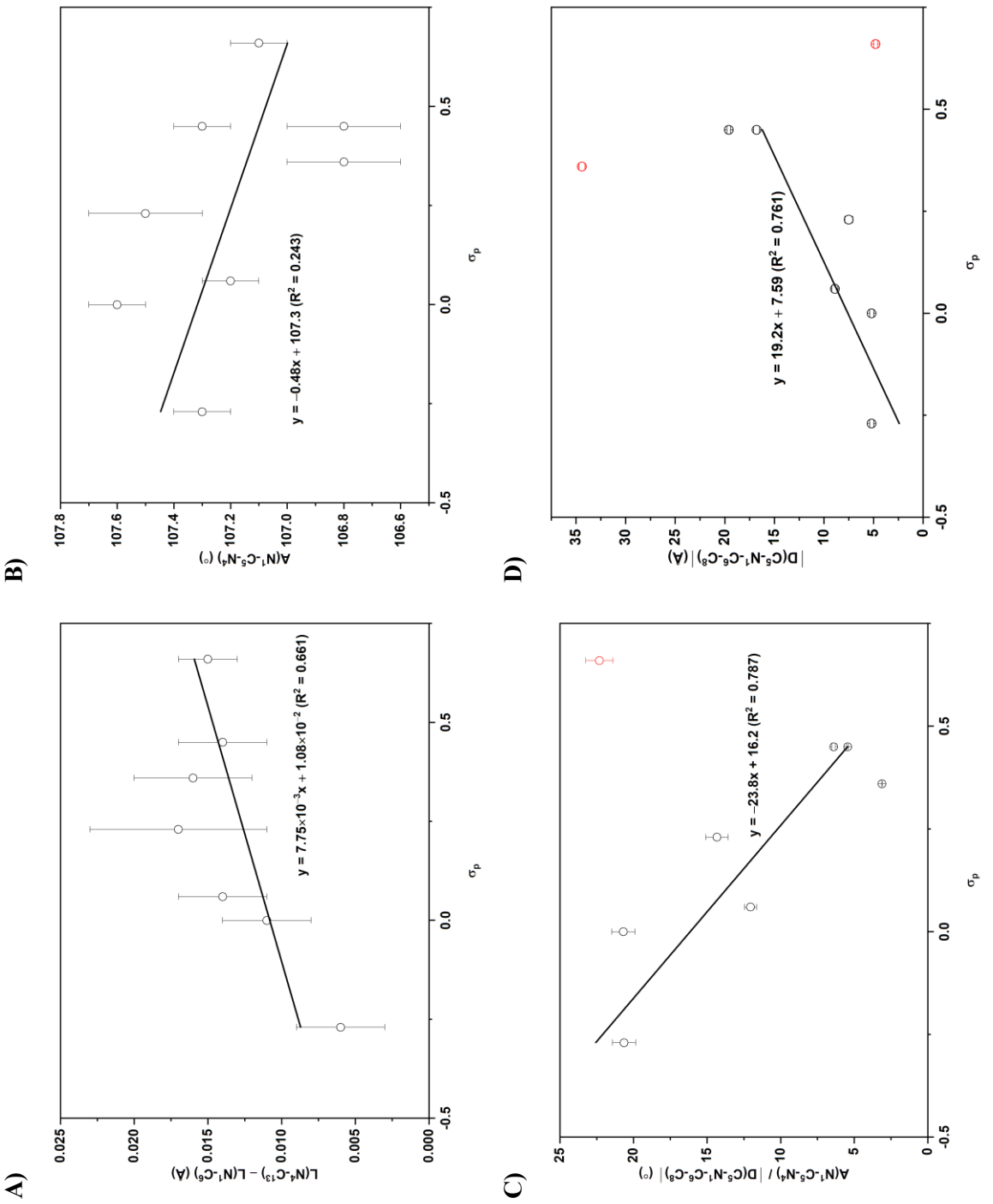


Figure 18 – Graphs comparing structural parameters determined by single crystal XRD to σ_p values obtained from literature. **A** – L(N^4-C^{13}) – L(N^1-C^6). **B** – A(N^1-C^5-N^4). **C** – A(N^1-C^5-N^4) / D(C^5-N^1-C^6-C^8). **D** – D(C^5-N^1-C^6-C^8). Data omitted from fits is shown in red.

Generally, the aryl rings bonded to N^1 and the exocyclic nitrogen on C^3 are close to planarity with the triazolium ring indicating effective conjugation can occur across the molecule. Whilst no clear trend is seen between σ_p and the planarity of the C^3-NHPh, investigated through analysis of D(N^2-C^3-N^9-C^{10}) and D(C^3-N^9-C^{10}-C^{12}), there is thought to be a linear relationship between the N^1-Ar dihedral angle and σ_p (**Figure 18D**). Where the aryl ring is significantly electron rich, a high level of electron donation into the π^*(N^1-C^5) orbital occurs and bond order is greater than 1 between N^1 and

C^6. Increasing values of σ_p result in increasing electron withdrawal from the aryl ring and thus less electron donation to the triazolium ring – bond order decreases and freedom to rotate around the N^1-C^6 bond increases leading to larger dihedral angles to relieve steric strain. Two datapoints (**83H·Cl** and **33jH·BF$_4$**) are omitted from the fit as there are additional considerations with these compounds – they are not deemed anomalous. **83H·Cl** has by far the most complicated substituent, and with this comes interactions with the group that can lead to significant distortions. A key interaction between the NH group of the amide bond in the substituent and chloride is observed, with interactions also seen with the exocyclic NH of the Nitron scaffold and the C^5-H position (**Figure 19**). For **33jH·BF$_4$** the electron withdrawal of the cyano group and additional withdrawal by the triazolium ring gives a very electron poor aryl ring. The cyano group is small, and triazolium planar, meaning that effective stacking can take place to give brick layer stacking between the N^1-Ar and C^3-NHAr rings (**Figure 20**). The N^4-Ar ring has a much greater dihedral angle and is highly variable, so no trend can be found with σ_p. The zwitterion **33m** has the smallest values for D(C^5-N^1-C^6-C^8) and D(C^5-C^4-C^{13}-C^{14}), and the C^3-NHPh group is also close to coplanar suggesting a significantly more conjugated structure than the protonated triazolium salts – this conjugation is seen through the bright yellow colour of the zwitterion. This planarity is thought to arise from the lack of proton on the C^3-N position, which not only slightly reduces the steric strain experienced by the N^4-Ph group but also increases the electron density of the triazolium ring leading to more favourable orbital interactions to delocalise this enhanced electron density.

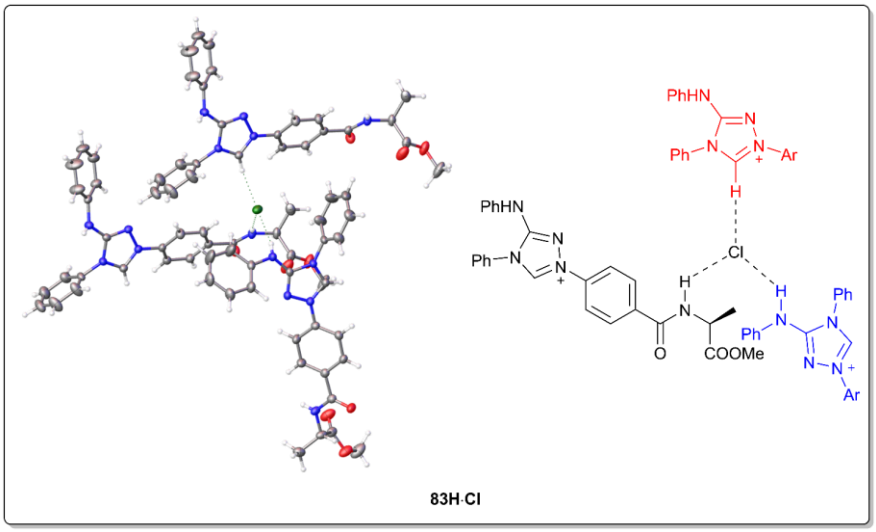


Figure 19 – A key interaction between the chloride counterion of **83H·Cl**, the NH of the R^2 substituent amido group, the exocyclic NH of the Nitron core scaffold, and the C(5)-H position has been identified that can explain the significant difference in D(C^5-N^1-C^6-C^8) for this compound.

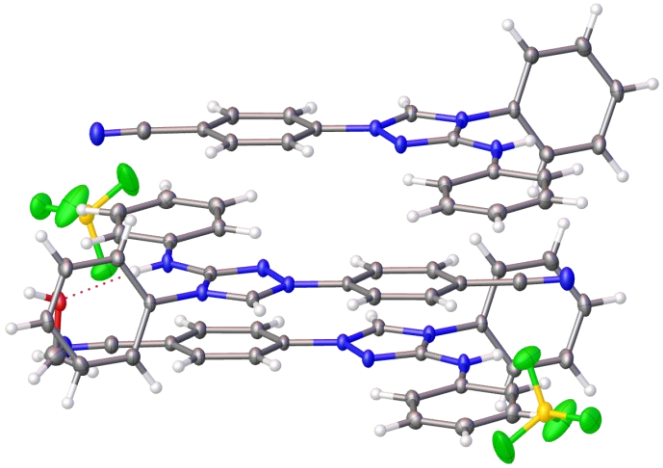


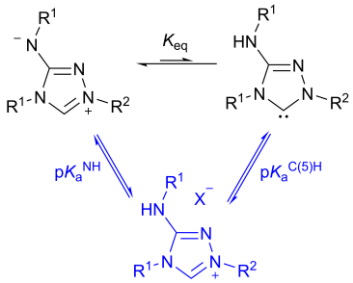
Figure 20 – Due to the highly electron poor N(1)-Ar group and little steric bulk surrounding the ring, brick layer stacking is observed between the N(1)-Ar and C(3)-NHAr ring of **33jH·BF$_4$** leading to a highly planar structure across this region of the molecule.

2.3.7 – Exploring the tautomerization of Nitron analogues

The ability of Nitron to convert to a NHC *in situ* is key to many of the known applications. This section will discuss how structural changes relate to the levels of carbenic tautomer present *in situ* through computational analysis of the two tautomers.

Density functional theory (DFT) calculations were performed upon the zwitterionic Nitron analogue and the corresponding carbenic tautomer using B3LYP and M06-2X functionals. B3LYP acts as a general functional for which many organic compounds are analysed within literature, and enables future comparison of structural elements to these literature values. M06-2X can be seen as an improvement over the B3LYP system for describing the Nitron tautomers, as it has been shown to better describe non-covalent interactions (such as the ionic interactions of the zwitterionic structure and hydrogen bonding) and main group thermochemistry.[167, 168] The 6-31+G(d,p) basis set was generally used, however the LANL2DZ basis set is necessary for calculations relating to the iodinated Nitron **33g** given that 6-31+G(d,p) does not accurately describe atoms of atomic number greater than 18. LANL2DZ is an effective core potential (ECP) model, explicitly treating only valence electrons within calculations, which describes up to a 60-electron system per atom and can be used to describe atoms up to atomic number 83 (apart from helium). Reliable results can be obtained for relative energies but should not be used where the core electrons are important to the properties of the molecule.[169, 170] A polarised continuum model (PCM) of acetonitrile or water are used to describe solvation. The methodologies used are summarised in **Table 3**, with full details of the calculations provided in Appendix B-2. The Gibbs free energy change related to tautomerisation (ΔG_{taut}) is calculated for each Nitron tautomer using **M1** and **M3-5** (apart from **33g** for which the ECP model **M2** is necessary). From this energy change an equilibrium constant (K_{eq}) can be obtained for the tautomerisation and used to determine the fraction of carbene molecules.

Table 3 – Details of the DFT methods used in this work.

Method code	Functional	Basis set	Solvation model	Description of K_{eq}
M1	B3LYP	6-31+G(d,p)	PCM(MeCN)	
M2	B3LYP	LANL2DZ	PCM(MeCN)	
M3	B3LYP	6-31+G(d,p)	PCM(H_2O)	
M4	M06-2X	6-31+G(d,p)	PCM(MeCN)	
M5	M06-2X	6-31+G(d,p)	PCM(H_2O)	

To calculate the fraction of carbene ($F_{carbene}$) present *in situ* from values of K_{eq}, **Equation 1** is generally used. Derivation of **Equation 1** is provided in Appendix B-3, by considering the relative concentrations of the zwitterionic and carbenic forms of the Nitron analogues. The acid-functionalised Nitron **33i**, in the overall neutral form, has three tautomers (**Figure 21**) and so a more complicated method considering the two tautomerisation processes (or, more accurately, the thermodynamic cycle of tautomers) is necessary to describe $F_{carbene}$ than **Equation 1**. Details relating to the necessary calculations for **33i** are given in Appendix B-3.

$$F_{Carbene} = \frac{K_{eq}}{1 + K_{eq}} \qquad \textbf{Equation 1}$$

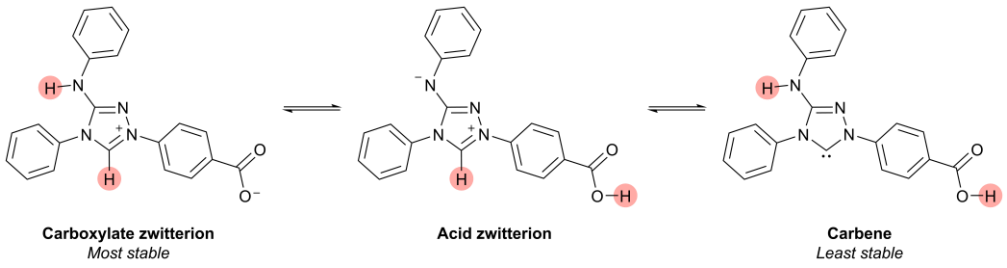


Figure 21 – **33i** has three tautomers in the neutral form. The most stable by DFT is the carboxylate zwitterion. Proton transfer from the exocyclic nitrogen to the carboxylate group gives the acid zwitterion, with a structure similar to that of other zwitterionic Nitron analogues. Finally, the least stable tautomer is the carbenic form resulting from proton transfer of the C(5)-H to the exocyclic nitrogen.

Table 4 provides the results for all methods undertaken during this work, however the trends discussed are seen regardless of the method used. Using the same functional and basis set, variation due to solvation is comparatively small – the larger effect arises from the change in functional. Comparing **33a** to **33d**, where variation is upon R^1 (the aryl rings derived from the thiourea), the move from electron-donating to electron-withdrawing substituent leads to a more negative

$\log[F_{carbene}]$ and a decrease in the percentage of carbene. It could be proposed that the opposite trend would be seen with electron withdrawing substituents decreasing $pK_a^{C(5)H}$, however the data suggests that stabilisation / destabilisation of the anionic charge plays a more significant role in the concentrations of carbenic tautomer (**Figure 22A**). With electron-withdrawing substituents the charge upon the exocyclic nitrogen is stabilised, leading to a decrease in pK_a^{NH}. $pK_a^{C(5)H}$ will also decrease, but from the data it can be suggested that this is a lesser effect and overall the difference in pK_a^{NH} and $pK_a^{C(5)H}$ increases with more-electron withdrawing substituents. The tautomerisation to the carbene therefore becomes less favourable, and $F_{carbene}$ decreases (decrease in $\log[F_{Carbene}]$). The opposite is the case with electron-donating substituents, with destabilisation of the exocyclic nitrogen increasing pK_a^{NH} and decreasing the difference *versus* $pK_a^{C(5)H}$ such that tautomerisation to the carbene becomes more favourable.

Considering variation at R^2, the expected trend in the data is seen with electron withdrawing substituents lowering the pK_a at C(5) and leading to higher levels of carbene. Conversely electron-donating substituents can stabilise the cationic charge of the triazolium ring and disfavour generation of the corresponding triazolylidine species (**Figure 22B**).

Looking at the data obtained using **M4**, as an example, the variation in $\log[F_{carbene}]$ seen by variation of R^1 is ± 2.438 (~280 fold difference in $F_{carbene}$) whilst by variation at R^2 the value is ± 1.771 (~60 fold difference in $F_{carbene}$). Additionally, the variation in σ_p for R_1 is ± 0.78 (−0.24 for OEt group, +0.54 for CF_3)[164] whilst for R_2 is ± 0.93 (−0.27 for OMe group, +0.66 for CN).[164] With a smaller variation in the substituent effect, the difference in fraction of carbene is over 4 times greater for R_1 than R_2 – it can be calculated that the difference in substituent effect is 5.54 times greater for R_1 than R_2 by accounting for the range of σ_p investigated. This is proposed to be a result of the exocyclic nitrogen stabilisation and destabilisation, suggesting a key role of the exocyclic nitrogen basicity in the tautomerisation to carbene.

Experimental work by Murray is in agreement with these computational findings (**Table 5**). The pK_a of the exocyclic nitrogen was determined by Murray using spectrophotometric titration, whilst the pK_a of the C(5)-H position could be obtained by single point H/D-exchange analysis at p*D* 1.09 within 10% v/v MeCN. Through determination of the pK_a at the exocyclic nitrogen and quantitative estimation of the C(5)-H pK_a values, values of pK_T (where K_T is the tautomerisation equilibrium constant, analogous to K_{eq} used in this work) could be obtained. Values of pK_T can be converted to $F_{carbene}$, and show the same trend upon alteration at the R^1 positions within experimental data as is seen in this work computationally.[127]

Table 4 – Summary of the data obtained by DFT analysis of the tautomers of Nitron analogues.

Analogue	K_{eq}					$\log[F_{carbene}]$				
	M1	M2	M3	M4	M5	M1	M2	M3	M4	M5
33a	1.82×10^{-5}	1.95×10^{-4}	1.52×10^{-5}	2.00×10^{-3}	1.67×10^{-3}	−4.74	−3.71	−4.82	−2.70	−2.78
33b	6.35×10^{-4}	- [a]	4.05×10^{-4}	1.67×10^{-2}	1.05×10^{-2}	−3.20	- [a]	−3.39	−1.79	−1.98
33c	2.63×10^{-7}	- [a]	1.87×10^{-7}	5.99×10^{-5}	3.78×10^{-5}	−6.58	- [a]	−6.73	−4.22	−4.42
33d	1.35×10^{-4}	- [a]	7.78×10^{-5}	9.62×10^{-3}	8.17×10^{-3}	−3.87	- [a]	−4.11	−2.02	−2.09
33e	2.96×10^{-5}	- [a]	3.08×10^{-5}	9.77×10^{-3}	7.09×10^{-3}	−4.53	- [a]	−4.51	−2.01	−2.15
33f	4.79×10^{-5}	3.57×10^{-4}	3.72×10^{-5}	9.42×10^{-3}	6.88×10^{-3}	−4.32	−3.45	−4.43	−2.03	−2.17
33g	- [a]	3.30×10^{-4}	- [a]	- [a]	- [a]	- [a]	-3.48	- [a]	- [a]	- [a]
33h	7.15×10^{-6}	- [a]	5.75×10^{-6}	1.43×10^{-3}	1.04×10^{-3}	−5.15	- [a]	−5.24	−2.85	−2.98
33i	1.48×10^{-6} [b]	- [a]	2.89×10^{-7} [b]	1.09×10^{-3} [b]	2.41×10^{-4} [b]	−5.83	- [a]	−6.54	−3.01	−3.64
33j	8.53×10^{-4}	- [a]	5.87×10^{-4}	6.08×10^{-2}	3.98×10^{-2}	−3.07	- [a]	−3.23	−1.24	−1.42
33k	9.35×10^{-6}	- [a]	6.53×10^{-6}	4.44×10^{-4}	1.17×10^{-4}	−5.03	- [a]	−5.19	−3.35	−3.93
33l	7.45×10^{-6}	- [a]	4.99×10^{-6}	1.24×10^{-3}	6.39×10^{-4}	−5.13	- [a]	−5.30	−2.91	−3.20
33m	4.11×10^{-8}	- [a]	2.78×10^{-8}	1.83×10^{-5}	1.53×10^{-5}	−7.39	- [a]	−7.56	−4.74	−4.81

[a] Method not used for this compound. [b] Values for the equilibrium between the carboxylate zwitterion and carbenic form.

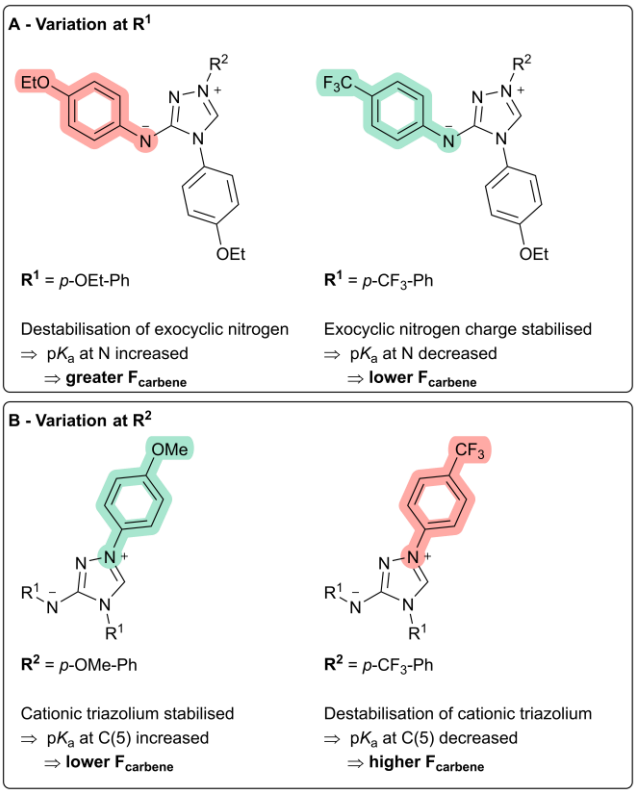


Figure 22 – The impact of substituents upon the fraction of carbene tautomer of Nitron present. **A** - Carbene levels are enhanced by the use of electron donating substituents at R^1 as there is an increase in the pK_a difference between the exocyclic nitrogen and C(5)-H. **B** – use of electron withdrawing substituents at R^2 destabilises the triazolium and decreases C(5)-H pK_a to lead to a higher fraction of carbene.

Table 5 – Experimental values of log $F_{carbene}$ determined by Murray.[127]

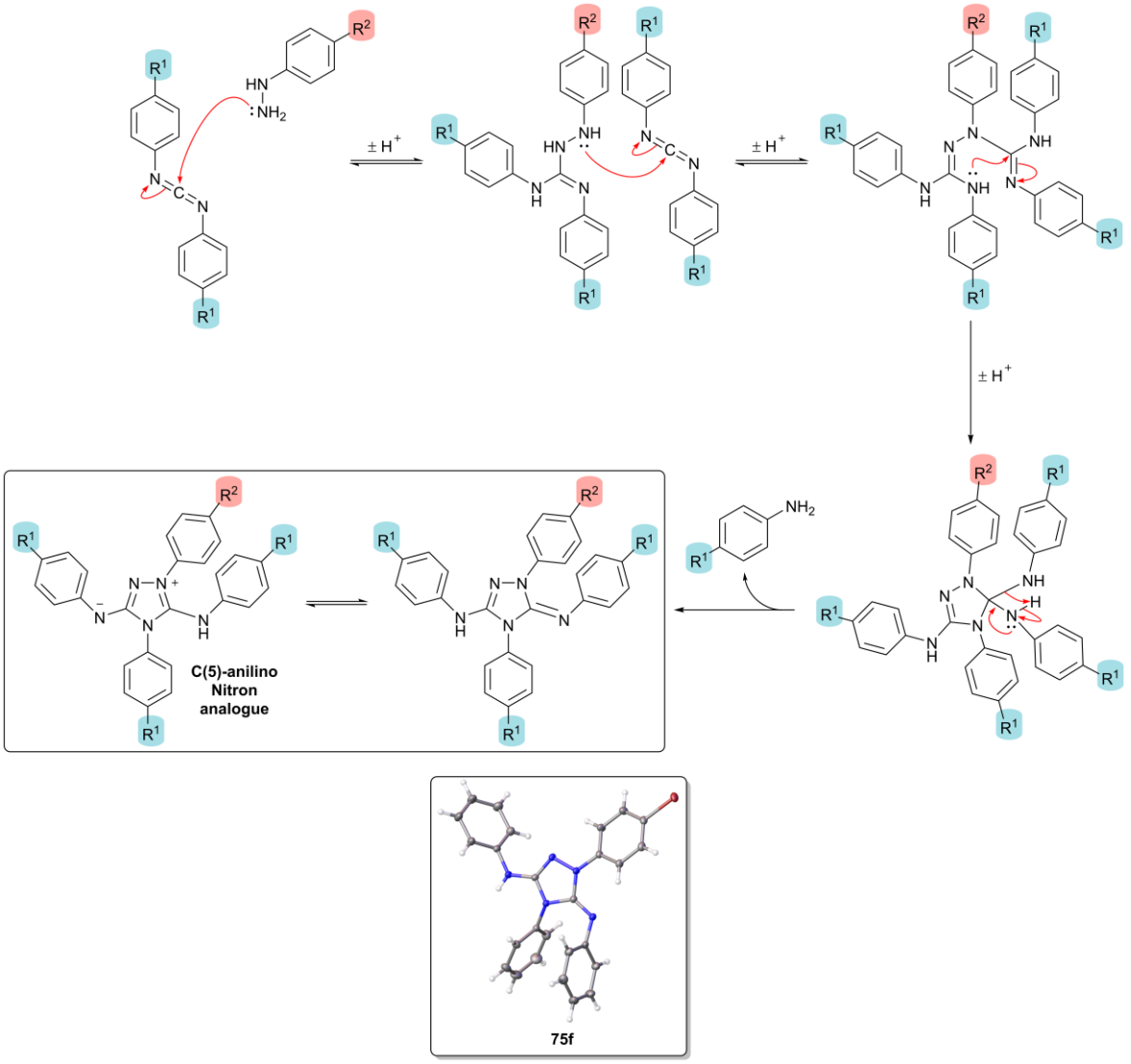
Analogue	R^1	R^2	p$K_a^{C(3)-NH}$	p$K_a^{C(5)-H}$ (30% v/v MeCN)	pK_T	log $[F_{carbene}]_{exp}$ [b]	log $[F_{carbene}]_{comp}$
33a	Ph	Ph	9.78 (± 0.04)	17.8	7.9	−7.9	−4.74 → −2.70
33c	*p*-CF_3-C_6H_4	Ph	8.85 (± 0.03)	17.1	8.3	−8.3	−6.73 → −4.22
33d	*p*-OEt-C_6H_4	Ph	10.4 (± 0.02)	18.1	7.7	− 7.7	−4.11 → −2.02

[a] Value not determined. [b] Fraction of carbene determined from values of pK_T obtained in the work of Murray.[127] [c] Range of values computationally determined for the fraction of carbene in this work.

2.3.8 – Synthesis of N^5-adducts

As mentioned in Section 2.3.2, the addition of carbodiimide too quickly to the solution of hydrazine can lead to the formation of a nitrogen-rich scaffold referred to as an N^5-adduct. The mechanism for formation of this by-product is the addition of a second carbodiimide molecule to anilinoamidrazone and then cyclisation through loss of aniline (**Scheme 44**). The yield of this species under the conditions used in our synthetic strategy to Nitron depend on the nature of R^1 and R^2 – electron-

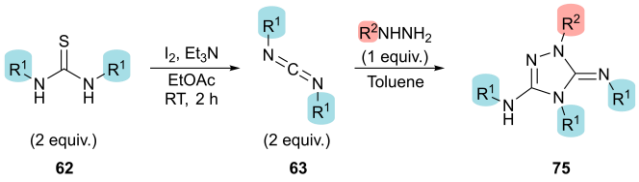
donating R^1 slows the formation of anilinoamidrazone such that N^5-adduct formation competes with anilinoamidrazone formation. Electron-withdrawing R^2 additionally slows the formation of anilinoamidrazone leading to competition for reaction with carbodiimide. Tautomerisation of the adduct reveals that the species can be considered a C(5)-anilino Nitron analogue, however with the carbenic position blocked most of the applications related to Nitron do not relate to these adducts.



Scheme 44 – Proposed mechanism for the formation of the N^5-adduct from the anilinoamidrazone intermediate of the Nitron analogue synthesis. The structure of the N^5-adduct **75f** obtained by X-ray diffraction, where R^1 = H and R^2 = Br, is also shown.

Through increasing the molar equivalents of carbodiimide, the synthetic strategy implemented to obtain anilinoamidrazones can be adapted to allow the reaction to proceed and give N^5-adducts in higher yields (**Scheme 45**). Variation of R^2, through alteration of the arylhydrazine used, was explored as part of this work; the analogues attempted to be prepared by this adapted route are detailed in **Table 6** alongside data collected by Murray.[127] Note that, due to the more electron withdrawing R^2 group, **75i** was not investigated in this adapted route. **75i** was observed by LC-MS

in the synthesis of **33iH·Cl** but only in trace amounts that could not be isolated, and it is thought that the yields of **75i** obtained in this adapted route may be lower than those obtained for **75f**.



Scheme 45 – By addition of excess carbodiimide, N^5 adducts can be generated in higher yields than that obtained from the synthetic route used to obtain Nitron analogues detailed in **Scheme 38**.

Table 6 – Summary of the yields obtained in the synthesis of N^5-adducts, shown in **Scheme 45**.

Analogue	R^1	R^2	Yield (%)[a]
75a [b]	Ph	Ph	57
75b [b]	*p*-Me-C_6H_4	Ph	34
75c [b]	*p*-CF_3-C_6H_4	Ph	63
75d [b]	*p*-OEt-C_6H_4	Ph	66
75e [b]	Ph	*p*-F-C_6H_4	41
75f [c]	Ph	*p*-Br-C_6H_4	5
75j [b]	Ph	*p*-CN-C_6H_4	37
75k [c]	Ph	Bn	- [d]

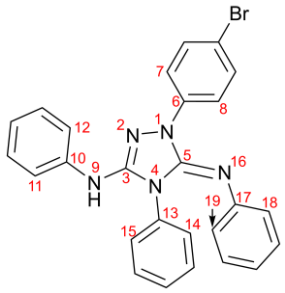
[a] Overall yield of full process. [b] Synthesized by J. Murray.[127] [c] This work. [d] Product not isolated, see discussion below for more details.

Purification of **75f** was possible by recrystallisation from isopropanol. For the benzyl analogue of the N^5-adduct, **75k**, product formation was observed by LC-MS with the loss of positive electrospray ionisation (ES+) peaks for the C(3)-anilino amidrazone intermediate indicating completion after 22 h. However, upon recrystallisation from IPA, LC-MS showed a complex mixture containing a variety of species believed to arise from the debenzylation of the adduct. Given that little evidence is available on these degradation species their structures have not included in this work, however LC-MS would indicate that the benzyl group can be lost through reaction with nucleophiles.

Only one crystal structure of an N^5-adduct, corresponding to **75f**, has been obtained as part of this work (see **Scheme 44**) with a further N^5-adduct analysed by XRD as part of the work by Murray (**75b**).[127] For this reason detailed structural analysis is not appropriate in this case, however some general comments can be made based on the structural data shown in **Table 7**. The data is compared to the triazolium salt **33fH·BF_4** with closely related structure. Bond lengths, bond angles and dihedral angles are denoted L, A and D respectively. The N^5-adduct has a distorted triazole core with shorter N^2-C^3 bond (resulting from less electron donation from N^9 into the neutral N^5-adduct ring *versus* the triazolium ring) and smaller N^1-C^5-N^4 internal angle (resulting from the C^5 position being pulled outwards to reduce the steric clash of the C^3-NAr group). Shorter N^1-Ar and N^4-Ph bonds are

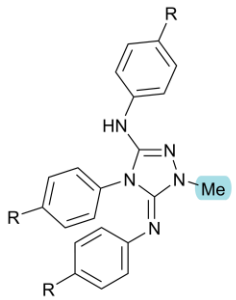
observed due to the ability of the neutral triazole ring to donate greater electron density to these bonds, however this is not through resonance given that the corresponding dihedral angles show both aromatic rings are out of plane due to the N^5 substituent. The C^3-NHAr group remains coplanar, shown in the value of $D(N^2\text{-}C^3\text{-}N^9\text{-}C^{10})$.

Table 7 – Structural analysis of the N^5-adduct **75f** and comparison to the values observed for the closely related triazolium salt **33fH·BF$_4$**.

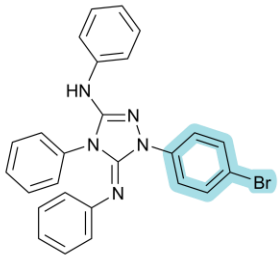


Structural element	Value	
	75f	**33fH·BF$_4$**
$L(N^1\text{-}C^6)$	1.405 ± 0.002 Å	1.434 ± 0.004 Å
$L(N^2\text{-}C^3)$	1.298 ± 0.002 Å	1.321 ± 0.004 Å
$L(C^3\text{-}N^9)$	1.352 ± 0.001 Å	1.342 ± 0.004 Å
$L(N^4\text{-}C^{13})$	1.436 ± 0.001 Å	1.449 ± 0.004 Å
$L(N^5\text{-}C^{16})$	1.293 ± 0.001 Å	-
$A(N^1\text{-}C^5\text{-}N^4)$	103.8 ± 0.1°	107.5 ± 0.2°
$D(C^5\text{-}N^1\text{-}C^6\text{-}C^8)$	−26.6 ± 0.2°	−7.5 ± 0.4°
$D(C^5\text{-}N^4\text{-}C^{13}\text{-}C^{14})$	−66.1 ± 0.1°	+62.7 ± 0.4°
$D(N^2\text{-}C^3\text{-}N^9\text{-}C^{10})$	+7.4 ± 0.2°	−2.2 ± 0.5°
$D(N^4\text{-}C^5\text{-}N^{16}C^{17})$	−17.8 ± 0.2°	-

This scaffold has been scarcely discussed within the literature and to our knowledge has not found a useful application. Some synthetic work has been undertaken by Sunderdiek and Zinner[171] on a related scaffold with an N(1)-Me group (**84**). It is hoped that these nitrogen-rich scaffolds are explored further and find application in the near future.



84
(R = H, Me)



75f

2.4 – Sulfur-substituted 1,2,4-triazolium salts from 1,2,4-triazoles

This chapter section explores the synthesis of 1,2,4-triazolium salts structurally related to Nitron, however bearing sulfur substituents, which are referred to as *S*-triazolium salts (**Figure 23**). There is little literature precedent for the *S*-triazolium scaffold and so is an interesting area for synthetic exploration and studies regarding their potential applications. The preparation of a library of 1,2,4-triazole precursors is discussed followed by the discovery of methods to allow for their conversion to triazolium salts. All species are fully characterised, including crystal structures to enable structural analysis. Computational analysis also aids understanding of the selectivity observed within 1,2,4-triazolium formation.

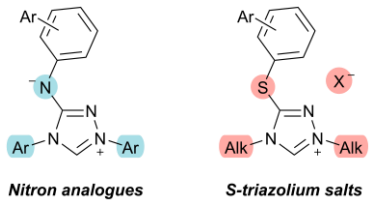


Figure 23 – Structural comparison of Nitron analogues with *S*-triazolium salts. Variation between the scaffolds is highlighted.

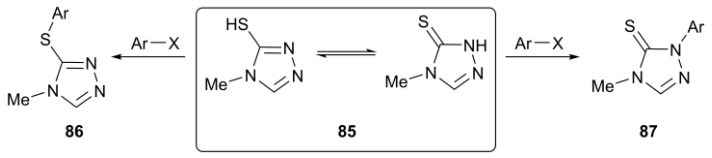
To our knowledge, the synthesis of *S*-triazolium salts has not been undertaken using a route *via* the 1,2,4-triazole, such as that reviewed in Section 2.2. The synthesis of sulfur-substituted 1,2,4-triazolium salts *via* an *S*-amidrazone intermediate would involve the use of varying isothiocyanates, which are a highly toxic class of compounds that pose a significant risk of fatality on contact with skin,[172] are carcinogenic and form adducts with body defence mechanisms such as glutathione,[173] and are known to be teratogenic.[174] By making one *S*-triazole analogue and converting this into the triazolium with varying groups, the frequency of contact with isothiocyanates can be minimised and risk potentially reduced. A small selection of *S*-triazoles are also commercially available at low cost (including 3-mercapto-1,2,4-triazole), whilst thiosemicarbazides are limited to a small library available at costs too high for common synthetic applications.

Herein is presented work towards the synthesis of *S*-triazolium salts *via* 1,2,4-triazole intermediates, with some optimisation of the synthetic route to *S*-triazoles and computational analysis to aid understanding of the selectivity observed in *S*-triazolium formation.

2.4.1 – Preparation of 1,2,4-triazole precursors

The commercially available 4-methyl-1,2,4-triazole-3-thiol (**85**) was chosen to test conditions for the synthesis of the 3-arylthio-1,2,4-triazole (*S*-triazole, **86**) precursor to *S*-triazolium salts. The methodologies within the literature for generation of S-Ar bonds are numerous and diverse,[175-177]

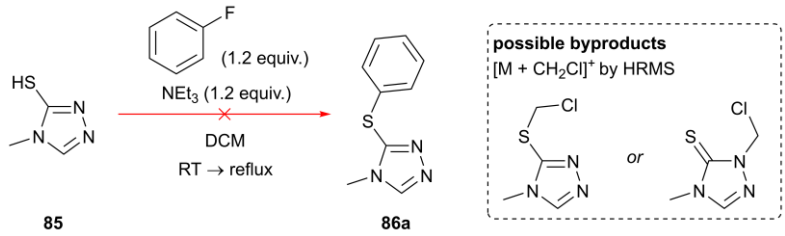
however the challenge in this case is the tautomerisation to the 1,2,4-triazole-3-thione (**Scheme 46**) which decreases reactivity at sulfur and may lead to issues with selectivity by reaction at nitrogen.



86 **85** **87**

Scheme 46 – Due to tautomerisation, the desired product **86** may be more challenging to access due to the less reactive sulfur. Product formation can also compete with formation of **87**.

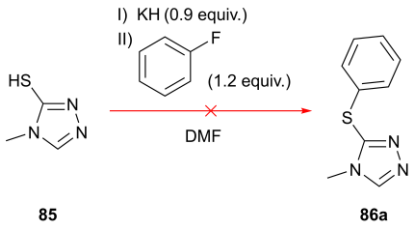
The use of nucleophilic aromatic substitution chemistry (S_NAr) was initially investigated as the most straightforward route to the desired compounds. Stirring, and then gently heating **85** in the presence of fluorobenzene in DCM (**Scheme 47**) was not successful in the formation of product. LC-MS and high resolution mass spectrometry (HRMS) of the reaction mixture evidenced the formation of the ion $[M + CH_2Cl]^+$ resulting from reaction with solvent. Use of THF as the solvent was attempted, and whilst the proposed reaction with solvent was not observed neither was the formation of product.



85 **86a**

Scheme 47 – Attempted synthesis of **86a** using S_NAr chemistry. The desired product was not observed.

The use of strong base to generate the thiolate, followed by addition of fluorobenzene, was then attempted (**Scheme 48**). A mixture of products were observed from this process, presumably resulting from the potential to deprotonate the thiol, the triazole nitrogen of the starting material tautomer, or the C(5)-H position to undertake further reaction. LC-MS suggests that starting material dimerization takes place, however this dimer could not be isolated.

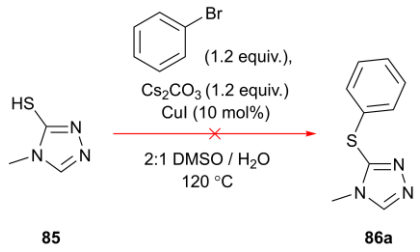


85 **86a**

Scheme 48 – Attempted synthesis of **86a** using sodium hydride. The desired product was not observed.

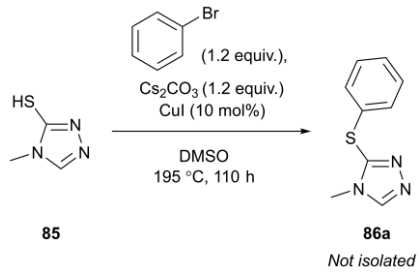
Ullmann coupling was then explored. Using the method of Zhao *et al*,[175] using copper(I) iodide and caesium carbonate, coupling of bromobenzene to **85** was attempted (**Scheme 49**). The reaction was tracked by LC-MS, however analysis after 90 h still did not show formation of product. A repeat of

this methodology scaled up the reaction to attempt isolation of species seen to form in trace amounts by LC-MS, however these compounds were never isolated.



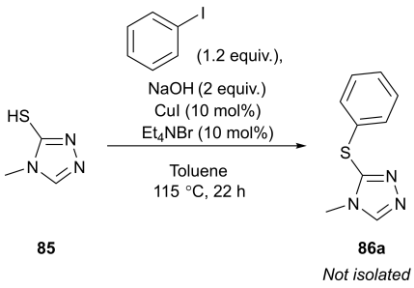
Scheme 49 – Attempted synthesis of **86a** using the method of Zhao *et al*. Product formation was not observed.

Given no product formation was seen, it was presumed that elevated temperatures may be necessary to enable the reaction to occur. Using the conditions detailed in **Scheme 50**, adapted from literature,[175] product formation was confirmed by LC-MS and HRMS. Isolation of the product was non-trivial – the solution was diluted with water and extracted with diethyl ether and DCM however effective product isolation was not possible from the DMSO/water mixture. The organic extracts were combined and the dried crude product recrystallised from IPA to obtain low yields of impure **86a**. In repeats of these reaction conditions a variety of methods were attempted to separate DMSO from **86a** or make the isolation easier: using less DMSO solvent; liquid extraction of ice cold DMSO/water mix; vacuum distillation to remove the majority of solvent – none of these methods were effective. The reaction was also attempted with 1-bromo-4-nitrobenzene to see if isolation was easier, however this was equally unsuccessful with low yields of an impure *S*-triazole. The need for high temperatures leads to the use of solvents such as DMSO, however the inability to effectively remove DMSO *in vacuo* or by a range of methods prevents its use in the formation of *S*-triazoles.



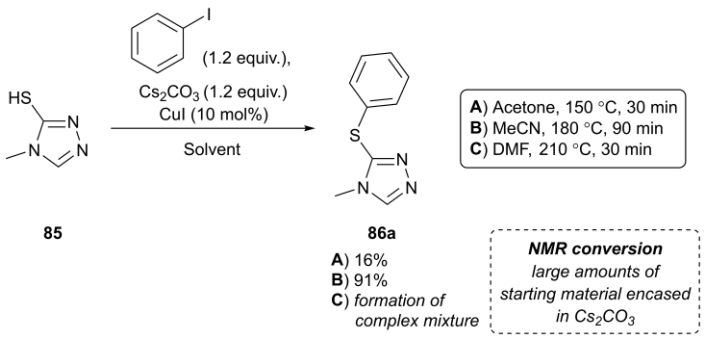
Scheme 50 – Synthesis of **86a** using adapted conditions from literature. Product formation was evidenced but the product could not be isolated.

Using the work of Chan *et al*,[176] using toluene instead of the previously employed DMSO and introducing a phase-transfer catalyst for sodium hydroxide (**Scheme 51**), low conversion was observed by LC-MS. Isolation of the product from starting material was unsuccessful by recrystallisation from methanol or column chromatography due to the small amount formed. This work, although showing low conversion, suggested that very high temperatures may not be necessary and that solvents other than DMSO can allow for this reaction to occur.



Scheme 51 – Synthesis of **86a** using the method of Chan *et al*. Small amounts of product formation could be verified by LC-MS, however the product was not isolated from the starting material.

The need for high temperatures in solvents that can be removed *in vacuo* led to the use of microwave chemistry (**Scheme 52**). Three solvents were investigated in this initial study (**A**, acetone; **B**, MeCN; **C**, DMF), and heated by microwave irradiation for 30 minutes. A pale grey mass of caesium salts was observed at the bottom of each vial that could not be fragmented with sonication at 40 °C, and so the solutions were analysed by LC-MS: all vials showed product formation. **A** showed minimal conversion and was not microwave irradiated further. **C** was a complex mixture and was also not taken further. **B** showed good conversion and was heated under the same conditions for a further 60 minutes to push the reaction to completion. NMR analysis of **A** and **B** gave approximate conversions of 16% and 91% respectively, however with most of the starting material trapped in the caesium salt the actual yields are significantly lower. This method, using acetone and acetonitrile, was chosen for optimisation to gain access to *S*-triazoles.



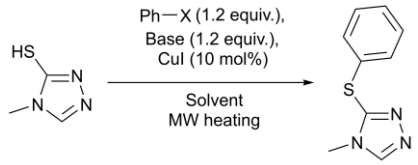
Scheme 52 – Synthesis of **86a** using microwave irradiation. Three solvent systems were tested: **A** – acetone; **B** – acetonitrile; **C** – Dimethylformamide.

2.4.1.1 – Optimisation of the microwave-assisted Ullmann coupling

Table 8 summarises the work towards an optimised synthesis of **86a**. Following the initial findings (runs **3** – **5**), noting the promise of acetone and acetonitrile as solvent, changes to the solvent system were explored. By use of 2:1 organic solvent / water mixtures (runs **6** and **7**) the formation of an insoluble mass was avoided, however the reaction was low yielding and the tendency for pressure build-up suggested the caesium salts were not fully dissolving even at the elevated temperatures. The use of potassium acetate (runs **17** and **18**) was better yielding than Cs_2CO_3 however pressure build up limited the temperatures that could be achieved. The use of triethylamine (runs **10** and **11**) led to

the best yields of the three bases and was therefore explored further. It should be noted that buffer solutions were explored in place of water (runs **19** and **20**) however showed little success.

Table 8 – Summary of the optimisation undertaken for the Microwave-assisted Ullmann coupling to give **86a**. All reactions undertaken using 200 mg **85**. MW = Microwave.



85 **86a**

Run	X	Base	Solvent	Temp. (°C)	Time (min)	Yield (%)
1	F	NEt_3	2:1 MeCN / water	150	60	*Trace* [a]
2	Br	NEt_3	2:1 MeCN / water	150	60	11
3	I	Cs_2CO_3	Acetone	150	30	16[b]
4	I	Cs_2CO_3	MeCN	180	90	91[b]
5	I	Cs_2CO_3	DMF	250	30	- [c]
6	I	Cs_2CO_3	2:1 acetone / water	150	30	9
7	I	Cs_2CO_3	2:1 MeCN / water	130	60	20
8	I	NEt_3	Acetone	150	60	14
9	I	NEt_3	MeCN	150	60	21
10	I	NEt_3	2:1 acetone / water	120	30	27
11	I	NEt_3	2:1 MeCN / water	120	60	37
12	I	NEt_3	2:1 MeCN / water	150	30	16
13	I	NEt_3	2:1 MeCN / water	150	60	44
14	I	NEt_3	2:1 MeCN / water	180	120	81
15	I	NEt_3	1:1 MeCN / water	150	30	11
16	I	NEt_3	1:1 MeCN / water	150	480	52
17	I	AcOK	2:1 acetone / water	140	40	13
18	I	AcOK	2:1 MeCN / water	140	60	26
19	I	2:1 acetone / phosphate buffer (p*H* = 7)[d]		140	60	- [e]
20	I	2:1 acetone / borate buffer (p*H* = 10)[d]		140	210	3

[a] Product observed by LC-MS, very small peaks by NMR – NMR conversion not appropriate and isolation not possible [b] NMR conversion, large mass of caesium salt preventing mixing of reagents. [c] Complex mixture formed. [d] Buffer used in place of water and base. [e] No reaction by LC-MS, product not observed.

Water is deemed necessary for the effective Ullmann coupling, as by using anhydrous solvents (runs **8** and **9**) there is a significant drop in the yield *versus* comparative conditions in 2:1 acetonitrile / water (runs **12** and **13**). However, equal volumes of water show a potential drop in the yield under comparative conditions (run **15**). It could be proposed that the increase in solvent polarity upon addition of water aids the solubility of triethylammonium salts, but in equiproportional solvent mixtures the lowered solubility of reagents limits the yield. Acetonitrile/water mixtures were chosen

to be explored further given the higher temperatures that can be safely reached and the higher yields that can be obtained under comparative conditions.

The choice of haloalkane is important – as may be expected yields are lowered for bromobenzene *versus* iodobenzene, and use of fluorobenzene gives only traces of product (compare runs **1**, **2** and **13**). The oxidative addition of copper to the carbon-halogen bond is slowed as the bond strength increases, and this is evidenced to reduce the yield.

A reduction in reaction time shows a significant drop in the yield (compare run **12** to run **13**), which though may seem obvious at first indicates that the moderate yields obtained are a result of reaction conditions and not isolation technique. By use of prolonged reaction time (compare run **15** to run **16**) conditions that may give poor yields can be significantly improved, however reaction times of this length are unappealing for library synthesis. Elevated temperatures improve yield (compare runs **11** and **13**) and are a more convenient alternative to longer reaction times – the possibility of pressure build-up however is paramount to consider for safety reasons.

By consideration of all the above, run **14** gives the highest yield in a 2-hour reaction time. This was deemed an appropriate optimised route given that diminishing improvements will be achieved under longer reaction times, and temperatures above 180 °C are deemed unsafe and likely to lead to byproduct formation (considering run **5**).

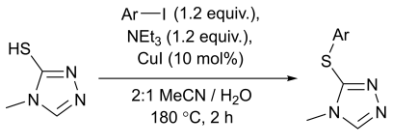
2.4.1.2 – Exploration of the scope of S-triazole synthesis

Table 9 lists the *S*-triazoles that were obtained from the microwave assisted Ullmann coupling based on the optimised conditions. The reaction proceeded without formation of byproducts, and so purification of the *S*-triazoles was generally straightforward. In cases where liquid aryl halides were used the reaction mixture was concentrated *in vacuo*, resuspended in DCM, washed with saturated aqueous sodium bicarbonate solution and concentrated *in vacuo* to afford the product. Solid aryl halides required column chromatography using 0 to 10% MeOH in DCM, with good separation of the product from starting materials. In the case of **86g** selectivity for the coupling was seen at the aryl iodide bond of 1-bromo-4-iodobenzene, with the *para*-iodinated *S*-triazole and/or triazole dimer not observed by LC-MS.

A further *S*-triazole, **86q**, could be obtained using pentafluoropyridine (PFP) (**Scheme 53**). PFP is a highly reactive species that allows for the facile addition of an electron withdrawing substituent, and has been implemented in the generation of acyl fluorides *in situ* for the synthesis of amide, ester and thioester bonds.[178, 179] S_NAr at the *para*-position of PFP occurs selectively, and purification is straightforward requiring only an aqueous wash of the crude product dissolved in DCM. Attempts were made to use this methodology on 3-mercapto-1-2,4-triazole (**88**), undertaking double arylation. *S*-arylation can occur, and a reasonable yield of **89** can be obtained, however these conditions cannot be used to undertake triazole *N*-arylation. The addition of *N*, *N'*-dimethylethylenediamine, which has

been successful within the literature,[180] enabled product formation based on LC-MS evidence but gave a mixture of isomers which could not be separated by column (10% MeOH in DCM). The synthetic procedure was therefore adjusted for *S*-arylation only (**Scheme 54**). Isolation of **89** required the use of ethylenediaminetetraacetic acid (EDTA) to scavenge copper ions chelated to the product.

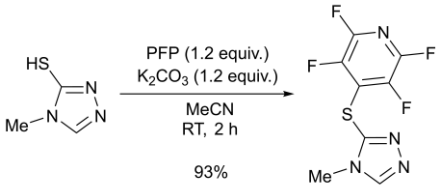
Table 9 – Summary of the *S*-triazoles synthesized using the optimised Ullmann coupling conditions.



85 **86a-p**

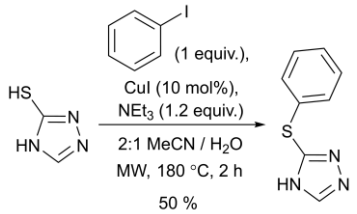
Compound	Ar	Yield (%)	Compound	Ar	Yield (%)
86a	Ph	81	**86i**	*p*-I-C_6H_4	40
86b	*p*-Me-C_6H_4	60	**86j**	*p*-CF_3-C_6H_4	69
86c	*p*-^{t}Bu-C_6H_4	40	**86k**	*p*-COH-C_6H_4	16
86d	*p*-OMe-C_6H_4 [a]	29	**86l**	*p*-COMe-C_6H_4	10
86e	*p*-NO_2-C_6H_4	91	**86m**	*p*-COOH-C_6H_4	97[b]
86f	*p*-CN-C_6H_4	12	**86n**	*p*-COOMe-C_6H_4	21
86g	*p*-F-C_6H_4	78	**86o**	2,6-Me-C_6H_4	72
86h	*p*-Br-C_6H_4	75	**86p**	Pyrid-2-yl	61

[a] Aryl bromide used. [b] NMR yield, with inseparable traces of starting material.



85 **86q**

Scheme 53 – Using pentafluoropyridine, the tetrafluoropyridyl *S*-triazole **86q** can be synthesized.

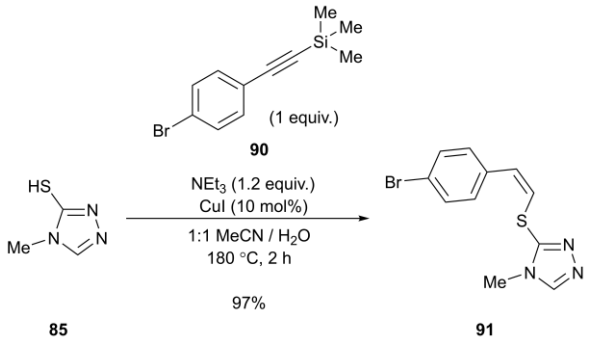


88 **89**

Scheme 54 – The arylation of 3-mercapto-1,2,4-triazole (**88**) selectively gave the *S*-arylation product **89** (based on ^{1}H NMR), with attempts on using an adapted route to undertake double arylation unsuccessful.

As part of work towards the bioconjugation of *S*-triazolium salts to amino acids, the generation of ethynyl-substituted *S*-triazoles was explored. It was proposed that the use of an alkyne without a terminal protecting group may lead to further reactions under the Ullmann coupling conditions, most

notably Glaser coupling[181] to give dimerization of either the aryl halide or the *S*-triazole product. For this reason the generation of the *S*-triazole was attempted using the trimethylsilyl-protected alkyne **90** (**Scheme 55**), however the product formed in high yields (**91**) arises from the attack of the thiol-substituted triazole onto the alkyne and loss of the trimethylsilyl group. Swapping to 4-bromophenylacetylene gives the same product, but was lower yielding (82%).



Scheme 55 – Attempted Ullmann coupling with the trimethylsilyl-protected phenylacetylene **90** leads to generation of the ethenyl-conjugated *S*-triazole **91** in very high yields.

S-triazoles were fully characterised using NMR spectroscopy and mass spectrometry in all cases. Where possible the compounds were also analysed by single crystal XRD (**Figure 24**). Suitable crystals were formed by slow evaporation of acetonitrile or methanol from the solution at room temperature. Detailed crystallographic information can be found in Appendix A. A selection of key bond lengths, bond angles and dihedral angles are given in **Table 10** based on the general structures provided and with C^9 being defined as the *ortho*-carbon closest to C^3. *S*-triazoles are seen to adopt a roughly perpendicular arrangement of the aryl and triazolyl rings.

Plots of the selected XRD structural elements against the σ_p values obtained from the literature[164] reveals trends which are shown in **Figure 25**. These trends consider the modulus of dihedral angles as deviation from planarity, consider only the major component for the structure of **86k**, and omit **86q** due to the differing substitution pattern. The strongest linear correlation to σ_p values is seen when looking at the N^2-C^3-S^6-C^7 dihedral, with an increase in σ_p (increasing electron withdrawal) showing a decrease in the dihedral angle (**Figure 25A**). Given that the dihedral angles are all between ± 89° and ± 112°, and there is no trend in L(C^3-S^6) against σ_p, the change in planarity is not thought to be due to varying conjugation across the Ar-S^6-triazole scaffold. A good correlation, excluding the anomalous result for **86a** (σ_p = 0), is seen for D(C^3-S^6-C^7-C^9) decreasing as σ_p increases (**Figure 25B**). This can be explained by enhanced donation of electron density through resonance from sulfur to the aryl ring as the *para*-substituent becomes more electron withdrawing – this is supported by decreasing S^6-C^7 bond length with increases in σ_p (1.783 ± 0.001 Å for **86b**, 1.775 ± 0.002 Å for **86a** and 1.770 ± 0.002 Å for **86e**). The smaller than expected dihedral bond angle for **86a** is potentially a

result of the lack of *para*-substituent affecting crystal packing. Returning to the consideration of D(N^2-C^3-S^6-C^7), with a proposed donation into the aryl ring from sulfur electron-withdrawing substituents will increase the cationic charge upon the sulfur atom. The decrease in dihedral angle such that the aryl and triazole rings are perpendicular is proposed to relieve unfavourable electronic interactions of the cationic sulfur with the triazole ring. With the aryl ring orientated such that it is close to the N^4-methyl group, there is also a possible CH-π interaction affecting D(N^2-C^3-S^6-C^7) however this is not deemed significant given the distance between and orientation of the groups.

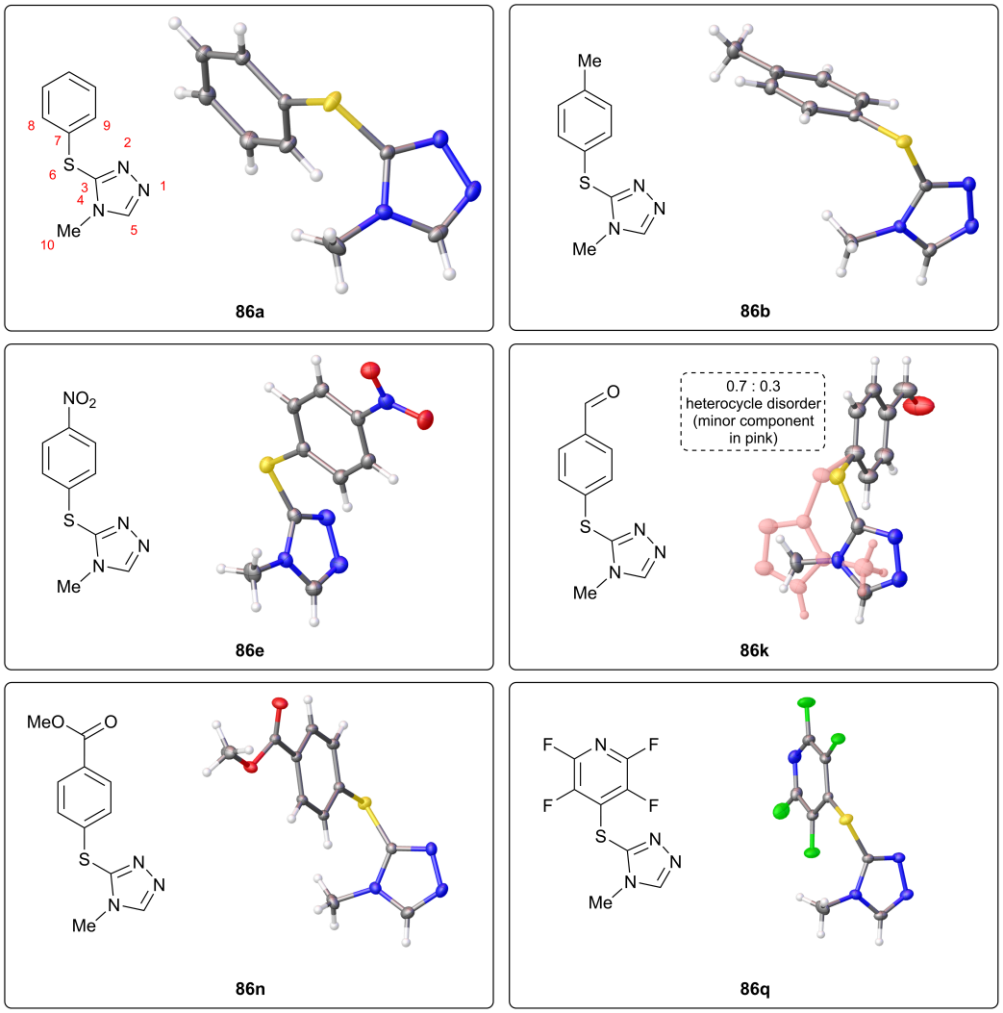
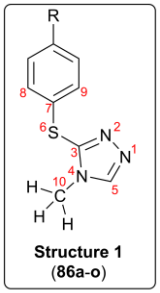
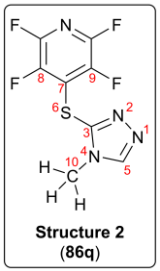


Figure 24 – The six *S*-triazole crystal structures obtained from single crystal XRD, with the numbering scheme used shown on the structure of **86a**. See Appendix A for detailed crystallographic information.

Increasing σ_p also shows a weak correlation with increasing A(N^1-C^5-N^4) (**Figure 25C**), which does not agree with trends recently discovered for the carbenic position of fused ring 1,2,4-triazolium salts where decreases in the angle were consistent with increased acidity.[166] A small change in the angle (110.8 → 111.6) is observed within the compounds analysed, and so the observed change may not be statistically significant.

Table 10 – Selected bond lengths, bond angles and dihedral angles of the *S*-triazoles analysed by XRD.

	Compound	86a	86b	86e	86k[a]	86n	86q
	σ_p [b]	0	−0.17	+0.78	+0.42	+0.45	- [c]
 Structure 1 (86a-o)	L(N^1-C^5) (Å)	1.313 (± 0.003)	1.314 (± 0.001)	1.313 (± 0.003)	1.314 (± 0.005) [*1.316 (± 0.012)*]	1.325 (± 0.003)	1.308 (± 0.002)
	L(C^4-C^5) (Å)	1.352 (± 0.002)	1.355 (± 0.001)	1.346 (± 0.003)	1.358 (± 0.008) [*1.360 (± 0.017)*]	1.347 (± 0.002)	1.351 (± 0.003)
	L(N^2-C^3) (Å)	1.312 (± 0.002)	1.317 (± 0.001)	1.316 (± 0.003)	1.323 (± 0.004) [*1.317 (± 0.011)*]	1.314 (± 0.002)	1.312 (± 0.003)
	L(C^3-S^6) (Å)	1.746 (± 0.002)	1.743 (± 0.001)	1.742 (± 0.002)	1.746 (± 0.004) [*1.739 (± 0.010)*]	1.748 (± 0.002)	1.752 (± 0.002)
 Structure 2 (86q)	L(N^4-C^{10}) (Å)	1.466 (± 0.002)	1.456 (± 0.001)	1.457 (± 0.003)	1.458 (± 0.007) [*1.447 (± 0.017)*]	1.458 (± 0.003)	1.455 (± 0.003)
	A(N^1-C^5-N^4) (°)	111.2 (± 0.2)	110.8 (± 0.1)	111.6 (± 0.2)	111.4 (± 0.5) [*110.6 (± 1.0)*]	110.9 (± 0.2)	111.4 (± 0.2)
	A(N^2-C^3-S^6) (°)	124.8 (± 0.1)	125.7 (± 0.1)	125.1 (± 0.2)	124.4 (± 0.3) [*124.6 (± 0.7)*]	124.2 (± 0.1)	125.1 (± 0.1)
	A(C^3-S^6-C^7) (°)	104.1 (± 0.1)	99.8 (± 0.1)	101.2 (± 0.1)	103.1 (± 0.2) [*105.3 (± 0.4)*]	102.8 (± 0.1)	100.7 (± 0.1)
	D(N^2-C^3-S^6-C^7) (°)	+98.8 (± 0.2)	+111.9 (± 0.1)	−93.3 (± 0.2)	+89.1 (± 0.3) [*−95.1 (± 0.7)*]	−97.0 (± 0.2)	+70.4 (± 0.2)
	D(C^3-S^6-C^7-C^9) (°)	+11.2 (± 0.2)	−48.7 (± 0.1)	−5.6 (± 0.2)	+19.8 (± 0.3) [*−12.4* (± 0.4)]	−34.5 (± 0.2)	+37.9 (± 0.2)

[a] Italicised data in square brackets for minor component. [b] Values taken from literature.[164] [c] Not included in analysis.

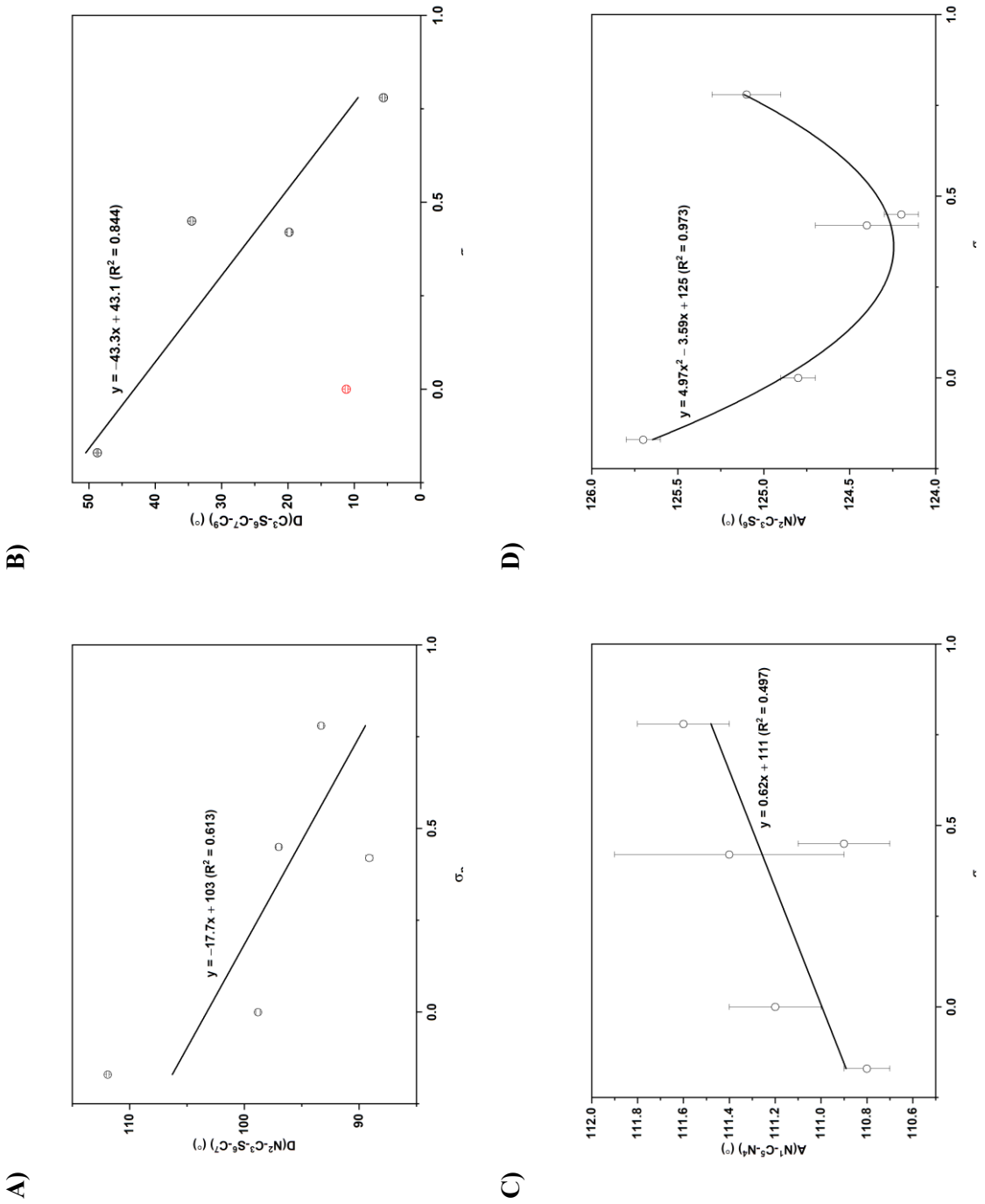


Figure 25 – Graphs of structural parameters determined by XRD against σ_p. **A** – D(N^2-C^3-S^6-C^7). **B** – D(C^3-S^6-C^7-C^9). **C** – A(N^1-C^5-N^4). **D** – a polynomial relationship is proposed for A(N^2-C^3-S^6). Data in red omitted from the fit.

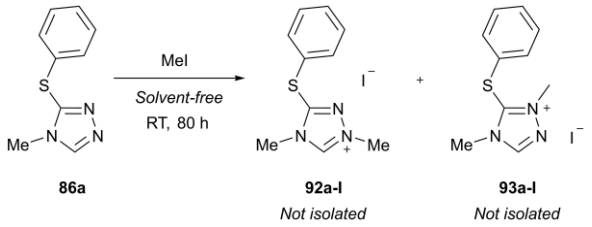
With 5 datapoints, polynomial relationships of the XRD data must be treated with caution. However, a very strong polynomial relationship is seen between A(N^2-C^3-S^6) and σ_p with the smallest angle of ~124.3° seen with slightly electron-withdrawing substituents (**Figure 25D**). The trend for lower values of σ_p is proposed to be a result of increased electron donation into the triazole ring by the electron donating substituent, leading to greater bond order between C^3 and S^6. The increase seen for **86e** is proposed to be a result of the electronic interactions discussed earlier, whereby the more

cationic sulfur arising from increased donation into the more electron-poor aryl ring orients itself as far away as possible from the triazole ring.

2.4.2 – Transformation of 1,2,4-triazoles to 1,2,4-triazolium salts

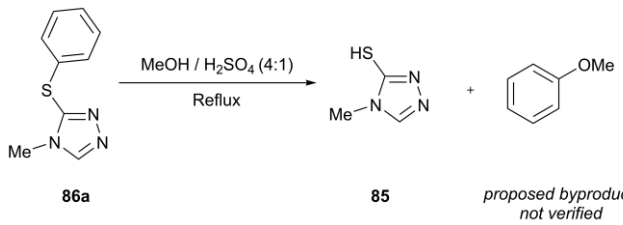
2.4.2.1 – Discovery of a route to dialkyl-S-triazolium salts

Discovery of an effective method to undertake formation of *S*-triazolium salts from the *S*-triazoles synthesized within this project explored some of the methods detailed within Section 2.1. Given that alkylation is significantly less challenging than arylation due to the low nucleophilicity of the triazole nitrogen, and the ability to undertake S_N2 chemistry over the more thermodynamically unfavourable S_NAr chemistry, the addition of alkyl groups to **86a** was investigated. Limited success was found by stirring **86a** in iodomethane (**Scheme 56**), the desired product *m/z* was observed by LC-MS and HRMS however ^{1}H NMR showed no clear evidence of triazolium formation with peaks barely distinguishable from baseline noise. Further analysis of the LC-MS trace showed two peaks of the same *m/z* that indicated selectivity was not observed in the site of methylation – the *S*-triazole scaffold bears two relatively unreactive nitrogen atoms, and so competing addition to the N^1 and N^2 position can occur to give **92a·I** and **93a·I**. Repeats of this procedure investigated addition of $NaBF_4$ as an alternative counterion, the use of THF and stoichiometric MeI to enable reflux, and the use of copper(I) iodide however none of these alterations led to significant product formation.



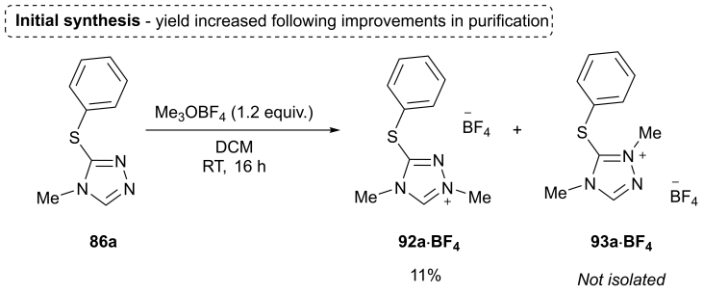
Scheme 56 – By stirring **86a** in iodomethane, evidence of a *S*-triazolium product was seen by LC-MS and HRMS. ^{1}H NMR indicated low conversion and poor methylation selectivity.

Using the method of Tucker,[182] alkylation under acidic conditions was attempted (**Scheme 57**). After 2 hours complete loss of **86a** was observed by LC-MS, with ^{1}H NMR showing the cleavage of the sulfur-aryl bond to regain **85**. A repeat of the reaction at room temperature also led to cleavage.



Scheme 57 - Attempted methylation under acidic conditions led to cleavage of the sulfur-aryl bond.

The use of trimethyloxonium tetrafluoroborate was the method which, in high yields and with a straightforward setup, gave access to **92a·BF$_4$** (**Scheme 58**). Purification was initially possible by allowing the reaction solvent to evaporate overnight at room temperature, giving crystalline solid in an oil. The crystals could be washed with chloroform to access pure **92a·BF$_4$** however in a low yield – NMR and mass spectrometry analysis was possible, however the crystals formed were of unsatisfactory quality for single-crystal XRD. The chloroform washings contained a mixture of **92a·BF$_4$** plus the N^2-methylated isomer **93a·BF$_4$**, which could not be separated by recrystallisation nor column chromatography using 10% MeOH in DCM eluent. A promising finding was that the chloroform washings were mostly one isomer, which agreed by ^{1}H NMR with the formed crystals – good selectivity can be achieved with this method.



Scheme 58 – Initial isolation of **92a·BF$_4$**. Using trimethyloxonium tetrafluoroborate, stirring overnight, complete conversion was observed by LC-MS to the desired product or the N^2-methylated product (**93a·BF$_4$**).

It should be noted that the isomer formed was not conclusively known when isolated – mass spectrometry is of little use and standard NMR techniques unable to definitively distinguish the two isomers. Two peaks for the C^5-H position were observed by ^{1}H NMR spectroscopy, with the peak of highest shift attributed to the desired isomer **92a·BF$_4$** based on the proximity to the cationic charge (distributed over N^1-C^5-N^4 instead of N^2-C^3-N^4 in **93a·BF$_4$**). ^{1}H-^{15}N heteronuclear multiple bond correlation (HMBC) NMR gave the first clear indication that the desired isomer was formed (**Figure 26**), with the data showing that the two methyl groups at 4.03 ppm and 3.79 ppm correlate to nitrogens of similar shift and furthermore share correlation to nitrogens adjacent to the C^5-H position (10.03 ppm). The correlation at (4.03 ppm, 299.5 ppm) corresponds to N^1-Me correlating to the N^2 position, indicated by the lack of correlation with the C^5-H environment. This additional correlation allows for verification of the NMR peak corresponding to each methyl group, and furthermore may suggest that the triazolium cationic charge mostly exists upon N^1.

Further evidence for the regioisomer formed came from the differing hydrogen exchange rates in protic deuterated solvents. Due to the lower pK_a of **92a·BF$_4$** (formation of normal NHC) *versus* **93a·BF$_4$** (formation of an abnormal carbene), NMR analysis of **92a·BF$_4$** in methanol-*d*^{4} shows a small peak for the C^5-H signal. **93a·BF$_4$** very slowly undergoes exchange of the C^5-H for deuterium in the same solvent, and so a large C^5-H signal can be seen. This straightforward test enables rapid verification of the formed triazolium, even without spectroscopic data relating to the other isomer.

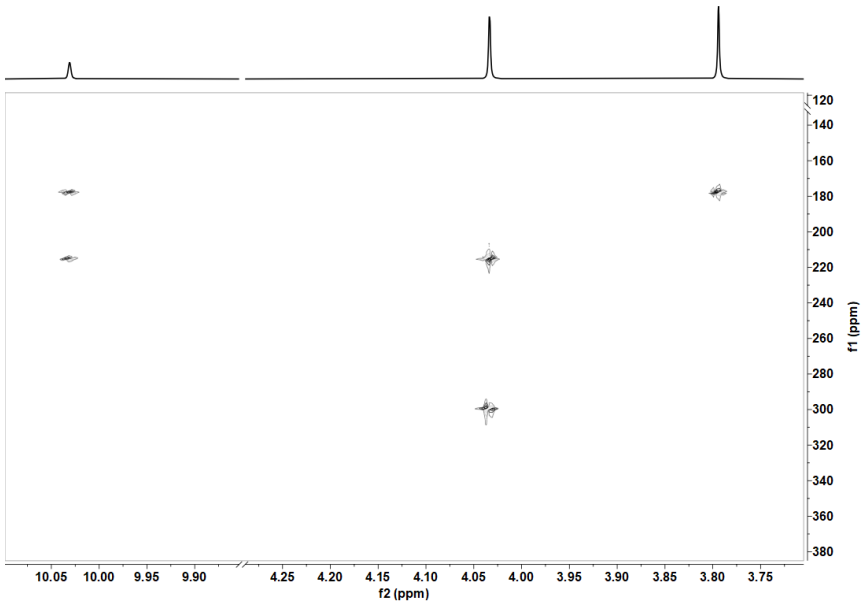


Figure 26 – ^{1}H-^{15}N HMBC NMR of **92a·BF$_4$**. Horizontal axis cut between 4.29 and 9.85 ppm for clarity.

Suitable crystals of **92a·BF$_4$** were obtained for single crystal XRD from the slow evaporation of acetonitrile from a solution of the *S*-triazolium. Acetonitrile was initially avoided due to concerns relating to hydrolytic ring opening (see previous work, **Scheme 32**) however no signs of the ring-opening were observed. The XRD crystal structure (**Figure 27**) verifies that N^1 methylation is the major product, adopting a similar arrangement observed within the *S*-triazoles with perpendicular aryl and triazolium rings.

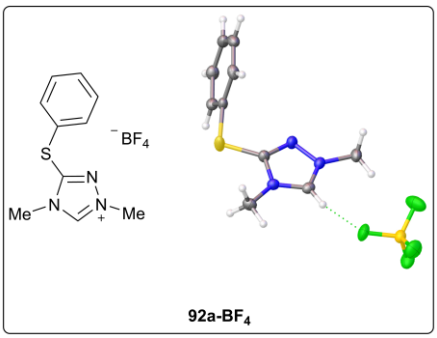
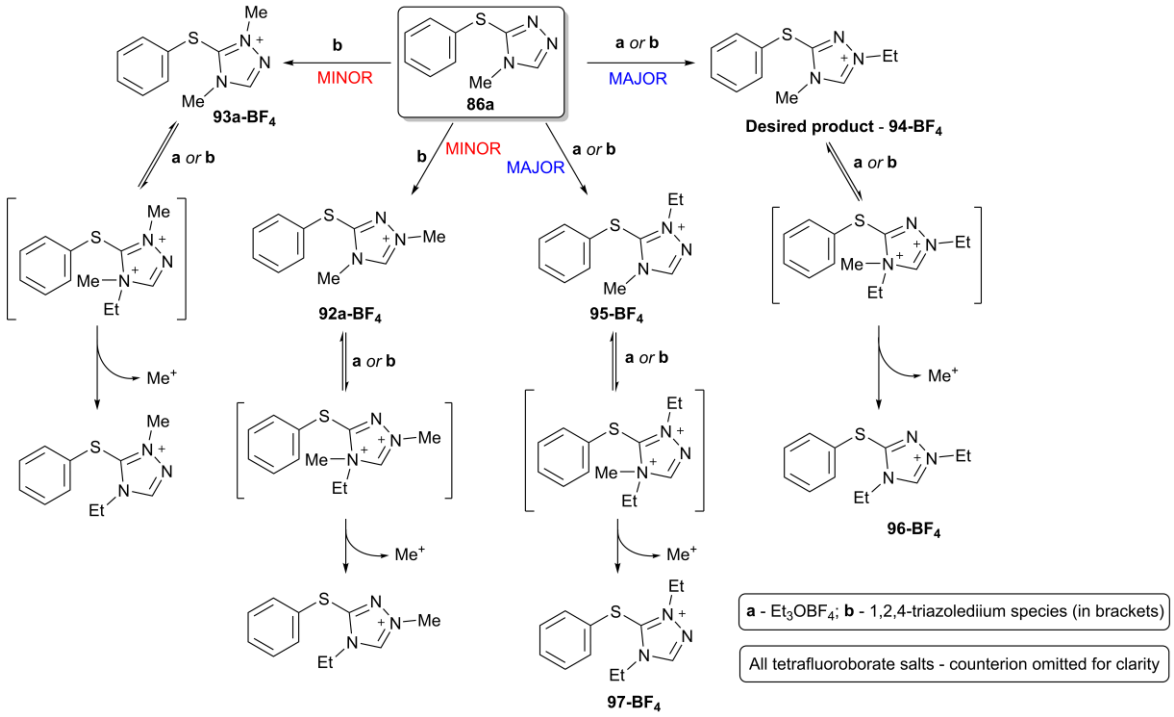


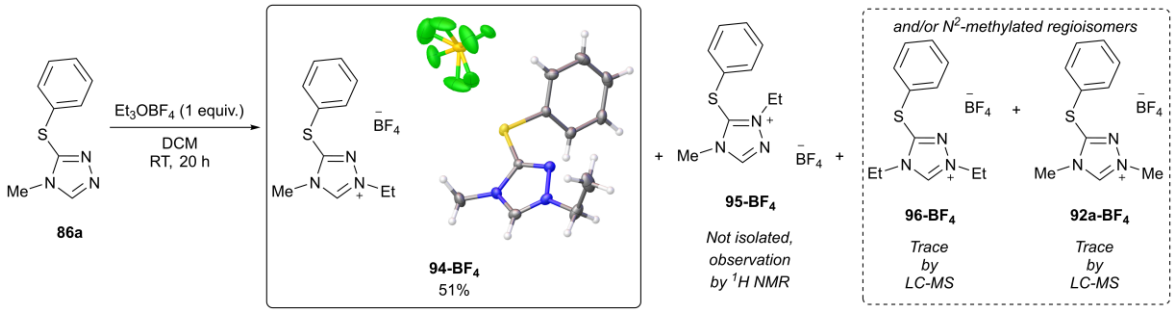
Figure 27 – Crystal structure of **92a·BF$_4$** from single crystal XRD, verifying formation of the desired isomer. Detailed crystallographic information can be found in Appendix A.

Swapping the alkylating agent to triethyloxonium tetrafluoroborate (to synthesize **94·BF$_4$** and **95·BF$_4$**) led to an additional challenge (**Scheme 59**). The *S*-triazolium salts generated in this work are proposed to undergo additional alkylation at the N^4-position to give a short-lived 1,2,4-triazolediium intermediate, which acts as an alkylating agent that can react with a triazole or triazolium. When using trimethyloxonium tetrafluoroborate this is not a significant issue, as the proposed triazolediium would lose one of the methyl groups and regenerate the dimethyl triazolium salt. However, ethylation leads to the possibility of methyl to ethyl exchange by this addition-elimination mechanism, explaining why LC-MS and HRMS evidence was obtained for formation of

the dimethyl triazolium salts (**92a·BF$_4$** and **93a·BF$_4$** – both also suggested to form by observing the C^5-H signals by ^{1}H NMR) and diethyl triazolium salts (**96·BF$_4$** and **97·BF$_4$**). The dialkylated *S*-triazolium salts prepared in this work do not show any sign of instability or isomerisation in aqueous or alcohol solvents by ^{1}H NMR tracking over a period of 15 days; the *S*-triazolium alone does not appear to be an alkylating agent. This process can be controlled through the stoichiometry of the reaction, with the reduction from 1.2 equivalents Et_3OBF_4 to equimolar amounts of **86a** and Et_3OBF_4 increasing the yield of **94·BF$_4$** from 27% to 51% (**Scheme 60**) – single crystal XRD verified formation of the desired isomer in agreement with the C^5-H NMR shift *versus* the minor yielding **95·BF$_4$**.



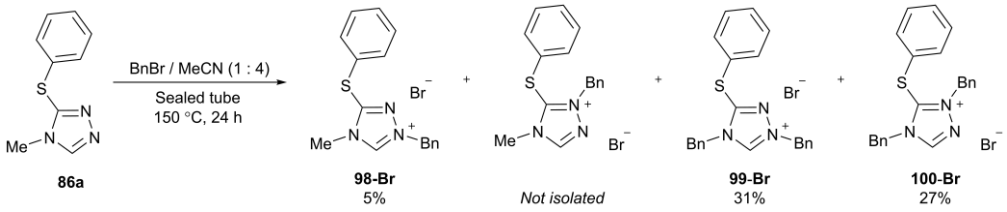
Scheme 59 – Ethylation of **86a** can lead to a complex set of pathways where a mixture of ethylated and methylated triazolium salts can be generated.



Scheme 60 – The synthesis of **94·BF$_4$** in good yields can be undertaken with 1 equivalent of triethyloxonium tetrafluoroborate. Verification of **94·BF$_4$** was possible by single crystal XRD, detailed crystallographic information is provided in Appendix A.

Alkylation using haloalkanes is a more interesting route to *S*-triazolium salts given the range of substituents which could be introduced. Only trimethyl and triethyloxonium salts are commercially

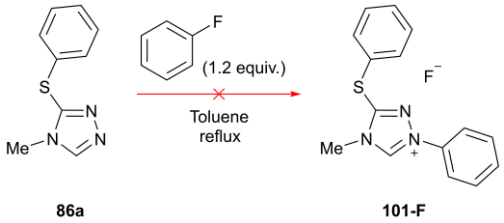
available, with the synthesis of further analogues limited to tripropyloxonium and tributyloxonium hexachloroantimonate salts using $SbCl_5$ and either trialkyl phosphate or ethyl diazoacetate.[183, 184] Using forcing conditions benzyl bromide can react with **86a** to give a mixture of products (**Scheme 61**), however due to the use of excess benzyl bromide the isolated yield of the 1-benzyl-4-methyl *S*-triazolium **98·Br** is only 5% and the major products are the two regioisomers of dibenzyl *S*-triazolium (**99·Br** and **100·Br**). This outcome, coupled with the stability of **99·Br** and **100·Br** by ^{1}H NMR in methanol-d^4 over a period of 5 days, gives further evidence of the generation of triazolediium alkylating agents *in situ* that enable the exchange of the N^4 methyl group.



Scheme 61 – The synthesis of benzylated triazolium salts in excess benzyl bromide leads to the 1,4-dibenzyl *S*-triazolium **99·Br** as the major product, with the 2,4-dibenzyl isomer **100·Br** having slightly lower yield. Small amounts of the monobenzylated *S*-triazolium salt **98·Br** were isolated.

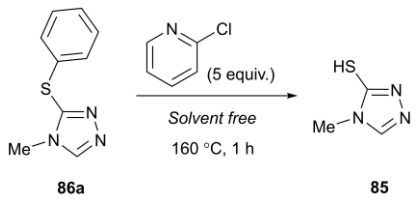
2.4.2.2 – Exploration of S-triazolium synthesis by arylation

The arylation of *S*-triazoles to *S*-triazolium salts was initially attempted using modified versions of the methodologies used in the synthesis of *S*-triazoles. Refluxing **86a** and fluorobenzene in toluene (**Scheme 62**) showed no clear evidence of product formation, forming a complex mixture with no LC-MS peak of *m/z* corresponding to **101·F**. A repeat of this reaction tried highly forcing conditions – microwave heating at 250 °C for 2 h in DMF, also forming a complex mixture with LC-MS suggesting trace levels of **101·F** present. Product isolation was not possible by RP-LC.



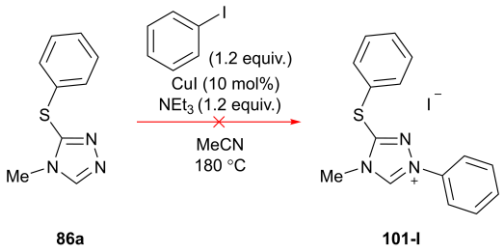
Scheme 62 - The attempted arylation of **86a** by S_NAr chemistry was unsuccessful, with no clear evidence of product formation.

As a variation to the method shown in **Scheme 62**, reaction of **86a** with 2-chloropyridine was explored (**Scheme 63**). The addition of triazole to the pyridine is proposed to be aided by the adjacent slightly more electronegative nitrogen (*versus* carbon), potentially facilitating a S_NAr mechanism. Under these conditions it was instead found that S-Ar bond cleavage occurs, regenerating the triazole starting material. A repeat of this reaction at 80 °C showed less *S*-triazole cleavage, however the *m/z* for the *S*-triazolium was not observed.



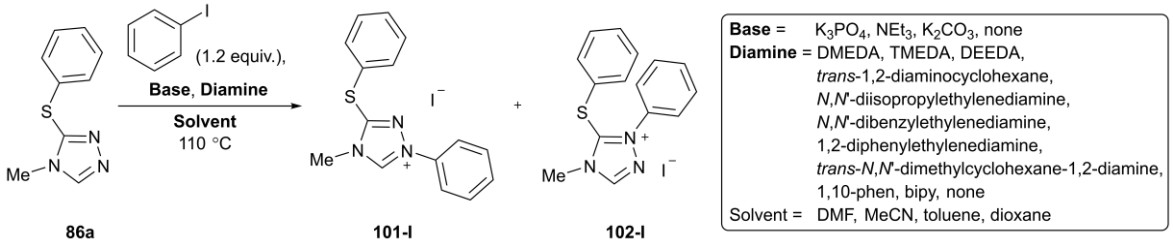
Scheme 63 – The attempted addition of a pyrid-2-yl group to **86a**. Product formation was not observed.

Ullmann coupling conditions similar to those used effectively to synthesize *S*-triazoles were explored (**Scheme 64**). After microwave heating the mixture for 5 hours **101·I** formation was not observed by LC-MS, and so forcing conditions like those investigated for S_NAr chemistry were explored. By switching to DMF and microwave heating for 3 hours at 200 °C, product formation was once again observed by LC-MS. However, ^{1}H NMR spectra of the reaction mixture showed no evidence of product and isolation of the observed *m/z* was not achieved.



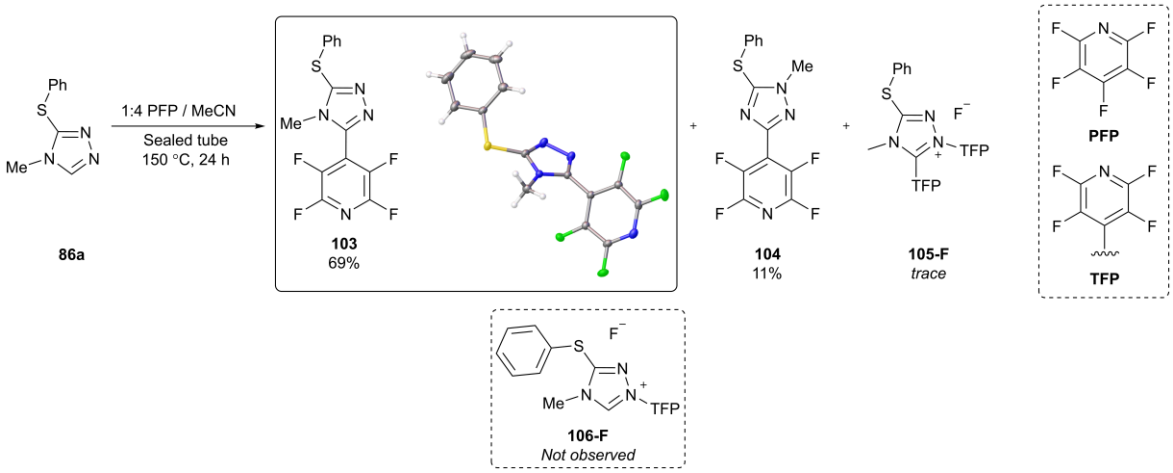
Scheme 64 – The attempted arylation of **86a** using Ullmann coupling conditions similar to those used in the generation of *S*-triazoles. Product formation was not observed.

An alteration to the Ullmann coupling was attempted, based on the work of Buchwald *et al*[180] who explored the arylation of unsubstituted 1,2,4-triazole amongst a range of other heterocycles. They report that the involvement of diamine ligands enables the effective *N*-arylation of heterocycles, particularly when using *N,N'*-dimethyl substituted ligands for which competitive arylation of the diamine ligand is supressed. As part of this work a variety of conditions were used (**Scheme 65**), with more details provided in Appendix B-4. It was found that 10 mol% CuI and 20 mol% of either 1,10-phenanthroline (1,10-phen) or *trans-N,N'*-dimethylcyclohexane-1,2-diamine, with 2 equivalents of K_3PO_4 in DMF, gave good conversion to the desired product. Unfortunately isolation of **101·I** was not possible by column chromatography using 10% v/v methanol in dichloromethane, or RP-LC, with the two regioisomers of the product impossible to separate and elution with residual iodobenzene often observed. RP-LC was the most promising method, with evidence of partial regioisomer separation by ^{1}H NMR using a 1% column load of product mixture on a 90 min gradient from 5 to 100% v/v methanol in water. *N,N'*-dimethylethylenediamine (DMEDA), found to be an effective ligand in the literature[180] for triazole arylation, was ineffective in this work showing significant ligand *N*-arylation. It can be proposed that the low reactivity of the substituted triazole leads to ligand arylation being preferential. Generally it was found that more rigid diamine ligands gave rise to better conversion based on LC-MS data, and exhibited less ligand *N*-arylation.

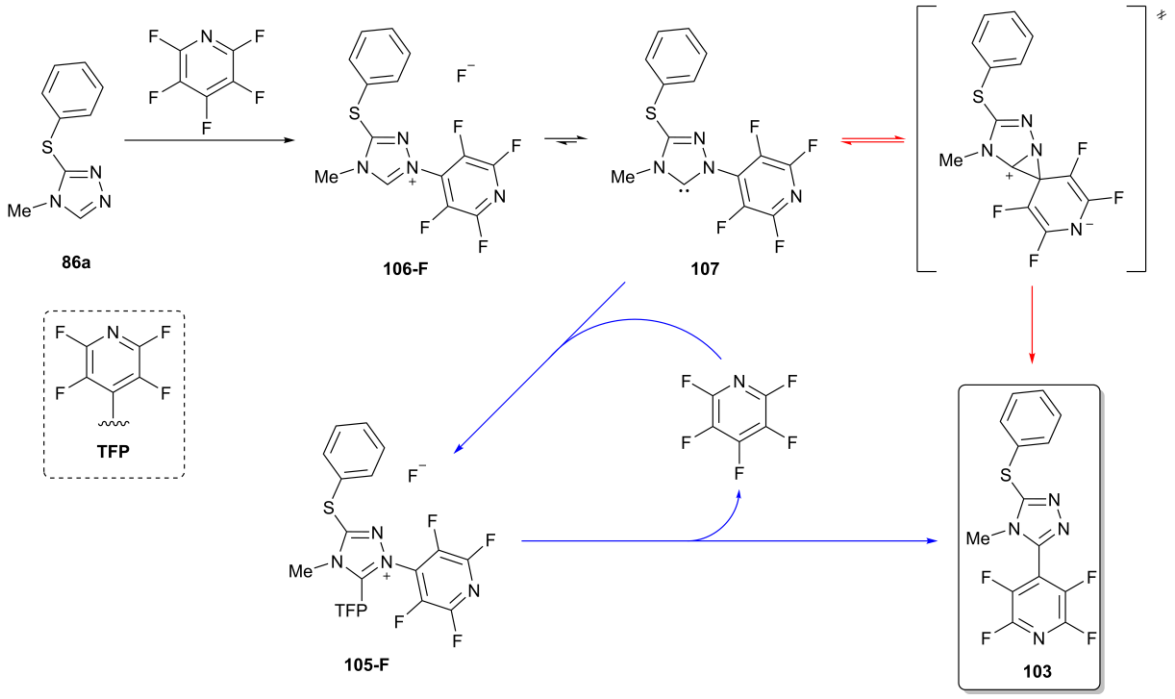


Scheme 65 – The attempted arylation of **86a** using a copper-diamine catalyst based on literature. Whilst conversion to the product was observed, separation of the two regioisomers **101·I** and **102·I** was not achieved by column chromatography or RP-LC.

The reaction of PFP with **86a** was explored, however an unexpected product was isolated. LC-MS showed formation of the product *m/z*, however following purification by RP-LC no signal could be observed for the C^5-H position by ^{1}H NMR in $CDCl_3$. Initial proposals were that the tetrafluoropyridyl substituent is so electron withdrawing that the carbene is highly favoured over the *S*-triazolium salt, however if this were the case double addition to PFP might be expected in significant amounts whilst LC-MS shows only traces of the corresponding *m/z*. Single crystal XRD verified the product formed, showing what could be simply described as the addition of PFP to the C^5 position (**103**, **Scheme 66**). The C^5 position of **86a** is not believed to be acidic enough for proton removal under the reaction conditions, and so such a description is misleading. A more reasonable explanation is that the desired *S*-triazolium (**106·F**) forms, and the electron withdrawing nature of the tetrafluoropyrid-4-yl (TFP) substituent leads to significant amounts of carbene (**107**) generation *in situ* (**Scheme 67**). This carbene could react with another molecule of PFP to give **105·F** and fragment at the N^1 position to give **103**, or alternatively the TFP substituent can undergo migration to the C^5 position. A repeat of this reaction was undertaken at room temperature to investigate if rearrangement could be avoided, however the same outcome was observed after stirring overnight.



Scheme 66 – The addition of PFP to **86a** gave rise to the unexpected C^5-substituted species **103** in good yields alongside **104** and **105·F**. Single crystal XRD was possible upon **103**, further crystallographic information can be found in Appendix A.

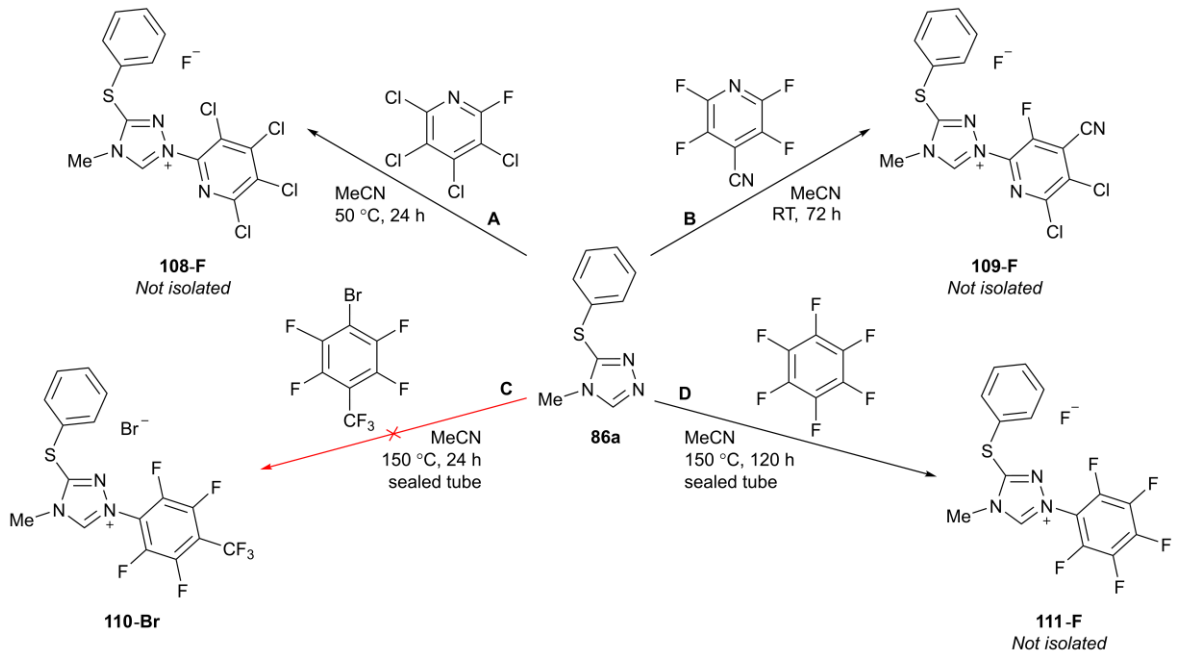


Scheme 67 – Two alternative pathways are proposed for the conversion of carbene **107** to the observed product **103**. **107** could react with another molecule of PFP (blue arrows) to give the double substituted triazolium **105·F**, which can eliminate PFP through fluoride attack to give **103**. The carbene could also react with the PFP substituent on N^1 (red arrows) to give a trigonal intermediate that irreversibly undergoes ring opening to **103**.

Less reactive halogenated aryl rings were explored for which the rearrangement reaction is less likely. Using 2-fluorotetrachloropyridine, addition of the tetrachloropyrid-2-yl group to **86a** was attempted (**Scheme 68A**). The promoted reaction at the *ortho*-position over the *para*-position observed for PFP, coupled with the use of less electronegative halogen substituents, was hoped to limit further reactivity of **108·F**. Product formation was observed in trace amounts by LC-MS and HRMS, however purification was not possible using RP-LC. A repeat of this reaction heated the reaction mixture to 150 °C for 24 h in a sealed tube, however a highly impure mixture containing small amounts of **108·F** was observed by LC-MS.

Ortho-substitution is also promoted with 2,3,5,6-tetrafluoro-4-pyridinecarbonitrile (**Scheme 68B**). Traces of *m/z* corresponding to **109·F** were observed by LC-MS, but this species could not be isolated by RP-LC. A repeat of this reaction investigated the use of a sealed tube, heating the reaction to 150 °C for 24 h, however an impure mixture was observed which could not be separated by RP-LC.

The trifluoromethyl group of 4-bromo-2,3,5,6-tetrafluorobenzotrifluoride, like the nitrogen of pyridine, can facilitate *ortho*-substitution. Reaction of this species with **86a** (**Scheme 68C**) however shows a low purity mixture by LC-MS, with no sign of **110·Br** *m/z* or the product arising from substitution of fluoride. ^{1}H and ^{19}F NMR also indicate that the reaction does not occur, with starting material peaks observed alongside peaks indistinguishable from the baseline noise.



Scheme 68 – Overview for the attempted addition of polyhalogenated pyrid-2-yl and aryl substituents to **86a**. **A** – 2-fluorotetrachloropyridine. **B** – 2,3,5,6-tetrafluoro-4-pyridinecarbonitrile. **C** – 4-bromo-2,3,5,6-tetrafluorobenzotrifluoride. **D** – hexafluorobenzene.

The reaction of hexafluorobenzene with **86a** (**Scheme 68D**) required prolonged heating, however slow product formation was evidenced by LC-MS and HRMS. LC-MS also showed no formation of byproducts, and thus was seen as an interesting reaction to explore further. ^{1}H and ^{19}F NMR analysis of the crude reaction mixture however shows no evidence of **111**·**F**. A repeat of this reaction explored the addition of CuI, heating at 135 °C under Ar for 24 h. **111**·**F** formation was once again observed with LC-MS suggesting greater levels of conversion than without copper catalyst, however product purification was not possible using RP-LC.

2.4.2.3 – Exploration of the scope of S-triazolium synthesis by alkylation

The scope of *S*-triazolium synthesis using Me_3OBF_4 was explored with the *S*-triazoles synthesized within this work. As expected, small scale investigations with **86m** confirm that methylation occurred also on the carboxylic acid group forming a mixture (4 peaks observed by LC-MS proposed to arise from both *S*-triazolium regioisomers of the carboxylate and methyl ester, alongside starting triazole). The complex mixture could not be purified. Methylation of ethenyl-conjugated *S*-triazole **91** was attempted, however only trace amounts of the triazolium salts **112**·$\mathbf{BF_4}$ and **113**·$\mathbf{BF_4}$ were observed.

The low yielding isolation of the *S*-triazolium isomers by preferential crystallisation was not widely applicable; the technique was ineffective in isolating **92d**·$\mathbf{BF_4}$ and **92e**·$\mathbf{BF_4}$, the two analogues initially explored. Alternative purification techniques were necessary to increase isolated yields and enable isolation of the N^2-methylated isomer to quantify alkylation selectivity. Access to RP-LC later in the project drastically improved the effectiveness of purification. **Figure 28** shows an example column absorbance trace obtained in the purification of **92l**·$\mathbf{BF_4}$ using 5 to 100% v/v MeOH in H_2O.

In all cases in this work, the N^2-methylated isomer elutes first from the reverse phase column. A standard procedure was developed for the isolation of *S*-triazolium salts, which enabled isolation of the two regioisomers plus residual starting material in all cases – this is detailed in **Table 11**.

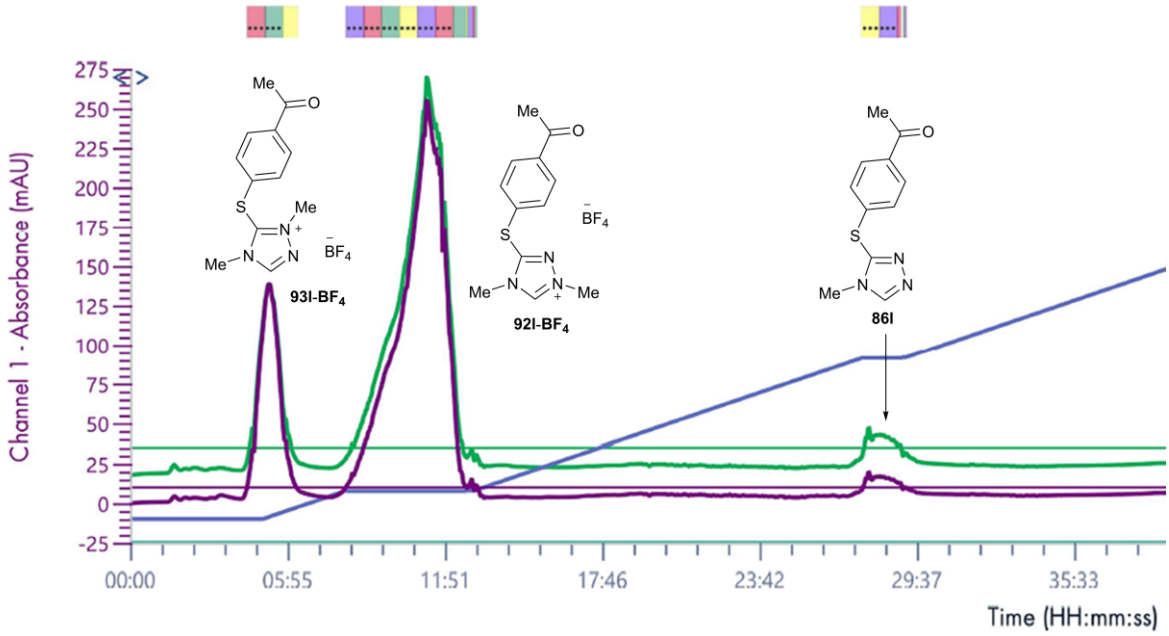


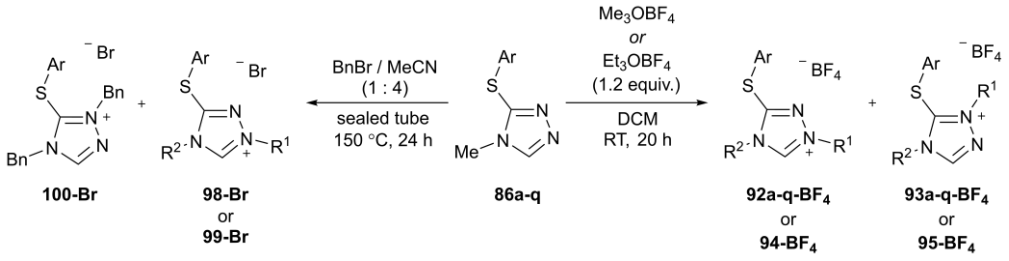
Figure 28 – RP-LC absorbance trace obtained in the purification of **92l·BF₄**, with structures shown of the compounds corresponding to each absorbance peak. The thick purple line shows absorbance at 254 nm, which was used to determine the threshold for fraction collection (thin purple line, 10 mAU). The green line is the averaged absorbance across the region 200 – 400 nm, and is scaled to match the absorbance at 254 nm (actual averaged absorbance values are lower than shown on vertical scale). The blue line shows the increase in percentage MeOH within the eluent, starting at 5% v/v MeOH in H_2O. **92l·BF₄** elutes at 11% v/v MeOH and **86l** at 39% v/v MeOH in H_2O. For clarity, the absorbance trace is cropped to show the region of interest.

Table 11 – Standard procedures for the purification of *S*-triazolium salts using RP-LC. Purification undertaken with Puriflash PF-50SIHC columns on a Puriflash PF-XS-520 system. To ensure effective separation, following manufacturers guidance, column loading was kept at 5% by weight of crude material (600 mg for 12 g column and 1250 mg for 25 g column).

Column size (g)	Flow rate (mL / min)	Time (min)	% v/v MeOH	% v/v H_2O
12	15	0	5	95
		5	5	95
		60	100	0
25	15	0	5	95
		10	5	95
		60	100	0

Table 12 summarises the series of *S*-triazolium salts that were isolated in this work using trialkyloxonium salts or benzyl bromide. Note the large improvement in yield of **92a·BF₄** (11% to 82%) with the use of RP-LC.

Table 12 – Summary of the *S*-triazolium salts synthesized during this work. TFP = tetrafluoropyrid-4-yl.



R^1	R^2	Ar	Starting material	Yield (%)		Ratio 1,4-triazolium : 2,4-triazolium
				1,4-triazolium	2,4-triazolium	
Me	Me	Ph	**86a**	**92a·BF$_4$**, 82	**93a·BF$_4$**, 4	95 : 5
Me	Me	*p*-Me-C$_6$H$_4$	**86b**	**92b·BF$_4$**, 47	**93b·BF$_4$**, 3	94 : 6
Me	Me	*p*-^{t}Bu-C$_6$H$_4$	**86c**	**92c·BF$_4$**, 35	**93c·BF$_4$**, - [a]	-
Me	Me	*p*-OMe-C$_6$H$_4$	**86d**	**92d·BF$_4$**, 80	**93d·BF$_4$**, 10	89 : 11
Me	Me	*p*-NO$_2$-C$_6$H$_4$	**86e**	**92e·BF$_4$**, 77	**93e·BF$_4$**, 5	94 : 6
Me	Me	*p*-CN-C$_6$H$_4$	**86f**	**92f·BF$_4$**, 23	**93f·BF$_4$**, 5	82 : 18
Me	Me	*p*-Br-C$_6$H$_4$	**86h**	**92h·BF$_4$**, 51	**93h·BF$_4$**, 1	98 : 2
Me	Me	*p*-I-C$_6$H$_4$	**86i**	**92i·BF$_4$**, 55	**93i·BF$_4$**, 4	93 : 7
Me	Me	*p*-COH-C$_6$H$_4$	**86j**	**92j·BF$_4$**, - [a]	**93j·BF$_4$**, - [a]	-
Me	Me	*p*-COMe-C$_6$H$_4$	**86l**	**92l·BF$_4$**, 68	**93l·BF$_4$**, 9	88 : 12
Me	Me	*p*-COOH-C$_6$H$_4$	**86m**	- [b]	- [b]	-
Me	Me	*p*-COOMe-C$_6$H$_4$	**86n**	**92n·BF$_4$**, 63	**93n·BF$_4$**, - [a]	-
Me	Me	2,6-Me-C$_6$H$_4$	**86o**	**92o·BF$_4$**, 44	**93o·BF$_4$**, 35	56 : 44
Me	Me	Pyrid-2-yl	**86p**	**92p·BF$_4$**, - [a]	**93p·BF$_4$**, - [c]	-
Me	Me	TFP	**86q**	**92q·BF$_4$**, 53	**93q·BF$_4$**, 1	98 : 2
Me	Me	CH=CH-(*p*-Br-C$_6$H$_4$)	**91**	**112·BF$_4$**, - [a]	**113·BF$_4$**, - [a]	-
Et	Me	Ph	**86a**	**94·BF$_4$**, 51[d]	**95·BF$_4$**, - [c]	-
Et	Et[e]	Ph	**86a**	**96·BF$_4$**, - [a]	**97·BF$_4$**, - [c]	-
Bn	Me	Ph	**86a**	**98·Br**, 5	- [a]	-
Bn	Bn[e]	Ph	**86a**	**99·Br**, 31	**100·Br**, 27	53 : 47
TFP	Me	Ph	**86a**	**106·F**, - [f]	- [g]	-

[a] Compound observed by LC-MS and ^{1}H NMR in trace amounts, not isolated. [b] Preferential methylation of acid group, target *S*-triazolium salt not isolated. [c] Product not observed in appreciable amounts to verify by ^{1}H NMR. [d] Yield obtained with the use of 1 equivalent Et_3OBF_4. [e] N^4 methyl group exchanged by alkylating agent. [f] Product proposed to rearrange following formation to C^5-substituted triazole, discussed earlier. [g] Species not observed.

With isolation of both regioisomers in the majority of cases, selectivity of the triazolium formation can be investigated – selectivities of 80% or greater can be achieved in the methylation of *S*-triazoles

bearing *para*-aryl substitution. The introduction of bulky *ortho*-substituents upon Ar leads to no selectivity in methylation, proposed to be due to the aryl orienting itself away from N^2 making the methylation of either position equally possible (considering steric effects only). No clear selectivity is also observed in the formation of dibenzylated *S*-triazolium salts, proposed to be a result of the forcing conditions used to undertake the reaction.

S-triazolium salts were fully characterised by NMR spectroscopy and mass spectrometry in all cases. In the majority of cases single crystal XRD analysis was also possible for the obtained 1,4-dialkyl triazolium salts (**Figure 29**).

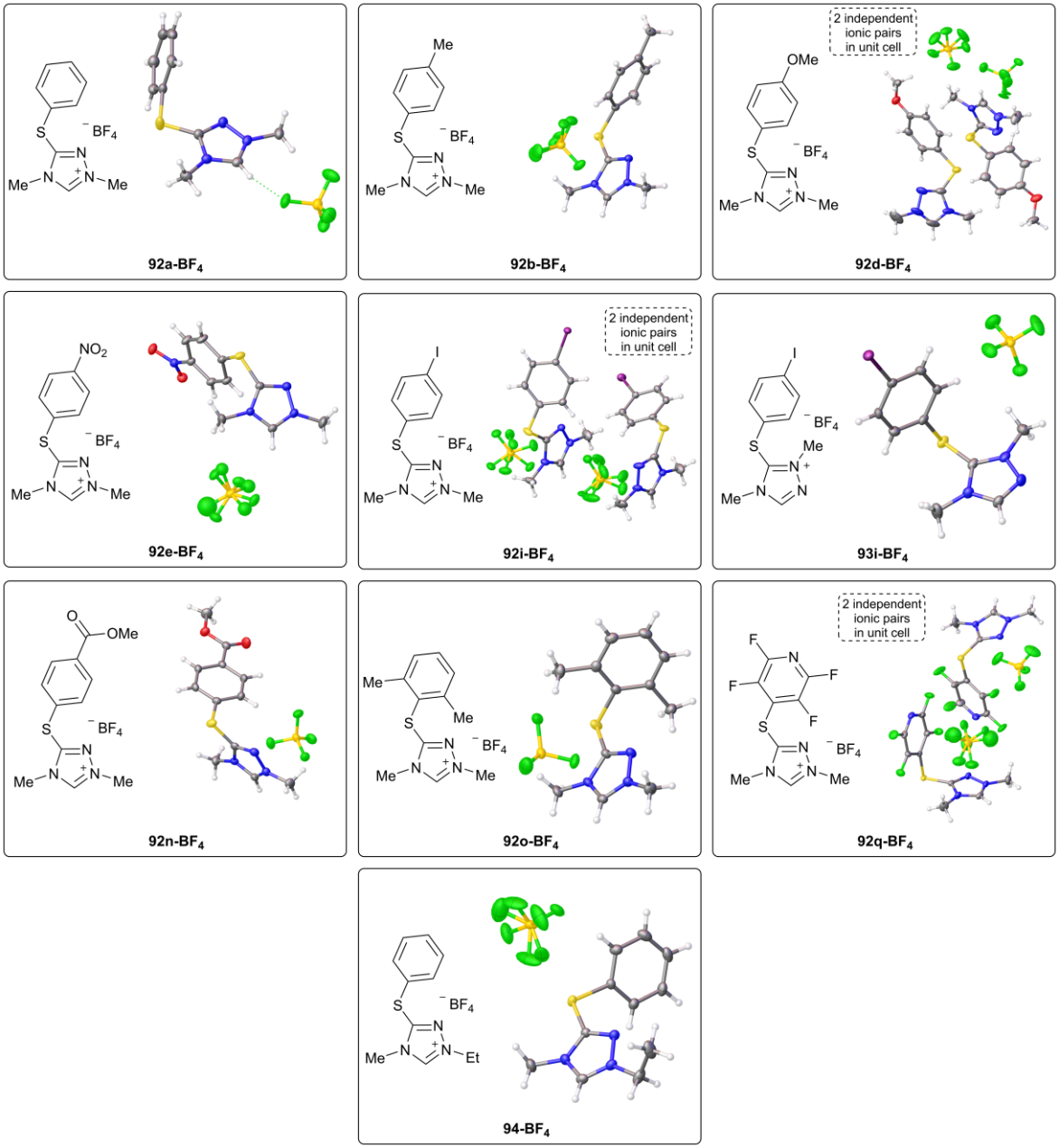


Figure 29 – The ten *S*-triazolium crystal structures obtained by single-crystal XRD. Detailed crystallographic information can be found in Appendix A.

Obtaining single crystals of 1,2-dialkyl triazolium salts was more challenging, with **93i·BF$_4$** being the only analogue analysed by XRD. Suitable crystals were formed by slow evaporation of the acetonitrile/water azeotropic mixture from an aliquot of the RP-LC effluent identified as the *S*-triazolium by LC-MS. Detailed crystallographic information can be found in Appendix A. A selection of key bond lengths, bond angles and dihedral angles are given in **Table 13** and **Table 14** based on the general structure provided and with C^9 being identified as the *ortho*-carbon closest to the plane of the triazolium ring. Consideration of C^9 as the *ortho*-position upon the aryl ring closest to N^2, as was used in the XRD analysis of *S*-triazoles, gives reduced quality fitting to a linear relationship against rate constants for H/D-exchange at the C^5 position (see Chapter 5). The poor fitting relates to an approximately 180° rotation about the N^2-C^3-S^6-C^7 dihedral in some crystal structures, to place the aryl ring close to the alkyl substituent upon N^4 (**Scheme 69**).

Data relating to *para*-substituted 1,4-dimethyl *S*-triazolium salts was plotted against values of σ_p taken from literature.[164] The data generally shows poorer fits than that seen with *S*-triazoles and Nitron analogues, indicating a high degree of conformational freedom in the crystal state. For this reason, XRD structural analysis will be not be explored in the same detail. D(C^3-S^6-C^7-C^9) shows by far the best linear trend (R^2 = 0.848), after omitting one of the crystallographically independent molecules in the XRD data for **92i·BF$_4$**. This omission is based on the datapoint lying significantly beyond the 95% confidence margins from the linear regression fit to the rest of the dataset. The plot of D(C^3-S^6-C^7-C^9) against σ_p shows a positive linear trend, with the dihedral becoming less negative (closer to planarity) as σ_p becomes more positive (**Figure 30**). Such an observation indicates that increasing electron withdrawal by the *para*-substituent upon the aryl ring leads to increased planarity of the triazolyl and aryl rings. This can be explained by the increased donation of non-bonding electrons from sulfur to give increased bond order and a more planar structure. The same trend was observed for *S*-triazoles, however the dihedral was becoming less positive given that all the dihedral angles were taken as positive values in the analysis.

Unlike Nitron analogues and *S*-triazoles, the *S*-triazolium salts analysed within this project have been investigated to obtain rate constants regarding H/D-exchange at the C^5 position. For this reason more detailed structure activity relationships can also be undertaken *versus* second order rate constants for proton transfer. Structure activity relationships are discussed in Chapter 5.

Table 13 – Selected bond lengths, bond angles and dihedral angles of the *S*-triazolium salts **92a**·BF_4 to **92i**·BF_4 analysed by single-crystal XRD.

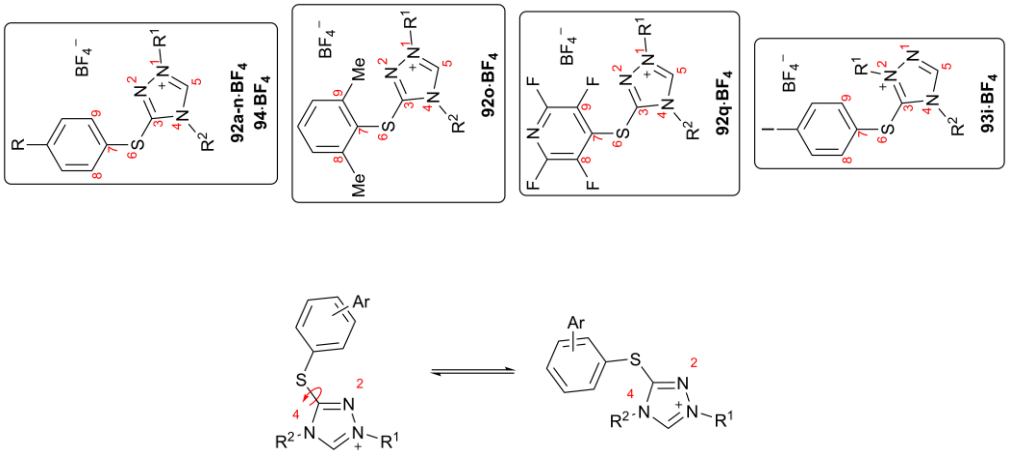
Compound	**92a**·BF_4	**92b**·BF_4	**92d**·BF_4 [a]	**92e**·BF_4	**92i**·BF_4 [a]
L(N^1-C^5) (Å)	1.313 (± 0.002)	1.314 (± 0.002)	1.306 (± 0.004) 1.301 (± 0.003)	1.313 (± 0.002)	1.307 (± 0.003) 1.307 (± 0.002)
L(N^4-C^5) (Å)	1.335 (± 0.002)	1.334 (± 0.002)	1.333 (± 0.004) 1.332 (± 0.003)	1.332 (± 0.002)	1.327 (± 0.002) 1.334 (± 0.002)
L(N^2-C^3) (Å)	1.314 (± 0.002)	1.312 (± 0.002)	1.308 (± 0.004) 1.311 (± 0.003)	1.308 (± 0.002)	1.304 (± 0.002) 1.305 (± 0.002)
L(C^3-S^6) (Å)	1.736 (± 0.001)	1.739 (± 0.002)	1.742 (± 0.003) 1.740 (± 0.002)	1.740 (± 0.001)	1.740 (± 0.002) 1.744 (± 0.002)
L(N^1-R^1) (Å)	1.459 (± 0.002)	1.458 (± 0.002)	1.468 (± 0.005) 1.472 (± 0.004)	1.460 (± 0.002)	1.458 (± 0.003) 1.452 (± 0.003)
L(N^4-R^2) (Å)	1.465 (± 0.002)	1.467 (± 0.002)	1.460 (± 0.004) 1.465 (± 0.003)	1.465 (± 0.002)	1.462 (± 0.003) 1.461 (± 0.002)
A(N^1-C^5-N^4) (°)	107.4 (± 0.1)	107.3 (± 0.1)	107.3 (± 0.3) 107.7 (± 0.2)	107.3 (± 0.1)	107.3 (± 0.2) 107.1 (± 0.1)
A(C^3-S^6-C^7) (°)	101.4 (± 0.1)	101.4 (± 0.1)	100.7 (± 0.1) 99.9 (± 0.1)	102.2 (± 0.1)	100.1 (± 0.1) 101.2 (± 0.1)
D(N^2-C^3-S^6-C^7) (°)	−8.6 (± 0.2)	−18.8 (± 0.2)	−11.9 (± 0.3) −7.6 (± 0.3)	+104.8 (± 0.1)	−112.8 (± 0.2) −11.2 (± 0.2)
D(C^3-S^6-C^7-C^9) (°)	−78.2 (± 0.1)	−64.1 (± 0.1)	−70.2 (± 0.2) −69.2 (± 0.2)	−6.5 (± 0.2)	+39.0 (± 0.2) −58.7 (± 0.1)

[a] Two independent ionic pairs within unit cell, values for both reported.

Table 14 – Selected bond lengths, bond angles and dihedral angles of the *S*-triazolium salts **93i·BF$_4$** to **94·BF$_4$** analysed by single-crystal XRD.

Compound	**93i·BF$_4$**	**92n·BF$_4$**	**92o·BF$_4$**	**92q·BF$_4$** [a]	**94·BF$_4$**
L(N^1-C^5) (Å)	1.304 (± 0.009)	1.304 (± 0.004)	1.308 (± 0.002)	1.312 (± 0.003) 1.307 (± 0.004)	1.306 (± 0.003)
L(N^4-C^5) (Å)	1.341 (± 0.009)	1.331 (± 0.004)	1.333 (± 0.002)	1.333 (± 0.004) 1.327 (± 0.004)	1.338 (± 0.003)
L(N^2-C^3) (Å)	1.318 (± 0.009)	1.304 (± 0.004)	1.316 (± 0.002)	1.309 (± 0.003) 1.310 (± 0.004)	1.311 (± 0.003)
L(C^3-S^6) (Å)	1.746 (± 0.007)	1.744 (± 0.003)	1.736 (± 0.001)	1.753 (± 0.003) 1.753 (± 0.003)	1.737 (± 0.002)
L(N^1-R^1) (Å)	1.466 (± 0.009) [a]	1.472 (± 0.004)	1.458 (± 0.002)	1.454 (± 0.004) 1.463 (± 0.004)	1.471 (± 0.003)
L(N^4-R^2) (Å)	1.473 (± 0.010)	1.460 (± 0.004)	1.465 (± 0.002)	1.467 (± 0.003) 1.463 (± 0.005)	1.467 (± 0.003)
A(N^1-C^5-N^4) (°)	112.0 (± 0.6)	107.6 (± 0.2)	107.7 (± 0.1)	107.2 (± 0.3) 107.2 (± 0.2)	107.3 (± 0.2)
A(C^3-S^6-C^7) (°)	100.0 (± 0.4)	100.0 (± 0.1)	99.3 (± 0.1)	98.1 (± 0.1) 98.3 (± 0.1)	101.5 (± 0.1)
D(N^2-C^3-S^6-C^7) (°)	−101.4 (± 0.8)	+117.4 (± 0.2)	−23.9 (± 0.1)	−92.6 (± 0.2) −93.0 (± 0.2)	+24.9 (± 0.2)
D(C^3-S^6-C^7-C^9) (°)	−97.7 (± 0.5)	−33.9 (± 0.3)	-100.5 (± 0.1)	+89.3 (± 0.3) +79.9 (± 0.2)	−126.2 (± 0.2)

[a] Two independent ionic pairs within unit cell, values for both reported. [b] L(N^2-R^1) quoted.



Scheme 69 – C-S bond rotation leads to roughly two conformations of the *S*-triazolium scaffold within the crystal lattice, where the aryl ring either arranges close to the N^2 or N^4-R^2 position.

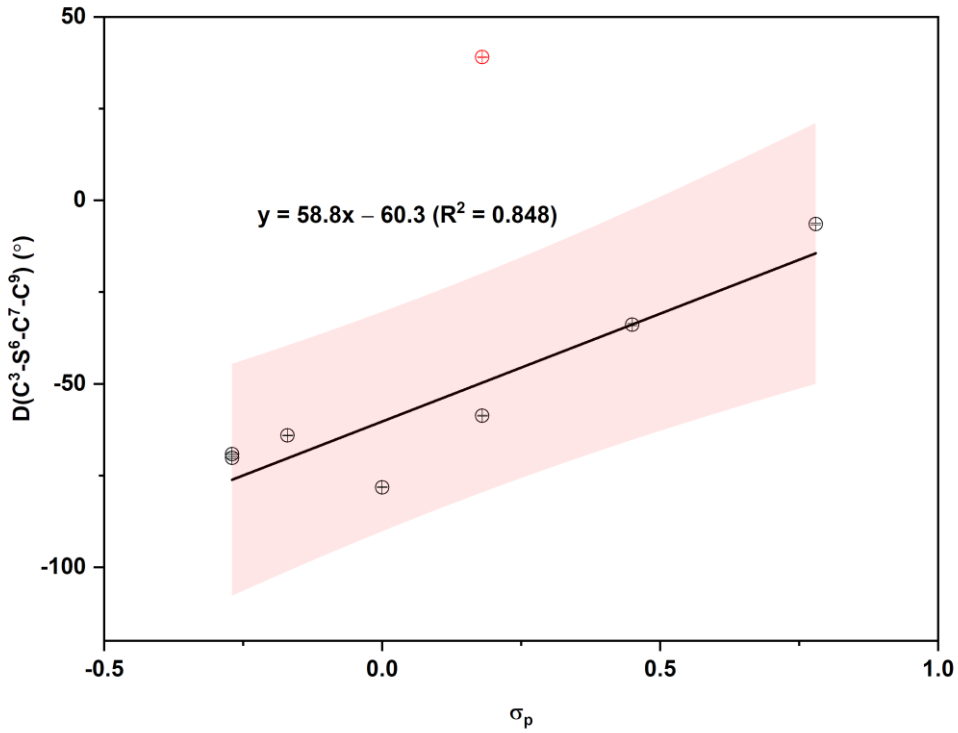
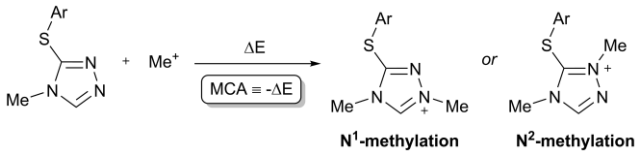


Figure 30 – Graph showing the trend between $D(C^3\text{-}S^6\text{-}C^7\text{-}C^9)$ and σ_p. The area in pink indicates the 95% confidence interval for the linear fitting to the data. The data point shown in red relates to one of the crystallographically independent molecules with the single crystal XRD data of **92i·BF₄** and is deemed anomalous, given it exists significantly above the 95% confidence interval, so is not included within the fit. Inclusion in the fit reduces R^2 to 0.354.

2.4.2.4 – Computational analysis of S-triazole methylation

The observed selectivity in the alkylation of *S*-triazoles was explored computationally using the 'Estimating Nucleophilicity and Electrophilicity' (EsNuEl) web application, developed by Jensen *et al.*[185] The application automatically identifies nucleophilic sites on the input structure by calculating methyl cation affinities (MCAs) (**Scheme 70**). Calculations start with a conformational search of the input structure, followed by r^2SCAN-3c SMD(DMSO) single-point calculations to determine the energy change upon addition of the methyl cation. Electrophilicity is determined by the platform in a analogous method considering methyl anion affinity.



Scheme 70 – Determination of methyl cation affinity, calculated in this work by the EsNuEl application.

Table 15 summarises the results of these calculations based on the process shown. Larger MCA values indicate methylation reactions that are more thermodynamically favourable. As expected, the introduction of electron-donating groups (e.g. *p*-OMe, **86d**) increases the nucleophilicity of the 1,2,4-triazole nitrogens making the methylation process more favourable, whilst electron withdrawing

groups (e.g. *p*-NO_2, **86e**) give lower MCA values (**Figure 31**). In all cases the calculations suggest N^1-methylation is favourable (considering ΔMCA), mirroring the experimentally observed results. However, the difference is very small for the pyrid-2-yl analogue **86p**. This is proposed to be a result of N^2-methylation being promoted by the pyrid-2-yl substituent given the increase in MCA. The pyridyl nitrogen could donate electron density into one of the sigma antibonding orbitals of the methyl group C-H bonds, increasing electron density on the methyl group carbon and reducing the build-up of positive charge on the N^2 position of the triazolium ring through inductive effects.

Table 15 – Summary of the methyl cation affinity values obtained using the EsNuEl web application

Compound	Ar	σ_p	MCA (kJ mol^{-1})		Relative MCA (kJ mol^{-1})		Δ MCA (N^1 vs. N^2) (kJ mol^{-1})
			N^1	N^2	N^1	N^2	
86a	Ph	0	532.04	526.38	0	0	−5.66
86b	*p*-Me-C_6H_4	−0.17	533.29	528.42	+1.25	+2.04	−4.87
86c	*p*-^{t}Bu-C_6H_4	−0.20	532.95	528.00	+0.91	+1.62	−4.95
86d	*p*-OMe-C_6H_4 [a]	−0.27	534.79	529.59	+2.75	+3.21	−5.20
86e	*p*-NO_2-C_6H_4	+0.78	515.38	504.62	−16.66	−21.76	−10.76
86f	*p*-CN-C_6H_4	+0.66	526.27	518.87	−5.77	−7.51	−7.40
86g	*p*-F-C_6H_4	+0.06	528.72	520.95	−3.32	−5.43	−7.77
86h	*p*-Br-C_6H_4	+0.23	530.45	523.86	−1.59	−2.52	−6.59
86i	*p*-I-C_6H_4	+0.18	531.56	525.41	−0.48	−0.97	−6.15
86j	*p*-CF_3-C_6H_4	+0.54	522.47	513.30	−9.57	−13.08	−9.17
86k	*p*-COH-C_6H_4	+0.42	521.56	513.16	−10.48	−13.22	−8.40
86l	*p*-COMe-C_6H_4	+0.50	523.22	515.08	−8.82	−11.30	−8.14
86m	*p*-COOH-C_6H_4	+0.45	523.04	514.65	−9.00	−11.73	−8.39
86n	*p*-COOMe-C_6H_4	+0.45	523.76	515.08	−8.28	−11.3	−8.68
86o	2,6-Me-C_6H_4	- [a]	534.56	528.91	+2.52	+2.53	−5.65
86p	Pyrid-2-yl	- [a]	528.43	528.05	−3.61	+1.67	−0.38
86q	TFP	- [a]	513.52	504.55	−18.52	−21.83	−8.97

[a] not included in fitting

The data does not explain the low selectivity for the 2,6-dimethylphenyl analogue **86o** (56% N^1-methylation observed experimentally) with a ΔMCA value almost identical to the *S*-phenyl 1,2,4-triazole **86a** which shows 95% N^1 methylation. Considering all MCA values, no trend is seen when plotted against experimental yields of either isomer or difference in yield between isomers. As such, the values obtained should be treated with caution.

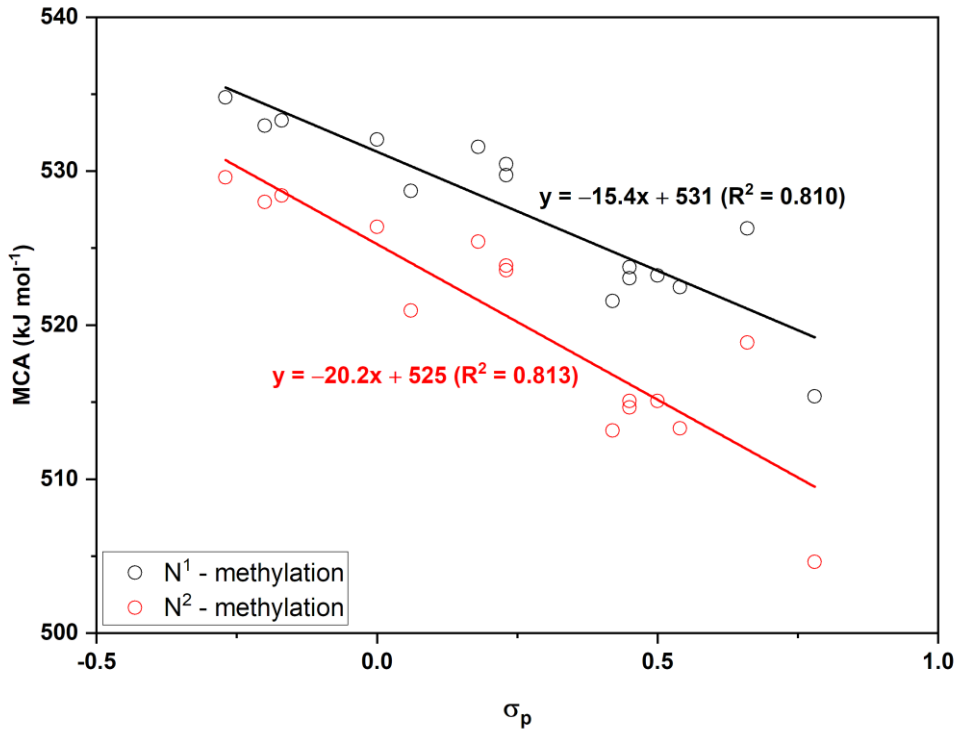


Figure 31 – Plot of MCA values against σ_p values from literature, considering *para*-substituted analogues only. The increase in σ_p (introduction of more electron withdrawing substituents is shown to correlate with decreased MCA.

In summary, the preference to undergo methylation upon N^1 over N^2 is supported by these calculations as formation of the thermodynamically favoured product. The calculations cannot describe the extent of selectivity accurately, and so calculations at a higher level of theory may be necessary to describe this. Alternatively, these results suggest the selectivity is predominantly affected by steric interactions, with the *S*-aryl substituent hindering addition at N^2. This would explain why the 2,6-dimethylphenyl analogue, with aryl ring forced out-of-plane from the triazole heterocycle, shows minimal selectivity.

2.5 – Bioconjugation of 1,2,4-triazolium salts to peptide and peptidomimetic scaffolds

This chapter section explores the conjugation of 1,2,4-triazolium salts to the *N*-terminus or R-group of amino acids, as a starting point towards incorporation into larger peptide or enzyme systems. In a parallel project, our group is interested in biocatalysis using NHC mimics of thiamine (vitamin B1). This approach could enable the bottom-up construction of triazolium-conjugated biocatalysts.

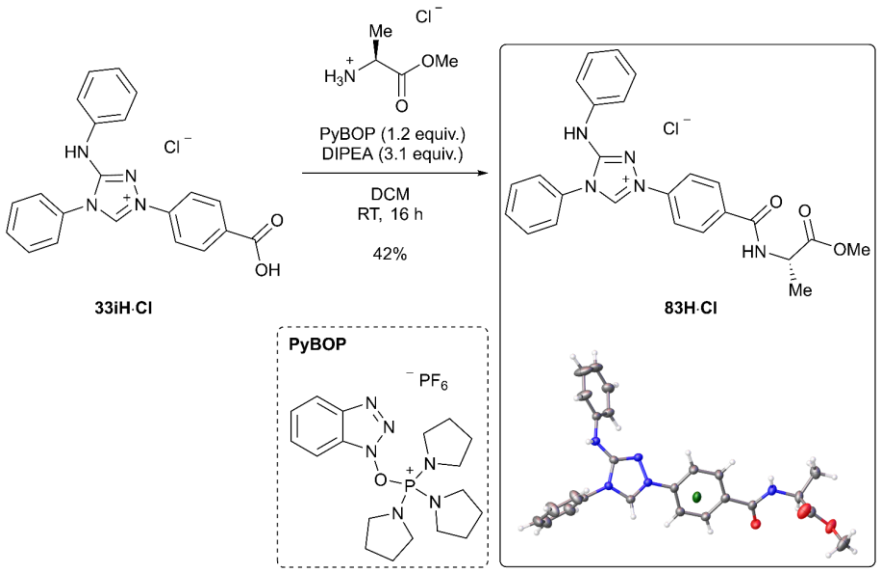
The exploration of *N*-terminus bioconjugation using carboxy-functionalised triazolium salts is described, followed by work towards the bioconjugation upon amino acid R-groups using a variety of methods.

2.5.1 – *N*-terminal bioconjugation of carboxy-functionalised triazolium salts

2.5.1.1 – Investigations into amide coupling methodologies

The carboxyl-functionalised Nitron **33iH·Cl** may be used as a nucleophilic handle by the generation of ester, thioester and amide linkages. By development of a method to generate amide bonds to amino acids, a library of bioconjugates could be generated by applying this technique to a range of applicable amino acids.

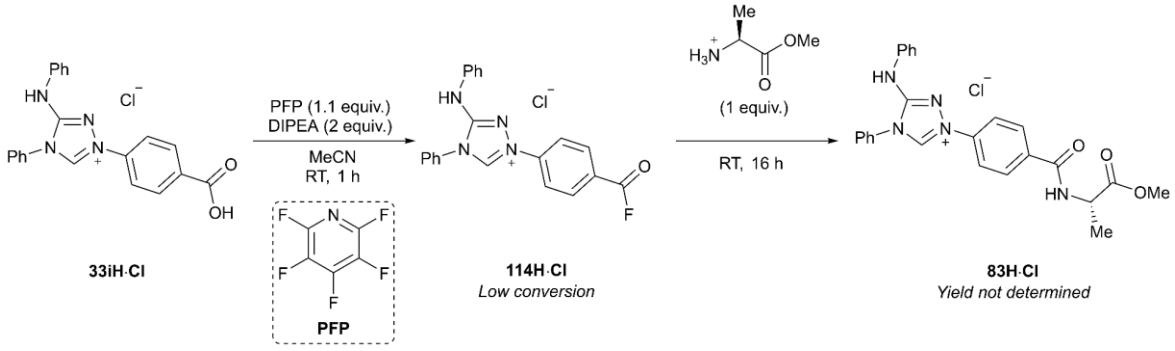
Using the amide coupling reagent PyBOP (benzotriazol-1-yloxytripyrrolidinophosphonium hexafluorophosphate), **33iH·Cl** was shown to form an amide bond to alanine methyl ester (**Scheme 71**). The product could be purified by column chromatography (0 to 10% MeOH in DCM) to obtain **83H·Cl** in 22% yield, however a yield of 42% could be obtained using RP-LC (MeOH / H_2O).



Scheme 71 – The formation of an amide bond between carboxy-functionalised Nitron **33iH·Cl** and alanine methyl ester was successfully undertaken using the amide coupling agent PyBOP. **83H·Cl** was verified by XRD, detailed crystallographic information can be found in Appendix A.

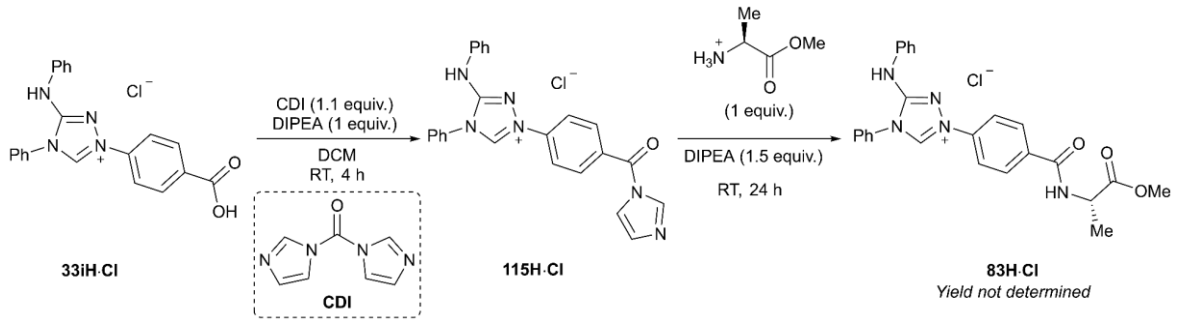
In collaboration with Katherine Deck, a 4th year MChem student under my supervision, alternative coupling strategies were explored to further improve the yield. Representative examples from the common coupling agent classes (halogenating agents, imidazoles and carbodiimides) were compared against the phosphonium salt PyBOP. Isolation of these bioconjugates is non-trivial – RP-LC of these compounds can require multiple repeats to attain pure compound and so the effectiveness of methods was determined by looking at the conversion by NMR, specifically the peak corresponding to the C^5-H position within the starting material and product.

The reaction of **33iH·Cl** with PFP, taken from the literature,[178] was shown to form the corresponding acyl fluoride **113** (**Scheme 72**). ^{19}F NMR analysis indicated low conversion from **33iH·Cl** to **114H·Cl**, with the major peaks corresponding to unreacted PFP. LC-MS analysis of the final reaction mixture shows low levels of **114H·Cl** formation and thus was not investigated further. The use of thionyl chloride in an analogous method, attempting to generate the acyl chloride, showed no product formation.



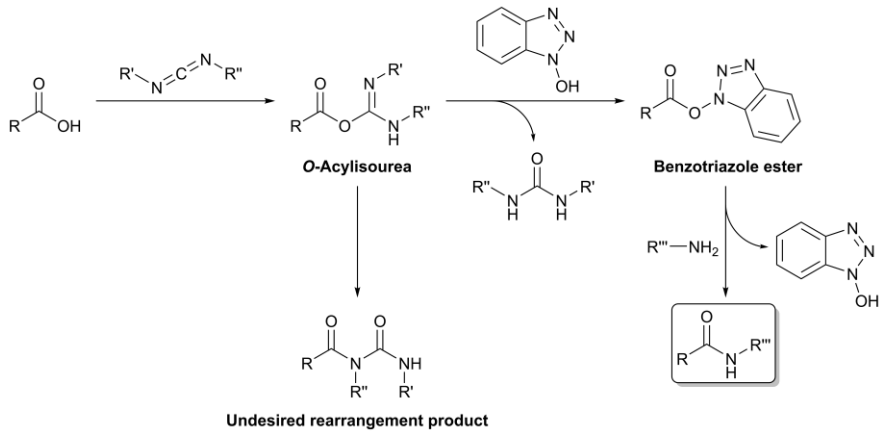
Scheme 72 – Attempted amide coupling of carboxy Nitron **33iH·Cl** to alanine methyl ester using PFP.

The reaction was then investigated using carbonyldimidazole (CDI), which should form a reactive imidazolyl amide (**115H·Cl**) that can be used to generate **83H·Cl** (**Scheme 73**). CDI was found to be the second most common amide coupling reagent used within the literature for large scale peptide synthesis.[186] A few hours after the addition of alanine to the intermediate proposed to form, a yellow solid precipitated onto the surface of the flask which was verified by LC-MS to be unreacted starting material. LC-MS analysis by Deck indicated low levels of conversion and in attempting to undertake LLE (DCM / H_2O) an emulsion formed that could not be separated even after several brine washes and attempted filtration. Independently analysing the findings of Deck, the formation of the emulsion and precipitated solid further supports that the reaction mixture contained large amounts of the zwitterionic (characteristically yellow) Nitron. The three non-polar aryl rings surrounding a polar triazolyl core may give rise to emulsifying properties and without acidification prevent the effective separation of layers in LLE.



Scheme 73 – The generation of a imidazolyl amide **115H·Cl** showed very low levels of conversion to **83H·Cl** and a persistent emulsion that made purification challenging.

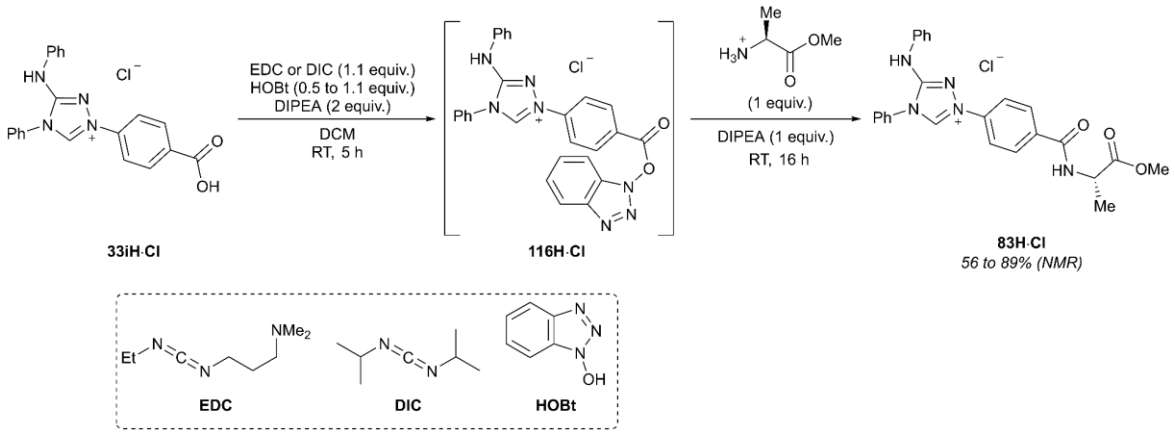
The most commonly used amide coupling reagent class for large-scale amidation reactions are the carbodiimides, of which 1-ethyl-3-(3-dimethylaminopropyl)carbodiimide (EDC), *N*,*N'*-dicyclohexylcarbodiimide (DCC) and *N*,*N'*-diisopropylcarbodiimide (DIC) are the 1st, 6th and 11th most popular coupling reagents respectively.[186] These reagents generate *O*-acylisourea intermediates that can react with amines to enable the generation of amide bonds. Additives are commonly used alongside the carbodiimide to prevent racemisation and suppress by-product formation, one of these being hydroxybenzotriazole (HOBt) that generates an activated benzotriazole ester from the *O*-acylisourea intermediate (**Scheme 74**).



Scheme 74 – General reaction pathway for coupling using a carbodiimide reagent in combination with HOBt. Carbodiimide reacts with the carboxylic acid to generate the *O*-acylisourea, which further reacts with HOBt to give the benzotriazole ester. Reaction of this activated ester with an amine allows for the formation of the desired amide. The use of HOBt to immediately react with the formed *O*-acylisourea limits or prevents the formation of the undesired rearrangement product.

EDC or DIC in combination with HOBt were explored within this work (**Scheme 75**). Use of DIC and HOBt led to a persistent emulsion during workup, and so focus moved to the use of EDC. EDC and HOBt still led to the formation of an emulsion, however it was to a lesser extent and could be separated by the use of brine. Previous reports noted significant differences in outcome between the use of catalytic and stoichiometric amounts of HOBt with EDC,[187] however within this work no significant changes were seen when increasing HOBt loading from 0.5 to 1.1 equivalents. **Table 16** summarises the NMR conversions observed for various conditions used with carbodiimide coupling;

although carbodiimide couplings give good to high levels of conversion by NMR, PyBOP coupling is the best method and is used to explore bioconjugate library synthesis. PyBOP is also preferable over carbodiimide couplings given that the formation of persistent emulsions of starting material were observed in most cases when using EDC or DIC.



Scheme 75 - The generation of amide bonds using a carbodiimide coupling reagent in combination with HOBt (giving benzotriazole ester **116H·Cl**) gave good conversion by NMR to the desired alanine bioconjugate.

Table 16 – Summary of the NMR yields obtained for the carbodiimide coupling methods tested, compared to PyBOP coupling

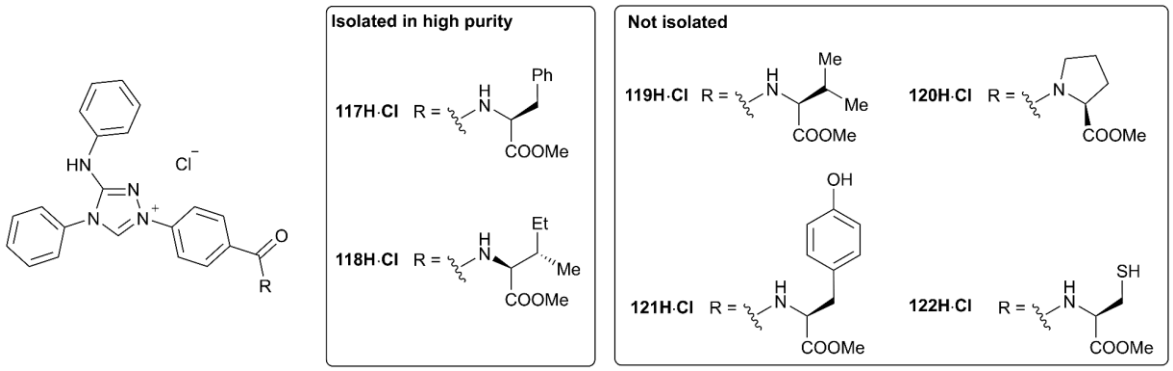
Conditions	NMR conversion (%)
EDC only	56
EDC, HOBt (1.1 equiv.)	78
EDC, HOBt (0.5 equiv.)	77
EDC, HOBt, catalytic DMF	- [a]
DIC, HOBt (1.1 equiv.)	89
PyBOP	94

[a] Not determined.

2.5.1.2 – Exploration of the scope of Nitron conjugation to amino acids

With PyBOP showing the highest conversion by NMR and no evidence of emulsion formation, the method was applied to a selection of amino acid methyl esters (**Scheme 76**). Conversion to the corresponding amide was seen by LC-MS and HRMS, however pure samples could only be obtained for the phenylalanine and isoleucine bioconjugates (**117H·Cl** and **118H·Cl**) with **119H·Cl** to **122H·Cl** impossible to isolate. Deck found that the *tris*(pyrrolidino)phosphine oxide byproduct of PyBOP coupling co-eluted with the product in most cases and attributed this to the triazolium salt forming electrostatic interactions with the phosphine oxide carbonyl group.

It should be noted that the work of Deck on synthesizing Nitron-peptide bioconjugates continued into the use of solid phase peptide methods in collaboration with Dr. William Brittain, which showed some promise for accessing bioconjugate analogues challenging to isolate by RP-LC. This work will not be discussed within this thesis.



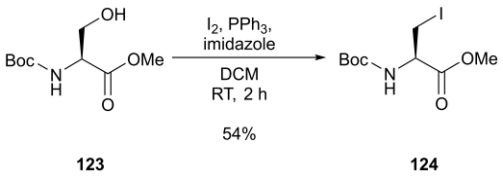
Scheme 76 – Scope of the PyBOP coupling products obtained using the method detailed in **Scheme 71**. Purification in many cases was challenging due to co-elution of the phosphine oxide byproduct of PyBOP in RP-LC purification.

2.5.2 – In-chain bioconjugation of 1,2,4-triazolium salts to amino acids

Bioconjugation methods that form a linkage to amino acid side chains enables the introduction of multiple scaffolds and will likely be of use to better mimic the complex environment of an enzyme active site. The generated unnatural amino acids could be implemented as a monomer within solid phase or solution phase peptide synthesis, enabling controlled distribution of the triazolium in the peptide. Alternatively, late-stage modification of a peptide or peptoid scaffold with a 1,2,4-triazolium may enable the modification of complex enzyme structures which cannot be synthesized due to complexity and solubility issues.[150]

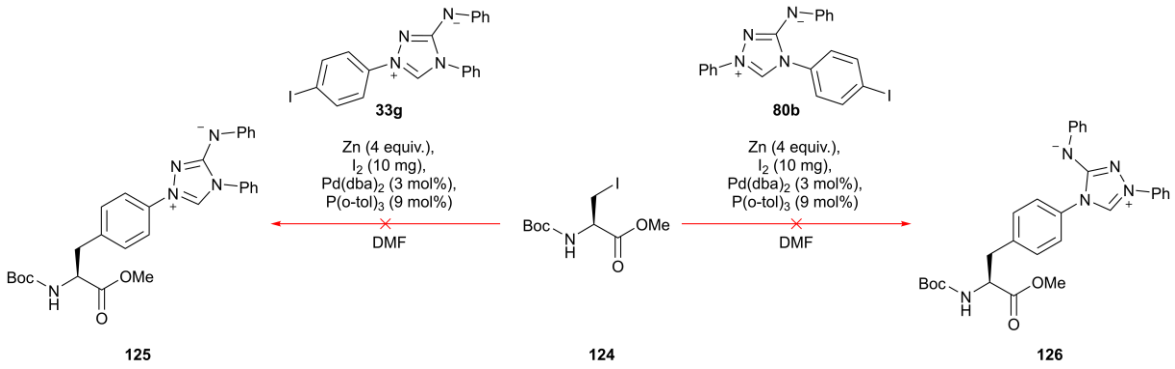
2.5.2.1 – Conjugation to alanine-based residues

The bioconjugation of 1,2,4-triazolium salts to alanine residues requires the development of a reactive analogue, and so *N*-Boc-iodoalanine methyl ester (**124**) was synthesized using the Appel reaction (**Scheme 77**). Following the method of Trost and Rudd,[188] *N*-Boc-serine methyl ester (**123**) was added to a stirring mixture of iodine, triphenylphosphine and imidazole. After 2 hours the concentrated reaction mixture could be purified using column chromatography (0 to 25% ethyl acetate in hexanes) to access the product, which could be verified by NMR. The photosensitivity of this compound required the reaction and purification to be undertaken in a darkened fume hood.



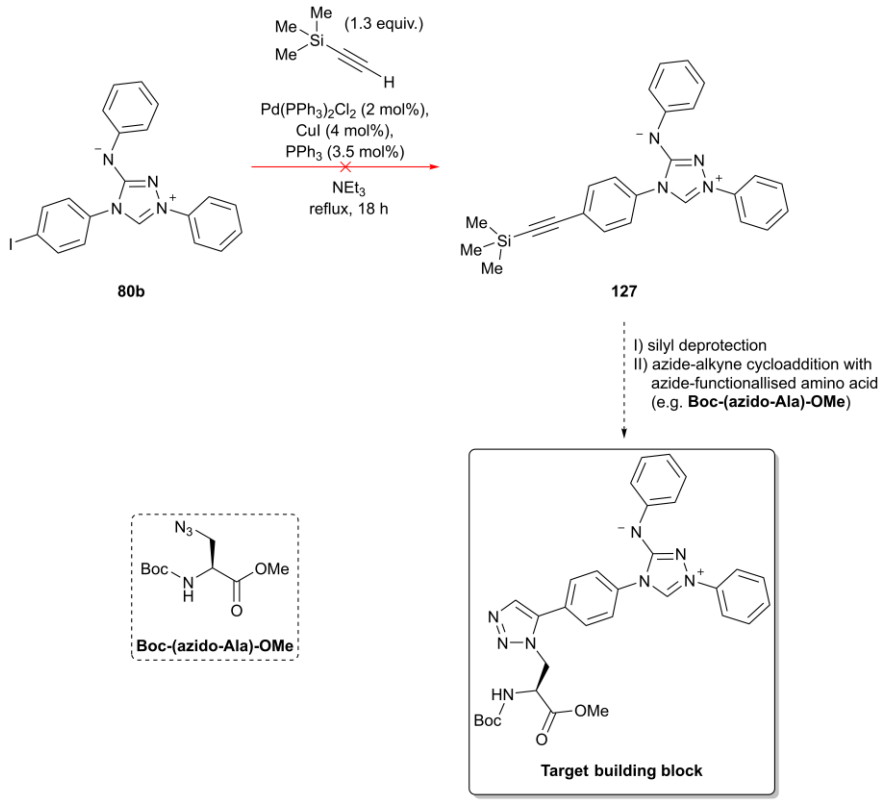
Scheme 77 – The application of the Appel reaction using iodine to gain access to protected iodoalanine **124** from protected serine **123**.

Using iodoalanine and the iodinated Nitron analogues (**33g** and **80b**), Negishi couplings were attempted (**Scheme 78**). LC-MS suggested low levels of conversion to the desired product occur, with evidence of triazolium ring opening. HRMS was unable to verify product formation for **125** and **126**, and RP-LC was unsuccessful in isolating either isomer.



Scheme 78 – Attempted Negishi coupling between iodoalanine **124** and iodinated Nitron analogues **33g** and **80b**.

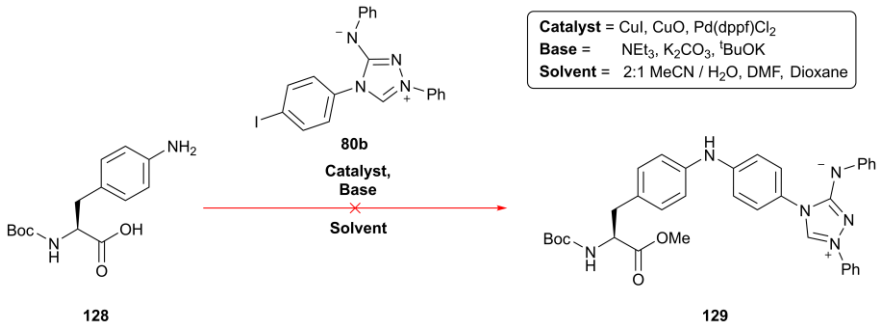
An alternative to routes proceeding *via* iodinated alanine is the generation of the corresponding azido-alanine, to allow azide-alkyne Huisgen cycloadditions[189] with alkyne-substituted triazolium salts (**Scheme 79**). The resulting building block from this cycloaddition consists of the triazolium salt attached to the amino acid side chain through a 1,2,3-triazole ring. The preparation of an alkyne-functionalised Nitron analogue was explored - Sonogashira coupling of trimethylsilylacetylene was attempted with **80b** based on the method of Brittain.[190] LC-MS showed no signs of **127** formation with evidence for the ring opening of **80b** to the corresponding triazabutadiene, analogous to observations seen in previous work within the group.[59]



Scheme 79 – Attempted Sonogashira coupling of iodinated Nitron **80b** with trimethylsilylacetylene. Evidence for the formation of **127** was not observed by LC-MS or ^{1}H NMR, with LC-MS indicating formation of the triazabutadiene derived from ring opening of **80b**. The planned next steps to an amino acid bioconjugate, if the Sonogashira coupling was successful, are also shown.

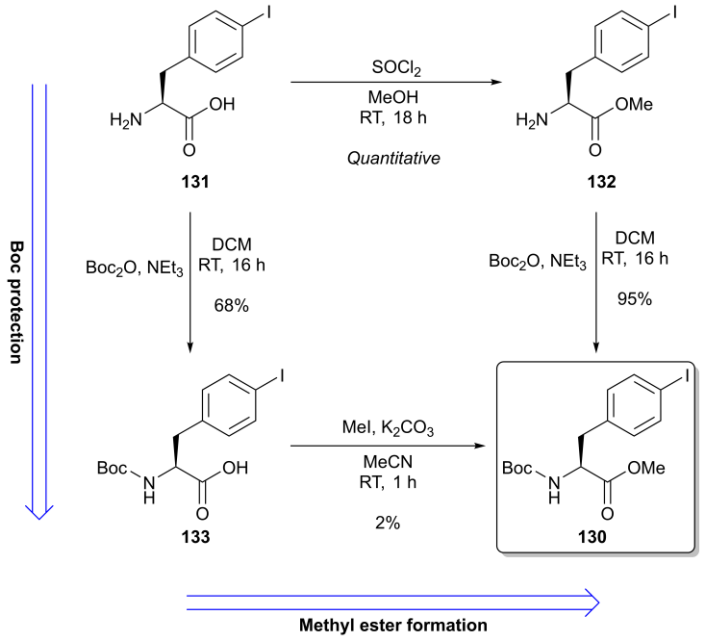
2.5.2.2 – Conjugation to phenylalanine-based residues

Using commercially available *N*-Boc-4-aminophenylalanine (**128**), conjugation of **80b** using Ullmann and Buchwald–Hartwig coupling conditions was investigated (**Scheme 80**). Using copper(I) iodide and triethylamine in 2:1 MeCN/H_2O, replicating the Ullmann coupling conditions used in *S*-triazole synthesis, no product formation was observed after 30 minutes microwave irradiation at 150 °C. A repeat at 180 °C for 2 hours showed a highly complex mixture and still no formation of **129**. Alteration of the base to potassium carbonate or potassium *tert*-butoxide led to the ring opening of **80b**, verified by HRMS. Copper(II) oxide nanoparticles were explored as an alternative catalyst, using potassium carbonate in DMF at 40 °C – no signs of product were observed. The conditions explored for Buchwald–Hartwig coupling were the use of Pd(dppf)Cl_2 and potassium *tert*-butoxide in dioxane, with microwave irradiation at 100 °C for 16 hours showing complete consumption of **128** by LC-MS; product formation was not observed.



Scheme 80 – Attempted Ullmann and Buchwald–Hartwig coupling between *N*-Boc-4-aminophenylalanine (**128**) and **80b**. No evidence for the formation of **129** was observed. Dppf = Bis(diphenylphosphino)ferrocene.

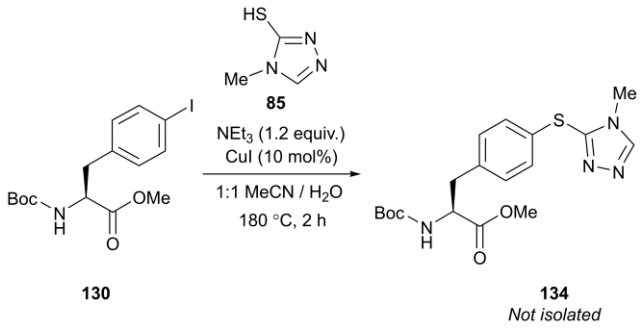
An alternative method was to use *N*-Boc-4-iodophenylalanine methyl ester (**130**) to undertake an Ullmann coupling identical to that undertaken in the synthesis of *S*-triazoles. 4-Iodophenylalanine (**131**) is commercially available, however **130** is not available. Without protecting groups it was proposed that side reactions may occur such as copper-catalysed dimerization between the amino group and iodobenzyl ring, or amide bond formation to the dipeptide species. **130** was synthesized from **131** by generation of the methyl ester **132** using thionyl chloride and subsequent Boc-protection (**Scheme 81**); undertaking the Boc-protection first (**133**) was significantly lower yielding.



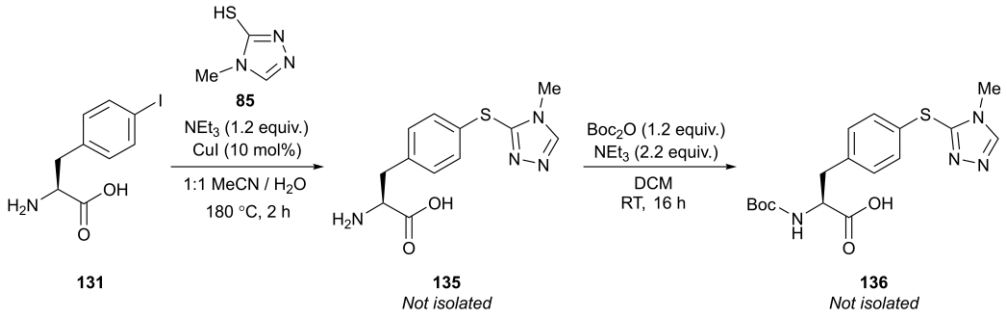
Scheme 81 – The two alternative routes to *N*-Boc-4-iodophenylalanine methyl ester (**130**).

The Ullmann coupling of **130** with 4-methyl-1,2,4-triazole-3-thiol was explored (**Scheme 82**). LC-MS showed the formation of an impure mixture containing the product, with deprotection of the amine and acid functionalities observed. Column chromatography (0 to 10% MeOH in DCM) was unsuccessful in isolating **134**, with the product and Boc-deprotected product co-eluting from the column based on ^{1}H NMR spectrophotometric analysis. A repeat of the reaction used the unprotected 4-iodophenylalanine **131** and was shown to form the product based on NMR and LC-MS evidence

(**Scheme 83**). The zwitterionic amino acid however was challenging to remove from the aqueous phase of the liquid-liquid extraction (LLE) used within the work-up, including after acidification to the hydrochloride salt. A further repeat was undertaken where the reaction mixture using **131** was concentrated and carried forward to a Boc protection without further purification. LC-MS verified formation of the intermediate **135** and then high levels of conversion to the product **136**. To remove the triethylamine present within the product, LLE with DCM and water was attempted however the same issues with aqueous solubility were observed. The aqueous and organic phases were concentrated separately, the aqueous phase by lyophilization, and purification attempted on each phase using RP-LC. Only traces of the product could be obtained from RP-LC of the aqueous and organic phase, which co-eluted with triethylamine.



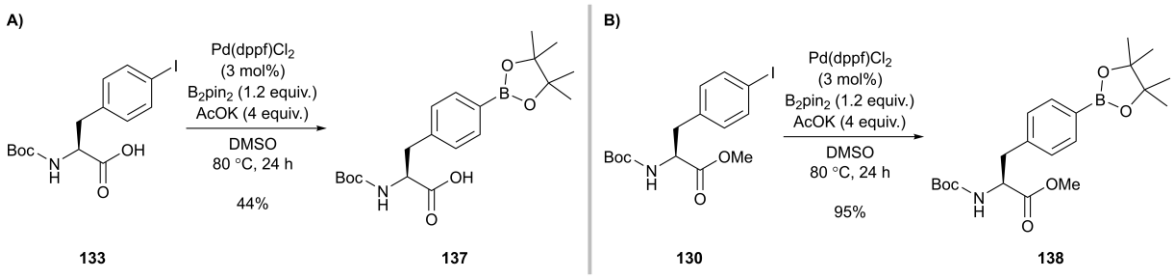
Scheme 82 – Ullmann coupling between *N*-Boc-4-iodophenylalanine methyl ester (**130**) and 4-methyl-1,2,4-triazole-3-thiol (**85**) showed the formation of **134**, however partial deprotection of the amino group led to a complex mixture that was not possible to purify.



Scheme 83 – Ullmann coupling between 4-iodophenylalanine **131** and 4-methyl-1,2,4-triazole-3-thiol **85** was successful, however attempts to isolate **135** were unsuccessful due to the high aqueous solubility. A repeat used crude **135** in the formation of the Boc-protected analogue **136**, however separation from triethylamine was unsuccessful.

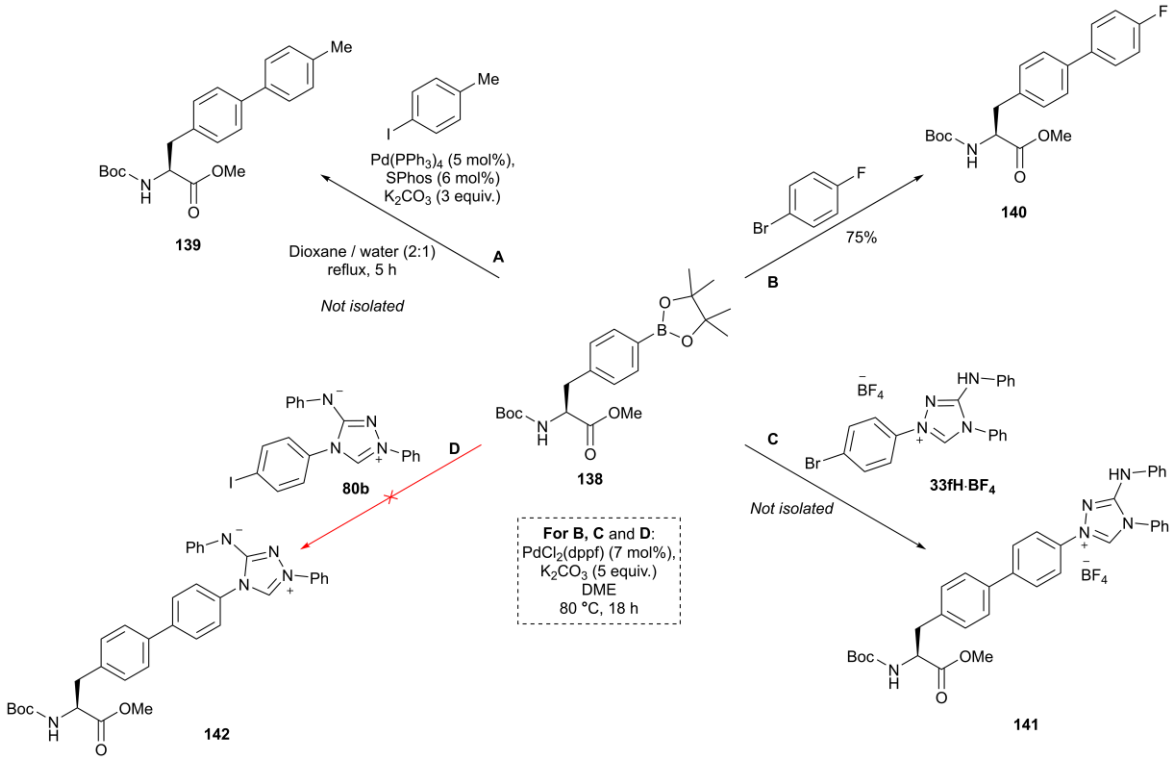
A third method of bioconjugation to phenylalanine-based residues was the Suzuki–Miyaura coupling of bromo and iodo Nitrons (**33fH·BF$_4$** and **80b**) to the boronic acid pinacol ester that can be generated from 4-iodophenylalanine. To generate the pinacol ester **137**, initial attempts used *N*-Boc 4-iodophenylalanine (**133**, **Scheme 84A**) however LC-MS indicated that only partial conversion occurred which was attributed to some of the potassium acetate base being used to deprotonate the amino acid. Column chromatography (2 to 10% MeOH in DCM) allowed isolation of **137**, however only in moderate yields. A repeat of the reaction used the methyl ester analogue **130** and achieved

much greater conversion by LC-MS (**Scheme 84B**). High yields of **138** were isolated and carried forward to the coupling with Nitron analogues.



Scheme 84 – The two attempts at generating a boronic acid pinacol ester analogue of phenylalanine for Suzuki–Miyaura coupling. **A**) using the free acid **B**) using the corresponding methyl ester.

A test coupling was initially undertaken to determine conditions to undertake the transformation. Coupling of 4-iodotoluene (**Scheme 85A**), using a procedure taken from literature,[191] suggested complete conversion by thin layer chromatography (TLC). Attempted **139** isolation using column chromatography (0 to 10% ethyl acetate in hexanes) gave only traces of impure product.



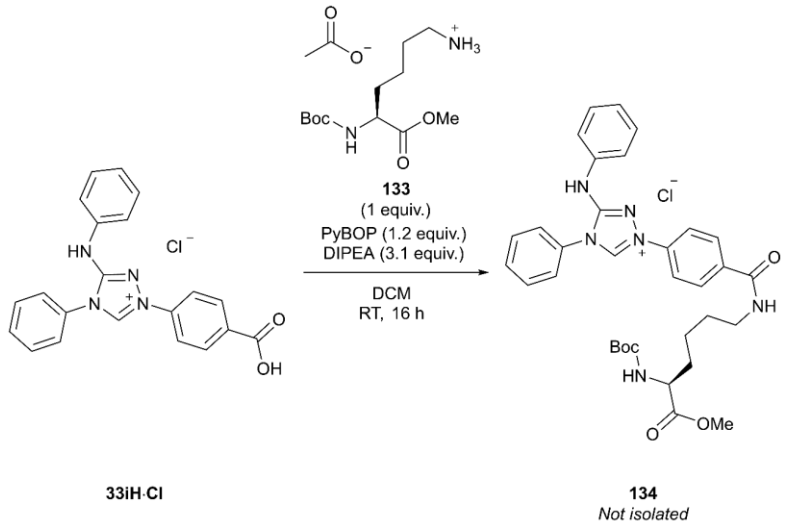
Scheme 85 – Exploration of the Suzuki–Miyaura coupling of **138**. **A** – attempts at coupling 4-iodotoluene gave only traces of impure **139**. **B** – coupling of 4-iodobenzene, with an alternative method, gave a high yield of **140**. **C** – coupling with **33fH·BF4** suggested some formation of product by LC-MS, however isolation was not possible. **D** – attempted coupling of the iodinated Nitron **80b** were unsuccessful.

Alternative conditions,[192] using $PdCl_2$(dppf), were explored for the coupling of 4-fluorobromobenzene (**Scheme 85B**). In this case the fluorinated biphenyl product **140** could be obtained in good yields with straightforward purification.

With a method discovered to undertake the coupling with phenylalanine, the coupling of brominated Nitron **33fH·BF$_4$** was explored (**Scheme 85C**). LC-MS suggested the formation of **141** *m/z*, however HRMS and NMR data did not support this finding. Attempted isolation of **141** was unsuccessful. The procedure was also attempted using the iodinated Nitron **80b** (**Scheme 85D**) however **142** formation could not be observed; NMR data showed a mixture of the two starting materials.

2.5.2.3 – Conjugation to lysine-based residues

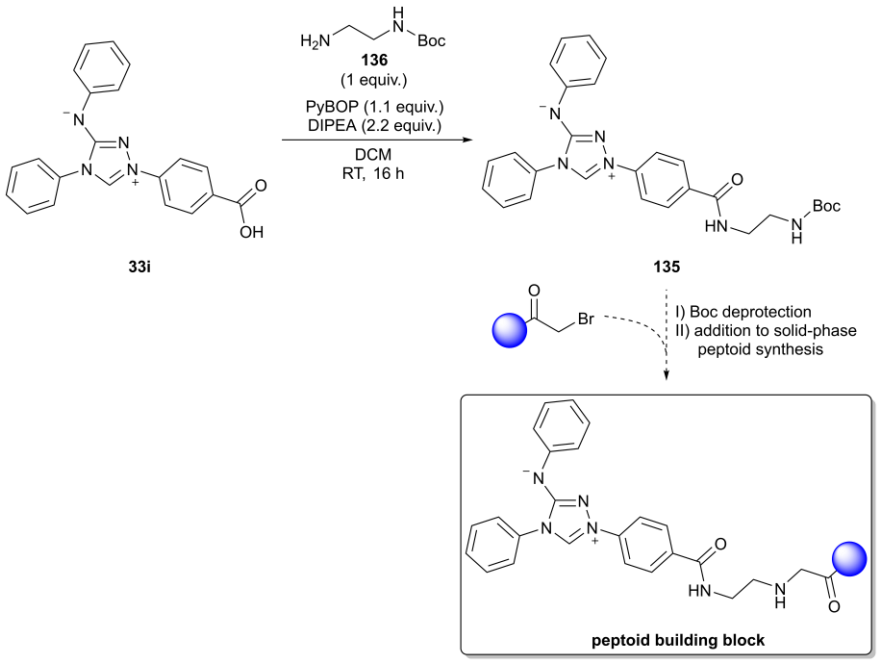
The coupling of carboxy-functionalised Nitron **33iH·Cl** to *N*-Boc lysine methyl ester (**133**) was attempted using the PyBOP coupling conditions used earlier to generate **134** (**Scheme 86**). LC-MS and HRMS verified product formation, however only partial conversion had occurred. Column chromatography (0 to 10% MeOH in DCM) was unsuccessful in isolating **134** – the product co-eluted with **133**. A repeat investigated the use of RP-LC (MeOH / H_2O) however the product could not be isolated without traces of either **133** or PyBOP-related byproducts.



Scheme 86 – Attempted PyBOP coupling of carboxy-functionalised Nitron **33iH·Cl** with lysine **133** gave traces of **134** which could not be isolated.

2.5.3 – Synthesis of peptidomimetic building blocks

By adding a diamine linker to the carboxy-functionalised Nitron **33i**, a building block would be developed that could be incorporated into peptoid scaffolds using a sub-monomer approach (**Scheme 87**). Using the PyBOP coupling conditions used for the conjugation to alanine, conjugation of carboxy-Nitron **33i** to *N*-Boc-ethylenediamine was explored. LC-MS and HRMS supported formation of **135**, however purification by column chromatography (0 to 10% MeOH in DCM) or RP-LC was unable to isolate the product.



Scheme 87 – The diamine coupled Nitron **135**, formed by PyBOP coupling of **33i** and **136**, could be observed by LC-MS but could not be isolated by column chromatography or RP-LC. The planned next steps to a peptoid building block, if isolation of **135** is possible, are also shown.

2.6 – Conclusions

A contemporary route to Nitron analogues has been presented within, showing an improved yield, tolerance of a range of functional groups, and avoidance of more hazardous reagents. An extended range of Nitron analogues have been prepared with this new route and have enabled structural analysis comparing single crystal XRD parameters to values of σ_p. The zwitterion to carbene tautomerisation has also been explored computationally to quantify the effects of substituents upon the concentration of carbene *in situ*.

A novel class of *S*-triazolium salts have been reported, synthesized by a generally high yielding Ullmann coupling followed by alkylation with either trialkyloxonium salts or benzyl bromide. The synthetic route to *S*-triazoles has been optimised in consideration of alkyl halide, solvent, base, reaction time and temperature used – 18 *S*-triazoles have then been prepared with this method. XRD structural analysis has been possible with the *S*-triazoles and trends found between structural parameters and σ_p. The observation of regioisomers in the formation of *S*-triazolium salts led to exploration of methods to differentiate these compounds with a range of analytical strategies, and then how to effectively isolate these compounds with RP-LC. 26 novel triazolium species with either 1,4- or 2,4-dialkyl substitution have been isolated, with 10 of these analogues verified by XRD.

The bioconjugation of triazolium salts to peptide and peptidomimetic scaffolds has been explored, and whilst successful isolation has been limited to three examples (**83H·Cl**, **117H·Cl** and **118H·Cl**) evidence has shown the ability to form a range of other bioconjugates by various methods *in situ*. The methods of undertaking *N*-terminal bioconjugation have been surveyed, with PyBOP coupling the most promising based on conversion levels and ease of handling. Purification challenges by RP-LC, considering *N*-terminal and R group bioconjugation, have however limited work within this area. Hopefully future work can address this issue and enable the exploration of mimicking enzymatic systems with the NHCs that can be generated from these triazolium salts.

3 – Synthesis and reactions of Blatter radicals

3.0 – Foreword

There has been no further exploration of the rearrangement of Nitron (**33a**) to Blatter-type radical (**37a**) since our original report,[59] yet this class of radicals is growing in interest particularly within the fields of materials chemistry – liquid crystalline photoconductors,[193-198] spintronics,[199-201] and organic batteries.[202, 203] The C(3)-N substitution of the 1,2,4-benzotriazinyl radical scaffold accessible by this method is difficult to obtain using other synthetic methodologies in the literature, and is also the same as that seen within the benzotriazinyl radical implicated in the mode of action of TPZ.[33, 204]

Using the expanded range of Nitron analogues available from the more contemporary Nitron synthesis, more detailed investigations can take place relating to the conversion of Nitron to Blatter radical (Section 3.3 for synthesis, and Section 3.3.3 for mechanism). The ability to further modify the radical scaffold is then explored to enable access to additional Blatter radicals (Section 3.4). Initial investigations of several synthetic applications of Blatter radicals will also be pursued within this work (Section 3.5). This chapter ends by considering the bioconjugation of Blatter radicals as either spin probes or anticancer agents (Section 3.6).

3.1 – Chapter contributions

The work presented in this chapter was undertaken in collaboration with the individuals listed below, with their contributions to this work noted. All other work detailed in this chapter was undertaken by the present author.

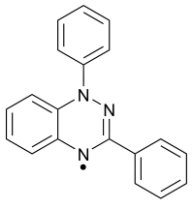
Katherine Deck (former O'Donoghue group 4th year MChem student): investigations into the conversion of Nitron bioconjugates into Blatter radicals; late-stage bioconjugation of Blatter radicals to amino acids.

Jacob Murray (former O'Donoghue group PhD student): synthesis of 8 novel Blatter radicals; development of rationale relating to the role of zwitterion-carbene tautomerization in Blatter radical formation.

Tom Richardson (former O'Donoghue group 4th year MChem student): synthesis of a Nitron analogue with exocyclic *N*-methylation; initial NMR investigations into the transformation of Nitron to Blatter radical.

3.2 – Introduction

1,2,4-benzotriazinyl radicals, also termed Blatter radicals (BRs), are an underexplored class of persistent organic radical discovered during the work of Blatter and Lukasewski.[205] Their initial report described two methods to access the 1,3-diphenyl-benzo[*e*][1,2,4]triazin-4-yl radical **137** (**Figure 32**), and even at this early stage commented on the broad potential of these compounds.[206, 207]



137

Figure 32 – Structure of Blatter's eponymous radical **137**, the original benzo[*e*][1,2,4]triazin-4-yl for which this class of radical is based upon.

BRs are bench stable radicals which can withstand moisture, air, low pressure and temperatures of over 400 °C.[208, 209] They characteristically exhibit functionalisation of the N(1) and C(3) positions of a 1,2,4-benzotriazine scaffold, generally with aryl substituents, however further derivatization has been undertaken within the literature.[210-214] They possess a SOMO centred about the N(1) position (**Figure 33a**), with smaller distribution at the N(2) and N(4) positions. The spin density of the radical exists across the benzotriazinyl scaffold, and is also present in significant amounts on the N(1)-aryl substituent which is key for the potential to tune radical character (**Figure 33b**). The fused ring and substitution pattern leads to significant delocalisation of the radical character – this can account for the stability and intriguing properties observed.[215]

a) **b)**

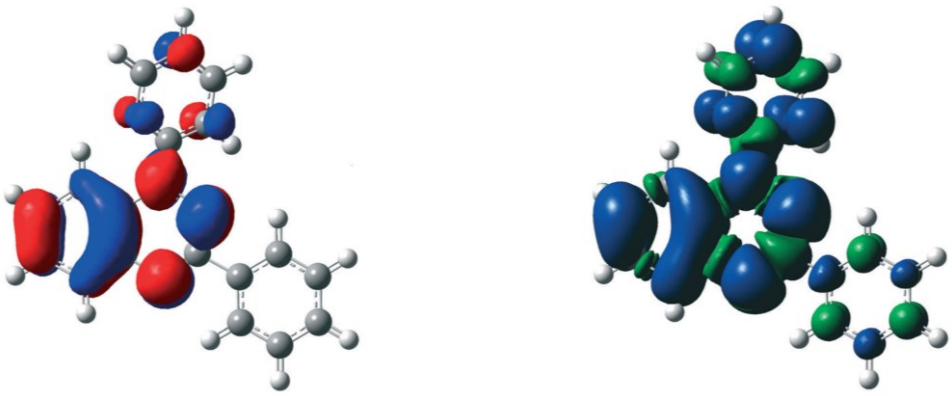


Figure 33 – **a)** – Graphical representation of the SOMO of **137** showing the major portion of the orbital is associated with the benzotriazinyl ring. **b)** – Graphical representation of the spin density of **137**. For **a)** and **b)**, graphical representations are obtained using UB3LYP/def2-TZVPP level of theory with isovalues of +0.03 and +0.004 respectively. Reprinted with permission from: C. P. Constantinides, D. B. Lawson, G. A. Zissimou, A. A. Berezin, A. Mailman, M. Manoli, A. Kourtellaris, G. M. Leitus, R. Clérac, H. M. Tuononen and P. A. Koutentis, *CrstEngComm*, 2020, **22**, 5453-5463. Copyright 2020 © The Royal Society of Chemistry.

The bulky aryl groups also give rise to changes in the solid-state packing. The N(1) aryl substituent generally has a large torsion angle (~50°) which leads to the π-slip-stacked arrangement observed within the crystal state.[216] This arrangement strongly affects the molecular packing, the stability of liquid crystalline phases (of importance for their optical properties), and the intermolecular spin-spin interactions helping to account for their bulk magnetic properties.[197, 216] **Figure 34** illustrates this arrangement considering the crystal structure of the 1-phenyl-3-(morpholin-4-yl) Blatter radical **138** synthesised by Kaszyński *et al*.[69]

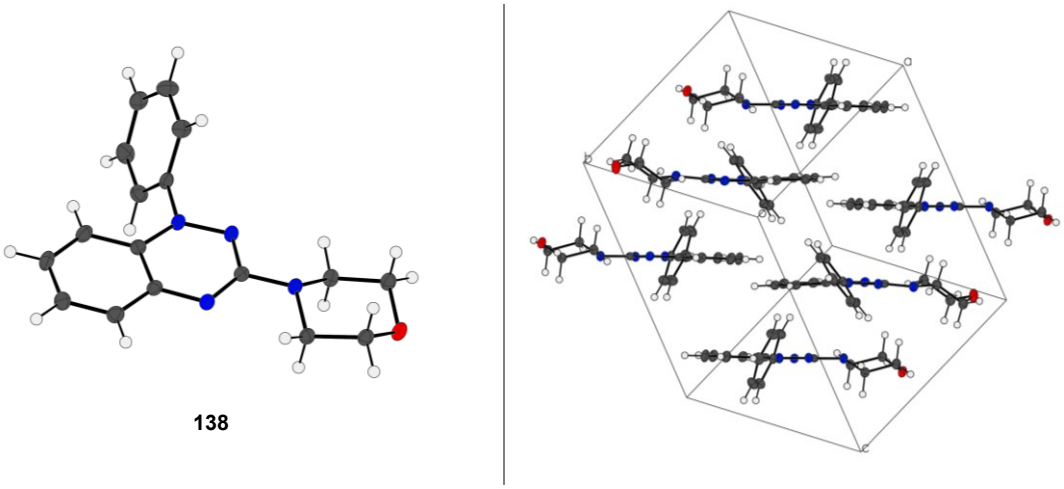


Figure 34 – Left: Cystal structure of one of the two crystallographically independent molecules observed within the single-crystal XRD data of the 1-phenyl-3-(morpholin-4-yl) Blatter radical **138**. Right: the unit cell of **138**. Data obtained from the Cambridge Crystallographic Data Centre: Database ID – BOPVOU. Data associated with the following publication: D. Pomikło, A. Bodzioch, A. Pietrzak and P. Kaszyński, *Org. Lett.*, 2019, **21**, 6995.

Due to the paramagnetic nature of Blatter radicals, characterisation is non-trivial using techniques such as NMR spectroscopy. Whilst the field of paramagnetic NMR has developed methodologies to exploit the rapid relaxation of spins, NMR parameters tailored to paramagnetic studies would be necessary[22] and have not yet been applied to BRs. Instead, BRs are analysed using techniques such as EPR spectroscopy and CV. An example of this analysis is shown from the work of Schubert *et al*,[217] who developed an alkyne-bearing Blatter radical **139** that could take part in copper-catalysed azide-alkyne cycloaddition (CuAAC) with an azide-functionalised norbornene. This monomer was then shown to undergo ring-opening metathesis polymerisation (ROMP) to give an electrochemically active polymer. The EPR spectrum of **139** (**Figure 35A**) consists of a seven-signal splitting pattern, observed in this case as a 12-mer, consistent with the coupling to the three benzotriazinyl nitrogens and the three fluorine atoms. The CV voltammogram of **139** (**Figure 35B**) was measured as a 1 mM solution in deoxygenated DCM and shows two electrochemical events, corresponding to one-electron reduction to the anion at the negative potential and one-electron oxidation to the cation near zero potential. The reversibility of the process makes Blatter radicals such as **139** of interest as active materials in organic thin-film batteries.[217]

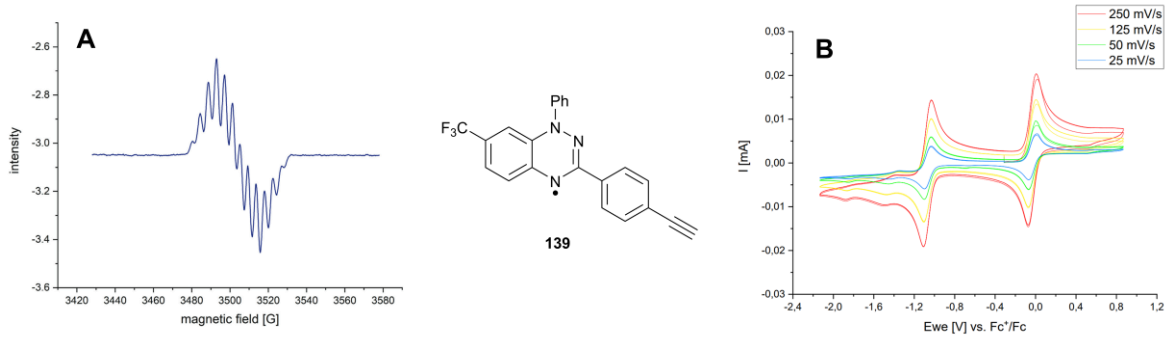


Figure 35 – Characterisation of the Blatter radical **139** used as a monomer precursor. **A** – EPR spectrum of **139** showing a seven-signal splitting pattern characteristic of CF_3-substituted Blatter radicals. **B** – CV voltammogram of **139** showing the reversible one-electron reduction and oxidation processes. The different coloured lines show the effect of scan rate on the observed current. Adapted with permission from: A. Saal, C. Friebe and U. S. Schubert, *Macromol. Chem. Phys.*, 222, **19**, 2100194. Copyright 2021 © Wiley-VCH GmbH.

3.2.1 – General applications of Blatter radicals

There is growing interest in the Blatter radical scaffold within areas such as photochemistry, magnetochemistry, electrochemistry and medicinal chemistry. **Figure 36** summarises the applications described in the literature for the Blatter radical; in the case of medicinal applications this also includes the literature around the *N*-oxide prodrug forms, and the benzotriazin-7-one obtained by the oxidation of BRs.

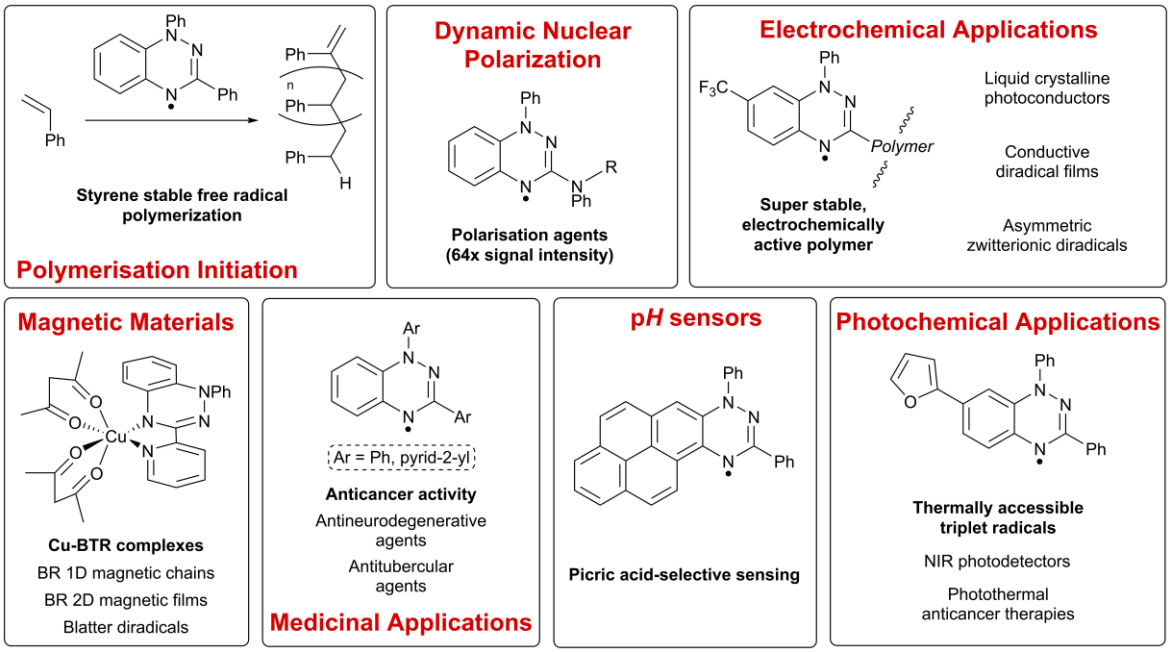
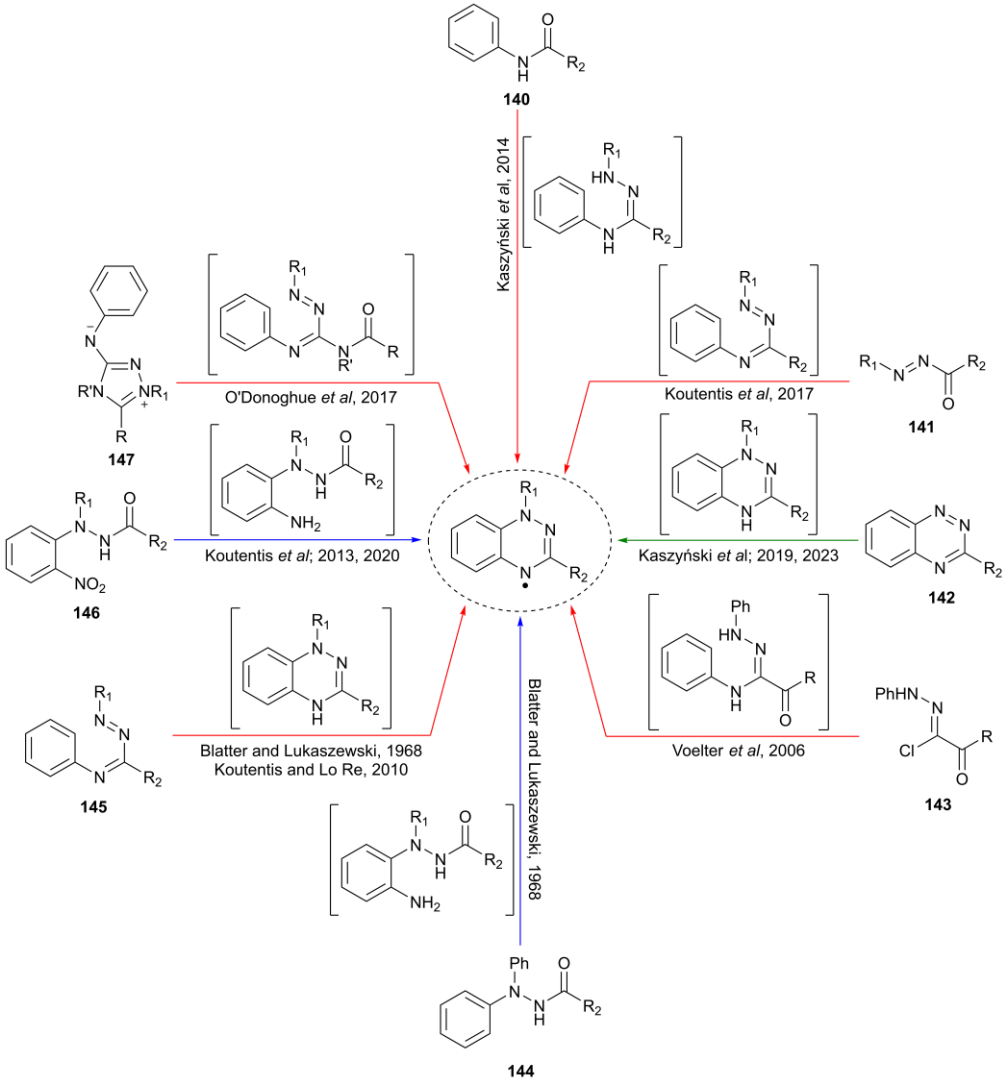


Figure 36 – Selected examples of the applications of BRs, with illustrated examples in bold. BRs have been shown to: catalyse styrene polymerisation;[218, 219] act as polarisation agents for dynamic nuclear polarisation;[220] show conductive properties of interest in organic electronics;[198, 200, 217, 221] can be used as a p*H* sensor;[212] show use in magnetic materials;[199, 212, 222-225] show interesting medicinal activity, often either as a product of an *N*-oxide or when oxidised to the benzotriazin-7-one;[204, 226-230] and/or show interesting photochemical properties.[201, 230-232]

3.2.2 – General syntheses of Blatter radicals

Although the Blatter radical was reported in the 1960s, the low yielding and time-consuming synthesis detracted from interest initially.[211] Recent developments, particularly within the work of Kaszyński[69, 70, 211, 233] and Koutentis,[234-237] has enabled a range of synthetic techniques to be applied to the generation of BRs. All synthetic routes to BRs fit into one of three methodologies: 6π-electrocyclization of *N*-aryltriazabutadienes, cyclocondensation of *N*-arylhydrazines, or the reaction of organometallic reagents with 1,2,4-benzotriazines (**Scheme 88**).



Scheme 88 – Summary of the synthetic methods used to obtain Blatter radicals. There are three known methods: 6π-electrocyclization of a *N*-aryltriazabutadiene (red arrows); cyclocondensation of *N*-aryl-*N'*-acylhydrazines (blue arrows); reaction of organometallic reagents with 1,2,4-benzotriazines (green arrow).

The most popular method within the literature, developed by Neugebauer *et al*,[238] is the oxidation of *N*-arylamidrazones and then electrocyclization of the corresponding triazabutadienes.[59, 205, 211, 235, 239, 240] The amidrazones are commonly accessed by reacting amides (**140**) with hydrazine,[211] hydrazones (**141**) and hydrazonyl chlorides (**143, 145**) with anilines,[239] or in the case of our group as a transient intermediate from 1,2,4-triazolium salts (**147**).[59] The electrocyclization of amidrazones to the

corresponding BR has been reported using various oxidants: mercury(II) oxide,[238] silver(II) oxide,[241] ruthenium(III) chloride,[239] potassium ferricyanide,[242] air[59] and palladium on carbon.[115, 235]

An alternative is the use of aryl halides to generate *N*-aryl-*N'*-acylhydrazines (**144**, **146**), which can then undergo cyclocondensation to give the BR.[205, 234, 243] This is an increasingly common route and avoids the challenging synthesis linked with amidrazones.[234]

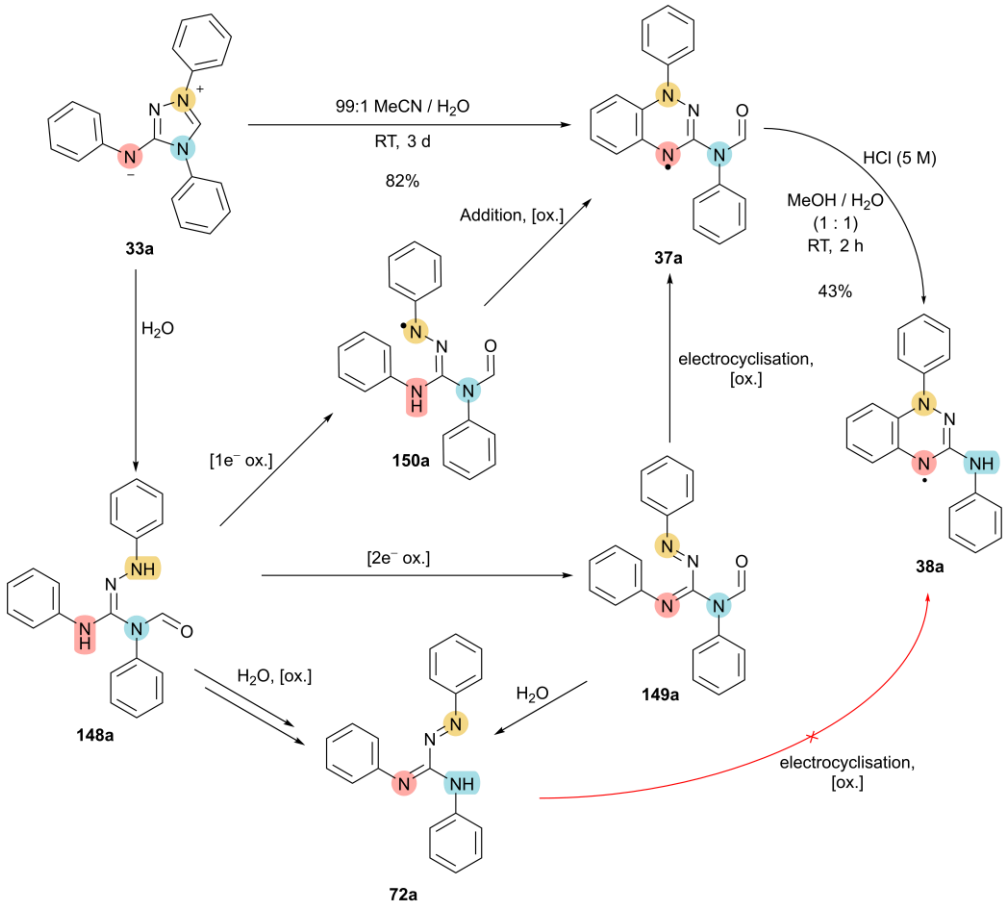
The final methodology, and one that has not received as much attention, is the reaction of organometallic reagents with C(3)-substituted 1,2,4-benzotriazines (**142**).[69, 70] By using routes based on the Arndt benzotriazine synthesis (discussed in detail in Chapter 4.2.1),[242, 244] 1,2,4-benzotriazine scaffolds can be generated to undergo this reaction.[245]

Only two of these routes are of relevance to the work discussed within this thesis, the synthesis from 1,2,4-triazolium salts discovered by our group[59] and the synthesis route from 1,2,4-benzotriazines.

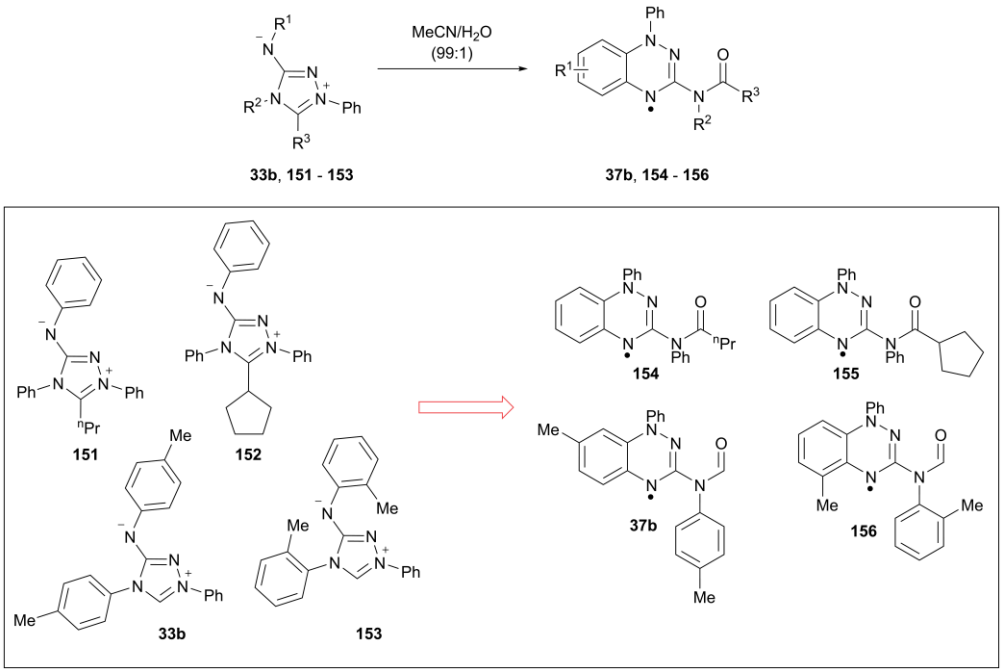
3.2.3 – Blatter radical synthesis from Nitron analogues

Given the intriguing tautomerisation of Nitron (**33a**) between the zwitterionic form and carbenic form,[58] the potential for Nitron to act as a NHC organocatalyst was investigated within our group. These studies[59] revealed the unusual rearrangement of Nitron to the C(3)-amido Blatter radical within wet acetonitrile over a period of 3 days. The proposed mechanism for this transformation is shown in **Scheme 89**, initiated by hydrolytic ring opening of Nitron to the *N*-formyl C(3)-anilino amidrazone intermediate **148a**. Previous work[59] showed that addition of ≤ 10% v/v water improved the isolated yield, however greater amounts of water led to significant *N*-formyl hydrolysis and oxidation to the triazabutadiene byproduct **72a**. From **148a**, there are two proposed pathways to give rise to **37a**. The most widely accepted, based on literature precedent,[205, 239, 240, 246] is the two-electron oxidation of C(3)-anilino amidrazone **148a** to *N*-formyl triazabutadiene **149a** followed by electrocyclization and oxidation to **37a**. The previous work[59] however cannot rule out a potential one-electron oxidation process to the hydrazyl radical **150a** that attacks into the anilino aryl ring and undergoes oxidation to **37a**. Hydrolysis of **37a** can be undertaken under acidic or basic conditions to give the C(3)-anilino radical **38a**, however attempts to cyclise triazabutadiene **72a** to **38a** under the standard experimental conditions, or by the addition of oxidants, were unsuccessful. The original 1-3,diphenyl Blatter radical **137** is proposed to be formed by the cyclisation of triazabutadiene,[205] and so in this case it is assumed that the anilino nitrogen of **72a** disfavours cyclisation.

A small selection of alkyl-substituted analogues were explored in our initial report (**33b**, **151** – **153**),[59] which are shown in **Scheme 90**. Previous to our work, the synthesis of analogues had not been explored, possibly as a result of the synthetic challenges of the traditional route to Nitron.[67] These analogues were found to proceed to the amido radicals (**37b**, **154** – **156**), however in the case of C(3)-functionalised Nitrons mild oxidant and base were necessary.



Scheme 89 – The mechanism previously published by our group for the transformation of Nitron (**33a**) to the C(3)-amido Blatter radical **37a**.



Scheme 90 – The scope of Nitron analogues and Blatter radicals synthesized within our previous work. In the case of **151** and **152** conversion to radical required the addition of potassium hydroxide and silver(I) oxide.

Despite the diverse applications of BRs detailed earlier, C(3)-N substituted radicals have not been considered in the literature until recently. A C(3)-amino substituent on the benzotriazinyl scaffold is found to be particularly effective in tuning the electrochemical properties of BRs.[70] Recently these radicals have been implemented as effective, switchable polarising agents for increasing NMR signal intensity.[220] The hyperpolarisation of nuclei can be used to overcome NMR insensitivity. Similar to contrast agents used within MRI, radicals enhance relaxation times using microwave-promoted transfer of spin polarisation to the analyte – this is governed by the Overhauser effect and therefore this technique is known as Overhauser dynamic nuclear polarisation (o-DNP). The unpaired electron also accelerates nuclear spin relaxation towards thermal equilibrium, and so being able to 'switch-off' the unpaired electron using electrochemical techniques can prevent rapid relaxation. Exploring **37a** and **38a** as o-DNP polarising agents (PAs), it was found that NMR signal intensity could be greatly enhanced (**Figure 37a**). The narrow electrochemical window of **37a** and **38a**, with both redox process for both radicals between −1.4 and 0.7 V, is favourable over 4-hydroxy-2,2,6,6-tetramethylpiperidin-1-oxyl (TEMPOL, **157**) which is commonly used for o-DNP. Only the oxidation potential of TEMPOL is within the region −1.4 to 0.7 V. Absolute signal enhancement from **37a** and **38a** is greater than that observed from TEMPOL (**Figure 37b**), and the BRs are stable and switchable over multiple cycles (**Figure 37c**) noting that the decreased variation of signal enhancement is likely a result of electrode fouling and not the radical stability.

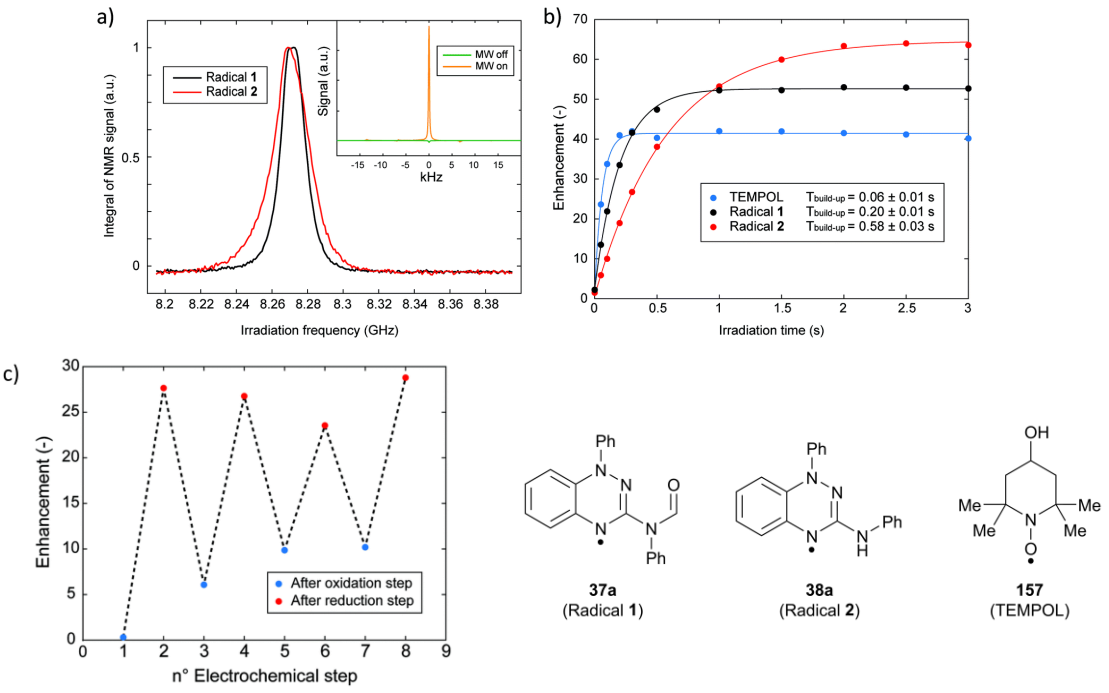


Figure 37 – O-DNP investigations into the C(3)-N substituted BRs **37a** and **37b**. **a)** – DNP MW frequency scans of the solvent ^{1}H signal, showing similar behaviour of both radicals. Inset: typical ^{1}H NMR spectrum with (orange line, 30 scans) and without (green line, 1000 scans) microwave irradiation at the optimal irradiation frequency. **b)** – Signal enhancement as a function of irradiation time, with maximum absolute enhancements of 42, 53 and 64 for TEMPOL, radical **1** and radical **2** respectively. **c)** – Electrochemical redox switching of the o-DNP enhancement provided by radical **1** (50 mM) in MeCN. Reprinted with permission from: F. Saenz, M. Tamski, J. Milani, C. Roussel, H. Frauenrath and J.-P. Ansermet, *Chem. Commun.*, 2022, **58**, 689-692. Copyright © 2022 The Royal Society of Chemistry.

The only other application of the radicals initially synthesized within the group that is currently in the literature is for the development of bipolar redox-flow battery materials. Otten *et al*[202] found however that the C(3)-amido radical **37a** underwent hydrolysis to the corresponding anilino radical **38a** following a charge / discharge cycle, proposed to result from decomposition of the closed shell anion formed upon Blatter radical reduction. **38a** shows a large discharge capacity fade rate, and so was not explored further.

The ease of synthesis and intriguing properties of the C(3)-N Blatter radicals is leading to a growth in interest. Analogues are limited to those synthesized by our group[59] and a small selection developed within the work of Kaszynski *et al*.[69, 70] With the expanded range of Nitron analogues and derivatives, coupled with computational studies and investigations regarding the conditions of efficient Blatter radical formation, this conversion can now be fully explored.

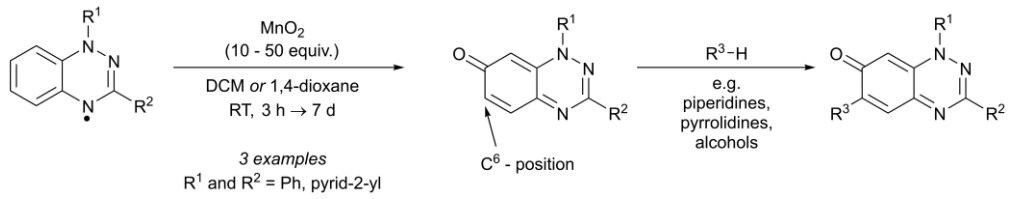
3.2.4 – The late-stage modification of Blatter radicals

There is also a significant amount of work into the late-stage modification of Blatter radicals, such as into the development of benzotriazine-7-one scaffolds of particular interest as anticancer agents[229, 247] and as an intermediate for further derivitisation.[248, 249] Ring contraction to benzimidazole scaffolds[250] and a range of metal-catalysed cross-couplings[211, 236] have also been effectively undertaken upon the radical.

3.2.4.1 – The oxidation of Blatter radicals

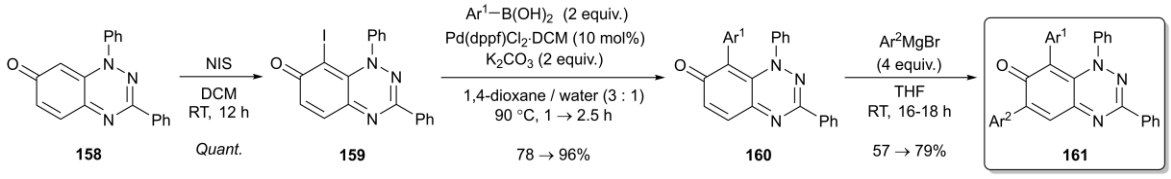
The oxidation of BRs to benzotriazin-7-ones, although generally undesirable as a byproduct in triazabutadiene cyclisation,[235, 251] has been shown to improve activity as an anticancer agent.[229, 247] Using manganese(IV) oxide (**Scheme 91**), good yields of the benzotriazine-7-one can be obtained and then derivatized at the C(6) position using a range of nucleophiles.[226, 229, 249, 252] Single-dose screening results of the two benzotriazine-7-ones against a panel of cancer cell lines shows promising growth inhibition, with cytotoxicity evaluation in the MTT assay showing over 95-fold increase in potency *versus* the corresponding BR against the MCF-7 cell line.[229] Evaluation of C(6)-substitution shows the development of derivatives with micromolar or even submicromolar potency.[247] The authors of this work, based on the National Cancer Institute COMPARE analysis, propose that the biological activity of benzotriazine-7-ones is closely related to that of the naturally occurring antibiotic, antifungal and anticancer agent pleurotin. Pleurotin is a potent inhibitor of the thioredoxin-thioredoxin reductase system, which is overexpressed in several cancers to aid cell proliferation and inhibit apoptosis.[247] As a planar polycyclic quinone, it is believed activity also arises as a DNA intercalating agent that strongly binds to the base pairs through π-interactions and hydrogen bonding.[252] Benzotriazine-7-ones have also shown promising activity as dual active antineurodegenerative agents, as inhibitors of β-amyloid peptide fibrillization (attributed to the

neurodegeneration observed in patients of Alzheimer's disease),[253] acetylcholinesterase and butyrylcholinesterase.[226]



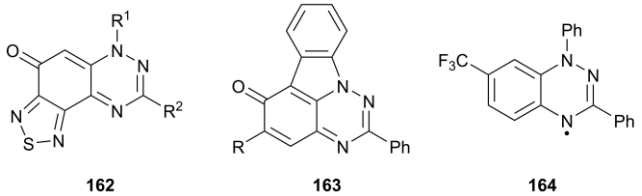
Scheme 91 – Using manganese(IV) oxide, BRs can be oxidised to the corresponding benzotriazine-7-one.

Alongside nucleophilic attack on the C(6)-position, the regioselective addition of electrophiles to the C(8) position is possible using *N*-chlorosuccinimide (NCS) and the analogues NBS and NIS in quantitative yields (**Scheme 92**). The introduction of iodine at C(8) of **158** (giving **159**) enabled Suzuki–Miyaura (**160)** and Stille couplings to take place, which when coupled with the use of a Grignard reagent allowed for the development of tetraarylbenzotriazine-7-ones (**161**), of interest as DNA intercalating agents.[252]



Scheme 92 – Regioselective iodination of benzotriazine-7-one **158** provides a position for Suzuki–Miyaura (shown in scheme) or Stille coupling to give 8-substituted benzotriazine-7-ones **160**. The 6-position can then be modified using a range of nucleophiles, such as Grignard reagents (**161**).

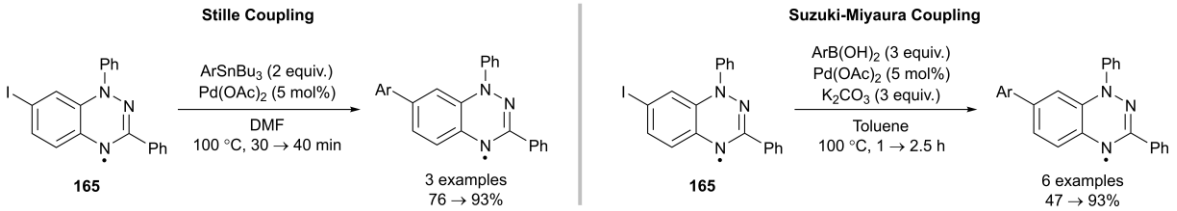
A range of other transformations have been undertaken upon benzotriazine-7-ones, or upon BRs to prevent benzotriazine-7-one formation. The reaction of tetrasulfur tetranitride with benzotriazine-7-ones gives rise to triazadiazolo-fused species **162**.[254] Pd-catalysed cyclisations of C(8)-iodinated benzotriazine-7-ones, and oxidative cyclisations of benzotriazine-7-ones mediated by copper and silver salts, give triazafluoranthenones **163**.[248] Finally, by blocking the C(7)-position, high oxidative stability can be achieved. The radical character of the 7-trifluoromethyl substituted radical **164** is left unchanged after refluxing with ten equivalents of $KMnO_4$ for two days.[251] This transformation is key to consider in regards to *in vivo* activity of the Blatter radical as an anticancer agent.



3.2.4.2 – Other transformations upon Blatter radicals

Derivatization of BRs to maintain radical character is less explored than the benzotriazine-7-one chemistry detailed in section 3.2.4.1, however several transformations have been successfully undertaken. The work of Kaszyński[211] provides the most instructive reference for late-stage BR derivatization, with examples from this study alongside other selected examples discussed below.

Stille and Suzuki–Miyaura couplings were successfully implemented in tests on the 7-iodo-1,3-diphenyl Blatter radical **165** (**Scheme 93**) by Loizou *et al*.[236] The Stille cross-coupling required optimisation to reduce the yield of the byproduct **158** – the optimised conditions led to yields of up to 11% of **158**. Only traces of **158** were observed in the Suzuki–Miyaura coupling, however longer reaction times were required. Yoshioka *et al*[246] implemented the Suzuki–Miyaura coupling conditions, in DMF, to introduce phenyl rings upon the *para*-positions of the N(1) and C(3) phenyl rings of BRs alongside the C(7)-phenylation illustrated in the discussed work of Loizou *et al*. Kaszyński further showed that Sonogashira and Heck couplings are possible upon iodinated Blatter radicals.[211]

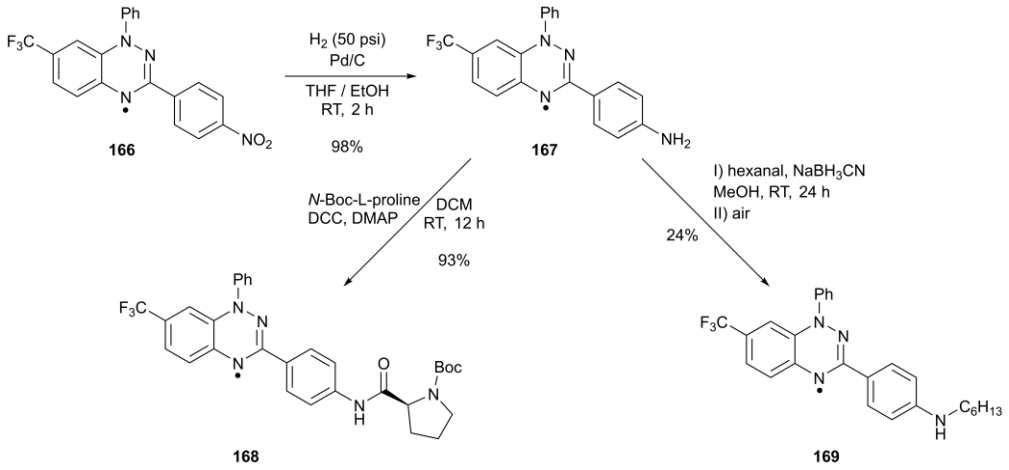


Scheme 93 – Optimised conditions for the Suzuki–Miyaura and Stille cross-coupling reactions upon iodinated Blatter radical **165**. In both cases the scope was explored showing good to excellent yields.

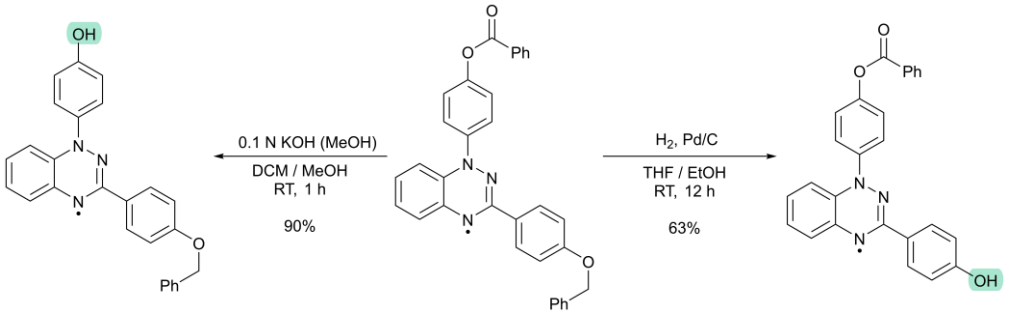
Catalytic hydrogenation of nitro-substituted Blatter radicals **166** was explored by Utecht *et al* (**Scheme 94**).[211] Reduction to the amino group (**167**) gives a handle for further derivatization – DCC coupling of L-proline (**168**) and the reductive amination with hexanal (**169**, with partial reduction of radical centre) were both shown.[211]

The selective deprotection of bisphenol Blatter radicals were also explored in the work of Utecht *et al* (**Scheme 95**).[211] Using benzyl and benzoyl functional groups, it was found that standard deprotection conditions can be implemented to selectively access monophenol products in good to excellent yields without reducing the benzotriazinyl core or initiating side reactions.

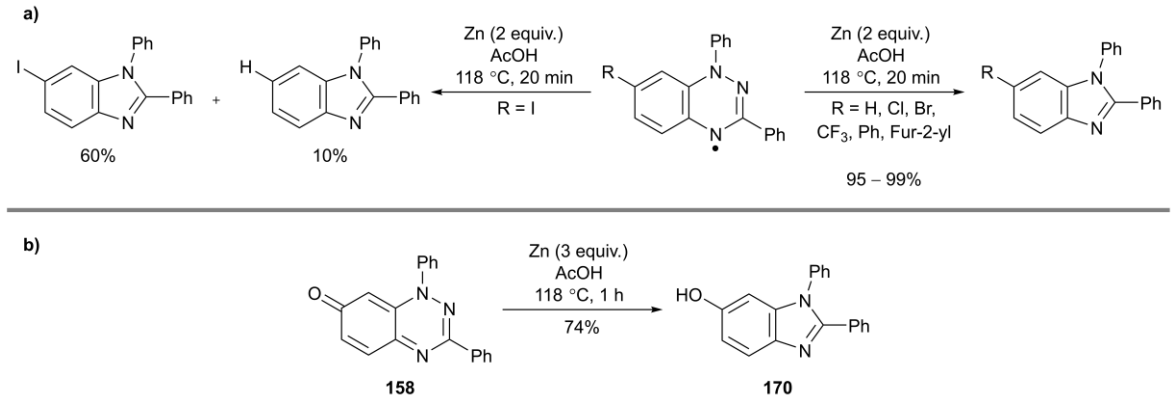
Although not maintaining the radical character, notably Koutentis *et al*[250] optimised the reductive ring contraction of Blatter radicals to benzimidazole scaffolds (**Scheme 96a**). Near quantitative yields of the desired product were obtained, providing an alternative route to 1,2-disubstituted benzimidazoles. They provide a tentative mechanism involving BR reduction and ring opening to a benzimidamide, followed by ring closure and loss of ammonia. Ring contraction of benzotriazine-7-ones was also demonstrated, allowing access to benzimidaz-6-ol species (**Scheme 96b**).



Scheme 94 – Pd-catalysed reduction of the 3-(4-nitrophenyl) group of **166** to the corresponding 4-aminophenyl group of **167** provides a handle for amide bond formation (**168**) or reductive amination (**169**).



Scheme 95 – Using standard deprotection conditions for benzyl and benzoyl groups, selective deprotection of the two phenolic groups can take place without affecting the benzotriazinyl core.



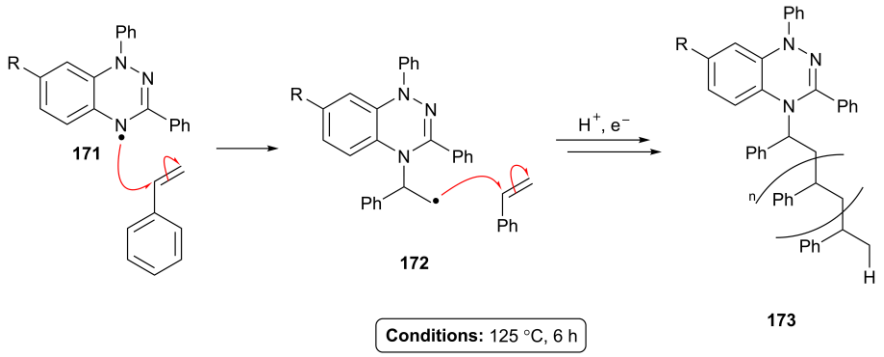
Scheme 96 – **a)** BRs can undergo reductive ring contraction using Zn powder to give rise to benzimidazoles. **b)** The same transformation is possible upon benzotriazine-7-ones **158**, albeit requiring greater equivalents of zinc powder in a longer reaction time and at lower yield, giving benzimidaz-6-ol species **170**.

3.2.5 – Synthetic application of Blatter radicals

BRs have been implemented in the initiation of reactions. Studies by Krasia-Christoforou *et al*[218] have shown the ability of BRs (**171**) to be used in stable free radical polymerisation (SFRP) of styrene (**Scheme 97**). Derivatization of the parent Blatter radical scaffold at the C(7)-position is shown to significantly affect polydispersity index (PDI) and number-average molecular weight: a PDI of 1.05

was achieved when R = Ph, observing 19% conversion; 34% conversion is observed when R = CF_3 with polydispersity of 1.25. Evidence also showed that **172** has low to moderate efficiency in initiating the polymerisation to **173**.

Work by Hawker *et al*[255] expanded on the above findings, obtaining the crystal structure for the unimolecular initiator **172** (R = H). The work also illustrated the ability to attain good PDI values when undertaking homopolymerisation with functional styrenic derivatives or copolymerisation with methyl methacrylate or butyl acrylate. Kuznetsova *et al*[219] showed that the induction period where **172** is generated can be avoided with the addition of the radical initiator azobisisobutyronitrile (AIBN), and that the BR remains attached to the end of the polymer chain – it does not have a catalytic role in polymerisation.



Scheme 97 – The mechanism of SFRP of styrene initiated by BRs **171**. The BR attacks into the alkene bond to generate the 1° radical initiator **172**. This unimolecular initiator undergoes reaction with further styrene molecules to lead to the final polystyrene **173**.

By developing synthetic applications of Blatter radicals that regenerate the radical at the end of the process, Blatter radicals may be useful as radical catalysts. Organocatalysis is a powerful tool to gain access to complex molecular architectures through a diverse range of transformations, however it is generally necessary to have substrates functionalised with polar groups to enable formation of non-covalent interactions with the organocatalyst. As a consequence, traditional organocatalysis implementing closed shell species cannot be applied to substrates that are poorly functionalised. Free radicals can complement closed shell organocatalysts by being able to react with non-polarised functional groups such as C-C multiple bonds, giving rise to reactive carbon-centred radical adducts. Covalent radical catalysis (CoRC), whereby formation of the radical adduct triggers a reaction cascade ending with the release of the catalyst, constitutes an efficient methodology to use simple building blocks not amenable to traditional organocatalysis to access complex architectures.[256] Recent reviews[257, 258] highlight the chemistry possible by nitrogen-centred radicals, however it should be noted that these reviews address the *in situ* generation of *N*-centred radicals as reactive starting materials and not as organocatalysts.

3.2.6 – Bioconjugation of persistent radicals

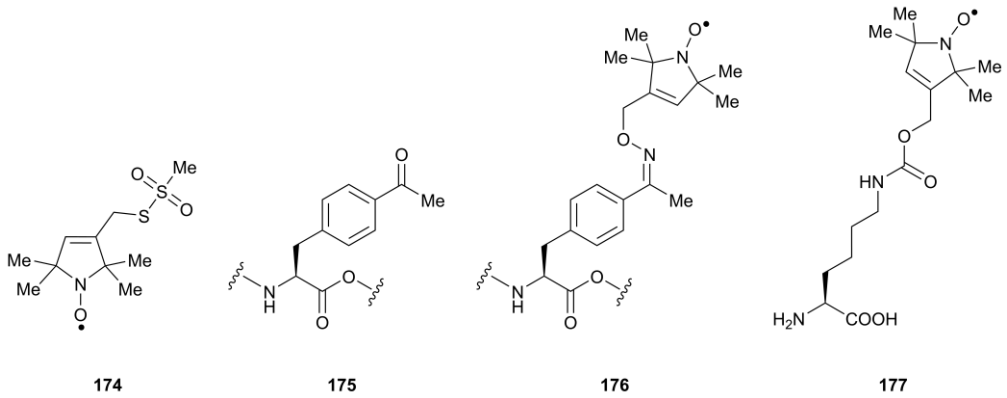
The topic of bioconjugation has already been introduced and discussed in regard to catalytic applications in Chapter 2.5.2. In this section the applications that relate to the potential benefits of Blatter radical bioconjugation are discussed – structural probes and medicinal applications.

3.2.6.1 – Radicals as spin labels

EPR spectroscopy has become an important tool in the structural elucidation of biomolecules, and for radical enzymes or certain metalloproteins can be undertaken directly upon the biomolecule. However, in most cases EPR analysis requires the introduction of persistent open shell systems (or 'spin labels') in a strategy referred to as site-directed spin labelling (SDSL). Nitroxide or trityl derivatives are common organic-based spin labels, the former being the most widely used of any spin label, however paramagnetic metal ions such as Cu(II) and Mn(II) have also found use as spin labels.[259] In the case of metalloenzymes that naturally contain paramagnetic metal ions, SDSL can yield information on the location of this metal within the active site.[260] It should be noted that SDSL can also be implemented in studies of the structure and function of other macromolecules, such as nucleic acids, lipids, and synthetic polymers – these applications are beyond the scope of this work.[261]

There are two methodologies to the introduction of spin labels. One possibility is to introduce the spin probe to a modified side chain within a protein, which is the more traditional form of SDSL pioneered by Hubbell *et al*.[262] Within this initial study, site-directed mutagenesis was used to introduce cysteine residues into bacteriorhodopsin that were reacted with the now commonly employed spin label (1-oxyl-2,2,5,5-tetramethylpyrroline-3-methyl)methanethiosulfonate (MTSSL, **Scheme 98**, **174**). EPR studies then revealed information about the location of the labelled residues, aiding understanding of the protein folding and tertiary structure. More recent studies by Hubbell *et al*[263] genetically encoded the 4-acetylphenylalanine amino acid **175** and used this in an orthogonal labelling strategy to introduce nitroxide radical **176**. The other method is to synthesize the spin-labelled amino acid, and then introduce this into a protein structure. Drescher and Summerer[264] reported the genetic encoding of spin-labelled amino acid (**177**) by *E. coli* into proteins, in response to the TAG stop codon, overcoming the limitations of the late-stage modification method such as multistep procedures and mutants that cannot contain cysteine residues.

A particularly useful EPR-based methodology is pulsed electron-electron double resonance (PELDOR, also referred to within the literature as DEER – double electron-electron resonance) that can measure nanometre-scale distances between two paramagnetic species within an immobilised system. Distances of typically 15 to 80 Å can be measured, which is typical for fluorescence-based methods such as FRET (discussed in Chapter 2.2.6.2) however benefits from the use of smaller labels that can be attached without the need for a linker group. PELDOR interprobe distance is therefore better defined, and can afford more detailed structural information as a result.[259]



Scheme 98 – Compounds involved in the introduction of spin labels to peptide scaffolds.

The change in spin-lattice relaxation time by EPR spectroscopy upon addition of a paramagnetic reagent to a spin labelled protein measures the diffusion-limited collision rate of the spin label with the reagent. Analysis of this variation can be used to measure the solvent accessibility in the spin label environment and thus can aid understanding of the secondary and tertiary structures of a protein, or understanding of protein dynamics.[265] Another application of SDSL is the analysis of protein dynamics using the characteristic spectral shapes arising from spin label rotation (rotation of the label itself, dynamics of the secondary structure bound to the spin label, and/or protein rotation).[261, 265]

An example of spin labelling is the determination of the Cu(II) ion location within the structure of azurin, comparing it to the known location from crystallographic data (**Figure 38**). Schiemann *et al*[260] expressed six cysteine mutants that were spin labelled with MTSSL and used PELDOR to determine the distance between the Cu(II) ion and the MTSSL labels. The values show the Cu(II) within the active site of azurin, with a difference of 2.6 Å from the XRD data of the non-modified protein. This variation can be somewhat explained by the spin density of an adjacent cysteine residue.[260]

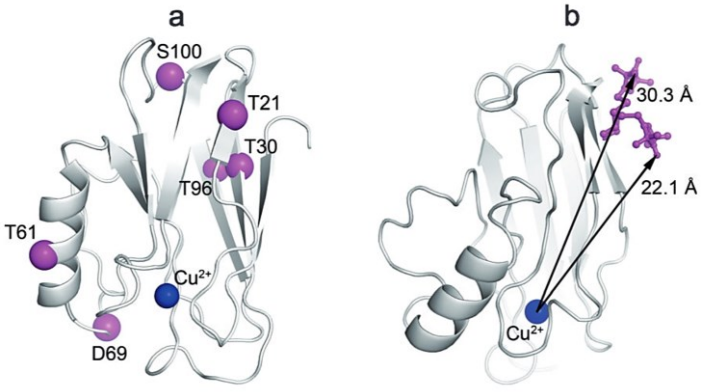


Figure 38 – a) The structure of azurin (PDB 1E67) and the chosen mutation labelling sites (pink spheres). B) The crystal structure of the azurin mutant $T21R_1$ (PDB 4BWW) with the two different conformations of MTSSL overlaid. The distance vectors connecting the Cu^{2+} ion with the oxygen atom of MTSSL in $T21R_1$ are shown by arrows. Reprinted with permission from: D. Abdullin, N. Florin, G. Hagelueken and O. Schiemann, *Angew. Chem. Int. Ed.*, **2015**, *54*, 1827 – 1831. Copyright 2015 © Wiley-VCH Verlag GmbH & Co.

For SDSL to be effective, the development of radicals with improved stability and spectroscopic properties is key. Furthermore, it is necessary to develop chemistry enabling efficient, orthogonal introduction of the spin label.[259] The high stability of Blatter radicals which can be further improved with structural modifications, and the diverse chemistry surrounding their synthesis and modification (detailed in Section 3.2.2 and 3.2.3), unlocks the possibility of tuning the Blatter radical scaffold to give species suitable for use *in vivo* and bearing functionalities that enable effective bioconjugation to peptides. Therefore, Blatter radicals may be an interesting species to implement within SDSL.

3.2.6.2 – Medicinal applications of bioconjugation

The combination of biomolecules such as proteins or nucleic acids with exogenous moieties leads to a wider range of functions and an enhanced efficacy, making bioconjugation an attractive methodology in the development of therapeutics.[148] The flexibility of bioconjugation over other drug delivery systems (nanoparticles, liposomes, vesicular systems etc.) further enhances interest within this area – they have a highly customisable design, higher stability, potentially lower cost and good reproducibility.[149]

One key example of bioconjugates, receiving a great deal of interest as promising modalities within oncology, are antibody-drug conjugates (ADCs) (**Figure 39**). The antibody is able to deliver payload to a specific target enabling selective antiproliferative or cytotoxic activity, thus reducing the side effects *versus* traditional anticancer agents. Whilst antibodies alone can serve as therapeutic agents, triggering immune system response, the introduction of a cytotoxic payload can overcome several limitations: the ineffectiveness observed where target antigen expression is low; the insufficient effect of the antibody alone; and the production costs for monoclonal antibodies (mAbs) that give rise to cytotoxic immune responses. There is a growth in interest around the development of suitable linker technology to attach the payload to the antibody. This includes consideration of non-cleavable linkers that keep the payload attached to the antibody in the presence of proteases, or instead releasing the payload once at the site of action.[148]

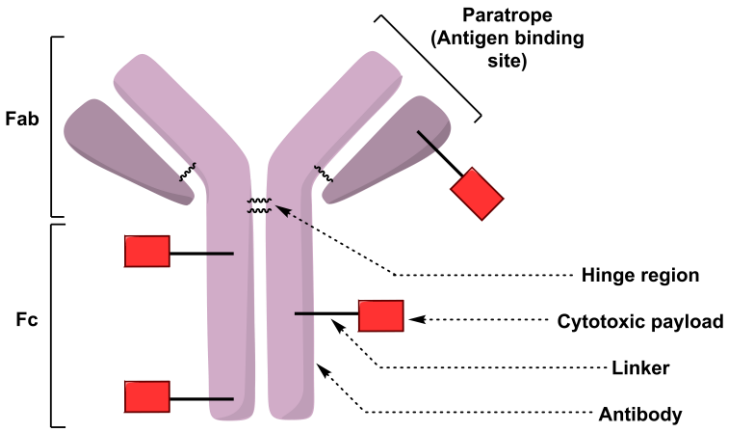
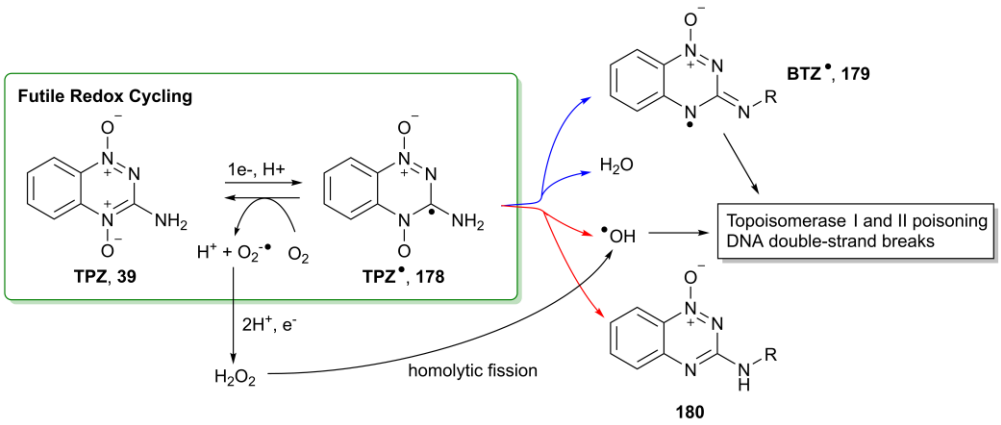


Figure 39 – General structure of an antibody-drug conjugate. Fc = fragment crystallisable. Fab = fragment antigen-binding.

Another key example to mention are the carbohydrate vaccines, which are glycan antigens that are covalently attached to a immunogenic carriers that can lead to an immune response.[266] Unlike the molecular recognition of exogenous proteins, the polysaccharides of the glycocalyx surrounding bacterial cells alone cannot elicit an immunological memory. As a result the immune response arising from carbohydrate recognition is slow and may lead to noticeable illness. Carbohydrate vaccines are conjugates of isolated glycocalyx carbohydrates with carriers, traditionally toxoids of the disease of interest, enabling delivery of the immune response to the bacterial pathogen.[267]

The relevance of peptide bioconjugation on the BR scaffold from a medicinal viewpoint is based on the findings for Tirapazamine (**TPZ**, **39**), an experimental anticancer prodrug. TPZ is proposed to act partially by formation of benzotriazinyl radicals *in vivo* (**BTZ•**, **178**, **Scheme 99**) that are structurally similar to BRs. The key point to note is that the implementation of TPZ as an anticancer treatment within clinical settings has been limited by poor extravascular penetration and very high aqueous solubility that leads to rapid clearance.[268] Although the high aqueous solubility can be attributed to the highly charged structure of TPZ, the potential active drug form BTZ• shares structural similarity to the synthesized BRs and is deemed of potential interest as part of the cellular assays undertaken within this work.



Scheme 99 – Proposed mode of action of Tirapazamine (**TPZ**, **39**). TPZ can undergo intracellular reduction to the radical species **178**, which can undergo dehydration to an active drug in the form of the benzotriazinyl radical (**BTZ•**, **179**, blue arrows). This radical can act through poisoning of topoisomerase, leading to DNA single or double strand breaks. An alternative is the loss of hydroxy radical to give the neutral benzotriazine **180** (red arrows), with the hydroxyl radical also a possible agent leading to DNA strand breaks.

3.3 – Synthesis of Blatter radicals from 1,2,4-triazolium salts

The parent Nitron (**33a**) is found to convert to Blatter radical **37a** in wet acetonitrile over 3 days, with high yields (82%) and only traces of byproduct. The simplicity of this method counteracts the long conversion timescale, and makes it an attractive route to probe the applications of BRs.

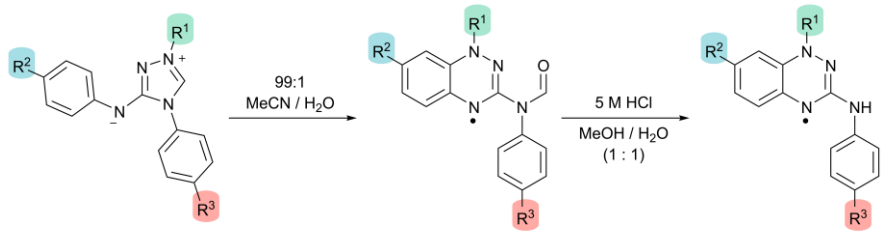
As was the case with **33a**, Nitron analogues were stirred at room temperature within wet acetonitrile and exposure to air. Air exposure was generally achieved using a needle through a rubber septum, preventing significant solvent evaporation, but on syntheses using ≥ 5 g Nitron analogue an open flask setup was used. Radical formation was monitored using LC-MS, before probing radical character using NMR spectroscopy, EPR spectroscopy and CV. Due to the synthetic challenges accessing the benzyl analogue of Nitron (**33k**), synthesis of the corresponding N(1)-benzyl Blatter radicals was not achieved.

The hydrolysis of C(3)-amido radicals **37**, **181** and **183** to the corresponding anilino radicals **38**, **182** and **184** was also achieved by stirring with 5 M HCl for 2 h in a methanol-water mixture.[59] In some cases reaction time was increased based upon LC-MS evidence. With the carboxy-functionalised Nitron **33i** a short reaction time is necessary due to partial conversion to the methyl ester **184a**. At 2 h a mixture was obtained of the methylated (**184a**) and non-methylated (**38i**) anilino radicals, and separations by column chromatography or recrystallisation (EtOH / H_2O) were unsuccessful. The methylation could be pushed significantly further by increasing the reaction time to 19 h, allowing for good yields of **184a**. LC-MS evidence after 1 h suggested good conversion of **37i** with minimal methylation, however, the higher aqueous solubility meant **38i** could not be extracted from the reaction solvent. Lyophilization of the reaction mixture followed by column chromatography (0 to 10% MeOH in DCM) was unsuccessful in isolating the radical. Hydrolysis of **37i** was also attempted using 1 M NaOH in 50 : 50 methanol / water, following the procedure previously published by our group,[59] however LC-MS indicated the degradation of the starting material with no formation of **38i**. In collaborative work with K. Deck, a 4th year MChem student under my supervision, hydrolysis of **183a** using lithium hydroxide in THF gave **38i** in good purity – this procedure was following the work of Karlsson *et al*.[269] **38i** was carried forward without isolation based on the above findings to studies regarding the bioconjugation of Blatter radicals detailed later.

Table 17 summarises the results independently obtained, and those obtained in collaborative work with Deck. Blatter radicals isolated by Murray[127] are also included as they will be explored in the XRD structure to activity relationships, and his findings are key to the discussion within this work. The results illustrate tolerance of substitution upon the R^1 position, with a large selection of Blatter radical analogues isolated bearing functionalisation at this position. Substitution at R^2 and R^3 however plays a significant role in the ability to form the radical; the electron-donating *p*-OEt-C_6H_4 analogue **33d** was able to form radical, but the electron-withdrawing trifluoromethyl group (**33c**, **33l**,

33m) leads to a stable Nitron analogue that did not form the desired radical based on LC-MS evidence. Slow hydrolytic ring opening to the C(3)-anilino triazabutadiene **72** was observed over several weeks, and as highlighted earlier (**Scheme 89**) these species do not undergo the electrocyclization to Blatter radicals under the general conditions.

Table 17 – Summary of the Blatter radicals isolated during this work.[a] Also included are the Blatter radicals synthesised or attempted to be synthesised in the work of J. Murray. [b]



33, 80, 81 37, 181, 183 38, 182, 184

Nitron Analogue	R^1	R^2	R^3	BR Yield (%)	
				C(3)-amido	C(3)-anilino
33a [a]	Ph	H	H	**37a**, 70 [a]	**38a**, 94 [a]
33b [b]	Ph	Me	Me	- [c]	- [d]
33c [b]	Ph	CF_3	CF_3	- [c]	- [d]
33d [b]	Ph	OEt	OEt	**37d**, 41 [b]	- [d]
33e [b]	*p*-F-C_6H_4	H	H	**37e**, 75 [b]	**38e** 88 [b]
33f [a]	*p*-Br-C_6H_4	H	H	**37f**, 93 [a]	**38f**, 69 [a]
33g [a]	*p*-I-C_6H_4	H	H	**37g**, 47 [a]	**38g**, 64 [a]
33h [b]	*p*-OMe-C_6H_4	H	H	**37h**, 45 [b]	**38h**, 76 [b]
33i [a]	*p*-COOH-C_6H_4	H	H	**37i**, 31 [a]	- [e]
33j [b]	*p*-CN-C_6H_4	H	H	**37j**, 60 [b]	**38j**, 80 [b]
33k [a]	Bn	H	H	- [d]	- [d]
33l [b]	*p*-CF_3-C_6H_4	CF_3	CF_3	- [c]	- [d]
33m [b]	*p*-OMe-C_6H_4	CF_3	CF_3	- [c]	- [d]
80a [a]	Ph	H	Br	- [d]	- [d]
80b [a]	Ph	H	I	**181b**, 50 [a]	**182b**, - [f]
81a [e]	*p*-COOMe-C_6H_4	H	H	**183a**, 42 [a]	**184a**, 24 [g]
81b [e]	*p*-COOEt-C_6H_4	H	H	**183b**, 26 [a]	- [d]

[a] This work. [b] Synthesized by J. Murray.[127] [c] Radical formation not observed. [d] Not synthesised. [e] Formation of methyl ester (**184a**) inseparable from the target radical. Alternative method used to obtain crude compound, see above. [f] Formation of inseparable mixture, see below. Isolation by alternative method detailed later. [g] Synthesized from **37i** with methylation under acidic conditions.

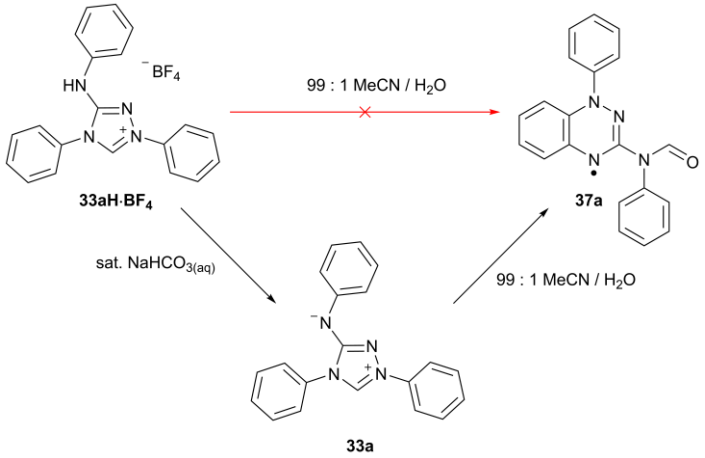
Murray[127] explored the use of sodium hydroxide and a range of oxidants on the analogues that did not form radicals, in the hope of accelerating hydrolytic ring opening and *N*-formyl C(3)-anilino amidrazone oxidation, however was unsuccessful. The addition of 10 mM NaOH slightly accelerated triazabutadiene formation, as the hydrolytic ring opening and undesirable *N*-formyl hydrolysis are

both promoted. Oxidants mostly had no noticeable effect, however the addition of hydrogen peroxide accelerated triazabutadiene formation.

The acid-catalysed hydrolysis of **181b** showed evidence of an intriguing isomerisation alongside anilino radical formation. LC-MS data for Blatter radicals characteristically show two peaks for the same *m/z* corresponding to product, which is proposed to arise from the separation of the radical from the protonated form. However, when **181b** was hydrolysed the observation of four *m/z* peaks corresponding to **182b** were observed. It is proposed that the extra peaks correspond to an isomerisation procedure however the product of this possible isomerisation is unknown – further details are provided in Appendix C.

3.3.1 – Blatter radical synthesis from the conjugate acid of Nitron

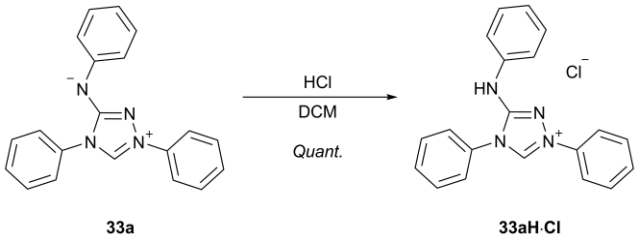
We investigated whether the Blatter radical (**37a**) could form from the conjugate acid of Nitron (**33aH·BF$_4$**). To enable Blatter radical formation following the route by Murray (**Scheme 100**),[127] it is necessary to firstly isolate the formally neutral form **33a** and then use this in a separate step of stirring within wet acetonitrile. Attempts to undertake the transformation to Blatter radical under standard conditions using the conjugate acid of Nitron analogues, synthesised in this work, led to no clear change by LC-MS over several weeks. From this it is suggested that the formally neutral form of Nitron analogues is necessary for the conversion to Blatter radical, and this stability of the protonated form is potentially useful for long-term storage. The focus of this work is if radicals can be obtained directly from the conjugate acid of Nitron by modification of the reaction conditions.



Scheme 100 – Under standard conditions, protonated Nitron salts (**33aH·BF$_4$**) show stability by LC-MS over several weeks. To enable the formation of Blatter radical **37a** an additional step of formally neutral Nitron analogue (**33a**) formation is necessary under the current procedure.

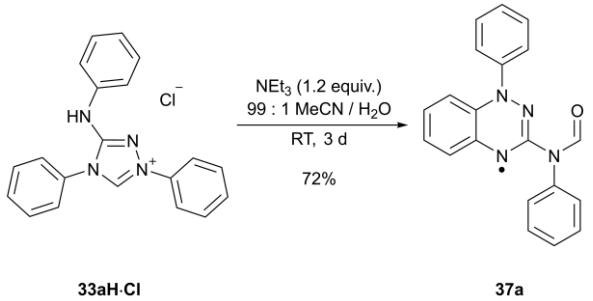
To further investigate this, the generation of the hydrochloride salt of Nitron **33aH·Cl** was undertaken from the commercially available formally neutral form (**Scheme 101**). It was verified to be stable over several weeks by ^{1}H NMR spectroscopy (see Section 3.3.3.1) and LC-MS in 99:1 MeCN/H$_2$O. The solution to this is the one-pot 'activation' and transformation of Nitron using base,

however as noted earlier the addition of base can accelerate the formation of triazabutadiene **72a** over long periods of time. **33aH·Cl** was tested using a series of bases; appropriate bases were selected as those which undertake the deprotonation without significant triazabutadiene formation after 24 h.



Scheme 101 – The formation of 'Nitron hydrochloride' (**33aH·Cl**) was undertaken in quantitative yields by dropwise addition of hydrochloric acid to a solution of Nitron. Disappearance of the yellow colour from the solution and precipitation of a white solid indicated formation of the hydrochloride salt.

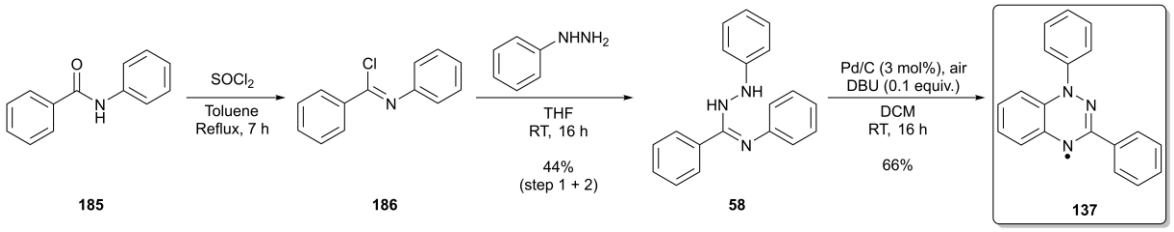
The solution, as would be expected, is to use weak base that will not significantly enhance triazabutadiene formation – triethylamine was chosen as most appropriate for this purpose given the low boiling point enabling removal of excess base *in vacuo* and the high aqueous solubility for effective removal by LLE. It was found that comparative yields to using zwitterionic Nitron were obtained from the use of Nitron hydrochloride and 1.2 equivalents of triethylamine over 3 days (**Scheme 102**). This method not only enables direct Blatter radical formation from the Nitron salt, reducing the number of synthetic steps, it also verifies that the Blatter radical formation can be 'switched on and off'. This illustrates the potential of Nitron as a *p*H sensor, indicating high *p*H values through the generation of the deep red amido radical **37a** or bright red triazabutadiene **72a**.



Scheme 102 – Using triethylamine, a one-pot Nitron hydrochloride 'activation' and Blatter radical formation was undertaken in comparative yields to the transformation of Nitron in solvent only.

3.3.2 – Characterisation of Blatter radicals

Isolated radicals were analysed by NMR spectroscopy; broadened spectra were observed (see Appendix C). A range of techniques were then used to explore the radical properties, which will be detailed within this section. Data is compared to the original C(3)-phenyl Blatter radical **137**, which was synthesized according to **Scheme 103**.[157]



Scheme 103 – Synthetic pathway used to access the parent Blatter radical **137**. The amidrazone **58** is synthesised from benzanilide **185** before oxidative cyclisation to **137**.

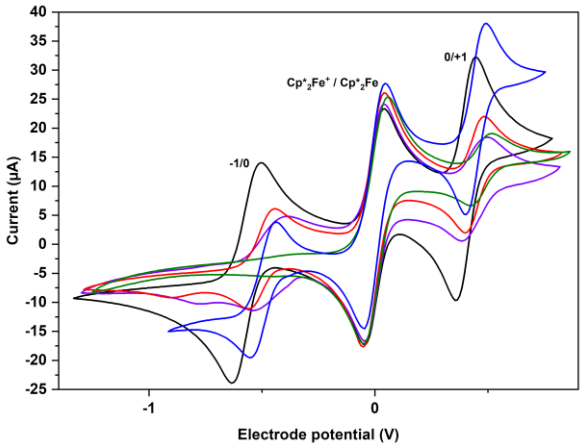
3.3.2.1 – Cyclic voltammetry

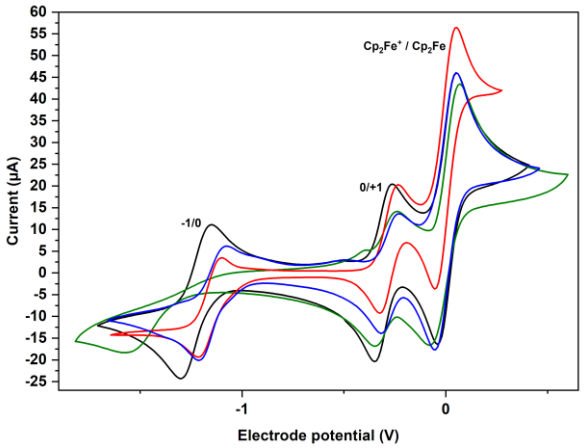
The reversible oxidation and reduction processes of the synthesized Blatter radicals were probed using cyclic voltammetry within acetonitrile, with platinum electrodes and tetrabutylammonium hexafluorophosphate electrolyte.[69] **Table 18** summarises the half-wave oxidation and reduction potentials relative to the ferrocene-based internal standard; C(3)-amido Blatter radicals see significant overlap with ferrocene, so decamethylferrocene is necessary in these cases. Decamethylferrocene has a half-wave potential of 0.50 V when compared to ferrocene, and so values for the amido-Blatter radicals are subject to a −0.50 V correction to enable comparisons to be made. Values obtained by Murray[127] are listed in **Table 19**.

Considering the data in **Table 18** and, ΔE values for the C(3)-amido and C(3)-anilino functionalised radicals are 0.93 V and 0.88 V respectively. Comparing radicals with the same aryl substitution, moving from amido to anilino functionalised radical gives a drop in ΔE between 0.05 (**37a** and **38a**, **37h** and **38h**) and 0.1 V (**37g** and **38g**). The smallest ΔE value is for **38j**, bearing the highly electron-withdrawing cyano group on the N(1) phenyl ring. The significantly higher half-wave reduction potential ($E^{-1/0}$) than any other tested C(3)-anilino radical indicates that the cyano group stabilises the anion formed upon reduction, further supported by the slightly higher $E^{-1/0}$ values for halogenated analogues **38f** and **38g**. For amido radicals the smallest ΔE appears to be that of **181b**, however it should be noted that a second smaller peak is observed upon reduction of the radical whilst scanning to negative potential (−0.69 V). This additional peak is attributed to two one-electron processes such as that observed by Murray for **38e**.[127] BRs with smaller values of ΔE are of particular interest given their promising activity as o-DNP PAs.[220] Conversely, **37d**, **37h** and **38h** with the electron-donating alkoxy substituents show the most negative $E^{-1/0}$ values due to destabilisation of the anionic reduced form of the radical. In comparison to the parent Blatter radical, all novel radicals synthesised within this work show significantly lower values of ΔE illustrating the potential benefit of C(3)-N substitution.

Table 18 – Summary of the half-wave oxidation and reduction potentials of isolated radicals, *versus* the ferrocene/ferrocenium half-wave potential, obtained as part of this work.

Radical	$E^{0/+1}$ (V)	$E^{-1/0}$ (V)	ΔE (V)	Cyclic voltammogram
C(3)-amido functionalised radicals[a]				
37a (—)	−0.10	−1.07	0.97	
37f (—)	−0.06	−1.00	0.94	
37g (—)	−0.02	−0.99	0.97	
37i (—)	−0.03	- [b]	-	
181b (—)	−0.06	−0.88	0.82	
C(3)-anilino functionalised radicals				
38a (—)	−0.31	−1.23	0.92	
38f (—)	−0.28	−1.16	0.88	
38g (—)	−0.28	−1.15	0.87	
182b (—)	−0.30	- [b]	-	





[a] Plotted values subject to −0.5 V correction for comparison to the Cp_2Fe^+/Cp_2Fe couple. [b] half-wave potential not observed.

Table 19 – Summary of the half-wave oxidation and reduction potentials of isolated radicals, *versus* the ferrocene/ferrocenium half-wave potential, obtained during the work of Murray.[127]

Radical	$E^{0/+1}$ (V)	$E^{-1/0}$ (V)	ΔE (V)	Radical	$E^{0/+1}$ (V)	$E^{-1/0}$ (V)	ΔE (V)
C(3)-amido functionalised radicals				**C(3)-anilino functionalised radicals**			
37a[a]	−0.10	−1.07	0.97	**38a**[a]	−0.31	−1.23	0.92
37d	−0.25	−1.15	0.90	**38e**	- [b]	- [b]	- [b]
37e	−0.07	−1.06	0.99	**38h**	−0.34	−1.30	0.96
37h	−0.13	−1.14	1.01	**38j**	−0.22	−0.99	0.77
37j	0.00	−0.83	0.83	**Parent Blatter radical**			
				137	−0.18	−1.25	1.07

[a] Radical also analysed during this work (Table 18), values in agreement. [b] Observation of two one-electron processes upon oxidation of the anion back to the neutral radical.

3.3.2.2 – Electron paramagnetic resonance spectroscopy

Electron paramagnetic resonance spectroscopy (EPR) spectra were acquired by Prof. Victor Chechik at the University of York, with representative examples shown in **Figure 40**. Data matched that previously reported for the C(3)-amido and C(3)-anilino radicals obtained from Nitron (**37a** and **38a**).[59] Simulated and experimental spectra are in close agreement, and the addition of a fourth hyperfine to consider the exocyclic nitrogen was found to give a slight improvement in the fit. This improvement could describe a small amount of radical character delocalised on this exocyclic nitrogen, further supported by the nonet splitting pattern for 4 equivalent $I = 1$ nuclei.[25]

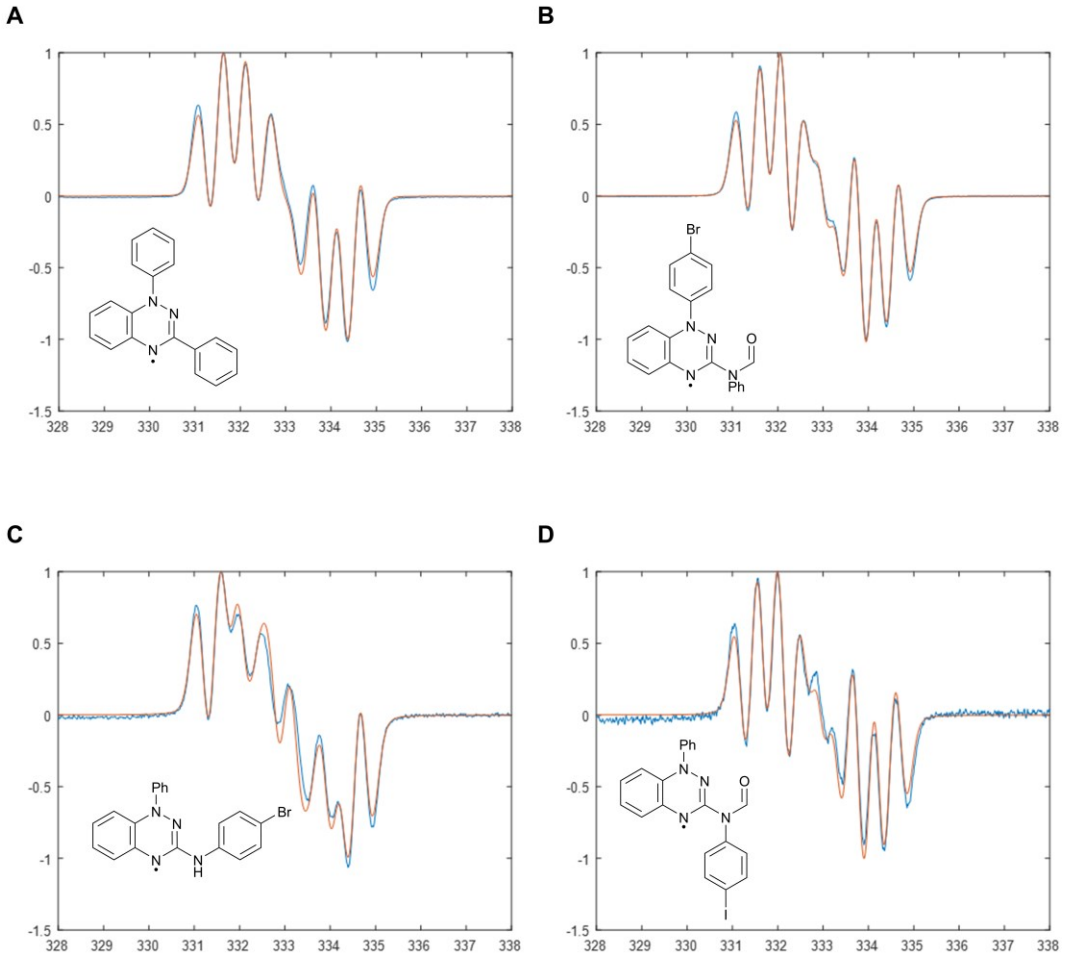


Figure 40 – Representative EPR spectra for Blatter radicals prepared as part of this work. **A** – parent Blatter radical (**137**). **B** – *p*-Br amido radical (**37f**). **C** – 4-bromoanilino radical (**182a**). **D** – iodinated amido radical (**181b**). Blue lines show experimental data, orange lines show simulated spectra.

Hyperfine coupling constants (HFCCs) give an indication of the location of spin density across the radicals; **Table 20** summarises the HFCCs for the radicals isolated during this work, and those obtained by Murray[127] for analysis. The constants show that radical character at the four nitrogens does not vary substantially with substituents, with a_N2 and a_N3 similar and a_N4 significantly lower than the others. To enable more detailed analysis, HFCCs can be attributed to particular nitrogen atoms based on computationally derived SOMO and spin density plots obtained by Dr. Mark Fox at

Durham University and those previously reported[59] (**Figure 41**, **Table 21**). Fox initially calculated HFCCs directly from UB3LYP/6-311+G(d,p) optimised geometries, then used B3LYP / EPR-II model chemistry on these optimised geometries to recalculate HFCC values. The later model is considered to be more suitable when predicting EPR parameters. Typically, larger SOMO contributions indicate greater stability of the radical character upon the four nitrogens in the scaffold. The calculations show the largest hyperfine coupling for N(1), with smaller coupling values to N(2) and N(4) – minimal radical character is calculated to exist upon the exocyclic nitrogen (N^{exo}). The largest contribution of radical character upon N(1) seen in these DFT calculations is supported by studies undertaken by Utecht *et al* on 7-trifluoromethyl-1,3-diaryl Blatter radicals.[211] The DFT calculations show only slight variation in SOMO contributions by each benzotriazinyl nitrogen, consistent with the EPR data, with destabilisation of all three nitrogens with a C(7)-ethoxy group (**37d**) and slight destabilisation of N(1) when introducing a cyano group upon the N(1)-aryl ring (**37j** and **38j**). DFT calculations have further highlighted that addition of a fourth coupling to EPR simulations must be verified as necessary to describe a chemical effect, rather than to improve the mathematical fitting to experimental data.

Table 20 – Summary of the hyperfine coupling constants obtained for the radicals isolated during this work.

Radical	a_N1 (Gauss)	a_N2 (Gauss)	a_N3 (Gauss)	a_N4 (Gauss)
137	7.55	5.22	4.78	0.72[a]
37a	8.04	5.10	4.63	0.98
37d[b]	7.31	5.29	4.73	1.31
37e[b]	7.58	5.56	4.31	1.06
37f	7.87	4.94	4.79	0.58
37g	7.85	5.10	4.66	0.44
37h[b]	8.18	5.06	4.49	1.00
37j[b]	7.38	5.18	4.69	0.56
38a	7.94	5.76	4.26	0.72
38e[b]	7.93	5.76	4.25	0.88
38f	7.75	5.75	4.28	0.58
38h[b]	8.13	5.65	4.13	1.13
38j[b]	7.25	5.81	4.30	0.76
181b	7.90	5.14	4.56	0.53
182a	8.01	5.58	4.24	0.67

[a] Although **137** does not have a exocyclic nitrogen, an improved fit was observed with a fourth hyperfine coupling constant which is included for consistency. [b] Radical synthesized by J. Murray.[127]

Based on the DFT studies: a_N1 describes N(1); a_N2 and a_N3 describe N(2) and N(4), however the similarity in values obtained relating to the two nitrogen atoms from EPR simulations of data and DFT mean the values cannot be assigned to a particular atom; a_N4 describes N^{exo}. Returning to the

data in **Table 20**, the addition of an electron-donating ethoxy group to the benzotriazinyl ring (**37d**) significantly decreases the contribution of N(1) whilst increasing N(2) and N(4) contribution. This can be explained by the stabilisation of radical character on N(2) and N(4) by electron donation from the ethoxy substituent *para* to the N(4) position. Electron donating substituents on the N(1) aryl ring (**37h** and **38h**) show increased N(1) contribution resulting from stabilisation of radical character, whilst **37j** and **38j** with the highly electron-withdrawing substituent on the N(1) aryl ring both show significantly lowered N(1) contributions resulting from destabilisation of radical character on N(1). Clear trends cannot be seen in the HFCC values corresponding to N(2), N(4) and N^{exo}.

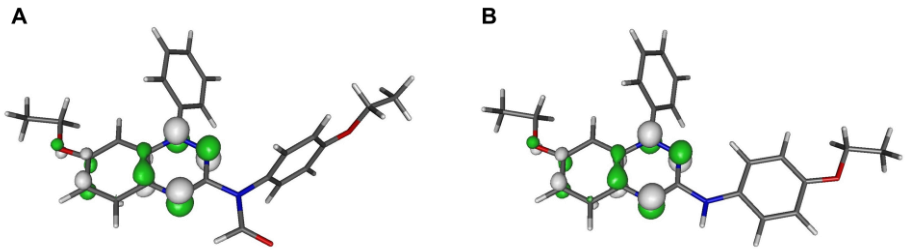
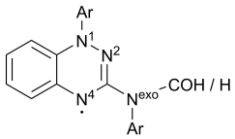


Figure 41 – Computed SOMO contributions of ethoxy-substituted Blatter radicals, showing the SOMO as mainly localised on the 3 benzotriazinyl nitrogens. **A** – amido Blatter radical (**37d**). **B** – anilino Blatter radical (**38d**). Determined by M. Fox using UB3LYP/6-311+G(d,p) level of theory.

Table 21 – Summary of the SOMO contributions, electron spin and HFCCs for a selection of Blatter radicals presented within this work. Determined by M. Fox using UB3LYP/6-311+G(d,p) level of theory.



Radical	Atom	SOMO (%)	Spin (e)	HFCC (Gauss)	EPR-II (Gauss)
137[a]	N(1)	18	0.22	4.43	5.31
	N(2)	20	0.37	3.27	4.11
	N(4)	18	0.32	3.51	4.36
37a[a]	N(1)	18	0.23	4.77	5.70
	N(2)	21	0.46	3.47	4.32
	N(4)	17	0.32	3.16	4.35
	N^{exo}	1	0.01	−0.17	−0.20
37d	N(1)	16	0.22	4.26	5.09
	N(2)	18	0.33	3.19	4.00
	N(4)	18	0.31	3.18	4.22
	N^{exo}	0	0.00	−0.26	−0.32
37j	N(1)	16	0.22	4.28	5.01
	N(2)	21	0.35	3.21	4.04
	N(4)	17	0.30	3.25	4.02
	N^{exo}	0	0	−0.29	−0.33
38a[a]	N(1)	18	0.26	4.70	5.62
	N(2)	19	0.33	3.28	4.16
	N(4)	18	0.30	3.27	4.05
	N^{exo}	0	−0.02	−0.47	−0.53
38j	N(1)	17	0.23	4.13	4.95
	N(2)	19	0.33	3.26	4.12
	N(4)	18	0.31	3.31	4.09
	N^{exo}	0	−0.02	−0.48	−0.55

[a] Values previously reported.

3.3.2.3 – Thermogravimetric analysis

The thermal stability of the radicals synthesized is a key consideration in regard to applications as a catalyst, within late-stage modification, or generally to probe the Blatter radicals to obtain evidence of their remarkable stability. Thermogravimetric analysis (TGA) of the radicals synthesized within the group have not previously been undertaken, however there are values available within the literature for Blatter radicals to provide as comparisons.[200, 208] **37a** and **38a** were investigated with the assumption that similar behaviour would be observed within the wider range of Blatter radical analogues synthesized within the group

TGA was undertaken with samples hermetically sealed in aluminium pans under a helium atmosphere, using heating rates of 10 °C / min to 300 °C followed by programmed cooling to 30 °C at a rate of 200 °C / min. **Figure 42A** shows the plot of percentage sample weight against time, which shows similar behaviour and losses from both **37a** and **38a**. The initial approximately 2% weight loss for **38a** can be attributed to the loss of water within the sample, as neither sample was stringently dried before analysis.

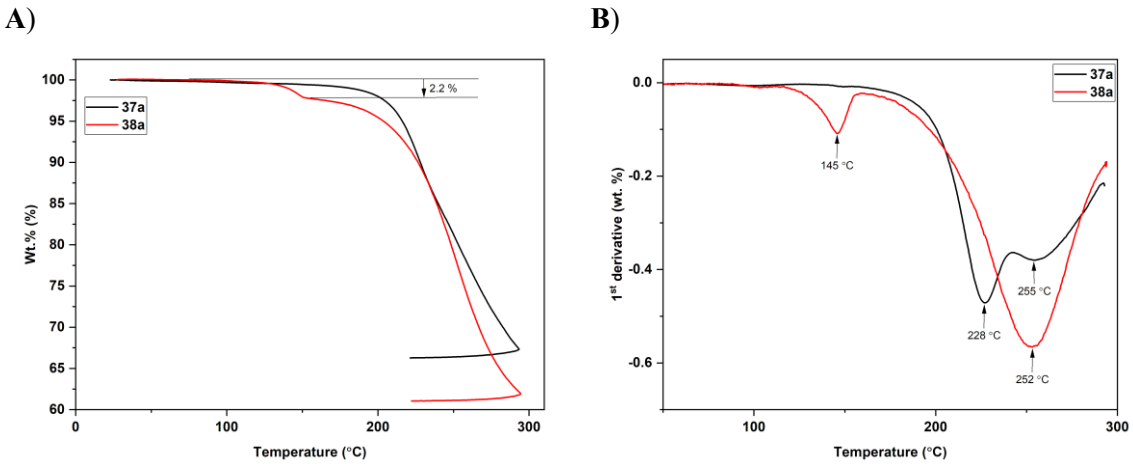
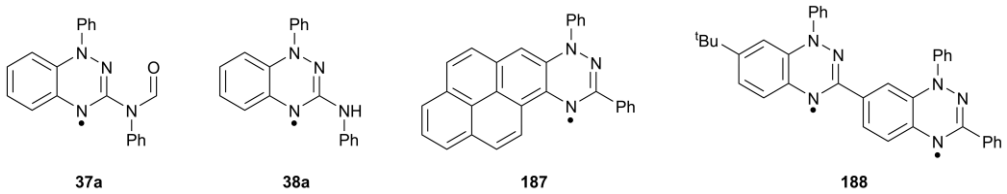


Figure 42 – **A**) TGA data, plotting percentage weight against the sample temperature, corresponding to the Blatter radicals **37a** and **38a**. In the case of **38a** the weight loss around 145 °C is labelled. **B**) The 1st order derivative of wt. % against sample temperature obtained by TGA. The labels shown correspond to the inflection points determined from a 2nd order derivative graph.

The first order derivative of the data is plotted in **Figure 42B**, with a 50-point adjacent averaging undertaken to provide a smooth plot. The inflection points for the labelled peaks were obtained from a second order derivative graph of the percentage weight (not shown). The mass loss relating to water is shown to occur around 145 °C, and the plot indicates that in the case of **37a** the drop in weight could contribute to two processes. The peak at 228 °C is only seen for the C(3)-amido radical **37a**, and may correspond to thermal decomposition to give **38a**. The event around 254 °C, observed with **37a** and **38a**, could correspond to decomposition of the anilino radical. **Table 22** provides decomposition onset values for the radicals analysed in this work alongside example Blatter radicals also analysed using TGA. There is limited TGA data within the literature, with DSC (differential scanning calorimetry) the more popular technique to probe temperature effects on Blatter radicals. The obtained values within this work are close to those reported within the literature[200, 208] for Blatter radicals described as showing 'robust thermal stability'. The values quantify the exceptional stability of the Blatter radicals synthesized within the group and also suggest that **37a** and **37b** can be safely used for applications even under high temperatures.

Table 22 – Decomposition onset values obtained within this work alongside comparative values from literature.

Radical	Decomposition onset (°C)	Source
37a	211	This work
38a	219	This work
187	250	Casu *et al* [208]
188	264	Rajca *et al* [200]



3.3.2.4 – Single crystal XRD

Where possible, Blatter radicals synthesized from Nitron analogues were also characterised by XRD (**Figure 43**). Suitable crystals were accessed by slow evaporation of methanol from the solution at room temperature. Detailed crystallographic information can be found in Appendix A. Radicals show variation in the orientation about the C(3)-N bond and a coplanar benzotriazinyl ring to the amido group. The aryl rings on N(1) and C(3)-N show significant deviation from planarity.

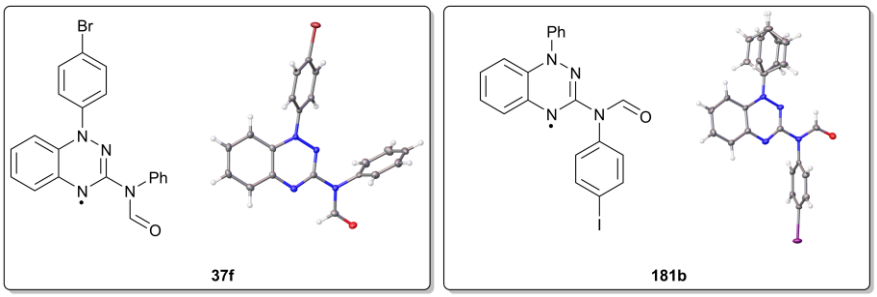


Figure 43 – The obtained crystal structures of Blatter radicals synthesized from the conversion of Nitron analogues. Detailed crystallographic information is provided in appendix A.

3.3.3 – Mechanistic insight into the conversion of Nitron and its analogues into Blatter radicals

Understanding the conversion of Nitron to a Blatter radical is key to designing new analogues that can favour the transformation, potentially making it possible under a broader range of conditions and thus unlocks the possibility of Nitron derivatives acting as an inactive species that can form radicals *in vivo* for a range of applications. Alternatively, by impeding radical formation, studies on the organocatalytic activity of Nitron derivatives may become possible.

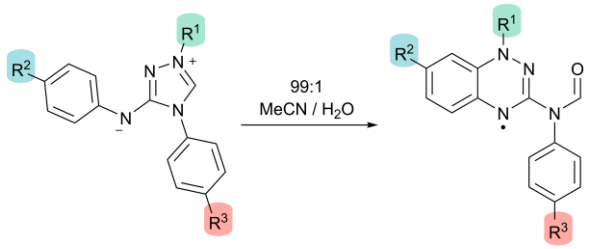
3.3.3.1 – Mechanistic insight from synthetic observations

The first consideration regarding how alteration of the Blatter radical scaffold affects the conversion to Blatter radicals is to look at the yields obtained within the synthetic work. **Table 23** provides selected examples of the C(3)-amido radicals synthesised as part of this work, or by Murray.[127] Variation of R^1 is tolerated (**33f**), although a significant drop in yield is observed by the introduction of electron-donating substituents (**33h**). This can be explained by the greater donation of electron density to the triazolium ring of Nitron, making nucleophilic attack less favourable. A similar result can be seen when introducing electron-donating substituents to R^1 and R^2 (**33d**), and so logically it would be expected that with electron-withdrawing substituents on R^1 and R^2 there would be enhanced radical formation due to the increased electrophilicity of the triazolium ring for attack by water. Instead, trifluoromethyl analogue **33c** shows no evidence of radical formation by LC-MS over a week with traces of triazabutadiene visible over subsequent weeks. Addition of electron-withdrawing substituents at R^1 to enhance nucleophilic attack of water (**33l**), or electron-donating substituents to partially counteract the effect of the trifluoromethyl group (**33m**), show no effect on the reaction outcome.

Given that the electron-withdrawing groups of **33c** are unexpectedly giving a highly stable Nitron analogue, the tendency to form Blatter radicals cannot be explained by simply considering the electrophilicity at the C(5) position of the Nitron analogue – another effect of substitution must have a significant contribution to radical formation. Given that an iodo substituent is tolerated upon R^3 (**80b**), albeit a weakly electron withdrawing group, it suggests R^2 substitution may have the major effect. R^2 substitution is therefore proposed to be the cause of the enhanced Nitron stability; the tautomerization that gives rise to the carbenic form of Nitron (**33a**) is dictated by R^2 through stabilisation or destabilisation of the exocyclic nitrogen (**Scheme 104**). Our observation of a stable Nitron analogue upon addition of a trifluoromethyl group can be explained as a result of stabilising the charge upon the exocyclic nitrogen, disfavouring the tautomerisation to the carbenic form that is proposed to undergo hydrolytic ring opening. In the majority of analogues, $R^2 = R^3$ and so an electron-withdrawing group is also present adjacent to the *N*-formyl group in the C(3)-anilino amidrazone intermediate. For the small amount of ring-opened intermediate (**148**) that does form,

the R^3 EWG leads to rapid *N*-formyl hydrolysis to triazabutadiene **72** and no Blatter radical formation. Rapid ring opening and slow *N*-formyl hydrolysis results from substitution with EDGs at R^2 and R^3 (**33d**). When only R^3 is substituted with a EWG (**80a** and **80b**) ring opening occurs to a significant level, but the *N*-formyl hydrolysis is accelerated leading to lower yields or, in the case of **80a**, only traces of Blatter radical **181a** formation.

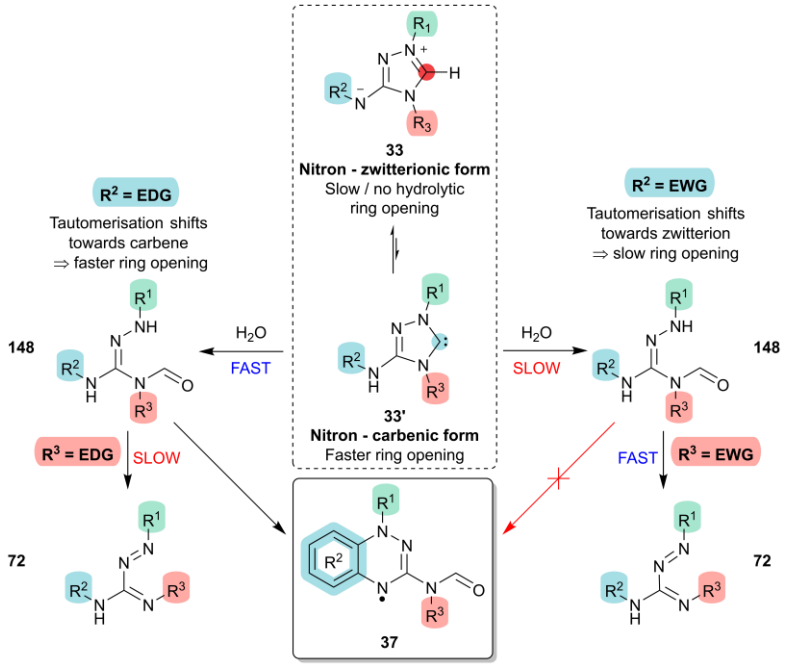
Table 23 – Selected examples of the Blatter radicals isolated during this work. The full summary of Blatter radicals synthesized is provided in **Table 17**.



33, 80 **37, 181**

Nitron Analogue	R^1	R^2	R^3	Yield (37, 181) (%)
33a	Ph	H	H	**37a**, 70
33c[a]	Ph	CF_3	CF_3	- [b]
33d[a]	Ph	OEt	OEt	**37d**, 41[a]
33f	*p*-Br-C_6H_4	H	H	**37f**, 93
33h[a]	*p*-OMe-C_6H_4	H	H	**37h**, 45[a]
33l[a]	*p*-CF_3-C_6H_4	CF_3	CF_3	- [b]
33m[a]	*p*-OMe-C_6H_4	CF_3	CF_3	- [b]
80a	Ph	H	Br	- [c]
80b	Ph	H	I	**181b**, 50

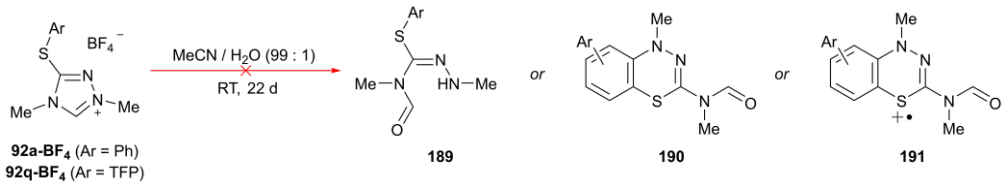
[a] Synthesized by J. Murray.[127] [b] Radical formation not observed. [c] Not synthesised.



Scheme 104 – The role of tautomerisation in Blatter radical **37** formation. It is proposed that the carbenic form **33'** preferentially undergoes hydrolytic ring opening to the *N*-formyl C(3)-anilino amidrazone **148**, and therefore the position of the zwitterion-carbene tautomerisation equilibrium holds a key role in the ring opening of Nitron analogues.

3.3.3.2 – Modification of the exocyclic nitrogen

To prove the role of the exocyclic nitrogen in the ability to form Blatter radical, alteration of the exocyclic nitrogen can be considered. The *S*-triazolium salts described in Chapter 2.4 are structurally similar to Nitron, with the two differences being that they are substituted with alkyl instead of aryl groups and have sulfur in place of nitrogen. The theoretical tautomerisation to the corresponding carbene would result in a highly unfavourable cationic sulfur atom. Consistent with expectations, a solution of **92a·BF$_4$** and **92q·BF$_4$** within wet acetonitrile (**Scheme 105**) showed no evidence of ring opening by LC-MS and ^{1}H NMR within a period of over three weeks. It should be noted that 1,3,4-benzothiadiazine species similar to **190** have been previously reported[270] as pale yellow solids, with no suggestion of radical character as a radical cation (**191**).

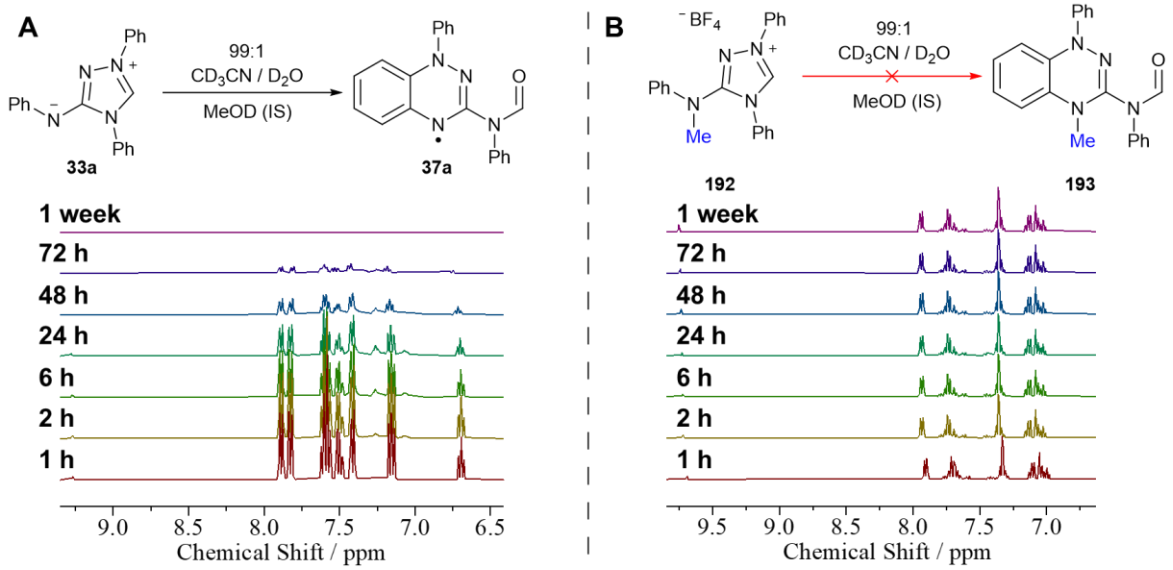


Scheme 105 – Attempts at undertaking hydrolytic ring opening upon two *S*-triazolium salts, and potentially forming thioamidrazone **189** or 1,3,4-benzothiadiazine species **190**, were unsuccessful with no evidence of reaction over a period of three weeks.

As was detailed in Chapter 3.3.1, the protonated salts of Nitron show no formation of ring opening products until converted to the corresponding Nitron zwitterion by treatment with base (**Scheme**

100). This observation is now explained as the inability to undergo tautomerisation to the carbene, and thus is a method to effectively 'switch-off' radical formation.

The final alteration explored is to alkylate the exocyclic nitrogen to permanently prevent Blatter radical formation. This work was undertaken by Tom Richardson, a previous 4th year MChem student.[127] *N*-methylated Nitron **192** was shown by ^{1}H NMR to be stable over a period of seven days, whilst Nitron **33a** showed complete loss of NMR signal corresponding to the starting material over the same time period (**Scheme 106**). Whilst radical formation was not expected for **192** owing to the *N*-methyl substituent, this NMR experiment did demonstrate that ring-opening of the cationic triazolium also did not occur to any significant extent. It can also be noted that the peak owing to C(5)-H at 9.7 ppm still remains at long reaction times for **192** showing that H/D exchange is relatively slow under these reaction conditions in 99:1 CD_3CN:D_2O



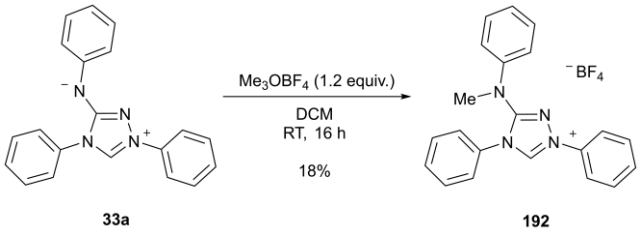
Scheme 106 – Work by T. Richardson[127] illustrated the stability of the Nitron derivative accessed by *N*-methylation of the exocyclic nitrogen. **A** – Over a period of 7 days complete disappearance of the NMR signal was observed for the conversion of Nitron to Blatter radical. **B** – The Nitron analogue with methylated exocyclic nitrogen showed no change by ^{1}H NMR over a period of 7 days.

These studies clearly implicate the role of tautomerisation to the NHC form of Nitron within ring opening and subsequent Blatter radical formation. By preventing tautomerization of Nitron through changes to the exocyclic nitrogen, analogues with dramatically increased stability are obtained.

3.3.3.3 – NMR studies of Blatter radical formation

Richardson's work described above illustrates that the formation of radical **37a** can be observed through the disappearance of starting material peaks, and so studies were undertaken to quantify the Blatter radical formation rates. The paramagnetic product is 'NMR silent', which aids NMR studies as there should be no NMR peaks corresponding to the product. The synthesis of *N*-methylated

Nitron tetrafluoroborate salt **192** was repeated using Richardson's method (**Scheme 107**), allowing for NMR studies as part of this work.



Scheme 107 – The synthesis of *N*-methylated Nitron **192** following the method of Richardson.[127]

The conversion of Nitron analogues (**Figure 44**) was tracked by observing the disappearance of a selected aryl peak. The integral of the selected peak was obtained as a function of time compared to the tetramethylammonium chloride (TMACl) internal standard (IS), which was set to an arbitrary figure of 1000. The fraction of starting material, f(s), was calculated as the y-intercept of the fit to the initial data (phase 1) – a stopwatch was used to determine the time between mixing and the start of data acquisition for the first datapoint. In the majority of cases, reactions were held within a thermostated bath at 25 °C and removed only for the time required for analysis; in the case of continuous NMR tracking, the sample was held within a thermostated spectrometer at 25.5 ± 0.2 °C

For clarity, the following discussion is presented for the parent Nitron (**33a**) with data for Nitron analogues provided in Appendix C. **Figure 45** shows the NMR overlay for Nitron under the experimental conditions. Unlike the work of Richardson, this reaction was undertaken within an NMR tube instead of taking aliquots from a stirring reaction mixture. This allows for consistency of the reaction concentration and removes error due to sampling. The NMR overlay shows the presence of additional peaks to starting material (highlighted in purple). The additional peaks are not seen to accumulate to a significant extent. Based on NMR integrals, it is clear that conversion to radical is the major reaction overall. Furthermore, these additional peaks are present at long reaction times again at low levels relative to the starting Nitron concentration. Based on recommendations within a recent review by Lloyd-Jones *et al*,[271] a repeat of the reaction was undertaken with vigorous horizontal agitation of the NMR tube following acquisition of each data point – there was no noticeable change in the reaction outcome.

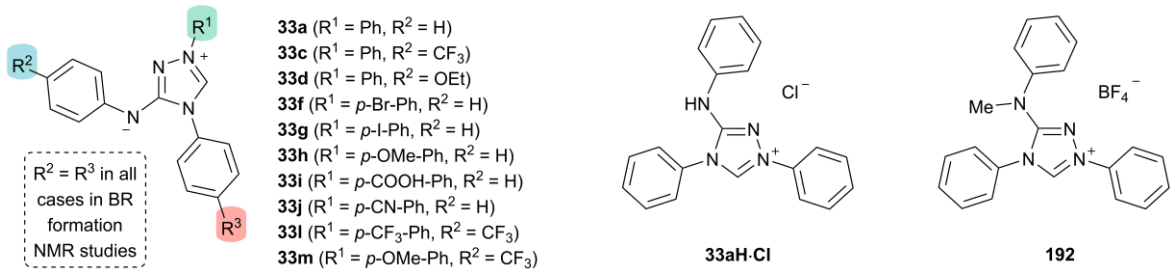


Figure 44 – Summary of the Nitron analogues analysed as part of the following NMR studies.

An isolated peak (highlighted in grey) in the aromatic region owing to substrate was monitored over time. **Figure 46A** shows the plot for fraction of remaining Nitron as a function of time, with data fitted to an exponential decay process. The data for day 1 (black) appears to be distinct from the values obtained for subsequent days (red), and is perhaps indicative of two consecutive processes. **Figure 46B** shows the semilogarithmic plot of f(s) data, showing two linear regions. This suggests two consecutive first order or pseudo first order processes.

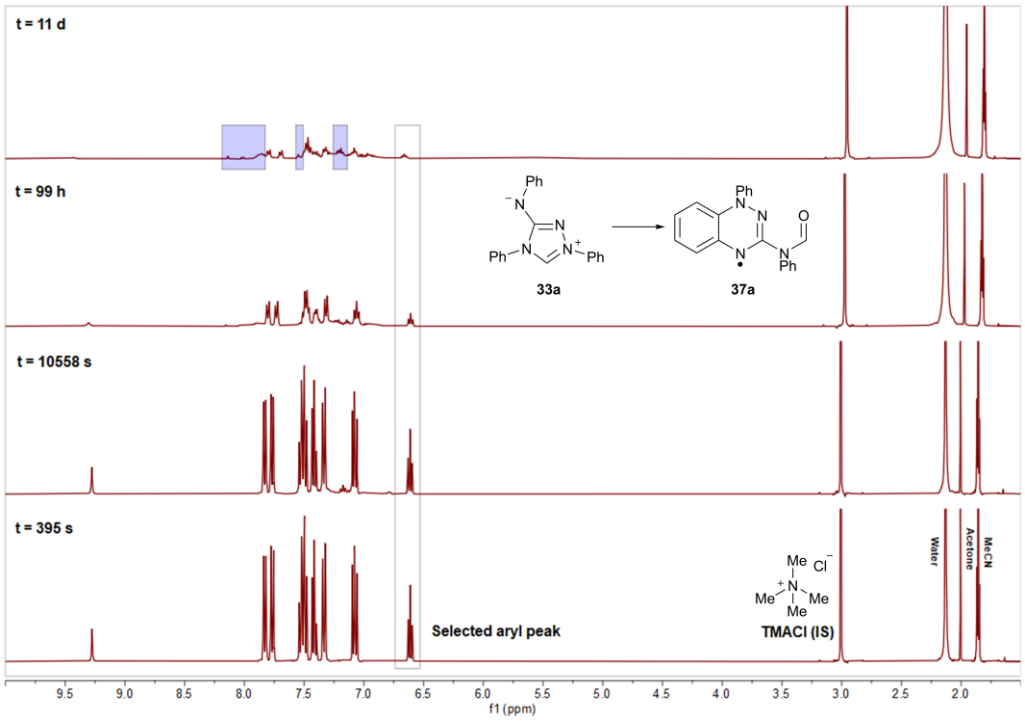


Figure 45 – NMR overlay for the reaction of Nitron (**33a**) to give the corresponding C(3)-amido Blatter radical (**37a**). The peak selected to track as an indicator of hydrolytic ring opening is shown within the box. Additional peaks formed after 11 days reaction highlighted in blue.

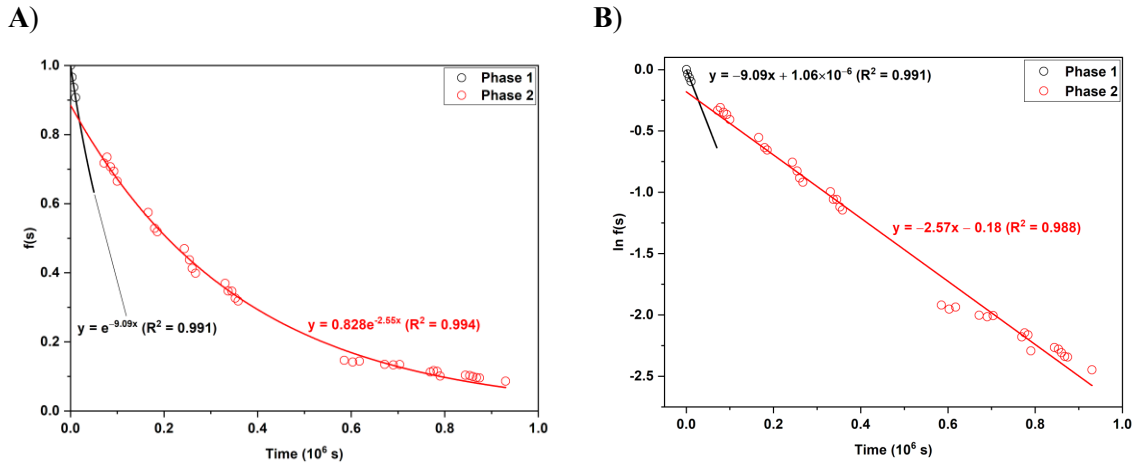


Figure 46 – **A**) Plot of the fraction of remaining starting material as a function of time for Nitron (**33a**) in 99:1 d_3-MeCN / D_2O. 400 MHz spectrometer, n = 8. The data seemingly fits to two separate processes with good R^2 values. **B**) Semilogarithmic plot of the fraction of remaining starting material as a function of time for Nitron (**33a**) in 99:1 d_3-MeCN / D_2O. 400 MHz spectrometer, n = 8.

The time difference between the final point of phase 1 and the first point attributed to phase 2 is large, and so continuous tracking in the NMR probe was then undertaken to accurately describe the change in starting material concentrations moving from phase 1 to phase 2. To do this quantitatively, it is important to allow for sufficient time between scans such that the vast majority of spins are fully relaxed – using ≥5 times T_1 for all protons of interest within the structure allows for ≥99.3% relaxation, and thus for experiments to be deemed quantitative.[272] T_1 values were therefore determined within dry acetonitrile using the inversion recovery technique, which will be explained in greater detail in Chapter 5.3.1, involving a 180° pulse being applied to the sample followed by a variable inversion time before acquisition by a 90 ° pulse. Fitting of the data showed that the T_1 values for phenyl protons in Nitron range from 3.58 to 4.17 s, with the C(5)-H T_1 being 5.44 s. A 35 second relaxation decay was therefore used. **Figure 47** shows the data obtained from the initial analysis, which again supports the existence of two distinct regions and consecutive processes.

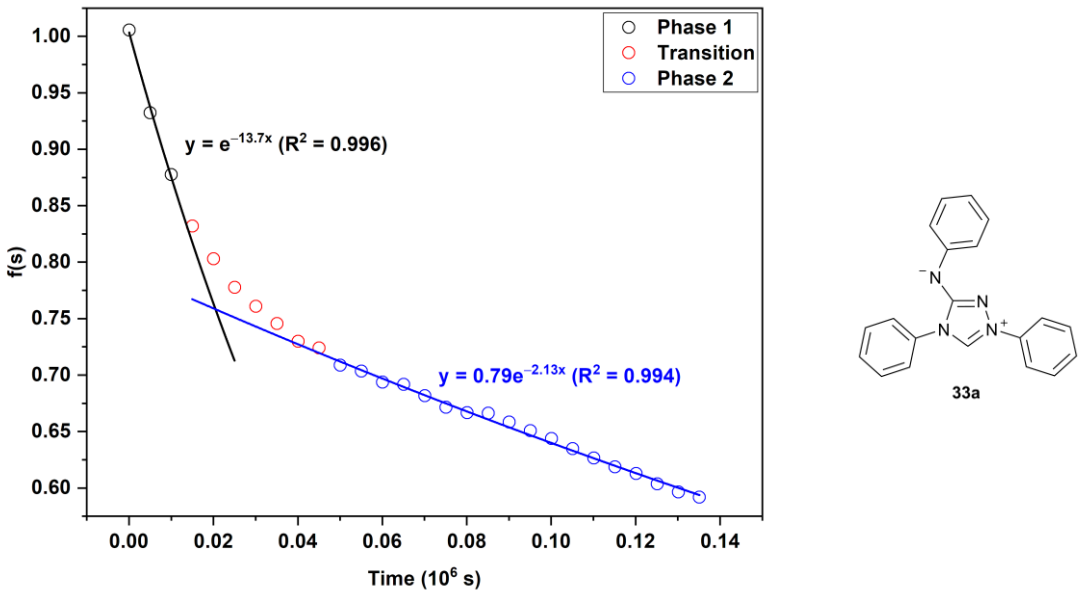
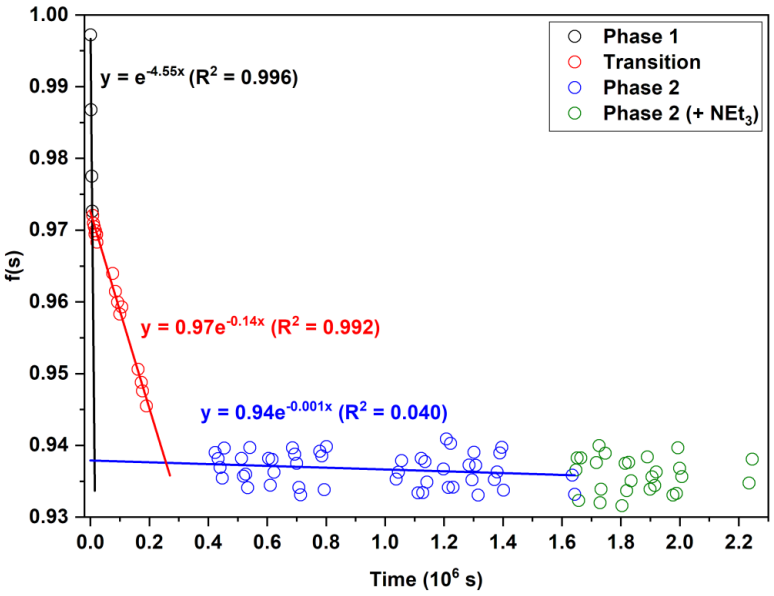
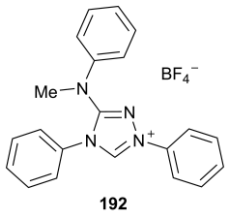


Figure 47 – Plot of the fraction of remaining starting material as a function of time for Nitron (**33a**) obtained using continuous ^{1}H NMR analysis, with the NMR tube in the probe of the instrument, enabled identification of a transition region between phase 1 and 2.

The analogues of zwitterionic Nitron explored in this work (**Figure 44**) generally show comparable behaviour with Nitron, with observation of two distinct phases. Variation between analogues is observed regarding the rate of the reaction phases and the extent of drop in f(s) before progressing to phase 2. The only anomalous data corresponds to **33d** and **33h**, where the peak integrals are seen to show poor fits to an exponential decay process due to significant peak overlap in all cases. The carboxy-functionalised Nitron analogue **33i** was also unable to be analysed for rate of radical formation due to poor solubility within the experimental conditions. Appendix C provides the plots of f(s) and ln f(s) against time for all analogues successfully analysed in this work.

A comparative NMR study with *N*-methylated Nitron **192** shows a smaller drop in the fraction of starting material in the first 80 minutes, before also observing a transition period. However the latter decay occurs over a longer time period than with **33a**, and is also fitted to an exponential decay process (**Figure 48**). There is a significantly smaller percentage drop in f(s) compared to **33a** (calculated by the intersection of the phase 1 and 2 fit lines). Following the transition period, f(s) remains relatively constant for a substantial period of time. Triethylamine (5 μL, neat) was added to attempt reaction progression, but led to no clear change.





192

Figure 48 – Plot of the fraction of remaining starting material as a function of time for *N*-methylated Nitron **192**. The graph shows a clear transition period alongside phases 1 and 2 (the latter of which showing no clear reaction taking place, even upon addition of triethylamine to promote ring opening).

The final example presented is for the Nitron hydrochloride salt **33aH·Cl** (**Figure 49**). The initial behaviour of this species is similar to **192** however there is no significant transition period observed and the drop before moving to phase 2 is very close to that obtained for **33a**. An interesting observation is that, though having a poor fit to an exponential decay process, there does appear to be a trend of decreasing f(s) during phase 2. A rate constant of 8.32×10^{-9} s^{-1} can be obtained for this hydrochloride salt, with magnitude greater than 4 times the standard deviation – a very slow reaction is taking place. The addition of 1.2 equivalents of triethylamine followed by vigorous horizontal agitation resulted in an immediate colour change from a colourless to bright yellow solution, indicative of liberating the zwitterionic form of Nitron. A rapid decrease in the fraction of starting material is observed, followed by the reaction rate decreasing to a rate comparable to that of **33a**. These findings quantitatively validate the ability to 'switch-on' radical formation from the protonated salt through liberation of the zwitterionic form.

Rate constants for the two processes (k_1 and k_2 corresponding to the phase 1 and 2 respectively), alongside the percentage drop of f(s) before intersection of the fit lines corresponding to phase 1 and

2, can be determined for all the Nitron analogues analysed in this way. **Table 24** summarises the data obtained, determined using the semilogarithmic plots. In all cases, k_1 is greater than k_2. k_1 is between 3.5 and 27 times faster than k_2, with the largest difference seen when there are 3 *p*-CF_3 groups on Nitron (**33l**). In cases where levels of $\%_{drop}$ seen are below 12 % (**33c**, **33l**, **192**), k_1^{rel} values are less than 0.7. All other cases $\%_{drop}$ values are 20% or greater, with k_1^{rel} values of 1.00 or greater. k_2^{rel} values are decreased compared to Nitron **33a** with the introduction of electron-withdrawing groups (**33c**, **f**, **j**, **l**, **m**), or by addition of a proton (**33aH·Cl**) or methyl group (**192**) to the exocyclic nitrogen. Increased k_2^{rel} is seen with the introduction of an iodo substituent (**33g**) or in the presence of triethylamine (**33aH·Cl**, following the initial rapid decrease upon NEt_3 addition).

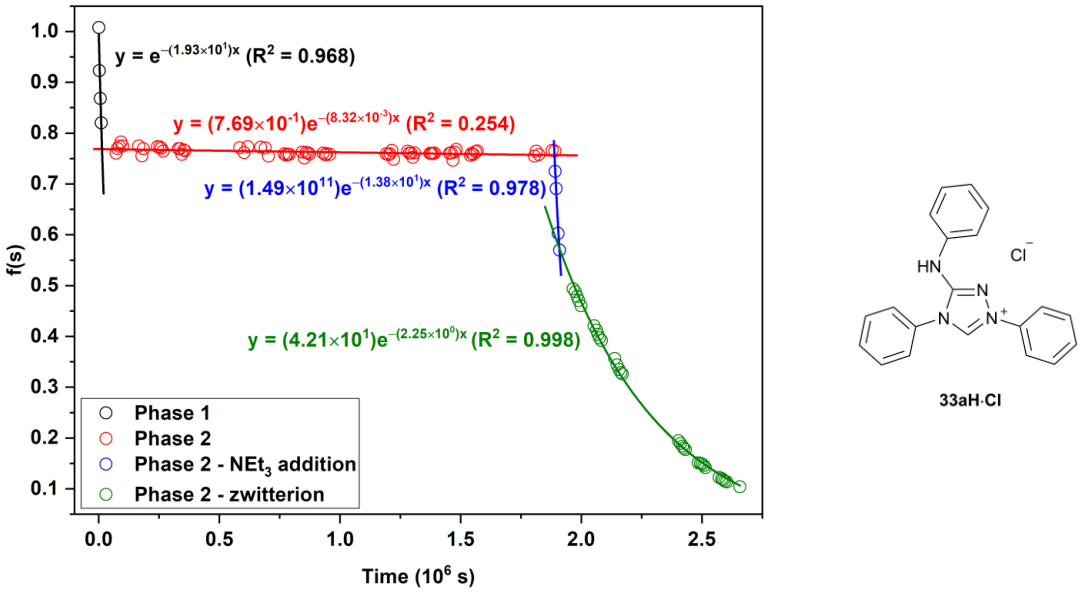


Figure 49 – Plot of the remaining fraction of starting material as a function of time for **33aH·Cl**. A slow reaction is observed for the hydrochloride salt, however upon addition of triethylamine to liberate the zwitterionic Nitron, a dramatic increase in rate is observed.

Nitron and all analogues synthesized within this work do not show peaks by NMR for the carbene when analysed within $CDCl_3$ and DMSO-d_6 for characterisation. Furthermore, DFT and experimental evaluation of the tautomeric distribution show small fractions of the carbene tautomer ($F_{Carbene}$) that are significantly below the values obtained for $\%_{drop}$. These observations suggest $\%_{drop}$ is likely not a direct measurement of the levels of carbene *in situ*.

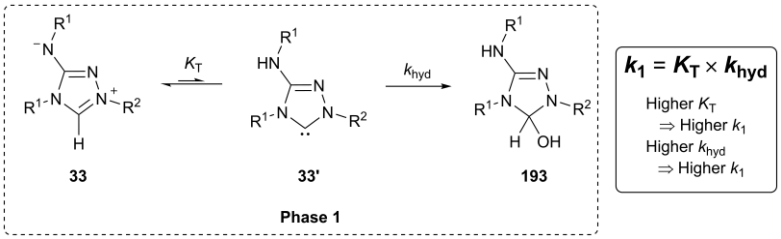
One option is that $\%_{drop}$ could relate to formation of hydrate **193** enabled by increased access to the NHC (**Scheme 108**). This explanation would therefore suggest k_1, which is seen to generally increase as $\%_{drop}$ increases, describes the overall rate of **193** formation starting with the tautomerisation between zwitterion and carbene as a pre-equilibrium described by K_T. This directly correlates to our predicted effect of substituent on K_T. The subsequent hydrate formation from **33'** is described by k_{hyd}. Considering other triazolium salts analysed within the group, a similar initial drop in integral is not observed in the H/D-exchange studies that could correspond to hydrate formation although these

studies are in predominantly aqueous solution with no more than 30% v/v acetonitrile co-solvent. A relevant example would be the *S*-triazolium salts **92·BF$_4$** analysed as part of this work in fully aqueous solution. Work by Murray[127] on the H/D-exchange of the C(5)-H position of Nitron analogues has also been undertaken. Within 30% v/v MeCN-d$_3$ in D$_2$O, at p*D* 1.09, Murray did not observe the same drop in integral. This indicates that the observed 2-phase behaviour is unlikely to be hydration of the cationic triazolium, with tautomerisation to the carbenic form of Nitron key to hydrate formation.

Table 24 – Summary of the rate constants, and percentage drop before start of phase 2, determined from semilogarithmic plots of the hydrolytic ring opening of Nitron towards Blatter radicals.

Analogue	k_1 (× 10^{-5} s^{-1})	k_1^{rel}	k_2 (× 10^{-8} s^{-1})	k_2^{rel}	k_1 / k_2	%$_{drop}$
33a	0.909 (± 0.06)	1.00	257 (± 5)	1.00	3.54	24
33aH·Cl	1.93 (± 0.25)	2.12	0.832 (± 0.179) [a] 230 (± 2) [b]	0.003 [a] 1.12 [b]	8.39 [b]	23
33c	0.211 (± 0.011)	0.23	35.1 (± 0.1)	0.14	6.01	8
33d	- [c]	- [c]	- [c]	- [c]	- [c]	- [c]
33f	1.45 (± 0.07)	1.60	75.5 (± 0.3)	0.29	19.2	32
33g	2.43 (± 0.24)	2.67	681 (± 3)	2.65	3.57	20
33h	- [c]	- [c]	- [c]	- [c]	- [c]	- [c]
33i	- [d]	- [d]	- [d]	- [d]	- [d]	- [d]
33j	1.06 (± 0.06)	1.17	91.1 (± 0.5)	0.35	11.6	26
33l	0.464 (± 0.006)	0.51	17.2 (± 0.1)	0.07	27.0	7
33m	0.673 (± 0.013)	0.74	38.2 (± 0.1)	0.15	17.6	12
192	0.454 (± 0.020)	0.50	- [e]	- [e]	- [e]	6

[a] Before addition of triethylamine [b] Following addition of triethylamine and rapid reaction. [c] Data unable to be fitted to decay process, discussed earlier. [d] Very poor solubility under experimental conditions. [e] No clear evidence of reaction during phase 2, proposed stable.



Scheme 108 – Option for phase 1 involving adjustment of the Nitron zwitterion (**33**) to carbene (**33'**) tautomerisation K_T, followed by hydrate (**193**) formation.

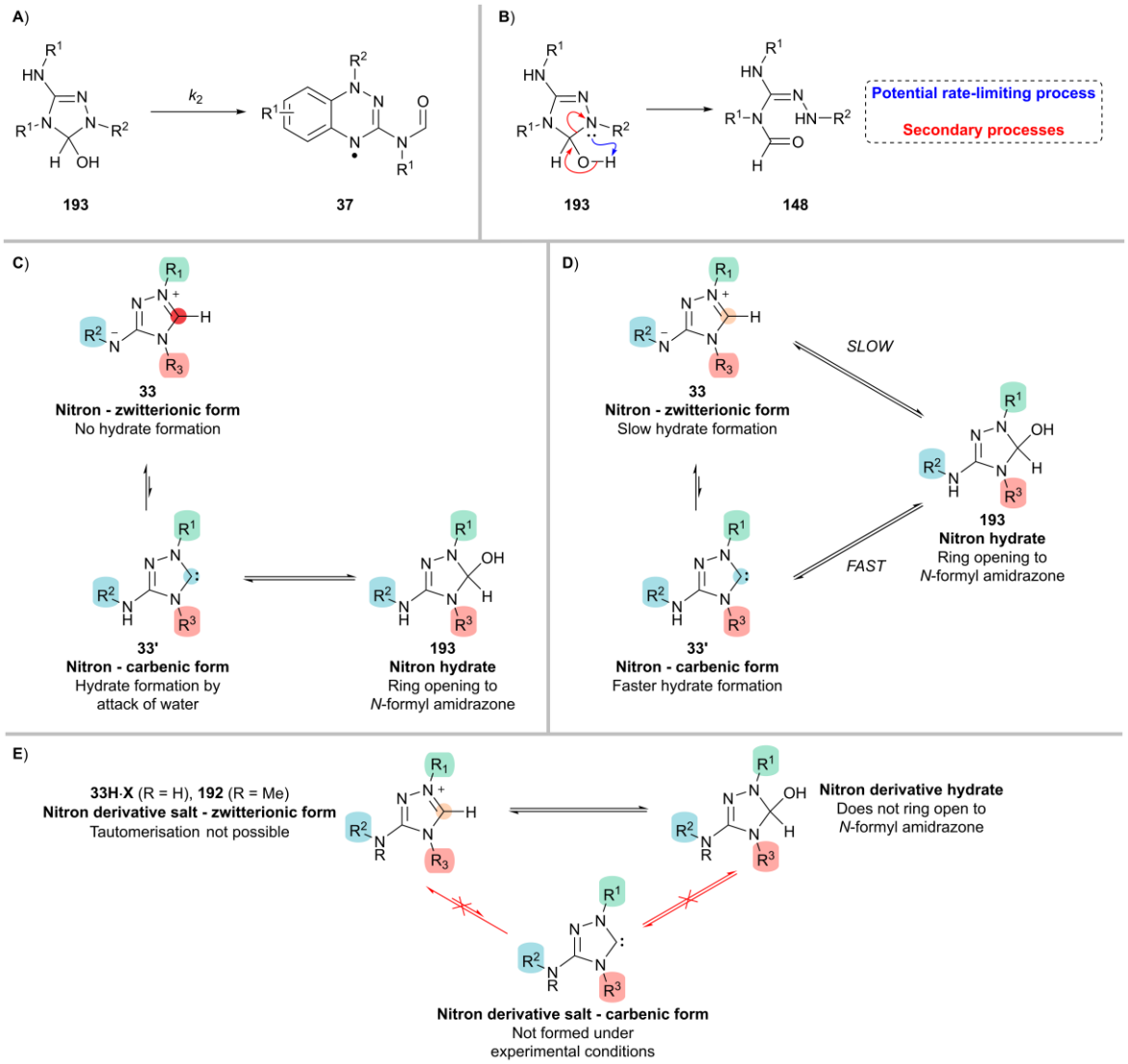
By obtaining the integral for the peak corresponding to the C(5)-H position, the H/D-exchange rate during the transformation can be estimated from **Equation 2**. Both the phenyl hydrogen and C(5)-H will decrease owing to radical formation, but an additional drop in C(5)-H would be indicative of H/D exchange. The exchange rate can be used as an indicator for the rate of tautomerisation. For Nitron, the obtained first order rate constant for C(5)-H exchange for deuterium (k_{ex}) is 2.30 × 10^{-6}

s^{-1} which is significantly lower than k_1 (9.09×10^{-6} s^{-1}) and so the tautomerisation between zwitterion and carbene is slower than the proposed hydrate formation. The estimate for k_{ex} is however comparable to k_2 (2.57×10^{-6} s^{-1}) and so it can be proposed that during phase 2 the rate of tautomerisation could limit the rate of ring opening to give Blatter radical. The rapid rate attributed to phase 1 could be due to higher levels of the carbenic form *in situ* that upon depletion leads into the transition to phase 2.

$$Ln\left(\frac{I^{Ar}{}_t}{I^{C(5)-H}{}_t}\right) = k_{ex}t \qquad \textbf{Equation 2}$$

As formation of **193** is key to further reaction occurring, phase 2 and k_2 could alternatively refer to the ring opening rate of **193** to undergo transformation to Blatter radical **37** (**Scheme 109A**). The kinetic analysis shows that k_2 decreases upon the introduction of electron withdrawing substituents to the N(1)-aryl ring (**33f**, **33j**), which would be expected to slow the ring opening owing to a decrease in N-basicity. Proton transfer during ring opening is potentially dependent on N-H bond formation, with C=O bond formation and C-N bond cleavage secondary processes in the asynchronous ring opening (**Scheme 109B**). With this additional hydration step being key, the mechanistic explanation from previous data requires updating to consider this step. One possibility is that this hydration occurs exclusively from the carbenic form of Nitron (**Scheme 109C**). The alternative is that hydrate formation leads to setup of a thermodynamic cycle (**Scheme 109D**) with the zwitterion able to undergo slow hydration and the carbene giving comparatively faster hydrate formation. The latter option explains why **192** and **33aH·Cl** also show an initial drop in integral with hydrate formed only from the zwitterion (**Scheme 109E**).

In general, all of the data in **Table 24** would be consistent with this explanation including the reaction of *N*-methylated Nitron **192**. The only experimental data difficult to rationalise by this mechanistic hypothesis is the NMR $\%_{drop}$ for the conjugate acid of Nitron **33aH·Cl**. The $\%_{drop}$ for **33a** and **33aH·Cl** are very similar (~23 %). In principle, the latter conjugate acid does not have the tautomerisation option and the formation of less carbene would be expected. The $\%_{drop}$ may instead be intrinsic to the whole scaffold, given that this similar drop is seen with Nitron and the conjugate acid form. It should be noted that Nitron analogues show unusual solubility profiles, however precipitation was not observed during these NMR experiments (apart from the carboxy-functionalised Nitron analogue **33i** which was not analysed). Another consideration is that solvent 'restructuring' occurs after the initial mixing, which could contribute to the initial drop although it is unlikely that this would vary substantially as a function of different Nitron derivatives.



Scheme 109 – **A** – k_2 is proposed to describe the ring opening and subsequent oxidative steps within the transformation to Blatter radical. **B** – The basicity at N(1) is postulated to dictate the rate of ring opening. **C** – Hydrate formation may exist as a secondary pre-equilibrium additional to the mechanism described with previous data. **D** – Consideration of hydrate formation may be more appropriate as a thermodynamic cycle. **E** – based on the observations with **192** and **33aH·Cl**, whereby slow hydrate formation can potentially occur from a Nitron derivative with modification at the exocyclic nitrogen, the potential hydrate formation from the zwitterionic form explains the observed change in integral.

Computational studies are in progress regarding the Nitron ring opening to Blatter radical. Transition state calculations suggest a possible reaction pathway whereby the carbenic form of Nitron deprotonates water to give a short-lived carbocation and hydroxide ion. From this transition state, hydroxide adds to the formed carbocation to give the proposed hydrate. Transition state calculations also support the feasibility of the proton transfer step to N(1), with an asynchronous proton transfer followed by breaking of the N(1)-C(5) bond. Full details of these calculations are planned to be discussed within a future publication.

3.3.3.4 – Revisiting computational studies of zwitterion-carbene tautomerisation

With an enhanced understanding of the role of zwitterion-carbene tautomerisation upon Blatter radical formation, the results discussed in Chapter 2.2.4 can be discussed in relation to the yield of Blatter radical that can be obtained from the Nitron analogue in question.

The lowest fraction of carbene is shown by DFT studies, regardless of method, to be for **33m** followed by **33c**. These analogues bear *p*-CF_3 groups upon the aryl ring attached to the exocyclic nitrogen and so the exocyclic nitrogen is stabilised in these cases. These two species were shown by Murray[127] to not afford the corresponding radical, and so DFT studies support the hypothesized effect of tautomerization when considering variation of the C(3)-NAr group.

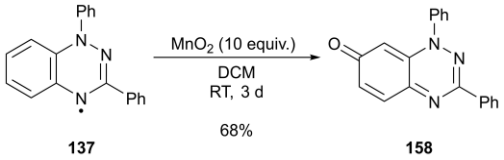
The introduction of electron-withdrawing groups upon N(1)-Ar was proposed in Chapter 2 to accelerate the formation of the Blatter radical by accelerating the hydrolytic ring opening, supported by an increased fraction of carbene in DFT studies. The updated mechanism additionally suggests that Blatter radical formation is impeded by introduction of electron-withdrawing groups on N(1)-Ar, due to the reduced basicity of N(1) in hydrate **193** during phase 2. In conclusion, whilst the tautomerism clearly influences the concentration of the more hydrolytically labile carbene tautomer, the role of substituents on overall radical formation is evidently more complex.

3.4 – Late-stage modification of Blatter radicals

This chapter section explores the possibility of undertaking late-stage functionalisation of Blatter radicals as a route to an expanded library of derivatives. Oxidation of Blatter radicals to the corresponding benzotriazine-7-one, electrophilic halogenation, and alkylation of the exocyclic nitrogen will be explored. The work will explore the derivatization of the C(3)-N substituted Blatter radical scaffold, which has not been investigated within the literature. The C(3)-N position is a useful nucleophilic handle that enables derivatization close to the benzotriazinyl core, and could enable more pronounced effects in the radical properties.

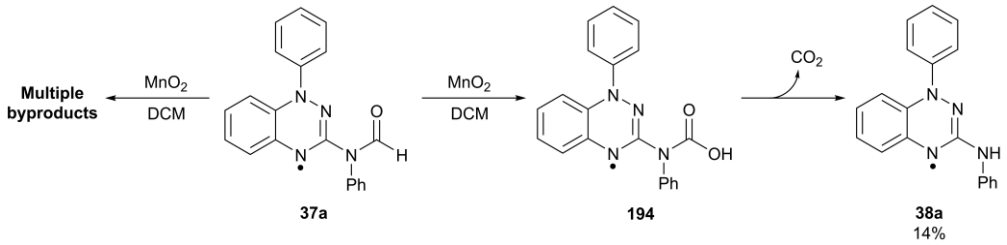
3.4.1 – Oxidation of Blatter radicals

Based on the literature procedure,[229] the benzotriazine-7-one of the parent BR was synthesized in good yields and with a straightforward isolation (**Scheme 110**). After 3 d the reaction mixture was filtered through celite and concentrated *in vacuo* to give the desired product. The yield obtained is slightly lower than that reported within the literature (82%).[235]



Scheme 110 – Using manganese(IV) oxide, the parent Blatter radical could be oxidised to the corresponding benzotriazine-7-one in good yields.

The oxidation of C(3)-amido radical **37a** initially prepared by our group was then explored, using the analogue obtained from Nitron to optimise the conditions. Unlike that seen in the oxidation of the parent radical **137**, LC-MS analysis indicated the formation of a wide variety of species with a large number of *m/z* peaks observed after 48 h. The reaction was repeated with hourly LC-MS monitoring, which showed that after 1 h a mixture of the amido (**37a**) and anilino radical (**38a**) is observed. Tracking from 1 h to 21 h shows the formation of a variety of *m/z* peaks, with no clear *m/z* peak that can be attributed to the formation of the benzotriazine-7-one. One proposal is that under the experimental conditions the carbamic acid **194** could be formed, which undergoes decarboxylation to give the anilino radical **38a** (**Scheme 111**). This oxidative decarboxylation method was explored as an alternative to using acid or base hydrolysis to gain the Blatter radical, however the partial conversion after 1 h and formation of a complex mixture following this meant that a yield of only 14% of **38a** could be obtained following column chromatography (0 → 10% MeOH in DCM). This method may be of use in cases where radicals are particularly p*H*-sensitive, but given the higher yields and more straightforward purification it is preferable to use the original base-catalysed deformylation to access **38a**.



Scheme 111 – Oxidation using manganese(IV) oxide is proposed to give the carbamic acid form of the Blatter radical, which can undergo decarboxylation to give the C(3)-anilino radical.

Attempts to undertake the oxidation upon the C(3) anilino radical **38a** were also unsuccessful. A peak for the *m/z* of the benzotriazin-7-one was observed by LC-MS during hourly tracking, however it indicated only traces of the product *m/z* which were not observed after 4 h. LC-MS also showed the formation of a complex mixture with a wide range of *m/z* values. Filtration through celite and removal of solvent *in vacuo* gave a viscous black oil, which by NMR showed the formation of various closed shell species that could not be separated by column chromatography. The *m/z* peaks observed in the reaction cannot be conclusively assigned to a structure, however possible byproducts from the oxidation (**Figure 50**) are thought to include the 1,3-diphenylbenzotriazine **196** and corresponding benzotriazine-7-one **158**.

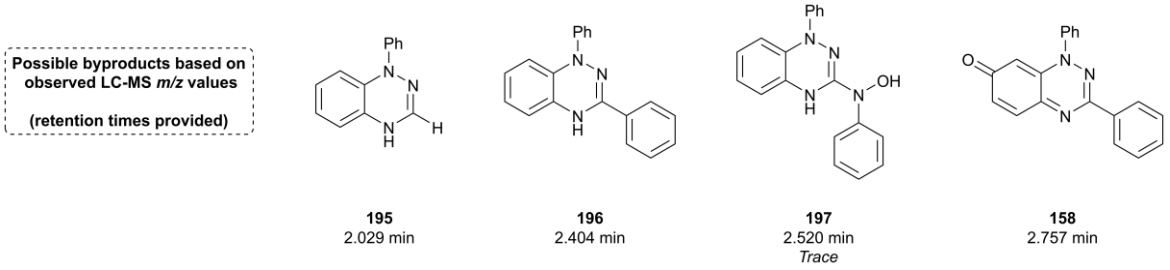
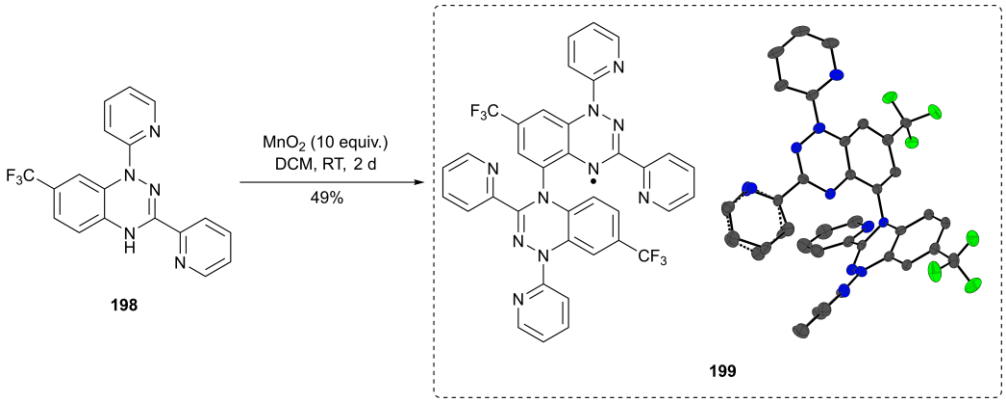


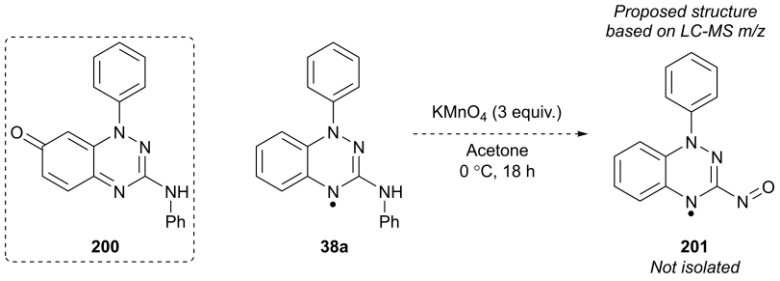
Figure 50 – Structures of the possible byproducts arising from MnO_2 oxidation of **36a**

Larger *m/z* peaks with mass varying by 314 units were also observed that indicate a polymeric product. There is literature evidence of radical dimerization under oxidative conditions (**Scheme 112**). Koutentis *et al*[234, 273] found that under oxidative conditions the 7-trifluoromethyl substituted benzotriazine **198** does not oxidise to give the expected BR, but instead forms a dimeric species (**199**) verified by single crystal XRD. The literature precedent for such reactions indicates that the oxidation of C(3)-amido / anilino radicals may give rise to addition products, and it is proposed that the potential of exocyclic *N*-oxidation can complicate the crude product mixture further.

Alternative conditions were explored for the transformation upon **38a**. Varying equivalents of MnO_2 did not lead to observation of the *m/z* corresponding to the desired product **200** by LC-MS. Changing the oxidant to $KMnO_4$ in acetone is suggested to form a nitroso-substituted radical (**201**) based on LC-MS evidence, however column chromatography (0 to 10% MeOH in DCM) was unsuccessful in isolating the species to further verify this (**Scheme 113**).



Scheme 112 – Oxidation of the pyrid-2-yl radical **198** has been validated by single crystal XRD to form the dimer **199**. XRD data reproduced with permission from: A. A. Berezin, G. Zissimou, C. P. Constantinides, Y. Beldjoudi, J. M. Rawson and P. A. Koutentis, *J. Org. Chem*, 2015, **80**, 8943 – 8944. Copyright © 2015 American Chemical Society.

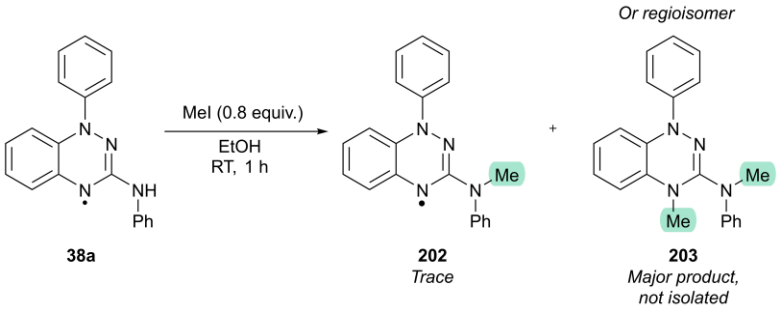


Scheme 113 – The oxidation of anilino radical **38a** with $KMnO_4$ is proposed to form the nitroso-substituted Blatter radical **201** based on LC-MS evidence. The product could not be isolated.

3.4.2 – Attempted alkylation and arylation of Blatter radicals

The addition of alkyl groups to the anilino Blatter radical **38a** using a generally applicable, high yielding methodology would provide a convenient route to a large library of Blatter radical analogues given the number of alkyl halides that are commercially available. However the potential of alkylation at the anilino nitrogen, N(4) position, or the N(2) position resulting from resonance from the exocyclic nitrogen makes the procedure particularly challenging.

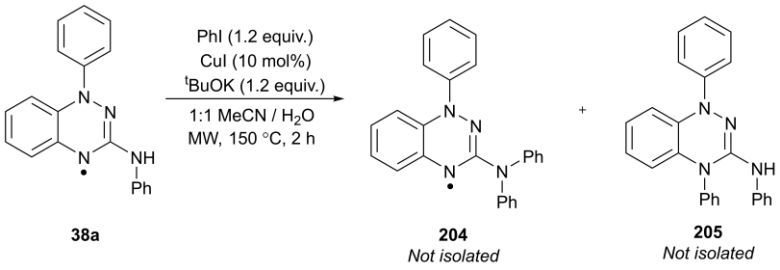
Using 0.8 equivalents of iodomethane to undertake the transformation resulted in evidence of several methylated products within 1 h reaction time (**Scheme 114**). The major species observed by LC-MS corresponds to the anilino radical starting material **38a** and the *m/z* of a dimethylated species with the possible structure **203**. This observation can be explained by the greater electron-donating character of the methylated nitrogen in the monomethylated radical **202**, which is structurally verified due to observation of the $[M]^+$ peak that indicates radical character. This more electron-donating amino group promotes further reaction with MeI, which outcompetes reaction with starting material. LC-MS shows only traces of the desired *m/z* corresponding to **202**, with column chromatography (0 to 10% MeOH in DCM) unable to isolate either species. As **203** could not be isolated, the site of methylation is not known.



Scheme 114 – Attempted methylation of anilino Blatter radical **38a**. LC-MS indicates that the major product is the dimethylated anilino benzotriazine, with one potential regioisomer shown as **203**; the other major peak corresponds to starting material. Traces of the monomethylated radical **202** *m/z* are observed.

Attempting the conditions shown in **Scheme 114** at 0 °C, or the addition of iodomethane portionwise, did not prevent double methylation seemingly being favoured over the methylation of **38a**. Me_3OBF_4 in DCM was used, hoping that the more reactive methylating agent may make starting material reaction compete with double addition, however the major product was once again the double addition species. In all attempts the double-methylated species **203** could not be separated from **202** or residual **38a** by DCM/MeOH column chromatography or recrystallisation from ethanol.

Ullmann coupling to introduce a phenyl group to the Blatter radical is seemingly more successful – clean conversion to the product *m/z* is observed by LC-MS and TLC indicates good separation from the starting anilino radical (**Scheme 115**). However, recrystallisation from ethanol, column chromatography (0 → 10% MeOH in DCM) or RP-LC did not afford a pure radical supporting the idea that multiple regioisomers are again observed. Further analysis of the LC-MS data from the isolated mixture shows two peaks for the product *m/z* with similar retention time, proposed to correspond to the desired product **204** and non-radical benzotriazine **205**.



Scheme 115 – Ullmann coupling to the anilino Blatter radical **38a** proceeds without the formation of byproduct, however forms inseparable, structurally similar species (**204** and **205**).

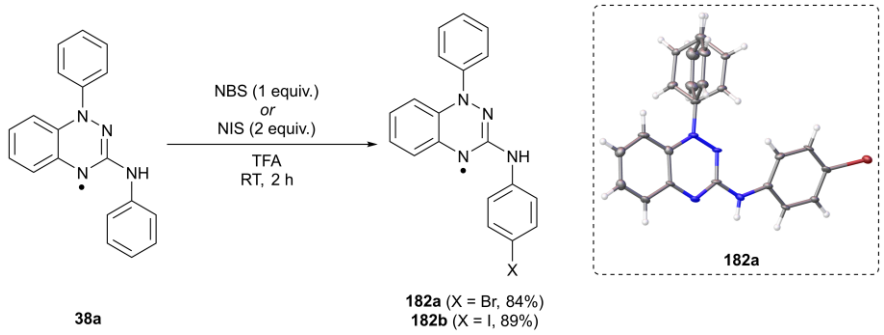
3.4.3 – Electrophilic halogenation of Blatter radicals

Under the conditions implemented in the halogenation of Nitron (Chapter 2.3.4),[165] electrophilic halogenation of Blatter radicals was attempted. Surprisingly, given the literature precedent for such a reaction on benzotriazine-7-ones,[252] there is no known discussion of Blatter radical halogenation

using *N*-halosuccinimide reagents. Halogen atoms are instead generally introduced by variation of the starting material.[211, 236, 246]

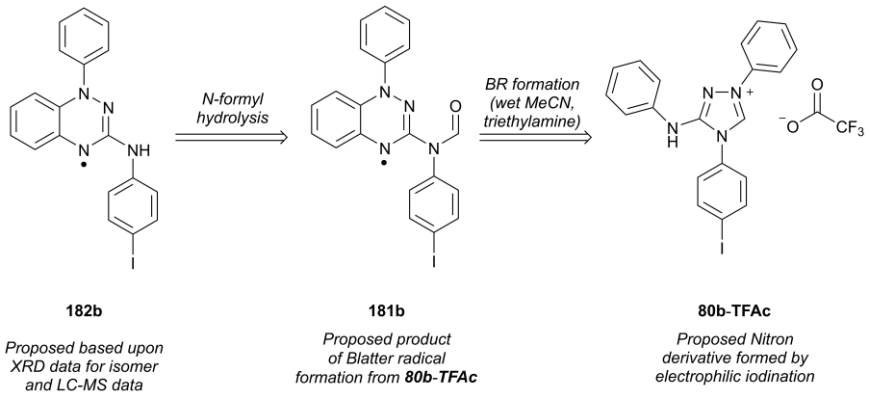
The electrophilic halogenation of amido Blatter radicals, as was expected, led to hydrolysis of the *N*-formyl group under the acidic conditions used. LC-MS did not show clear evidence for iodination of the amido radical, verifying that the hydrolysis is preferable over electrophilic halogenation.

Regioselective addition of a bromo or iodo group to the anilino ring of **38a** is observed in high yields under the electrophilic halogenation conditions (**Scheme 116**). The location of the halogen atom is verified by single-crystal XRD for **182a**, and it is assumed that the same substitution will be observed in **182b** (supported by the LC-MS data of **182b** being distinct from that of the isomer with N(1)-aryl iodination, **38g**).



Scheme 116 – Electrophilic halogenation of **38a** gives regioselective addition to the anilino ring in high yields. Single crystal XRD of **182a** verifies the structure.

With the structure of **182b** proposed based on XRD and LC-MS evidence, known to be identical to the major product in the hydrolysis of **181b** based on identical LC-MS retention times, it can be proposed with good evidence that the location of the halogen atom in **80bH·TFAc** is on the N(4)-ring (**Scheme 117**).



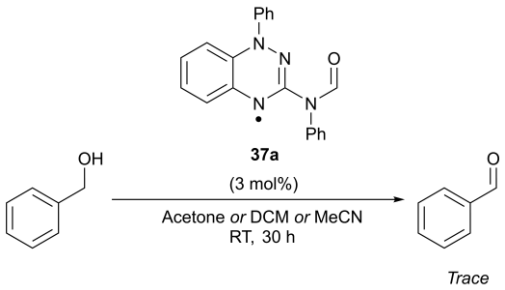
Scheme 117 – Based on single crystal XRD data of **182a**, and variation in LC-MS data between **38g** and **182b**, it can be proposed that the iodine of **182b** is also on the anilino ring. LC-MS retention times for **182b** are the same as the major product obtained from acid-catalysed hydrolysis of **181b**, and so it can be proposed that they are structurally identical. Thus, the amido radical used in the acid-catalysed hydrolysis must have the structure **181b** and be derived from the Nitron analogue with the structure **80bH·TFAc**. With the same logic, it can be proposed **80aH·TFAc** also bears a bromine atom in the *para*-position of the N(4)-ring.

3.5 – The organocatalytic applications of Blatter radicals

Radical-mediated reactions have emerged as a key tool in synthetic chemistry due to the ability to undertake chemoselective carbon-carbon and carbon-heteroatom bond formation.[274] Despite this, to our knowledge little work has been undertaken in the area of organocatalysis using Blatter radicals. This chapter section will undertake exploration of the organocatalytic potential provided by this persistent class of radicals, based around the oxidation of benzyl alcohol to benzaldehyde. This work hopes to somewhat address the lack of information within the literature regarding Blatter radical organocatalysis, with hopes of initiating an area of research that may uncover efficient transformations of synthetic or even industrial interest.

3.5.1 – The oxidation of benzyl alcohol

One transformation investigated was the oxidation of benzyl alcohol to benzaldehyde using the C(3)-amido radical derived from Nitron (**Scheme 118**). The reaction was attempted using 0.1 mL benzyl alcohol in three different solvents with 3 mol% **37a**. A control was also undertaken, stirring only benzyl alcohol in each of the solvents. Reaction monitoring every 1 – 2 h was undertaken using TLC (EtOAc / hexane) for the first 8 h, however no clear spot could be seen for the product in any of the three reactions. After 30 h of stirring, each of the reaction mixtures was concentrated *in vacuo* and analysed in ^{1}H NMR spectroscopy with 128 scans. As was expected, given that oxidation catalysts and occasionally forcing conditions are required for the oxidation of benzyl alcohol to benzaldehyde,[275] evidence for the oxidation of benzyl alcohol after 30 h stirring within solvent is negligible with integrals of the methylene protons varying by <1% *versus* the starting material (**Figure 51A**). In the presence of 3 mol% **37a**, the methylene integral drops by approximately 5% and there is growth of the peak corresponding to the aldehydic proton in all three cases (**Figure 51B**), considering data from the reaction in acetone. It is crucial to point out that these results do not verify that oxidation is taking place – with a delay time of only 5.09 seconds between scans this is shorter than, for example, the 5.72 s T_1 value for the aldehydic proton determined by Mehrotra *et al* also within $CDCl_3$.[276] NMR values cannot be seen as quantitative without a delay of greater than 5 × T_1 for all protons of interest in the molecule.[272] The presence of Blatter radical *in situ* is proposed to promote rapid relaxation of spins and thus reduce the T_1 value, however the magnitude of this change is unknown. The integral changes observed are also not proportional to the change expected from the reaction. Finally, with such small changes it is also important to consider errors in integrating peaks. These findings are therefore considered as indication, but not evidence, of Blatter radicals potentially catalysing the oxidation of benzyl alcohol.



Scheme 118 – Using the C(3)-amido radical **37a**, potential evidence for the oxidation of benzyl alcohol to benzaldehyde was observed.

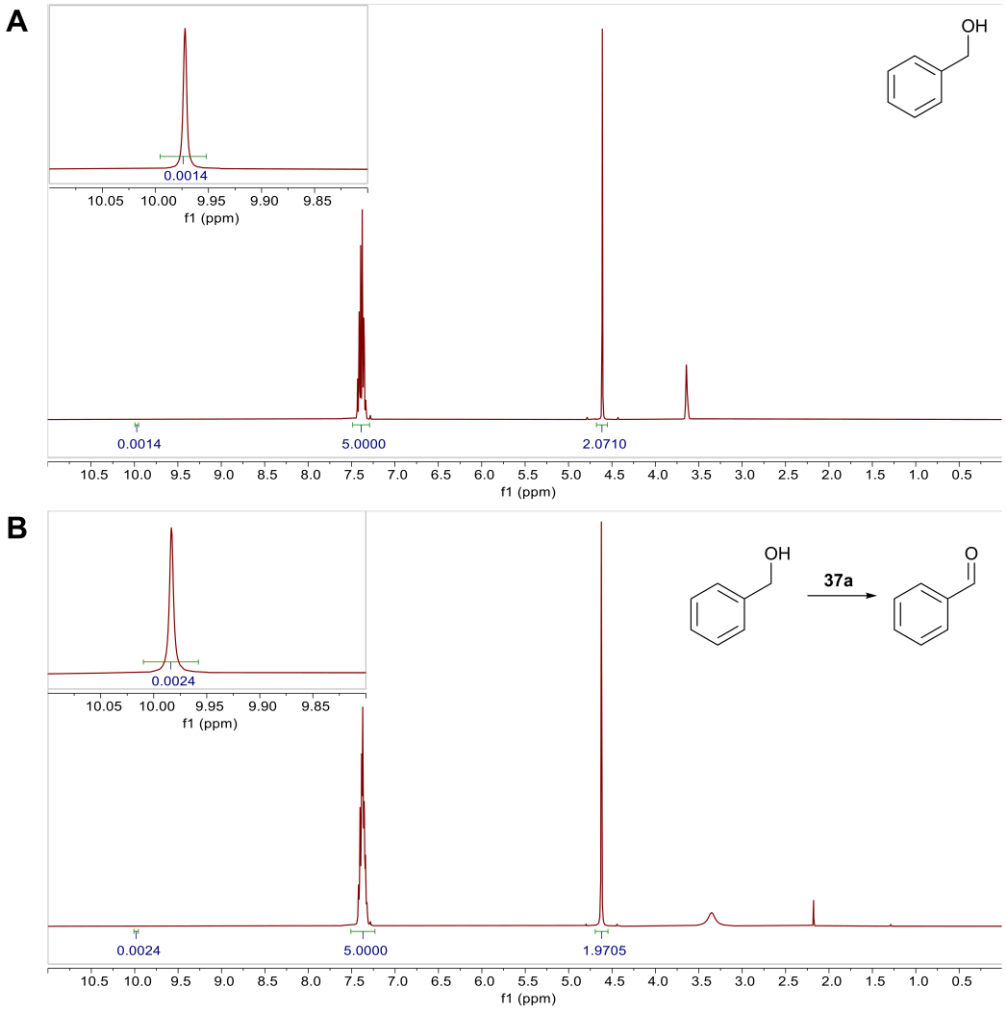
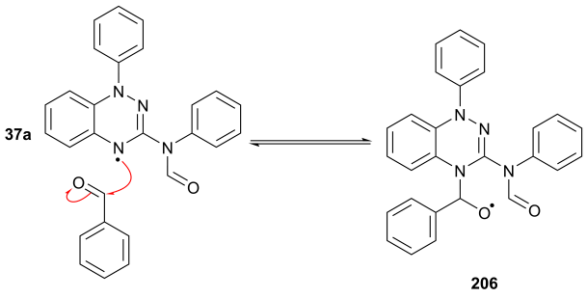


Figure 51 – ^{1}H NMR spectra investigating the oxidation of benzyl alcohol by **37a** in acetone. **A** – NMR of the benzyl alcohol starting material following 30 h stirring within acetone. **B** – NMR of the reaction mixture obtained after stirring benzyl alcohol and 3 mol% **37a** for 30 h. The $CDCl_3$ peak is adjacent to the aromatic multiplet and is not included within the arbitrary integral for aromatic protons. Data collected from 128 scan ^{1}H NMRs with a delay of 5.09 s between scans.

In repeats of the conditions shown in **Scheme 118** use of a photoreactor at 420 nm and the use of 1 equivalent H_2O_2 (enabling proposed oxidation of the Blatter radical *in situ* to the *N*-oxide) were explored, however substantial oxidation was not seen by ^{1}H NMR spectroscopy after 28 h in both cases.

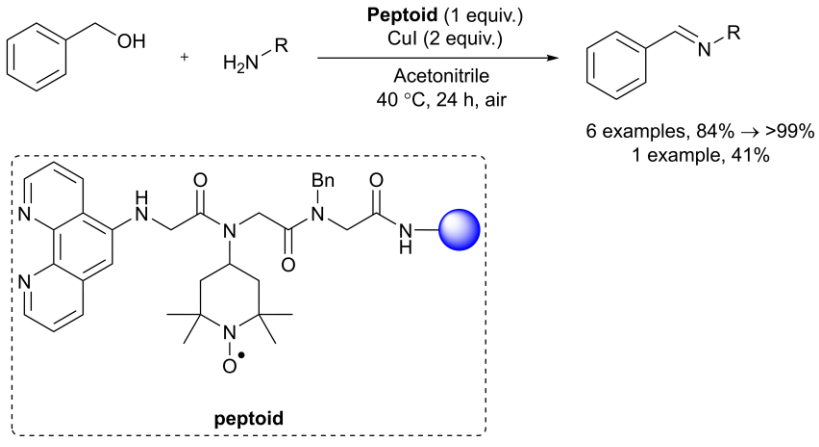
One possibility for the low conversion levels may be that the aldehyde product is able to form a radical adduct with **37a** (**206**), similar in the manner to that discussed with CoRC, which would lead to poisoning of the catalyst (**Scheme 119**). It would also explain why, if there are further reactions, there is no additional NMR peaks for a byproduct. Investigating further reactions upon the formed aldehyde were therefore of interest, and so oxidative coupling to amines was explored.



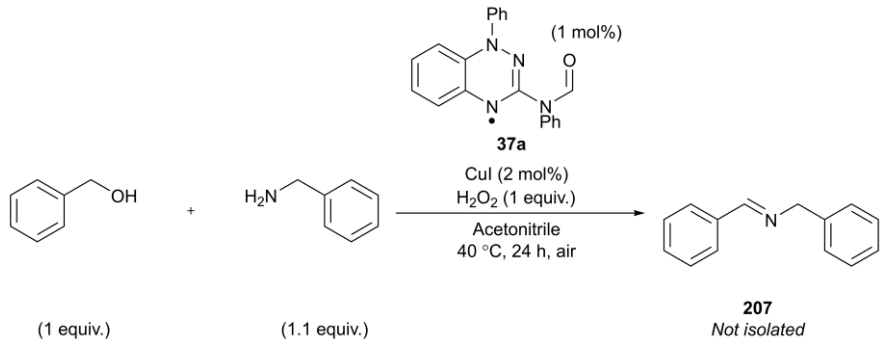
Scheme 119 – The potential formation of a radical adduct **206** by addition of **37a** into the formed benzaldehyde molecules. The adduct would not be expected to undertake benzyl alcohol oxidation. Given the configuration of the adduct drawn, it may also be possible for further reactivity with the C(3)-amido group to generate a 1,3,5-oxadiazinane ring.

3.5.2 – Oxidative coupling of benzyl alcohol and benzylamine

Work by Stamatin and Maayan[277] explored the oxidative coupling of benzyl alcohol to a range of amines, using a peptoid scaffold functionalised with a phenanthroline group (which chelates to copper) and TEMPO (2,2,6,6-tetramethyl-1-piperidinyloxy radical) (**Scheme 120**). TEMPO is structurally related to Blatter radicals following oxidation of the N(4) position, which is proposed to be accessible in small amounts by addition of hydrogen peroxide to a solution of the radical. Therefore, the mimicking of the peptoid system shown in **Scheme 120** by using CuI, Blatter radical and hydrogen peroxide was investigated (**Scheme 121**).



Scheme 120 – Summary of the oxidative coupling of benzyl alcohol to amines implementing a peptoid functionalised with two catalytic side chains, undertaken by Stamatin and Maayan. Percentages of product correspond to the conversion observed by gas chromatography (GC).



Scheme 121 – Summary of the oxidative coupling method explored within this work. The Blatter radical **37a** is proposed to be oxidised to give an activated catalyst similar in structure to TEMPO, which can react with the benzyl alcohol to generate benzaldehyde *in situ*. The generated benzaldehyde can then react with amine to give the imine product **207**.

After 19 h stirring at RT, gas chromatography-mass spectrometry (GC-MS) indicates formation of the desired product, and after 24 h ^{1}H NMR spectroscopy indicates 9% conversion (comparison of methylene group in alcohol to imine proton). The reaction was checked after 3 d showing minimal change, so was terminated after 29 d stirring at RT – 13% conversion was observed at this time.

Given that unsatisfactory conversion was observed, the reaction shown in **Scheme 121** was repeated over a similar time period with varying conditions detailed in **Table 25** to explore the effects of adding radical, hydrogen peroxide and copper(I) iodide alongside allowing or excluding air. Reactions were analysed by ^{1}H NMR spectroscopy: a 0.1 mL aliquot of the reaction mixture was concentrated *in vacuo*, before resuspending in 0.8 mL of deuterated chloroform. Reaction progress was quantified by analysing the integrals of the methylene peaks corresponding to the methylene group of benzyl alcohol and the methylene group of the imine product (**Figure 52**).

Table 25 – Summary of the conditions used to optimise the oxidative coupling for the amido radical. All runs use benzyl alcohol (1 equiv.) and benzylamine (1.1 equiv.) in acetonitrile (2 mL). Where radical is added, 1 mol% is used. Where H_2O_2 is added, 1 equiv. is used. Where air exposure is permitted, a needle through a rubber septum is used. Where CuI is added, 2 mol% is used.

Run	Radical	H_2O_2	Reaction atmosphere	Copper(I) iodide	NMR conversion – 42 d (%)
A	None	✗	Air	✗	1 [a]
B	None	✓	Argon	✗	2 [a]
C	**37a**	✗	Air	✗	7
D	None	✗	Air	✓	10
E	**37a**	✓	Argon	✗	2 [a]
F	None	✓	Argon	✓	18
G	**37a**	✗	Air	✓	21
H	**37a**	✓	Argon	✓	16

[a] Conversion after 14 d.

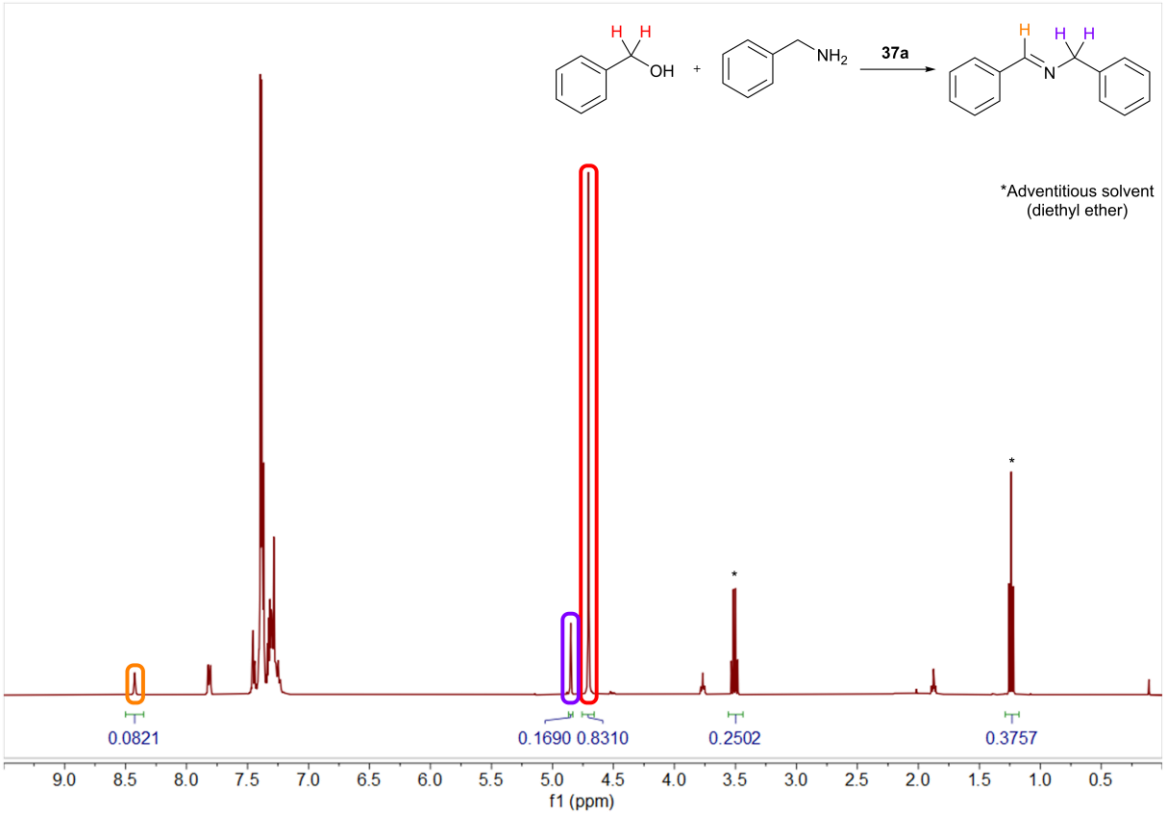


Figure 52 – Example NMR (run **G**, 341 h) showing the method for reaction quantification. The two peaks corresponding to the methylene bridge of benzyl alcohol (4.70 ppm) and the methylene bridge of the imine product (4.85 ppm) are integrated and set to a total integral of 1, giving the fraction of product as 0.169 in this case. No clear peaks (such as the proton corresponding to benzaldehyde) were observed outside of this region.

Figure 53A shows the change in fraction of substrate throughout the reaction monitoring. As is expected runs where the starting materials are stirred in the presence of air or H_2O_2 (runs **A** and **B**, respectively) show little conversion, with the imine formation observed explained by aldehyde present within the benzyl alcohol. Adding **37a** and stirring within air shows steady product formation (run **C**) however the use of peroxide was not effective (run **E**). CuI also shows steady product formation within air (run **D**), however by using CuI and H_2O_2 (run **F**) rapid initial conversion was observed and a steady increase followed this to reach approximately 18% conversion within the reaction timeframe. Finally, by using CuI and **37a** in air (run **G**) a conversion of approximately 21% is achieved within the reaction timeframe, the best within those tested; using hydrogen peroxide under argon (run **H**) gave approximately 16% conversion. Note that the use of H_2O_2 under an air atmosphere, in the presence of CuI and **37a**, gave approximately 13% conversion after 29 d (~700 h) in the initial test. Runs **F**, **G** and **H** all showed greater conversion within a similar timeframe than the initial test.

The same procedure was then implemented on the corresponding anilino radical (**38a**). **Table 26** summarises the runs undertaken whilst **Figure 53B** shows the change in fraction of imine over time. As was seen with **37a**, the use of air, CuI and **38a** gave the best conversion with 27% imine formation within the reaction timeframe. Considering tracking relating to **38a** was only undertaken for 681 h

versus 1017 h for **37a**, **38a** gives a 1.3 times greater conversion under the best conditions (run **G** *versus* **K**). The other results are also generally in agreement with that seen for **37a**.

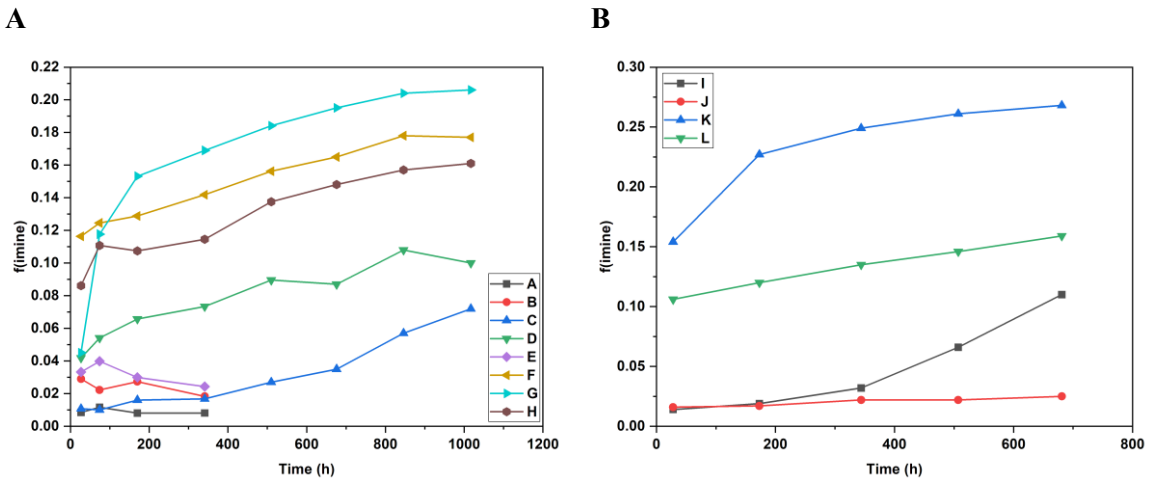


Figure 53 – **A** – Summary of the fraction of imine product observed within the reaction mixture (determined by ^{1}H NMR) as a function of time. The letters provided within the legend correspond to the run identifiers provided in **Table 25**. Runs **A**, **B** and **E** were terminated after 341 h due to low conversion rates and drops in the fraction of imine indicating a catalytic process was not taking place. **B** – Summary of the fraction of imine product observed within the reaction mixture (determined by ^{1}H NMR) as a function of time. The letters provided within the legend correspond to the run identifiers provided in **Table 26**.

Table 26 – Summary of the conditions used to optimise the oxidative coupling for the anilino radical. All runs use **38a** (1 mol%), benzyl alcohol (1 equiv.) and benzylamine (1.1 equiv.) in acetonitrile (2 mL). Where H_2O_2 is added, 1 equiv. is used. Where air exposure is permitted, a needle through a rubber septum is used. Where CuI is added, 2 mol% is used.

Run	Radical	H_2O_2	Reaction atmosphere	Copper(I) iodide	NMR conversion – 28 d (%)
I	**38a**	✗	Air	✗	11
J	**38a**	✓	Argon	✗	3
K	**38a**	✗	Air	✓	27
L	**38a**	✓	Argon	✓	16

The data within air shows that CuI has a dual role under the experimental conditions. When CuI alone is stirred with benzylamine and benzyl alcohol, conversion to the imine is observed that is potentially catalysed by CuI – 10% conversion is seen after 42 d (run **D**). The second role is enhancing the effect of Blatter radical addition on imine formation. **37a** leads to 7% conversion after 42 d (run **C**), which is increased to 21% by addition of CuI (run **G**). The same is seen with **38a**, albeit within 28 d instead of 42 d (11% → 27% by addition of CuI, runs **I** and **K** respectively). There is an additive effect observed, with the addition of CuI and radical showing greater conversion than the addition of one species – this is true for **37a** and **38a**.

With addition of 1 mol% radical, conversions significantly greater than 1% would suggest that the radical is not a stoichiometric reagent, and instead is regenerated as part of a catalytic cycle.

Considering the examples using radical only within air (run **C** and **I** for **37a** and **38a**, respectively), conversions of 7% and 11% are observed. Whilst regeneration of the catalyst is not directly evidenced, the conversions would suggest 7 and 11 turnovers respectively of each radical occur and so the Blatter radicals have a potential organocatalytic activity. Furthermore, with a conversion of less than 1% by stirring in air after 14 d, and no indication of increasing imine formation, the observed imine formation in runs **C** and **I** (2% for **37a**, 3% for **38a**, after 14 d) can be attributed to the Blatter radical over reaction resulting from stirring within air. The additive effect seen with CuI may be catalysing the oxidation of the reduced Blatter radical following imine formation, accelerated over undertaking the oxidation of the benzotriazine alone in air.

The reaction times used and conversions observed are not particularly convenient for synthetic or industrial application, however it must be highlighted that these reactions were undertaken with catalyst loadings of 1 and 2 mol% for the radical and CuI respectively. Furthermore, considering that 100 and 200 mol% loading was used in the reference work for the peptoid and CuI respectively,[277] 100-fold greater than that used within this work, there is a great deal of flexibility within the catalyst loadings to optimise this procedure. The findings have shown that the Blatter radical can be considered as a potential organocatalyst with results showing the radical can undergo 6 or 11 catalytic cycles on average for **37a** and **38a** respectively (runs **C** and **I**, respectively).

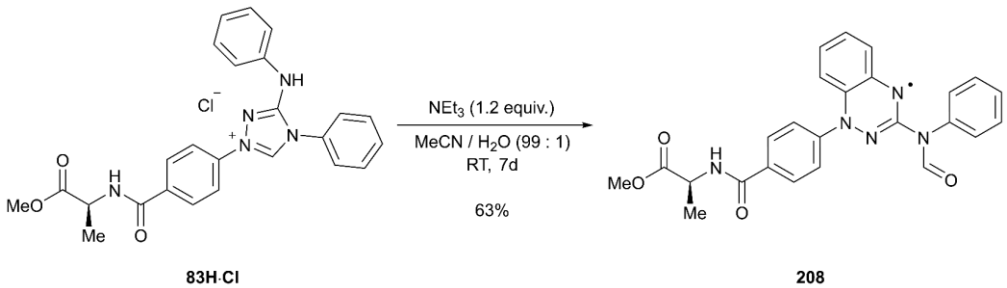
3.6 – Bioconjugation of Blatter radicals

The ability to introduce Blatter radicals to specific locations of a protein scaffold unlocks the possibility of analysing the protein structure, binding interactions and dynamic behaviour by EPR,[259] using the Blatter radical as a spin label. Furthermore, given the proposed role of a benzotriazinyl radical in the mechanism of the experimental anticancer prodrug Tirapazamine, the bioconjugation of Blatter radicals may be of medicinal benefit to enhance bioavailability. This chapter section explores the bioconjugation of Blatter radicals to peptide scaffolds to direct future studies on the development of Blatter radicals as spin labels.

3.6.1 – 'On-bioconjugate' conversion of 1,2,4-triazolium salts to Blatter radicals

One methodology to obtain Blatter radical bioconjugates is the conversion of Nitron analogue bioconjugates within wet acetonitrile. The mild conditions used within the transformation should not impact the peptide structure, and may be beneficial as to prevent side reactions by the Blatter radical during peptide synthesis.

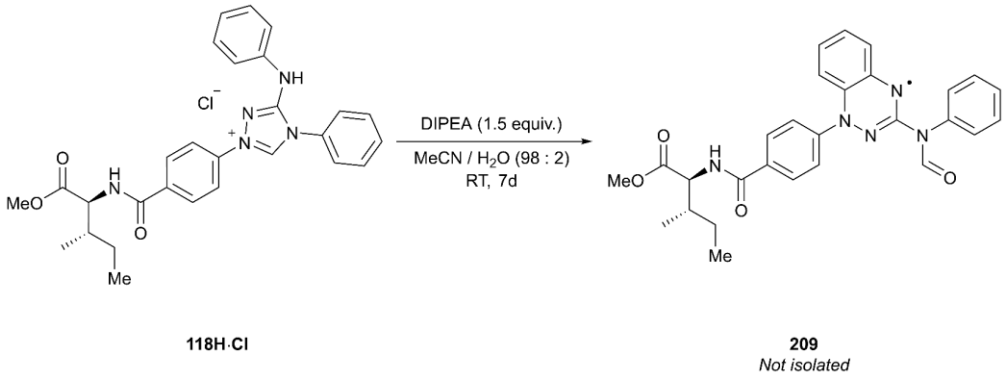
Using the Nitron alanyl conjugate **83H·Cl**, the 'on-bioconjugate' conversion to Blatter radical **208** was verified by LC-MS and HRMS (**Scheme 122**). Recrystallisation of the crude product using the standard conditions for C(3)-amido radicals of hot ethanol indicated instability of the product, and undertaking the procedure with room temperature ethanol amongst a range of other solvent mixtures was not successful in removing residual starting material. Column chromatography (0 → 10% MeOH in DCM) was not successful either, with only traces of product eluted from the column. Instead, the use of DCM/ether and cooling to −20 °C was able to precipitate the residual starting material amongst small amounts of the product, enabling isolation of the Blatter radical bioconjugate in good yields.



Scheme 122 – The conversion of the Nitron alanyl conjugate **83H·Cl** to the corresponding Blatter radical **208** was achieved in good yields. Verification by XRD was not possible.

In collaboration with Katherine Deck, a 4th year MChem student under my supervision, the transformation of the Nitron isoleucinyl conjugate **118H·Cl** into the corresponding Blatter radical was explored. The formation of **209** was verified based on LC-MS and HRMS evidence, however

unlike with the alanyl analogue additional peaks were observed that were linked to byproduct formation. The Blatter radical could not be isolated.

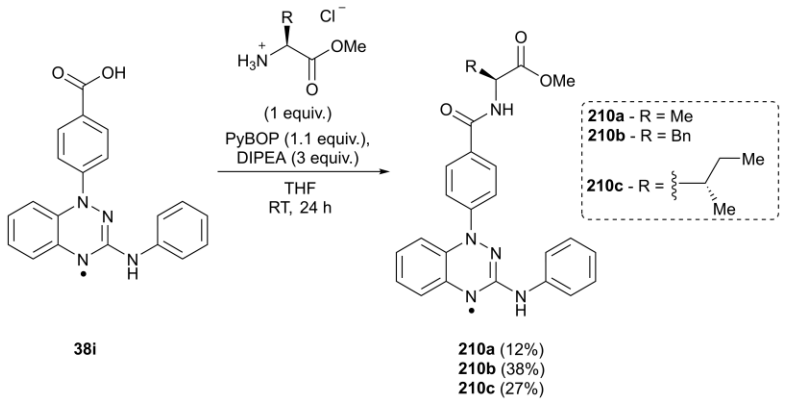


Scheme 123 – The conversion of Nitron isoleucinyl conjugate **118H·Cl** to the corresponding Blatter radical **209**. The product could not be isolated.

3.6.2 – Late-stage bioconjugation of Blatter radicals

The alternative to 'on-bioconjugate' Blatter radical formation is the bioconjugation of a Blatter radical to a peptide scaffold at the late-stages of a synthetic process. By using this methodology the chances of side reactions by the radical are limited, and there will be less waste given that the conversion of Nitron to Blatter radical is far from quantitative; some of the bioconjugated Nitron will form the undesired triazabutadiene.

In collaboration with Deck, a series of amide couplings were possible upon the carboxy-functionalised C(3)-anilino radical **38i** to give bioconjugated BRs **210a**–**c** (**Scheme 124**). It was assumed that the coupling procedure would be most effective under the optimised conditions discovered for the coupling of amino acids to Nitron analogues. Radical bioconjugates were isolable using RP-LC and verified by LC-MS and HRMS.



Scheme 124 – Summary of the Blatter radical bioconjugates that were synthesized by PyBOP coupling

3.7 – Conclusions

The Blatter radical is a persistent species that is of interest for a variety of applications primarily focussed within the area of materials chemistry. By better understanding the synthesis and properties of Blatter radicals, the structures can be tailored to enable design of efficient, multifunctional, stable radical materials.

Expansion of the library of Blatter radicals synthesised from Nitron analogues and characterisation by standard techniques enabled property to structure relationships to be made to direct future radical design. The previously unexplored thermal stability by TGA showed a robust stability comparable to radicals intentionally designed for stability at high temperatures.

Mechanistic studies illustrate the role of zwitterion-carbene tautomerisation in Blatter radical formation. The tautomerisation to the carbenic form of Nitron is thought to play a major role in Nitron hydrate formation, that can generally be an indicator for the rate of Blatter radical formation. Complexities arise when considering the effect of substitution upon the N(1)-Ar ring, which is proposed to reduce the basicity of the N(1) position and impede the proton transfer involved in hydrate ring opening.

Late-stage derivatization showed the ability to undertake regioselective halogenation of the Blatter radical, however attempts to alkylate or oxidise the Blatter radical led to significant issues from side-reactions.

Synthetic, potentially organocatalytic, applications of Blatter radicals show promise in the area of oxidative coupling of alcohols to amines. With 1 mol% radical and 2 mol% CuI, conversions of up to 27% were observed by stirring under air. It is hoped that this can be optimised in the near future as an effective C-N bond forming methodology. The low catalyst loading used in these initial studies gives a great deal of flexibility in improving this process.

Finally, Blatter radical bioconjugates have been prepared as a ‘proof-of-principle’ as a derivative with potentially improved medicinal properties or that can be expanded to the implementation of Blatter radicals as spin probes.

4 – The syntheses of 1,2,4-benzotriazines and their related N-oxides

4.0 – Foreword

1,2,4-Benotriazine *N*-oxide scaffolds have shown promise as anticancer[204, 228] and antimicrobial[227, 278] agents. One key example for this work is the experimental anticancer prodrug Tirapazamine.[279] The mode of action for these compounds has been proposed to involve *N*-centred benzotriazinyl radicals, structurally similar to Blatter radicals, as the active drug.[204] There is not a clear link within the literature between the fields of Blatter radical synthesis and the cytotoxicity of Tirapazamine and related prodrugs.

Following a brief discussion of relevant literature (Section 4.2), work in this chapter will explore the synthesis of benzotriazines and their *N*-oxides. Through the synthesis of 1,2,4-benzotriazines-1-oxides by the Arndt benzotriazine synthesis (Section 4.3), Tirapazamine can be accessed through oxidation (Section 4.4.1). The gram-scale synthesis of Tirapazamine allows for late-stage derivatisation such as bioconjugation and for use in cellular assays. Reduction of the 1-oxide gives a key intermediate identified in the synthesis of Blatter radicals (Section 4.4.2), however these studies show that the addition of organolithium reagents following published conditions leads to an unexpected transformation described in Section 4.5.

4.1 – Chapter contributions

All work detailed in this chapter was undertaken by the present author.

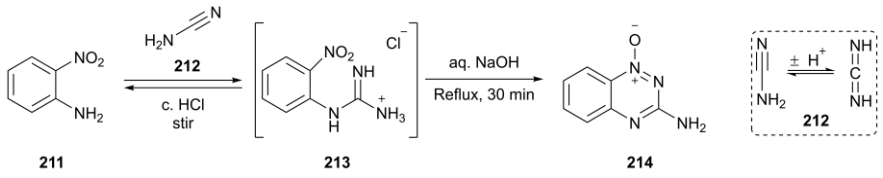
4.2 – Introduction

The 1,2,4-benzotriazine scaffold is an important heterocycle due to the diverse biological activity exhibited[280-283] and more recent interest in the synthesis of Blatter radicals.[69, 70] A diverse range of routes to benzotriazine analogues have been described within the literature,[68, 284, 285] however the Arndt benzotriazine synthesis (ABS) discussed below is the only synthetic route relevant to this work.

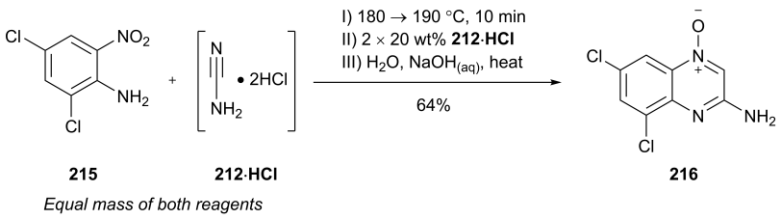
4.2.1 – Arndt benzotriazine synthesis

The condensation of 2-nitroanilines **211** with cyanamide **212** was illustrated by Fritz Arndt[244, 286] to give rise to a C(3)-substituted 1,2,4-benzotriazine-1-oxide scaffold (**Scheme 125**). This transformation required the melting of **211** and **212** together, before treating with concentrated HCl to initiate the highly exothermic process of guanidine (**213**) formation. The solution of **213** is further treated with concentrated aqueous NaOH and heated at reflux to precipitate the formed benzotriazine-1-oxide **214**.[286] The reaction is effective due to the carbodiimide tautomer of **212** – this tautomerisation weakens the C-N triple bond allowing for efficient reaction with aniline.

The exploration of benzotriazines as antimalarials by Wolf and coworkers[286] adapted Arndt's conditions to use acetic acid as solvent, enabling larger scale and higher yielding synthesis of **214**. In cases where the guanidine formation was unsuccessful, where electron-withdrawing groups are upon the aniline, cyanamide dihydrochloride **212·HCl** was used and the reaction was briefly heated (**Scheme 126**).



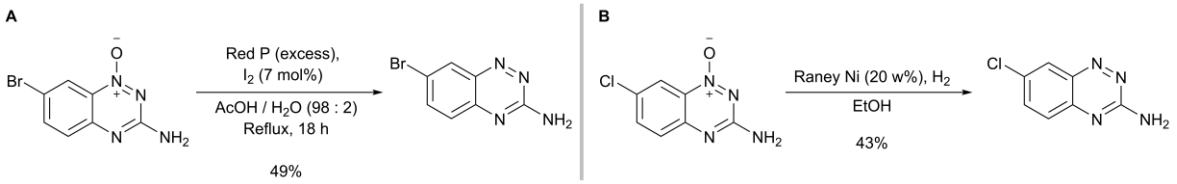
Scheme 125 – The Arndt benzotriazine synthesis. 2-nitroaniline (**211**) is reacted with cyanamide (**212**) to give the benzotriazine-1-oxide **214**.



Scheme 126 – Wolf's benzotriazine synthesis, adapted from the work of Arndt.

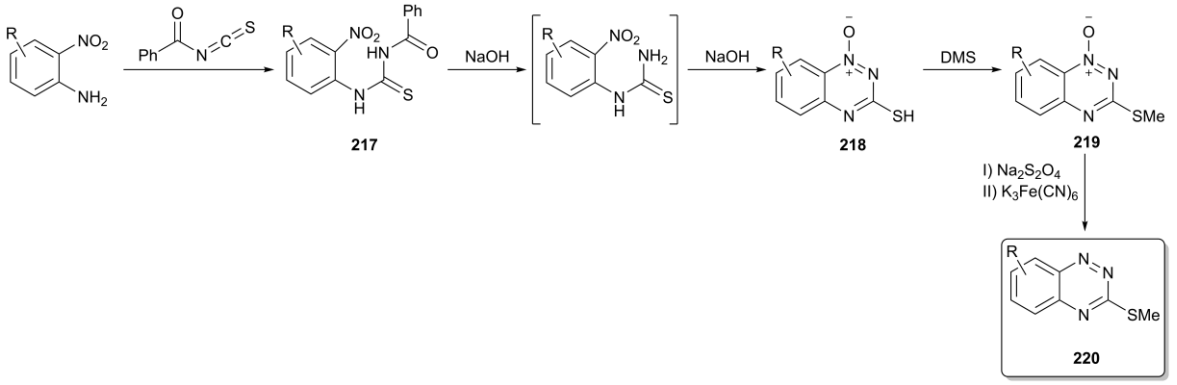
Arndt showed that the benzotriazine-1-oxides accessed by this route could be reduced to the corresponding benzotriazine using tin.[244, 286] Wolf and coworkers further showed that the use of phosphorous, iodine and water, or catalytic hydrogenation with Raney nickel, could also reduce the

1-oxide (**Scheme 127**).[286] Other methods have been implemented to undertake this reduction: H_2 and Pd/C,[70, 245] Zn and NH_4Cl,[245] and sodium dithionite.[287-289]



Scheme 127 – Reduction of benzotriazine-1-oxides by Wolf and coworkers. **A** – using phosphorous, iodine and water. **B** – catalytic hydrogenation using Raney nickel.

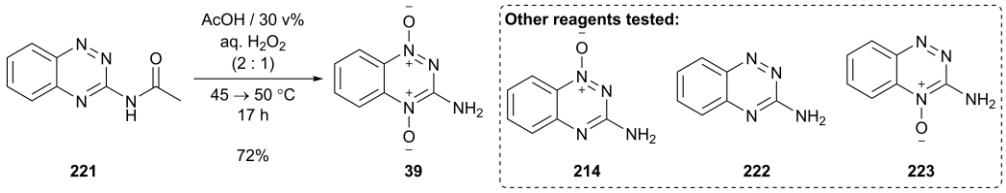
Work by Arndt and Rosenau[289, 290] modified the original ABS procedure by generating a thiourea instead of the guanidine intermediate, which was shown to cyclise to the corresponding 3-mercapto-1,2,4-benzotriazine. Pallos *et al*[289] simplified the route, finding that the *N*-benzoylthioureas (**217**) can undergo hydrolysis and ring closure within hydroxide to afford the corresponding benzotriazine-1-oxide **218** (**Scheme 128**). Due to the rapid oxidation of **218** in air, alkylation was immediately undertaken using either DMS or methyl iodide to give **219**. Dithionite reduction gave the desired benzotriazines **220** in yields between 50 and 87% across all 4 steps.



Scheme 128 – Route to 3-methylthio-1,2,4-benzotriazines **220** by Pallos *et al*.

4.2.2 – Oxidation to 1,2,4-benzotriazine-1,4-di-*N*-oxides

Robbins and Schofield,[291] as part of studies to generate 1,2,4-benzotriazine analogues bearing electron-withdrawing substituents, first showed that 1,2,4-benzotriazines can undergo oxidation using peracetic acid to give the 1,4-di-*N*-oxide **39** (**Scheme 129**). Their discovery in 1957 was not explored further within the literature until 13 years later, where Mason and Tennant[288] determined oxidation of **222** at room temperature gives the 2-oxide **223** based on NMR analysis. Interest in this transformation has slowly grown over time due to the medicinal properties of **39** (now known as Tirapazamine). These properties were first illustrated using this transformation within *in vivo* cell survival assays against squamous cell carcinoma (SCC) by Zeman and coworkers.[292]

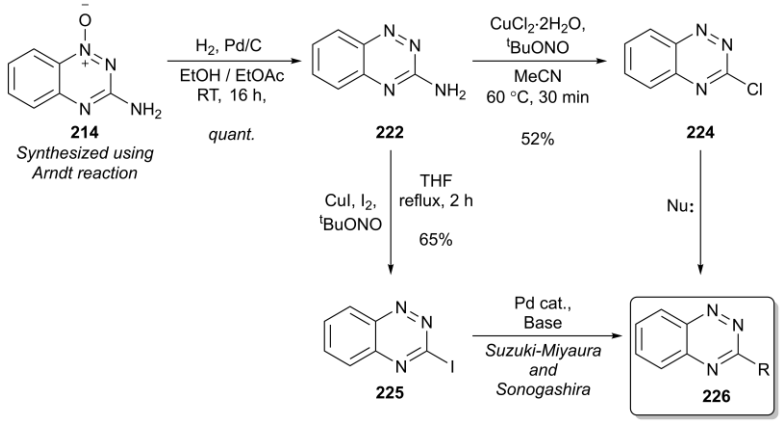


Scheme 129 – 3-Acetamido-1,2,4-benzotriazine **221** was successfully oxidised to the 1,4-dioxide analogue **39** in good yields by Robbins and Schofield. Analogues of **221** were also successfully oxidised to **39** (see box).

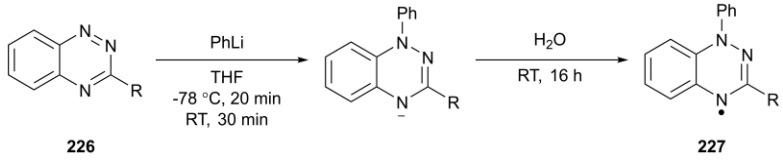
Other reagents have been used since the work of Robbins and Schofield[291] to undertake this oxidation: *meta*-chloroperbenzoic acid (mCPBA)[293] and hypofluorous acid.[294] The latter is of interest for rapid ^{18}O labelling as a mechanistic tool for the mode of action of Tirapazamine.

4.2.3 – Blatter radical synthesis from benzotriazines

Kaszyński *et al*[69, 245] reported in 2019 that Blatter radicals can be synthesized from the 1,2,4-benzotriazine scaffold bearing a variety of substituents at the C(3)-position. ABS was used to gain access to 3-amino-1,2,4-benzotriazines **222**, which were then halogenated using a diazotization reaction (**224**, **225**) and underwent either S_NAr or Pd-catalysed cross-coupling to give analogues **226** (**Scheme 130**). Using PhLi, N(1) addition gave an anionic benzotriazinyl scaffold that oxidised in air overnight to the BR (**Scheme 131**). Their work found that when R = NHPh, the addition of PhLi gave an unidentified species that did not agree with the expected mass data by HRMS and was found to give clear NMR signals. This closed shell species was observed in higher yields upon increasing equivalents of PhLi addition (6 → 35% when 1.3 → 4 equiv. PhLi used).



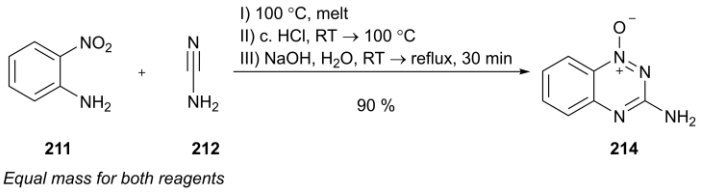
Scheme 130 – Synthesis of C(3)-derivatised benzotriazines *via* halogenated analogues by Kaszyński *et al*.



Scheme 131 – The synthesis of Blatter radicals **227** from 1,2,4-benzotriazines **226** using phenyllithium, by Kaszyński *et al*.

4.3 – Synthesis of 1,2,4-benzotriazines

Using the conditions described by Mason and Tennant,[288] 3-aminobenzotriazine-1-oxide **214** was synthesized in high yields (**Scheme 132**). Slow addition was required when treating the hydrochloric acid solution with aqueous hydroxide to avoid significant effervescence; in larger scale syntheses (≥2 g of each reagent) the use of a water bath at room temperature was found to be effective. Recrystallisation of the crude product from acetic acid, following the literature procedure, was ineffective in removing residual **211**. An alternative procedure was developed whereby the crude product was placed on a short pad of silica topped with 2 wetted filter papers and flushed with 10% MeOH in DCM until **211** was no longer observed by TLC. The purified product, sparingly soluble in the eluent, could be recovered from atop the silica pad and effectively crystallised in acetic acid.



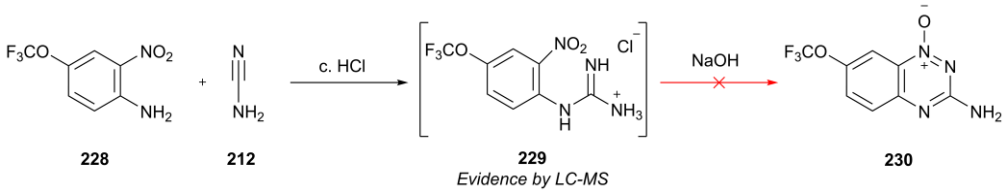
Scheme 132 – The synthesis of 3-amino-1,2,4-benzotriazine-1-oxide (**214**) following the method of Mason and Tennant.

4.3.1 – Alteration of the 2-nitroaniline reagent

Synthesis of analogues with ABS generally involves alteration of the aniline reagent,[283] and so by using a series of 2-nitroaniline compounds bearing a selection of substituents, the reaction with cyanamide was explored.

2-Nitro-4-(trifluoromethoxy)aniline **228** showed formation of the guanidine intermediate **229** by stirring in hydrochloric acid at room temperature for 5 minutes, however the addition of sodium hydroxide did not clearly form any of the 1-oxide product **230** based on ^{1}H and ^{19}F NMR spectroscopic analysis alongside LC-MS (**Scheme 133**). The reaction mixture mostly contained starting material, believed to indicate partial reaction rather than **229** reverting to the aniline, and so in a repeat of this reaction the mixture of starting materials in hydrochloric acid were heated to 50 °C for 30 minutes. **230** was observed by LC-MS in trace amounts, however NMR analysis of a sample spiked with **228** verified that this was the major species within the crude reaction mixture. The third attempt of this transformation stirred the aniline-cyanamide mixture at 60 to 70 °C for 40 minutes before the addition of HCl, which led to an exothermic process indicative of **229** formation. However, the addition of NaOH did not lead to significant ring closure based on LC-MS. Impure product samples were obtained from the reaction mixture following RP-LC, however too little product was formed to attempt further isolation. A fourth attempt added a greater excess of sodium hydroxide to ensure **229** is deprotonated, with the product seen to form a significant peak by LC-MS, however the precipitated product was significantly impure and unable to be isolated by RP-LC.

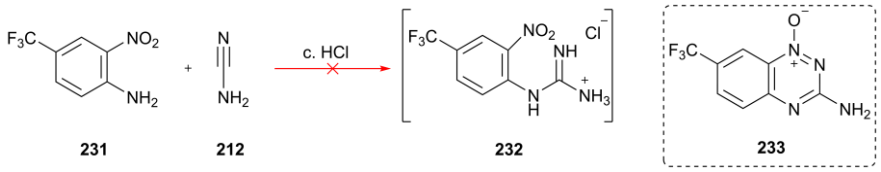
Throughout all the attempts, LC-MS evidence indicated that the trifluoromethyl group of the trifluoromethoxy substituent may be lost under the reaction conditions from **228**, however HRMS could not verify this. It was favourable to therefore focus on groups that would not be susceptible to hydrolysis.



228 **212** **229** *Evidence by LC-MS* **230**

Scheme 133 – Attempted synthesis of the 7-trifluoromethoxy analogue of the benzotriazine-1-oxide (**230**).

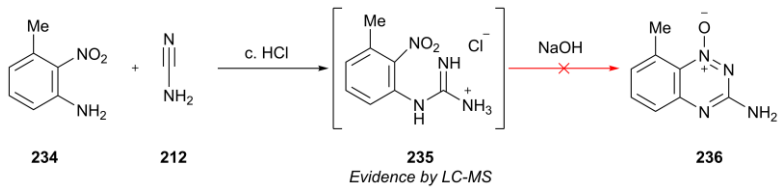
The 7-trifluoromethyl aniline analogue **233** was also investigated in ABS (**Scheme 134**). After treating the oil of **231** and **212** with concentrated hydrochloric acid, the formation of a pale orange precipitate was observed. Following addition of sodium hydroxide the mixture was heated at reflux overnight, however LC-MS alongside ^{1}H, $^{13}C\{^{1}H\}$ and ^{19}F NMR spectroscopy gave no clear indication of guanidine (**232**) formation. The pale orange precipitate was found to be the starting aniline based on LC-MS.



231 **212** **232** **233**

Scheme 134 – Attempted synthesis of the 7-trifluoromethyl analogue of the benzotriazine-1-oxide (**233**). The guanidine intermediate **232** was not observed in this case. The desired product **233** is also shown (box).

Use of 3-methyl-2-nitroaniline **234** to give the 8-methyl analogue of the benzotriazine-1-oxide **236** was the only other aniline explored (**Scheme 135**). The addition of concentrated HCl to the stirring oil gave a milky white solution that was proposed to be the guanidine chloride salt **235**, and after 5 minutes stirring NaOH was added giving a colour change to clear orange. The mixture was heated at reflux for 40 minutes, leading to precipitate formation, however LC-MS shows peaks of *m/z* corresponding to **234** and **235**. Filtration of the precipitate gave high purity **234** by LC-MS, with traces of **235** observed in the filtrate and no signs of **236** formation. A repeat using a greater excess of sodium hydroxide showed the *m/z* that corresponds to **236**, however only in trace amounts that could not be isolated by RP-LC.

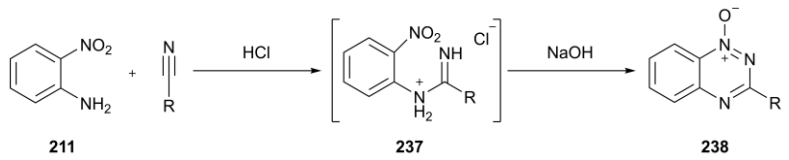


234 **212** **235** *Evidence by LC-MS* **236**

Scheme 135 – Attempted synthesis of the 8-methyl analogue of the benzotriazine-1-oxide.

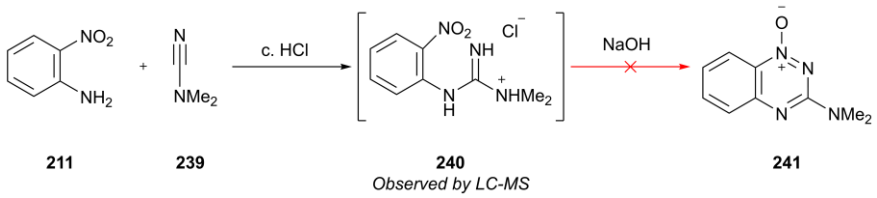
4.3.2 – Alteration of the nitrile reagent

As an alternative to the work within the literature,[244, 245, 286] ABS was also explored using alternative nitrile containing species. With the effectiveness of the reaction relying partly on the carbodiimide tautomer of **212** that can readily react with the aniline to give the guanidine intermediate (**Scheme 125**), swapping the amino group on **212** would require forcing conditions to give the corresponding amidine intermediate (**237**, **Scheme 136**). Furthermore, **237** may be less stable depending on the introduced group due to lack of tautomerisation – reversion to the aniline and nitrile may be more favourable which may impact the yield. These effects were considered when choosing alternative nitrile reagents and synthetic conditions.



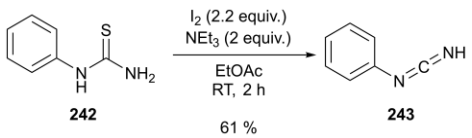
Scheme 136 – Modified ABS using a variety of nitrile containing species would occur *via* the amidine **237**, before obtaining a selection of C(3) substituted benzotriazine-1-oxides (**238**).

Use of dimethylcyanamide **239**, with the introduction of electron-donating substituents, was proposed to be a sensible alternative to cyanamide (**Scheme 137**). The reagent oil was treated with concentrated hydrochloric acid and stirred for 15 minutes before hydroxide addition and subsequent 1 h heating at reflux. LC-MS indicated **240** and **241** formation, however NMR analysis showed that the obtained product was mostly **211**. **240** and **241** could not be isolated by RP-LC.



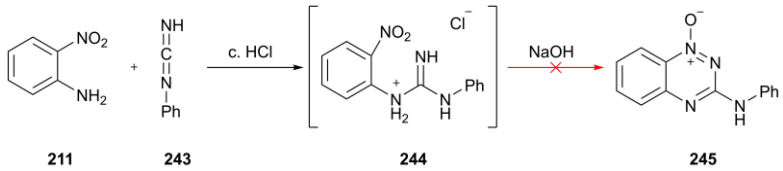
Scheme 137 – The reaction of **211** with dimethylcyanamide **239** showed traces of **240** and **241** formation from LC-MS and ^{1}H NMR evidence.

Using *N*-phenylthiourea **242**, and the carbodiimide formation developed by Murray, *N*-phenylmethanediimine (**243**) was synthesized in good yield (**Scheme 138**). Purification was less successful than with the diarylcarbodiimides discussed in Chapter 2.3.3, with polymer seen to be sparingly soluble in the hexane mixture explaining the lower isolated yield. **243** is a tautomer of *N*-phenylcyanamide, and so it was thought comparative success would be achieved.



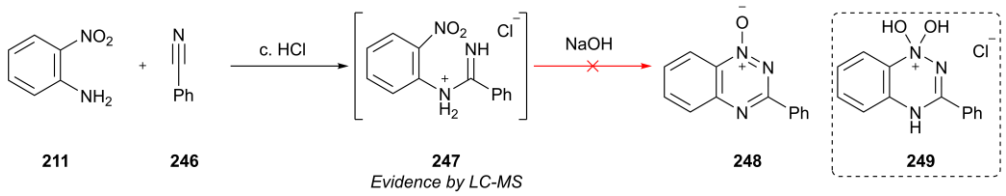
Scheme 138 – Desulfurization of *N*-phenylthiourea (**242**) gives *N*-phenylmethanediimine **243** in good yields.

243 was combined with 2-nitroaniline and concentrated HCl in efforts to generate the *N*-phenylbenzotriazine product **245** (**Scheme 139**). An exothermic process was seen upon addition of the acid, and following addition of sodium hydroxide the reaction mixture was refluxed overnight to force any guanidine **244** to cyclise. LC-MS evidence however did not show evidence of ring closure, and so a sample of the reaction mixture was microwave irradiated (10 min, 150 °C) based on Wolf's benzotriazine synthesis.[286] The irradiated sample showed a significant increase in the species observed by LC-MS, including traces of a species with *m/z* that could agree with **245**, however isolation by RP-LC was unsuccessful. The remaining reaction mixture was refluxed for a further 3 days with no clear evidence of reaction progression. In a repeat of the reaction a higher excess of sodium hydroxide was used to force **244** ring closure, however no noticeable change in the reaction outcome was observed.



Scheme 139 – Attempted synthesis of *N*-phenyl-1,2,4-benzotriazine-1-oxide (**245**) only showed generation of the guanidine intermediate **244**.

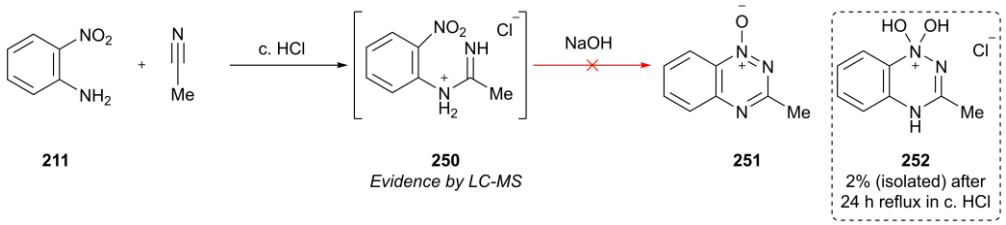
Benzonitrile **246** was also seen to generate the guanidine intermediate (**247**) following a 15 minute stir in concentrated hydrochloric acid, treatment with sodium hydroxide, and reflux for 30 minutes (**Scheme 140**). The desired 1-oxide **248** was not observed under these conditions, and **247** was only seen in trace amounts, so reflux in concentrated hydrochloric acid was undertaken for 24 h to see if the reaction could be pushed towards completion. LC-MS and HRMS indicated that, under these forcing conditions, the *N,N*-dihydroxydihydro-1,2,4-benzotriazinium species **249** is generated. Isolation of **249** was not possible by column chromatography (10% AcOH in DCM). The forcing conditions did not significantly improve formation of **247** by LC-MS.



Scheme 140 – Attempted synthesis of 3-phenyl-1,2,4-benzotriazine-1-oxide (**248**). Under prolonged reflux, **249** is proposed to form based on LC-MS and HRMS evidence.

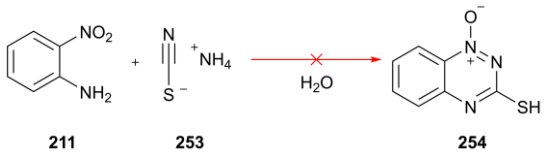
Acetonitrile was also investigated in this process, with a similar outcome to benzonitrile (**Scheme 141**). Formation of the analogous dihydroxydihydrobenzotriazinium species **252** was evidenced by LC-MS, but in this case could be isolated by column chromatography (0 to 50% AcOH in DCM) in 2% yield. LC-MS, HRMS and NMR characterisation of **252** was possible. Treatment of **252** under acidic (c. HCl) or basic (excess NaOH) conditions at room temperature for 1 hour, or stirring in water

for 16 h, did not show formation of **251**. It is proposed that N(4)-donation is not completely responsible for the loss of water/hydroxide in ABS, with the resonance possible by the 3-amino / 3-mercapto group playing a key role in 1-oxide formation.



Scheme 141 – Attempted synthesis of 3-methyl-1,2,4-benzotriazine-1-oxide (**251**). Under prolonged reflux, **252** is shown to form based on LC-MS, HRMS and NMR evidence.

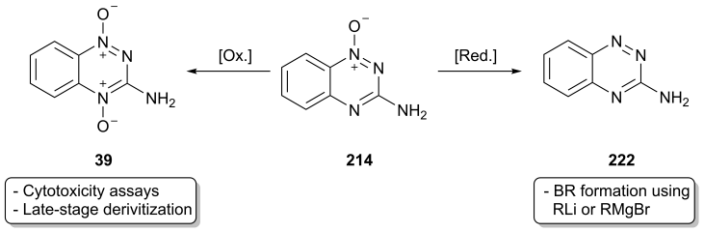
An alteration to Messmer's benzotriazine synthesis,[289] the reaction of **211** with ammonium thiocyanate **253**, was also attempted (**Scheme 142**). Unlike other benzotriazine syntheses, hydrochloric acid was not added so as to avoid thiocyanic acid formation. Thiocyanic acid is known to form toxic gases including hydrogen cyanide upon heating, and so must be avoided.[295] By having the thiocyanate ion, resonance to the isothiocyanate ion structurally similar to the carbodiimide was also possible. The mixture was stirred for 24 h to ensure any reaction was complete, before addition of hydroxide and stirring overnight. The resultant mixture showed no signs of reaction by ^{1}H NMR spectroscopy and LC-MS. The reaction was reattempted by heating the reaction mixture at reflux for 2 h, however LC-MS evidence showed formation of a mixture of species that could not be identified or purified by RP-LC.



Scheme 142 – Attempted 3-mercapto-1,2,4-benzotriazine (**254**) synthesis using ammonium thiocyanate **253**.

4.4 – Further reactions from 1,2,4-benzotriazine-1-oxide

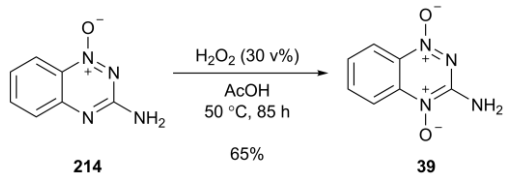
The benzotriazine 1-oxide synthesized from the Arndt reaction (**214**) can be transformed into two species of interest within this project (**Scheme 143**). Oxidation using peracetic acid enables synthesis of the 1,4-dioxide analogue commonly known as Tirapazamine (**39**), an experimental anticancer prodrug[296, 297] that is proposed to act *via* a benzotriazinyl radical.[204] Gram-scale synthesis of **39** allows for late-stage derivatization to be explored. Alternatively, by reducing **214** to 3-amino-1,2,4-benzotriazine **222**, this can be potentially used in Kaszyński's Blatter radical synthesis using organometallic reagents.[69, 70]



Scheme 143 – The oxidation and reduction of the benzotriazine-1-oxide **214** leads to two species of interest within this work (see boxes).

4.4.1 – Oxidation to the 1,4-dioxide (Tirapazamine)

214 was oxidised to the 1,4-dioxide **39** following the literature procedure of Mason and Tennant (**Scheme 144**).[288] After stirring for 85 h, solid sodium bicarbonate was cautiously added to neutralise the mixture and the inorganic salts were filtered from the solution. **39** could be extracted from the aqueous solution in good yields as a bright red solid, using DCM.

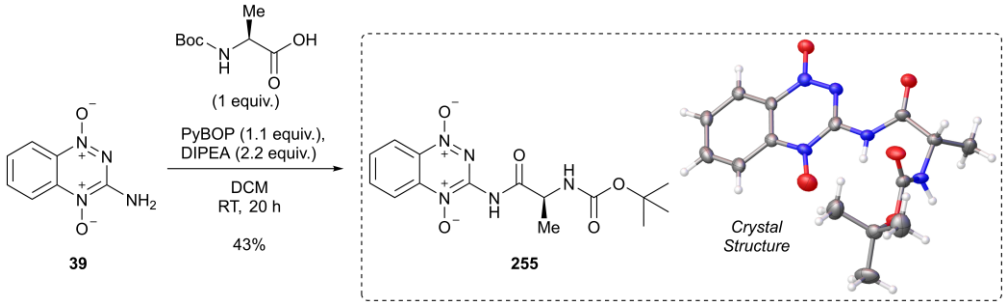


Scheme 144 – Oxidation of 3-amino-1,2,4-benzotriazine **214** to Tirapazamine **39**.

One of the major issues observed with Tirapazamine, on account of the highly charged structure, is a very high aqueous solubility that limits cellular penetration and also leads to rapid clearance.[268] This can be overcome by developing drug delivery systems such as gelatin nanoparticles,[298] gold nanoparticles,[299] poly(anhydrides)[300] and metal-organic frameworks (MOFs).[301] Given the implementation of bioconjugation for triazolium and Blatter radical scaffolds earlier in this work, bioconjugation was also attempted upon Tirapazamine.

Using the PyBOP coupling methodology used to generate Nitron bioconjugates, Tirapazamine was successfully added to the C-terminus of alanine (**Scheme 145**). RP-LC (5 to 100% MeCN in H_2O) enabled isolation of the compound, which was dried in air to give orange crystals that could be

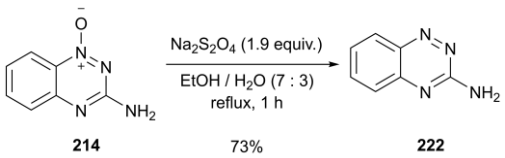
analysed by single crystal XRD. LC-MS of other column chromatography effluent fractions indicated formation of the benzotriazine-1-oxide bioconjugate, indicating that the reaction conditions may lead to Tirapazamine reduction, however this species was not isolated.



Scheme 145 – PyBOP coupling of Tirapazamine **39** to *N*-Boc-alanine was possible to give **255** in good yields. The obtained crystal structure of **255** is also shown.

4.4.2 – Reduction to 1,2,4-benzotriazine

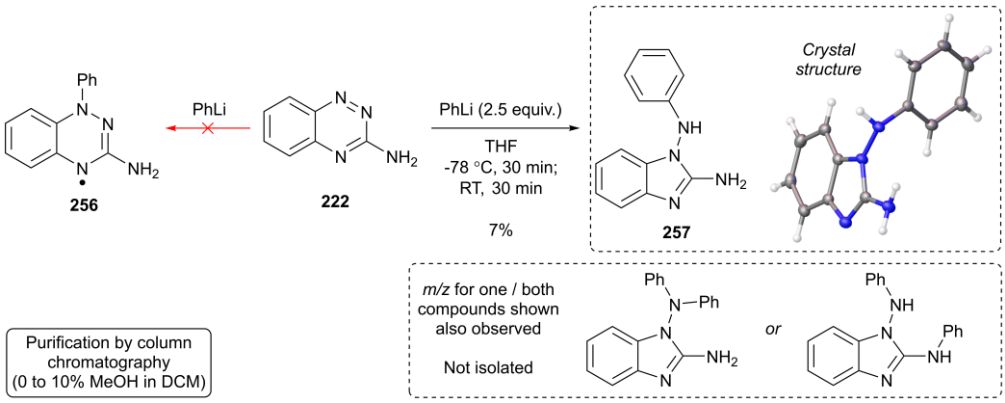
Reduction of **214** to **222** was undertaken following the procedure of Mason and Tennant (**Scheme 146**).[288] Using twice the mass of sodium dithionite to **214**, the mixture was heated at reflux for 1 h. Following hot filtration and concentrating *in vacuo*, the product could be isolated by washing the resultant yellow solid with water. Recrystallisation from hot ethanol was required to remove residual **214**.



Scheme 146 – Sodium dithionite reduction of **214** gave the corresponding benzotriazine **222** in good yields.

4.5 – Reaction of 1,2,4-benzotriazines with organometallic reagents

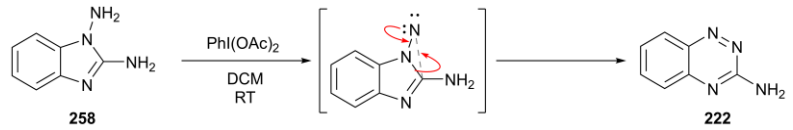
Following the method of Kaszyński,[69] phenyllithium was reacted with **222**. After stirring for an hour in total the reaction mixture was vented with a needle and water added cautiously to the mixture and stirred overnight at room temperature. LC-MS however indicated that a product with *m/z* 2 units greater than expected had formed, verified by HRMS, with only a small peak that could be assigned to the desired product **256**. Isolation of the species of higher *m/z* was possible using column chromatography (0 to 10% MeOH in DCM) with the effluent left to dry in air to give dark red crystals – the species with *m/z* consistent with the Blatter radical was not isolated. Single-crystal XRD showed that the unknown *m/z* corresponds to a 1,2-diaminobenzimidazole scaffold (**257**, **Scheme 147**). Although highly coloured, indicative of a Blatter radical, this species is verified to be non-radical by NMR. Further analysis of the column chromatography effluent also shows formation of the *m/z* corresponding to the presence of a second phenyl ring in place of a hydrogen, with two peaks observed by positive electrospray ionisation (ES+) with similar retention times, however the isolation of this *m/z* was not possible.



Scheme 147 – Reaction of phenyllithium with **222** did not clearly lead to formation of the Blatter radical in this work, instead ring contraction to **257** was observed.

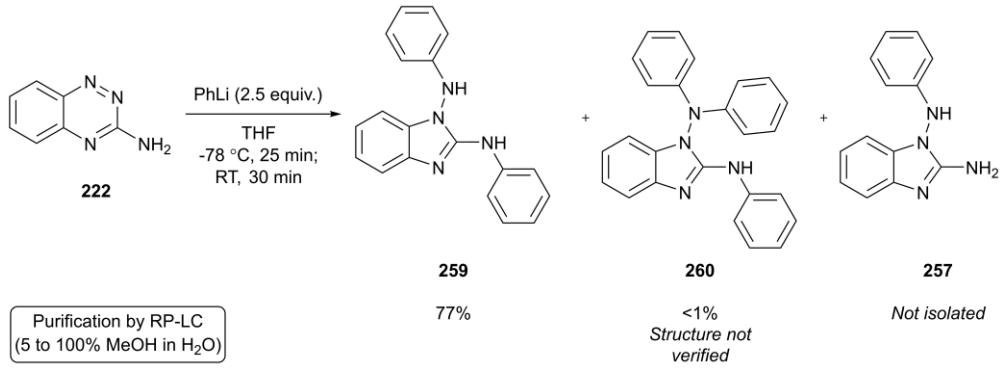
The 1,2-diaminobenzimidazole scaffold is of interest as a selective inhibitor of nitric oxide synthases (NOS), and therefore is of interest as an anti-inflammatory or treatments against stroke or morphine addiction.[302] 2-Amido benzimidazoles have also been identified as potent agonists of stimulator of interferon genes (STING), which is effective in the treatment of severe acute respiratory syndrome coronavirus 2 (SARS-CoV-2).[303]

It should also be noted that the reverse of this ring-contraction has been previously described by Kumar *et al*,[304] who found iodobenzene diacetate can undertake ring expansion of 1,2-diaminobenzimidazole **258** to **222** (**Scheme 148**). They propose the generation of a nitrene at the 1-position which leads to **222** formation.



Scheme 148 – Kumar *et al* illustrated the ring expansion of 1,2-diaminobenzimidazole **258** to benzotriazine **222** using a hypervalent iodine species.

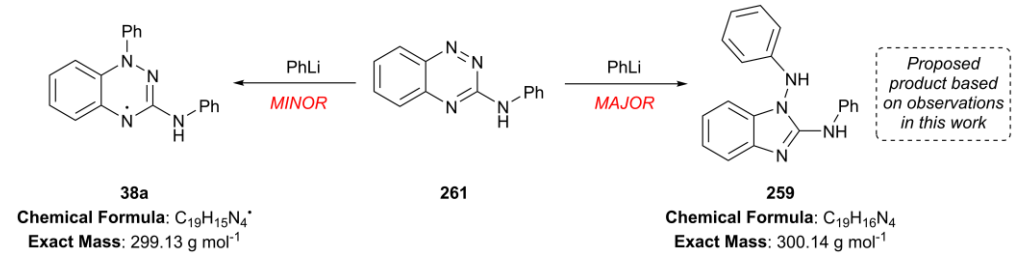
Optimisation of the reaction conditions was explored, to see if the 7% yield of **257** could be improved. Use of 1.3 equivalents phenyllithium was tested given that the disubstituted species was observed using 2.5 equivalents, however only partial conversion was observed with significant amounts of **222** present by LC-MS. 1.8 equivalents of phenyllithium led to only traces of **222** by LC-MS, however the double arylated species was also observed in trace amounts and the yield of **257** was slightly lowered (5%). The initial conditions using 2.5 equivalents were therefore used moving forward. The procedure summarised in **Scheme 147** was repeated, however with the reaction warmed to room temperature after 25 minutes instead of 30. LC-MS of the crude product mixture showed a greater amount of double arylated product *m/z* than in previous runs, and following purification by RP-LC the double arylated species **259** was isolated in high yield (**Scheme 149**). The triple arylated species **260** was also isolated, however in a yield less than 1% (2 mg) – analysis by ^{1}H NMR spectroscopy suggested isolation of pure compound with integrals in agreement with **260**, however verification of the structure was not possible and the given structure is deemed the most likely species to have formed. The significant change in reaction outcome by LC-MS and isolated yield indicates a significant effect in the outcome depending on the reaction time at −78 °C, however further studies would be required to verify this.



Scheme 149 – The reaction of phenyllithium with **222** gave high yields of the 1,2-dianilinobenzimidazole **259** which could be effectively isolated using RP-LC.

Kaszyński *et al*[69] report a 13% yield of **256** as a dark red solid, which has been verified by HRMS and elemental analysis to agree with the Blatter radical. Kaszyński's HRMS data is also distinct from that collected within this work for **257**, and so it is concluded that a change in setup between Kaszyński's work and this work has led to change in the major product. Given that low yields were obtained in both cases it is felt feasible that Kaszyński also formed **257**, but as a minor species that was not explored further or not structurally verified.

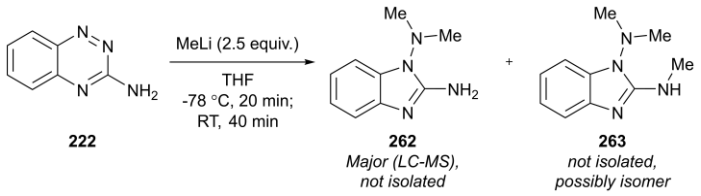
It is key to note that Kaszyński observed a non-radical species when reacting phenyllithium with 3-anilino-1,2,4-benzotriazine **261**, which could be attributed to a product analogous to **259** (**Scheme 150**). ^{1}H and $^{13}C\{^{1}H\}$ NMR analysis of the species shows sharp peaks, however with a large number of aromatic environments and no access to 2-dimensional NMR it is challenging to conclusively assign Kaszyński's data to **259**. It should be noted that a singlet at 6.84 ppm is observed with integral significantly less than one, which may correspond to the 2-amino NH group (6.45 ppm in data collected within this work for **257**, where the 2-amino group is not arylated). Given the non-radical nature, Kaszyński interprets the HRMS data as the $[M + H]^+$ ion of a species with formula $C_{19}H_{14}N_4$. However, the data could also be analysed as the $[M]^+$ peak for **38a** given that the molecular ion peak is commonly observed for BRs by HRMS. It is therefore proposed that **259** exists in the crude product mix and is seen by NMR spectroscopy, with a small amount of **38a** that is the species analysed by HRMS.



Scheme 150 – Kaszyński *et al* found that reaction of phenyllithium with **261** gave a non-radical species, proposed to be the benzimidazole species **259**.

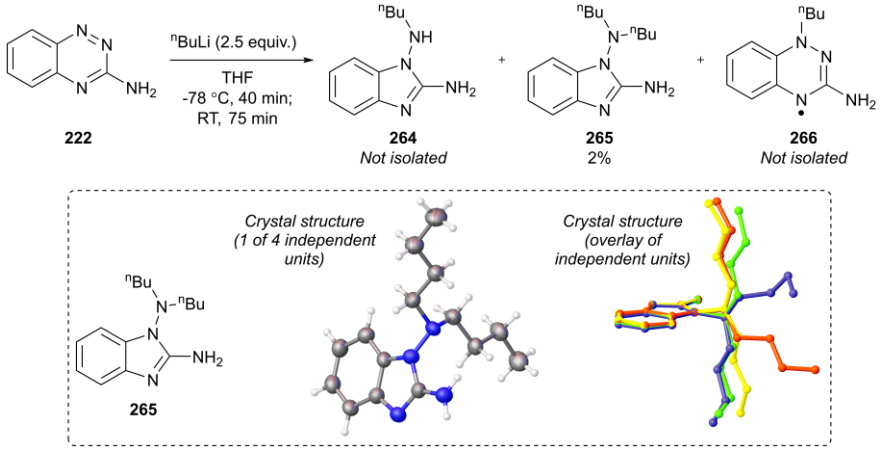
4.5.1 – Exploring the scope of benzotriazine ring-contraction

Alternative organometallic reagents to phenyllithium were explored to see if the transformation could be used to give a broader range of benzimidazole species. The reaction of methyllithium with **222** was only successful in part, with low conversion and challenging purification (**Scheme 151**). After the 1 hour reaction time the reaction was quenched with water, which unlike phenyllithium resulted in significant effervescence. LC-MS analysis of the reaction mixture showed a series of poorly resolved peaks with similar retention times consistent with **222** (major), **262** and **263** (trace). Purification by RP-LC was unsuccessful in isolating the products. In a repeat of the reaction, the mixture was held at −78 °C for 1 hour before warming to RT and stirring for a further hour. LC-MS analysis of this repeat indicated potential improvement in conversion to **262**, however **222** still appeared to be the major species and isolation was not possible.



Scheme 151 – The reaction of **222** with methyllithium showed little success, with only traces of alkylated benzimidazole.

The reaction with n-butyllithium showed evidence of formation of a mixture of mono- and di-alkylated products (**264** and **265**, respectively), and also a small peak for the Blatter radical **266**, by LC-MS. LC-MS also showed a large ES+ peak for polymeric material, with *m/z* varying by 44 units and the lowest *m/z* peak that could be identified at *m/z* = 297. The variation of 44 units points towards the addition of successive ethenolate units generated from the cycloreversion of THF solvent,[305] however the exact structure of this polymer is not known. The dialkylated product **265** could be isolated in low yields after two purifications by column chromatography (0 to 10% MeOH in DCM) (**Scheme 152**). Single-crystal XRD was also possible in this case, with the butyl chains of the 4 crystallographically independent units showing significant disorder. In a repeat of this reaction the solvent volume was tripled to see if **264** could be obtained in isolable amounts, however there was no noticeable change in the reaction outcome.

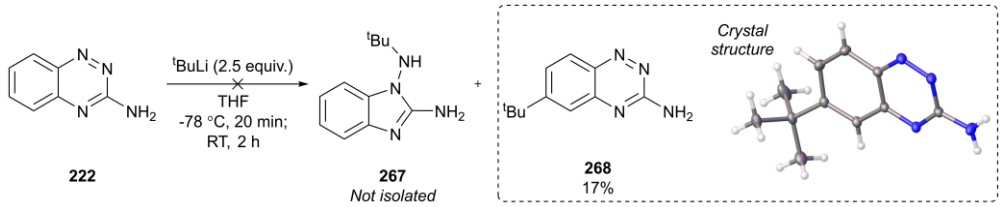


Scheme 152 – The reaction of **222** with n-butyllithium gave traces of the monoalkylated benzimidazole **264** and Blatter radical **266**, but the only isolated species is the dialkylated benzimidazole **265** that was analysed by single-crystal XRD (box).

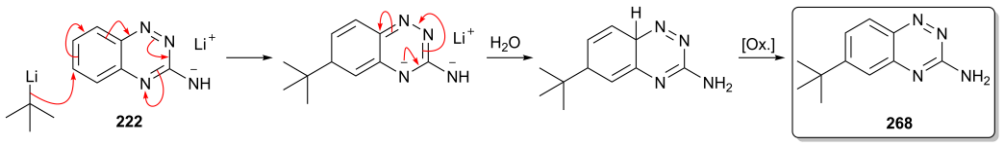
The use of *tert*-butyllithium led to an additional, unexpected reaction (**Scheme 153**). LC-MS analysis of the quenched reaction mixture shows formation of a *m/z* 1 less than the benzotriazine **267** as the major product, with **267** also observed in small amounts. RP-LC enabled isolation of the species of unknown *m/z*, which was recrystallised from methanol to enable XRD analysis – formation of the C(6)-alkylated benzotriazine **268** was shown. To our knowledge, C(6)-alkylation of the benzotriazine scaffold has not been previously reported. Reaction of organometallic reagents at this position is however known for benzotriazin-7-ones.[252] A mechanism for this transformation is proposed in

Scheme 154, with alkylation at this position favourable due to the push of electron density onto the N(4) position.

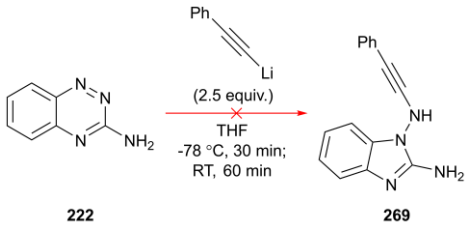
The use of organolithium reagents with sp^3 and sp^2-hybridised carbons had been explored, and so the last organolithium reagent of interest was lithium phenylacetylide (**Scheme 155**). LC-MS of the reaction mixture showed only a peak for **269**, with no evidence of reaction. Given the comparatively long reaction time it is proposed that evidence of reaction to **269** should be observed under these conditions, if reaction can occur, so this transformation was not explored further.



Scheme 153 – The reaction of *tert*-butyllithium with the benzotriazine **222** led to C(6) alkylation, which was verified by single-crystal XRD.

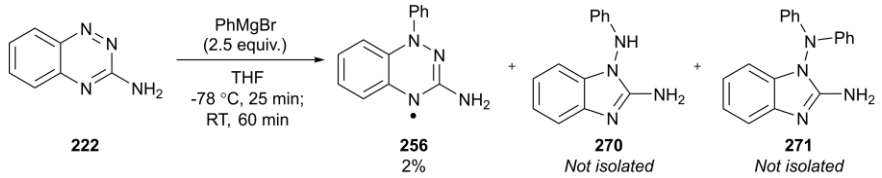


Scheme 154 – Proposed mechanism for the generation of **268**.



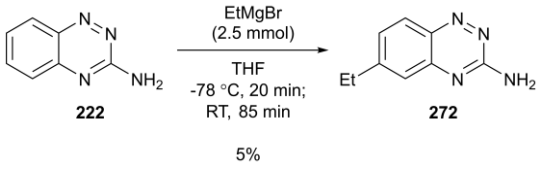
Scheme 155 – The addition of lithium phenylacetylide to **222** led to no clear reaction taking place.

Use of Grignard reagents was then explored in the transformation. The reaction of **222** with phenylmagnesium bromide also showed formation of single and double arylation products, but allowed for isolation of possible Blatter radical **256** (**Scheme 156**). LC-MS of the reaction mixture after quenching showed a mixture of **222** and the three reaction products (**256**, **270**, **271**), with a very small amount of **256** proposed to be isolated. A broadened ^{1}H NMR spectrum, alongside LC-MS and HRMS evidence, was obtained to support **256** formation.



Scheme 156 – Using phenylmagnesium bromide, the 1-phenyl-3-amino Blatter radical **256** is suggested to form from **222** in low yields.

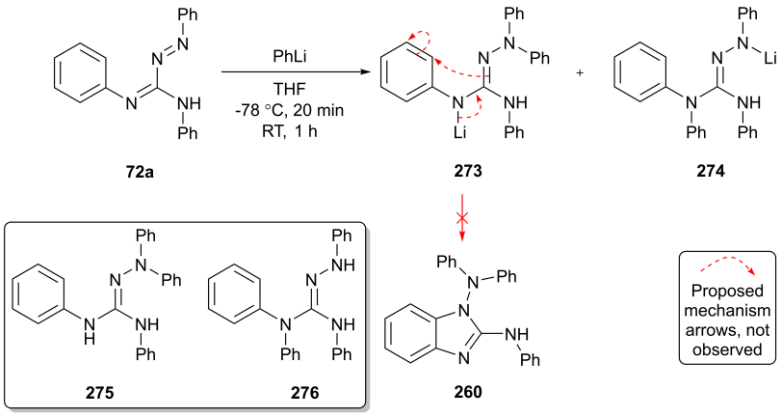
Using ethylmagnesium bromide, formation of the C(6)-alkylated benzotriazine **272** was observed (**Scheme 157**). LC-MS of the quenched reaction mixture showed the substituted benzotriazine as the only product, in a mixture with **222**. RP-LC (5 to 100% MeOH in water) was able to isolate only 8 mg of the compound, however this allowed for full characterisation.



Scheme 157 – Ethylmagnesium bromide is seen to generate a C(6) alkylated benzotriazine **272** from **222** like that seen when using *tert*-butyllithium.

The final alteration to the benzotriazine ring contraction was not made to optimise yield, but from a sustainability perspective. 2-Methyltetrahydrofuran (MeTHF) is a good substitute for THF given that the solvent can be derived from renewable resources (the hydrogenation of 2-furaldehyde produced from agricultural waste) and gives better phase separations from water.[306] The reaction of **222** with phenyllithium and phenylmagnesium bromide showed formation of mono- and di-arylated benzimidazole by LC-MS in both cases – product could only be isolated from the reaction using phenyllithium, achieving a 1% yield of the diarylated benzimidazole **259**.

As a potential alternative to undertaking the reaction with benzotriazines, the reaction of phenyllithium with the triphenyl triazabutadiene **72a** was investigated (**Scheme 158**). Arylation occurred on each end of the triazabutadiene scaffold, leading to formation of **273** and **274**, based on two ES+ peaks by LC-MS. It was initially proposed that **273** may undergo ring closure *via* the mechanism shown with the dashed arrows to give **260**, however after quenching the reaction mixture with water a mixture of **275** and **276** with some residual **72a** was observed by LC-MS. Purification by RP-LC (5 to 100% MeOH in H_2O) allowed for enriched isomer samples of **275** and **276** to be obtained, however after 3 total runs of RP-LC and attempts using recrystallisation (hot MeOH), the amidrazone products could not be isolated.

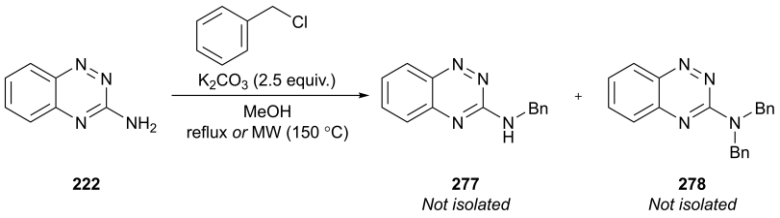


Scheme 158 – The reaction of phenyllithium with the triazabutadiene **72a** gives a mixture of amidrazone **275** and **276**. Ring closure to **260** *via* the proposed mechanism is not observed.

4.5.2 – 3-Amino functionalisation

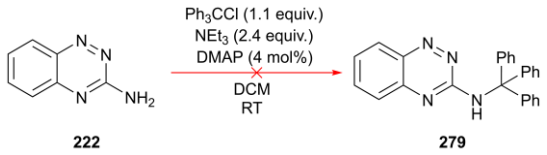
It is proposed, given evidence for the ring contraction in **222** and **261**, that the exocyclic nitrogen is key within the mechanism of benzotriazine ring contraction to benzimidazole. Substitution of the 3-amino position of **222** was therefore explored to see if this would impact the outcome of reaction with organometallic reagents. The introduction of a protecting group that could be removed was key to the process, as this would allow for a C(3)-NH_2 group that can act as a nucleophilic handle for late-stage modification.

Benzylation of **222** was attempted several times, however low conversion was observed by LC-MS to the possible products **277** and **278** using conventional heating or microwave irradiation (**Scheme 159**). Purification by recrystallisation seemingly led to product decomposition, whilst column chromatography was also unsuccessful.



Scheme 159 – Attempts at benzylating **222** led to minimal conversion and no isolated product across multiple attempts.

The other attempted method was the introduction of a trityl group, however this was also unsuccessful (**Scheme 160**). The reaction was initially stirred for 48 h at RT, and with no reaction observed by LC-MS the reaction flask was gently heated to reflux – this did not lead to observable product **279** formation by LC-MS or NMR spectroscopy.



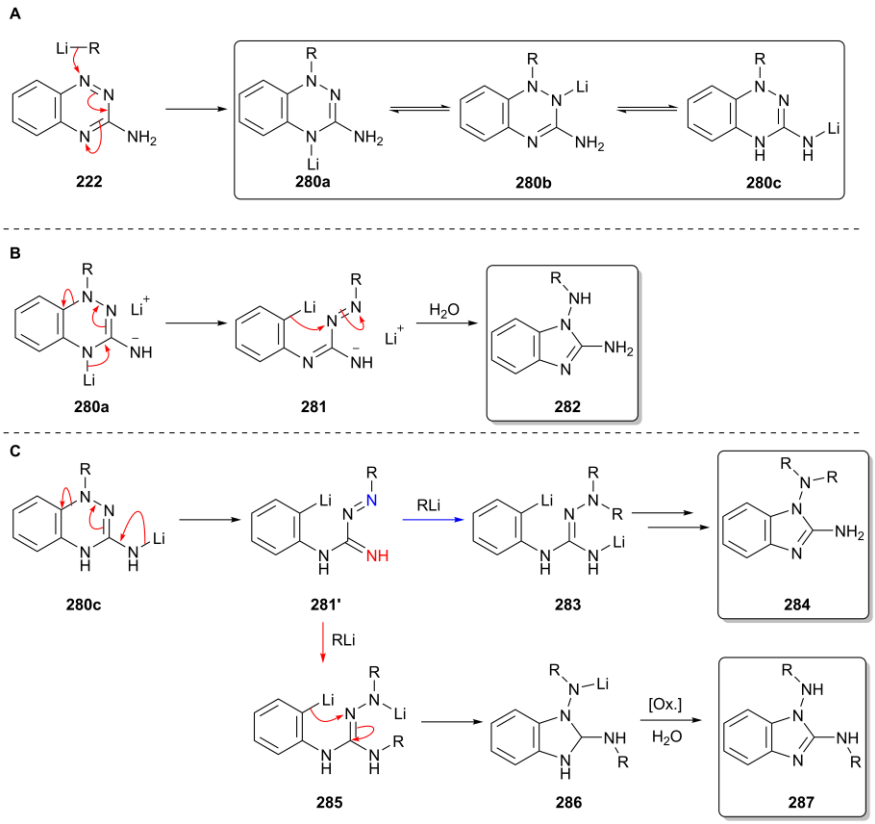
Scheme 160 – Attempted introduction of a trityl group upon the benzotriazine **222** was unsuccessful. DMAP = 4-dimethylaminopyridine.

The unsuccessful addition of a benzyl or trityl group is attributed to the low nucleophilicity of the amino group due to resonance across the benzotriazine ring system, in particular the guanidine moiety containing the 3-amino group.

4.5.3 – Mechanistic evaluation

The mechanism proposed for the formation of benzimidazoles using organolithium reagents is shown in **Scheme 161**. The addition of the organolithium reagent is thought to occur in the same way as is reported in the route to Blatter radicals,[69] however, owing to the exocyclic nitrogen there are now three instead of two lithiated intermediates which can stabilise the dihydrobenzotriazinide salt (**280**) making it less susceptible to oxidation (**Scheme 161A**). The formation of monosubstituted benzotriazine **282** (**Scheme 161B**) is proposed to occur by ring opening to the aryllithium triazabutadiene **281**, the reverse of the route to form Blatter radicals from amidrazone intermediates. **281** will preferentially adopt the *s*-trans configuration, giving the correct orientation of groups for the aryllithium moiety to attack into the N-N double bond and give the product.

Disubstituted benzimidazoles are formed preferentially with slightly more reactive organolithium reagents based on the findings in Section 4.5.1 – these more reactive organolithium reagents may add a second time to the triazabutadiene intermediate **281'** to give amidrazones **283** and **285** (**Scheme 161C**). The obtained amidrazone depends on which end of the triazabutadiene scaffold organolithium addition occurs. Amidrazones **283** and **285** cyclise through attack of the aryllithium substituent, which then oxidise to **284** and **287** respectively within air. The mixture of products obtained is a result of the two competing mechanisms, more specifically the relative rates of ring opening to **281** or organolithium addition to give **283** / **285**.



Scheme 161 – Proposed mechanism of benzimidazole formation. **A** – Generation of resonance-stabilised dihydrobenzotriazinide salt. **B** – route to monosubstituted benzimidazole, with slightly less reactive organolithium reagents (e.g. PhLi). **C** – route to disubstituted benzimidazoles, favoured with more reactive organolithium reagents (e.g. ^{n}BuLi).

Based on the work of Kaszyński,[69] changing the 3-amino substituent to an alkyl, aryl or alkylthio group leads to the formation of Blatter radical in yields between 29 and 81%. With only one case of possible Blatter radical formation within this work, using a Grignard reagent instead of PhLi used in the literature,[69] it is proposed that the 3-amino substituent is key to the ring contraction to benzimidazole. The amino group is proposed to stabilise the lithiated intermediate **280**, with three intermediates in equilibrium, such that ring opening to the triazabutadiene outcompetes the oxidation to the Blatter radical. Once the triazabutadiene-aryllithium species is formed, the benzimidazole ring formation is thought to be a readily occurring process given the arrangement and proximity of groups poised for ring closure. Furthermore, no evidence of the triazabutadiene is obtained in this work suggesting (if this is the mechanism of benzimidazole formation) that this species is short-lived *in situ*.

4.6 – Conclusions

Using the Arndt benzotriazine synthesis, 3-amino-1,2,4-benzotriazine-1-oxide **214** was successfully synthesized. Variation of the aniline and nitrile starting materials led to issues in cyclisation, and so the target benzotriazine-1-oxide analogues could not be prepared. Under forcing conditions the formation of a benzotriazinium salt was observed and this species could be isolated and characterised in very low yields. Oxidation and reduction of the 1-oxide species **214** gave access to the 1,4-dioxide **39** (Tirapazamine) and 3-amino-1,2,4-benzotriazine **222**, the former of which has been successfully coupled to alanine as a 'proof of concept' for Tirapazamine bioconjugation.

The addition of phenyllithium to **222** was seen to lead to ring contraction to 1,2-diaminobenzimidazoles. The mechanism of this transformation has been proposed and most likely involves an initial conjugate addition of PhLi, subsequent 6-membered ring opening to a triazabutadiene-aryllithium, followed by closure to a 5-membered ring. A series of analogues have been explored, with the benzimidazole **265** obtained from reaction with ^{n}BuLi isolated and verified by XRD. A novel regioselective C(6)-alkylation of benzotriazines is also reported using organolithium and Grignard reagents, albeit in low overall yields after purification.

5 – Kinetic studies of 1,2,4-triazolium salts in organocatalysis

5.0 – Foreword

The *N*-heterocyclic carbenes (NHCs) of 1,2,4-triazolium salts, accessed by deprotonation at the precarbenic site, have found applications in a variety of fields: as ligands for metal catalysts;[96, 307] treatments for a broad range of diseases as metal-NHC complexes,[308] and within organocatalysis.[40, 309] The rate of the deprotonation step is key to the range of applications that NHCs can exhibit; it dictates the accessibility of the NHC from the triazolium salt and furthermore gives an indication of NHC stability. Organocatalysis using stable carbenes is now dominated by the triazolylidine carbene, particularly in the area of asymmetric NHC-catalysed reactions.[309]

This chapter will focus on the key deprotonation step for the *S*-triazolium salts prepared within this work. Following a brief overview of the organocatalytic applications of 1,2,4-triazolium salts (Section 5.2), the methodology used to analyse the deprotonation step is described including consideration of rate constant accuracy (Section 5.3). The first and second order rate constants obtained in this work are then detailed (Section 5.4) followed by structure-activity data evaluation *via* Hammett analysis (Section 5.4.1). With single-crystal XRD data for many of the *S*-triazolium salts, relationships between XRD structural elements and the rate constants for deprotonation are evaluated (Section 5.5). pK_a values of the triazolium salts in water can be estimated through this work, and are described in Section 5.6. Finally, an initial exploration of the organocatalytic properties of *S*-triazolium salts is detailed in Section 5.7.

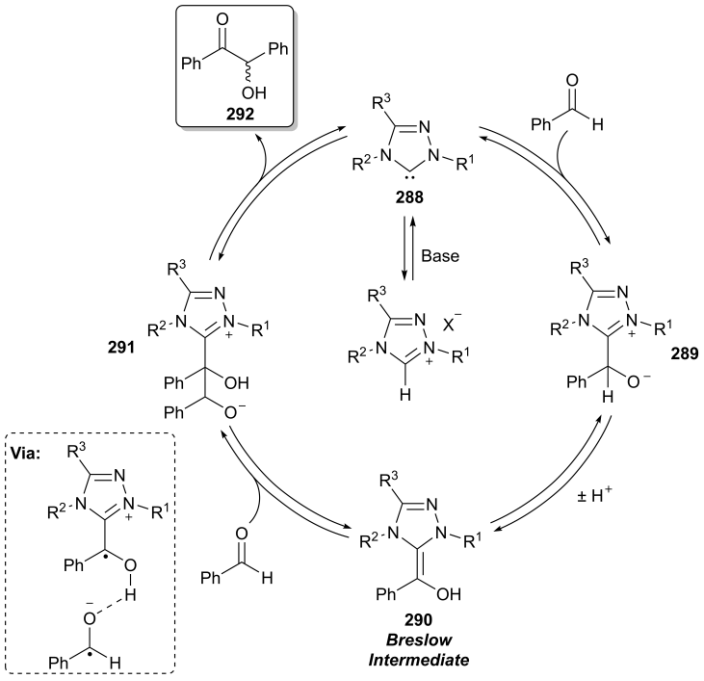
5.1 – Chapter contributions

All work detailed in this chapter was undertaken by the present author.

5.2 – Introduction

5.2.1 – NHC organocatalysis of the benzoin and Stetter reactions

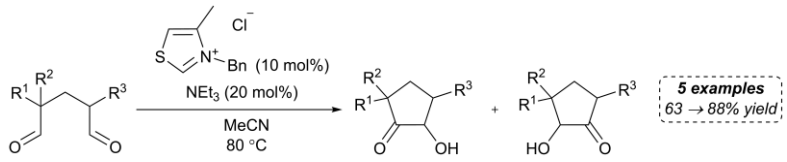
The benzoin reaction is one of the most widely studied reactions employing NHCs, discovered by Wöhler and Liebig using catalytic cyanide[310] before later being shown using thiazolylidine carbenes by Ukai and coworkers.[311] The reaction cycle (**Scheme 162**) starts by addition of an aldehyde molecule to the NHC **288** to give the zwitterionic adduct **289**. Removal of the charge separation occurs *via* tautomerisation to the enaminol intermediate **290** first proposed by Breslow and now known as the Breslow intermediate.[312] The Breslow intermediate then reacts with a second molecule of aldehyde to give the secondary adduct **291**. The original mechanism for this step involves 2-electron attack into the second aldehyde molecule, resulting from the push of electron density from the nitrogen of the enaminol group. Recent work on thiazolylidine carbenes suggests an alternative option for secondary adduct formation is by single electron transfer (SET) to the aldehyde to give a radical ion pair.[313] Collapse of the secondary adduct regenerates the carbene catalyst **288** whilst releasing the α-hydroxyketone product **292**. The reaction is an example of umpolung acyl-anion catalysis, whereby the electrophilic aldehyde reagent is converted to a nucleophilic acyl-anion equivalent for addition to a second aldehyde molecule.[309]



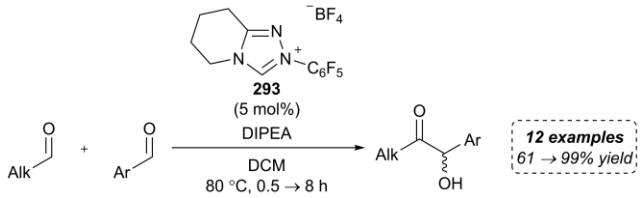
Scheme 162 – The mechanism of the triazolylidine-catalysed benzoin reaction. The NHC **288** generates an acyl anion intermediate (Breslow intermediate, **290**) that reacts with a second aldehyde molecule to give the α-hydroxyketone product **292**.

Through the use of two different aldehydes, cross-benzoin reactions have been successfully undertaken. Cookson and Lane[314] first reported the cross-benzoin in the cyclisation of glutaraldehyde

analogues, with the formation of both isomers observed (**Scheme 163**). One of the major issues with this transformation is the chemoselectivity, which becomes even more of a challenge when considering intermolecular cross-benzoin reactions that can form four different products. Work by Yang *et al*[315, 316] found that alteration of the NHC can alter the Breslow intermediate preferred between aromatic and aliphatic aldehydes, giving selectivities of up to 98% – triazolylidine carbenes preferentially generate Breslow intermediates with the aliphatic aldehyde, whilst thiazolylidines prefer the Breslow intermediate generated from aromatic aldehydes.[309] Gravel *et al*[317] improved on Yang's results (**Scheme 164**), finding that the fused piperidine catalyst **293** gives even greater chemoselectivity with low catalyst loading.

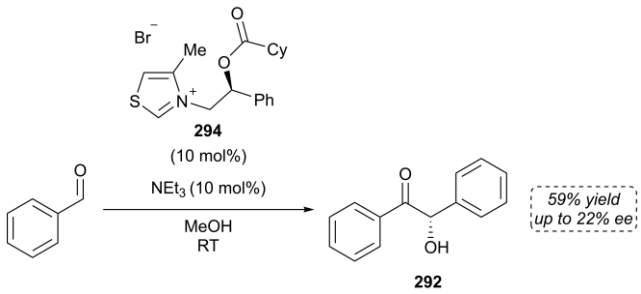


Scheme 163 – The intramolecular cross-benzoin was first shown by Cookson and Lane using glutaraldehyde analogues.

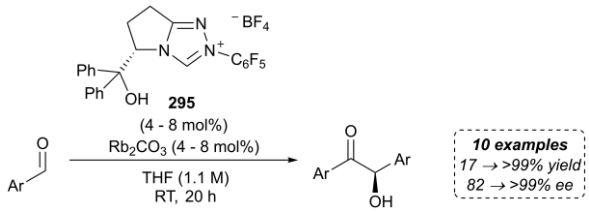


Scheme 164 – Gravel and coworkers found that chemoselectivity of the formed Breslow intermediate can be optimised through catalyst design.

Stereoselectivity of the benzoin reaction was first indicated to be possible through the work of Sheehan and Hunneman, who obtained an enantiomeric excess (*ee*) of 22% using a thiazolium salt precatalyst (**294**, **Scheme 165**).[318] Since this report the yields and selectivity of the transformation have been significantly improved, most notably by moving from thiazolylidine to triazolylidine carbene catalysts.[309, 319] Enantioselective benzoin condensations with *ee* values greater than 90% have been recently reported using triazolylidine carbenes by multiple groups,[320-323] however the most promising report is that of Connon and Zeitler[324] where up to quantitative conversion and *ee* greater than 99% was achieved using the pentafluorophenyl substituted triazolium **295** (**Scheme 166**). The stereoselectivity observed is attributed to the incorporation of a hydrogen-bonding alcohol close to the carbenic centre.[309]

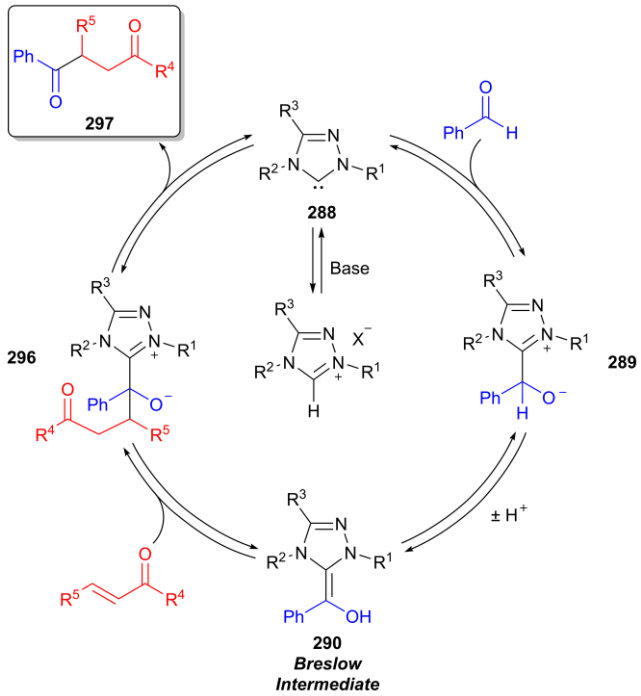


Scheme 165 – The first reported example of an asymmetric benzoin condensation by Sheehan and Hunneman.



Scheme 166 – The enantioselective benzoin reaction undertaken by Connon and Zeitler, the more effective catalytic system to date for this transformation.

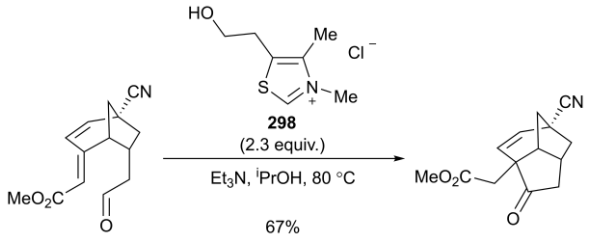
The Stetter reaction is mechanistically identical to the benzoin reaction up to the stage of Breslow intermediate formation, however the acyl anion now undergoes conjugate addition to an activated carbon-carbon double bond such as an α,β-unsaturated system (**Scheme 167**).



Scheme 167 – The mechanism of the triazolylidine-catalysed Stetter reaction. The Breslow intermediate reacts with an α,β-unsaturated carbonyl-containing species to generate the secondary adduct **296**, which collapses to give the 1,4-dicarbonyl compound **297** and NHC **288**.

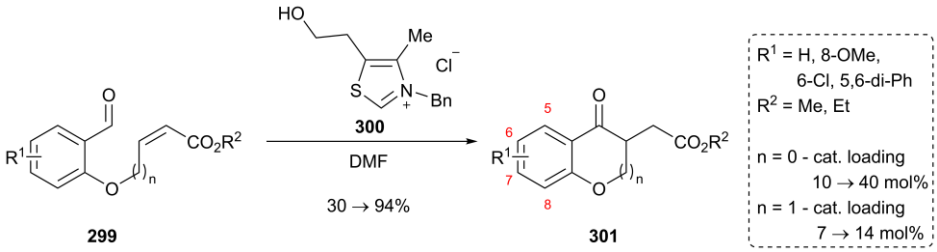
Stetter first described this reaction using thiazolylidine carbenes in the 1970's, successfully applying the process to the synthesis of di-, tri- and tetraketones, 4-oxo nitriles and dioxo carboxylic esters.[325,

[326] Since this initial report, a large amount of work has been undertaken in the development of intramolecular Stetter reactions – applying this transformation to generate cyclic ketone scaffolds within biologically relevant compounds.[309] Trost and coworkers,[327] using a thiazolium salt, performed the first intramolecular Stetter reaction in 1979 (**Scheme 168**). However, their conditions do not suggest use of the thiazolium salt in catalytic amount but instead as a stoichiometric reagent.



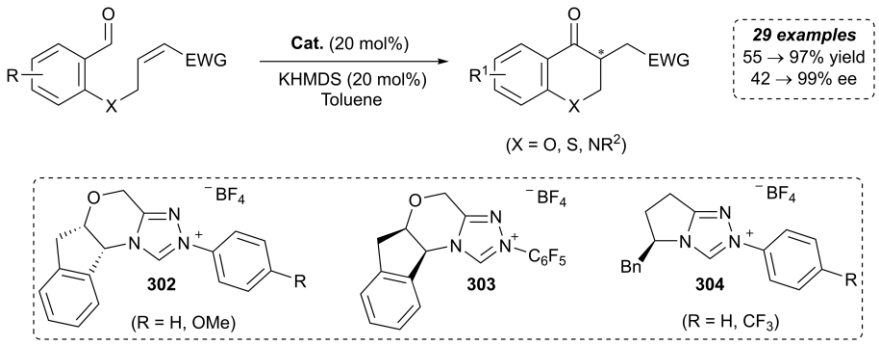
Scheme 168 – The first report of an intramolecular Stetter reaction, by Trost and coworkers.

Ciganek[328] was the first to report an intramolecular Stetter reaction under catalytic conditions, 20 years after Stetter's initial work (**Scheme 169**). Although catalyst loading was as high as 40 mol% in some cases, satisfactory to very high yields of chromanone **301** were achieved with **300** in the absence of base. Thiazolylidine generation is presumed by Ciganek to occur through deprotonation by DMF, however the very low pK_aH of DMF (−0.3) raises significant doubt about this assumption. The 2-formylphenoxycrotonate starting material **299**, along with 2-formylphenoxyacrylates, are known to be highly active substrates for the Stetter reaction. These substrates are now seen as benchmark reactions for the development of new carbene catalysts.[319]



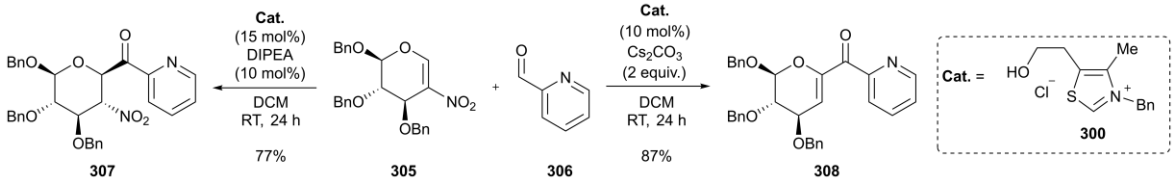
Scheme 169 – The first report of an intramolecular Stetter reaction undertaken under catalytic conditions, by Ciganek.

More recent work on intramolecular Stetter reactions has considered the stereoselectivity of the process. Rovis *et al*[329] have undertaken a great deal of work in this area, enabling variation of the chromanone product commonly explored in Stetter reaction development using a series of chiral triazolium salts **302** – **304** (**Scheme 170**). This has also included work in the introduction of phosphorous-containing electron-withdrawing groups.[330] Other notable contributions to the development of intramolecular Stetter reactions include transformations with 1,6-conjugate acceptors by Law and McErlean[331] and the development of immobilised NHC precursors that undertake stereoselective transformations by Zeitler and Mager.[332]



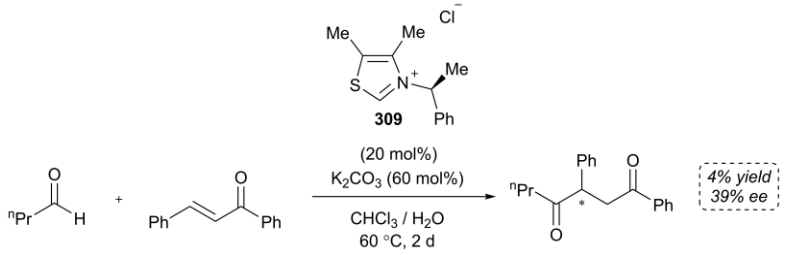
Scheme 170 – Asymmetric intramolecular Stetter reaction by Rovis *et al*.

Intermolecular Stetter reactions have also shown application in the development of a range of organic precursors and natural products.[309, 319] Following Stetter's initial work,[325, 326] the intermolecular Stetter reaction has not seen a large amount of interest within the literature until recently. One example is the work by Liu *et al*[333] on *C*-glycosylation using 2-nitroglucal **305** (**Scheme 171**). Variation of the base used within the transformation can either enable the Stetter reaction (**307**), or proceed to give the corresponding enone **308**.

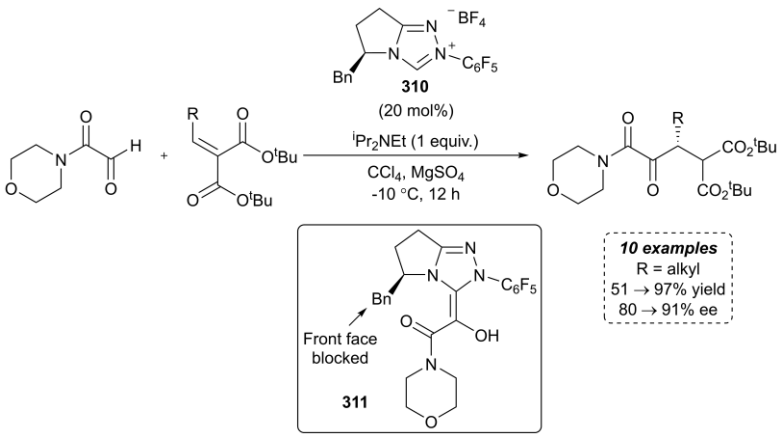


Scheme 171 – *C*-glycosylation of heteroaromatic aldehydes by intermolecular Stetter reaction, by Liu *et al*.

Enders[334] reported the first asymmetric intermolecular Stetter reaction in 1989 using thiazolium precatalyst **309**, obtaining a good *ee* for an initial report however low yields were achieved (**Scheme 172**). Progress in this area did not begin to gain significant attention until 2008, where the first reports using triazolium-based NHCs were made by Rovis[335, 336] and Enders.[337, 338] The catalysts used in these reports share a bicyclic, pyrrolidino-fused scaffold that enables the introduction of chirality or directing groups close to the precarbenic centre. As an example, Rovis[336] illustrated the enantioselective reaction between alkylidemalonates and glyoxamide (**Scheme 173**) using the benzyl-functionalised triazolium scaffold **310**, which can direct the product structure formed through favouring rear-side attack of the Breslow intermediate **311**.



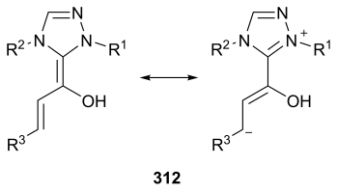
Scheme 172 – The first report of an asymmetric intermolecular Stetter reaction by Enders.



Scheme 173 – Triazolylidine-catalysed asymmetric intermolecular Stetter reaction by Rovis *et al*.

5.2.2 – Other triazolylidine-catalysed reactions

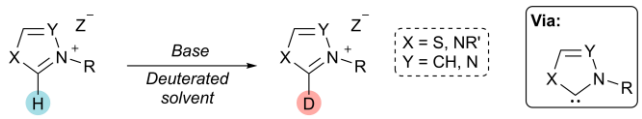
The benzoin and Stetter reactions are the only two transformations explored within this work, however there are a broad range of other transformations catalysed by triazolylidines noted within the literature. For example, α,β-unsaturated aldehydes can undergo direct addition to generate extended Breslow intermediate scaffolds (**312**) that can react with electrophiles to give β-substituted carbonyl compounds.[309] Recent reviews[309, 339] provide a detailed overview of the broader applications known.



312

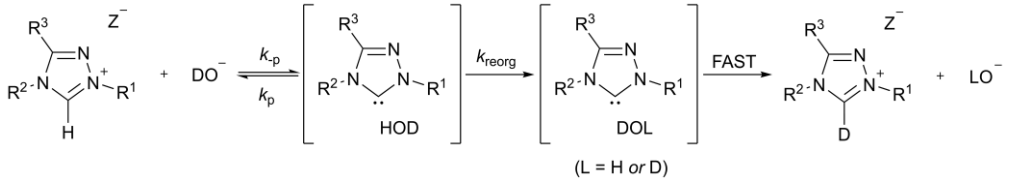
5.3 – Evaluation of NHC carbon acidity using H/D-exchange

The formation of carbene through deprotonation of the corresponding triazolium ion is key to all NHC-catalysed reactions. Knowledge of the relative acidities of triazolium ions, or azolium ions in general, is key to understanding their catalytic potential including reactivity with substrate and stability in solvent. The rate constant for deprotonation by base, commonly defined as kinetic acidity or protofugality, may be accessed experimentally by hydrogen-deuterium (C-H / C-D) exchange kinetic analysis (**Scheme 174**). Within this work, the term 'protofugality' is used to avoid confusion discussed within the literature[340] regarding reference to 'kinetic acidity'.



Scheme 174 – General scheme for the hydrogen-deuterium exchange upon azolium ions.

The protofugality can be estimated at a known p*D* value (known concentration of deuteroxide) as k_{ex}, which is the first order rate constant for exchange of hydrogen for deuterium within deuterated solvent (**Scheme 175**).[341] The deprotonation step is considered as a pre-equilibrium with rate constants k_{-p} and k_p, which is then followed by the solvent reorganisation step with rate constant k_{reorg}. Both steps contribute to the rate of exchange, with the rate constant for the reverse protonation step (k_p) evidenced to be fast and non-rate limiting.[342-344] The rate of the reverse protonation step is close to that for the dielectric relaxation of solvent ($k_p = k_{reorg} \approx 10^{11}$ s^{-1}), and by considering the principle of microscopic reversibility the overall rate constant for the deuteration of carbene can be estimated as the rate constant for solvent reorganisation (~10^{11} s^{-1})



Scheme 175 – Deuteroxide dependent H/D exchange of triazolium ions. A pre-equilibrium leads to the carbene-HOD complex, followed by solvent reorganisation (k_{reorg}) and rapid deuteration by DOL.

Comparing k_{ex} as a function of deuteroxide concentration, or log k_{ex} against p*D*, allows for the determination of k_{DO} – the second-order rate constant for deprotonation. Our group have previously reported k_{ex} and k_{DO} values for a large series of azolium salts in aqueous solution (**Figure 54**).[64, 65, 127, 166, 345-347] The data collected shows the clear increase in protofugality moving from imidazolium to triazolium salts. This is attributed to the role of the additional ring heteroatom destabilising the cationic triazolium relative to the formally neutral NHC.

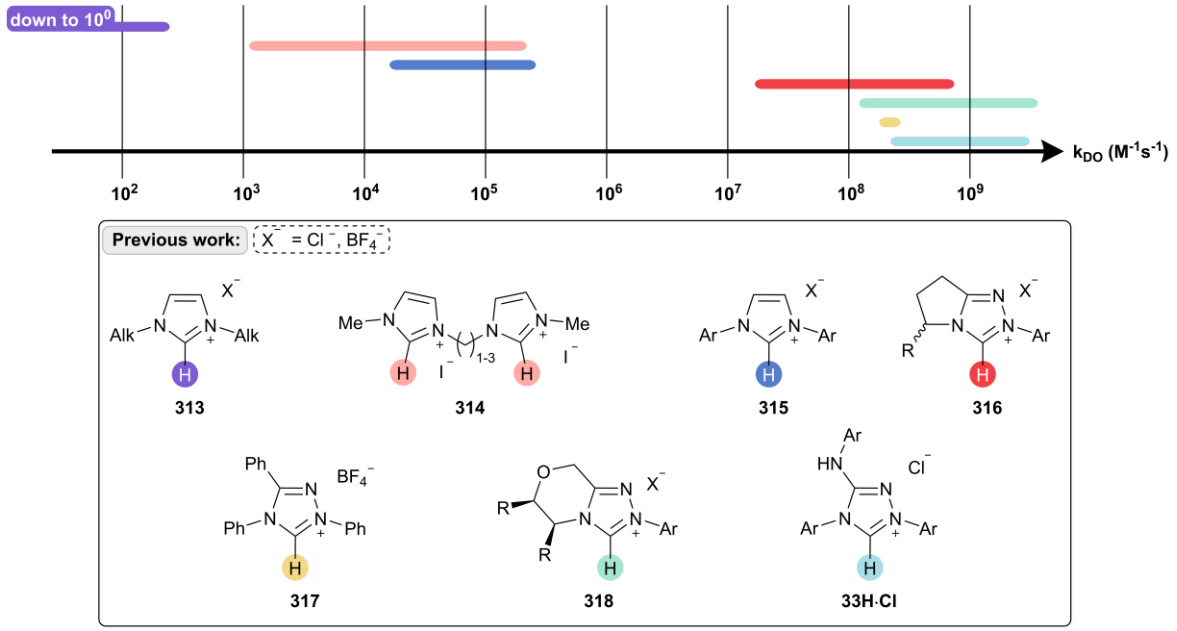
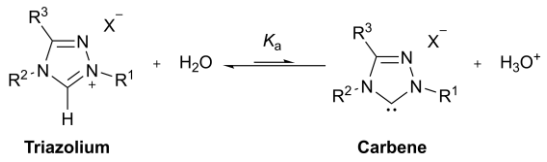


Figure 54 – Previously determined k_{DO} values for a selection of azolium ions in aqueous solution. Note that the data for **33H·Cl** was obtained with the addition of 30% v/v MeCN.

Considering the deprotonation of triazolium ions in water (**Scheme 176**), the equilibrium can be described with the constant K_a (**Equation 3**) which is more commonly expressed as pK_a (**Equation 4**).



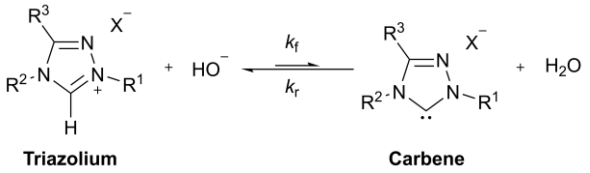
Scheme 176 – The acid dissociation of triazolium ions in water, defined by the acid dissociation constant K_a.

$$K_a = \frac{[Carbene][H_3O^+]}{[Triazolium]} \qquad \textbf{Equation 3}$$

$$pK_a = -\log_{10} K_a \qquad \textbf{Equation 4}$$

Approaches to determine pK_a values for strong carbon acids attempt to observe equilibrium concentrations of acid and the conjugate base using spectrophotometric, calorimetric or potentiometric techniques.[348] However, the basicity of triazolylidine NHCs (pK_aH ~ 17 in aqueous solution)[65] *versus* water results in a rapid and near complete reprotonation to give the triazolium salt, an example of the solvent levelling effect. Due to the levels of carbene being below detectable limits, the approaches commonly used for strong acids cannot be used. Instead, the pK_a values of weak carbon acids are determined using a kinetic approach (**Scheme 177**) where the acid dissociation is expressed in terms of the rate constants for the forward reaction (deprotonation, k_f, M^{-1} s^{-1}) and the

reverse reaction (reprotonation by solvent, k_r, s^{-1}) (**Equation 5**). The forward reaction is usually accessed by H/D exchange, and the reverse by estimation or fast reaction spectroscopy.



Scheme 177 – The acid dissociation of triazolium ions in water, defined by the rates of forward (k_f) and reverse (k_r) reactions.

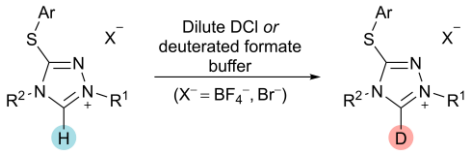
$$K_a = \frac{k_f}{k_r} \qquad \textbf{Equation 5}$$

5.3.1 – Experimental details

Within this work, first and second order rate constants for exchange of the C(5)-H of 1,4-dialkyl *S*-triazolium salts for deuterium were determined in solutions of DCl in D_2O, and in formate buffer, at 25 °C and ionic strength (I) = 1.0 (KCl). Further details on the NMR spectrometer setup and data processing can be found in Appendix D. For reference, **Table 27** summarises the *S*-triazolium salts analysed during this work.

Table 27 – Summary of the *S*-triazolium salts analysed during this work.

Analogue	R^1	R^2	Ar	General structure
92a·BF$_4$	Me	Me	Ph	
92b·BF$_4$	Me	Me	*p*-Me-C$_6$H$_4$	
92d·BF$_4$	Me	Me	*p*-OMe-C$_6$H$_4$	
92e·BF$_4$	Me	Me	*p*-NO$_2$-C$_6$H$_4$	
92h·BF$_4$	Me	Me	*p*-Br-C$_6$H$_4$	
92i·BF$_4$	Me	Me	*p*-I-C$_6$H$_4$	
92n·BF$_4$	Me	Me	*p*-COOMe-C$_6$H$_4$	
92o·BF$_4$	Me	Me	2,6-Me-C$_6$H$_4$	
92q·BF$_4$	Me	Me	TFP	
94·BF$_4$	Et	Me	Ph	
99·Br	Bn	Bn	Ph	



TFP = tetrafluoropyrid-4-yl

In pure aqueous buffers, p*D* values were calculated from the p*H* values by correcting observed readings from the p*H* probe used based on literature values[349] (**Equation 6**). Deuteroxide concentration could therefore be determined using **Equation 7**, where $K_W = 10^{-14.87}$ M^2 is the ion product of D_2O at 25 °C[350] and $\gamma_{DO} = 0.696 \pm 0.005$ is the apparent activity coefficient of deuteroxide

under our experimental conditions. γ_{DO} was determined from the measured p*H* of solutions of known [HO^-] in water at I = 1.0 (KCl) and 25 °C, with the assumption that $\gamma_{DO} = \gamma_{HO}$.

In 20% d_3-MeCN within D_2O buffers, an additional subtraction of $\delta = 0.067$ (a constant based on values calculated in the literature)[350, 351] is required to account for p*D* variation arising from the use of pure aqueous standards for calibration with subsequent p*D* measurements in 2:8 d_3-MeCN / D_2O (**Equation 8**). The deuteroxide concentration was calculated from **Equation 9**, where pK_{AP}(MeCN-D_2O) = 15.36 is the autoprotolysis value of water in a mixture of 2:8 MeCN / D_2O and $\gamma_{DO} = 0.893$ is the apparent activity coefficient of deuteroxide under our experimental conditions. The determination of these values is non-trivial and is therefore discussed in Appendix D.

$$pD_{Corr} = pH\ meter\ reading + 0.4 \qquad \textbf{Equation 6}$$

$$[DO^-] = \frac{10^{pD_{corr} - pK_w}}{\gamma_{DO}} \qquad \textbf{Equation 7}$$

$$pD_{Corr} = pH\ meter\ reading + 0.4 - \delta \qquad \textbf{Equation 8}$$

$$[DO^-] = \frac{10^{pD_{corr} - pK_{AP}(MeCN - D_2O)}}{\gamma_{DO}} \qquad \textbf{Equation 9}$$

p*D* values were obtained at the beginning and end of the H/D exchange reaction, with the maximum variation in p*D* being ± 0.04. In general, p*D* variation across experiments was ± 0.02 corresponding to no observed change in p*D* within the error of the electrode. For consistency, the p*D* at the start of the reaction was used in data analysis.

5.3.2 – Determination of T_1 values

Quantitative NMR (qNMR) is a valuable tool for determination of compound purity, mechanistic analysis, and physical-organic studies. For reliable quantitation of NMR signals it is important to consider the acquisition parameters; with NMR frequently being semi- or fully-automated process the required conditions for quantitation are often not met. One parameter often overlooked is the spin-lattice decay (T_1), with its magnitude placing a limit on acquisition rates of consecutive scans. For experiments in which 90° pulses are applied, the time between consecutive excitation pulses (also known as the repetition time, t_R) must be at least $5 \times T_1$ as this allows for ≥ 99.3% relaxation of spins. Failure to adhere to this leads to unevenly relaxed spins within the analyte, and thus can lead to inaccurate quantitation.[272]

Figure 55 shows an example of the effect of incorrect T_1 values on the inverse-gated proton-decoupled ^{13}C NMR of 1,1-diphenyl-2-propyn-1-ol, an experiment that enables quantitation of signals through minimisation of nuclear Overhauser effect (NOE) enhancements. Only when $t_R \geq 5$

× T_1 is the spin-lattice relaxation near complete, and when coupled with the minimised NOEs this allows for quantitation of $^{13}C\{^1H\}$ environments.[272]

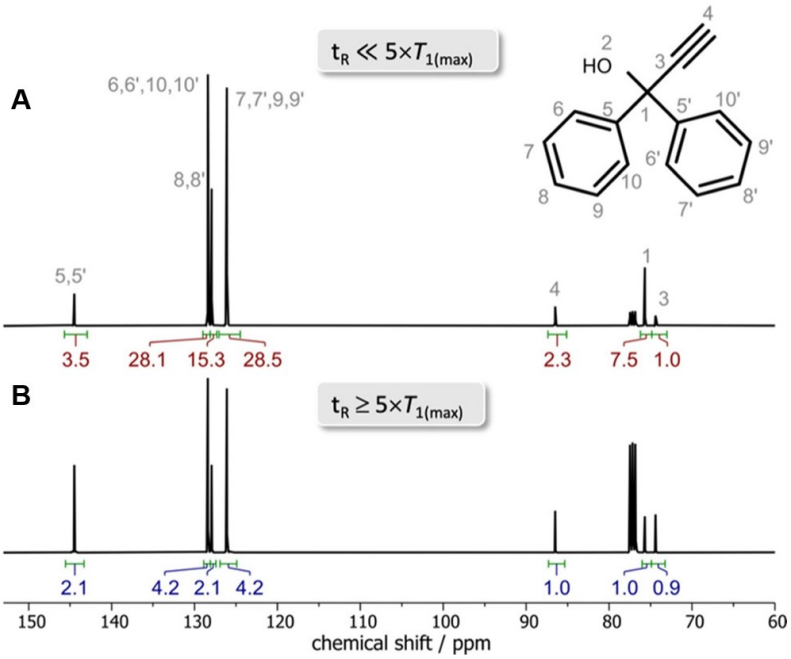


Figure 55 – **A** – Inverse-gated, proton-decoupled ^{13}C NMR spectrum of 1,1-diphenyl-2-propyn-1-ol (pictured) with $t_R << 5 \times T_1$. **B** – same spectrum, acquired using $t_R \geq 5 \times T_1$ for all $^{13}C\{^1H\}$ environments such that qNMR is established. Modified with permission from R. Wei, C. L. Dickson, D. Uhrín and G. C. Lloyd-Jones, *J. Org. Chem.*, 2021, **86**, *13*, 9023 – 9029. Copyright 2021 © American Chemical Society.

T_1 is typically influenced by the nucleus of interest, as well as the surrounding nuclei that can provide alternative pathways of relaxation. Therefore, determination of T_1 is necessary for all nuclei of interest in kinetic experiments. **Figure 56** summarises some of the ways in which T_1 can be quantified. Inversion recovery (**Figure 56A**) is the most widely used methodology, and on nearly all spectrometers is a pre-defined pulse sequence.[272] The process starts with a 180° pulse, followed by a delay period of time τ before a 90° pulse and acquisition of the free induction decay (FID).[352, 353] The integral of the partially relaxed environments can be determined as a function of τ, and plotted to give T_1 through fitting to an exponential model. Saturation recovery (**Figure 56B**) involves fully saturating the signal using equally spaced 90° pulses before alteration of τ to determine T_1.[272] This methodology has been used in the determination of T_1 values for paramagnetic species, such as nitroxide[354] and phenoxyl[355] radicals. Progressive saturation (**Figure 56C**) uses a 90° pulse train, with variation of τ allowing the sampling of a recovery curve from the steady state.[356] Finally, a modern approach is termed 'Faster longitudinal relaxation investigated by progressive saturation' or FLIPS (**Figure 56D**). In this method a scan is acquired after every excitation pulse, which allows for a much faster acquisition of T_1 with all data collected in a single experiment, however this method is less accurate than techniques such as the commonly used inversion recovery.[272]

T_1 values of the resonance accounting for C(5)-H were determined for all salts tested using the inversion recovery method. A FID array was undertaken where a 180° pulse was applied and inversion time from 0.0625 to 32 s waited before a 90° pulse and FID obtained. Further details of the method to obtain T_1 values is given in the experimental (Chapter 8).

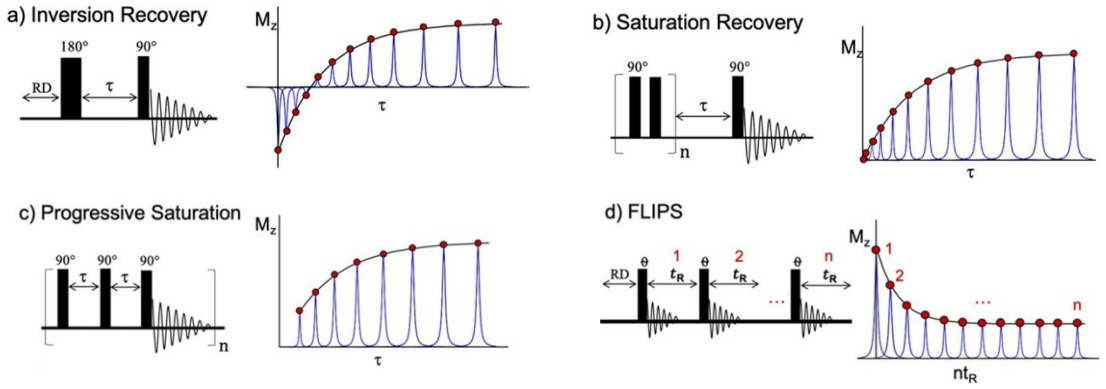


Figure 56 – Pulse sequences and the resultant data fitting used to derive values of T_1. Modified with permission from R. Wei, C. L. Dickson, D. Uhrín and G. C. Lloyd-Jones, *J. Org. Chem.*, 2021, **86**, *13*, 9023 – 9029. Copyright 2021 © American Chemical Society.

The determined T_1 values are summarised in **Table 28**. Data was collected for [DCl] = 1.00×10^{-1} M as all salts were shown to have H/D-exchange half-lives significantly longer than the experiment time (~15 minutes) in initial studies. Given significant differences in T_1 between salts it is deemed necessary to consider every compound tested. The effect of altering [DCl], and the effect of 20% v/v MeCN as was used in some experiments, was also explored.

Table 28 – Summary of the T_1 values determined within this work using the inversion recovery method.

Analogue	[DCl] (mM)	Solvent	T_1 (s)	Analogue	[DCl] (mM)	Solvent	T_1 (s)
92a·BF$_4$	10	D_2O	6.73	**92i·BF$_4$**	100	D_2O	5.67
92a·BF$_4$	100	D_2O	6.51	**92n·BF$_4$**	100	D_2O	5.75
92a·BF$_4$	100	2:8 d_3-MeCN / D_2O	6.68	**92o·BF$_4$**	100	D_2O	4.49
92b·BF$_4$	100	D_2O	5.56	**92q·BF$_4$**	100	D_2O	5.90
92d·BF$_4$	100	D_2O	5.67	**94·BF$_4$**	100	D_2O	4.97
92e·BF$_4$	100	D_2O	6.25	**99·Br**	100	2:8 d_3-MeCN / D_2O	3.00
92e·BF$_4$	100	2:8 d_3-MeCN / D_2O	6.56	TMACl (IS)	100	D_2O	7.54
92h·BF$_4$	100	D_2O	4.86				

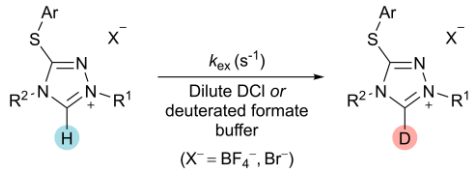
All salts have T_1 values for the C(5)-H position of less than 7 s in 1.00×10^{-1} M DCl, thus a relaxation delay of 35 s is used as this is greater than 5 times the value of T_1 for all *S*-triazolium salts. Data obtained for **92a·BF$_4$** at 1.00×10^{-2} DCl, the highest concentration DCl used in these experiments, indicates a slightly increased T_1 and as such there is a possibility in some cases that t_R is not greater

than $5 \times T_1$. Accurate determination of T_1 values at lower DCl concentrations is non-trivial, given the relatively fast H/D-exchange that will impact the inversion recovery experiments. Furthermore, T_1 values at 1.00×10^{-1} DCl are generally lower than that for **92a·BF$_4$**. As a balance between precision and ability to acquire reliable data, a 35 s delay is used.

The internal standard T_1 is greater than 7 s, therefore $t_R = d_1 + at < 5T_1$ (where d_1 is the relaxation delay and 'at' is the acquisition time) and the integral of the internal standard peak cannot be considered quantitative. Under these conditions relaxation will be less than 99.3% and the internal standard peak will be supressed.[272] However, all values are relative to this internal standard peak which has a constant integral for all spectra (apart from slight increases in integral, consistently < 0.3% across a 64 spectra array, as a result of solvent evaporation that effects all spectra signals proportionally). As such, absolute quantitation is not deemed necessary for the internal standard.

5.4 – Determination of first and second order rate constants for C^5-H/D exchange

The overall H/D exchange process is first order in dilute aqueous solution. k_{ex} values (**Scheme 178**) were determined from the slope of a plot of ln f(s) against time, fitted using the least squares method, where f(s) was determined using **Equation 10**. Errors in the value of k_{ex} stated in this work are the standard errors obtained from the linear fit. To determine the fraction of remaining substrate, f(s), the peak integral corresponding to the C(5)-H position was compared to the peak of the internal standard (tetramethylammonium chloride) that was set to an arbitrary figure of 1000. The integral of the C(5)-H position in the first spectrum of the array was taken as I(0), and f(s) values at time 't' determined using **Equation 10**. The second order rate constant, k_{DO} ($M^{-1}s^{-1}$), was obtained for each *S*-triazolium salt from plots according to **Equation 12** and **Equation 13** where $K_w = 10^{-14.87}$ and γ_{DO} is defined based on the solvent used as described earlier.



Scheme 178 – Determination of protofugality, described by the first-order rate constant k_{ex}, for the *S*-triazolium salts analysed in this work.

$$f(s) = \frac{I(t)}{I(0)} \qquad \textbf{Equation 10}$$

For clarity, this discussion will focus on the *S*-phenyl 1,4-dimethyl triazolium salt **92a·BF₄** as a representative example. Tabulated data and plots relating to all *S*-triazolium salts are provided in Appendix D. **Figure 57** shows a representative NMR overlay at 500 MHz for **92a·BF₄**, using 2 mM DCl (pD_{Corr} = 2.87), obtained during exchange of the C(5)-H proton (s, 9.81 ppm) for deuterium in D_2O at 25 °C and I = 1.0 (KCl). The internal standard, TMACl, is present as a singlet at 3.31 ppm. Disappearance of the peak corresponding to C(5)-H occurs over time, with no other changes observed and this was the case for all *S*-triazolium salts analysed during this work.

Figure 58A shows a representative plot of the fraction of unexchanged substrate against time for the deuterium exchange reaction of **92a·BF₄** within 2 mM DCl. The data fits well to an exponential decay process. A plot of ln f(s) as a function of time (**Figure 58B**) gives a linear fit, indicative of a first-order or pseudo first-order process. As [DCl] is close to constant throughout the experiment, the H/D-exchange reaction is confirmed to be first order from **Figure 58B**. Values of k_{ex} can be obtained from the slope of the ln f(s) plot according to **Equation 11** and are tabulated in Appendix D.

$$\ln f(s) = -kt \qquad \textbf{Equation 11}$$

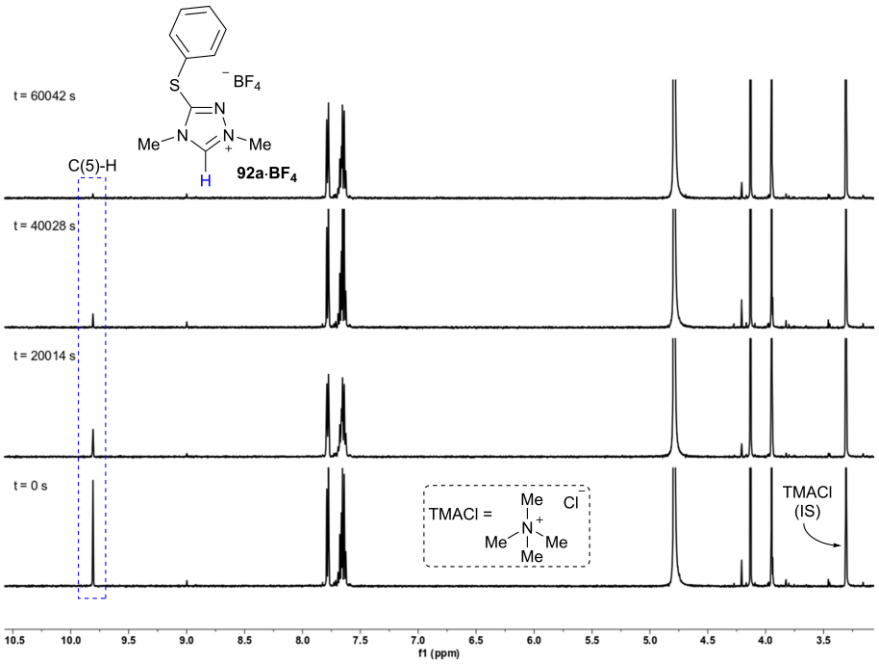


Figure 57 – Representative NMR overlay for **92a·BF$_4$** at 2 mM DCl (pD_{Corr} = 2.87).

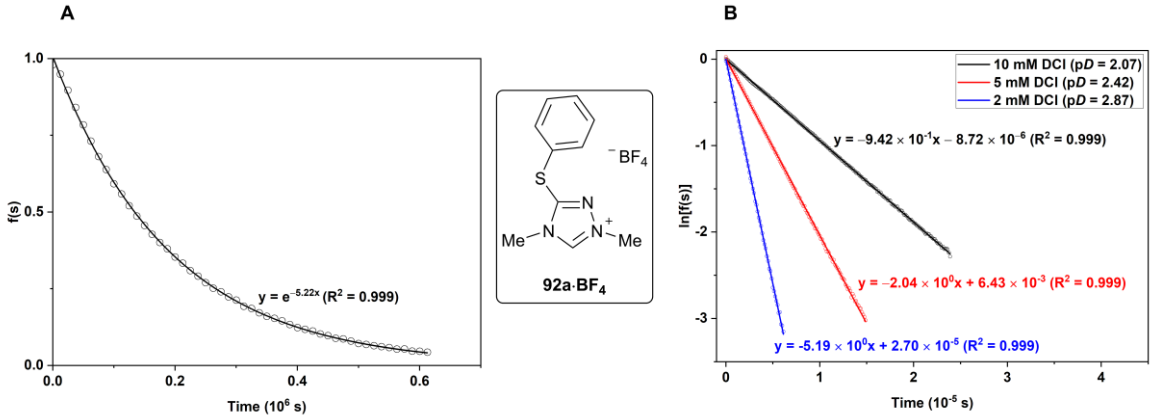


Figure 58 – Plots relating to the fraction of remaining **92a·BF$_4$** within H/D-exchange experiments. **A**) plot of fraction of remaining substrate as a function of time. **B**) semilogarithmic plot of fraction of remaining substrate as a function of time, relating to experiments within dilute DCl.

Finally, the second order rate constant k_{DO} ($M^{-1}s^{-1}$) was obtained for each *S*-triazolium salt from plots according to **Equation 12** and **Equation 13** where $K_w = 10^{-14.87}$ and γ_{DO} is defined based on the solvent used as described in Section 5.3.1 (γ_{DO} = 0.696 in D_2O, γ_{DO} = 0.893 in 20% v/v d_3-MeCN in D_2O). Representative plots are shown in **Figure 59** corresponding to **92a·BF$_4$**, with tabulated values of k_{DO} for each *S*-triazolium salt provided in **Table 29**. Calculation of errors relating to log k_{DO} values is discussed in Chapter 8.8.3. The slope of unity for plots according to **Equation 13** confirms a first order dependence on deuteroxide ion. With two equations used to describe the value of k_{DO}, these will be described as k_{ex} – [DO^-] plots (**Equation 12**) and log k_{ex} – p*D* plots (**Equation 13**) for clarity. Log k_{DO} values are also reported for comparison in the following section.

$$k_{ex} = k_{DO}[DO^-] \qquad \textbf{Equation 12}$$

$$\log_{10} k_{ex} = \log_{10}\left(\frac{k_{DO}K_w}{\gamma_{DO}}\right) + pD \qquad \textbf{Equation 13}$$

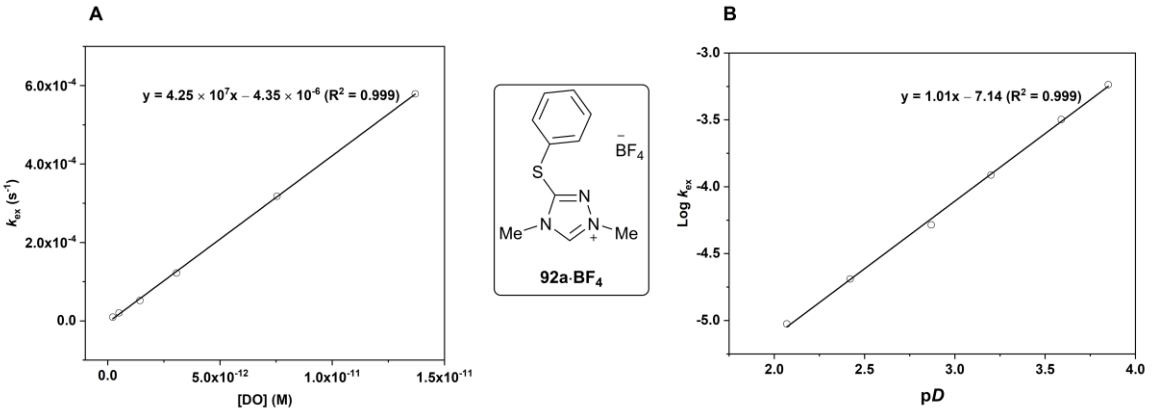
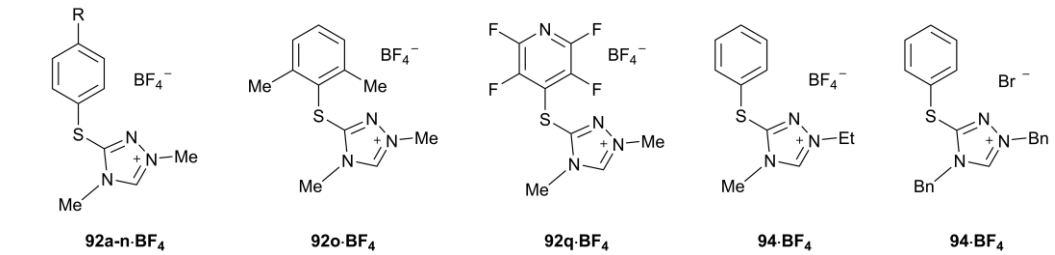


Figure 59 – Plots to determine k_{DO} for **92a·BF$_4$**. **A**) plot as a function of [DO$^-$] according to **Equation 12**. **B**) plot as a function of p*D* according to **Equation 13**.

Table 29 – Summary of the k_{DO} values obtained from plots according to **Equation 12** (k_{ex} – [DO$^-$]) and **Equation 13** (log k_{ex} – p*D*). Note that log k_{DO} values are reported here to 4 significant figures consistent with the level of standard error calculated, however are reported from this point onwards to 3 significant figures consistent with the level of accuracy in reported values of k_{DO}.

Analogue	R	k_{DO} ($\times 10^7$ M^{-1}s^{-1})		log k_{DO}	
		k_{ex} – [DO$^-$]	log k_{ex} – p*D*	k_{ex} – [DO$^-$]	log k_{ex} – p*D*
92a·BF$_4$	H	4.25 (± 0.03)	3.74 (± 0.03)	7.628 (± 0.003)	7.573 (± 0.003)
92b·BF$_4$	Me	3.27 (± 0.03)	2.67 (± 0.05)	7.515 (± 0.004)	7.427 (± 0.008)
92d·BF$_4$	OMe	2.70 (± 0.07)	2.84 (± 0.06)	7.431 (± 0.011)	7.453 (± 0.009)
92e·BF$_4$	NO$_2$	9.20 (± 0.36)	8.29 (± 0.08)	7.964 (± 0.017)	7.919 (± 0.004)
92h·BF$_4$	Br	4.43 (± 0.02)	5.42 (± 0.03)	7.646 (± 0.002)	7.734 (± 0.002)
92i·BF$_4$	I	4.60 (± 0.05)	4.63 (± 0.04)	7.663 (± 0.005)	7.666 (± 0.004)
92n·BF$_4$	COOMe	6.61 (± 0.13)	7.46 (± 0.10)	7.820 (± 0.009)	7.873 (± 0.006)
92o·BF$_4$	-	2.16 (± 0.13)	0.584 (± 0.009)	7.334 (± 0.026)	6.766 (± 0.007)
92q·BF$_4$	-	16.2 (± 0.4)	14.5 (± 0.02)	8.210 (± 0.011)	8.161 (± 0.006)
94·BF$_4$	-	3.38 (± 0.03)	2.88 (± 0.01)	7.529 (± 0.004)	7.459 (± 0.002)
99·Br	-	45.1 (± 1.0)	32.9 (± 0.6)	8.654 (± 0.010)	8.517 (± 0.008)



The k_{DO} values obtained describe the protofugality, an updated term for kinetic acidity that hopes to remove confusion from intermixing terms for kinetic and thermodynamic properties.[340] Protofugality

is the second-order rate constant for 'loss of proton' by transfer to a common base, which in this case is transfer to the conjugate base of solvent – deuteroxide. Comparisons can be made to the term nucleofugality, in reference to loss of a leaving group. Values obtained from the two methods of k_{DO} determination show similarity in almost all cases, with the data for **92o·BF$_4$** being the only example where log k_{DO} variation between methods is greater than 0.13. The reason for this larger variance is unclear, however for this particular compound the H/D-exchange was only investigated at three p*D* values and so further analysis at a larger range of p*D* values may decrease the variation.

5.4.1 – Comparison of second order rate constants: Exchange rate scales and Hammett structure-activity analysis

The log k_{DO} values reported in this work from k_{ex} – [DO$^-$] plots (**Equation 12**) are summarised in **Figure 60**. Also reported are a series of azolium salts previously analysed within the group.[64, 65]

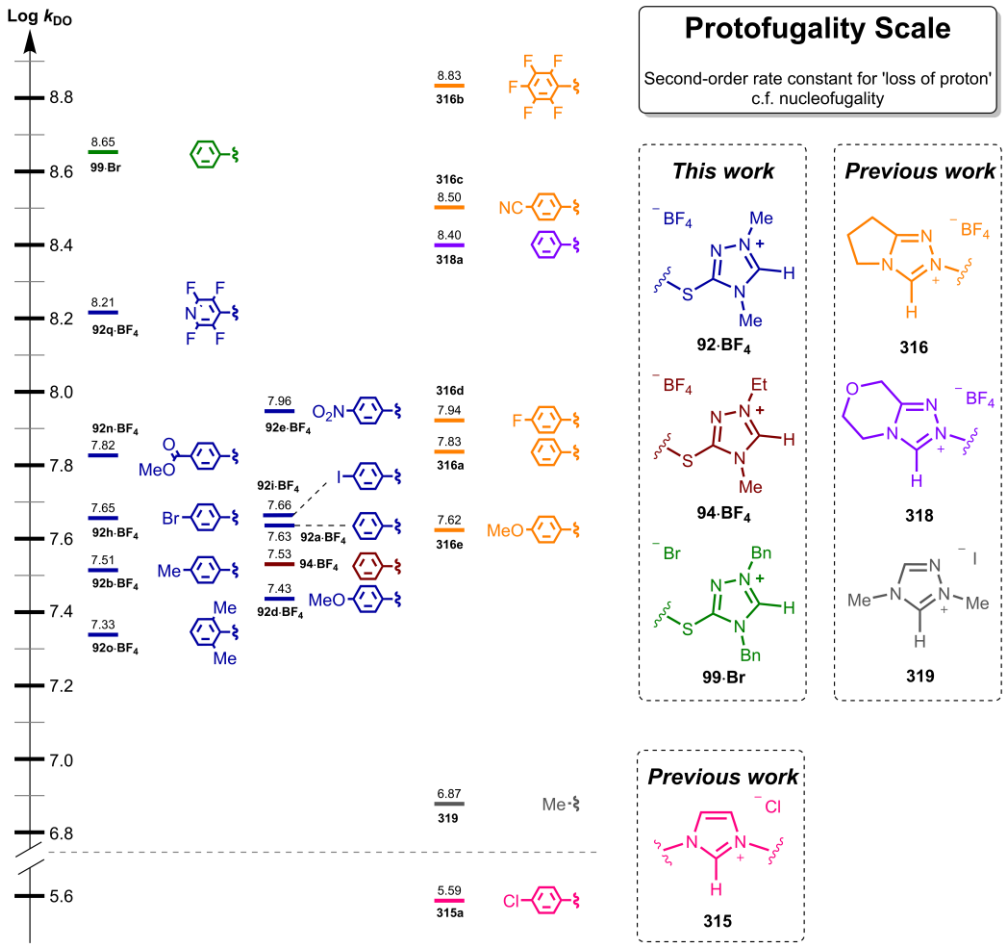


Figure 60 – Protofugality scale for the *S*-triazolium salts analysed in this work. Example k_{DO} values from previous work in the group are also provided: pyrrolidine-fused triazolium salts **316**,[65] morpholine-fused triazolium salts **318**,[65] 1,4-dimethyl-1,2,4-triazolium iodide **319**[357] and imidazolium **315**.[64]

The introduction of aryl substituents on the adjacent nitrogen is known to increase k_{DO} values significantly, for example 1,4-dimethyltriazolium iodide (**319**) has been shown to have a log k_{DO}

value of 6.87 in previous work within the group.[357] Introduction of one *N*-phenyl substituent, such as that seen in **316a**, shows an increase in log k_{DO} by one unit or a 10-fold increase in k_{DO} *versus* **319**. All of the *S*-triazolium ions **92·BF$_4$** have significantly higher protofugalities than **319** by 0.5 to 1.5 log k_{DO} units, demonstrating the acidifying effect of the *S*-Ar substituent.

The introduction of electron-withdrawing substituents upon the aryl ring of *S*-triazolium salts shows the expected increase in protofugality, whilst electron donating substituents lower k_{DO} relative to *S*-phenyl analogue **92a·BF$_4$**. For example, changing from a *para*-methyl substituent (**92b·BF$_4$**) to a *para*-methoxycarbonyl substituent (**92n·BF$_4$**) increases log k_{DO} by 0.32 – this corresponds to a 2-fold increase in k_{DO}. The introduction of an ethyl substituent in place of one of the *N*-methyl groups (**94·BF$_4$**) shows a small change in k_{DO} (*c.f.* **92a·BF$_4$**), however the dibenzyl triazolium **99·Br** has the highest k_{DO} value of the compounds analysed in this work.

Finally, in comparison to previous work,[64, 65] similar k_{DO} values are obtained for *S*-triazolium salts (**92·BF$_4$**, **94·BF$_4$**, **99·Br**) and triazolium salts with an aryl substituent adjacent to the precarbenic centre (**316**, **318**). The scale clearly shows the significantly increased protofugality of triazolium salts *versus* imidazolium salts (e.g. **315a**), with a log k_{DO} value roughly 2 less than the triazolium salts analysed within the group. Importantly, the *S*-aryl substituent is demonstrated to significantly affect the protofugality of dialkyl triazolium salts, resulting in species with protofugality values similar to those bearing aryl substituents adjacent to the precarbenic centre. These *N*-aryl triazolium salts have seen wide application for organocatalysis,[358, 359] indicating that the *S*-triazolium scaffold may also be of interest as an organocatalyst as the acidities are similar.

Hammett analysis of the 1,4-dimethyl triazolium salts prepared in this work has been undertaken, with relevant data tabulated in **Table 30**. For consistency with the protofugality scale, the data from k_{ex} – [DO$^-$] plots (**Equation 12**) is analysed. Based on work by Charton,[360] analogues bearing *ortho*-substituents are described by multiplying the value of σ_p by 0.736. σ_m and σ_p values were obtained from the literature.[164]

Table 30 – Data relevant to Hammett analysis of *S*-triazolium salts analysed in this work. σ_{Ar} corresponds to the appropriate value of σ_p from the literature, unless otherwise stated.

Analogue	log k_{DO}	σ_{Ar}	Analogue	log k_{DO}	σ_{Ar}
92a·BF$_4$	7.63	0.00	**92i·BF$_4$**	7.66	+0.18
92b·BF$_4$	7.51	−0.17	**92n·BF$_4$**	7.82	+0.45
92d·BF$_4$	7.43	−0.27	**92o·BF$_4$**	7.33	−0.25[a]
92e·BF$_4$	7.96	+0.78	**92q·BF$_4$**	8.21	+1.22[b]
92h·BF$_4$	7.65	+0.23			

[a]Value obtained by taking the sum of σ_p values for the groups and multiplying by 0.736. [b]Value obtained by taking the difference in σ_p values between phenyl (−0.01) and pyrid-4-yl (+0.44), then determining the sum of this value and the substituent effects of the four fluorines with the two *ortho*-fluorines accounted for by using 1.472σ_p.

Figure 61 shows the Hammett plot obtained from the log k_{DO} data obtained from the k_{ex} – [DO^-] plots. Linear fits are shown for the *para*-substituted *S*-triazolium salts only and also for all 1,4-dimethyl *S*-triazolium salts synthesized in this work. The fits are relatively similar, indicating that Charton's modification[360] for *ortho*-substituted aryl rings applies well to the *S*-triazolium salts. ρ values of +0.48 and +0.53 are obtained depending on the fit used, with both values consistent with the H/D-exchange mechanism where an electron density increase in the intermediate is seen near the substituted aryl ring 'Ar' (cationic triazolium salt forming a neutral carbene). The magnitude indicates that there is a substantial substituent effect, but the value is significantly less than 1. Values less than 1 indicate that the exchange is less sensitive to substitution than the reference *para*-substituted benzoic acid dissociation in water (**Scheme 179**) – this is to be expected given the distance of the *S*-aryl substituent from the precarbenic site.

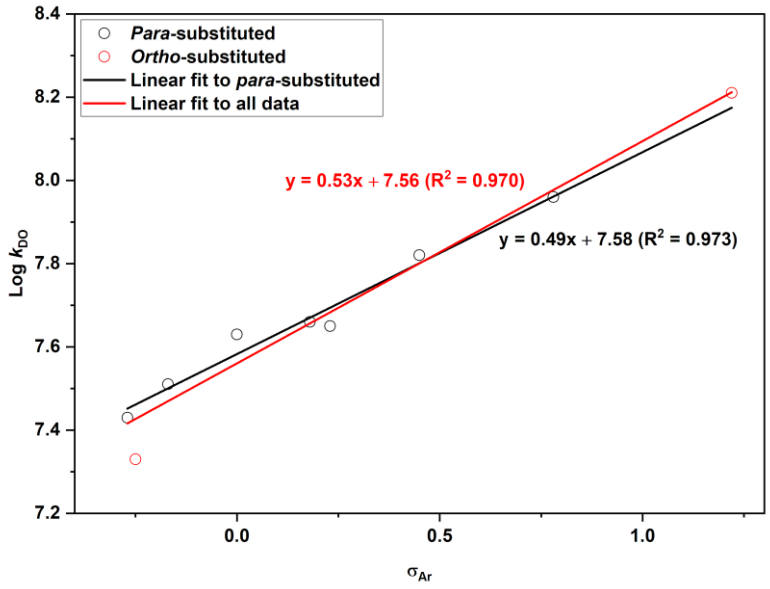
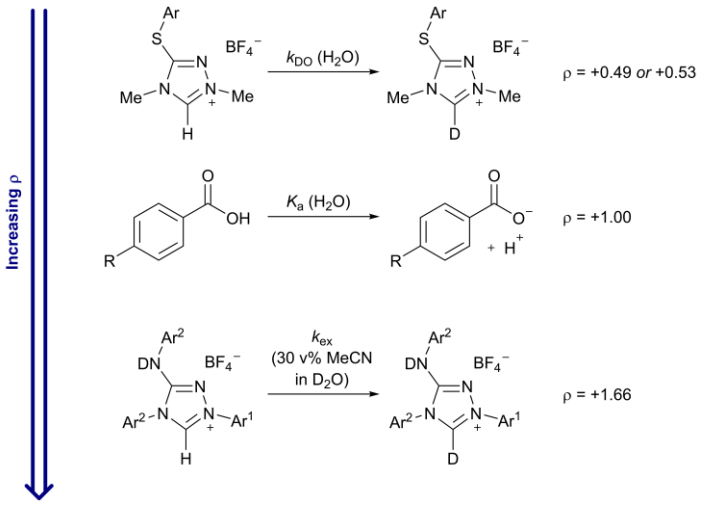


Figure 61 – Hammett plot of the log k_{DO} data obtained from the k_{ex} – [DO^-] plots. Fits to *para*-substituted salts only, and to all salts, are shown.

Scheme 179 also shows the ρ-value estimated by Murray relating to the H/D-exchange of Nitron analogues in 30% v/v MeCN in D_2O. Due to the ring opening of Nitron, which was found to occur at p*D* values greater than 3, Murray investigated the exchange at *p*D 1.09 only and used the obtained k_{ex} values to obtain a value for ρ as +1.66 (σ value estimated as the sum of substituents on Ar^1 and Ar^2). This value is significantly greater than that obtained for the *S*-triazolium salts in this work, however this is expected given that the substitution investigated is partly upon the N(1) and N(4)-aryl rings adjacent to the precarbenic site.



Scheme 179 – Comparison of Hammett *ρ*-value obtained in this work (top) to the reference reaction (middle) and the H/D-exchange process experimentally estimated by Murray on Nitron analogues (bottom).

5.5 – XRD structure to activity relationships

By analysis of XRD data, it is hoped relationships can be found between the structural parameters and the values of k_{DO}. The data analysed in this section relates to the crystal structures shown in Chapter 2.3.2.3. **Figure 62** shows the structures of the *S*-triazolium salts analysed during this work – apart from **92o·BF$_4$** and **92q·BF$_4$**, all *S*-triazolium salts correspond to the general structure.

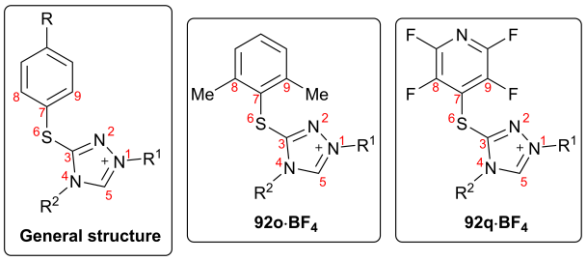


Figure 62 – General structures of the *S*-triazolium salts with the atom numbering used throughout this chapter section.

Given that the majority of *S*-triazolium salts prepared in this work are 1,4-dimethyl triazolium salts bearing substitution on the *para*-position of the aryl ring, analysis of relationships between only these analogues was undertaken whereby alterations in the crystal structure, considering the structural parameters shown in **Figure 63**, can be attributed to the effect of the aryl substituent.

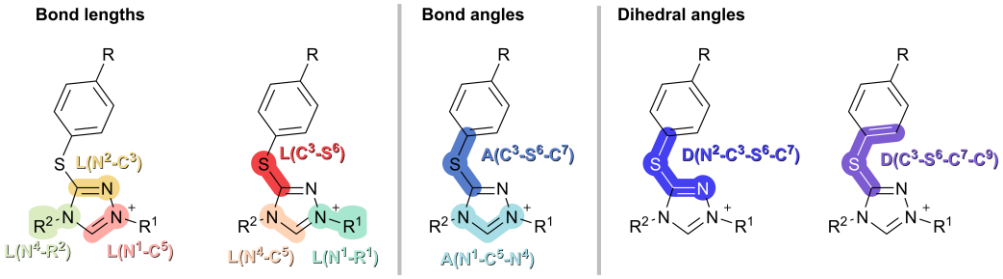


Figure 63 – Structural parameters explored in this work, shown on the general structure. Within this section $R^1 = R^2 = Me$.

The modulus of D(C^3-S^6-C^7-C^9) shows the best linear fit to k_{DO} values (**Figure 64A**). This overall trend involves an increase in k_{DO} with decreasing |D(C^3-S^6-C^7-C^9)|. Variation between experimental k_{DO} values and those calculated from the linear fits in **Figure 64A** are generally ± 30%, with one example from each fit showing variation of ± 39%. The k_{DO} values determined using this method are therefore not a replacement for experimental determination and should be used as an approximation. There is an increase in electron density from the cationic triazolium to neutral carbene, and so the trend can be rationalised as increased stabilisation of the carbene intermediate within the H/D-exchange process by delocalisation. The smaller the value of |D(C_3-S_6-C_7-C_9)|, the more co-planar the triazolyl and phenyl rings. This perhaps maximises the inductive electron withdrawing effect, which stabilises the neutral NHC relative to the cationic triazolium salt.

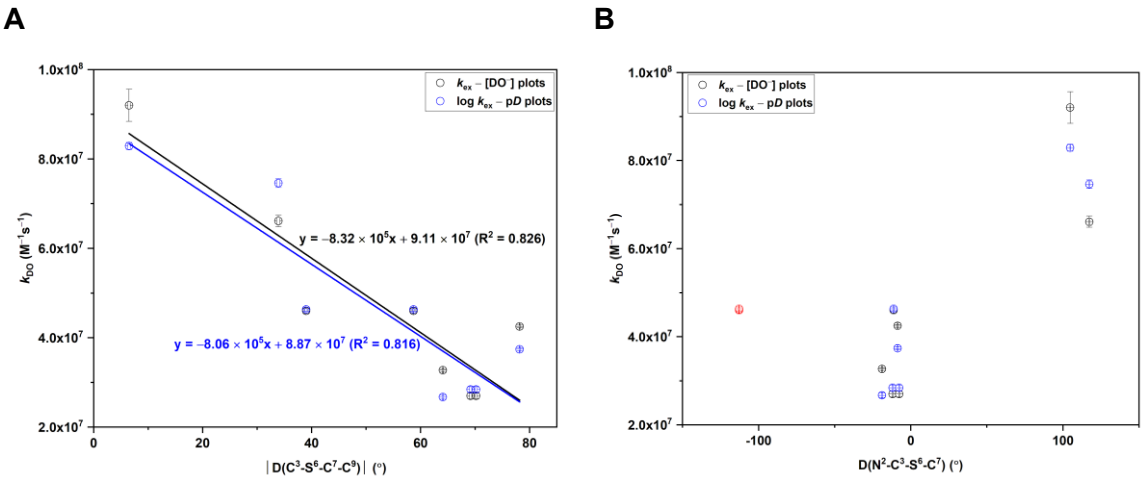


Figure 64 – Structure-activity plots for *para*-substituted 1,4-dimethyl salts. **A** – $|D(C_3\text{-}S_6\text{-}C_7\text{-}C_9)|$, showing the strongest linear fit. **B** – $D(N_2\text{-}C_3\text{-}S_6\text{-}C_7)$ has a good linear fit after omitting one of the crystallographically independent units of **92i·BF₄** (shown in red).

An increase in $D(N^2\text{-}C^3\text{-}S^6\text{-}C^7)$ also correlates to an increase in k_{DO}, after omitting one of the data points corresponding to one of the crystallographically-independent units of **92i·BF₄** (**Figure 64B**). Given that the data generally forms two clusters around 0 and 100°, it is not appropriate to describe this as a linear trend. Instead there appears to be a conformational switch that correlates to a change in k_{DO} – deviation from planarity is linked to an increase in k_{DO}. Only the two analogues with the most electron withdrawing groups (**92e·BF₄** and **92n·BF₄**) show this deviation from planarity, with the point of variation occurring between σ_p values of +0.23 (**92h·BF₄**, *p*-Br-C_6H_4) and +0.45 (**92n·BF₄**, *p*-COOMe-C_6H_4).[164] It is proposed that there is a point at which electron withdrawal by the *para*-substituent leads to resonance between the aryl and triazolyl ring to become unfavourable. The aryl ring can therefore rotate out of plane with the triazolyl ring, possibly to relieve steric interactions between the two rings.

Linear plots of k_{DO} values against other structural parameters show substantially poorer fits, with the next best fit being a negative trend between k_{DO} and $L(N_2\text{-}C_3)$ ($R^2 \sim 0.2$ for both sets of k_{DO} values).

The inclusion of *S*-triazolium analogues bearing *ortho*-substitution upon the aryl ring, or variation of the *N*-alkyl groups, increases the complexity of the modelling and leads to weaker linear fits than those seen within the previous section. JMP (John's Macintosh Program) software is therefore used to provide an accurate model that enables reasonable correlations of k_{DO} values from XRD data.

Plots of k_{DO} values against each bond length, bond angle and dihedral angle within the *S*-triazolium scaffold were made and fit to a linear model. This allows for identification of parameters that correlate best to k_{DO} values; overparameterization leads to issues in refining a model. Only fits achieving an R^2 value greater than 0.6 are deemed to be of interest, a threshold deemed sensible given that only three of the parameters give fits exceeding $R^2 = 0.6$ (**Figure 65A – C**). A fourth fit against $|D(N_2\text{-}C_3\text{-}S_6\text{-}C_7)|$ is shown as the next best linear fit based on R^2 values (**Figure 65D**) however shows

data grouping not appropriate to analyse as a linear correlation. |D(N_2-C_3-S_6-C_7)| is not involved in additional studies.

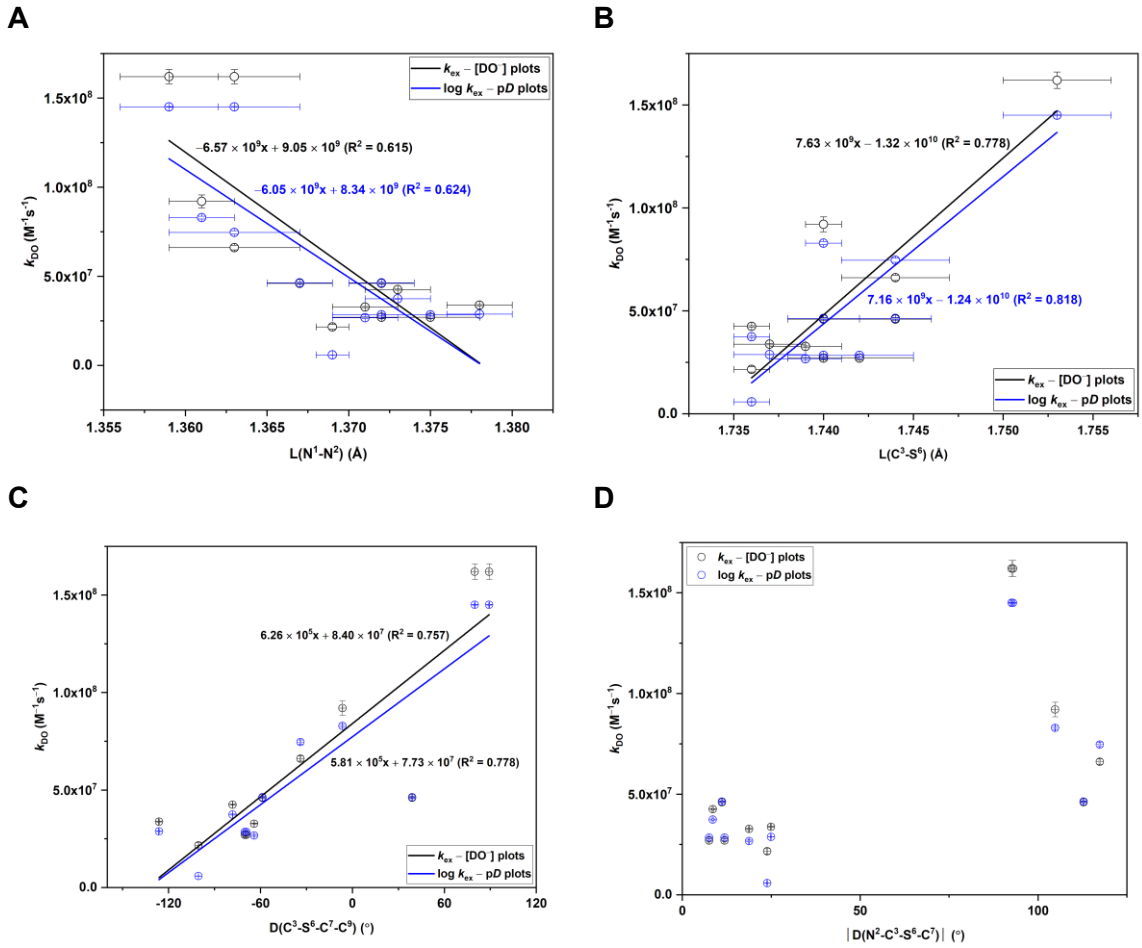
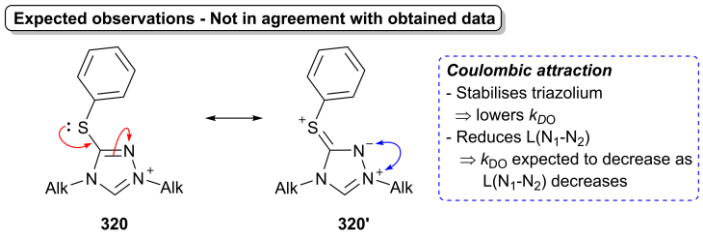


Figure 65 – Structure-activity plots for all *S*-triazolium salts analysed by XRD and H/D-exchange kinetics within this work. **A** – L(N_1-N_2); **B** – L(C_3-S_6); **C** – D(C_3-S_6-C_7-C_9), showing the best fit to k_{DO} values. **D** – |D(N_2-C_3-S_6-C_7)|, with data group not appropriate to analyse by a linear fit.

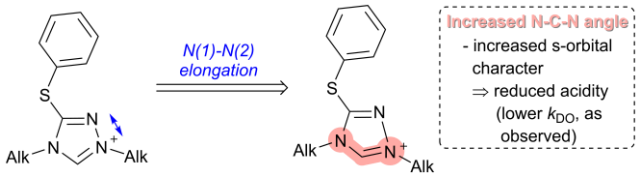
The negative trend between k_{DO} and L(N_1-N_2) (**Figure 65A**) is challenging to rationalise. It would be expected that analogues with lower k_{DO} values would show greater stabilisation of the cationic nitrogen by electron donation from N(2) (**Scheme 180**). The coulombic attraction within the highly charged resonance form **320'** would also be expected to lead to decreased length of the N(1)-N(2) bond, and so a decrease in the bond length would be expected to correlate with decreased k_{DO}. With the opposite trend observed, one alternative option is that lengthening of the N(1)-N(2) bond allows for a triazolyl ring distortion that allows for increases in the angle about the precarbenic site (**Scheme 181**). Increases in this angle are consistent with increased acidity / enhanced k_{DO} based on previous work within the group.[166]

The positive trend between k_{DO} and L(C_3-S_6) (**Figure 65B**) can be proposed to describe the electron donation from the *S*-aryl ring. Increased length of the C(3)-S(6) bond indicates less electron donation into the triazolyl ring, which means less stabilisation of the cationic triazolium salt and increased propensity to form the carbene intermediate.

The positive trend between k_{DO} and D(C_3-S_6-C_7-C_9) (**Figure 65C**) can be explained in the same manner as with *para*-substituted 1,4-dimethyl *S*-triazolium salts. The increase in planarity from −144° to −6° correlates with increased k_{DO} due to maximisation of the inductive electron withdrawing effect that stabilises the neutral NHC relative to the cationic triazolium salt. The only anomalous results arise at positive dihedrals, corresponding to the two independent ionic pairs within the crystal structure of **92q·BF$_4$**. This analogue bears the highly electron-withdrawing, *ortho*-substituted tetrafluoropyrid-4-yl group that may adopt this conformation due to the electronic repulsion of the *ortho*-fluorine groups and N(2) position.



Scheme 180 – It was expected that a positive trend between k_{DO} and L(N_1-N_2) would be seen, rationalised by the changes in the coulombic attraction visualised in the resonance form.



Scheme 181 – Explanation for the lowering of k_{DO} values as N(1)-N(2) length increases.

Finally, the deviation from planarity relating to D(N^2-C^3-S^6-C^7) is seen to correlate to increased k_{DO} (**Figure 65D**). The same clustering described earlier for *para*-substituted 1,4-dimethyl *S*-triazolium salts is seen, however in this case the modulus of dihedral angle values gives the better fit. The explanation of a threshold electron withdrawal by substituents, that leads to deviation from planarity becoming more favourable than resonance through the Ar-S-triazolyl moiety, still applies.

With single parameter trends observed, more complex trends were explored using JMP. The models are evaluated by consideration of the 'p-value' and 'F-ratio'. The p-value is a measure of the probability of obtaining the observed relationship between the structural parameter and k_{DO}, assuming the null hypothesis that in reality there is no link between the parameter in question and k_{DO}. Lower p-values indicate trends that are less likely to be due to chance, and that there is a genuine relationship between the structural parameter and k_{DO}. The F-ratio is the ratio of mean square values between the observed effect and the error, the value describes if the structural parameter supports or disproves the null hypothesis when part of the fitting model. F-ratio values significantly larger than 1 indicate that the variation observed is more than would be expected by chance, and inclusion of the structural parameter in the model rejects the null hypothesis. F-ratio values of 1 support the null

hypothesis, whilst F-ratio values less than 1 simply show a non-rejection of the null hypothesis (the inclusion of the parameter in the model cannot prove or disprove the null hypothesis).

The two sets of k_{DO} values obtained were fitted to a model with standard least squares fitting considering the three key parameters L(N^1-N^2), L(C^3-S^6) and D(C^3-S^6-C^7-C^9) (**Figure 66**). It was expected that with the decrease in C(3)-S(6) bond length that an increase in N(2)-C(3) would be observed, and therefore this parameter was also included in the model. For clarity, this model is described as Fit 1 (F_1). Details of F_1 for each set of k_{DO} values are shown in **Table 31** and **Table 32**. Plots of the k_{DO} data against values obtained from F_1 are shown in **Figure 67**. Finally, **Equation 14** and **Equation 15** describe the F_1 models.

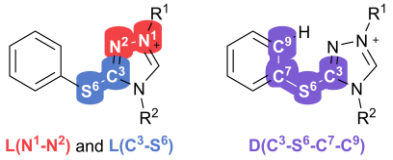


Figure 66 – Representations of the three key parameters identified in single-parameter fits.

Table 31 – Details of the standard least squares fitting of k_{DO} values determined from k_{ex} – [DO^-] plots to four selected XRD parameters.

Variable	L(N^1-N^2)	L(N^2-C^3)	L(C^3-S^6)	D(C^3-S^6-C^7-C^9)	Intercept
p-value	0.16	0.55	0.21	0.41	/
Estimated value	-2.48×10^9	1.42×10^9	3.92×10^9	2.18×10^5	-5.22×10^9
Standard error	1.60×10^9	2.29×10^9	2.82×10^9	2.46×10^5	6.82×10^9
F-ratio	2.41	0.39	1.94	0.78	/

Table 32 – Details of the standard least squares fitting of k_{DO} values determined from log k_{ex} – p*D* plots to four selected XRD parameters.

Variable	L(N^1-N^2)	L(N^2-C^3)	L(C^3-S^6)	D(C^3-S^6-C^7-C^9)	Intercept
p-value	0.24	0.76	0.27	0.27	/
Estimated value	-1.79×10^9	-6.45×10^8	2.97×10^9	2.58×10^5	-1.80×10^9
Standard error	1.40×10^9	2.00×10^9	2.46×10^9	2.15×10^5	5.96×10^9
F-ratio	1.65	0.10	1.45	1.46	/

The p-values for F_1 show that there is a relatively low possibility for the trends in k_{DO} against L(N^1-N^2), L(C^3-S^6) and D(C^3-S^6-C^7-C^9) to be due to chance, however the p-value for L(N^2-C^3) indicates a statistically insignificant trend. The F-ratio for L(N^2-C^3) further shows that the obtained data does not support or disprove a link between the length of the N(2)-C(3) bond and k_{DO}. It should be noted that large standard errors are observed in the fits due to the size of the dataset used in the model and the number of parameters used. Plots corresponding to F_1 show significantly improved

R^2 values over the single parameter fits, though it is important to consider that increases in R^2 would be expected when optimising to multiple parameters. In relation to using F_1 to approximate k_{DO} values, **Table 33** details the variation between experimental and calculated values calculated using **Equation 16** – the use of these equations to approximate k_{DO} is unsatisfactory.

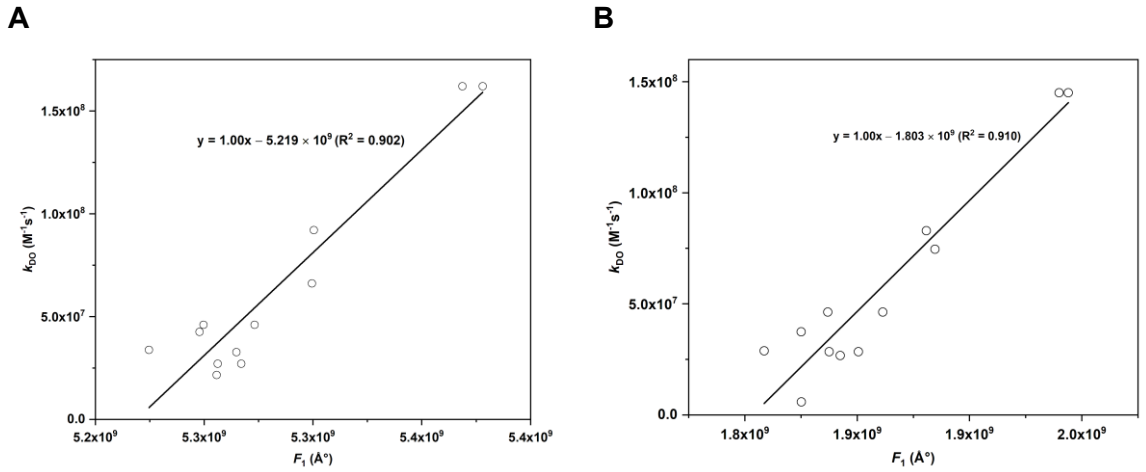


Figure 67 – Fit of k_{DO} data against the model F_1 obtained using JMP software. **A** – k_{DO} values plotted and model developed upon values from k_{ex} – [DO^-] plots. **B** – k_{DO} values plotted and model developed upon values from log k_{ex} – pD plots.

$$k_{DO} = (-2.48 \times 10^9)L_{N^1-N^2} + (1.42 \times 10^9)L_{N^2-C^3} + (3.92 \times 10^9)L_{C^3-S^6} + (2.18 \times 10^5)D_{C^3-S^6-C^7-C^9} - (5.22 \times 10^9)$$

From k_{ex} – [DO^-] plots **Equation 14**

$$k_{DO} = (-1.79 \times 10^9)L_{N^1-N^2} - (6.45 \times 10^8)L_{N^2-C^3} + (2.97 \times 10^9)L_{C^3-S^6} + (2.58 \times 10^5)D_{C^3-S^6-C^7-C^9} - (1.80 \times 10^9)$$

From log k_{ex} – pD plots **Equation 15**

Table 33 – Details of the difference between k_{DO} values obtained from F_1 and those experimentally determined.

F_1	**Max. positive difference**	**Max. negative difference**	**Mean difference**
k_{ex} – [DO^-] plots	+78%	−83%	15%
log k_{ex} – pD plots	+280%	−81%	33%

$$Difference = \left(\left(\frac{{k_{DO}}^{Fit}}{{k_{DO}}^{Experimental}}\right) \times 100\%\right) - 100\% \quad \textbf{Equation 16}$$

As a final investigation of XRD parameter relationships to k_{DO}, a full factorial model of L(N^1-N^2), L(C^3-S^6) and D(C^3-S^6-C^7-C^8) was prepared by least squares fitting to k_{DO} data. The methodology

differs depending on the k_{DO} values used, and so each set of values will be discussed separately. Initial investigations were undertaken looking at the p-values obtained when fitting to k_{DO} values obtained from k_{ex} – [DO^-] plots (**Equation 12**). It was determined that the relationship of $L(N^1\text{-}N^2) \times L(C^3\text{-}S^6)$, and by extension the relationship of the product of all parameters, shows low probability of statistically relevant correlation. With the removal of these two terms from the fitting, Fit 2 (F_2) was obtained and is described in **Table 34**. **Equation 17** shows the full form of the model, however this can be simplified to **Equation 18** by combining fitting terms. Finally, **Figure 68** shows a plot of the F_2 model (**Equation 18**) to the relevant k_{DO} values. The p-values obtained for F_2 are improved over F_1, with $L(C^3\text{-}S^6)$ now having the least statistically significant relationship to the model. $L(C^3\text{-}S^6)$ also is the only term where F-ratio remains below 1. The plot of F_2 shows an improved fit to k_{DO} over F_1 based on the R^2 values.

With the k_{DO} values obtained from log k_{ex} – pD plots (**Equation 13**), a significantly different modified full factorial model fit was found. In an initial investigation all two-parameter terms show p-values greater than 0.58 and so were removed, alongside the all-parameter term. Note that the R^2 value for linear fitting of k_{DO} against this preliminary model is 0.957.

Table 34 – Details of the full factorial modelling of k_{DO} values obtained from k_{ex} – [DO^-] plots to 5 parameters identified within the model optimisation

Variable	$L(N^1\text{-}N^2)$	$L(C^3\text{-}S^6)$	$D(C^3\text{-}S^6\text{-}C^7\text{-}C^9)$	$L(N^1\text{-}N^2) \times D(C^3\text{-}S^6\text{-}C^7\text{-}C^9)$[a]	$L(C^3\text{-}S^6) \times D(C^3\text{-}S^6\text{-}C^7\text{-}C^9)$[b]	Intercept[c]
p-value	0.03	0.50	0.25	0.24	0.23	/
Estimated value	-2.78×10^9	1.16×10^9	1.75×10^9	-2.45×10^7	2.12×10^7	1.84×10^9
Standard error	1.01×10^9	1.61×10^9	1.37×10^5	1.88×10^7	1.58×10^7	3.24×10^9
F-ratio	7.58	0.52	1.64	1.69	1.82	/

[a] Model parameters relate to the term ($L(N^1\text{-}N^2)$ − 1.36858 Å) × ($D(C^3\text{-}S^6\text{-}C^7\text{-}C^9)$ + 48.579°). [b] Model parameters relate to the term ($L(C^3\text{-}S^6)$ − 1.742 Å) × ($D(C^3\text{-}S^6\text{-}C^7\text{-}C^9)$ + 48.579°). [c] Quoted values differ from the simplified equation (**Equation 18**) which is plotted in **Figure 68**.

$$k_{DO} = -(2.78 \times 10^9)L_{N^1-N^2} + (1.16 \times 10^9)L_{C^3-S^6} + (1.75 \times 10^5)D_{C^3-S^6-C^7-C^9} + (L_{N^1-N^2} - 1.37)\left((D_{C^3-S^6-C^7-C^9} + 48.6) \times (-2.45 \times 10^7)\right) + (L_{C^3-S^6} - 1.74)\left((D_{C^3-S^6-C^7-C^9} + 48.6) \times (2.12 \times 10^7)\right) + (1.84 \times 10^9)$$

Equation 17

$$k_{DO} = -(2.45 \times 10^7)L_{N^1-N^2}D_{C^3-S^6-C^7-C^9} + (2.12 \times 10^7)L_{C^3-S^6}D_{C^3-S^6-C^7-C^9} - (3.97 \times 10^9)L_{N^1-N^2} + (2.19 \times 10^9)L_{C^3-S^6} - (3.28 \times 10^6)D_{C^3-S^6-C^7-C^9} + (1.67 \times 10^9)$$

Equation 18

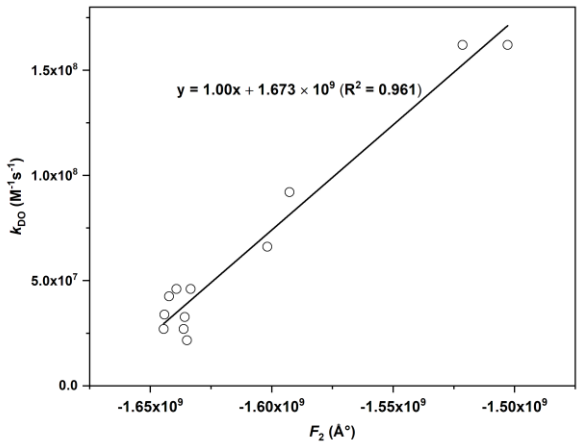


Figure 68 – Fit of k_{DO} data obtained from k_{ex} – [DO^-] plots against the model F_2 obtained using JMP software.

The final fit to this set of k_{DO} values was therefore made with single-parameter variables, however the R^2 for the linear fit to the model dropped to 0.909. To give a higher R^2 value the squares of the three parameters were also considered – this resulted in F_2 version A (F_{2A}). **Table 35** describes this fit, with **Equation 19** showing the full form of the model and **Equation 20** giving the simplified form. The data is shown graphically in **Figure 69A**. F_{2A} gives a linear fit to the k_{DO} values with R^2 = 0.964, and the model has p-values of 0.24 or less for 4 of the 6 terms. However, the two highest p-values are for $L(C^3\text{-}S^6)$ and $[L(C^3\text{-}S^6)]^2$ and furthermore these terms have F-ratios less than 1. These model parameters indicate terms relating to the length of the C(3)-S(6) bond are seen as less statistically relevant to the fit than the other 4 terms.

Table 35 – Details of the full factorial modelling of k_{DO} values obtained from k_{ex} – [DO^-] plots to 5 parameters identified within the model optimisation

Variable	p-value	Estimated value	Standard error	F-ratio
$L(N^1\text{-}N^2)$	0.20	-1.60×10^9	1.09×10^9	2.16
$L(C^3\text{-}S^6)$	0.53	1.29×10^9	1.90×10^9	0.46
$D(C^3\text{-}S^6\text{-}C^7\text{-}C^9)$	0.17	3.09×10^5	1.93×10^5	2.56
$[L(N^1\text{-}N^2)]^2$ [a]	0.24	1.91×10^{11}	1.43×10^{11}	1.78
$[L(C^3\text{-}S^6)]^2$ [b]	0.44	-2.53×10^{11}	2.99×10^{11}	0.72
$[D\ (C^3\text{-}S^6\text{-}C^7\text{-}C^9)]^2$ [c]	0.19	2.90×10^3	1.90×10^3	2.34
Intercept [d]	/	3.52×10^6	3.26×10^9	/

[a] The model parameters relate to the term $[L(N^1\text{-}N^2) - 1.36858\ Å]^2$. [b] The model parameters relate to the term $[L(C^3\text{-}S^6) - 1.742\ Å]^2$. [c] The model parameters relate to the term $[D(C^3\text{-}S^6\text{-}C^7\text{-}C^9) + 48.579°]^2$. [d] The quoted values are the intercept according to the plot of **Equation 19**, and does not equal the intercept of the simplified equation (**Equation 20**) which is plotted in **Figure 69A**.

$$k_{DO} = (-1.60 \times 10^{9})L_{N^1-N^2} + (1.29 \times 10^{9})L_{C^3-S^6} + (3.09 \times 10^{5})D_{C^3-S^6-C^7-C^9} + (1.91 \times 10^{11})(L_{N^1-N^2} - 1.37)^2 - (2.53 \times 10^{11})(L_{C^3-S^6} - 1.74)^2 + (2.90 \times 10^{3})(D_{C^3-S^6-C^7-C^9} + 48.6)^2 + (3.52 \times 10^{6})$$

Equation 19

$$k_{DO} = 10^{11}L_{N^1-N^2}(1.91L_{N^1-N^2} - 5.23) + 10^{11}L_{C^3-S^6}(-2.53L_{C^3-S^6} + 8.81) + 10^{3}D_{C^3-S^6-C^7-C^9}(2.90D_{C^3-S^6-C^7-C^9} + 591) - (4.10 \times 10^{11})$$

Equation 20

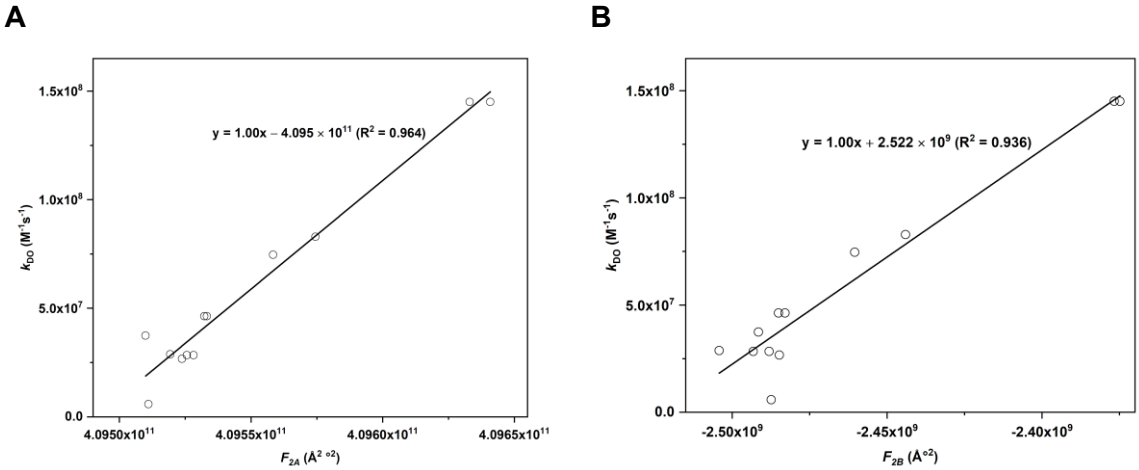


Figure 69 – Fit of k_{DO} data obtained from log k_{ex} – pD plots to statistical models obtained using JMP software. **A** – F_{2A}. **B** – F_{2B}.

Removal of parameters relating to the C(3)-S(6) bond length gave a good fit, but the p-value of $[L(N^1\text{-}N^2)]^2$ was 0.25 whilst all other parameters had p-values less than 0.08. A second version of the fit (F_{2B}) therefore included terms for $L(N^1\text{-}N^2)$, $D(C^3\text{-}S^6\text{-}C^7\text{-}C^8)$ and $[D(C^3\text{-}S^6\text{-}C^7\text{-}C^8)]^2$ only, and is detailed in **Table 36**. The model is shown in the full form in **Equation 21**, and can be simplified to give **Equation 22**. **Figure 69B** graphically shows the model.

Table 36 – Details of the full factorial modelling of k_{DO} values obtained from k_{ex} – $[DO^-]$ plots to 5 parameters identified within the model optimisation

Variable	$L(N^1\text{-}N^2)$	$D(C^3\text{-}S^6\text{-}C^7\text{-}C^9)$	$[D(C^3\text{-}S^6\text{-}C^7\text{-}C^9)]^2$ [a]	Intercept [b]
p-value	0.11	0.01	0.02	/
Estimated value	-1.79×10^9	3.32×10^5	2.38×10^3	2.52×10^9
Standard error	9.92×10^8	8.90×10^4	7.84×10^2	1.36×10^9
F-ratio	3.27	13.9	9.21	/

[a] The model parameters relate to the term $[D(C^3\text{-}S^6\text{-}C^7\text{-}C^9) + 48.579°]^2$. [b] The quoted values are the intercept according to the plot of **Equation 21**, and does not equal the intercept of the simplified equation (**Equation 22**) which is plotted in **Figure 69B**.

$$k_{DO} = (-1.79 \times 10^9)L_{N^1-N^2} + (3.32 \times 10^5)D_{C^3-S^6-C^7-C^9} + (2.38 \times 10^3)(D_{C^3-S^6-C^7-C^9} + 48.6)^2 + (2.52 \times 10^9)$$

Equation 21

$$k_{DO} = D_{C^3-S^6-C^7-C^9}\left((2.38 \times 10^3)D_{C^3-S^6-C^7-C^9} + (5.63 \times 10^5)\right) - (1.79 \times 10^9)L_{N^1-N^2} + (2.52 \times 10^9)$$

Equation 22

The fit gives a p-values less than 0.11 and all F-ratio values significantly above 1, indicating that all three parameters have a significant role in the model based on the obtained k_{DO} values. R^2 is slightly reduced to 0.936, however a drop is expected moving from a 6-term model to 3-term model.

Finally, the use of the models F_2, F_{2A} or F_{2B} to approximate k_{DO} is considered in **Table 37** by consideration of the differences between values experimentally determined and those approximated by the statistical models (determined using **Equation 16**). F_2 gives a very good approximation of k_{DO} in comparison to F_1, with a small mean difference and all values existing within a range of ± 80%. F_{2A} provides an unsatisfactory fit, mostly due to very high calculated values corresponding to the 2,6-dimethylphenyl *S*-triazolium **92o·BF$_4$** and the 1-ethyl-4-methyl *S*-phenyl triazolium **94·BF$_4$**. Removal of these values from the comparison gives a difference range of −4% to −78% with mean difference of −40%. A similar outcome is seen with F_{2B}, and in this case removing values for **92o·BF$_4$** and **94·BF$_4$** gives a difference range of +31% to −78% with mean difference of −17%.

Table 37 – Details of the difference between k_{DO} values obtained from F_2 (k_{ex} – [DO$^-$] plots), F_{2A} and F_{2B} (log k_{ex} – p*D*), and those experimentally determined.

Model	Max. positive difference	Max. negative difference	Mean difference
F_2	76%	−28%	9%
F_{2A}	900%	−78%	74%
F_{2B}	954%	−78%	99%

From the data it can be concluded that k_{DO} values derived from k_{ex} – [DO$^-$] plots can be approximated with reasonable accuracy using XRD data. However, the models still give a wide range of k_{DO} values as a result of the range of structural variation seen in the *S*-triazolium salt dataset. When looking at *para*-Ar substituted 1,4-dimethyl *S*-triazolium salts only, better fits can be obtained by considering a single parameter. With more *S*-triazolium salt analogues the fitting to a more complex model could be accomplished that considers all parameters of the structure, instead of selecting parameters to include in the model. F_2 is the best model for all *S*-triazolium salts, and when using to approximate k_{DO} the differences to experimental values described in **Table 37** should be considered.

5.6 – Estimation of C^5-H pK_a values

The carbon acid pK_a values for the *S*-triazolium salts may be obtained using **Equation 23**, where $K_w = 10^{-14}$ is the equilibrium constant for the autoionization of water, k_{HO} is the rate constant for deprotonation by hydroxide ion and k_{HOH} the reverse protonation by water. k_{HO} values can be calculated from the corresponding k_{DO} values using a secondary solvent isotope effect (**Equation 24**)[361] for proton transfer largely limited by solvent reorganisation. The reverse protonation is limited by solvent reorganisation, and so a value of 1×10^{11} s^{-1} which was previously determined[64, 344] can be assumed. Calculation of errors in k_{HO} and pK_a are described in the experimental (Chapter 8.8).

$$pK_a = pK_w + \log\left[\frac{k_{HOH}}{k_{HO}}\right] \qquad \textbf{Equation 23}$$

$$\frac{k_{DO}}{k_{HO}} = 2.4 \qquad \textbf{Equation 24}$$

Table 38 provides the values of k_{HO} and pK_a calculated from the two sets of k_{DO} values. pK_a is seen to range from 16.7 to 18.6 across the two sets of k_{DO} values, this small span reflects a small substituent effect on protofugality towards deuteroxide.

Table 38 – k_{HO} and pK_a values calculated from k_{DO}.

Analogue	k_{HO} ($\times 10^7$ $M^{-1}s^{-1}$)		pK_a	
	k_{ex} – [DO^-]	log k_{ex} – p*D*	k_{ex} – [DO^-]	log k_{ex} – p*D*
92a·BF_4	1.77 (± 0.05)	1.56 (± 0.04)	17.7 (± 0.04)	17.8 (± 0.05)
92b·BF_4	1.36 (± 0.04)	1.11 (± 0.04)	17.9 (± 0.05)	18.0 (± 0.05)
92d·BF_4	1.13 (± 0.04)	1.18 (± 0.04)	18.0 (± 0.05)	17.9 (± 0.05)
92e·BF_4	3.83 (± 0.18)	3.45 (± 0.35)	17.4 (± 0.05)	17.5 (± 0.06)
92h·BF_4	1.85 (± 0.05)	2.26 (± 0.06)	17.7 (± 0.04)	17.7 (± 0.04)
92i·BF_4	1.92 (± 0.05)	1.93 (± 0.05)	17.7 (± 0.05)	17.7 (± 0.05)
92n·BF_4	2.75 (± 0.09)	3.11 (± 0.09)	17.6 (± 0.05)	17.5 (± 0.05)
92o·BF_4	0.900 (± 0.059)	0.243 (± 0.038)	18.1 (± 0.05)	18.6 (± 0.08)
92q·BF_4	6.75 (± 0.24)	6.04 (± 0.18)	17.2 (± 0.05)	17.2 (± 0.05)
94·BF_4	1.41 (± 0.04)	1.20 (±0.03)	17.9 (± 0.05)	17.9 (± 0.04)
99·Br	18.8 (± 0.6)	13.7 (± 0.4)	16.7 (± 0.05)	16.9 (± 0.05)

Figure 70 compares the pK_a values obtained in this work to values previously reported by our group.[64, 65, 127, 166, 345-347] Similar pK_a values are obtained for the *S*-triazolium salts and Nitron analogues (**33H·X**), with the only variations being the swap of the bridging nitrogen in Nitron for sulfur and the swap of the 1,4-diaryl groups in Nitron for alkyl groups. This indicates that the swap of bridging nitrogen to a bridging sulfur counteracts the expected drop in pK_a moving from aryl to alkyl substituents. Similar values are also obtained for scaffolds previously employed in benzoin

condensations (**316**)[65, 324, 358] which further suggests possible organocatalytic activity for *S*-triazolium salts.

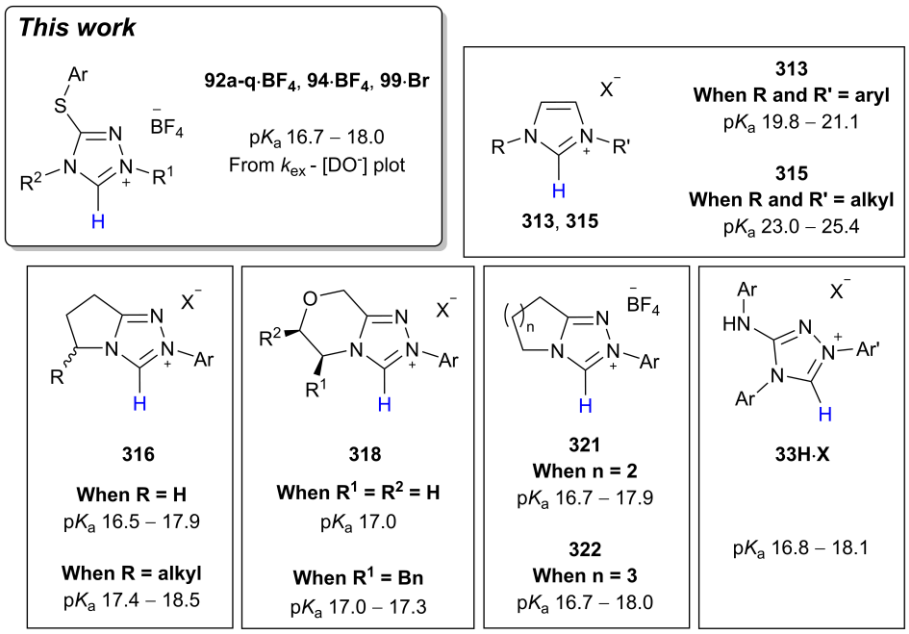
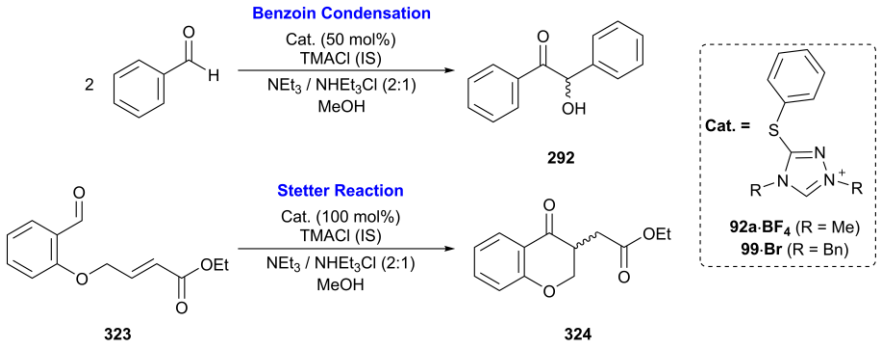


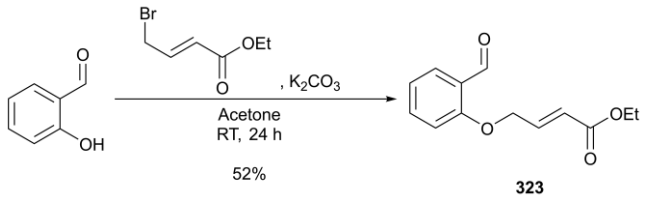
Figure 70 – pK_a values obtained in this work compared to previously reported values from our group: imidazoliums **313** and **315**,[64] pyrrolidino-fused triazolium salts **316**,[65, 345-347] morpholino-fused triazolium salts **318**,[65] piperidino-fused (**321**) and azepano-fused triazolium salts **322**,[166] and Nitron analogues **33H·X**.[127]

5.7 – Initial organocatalytic evaluation

Two *S*-triazolium salts were investigated within the benzoin condensation of benzaldehyde and the Stetter reaction of **323** (**Scheme 182**). As this work is an initial exploration of possible organocatalytic activity, high catalyst loadings up to stoichiometric amounts of the *S*-triazolium salt were used to promote observable reaction. The 2-formylphenoxycrotonate **323** was selected for the Stetter reaction as it has been shown as a highly active substrate with considerably enhanced reactivity over intermolecular Stetter reactions.[319] Synthesis of **323** was undertaken from salicylaldehyde, achieving good yields (**Scheme 183**). Due to the protofugality of **99·Br** being the highest of all analysed *S*-triazolium salts, it was predicted that this salt would form the most stable carbene and therefore be likely to give the highest catalytic rate.



Scheme 182 – The two transformations explored using *S*-triazolium salts as organocatalysts.



Scheme 183 – Synthesis of the intramolecular Stetter reaction substrate **323**.

Considering the benzoin condensation, 20 μmol of benzaldehyde was added to a 1 mL solution of *S*-triazolium salt (10 μmol) within triethylamine buffer. The reaction was tracked by ^{1}H NMR with the integral of peaks corresponding to product **292** compared to the internal standard TMACl, which was set to an arbitrary integral of 1000. The first NMR spectrum obtained is set as t = 0 and reaction time is determined in comparison to this NMR spectrum. **Figure 71** shows an NMR spectrum overlay of the benzoin reaction using **92a·BF$_4$**, with growth of a peak at 6.12 ppm corresponding to the proton environment highlighted in red for **292**.

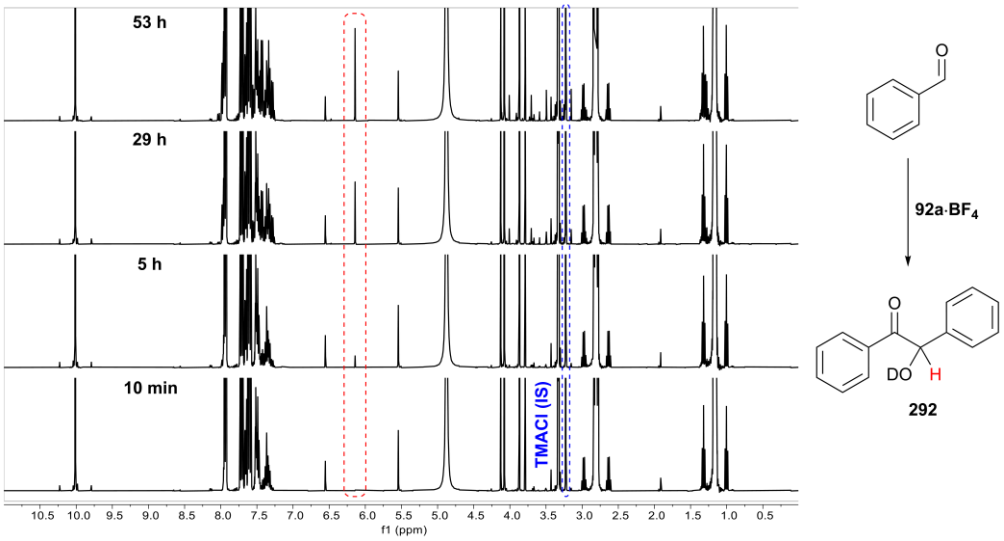


Figure 71 – NMR overlay showing the formation of benzoin **292** from benzaldehyde catalysed by **92a·BF$_4$**.

Using the known concentration of TMACl within the reaction mixture (2 mM), the integral of the peak corresponding to benzoin at 6.12 ppm ($I^{Benzoin}$) can be converted into concentrations of benzoin product using **Equation 25**. $I^{Benzoin}$ is multiplied by 12 to account for the 12 protons within the internal standard, then divided by 1000 as the peak for TMACl is set to the arbitrary figure of 1000. This gives the fraction of benzoin compared to the internal standard. This fraction is further multiplied by the concentration of internal standard to give the product concentration. **Figure 72** shows a plot of the concentration of benzoin formed as a function of time. The data shows the reaction is zero-order in respect of aldehyde concentration, consistent with a catalysed process whereby reaction rate is limited by free catalyst concentration, with a downward deviation in integral values after 1.1 × 10^5 s. A similar experimental process was used for investigating the *S*-triazolium salt catalysed Stetter reaction, however in this case 10 μmol of **323** was added to the buffered *S*-triazolium salt solution. The peak tracked by ^{1}H NMR spectroscopy was the CH_2 environment of the ethyl ester group in **324** (q, 3.62 ppm) and so **Equation 26** is used. Graphs for the benzoin reaction using **99·Br**, and the Stetter reaction with **94a·BF$_4$**, are provided in Appendix D.

$$[Benzoin]_t = \frac{(I^{Benzoin}{}_t \times 12)}{1000} \times (2 \times 10^{-3}\ mol\ dm^{-3}) \qquad \textbf{Equation 25}$$

$$[Chromanone]_t = \frac{(I^{Chromanone}{}_t \times 6)}{1000} \times (2 \times 10^{-3}\ mol\ dm^{-3}) \qquad \textbf{Equation 26}$$

Table 39 shows the initial rates within each reaction. A relative rate constant (k_{rel}) is also provided considering catalyst concentration within the reaction mixture. Catalytic activity is seen in both the benzoin and Stetter reactions from *S*-triazolium salts, with the benzoin reaction potentially favoured

based on these results however further studies would be necessary to verify this. Unexpectedly **99·Br** shows a significantly lower rate than **92a·BF$_4$** in the benzoin condensation, which is proposed to be a result of the sterically crowded adduct that would need to form with benzaldehyde.

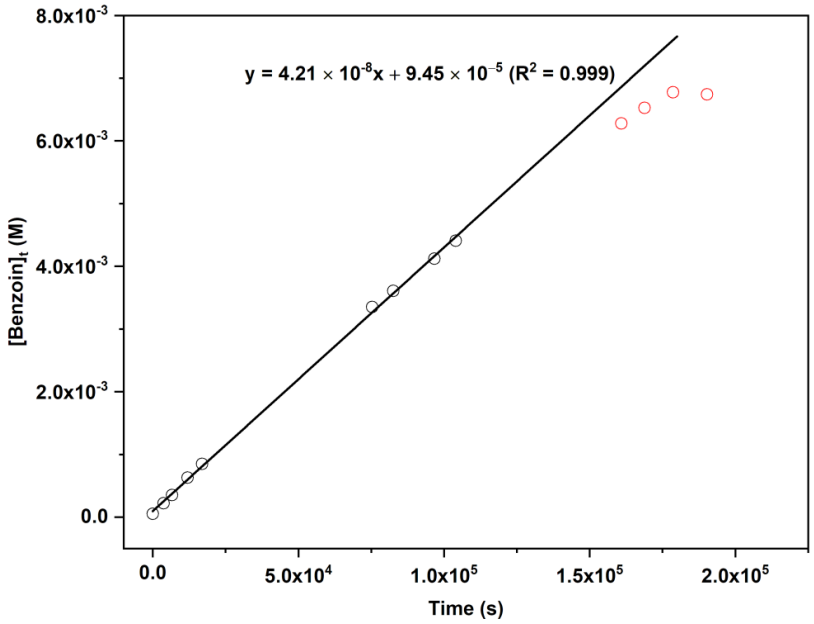


Figure 72 – Plot of [benzoin], corrected *versus* TMACl internal standard, as a function of time. Linear fit shown for data points over first 1.1 × 10^5 s, data points in red not included in fit.

Table 39 – Summary of the catalytic rates observed for *S*-triazolium salts in the benzoin and Stetter reactions.

Reaction	Cat.	Initial rate (M s^{-1})	[Cat.] (mM)	k_{rel} [a]
Benzoin	**92a·BF$_4$**	4.21 × 10^{-8}	10.19	13.52
	99·Br	3.72 × 10^{-9}	8.34	1.46
Stetter	**92a·BF$_4$**	2.61 × 10^{-9}	8.54	1.00

[a] Relative rate corrected for equal [Cat.].

5.8 – Conclusions

The work within this chapter describes the methodology to track H/D-exchange on the *S*-triazolium scaffold, paying particular care to ensure that the data collection is deemed quantitative through consideration of T_1 values and experimental setup. A series of 1st and 2nd order rate constants for the exchange process have been obtained, and compared through a protofugality scale and Hammett plot. The Hammett plot shows the expected positive value of ρ consistent with the H/D-exchange mechanism *via* the carbene intermediate.

XRD structure to activity relationships have given greater insight into the effect of structural variation on k_{DO}. One example is how delocalisation of charge through the Ar-S-triazolyl system, quantified by greater planarity of the aryl and triazolyl rings, correlates with increased k_{DO}. The fits also provide models to approximate k_{DO}, from simple descriptions using one XRD parameter for *para*-substituted 1,4-dimethyl *S*-triazolium salts to multi-parameter statistical models that provide an approximation of k_{DO} for any 1,4-dialkyl *S*-triazolium.

pK_a values have been calculated for the *S*-triazolium salts, and compared against previously studied triazolium salts – in particular Nitron analogues which were discussed in previous chapters. The pK_a values obtained indicate that the introduction of a sulfur bridge in place of the nitrogen in Nitron can counteract the expected drop in pK_a changing 1,4-diaryl substituents in Nitron to 1,4-dialkyl substituents in the *S*-triazolium. With alkyl-substituted triazolium salts that have promising protofugality / pK_a values, there arises the opportunity to explore the use of chiral alkyl substituents in the development of enantioselective transformations through asymmetric organocatalysis.

Finally, initial organocatalytic evaluation has been undertaken that verifies the formed triazolium salts show activity in the benzoin and Stetter reactions. These studies will hopefully be expanded upon within future work in the group.

6 – The evaluation of antiproliferative and antioxidant activity of Blatter radicals, 1,2,4-triazolium salts and related species

6.0 – Foreword

Through cell-based assays, such as the sulforhodamine B (SRB) assay, the antiproliferative or cytotoxic activity of compounds can be quantified. The SRB assay in particular is an efficient, cost-effective assay for the toxicity screening of compounds[362] and can therefore be a useful methodology for the identification of hit compounds in drug discovery programmes.

This chapter explores the antiproliferative activity of Blatter radicals, structurally related benzotriazine species such as Tirapazamine, Nitron analogues as precursors to Blatter radicals, and selected examples of other scaffolds prepared as part of this work. Following a review of the literature (Section 6.2) the toxicity evaluation of compounds by the SRB assay is undertaken (Section 6.3). Finally, a brief discussion of preliminary work into the application of our new Blatter radicals as reactive oxygen species scavengers is provided in Section 6.4.

6.1 – Chapter contributions

The work presented in this chapter was undertaken in collaboration with the individuals listed below, with their contributions to this work detailed. All other work detailed in this chapter was undertaken by the present author.

Dominic Black (Durham University PhD student, Prof. Robert Pal group): viability studies for cells in the presence of low concentrations of Blatter radicals.

Katherine Deck (former O'Donoghue group 4th year MChem student): providing samples for biological evaluation (4 Blatter radicals, 3 Nitron analogues).

Jacob Murray (former O'Donoghue group PhD student): providing samples for biological evaluation (7 Blatter radicals, 2 Nitron analogues).

6.2 – Introduction

The oxygen demand from uncontrolled cell proliferation of solid cancerous tumours often exceeds the ability of dysfunctional microvasculature to supply oxygen. As a result, tumour microenvironments (TMEs) often become hypoxic (**Figure 73**) and this dictates the evolution of the tumour.[363] Hypoxia was first postulated by Thomlinson and Gray, based on the observation of rings of intact tumour cells encapsulating necrotic areas where capillaries are unable to penetrate.[364] The chronic, diffusion-limited hypoxia resulting from inadequate vasculature can also be accompanied with acute, perfusion-limited hypoxia resulting from variable blood flow within tumour vessels or their temporary occlusion.[365] Acute hypoxia has been shown to lead to dihydrofolate reductase gene overexpression and DNA overreplication following re-exposure to oxygen, further leading to enhanced resistance to the anticancer agent methotrexate.[366] There is therefore an unmet need in oncology to either reverse the effects of tumour hypoxia, or develop agents that target hypoxic regions for chemotherapy – the latter will be detailed in this section.[367]

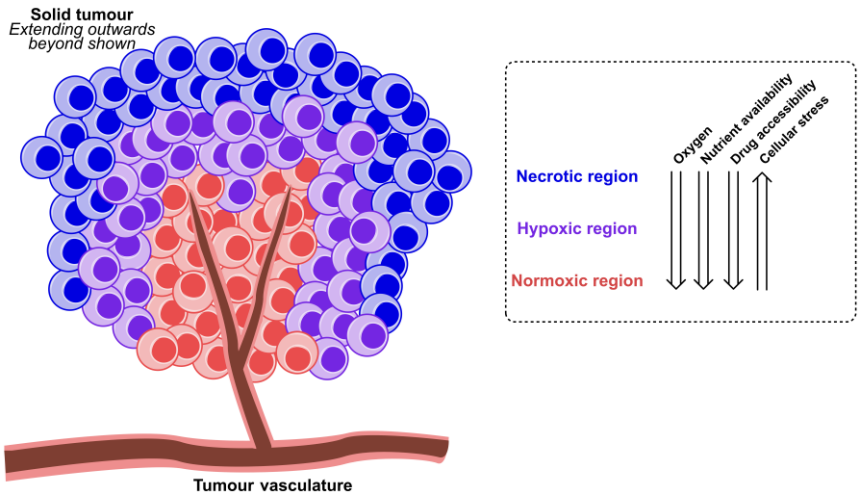


Figure 73 – The tumour microenvironment and impacts of inadequate vasculature. Solid tumours characteristically have abnormal vascularization as a result of angiogenesis not being able to generate sufficient microvasculature to support the tumour, which leads to areas of hypoxic and necrotic cells. As blood supply from the tumour vasculature decreases further inside the tumour, where the capillary network is unable to penetrate, the functions of the vasculature are impeded and cellular stress increases.

Tumour hypoxia is often accompanied by other consequences of vascular dysfunction, such as acidosis and nutrient deficiencies. These additional effects exacerbate the TME stress and have implications for tumour biology.[363] Hypoxic melanoma and breast cancer cells show enhanced macrophage recruitment, reduced M1 expression, and enhanced proliferation over hypoxic kidney cells. Melanoma cells further showed enhanced vascular endothelial growth factor A (VEGFA) gene expression, responsible for angiogenesis, under hypoxic conditions.[368]

Predicting the prevalence of hypoxia in tumours is made possible through understanding of hypoxic gene expression, with studies[369, 370] demonstrating that squamous cell carcinomas (SCCs) of the lung, cervix, neck and head express the greatest number of hypoxia-regulated genes. More importantly

these studies, which profiled over 9,000 individual tumours, show that a subset of all tumour types have evidence of hypoxia.[371] The direct measurement of hypoxia through oxygen partial pressure (pO_2) has been shown possible through the use of needle electrodes consisting of a gold wire microcathode (electrically insulated by a layer of glass and cement) recessed within a stainless steel shaft, quantitatively showing that mean pO_2 is significantly lower in human breast cancers *versus* normal breast tissue.[372] Computed tomography (CT) measurements on head and neck SCCs have further shown the decreasing oxygen gradient in relation to tumour depth.[373, 374]

6.2.1 – Challenges and solutions in the effective treatment of hypoxic tumours

The effectiveness of treatments is also impacted by vascular dysfunction. Anticancer drug resistance is observed as a result of inadequate exposure, resulting from tumour cells distant from blood vessels and blood flow stasis. Tumour penetration therefore is a key property to be considered in the development of anticancer drugs, given that limited penetration can be a dominant resistance mechanism in solid tumours.[375] Another consideration is that proliferation of cells decreases as a function of the distance from vasculature, which was linked to the extent of hypoxia,[376] and so agents that target the rapid proliferation associated with cancerous tumours may show decreased selectivity. Some anticancer agents also show enhanced cytotoxicity when the DNA lesions made can further react with oxygen, such as bleomycin, vincristine and esperamicin A1.[377, 378]

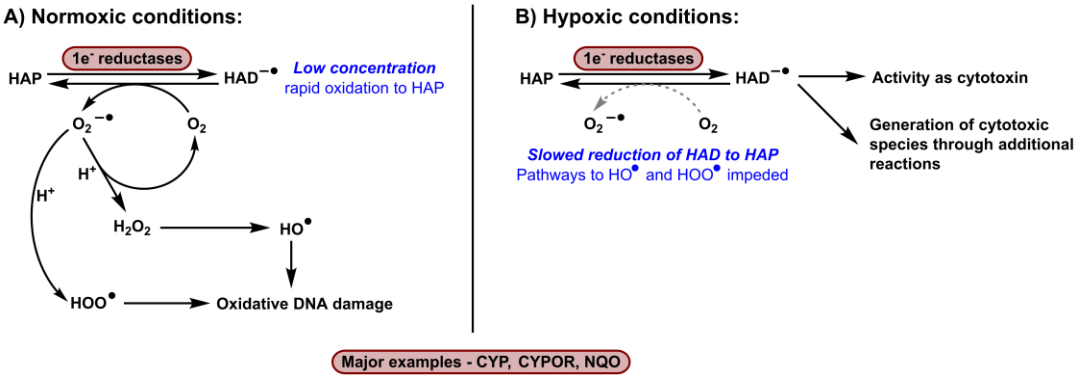
The low oxygen supply to cancerous tumours additionally limits the effectiveness of radiotherapy, particularly in head and neck SCCs. Without the presence of O_2, radiation-induced DNA radicals are unable to be oxidised which prevents the complex DNA lesions that arise from single-strand and double-strand breaks or base oxidation.[363]

The prevalence of hypoxia is particularly dependent on the prevalence of the hypoxia-inducible factor (HIF)-1 gene, which regulates angiogenesis and is an attractive target for oncological treatments.[371, 379] Co-regulation of HIF-1 activity occurs through many intracellular signalling pathways, but the two main pathways are the phosphatidylinositol-3-kinase (PI3K) / protein kinase B (Akt) / mammalian target of rapamycin (mTOR) pathway which mediates HIF-1α synthesis and stability, and the extracellular regulated kinase (ERK) / mitogen-activated protein kinase (MAPK) pathway which mediates the function of HIF-1α.[379] A series of 6-aminopyridines have shown inhibitory activity against the α, β, δ and γ forms of PI3K, and furthermore show growth inhibition of colorectal tumour cells.[380] HIF-1 can also bind to the multidrug resistance 1 (MDR1) gene, which leads to upregulation of the P-glycoprotein gene product under hypoxia. P-glycoprotein is associated with tumour resistance to chemotherapy, thus the effective inhibition of HIF-1 activity also acts as a method to enhance the effectiveness of other cancer chemotherapeutics.[381]

6.2.2 – Hypoxia-activated prodrugs: selective agents to treat resistant tumours

A new class of drugs has been developed that exploits the hypoxia present within tumours, referred to as hypoxia-activated prodrugs (HAPs) or hypoxic cytotoxins. Given that hypoxia is one of the major differences between tumours and normal tissues, these drugs would show selectivity towards the tumour and thus may result in reduced side effects. Furthermore, given that the HAP would target the cells most resistant to current therapies, these agents would overcome the resistance to standard therapies as part of therapeutic regime also including another chemotherapeutic treatment or in combination with radiotherapy.[382]

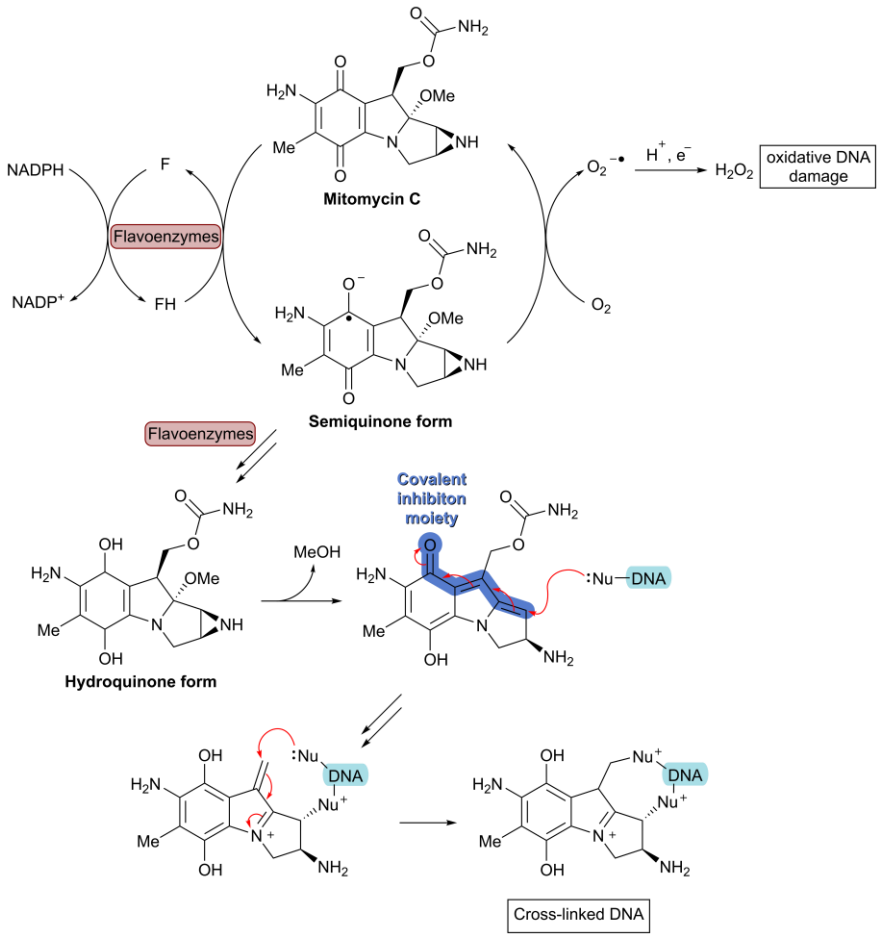
The common mechanism for HAP activation (**Scheme 184**) starts with the one-electron reduction of the relatively low toxicity prodrug (HAP) to a radical species – a hypoxia-activated drug (HAD).[365] Cellular reductases such as cytochrome P450 (CYP),[383] NADPH-cytochrome P450 oxidoreductase (CYPOR)[383, 384] and NADPH : quinone acceptor oxidoreductase (NQO)[385] have been shown to activate these compounds. Under normoxic conditions, where oxygen levels are equal to those within normal tissue, the formed HAD becomes a substrate for back-oxidation to the prodrug and thus a process of futile redox cycling is initiated that results in the generation of superoxide.[365] The superoxide generated can be protonated to give the hydroperoxyl ($HOO^{\bullet}$) radical and potentially protonated again to give hydrogen peroxide. Both the hydroperoxyl radical, and the hydroxyl radicals generated from hydrogen peroxide, can potentially lead to DNA double strand breaks through oxidative DNA damage.[279] Reactive oxygen species (ROS) such as hydroxyl and hydroperoxyl radicals are however continually produced in aerobic organisms through respiration, and so antioxidant systems and redox state modulating enzymes continually manage cellular ROS levels.[386] For this reason the cytotoxicity of HAP-HAD redox cycling is low, and only minor side-effects such as muscular cramping are seen in normoxic tissue.[387] However, under hypoxic conditions the futile redox cycling process is inhibited and a build-up of HAD occurs. If the HAD generated under hypoxic conditions is much more toxic than the ROS generated under normoxic conditions, which is commonly the case due to cellular antioxidant systems, hypoxia-dependent cytotoxicity arises.[365] The HAD can, theoretically, itself act as a cytotoxin however commonly further reactions occur to HAD to give the species that causes cytotoxicity.[279, 365]



Scheme 184 – The mechanism of action for hypoxic cytotoxins under normoxic and hypoxic conditions. **A**) under normoxic conditions, the HAP activation by cellular reductases is followed by the back-oxidation to HAP by oxygen. **B**) under hypoxic conditions, the back-oxidation of HAD to HAP is slowed and accumulation of HAD occurs.

6.2.2.1 – Mitomycin C

The first identified agent of this class is mitomycin C, for which enzymatic reduction implementing NADPH was found to be a prerequisite for its activity in cross-linking complimentary DNA strands (**Scheme 185**). The reduced form was found to be highly unstable and loses biological activity upon oxidation.[388] Mitomycin is consecutively reduced by two one-electron processes made possible by a variety of flavoenzymes, with the semiquinone form generated able to take part in futile redox-cycling.[389, 390] The hydroquinone formed after the second reduction process can lose methanol to generate a species able to cross-link DNA over two consecutive reactions with nucleophilic DNA residues.[389] Mitomycin C has shown antitumour activity in combination therapies and since 1958 has been in clinical use.[382, 391] The cross-linking capability of mitomycin C also has been shown to give rise to TrxR inhibition.[392]



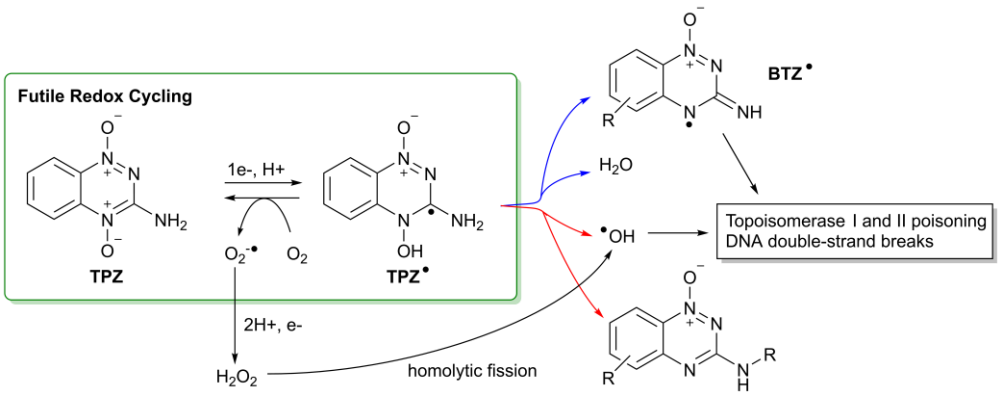
Scheme 185 – Mechanism of action of mitomycin C.

6.2.2.2 – Tirapazamine and other benzotriazine-1,4-di-N-oxides

Tirapazamine (TPZ) is the first compound specifically developed as a HAP,[393] and is of particular interest in this work due to generation of benzotriazinyl radicals structurally similar to Blatter radicals. TPZ is part of the family of benzotriazine-1,4-di-*N*-oxides (BTOs), which have shown applications as antineurodegenerative[226] and antitubercular[227] agents.

Reduction of TPZ to the carbon-centred radical TPZ• (**Scheme 186**) can occur by a range of cellular reductases – xanthine oxidase, DT diaphorase and NADPH:cytochrome P450 reductase all are known to be able to undertake the reduction. NADPH:cytochrome P450 reductase has however been evidenced to not mediate TPZ metabolism or nuclear DNA damage.[394] As is common with HAPs, TPZ• can then undergo a process of futile redox cycling when under normoxic conditions to generate superoxide and subsequently hydrogen peroxide.[365] This cycling process is known to limit the dosing of TPZ, as a variety of side effects arise from this – most notably these include muscle cramping, ototoxicity and fatigue.[387] Under hypoxic conditions, build-up of TPZ• leads to loss of the hydroxyl radical (HO•) to give the benzotriazine-*N*-oxide or, more importantly to this work, dehydration to give rise to the benzotriazinyl (BTZ•) radical. HO• and BTZ• are both implicated in the mode of

action, where topoisomerase I and II (topo I and II) become poisoned, and DNA single-strand breaks (SSBs) and double-strand breaks (DSBs) are produced.[279, 365]



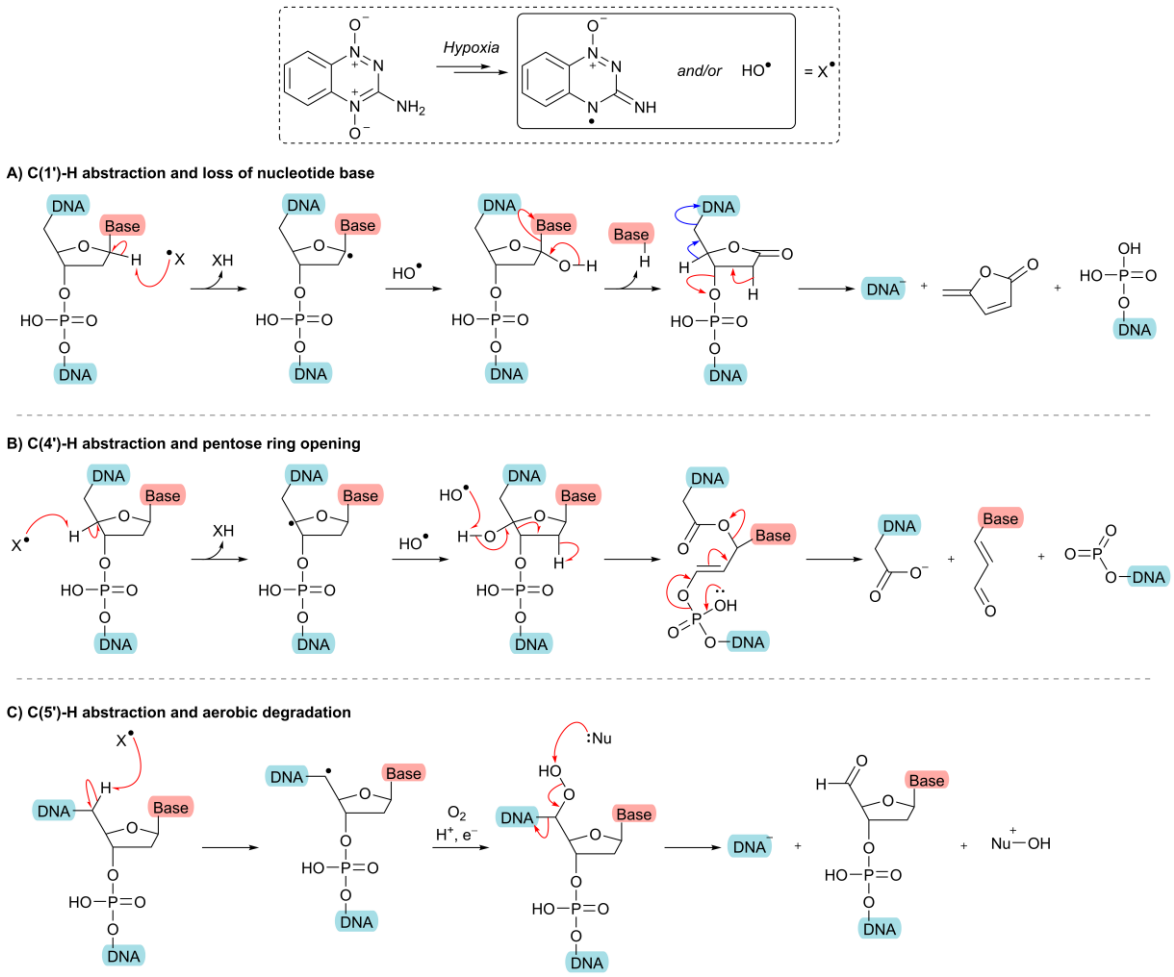
Scheme 186 – The mechanism of action of tirapazamine (TPZ).

Work by Peters and Brown[395] has shown that topo II in human lung cancer cells has significantly reduced activity when treated with TPZ, and that the number of DSBs are related to the levels of nuclear topo II. Furthermore, they show that topo IIα covalently binds to DNA after treatment with TPZ to form highly stable cleavage complexes. These findings indicate that the cytotoxicity seen by TPZ is, at least in part, through topo II poisoning.

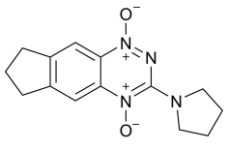
Alongside stabilising the Topo II cleavage complex, TPZ is known to directly cause DNA single strand breaks (SSBs) *via* a variety of methods initiated by hydrogen atom abstraction (**Scheme 187**). The species that undertakes H-abstraction could be the benzotriazinyl or hydroxyl radical, and so the mechanisms shown define an acting radical as X•. Abstraction of the C(1')-H (**Scheme 187A**) leads to loss of the nitrogenous base from the nucleotide unit to generate the lactone intermediate, which can undergo thermal decomposition to the cleaved DNA and 2-furanone. C(4')-H abstraction (**Scheme 187B**) results in the ring opening of the pentose sugar, followed by a transfer of electron density to give an α,β-unsaturated aldehyde functionalised with the base, and the separated DNA stands. Finally, C(5')-H abstraction (**Scheme 187C**) can undergo aerobic degradation to break the DNA sugar-phosphate backbone – further H-abstraction steps are known to lead to formation of furfural.[396, 397] All three of these mechanisms are supported by findings within the literature.[397]

BTOs such as TPZ have found wider application as medicinally active agents for a range of targets alongside cancerous tumours. Madrid *et al*[227] found that the BTO class of compounds are potent against replicating and nonreplicating *Mycobacterium tuberculosis* (Mtb), and undertook structural optimisation to identify the lead compound (**325**). **325** shows good selectivity for Mtb over mammalian cells, and also other pathogenic bacterial strains, with low potential for genetic toxicity. Several studies[278, 398] have further shown that TPZ has bactericidal activity against *E.coli*, *S. aureus* (methicillin-sensitive and methicillin-resistant strains), *S. enterica* and *C. difficile*. Antifungal action has also been reported against *S. cerevisiae* by Turcotte *et al*.[399] The mechanism of antibacterial and

antifungal action is proposed within the literature to be identical to that described for anticancer activity (**Scheme 187**).[227, 278, 398, 399]



Scheme 187 – The mechanisms of DNA degradation by TPZ. **A**) C(1')-H abstraction and loss of the nitrogenous base from the nucleotide unit. **B**) C(4')-H abstraction and ring opening of the pentose sugar. **C**) C(5')-H abstraction and aerobic degradation.



325

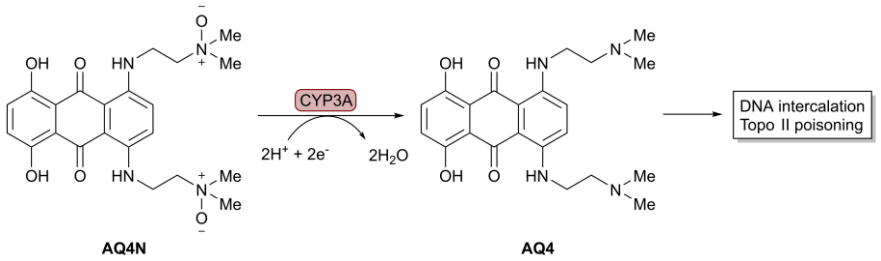
Whilst reports of the medicinal activity of BTOs is limited, the structurally related quinoxaline-1,4-di-*N*-oxides (QdNOs) have seen a wide range of applications reported within the literature – anticancer, antinflammatory, antioxidant, antimalarial and antibacterial activity.[400] The activity of QdNOs to cleave DNA, analogous to BTOs, was reported by Gates *et al*.[401]

It is important to consider that, if the active species of BTOs is the benzotriazinyl radical, comparison to reports of the quinoxalinyl radical activity may differ significantly. Madrid *et al*'s studies[227] on

activity against Mtb shows QdNOs have a minimal inhibitory concentration over 7-times greater than TPZ.

6.2.2.3 – AQ4N

The only other HAP in clinical trials, to our knowledge, is the anthraquinone AQ4N. AQ4N undergoes reduction of its amine *N*-oxide groups to AQ4, which acts as a potent DNA intercalator and Topo II poison – the *N*-oxide groups mask the binding of the HAP.[365, 402] Instead of futile redox cycling, O_2 directly competes with AQ4N in binding to CYP3A which undertakes the two-electron reduction (unlike the one-electron reduction usually seen).[403, 404]



Scheme 188 – the mechanism of action of AQ4N. The HAP undergoes a two-electron reduction to the active AQ4 form by CYP3A, which unmasks the tertiary amine groups involved in DNA intercalation and also poisoning of topoisomerase II.

There are multiple other areas of development beyond the scope of this thesis where HAPs are showing promise. Attachment of a DNA-targeting moiety to a unit known to undertake damage within hypoxic cells, an example of the latter being 2-nitroimidazoles, has led to compounds that are approaching anticancer clinical trials[405, 406] alongside showing antitubercular activity.[407] The development of compounds only activated under very hypoxic conditions, which can allow for influence on the cells surrounding it, overcomes the issues of tumour heterogeneity and allows for more widespread tumour targeting. Nitrogen mustards attached to nitrobenzene units have allowed for a 'bystander effect' where the alkylating agent is activated at very low oxygen levels and can interact with the DNA of the cell or the surrounding cells.[408, 409] Finally, one of the major issues in HAP development is visualisation of prodrug delivery and determining the site of activation. A new prodrug, EF5-Pano, has been recently developed which undergoes hypoxia-related release of the epitope of EF5 (an antibody-based hypoxia imaging agent) and the lysine deacetylase (KDAC) inhibitor Panobinostat.[367]

6.2.3 – Medicinal activity of 1,2,4-triazolium salts

There have been multiple reports of 1,2,4-triazolium salts possessing bioactivity against a variety of targets (**Figure 74**).[86] Hybrid compounds **326**, combining the cytotoxicity of triazole derivatives and the anticancer activity of 2-phenyl-3-alkylbenzofurans, were shown to have good cytotoxicity against a range of cancerous cell lines.[410] Dibenzofuran analogues **327** are seen to have improved cytotoxicity

over **326** through induced cell cycle arrest at the G2/M phase – R group modification is assumed significant with these compounds.[411] Work has also shown 1,4-dinaphthylmethyl substituted 1,2,4-triazolium salts **328** exhibit promising activity against breast and prostate cancer cell lines.[412] 1,2,4-triazolium containing drugs have also been approved for use, such as Isavuconazonium sulfate (Cresemba, **329**) – a prodrug of the antifungal agent isavuconazole.[413] The antibacterial agent biapenem **330** implements the triazolium scaffold to improve the pharmacokinetic profile, and has shown activity against tuberculosis[414] alongside being effective against particulate-matter induced lung damage.[415]

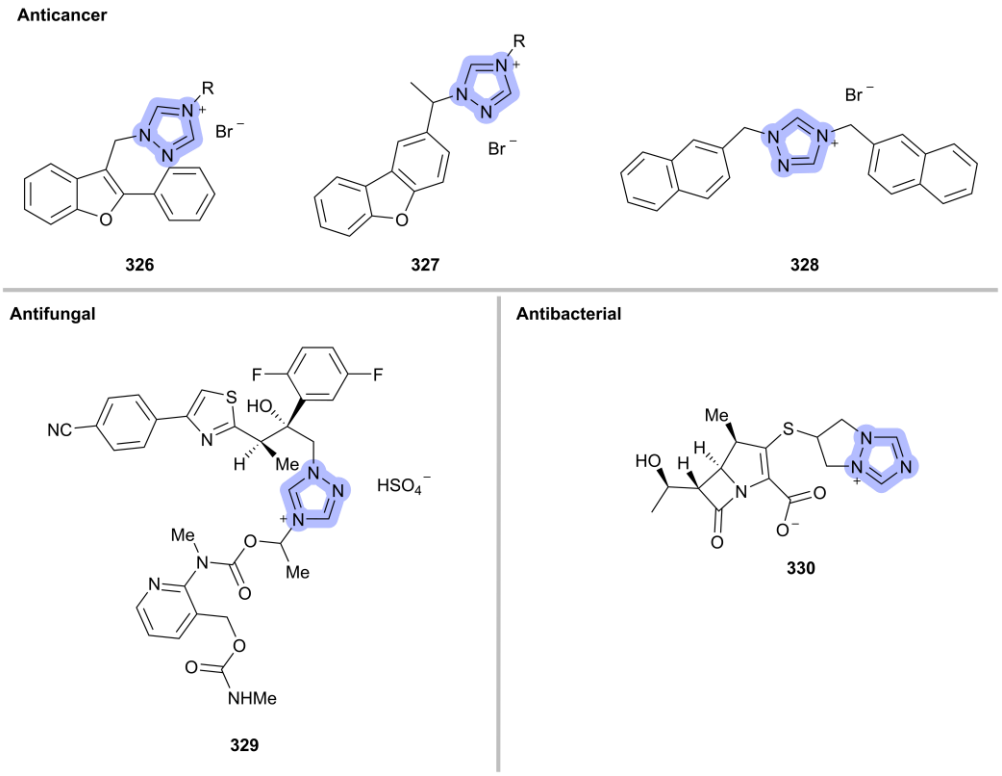
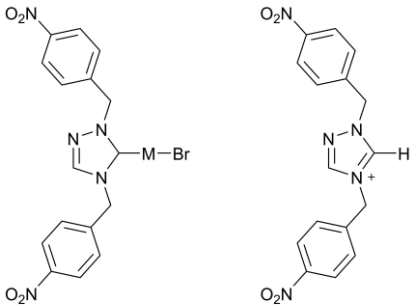


Figure 74 – The structures of a selection of triazolium salts showing medicinal activity.

Metal NHC complexes have been implemented as medicinal agents against a variety of targets.[99-102] Silver complexes of NHCs have shown antioxidant and antihaemolytic activity through scavenging of reactive oxygen species,[416] alongside uses in the treatment of cystic fibrosis and open wounds.[417, 418] Metal-NHC complexes have also shown anticancer activity (**Figure 75**) – silver, gold and copper complexes (**331a** – **c**) of the dibenzyl triazolium (**332**) show significantly greater activity across a series of anticancer cell lines *versus* the triazolium alone.[419]



331a (M = Ag)
331b (M = Au)
331c (M = Cu)

332

Figure 75 – Structures of 1,2,4-triazolylidine NHCs which show medicinal activity

6.3 – Evaluation of antiproliferative and cytotoxic activity

The Blatter radicals, Nitron analogues, benzotriazine compounds, *S*-triazoles, *S*-triazolium salts, and a selection of other compounds have been analysed by the sulforhodamine B (SRB) assay. These assays have been undertaken at the Centre for Cancer, Newcastle University, under the supervision of Prof. Ian Hickson. The assay enables straightforward quantification of antiproliferative and cytotoxic activity, which can then guide future development of analogues with potent anticancer activity.

The SRB assay, developed in 1990,[420] can be used to screen various cell types in an efficient and inexpensive manner.[362] The method is reliant on stoichiometric binding of the SRB dye to proteins under acidic conditions and subsequent extraction of these proteins under basic conditions. Relative cell mass is assumed to correlate with the amount of bound dye, which can be averaged per well in the 96-well plate setup. Interpolation of the data allows for the quantification of cell proliferation as GI_{50} (half-maximal growth inhibition). The SRB assay also has applications in evaluating gene expression modulation events (upregulation and gene knockdown), and studies of proliferation changes from replacing micro-ribonucleic acid involved in oncogenic pathways.[421, 422]

6.3.1 – Assay procedure

The SRB assay protocol (**Figure 76**) can be divided into five steps: cell preparation, treatment preparation, cell incubation, fixation and staining, and finally absorbance measurement. Cell preparation involves preparation of 96-well plates of the cell line of interest, starting with removal of growth medium from a colony of cells and dissociation of the cell monolayer with trypsin. The dissociated cells are resuspended in growth medium and plated at an appropriate cell concentration using hemocytometry – the use of a glass slide with precise volume chamber that allows cell counting using a microscope.[422] The concentration of cells plated is dependent on the cell line and incubation time. The standard procedure within this work involved plating at 31,250 cells mL^{-1}, corresponding to 2,500 cells per well. The plated cells are incubated for approximately 24 h to allow for the cells to establish monolayer colonies.

Treatment preparation initially involves the formation of stock solutions (50 μM to 50 mM) for the compound of interest. These stocks are prepared in a solvent of low toxicity to cells, and then diluted with a constant solvent concentration of 3% v/v to give 1 mL of treatment solution ready for dosing cells (**Table 40**). A range of treatment concentrations are used to determine concentration-dependent effects. Within this work, DMSO was the solvent of choice which showed good solubility of all compounds.[422]

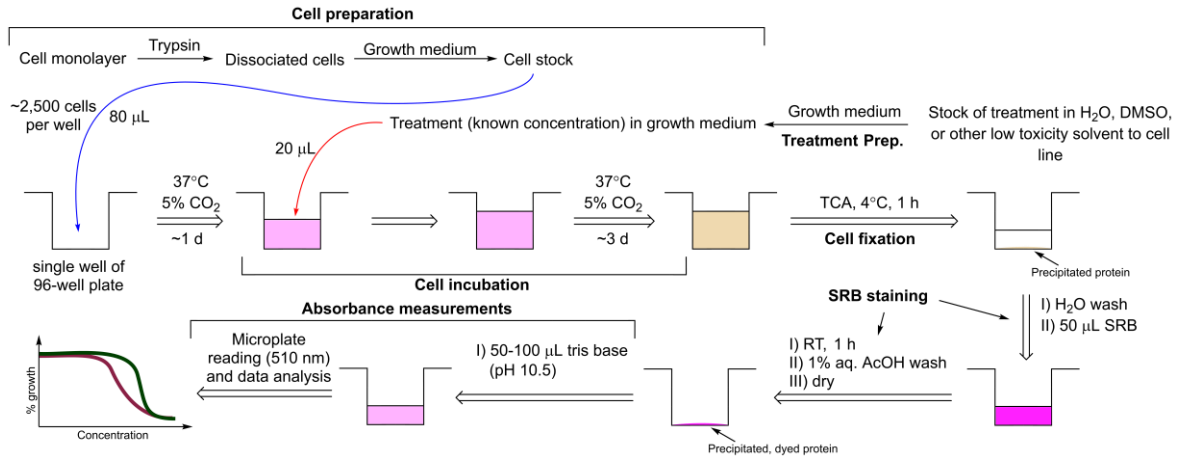


Figure 76 – Overview of the Sulforhodamine B assay procedure.

Table 40 – Details for the preparation of treatment solutions.

[Treatment] (µM)	Final concentration (µM) [a]	[Stock] (mM)	Stock volume (µL)	DMSO volume (µL)	Growth medium volume (µL)
0	0	- [b]	- [b]	30	
0.5	0.1	0.05	10	20	
1.5	0.3	0.05	30	0	
5	1	0.5	10	20	
15	3	0.5	30	0	970
50	10	5	10	20	
150	30	5	30	0	
500	100	50	10	20	
1500	300	50	30	0	

[a] 20 µL of treatment solution added to 80 µL cell stock. [b] No compound of interest added.

The cell incubation step involves the addition of treatment solution to the cell medium within the 96-well plate. A 10 × 6 grid of wells is treated, with two compounds analysed per plate (**Figure 77**). The plates are then placed in an incubator – within this work this is generally for 3 days. The appropriate incubation time is dependent on the compound of interest, the cell proliferation rate, and the starting cell concentration.[422]

Following incubation, the cells are fixed by the addition of trichloroacetic acid (TCA) to each well and refrigerated for at least 1 hour. The addition of TCA causes the precipitation of proteins from the incubated cells, giving a protein layer at the bottom of the wells.[423] The plates are washed with water to remove other cell contents, then the SRB dye added to stain the protein layer. Dilute acetic acid is used to remove residual dye after 1 hour, and the dyed protein layers are then dried.[422]

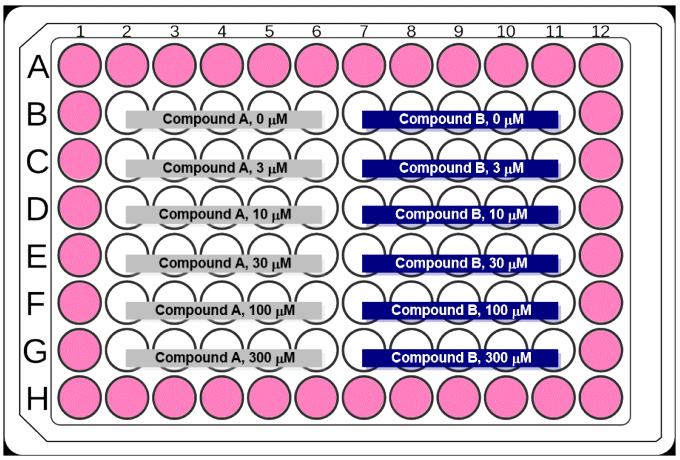


Figure 77 – Cell dosing layout on a 96-well plate, with two compounds analysed per plate. The commonly used dosing range of 3 to 300 μM compound is shown.

Absorbance measurements involve the addition of tris base solution to each well, then use of a microplate reader to measure SRB absorbance at 510 nm. The collected data from each well is averaged for each concentration, and then plotted to give dose response curves such as those shown in **Figure 78**. Cell number growth over the incubation period (determined by comparison to an additional plate of cells fixed at the time of treatment) is compared for each concentration of treatment to a control, where no compound of interest is added. The data is plotted as percentage growth over the time period *versus* the control, against [Compound]. At 100% growth, the compound has no effect on cell number growth. Percentage values between 0% and 100% correspond to reduced growth due to the antiproliferative effects of the compound. At 0% growth the concentration of compound is maintaining cell numbers at the initial value, whilst negative percentage values correspond to cytotoxic activity on the established cell colonies. The plot shows the connection of data points with straight lines, however to determine values of GI_{50} the data is fitted to a 50-interval Akima spline and interpolated to determine the concentration of compound when 50% growth is seen *versus* the control. The Akima spline is a type of non-smoothing spline that fits well to data with rapid variation. It also has the advantage of being stable to outlier values – unlike other cubic spline methodologies, the Akima spline is designed to give a more natural curve that avoids overshooting through making an overly smoothed curve. The method is good for fitting to the assay data due to the rapid changes in GI_{50} values and because it deals with the 'bottoming-out' of data resulting from highly cytotoxic activity well. The 82 dose response curves resulting from this work are shown in Appendix E.

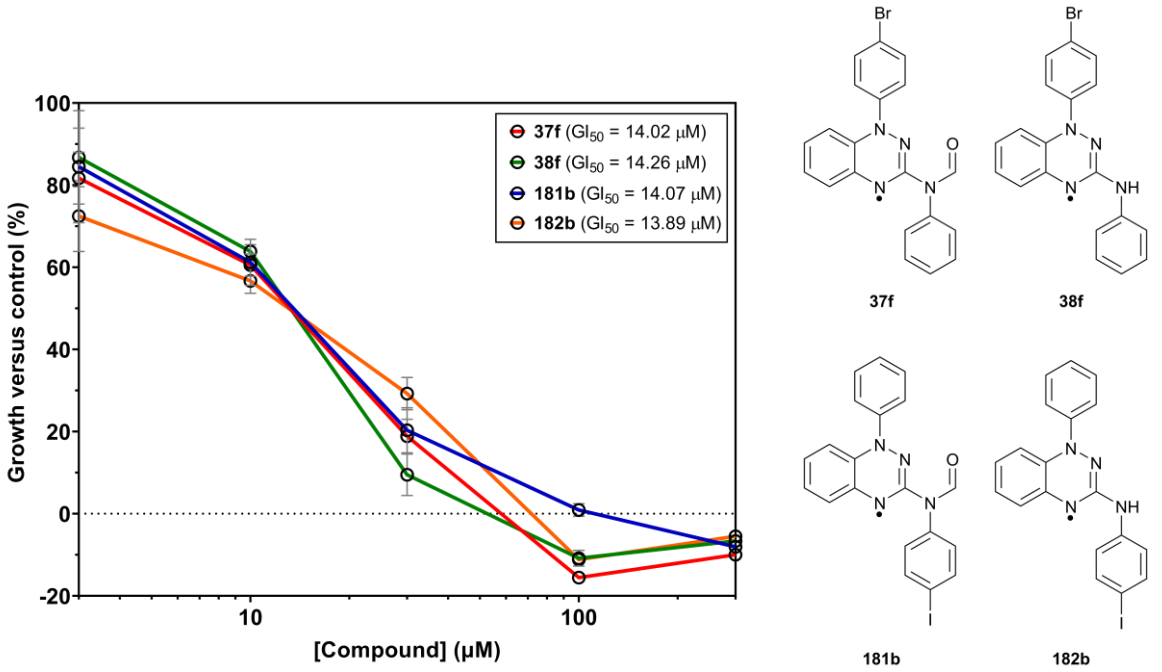


Figure 78 – An example dose-response curve (Experiment 3 – GB-1 cell line).

6.3.2 – Growth inhibition results

The following section describes the SRB assay results for each set of compounds, after 3 days incubation. Three cell lines are used as part of this work: SJSA-1 (human femoral osteosarcoma), MCF-7 (human mammary gland adenocarcinoma) and GB-1 (human glioblastoma). The MCF-7 cell line was selected given that previous work by Aldabbagh *et al*[229] used this cell line to explore the cytotoxicity of 2 Blatter radicals and 3 benzotriazine-7-one species. The GB-1 and SJSA-1 cell lines were selected given they are commonly associated with the development of hypoxic conditions[424-427] and so are of particular relevance when considering the HAP Tirapazamine and Blatter radicals structurally similar to the activated form of TPZ.

Values are reported as an average of triplicates, with standard errors, unless stated otherwise. All compounds were initially analysed at 3, 10, 30, 100 and 300 μM final concentration. Highly potent compounds, where GI_{50} values less than 3 μM were obtained, were further analysed at 0.1, 0.3, 1, 3 and 10 μM final concentration. Compounds with GI_{50} values greater than 300 μM after triplicate experiments were not explored further.

6.3.2.1 – Benzotriazines

GI_{50} values are given in **Table 41** for the benzotriazine compounds shown in **Figure 79**. 3-amino-1,2,4-benzotriazine **222** and the 1-oxide **214** show weak antiproliferative activity, however a significant increase in growth inhibition is seen for the 1,4-di-*N*-oxide TPZ (**39**). The benzotriazin-7-one **158** shows potent antiproliferative activity at submicromolar concentrations, and has the lowest GI_{50} value of all the compounds analysed in this work. The remarkable antiproliferative activity of

39 and **158** has been previously shown in the literature. TPZ (**39**) is the subject of many recent reports regarding activity as an experimental anticancer prodrug under hypoxic conditions.[279, 299, 301, 428, 429] Work by Tano *et al*[279] showed that TPZ leads to the accumulation of cytosolic superoxide and ROS, and can also induce DNA damage that is amplified under hypoxic conditions – potentially a result of hypoxia-selective trapping of Topo I. Aldabbagh *et al*[229] report SRB assays for **158**, with results for the MCF-7 cell line in close agreement with those obtained in this work using a similar method.

Table 41 – GI_{50} values for benzotriazine compounds.

	GI_{50} (µM)			GI_{50} (µM)	
	MCF-7	**GB-1**		**MCF-7**	**GB-1**
214	255.09 [a]	258.47 (± 27.54)	**39**	32.95 (± 16.08)	25.52 (± 2.88)
222	204.24 (± 33.70)	247.01 [a]	**158**	0.68 [a]	0.76 [a]

[a] Single experiment value

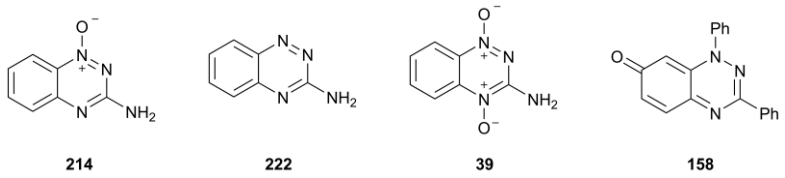


Figure 79 – Structures of the benzotriazine species analysed in this work. The synthesis of **214**, **222** and **39** was described in Chapter 4, Section 4.2 and 4.3. The synthesis of **158** was described in Chapter 3, Section 3.4.

6.3.2.2 – Blatter radicals

Data for the BRs analysed in this work is shown in **Table 42** for the SJSA-1 cell line and **Table 43** for the MCF-7 and GB-1 cell lines – the corresponding structures are shown in **Figure 80**. Studies of the effect of hypoxic conditions for **37a** and **38a** were explored against the SJSA-1 cell line, a significant drop in antiproliferative activity was observed in both cases. Although the generation of Blatter-type radicals is one of the cytotoxic species formed from TPZ under hypoxic conditions, the data suggests that the formed BTZ radicals from TPZ may have reduced activity under hypoxic conditions. One explanation for this reduced activity is that the SJSA-1 cells show slowed replication rate under hypoxic conditions, and so there are less cell divisions where the BRs can apply their antiproliferative activity.

Table 42 – GI_{50} values for Blatter radicals against the SJSA-1 cell line.

	GI_{50} – SJSA-1 (µM)	
	Normoxic	**Hypoxic**
37a	6.61 (± 0.02)	25.92 [a]
38a	30.38 (± 1.11)	68.07 [a]

[a] Single experiment value

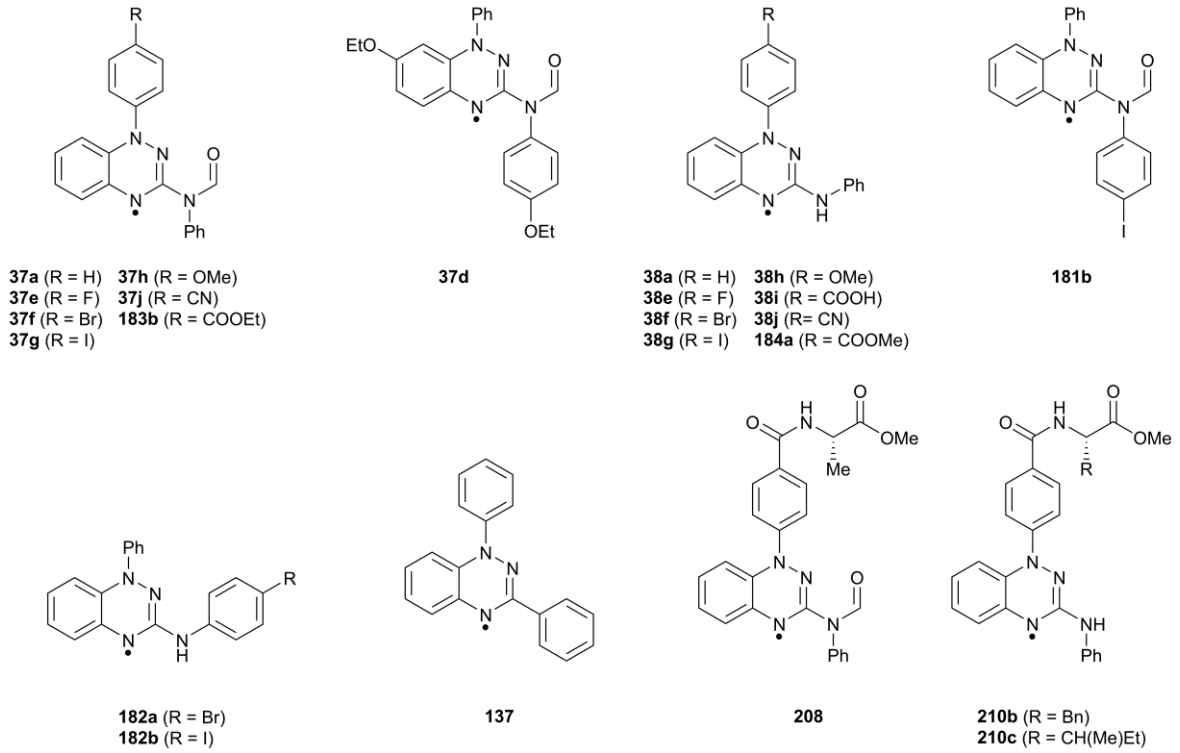


Figure 80 – Structures of the Blatter radicals analysed in this work. The synthesis of all Blatter radicals was described in Chapter 3.

Apart from **38i** and **184a**, all Blatter radicals show greater antiproliferative activity against the MCF-7 and GB-1 cell lines than TPZ **39**. Such an observation may be explained by the Blatter-type radical being the highly potent antiproliferative agent formed from TPZ, and that the loss of hydroxyl radical to give the benzotriazine 1-oxide (**Scheme 186**) is a pathway to less cytotoxic agents. In other words, the species responsible for the antiproliferative activity is the formed BTZ radical. The data could however be explained as a result of normoxic conditions, preventing the generation of the HAD in significantly high concentrations. **38h** is the most antiproliferative Blatter radical tested within this work, with activity over 18× greater than TPZ against the MCF-7 cell line and over 6× greater against the GB-1 cell line (based on GI_{50} value difference). **38h** is also the anilino radical with the most electron-donating substituent, and so the higher energy SOMO may account for the increased activity. There is not a consistent change in antiproliferative activity moving from amido to anilino radicals, however in most cases the amido radicals show greater activity. The original C(3)-phenyl Blatter radical **137** shows similar GI_{50} values to the C(3)-amido and anilino radicals (4.39 μM for MCF-7 and 4.37 μM for GB-1), with removal of the nitrogen at the C(3)-position slightly increasing antiproliferative activity (c.f. **38a** – 7.66 μM for MCF-7 and 8.32 μM for GB-1). Finally, bioconjugates of the C(3)-amido and anilino radicals (**208**, **210b** and **210c**) show similar activity to the other Blatter radicals tested, suggesting no significant improvement in the antiproliferative properties from conjugating amino acids to the radicals. The SRB assay however does not model the pharmacokinetic profile of the Blatter radicals, where bioconjugation may aid absorption into the bloodstream and/or distribution to the tumour site.

Table 43 – GI_{50} values for Blatter radicals against the MCF-7 and GB-1 cell lines.

	GI_{50} (μM)			GI_{50} (μM)	
	MCF-7	**GB-1**		**MCF-7**	**GB-1**
37a	4.59 (± 0.69)	5.48 (± 0.45)	**38i**	49.82 (± 2.49)	57.51 (± 1.40)
37d	4.20 (± 3.26)	7.92 (± 5.28)	**38j**	6.82 (± 1.17)	11.56 (± 2.53)
37e	4.02 (± 0.59)	6.26 (± 1.02)	**181b**	8.84 (± 3.75)	13.82 (± 6.62)
37f	17.91 (± 5.85)	24.93 (± 1.56)	**182a**	7.50 (± 2.75)	5.13 (± 1.09)
37g	11.94 (± 9.77)	10.87 (± 5.00)	**182b**	10.27 (± 2.80)	17.70 (± 1.34)
37h	3.35 (± 1.09)	17.38 (± 18.36)	**183b**	13.25 (± 4.24)	22.39 (± 9.24)
37j	5.92 (± 1.97)	8.27 (± 3.86)	**184a**	70.36 (± 13.36)	56.52 (± 13.42)
38a	7.66 (± 0.97)	8.32 (± 2.20)	**137**	4.39 (± 0.04)	4.37 (± 0.31)
38e	6.63 (± 2.37)	7.41 (± 0.64)	**208**	4.47 (± 0.57)	9.28 (± 0.33)
38f	11.82 (± 1.76)	16.26 (± 1.31)	**210b**	19.92 (± 4.61)	16.33 (± 5.80)
38g	23.92 (± 15.37)	16.64 (± 8.63)	**210c**	10.37 (± 0.42)	6.14 (± 0.74)
38h	1.82 (± 0.78)	3.90 (± 0.68)			

Aldabbagh *et al*[229] provide the only known report within the literature for the anticancer activity of BRs (**Figure 81**). Using the MTT assay, the pyrid-2-yl Blatter radicals **333** and **334** are tested against the MCF-7 cell line alongside the DU-145 (prostate) cell line. The GI_{50} values obtained are higher than the majority of radicals analysed as part of this work, however this may be attributed to the different assay used.

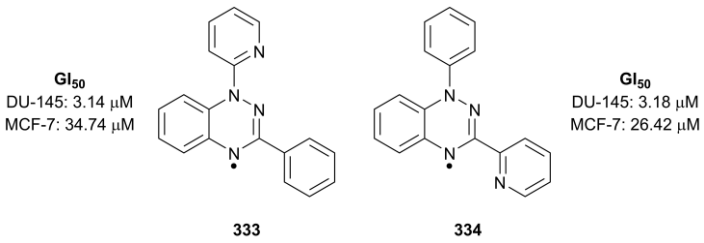


Figure 81 – GI_{50} values for the two pyrid-2-yl substituted Blatter radicals analysed by Aldabbagh *et al*.

Figure 82 shows a growth inhibition scale considering the antiproliferative activity of all Blatter radicals synthesized and subsequently analysed as part of this work. Values are directly compared to Tirapazamine (**39**) and the Blatter radicals analysed by Aldabbagh *et al*[229] (**333** and **334**).

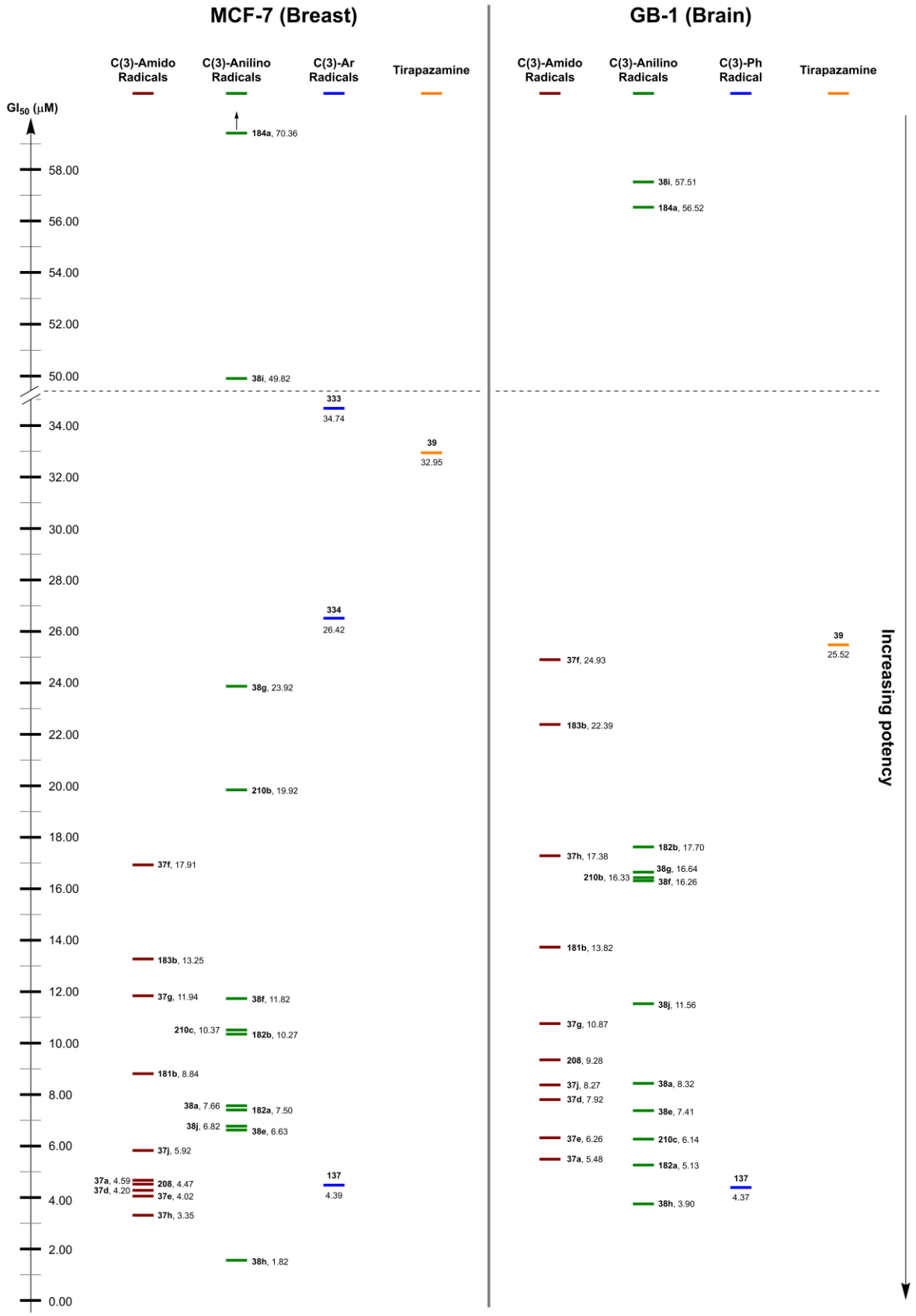


Figure 82 – Growth inhibition scale for Blatter radicals synthesized and subsequently analysed in cellular assays against the MCF-7 and GB-1 cell lines within this work. Values compared to Tirapazamine (**39**), also synthesized and analysed in this work, and the values for **333** and **334** obtained by Aldabbagh *et al*.[229] Upward arrow denotes GI_{50} values that are above the maximum GI_{50} value on the scale.

6.3.2.3 – Nitron analogues

Data for the Nitron analogues is shown in **Table 44**, corresponding to the compounds shown in **Figure 83**. Compared to the Blatter radicals, Nitron analogues show reduced antiproliferative activity – this may be beneficial in the development of Nitron analogues as a prodrug that can form Blatter radicals *in vivo*. In some cases, the zwitterionic Nitron analogue and protonated salt were both tested for antiproliferative activity. GI_{50} values for the protonated salts (**33f·BF$_4$**, **80bH·TFAc**) show similar or slightly increased antiproliferative activity *versus* the zwitterionic salts (**33f**, **80b**). Interestingly, **33dH·BF$_4$** has a comparatively low GI_{50} value which may be a result of the electron donating ethoxy groups favouring the carbenic form of Nitron. Increased levels of carbene *in situ* have been linked to the transformation to give Blatter radical **37d.** The carbenic form of **33d**, the Blatter radical formed from the carbene (**37d**), or the corresponding triazabutadiene byproduct (**72d**) may be responsible for the increased antiproliferative activity.

Table 44 – GI_{50} values for Nitron analogues.

	GI_{50} (μM)			**GI_{50} (μM)**	
	MCF-7	**GB-1**		**MCF-7**	**GB-1**
33a	26.34 (± 7.64)	43.99 (± 8.21)	**80b**	7.64 (± 1.81)	11.69 (± 4.20)
33dH·BF$_4$	6.80 [a]	9.47 [a]	**80bH·TFAc**	5.42 (± 0.36)	5.70 (± 0.36)
33f	14.78 (± 2.17)	18.64 (± 1.03)	**81aH·Cl**	25.71 (± 6.78)	23.74 (± 4.22)
33fH·BF$_4$	15.49 (± 0.87)	18.35 ± (3.05)	**81bH·Cl**	26.54 (± 10.01)	29.31 (± 10.76)
33g	8.07 [a]	14.53 [a]	**83**	150.06 (± 26.47)	184.56 (± 4.80)
33h	19.50 [a]	23.46 [a]	**117**	56.31 (± 11.03)	84.17 (± 16.48)
33i	50.60 (± 8.28)	109.90 (± 1.13)	**118**	113.14 (± 37.93)	141.15 (± 51.97)
33i·Cl	- [b]	- [b]	**192**	29.05 (± 1.10)	76.02 (± 9.01)

[a] Single experiment value. [b] GI_{50} value greater than 300 μM.

Table 45 provides cytotoxicity data for the 1,2,4-triazolium salts **326** – **328** described within the literature[410-412] as anticancer compounds. Where possible, the average GI_{50} value of the five most cytotoxic analogues is given for comparison. The data shows that the Nitron analogues demonstrate similar cytotoxicity as triazolium-containing anticancer agents within the literature, and furthermore there may be interest in exploring the cytotoxicity of Nitron analogues against the leukaemia cell line HL-60 given promising results described within the literature.[410, 411]

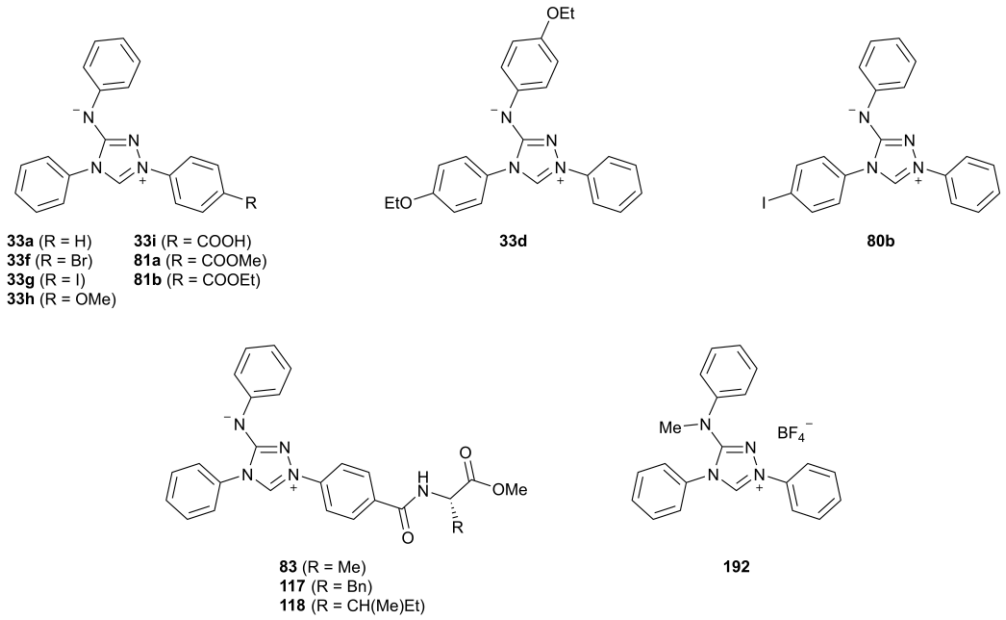


Figure 83 – Structures of the Nitron analogues analysed during this work. The synthesis of all Nitron analogues was described in Chapter 2, Section 2.2 and 2.4.

Table 45 – Cytotoxicity values for the 1,24-triazolium salts described within the literature as having anticancer activity. General class of cancer is provided for clarity. Values in brackets give the average cytotoxicity of the 5 most potent analogues described where possible.

	GI_{50} (µM)			
	MCF-7 (breast)	**MDA-MB-468 (breast)**	**GB-1 (brain)**	**HL-60 (blood)**
326	3.11 - >40 (11.90)	- [a]	- [a]	2.33 - >40 (5.55)
327	- [a]	- [a]	1.76	0.80
328	- [a]	5.0 - 100 (43.38)	- [a]	- [a]
This work	5.42 - 150.06 (9.49)	- [a]	5.70 - 184.56 (11.95)	- [a]

[a] Not analysed.

6.3.2.4 – S-triazoles and S-triazolium salts

Table 46 shows the GI_{50} values corresponding to the *S*-triazoles and *S*-triazolium salts shown in **Figure 84**. The antiproliferative activities of the *S*-triazoles are too weak to obtain GI_{50} values under the standard setup, and so were not explored further. Low potency is seen with the *S*-triazolium salts when compared to other compounds analysed within this work, and there is a clear improvement in activity when added to MCF-7 cells over GB-1 cells. Considering that Nitron analogues show promising cytotoxic activity, the low potency of *S*-triazolium salts is proposed to be a result of the inability to access the carbenic form – unlike Nitron analogues the *S*-triazolium salts cannot undergo tautomerisation to give the corresponding NHC. The *S*-triazolium salts could give rise to a short-

lived NHC *in vivo* through base deprotonation, which may describe the observed cytotoxicity. Both scaffolds do not show promise for further studies.

Table 46 – GI_{50} values for *S*-triazoles and *S*-triazolium salts.

	GI_{50} (μM)			GI_{50} (μM)	
	MCF-7	**GB-1**		**MCF-7**	**GB-1**
86a	- [a]	- [a]	**86p**	- [a]	- [a]
86b	- [a]	- [a]	**89**	- [a]	- [a]
86d	- [a]	- [a]	**92a·BF_4**	299.35 (± 0.65)	- [a]
86e	- [a]	- [a]	**92d·BF_4**	100.31 [b]	- [a]
86f	- [a]	- [a]	**92e·BF_4**	110.91 (± 9.46)	79.11 (± 12.32)
86h	- [a]	- [a]	**99·Br**	73.18 (± 4.78)	- [a]
86o	- [a]	- [a]			

[a] GI_{50} value greater than 300 μM. [b] Single experiment value

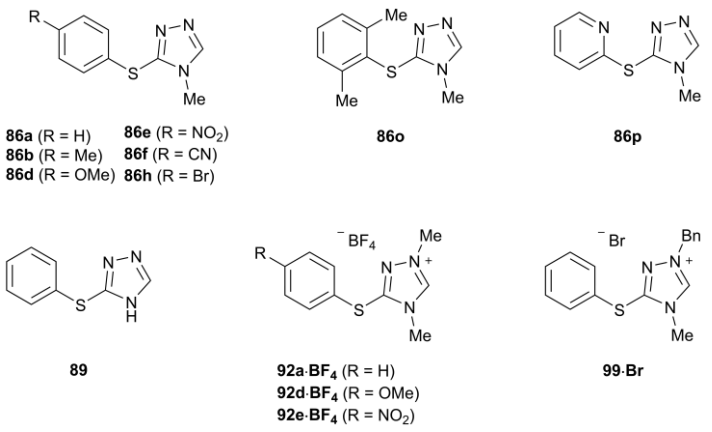


Figure 84 – Structures of the *S*-triazoles and *S*-triazolium salts analysed during this work. The synthesis of both scaffolds was described in Chapter 2, Section 2.3.

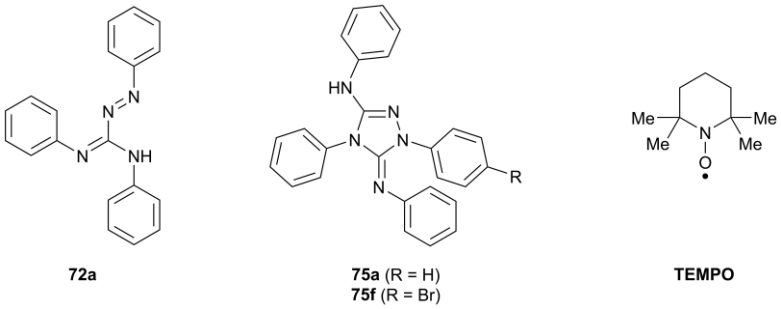
6.3.2.5 – Other compounds

A selection of other compounds were analysed as part of this work, detailed in **Table 47** and shown in **Figure 85**. The triazabutadiene **72a** was analysed as a potential degradation product of Nitron. The antiproliferative activity of **72a** is significantly greater than Nitron (**33a**), and so analogues of Nitron could also act as a prodrug form of triazabutadienes. The N^5-adducts **75a** and **75f** show good potency, and so medicinal activity may be a promising area of study for these scaffolds that have not found application within the literature. Finally, the TEMPO radical was also explored in this work as a well-documented persistent radical, with anticancer properties shown by TEMPO and closely related analogues.[430-432] This work does not indicate good antiproliferative activity by TEMPO, however it should be noted this is a single experiment value.

Table 47 – GI_{50} values for other compounds analysed during this work that do not fall into one of the previous categories.

	GI_{50} (μM)			**GI_{50} (μM)**	
	MCF-7	**GB-1**		**MCF-7**	**GB-1**
72a	17.57 (± 4.48)	15.64 (± 0.85)	**75f**	20.40 [a]	70.96 [a]
75a	23.75 [a]	130.06 [a]	**TEMPO**	296.55 [a]	- [b]

[a] Single experiment value. [b] GI_{50} value greater than 300 μM.



72a **75a** (R = H) **75f** (R = Br) **TEMPO**

Figure 85 – Structures of the other compounds analysed during this work that do not fall into one of the previous categories.

Figure 86 summarises all the GI_{50} values obtained with a 3 day incubation time. The summary illustrates that similar activity is generally seen against the MCF-7 and GB-1 cell lines for all compound classes.

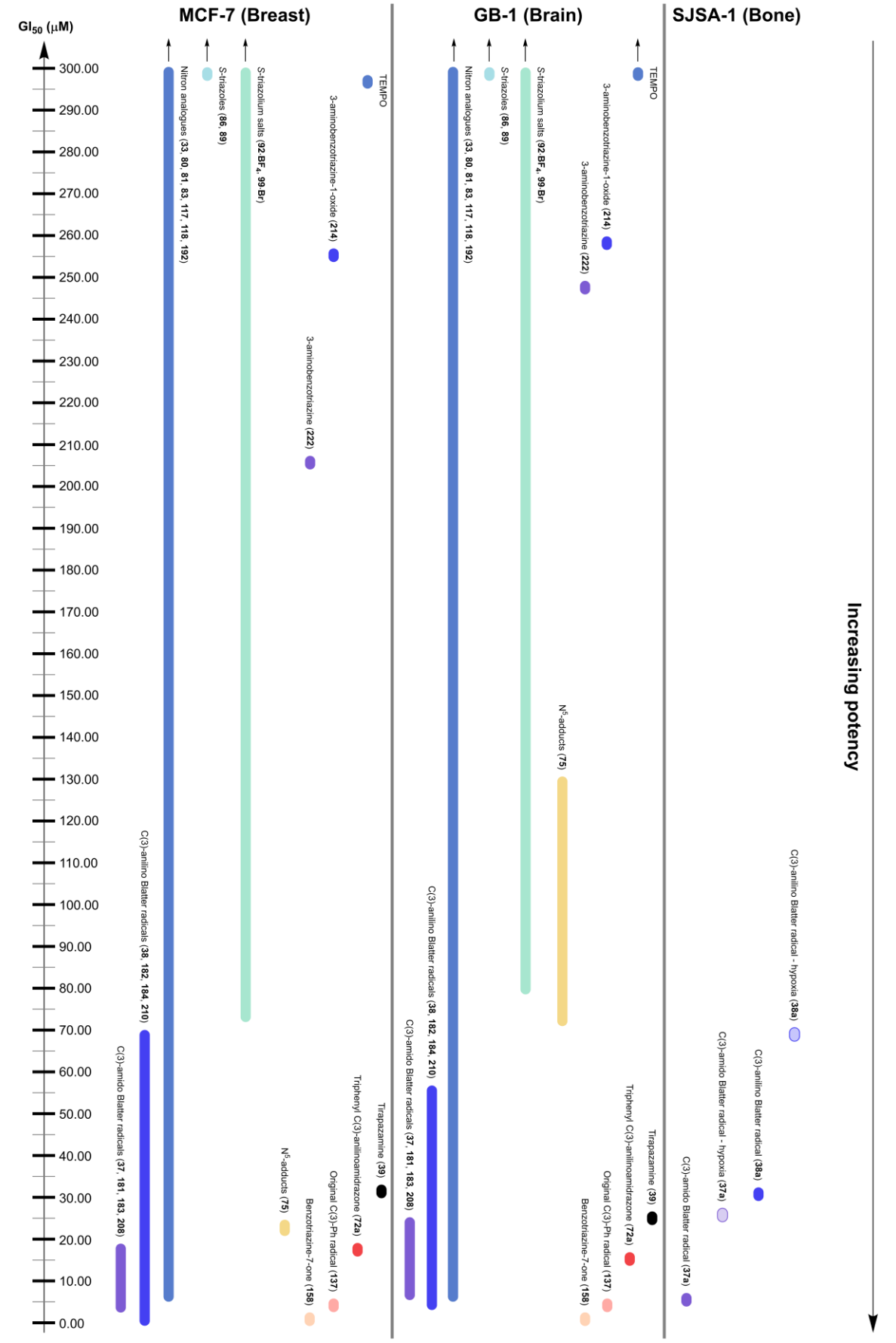


Figure 86 – Summary of cytotoxicity values obtained in this work using a 3-day incubation time. Upward arrows indicate compounds with potency too low to be observed in the SRB assay (GI_{50} > 300 μM).

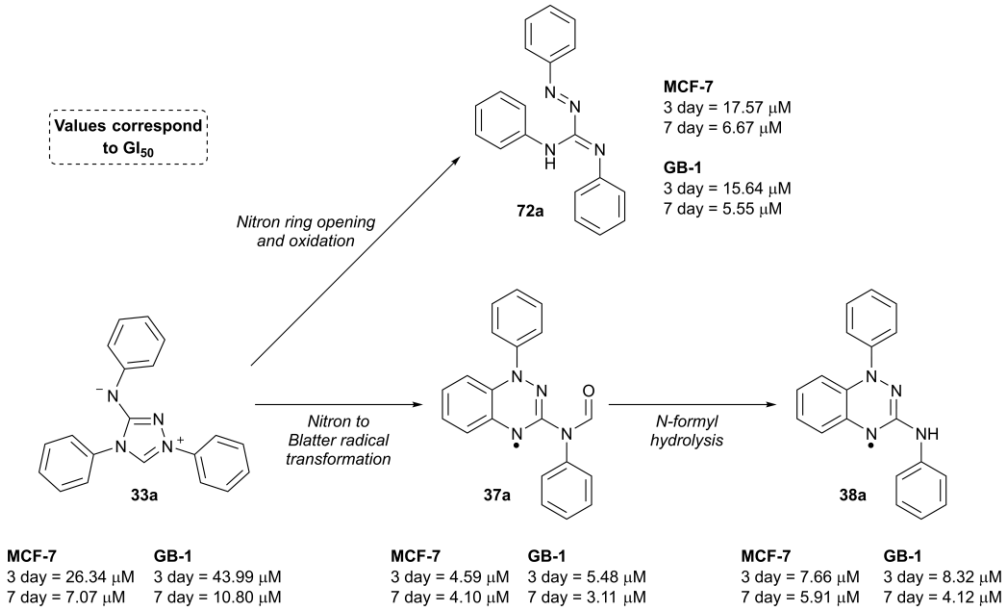
6.3.3 – Prolonged incubation studies

As a final study using the SRB assay, the effect of increasing incubation time to 7 days was explored with the results provided in **Table 48**. The antiproliferative effect of Blatter radicals (**37a**, **38a** and **38h)** generally increases as incubation time is increased suggesting a prolonged effect on growth. Apart from **38h** against the MCF-7 cell line, GI_{50} values decrease between 11% and 50%. The triazabutadiene **72a** shows over 60% decrease in GI_{50} for both cell lines, also indicating a maintained antiproliferative effect for several days. Nitron (**33a**) and the methoxy-substituted analogue **33h** both show very large increases in potency, with GI_{50} values generally decreasing by over 70%. This may suggest that over time the more potent Blatter radical or triazabutadiene species are formed in the cells (**Scheme 189**), however these initial studies are unable to verify formation of these species. Furthermore, the exocyclic *N*-methylated analogue of Nitron (**192**) also shows a substantial decrease in GI_{50} value upon increasing incubation time to 7 days, and this species has been shown in Chapter 3.4 to not undergo the ring opening to triazabutadiene or Blatter radical. It may instead by proposed that the Nitron analogue itself is showing antiproliferative activity. These findings do support further exploration of Nitron derivatives as anticancer prodrugs.

Table 48 – GI_{50} values of selected compounds after 3 and 7 days. Percentage change in GI_{50} value when moving from 3 to 7 days is also provided.

	GI_{50} – MCF-7 (µM)		**GI_{50} – GB-1 (µM)**		**Change (%)**	
	3 days	**7 days**	**3 days**	**7 days**	**MCF-7**	**GB-1**
33a	26.34 (± 7.64)	7.07 (± 1.75)	43.99 (± 8.21)	10.80 (± 7.36)	− 73	− 75
33h	19.50 [a]	4.16 [a]	23.46 [a]	13.81 [a]	− 79	− 41
37a	4.59 (± 0.69)	4.10 (± 0.91)	5.48 (± 0.45)	3.11 (± 0.07)	− 11	− 43
38a	7.66 (± 0.97)	5.91 (± 1.63)	8.32 (± 2.20)	4.12 (± 0.63)	− 23	− 50
38h	1.82 (± 0.78)	2.17 (± 0.76)	3.90 (± 0.68)	2.15 (± 0.10)	+ 19	− 45
72a	17.57 (± 4.48)	6.67 (± 1.93)	15.64 (± 0.85)	5.55 (± 0.91)	− 62	− 65
192	29.05 (± 1.10)	12.95 (± 3.72)	76.02 (± 9.01)	41.98 (± 8.61)	− 55	− 45

[a] Single experiment value

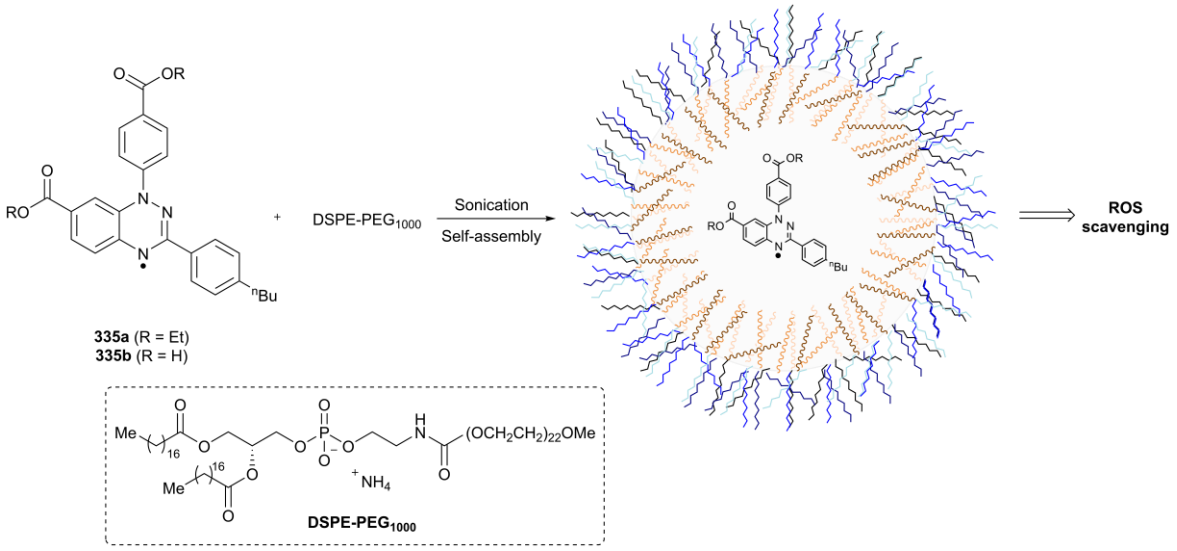


Scheme 189 – Summary of the change in GI_{50} value from Nitron **33a** to the triazabutadiene **72a** or the Blatter radicals **37a** and **38a**. Increased cytotoxicity for **72a**, **37a** and **38a** suggest a potential use of **33a** as a prodrug.

6.4 – Blatter radicals as reactive oxygen species scavengers

Reactive oxygen species (ROS) have a key role in activating gene transcription, inhibiting and activating proteins, and DNA mutagenesis. However, excessive ROS production or exposure, for prolonged periods of time, can lead to a range of negative effects: irreversible impairment of cellular function; pathological gain of function; development of malignant cells; and death. The human body combats these negative effects through regulating ROS production, repair of ROS-mediated damage (degradation of damaged macromolecules and re-synthesis, or sequester macromolecules with chaperones) and the catabolism of ROS by antioxidant systems.[433] However, the use of exogeneous agents to guarantee redox homeostasis and reduce the incidence of cellular ROS overproduction are sometimes necessary. A range of antioxidant systems have been investigated to reduce overproduction of cellular ROS, such as glutathione, TEMPO, NADH, and vitamins C and E – such species commonly suffer from short retention time, rapid elimination and low delivery efficiency. The development of new antioxidants is therefore an attractive area of research for disease prevention.

Initial investigations have been undertaken as part of this work based on the recent report by Hu *et al*,[71] who have reported the first case of Blatter radicals being implemented in the scavenging of ROS (**Scheme 190**). The self-assembly of nanoparticles (NPs) was possible upon sonication with the biocompatible amphiphilic DSPE-PEG$_{1000}$ (1,2-distearoyl-sn-glycero-3-phosphoethanol-amine-*N*-[methoxy-(polyethylene glycol)-1000]). NPs of **335b** were unstable and showed little effect on ROS concentrations in model cells, however **335a** formed stable ~25 mm NPs with no evidence of aggregation and good water dispersibility. **335a** NPs scavenged excessive ROS in the model system to give obtain normal concentrations.



Scheme 190 – Overview of the Blatter radical nanoparticle preparation for ROS scavenging by Hu *et al*.

These interesting results led to considering the use of radicals synthesized within our group as ROS scavengers, and how the C(3)-*N* substituent may affect activity given that this substituent is found to be particularly effective in tuning the electrochemical properties of Blatter radicals.[70] In collaboration with Prof. Robert Pal of Durham University, work has taken place towards the preparation of nanoparticles encapsulating Blatter radicals synthesized within our group.

Hu *et al*[71] found that cell viability was not clearly changed after incubating with NP concentrations up to 100 μg mL^{-1}. With a radical / PEG ratio of 1 : 5 by weight in the NPs, the concentration of BR is approximately 17 μg mL^{-1} or 0.04 to 0.06 μM. These concentrations are significantly lower than those used in the SRB assays (0.1 to 300 μM) to observe antiproliferative effects, and so the findings of Section 6.3 are in agreement with the observations of Hu and coworkers.[71]

Dominic Black, a PhD student in the group of Prof. Robert Pal, undertook viability studies of **37a** and **38a** against the NIH-3T3 (mouse embryonic fibroblasts) cell line (**Figure 87**). At 10 μg mL^{-1} both Blatter radicals are stable within cells, with no visible impairment of cell viability. Above 10 μg mL^{-1} the radicals crystallise from the cellular media, with the cells serving as a nucleation point for crystallisation. This crystallisation from media is not a surprise, given that the amphiphilic nanoparticles employed by Hu and coworkers[71] were developed to combat low aqueous solubility.

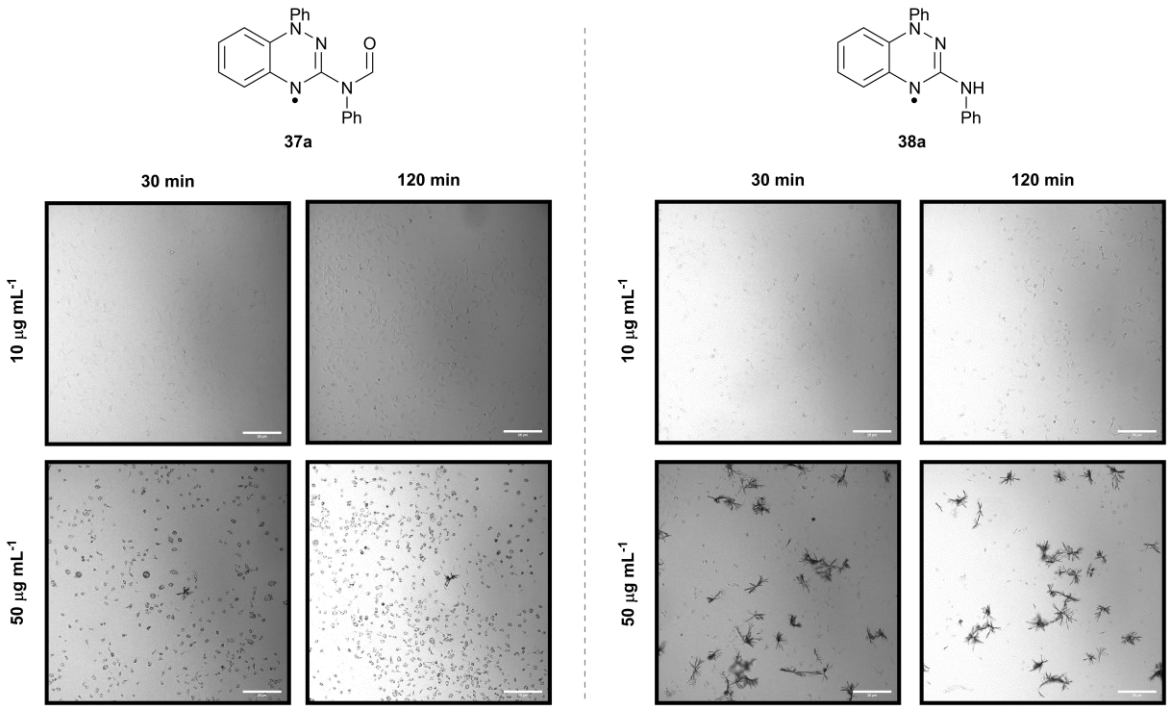


Figure 87 – Cell viability studies of **37a** and **38a**. Cell microscopy images were obtained using a custom built microscope modified from a Zeiss Axiovert 200M, using a Zeiss APOCHROMAT 63x/1.40 NA objective.

With cell viability impairment not observed for **37a** and **38a** at the tested concentrations, this initial study acts as a starting point in the development of nanoparticles analogous to those described within the literature.[71]

6.5 – Conclusions

Benzotriazinyl radicals structurally similar to Blatter radicals have been implicated in the mode of action of TPZ,[204] however direct studies of Blatter radicals as anticancer agents is not described within the literature. This is despite many recent reports regarding Blatter radical synthesis through a variety of methods.[59, 69, 70, 234, 240] These studies may also aid the ongoing discussion within the literature[434] regarding the reactive species responsible for the activity of TPZ.

This work illustrates that the Blatter radical is a potent antiproliferative agent, with up to 18-fold greater activity than TPZ under normoxic conditions. GI_{50} values of the majority of Blatter radicals are below that of TPZ for the MCF-7 and GB-1 cell lines. Blatter radicals are also shown to maintain antiproliferative activity for 7 days in cellular assays. Initial investigations into the use of Nitron analogues as prodrugs, based on incubation time dependent GI_{50} value tracking, shows on average a 70% increase in potency for Nitron comparing 3 and 7 day incubation times.

Initial studies of Blatter radicals as ROS scavengers have shown Blatter radicals at concentrations of 10 μg mL^{-1} do not show visible antiproliferative activity. Based on previous work within the literature,[71] the new Blatter radicals synthesized within the group can now be explored as antioxidants for disease prevention.

7 – Conclusions and future work

7.1 – Conclusions

1,2,4-triazolium salts have shown a broad range of applications within the literature, including medicinal activity and the development of ionic liquids. The triazolylidine NHC, generated by deprotonation of the 1,2,4-triazolium salt, has further applications in the fields of organocatalysis and organometallic catalysis. As part of this work the synthesis of 1,2,4-triazolium salts bearing *N*- or *S*-substitution has allowed for the exploration of a range of applications. Most notably these include the transformation of *N*-substituted triazolium salts (Nitron analogues) to Blatter radicals, alongside the protofugality and organocatalytic activity of *S*-triazolium salts.

Chapter 2 explored the synthesis of Nitron analogues (**33**), a class of 1,2,4-triazolium salt with a C(3)-anilino substituent. The intriguing tautomerisation of Nitron into the carbenic form *in situ* prompted studies in the group by Murray[127] into the development of an updated synthetic methodology. Prior to our previous report,[59] the synthesis of Nitron was limited to a single route[67] using carcinogenic reagents – there were no reports regarding the preparation of Nitron analogues. As part of this work, a higher yielding route with broader scope and use of less hazardous reagents was developed. In work by the author, late-stage modification by halogenation (**80**) or esterification (**81**) was also undertaken. The halogenation of Nitron analogues is particularly of interest in the development of analogues with substitution selectively upon the N(4)-Ar ring – this is difficult to achieve within the synthesis of Nitron analogues. A survey of the methods to undertake bioconjugation of Nitron analogues to peptide and peptidomimetic scaffolds is also described, with three amino acid bioconjugates isolated. Tautomerisation of Nitron analogues to the carbenic form was also explored through DFT, to describe the effects of substituents on the fraction of carbene *in situ*. The Nitron analogue single-crystal XRD data obtained in this work has also enabled the exploration of substituent effects on structure of the analogues.

Chapter 2 also presented the synthesis of a series of *S*-triazolium salts (**92·BF$_4$**, **94·BF$_4$**, **99·Br**) *via* *S*-substituted 1,2,4-triazoles. The microwave-assisted Ullmann coupling to *S*-triazoles is evaluated through the tuning of reaction conditions to give a versatile and generally high-yielding method with straightforward purification. The identification of *S*-triazolium salt isomer formed has been described by a series of methods, with the isolation and characterisation of both isomers effectively undertaken through RP-LC. In total, 26 novel *S*-triazolium species have been isolated within this work. The observed selectivity, pleasingly for the desired 1,4-dialkyl triazolium, is described through consideration of *S*-triazole methyl cation affinity.

Chapter 3 discussed synthetic and mechanistic studies into the transformation of Nitron analogues (**33**, **80**, **81**) into Blatter radicals (**37**, **38**, **181** – **184**). Blatter radicals demonstrate remarkable bench stability over several years, with no indication of sensitivity to air or moisture. This stability is attributed to the SOMO stabilisation across the bicyclic benzotriazine core, in particular the three

triazinyl nitrogens that all show significant levels of radical character. Recently the radicals synthesized within the group have shown promising activity as signal enhancement agents in dynamic nuclear polarisation[220] and have also been investigated within organic batteries.[202] Using the rearrangement of Nitron analogues first reported by our group in 2017,[59] the range of C(3)-N substituted Blatter radicals is dramatically improved – this substitution is difficult to achieve using other methods within the literature. Furthermore, studies into the late-stage halogenation of Blatter radicals has enabled the development of analogues in high yields with selective C(3)-N-Ar halogenation. Bioconjugation of Blatter radicals to amino acids has also been undertaken and acts as an initial step towards the implementation of Blatter radicals as spin probes or as peptide conjugates with improved medicinal activity. The diverse range of characterisation techniques undertaken has enabled property to structure relationships to be explored, and has shown the previously unexplored robust thermal stability of C(3)-N substituted Blatter radicals.

The mechanistic studies in Chapter 3 expanded on the previously described role of zwitterion-carbene tautomerisation in Blatter radical formation, including through NMR studies of the formation of Blatter radical to give describe relative rates of formation. An intriguing 2-phase behaviour is observed within these studies that is tentatively ascribed to the formation of a hydrated Nitron intermediate that can undergo ring opening towards Blatter radical. The role of N(1)-Ar substitution is also discussed, with the introduction of electron withdrawing groups proposed to reduce N(1) basicity and impede ring opening.

The potential of Blatter radicals as organocatalysts within the oxidative coupling of amines and alcohols is also described. Conversions indicative of Blatter radical catalysing imine formation are obtained in these initial studies, with 1 mol% loading alongside 2 mol% CuI achieving up to 27% NMR conversion.

Chapter 4 presents the synthesis of benzotriazines, including Tirapazamine **39** currently under consideration as an experimental anticancer prodrug. **39** is proposed to generate benzotriazinyl radicals under hypoxic conditions, structurally similar to Blatter radicals, as the drug form. 3-Amino-1,2,4-benzotriazine-1-oxide **214** was synthesized using the Arndt benzotriazine synthesis. Attempts to prepare analogues through variation of the aniline and nitrile starting materials are also described, however issues in cyclising the guanidine intermediates resulted in no analogues being isolated. The formation of 2 benzotriazinium salts were evidenced by LC-MS through prolonged reflux in concentrated HCl, with one example isolated in low yields and characterised. Oxidation to Tirapazamine **39** and reduction to the 1,2,4-benzotriazine **222** were also successfully undertaken, with the generation of an alanyl bioconjugate of **39** also reported.

Chapter 4 also describes the previously unidentified ring contraction of 3-amino-1,2,4-benzotriazine **222** to 1,2-diaminobenzimidazoles upon addition of organolithium reagents. The initial conjugate

addition of the organolithium reagent is proposed to lead to ring opening to a triazabutadiene-aryllithium, which undergoes ring closure to give the benzimidazole product. When using *tert*-butyllithium and phenylmagnesium bromide, a novel regioselective C(6)-addition to **222** is instead observed which is supported by XRD data.

Chapter 5 explores the H/D-exchange of *S*-triazolium salts **92a – q·BF$_4$**, **94·BF$_4$** and **99·Br** as a means to describe the protofugality (kinetic acidity) in a series of deuterated buffers or dilute DCl solutions. The 1st and 2nd order rate constants for the exchange process are comparable to values obtained for arylated 1,2,4-triazolium salts implemented within organocatalytic applications. These findings indicate the expected drop in C(5)-H protofugality from swapping aryl substituents for alkyl can be effectively counteracted by the introduction of the C(3)-SAr substituent. Furthermore, the introduction of substituents upon the C(3)-SAr ring can tailor the protofugality. This is shown through Hammett structure-activity analysis, obtaining values for ρ around +0.5 depending on the inclusion of *para*-substituted C(3)-SAr analogues. pK_a values of the 11 *S*-triazolium salts analysed in this work have been calculated as between 16.7 and 19.0 in water. These values may be compared with values obtained previously within the group, including studies on the C(5)-H of Nitron analogues **33H·X**. These studies indicate the sulfur bridge of *S*-triazolium salts can counteract the pK_a drop expected moving from 1,4-diaryl to 1,4-dialkyl triazolium salts. This could be used in the design of alternative triazolium-derived NHC organocatalysts as there is a move towards catalysts of lower pK_a that can function in aqueous solution. With a series of second-order rate constants for the C(5)-hydrogen exchange for deuterium, XRD structural parameters were used within structure to protofugality relationships. Multi-parameter statistical models provide an approximation of k_{DO} applicable for all 1,4-dialkyl *S*-triazolium salts analysed within this work.

Initial organocatalytic evaluation is also undertaken in Chapter 5, considering the benzoin and Stetter reaction. *S*-triazolium salts show activity in both transformations, with initial rate constants obtained and evaluated.

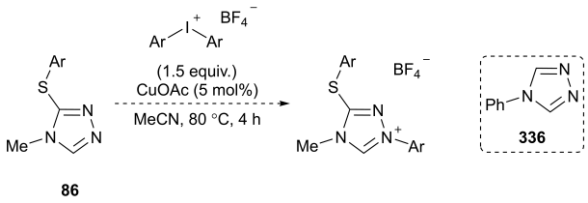
Chapter 6 explores the antiproliferative activity of all compounds analysed as part of this work. Particularly of interest are the Blatter radicals, which have been implicated in the mode of action of Tirapazamine **39**[204] but are only described once within the literature as anticancer agents.[229] This report is however limited to 2 radicals which do not bear the C(3)-N substitution seen in **39**. This work shows the Blatter radical is a potent antiproliferative agent under normoxic conditions, with activity greater than that seen for **39**. Nitron analogues also show promising activity, however *S*-triazoles and *S*-triazolium salts do not show promise for further studies. Prolonged incubation studies show a dramatic improvement in cytotoxicity for Nitron **33a** and **33h**, which may be attributed to ring opening to the triazabutadiene **72a** or Blatter radical **37a** given the comparable cytotoxicity after 7 days. These findings indicate a potential use of Nitron as an anticancer prodrug. Chapter 6 also

describes initial studies of Blatter radicals **37a** and **38a** as ROS scavengers, with cell viability studies indicating that Blatter radicals do not show antiproliferative activity at 10 μg mL^{-1}.

This thesis combines synthetic development, kinetic and mechanistic analysis, computational methods and cellular assays to give an greater understanding of 1,2,4-triazolium salts for organocatalysis and Blatter radical synthesis.

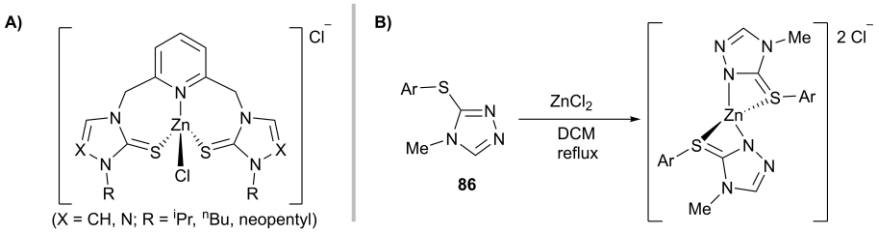
7.2 – Future work

The novel *S*-triazolium salts described in Chapter 2 have so far been limited to 1,4-dialkyl analogues, the introduction of an aryl substituent would be expected to significantly increase protofugality as has been illustrated in other 1,2,4-triazolium salts synthesized within the group. Arylation of *S*-triazoles has been attempted as part of this work and not shown a great deal of promise, however there are other methodologies that may provide a route to these analogues. Of particular interest is the use of diaryliodonium salts (**Scheme 191**) which is reported by Bolliger *et al*.[110] They describe formation of the desired 1,4-diarylated triazolium isomer in isolated yields of between 52% and 96% when using 4-phenyl-1,2,4-triazole **336** and a series of diaryliodonium salts.



Scheme 191 – Proposed use of diaryliodonium salts to give arylated *S*-triazolium salts.

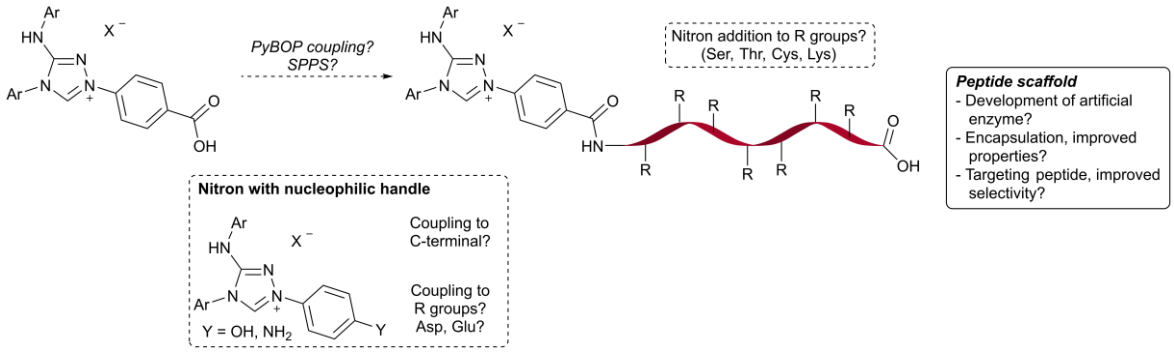
Modelling the active site of LADH using thiol-substituted 1,2,4-triazole zinc complexes (**Scheme 192A**) is an interesting application described within Chapter 2.4.[145] The preparation of *S*-triazole analogues within this work provide an expanded scope of scaffolds that could be explored in complexation to zinc (**Scheme 192B**), including investigations of the reduction of aldehydes mirroring those with literature precedent.[145]



Scheme 192 – Development of LADH active site models. **A** – the zinc active site model synthesized by Miecznikowski and coworkers. **B** – proposed future work involving the *S*-triazoles **86** synthesized as part of this work.

The initial bioconjugation studies undertaken on Nitron analogues in Chapter 2 are also ripe for future exploration. With a known route to amino acid bioconjugates using PyBOP coupling, alongside promising work undertaken in this project on solid-phase peptide synthesis (SPPS) in collaboration with Deck, Nitron analogues could be incorporated into larger peptide scaffolds in work towards the development of artificial enzymes (**Scheme 193**). Use of peptide scaffolds that encapsulate the compound may improve the physiological properties, and thus may improve the cytotoxicity as a potential anticancer agent; this may include activity as a prodrug. The use of a targeting peptide may also enable more selective treatment, particularly useful when considering the potential of prodrug

use towards a more cytotoxic Blatter radical that inherently may show little selectivity. The *in situ* generation of carbene through Nitron tautomerisation may prove to be a promising property of these compounds for both organocatalysis and ring opening to anticancer agents.



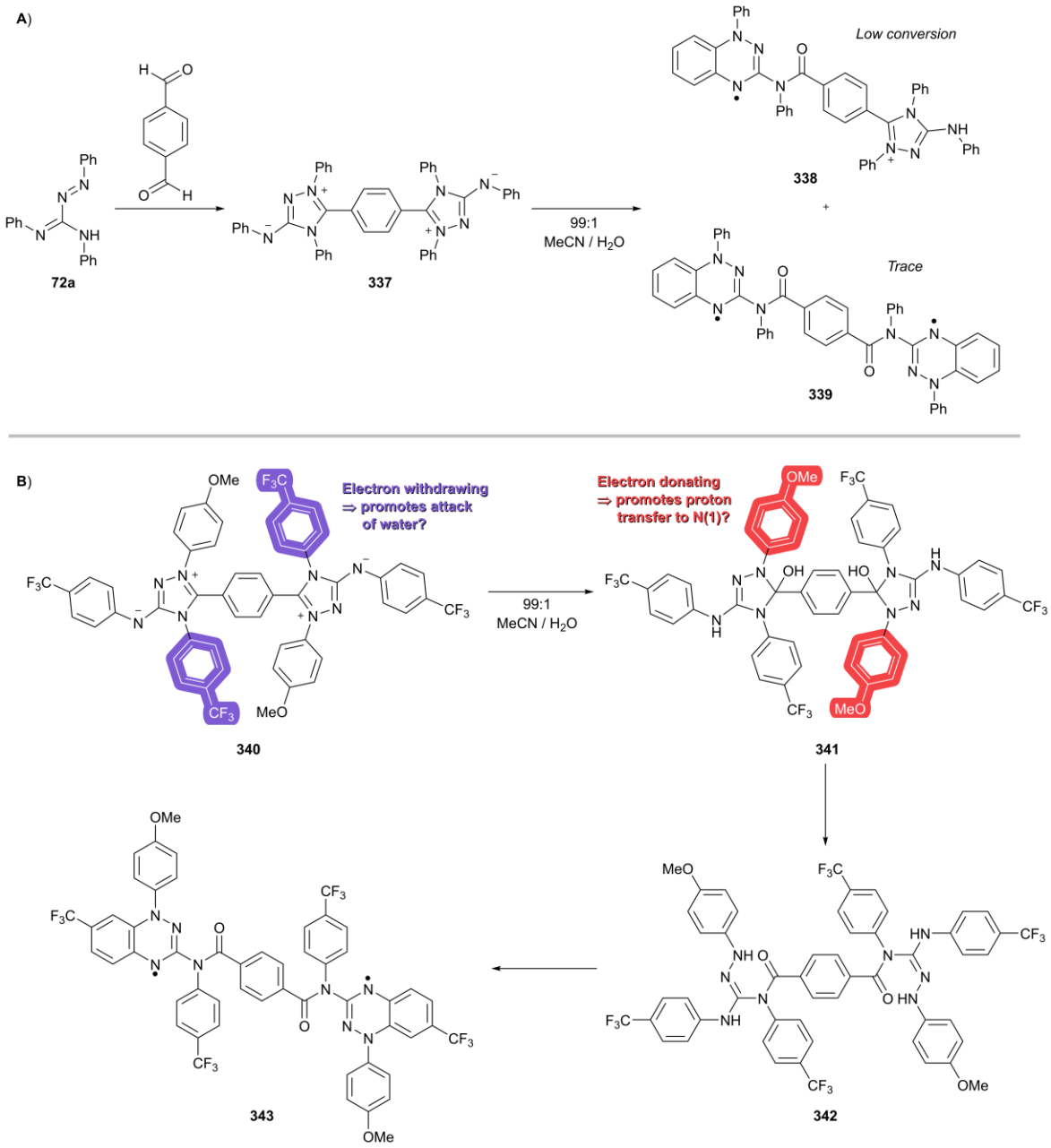
Scheme 193 – Using solution phase techniques, such as PyBOP coupling, a Nitron-amino acid bioconjugate could be prepared and subsequently introduced into a peptide scaffold. The Nitron analogue could also be introduced using solid-phase peptide synthesis.

Chapter 3 expanded on previous findings regarding the mechanism of Blatter radical formation from Nitron analogues. Further studies on the mechanism would be of benefit to provide evidence for the 2-phase behaviour observed, and potentially validate the mechanism underlying this behaviour. The initial drop may be assessed by NMR studies using variable % v/v water in MeCN, including tracking any changes in MeCN only.

There is growing interest within the literature regarding the development of Blatter diradicals exhibiting interesting electronic, magnetic and photochemical properties.[200, 230, 435] Work is ongoing within our group towards the development of Blatter diradicals from di-Nitron analogues, implementing our updated synthetic route and reported conditions to obtain Blatter radicals.[59] Murray[127] reported the synthesis of di-Nitron **337** by undertaking the ring closure of triazabutadiene **72a** (**Scheme 194A**) however observed slow, partial conversion to a mixture of **338** and **339** by LC-MS. Addition of mild oxidant and base was found to potentially increase the rate of Blatter radical formation, but also led to a complex mixture from which **339** could not be isolated. A slow reaction is to be expected with the ability to undergo tautomerisation to the carbenic form now not possible, however it may still be possible for Blatter radicals to be isolated implementing this method. Our group have previously reported the isolation of C(3)-alkylated analogues of Nitron **151** and **152**, which were successfully converted to the corresponding Blatter radicals **154** and **155** albeit in low yields requiring KOH and Ag_2O (Chapter 3, **Scheme 90**). To aid the ring opening, the introduction of electron withdrawing groups on N(4)-Ar may promote the attack of water to generate the hydrated intermediate **341** (**Scheme 194B**), with the electron donating group on N(1)-Ar increasing the basicity to promote the proton transfer required for ring opening. These changes are hoped to translate to greater levels of Blatter radical formation under our reported base-free and oxidant-free

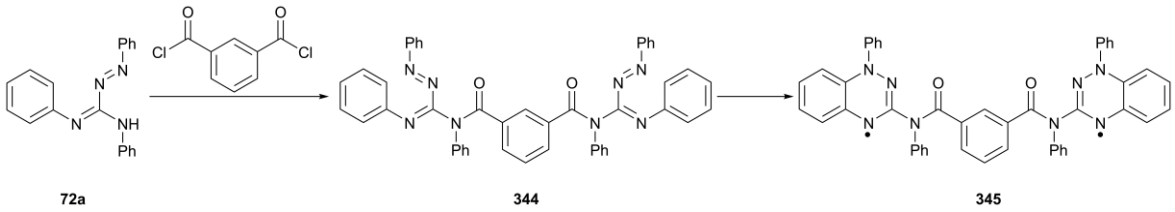
conditions, allowing for more straightforward isolation. A change in experimental conditions, such as the implementation of electrochemical techniques, may also yield promising results.

Alongside alterations of the Nitron starting material, there is a possibility that the C(3)-N position could be used as a handle for dimerization. Studies within the group in this area have shown limited promise, for example the use of oxalyl chloride lead to formation of a imidazolidine ring between C(3)-N and the N(4) radical center. It may instead be beneficial to use the triazabutadiene **72** and undertake reactions on the anilino nitrogen that promote cyclisation to Blatter radical (**Scheme 195**).



Scheme 194 – Work towards the isolation of Blatter diradicals from di-Nitron species. **A**) Previous work by Murray showed formation of di-Nitron **337**, however conversion under our reported conditions led to low conversion to Blatter radical **338** and traces of Blatter diradical **339** evidenced by LC-MS. **B**) Proposed analogue of **337** (**340**) bearing substituents to promote formation of hydrate **341** and subsequently promote ring opening to **342** – this is hoped to translate to greater yields of the Blatter radical **343**.

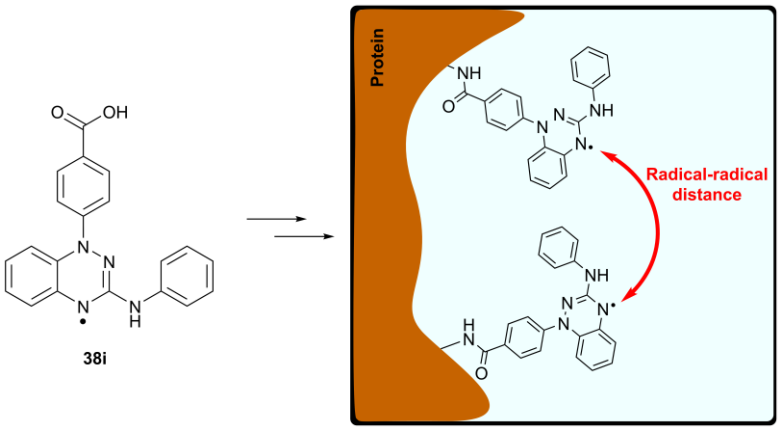
A third option is to use substituents upon the aryl rings of Nitron analogues to undertake dimerization, for example metal-catalysed cross-couplings of halogenated Nitron analogues or the use of amide coupling methods described in the bioconjugation section to form diradicals of the carboxy-functionalised Blatter radical **38i**.



Scheme 195 – Proposed formation of Blatter diradical **345** by reaction of triazabutadiene **72a** with isophthaloyl dichloride followed by cyclisation of the di-triazabutadiene **344**.

As discussed in Chapter 3, the radicals reported by our group (**37a**, **38a**) have shown promising activity as o-DNP polarising agents better than the commonly used TEMPOL radical. The Blatter radical transfers polarisation of the unpaired electron to the compound of interest allowing for increased signal intensity, with a small electrochemical window between oxidation and reduction processes. The work reported herein has allowed for the synthesis of additional analogues that show smaller electrochemical windows than the C(3)-amido radical **37a** and C(3)-anilino radical **38a** (ΔE = 0.97 and 0.92 V, respectively). Examples include the iodinated C(3)-amido radical **181b** (ΔE = 0.82 V) and the *p*-CN anilino radical **38j** (ΔE = 0.77 V). It would be of interest to explore these radicals as o-DNP polarising agents as it would be expected that even greater signal enhancement may be observed.

Finally in relation to the work in Chapter 3, the initial bioconjugation work can act as the initial studies towards the development of Blatter radicals as spin probes (**Scheme 196**). PyBOP coupling was shown to generate amino acid bioconjugates, which could be introduced into a peptide scaffold as a radical monomer using SPPS methods. The generation of Blatter radical bioconjugates may also be beneficial for improved bioavailability or targeting, considering the use of Blatter radicals as antiproliferative agents.



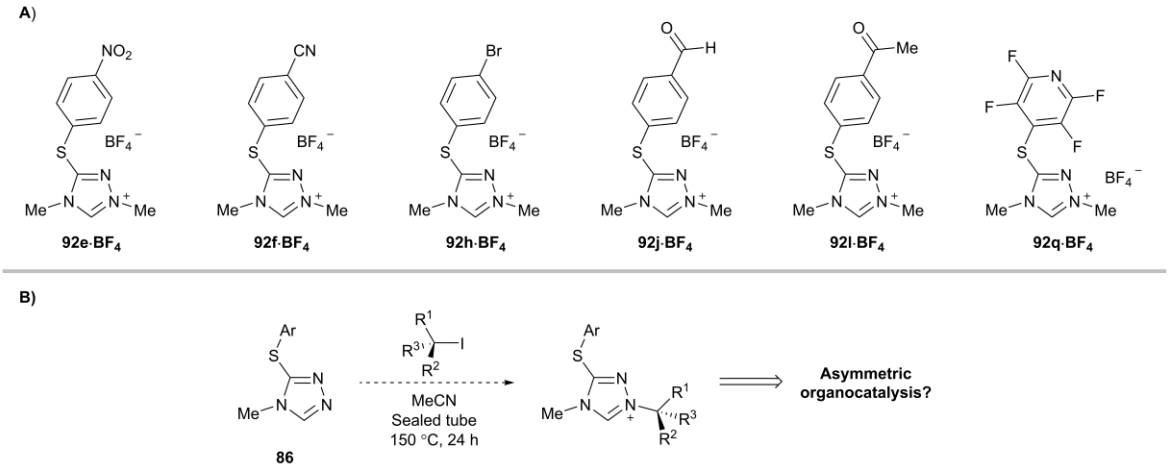
Scheme 196 – Using the carboxy-functionalised Blatter radical **38i** and knowledge regarding the PyBOP coupling of Blatter radicals to amino acids, the introduction of Blatter radicals as spin probes could be undertaken.

Chapter 4 presented the unexpected synthesis of 1,2-diaminobenzimidazoles from the addition of organolithium species to benzotriazine. Within the literature 1,2-diaminobenzimidazoles have been implemented in the development of zeolite imidazole frameworks (ZIFs) containing cobalt used for CO_2 capture,[436] fluorescent chemosensors for a range of anions and cations,[437] and as NOS inhibitors for the treatment of stroke, inflammation or morphine addiction.[302] The aminobenzimidazole scaffold is also key in a series of STING antagonists effective in treatment of SARS-CoV-2[303] and agonists key in the development of antitumour immunity treatments that supress tumour progression.[438] All of these applications may benefit from this novel route to benzimidazole species if further explored.

Chapter 5 described the protofugality of *S*-triazolium salts, which were found to be similar to previously described organocatalysts within our group.[63] Initial organocatalytic studies showed activity in both the benzoin and Stetter reaction, however only two salts were investigated. Future studies investigating the introduction of electron-withdrawing substituents upon the aryl ring (**Scheme 197A**) may prove to be effective organocatalysts for this transformation, with low steric hindrance about the precarbenic site. Furthermore, with promising protofugality of the 1,4-dialkyl *S*-triazolium salts, the synthesis of chiral *S*-triazolium salts may show stereoselective catalytic activity (**Scheme 197B**). It is proposed that the addition of a tertiary iodoalkane would require forcing conditions, with a good starting point being the conditions used in the synthesis of benzylated *S*-triazolium **99·Br** (sealed tube at 150 °C).

Chapter 6 presented studies undertaken regarding the antiproliferative activity of the range of compounds described in this work. These studies were limited to the SRB assay due to constraints on the project, with other assays planned given further time. The comet assay, also known as single cell gel electrophoresis (SCGE) is a simple method to measure DNA SSBs in eukaryotic cells. The assay involves embedding cells in agarose gel, cell lysis through the addition of detergent and brine, then electrophoresis resulting in the formation of tails made of relaxed DNA that is no longer

supercoiled due to the SSBs.[439] This assay would be of use to investigate whether Blatter radicals, and other compounds analysed in this work, apply their cytotoxic activity through cleavage of the phosphodiester backbone of DNA. Additional exploration may involve the implementation of *in vivo* models based on the expertise of Prof. Ian Hickson, which would give greater insight into the potential use of Blatter radicals as anticancer drugs.



Scheme 197 – Expansion of organocatalysis by *S*-triazolium salts. **A** – Electron-withdrawing substituents are proposed to show promise as organocatalysts given their higher protofugality and lack of steric hindrance about the precarbenic centre. **B** – the introduction of a chiral substituent may allow for asymmetric organocatalysis in benzoin and Stetter reactions.

Nitron analogues **33** are shown to have a dramatic increase in cytotoxicity changing the incubation time from 3 days to 7 days. This is attributed to the ring opening of Nitron to either triazabutadienes **72** or Blatter radicals **37** and **38**. The ability of Nitron to act as a prodrug form requires further exploration, one example being the use of mass spectrometric techniques to investigate the compounds present in the experimental setup following incubation. Consideration of the ability to undergo Blatter radical formation under physiological conditions, in particular the conditions of the cancer TME (**Figure 88**), may allow for Nitron to convert to a cytotoxic species at the tumour site. Effective implementation of Nitron as a prodrug would hopefully lead to less side effects, and therefore a better outcome for a potential patient.

Finally, the initial studies in Chapter 6 regarding ROS scavenging by Blatter radicals can also be expanded based on the initial cell viability studies undertaken in this work. With Blatter radicals not impacting cell viability at concentrations up to 10 μg mL^{-1}, the new Blatter radicals synthesised within the group can now undergo exploration as antioxidants for the prevention of disease.

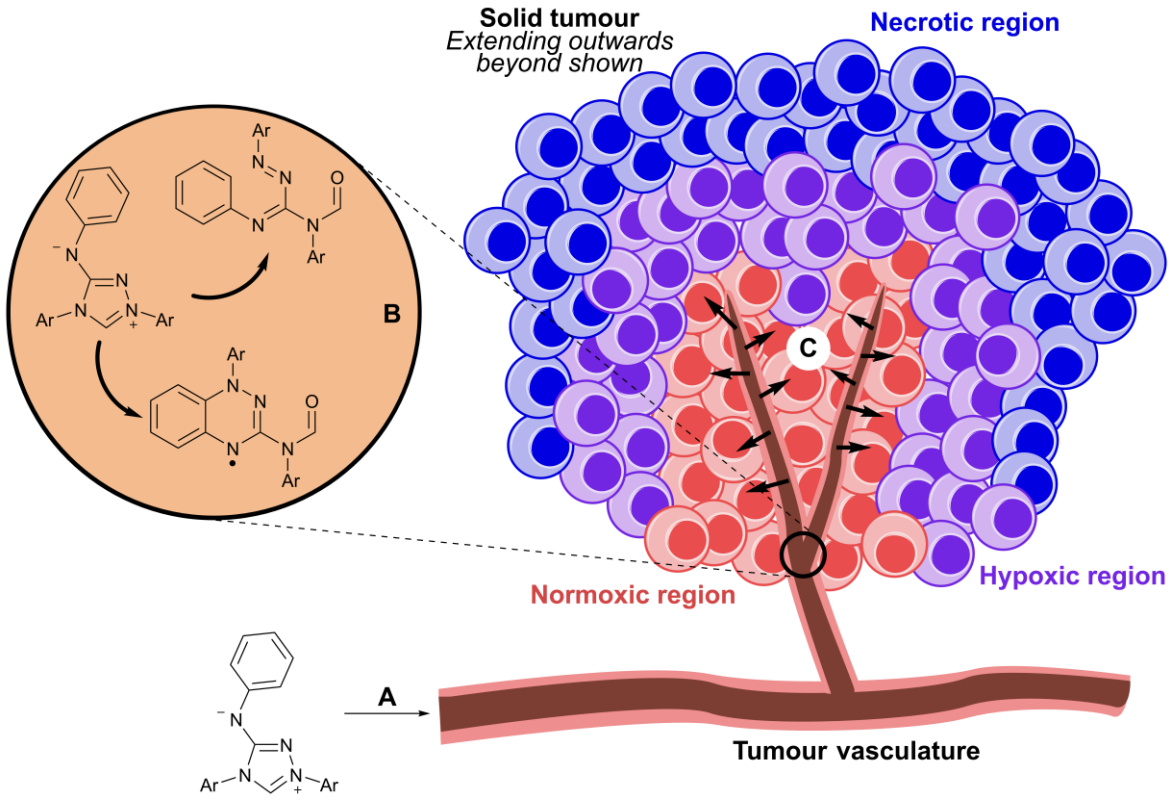


Figure 88 – The potential of Blatter radicals as anticancer prodrugs. **A** – Following administration of Nitron, possibly as the conjugate acid salt, the compound travels *via* the bloodstream to the tumour site. **B** – within close proximity of the cancer tumour, Nitron converts to the Blatter radical or the triazabutadiene. **C** – the ring opened form of Nitron enters the tumour and applies the cytotoxic activity. An alternative to the above is the ring opening of Nitron once within tumour cells.

Additional to the areas described above, many areas of research described in this thesis show promise for future exploration. One example is synthetic expansion towards the development of Blatter radicals with promising antiproliferative activity. The development of new Nitron analogues, described in Chapter 2 and directed by the cytotoxicity data in Chapter 6, can allow for an increased scope of Blatter radicals using the method described in Chapter 3. These radicals can then be analysed in cellular assays towards the development of potent anticancer agents.

8 – Experimental

8.1 – General experimental information – chemistry work

8.1.1 – Materials used

Materials were obtained from Alfa Aesar, Apollo Scientific, Fluorochem, Key Organics, Merck and Tokyo Chemical Industry. The commercial material was used with no further purification or characterisation, apart from the two exceptions detailed below. Deuterated solvents were used from Cambridge isotope laboratories.

2-methyltetrahydrofuran was dried before use: to an evacuated 20 mL microwave vial, containing ~25 3 Å molecular sieves, hydrous 2-methyltetrahydrofuran was added. The solvent was left to stand overnight before first use.

Commercial pentafluoropyridine was distilled before use due to impurities observed by ^{19}F NMR spectroscopy. The fraction afforded at 85 °C was collected and the pure pentafluoropyridine used in experiments.

8.1.2 – Experimental methods and related notation

8.1.2.1 – Microwave-assisted synthesis

Synthesis involving microwave heating was undertaken using a Biotage Initiator system. Reactions were pre-stirred for 5 seconds before heating, with the quoted reaction times referring to the length of time held at the target temperature (fixed hold time).

8.1.2.2 – Photochemical synthesis

Synthesis involving UV light was undertaken using a Penn PhD photoreactor m2, with the light source used noted in the experimental. Light intensity was at 100% for all runs.

8.1.2.3 – Electrochemical synthesis

Electrosynthesis was undertaken using an IKA Electrosyn 2.0 system with graphite, nickel or platinum electrodes. Reactions were undertaken with a constant current, with reaction time determined by the amount of charge supplied. Unless stated otherwise, the current within the solution was flipped every 2 minutes to limit electrode fouling.

Before and after use, the electrodes were cleaned by rinsing with deionised water and acetone, gently scraping the surface with a metal spatula, and then once again rinsing with deionised water followed by acetone. When cleaning prior to use, electrodes were dried using a flow of argon gas.

8.1.2.4 – Flash column chromatography

Flash column chromatography was undertaken with a Puriflash XS520 plus system with fraction collection based upon absorption at 254 nm and implementation of intelligent isocratic mixing. Standard phase flash column chromatography implemented Puriflash high capacity 15 μm silica columns between 4 g and 25 g in size. Reverse phase column chromatography implemented Puriflash biological grade C18-XS 15 μm silica 12 g columns. All organic solvents used were of HPLC grade apart from dichloromethane, which was of analytical reagent grade. Ultrapure water used in reverse phase chromatography was obtained using a PURELAB Chorus 1 system.

8.1.2.5 – Thin layer chromatography

Thin layer chromatography was undertaken using Macherey-Nagel Polygram® Cel 300 plates. Plates were visualized using a UV lamp.

8.1.2.6 – Nuclear magnetic resonance spectroscopy

Unless otherwise noted, nuclear magnetic resonance (NMR) spectra were recorded on a Varian VNMRS-600 spectrometer with operating frequencies of 599.42 MHz for ^{1}H, 92.01 MHz for ^{2}H, 150.72 MHz for ^{13}C{^{1}H} and 60.75 MHz for ^{15}N.

Other spectra were obtained on the following machines, noted within the experimental by the provided codes:

> **A4**: Bruker Avance III-HD-400 spectrometer with operating frequencies of 399.95 MHz for ^{1}H, 128.32 MHz for ^{11}B, 100.57 MHz for ^{13}C{^{1}H}, 376.33 MHz for ^{19}F, 161.90 MHz for ^{31}P
>
> **B4**: Bruker Avance III-HD-400 spectrometer with operating frequencies of 400.07 MHz for ^{1}H, 128.36 MHz for ^{11}B, 100.60 MHz for ^{13}C{^{1}H}, 376.45 MHz for ^{19}F, 161.95 MHz for ^{31}P
>
> **N4**: Bruker Neo-400 spectrometer with operating frequencies of 400.13 MHz for ^{1}H, 128.40 MHz for ^{11}B, 100.63 MHz for ^{13}C{^{1}H}, 376.57 MHz for ^{19}F, 162.00 MHz for ^{31}P
>
> **C5**: Varian DD2-500 spectrometer with operating frequencies of 499.44 MHz for ^{1}H, 76.68 MHz for ^{2}H, 125.61 MHz for ^{13}C{^{1}H}, 470.03 MHz for ^{19}F, 202.21 MHz for ^{31}P

In all cases regardless of machine used, operating frequencies for the elemental isotope of interest are provided in Hz to the nearest integer alongside the observed peaks.

Data was analysed using Mestrelab Research MestReNova software. The notation used in reference to ^{1}H NMR spectra is as follows: s = singlet, d = doublet, t = triplet, q = quartet, qu = quintet, sext = sextet, sept = septet and m = multiplet (spitting unknown); combinations of characters denote

complex splitting (e.g., dt = doublet of triplets) with the splitting patterns given in order from largest to smallest coupling constant. w = weak, br = broad signal. For $^{13}C\{^{1}H\}$NMR, all peaks are singlets unless otherwise noted. Coupling constants (and integrals to the nearest integer where appropriate) are provided for each spectrum peak. The solvent for each experiment is noted, with ^{1}H and $^{13}C\{^{1}H\}$ NMR shift values in ppm relative to the solvent peak. ^{15}N and ^{19}F NMR shift values were not referenced to an internal standard, and so absolute values should be interpreted with caution. Note that ^{15}N NMR shifts are extracted from ^{1}H-^{15}N HMBC experiments.

8.1.2.7 – Electron paramagnetic resonance spectroscopy

EPR spectra were obtained using a Bruker EMX-Micro operating at X-band (9.5 GHz frequency), power 5 mW, modulation frequency 100 kHz, modulation amplitude 1 G. The spectra were recorded at room temperature using 0.1 mM solutions of radicals in degassed toluene.

8.1.2.8 – Infra-red spectroscopy

Infrared spectra were obtained using neat liquid or solid samples on a Perkin Elmer FT-IR Frontier spectrometer.

8.1.2.9 – Liquid chromatography-mass spectrometry

Liquid chromatography-mass spectrometry (LC-MS) data were obtained using a Water Aquity UPLC system with electrospray ionisation (ES+ and ES−) and single quadrupolar detection. Mass spectrometer operating range is between 100 and 2000 amu, with photodiode array detection of absorbance from 210 to 400 nm.

All data is given from either a C_{18} MeOH or MeCN column; Acquity UPLC BEH C_{18} 1.7 µm (2.1 × 50 mm) column with (H_2O/HCO_2H 99.9 : 0.1% v/v): MeOH or MeCN mobile phase. The compound's molecular mass peak is noted alongside the retention time according to the positive electrospray trace.

8.1.2.10 – Liquid chromatography – mass spectrometry – mass spectrometry

Liquid chromatography – mass spectrometry – mass spectrometry (LC-MS-MS) data were obtained using a Waters Acquity UPLC system with electrospray ionisation (ES+ and ES−) and triple quadrupolar detection. The isolated target ion from Q1 is passed through a collision cell (Q2) with 25 eV applied to initiate excitation and collision with Ar gas within the cell. Collision initiates fragmentation scanned within Q3. Mass spectrometer operating range in Q1 and Q3 is between 100 and 2000 amu, with photodiode array detection of absorbance from 210 to 400 nm.

All data is given from either a C_{18} MeOH or MeCN column; Acquity UPLC BEH C_{18} 1.7 µm (2.1 × 50 mm) column with (H_2O/HCO_2H 99.9 : 0.1% v/v): MeOH or MeCN mobile phase. The

compound's molecular mass peak is noted alongside the retention time according to the positive electrospray trace.

8.1.2.11 – Gas chromatography – mass spectrometry

Gas chromatography – mass spectrometry (GC-MS) data was undertaken on a Shimadzu QP2010-Ultra system with a Rxi-5Sil MS column and Helium carrier gas (0.41 mL min^{-1}). A temperature gradient of 30 °C to 300 °C is used with 50 °C min^{-1} temperature increase; a 5 min hold time at 300 °C is used.

8.1.2.12 – High resolution mass spectrometry

High resolution mass spectrometry (HRMS) data was obtained using a FIA Waters Acquity UPLC system with electrospray ionisation (ES+ and ES−) and QtoF Premier mass spectrometer detection. Mass spectrometer operating range is between 100 and 2000 mDa, with photodiode array detection of absorbance from 210 to 400 nm.

All data is given from either a C_{18} MeOH or MeCN column; Acquity UPLC BEH C_{18} 1.7 µm (2.1 × 50 mm) column with (H_2O/HCO_2H 99.9 : 0.1% v/v): MeOH or MeCN mobile phase. Exact mass measurements are processed using Elemental Composition 4.0 embedded within MassLynx 4.1 (Waters Ltd, UK). The compound's experimental molecular mass peak is given alongside the predicted mass for the expected formula, the difference in these values is also provided in mDa.

8.1.2.13 – UV/Vis spectrometry

UV/Vis spectra collected for the purpose of compound characterisation were obtained using a Cary 100 system at 25 °C. Scans were run from 800 to 200 nm at 600 nm min^{-1} (1 nm interval, 0.1 s average time) with a baseline correction before each spectrum was collected. Spectra were obtained in methanol unless stated otherwise.

8.1.2.14 – Single crystal X-ray crystallography

The X-ray crystal data for compounds in this work were either collected on a Bruker D8Venture (Photon100 CMOS detector IµS-microsource, focusing mirrors) 3-circle diffractometer or an Agilent XCalibur (Sapphire-3 CCD detector, fine-focus sealed tube, graphite monochromator) 4-circle diffractometer.

Λ MoKα radiation (λ = 0.71073 Å) was used for all compounds. The temperature on the crystals (120.0 ± 0.2 K) was maintained by an Oxford Cryosystems CryostreamPlus open-flow N_2 cooling device. Corresponding instrument software was used for cell refinement, data collection, data reduction and empirical absorption correction. All structures were solved by either direct or intrinsic phase methods and refined by full-matrix least squares on F^2 for all data using Olex2[440] and

SHELXTL[441] software. All non-disordered non-hydrogen atoms were placed in the calculated positions and refined in riding mode.

8.1.2.15 – Cyclic voltammetry

A potentiostat (PalmSens EmStat3) interfaced with a computer was used for the electrochemical measurements. A three-electrode cell containing a Pt working electrode, Pt counter electrode and Pt wire pseudo-reference electrode were used.

Cyclic voltammetry measurements were carried out on amido and amino Blatter radicals as 2 mM quantities in dried, degassed acetonitrile containing Bu_4NPF_6 electrolyte (0.1 M) which was dried before use. Inert conditions were maintained during measurements. Decamethylferrocene and ferrocene were used as internal references for amido and amino radical respectively. A scan rate of 50 mV s^{-1} was used for measurements. All potentials are quoted relative to the ferrocenium / ferrocene (Cp_2Fe^+ / Cp_2Fe) couple. The decamethylferrocenium / decamethylferrocene ($Cp^*_2Fe^+$ / Cp^*_2Fe) couple has a half-cell potential of −0.50 V relative to the Cp_2Fe^+ / Cp_2Fe couple in this setup. Data was analysed using PSTrace 5.9 software. 5 complete cycles were undertaken in each case, with the data for the third cycle analysed to obtain the potentials.

8.1.2.16 – Elemental analysis

Solid analyte was used for elemental analysis on an Exeter CE-440 Elemental Analyser. Samples were dried *in vacuo* for 24 h before analysis.

8.1.2.17 – Thermogravimetric analysis

Solid analyte was used for thermogravimetric analysis (TGA) on a Perkin Elmer Pyris 1 N5378101 system. Samples were hermetically sealed in aluminium pans with a constant flow of helium (20 mL min^{-1}). The machine was heated from 30 to 300 °C at a rate of 10 °C min^{-1}, followed by cooling at a rate of 200 °C min^{-1} to 30 °C. Sample temperatures were around 220 °C at the end of the experiment. Two-point temperature calibration against nickel (354 °C) and iron (780 °C) was used. Corresponding instrument software was used for obtaining data reports.

8.1.2.18 – In-lab experimental methods

8.1.2.18.1 – T_1 measurements

T_1 values were determined for all *S*-triazolium salts analysed during this work by the inversion recovery method. A free induction decay (FID) array was undertaken where a 180° pulse was applied, and inversion time from 0.0625 and 32 s waited before applying a 90° pulse and an FID obtained. The integral for the signal corresponding to the C(5)-H position was fitted using MestReNova software to a three-parameter exponential fit of the form shown in **Equation 27**. This fit can be compared to a model describing the inversion recovery procedure (**Equation 28**), obtained from the

literature.[442] For **Equation 28**, 'a' and 'b' are complex parameters. A plot of $S(TI_n)$, a sample of the resulting FID at inversion time 'n', against the inversion time gives a three-parameter exponential fit with 'G-value' equal to $1/T_1$ comparing **Equation 28** to the form of **Equation 27**. T_1 values are therefore obtained from the reciprocal of the G-value from fitting experimental data to **Equation 27**.

$$Y' = B + Fe^{-Gx} \qquad \textbf{Equation 27}$$

$$S(TI_n) = a + be^{\frac{TI_n}{T_1}} \qquad \textbf{Equation 28}$$

~2 mg (10 μmol, 10 mM) of *S*-triazolium salts were dissolved dilute DCl solution. To ensure minimal change in the integral of C(5)-H attributable to H/D-exchange, 100 mM DCl was commonly used.

8.1.2.18.2 – C(5)-H/D Exchange Experiments

~2 mg (10 μmol, 10 mM) of *S*-triazolium salts were dissolved in either dilute DCl solution or deuterated formate buffers – a timer was started upon mixing. Tetramethylammonium chloride (TMACl) internal standard (2 μmol, 2 mM) was added and the sample thoroughly mixed using vortex stirring to give 1 mL of reaction mixture. 700 μL of the reaction mixture was placed within an NMR tube, with the remaining 300 μL transferred to an Eppendorf vial and placed in a thermostatted water bath at 25.00 °C. The NMR tube sample was analysed by continuous NMR analysis within a thermostatted instrument at 25.5 ± 0.2 °C – NMR experiment details are provided in **Table 49**. The timer was stopped upon acquisition time starting – a delay time between initial mixing and first spectrum was generally between 4 and 7 minutes. p*D* measurements were taken at the start and end of the experiment using the sample within the Eppendorf tube and were found to vary by a maximum of ± 0.03 units.

Table 49 – Experimental parameters for C(5)-H/D exchange experiments

Parameter	Value
Spectrometer model	Varian DD2-500
Spectrometer probe	5mmSW
Spectrometer frequency for ^{1}H NMR	499.44 Hz
Number of scans	32
Receiver gain	40 Hz
Relaxation delay	35 s
Pulse width	11.4 s
Acquisition time	4.0894 s

8.1.2.18.3 – Initial organocatalytic investigations

~3 mg (10 μmol, 10 mM) of the *S*-triazolium salts were dissolved in 1 mL of triethylamine buffer (NEt_3 / NEt_3HCl, 2 :1, MeOH). TMACl (2 μmol, 2 mM) was added followed by the starting material. The mixture was transferred to an NMR tube and regularly analysed, with the tube held in a thermostatted water bath when not in use. NMR experiment details are provided in **Table 50**.

Table 50 – Experimental parameters for initial organocatalytic experiments

Parameter	Value
Spectrometer model	Bruker Neo-400
Spectrometer probe	Bruker CPP BBO 400S 1 BB-H&F-D-05 Z
Spectrometer frequency for ^{1}H NMR	400.13
Number of scans	1
Receiver gain	20.2 Hz
Relaxation delay	0.1 s
Pulse width	12 s
Acquisition time	4 s

8.1.2.19 – Computational methods and specialist software

DFT calculations were undertaken using the Gaussian 16 interface with GaussView 6 software. Calculations were ran using the Hamilton high-performance computing (HPC) Service of Durham University. Methyl cation affinity (MCA) studies were conducted using the 'Estimating Nucleophilicity and Electrophilicity' (EsNuEl) web application.[185]

Graphs for chemistry-related work (Chapter 2 – 5) were made using OriginLab software, with data fit to in-built linear and non-linear models. Quoted values are reported directly from the software.

8.2 – Syntheses from Chapter 2

8.2.1 – General procedures

8.2.1.1 – General procedure A: Synthesis of amidrazones and triazabutadienes

Hydrazine (1 equiv.) placed in an Ar-filled flask. Toluene (30 mL) was added and the mixture degassed (30 min). Diphenylmethanediimine (**63a**) (1 equiv.) and triethylamine (1.1 equiv.) added, then mixture stirred (RT, 16 h). The mixture was filtered to give the crude product, with further steps discussed for each compound.

8.2.1.2 – General procedure B: Synthesis of Nitron analogues

Ammonium tetrafluoroborate (1 equiv.) combined with amidrazone (1 equiv.) under Ar in a reflux apparatus. Trimethyl orthoformate (40 mL) added and mixture refluxed (16 h), then cooled to RT. Further steps are discussed for each compound.

8.2.1.3 – General procedure C: Synthesis of Nitron esters

To a solution of 1-(4-carboxyphenyl)-4-phenyl-3-(phenylamino)-4*H*-1,2,4-triazol-1-ium chloride (**33iH·Cl**) (1 equiv.) in alcohol (10 mL), cooled on ice, thionyl chloride was added dropwise. The mixture was allowed to warm to RT and then stirred under the conditions given for each compound. The reaction mixture was concentrated *in vacuo*, resuspended in toluene (10 mL), and then concentrated *in vacuo* – this procedure was repeated a further time to give the title compound.

8.2.1.4 – General procedure D: Synthesis of S-triazoles

4-methyl-4*H*-1,2,4-triazole-3-thiol (**85**) (500 mg, 4.35 mmol, 1 equiv.) was combined with copper(I) iodide (82 mg, 0.43 mmol, 10 mol%) and solid aryl halides (1 equiv.) under an Ar atmosphere within a MW vial. Triethylamine (0.67 mL, 4.8 mmol, 1.2 equiv.), acetonitrile (5 mL), water (5 mL) and liquid aryl halides (1 equiv.) added. The mixture was heated (MW, 180 °C, 2 h), then concentrated *in vacuo*. Purification is discussed for each compound.

8.2.1.5 – General procedure E: Synthesis of S-triazolium salts

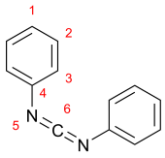
Triazole (1 equiv.) and trimethyloxonium tetrafluoroborate (1.2 equiv.) placed in a MW vial under an Ar atmosphere. DCM (5 mL) added, reaction mixture stirred (RT, 20 h) then concentrated *in vacuo*. The crude product was purified by reverse phase liquid chromatography (10 → 100% MeOH in H_2O) to give the title compound.

8.2.1.6 – General procedure F: Synthesis of Nitron bioconjugates

L-amino acid methyl ester hydrochloride salt (1 equiv.), 1-(4-carboxyphenyl)-4-phenyl-3-(phenylamino)-4*H*-1,2,4-triazol-1-ium chloride (**33iH·Cl**) (1 equiv.) and PyBOP (1.1 equiv.) were

dissolved in DCM (10 mL) within a sealed vial. DIPEA (3.5 equiv.) added, reaction mixture stirred (RT, 24 h). Purification is discussed for each compound.

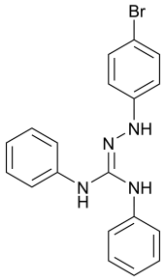
8.2.2 – Diphenylmethanediimine (**63a**)



N,N'-Diphenylthiourea (2.02 g, 8.85 mmol, 1 equiv.) was dissolved in EtOAc (70 mL), and the solution was cooled on ice. Triethylamine (2.45 mL, 17.5 mmol 2 equiv.) was added followed by portionwise addition of I_2 (4.90 g, 19.3 mmol 2.2 equiv.) over 15 min. The mixture was allowed to warm to RT, then stirred (2 h). The resulting mixture was filtered *in vacuo*, the filtrate was washed with aqueous $Na_2S_2O_3$ (1 M, 80 mL), dried over Na_2SO_4, then concentrated *in vacuo*. The resultant oil was diluted in hexanes to precipitate out poly(diphenylmethanediimine), filtered through celite with hexanes as the eluent, then concentrated *in vacuo* to afford diphenylmethanediimine (1.69 g, 8.71 mmol, 98%) as an orange oil.

^{1}H NMR (600 MHz, $CDCl_3$): δ_H 7.17 – 7.23 (6H, m, C^1 and C^3); 7.36 (4H, td, 7.9 and 2.0 Hz, C^2). **^{13}C{^{1}H} NMR (150 MHz, $CDCl_3$):** δ_C 124.3 (C^3); 125.7 (C^1); 129.6 (C^2); 135.4 (C^6); 138.6 (C^4). **LC-MS (MeOH/H_2O):** 213.213, 100%, $[M + H_3O]^+$; 214.239, 13%, $[M + H_4O]^+$; 215.227, 1%, $[M + H_5O]^+$ (2.170 min). 195.198, 100%, $[M + H]^+$; 196.186, 16%, $[M + 2H]^+$; 197.288, 1%, $[M + 3H]^+$; 389.366, 72%, $[2M + 2H]^+$; 390.316, 20%, $[2M + 3H]^+$; 391.342, 3%, $[2M + 4H]^+$ (3.584 min). 227.161, 2%, $[M + CH_5O]^+$; 421.327, 100%, $[2M + CH_5O]^+$; 422.353, 31%, $[2M + CH_6O]^+$; 423.341, 10%, $[2M + CH_7O]^+$; 424.329, 2%, $[2M + CH_8O]^+$ (3.661 min). **GCMS (DCM):** 77.05, 30%, $[M – C_7H_5N_2]^+$; 91.05, 23%, $[M – C_7H_5N]^+$; 104.10, 6%, $[M – C_6H_4N]^+$; 118.10, 3%, $[M – C_6H_5]^+$; 192.10, 2%, $[M – 2H]^+$; 193.10, 10%, $[M – H]^+$; 194.10, 100%, $[M]^+$; 195.10, 15%, $[M + H]^+$; 196.10, 1%, $[M + 2H]^+$ (4.913 min). **HRMS:** 195.0919, $[M + H]^+$ (195.0922 expected for $C_{13}H_{11}N_2$, −0.3 mDa).

8.2.3 – Carbono(*N*-(4-bromophenyl))hydrazonic *N,N'*-diphenyldiamide (**54f**)

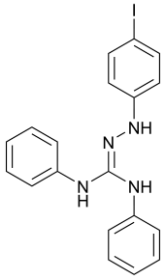


Following general procedure A, 4-bromophenylhydrazine hydrochloride (2.55 g, 11.4 mmol) gave a deep red filtrate and orange solid. The solid was redissolved in DCM (50 mL), washed with saturated

$NaHCO_3$ solution (3 × 20 mL) and then concentrated *in vacuo* to give carbono(*N*-(4-bromophenyl))hydrazonic *N*,*N*'-diphenyldiamide (3.90 g, 10.3 mmol, 90%) as a pale yellow solid. The oxidatively unstable compound was taken forward without further analysis.

LC-MS (MeOH/H_2O): (for ^{79}Br isotopologue) 381.347, 100%, $[M]^+$; 382.411, 40%, $[M + H]^+$; (for ^{81}Br isotopologue) 383.361, 96%, $[M]^+$; 384.426, 37%, $[M + H]^+$; 385.414, 4%, $[M + 2H]^+$ (2.453 min). **HRMS:** 381.0710, $[M + H]^+$ (381.0715 expected for $C_{19}H_{18}N_4{}^{79}Br$, −0.5 mDa).

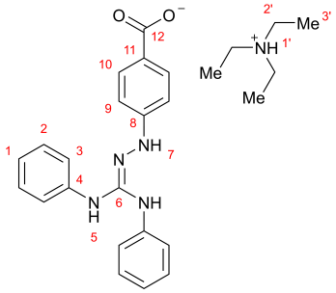
8.2.4 – Carbono(*N*-(4-iodophenyl))hydrazonic *N*,*N*'-diphenyldiamide (**54g**)



Following general procedure A, 4-iodophenylhydrazine hydrochloride (3.83 g, 14.1 mmol) gave the crude product as a yellow solid. The resultant solid was dissolved in DCM (40 mL), washed with saturated $NaHCO_3$ solution (3 × 20 mL) and concentrated *in vacuo* to give carbono(*N*-(4-bromophenyl))hydrazonic *N*,*N*'-diphenyldiamide (5.781 g) with notable amounts of the triazabutadiene byproduct **72g**. The oxidatively unstable compound was taken forward without further analysis.

LC-MS (MeOH/H_2O): 429.187, 100%, $[M + H]^+$; 430.251, 59%, $[M + 2H]^+$; 431.315, 10%, $[M + 3H]^+$ (2.592 min). **HRMS:** 429.0591, $[M + H]^+$ (429.0576 expected for $C_{19}H_{18}N_4{}^{127}I$, +1.5 mDa).

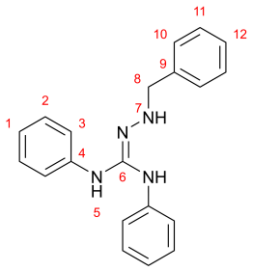
8.2.5 – Triethylammonium 4-(2-(*bis*(phenylamino)methylene)hydrazinyl)-benzoate (**54i**)



Following general procedure A, 4-hydrazinobenzoic acid (3.33 g, 21.9 mmol) gave triethylammonium 4-(2-(*bis*(phenylamino)methylene)hydrazinyl)-benzoate (9.57 g, 21.4 mmol, 98%) as a white solid.

^{1}H NMR (599 MHz, d_6-DMSO): δ_H 1.00 (9 H, t, J = 7.2 Hz, $C^{3'}$); 2.62 (6 H, q, J = 7.2 Hz, $C^{2'}$); 6.81 (2 H, tt, J = 7.5 and 1.2 Hz, C^{1}); 6.91 (2 H, d, J = 8.8 Hz, C^{10}); 7.18 (4 H, td, 7.5 and 1.9 Hz, C^{2}); 7.22 – 7. 51 (4 H, m, C^{3}); 7.70 (2 H, J = 8.8 Hz, C^{9}); 8.25 (2 H, br. s, N^{5}); 8.72 (1 H, s, N^{7}). **^{13}C{^{1}H} NMR (151 MHz, d_6-DMSO):** δ_C 10.7 ($C^{3'}$); 45.5 ($C^{2'}$); 109.8 (C^{4}); 110.5 (C^{10}); 117.0 (C^{8}); 119.9 (C^{1}); 128.7 (C^{2}); 130.8 (C^{3}); 130.9 (C^{9}); 150.6 (C^{11}); 155.8 (C^{12}); 167.6 (C^{6}). **LC-MS (MeCN/H_2O):** 347.447, 100%, $[M + H]^+$; 348.474, 22%, $[M + 2H]^+$; 349.500, 3%, $[M + 3H]^+$ (1.528 min). **HRMS:** 347.1501, $[M + H]^+$ (347.1508 expected for $C_{20}H_{19}N_4O_2$, −0.7 mDa).

8.2.6 – Carbono(*N*-benzyl)hydrazonic *N*,*N*'-diphenyldiamide (**54k**)

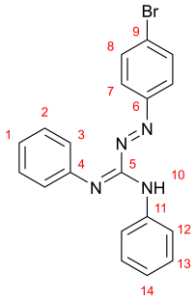


Following general procedure A, benzylhydrazine dihydrochloride (1.70 g, 8.71 mmol) and triethylamine (2.70 mL, 19.4 mmol, 2.2 equiv. – increased over the general procedure due to hydrazine dihydrochloride salt) gave crude carbono(*N*-benzyl)hydrazonic *N*,*N*'-diphenyldiamide (2.19 g) as a white solid also containing small amounts of *N*-heterocyclic by-product and triethylammonium chloride. The crude product (3.27 g) was taken forward to the next step without further purification due to oxidative instability of the amidrazone.

A sample of this crude mixture (~30 mg) was redissolved in DCM (10 mL), washed with saturated $NaHCO_3$ solution (15 mL) and water (10 mL) then dried *in vacuo*. The resultant white solid was used to characterise the compound.

^{1}H NMR (600 MHz, $CDCl_3$): δ_H 3.87 (2H, s, N^{5}); 4.64 (2H, s, C^{8}); 5.30 (1H, s, N^{7}); 6.89 (2H, t, 7.4 Hz, C^{1}); 6.93 (4H, d, J = 7.9 Hz, C^{3}); 7.16 (4H, td, J = 8.5 and 7.3 Hz, C^{2}); 7.29 – 7.33 (3H, m, C^{10} and C^{12}); 7.35 (2H, dd, J = 7.4 and 2.3 Hz, C^{11}). **^{13}C{^{1}H} NMR (150 MHz, $CDCl_3$):** δ_C 56.5 (C^{8}); 121.2 (C^{3}); 122.3 (C^{1}); 127.8 (C^{10}); 128.6 (C^{9}); 128.7 (C^{12}); 128.8 (C^{11}); 129.1 (C^{2}); 137.0 (C^{4}); 151.8 (C^{6}). **LC-MS (MeCN/H_2O):** 317.424, 100%, $[M + H]^+$; 318.450, 58%, $[M + 2H]^+$; 319.476, 9%, $[M + 3H]^+$; 320.464, 1%, $[M + 4H]^+$ (1.862 min). **HRMS:** 317.1772, $[M + H]^+$ (317.1766 expected for $C_{20}H_{21}N_4$, +0.6 mDa).

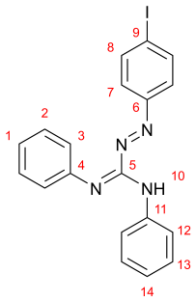
8.2.7 – 2-(4-Bromophenyl)-*N*,*N*'-diphenyldiazene-1-carboximidamide (**72f**)



Following general procedure A, 4-bromophenylhydrazine hydrochloride (2.55 g, 11.4 mmol) gave the impure amidrazone **54f** as an orange solid. A sample of the amidrazone (30 mg) was dissolved in MeOH (2 mL) and left in a vial open to air (RT, 16 h). The solvent was removed by flowing air across the sample, then recrystallised (MeOH) to give 2-(4-bromophenyl)-*N*,*N*'-diphenylhydrazine-1-carboximidamide (7 mg, 0.02 mmol, <1 %) as a red solid.

^{1}H NMR (400 MHz, N4, $CDCl_3$): δ_H 5.83 (1 H, br. s, N^{10}); 7.10 (1 H, tt, J = 7.4 and 0.9 Hz, C^{14}); 7.38 (2 H, td, J = 8.0 and 1.2 Hz, C^{12}); 7.46 – 7.53 (4 H, m, C^{7} and C^{13}); 7.54 – 7.62 (3 H, m, C^{1} and C^{8}); 7.66 (2 H, td, J = 7.3 and 1.6 Hz, C^{3}); 8.00 (2 H, dt, J = 8.9 and 2.5 Hz, C^{2}). **LC-MS (MeOH/H_2O):** (for ^{79}Br isotopologue) 379.333, 100%, $[M + H]^+$; 380.397, 28%, $[M + 2H]^+$; (for ^{81}Br isotopologue) 381.347, 94%, $[M + H]^+$; 382.373, 30%, $[M + 2H]^+$; 383.361, 5%, $[M + 3H]^+$ (3.738 min). **HRMS:** 379.0551, $[M + H]^+$ (379.0558 expected for $C_{19}H_{16}N_4{}^{79}Br$, −0.7 mDa).

8.2.8 – 2-(4-Iodophenyl)-*N*,*N*'-diphenyldiazene-1-carboximidamide (**72g**)

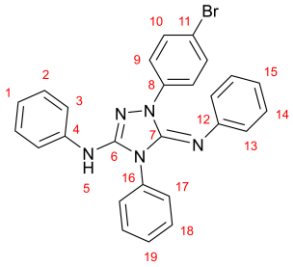


Following general procedure A, 4-iodophenylhydrazine hydrochloride (4.21 g, 15.6 mmol) gave impure amidrazone **54g** as a yellow solid. The crude product was purified by column chromatography (0 → 10% MeOH in DCM) to give 2-(4-iodophenyl)-*N*,*N*'-diphenyldiazene-1-carboximidamide (14 mg, 0.03 mmol, <1%) as a red solid.

^{1}H NMR (599 MHz, $CDCl_3$): δ_H 5.79 (1 H, s, N^{10}); 7.07 (1 H, tt, J = 7.4 and 1.1 Hz, C^{14}); 7.35 (2 H, td, J = 7.7 and 1.2 Hz, C^{12}); 7.46 (2 H, dt, J = 7.6 and 1.1 Hz, C^{13}); 7.48 (2 H, dt, J = 7.0 and 1.1 Hz, C^{3}); 7.57 (1 H, tt, J = 7.7 and 2.2 Hz, C^{1}); 7.63 (2 H, td, J = 7.7 and 1.0 Hz, C^{2}); 7.74 (2 H, dt, J = 9.1 and 2.1 Hz, C^{8}); 7.86 (2 H, dt, J = 9.0 and 2.0 Hz, C^{7}). **^{13}C{^{1}H} NMR (151 MHz, $CDCl_3$):** δ_C

118.0 (C^{13}); 120.1 (C^{7}); 123.1 (C^{14}); 127.7 (C^{3}); 129.5 (C^{12}); 130.2 (C^{1}); 130.7 (C^{2}); 130.8 (C^{11}); 138.0 (C^{8}); 138.0 (C^{4}); 138.1 (C^{6}); 142.6 (C^{9}); 183.3 (C^{5}). **LC-MS (MeOH/H_2O):** 427.172, 100%, $[M + H]^+$; 428.236, 57%, $[M + 2H]^+$; 429.263, 10%, $[M + 3H]^+$; 430.289, 1%, $[M + 4H]^+$ (3.703 min). **HRMS:** 427.0419, $[M + H]^+$ (427.0420 expected for $C_{19}H_{16}N_4{}^{127}I$, −0.1 mDa).

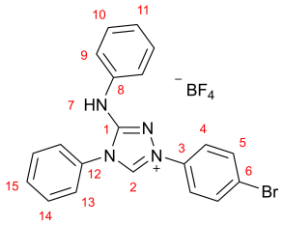
8.2.9 – 1-(4-Bromophenyl)-*N*,4-diphenyl-5-(phenylimino)-4,5-dihydro-1*H*-1,2,4-triazol-3-amine (**75f**)



Toluene (30 mL) was degassed under an Ar atmosphere (30 min), then diphenylmethanediimine (**62a**) (1.70 g, 8.73 mmol, 2 equiv.), 4-bromophenylhydrazine hydrochloride (0.972 g, 4.35 mmol, 1 equiv.) and triethylamine (0.67 mL, 4.8 mmol, 1.1 equiv.) added. Mixture stirred (RT, 19 h) then was concentrated *in vacuo*. The crude product was recrystallised (IPA) to give 1-(4-bromophenyl)-*N*,4-diphenyl-5-(phenylimino)-4,5-dihydro-1*H*-1,2,4-triazol-3-amine (211 mg, 0.439 mmol, 10%) as a red solid.

^{1}H NMR (600 MHz, $CDCl_3$): δ_H 5.63 (1 H, s, N^5); 6.60 (2 H, d, J = 8.3 Hz, C^3); 6.62 (1H, tt, J = 7.3 and 1.3 Hz, C^1); 6.86 (2H, td, J = 6.9 and 1.8 Hz, C^2); 7.08 (1H, tt, J = 7.3 and 1.2 Hz, C^{19}); 7.20 (2 H, dt, J = 5.6 and 4.0 Hz, C^{14}) 7.28 – 7.30 (3 H, m, C^{13} and C^{15}); 7.36 (2 H, td, J = 7.1 and 1.3 Hz, C^{18}); 7.45 (2H, dd, J = 8.7 and 1.3 Hz, C^{17}); 7.51 (2 H, d, J = 9.0 Hz, C^{10}); 8.12 (2 H, d, J = 9.0 Hz, C^9). **^{13}C{^{1}H} NMR (150 MHz, $CDCl_3$):** δ_C 116.4 (C^{11}); 117.7 (C^{17}); 120.8 (C^1); 120.9 (C^9); 122.3 (C^3); 122.8 (C^{19}); 128.2 (C^2); 128.5 (C^{14}); 129.3 (C^{18}); 129.5 (C^{13}); 129.9 (C^{15}); 131.5 (C^{10}); 132.2 (C^{12}); 138.2 (C^{16}); 138.6 (C^8); 140.7 (C^6); 143.7 (C^7); 146.7 (C^4). **LC-MS (MeOH/H_2O):** For ^{79}Br isotopologue – 482.398, 100%, $[M + H]^+$; 483.424, 22%, $[M + 2H]^+$. For ^{81}Br isotopologue – 484.412, 97%, $[M + H]^+$; 485.438, 24%, $[M + 2H]^+$; 486.426, 4%, $[M + 3H]^+$ (2.967 min) **HRMS:** 482.1002, $[M + H]^+$ (482.0980 expected for $C_{26}H_{21}N_5{}^{79}Br$, + 2.2 mDa). **XRD:** Structure verified by XRD, see Appendix A.

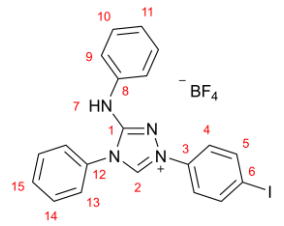
8.2.10 – 1-(4-Bromophenyl)-4-phenyl-3-(phenylamino)-4*H*-1,2,4-triazol-1-ium tetrafluoroborate (**33fH·BF$_4$**)



Following general procedure B, carbono(*N*-(4-bromophenyl))hydrazonic *N*,*N*'-diphenyldiamide (**54f**) (6.24 g, 16.4 mmol) gave a yellow solution. Air was flowed over the solution to give an orange oil. IPA (10 mL) was added to the oil to precipitate 1-(4-bromophenyl)-4-phenyl-3-(phenylamino)-4*H*-1,2,4-triazol-1-ium tetrafluoroborate (2.48 g, 5.18 mmol, 32%) as a white solid.

^{1}H NMR (599 MHz, d$_6$-DMSO): δ_H 7.13 (1 H, tt, *J* = 7.3 and 1.1 Hz, C^{11}); 7.41 (2 H, tdd, *J* = 7.5, 2.0 and 1.2 Hz C^{10}); 7.64 (2 H, dtd, *J* = 7.8, 1.1 and 1.0 Hz, C^9); 7.72 – 7.80 (3 H, m, C^{14} and C^{15}); 7.81 – 7.88 (2 H, m, C^{13}); 7.92 – 7.99 (4 H, m, C^4 and C^5); 9.75 (1 H, s, N^7); 10.90 (1 H, s, C^2). **^{13}C{^{1}H} NMR (151 MHz, d$_6$-DMSO):** δ_C 119.24 (C^9) 122.0 (C^5); 123.0 (C^6); 123.5 (C^{11}); 126.8 (C^{13}); 129.1 (C^{10}); 130.3 (C^{14}); 130.6 (C^{12}); 131.4 (C^{15}); 133.2 (C^4); 134.4 (C^3); 138.3 (C^8); 139.7 (C^2); 150.6 (C^1). **LC-MS (MeOH/H$_2$O):** (For ^{79}Br isotopologue) 391.342, 100%, $[M - BF_4]^+$; 392.368, 22%, $[M + H - BF_4]^+$; (For ^{81}Br isotopologue) 393.356, 97%, $[M - BF_4]^+$; 394.383, 23%, $[M + H - BF_4]^+$ (2.016 min). **HRMS:** 391.0560, $[M - BF_4]^+$ (391.0558 expected for $C_{20}H_{16}N_4{}^{79}Br$, +0.2 mDa). **XRD:** Structure verified by XRD, see Appendix A.

8.2.11 – 1-(4-Iodophenyl)-4-phenyl-3-(phenylamino)-4*H*-1,2,4-triazol-1-ium tetrafluoroborate (**33gH·BF$_4$**)

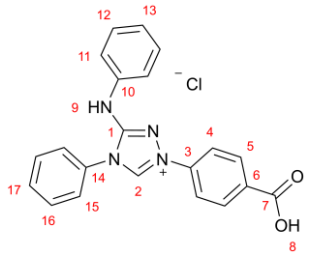


Following general procedure B, carbono(*N*-(4-iodophenyl))hydrazonic *N*,*N*'-diphenyldiamide (6.05 g, 14.1 mmol) led to formation of solid upon cooling. The mixture was filtered to give 1-(4-iodophenyl)-4-phenyl-3-(phenylamino)-4*H*-1,2,4-triazol-1-ium tetrafluoroborate (4.15 g, 7.89 mmol, 56%) as a grey solid.

^{1}H NMR (599 MHz, d$_6$-DMSO): δ_H 7.12 (1 H, tt, *J* = 7.5 and 1.1 Hz, C^{11}); 7.40 (2 H, tt, 8.5 and 2.1 Hz, C^9); 7.62 (2 H, dt, *J* = 8.7 and 2.1 Hz, C^{10}); 7.72 – 7.80 (5 H, m, C^5, C^{14} and C^{15}); 7.82 – 7.85 (2 H, m, C^{13}); 8.09 (2 H, dt, *J* = 8.9 and 2.0 Hz, C^4); 9.73 (1 H, s, N^7); 10.88 (1H, s, C^2). **^{13}C{^{1}H} NMR**

(151 MHz, d_6-DMSO): δ_C 96.3 (C^6); 119.2 (C^{10}); 121.8 (C^5); 123.5 (C^{11}); 126.8 (C^{13}); 129.1 (C^9); 130.3 (C^{14}); 130.6 (C^{12}); 131.4 (C^{15}); 134.7 (C^3); 138.3 (C^8); 138.9 (C^4); 139.6 (C^2); 150.6 (C^1). **LC-MS (MeCN/H_2O):** 439.181, 100%, $[M - BF_4]^+$; 440.246, 59%, $[M + H - BF_4]^+$; 441.272, 10%, $[M + 2H - BF_4]^+$; 442.412, 1%, $[M + 3H - BF_4]^+$ (2.313 min). **HRMS:** 439.0411, $[M - BF_4]^+$ (439.0420 expected for $C_{20}H_{16}N_4{}^{127}I$, −0.9 mDa).

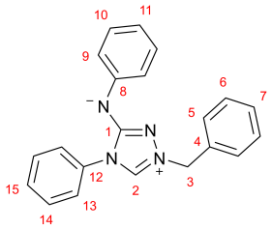
8.2.12 – 1-(4-Carboxyphenyl)-4-phenyl-3-(phenylamino)-4*H*-1,2,4-triazol-1-ium chloride (**33iH·Cl**)



Following general procedure B, triethylammonium 4-(2-(bis(phenylamino)methylene)hydrazinyl)-benzoate (**54i**) (9.57 g, 21.4 mmol) gave a yellow solution containing precipitate. The reaction mixture was filtered, with the solid resuspended in DCM (100 mL) and washed with saturated $NaHCO_3$ solution (5 × 30 mL). The combined aqueous phases were acidified to p*H* 1 by dropwise addition of concentrated HCl to the stirring aqueous phase, to form a precipitate. The aqueous phase was filtered *in vacuo* to afford 1-(4-carboxyphenyl)-4-phenyl-3-(phenylamino)-4*H*-1,2,4-triazol-1-ium chloride (5.14 g, 13.1 mmol, 61%) as a pale pink solid.

^{1}H NMR (599 MHz, CD_3OD): δ_H 7.14 (1 H, tt, *J* = 7.4 and 1.1 Hz, C^{13}); 7.39 (2 H, dt, *J* = 7.5 and 2.0 Hz, C^{11}); 7.64 (2 H, dt, *J* = 7.6 and 1.0 Hz, C^{12}); 7.73 – 7.78 (3 H, m, C^{15} and C^{17}); 7.83 (2 H, dt, *J* = 7.6 and 2.5 Hz, C^{16}); 7.94 (2 H, dt, *J* = 8.8 and 2.0 Hz, C^4); 8.16 (2 H, dt, *J* = 8.8 and 2.3 Hz, C^5); 9.13 (<1 H, s, N^9); 10.61 (<1 H, s, C^2). **^{13}C{^{1}H} NMR (151 MHz, CD_3OD):** δ_C 120.6 (C^4); 120.9 (C^{12}); 125.2 (C^{13}); 127.8 (C^{16}); 130.2 (C^{11}); 131.8 (C^{15}); 132.0 (C^{10}); 132.0 (C^5); 132.9 (C^{17}); 137.6 (C^{14}); 139.4 (C^6); 141.3 (C^2); 152.8 (C^1); 173.0 (C^7). **LC-MS (MeOH/H_2O):** 357.405, 100%, $[M - Cl]^+$; 358.507, 52%, $[M + H - Cl]^+$; 359.495, 9%, $[M + 2H - Cl]^+$; 360.483, 1%, $[M + 3H - Cl]^+$ (2.042 min). **HRMS:** 357.1348, $[M - Cl]^+$ (357.1352 expected for $C_{21}H_{17}N_4O_2$, −0.4 mDa).

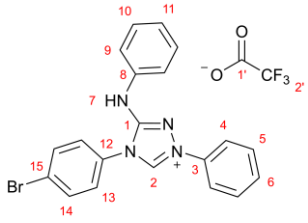
8.2.13 – (1-Benzyl-4-phenyl-4*H*-1,2,4-triazol-1-ium-3-yl)(phenyl)amide (**33k**)



Following general procedure B, carbono(*N*-benzyl)hydrazonic *N*,*N*'-diphenyldiamide (crude, 3.27 g ~8.00 mmol) gave a yellow solution containing precipitate. The crude tetrafluoroborate salt of the title product (**33kH·BF$_4$**) was obtained by filtration of the solution, as a pale grey solid. The tetrafluoroborate salt was dissolved in DCM (40 mL), washed with saturated $NaHCO_3$ solution (2 × 10 mL) and water (2 × 30 mL). The combined organic phases were concentrated *in vacuo* to give impure title product (1.35g, 4.14 mmol, 52%) as a yellow oil. The oil was triturated with diethyl ether (~1 mL), cooled (0 °C, 16 h), then filtered to give (1-benzyl-4-phenyl-4*H*-1,2,4-triazol-1-ium-3-yl)(phenyl)amide (338 mg, 1.04 mmol, 12% based on 8.76 mmol thiourea starting material) as a yellow solid.

^{1}H NMR (599 MHz, CDCl$_3$): δ_H 4.88 (2H, s, C^3); 6.72 (2H, dd, 7.0 and 1.4 Hz, C^5); 6.75 (1H, tt, 7.3 and 1.3 Hz, C^7) 7.01 (2H, td, 7.8 Hz and 1.9 Hz, C^6); 7.18 – 7.22 (3H, m, C^{10} and C^{11}); 7.24 – 7.32 (5H, m, C^9, C^{13} and C^{15}); 7.35 (2H, dt, 8.0 and 2.0 Hz, C^{14}); 7.48 (1H, s, C^2). **^{13}C{^{1}H} NMR (151 MHz, CDCl$_3$):** δ_C 51.5 (C^3); 120.8 (C^7); 122.3 (C^5); 123.9 (C^{14}); 127.5 (C^{10}); 127.7 (C^9); 128.1 (C^{11}); 128.6 (C^{13}); 128.6 (C^6); 129.2 (C^{15}); 134.9 (C^8); 136.6 (C^2); 136.8 (C^4); 144.2 (C^{12}); 148.3 (C^1). **LC-MS (MeOH/H$_2$O):** 327.343, 100%, $[M + H]^+$; 328.445, 61%, $[M + 2H]^+$; 329.433, 12%, $[M + 3H]^+$; 330.421, 1%, $[M + 4H]^+$ (1.707 min). **HRMS:** 327.1620, $[M + H]^+$ (327.1610 expected for $C_{21}H_{19}N_4$, +1.0 mDa).

8.2.14 – 4-(4-Bromophenyl)-1-phenyl-3-(phenylamino)-4*H*-1,2,4-triazol-1-ium trifluoroacetate (**80aH·TFAc**)

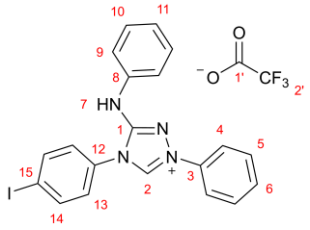


Nitron (200 mg, 0.640 mmol, 1 equiv.) was dissolved in trifluoroacetic acid (conc., 10 mL). *N*-bromosuccinimide (116 mg, 0.652 mmol, 1 equiv.) was added then the reaction mixture was stirred

(RT, 2 h). The reaction mixture was concentrated *in vacuo* to an oil. Trituration of the oil with diethyl ether afforded 4-(4-bromophenyl)-1-phenyl-3-(phenylamino)-4*H*-1,2,4-triazol-1-ium trifluoroacetate (129 mg, 0.255 mmol, 40%) as a white solid.

^{1}H NMR (599 MHz, d$_6$-DMSO): δ_H 7.58 (2 H, dt, C^{13}); 7.61 – 7.65 (3 H, m, C^{14} and C^6); 7.72 (2 H, t, *J* = 7.97 Hz, C^4); 7.74 – 7.79 (3 H, m, C^9 and C^{11}); 7.85 (2 H, dt, *J* = 7.08 and 2.08 Hz, C^{10}); 8.00 (2 H, dt, *J* = 7.70 and 1.46 Hz, C^5); 9.89 (1 H, s, N^7); 10.90 (1 H, s, C^2). **^{13}C{^{1}H} NMR (151 MHz, d$_6$-DMSO):** δ_C 40.1 (C$^{2'}$); 115.0 (C^{12}); 120.0 (C^5); 121.1 (C^{14}); 126.8 (C^{10}); 130.2 (C^4); 130.2 (C^6); 130.2 (C^9); 130.5 (C^8); 131.4 (C^{11}); 131.8 (C^{13}); 134.9 (C^3); 137.9 (C^{15}); 139.5 (C^2); 150.3 (C^1); 157.6 (w q, *J* = 30.55 Hz, C$^{1'}$). **LC-MS (MeOH/H$_2$O):** (For ^{79}Br isotopologue) 391.221, 99%, [M – $CF_3COO]^+$; 392.285, 54%, [M + H – $CF_3COO]^+$ (For ^{81}Br isotopologue) 393.197, 100%, [M – $CF_3COO]^+$; 394.261, 51%, [M + H – $CF_3COO]^+$ (1.829 min). **HRMS:** 391.0561, [M – $CF_3COO]^+$ (391.0558 expected for $C_{20}H_{16}N_4{}^{79}Br$, +0.3 mDa).

8.2.15 – 4-(4-Iodophenyl)-1-phenyl-3-(phenylamino)-4*H*-1,2,4-triazol-1-ium trifluoroacetate (**80bH·TFAc**)

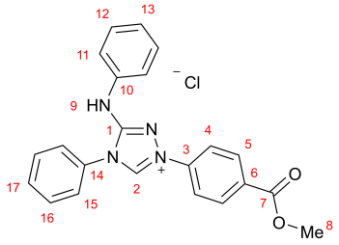


Nitron (2.02 g, 6.46 mmol, 1 equiv.) was dissolved in trifluoroacetic acid (conc., 100 mL). *N*-iodosuccinimide (1.44 g, 6.40 mmol, 1 equiv.) was added then the mixture was stirred (RT, 2 h). The reaction mixture was concentrated *in vacuo*, then diluted in EtOAc (100 mL) and washed with aqueous $Na_2S_2O_3$ (1 M, 2 × 70 mL). The organic phase was dried over Na_2SO_4, then concentrated *in vacuo* to a brown oil. The oil was resuspended in EtOH (100 mL) and filtered into a conical flask, then water (200 mL) was added to the flask to afford a grey precipitate. The flask was swirled briefly to increase the precipitate formed, then the mixture filtered *in vacuo* to give 4-(4-iodophenyl)-1-phenyl-3-(phenylamino)-4*H*-1,2,4-triazol-1-ium trifluoroacetate (2.70 g, 4.89 mmol, 76%) as a grey solid.

^{1}H NMR (600 MHz, d$_6$-DMSO): δ_H 7.49 (2 H, dt, *J* = 8.4 and 1.9 Hz, C^{13}); 7.63 (1 H, t, *J* = 7.9 Hz, C^{11}); 7.70 – 7.78 (7 H, m, C^5, C^6, C^{14} and C^{10}); 7.84 (2 H, dt, *J* = 7.1 and 2.1 Hz, C^9); 8.00 (2 H, dd, C^4); 9.84 (1 H, s, N^7); 10.88 (1 H, s, C^2). **^{13}C{^{1}H} NMR (150 MHz, d^6-DMSO):** δ_C 120.0 (C^4); 120.8 (C^8); 121.4 (C^{13}); 123.6 (C$^{2'}$); 126.8 (C^9); 129.6 (C^1); 130.2 (C^5); 130.2 (C^6); 130.3 (C^{10}); 130.5 (C^{15}); 131.4 (C^{11}); 134.9 (C^3); 137.7 (C^{14}); 138.3 (C^{12}); 139.5 (C^2); 150.2 (C$^{1'}$). **^{19}F NMR (376 MHz, d$_6$-DMSO):** −73.5 (3F, s, C$^{2'}$). **LC-MS (MeCN/H$_2$O):** 313.395, 4%, [M – I – $CF_3COO]^+$; 314.383, 1%,

$[M + H - I - CF_3COO]^+$; 439.227, 100%, $[M - CF_3COO]^+$; 440.291, 55%, $[M + H - CF_3COO]^+$; 441.279, 7%, $[M + 2H - CF_3COO]^+$; 442.229, 1%, $[M + 3H - CF_3COO]^+$ (2.273 min). **HRMS:** 439.0425, $[M - CF_3COO]^+$ (439.0420 expected for $C_{20}H_{16}N_4{}^{127}I$, +0.5 mDa). **UV/Vis**: λ_{max} = 262 nm (216 nm).

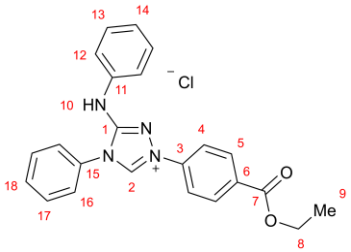
8.2.16 – 1-(4-(Methoxycarbonyl)phenyl)-4-phenyl-3-(phenylamino)-4*H*-1,2,4-triazol-1-ium chloride (**81aH·Cl**)



Following general procedure C, using methanol, thionyl chloride (4 equiv.) and stirring (RT, 16 h), 1-(4-(methoxycarbonyl)phenyl)-4-phenyl-3-(phenylamino)-4*H*-1,2,4-triazol-1-ium chloride (82 mg, 0.20 mmol, 81%) was obtained as an orange solid.

^{1}H NMR (400 MHz, N4, CD$_3$OD): δ_H 3.99 (3 H, s, C^8); 7.18 (1 H, tt, J = 7.4 and 1.1 Hz, C^{13}); 7.40 – 7.45 (2 H, m); 7.66 (2 H, dd, J = 8.9 and 1.1 Hz); 7.87 – 7.76 (5 H, m); 8.15 (2 H, dt, J = 8.9 and 2.3 Hz); 8.33 (2 H, dt, J = 8.9 and 2.3 Hz); 10.75 (<1 H, s, C^2). **^{13}C{^{1}H} NMR (101 MHz, N4, CD$_3$OD):** δ_C 51.7 (C^8), 119.6, 119.9, 124.0, 126.4, 128.8, 130.5, 131.1, 131.7, 137.9, 138.4, 165.5 (C^7). **IR:** 753, 1109, 1285 (C-O), 1500, 1589 (C=C), 1715 (C=O), 2921 (C-H) cm^{-1} . **LC-MS:** 371.9, $[M - Cl]^+$ (2.33 min). **HRMS:** 371.1494, $[M - Cl]^+$ (371.1508 expected for $C_{22}H_{19}N_4O_2$, −1.4 mDa). **XRD:** structure verified by XRD, see Appendix A.

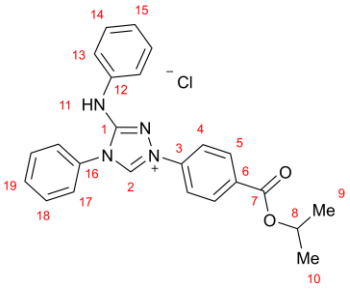
8.2.17 – 1-(4-(Ethoxycarbonyl)phenyl)-4-phenyl-3-(phenylamino)-4*H*-1,2,4-triazol-1-ium chloride (**81bH·Cl**)



Following general procedure C, using ethanol, thionyl chloride (5 equiv.) and stirring (RT, 7 d), 1-(4-(ethoxycarbonyl)phenyl)-4-phenyl-3-(phenylamino)-4*H*-1,2,4-triazol-1-ium chloride (83 mg, 0.20 mmol, 79%) was obtained as a pale yellow solid.

^{1}H NMR (400 MHz, N4, CD_3OD): δ_H 1.44 (3 H, t, *J* = 7.0 Hz, C^9); 4.45 (2 H, q, *J* = 7.2 Hz, C^8); 7.18 (1 H, tt, *J* = 7.5 and 1.1 Hz, C^{14}); 7.40 – 7.45 (2 H, m); 7.66 (2 H, dd, *J* = 8.9 and 1.1 Hz); 7.77 – 7.86 (5 H, m); 8.14 (2 H, dt, *J* = 8.9 and 2.0 Hz); 8.33 (2 H, dt, *J* = 8.9 and 2.0 Hz); 10.73 (1 H, s, C^2). **^{13}C{^{1}H} NMR (101 MHz, N4, CD_3OD):** δ_C 13.2 (C^9); 61.4 (C^8); 119.6; 119.9; 124.0; 126.4; 128.8; 130.5; 131.0; 131.7; 131.9; 137.9; 138.4; 139.3; 151.6; 165.1 (C^7). **IR:** 752, 1130, 1283 (C-O), 1500, 1626 (C=C), 1711 (C=O), 2905 (C-H) cm^{-1}. **LC-MS:** 385.7, $[M - Cl]^+$ (2.54 min). **HRMS:** 385.1670, $[M - Cl]^+$ (385.1665 expected for $C_{23}H_{21}N_4O_2$, +0.5 mDa).

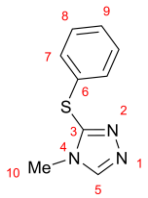
8.2.18 – 1-(4-(Isopropoxycarbonyl)phenyl)-4-phenyl-3-(phenylamino)-4*H*-1,2,4-triazol-1-ium chloride (**81cH·Cl**)



Following general procedure C, using isopropanol, thionyl chloride (10 equiv.) and stirring (70 °C, 5 d), 1-(4-(isopropoxycarbonyl)phenyl)-4-phenyl-3-(phenylamino)-4*H*-1,2,4-triazol-1-ium chloride (75 mg, 0.17 mmol, 69%) was obtained as a light brown solid.

^{1}H NMR (400 MHz, N4, CD_3OD): δ_H 1.43 (6 H, d, *J* = 6.3 Hz, C^9 and C^{10}); 5.29 (1 H, sept, *J* = 6.3 Hz, C^8); 7.18 (1 H, t, *J* = 7.4 Hz, C^{15}); 7.42 (2H, t, *J* = 7.9 Hz); 7.66 (2 H, d, *J* = 7.9 Hz); 7.78 – 7.87 (5 H, m); 8.14 (2 H, d, *J* = 8.6 Hz); 8.31 (2 H, d, *J* = 8.6 Hz). **^{13}C{^{1}H} NMR (101 MHz, N4, CD_3OD):** δ_C 20.7 (C^{10}); 21.9 (C^9); 69.3 (C^8); 119.6; 119.8; 124.0; 126.4; 128.8; 130.5; 131.0; 131.7; 132.3; 137.9; 138.3; 151.5; 164.5 (C^7). **IR:** 692, 751, 1102, 1281 (C-O), 1499, 1709 (C=O), 2853 (C-H), 2921 (C-H), 3236 (N-H) cm^{-1}. **LC-MS:** 399.8, $[M - Cl]^+$ (1.8 min). **HRMS:** 399.1826, $[M - Cl]^+$ (399.1821 expected for $C_{24}H_{23}N_4O_2$, +0.5 mDa).

8.2.19 – 4-Methyl-3-(phenylthio)-4*H*-1,2,4-triazole (**86a**)

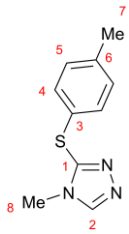


Following general procedure D, iodobenzene (0.49 mL, 4.4 mmol) gave the crude product as a white solid. The crude product was resuspended in DCM (50 mL) and washed with saturated $NaHCO_3$

solution (2 × 20 mL) and water (20 mL). The organic phase was dried (Na_2SO_4) and concentrated *in vacuo* to give 4-methyl-3-(phenylthio)-4*H*-1,2,4-triazole (673 mg, 3.51 mmol, 81%) as a white solid.

^{1}H NMR (600 MHz, d_6-DMSO): δ_H 3.57 (3H, s, C^{10}); 7.24 (2H, ddd, 8.5, 2.4 and 1.2 Hz, C^7); 7.31 (1 H, tt, 7.4 and 1.2 Hz, C^9); 7.37 (2H, tdd, 15.6, 2.2 and 1.6 Hz, C^8); 8.73 (1 H, s, C^5). **^{13}C{^{1}H} NMR (150 MHz, d_6-DMSO):** δ_C 31.3 (C^{10}); 127.5 (C^9); 128.6 (C^7); 129.7 (C^8); 132.1 (C^6); 146.3 (C^3); 147.3 (C^5). **^{15}N NMR (71 MHz, d_6-DMSO):** δ_N 170.9 (N^4); 325.2 (N^1); 335.4 (N^2). **LC-MS (MeOH / H_2O):** 109.082, 78%, $[M - C_3N_3H_4]^+$; 150.164, 30%, $[M - C_2NH_3]^+$ 192.159, 100%, $[M + H]^+$; 193.223, 65%, $[M + 2H]^+$; 194.211, 36%, $[M + 3H]^+$; 195.199, 4%, $[M + 4H]^+$ (1.413 min) **HRMS:** 192.0590 (192.0595 expected for $C_9H_{10}N_3S$, −0.5 mDa). **TLC (9:1 DCM/MeOH):** R_f = 0.48. **XRD:** Structure verified by XRD, see Appendix A.

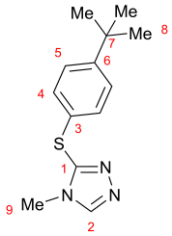
8.2.20 – 4-Methyl-3-(*p*-tolylthio)-4*H*-1,2,4-triazole (**86b**)



Following general procedure D, 4-iodotoluene (948 mg, 4.35 mmol) gave the crude product as a yellow solid. The crude product was redissolved in DCM (50 mL) and washed with saturated $NaHCO_3$ solution (3 × 20 mL). The organic phase was concentrated *in vacuo* to afford 4-methyl-3-(*p*-tolylthio)-4*H*-1,2,4-triazole (534 mg, 2.60 mmol, 60%) as a pale yellow solid.

^{1}H NMR (600 MHz, $CDCl_3$): δ_H 2.29 (3H, s, C^7); 3.55 (3H, s, C^8); 7.09 (2H, dd, 7.9 and 0.7 Hz, C^4); 7.23 (2H, dd, 8.3 and 2.3 Hz, C^5); 8.20 (1H, s, C^2). **^{13}C{^{1}H} NMR (150 MHz, $CDCl_3$):** δ_C 21.2 (C^7); 31.7 (C^8); 127.5 (C^3); 130.5 (C^4); 130.7 (C^5); 138.5 (C^6); 146.1 (C^2); 149.0 (C^1). **LC-MS ($MeOH/H_2O$):** 206.106, 100%, $[M + H]^+$; 207.170, 66%, $[M + 2H]^+$; 208.158, 47%, $[M + 3H]^+$; 209.146, 5%, $[M + 4H]^+$; 210.172, 1%, $[M + 5H]^+$; 228.149, 3%, $[M + Na]^+$ (2.299 min). **XRD:** Structure verified by XRD, see Appendix A.

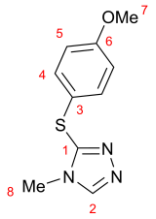
8.2.21 – 3-((4-(*Tert*-butyl)phenyl)thio)-4-methyl-4*H*-1,2,4-triazole (**86c**)



Following general procedure D, 1-(*tert*-butyl)-4-iodobenzene (0.85 mL, 4.78 mmol, 1.1 equiv.) gave the crude product as a pale yellow solid. The reaction mixture was redissolved in DCM (20 mL) and washed with saturated $NaHCO_3$ solution (2 × 10 mL), then the organic phase concentrated *in vacuo*. The crude product was purified by column chromatography (0 → 10% MeOH in DCM) to give 3-((4-(*tert*-butyl)phenyl)thio)-4-methyl-4*H*-1,2,4-triazole (425 mg, 1.72 mmol, 40%) as a colourless solid.

^{1}H NMR (700 MHz, E7, $CDCl_3$): δ_H 1.18 (9 H, s, C^8); 3.52 (3 H, s, C^9); 7.18 (2 H, dd, J = 8.4 and 2.3 Hz, C^4); 7.23 (2 H, dd, J = 8.5 and 2.3 Hz, C^5); 8.21 (1 H, s, C^2). **^{13}C{^{1}H} NMR (176 MHz, E7, $CDCl_3$):** δ_C 31.0 (C^8); 31.6 (C^9); 34.4 (C^7); 126.5 (C^5); 127.3 (C^3); 130.0 (C^4); 146.1 (C^2); 148.5 (C^1); 151.2 (C^6). **LC-MS (MeOH/H_2O):** 248.250, 100%, $[M + H]^+$; 349.276, 21%, $[M + 2H]^+$; 250.302, 7%, $[M + 3H]^+$ (3.148 min). **HRMS:** 248.1239, $[M + H]^+$ (248.1221 expected for $C_{13}H_{18}N_3S$, +1.8 mDa).

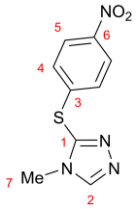
8.2.22 – 3-((4-Methoxyphenyl)thio)-4-methyl-4*H*-1,2,4-triazole (**86d**)



Following general procedure D, 4-iodoanisole (1.21 g, 5.16 mmol, 1.2 equiv.) gave the crude product as a white solid. The crude product was purified by column (0 → 10% MeOH in DCM), with the product fractions concentrated *in vacuo*. The product was redissolved in DCM (40 mL), washed with saturated $NaHCO_3$ solution (2 × 20 mL) and water (20 mL), then concentrated *in vacuo* to give 3-((4-methoxyphenyl)thio)-4-methyl-4*H*-1,2,4-triazole (279 mg, 1.26 mmol, 29%) as a white solid.

^{1}H NMR (599 MHz, $CDCl_3$): δ_H 3.59 (3 H, s, C^8); 3.78 (3 H, s, C^7); 6.85 (2 H, d, 8.9 Hz, C^5); 7.40 (2 H, d, 8.7 Hz, C^4); 8.22 (1 H, s, C^2). **^{13}C{^{1}H} NMR (151 MHz, $CDCl_3$):** δ_C 31.6 (C^8); 55.4 (C^7); 115.2 (C^5); 120.7 (C^3); 149.6 (C^1); 133.5 (C^4); 145.8 (C^2); 160.1 (C^6). **LC-MS (MeOH/H_2O):** 222.220, 100%, $[M + H]^+$; 223.284, 24%, $[M + 2H]^+$; 225.261, 1%, $[M + 3H]^+$; 244.264, 2%, $[M + Na]^+$ (2.042 min). **HRMS:** 222.0721, $[M + H]^+$ (222.0701 expected for $C_{10}H_{12}N_3OS$, +2.0 mDa).

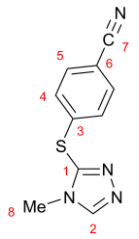
8.2.23 – 4-Methyl-3-((4-nitrophenyl)thio)-4*H*-1,2,4-triazole (**86e**)



Following general procedure D, 1-bromo-4-nitrobenzene (1.08 g, 4.35 mmol) gave the crude product as a yellow solid. The solid was partitioned between DCM (50 mL) and saturated $NaHCO_3$ solution (30 mL), the aqueous phase further washed with DCM (20 mL), and the combined organic phases concentrated *in vacuo* to afford 4-methyl-3-((4-nitrophenyl)thio)-4*H*-1,2,4-triazole (969 mg, 3.98 mmol, 91%) as a yellow solid.

^{1}H NMR (700 MHz, E7, $CDCl_3$): δ_H 3.67 (3 H, s, C^7); 7.36 (2 H, dt, 9.7 and 2.4 Hz, C^5); 8.15 (2 H, ddd, 9.7 and 2.4 Hz, C^4); 8.37 (1 H, s, C^2). **^{13}C{^{1}H} NMR (176 MHz, E7, $CDCl_3$):** δ_C 31.9 (C^7); 124.7 (C^4); 128.3 (C^5); 141.2 (C^3); 145.9 (C^1); 146.8 (C^2); 147.0 (C^6). **IR:** 1342 (N-O); 1505 (N-O); 1575 (C=C); 1597 (C=N); 2927 (C-H, aliphatic); 3094 cm^{-1} (C-H, aromatic). **LC-MS (MeOH / H_2O):** 191.171, 82%, $[M - NO_2]^+$; 207.209, 14%, $[M - C_2NH_3]^+$; 237.194, 100%, $[M + H]^+$; 238.220, 62%, $[M + 2H]^+$; 239.208, 41%, $[M + 3H]^+$; 240.196, 5%, $[M + 4H]^+$; 241.260, 1%, $[M+ 5H]^+$ (1.783 min). **HRMS:** 237.0443, $[M+H]^+$ (237.0446 expected for $C_9H_9N_4O_2S$, −0.3 mDa). **TLC (9:1 DCM/MeOH):** R_f = 0.52. **XRD:** Structure verified by XRD, see Appendix A.

8.2.24 – 4-((4-Methyl-4*H*-1,2,4-triazol-3-yl)thio)benzonitrile (**86f**)

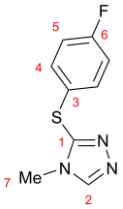


Following general procedure D, 4-bromobenzonitrile (793 mg, 4.35 mmol) gave the crude product as a yellow solid. The crude product was purified by column chromatography (0 → 10% MeOH in DCM), with the product fractions concentrated *in vacuo*. The purified product was redissolved in DCM (30 mL), washed with saturated $NaHCO_3$ solution (2 × 20 mL) and concentrated *in vacuo* to afford 4-((4-methyl-4*H*-1,2,4-triazol-3-yl)thio)benzonitrile (115 mg, 0.532 mmol, 12%) as a pale yellow solid.

^{1}H NMR (599 MHz, $CDCl_3$): δ_H 3.65 (3 H, s, C^8); 7.34 (2 H, dtd, J = 8.2, 1.9 and 0.5 Hz, C^4); 7.58 (2 H, dtd, J = 8.2, 2.0 and 0.5 Hz, C^5); 8.34 (1 H, s, C^2). **^{13}C{^{1}H} NMR (151 MHz, $CDCl_3$):** δ_C 31.9 (C^8); 111.3 (C^3); 118.2 (C^7); 128.7 (C^4); 133.1 (C^5); 139.0 (C^6); 146.1 (C^1); 146.7 (C^2). **LC-MS**

(MeOH/H_2O): 217.166, 100%, $[M + H]^+$; 218.268, 33%, $[M + 2H]^+$; 219.218, 14%, $[M + 3H]^+$; 220.244, 1%, $[M + 4H]^+$ (1.579 min). **HRMS:** 217.0543, $[M + H]^+$ (217.0548 expected for $C_{10}H_9N_4S$, −0.5 mDa).

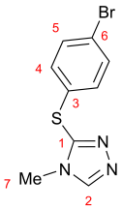
8.2.25 – 3-((4-Fluorophenyl)thio)-4-methyl-4*H*-1,2,4-triazole (**86g**)



Following general procedure D, 1-bromo-4-fluorobenzene (0.53 mL, 4.78 mmol, 1.1 equiv.) gave the crude product as a pale yellow solid. The reaction mixture was resuspended in DCM (20 mL), washed with saturated $NaHCO_3$ solution (2 × 20 mL) and water (10 mL), then the organic phase concentrated *in vacuo*. The crude product was purified by column chromatography (0 → 10% MeOH in DCM) to give 3-((4-fluorophenyl)thio)-4-methyl-4*H*-1,2,4-triazole (712 mg, 3.39 mmol, 78%) as a colourless solid.

^{1}H NMR (400 MHz, B4, $CDCl_3$): δ_H 3.61 (3 H, s, C^7); 7.01 (2 H, td, J = 8.6, C^4); 7.41 (2 H, dddd, J = 9.0, 5.1, 3.2 and 2.1 Hz, C^5); 8.30 (1H, s, C^2). **^{13}C{^{1}H} NMR (101 MHz, B4, $CDCl_3$):** δ_C 31.8 (C^7); 117.0 (d, J = 22.2 Hz, C^5); 125.8 (d, J = 3.4 Hz, C^3); 133.2 (d, J = 8.4 Hz, C^4); 141.6 (C^2); 146.2 (C^1); 162.9 (d, J = 249.4 Hz, C^6). **^{19}F NMR (376 MHz, B4, $CDCl_3$):** δ_F −112.4 (tt, J = 8.4 and 5.1 Hz, C^6). **LC-MS (MeOH/H_2O):** 210.207, 100%, $[M + H]^+$; 211.195, 12%, $[M + 2H]^+$; 212.183, 5%, $[M + 3H]^+$ (2.141 min). **HRMS:** 210.0512, $[M + H]^+$ (210.0501 expected for $C_9H_9N_3FS$, +1.1 mDa).

8.2.26 – 3-((4-Bromophenyl)thio)-4-methyl-4*H*-1,2,4-triazole (**86h**)

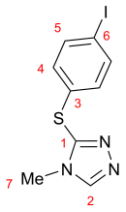


Following general procedure D, 4-bromoiodobenzene (1.23 g, 4.35 mmol, 1 equiv.) gave the crude product as a colourless solid. The reaction mixture was redissolved in DCM (30 mL), washed with saturated $NaHCO_3$ solution (2 × 20 mL) and concentrated *in vacuo* to give 3-((4-bromophenyl)thio)-4-methyl-4*H*-1,2,4-triazole (352 mg, 1.31 mmol, 75%) as a white solid.

^{1}H NMR (600 MHz, $CDCl_3$): δ_H 3.59 (3 H, s, C^7); 7.18 (2 H, dd, J = 6.6 and 2.1 Hz, C^5); 7.40 (2 H, dd, J = 6.6 and 2.0 Hz, C^4); 8.25 (1 H, s, C^2). **^{13}C{^{1}H} NMR (151 MHz, $CDCl_3$):** δ_C 31.7 (C^7); 122.3 (C^3); 130.5 (C^6); 131.5 (C^5); 132.8 (C^4); 146.3 (C^2); 147.8 (C^1). **LC-MS (MeOH/H_2O):** (For ^{79}Br

isotopologue) 270.145, 100%, $[M + H]^+$; 271.210, 22%, $[M + 2H]^+$; (For ^{81}Br isotopologue) 272.160, 98%, $[M + H]^+$; 273.224, 20%, $[M + 2H]^+$ (2.401 min).

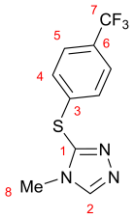
8.2.27 – 3-((4-Iodophenyl)thio)-4-methyl-4*H*-1,2,4-triazole (**86i**)



Following general procedure D, 1,4-diiodobenzene (1.43 g, 4.34 mmol) gave the crude product as a yellow solid. The crude product was purified by column chromatography (0 → 10% MeOH in DCM) to give 3-((4-iodophenyl)thio)-4-methyl-4*H*-1,2,4-triazole (547 mg, 1.73 mmol, 40%) as a colourless solid.

^{1}H NMR (599 MHz, $CDCl_3$): δ_H 3.60 (3 H, s, C^7); 7.06 (2 H, ddd, J = 8.58, 2.58 and 1.92 Hz, C^5); 7.62 (2 H, ddd, J = 8.57, 2.55 and 2.04 Hz, C^4); 8.26 (1 H, s, C^2). **^{13}C{^{1}H} NMR (151 MHz, $CDCl_3$):** δ_C 31.8 (C^7); 93.6 (C^6); 131.5 (C^3); 131.6 (C^5); 138.7 (C^4); 146.5 (C^1); 147.8 (C^2). **LC-MS ($MeOH/H_2O$):** 318.064, 100%, $[M + H]^+$; 319.128, 41%, $[M + 2H]^+$; 320.116, 21%, $[M + 3H]^+$; 321.218, 2%, $[M + 4H]^+$ (2.540 min). **HRMS:** 317.9567, $[M + H]^+$ (317.9562 expected for $C_9H_9N_3S^{127}I$, +0.5 mDa).

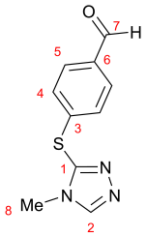
8.2.28 – 4-Methyl-3-((4-(trifluoromethyl)phenyl)thio)-4*H*-1,2,4-triazole (**86j**)



Following general procedure D, 4-iodobenzotrifluoride (0.70 mL, 4.78 mmol, 1.1 equiv.) gave the crude product as a pale yellow solid. The reaction mixture was redissolved in DCM (30 mL) and washed with saturated $NaHCO_3$ solution (20 mL), with the organic phase concentrated *in vacuo*. The crude product was purified by column chromatography (0 → 10% MeOH in DCM) to give 4-methyl-3-((4-(trifluoromethyl)phenyl)thio)-4*H*-1,2,4-triazole (774 mg, 2.99 mmol, 69%) as a colourless solid.

^{1}H NMR (400 MHz, B4, $CDCl_3$): δ_H 3.60 (3 H, s, C^8); 7.29 (2 H, d, 8.1 Hz, C^4); 7.49 (2 H, d, 8.2 Hz, C^5); 8.34 (1 H, s, C^2). **^{19}F NMR (376 MHz, B4, $CDCl_3$):** δ_F −62.8 (t, J = 0.8 Hz, C^7). **LC-MS ($MeOH/H_2O$):** 260.183, 100%, $[M + H]^+$; 261.247, 11%, $[M + 2H]^+$; 262.159, 6%, $[M + 3H]^+$ (2.662 min). **HRMS:** 260.0489, $[M + H]^+$ (260.0469 expected for $C_{10}H_9N_3F_3S$, +2.0 mDa).

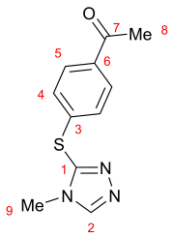
8.2.29 – 4-((4-Methyl-4*H*-1,2,4-triazol-3-yl)thio)benzaldehyde (**86k**)



Following general procedure D, 4-bromobenzaldehyde (805 mg, 4.35 mmol) gave the crude product as a pale yellow solid. The reaction mixture was concentrated *in vacuo* and purified by column chromatography (0 → 10% MeOH in DCM). The product fractions were concentrated *in vacuo*, redissolved in DCM (20 mL), and washed with saturated $NaHCO_3$ solution (2 × 10 mL). The organic phase was concentrated *in vacuo* to give 4-((4-methyl-4*H*-1,2,4-triazol-3-yl)thio)benzaldehyde (158 mg, 0.721 mmol, 17%) as a white solid.

^{1}H NMR (599 MHz, $CDCl_3$): δ_H 3.64 (3 H, s, C^8); 7.34 (2 H, dt, J = 8.3 and 1.8 Hz, C^4); 7.78 (2 H, dt, J = 8.6 and 2.0 Hz, C^5); 8.35 (1 H, s, C^2); 9.94 (1 H, s, C^7). **^{13}C{^{1}H} NMR (151 MHz, $CDCl_3$):** δ_C 31.8 (C^8); 128.3 (C^4); 130.7 (C^5); 135.2 (C^6); 140.3 (C^3); 146.4 (C^1); 146.7 (C^2); 191.0 (C^7). **LC-MS (MeOH/H_2O):** 220.168, 100%, $[M + H]^+$; 221.270, 39%, $[M + 2H]^+$; 222.258, 18%, $[M + 3H]^+$ (1.553 min). **HRMS:** 220.0545, $[M + H]^+$ (220.0545 expected for $C_{10}H_{10}N_3OS$, 0 mDa). **XRD:** Product verified by XRD, see Appendix A.

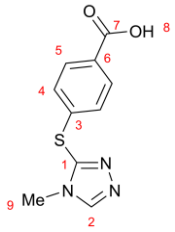
8.2.30 – 1-(4-((4-Methyl-4*H*-1,2,4-triazol-3-yl)thio)phenyl)ethan-1-one (**86l**)



Following general procedure D, 4-bromoacetophenone (864 mg, 4.34 mmol) gave the crude product as a bright-yellow solid. The reaction mixture was redissolved in DCM (20 mL) and washed with saturated $NaHCO_3$ solution (2 × 10 mL), with the organic phase concentrated *in vacuo*. The crude product was purified by column chromatography (0 → 10% MeOH in DCM) to give 1-(4-((4-methyl-4*H*-1,2,4-triazol-3-yl)thio)phenyl)ethan-1-one (99 mg, 0.42 mmol, 10%) as a pale yellow solid.

^{1}H NMR (700 MHz, E7, $CDCl_3$): δ_H 2.54 (3 H, s, C^8); 3.61 (3 H, s, C^9); 7.27 (2 H, d, J = 8.4 Hz, C^4); 7.85 (2 H, d, J = 8.5 Hz, C^5); 8.36 (1 H, s, C^2). **^{13}C{^{1}H} NMR (176 MHz, E7, $CDCl_3$):** δ_C 26.6 (C^8); 31.8 (C^9); 128.3 (C^4); 129.5 (C^5); 136.0 (C^6); 138.3 (C^3); 146.7 (C^2); 146.8 (C^1); 197.0 (C^7). **LC-MS (MeOH/H_2O):** 234.188, 100%, $[M + H]^+$; 235.252, 11%, $[M + 2H]^+$; 236.240, 6%, $[M + 3H]^+$ (1.881 min). **HRMS:** 234.0722, $[M + H]^+$ (234.0701 expected for $C_{11}H_{12}N_3OS$, +2.1 mDa).

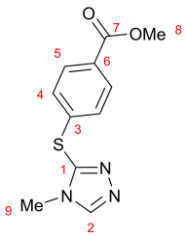
8.2.31 – 4-((4-Methyl-4*H*-1,2,4-triazol-3-yl)thio)benzoic acid (**86m**)



Following general procedure D, 4-bromobenzoic acid (875 mg, 4.35 mmol) and triethylamine (1.33 mL, 9.58 mmol, 2.2 equiv.) gave the crude product (1.15 g) as a colourless solid. The mixture was verified by ^{1}H NMR to be crude 4-((4-methyl-4*H*-1,2,4-triazol-3-yl)thio)benzoic acid with 97% product and 3% residual 4-methyl-*4H*-1,2,4-triazole-3-thiol.

LC-MS (MeCN/H$_2$O): 236.164, 100%, $[M + H]^+$; 237.228, 21%, $[M + 2H]^+$; 238.216, 12%, $[M + 3H]^+$; 239.356, 2%, $[M + 4H]^+$ (1.134 min). **HRMS:** 236.0500, $[M + H]^+$ (236.0494 expected for $C_{10}H_{10}N_3O_2S$, +0.6 mDa).

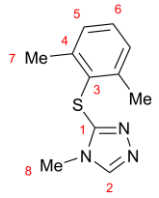
8.2.32 – Methyl 4-((4-methyl-4*H*-1,2,4-triazol-3-yl)thio)benzoate (**86n**)



Following general procedure D, methyl 4-iodobenzoate (1.14 g, 4.34 mmol) gave the crude product as a pale yellow solid. The reaction mixture was redissolved in DCM (20 mL), washed with saturated $NaHCO_3$ solution (2 × 10 mL) and the organic phase concentrated *in vacuo*. The crude product was purified by column chromatography (0 → 10% MeOH in DCM) to give methyl 4-((4-methyl-4*H*-1,2,4-triazol-3-yl)thio)benzoate (228 mg, 0.915 mmol, 21%) as a white solid.

^{1}H NMR (700 MHz, E7, CDCl$_3$): δ_H 3.63 (3 H, s, C^9); 3.90 (3 H, s, C^8); 7.29 (2 H, d, J = 8.4 Hz, C^4); 7.96 (2 H, d, J = 8.2 Hz, C^5); 8.41 (1 H, s, C^2). **^{13}C{^{1}H} NMR (176 MHz, E7, CDCl$_3$):** δ_C 31.9 (C^9); 52.5 (C^8); 128.4 (C^4); 129.5 (C^3); 130.8 (C^5); 137.9 (C^6); 146.6 (C^2); 166.3 (C^7); C^1 not observed due to low signal-to-noise ratio. **LC-MS (MeOH/H$_2$O):** 250.188, 100%, $[M + H]^+$; 251.252, 57%, $[M + 2H]^+$; 252.240, 26%, $[M + 3H]^+$; 253.228, 3%, $[M + 4H]^+$; 272.154, 1%, $[M + Na]^+$; 499.303, 74%, $[2M + H]^+$; 500.329, 24%, $[2M + 2H]^+$; 501.279, 12%, $[2M + 3H]^+$; 502.381 $[2M + 4H]^+$; 503.521, 1%, $[2M + 5H]^+$ (2.176 min). **HRMS:** 250.0663, $[M + H]^+$ (250.0650 expected for $C_{11}H_{12}N_3O_2S$, +1.3 mDa). **XRD:** Structure verified by XRD, see Appendix A.

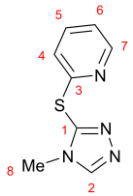
8.2.33 – 3-((2,6-Dimethylphenyl)thio)-4-methyl-4*H*-1,2,4-triazole (**86o**)



Following general procedure D, 2-iodo-1,3-dimethylbenzene (0.63 mL, 4.4 mmol) gave the crude product as a light yellow solid. The crude product was redissolved in DCM (40 mL), washed with saturated $NaHCO_3$ solution (2 × 10 mL) and the organic phase concentrated *in vacuo* to afford 3-((2,6-dimethylphenyl)thio)-4-methyl-4H-1,2,4-triazole (689 mg, 3.14 mmol, 72%) as a light yellow solid.

^{1}H NMR (599 MHz, $CDCl_3$): δ_H 2.47 (6 H, s, C^7); 3.55 (3 H, s, C^8); 7.14 (2 H, dq, 7.3 and 0.7 Hz, C^5); 7.21 (1 H, dd, 8.2 and 6.8 Hz, C^6); 8.10 (1 H, s, C^2). **^{13}C{^{1}H} NMR (151 MHz, $CDCl_3$):** δ_C 22.2 (C^7); 31.3 (C^8); 127.34 (C^4); 129.0 (C^5); 130.0 (C^6); 143.1 (C^3); 145.2 (C^2); 149.8 (C^1). **LC-MS (MeCN/H_2O):** 220.244, 100%, $[M + H]^+$; 221.346, 40%, $[M + 2H]^+$; 222.296, 17%, $[M + 3H]^+$; 223.322, 2%, $[M + 4H]^+$ (2.478 min). **HRMS:** 220.0899, $[M + H]^+$ (220.0908 expected for $C_{11}H_{14}N_3S$, −0.9 mDa).

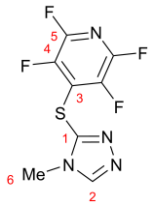
8.2.34 – 2-((4-Methyl-4*H*-1,2,4-triazol-3-yl)thio)pyridine (**86p**)



Following general procedure D, 2-bromopyridine (0.425 mL, 4.35 mmol) gave the crude product as a pale yellow solid. The crude product was redissolved in DCM (30 mL), washed with H_2O (20 mL) and saturated $NaHCO_3$ solution (2 × 10 mL), then concentrated *in vacuo* to afford 2-((4-methyl-4*H*-1,2,4-triazol-3-yl)thio)pyridine (510 mg, 2.65 mmol, 61%) as a white solid.

^{1}H NMR (700 MHz, E7, $CDCl_3$): δ_H 3.70 (3 H, s, C^8); 7.08 (1 H, ddd, J = 7.6, 4.8 and 1.0 Hz, C^6); 7.16 (1 H, dd, J = 8.0 and 1.1 Hz, C^4); 7.56 (1 H, td, J = 7.8 and 1.9 Hz, C^5); 8.34 (1 H, dd, J = 5.0 and 1.9 Hz, C^7); 8.35 (1 H, s, C^2). **^{13}C{^{1}H} NMR (176 MHz, E7, $CDCl_3$):** δ_C 32.0 (C^8); 121.5 (C^6); 122.1 (C^4); 137.4 (C^5); 146.2 (C^3); 146.7 (C^2); 150.2 (C^7); 155.9 (C^1). **LC-MS (MeOH/H_2O):** 193.184, 100%, $[M + H]^+$; 194.286, 27%, $[M + 2H]^+$ 195.274, 12%, $[M + 3H]^+$; 196.224, 1%, $[M + 4H]^+$ (1.219 min). **HRMS:** 193.0549, $[M + H]^+$ (193.0548 expected for $C_8H_9N_4S$, +0.1 mDa).

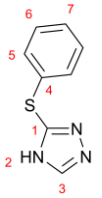
8.2.35 – 2,3,5,6-Tetrafluoro-4-((4-methyl-4*H*-1,2,4-triazol-3-yl)thio)pyridine (**86q**)



4-methyl-*4H*-1,2,4-triazole-3-thiol (500 mg, 4.34 mmol, 1 equiv.) and K_2CO_3 (720 mg, 5.21 mmol, 1.2 equiv.) were dissolved in MeCN (20 mL). Pentafluoropyridine (0.57 mL, 5.21 mmol, 1.2 equiv.) was added then the mixture was stirred (RT, 150 min). The reaction mixture was concentrated *in vacuo*, resuspended in DCM (50 mL), washed with water (2 × 20 mL) then concentrated *in vacuo* to give 2,3,5,6-tetrafluoro-4-((4-methyl-4*H*-1,2,4-triazol-3-yl)thio)pyridine (1.07 g, 4.05 mmol, 93%) as a white solid.

^{1}H NMR (599 MHz, $CDCl_3$): δ_H 3.83 (3 H, s, C^6); 8.31 (1 H, s, C^2). **$^{13}C\{^1H\}$ NMR (151 MHz, $CDCl_3$):** δ_C 32.1 (C^6); 126.0 (t, J = 16.9 Hz, C^3); 140.9 (ddd, J = 259.8, 28.8 and 9.8 Hz, C^5); 143.3 (C^1); 143.7 (dtt, J = 248.3, 13.6 and 3.6 Hz, C^4); 146.6 (C^2). **^{19}F NMR (A4, 376 MHz, $CDCl_3$):** δ_F −137.4 (C^4); −88.5 (C^5). **LC-MS ($MeOH/H_2O$):** 265.124, 100%, $[M + H]^+$; 266.188, 55%, $[M + 2H]^+$; 267.138, 36%, $[M + 3H]^+$; 268.202, 4%, $[M + 4H]^+$ (1.534 min). **HRMS:** 265.0167, $[M + H]^+$ (265.0171 expected for $C_8H_5N_4SF_4$, −0.4 mDa). **XRD:** Structure verified by XRD, see Appendix A.

8.2.36 – 3-(Phenylthio)-4*H*-1,2,4-triazole (**89**)

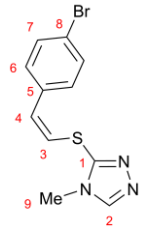


3-mercapto-1,2,4-triazole (500 mg, 4.94 mmol, 1 equiv.) and copper(I) iodide (95 mg, 0.50 mmol, 10 mol%) were added to a microwave vial which was stringently evacuated and backfilled with Ar. MeCN (7 mL), H_2O (7 mL), triethylamine (0.83 mL, 6.0 mmol, 1.2 equiv.) and iodobenzene (0.55 mL, 4.9 mmol, 1 equiv.) were added to the vial. The vial was heated (MW, 180 °C, 2 h), then the solvent removed *in vacuo* to give a pale yellow solid. The reaction mixture was resuspended in DCM (40 mL), washed with concentrated $NaHCO_3$ solution (2 × 20 mL), aqueous EDTA solution (5 w%, 2 × 10 mL), then filtered through celite. The filtrate was concentrated *in vacuo* to give 3-(phenylthio)-4*H*-1,2,4-triazole (440 mg, 2.49 mmol, 50%) as a white solid.

^{1}H NMR (600 MHz, $CDCl_3$): δ_H 7.33 – 7.40 (3H, m, C^5 and C^7); 7.54 (2H, dd, 7.8 and 1.9 Hz, C^6); 8.05 (1H, s, C^3); 11.76 (1H, br. s, N^2). **$^{13}C\{^1H\}$ NMR (150 MHz, $CDCl_3$):** δ_C 129.1 (C^7); 129.8 (C^5);

130.3 (C^4); 133.0 (C^6); 147.7 (C^3); 156.5 (C^1, weak). **IR:** 1580 (C=C); 1652 (C=N); 1745 (C-H bend, overtone); 3060 cm (C-H); 3117 cm^{-1} (N-H). **LC-MS (MeOH/H_2O):** 152.099, 1%, $[M - CN]^+$; 178.095, 100%, $[M + H]^+$; 179.159, 25%, $[M + 2H]^+$; 180.148, 13%, $[M + 3H]^+$; 181.212, 1%, $[M + 4H]^+$; 183.074, 1%, $[M + 5H]^+$; 200.101, 1%, $[M + Na]^+$ (1.425 min). **HRMS:** 178.0442, $[M + H]^+$ (178.0439 expected for $C_8H_8N_3S$, +0.3 mDa).

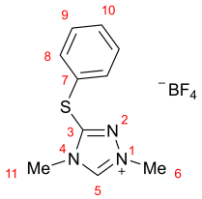
8.2.37 – (*Z*)-3-((4-Bromostyryl)thio)-4-methyl-4*H*-1,2,4-triazole (**91**)



Following general procedure D, (4-bromophenylethynyl)trimethylsilane (1.10 g, 4.35 mmol, 1 equiv.) gave the crude product as a yellow solid. The crude product was redissolved in DCM (20 mL), washed with water (2 × 10 mL) then concentrated *in vacuo* to give (*Z*)-3-((4-bromostyryl)thio)-4-methyl-4*H*-1,2,4-triazole (498 mg, 1.69 mmol, 97%) as a pale yellow solid.

^{1}H NMR (600 MHz, $CDCl_3$): δ_H 3.65 (3 H, s, C^9); 6.72 (1 H, d, J = 10.5 Hz, C^3); 6.89 (1 H, d, J = 10.5 Hz, C^4); 7.33 (2 H, dt, J = 8.4 and 1.7 Hz, C^6); 7.53 (2 H, dt, J = 8.6 and 2.0 Hz, C^7); 8.26 (1 H, s, C^2). **^{13}C{^{1}H} NMR (151 MHz, $CDCl_3$):** δ_C 31.5 (C^9); 99.3 (C^2); 120.1 (C^4); 122.0 (C^8); 129.0 (C^3); 130.3 (C^6); 131.9 (C^7); 131.9 (C^1); 134.6 (C^5). **LC-MS (MeOH/H_2O):** (For ^{79}Br isotopologue) 296.097, 80%, $[M + H]^+$ (For ^{81}Br isotopologue) 297.921, 100%, $[M + H]^+$; 299.137, 24%, $[M + 2H]^+$; 300.126, 9%, $[M + 3H]^+$; 301.190, 1%, $[M + 4H]^+$ (2.922 min). **HRMS:** 295.9864, $[M + H]^+$ (295.9857 expected for $C_{11}H_{11}N_3S^{79}Br$, +0.7 mDa).

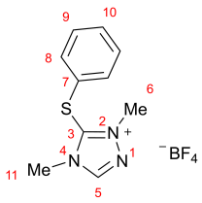
8.2.38 – 1,4-Dimethyl-3-(phenylthio)-4*H*-1,2,4-triazol-1-ium tetrafluoroborate (**92a**·$\mathbf{BF_4}$)



Following general procedure E, 4-methyl-3-(phenylthio)-4*H*-1,2,4-triazole (**86a**) (501 mg, 2.62 mmol) gave 1,4-dimethyl-3-(phenylthio)-4*H*-1,2,4-triazol-1-ium tetrafluoroborate (529 mg, 1.80 mmol, 69%) as colourless crystals.

^{1}H NMR (700 MHz, E7, d_6-DMSO): δ_H 3.79 (3 H, s, C^{11}); 4.03 (3 H, s, C^{6}); 7.46 – 7.52 (3 H, m, C^{8} and C^{10}); 7.59 (2 H, dt, J = 5.3 and 2.1 Hz, C^{9}); 10.02 (1 H, s, C^{5}). **^{13}C{^{1}H} NMR (176 MHz, E7, d_6-DMSO):** δ_C 33.7 (C^{11}); 39.0 (C^{6}); 127.1 (C^{7}); 129.8 (C^{10}); 130.1 (C^{8}); 132.3 (C^{9}); 145.4 (C^{5}); 151.9 (C^{3}). **^{15}N NMR (71 MHz, E7, d_6-DMSO):** δ_N 177.7 (N^{4}); 215.0 (N^{2}); 299.4 (N^{1}). **LC-MS (MeOH / H_2O):** 109.120, 16%, $[M - C_4N_3H_7]^+$; 205.195, 1%, $[M - H]^+$; 206.221, 100%, $[M]^+$; 207.247, 18%, $[M + H]^+$; 208.273, 8%, $[M + 2H]^+$; 209.261, 1%, $[M + 3H]^+$; 210.211, 1%, $[M + 4H]^+$ (0.255 min). **HRMS:** 206.0744, $[M]^+$ (206.0752 expected for $C_{10}H_{12}N_3S$, −0.8 mDa). **XRD:** Structure verified by XRD, see Appendix A

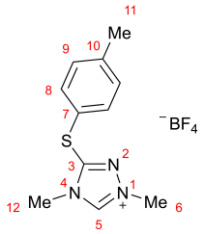
8.2.39 – 1,4-Dimethyl-5-(phenylthio)-4*H*-1,2,4-triazol-1-ium tetrafluoroborate (**93a**·BF_4)



Following general procedure E, 4-methyl-3-(phenylthio)-4*H*-1,2,4-triazole (**86a**) (501 mg, 2.62 mmol) gave 1,4-dimethyl-5-(phenylthio)-4*H*-1,2,4-triazol-1-ium tetrafluoroborate (26 mg, 0.13 mmol, 5%) as a white solid.

^{1}H NMR (700 MHz, E7, d_6-DMSO): δ_H 3.78 (3 H, s, C^{11}); 4.05 (3 H, s, C^{6}); 7.47 – 7.51 (3 H, m, C^{8} and C^{10}); 7.62 (2 H, dt, J = 7.8 and 2.4 Hz, C^{9}); 9.29 (1 H, s, C^{5}). **^{13}C{^{1}H} NMR (176 MHz, E7, d_6-DMSO):** δ_C 34.5 (C^{11}); 39.0 (C^{6}); 127.7 (C^{7}); 129.0 (C^{10}); 130.4 (C^{8}); 132.1 (C^{9}); 146.5 (C^{5}); 206.5 (C^{3}). **^{15}N NMR (71 MHz, E7, d_6-DMSO):** δ_N 182.2 (N^{4}); 222.1 (N^{1}); 301.0 (N^{2}). **LC-MS (MeOH / H_2O):** 109.120, 14%, $[M - C_4N_3H_7]^+$; 114.098, 7%, $[M - C_6H_5]^+$; 206.259, 100%, $[M]^+$; 207.247, 11%, $[M + H]^+$; 208.273, 6%, $[M + 2H]^+$; 209.185, 1%, $[M + 3H]^+$ (1.004 min).

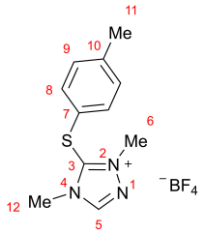
8.2.40 – 1,4-Dimethyl-3-(*p*-tolylthio)-4*H*-1,2,4-triazol-1-ium tetrafluoroborate (**92b**·BF_4)



Following general procedure E, 4-methyl-3-(*p*-tolylthio)-4*H*-1,2,4-triazole (**86b**) (202 mg, 0.984 mmol) gave 1,4-dimethyl-3-(*p*-tolylthio)-4*H*-1,2,4-triazol-1-ium tetrafluoroborate (102 mg, 0.332 mmol, 34%) as colourless crystals.

^{1}H NMR (599 MHz, $CDCl_3$): δ_H 2.39 (3 H, s, C^{11}); 3.85 (3 H, s, C^{12}); 4.05 (3 H, s, C^6); 7.26 (2 H, d, J = 7.8 Hz, C^8); 7.44 (2 H, d, J = 8.3 Hz, C^9) 9.77 (1 H, s, C^5). **^{13}C{^{1}H} NMR (151 MHz, $CDCl_3$):** δ_C 21.5 (C^{11}); 34.0 (C^{12}); 39.5 (C^6); 121.4 (C^7); 131.2 (C^8); 133.9 (C^9); 141.4 (C^{10}); 145.5 (C^5); 154.3 (C^3). **LC-MS (MeOH/H_2O):** 220.202, 100%, $[M]^+$; 221.266, 42%, $[M + H]^+$; 222.254, 17%, $[M + 2H]^+$; 223.280, 2%, $[M + 3H]^+$ (1.777 min). **HRMS:** 220.0904, $[M]^+$ (220.0908 expected for $C_{11}H_{14}N_3S$, −0.4 mDa). **XRD:** Structure verified by XRD, see Appendix A.

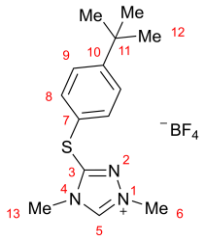
8.2.41– 1,4-Dimethyl-5-(*p*-tolylthio)-4*H*-1,2,4-triazol-1-ium tetrafluoroborate (**93b**·BF_4)



Following general procedure E, 4-methyl-3-(*p*-tolylthio)-4*H*-1,2,4-triazole (**86b**) (202 mg, 0.984 mmol) gave 1,4-dimethyl-5-(*p*-tolylthio)-4*H*-1,2,4-triazol-1-ium tetrafluoroborate (17 mg, 0.055 mmol, 7%) as a colourless solid.

^{1}H NMR (700 MHz, E7, $CDCl_3$): δ_H 2.35 (3 H, s, C^{11}); 3.83 (3 H, s, C^{12}); 3.99 (3 H, s, C^6); 7.25 (2 H, d, J = 8.1 Hz, C^9); 7.36 (2 H, d, J = 7.9 Hz, C^8); 8.77 (1 H, s, C^5). **^{13}C{^{1}H} NMR (176 MHz, E7, $CDCl_3$):** δ_C 21.4 (C^{11}); 34.9 (C^{12}); 39.3 (C^6); 121.2 (C^{10}); 131.8 (C^9); 133.0 (C^8); 141.8 (C^7); 146.2 (C^5); 148.9 (C^3). **LC-MS (MeOH/H_2O):** 220.202, 100%, $[M]^+$; 221.266, 26%, $[M + H]^+$; 222.292, 11%, $[M + 2H]^+$; 223.242, 2%, $[M + 3H]^+$ (1.429 min).

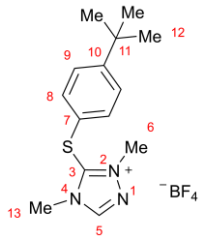
8.2.42 – 3-((4-(*Tert*-butyl)phenyl)thio)-1,4-dimethyl-4*H*-1,2,4-triazol-1-ium tetrafluoroborate (**92c**·BF_4)



Following general procedure E, 3-((4-(*tert*-butyl)phenyl)thio)-4-methyl-4*H*-1,2,4-triazole (**86c**) (341 mg, 1.38 mmol) gave 3-((4-(*tert*-butyl)phenyl)thio)-1,4-dimethyl-4*H*-1,2,4-triazol-1-ium tetrafluoroborate (167 mg, 0.478 mmol, 35%) as a colourless solid.

^{1}H NMR (700 MHz, E7, $CDCl_3$): δ_H 1.30 (9 H, s, C^{12}); 4.00 (3 H, s, C^{13}); 4.09 (3 H, s, C^6); 7.32 (2 H, d, J = 8.5 Hz, C^9); 7.42 (2 H, d, J = 8.4 Hz, C^8); 9.99 (1 H, s, C^5). **LC-MS (MeOH/H_2O):** 262.311, 100%, $[M - BF_4]^+$; 263.299, 16%, $[M + H - BF_4]^+$; 264.287, 6%, $[M + 2H - BF_4]^+$ (2.627 min). **HRMS:** 262.1387, $[M]^+$ (262.1378 expected for $C_{14}H_{20}N_3S$, +0.9 mDa).

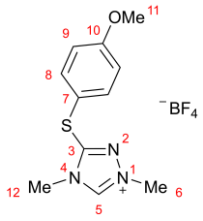
8.2.43 – 5-((4-(*Tert*-butyl)phenyl)thio)-1,4-dimethyl-4*H*-1,2,4-triazol-1-ium tetrafluoroborate (**93c**·BF_4)



Following general procedure E, 3-((4-(*tert*-butyl)phenyl)thio)-4-methyl-4*H*-1,2,4-triazole (**86c**) (341 mg, 1.38 mmol) gave 5-((4-(*tert*-butyl)phenyl)thio)-1,4-dimethyl-4*H*-1,2,4-triazol-1-ium tetrafluoroborate (32 mg, 0.092 mmol, 7%) as a colourless solid.

^{1}H NMR (700 MHz, E7, $CDCl_3$): δ_H 1.28 (9 H, s, C^{12}); 3.89 (3 H, s, C^{13}); 4.02 (3 H, s, C^6); 7.38 (2 H, d, J = 8.5 Hz, C^9); 7.44 (2 H, d, J = 8.5 Hz, C^8); 9.04 (1 H, s, C^5). **^{13}C{^{1}H} NMR (176 MHz, E7, $CDCl_3$):** δ_C 31.1 (C^{12}); 34.9 (C^{11}); 35.1 (C^{13}); 39.3 (C^6); 121.6 (C^7); 128.2 (C^8); 132.6 (C^9); 146.5 (C^5); 148.8 (C^3); 154.7 (C^{10}). **^{15}N NMR (71 MHz, $CDCl_3$):** 181.2 (N^4); 220.3 (N^1); 302.8 (N^2). **LC-MS (MeOH/H_2O):** 262.273, 100%, $[M]^+$; 263.337, 58%, $[M + H]^+$; 264.287, 19%, $[M + 2H]^+$; 265.314, 3%, $[M + 3H]^+$ (2.245 min).

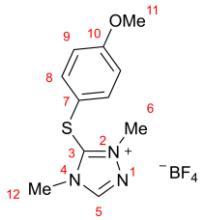
8.2.44 – 3-((4-Methoxyphenyl)thio)-1,4-dimethyl-4*H*-1,2,4-triazol-1-ium tetrafluoroborate (**92d**·BF_4)



Following general procedure E, 3-((4-methoxyphenyl)thio)-4-methyl-4*H*-1,2,4-triazole (**86d**) (204 mg, 0.922 mmol) gave 3-((4-methoxyphenyl)thio)-1,4-dimethyl-4*H*-1,2,4-triazol-1-ium tetrafluoroborate (73 mg, 0.23 mmol, 25%) as a white solid.

^{1}H NMR (600 MHz, d_6-DMSO): δ_H 3.79 (3 H, s, C^{12}); 3.80 (3 H, s, C^{11}); 3.98 (3 H, s, C^6); 7.07 (2 H, dd, *J* = 6.7 and 2.1 Hz, C^9); 7.59 (2 H, dd, *J* = 6.7 and 2.2 Hz, C^8); 9.96 (1 H, s, C^5). **^{13}C{^{1}H} NMR (151 MHz, d_6-DMSO):** δ_C 33.6 (C^{12}); 38.9 (C^6); 55.5 (C^{11}); 115.7 (C^9); 115.9 (C^{10}); 135.8 (C^8); 145.1 (C^5); 153.5 (C^3); 161.0 (C^{10}). **LC-MS (MeOH/H_2O):** 236.206, 100%, $[M - BF_4]^+$; 237.233, 39%, $[M + H - BF_4]^+$; 238.221, 17%, $[M + 2H - BF_4]^+$; 239.171, 2%, $[M + 3H - BF_4]^+$ (1.450 min). **HRMS:** 236.0858, $[M - BF_4]^+$ (236.0858 expected for $C_{11}H_{14}N_3OS$, +1.1 mDa).

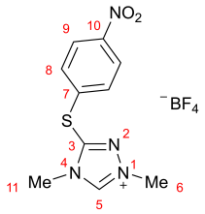
8.2.45– 5-((4-Methoxyphenyl)thio)-1,4-dimethyl-4*H*-1,2,4-triazol-1-ium tetrafluoroborate (**93d**·BF_4)



Following general procedure E, 3-((4-methoxyphenyl)thio)-4-methyl-4*H*-1,2,4-triazole (204 mg, 0.922 mmol) gave 5-((4-methoxyphenyl)thio)-1,4-dimethyl-4*H*-1,2,4-triazol-1-ium tetrafluoroborate (24 mg, 0.074 mmol, 8%) as a white solid.

^{1}H NMR (700 MHz, E7, $CDCl_3$): δ_H 3.82 (3 H, s, C^8); 3.84 (3 H, s, C^9); 3.99 (3 H, s, C^3); 6.97 (2 H, d, *J* = 8.4 Hz, C^5); 7.49 (2 H, d, *J* = 8.3 Hz, C^6); 8.73 (1 H, s, C^2). **^{13}C{^{1}H} NMR (176 MHz, E7, $CDCl_3$):** δ_C 35.0 (C^8); 39.3 (C^3); 55.8 (C^9); 113.9 (C^4); 116.7 (C^5); 135.9 (C^6); 146.1 (C^2); 149.3 (C^1); 162.2 (C^7). **LC-MS (MeOH/H_2O):** 236.202, 100%, $[M]^+$; 237.266, 23%, $[M + H]^+$; 238.216, 9%, $[M + 2H]^+$; 239.280, 1%, $[M + 3H]^+$ (1.308 min).

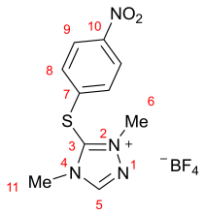
8.2.46 – 1,4-Dimethyl-3-((4-nitrophenyl)thio)-4*H*-1,2,4-triazol-1-ium tetrafluoroborate (**92e**·BF_4)



Following general procedure E, 4-methyl-3-((4-nitrophenyl)thio)-4*H*-1,2,4-triazole (**86e**) (250 mg, 1.06 mmol) gave 1,4-dimethyl-3-((4-nitrophenyl)thio)-4*H*-1,2,4-triazol-1-ium tetrafluoroborate (207 mg, 0.612 mmol, 58%) as colourless crystals.

^{1}H NMR (599 MHz, d_6-DMSO): δ_H 3.81 (3 H, s, C^{11}); 4.10 (3 H, s, C^6); 7.75 (2 H, dt, J = 9.2 and 2.4 Hz, C^9); 8.25 (2 h, dt, J = 9.0 and 2.4 Hz, C^8); 10.14 (1 H, s, C^5). **^{13}C{^{1}H} NMR (151 MHz, d_6-DMSO):** δ_C 33.9 (C^{11}); 39.2 (C^6); 124.6 (C^8); 130.7 (C^9); 137.5 (C^7); 146.0 (C^5); 147.3 (C^{10}); 149.7 (C^3). **LC-MS (MeOH / H_2O):** 251.158, 100%, $[M]^+$; 252.108, 21%, $[M + H^+]^+$; 253.096, 9%, $[M + 2H]^+$; 254.074, 1%, $[M + 3H]^+$ (1.041 min). **HRMS:** 251.0602, $[M]^+$ (251.0603 expected for $C_{10}H_{11}N_4O_2S$, −0.1 mDa). **XRD:** Structure verified by XRD, see Appendix A.

8.2.47 – 1,4-Dimethyl-5-((4-nitrophenyl)thio)-4*H*-1,2,4-triazol-1-ium tetrafluoroborate (**93e**·BF_4)

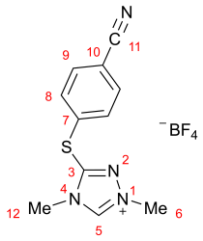


Following general procedure E, 4-methyl-3-((4-nitrophenyl)thio)-4*H*-1,2,4-triazole (**86e**) (250 mg, 1.06 mmol) gave 1,4-dimethyl-5-((4-nitrophenyl)thio)-4*H*-1,2,4-triazol-1-ium tetrafluoroborate (12 mg, 0.035 mmol, 3%) as a white solid.

^{1}H NMR (599 MHz, d_6-DMSO): δ_H 3.80 (3 H, s, C^{11}); 4.08 (3 H, s, C^6); 7.77 (2 H, ddd, J = 9.1, 2.9 and 2.1 Hz, C^9); 8.25 (2 H, ddd, J = 9.0, 2.9 and 2.1 Hz, C^8); 9.41 (1 H, s, C^5). **^{13}C{^{1}H} NMR (151 MHz, d_6-DMSO):** δ_C 34.6 (C^{11}); 39.2* (C^6); 124.9 (C^8); 131.1 (C^9); 135.7 (C^7); 146.4 (C^3); 146.9 (C^5); 147.6 (C^{10}). **LC-MS (MeCN/H_2O):** 251.120, 100%, $[M]^+$; 252.108, 16%, $[M + H]^+$; 253.286, 1%, $[M + 2H]^+$ (0.768 min).

*This signal is significantly obscured by d_6-DMSO and only a small peak can be seen within the solvent peak. HSQC evidence verifies that the peak exists at the provided shift value.

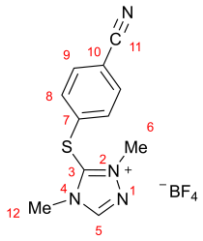
8.2.48 – 3-((4-Cyanophenyl)thio)-1,4-dimethyl-4*H*-1,2,4-triazol-1-ium tetrafluoroborate (**92f·BF$_4$**)



Following general procedure E, 4-((4-methyl-4*H*-1,2,4-triazol-3-yl)thio)benzonitrile (**86f**) (174 mg, 0.805 mmol) gave 3-((4-cyanophenyl)thio)-1,4-dimethyl-4*H*-1,2,4-triazol-1-ium tetrafluoroborate (59 mg, 0.19 mmol, 24%) as a colourless solid.

^{1}H NMR (700 MHz, E7, CD$_3$OD): δ_H 3.87 (3 H, s, C^{13}); 4.11 (3 H, s, C^6); 7.71 (2H, ddd, J = 8.7, 1.9 and 1.4 Hz, C^8); 7.81 (2 H, ddd, J = 8.7, 2.0 and 1.5 Hz, C^9); 9.91 (<1 H, s, C^5). **^{13}C{^{1}H} NMR (176 MHz, E7, CD$_3$OD):** δ_C 34.47 (C^{13}); 39.8 (C^6); 114.3 (C^7); 118.7 (C^{10}); 133.3 (C^8); 134.6 (C^9); 135.2 (C^{11}); 146.6 (C^5); 152.9 (C^3). **^{15}N NMR (71 MHz, E7, CD$_3$OD):** δ_N 177.9 (N^4); 216.2 (N^2); 303.0 (N^1). **LC-MS (MeOH/H$_2$O):** 231.185, 100%, [M]$^+$; 232.250, 27%, [M + H]$^+$; 233.238, 11%, [M + 2H]$^+$; 234.302, 1%, [M + 3H]$^+$ (1.221 min).

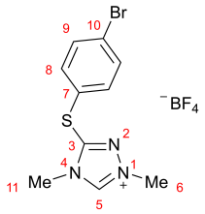
8.2.49 – 5-((4-Cyanophenyl)thio)-1,4-dimethyl-4*H*-1,2,4-triazol-1-ium tetrafluoroborate (**93f·BF$_4$**)



Following general procedure E, 4-((4-methyl-4*H*-1,2,4-triazol-3-yl)thio)benzonitrile (**86f**) (174 mg, 0.805 mmol, 1 equiv.) gave 5-((4-cyanophenyl)thio)-1,4-dimethyl-4*H*-1,2,4-triazol-1-ium tetrafluoroborate (13 mg, 0.041 mmol, 5%) as a colourless solid.

^{1}H NMR (700 MHz, E7, CD$_3$OD): δ_H 3.88 (3 H, s, C^{13}); 4.14 (3 H, s, C^6); 7.66 (2H, ddd, J = 8.8, 2.1 and 2.0 Hz, C^8); 7.81 (2 H, ddd, J = 8.8, 2.0 and 2.0 Hz, C^9); 9.12 (1 H, s, C^5). **^{13}C{^{1}H} NMR (176 MHz, E7, CD$_3$OD):** δ_C 35.3 (C^{13}); 39.9 (C^6); 114.9 (C^7); 118.5 (C^{10}); 132.7 (C^8); 135.2 (C^9); 133.9 (C^{11}); 148.0 (C^5); 148.5 (C^3). **^{15}N NMR (71 MHz, E7, CD$_3$OD):** δ_N 182.8 (N^4); 224.4 (N^2); 304.3 (N^1). **LC-MS (MeOH/H$_2$O):** 231.223, 100%, [M]$^+$; 232.212, 12%, [M + H]$^+$; 233.276, 5%, [M + 2H]$^+$; (0.857 min).

8.2.50 – 3-((4-Bromophenyl)thio)-1,4-dimethyl-4*H*-1,2,4-triazol-1-ium tetrafluoroborate (**92h**·BF_4)



Following general procedure E, 3-((4-bromophenyl)thio)-4-methyl-4*H*-1,2,4-triazole (**86h**) (200 mg, 0.740 mmol) gave 3-((4-bromophenyl)thio)-1,4-dimethyl-4*H*-1,2,4-triazol-1-ium tetrafluoroborate (109 mg, 0.293 mmol, 40%) as a pale yellow solid.

^{1}H NMR (599 MHz, $CDCl_3$): δ_H 3.87 (3 H, s, C^{11}); 4.06 (3 H, s, C^6); 7.42 (2 H, dt, J = 8.4 and 1.8 Hz, C^9); 7.58 (2 H, dt, J = 8.5 and 1.8 Hz, C^8); 9.84 (1 H, s, C^5). **^{13}C{^{1}H} NMR (151 MHz, $CDCl_3$):** δ_C 34.01 (C^{11}); 39.53 (C^6); 124.43 (C^7); 125.48 (C^{10}); 133.66 (C^8); 135.03 (C^9); 146.09 (C^5); 153.17 (C^3). **LC-MS (MeOH/H_2O):** (For ^{79}Br isotopologue) 284.088, 86%, $[M - BF_4]^+$; (For ^{81}Br isotopologue) 285.988, 100%, $[M - BF_4]^+$; 287.166, 22%, $[M + H - BF_4]^+$; 288.154, 8%, $[M + 2H - BF_4]^+$; 289.256, 1%, $[M + 3H - BF_4]^+$ (1.638 min). **HRMS:** 283.9860, $[M - BF_4]^+$ (283.9857 expected for $C_{10}H_{11}N_3S^{79}Br$, +0.3 mDa).

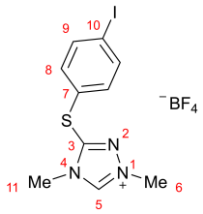
8.2.51– 5-((4-Bromophenyl)thio)-1,4-dimethyl-4*H*-1,2,4-triazol-1-ium tetrafluoroborate (**93h**·BF_4)



Following general procedure E, 3-((4-bromophenyl)thio)-4-methyl-4*H*-1,2,4-triazole (**86h**) (200 mg, 0.740 mmol) gave 5-((4-bromophenyl)thio)-1,4-dimethyl-4*H*-1,2,4-triazol-1-ium tetrafluoroborate (4 mg, 0.01 mmol, 1%) as a pale yellow solid.

^{1}H NMR (599 MHz, d_6-DMSO): δ_H 3.78 (3 H, s, C^{11}); 4.06 (3 H, s, C^6); 7.57 (2 H, dt, J = 8.8 and 2.1 Hz, C^9); 7.68 (2 H, dt, J = 8.6 and 2.0 Hz, C^8); 9.29 (1 H, s, C^5). **^{13}C{^{1}H} NMR (151 MHz, d_6-DMSO):** δ_C 34.5 (C^{11}); 39.0 (C^6); 123.8 (C^{10}); 125.8 (C^7); 133.2 (C^8); 134.1 (C^9); 146.5 (C^5); 147.4 (C^3). **LC-MS (MeCN/H_2O):** (For ^{79}Br isotopologue) 284.088, 88%, $[M - BF_4]^+$; (For ^{81}Br isotopologue) 285.988, 100%, $[M - BF_4]^+$; 287.128, 19%, $[M + H - BF_4]^+$; 288.116, 8%, $[M + 2H - BF_4]^+$; 289.180, 1%, $[M + 3H - BF_4]^+$ (1.186 min).

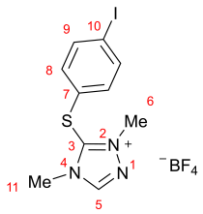
8.2.52 – 3-((4-Iodophenyl)thio)-1,4-dimethyl-4*H*-1,2,4-triazol-1-ium tetrafluoroborate (**92i**·BF_4)



Following general procedure E, 3-((4-iodophenyl)thio)-4-methyl-4*H*-1,2,4-triazole (**86i**) (200 mg, 0.631 mmol, 1 equiv.) gave 3-((4-iodophenyl)thio)-1,4-dimethyl-4*H*-1,2,4-triazol-1-ium tetrafluoroborate (116 mg, 0.276 mmol, 44%) as a pale yellow solid.

^{1}H NMR (700 MHz, E7, d_6-DMSO): δ_H 3.78 (3 H, s, C^{11}); 4.02 (3 H, s, C^6); 7.36 (2 H, ddd, J = 8.5, 2.6 and 1.9 Hz, C^8); 7.84 (2 H, ddd, J = 8.5, 2.5 and 2.0 Hz, C^9); 10.05 (1 H, s, C^5). **^{13}C{^{1}H} NMR (171 MHz, E7, d_6-DMSO):** δ_C 33.8 (C^{11}); 39.0 (C^6); 96.8 (C^7); 127.3 (C^{10}); 134.1 (C^8); 138.8 (C^9); 145.5 (C^5); 151.5 (C^3). **LC-MS (MeCN/H_2O):** 332.087, 100%, $[M - BF_4]^+$; 333.189, 29%, $[M + H - BF_4]^+$; 334.139, 12%, $[M + 2H - BF_4]^+$ (1.568 min). **HRMS:** 331.9726, $[M]^+$ (331.9718 expected for $C_{10}H_{11}N_3SI$, +0.8 mDa). **XRD:** Structure verified by XRD, see Appendix A.

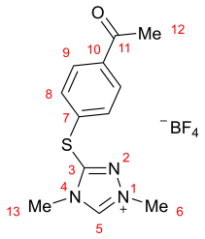
8.2.53 – 5-((4-Iodophenyl)thio)-1,4-dimethyl-4*H*-1,2,4-triazol-1-ium tetrafluoroborate (**93i**·BF_4)



Following general procedure E, 3-((4-iodophenyl)thio)-4-methyl-4*H*-1,2,4-triazole (**86i**) (200 mg, 0.631 mmol) gave 5-((4-iodophenyl)thio)-1,4-dimethyl-4*H*-1,2,4-triazol-1-ium tetrafluoroborate (9 mg, 0.02 mmol, 3%) as a pale yellow solid.

^{1}H NMR (700 MHz, E7, d_6-DMSO): δ_H 3.77 (3 H, s, C^{11}); 4.05 (3 H, s, C^6); 7.40 (2 H, d, J = 8.5 Hz, C^8); 7.83 (2 H, d, J = 8.5 Hz, C^9); 9.30 (1 H, s, C^5). **^{13}C{^{1}H} NMR (176 MHz, E7, d_6-DMSO):** δ_C 34.5 (C^{11}); 39.0 (C^6); 97.3 (C^7); 126.3 (C^{10}); 133.9 (C^8); 139.0 (C^9); 146.5 (C^5); 147.4 (C^3). **LC-MS (MeCN/H_2O):** 332.087, 100%, $[M - BF_4]^+$; 333.189, 11%, $[M + H - BF_4]^+$; 334.101, 5%, $[M + 2H - BF_4]^+$ (1.603 min). **XRD:** Structure verified by XRD, see Appendix A.

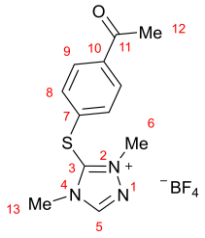
8.2.54 – 3-((4-Acetylphenyl)thio)-1,4-dimethyl-4*H*-1,2,4-triazol-1-ium tetrafluoroborate (**92l**·BF_4)



Following general procedure E, 1-(4-((4-methyl-4*H*-1,2,4-triazol-3-yl)thio)phenyl)ethan-1-one (**86l**) (61 mg, 0.26 mmol, 1 equiv.) gave 3-((4-acetylphenyl)thio)-1,4-dimethyl-4*H*-1,2,4-triazol-1-ium tetrafluoroborate (13 mg, 0.039 mmol, 15%) as a pale yellow solid.

^{1}H NMR (700 MHz, E7, $CDCl_3$): δ_H 2.60 (3 H, s, C^{12}); 3.87 (3 H, s, C^{13}); 4.11 (3H, s, C^6); 7.57 (2 H, d, J = 8.1 Hz, C^8); 7.98 (2 H, d, J = 8.2 Hz, C^9); 9.95 (1 H, s, C^5). **^{13}C{^{1}H} NMR (176 MHz, E7, $CDCl_3$):** δ_C 26.8 (C^{12}); 34.2 (C^{13}); 39.7 (C^6); 130.0 (C^9); 132.0 (C^8); 132.1 (C^{10}); 138.0 (C^7); 146.2 (C^5); 152.0 (C^2); 197.0 (C^{11}). **^{15}N NMR (71 MHz, E7, $CDCl_3$):** δ_N 176.6 (N^4); 215.6 (N^2); 301.6 (N^1). **LC-MS (MeOH/H_2O):** 248.174, 100%, $[M]^+$; 249.276, 27%, $[M + H]^+$; 260.264, 12%, $[M + 2H]^+$; 251.252, 1%, $[M + 3H]^+$ (1.412 min). **HRMS:** 248.0864, $[M]^+$ (248.0858 expected for $C_{12}H_{14}N_3OS$, +0.6 mDa).

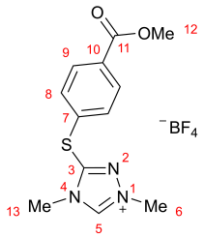
8.2.55 – 5-((4-Acetylphenyl)thio)-1,4-dimethyl-4*H*-1,2,4-triazol-1-ium tetrafluoroborate (**93l**·BF_4)



Following general procedure E, 1-(4-((4-methyl-4*H*-1,2,4-triazol-3-yl)thio)phenyl)ethan-1-one (**86l**) (61 mg, 0.26 mmol) gave 5-((4-acetylphenyl)thio)-1,4-dimethyl-4*H*-1,2,4-triazol-1-ium tetrafluoroborate (8 mg, 0.02 mmol, 9%) as a pale yellow solid.

^{1}H NMR (700 MHz, E7, d_6-DMSO): δ_H 2.59 (3 H, s, C^{12}); 3.78 (3 H, s, C^{13}); 4.06 (3H, s, C^6); 7.66 (2 H, ddd, J = 8.6, 2.3 and 2.0 Hz, C^8); 7.98 (2 H, ddd, J = 8.7, 2.2 and 2.1 Hz, C^9); 9.37 (1 H, s, C^5). **^{13}C{^{1}H} NMR (176 MHz, E7, d_6-DMSO):** δ_C 26.8 (C^{12}); 34.6 (C^{13}); 39.1 (C^6); 129.7 (C^9); 130.8 (C^8); 137.1 (C^7); 132.6 (C^{10}); 146.8 (C^5); 147.0 (C^3); 197.2 (C^{11}). **^{15}N NMR (71 MHz, E7, d_6-DMSO):** δ_N 183.4 (N^4); 223.6 (N^1); 302.0 (N^2). **LC-MS (MeOH/H_2O):** 248.212, 100%, $[M]^+$; 249.238, 13%, $[M + H]^+$ 250.226, 7%, $[M + 2H]^+$; 251.290, 1% (1.082 min).

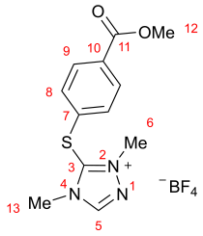
8.2.56 – 3-((4-(Methoxycarbonyl)phenyl)thio)-1,4-dimethyl-4*H*-1,2,4-triazol-1-ium tetrafluoroborate (**92n**·BF_4)



Following general procedure E, methyl 4-((4-methyl-4*H*-1,2,4-triazol-3-yl)thio)benzoate (**86n**) (200 mg, 0.803 mmol) gave 3-((4-(methoxycarbonyl)phenyl)thio)-1,4-dimethyl-4*H*-1,2,4-triazol-1-ium tetrafluoroborate (153 mg, 0.436 mmol, 54%) as pale yellow crystals.

^{1}H NMR (700 MHz, E7, CD_3OD): δ_H 3.85 (3 H, s, C^{13}); 3.92 (3 H, s, C^{12}); 4.10 (3 H, s, C^6); 7.66 (2 H, ddd, *J* = 8.6, 2.2 and 1.9 Hz, C^8); 8.07 (2 H, ddd, *J* = 8.7, 2.1 and 2.0 Hz, C^9); 9.86 (<1 H, s, C^5). **^{13}C{^{1}H} NMR (176 MHz, E7, CD_3OD):** δ_C 34.4 (C^{13}); 39.7 (C^6); 53.0 (C^{12}); 131.9 (C^9); 132.9 (C^8); 132.5 (C^7); 134.3 (C^{10}); 146.8 (C^5); 153.5 (C^3); 167.4 (C^{11}). **LC-MS (MeOH/H_2O):** 264.173, 100%, $[M]^+$; 265.238, 36%, $[M + H]^+$; 266.264, 14%, $[M + 2H]^+$; 267.290, 2%, $[M + 3H]^+$ (1.672 min). **HRMS:** 264.0820, $[M]^+$ (264.0807 expected for $C_{12}H_{14}N_3O_2S$, +1.3 mDa). **XRD:** Structure verified by XRD, see Appendix A.

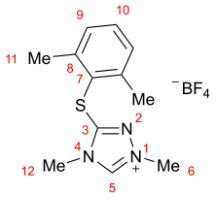
8.2.57 – 5-((4-(Methoxycarbonyl)phenyl)thio)-1,4-dimethyl-4*H*-1,2,4-triazol-1-ium tetrafluoroborate (**93n**·BF_4)



Following general procedure E, methyl 4-((4-methyl-4*H*-1,2,4-triazol-3-yl)thio)benzoate (**86n**) (200 mg, 0.803 mmol) gave 5-((4-(methoxycarbonyl)phenyl)thio)-1,4-dimethyl-4*H*-1,2,4-triazol-1-ium tetrafluoroborate (15 mg, 0.043 mmol, 5%) as a pale yellow solid.

^{1}H NMR (700 MHz, E7, CD_3OD): δ_H 3.87 (3 H, s, C^{13}); 3.92 (3 H, s, C^{12}); 4.13 (3 H, s, C^6); 7.62 (2 H, ddd, *J* = 8.9, 2.1 and 2.1 Hz, C^8); 8.09 (2 H, ddd, *J* = 8.8, 2.1 and 2.1 Hz, C^9); 9.09 (<1 H, s, C^5). **^{13}C{^{1}H} NMR (176 MHz, E7, CD_3OD):** δ_C 35.3 (C^{13}); 39.8 (C^6); 53.0 (C^{12}); 132.4 (C^8); 132.5 (C^9); 132.9 (C^7); 133.1 (C^{10}); 147.8 (C^5); 149.0 (C^3); 167.1 (C^{11}). **LC-MS (MeOH/H_2O):** 264.211, 100%, $[M]^+$; 265.276, 25%, $[M + H]^+$; 266.226, 10%, $[M + 2H]^+$; 267.328, 2%, $[M + 3H]^+$ (1.100 min).

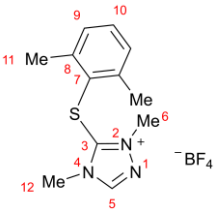
8.2.58 – 3-((2,6-Dimethylphenyl)thio)-1,4-dimethyl-4*H*-1,2,4-triazol-1-ium tetrafluoroborate (**92o**·BF_4)



Following general procedure E, 3-((2,6-dimethylphenyl)thio)-4-methyl-4*H*-1,2,4-triazole (**86o**) (500 mg, 2.28 mmol) gave 3-((2,6-dimethylphenyl)thio)-1,4-dimethyl-4*H*-1,2,4-triazol-1-ium tetrafluoroborate (233 mg, 0.726 mmol, 32%) as colourless crystals.

^{1}H NMR (599 MHz, d_6-DMSO): δ_H 2.44 (6 H, s, C^{11}); 3.84 (3 H, s, C^{12}); 3.90 (3 H, s, C^6); 7.29 (2 H, d, J = 7.3 Hz, C^9); 7.37 (1 H, dd, J = 8.1 and 7.0 Hz, C^{10}); 9.93 (1 H, s, C^5). **^{13}C{^{1}H} NMR (151 MHz, d_6-DMSO):** δ_C 21.4 (C^{11}); 33.4 (C^{12}); 38.7 (C^6); 124.3 (C^8); 128.9 (C^9); 131.1 (C^{10}); 143.4 (C^7); 144.9 (C^5); 153.1 (C^3). **LC-MS (MeCN/H_2O):** 234.188, 100%, $[M - BF_4]^+$; 235.252, 59%, $[M + H - BF_4]^+$; 236.240, 31%, $[M + 2H - BF_4]^+$; 237.342, 2%, $[M + 3H - BF_4]^+$ (1.377 min). **HRMS:** 234.1056, $[M]^+$ (234.1065 expected for $C_{12}H_{16}N_3S$, −0.9 mDa). **XRD:** Structure verified by XRD, see Appendix A.

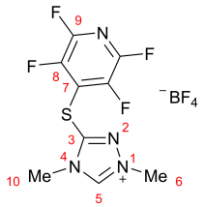
8.2.59 – 5-((2,6-Dimethylphenyl)thio)-1,4-dimethyl-4*H*-1,2,4-triazol-1-ium tetrafluoroborate (**93o**·BF_4)



Following general procedure E, 3-((2,6-dimethylphenyl)thio)-4-methyl-4*H*-1,2,4-triazole (**86o**) (500 mg, 2.28 mmol) gave 5-((2,6-dimethylphenyl)thio)-1,4-dimethyl-4*H*-1,2,4-triazol-1-ium tetrafluoroborate (185 mg, 0.576 mmol, 25%) as a white solid.

^{1}H NMR (599 MHz, $CDCl_3$): δ_H 2.38 (6 H, s, C^{11}); 3.65 (3 H, s, C^{12}); 3.78 (3 H, s, C^6); 7.23 (2 H, d, J = 7.6 Hz, C^9); 7.34 (1 H, t, J = 7.6 Hz, C^{10}); 8.71 (1 H, s, C^5). **^{13}C{^{1}H} NMR (151 MHz, $CDCl_3$):** δ_C 22.1 (C^{11}); 34.3 (C^{12}); 38.7 (C^6); 122.5 (C^7); 130.1 (C^9); 131.9 (C^{10}); 143.1 (C^8); 146.0 (C^1); 149.4 (C^3). **LC-MS (MeCN/H_2O):** 234.188, 100%, $[M - BF_4]^+$; 235.252, 55%, $[M + H - BF_4]^+$; 236.240, 24%, $[M + 2H - BF_4]^+$; 237.304, 3%, $[M + 3H - BF_4]^+$ (1.134 min). **HRMS:** 234.1056, $[M]^+$ (234.1065 expected for $C_{12}H_{16}N_3S$, −0.9 mDa).

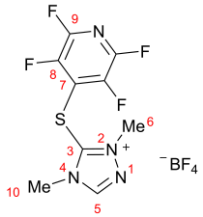
8.2.60 – 1,4-Dimethyl-3-((perfluoropyridin-4-yl)thio)-4*H*-1,2,4-triazol-1-ium tetrafluoroborate (**92q**·**BF$_4$**)



Following general procedure E, 2,3,5,6-tetrafluoro-4-((4-methyl-4*H*-1,2,4-triazol-3-yl)thio)pyridine (**86q**) (500 mg, 1.89 mmol) gave 1,4-dimethyl-3-((perfluoropyridin-4-yl)thio)-4*H*-1,2,4-triazol-1-ium tetrafluoroborate (283 mg, 0.773 mmol, 41%) as colourless crystals.

^{1}H NMR (599 MHz, d$_6$-DMSO): δ_H 3.92 (3 H, s, C^{10}); 4.07 (3 H, s, C^6); 10.09 (1 H, s, C^5). **^{13}C{^{1}H} NMR (151 MHz, d$_6$-DMSO):** δ_C 34.2 (C^{10}); 39.3 (C^6); 123.6 (t, *J* = 18.7 Hz, C^7); 141.8 (ddd, *J* = 258.9, 35.5 and 7.4 Hz, C^8); 142.6 (dt, *J* = 243.9 and 17.0 Hz, C^9); 145.6 (C^5); 147.9 (C^3). **^{19}F NMR (376 MHz, d$_6$-DMSO):** δ_F −148.4 and −148.4 (BF_4 counteranion); −134.0 (C^8); −90.3 (C^9). **LC-MS (MeCN/H$_2$O):** 279.109, 100%, $[M - BF_4]^+$; 280.135, 59%, $[M + H - BF_4]^+$; 281.123, 26%, $[M + 2H - BF_4]^+$; 282.188, 2%, $[M + 3H - BF_4]^+$ (0.944 min). **HRMS:** 279.0337, $[M]^+$ (279.0328 expected for $C_9H_7N_4F_4S$, +0.9 mDa). **XRD:** Product verified by XRD, see Appendix A.

8.2.61– 1,4-Dimethyl-5-((perfluoropyridin-4-yl)thio)-4*H*-1,2,4-triazol-1-ium tetrafluoroborate (**93q**·**BF$_4$**)



Following general procedure E, 2,3,5,6-tetrafluoro-4-((4-methyl-4*H*-1,2,4-triazol-3-yl)thio)pyridine (**86q**) (500 mg, 1.89 mmol, 1 equiv.) gave 1,4-dimethyl-5-((perfluoropyridin-4-yl)thio)-4*H*-1,2,4-triazol-1-ium tetrafluoroborate (6 mg, 0.02 mmol, 1%) as a colourless solid.

^{1}H NMR (599 MHz, d$_6$-DMSO): δ_H 3.88 (3 H, s, C^{10}); 4.17 (3 H, s, C^6); 9.38 (1 H, s, C^5). **^{13}C{^{1}H} NMR (151 MHz, d$_6$-DMSO):** δ_C 34.5 (C^{10}); 39.2 (C^6); 121.0 (t, *J* = 18.7 Hz, C^7); 142.1 (ddd, *J* = 257.9, 29.2 and 7.5 Hz, C^8); 142.7 (dtd, *J* = 243.6, 14.8 and 3.6 Hz, C^9); 144.2 (C^3); 146.7 (C^5). **^{19}F NMR (376 MHz, d$_6$-DMSO):** δ_F −148.5 and −148.4 (BF_4 counteranion); −133.4 (C^8); −90.0 (C^9). **LC-MS (MeCN/H$_2$O):** 279.109, 100%, $[M - BF_4]^+$; 280.173, 28%, $[M + H - BF_4]^+$; 281.123, 12%,

$[M + 2H - BF_4]^+$; 282.188, 1%, $[M + 3H - BF_4]^+$ (0.753 min). **HRMS:** 279.0337, $[M]^+$ (279.0328 expected for $C_9H_7N_4F_4S$, +0.9 mDa).

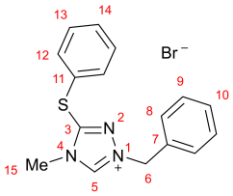
8.2.62 – 1-Ethyl-4-methyl-3-(phenylthio)-4*H*-1,2,4-triazol-1-ium tetrafluoroborate (**94·BF$_4$**)



Following general procedure E, changing trimethyloxonium tetrafluoroborate for triethyloxonium tetrafluoroborate (1.2 equiv.), 4-methyl-3-(phenylthio)-4*H*-1,2,4-triazole (**86a**) (500 mg, 2.62 mmol) gave 1-ethyl-4-methyl-3-(phenylthio)-4*H*-1,2,4-triazol-1-ium tetrafluoroborate (411 mg, 1.34 mmol, 51%) as colourless crystals.

^{1}H NMR (600 MHz, CDCl$_3$): δ_H 1.52 (3 H, t, J = 7.3 Hz, C^7); 3.82 (3 H, s, C^{12}); 4.34 (2 H, q, J = 7.3 Hz, C^6); 7.37 – 7.44 (3 H, m, C^{10} and C^{11}); 7.50 (2 H, td, J = 3.9 and 0.9 Hz, C^9); 9.67 (1 H, s, C^5). **^{13}C{^{1}H} NMR (151 MHz, CDCl$_3$):** δ_C 13.6 (C^7); 34.0 (C^{12}); 48.5 (C^6); 126.0 (C^8); 130.2 (C^{11}); 130.3 (C^{10}); 133.1 (C^9); 144.7 (C^5); 153.2 (C^3). **LC-MS (MeOH/H$_2$O):** 220.164, 100%, $[M - BF_4]^+$; 221.228, 55%, $[M + H - BF_4]^+$; 222.216, 27%, $[M + 2H - BF_4]^+$; 223.242, 3%, $[M + 3H - BF_4]^+$ (1.360 min). **HRMS:** 220.0907, $[M]^+$ (220.0908 expected for $C_{11}H_{14}N_3S$, −0.1 mDa). **XRD:** Structure verified by XRD, see Appendix A.

8.2.63 – 1-Benzyl-4-methyl-3-(phenylthio)-4*H*-1,2,4-triazol-1-ium bromide (**98·Br**)

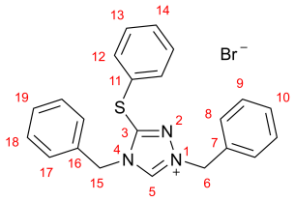


4-Methyl-3-(phenylthio)-4*H*-1,2,4-triazole (**86a**) (500 mg, 2.62 mmol, 1 equiv.) was dissolved in MeCN (25 mL) and BnBr (5 mL, 42.1 mmol, excess) within a pressure tube. The reaction mixture was heated (150 °C, 28 h) then concentrated *in vacuo*. The crude product was purified by reverse phase liquid chromatography (10 → 100% MeOH in H_2O) to give 1-benzyl-4-methyl-3-(phenylthio)-4*H*-1,2,4-triazol-1-ium bromide (47 mg, 0.13 mmol, 5%) as a white solid.

^{1}H NMR (599 MHz, CDCl$_3$): δ_H 3.95 (3 H, s, C^{15}); 5.64 (2 H, s, C^6); 7.37 – 7.39 (3 H, m, C^9 and C^{10}); 7.45 (2 H, dt, J = 6.9 and 2.0 Hz, C^{13}); 7.48 – 7.51 (3 H, m, C^{12} and C^{14}); 7.53 – 7.55 (2 H, m,

C^8); 12.11 (1 H, s, C^5). **$^{13}C\{^1H\}$ NMR (151 MHz, $CDCl_3$):** δ_C 34.4 (C^{15}); 56.7 (C^6); 125.3 (C^7); 129.4 (C^9); 129.6 (C^8); 129.9 (C^{10}); 130.5 (C^{13}); 130.8 (C^{14}); 131.8 (C^{11}); 133.4 (C^{12}); 145.6 (C^5); 153.6 (C^3). **LC-MS (MeOH/H_2O):** 192.310, 27%, $[M - C_7H_6 - Br]^+$; 193.298, 3%, $[M - C_7H_5 - Br]^+$; 282.345, 100%, $[M - Br]^+$; 283.409, 22%, $[M + H - Br]^+$; 284.397, 8%, $[M + 2H - Br]^+$; 285.386, 1%, $[M + 3H - Br]^+$ (1.836 min). **HRMS:** 282.1050, $[M]^+$ (282.1065 expected for $C_{16}H_{16}N_3S$, −1.5 mDa).

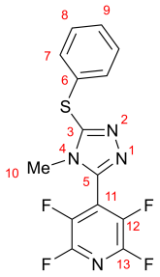
8.2.64 – 1,4-Dibenzyl-3-(phenylthio)-4*H*-1,2,4-triazol-1-ium bromide (**99·Br**)



4-Methyl-3-(phenylthio)-4*H*-1,2,4-triazole (**86a**) (500 mg, 2.62 mmol, 1 equiv.) was dissolved in MeCN (25 mL) and BnBr (5 mL, 42.1 mmol, excess) within a pressure tube. The reaction mixture was heated (150 °C, 28 h) then concentrated *in vacuo*. The crude product was purified by reverse phase liquid chromatography (10 → 100% MeOH in H_2O) to give 1,4-dibenzyl-3-(phenylthio)-4*H*-1,2,4-triazol-1-ium bromide (356 mg, 0.812 mmol, 31%) as a pale yellow solid.

^1H NMR (599 MHz, $CDCl_3$): δ_H 5.59 (2 H, s, C^{15}); 5.62 (2 H, s, C^6); 7.33 – 7.42 (8 H, m, C^9, C^{10}, C^{13}, C^{14} and C^{18}); 7.42 – 7.46 (3 H, m, C^{17} and C^{19}); 7.46 – 7.51 (4 H, m, C^8 and C^{12}); 12.11 (1 H, s, C^5). **$^{13}C\{^1H\}$ NMR (151 MHz, $CDCl_3$):** δ_C 51.6 (C^{15}); 56.7 (C^6); 125.5 (C^{16}); 129.1 (C^{12}); 129.3 (C^{18}); 129.6 (C^8); 129.7 (C^{14}); 129.8 (C^{10}); 129.6 (C^{13}); 130.3 (C^9); 130.7 (C^{19}); 131.7 (C^{11}); 131.8 (C^7); 133.6 (C^{17}); 144.9 (C^5); 153.7 (C^3). **LC-MS (MeOH/H_2O):** 358.234, 100%, $[M - Br]^+$; 359.336, 63%, $[M + H - Br]^+$; 360.324, 35%, $[M + 2H - Br]^+$; 361.350, 6%, $[M + 3H - Br]^+$; 362.338, 1%, $[M + 4H - Br]^+$ (2.506 min). **HRMS:** 358.1385, $[M]^+$ (358.1378 expected for $C_{22}H_{20}N_3S$, +0.7 mDa).

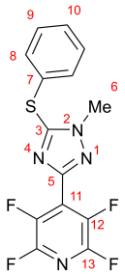
8.2.65 – 2,3,5,6-Tetrafluoro-4-(4-methyl-5-(phenylthio)-4*H*-1,2,4-triazol-3-yl)pyridine (**103**)



4-Methyl-3-(phenylthio)-4*H*-1,2,4-triazole (**86a**) (300 mg, 1.57 mmol, 1 equiv.) was dissolved in MeCN (15 mL) and pentafluoropyridine (3 mL) within a pressure tube. The reaction mixture was heated (150 °C, 18 h) then concentrated *in vacuo*. The reaction mixture was then purified by reverse phase column chromatography (5 → 100% MeCN in H_2O) to afford 2,3,5,6-tetrafluoro-4-(4-methyl-5-(phenylthio)-4*H*-1,2,4-triazol-3-yl)pyridine (372 mg, 1.09 mmol, 69%) as colourless crystals.

^{1}H NMR (599 MHz, $CDCl_3$): δ_H 3.55 (3 H, t, J = 1.1 Hz, C^{10}); 7.31 – 7.40 (3 H, m, C^7 and C^9); 7.42 – 7.47 (2 H, m, C^8). **^{13}C{^{1}H} NMR (151 MHz, $CDCl_3$):** δ_C 32.0 (t, J = 2.6 Hz, C^{10}); 128.8 (C^9); 130.0 (C^6); 130.0 (C^7); 130.9 (C^8); 138.8 (C^{11}); 139.8 (dd, J = 266.5 and 36.1 Hz, C^{12}) 143.8 (dt, J = 252.9 and 12.3 Hz, C^{13}); 143.8 (C^5); 152.0 (C^3). **^{19}F NMR (B4, 376 MHz, $CDCl_3$):** δ_F −138.6 (C^{12}); −87.3 (C^{13}). **LC-MS (MeOH/H_2O):** 341.170, 100%, $[M + H]^+$; 342.272, 36%, $[M + 2H]^+$; 343.222, 14%, $[M + 3H]^+$; 344.210, 3%, $[M + 4H]^+$ (2.714 min). **HRMS:** 341.0493, $[M + H]^+$ (341.0484 expected for $C_{14}H_9N_4F_4S$, +0.9 mDa). **XRD:** Structure verified by XRD, see Appendix A.

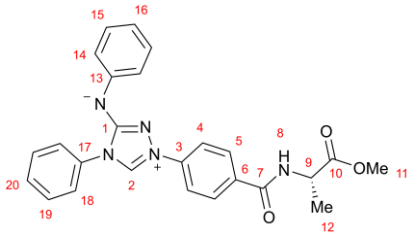
8.2.66 – 2,3,5,6-Tetrafluoro-4-(1-methyl-5-(phenylthio)-1*H*-1,2,4-triazol-3-yl)pyridine (**104**)



4-Methyl-3-(phenylthio)-4*H*-1,2,4-triazole (**86a**) (300 mg, 1.57 mmol, 1 equiv.) was dissolved in MeCN (15 mL) and pentafluoropyridine (3 mL) within a pressure tube. The reaction mixture was heated (150 °C, 18 h) then concentrated *in vacuo*. The reaction mixture was then purified by reverse phase column chromatography (5 → 100% MeCN in H_2O) to afford 2,3,5,6-tetrafluoro-4-(1-methyl-5-(phenylthio)-1*H*-1,2,4-triazol-3-yl)pyridine (47 mg, 0.14 mmol, 11%) as a white solid.

^{1}H NMR (599 MHz, $CDCl_3$): δ_H 3.26 (3 H, s, C^6); 7.36 – 7.45 (3 H, m, C^8 and C^{10}); 7.46 – 7.53 (2 H, m, C^9). **^{13}C{^{1}H} NMR (151 MHz, $CDCl_3$):** δ_C 28.9 (C^6); 127.6 (C^7); 129.6 (C^{10}); 130.1 (C^8); 131.9 (C^{11}); 132.0 (C^9); 137.7 (dt, J = 267.4 and 6.4 Hz, C^{12}); 143.8 (dtd, J = 246.3, 15.1 and 3.8 Hz, C^{13}); 146.9 (C^5); 151.8 (C^3). **^{19}F NMR (B4, 376 MHz, $CDCl_3$):** δ_F −144.0 (C^{12}); −87.8 (C^{13}). **LC-MS (MeOH/H_2O):** 341.170, 100%, $[M + H]^+$; 342.234, 26%, $[M + 2H]^+$; 343.260, 10%, $[M + 3H]^+$; 344.324, 1%, $[M + 4H]^+$ (2.020 min). **HRMS:** 341.0495, $[M]^+$ (341.0484 expected for $C_{14}H_9N_4SF_4$, +1.1 mDa).

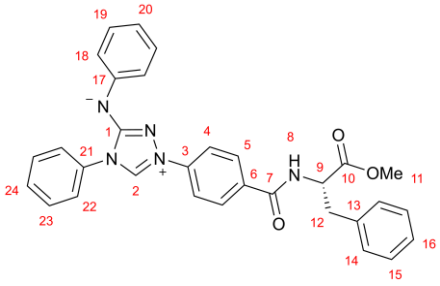
8.2.67 – (*S*)-(1-(4-((1-Methoxy-1-oxopropan-2-yl)carbamoyl)phenyl)-4-phenyl-4*H*-1,2,4-triazol-1-ium-3-yl)(phenyl)amide (**83**)



Following general procedure F, L-alanine methyl ester hydrochloride (71 mg, 0.51 mmol) gave the crude product as a yellow solution. The crude product was concentrated *in vacuo* and purified by reverse phase liquid chromatography (5 → 100% MeCN in H_2O) to afford (1-(4-((1-methoxy-1-oxopropan-2-yl)carbamoyl)phenyl)-4-phenyl-4*H*-1,2,4-triazol-1-ium-3-yl)-(phenyl)amide (101 mg, 0.23 mmol, 45%) as a yellow solid. XRD data was possible as the protonated chloride salt (**83H·Cl**), obtained by dissolving a sample (~20 mg) in DCM (10 mL) and washing with HCl (1 M, 10 mL) – the organic phase was left to slow dry in air giving colourless crystals.

^{1}H NMR (600 MHz, CD_3OD): δ_H 1.55 (3 H, d, J = 7.3 Hz, C^{12}); 3.78 (3 H, s, C^{11}); 4.67 (1 H, q, J = 7.3 Hz, C^9); 7.18 (1 H, tt, J = 7.4 and 1.1 Hz, C^{16}); 7.42 (2 H, tdd, J = 7.4, 3.2 and 2.1 Hz, C^{14}); 7.66 (2 H, dtd, J = 7.6, 2.0 and 0.9 Hz, C^{15}); 7.75 – 7.83 (3 H, m, C^{18} and C^{20}); 7.85 (2 H, dt, J = 6.2 and 1.7 Hz, C^{19}); 8.12 (2 H, dt, J = 8.9 and 2.1 Hz, C^4); 8.17 (2 H, dt, J = 9.0 and 2.2 Hz, C^5); 10.70 (1 H, s, C^2). **^{13}C{^{1}H} NMR (151 MHz, CD_3OD):** δ_C 17.2 (C^{12}); 50.3 (C^9); 52.9 (C^{11}); 121.0 (C^{15}); 121.3 (C^4); 125.4 (C^{16}); 127.7 (C^{19}); 130.2 (C^{14}); 130.6 (C^5); 131.7 (C^{17}); 131.8 (C^2); 131.9 (C^{18}); 133.1 (C^{20}); 136.9 (C^3); 138.9 (C^6); 139.3 (C^{13}); 153.0 (C^1); 168.3 (C^7); 174.7 (C^{10}). **LC-MS (MeCN/H_2O):** 442.457, 100%, $[M + H]^+$; 443.521, 63%, $[M + 2H]^+$; 444.509, 16%, $[M + 3H]^+$; 445.535, 2%, $[M + 4H]^+$ (2.067 min). **HRMS:** 442.1856, $[M + H]^+$ (442.1879 expected for $C_{25}H_{24}N_5O_3$, −2.3 mDa).

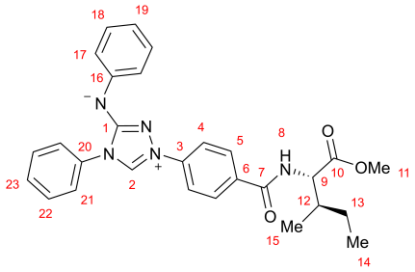
8.2.68 – (*S*)-(1-(4-((1-Methoxy-1-oxo-3-phenylpropan-2-yl)carbamoyl)phenyl)-4-phenyl-4*H*-1,2,4-triazol-1-ium-3-yl)(phenyl)-amide (**117**)



Following general procedure F, L-phenylalanine methyl ester hydrochloride (56 mg, 0.26 mmol) gave the crude product. The reaction mixture was washed with water (3 × 50 mL) and the combined organic phases dried with Na_2SO_4. The solvent was removed *in vacuo* and purified by reverse phase liquid chromatography (5 → 100% MeOH in H_2O) to give (*S*)-(1-(4-((1-methoxy-1-oxo-3-phenylpropan-2-yl)carbamoyl)phenyl)-4-phenyl-4*H*-1,2,4-triazol-1-ium-3-yl)(phenyl)-amide (16 mg, 0.031 mmol, 12%) as a pale yellow solid.

^{1}H NMR (400 MHz, N4, CD_3OD): δ_H 3.18 (2 H, d, *J* = 3.7 Hz, C^{12}); 3.37 (1 H, t, *J* = 5.6 Hz, C^9); 3.77 (3 H, s, C^{11}); 7.18 (1 H, tt, *J* = 7.4 and 1.1 Hz); 7.23 – 7.26 (1 H, m); 7.28 – 7.31 (4 H, m); 7.40 – 7.44 (2 H, m); 7.63 – 7.67 (2 H, m); 7.77 – 7.80 (3 H, m); 7.82 – 7.85 (2 H, m); 8.03 (2 H, dt, *J* = 8.9 and 2.1 Hz); 8.08 (2 H, dt, *J* = 8.9 and 2.1 Hz). **IR:** 840, 1216, 1459, 1633 (C=O, amide), 1723 (C=O, ester), 2966 cm^{-1} (C-H). **LC-MS:** 518.8, $[M + H]^+$ (2.75 min). **HRMS:** 518.2195, $[M + H]^+$ (518.2192 expected for $C_{31}H_{28}N_5O_3$, +0.3 mDa).

8.2.69 – (1-(4-(((2*S*,3*R*)-1-Methoxy-3-methyl-1-oxopentan-2-yl)carbamoyl)-phenyl)-4-phenyl-4*H*-1,2,4-triazol-1-ium-3-yl)(phenyl)amide (**118**)

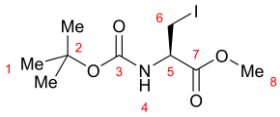


Following general procedure F, L-isoleucine methyl ester hydrochloride (46 mg, 0.25 mmol) gave the crude product. The reaction mixture was washed with water (3 × 50 mL) and the combined organic phases dried with Na_2SO_4. The solvent was removed *in vacuo* and purified by reverse phase liquid chromatography (20 → 100% MeOH in H_2O) to give (1-(4-(((2*S*,3*R*)-1-methoxy-3-methyl-1-

oxopentan-2-yl)carbamoyl)phenyl)-4-phenyl-4*H*-1,2,4-triazol-1-ium-3-yl)(phenyl)amide (30 mg, 0.062 mmol, 25%) as a white solid.

^{1}H NMR (400 MHz, N4, CD_3OD): δ_H 1.00 (3 H, t, *J* = 7.5 Hz, C^{14}); 1.04 (3 H, d, *J* = 6.9 Hz, C^{15}); 3.78 (3 H, s, C^{11}); 4.61 (1 H, d, *J* = 6.9 Hz, C^{12}); 7.18 (1 H, t, *J* = 7.4 and 1.1 Hz); 7.39 – 7.45 (2 H, m); 7.65 (2 H, dd, *J* = 8.7 and 1.1 Hz); 7.77 – 7.86 (5 H, m); 8.10 – 8.17 (4 H, m). **IR:** 843, 1209, 1485, 1640 (C=O, amide), 1723 (C=O, ester), 2970 (C-H) cm^{-1}.

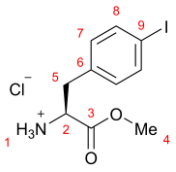
8.2.70 – Methyl (*R*)-2-((*tert*-butoxycarbonyl)amino)-3-iodopropanoate (**124**)



Triphenylphosphine (1.20 g, 4.56 mmol, 1 equiv.) and imidazole (310 mg, 4.56 mmol, 1 equiv.) was dissolved in DCM (10 mL). Iodine (1.39 g, 5.47 mmol, 1.2 equiv.) was added, then the mixture stirred (RT, 5 min). Boc-Ser-OMe (1.00 g, 4.56 mmol, 1 equiv.) dissolved in DCM (5 mL) was added to the reaction mixture. The mixture was stirred (RT, 2 h) without exposure to light, then washed with water (2 × 10 mL), saturated $Na_2S_2O_3$ solution (10 mL) and brine (10 mL) within a dark fume hood. The organic phase was concentrated *in vacuo* and purified by column chromatography (0 → 25% EtOAc in hexane) with minimal exposure to light to afford methyl (*R*)-2-((*tert*-butoxycarbonyl)amino)-3-iodopropanoate (812 mg, 2.47 mmol, 54%) as a yellow oil.

^{1}H NMR (400 MHz, $CDCl_3$): δ_H 1.38 (9H, s, C^1); 3.72 (3H, s, C^8); 3.49 (2H, t, *J* = 3.8 Hz, C^6) 4.45 (1H, dt, *J* = 7.9 and 4.0 Hz, C^5); 5.39 (1H, d, *J* = 7.7 Hz, N^4). **^{13}C{^{1}H} NMR (100 MHz, $CDCl_3$):** δ_C 7.8 (C^6); 28.2 (C^1); 53.0 (C^8); 53.7 (C^2); 80.3 (C^5); 154.8 (C^7); 170.0 (C^3). **TLC (25:75 EtOAc/Hexane):** R_f = 0.58.

8.2.71– (*S*)-3-(4-Iodophenyl)-1-methoxy-1-oxopropan-2-aminium chloride (**132**)

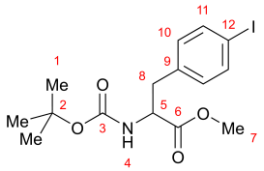


4-Iodo-L-phenylalanine (2.00 g, 6.87 mmol, 1 equiv.) was dissolved in MeOH (50 mL) and cooled on ice. $SOCl_2$ (1.00 mL, 13.7 mmol, 2 equiv.) was added cautiously with stirring, then the reaction mixture was stirred (0 °C, 5 min). The mixture was warmed to RT and stirred (RT, 16 h). The reaction mixture was concentrated *in vacuo*, then the crude product was resuspended in toluene (30 mL) and concentrated *in vacuo*. The product was again resuspended in toluene (30 mL) and concentrated *in*

vacuo to afford (*S*)-3-(4-iodophenyl)-1-methoxy-1-oxopropan-2-aminium chloride (2.18 g, 6.37 mmol, 93%) as a white solid.

LC-MS (MeOH/H_2O): 306.212, 100%, $[M+H]^+$; 307.314, 30%, $[M + 2H]^+$; 308.303, 3%, $[M + 3H]^+$ (1.193 min). **HRMS:** 305.9999, $[M + H]^+$ (305.9991 expected for $C_{10}H_{13}NO_2I$, +0.8 mDa).

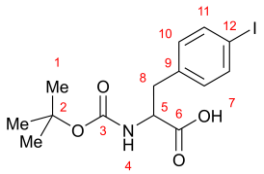
8.2.72 – Methyl (*S*)-2-((*tert*-butoxycarbonyl)amino)-3-(4-iodophenyl)-propanoate (**130**)



(*S*)-3-(4-Iodophenyl)-1-methoxy-1-oxopropan-2-aminium chloride (**132**) (2.20 g, 6.44 mmol, 1 equiv.) was dissolved in DCM (50 mL). Triethylamine (1.98 mL, 14.2 mmol, 2.2 equiv.) and di-*tert*-butyl dicarbonate (1.69 g, 7.73 mmol, 1.2 equiv.) were added. The reaction mixture was stirred (RT, 15 h), then washed with saturated $NaHCO_3$ solution (2 × 20 mL). The organic phase was concentrated *in vacuo* to give methyl (*S*)-2-((*tert*-butoxycarbonyl)amino)-3-(4-iodophenyl)-propanoate (2.483 g, 6.13 mmol, 95%) as a colourless solid.

^{1}H NMR (600 MHz, $CDCl_3$): δ_H 1.41 (9 H, s, C^1); 2.97 (1 H, dd, J = 13.8 and 6.2 Hz, C^8); 3.07 (1 H, dd, J = 13.9 and 5.8 Hz, C^8); 3.71 (3 H, s, C^7); 4.56 (1 H, q, J = 10.1 Hz, C^5); 4.97 (1 H, d, J = 8.2 Hz, N^4); 6.87 (2 H, d, J = 7.9 Hz, C^{11}); 7.61 (2 H, d, J = 8.3 Hz, C^{10}). **^{13}C{^{1}H} NMR (151 MHz, $CDCl_3$):** δ_C 28.4 (C^1); 38.1 (C^8); 52.5 (C^7); 54.3 (C^5); 80.2 (C^2); 92.6 (C^{12}); 131.5 (C^{11}); 135.9 (C^9); 137.7 (C^{10}); 155.1 (C^3); 172.2 (C^6). **LC-MS (MeOH/H_2O):** 306.174, 100%, $[M + H - Boc]^+$; 307.276, 24% $[M + 2H - Boc]^+$; 308.303, 2%, $[M + 3H - Boc]^+$; 406.316, 2%, $[M + H]^+$ (3.429 min).

8.2.73– 2-((*Tert*-butoxycarbonyl)amino)-3-(4-iodophenyl)propanoic acid (**133**)

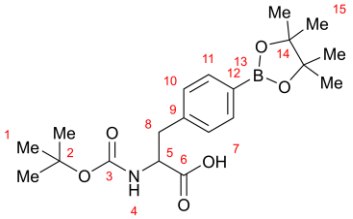


4-Iodo-L-phenylalanine (2.00 g, 6.87 mmol, 1 equiv.) was dissolved in DCM (50 mL). Triethylamine (1.15 mL, 8.24 mmol, 1.2 equiv.) and di-*tert*-butyl dicarbonate (1.82 g, 8.24 mmol, 1.2 equiv.) were added. The reaction mixture was stirred (RT, 16 h) then concentrated *in vacuo*. The crude product was purified by column chromatography (10% MeOH in DCM) to give 2-((*tert*-

butoxycarbonyl)amino)-3-(4-iodophenyl)propanoic acid (1.82 g, 4.66 mmol, 68%) as a colourless solid.

^{1}H NMR (600 MHz, $CDCl_3$): *(Major rotamer, 65% by ^{1}H NMR)* δ_H 1.42 (9 H, s, C^1); 3.02 (1 H, dd, J = 14.1 and 6.4 Hz, C^8); 3.11 – 3.21 (1 H, m, C^8); 4.59 (1 H, dd, J = 13.0 and 6.3 Hz, C^5); 4.95 (1 H, d, J = 8.0 Hz, N^4); 6.86 – 7.01 (2 H, m, C^{10}); 7.55 – 7.66 (2 H, m, C^{11}). *(Minor rotamer, 35% by ^{1}H NMR)* δ_H 1.29 (9 H, s, C^1); 2.86 (1 H, dd, J = 12.1 and 8.8 Hz, C^8); 3.11 – 3.21 (1 H, m, C^8); 4.36 (1 H, s, C^5); 6.58 (1 H, d, J = 4.3 Hz, N^4); 6.86 – 7.01 (2 H, m, C^{10}); 7.55 – 7.66 (2 H, m, C^{11}). **^{13}C{^{1}H} NMR (176 MHz, $CDCl_3$):** *(Major rotamer, 65%)* δ_C 28.4 (C^1); 37.5 (C^8); 54.2 (C^5); 80.7 (C^2); 92.8 (C^{12}); 131.5 (C^{10}); 135.6 (C^9); 137.8 (C^{11}); 155.5 (C^6); 176.0 (C^3). *(Minor rotamer, 35%)* δ_C 28.1 (C^1); 39.1 (C^8); 55.9 (C^5); 82.0 (C^2); 92.6 (C^{12}); 131.7 (C^{10}); 136.3 (C^9); 137.7 (C^{11}); 156.5 (C^6); 175.4 (C^3). **LC-MS (MeCN/H_2O):** 290.250, 18%, $[M + H - Boc]^+$; 292.226, 100%, $[M + 2H - Boc]^+$; 293.253, 10%, $[M + 3H - Boc]^+$ (2.684 min). **HRMS:** 414.0163, $[M + Na]^+$ (414.0178 expected for $C_{14}H_{18}NO_4Na^{127}I$, −1.5 mDa). **TLC (9:1 DCM/MeOH):** R_f = 0.88.

8.2.74 – 2-((*Tert*-butoxycarbonyl)amino)-3-(4-(4,4,5,5-tetramethyl-1,3,2-dioxaborolan-2-yl)phenyl)propanoic acid (**137**)

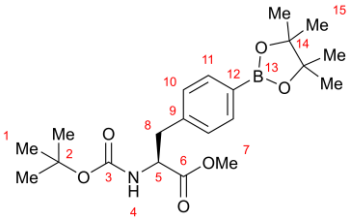


2-((*tert*-butoxycarbonyl)amino)-3-(4-iodophenyl)propanoic acid (**133**) (2.00 g, 5.11 mmol, 1 equiv.), bis(pinacolato)diboron (1.48 g, 5.84 mmol, 1.14 equiv.), [$PdCl_2$(dppf)] (114 mg, 0.156 mmol, 3 mol%) and potassium acetate (2.01 g, 20.5 mmol, 4 equiv.) were placed in Ar filled Schlenk tube. DMSO (50 mL) was added, then the reaction mixture heated (80 °C, 24 h) then cooled to RT. The reaction mixture was diluted with EtOAc (50 mL) then washed with HCl (1 M, 2 × 20 mL) and water (20 mL). The organic phase was concentrated *in vacuo* and purified by column chromatography (2 → 10% MeOH in DCM) to give 2-((*tert*-butoxycarbonyl)amino)-3-(4-(4,4,5,5-tetramethyl-1,3,2-dioxaborolan-2-yl)phenyl)propanoic acid (882 mg, 2.25 mmol, 44%) as a colourless solid.

^{1}H NMR (400 MHz, B4, $CDCl_3$): (*Major rotamer, 87% by ^{1}H NMR*) δ_H 1.29 (12 H, s, C^{15}); 1.37 (9 H, s, C^1); 3.06 (1 H, dd, J = 13.8 and 6.3 Hz, $C^{8'}$); 3.18 (1 H, dd, J = 14.0 and 7.5 Hz, $C^{8''}$); 4.55 (1 H, ddd, J = 6.7, 6.5 and 6.5 Hz, C^5); 5.10 (1 H, d, 8.1 Hz, N^4); 7.17 (2 H, d, J = 7.4 Hz, C^{10}); 7.70 (2 H, d, J = 7.4 Hz, C^{11}). (*Minor rotamer, 13% by ^{1}H NMR*) δ_H 1.19 (12 H, s, C^{15}); 1.22 (9 H, s, C^1); 2.88 (1 H, dd, J = 12.4 and 7.8 Hz, $C^{8'}$); 2.96 (1 H, dd, J = 13.2 and 5.6 Hz, $C^{8''}$); 4.27 – 4.38 (1 H, m, C^5); 5.17 (1 H, d, J = 8.2 Hz, N^4); 6.90 (2 H, d, J = 8.0 Hz, C^{10}); 7.56 (2 H, d, J = 7.7 Hz, C^{11}).

LC-MS (MeCN/H_2O): 291.504, 23%, $[M - Boc]^+$; 292.492, 92%, $[M + H - Boc]^+$; 293.519, 14%, $[M + 2H - Boc]^+$ (3.404 min). **HRMS:** 291.1742, $[M - Boc]^+$ (291.1756 expected for $C_{15}H_{23}NO_4B$, −1.4 mDa). **TLC (9:1 DCM/MeOH):** $R_f = 0.80$.

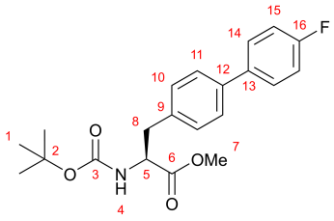
8.2.75 – Methyl (*S*)-2-((*tert*-butoxycarbonyl)amino)-3-(4-(4,4,5,5-tetramethyl-1,3,2-dioxaborolan-2-yl)phenyl)propanoate (**138**)



Methyl (*S*)-2-((*tert*-butoxycarbonyl)amino)-3-(4-iodophenyl)propanoate (**130**) (2.01 g, 4.94 mmol, 1 equiv.), bis(pinacolato)diboron (1.44 g, 5.68 mmol, 1.15 mmol), $[PdCl_2(dppf)]$ (111 mg, 0.152 mmol, 3 mol%) and potassium acetate (1.94 g, 19.8 mmol, 4 equiv.) were placed in an Ar-filled Schlenk tube. DMSO (20 mL) was added, then the reaction mixture stirred (80 °C, 24 h) then cooled to RT. EtOAc (20 mL) was added to the reaction mixture, then the mixture washed with HCl (1 M, 2 × 20 mL) and water (2 × 20 mL). The organic phase was concentrated *in vacuo*. The reaction mixture was purified by column chromatography (0 → 10% MeOH in DCM) to give methyl (*S*)-2-((*tert*-butoxycarbonyl)amino)-3-(4-(4,4,5,5-tetramethyl-1,3,2-dioxaborolan-2-yl)phenyl)propanoate (1.10 g, 2.70 mmol, 55%) as a colourless solid.

^{1}H NMR (600 MHz, $CDCl_3$): *(Major isomer, 85%)* δ_H 1.28 – 1.31 (12 H, m, C^{15}); 1.38 (9 H, s, C^1); 3.04 (1 H, dd, J = 13.7 and 9.0 Hz, C^8); 3.10 (1 H, dd, J = 13.7 and 5.7 Hz, C^8); 3.64 – 3.69 (3 H, m, C^7); 4.55 (1 H, td, J = 2.1 and 7.5, C^5); 5.02 (1 H, d, J = 8.9 Hz, N^4); 7.10 (2 H, d, J = 7.5 Hz, C^{11}); 7.68 – 7.73 (2 H, m, C^{10}). *(Minor isomer, 15%)* δ_H 1.23 (9 H, s, C^1); 1.28 – 1.31 (12 H, m, C^{15}); 2.86 – 2.96 (2 H, m, C^8); 3.64 – 3.69 (3 H, m, C^7); 4.26 – 4.39 (1 H, m, C^5); 5.34 – 5.56 (1 H, m, N^4); 7.11 – 7.16 (2 H, m, C^{11}); 7.68 – 7.73 (2 H, m, C^{10}). **^{13}C{^{1}H} NMR (151 MHz, $CDCl_3$):** *(Major isomer, 85%)* δ_C 24.9 (C^{15}); 28.3 (C^1); 38.4 (C^8); 52.2 (C^7); 54.4 (C^5); 79.9 (C^2); 83.8 (C^{14}); 127.5 (C^{12}); 128.7 (C^{11}); 135.0 (C^{10}); 139.3 (C^9); 155.1 (C^3); 172.2 (C^6). *(Minor isomer, 15%)* δ_C 24.9 (C^{15}); 25.0 (C^1); 39.0 (C^8); 52.2 (C^7); 56.1 (C^5); 83.7 (C^{14}); 127.7 (C^{12}); 128.7 (C^{11}); 135.0 (C^{10}); 139.3 (C^9); 155.1 (C^3); 172.2 (C^6); 83.5 (C^2).**^{11}B NMR (128 MHz, $CDCl_3$):** *(For major and minor isomer)* δ_B 30.7 (s, B^{13}). **LC-MS (MeCN/H_2O):** 305.452, 52%, $[M + H - Boc]^+$; 306.364, $[M + 2H - Boc]^+$; 307.466, 38%, $[M + 3H - Boc]^+$; 405.442, 3%, $[M + H]^+$; 406.430, 15%, $[M + 2H]^+$; 833.589, 100%, $[2M + Na]^+$; 834.653, 50%, $[2M + H + Na]^+$ (3.558 min). **HRMS:** 405.2439, $[M + H]^+$ (405.2437 expected for $C_{21}H_{33}NO_6{}^{10}B$, +0.2 mDa). **TLC (9:1 DCM/MeOH):** $R_f = 0.96$.

8.2.76 – Methyl (*S*)-2-((*tert*-butoxycarbonyl)amino)-3-(4'-fluoro-[1,1'-biphenyl]-4-yl)propanoate (**140**)



Methyl (*S*)-2-((*tert*-butoxycarbonyl)amino)-3-(4-(4,4,5,5-tetramethyl-1,3,2-dioxaborolan-2-yl)-phenyl)propanoate (**138**) (100 mg, 0.247 mmol, 1 equiv.), [$PdCl_2$(dppf)] (13 mg, 0.017 mmol, 7 mol%) and potassium carbonate (171 mg, 1.24 mmol, 5 equiv.) were placed in MW vial under Ar. DME (5 mL) and 4-fluorobromobenzene (0.03 mL, 0.3 mmol, 1.2 equiv.) were added. The reaction mixture was heated (80 °C, 18 h) then cooled to RT. The reaction mixture was partitioned between EtOAc (20 mL) and water (20 mL), with the organic phase concentrated *in vacuo* to give methyl (*S*)-2-((*tert*-butoxycarbonyl)amino)-3-(4'-fluoro-[1,1'-biphenyl]-4-yl)propanoate (69 mg, 0.19 mmol, 77%) as a colourless solid.

^{1}H NMR (600 MHz, $CDCl_3$): *(Major isomer, 83% by ^{1}H NMR)* δ_H 1.42 (9 H, s, C^1); 3.08 (1 H, dd, *J* = 14.3 and 6.0 Hz, C^8); 3.16 (1 H, dd, *J* = 13.9 and 5.7 Hz, C^8); 3.74 (3 H, s, C^7); 4.62 (1 H, td, *J* = 6.9 and 3.7 Hz, C^5); 5.02 (1 H, d, *J* = 8.3 Hz, N^4); 7.11 (2 H, dd, *J* = 8.6 and 4.8 Hz, C^{14}); 7.19 (2 H, d, *J* = 7.7 Hz, C^{10}); 7.47 (2 H, d, *J* = 7.7 Hz, C^{11}); 7.52 (2 H, dd, *J* = 8.4 and 5.4 Hz, C^{15}). *(Minor isomer, 17% by ^{1}H NMR)* δ_H 1.39 (9 H, s, C^1); 2.92 – 3.03 (2 H, m, C^8); 3.74 (3 H, s, C^7); 4.36 – 4.49 (1 H, m, C^5); 4.71 – 4.78 (1 H, m, N^4); 7.11 (2 H, dd, *J* = 8.6 and 4.8 Hz, C^{14}); 7.19 (2 H, d, *J* = 7.7 Hz, C^{10}); 7.47 (2 H, d, *J* = 7.7 Hz, C^{11}); 7.52 (2 H, dd, *J* = 8.4 and 5.4 Hz, C^{15}). **^{13}C{^{1}H} NMR (151 MHz, $CDCl_3$):** *(Major isomer, 83%)* δ_C 28.4 (C^1); 38.1 (C^8); 52.4 (C^7); 54.5 (C^5); 80.1 (C^2); 115.7 and 115.8 (C^{14}); 127.2 (C^{11}); 128.7 (C^{15}); 129.9 (C^{10}); 135.3 (C^{12}); 137.0 (C^{13}); 139.1 (C^9); 155.2 (C^3); 163.4 (C^{16}); 172.5 (C^6). *(Minor isomer, 17%)* δ_C 28.3 (C^1); 38.1 (C^8); 52.4 (C^7); 56.1 (C^5); 80.1 (C^2); 115.7 and 115.8 (C^{14}); 127.2 (C^{11}); 128.7 and 128.7 (C^{15}); 129.9 (C^{10}); 135.3 (C^{12}); 137.0 (C^{13}); 139.1 (C^9); 155.2 (C^3); 163.4 (C^{16}); 172.5 (C^6). **^{19}F NMR (376 MHz, $CDCl_3$):** δ_F −115.8 (tt, *J* = 8.8 and 5.2 Hz, F^{17})**. LC-MS (MeOH/H_2O):** 274.250, 85%, $[M + 2H – Boc]^+$; 275.314, 49%, $[M + 3H – Boc]^+$; 374.354, 6%, $[M + H]^+$; 769.488, 100%, $[2M + Na]^+$; 770.476, 77%, $[2M + H + Na]^+$ (3.609 min). **HRMS:** 374.1774, $[M + H]^+$ (374.1768 expected for $C_{21}H_{25}NO_4F$, +0.6 mDa).

8.3 – Syntheses from Chapter 3

8.3.1 – General procedures

8.3.1.1 – General procedure G: Synthesis of C(3)-amido Blatter radicals

Nitron analogue (1 equiv.) was dissolved in a mixture of acetonitrile and water (99:1, 10 g L^{-1}). The reaction mixture was stirred at room temperature with exposure to air for the time given, then concentrated *in vacuo* to a deep red coloured solid. The crude product was recrystallised from hot ethanol with the addition of water, allowing to cool to RT before storing at 2 °C for 16 h, to give the title compound.

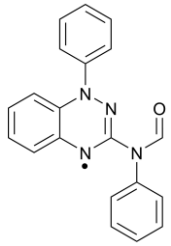
8.3.1.2 – General procedure H: Synthesis of C(3)-anilino Blatter radicals

C(3)-amido Blatter radical (1 equiv.) was dissolved in a HCl solution (5 M, 1:1 MeOH / H_2O, 5 g L^{-1}), then stirred at room temperature for the time given. The reaction mixture was concentrated *in vacuo*, with purification discussed for each compound.

8.3.1.3 – General procedure I: Synthesis of Blatter radical bioconjugates

L-amino acid methyl ester hydrochloride (1 equiv.), 1-(4-carboxyphenyl)-3-anilino-1,4-dihydrobenzo[*e*][1,2,4]triazin-4-yl radical (**38i**) (1 equiv.) and PyBOP (1.1 equiv.) were dissolved in THF. DIPEA (3 equiv.) added, mixture stirred (RT, 24 h). The reaction mixture was filtered, with the filtrate concentrated *in vacuo*. The crude product was purified by reverse phase liquid chromatography (10 → 100% MeOH in H_2O) to give the title compound.

8.3.2 – 1-Phenyl-3-(*N*-formylanilino)-1,4-dihydrobenzo[*e*][1,2,4]triazin-4-yl radical (**37a**)

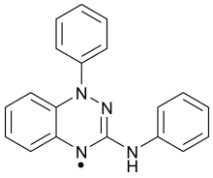


Following general procedure G, Nitron (**33a**, 9.99 g, 32.0 mmol) was stirred (RT, 94 h) to give 1-phenyl-3-(*N*-formylanilino)-1,4-dihydrobenzo[*e*][1,2,4]triazin-4-yl radical (7.31 g, 22.34 mmol, 70%) as a dark red powder.

IR: 1586 (C=N), 1681 (C=O), 2925 (C-H, aldehyde), 3069 and 3059 cm^{-1} (C-H, aromatic); 3355 (O-H, EtOH from recrystallisation) cm^{-1} **LC-MS (MeCN / H_2O):** 299.226, 4%, $[M - CO]^+$; 327.573, 44%, $[M]^+$; 328.181, 100%, $[M + H]^+$; 329.169, 21%, $[M + 2H]^+$; 330.347, 2%, $[M + 3H]^+$ (1.449

min). 209.131, 41%, $[M - NPhCOH]^+$; 328.219, 76%, $[M+H]^+$; 328.827, 54%, $[M + 2H]^+$; 330.461, 66%, $[M + 3H]^+$; 331.259, 22%, $[M + 4H]^+$; 351.170, 4%, $[M + Na]^+$ (2.906 min). **HRMS:** 327.1242, $[M]^+$ (327.1246 expected for $C_{20}H_{15}N_4O$, -0.4 mDa). **UV/Vis**: λ_{max} = 254 nm (210, 319 and 368 nm). **CV ($Cp^*_2Fe^+$ / Cp^*_2Fe, −0.5 V):** $E^{0/+1}$ = −0.10 V; $E^{-1/0}$ = −1.07 V; ΔE = 0.97 V. **EPR:** a_N1 = 8.04 G, a_N2 = 5.10 G, a_N3 = 4.63 G, a_N4 = 0.98 G. **Elemental Analysis:** %C = 72.80 (73.38% expected, −0.58%); %H = 4.64 (4.62% expected,+ 0.02%); %N = 16.79 (17.11% expected, −0.32%) . **TLC (98:2 DCM/MeOH):** R_f = 0.5.

8.3.3 – 1-Phenyl-3-anilino-1,4-dihydrobenzo[*e*][1,2,4]triazin-4-yl radical (**38a**)

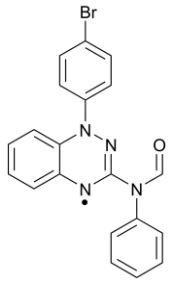


Following general procedure H, 1-phenyl-3-(*N*-formylanilino)-1,4-dihydrobenzo[*e*][1,2,4]triazin-4-yl radical (**37a**) (199 mg, 0.608 mmol) was stirred (RT, 28 h). The resultant solid was redissolved in DCM (150 mL), washed with Na_2CO_3 solution (1M, 50 mL), water (2 × 50 mL) and brine (50 mL). The organic phase was dried *in vacuo* and recrystallised (EtOH) to afford 1-phenyl-3-anilino-1,4-dihydrobenzo[*e*][1,2,4]triazin-4-yl radical (173 mg, 0.577 mmol, 94%) as a dark green solid.

IR: 1529 (C=N), 1599 (N-H bend), 2927 (C-H), 3303 (broad, N-H) cm^{-1} **LC-MS (MeOH / H_2O):** 299.295, 59%, $[M]^+$; 300.322, 42%, $[M + H]^+$; 301.272, 100%, $[M + 2H]^+$; 302.336, 35%, $[M + 3H]^+$; 303.324, 6%, $[M + 4H]^+$ (2.376 min). **HRMS:** 299.1299 (299.1297 expected for $C_{19}H_{15}N_4$, +0.2 mDa). **UV/Vis**: λ_{max} = 280 nm (205 and 591 nm). **CV (Cp_2Fe^+ / Cp_2Fe, 0 V):** $E^{0/+1}$ = −0.31 V; $E^{-1/0}$ = −1.23 V; ΔE = 0.92 V. **EPR:** a_N1 = 7.94 G, a_N2 = 5.76 G, a_N3 = 4.26 G, a_N4 = 0.72 G. **Elemental Analysis*:** %C = 72.79 (76.23% expected, −3.44%); %H = 4.95% (5.05% expected, −0.1%); %N = 17.49% (18.72% expected, −1.23%). **TLC (98:2 DCM/MeOH):** R_f = 0.35.

* The elemental analysis of this compound is an issue due to ineffective combustion within the elemental analysis instrumentation, including within an enriched oxygen environment.

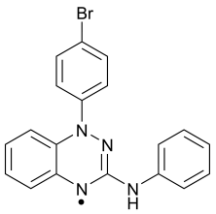
8.3.4 – 1-(4-Bromophenyl)-3-(*N*-formylanilino)-1,4-dihydrobenzo[*e*][1,2,4]triazin-4-yl radical (**37f**)



Following general procedure G, 1-(4-bromophenyl)-4-phenyl-3-(phenylamino)-4*H*-1,2,4-triazol-1-ium tetrafluoroborate (**33fH·BF$_4$**) (500 mg, 1.28 mmol) and triethylamine (0.18 mL, 1.3 mmol, 1 equiv.) were stirred (RT, 9 d) to give 1-(4-bromophenyl)-3-(*N*-formylanilino)-1,4-dihydrobenzo[*e*][1,2,4]triazin-4-yl radical (480 mg, 1.19 mmol, 93%) as a dark red solid.

LC-MS (MeOH/H$_2$O): (For ^{79}Br isotopologue) 405.290, 100%, $[M]^+$; 406.354, 60%, $[M + H]^+$; (For ^{81}Br isotopologue) 407.266, 99%, $[M]^+$; 408.330, 60%, $[M + 2H]^+$; 409.356, 12%, $[M + 3H]^+$; 410.344, 1%, $[M + 4H]^+$ (3.789 min). **HRMS:** 407.0505, $[M + 2H]^+$ – Protonated *leuco* form (407.0507 expected for $C_{20}H_{16}N_4O^{79}Br$, −0.2 mDa). **CV (Cp*$_2$Fe$^+$ / Cp*$_2$Fe, −0.5 V):** $E^{0/+1}$ = −0.06 V, $E^{-1/0}$ = −1.00 V; ΔE = 0.94 V. **EPR:** a_N1 = 7.87 G, a_N2 = 4.94 G, a_N3 = 4.79 G, a_N4 = 0.58 G. **XRD:** Structure verified by XRD, see Appendix A.

8.3.5 – 1-(4-Bromophenyl)-3-anilino-1,4-dihydrobenzo[*e*][1,2,4]triazin-4-yl radical (**38f**)

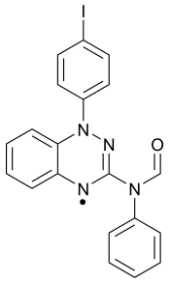


Following general procedure H, 1-(4-bromophenyl)-3-(*N*-formylanilino)-1,4-dihydrobenzo[*e*][1,2,4]triazin-4-yl radical (**37f**) (200 mg, 0.492 mmol) was stirred (RT, 27 h). Mixture redissolved in DCM (50 mL), washed with aqueous K_2CO_3 (1 M, 2 × 20 mL) and water (20 mL), then the organic phase concentrated *in vacuo*. The crude product was recrystallised (EtOH) to give 1-(4-bromophenyl)-3-anilino-1,4-dihydrobenzo[*e*][1,2,4]triazin-4-yl radical (130 mg, 0.344 mmol, 70%) as a dark green solid.

LC-MS (MeOH/H$_2$O): (For ^{79}Br isotopologue) 377.319 , 15%, $[M]^+$; 378.345, 24%, $[M + H]^+$; 379.295, 100%, $[M + 2H]^+$; (For ^{81}Br isotopologue) 380.359, 45%, $[M + H]^+$; 381.309, 92%, $[M + 2H]^+$; 382.373, 27%, $[M + 3H]^+$; 383.361, 5%, $[M + 4H]^+$ (2.196 min). **HRMS:** 377.0391, $[M]^+$

(377.0402 expected for $C_{19}H_{14}{}^{79}BrN_4$, −1.1 mDa). **CV (Cp_2Fe^+ / Cp_2Fe, 0 V):** $E^{0/+1}$ = −0.28 V; $E^{-1/0}$ = −1.16 V; ΔE = 0.88 V. **EPR:** a_N1 = 7.75 G, a_N2 = 5.75 G, a_N3 = 4.28 G, a_N4 = 0.58 G.

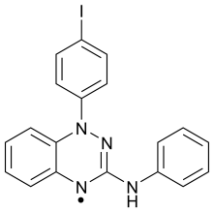
8.3.6 – 1-(4-Iodophenyl)-3-(*N*-formylanilino)-1,4-dihydrobenzo[*e*][1,2,4]triazin-4-yl radical (**37g**)



Following general procedure G, 1-(4-iodophenyl)-4-phenyl-3-(phenylamino)-4*H*-1,2,4-triazol-1-ium tetrafluoroborate (**33gH·BF_4**) (100 mg, 0.190 mmol) and triethylamine (0.03 mL, 0.2 mmol, 1.2 equiv.) were stirred (RT, 3 d). The crude product was purified by column chromatography (0 → 10% MeOH in DCM) and recrystallised (EtOH) to give 1-(4-iodophenyl)-3-(*N*-formylanilino)-1,4-dihydrobenzo[e][1,2,4]triazin-4-yl radical (39 mg, 0.086 mmol, 45%) as a dark red solid.

LC-MS (MeOH/H_2O): 453.167, 100%, $[M]^+$; 454.193, 63%, $[M + H]^+$; 455.257, 11%, $[M + 2H]^+$; 456.359, 1%, $[M + 3H]^+$ (3.842 min). **CV ($Cp^*_2Fe^+$ / Cp^*_2Fe, −0.5 V):** $E^{0/+1}$ = −0.02 V; $E^{-1/0}$ = −0.99; ΔE = 0.97 V. **EPR:** a_N1 = 7.85 G, a_N2 = 5.10 G, a_N3 = 4.66 G, a_N4 = 0.44 G.

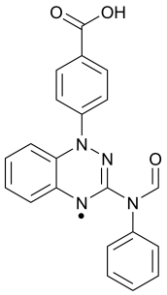
8.3.7 – 1-(4-Iodophenyl)-3-anilino-1,4-dihydrobenzo[*e*][1,2,4]triazin-4-yl radical (**38g**)



Following general procedure H, 1-(4-iodophenyl)-3-(*N*-formylanilino)-1,4-dihydrobenzo[*e*][1,2,4]-triazin-4-yl radical (**37g**) (10 mg, 0.022 mmol) were stirred (RT, 18 h). The crude product was redissolved in DCM (10 mL), washed with saturated $NaHCO_3$ solution (5 mL) and water (2 × 5 mL), then concentrated *in vacuo* to give 1-(4-iodophenyl)-3-anilino-1,4-dihydrobenzo[*e*][1,2,4]triazin-4-yl radical (6 mg, 0.01 mmol, 50%) as a dark green solid.

LC-MS (MeCN/H_2O): 425.196, 100%, $[M]^+$; 426.184, 24%, $[M + H]^+$; 427.210, 8%, $[M + 2H]^+$; 428.350, 2%, $[M + 3H]^+$ (2.471 min). **HRMS:** 425.0268, $[M]^+$ (425.0263 expected for $C_{19}H_{14}N_4I$, +0.5 mDa). **CV (Cp_2Fe^+ / Cp_2Fe, 0 V):** $E^{0/+1}$ = −0.28 V; $E^{-1/0}$ = −1.15 V; ΔE = 0.87 V.

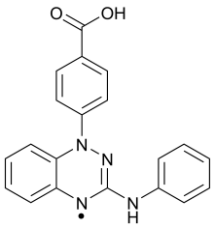
8.3.8 – 1-(4-Carboxyphenyl)-3-(*N*-formylanilino)-1,4-dihydrobenzo[*e*][1,2,4]triazin-4-yl radical (**37i**)



Following general procedure G, 1-(4-carboxyphenyl)-4-phenyl-3-(phenylamino)-4*H*-1,2,4-triazol-1-ium chloride (**33iH·BF$_4$**) (1.00 g, 2.55 mmol) and triethylamine (0.79 mL, 5.6 mmol, 2.2 equiv.) were stirred (RT, 6 d). The crude product was redissolved in DCM (70 mL), washed with water (2 × 30 mL), and concentrated *in vacuo*. The crude product was recrystallised from hot EtOH to give 1-(4-carboxyphenyl)-3-(*N*-formylanilino)-1,4-dihydrobenzo[*e*][1,2,4]triazin-4-yl radical (298 mg, 0.803 mmol, 31%) as a dark red solid.

LC-MS (MeCN/H$_2$O): 371.390, 100%, $[M]^+$; 372.378, 49%, $[M + H]^+$; 373.366, 16%, $[M + 2H]^+$; 374.354, 2%, $[M + 3H]^+$ (2.272 min). **HRMS:** 371.1134, $[M]^+$ (371.1144 expected for $C_{21}H_{15}N_4O_3$, −1.0 mDa). **CV (Cp*$_2$Fe$^+$ / Cp*$_2$Fe, −0.5 V):** $E^{0/+1} = -0.03$; −1/0 half-wave not observed. **TLC (9:1 DCM/MeOH):** $R_f = 0.4$.

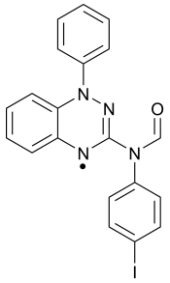
8.3.9 – 1-(4-Carboxyphenyl)-3-anilino-1,4-dihydrobenzo[*e*][1,2,4]triazin-4-yl radical (**38i**)



1-(4-(methoxycarbonyl)phenyl)-3-(*N*-formylanilino)-1,4-dihydrobenzo[*e*][1,2,4]triazin-4-yl radical (**183a**) (327 mg, 0.848 mmol, 1 equiv.) was dissolved in 20% aqueous THF (20 mL). Lithium hydroxide monohydrate (72 mg, 1.7 mmol, 2 equiv.) was added, then the reaction mixture was stirred (RT, 18 h). The reaction mixture was concentrated *in vacuo* to give 1-(4-carboxyphenyl)-3-anilino-1,4-dihydrobenzo[*e*][1,2,4]triazin-4-yl radical as a dark green solid, which was used directly in the next step without further purification.

IR: 736, 1173, 1413, 1496, 1637 (C=O), 3370 (C-H) cm^{-1} (assign.). **LC-MS:** 343.30, $[M]^+$ (1.52 min). **HRMS:** 343.1196, $[M]^+$ (343.1195 expected for $C_{20}H_{15}N_4O_2$, +0.1 mDa).

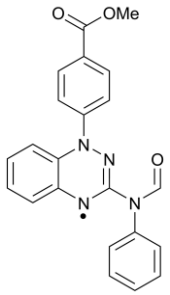
8.3.10 – 1-Phenyl-3-(*N*-formyl-4-iodoanilino)-1,4-dihydrobenzo[*e*][1,2,4]triazin-4-yl radical (**181b**)



(1,4-diphenyl-4*H*-1,2,4-triazol-1-ium-3-yl)(4-iodophenyl)amide (**80b**) (200 mg, 0.456 mmol, 1 equiv.) was dissolved in MeCN (19.8 mL) and water (0.2 mL). The reaction mixture was stirred (RT, 6 d) then dried *in vacuo*. The crude product was purified by reverse phase liquid chromatography (5 → 100% MeCN in H_2O) to give 1-phenyl-3-(*N*-formyl-4-iodoanilino)-1,4-dihydrobenzo[*e*][1,2,4]triazin-4-yl radical (104 mg, 0.229 mmol, 50%) as dark purple crystals.

LC-MS (MeCN/H_2O): 453.250, 100%, $[M]^+$; 454.276, 28%, $[M + H]^+$; 455.264, 9%, $[M + 2H]^+$; 456.290, 2%, $[M + 3H]^+$ (3.224 min). **HRMS:** 453.0210, $[M]^+$ (453.0212 expected for $C_{20}H_{14}N_4O^{127}I$, −0.2 mDa). **CV (Cp*$_2$Fe$^+$ / Cp*$_2$Fe, −0.5 V):** $E^{0/+1} = -0.06$ V; $E^{-1/0} = -0.88$ V; $\Delta E = 0.82$ V. **EPR:** $a_N1 = 7.90$ G, $a_N2 = 5.14$ G, $a_N3 = 4.56$ G, $a_N4 = 0.53$ G. **TLC (98:2 DCM/MeOH):** $R_f = 0.51$. **XRD:** Structure verified by XRD, see Appendix A.

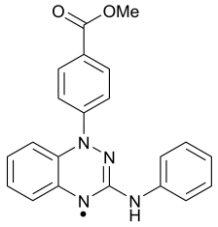
8.3.11– 1-(4-(Methoxycarbonyl)phenyl)-3-(*N*-formylanilino)-1,4-dihydrobenzo[*e*][1,2,4]triazin-4-yl radical (**183a**)



Following general procedure G, 1-(4-(methoxycarbonyl)phenyl)-4-phenyl-3-(phenylamino)-4*H*-1,2,4-triazol-1-ium chloride (**81aH·Cl**) (40 mg, 0.098 mmol) and DIPEA (25 μL, 0.15 mmol, 1.5 equiv.) was stirred (RT, 4 d). The crude product was purified by reverse phase liquid chromatography (10 → 100% MeOH in H_2O) to give 1-(4-(methoxycarbonyl)phenyl)-3-(*N*-formylanilino)-1,4-dihydrobenzo[*e*][1,2,4]triazin-4-yl radical (16 mg, 0.042 mmol, 43%) as a dark brown solid.

IR: 722, 1103, 1279 (C-O), 1411, 1499, 1684, 1719 (C=O), 2929 (C-H) cm^{-1}. **LC-MS (MeOH/H_2O):** 385.330, 100%, $[M]^+$; 386.319, 49%, $[M + H]^+$; 387.345, 16%, $[M + 2H]^+$ 388.447, 4%, $[M + 3H]^+$ (3.391 min). **HRMS:** 385.1313, $[M]^+$ (385.1301 expected for $C_{22}H_{17}N_4O_3$, +1.2 mDa).

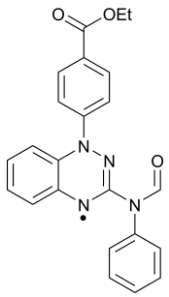
8.3.12 – 1-(4-(Methoxycarbonyl)phenyl)-3-anilino-1,4-dihydrobenzo[*e*][1,2,4]triazin-4-yl radical (**184a**)



Following general procedure H, 1-(4-carboxyphenyl)-3-(*N*-formylanilino)-1,4-dihydrobenzo[*e*][1,2,4]triazin-4-yl radical (**37i**) (200 mg, 0.54 mmol) was stirred (RT, 19 h). The reaction mixture was redissolved in DCM (20 mL), washed with saturated sodium bicarbonate solution (20 mL), then concentrated *in vacuo* to give 1-(4-(methoxycarbonyl)phenyl)-3-anilino-1,4-dihydrobenzo[*e*][1,2,4]triazin-4-yl radical (45 mg, 0.13 mmol, 24%) as a dark green solid.

LC-MS (MeCN/H_2O): 357.360, 18%, $[M]^+$; 359.336, 100%, $[M + 2H]^+$; 360.362, 20%, $[M + 3H]^+$; 361.388, 3%, $[M + 4H]^+$ (1.985 min). **HRMS:** 357.1351, $[M]^+$ (357.1352 expected for $C_{21}H_{17}N_4O_2$, −0.1 mDa).

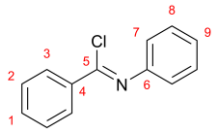
8.3.13 – 1-(4-(Ethoxycarbonyl)phenyl)-3-(*N*-formylanilino)-1,4-dihydrobenzo[*e*][1,2,4]triazin-4-yl radical (**183b**)



Following general procedure G, 1-(4-(ethoxycarbonyl)phenyl)-4-phenyl-3-(phenylamino)-4*H*-1,2,4-triazol-1-ium chloride (**81b**) (25 mg, 0.059 mmol) was stirred (RT, 8 d). The crude product was purified by reverse phase liquid chromatography (10 → 100% MeOH in H_2O) to give 1-(4-(ethoxycarbonyl)phenyl)-3-(*N*-formylanilino)-1,4-dihydrobenzo[*e*][1,2,4]triazin-4-yl radical (7 mg, 0.02 mmol, 30%) as a dark brown solid.

IR: 693, 759, 1014, 1269 (C-O), 1585, 1684, 1715 (C=O), 2937 (C-H) cm^{-1}. **LC-MS:** 400.61 $[M + H]^+$ (2.99 min). **HRMS:** 399.1462, $[M]^+$ (399.1457 expected for $C_{23}H_{19}N_4O_3$, +0.5 mDa).

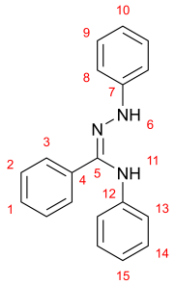
8.3.14 – *N*-phenylbenzimidoyl chloride (**186**)



N-phenylbenzamide (1.00 g, 5.07 mmol) was dissolved in anhydrous toluene (10 mL), then thionyl chloride (1.10 mL, 15.2 mmol, 3, equiv.) added. The reaction mixture was vigorously refluxed (8 h) then concentrated *in vacuo* to give *N*-phenylbenzimidoyl chloride (1.08g, 5.01 mmol, 99%) as a bright yellow solid.

LC-MS (H_2O quench, MeCN/H_2O): 198.197, 100%, $[M – Cl + OH + H]^+$; 199.261, 15%, $[M – Cl + OH + 2H]^+$; 200.287, 1%, $[M – Cl + OH + 3H]^+$ (2.106 min).

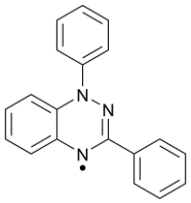
8.3.15– *N*,*N*'-diphenylbenzohydrazonamide (**58**)



N-phenylbenzimidoyl chloride (**186**) (1.08 g, 5.01 mmol, 1 equiv.) was dissolved in THF (10 mL) under an argon atmosphere. Triethylamine (1.06 mL, 7.61 mmol, 1.5 equiv.) was added, then the reaction mixture was cooled on ice. Phenylhydrazine (0.50 mL, 5.1 mmol, 1 equiv.) was added slowly to the reaction mixture, then the mixture was warmed to RT. The reaction mixture was stirred (RT, 16 h), then concentrated *in vacuo*. The reaction mixture was redissolved in 2% AcOH in H_2O (20 mL), then refluxed (30 min) before cooling to RT. The precipitate was filtered, then washed with water (5 mL) and MeOH (2 mL) to give *N*,*N*'-diphenylbenzohydrazonamide (637 mg, 2.21 mmol, 44%) as a colourless solid.

^{1}H NMR (400 MHz, N4, $CDCl_3$): δ_H 6.72 (2 H, dt, J = 8.6 and 1.0 Hz, C^{14}); 6.87 (1 H, tt, J = 7.3 and 1.2 Hz, C^{15}); 6.92 (1 H, tt, J = 7.4 and 1.1 Hz, C^{10}); 7.12 (2 H, dt, J = 8.5 Hz and 2.1 Hz, C^9); 7.20 – 7.30 (4 H, m, C^8 and C^{13}); 7.33 – 7.40 (3 H, m, C^1 and C^3); 7.73 (2 H, dt, J = 5.2 and 2.9 Hz, C^2). **LC-MS (MeOH/H_2O):** 288.268, 100%, $[M + H]^+$; 289.294, 53%, $[M + 2H]^+$; 290.321, 6%, $[M + 3H]^+$ (1.655 min). **HRMS:** 288.1502, $[M + H]^+$ (288.1501 expected for $C_{19}H_{18}N_3$, +0.1 mDa).

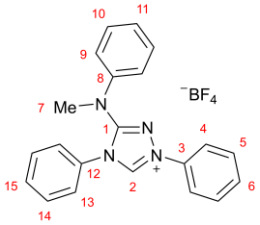
8.3.16 – 1,3-Diphenyl-1,4-dihydrobenzo[*e*][1,2,4]triazin-4-yl radical (**137**)



N,*N*'-diphenylbenzohydrazonamide (**58**) (200 mg, 0.696 mmol, 1 equiv.) was dissolved in DCM (10 mL). DBU (0.01 mL, 0.07 mmol, 10 mol%) and palladium on carbon (2.23 mg, 10 wt% loading, 0.002 mmol, 0.3 mol%) were added to the reaction mixture. The reaction mixture was stirred (RT, 3 d), then filtered through celite and concentrated *in vacuo*. The crude product was recrystallised (IPA) to give 1,3-diphenyl-1,4-dihydrobenzo[*e*][1,2,4]triazin-4-yl radical (168 mg, 0.591 mmol, 84%) as a dark brown solid.

LC-MS (MeCN/H_2O): 284.240, 29%, $[M]^+$; 285.228, 100%, $[M + H]^+$; 286.216, 82%, $[M + 2H]^+$; 287.280, 13%, $[M + 3H]^+$; 288.268, 1%, $[M + 4H]^+$ (3.165 min). **HRMS:** 2.71 min, 284.1191, $[M]^+$ (284.1188 expected for $C_{19}H_{14}N_3$, +0.3 mDa); 4.79 min, 285.1266, $[M + H]^+$ (285.1261 expected for $C_{19}H_{15}N_3$, +0.5 mDa). **CV (Cp_2Fe^+ / Cp_2Fe, 0 V):** $E^{0/+1}$ = −0.18 V; $E^{-1/0}$ = −1.25 V; ΔE = 1.07 V. **EPR**: a_N1 = 7.55 G; a_N2 = 5.22 G; a_N3 = 4.78 G; a_N4 = 0.72 G.

8.3.17 – 3-(Methyl(phenyl)amino)-1,4-diphenyl-4*H*-1,2,4-triazol-1-ium tetrafluoroborate (**192**)

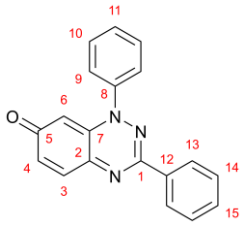


Nitron (1.00 g, 3.20 mmol, 1 equiv.) and trimethyloxonium tetrafluoroborate (568 mg, 3.84 mmol, 1.2 equiv.) was dissolved in DCM (40 mL) under an argon atmosphere. The reaction mixture was stirred (RT, 16 h), then quenched with water (10 mL). The two phases were separated, with the organic phase further washed with water (10 mL) and concentrated *in vacuo*. The crude product was redissolved in minimal hot IPA, filtered, then cooled to −20 °C overnight. The mixture was filtered to give 3-(methyl(phenyl)amino)-1,4-diphenyl-4*H*-1,2,4-triazol-1-ium tetrafluoroborate (237 mg, 0.573 mmol, 15%) as a pale grey solid.

^{1}H NMR (599 MHz, $CDCl_3$): δ_H 3.53 (3 H, s, C^7); 6.94 (2 H, dt, *J* = 7.4 and 1.1 Hz, C^{10}); 6.97 (1 H, tt, *J* = 7.4 and 1.1 Hz, C^{11}); 7.07 (2 H, td, *J* = 7.6 and 2.0 Hz, C^9); 7.16 (2 H, td, *J* = 7.5 and 1.5 Hz, C^{13}); 7.19 (1 H, tt, *J* = 7.4 and 2.2 Hz, C^{15}); 7.33 (2 H, dt, *J* = 7.2 and 1.8 Hz, C^{14}); 7.48 – 7.57

(3 H, m, C^4 and C^6); 7.98 (2 H, dt, J = 7.1 and 2.2 Hz, C^5); 9.78 (1 H, s, C^2). **$^{13}C\{^1H\}$ NMR (151 MHz, $CDCl_3$):** δ_C 43.0 (C^7); 121.0 (C^5); 124.7 (C^{10}); 125.9 (C^{14}); 127.0 (C^{11}); 129.7 (C^{13}); 129.8 (C^9); 130.2 (C^4); 130.6 (C^{15}); 130.8 (C^6); 131.2 (C^{12}); 135.0 (C^3); 138.8 (C^2); 142.6 (C^8); 154.7 (C^1). **LC-MS ($MeOH/H_2O$):** 327.261, 100%, $[M]^+$; 328.287, 61%, $[M + H]^+$; 329.351, 7%, $[M + 2H]^+$; 330.453, 1%, $[M + 3H]^+$ (2.263 min). **HRMS:** 327.1608, $[M]^+$ (327.1610 expected for $C_{21}H_{19}N_4$, −0.2 mDa).

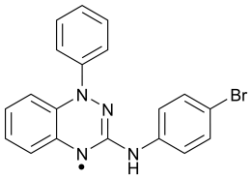
8.3.18 – 1,3-Diphenylbenzo[*e*][1,2,4]triazin-7(1*H*)-one (**158**)



1,3-diphenyl-1,4-dihydrobenzo[*e*][1,2,4]triazin-4-yl radical (**137**) (90 mg, 0.32 mmol, 1 equiv.) was dissolved in DCM (10 mL). MnO_2 (276 mg, 3.17 mmol, 10 equiv.) was added to the reaction mixture. The reaction mixture was stirred (RT, 3 d), filtered through celite and concentrated *in vacuo* to give 1,3-diphenylbenzo[*e*][1,2,4]triazin-7(1*H*)-one (64 mg, 0.21 mmol, 68%) as a deep purple solid.

^1H NMR (599 MHz, $CDCl_3$): δ_H 6.11 (1 H, d, J = 2.1 Hz, C^6); 7.31 (1 H, dd, J = 9.7 and 2.1 Hz, C^4); 7.46 – 7.52 (3 H, m, C^{11} and C^{14}); 7.55 – 7.64 (5 H, m, C^9, C^{10} and C^{15}); 7.72 (1 H, d, J = 9.7 Hz, C^3); 8.27 (2 H, td, J = 6.1 and 1.3 H, C^{13}). **$^{13}C\{^1H\}$ NMR (151 MHz, $CDCl_3$):** δ_C 97.8 (C^6); 125.7 (C^{10}); 126.8 (C^{13}); 128.9 (C^{14}); 130.1 (C^9); 130.3 (C^{15}); 130.7 (C^{11}); 132.2 (C^3); 133.9 (C^1); 136.6 (C^7); 141.1 (C^8); 142.5 (C^4); 150.9 (C^{12}); 155.0 (C^2); 182.1 (C^5). **LC-MS ($MeOH/H_2O$):** 300.202, 100%, $[M + H]^+$; 301.266, 25%, $[M + 2H]^+$; 302.292, 3%, $[M + 3H]^+$ (2.540 min). **HRMS:** 300.1133, $[M + H]^+$ (300.1137 expected for $C_{19}H_{14}N_3O$, −0.4 mDa).

8.3.19 – 1-Phenyl-3-(4-bromoanilino)-1,4-dihydrobenzo[*e*][1,2,4]triazin-4-yl radical (**182a**)

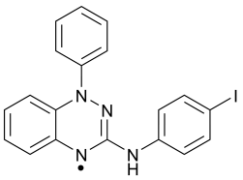


1-phenyl-3-anilino-1,4-dihydrobenzo[*e*][1,2,4]triazin-4-yl radical (**38a**) (400 mg, 1.34 mmol, 1 equiv.) was dissolved in TFA (10 mL). *N*-bromosuccinimide (238 mg, 1.34 mmol, 1 equiv.) was added to the reaction mixture, then the reaction mixture was stirred (RT, 2 h) then concentrated *in vacuo*. The crude product was recrystallized (DCM / diethyl ether, RT to 2 °C) to give the product,

with the mother liquor concentrated *in vacuo* and the recrystallisation process repeated to give further product. The recrystallised product was combined to give 1-phenyl-3-(4-bromoanilino)-1,4-dihydrobenzo[*e*][1,2,4]triazin-4-yl radical (426 mg, 1.13 mmol, 84%) as a dark green solid.

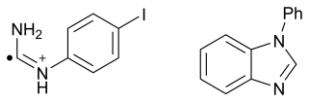
LC-MS (MeCN/H_2O): (For ^{79}Br isotopologue) 377.198, 97%, $[M]^+$; 378.224, 17%, $[M + H]^+$; (For ^{81}Br isotopologue) 379.212, 100%, $[M]^+$; 380.200, 25%, $[M + H]^+$; 381.302, 3%, $[M + 2H]^+$ (1.829 min). **HRMS:** 377.0402, $[M]^+$ (377.0402 expected for $C_{19}H_{14}N_4{}^{79}Br$, ± 0 mDa). **EPR:** a_N1 = 8.01 G, a_N2 = 5.58 G, a_N3 = 4.24 G, a_N4 = 0.67 G. **XRD:** Structure verified by XRD, see Appendix A.

8.3.20 – 1-Phenyl-3-(4-iodoanilino)-1,4-dihydrobenzo[*e*][1,2,4]triazin-4-yl radical (**182b**)



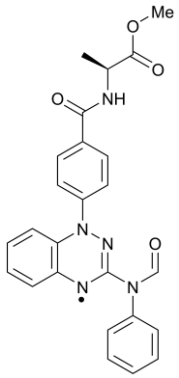
1-phenyl-3-anilino-1,4-dihydrobenzo[*e*][1,2,4]triazin-4-yl radical (**38a**) (200 mg, 0.669 mmol) was dissolved in trifluoroacetic acid (10 mL), *N*-iodosuccinimide (300 mg, 1.34 mmol, 2 equiv.) was added to the reaction mixture. The reaction mixture was stirred (RT, 2 h) before concentration *in vacuo* to a black oil. The oil was resuspended in EtOAc (40 mL), washed with $Na_2S_2O_3$ (1 M, 2 × 20 mL) and dried *in vacuo* to afford 1-phenyl-3-(4-iodoanilino)-1,4-dihydrobenzo[*e*][1,2,4]triazin-4-yl radical (254 mg, 0.598 mmol, 89%) as a dark purple solid.

LC-MS (MeOH / H_2O): 425.279, 100%, $[M]^+$; 426.306, 77%, $[M + H]^+$; 427.332, 68%, $[M + 2H]^+$; 428.358, 14%, $[M + 3H]^+$; 429.346, 3%, $[M + 4H]^+$; 430.296, 1%, $[M + 5H]^+$ (2.838 min). **LC-MS-MS (MeCN / H_2O):** 425.0, $[M]^+$; 298.2, $[M – I]^+$; 297.2, $[M – HI]^+$; 246.2, [**A**]$^+$; 221.1, $[M – C_6H_4I]^+$; 206.2, $[M – NHC_6H_4I]^+$; 193.2, [**B**]$^+$; 181.1, $[M – NCNHC_6H_4I]^+$; 118.1, [**B** – Ph]$^+$



HRMS: 425.0261, $[M]^+$ (425.0263 expected for $C_{19}H_{14}N_4{}^{127}I$, −0.2 mDa). **CV (Cp_2Fe^+ / Cp_2Fe, 0 V):** $E^{0/+1}$ = −0.30 V, −1/0 half wave not observed. **TLC (98:2 DCM/MeOH):** R_f = 0.63.

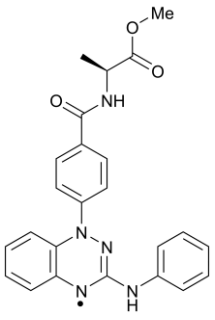
8.3.21 – (*S*)-1-(4-((1-Methoxy-1-oxopropan-2-yl)carbamoyl)phenyl)-3-(*N*-formylanilino)-1,4-dihydrobenzo[e][1,2,4]triazin-4-yl radical (**208**)



1-(4-carboxyphenyl)-3-(*N*-formylanilino)-1,4-dihydrobenzo[*e*][1,2,4]triazin-4-yl radical (**37i**) (50 mg, 0.11 mmol), triethylamine (18 μL, 0.12 mmol, 1.2 equiv.), MeCN (9.9 mL) and H_2O (0.1 mL) were combined in a reaction vial. The reaction mixture was stirred (RT, 7d), concentrated *in vacuo*, then partitioned between DCM (10 mL) and water (10 mL). The organic phase was concentrated in vacuo then recrystallised (DCM / diethyl ether, −20 °C) to remove residual starting material. The mother liquor was concentrated *in vacuo* to afford (*S*)-1-(4-((1-methoxy-1-oxopropan-2-yl)carbamoyl)phenyl)-3-(*N*-formylanilino)-1,4-dihydrobenzo[e][1,2,4]triazin-4-yl radical (30 mg, 0.066 mmol, 63%) as a dark red solid.

LC-MS (MeOH/H_2O): 456.518, 100%, $[M]^+$; 457.544, 31%, $[M + H]^+$; 458.494, 7%, $[M + 2H]^+$; 459.634, 1%, $[M + 3H]^+$ (2.967 min). **HRMS:** 456.1656, $[M]^+$ (456.1672 expected for $C_{25}H_{22}N_5O_4$, −1.6 mDa).

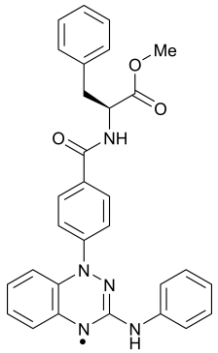
8.3.22 – 1-(4-((2*S*)-1-Methoxy-1-oxopropan-2-yl)carbamoyl)phenyl)-3-anilino-1,4-dihydrobenzo[*e*][1,2,4]triazin-4-yl radical (**210a**)



Following general procedure I, L-alanine methyl ester hydrochloride (46 mg, 0.33 mmol) gave 1-(4-((2*S*)-1-methoxy-1-oxopropan-2-yl)carbamoyl)phenyl)-3-anilino-1,4-dihydrobenzo[*e*][1,2,4]-triazin-4-yl radical (8 mg, 0.02 mmol, 6%) as a pale green solid.

IR: 693, 749, 837, 1089, 1483, 1600 (C-C, aromatic), 1632 (C=O, amide), 1736 (C=O, ester), 2954 (C-H), 3305 (N-H) cm^{-1}. **LC-MS:** 428.27, $[M]^+$ (2.03 min). **HRMS:** 428.1731, $[M]^+$ (428.1723 expected for $C_{24}H_{22}N_5O_3$, +0.8 mDa).

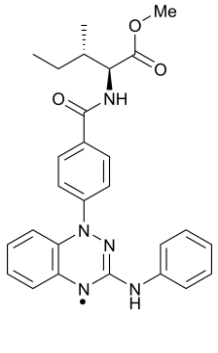
8.3.23 – 1-(4-(((2*S*)-1-Methoxy-1-oxo-3-phenylpropan-2-yl)carbamoyl)phenyl)-3-anilino-1,4-dihydrobenzo[*e*][1,2,4]triazin-4-yl radical (**210b**)



Following general procedure I, L-phenylalanine methyl ester hydrochloride (90 mg, 0.42 mmol) gave 1-(4-(((2*S*)-1-methoxy-1-oxo-3-phenylpropan-2-yl)carbamoyl)phenyl)-3-anilino-1,4-dihydrobenzo-[*e*][1,2,4]triazin-4-yl radical (76 mg, 0.15 mmol, 36%) as a dark green solid.

IR: 693, 748, 849, 1217, 1483, 1528, 1600 (C-C, aromatic), 1638 (C=O, amide), 1735 (C=O, ester), 2981 (C-H) cm^{-1}. **LC-MS:** 504.4, $[M]^+$ (2.84 min). **HRMS:** 504.2034, $[M]^+$ (504.2036 expected for $C_{30}H_{26}N_5O_3$, −0.2 mDa).

8.3.24 – 1-(4-(((2*S*,3*S*)-1-Methoxy-3-methyl-1-oxopentan-2-yl)carbamoyl)phenyl)-3-anilino-1,4-dihydrobenzo[*e*][1,2,4]triazin-4-yl radical (**210c**)

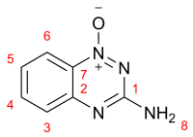


Following general procedure I, L-isoleucine methyl ester hydrochloride (75 mg, 0.35 mmol) gave 1-(4-(((2*S*,3*S*)-1-methoxy-3-methyl-1-oxopentan-2-yl)carbamoyl)phenyl)-3-anilino-1,4-dihydro-benzo[*e*][1,2,4]triazin-4-yl radical (50 mg, 0.11 mmol, 31%) as a dark green solid.

IR: 693, 749, 856, 1226, 1325, 1483, 1528, 1601 (C-C, aromatic), 1648 (C=O, amide), 1735 (C=O, ester), 2968 (C-H) cm^{-1}. **LC-MS:** 470.38, $[M]^+$ (2.59 min). **HRMS:** 470.2192, $[M]^+$ (470.2178 expected for $C_{27}H_{28}N_5O_3$, +1.4 mDa).

8.4 – Syntheses from Chapter 4

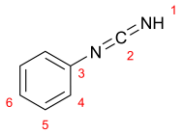
8.4.1 – 3-Aminobenzo[*e*][1,2,4]triazine-1-oxide (**214**)



2-nitroaniline (20.0 g, 145 mmol, 1 equiv.) and cyanamide (20.0 g, 476 mmol, 3.3 equiv.) were melted together to a dark brown oil. The oil was cooled to RT before addition of HCl (conc., 50 mL), a highly exothermic reaction is observed. A reflux condenser was quickly installed, with the resultant mixture stirred until at RT. A 20 M solution of NaOH (40.0 g, 1.00 mol) in H_2O (50 mL) was added dropwise to the reaction before reflux (30 min). The reaction mixture was cooled to RT, diluted with H_2O (100 mL) and filtered. The solid was washed with water (30 mL), transferred to a sintered funnel containing a filter paper atop celite, then purified by column chromatography (9:1 DCM / MeOH). Once residual 2-nitroaniline was no longer seen by TLC, the solid remaining atop the celite pad was removed and combined with column fractions of product to obtain 3-aminobenzo[*e*][1,2,4]triazine-1-oxide (21.3 g, 131 mmol, 90%) as a yellow solid.

^{1}H NMR (600 MHz, $CDCl_3$): δ_H 5.14 (2H, s, N^8); 7.36 (1H, ddd, 9, 7.2 and 1.2 Hz, C^5); 7.60 (1H, dd, 8.5 and 1.2 Hz, C^3); 7.74 (1H, ddd, 8.4, 6.9 and 1.5 Hz, C^4); 8.28 (1H, dd, 8.6 and 1.5 Hz, C^6). **^{13}C{^{1}H} NMR (150 MHz, $CDCl_3$):** δ_C 120.4 (C^6); 125.8 (C^5); 126.5 (C^3); 135.8 (C^4) (C^1, C^2 and C^7 unable to be assigned due to weak sample. **IR:** 1249 (C-N); 1350 (N-O); 1540 (C=N); 1570 (N-O); 1613 (N-H bend); 1651 (C=C); 3120 (C-H); 3339 and 3312 cm^{-1} (N-H). **LC-MS (MeOH/H_2O):** 107.181, 14%, $[M - CN_3H]^+$; 118.165, 30%, $[M - CN_2H_4]^+$; 133.177, 40%, $[M - CNH_3]^+$; 163.162, 100%, $[M + H]^+$; 164.188, 23%, $[M + 2H]^+$; 165.252, 2%, $[M + 3H]^+$ (1.106 min). **HRMS:** 163.0616, $[M+H]^+$ (163.0620 expected for $C_7H_7N_4O$, −0.4 mDa). **UV/Vis**: λ_{max} = 239 nm (258, 205 and 412 nm).

8.4.2 – *N*-Phenylmethanediimine (**243**)

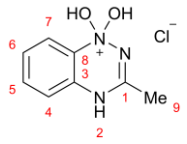


N-phenylthiourea (2.00 g, 13.1 mmol, 1 equiv.) was suspended in EtOAc (60 mL). Triethylamine (3.70 mL, 26.3 mmol, 2 equiv.) was added to the reaction mixture, followed by portionwise addition of I_2 (7.34 g, 28.9 mmol, 2.2 equiv.). The reaction mixture was stirred (RT, 2 h) then filtered *in vacuo* with the resultant solution washed with aqueous $Na_2S_2O_3$ (1 M, 2 × 30 mL) and the organic phase dried over Na_2SO_4. The organic phase was concentrated *in vacuo*, resuspended in hexanes (20 mL),

filtered through celite and concentrated *in vacuo*. The oil product was extracted from residual polymeric impurities by pipette to give *N*-phenylmethanediimine (0.944 g, 8.00 mmol, 61%) as an orange oil.

^{1}H NMR (B4, 400 MHz, $CDCl_3$): δ_H 7.01 – 7.07 (3 H, m, C^4 and C^6); 7.29 (2 H, tdd, J = 7.2, 2.5 and 1.3 Hz, C^5); 7.81 (1 H, br. s, N^1). **^{13}C{^{1}H} NMR (B4, 101 MHz, $CDCl_3$):** δ_C 115.4 (C^5); 123.4 (C^6); 129.6 (C^4); 137.6 (C^3); 209.0 (C^2). **LC-MS (MeOH/H_2O):** 109.112, 3%, $[M - CN + O]^+$ (hydrolysis product); 119.031, 100%, $[M + H]^+$; 120.133, 15%, $[M + 2H]^+$; 139.060, 24%, $[M + H_4O]^+$ (1.90 min). **GCMS (DCM):** 40.00, 15%, $[M - C_6H_6]^+$; 51.05, 15%, $[M - C_3H_3N_2]^+$; 65.05, 13%, $[M - C_2H_2N_2]^+$; 77.05, 24%, $[M - CHN_2]^+$; 91.05, 83%, $[M - CHN]^+$; 118.10, 100%, $[M]^+$ (4.29 min) **HRMS:** 119.0583, $[M + H]^+$ (119.0609 expected for $C_7H_7N_2$, −2.6 mDa).

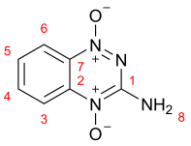
8.4.3 – 1,1-Dihydroxy-3-methyl-1,4-dihydrobenzo[*e*][1,2,4]triazin-1-ium chloride (**252**)



2-nitroaniline (2.00 g, 14.5 mmol) was stirred into MeCN (10 mL) to afford an oil. The obtained oil was treated with hydrochloric acid (5 mL) then heated to reflux (24 h). The reaction mixture was filtered, with the filtrate poured over DCM (40 mL). The organic phase was further washed with water (2 × 20 mL) then dried *in vacuo*. The crude product was purified by column chromatography (0 → 50% AcOH in DCM) to afford 1,1-dihydroxy-3-methyl-1,4-dihydrobenzo[*e*][1,2,4]triazin-1-ium chloride (41 mg, 0.23 mmol, 2%) as a brown solid.

^{1}H NMR (600 MHz, $CDCl_3$): δ_H 2.27 (3H, s, C^9); 7.15 (1 H, ddd, 8.6, 8.1 and 1.4 Hz, C^6); 7.62 (1H, ddd, 8.6, 7.2 and 1.6 Hz, C^5); 8.17 (1H, dd, 8.4 and 1.6 Hz, C^4); 8.73 (1H, dd, 8.6 and 1.4 Hz, C^7); 10.28 (1H, s, N^2). **^{13}C{^{1}H} NMR (150 MHz, $CDCl_3$):** δ_C 25.7 (C^9); 122.2 (C^9); 123.3 (C^7); 125.8 (C^6); 134.9 (C^5); 136.0 (C^8); 136.4 (C^{10}); 169.1 (C^3). **LC-MS (MeOH/H_2O):** 181.36, 100%, $[M + H]^+$; 182.162, 12%, $[M + 2H]^+$; 183.150, 1%, $[M + 3H]^+$ (1.682 min). **HRMS:** 180.0794, $[M]^+$ (180.0773 expected for $C_8H_{10}N_3O_2$, +2.1 mDa).

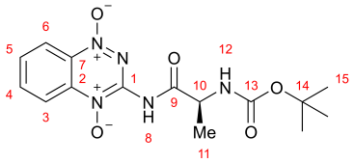
8.4.4 – 3-Aminobenzo[*e*][1,2,4]triazine 1,4-dioxide (Tirapazamine) (**39**)



3-aminobenzo[*e*][1,2,4]triazine-1-oxide (**214**) (1.00 g, 6.17 mmol) was dissolved in AcOH (40 mL) and 30% aq. H_2O_2 solution (25 mL). The reaction mixture was stirred (50 °C, 85 h) before solid $NaHCO_3$ added until roughly pH 7. The solid was filtered from the mixture with the resultant filtrate extracted with DCM (5 × 30 mL). The washings were combined, dried over Na_2SO_4 then *in vacuo* to afford 3-aminobenzo[*e*][1,2,4]triazine 1,4-dioxide (714 mg, 4.01 mmol, 65%) as a bright red solid.

^{1}H NMR (600 MHz, d_6-DMSO): δ_H 7.56 (1H, ddd, 8.2, 6.4 and 1.2 Hz, C^3); 7.94 (1H, ddd, 9.4, 6.9 and 1.2 Hz, C^4); 8.04 (2H, s, N^8); 8.14 (1H, dd, 8.6 and 0.5 Hz, C^3); 8.20 (1H, dd, 8.7 and 0.6 Hz, C^6). **^{13}C{^{1}H} NMR (150 MHz, d_6-DMSO):** δ_C 117.0 (C^3); 121.0 (C^6); 126.9 (C^5); 130.6 (C^2); 135.4 (C^4); 138.4 (C^7); 151.4 (C^1). **IR:** 1255 (C-N); 1352 (N-O); 1535 (C=N); 1590 (N-O); 1604 (N-H bend); 1730 and 1720 (C-H bend, overtone); 3101 (C-H); 3305 and 3262 cm^{-1} (N-H). **LC-MS (MeCN/H_2O):** 102.210, 6%, $[M - C_6H_4]^+$; 146.246, 1%, $[M - O_2]^+$; 162.171, 4%, $[M - O]^+$; 179.083, 100%, $[M + H]^+$; 180.148, 23%, $[M + 2H]^+$; 181.098, 2%, $[M + 3H]^+$ (0.268 min). **HRMS:** 179.0565, $[M + H]^+$ (179.0569 expected for $C_7H_7N_4O_2$, [−0.4 mDa]). **UV/Vis**: λ_{max} = 269 nm (221 and 469 nm). **TLC (9:1 DCM/MeOH):** R_f = 0.72.

8.4.5 – (S)-3-(2-((*Tert*-butoxycarbonyl)amino)propanamido)benzo[e][1,2,4]-triazine 1,4-dioxide (**255**)

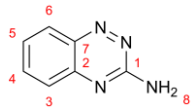


N-Boc alanine (100 mg, 0.529 mmol, 1 equiv.), 3-aminobenzo[*e*][1,2,4]triazine 1,4-dioxide (**39**) (95 mg, 0.53 mmol, 1 equiv.), PyBOP (305 mg, 0.586 mmol, 1.1 equiv.) and DCM (15 mL) were combined in a round bottomed flask. DIPEA (0.20 mL, 1.2 mmol, 2.2 equiv.) was added to the reaction mixture then the mixture was stirred (RT, 20 h). The crude product was concentrated *in vacuo,* then purified by reverse phase liquid chromatography (5 → 100% MeCN in H_2O) to give (S)-3-(2-((*tert*-butoxycarbonyl)amino)propanamido)benzo[e]-[1,2,4]-triazine 1,4-dioxide (80 mg, 0.23 mmol, 43%) as orange crystals.

^{1}H NMR (400 MHz, N4, $CDCl_3$): δ_H 1.47 (9 H, s, C^{15}); 1.50 (3 H, d, J = 7.3 Hz, C^{11}); 4.54 (1 H, m, C^{10}); 5.13 (1 H, d, J = 7.05 Hz, N^{12}); 7.75 (1 H, ddd, J = 8.6, 7.1 and 1.2 Hz, C^5); 7.99 (1 H, ddd, 8.5,

7.0 and 1.3 Hz, C^4); 8.44 (2 H, ddd, J = 8.3, 5.1 and 0.7 Hz, C^3 and C^6); 10.50 (1 H, br. s, N^8). **LC-MS (MeCN/H_2O):** 179.149, 8%, $[M - C_8H_{12}NO_3]^+$ 294.222, 33%, $[M - C_4H_7]^+$; 350.324, 100%, $[M + H]^+$; 351.366, 16%, $[M + 2H]^+$; 699.479, 7% $[2M + H]^+$ (1.690 min). **HRMS:** 350.1467, $[M + H]^+$ (350.1464 expected for $C_{15}H_{20}N_5O_5$, +0.3 mDa). **XRD:** Structure verified by XRD, see Appendix A.

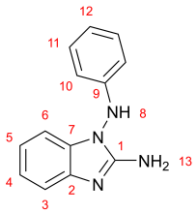
8.4.6 – Benzo[*e*][1,2,4]triazin-3-amine (**222**)



3-aminobenzo[*e*][1,2,4]triazine-1-oxide (**214**) (5.00 g, 30.9 mmol) was dissolved in EtOH (450 mL) and H_2O (200 mL). $Na_2S_2O_4$ (10.0 g, 57.4 mmol, 1.9 equiv.) was added to the reaction mixture before heating to reflux (1 h). The reaction mixture was separated by hot filtration and dried *in vacuo*. The crude product was resuspended in water, filtered, and dried by suction to afford Benzo[*e*][1,2,4]triazin-3-amine (3.30 g, 22.6 mmol, 73%) as a yellow solid.

^{1}H NMR (600 MHz, $CDCl_3$): δ_H 5.59 (2H, s, N^{11}); 7.51 (1H, ddd, 11.3, 6.8 and 1.2 Hz, C^8); 7.62 (1H, dd, 2.5 and 0.4 Hz, C^6); 7.78 (1H, ddd, 8.6, 6.9 and 1.4 Hz, C^7); 8.30 (1H, dd, 8.4 and 1.4 Hz, C^9). **^{13}C{^{1}H} NMR (150 MHz, $CDCl_3$):** δ_C 126.1 (C^8); 126.5 (C^6); 130.0 (C^9); 136.0 (C^7); 142.2 (C^5); 143.7 (C^{10}); 159.7 (C^3). **IR:** 1358 (N-O); 1548 (C=N); 1611 (N-H bend); 1672 (C=C); 3124 (C-H); 3347 and 3264 cm^{-1} (N-H). **LC-MS (MeOH/H_2O):** 147.120, 100%, $[M + H]^+$; 148.146, 17%, $[M + 2H]^+$; 149.134, 1%, $[M + 3H]^+$ (1.502 min). **HRMS:** 147.0659, $[M + H]^+$ (147.0671 expected for $C_7H_7N_4$, −1.2 mDa). **UV/Vis**: λ_{max} = 235 nm (207, 394 and 300 nm). **TLC (9:1 DCM/MeOH):** R_f = 0.70.

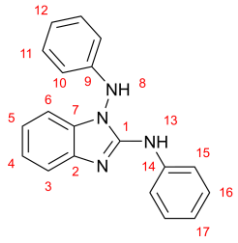
8.4.7 – N^1-phenyl-1*H*-benzo[*d*]imidazole-1,2-diamine (**257**)



Benzo[*e*][1,2,4]triazin-3-amine (**222**) (146 mg, 1.00 mmol, 1 equiv.) was dissolved in dry THF (3 mL) and cooled to −78 °C. PhLi (1.32 mL, 1.9 M in dibutyl ether, 2.5 mmol, 2.5 equiv.) was added dropwise to the stirring solution, then the reaction mixture was stirred (−78 °C, 30 min; RT, 30 min). The reaction mixture was vented with a needle then water (1 mL) added. The reaction mixture was further stirred (RT, 16 h) then concentrated *in vacuo* and purified by column chromatography (0 → 10% MeOH in DCM) to give N^1-phenyl-1*H*-benzo[*d*]imidazole-1,2-diamine (15 mg, 0.066 mmol, 7%) as dark red crystals.

^{1}H NMR (600 MHz, d$_6$-DMSO): δ_H 6.45 (2 H, s, N^{13}); 6.49 (2 H, ddd, J = 8.6, 3.1 and 2.1 Hz, C^{11}); 6.75 (1 H, dd, J = 7.8 and 1.3 Hz, C^{3}); 6.77 – 6.84 (2 H, m, C^{12} and C^{5}); 6.95 (1 H, td, J = 7.5 and 1.3 Hz, C^{4}); 7.15 – 7.21 (3 H, m, C^{6} and C^{10}); 8.98 (1 H, s, N^{8}). **^{13}C{^{1}H} NMR (151 MHz, d$_6$-DMSO):** δ_C 107.4 (C^{3}); 112.7 (C^{11}); 115.4 (C^{6}); 118.3 (C^{5}); 120.2 (C^{12}); 121.0 (C^{4}); 129.1 (C^{10}); 132.5 (C^{7}); 140.9 (C^{2}); 146.7 (C^{9}); 154.9 (C^{1}). **LC-MS (MeOH/H$_2$O):** 132.110, 26%, [M – C$_6$H$_6$N]$^+$; 210.249, 9%, [M – NH]$^+$; 225.221, 100%, [M + H]$^+$; 226.246, 48%, [M + 2H]$^+$ (1.862 min). **HRMS:** 225.1137, [M + H]$^+$ (225.1140 expected for C$_{13}$H$_{13}$N$_4$, −0.3 Da. **XRD:** Structure verified by XRD, see Appendix A.

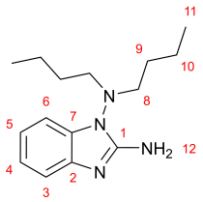
8.4.8 – N^1,N^2-diphenyl-1*H*-benzo[*d*]imidazole-1,2-diamine (**259**)



Benzo[*e*][1,2,4]triazin-3-amine (**222**) (146 mg, 1.00 mmol, 1 equiv.) was dissolved in dry THF (3 mL). The reaction mixture was cooled to −78 °C then PhLi (1.32 mL, 1.9 M in dibutyl ether, 2.5 mmol, 2.5 equiv.) was added dropwise to the reaction mixture. The reaction mixture was stirred (−78 °C, 25 min; RT, 30 min) then vented with a needle. Water (1 mL) was added, then the reaction mixture was stirred (RT, 5 h). The reaction mixture was partitioned between DCM (20 mL) and water (20 mL), with the organic phase concentrated *in vacuo* and purified by reverse phase liquid chromatography (5 → 100% MeOH in H$_2$O) to give N^1,N^2-diphenyl-1*H*-benzo[*d*]imidazole-1,2-diamine (301 mg, 0.769 mmol, 77%) as a red solid.

^{1}H NMR (599 MHz, d$_6$-DMSO): δ_H 6.93 – 6.99 (3 H, m, C^{5}, C^{12} and C^{17}); 7.02 (1 H, dd, J = 7.89 and 1.45 Hz, C^{6}); 7.11 (1 H, dd, J = 7.67 and 1.46 Hz, C^{3}); 7.14 (2 H, dt, J = 7.86 and 1.11 Hz, C^{10}); 7.21 (2 H, br. s, N^{8} and N^{13}); 7.23 – 7.30 (7 H, m, C^{4}, C^{11}, C^{15} and C^{16}). **^{13}C{^{1}H} NMR (151 MHz, d$_6$-DMSO):** δ_C 113.7 (C^{10}); 116.7 (C^{11}); 121.2 (C^{17}); 121.6 (C^{12}); 122.2 (C^{6}); 122.5 (C^{5}); 124.7 (C^{15}); 126.4 (C^{3}); 129.0 (C^{16}); 129.0 (C^{4}); 131.8 (C^{7}); 140.7 (C^{2}); 145.0 (C^{14}); 148.9 (C^{9}); 152.2 (C^{1}). **LC-MS (MeCN/H$_2$O):** 208.225, 2%, [M – C$_6$H$_6$N]$^+$; 301.292, 100%, [M + H]$^+$; 302.333, 34%, [M + 2H]$^+$; 303.363, 4%, [M + 3H]$^+$ (2.072 min). **HRMS:** 301.1460, [M + H]$^+$ (301.1453 expected for C$_{19}$H$_{17}$N$_4$, +0.7 mDa).

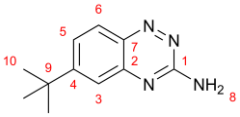
8.4.9 – N^1, N^1-dibutyl-1*H*-benzo[*d*]imidazole-1,2-diamine (**265**)



Benzo[*e*][1,2,4]triazin-3-amine (**222**) (146 mg, 1.00 mmol, 1 equiv.) was dissolved in dry THF (3 mL) in a microwave vial under Ar. The vial was cooled to −78 °C before addition of n-butyllithium (2.5 M in hexanes, 1 mL, 2.5 mmol, 2.5 equiv.) dropwise to the reaction mixture. The reaction mixture was stirred (−78 °C, 40 min; RT, 75 min) then was vented with a needle. Water (1 mL) was added to the reaction mixture, then the reaction mixture was stirred (RT, 1 h) and then concentrated *in vacuo*. The crude product was purified by column chromatography (0 → 10% MeOH in DCM) to afford N^1, N^1-dibutyl-1*H*-benzo[*d*]imidazole-1,2-diamine (5 mg, 0.02 mmol, 2%) as red crystals.

^{1}H NMR (599 MHz, CD_3OD): δ_H 0.87 (6 H, t, J = 7.4 Hz, C^{11}); 1.16 – 1.25 (2 H, m, $C^{9'}$); 1.27 – 1.42 (4 H, m, C^{10}); 1.48 (2 H, dtt, J = 12.8, 9.1 and 5.9 Hz, $C^{9''}$); 3.12 (2 H, ddd, J = 12.2, 9.4 and 6.1 Hz, $C^{8'}$); 3.50 (2 H, ddd, J = 12.2, 9.2 and 5.2 Hz, $C^{8''}$) 6.97 (1 H, td, J = 7.6 and 1.1 Hz, C^5); 7.06 (1 H, td, J = 7.7 and 1.1 Hz, C^4); 7.26 (1 H, dt, J = 7.9 and 0.9 Hz, C^3); 7.36 (1 H, d, J = 7.8 Hz, C^6). **^{13}C{^{1}H} NMR (151 MHz, CD_3OD):** δ_C 14.3 (C^{11}); 21.3 (C^{10}); 30.7 (C^9); 56.6 (C^8); 110.7 (C^6); 116.9 (C^3); 120.3 (C^5); 122.6 (C^4); 131.2 (C^2); 141.1 (C^7); 157.0 (C^1). **LC-MS (MeOH/H_2O):** 203.335, 3%, $[M - C_4H_9]^+$; 261.396, 100%, $[M + H]^+$; 262.457, 32%, $[M + 2H]^+$; 263.424, 3%, $[M + 3H]^+$ (2.607 min). **HRMS:** 261.2067, $[M + H]^+$ (261.2079 expected for $C_{15}H_{25}N_4$, −1.2 mDa). **XRD:** Structure verified by XRD, see Appendix A (4 crystallographically independent structures within unit cell).

8.4.10 – 6-(*Tert*-butyl)benzo[*e*][1,2,4]triazin-3-amine (**268**)

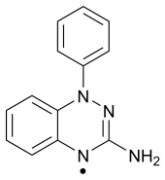


Benzo[*e*][1,2,4]triazin-3-amine (**222**) (146 mg, 1.00 mmol) was dissolved in dry THF (3 mL) under an argon atmosphere within a sealed vial. The reaction mixture was cooled to −78 °C, then *tert*-butyllithium (1.32 mL, 1.9 M in pentane, 2.5 mmol, 2.5 equiv.) was added dropwise to the reaction mixture. The reaction mixture was stirred (−78 °C, 20 min; RT, 2 h) then needle pierced through the vial septum and stirred until effervescence ceased. Water (1 mL) was added to the reaction mixture, then the reaction mixture was stirred (RT, 16 h). The mixture was partitioned between DCM (20 mL) and water (20 mL), with the organic phase concentrated *in vacuo*. The crude product was purified by reverse phase liquid chromatography (5 to 100% MeOH in water), then recrystallised from hot

MeOH to give 6-(*tert*-butyl)benzo[*e*][1,2,4]triazin-3-amine (34 mg, 0.17 mmol, 17%) as a yellow solid.

^{1}H NMR (599 MHz, $CDCl_3$): δ_H 1.38 (9 H, s, C^{10}); 5.97 (2 H, br. s, N^8); 7.51 (1 H, d, J = 1.89 Hz, C^3); 7.56 (1 H, dd, J = 8.90 and 1.98 Hz, C^5); 8.18 (1 H, d, J = 8.89 Hz, C^6). **^{13}C{^{1}H} NMR (151 MHz, $CDCl_3$):** δ_C 30.8 (C^{10}); 35.9 (C^9); 121.2 (C^3); 125.3 (C^5); 129.2 (C^6); 142.5 (C^4); 142.5 (C^2); 160.2 (C^7); 160.2 (C^1). **LC-MS (MeCN/H_2O):** 203.258, 100%, $[M + H]^+$; 204.316, 29%, $[M + 2H]^+$; 205.315, 2%, $[M + 3H]^+$ (2.731 min). **HRMS:** 203.1321, $[M + H]^+$ (203.1297 expected for $C_{11}H_{15}N_4$, +2.4 mDa). **XRD:** Structure verified by XRD, see Appendix A.

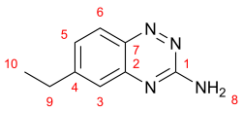
8.4.11– 1-Phenyl-3-amino-1,4-dihydrobenzo[*e*][1,2,4]triazin-4-yl radical (**256**)



Benzo[*e*][1,2,4]triazin-3-amine (**222**) (146 mg, 1.00 mmol) was dissolved in anhydrous THF (3 mL) and cooled to −78 °C. Phenylmagnesium bromide (0.83 mL, 3.0 M in diethyl ether, 2.5 mmol, 2.5 equiv.) was added to the reaction mixture, then the mixture was stirred (−78 °C, 25 min; RT, 60 min). Water (2 mL) was added to the reaction mixture, then the reaction mixture stirred (RT, 2 h). The reaction mixture was partitioned between DCM (20 mL) and water (20 mL), with the organic phase concentrated *in vacuo*. The crude product was purified by reverse phase liquid chromatography (5 → 100% MeOH in H_2O) to give 1-phenyl-3-amino-1,4-dihydrobenzo[*e*][1,2,4]triazin-4-yl radical (4 mg, 20 μmol, 2%) as a dark red solid.

LC-MS (MeCN/H_2O): 223.263, 100%, $[M]^+$; 224.272, 19%, $[M + H]^+$; 225.254, 1%, $[M + 3H]^+$ (0.857 min). **HRMS:** 223.0988, $[M]^+$ (223.0984 expected for $C_{13}H_{11}N_4$, +0.4 mDa).

8.4.12 – 6-Ethylbenzo[*e*][1,2,4]triazin-3-amine (**272**)



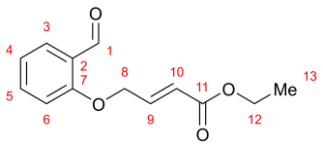
Benzo[*e*][1,2,4]triazin-3-amine (**222**) (146 mg, 1.00 mmol) was dissolved in anhydrous THF (3 mL), then cooled to −78 °C. Ethylmagnesium bromide (0.83 mL, 3.0 M in diethyl ether, 2.5 mmol, 2.5 equiv.) was added dropwise to the reaction mixture, then the mixture stirred (−78 °C, 20 min; RT, 85 min). Water (2 mL) was added to the reaction mixture, then the mixture was stirred (RT, 90 min). The reaction mixture was diluted with DCM (20 mL) and water (20 mL), leading to formation of an

emulsion. The emulsion was left to settle for 30 min, with isolation of the organic phase possible. The organic phase was dried over Na_2SO_4, filtered, and concentrated *in vacuo*. The crude product was purified by reverse phase liquid chromatography (5 → 100% MeOH in H_2O) to give 6-ethylbenzo[*e*][1,2,4]triazin-3-amine (8 mg, 0.05 mmol, 5%) as a yellow solid.

^{1}H NMR (599 MHz, $CDCl_3$): δ_H 1.32 (3 H, t, *J* = 7.58 Hz, C^{10}); 2.82 (2 H, q, *J* = 7.56 Hz, C^9); 5.52 (2 H, br. s, N^8); 7.34 (1 H, dd, *J* = 8.63 and 1.80 Hz, C^5); 7.37 (1 H, d, *J* = 1.43 Hz, C^3); 8.17 (1 H, d, *J* = 8.59 Hz, C^6). **^{13}C{^{1}H} NMR (151 MHz, $CDCl_3$):** δ_C 14.7 (C^{10}); 29.7 (C^9); 123.6 (C^3); 127.8 (C^5); 129.6 (C^6); 142.7 (C^7); 142.9 (C^4); 153.6 (C^2); 159.9 (C^1). **LC-MS (MeCN/H_2O):** 175.170, 100%, $[M + H]^+$; 176.229, 15%, $[M + 2H]^+$; 177.259, 1%, $[M + 3H]^+$ (1.603 min). **HRMS:** 175.1009, $[M + H]^+$ (175.0984 expected for $C_9H_{11}N_4$, +2.5 mDa).

8.5 – Syntheses from Chapter 5

8.5.1 – Ethyl (*E*)-4-(2-formylphenoxy)but-2-enoate (**323**)



Salicylaldehyde (0.54 mL, 5.2 mmol, 1 equiv.) and potassium carbonate (1.1 g, 7.8 mmol, 1.5 equiv.) were dissolved in acetone (20 mL). Ethyl 4-bromocrotonate (0.71 mL, 5.2 mmol, 1 equiv.) was added to the reaction mixture. The reaction mixture was stirred (RT, 16 h), then concentrated *in vacuo*. The resultant mixture was partitioned between diethyl ether (40 mL) and water (20 mL), with the organic phase washed with water (20 mL), then brine (10 mL), and concentrated *in vacuo*. The crude product was purified by column chromatography (0 to 20% EtOAc in hexanes), with the product crystallised from the column effluent by slow evaporation in air, affording ethyl (*E*)-4-(2-formylphenoxy)but-2-enoate (640 mg, 2.7 mmol, 52%) as large yellow crystals.

^{1}H NMR (599 MHz, $CDCl_3$): δ_H 1.29 (3 H, td, J = 7.2 and 0.7 Hz, C^{13}); 4.20 (2 H, qd, J = 7.2 and 0.7 Hz, C^{12}); 4.81 (2 H, dd, J = 4.1 and 2.1 Hz, C^{8}); 6.20 (1 H, ddt, J = 15.8, 2.1 and 0.6 Hz, C^{9}); 6.93 (1 H, d, J = 8.4 Hz, C^{6}); 7.02 – 7.11 (2 H, m, C^{10} and C^{4}); 7.52 (1 H, dddd, J = 8.3, 7.4, 1.9 and 0.6 Hz, C^{5}) 7.83 (1 H, dd, J = 7.7 and 1.9 Hz, C^{3}); 10.53 (1 H, t, J = 0.7 Hz, C^{1}). **^{13}C{^{1}H} NMR (151 MHz, $CDCl_3$):** δ_C 14.3 (C^{13}); 60.8 (C^{12}); 66.9 (C^{8}); 112.6 (C^{6}); 121.5 (C^{4}); 122.6 (C^{9}); 125.2 (C^{7}); 128.9 (C^{3}); 136.0 (C^{5}); 141.3 (C^{10}); 160.3 (C^{2}); 165.9 (C^{11}); 189.3 (C^{1}). **LC-MS (MeOH/H_2O):** 113.140, 74%, $[M - C_7H_5O_2]^+$; 161.104, 92%, $[M - C_3H_5O_2]^+$; 189.152, 58%, $[M - C_2H_5O]^+$; 235.214, 100%, $[M + H]^+$; 236.278, 25%, $[M + 2H]^+$; 237.266, 3%, $[M + 3H]^+$; 257.219, 16%, $[M + Na]^+$ (2.922 min). **HRMS:** 235.0990, $[M + H]^+$ (235.0970 expected for $C_{13}H_{15}O_4$, +2.0 mDa).

8.6 – General experimental information – biology work

8.6.1 – Materials used

Chemicals used were obtained from Merck and Thermo Fisher Scientific, with no further purification. All cell lines were supplied by the Centre for Cancer, Newcastle University from frozen cultures.

8.6.2 – Experimental methods and related notation

8.6.2.1 – Cell incubation

When not being manipulated, cells were held in an incubator at 37 °C and 5% CO_2 enriched air. In the case of experiments undertaken under hypoxic conditions, the plated cells were placed in a hypoxia chamber filled with 5% O_2 in N_2 following the addition of treatment.

8.6.2.2 – Hemocytometry

Determination of cell concentration for preparation of seeded plates used a Marienfield Neubauer counting chamber. Cells were manually counted using a microscope and tally counter.

8.6.2.3 – Plate reader

Spectrophotometric analysis of SRB assays was undertaken using a FLUOstar OMEGA plate reader consoled to a computer. Readings were undertaken as the absorbance at 570nm and reported as the optical density (OD) per well.

8.7 – SRB assay methodology

8.7.1 – Cell preparation

Cell stocks checked by microscope for 50% to 80% confluence. Media aspirated from flask then cells washed with phosphate-buffered saline (PBS). PBS aspirated from cells, then trypsin (1 mL) added and cells incubated (5 min). Roswell Park Memorial Institute (RPMI) 1640 medium (9 mL) washed across the surface of flask several times, then the cell suspension was transferred to a universal tube. The cell stock was analysed by hemocytometry, and then a sample of the cell stock diluted to give a stock for plating – for SJSA and MCF-7, RPMI medium used; for GB-1, Dulbecco's Modified Eagle Medium (DMEM) used. Plating stock (80 μL) added to each of the 60 middle wells of a 96-well plate needed for compound dosing. Outer wells filled with the appropriate growth medium for the cell line. An additional plate (t=0 plate) made with plating stock (80 μL) of each tested cell line in a 10-well line across the inner wells. All plates placed in incubator (1 d)

8.7.2 – Treatment preparation

Compound for analysis (up to 10 mg) dissolved in DMSO to give 50 mM stock. Sample of 50 mM stock (10 μL) diluted 10-fold to give 5 mM stock, process repeated with 5 mM stock to give 500 μM stock. Dosing stocks (1 mL) prepared by diluting to 5 times desired dosing concentration in RPMI growth medium – volume of DMSO used maintained at 30 μL (See **Table 40**, Chapter 6.2.1).

8.7.3 – Cell incubation

't=0 plate' fixed with TCA (50 % v/v in H_2O, 20 μL) and placed in fridge until end of incubation time. Compounds dosed onto the compound dosing plates (20 μL, 5 replicates, 6 lines of varying [compound] including control were [compound] = 0, 2 compounds per plate). Dosed plates placed in incubator for the desired incubation time.

8.7.4 – Fixation and staining

TCA (50 % v/v in H_2O, 20 μL) added to each plate, plates placed in fridge (1 h). 't = 0' and dosing plates all removed from fridge and TCA poured down sink into flow of water from tap. Plates washed with water 5 times and blotted dry on tissue paper. SRB dye (100 μL) added to each well, leave to stand (RT, 30 min). Dye splashed down sink, then acetic acid (0.1% v/v) added to each well 5 times. Plates blotted with tissue paper then dried either using a drying oven or by leaving exposed to air overnight.

8.7.5 – Absorbance measurement and data analysis

Tris base (10 mM, 100 μL) added to each well, plates gently agitated then placed in a plate reader. Absorbance measurements taken for all wells at 570 nm to give array of well-specific OD values.

OD readings for t=0 plate subtracted from dosing plate OD values to give difference during incubation time with compound (corrected OD). Control line where [compound] = 0 for both compounds on plate (10 wells) averaged. Percentage growth *versus* the control line calculated for each well using **Equation 29**. Percentage growth values for each well averaged and plotted with error bars corresponding to standard error.

$$Percentage\ growth\ versus\ control = \frac{Corrected\ OD}{Averaged\ control\ OD} \times 100\% \qquad \textbf{Equation 29}$$

8.8 – Determination of Error

The following section summarises the errors from the work discussed in Chapters 2 and 5.

8.8.1 – XRD structural analysis

For XRD structural analysis of Nitron analogues, the calculation of error in the value of L(N^4-C^{13}) – L(N^1-C^6) ($s_{variance}$) was determined using **Equation 30**. The calculation of error in the value of A(N^1-C^5-N^4) / D(C^5-N^1-C^6-C^8) (s_{ESE}, ESE = effective substituent effect) was determined using **Equation 31**.

$$s_{variance} = \sqrt{\left(s_{L(N^4-C^{13})}\right)^2 + \left(s_{L(N^1-C^6)}\right)^2} \qquad \textbf{Equation 30}$$

$$s_{ESE} = \frac{A(N^1 - C^5 - N^4)}{D(C^5 - N^1 - C^6 - C^8)} \times \sqrt{\left(\frac{s_{A(N^1-C^5-N^4)}}{A(N^1 - C^5 - N^4}\right)^2 + \left(\frac{s_{D(C^5-N^1-C^6-C^8)}}{D(C^5 - N^1 - C^6 - C^8)}\right)^2} \qquad \textbf{Equation 31}$$

8.8.2 – First order rate constants (k_{ex}, s^{-1})

The maximum percentage error in k_{ex} is estimated to be 3%, based on the standard error in the fit of ln f(s) – time data for **99·Br** at 2 mM DCl (p*D* = 3.00) in 2:8 d_3-MeCN / D_2O, having the lowest R^2 value (0.994). For exchange experiments undertaken in D_2O without the addition of co-solvent the maximum percentage error is reduced to 0.6%, estimated with the same method (R^2 = 0.998). In general, errors in the range 0.2% to 0.6% were obtained.

8.8.3 – Second order rate constants for deuteroxide-catalysed exchange (k_{DO}) and pK_a

When considering k_{DO} values obtained from **Equation 12** (k_{ex} – [DO^-] plots), it is assumed that the error in k_{DO} (s_{DO}) equals the standard error in the slope obtained from the fits of k_{ex} – [DO^-] data to **Equation 12**. This assumption is based on the errors in K_w and γ_{DO}, used to calculate [DO^-], being less than 1%.[443] Errors obtained were in the range 0.4% to 6.0% with an average error of 2.1%

When considering k_{DO} values obtained from **Equation 13** (log k_{ex} – p*D* plots), it is assumed that the error in k_{DO} (s_{DO}) equals the standard error in the value of ($k_{DO} \times K_w$) / γ_{DO} obtained from the fits of log k_{ex} – p*D* data to **Equation 13**. This assumption is based on the errors in K_w and γ_{DO} being less than 1%.[443] Errors obtained were in the range 0.2% to 1.9% with an average error of 1.0%.

When considering log k_{DO}, the calculation of error in the value of log k_{DO} (s_{logDO}) was undertaken using **Equation 32**.

$$s_{logDO} = \frac{s_{DO}}{\ln 10 \times k_{DO}}$$ **Equation 32**

C(5)-H pK_a values for all *S*-triazolium salts were calculated using **Equation 24**. The standard error in k_{HO} (s_{HO}) was calculated using **Equation 33**. The standard error in the ratio k_{HOH} / k_{HO}, denoted s_r, is obtained using **Equation 34**. This equation considers the error in k_{HOH}, which equals 1 (± 0.1) × 10^{11}.[444] The standard error in pK_a (s_{pKa}) was calculated using **Equation 35**, the error in pK_w is negligible and so is excluded from this calculation.[443]

$$s_{HO} = k_{HO} \times \sqrt{\left(\frac{0.0631}{2.40}\right)^2 + \left(\frac{s_{DO}}{k_{DO}}\right)^2}$$ **Equation 33**

$$s_r = \frac{k_{HOH}}{k_{HO}} \times \sqrt{\left(\frac{1 \times 10^{10}}{1 \times 10^{11}}\right)^2 + \left(\frac{s_{HO}}{k_{HO}}\right)^2}$$ **Equation 34**

$$s_{pK_a} = 0.434 \times \frac{s_r}{\left({}^{k_{HOH}}/_{k_{HO}}\right)}$$ **Equation 35**

8.8.4 – Structure activity relationships

For the single-parameter fits of k_{DO} values relating to *para*-substituted 1,4-dimethyl *S*-triazolium salts, the error in slope and intercept are summarised in **Table 51**. Due to the large standard errors in the fit, these trends are not analysed quantitatively. The linear fit corresponding to D(C_3-S_6-C_7-C_9) is suggested to give approximations of k_{DO} with straightforward calculations, but that the value obtained should only be used to suggest appropriate parameters for H/D-exchange NMR kinetics (experiment time, number of transients).

Table 51 – Errors relating to the single-parameter fits undertaken for the three XRD parameters with highest R^2 value.

Parameter	Slope		Intercept	
	k_{ex} – [DO^-]	log k_{ex} – p*D*	k_{ex} – [DO^-]	log k_{ex} – p*D*
D(C_3-S_6-C_7-C_9)	−8.32 (± 1.56) × 10^5	−8.06 (± 1.56) × 10^5	9.11 (± 0.89) × 10^7	8.87 (± 0.89) × 10^7
D(N_2-C_3-S_6-C_7)	3.49 (± 0.84) × 10^5	3.67 (± 0.56) × 10^5	3.94 (± 0.51) × 10^7	3.78 (± 0.33) × 10^7

For the single-parameter fits of all k_{DO} values against the three identified XRD parameters of highest R^2, the error in slope and intercept are summarised in **Table 52**. Due to the large standard errors in the fit, these trends are not analysed quantitatively.

Table 52 – Errors relating to the single-parameter fits undertaken for the three XRD parameters with highest R^2 value.

Parameter	Slope		Intercept	
	k_{ex} – [DO$^-$]	log k_{ex} – pD	k_{ex} – [DO$^-$]	log k_{ex} – pD
L(N_1-N_2)	−6.56 (± 1.64) × 10^9	−6.05 (± 1.49) × 10^9	9.05 (± 2.25) × 10^9	8.34 (± 2.03) × 10^9
L(C_3-S_6)	7.63 (± 1.29) × 10^9	7.16 (± 1.07) × 10^9	−1.32 (± 0.23) × 10^{10}	−1.24 (± 0.19) × 10^{10}
D(C_3-S_6-C_7-C_9)	6.33 (± 0.88) × 10^5	5.73 (± 0.84) × 10^5	9.40 (± 0.74) × 10^7	8.58 (± 0.71) × 10^7

For the statistical modelling using JMP, large standard errors similar in magnitude to the estimated parameters are obtained in most cases. Because of the large uncertainty, the values of the estimated parameters are not analysed quantitatively. The errors in the slope and intercept of the linear fits of these models are summarised in **Table 53**. The maximum percentage error in the slope and intercept is 10% and 10.5% respectively. With the higher complexity F_2 models the percentage errors in slope and intercept are within the range of 6% to 8%.

Table 53 – Errors relating to the statistical modelling undertaken using JMP for the three XRD parameters with highest R^2 value.

Fit	Slope		Intercept	
	k_{ex} – [DO$^-$]	log k_{ex} – pD	k_{ex} – [DO$^-$]	log k_{ex} – pD
F_1	1.00 (± 0.10)	1.00 (± 0.10)	−5.22 (± 0.55) × 10^9	−1.80 (± 0.18) × 10^9
F_{2A}	1.00 (± 0.06)	1.00 (± 0.06)	−1.67 (± 0.10) × 10^9	−4.09 (± 0.25) × 10^{11}
F_{2B}	1.00 (± 0.06)	1.00 (± 0.06)	−1.67 (± 0.10) × 10^9	2.52 (± 0.20) × 10^9

The large standard error values obtained in the structure activity relationships is a result of the dataset size, the small range of values in the case of bond lengths, possible polymorphism, and the error relating to the XRD acquisition and refinement. For the dihedral angles, a large variance may be expected as a result of polymorphism relating to rotatable bonds that can give a complex range of molecular conformations in the crystal state. The error could be improved by collecting a larger dataset, which may additionally allow for accurate modelling of monomorphic groups of crystals.

Appendix A - Crystallographic information

A-1 – XRD data from Chapter 2

A-1.1 – 1-(4-Bromophenyl)-4-phenyl-3-(phenylamino)-4*H*-1,2,4-triazol-1-ium tetrafluoroborate (**33fH·BF$_4$**)

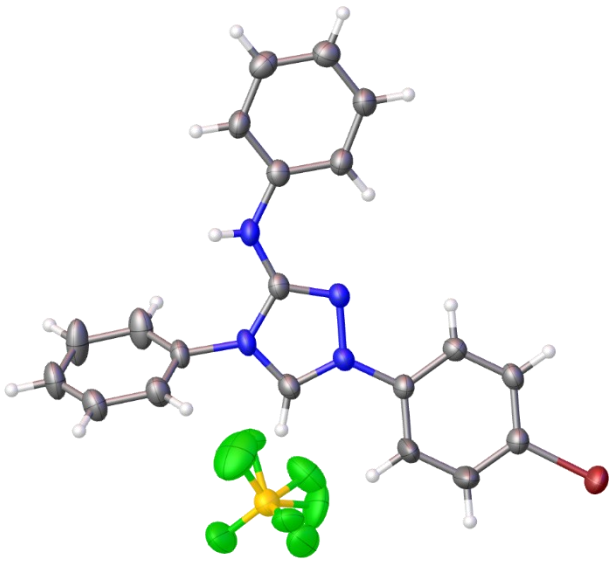


Table S1 – Crystal data and structure refinement for **33fH·BF$_4$**.

Identification code	21srv403	**ρ_{calc}g/cm^3**	1.536
Empirical formula	$C_{21}H_{20}BBrF_4N_4O$	**μ/mm^{-1}**	1.914
Formula weight	511.13	**F(000)**	516.0
Temperature/K	150.0	**Crystal size/mm^3**	0.09 × 0.08 × 0.04
Crystal system	triclinic	**Radiation**	Mo Kα (λ = 0.71073)
Space group	P-1	**2Θ range for data collection/°**	4.224 to 52
a/Å	9.7507(4)	**Index ranges**	−12 ≤ h ≤ 12, −13 ≤ k ≤ 13, −13 ≤ l ≤ 13
b/Å	10.7364(4)	**Reflections collected**	14802
c/Å	10.7979(4)	**Independent reflections**	4342 [R_{int} = 0.0428, R_{sigma} = 0.0508]
α/°	81.368(2)	**Data/restraints/parameters**	4342/51/321
β/°	81.474(2)	**Goodness-of-fit on F^2**	1.038
γ/°	88.217(2)	**Final R indexes [I>=2σ (I)]**	R_1 = 0.0425, wR_2 = 0.0845
Volume/Å^3	1105.20(7)	**Final R indexes [all data]**	R_1 = 0.0652, wR_2 = 0.0914
Z	2	**Largest diff. peak/hole / e Å^{-3}**	0.30/−0.36

A-1.2 – 1-(4-Carboxyphenyl)-4-phenyl-3-(phenylamino)-4*H*-1,2,4-triazol-1-ium chloride (**33iH·Cl**)

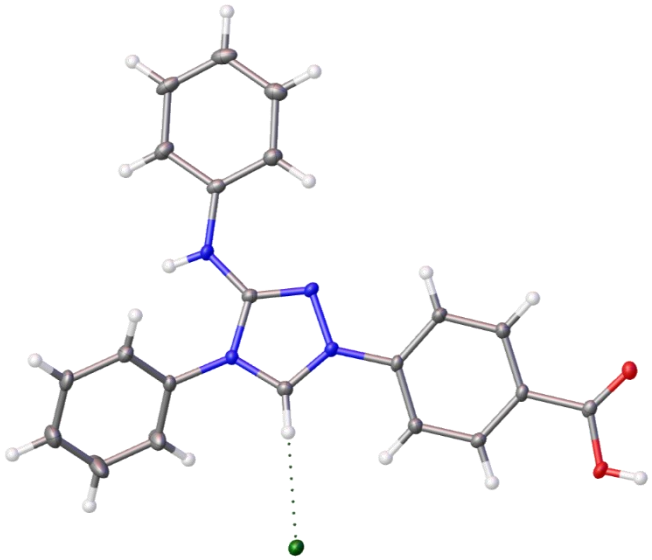


Table S2 – Crystal data and structure refinement for **33iH·BF$_4$**.

Identification code	21srv480	**ρ_{calc}g/cm^3**	1.437
Empirical formula	$C_{21}H_{22}ClN_4O_{4.5}$	**μ/mm^{-1}**	0.229
Formula weight	437.87	**F(000)**	458.0
Temperature/K	120.0	**Crystal size/mm^3**	0.36 × 0.05 × 0.01
Crystal system	triclinic	**Radiation**	Mo Kα (λ = 0.71073)
Space group	P-1	**2Θ range for data collection/°**	4.058 to 59.998
a/Å	6.4285(2)	**Index ranges**	$-9 \leq h \leq 9$, $-15 \leq k \leq 15$, $-22 \leq l \leq 22$
b/Å	10.6816(4)	**Reflections collected**	24113
c/Å	15.7635(5)	**Independent reflections**	5885 [R_{int} = 0.0758, R_{sigma} = 0.0697]
α/°	102.5480(10)	**Data/restraints/parameters**	5885/6/300
β/°	95.5130(10)	**Goodness-of-fit on F^2**	1.051
γ/°	104.0420(10)	**Final R indexes [I>=2σ (I)]**	R_1 = 0.0554, wR_2 = 0.1248
Volume/Å^3	1012.27(6)	**Final R indexes [all data]**	R_1 = 0.0718, wR_2 = 0.1330
Z	2	**Largest diff. peak/hole / e Å^{-3}**	0.43/−0.57

A-1.3 – 1-(4-(Methoxycarbonyl)phenyl)-4-phenyl-3-(phenylamino)-4*H*-1,2,4-triazol-1-ium chloride (**81a·Cl**)

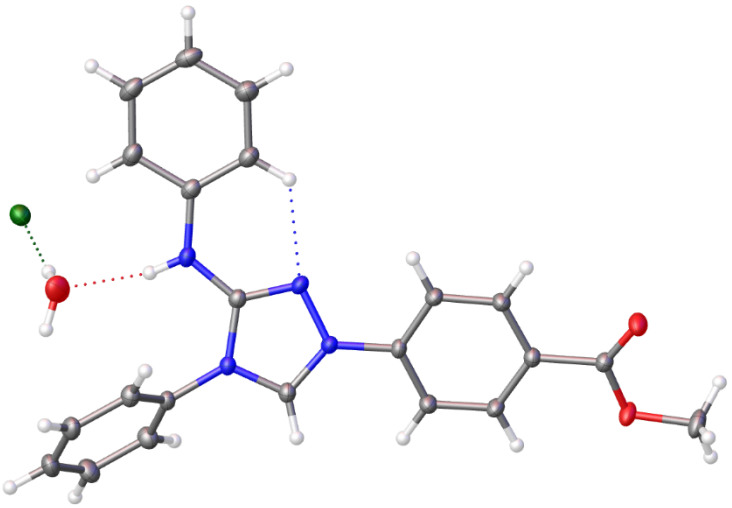


Table S3 – Crystal data and structure refinement for **81a·Cl**.

Identification code	23srv211	**ρ_{calc}g/cm^3**	1.398
Empirical formula	$C_{22}H_{21}ClN_4O_3$	**μ/mm^{-1}**	0.222
Formula weight	424.88	**F(000)**	444.0
Temperature/K	120.00	**Crystal size/mm^3**	0.199 × 0.055 × 0.039
Crystal system	triclinic	**Radiation**	Mo Kα (λ = 0.71073)
Space group	P-1	**2Θ range for data collection/°**	4.824 to 66.284
a/Å	5.89410(10)	**Index ranges**	−9 ≤ h ≤ 9, −13 ≤ k ≤ 13, −31 ≤ l ≤ 31
b/Å	8.6637(2)	**Reflections collected**	29509
c/Å	20.2806(5)	**Independent reflections**	7633 [R_{int} = 0.0498, R_{sigma} = 0.0550]
α/°	98.9440(10)	**Data/restraints/parameters**	7633/0/279
β/°	91.4750(10)	**Goodness-of-fit on F^2**	1.017
γ/°	99.0040(10)	**Final R indexes [I>=2σ (I)]**	R_1 = 0.0477, wR_2 = 0.1160
Volume/Å^3	1009.09(4)	**Final R indexes [all data]**	R_1 = 0.0748, wR_2 = 0.1294
Z	2	**Largest diff. peak/hole / e Å^{-3}**	0.58/−0.30

A-1.4 – 1-(4-Bromophenyl)-*N*,4-diphenyl-5-(phenylimino)-4,5-dihydro-1*H*-1,2,4-triazol-3-amine (**75f**)

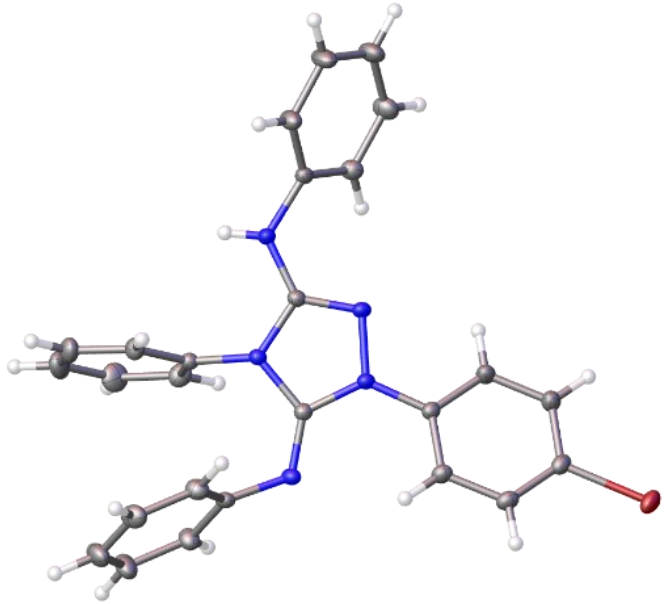


Table S4 – Crystal data and structure refinement for **75f**.

Identification code	23srv176	**ρ_{calc}g/cm^3**	1.473
Empirical formula	$C_{26}H_{20}BrN_5$	**μ/mm^{-1}**	1.914
Formula weight	482.38	**F(000)**	984.0
Temperature/K	120.00	**Crystal size/mm^3**	0.264 × 0.201 × 0.06
Crystal system	monoclinic	**Radiation**	Mo Kα (λ = 0.71073)
Space group	$P2_1/c$	**2Θ range for data collection/°**	4.258 to 73.684
a/Å	11.7640(5)	**Index ranges**	$-18 \leq h \leq 19$, $-24 \leq k \leq 24$, $-22 \leq l \leq 22$
b/Å	14.6387(6)	**Reflections collected**	104717
c/Å	13.6219(6)	**Independent reflections**	10637 [R_{int} = 0.0371, R_{sigma} = 0.0248]
α/°	90	**Data/restraints/parameters**	10637/0/293
β/°	111.962(2)	**Goodness-of-fit on F^2**	1.032
γ/°	90	**Final R indexes [I>=2σ (I)]**	R_1 = 0.0322, wR_2 = 0.0747
Volume/Å^3	2175.59(16)	**Final R indexes [all data]**	R_1 = 0.0471, wR_2 = 0.0794
Z	4	**Largest diff. peak/hole / e Å^{-3}**	0.53/−0.54

A-1.5 – 4-Methyl-3-(phenylthio)-4*H*-1,2,4-triazole (**86a**)

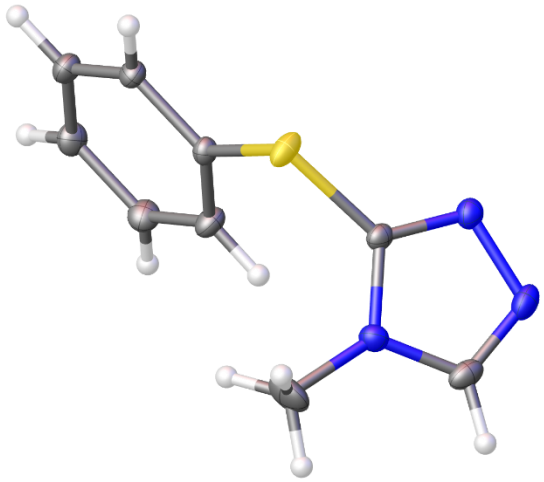


Table S5 – Crystal data and structure refinement for **86a**.

Identification code	20srv076	**ρ_{calc}g/cm^3**	1.408
Empirical formula	$C_9H_9N_3S$	**μ/mm^{-1}**	0.310
Formula weight	191.25	**F(000)**	400.0
Temperature/K	120.0	**Crystal size/mm^3**	0.27 × 0.18 × 0.11
Crystal system	orthorhombic	**Radiation**	Mo Kα (λ = 0.71073)
Space group	$P2_12_12_1$	**2Θ range for data collection/°**	5.862 to 58.998
a/Å	9.2964(12)	**Index ranges**	−12 ≤ h ≤ 12, −13 ≤ k ≤ 13, −14 ≤ l ≤ 14
b/Å	9.3889(11)	**Reflections collected**	14473
c/Å	10.3388(12)	**Independent reflections**	2518 [R_{int} = 0.0329, R_{sigma} = 0.0231]
α/°	90	**Data/restraints/parameters**	2518/0/119
β/°	90	**Goodness-of-fit on F^2**	1.061
γ/°	90	**Final R indexes [I>=2σ (I)]**	R_1 = 0.0283, wR_2 = 0.0711
Volume/Å^3	902.40(19)	**Final R indexes [all data]**	R_1 = 0.0316, wR_2 = 0.0726
Z	4	**Largest diff. peak/hole / e Å^{-3}**	0.56/−0.22

A-1.6 – 4-Methyl-3-(*p*-tolylthio)-4*H*-1,2,4-triazole (**86b**)

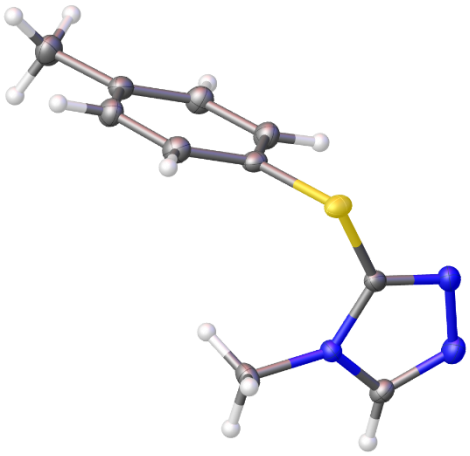


Table S6 − Crystal data and structure refinement for **86b**.

Identification code	22srv143	**ρ_{calc}g/cm^3**	1.377
Empirical formula	$C_{10}H_{11}N_3S$	**μ/mm^{-1}**	0.288
Formula weight	205.28	**F(000)**	432.0
Temperature/K	120.00	**Crystal size/mm^3**	0.21 × 0.18 × 0.16
Crystal system	monoclinic	**Radiation**	Mo Kα (λ = 0.71073)
Space group	$P2_1/c$	**2Θ range for data collection/°**	9.474 to 59.988
a/Å	11.2316(2)	**Index ranges**	$-15 \leq h \leq 15$, $-12 \leq k \leq 12$, $-14 \leq l \leq 14$
b/Å	9.0067(2)	**Reflections collected**	28073
c/Å	10.0453(2)	**Independent reflections**	2849 [R_{int} = 0.0280, R_{sigma} = 0.0143]
α/°	90	**Data/restraints/parameters**	2849/0/129
β/°	103.0710(8)	**Goodness-of-fit on F^2**	1.080
γ/°	90	**Final R indexes [I>=2σ (I)]**	R_1 = 0.0291, wR_2 = 0.0762
Volume/Å^3	989.85(3)	**Final R indexes [all data]**	R_1 = 0.0308, wR_2 = 0.0773
Z	4	**Largest diff. peak/hole / e Å^{-3}**	0.37/−0.25

A-1.7 – 4-Methyl-3-((4-nitrophenyl)thio)-4*H*-1,2,4-triazole (**86e**)

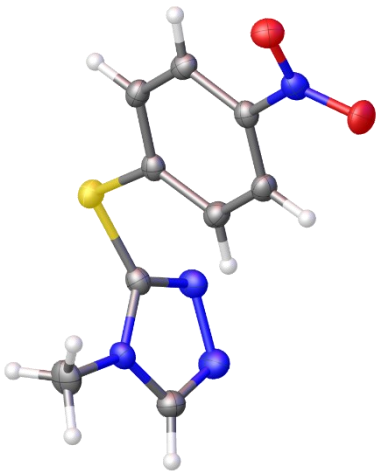
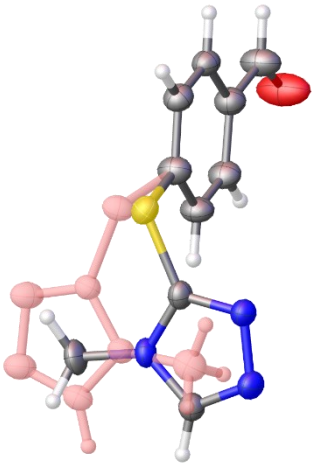


Table S7 – Crystal data and structure refinement for **86e**.

Identification code	20srv052	**ρ_{calc}g/cm^3**	1.559
Empirical formula	$C_9H_8N_4O_2S$	**μ/mm^{-1}**	0.311
Formula weight	236.25	**F(000)**	488.0
Temperature/K	120.0	**Crystal size/mm^3**	0.42 × 0.13 × 0.04
Crystal system	monoclinic	**Radiation**	Mo-Kα (λ = 0.71073)
Space group	$P2_1/c$	**2Θ range for data collection/°**	5.17 to 57.998
a/Å	10.1527(5)	**Index ranges**	−13 ≤ h ≤ 13, −17 ≤ k ≤ 18, −10 ≤ l ≤ 10
b/Å	13.2170(4)	**Reflections collected**	12529
c/Å	7.7599(3)	**Independent reflections**	2674 [R_{int} = 0.0634, R_{sigma} = 0.0537]
α/°	90	**Data/restraints/parameters**	2674/0/177
β/°	104.807(5)	**Goodness-of-fit on F^2**	1.032
γ/°	90	**Final R indexes [I>=2σ (I)]**	R_1 = 0.0431, wR_2 = 0.0906
Volume/Å^3	1006.70(8)	**Final R indexes [all data]**	R_1 = 0.0667, wR_2 = 0.1038
Z	4	**Largest diff. peak/hole / e Å^{-3}**	0.40/−0.38

A-1.8 – 4-((4-Methyl-4*H*-1,2,4-triazol-3-yl)thio)benzaldehyde (**86k**)



0.7 : 0.3 heterocycle disorder, minor component shown in pink.

Table S8 – Crystal data and structure refinement for **86k**.

Identification code	22srv012	**ρ_{calc}g/cm^3**	1.464
Empirical formula	$C_{10}H_9N_3OS$	**μ/mm^{-1}**	0.299
Formula weight	219.26	**F(000)**	456.0
Temperature/K	120.00	**Crystal size/mm^3**	0.43 × 0.07 × 0.04
Crystal system	monoclinic	**Radiation**	Mo Kα (λ = 0.71073)
Space group	$P2_1/c$	**2Θ range for data collection/°**	5.55 to 54.998
a/Å	10.1499(4)	**Index ranges**	$-13 \leq h \leq 13$, $-8 \leq k \leq 8$, $-19 \leq l \leq 19$
b/Å	6.6753(3)	**Reflections collected**	14526
c/Å	15.1851(6)	**Independent reflections**	2283 [R_{int} = 0.0731, R_{sigma} = 0.0516]
α/°	90	**Data/restraints/parameters**	2283/42/200
β/°	104.845(2)	**Goodness-of-fit on F^2**	1.074
γ/°	90	**Final R indexes [I>=2σ (I)]**	R_1 = 0.0606, wR_2 = 0.1600
Volume/Å^3	994.51(7)	**Final R indexes [all data]**	R_1 = 0.0809, wR_2 = 0.1753
Z	4	**Largest diff. peak/hole / e Å^{-3}**	0.55/−0.52

A-1.9 – Methyl 4-((4-methyl-4*H*-1,2,4-triazol-3-yl)thio)benzoate (**86n**)

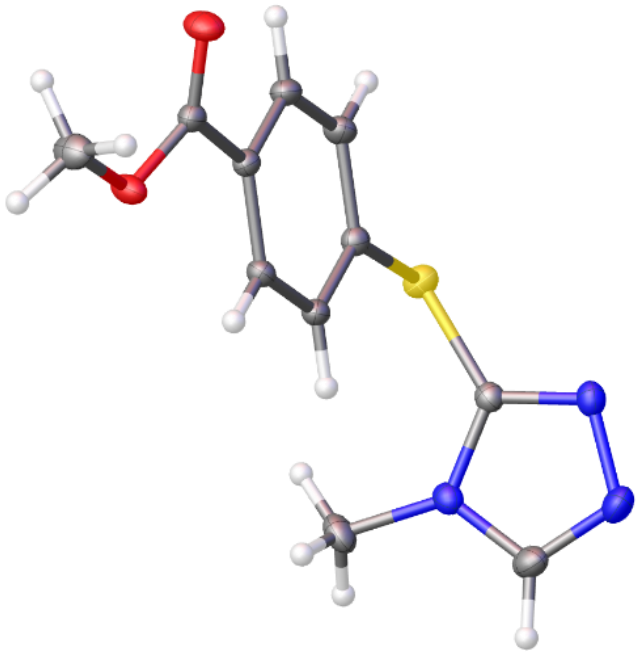


Table S9 – Crystal data and structure refinement for **86n**.

Identification code	22srv282	**ρ_{calc}g/cm^3**	0.277
Empirical formula	$C_{11}H_{11}N_3O_2S$	**μ/mm^{-1}**	260.0
Formula weight	249.29	**F(000)**	0.468 × 0.342 × 0.124
Temperature/K	120.00	**Crystal size/mm^3**	Mo Kα (λ = 0.71073)
Crystal system	monoclinic	**Radiation**	5.286 to 74.372
Space group	$P2_1$	**2Θ range for data collection/°**	−7 ≤ h ≤ 7, −15 ≤ k ≤ 15, −21 ≤ l ≤ 20
a/Å	4.58680(10)	**Index ranges**	17364
b/Å	9.5707(2)	**Reflections collected**	5219 [R_{int} = 0.0434, R_{sigma} = 0.0534]
c/Å	13.0035(3)	**Independent reflections**	5219/1/156
α/°	90	**Data/restraints/parameters**	1.046
β/°	91.8360(10)	**Goodness-of-fit on F^2**	R_1 = 0.0381, wR_2 = 0.0851
γ/°	90	**Final R indexes [I>=2σ (I)]**	R_1 = 0.0560, wR_2 = 0.0913
Volume/Å^3	570.55(2)	**Final R indexes [all data]**	0.37/−0.25
Z	2	**Largest diff. peak/hole / e Å^{-3}**	0.03(3)

A-1.10 – 2,3,5,6-Tetrafluoro-4-((4-methyl-4*H*-1,2,4-triazol-3-yl)thio)pyridine (**86q**)

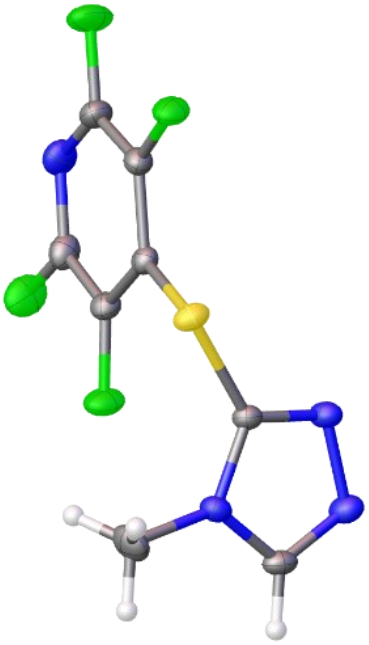


Table S10 – Crystal data and structure refinement for **86q**.

Identification code	22srv105	**ρ_{calc}g/cm^3**	1.761
Empirical formula	$C_8H_4F_4N_4S$	**μ/mm^{-1}**	0.366
Formula weight	264.21	**F(000)**	264.0
Temperature/K	120.00	**Crystal size/mm^3**	0.31 × 0.19 × 0.06
Crystal system	monoclinic	**Radiation**	Mo Kα (λ = 0.71073)
Space group	$P2_1$	**2Θ range for data collection/°**	4.18 to 59.998
a/Å	7.3051(3)	**Index ranges**	$-10 \leq h \leq 10$, $-9 \leq k \leq 9$, $-14 \leq l \leq 14$
b/Å	7.0003(3)	**Reflections collected**	11173
c/Å	10.1565(4)	**Independent reflections**	2888 [R_{int} = 0.0268, R_{sigma} = 0.0236]
α/°	90	**Data/restraints/parameters**	2888/1/170
β/°	106.4130(10)	**Goodness-of-fit on F^2**	1.050
γ/°	90	**Final R indexes [I>=2σ (I)]**	R_1 = 0.0237, wR_2 = 0.0582
Volume/Å^3	498.22(4)	**Final R indexes [all data]**	R_1 = 0.0250, wR_2 = 0.0590
Z	2	**Largest diff. peak/hole / e Å^{-3}**	0.24/−0.20

A-1.11 – 2,3,5,6-Tetrafluoro-4-(4-methyl-5-(phenylthio)-4*H*-1,2,4-triazol-3-yl)pyridine (**103**)

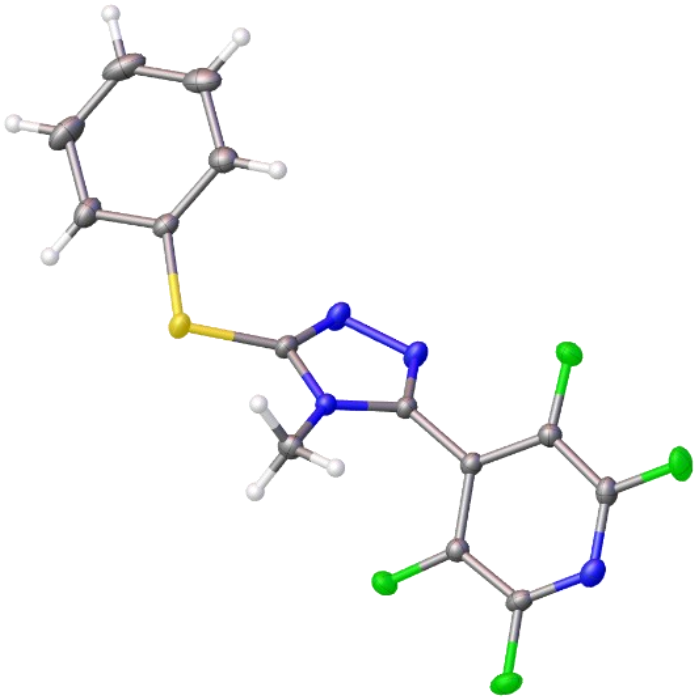


Table S11 – Crystal data and structure refinement for **103**.

Identification code	22srv109	**ρ_{calc}g/cm^3**	4
Empirical formula	$C_{14}H_8F_4N_4S$	**μ/mm^{-1}**	1.672
Formula weight	340.30	**F(000)**	0.291
Temperature/K	120.00	**Crystal size/mm^3**	688.0
Crystal system	monoclinic	**Radiation**	0.19 × 0.18 × 0.13
Space group	$P2_1/n$	**2Θ range for data collection/°**	Mo Kα (λ = 0.71073)
a/Å	11.0609(3)	**Index ranges**	5.23 to 59.992
b/Å	11.7404(3)	**Reflections collected**	$-15 \leq h \leq 15$, $-16 \leq k \leq 16$, $-16 \leq l \leq 16$
c/Å	11.5867(3)	**Independent reflections**	31726
α/°	90	**Data/restraints/parameters**	3938 [R_{int} = 0.0334, R_{sigma} = 0.0189]
β/°	116.0308(8)	**Goodness-of-fit on F^2**	3938/0/240
γ/°	90	**Final R indexes [I>=2σ (I)]**	1.039
Volume/Å^3	1352.01(6)	**Final R indexes [all data]**	R_1 = 0.0312, wR_2 = 0.0809
Z	4	**Largest diff. peak/hole / e Å^{-3}**	R_1 = 0.0353, wR_2 = 0.0834

A-1.12 – 1,4-Dimethyl-3-(phenylthio)-4*H*-1,2,4-triazol-1-ium tetrafluoroborate (**92a·BF$_4$**)

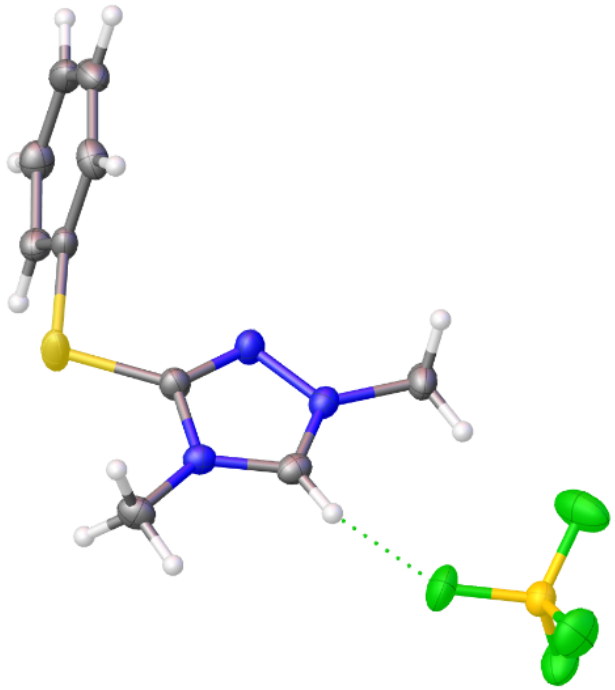


Table S12 – Crystal data and structure refinement for **92a·BF$_4$**.

Identification code	21srv411	**ρ_{calc}g/cm^3**	1.520
Empirical formula	$C_{10}H_{12}BF_4N_3S$	**μ/mm^{-1}**	0.289
Formula weight	293.10	**F(000)**	1200.0
Temperature/K	120.0	**Crystal size/mm^3**	0.32 × 0.3 × 0.24
Crystal system	orthorhombic	**Radiation**	Mo Kα (λ = 0.71073)
Space group	Pbca	**2Θ range for data collection/°**	3.856 to 59.998
a/Å	10.9810(3)	**Index ranges**	−15 ≤ h ≤ 15, −15 ≤ k ≤ 15, −29 ≤ l ≤ 29
b/Å	11.0467(3)	**Reflections collected**	57369
c/Å	21.1225(6)	**Independent reflections**	3713 [R_{int} = 0.0438, R_{sigma} = 0.0174]
α/°	90	**Data/restraints/parameters**	3713/0/220
β/°	90	**Goodness-of-fit on F^2**	1.074
γ/°	90	**Final R indexes [I>=2σ (I)]**	R_1 = 0.0440, wR_2 = 0.1078
Volume/Å^3	2562.24(12)	**Final R indexes [all data]**	R_1 = 0.0483, wR_2 = 0.1106
Z	8	**Largest diff. peak/hole / e Å^{-3}**	0.57/−0.47

A-1.13 – 1,4-Dimethyl-3-(*p*-tolylthio)-4*H*-1,2,4-triazol-1-ium tetrafluoroborate (**92b·BF$_4$**)

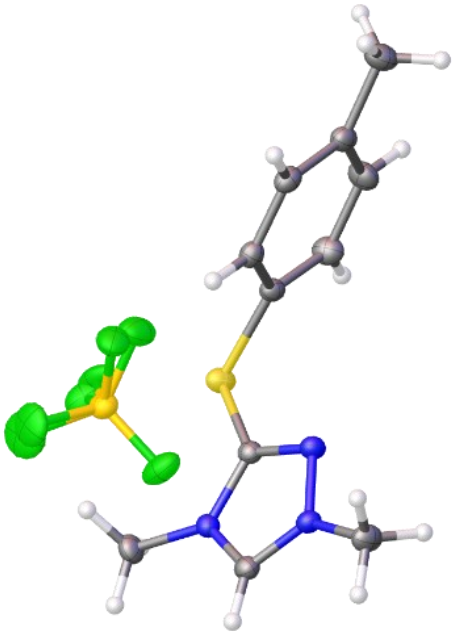
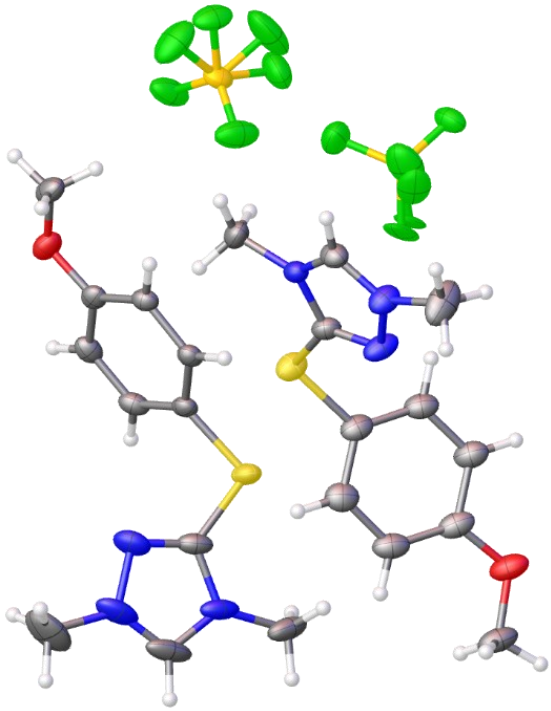


Table S13 – Crystal data and structure refinement for **92b·BF$_4$**.

Identification code	23srv263	**ρ_{calc}g/cm^3**	1.482
Empirical formula	$C_{11}H_{14}BF_4N_3S$	**μ/mm^{-1}**	0.273
Formula weight	307.12	**F(000)**	1264.0
Temperature/K	120.00	**Crystal size/mm^3**	0.32 × 0.24 × 0.12
Crystal system	orthorhombic	**Radiation**	Mo Kα (λ = 0.71073)
Space group	Pbca	**2Θ range for data collection/°**	4 to 57.998
a/Å	11.4673(4)	**Index ranges**	−15 ≤ h ≤ 15, −16 ≤ k ≤ 16, −27 ≤ l ≤ 27
b/Å	11.7845(4)	**Reflections collected**	82126
c/Å	20.3659(8)	**Independent reflections**	3651 [R_{int} = 0.0493, R_{sigma} = 0.0157]
α/°	90	**Data/restraints/parameters**	3651/33/211
β/°	90	**Goodness-of-fit on F^2**	1.133
γ/°	90	**Final R indexes [I>=2σ (I)]**	R_1 = 0.0438, wR_2 = 0.0967
Volume/Å^3	2752.17(17)	**Final R indexes [all data]**	R_1 = 0.0493, wR_2 = 0.0995
Z	8	**Largest diff. peak/hole / e Å^{-3}**	0.34/−0.27

A-1.14 – 3-((4-Methoxyphenyl)thio)-1,4-dimethyl-4*H*-1,2,4-triazol-1-ium tetrafluoroborate (**92d**·BF_4)



2 crystallographically independent ionic pairs are present within the unit cell.

Table S14 – Crystal data and structure refinement for **92d**·BF_4.

Identification code	23srv262	**ρ_{calc}g/cm^3**	1.490
Empirical formula	$C_{11}H_{14}BF_4N_3OS$	**μ/mm^{-1}**	0.270
Formula weight	323.12	**F(000)**	664.0
Temperature/K	120.00	**Crystal size/mm^3**	0.16 × 0.13 × 0.05
Crystal system	triclinic	**Radiation**	Mo Kα (λ = 0.71073)
Space group	P-1	**2Θ range for data collection/°**	4.298 to 54.99
a/Å	7.6746(5)	**Index ranges**	$-9 \leq h \leq 9$, $-14 \leq k \leq 14$, $0 \leq l \leq 21$
b/Å	11.3644(7)	**Reflections collected**	12203
c/Å	16.5366(10)	**Independent reflections**	12203 [R_{int} = 0.0612, R_{sigma} = 0.0372]
α/°	88.457(3)	**Data/restraints/parameters**	12203/76/421
β/°	87.928(2)	**Goodness-of-fit on F^2**	1.068
γ/°	88.754(2)	**Final R indexes [I>=2σ (I)]**	R_1 = 0.0496, wR_2 = 0.1243
Volume/Å^3	1440.50(16)	**Final R indexes [all data]**	R_1 = 0.0702, wR_2 = 0.1373
Z	4	**Largest diff. peak/hole / e Å^{-3}**	0.60/−0.41

A-1.15 – 1,4-Dimethyl-3-((4-nitrophenyl)thio)-4*H*-1,2,4-triazol-1-ium tetrafluoroborate (**92e·BF$_4$**)

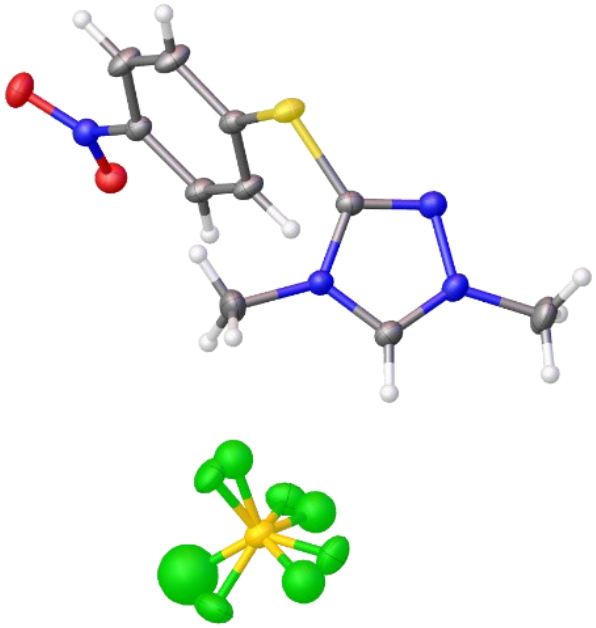
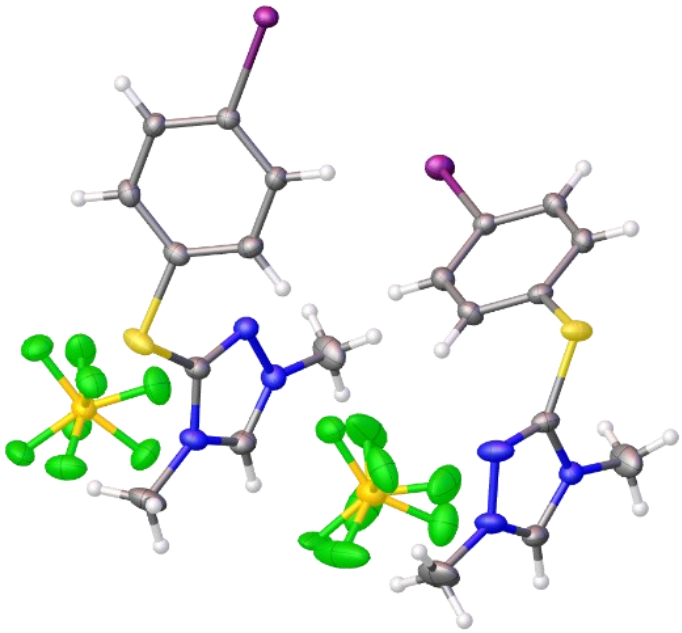


Table S15 – Crystal data and structure refinement for **92e·BF$_4$**.

Identification code	21srv469	**ρ_{calc}g/cm^3**	1.545
Empirical formula	$C_{11}H_{15}BF_4N_4O_3S$	**μ/mm^{-1}**	0.266
Formula weight	370.14	**F(000)**	380.0
Temperature/K	120.0	**Crystal size/mm^3**	0.24 × 0.19 × 0.06
Crystal system	triclinic	**Radiation**	Mo Kα (λ = 0.71073)
Space group	P-1	**2Θ range for data collection/°**	5.374 to 59.996
a/Å	7.5963(2)	**Index ranges**	−10 ≤ h ≤ 10, −11 ≤ k ≤ 11, −18 ≤ l ≤ 18
b/Å	8.4230(2)	**Reflections collected**	18553
c/Å	13.0782(4)	**Independent reflections**	4596 [R_{int} = 0.0307, R_{sigma} = 0.0264]
α/°	77.0850(10)	**Data/restraints/parameters**	4596/29/239
β/°	88.0220(10)	**Goodness-of-fit on F^2**	1.031
γ/°	77.2700(10)	**Final R indexes [I>=2σ (I)]**	R_1 = 0.0423, wR_2 = 0.1138
Volume/Å^3	795.48(4)	**Final R indexes [all data]**	R_1 = 0.0469, wR_2 = 0.1171
Z	2	**Largest diff. peak/hole / e Å^{-3}**	0.61/−0.44

A-1.16 – 3-((4-Iodophenyl)thio)-1,4-dimethyl-4*H*-1,2,4-triazol-1-ium tetrafluoroborate (**92i·BF$_4$**)



2 crystallographically independent ionic pairs are present within the unit cell.

Table S16 – Crystal data and structure refinement for **92i·BF$_4$**.

Identification code	22srv311	**ρ_{calc}g/cm^3**	1.912
Empirical formula	$C_{10}H_{11}BF_4IN_3S$	**μ/mm^{-1}**	2.378
Formula weight	418.99	**F(000)**	808.0
Temperature/K	120.00(10)	**Crystal size/mm^3**	0.41 × 0.13 × 0.07
Crystal system	triclinic	**Radiation**	Mo Kα (λ = 0.71073)
Space group	P-1	**2Θ range for data collection/°**	3.396 to 74.3
a/Å	7.06800(10)	**Index ranges**	−11 ≤ h ≤ 11, −21 ≤ k ≤ 20, −28 ≤ l ≤ 29
b/Å	12.5501(2)	**Reflections collected**	56449
c/Å	17.2321(2)	**Independent reflections**	13530 [R_{int} = 0.0292, R_{sigma} = 0.0303]
α/°	72.9070(10)	**Data/restraints/parameters**	13530/64/439
β/°	85.1220(10)	**Goodness-of-fit on F^2**	1.030
γ/°	88.0370(10)	**Final R indexes [I>=2σ (I)]**	R_1 = 0.0288, wR_2 = 0.0570
Volume/Å^3	1455.68(4)	**Final R indexes [all data]**	R_1 = 0.0441, wR_2 = 0.0618
Z	4	**Largest diff. peak/hole / e Å^{-3}**	0.83/−0.73

A-1.17 – 5-((4-Iodophenyl)thio)-1,4-dimethyl-4*H*-1,2,4-triazol-1-ium tetrafluoroborate (**93i·BF$_4$**)

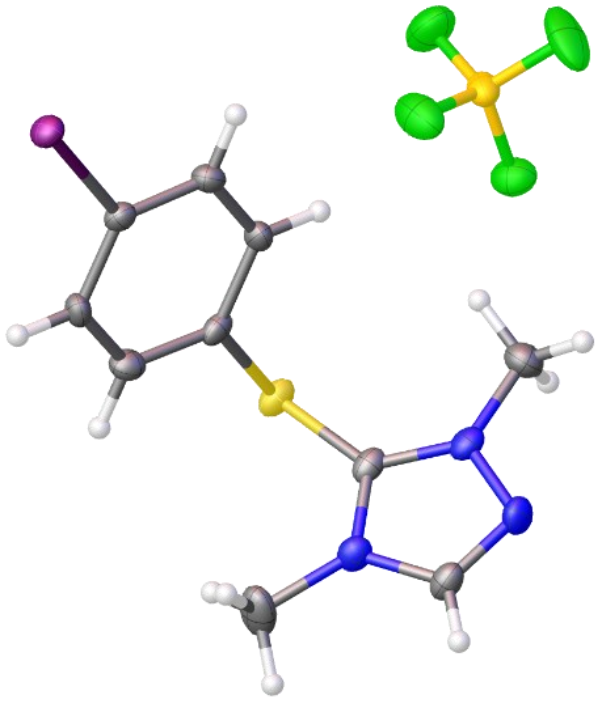


Table S17 – Crystal data and structure refinement for **93i·BF$_4$**.

Identification code	22srv304	**ρ_{calc}g/cm^3**	1.959
Empirical formula	$C_{10}H_{11}BF_4IN_3S$	**μ/mm^{-1}**	2.436
Formula weight	418.99	**F(000)**	404.0
Temperature/K	120.00	**Crystal size/mm^3**	0.069 × 0.057 × 0.016
Crystal system	triclinic	**Radiation**	Mo Kα (λ = 0.71073)
Space group	P-1	**2Θ range for data collection/°**	5.282 to 59.28
a/Å	8.0142(9)	**Index ranges**	−11 ≤ h ≤ 10, −11 ≤ k ≤ 11, −16 ≤ l ≤ 16
b/Å	8.3400(10)	**Reflections collected**	19473
c/Å	11.5895(13)	**Independent reflections**	3989 [R_{int} = 0.0733, R_{sigma} = 0.0631]
α/°	87.147(4)	**Data/restraints/parameters**	3989/0/183
β/°	82.733(4)	**Goodness-of-fit on F^2**	1.151
γ/°	67.612(4)	**Final R indexes [I>=2σ (I)]**	R_1 = 0.0703, wR_2 = 0.1514
Volume/Å^3	710.48(14)	**Final R indexes [all data]**	R_1 = 0.0855, wR_2 = 0.1573
Z	2	**Largest diff. peak/hole / e Å^{-3}**	2.61/−3.07

A-1.18 – 3-((4-(Methoxycarbonyl)phenyl)thio)-1,4-dimethyl-4*H*-1,2,4-triazol-1-ium tetrafluoroborate (**92n·BF$_4$**)

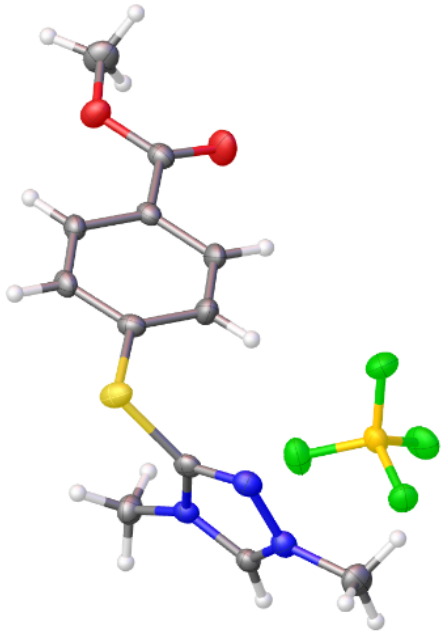


Table S18 – Crystal data and structure refinement for **92n·BF$_4$**.

Identification code	23srv271	**ρ_{calc}g/cm^3**	1.488
Empirical formula	$C_{12}H_{14}BF_4N_3O_2S$	**μ/mm^{-1}**	0.259
Formula weight	351.13	**F(000)**	360.0
Temperature/K	120.00	**Crystal size/mm^3**	0.33 × 0.07 × 0.02
Crystal system	triclinic	**Radiation**	Mo Kα (λ = 0.71073)
Space group	P-1	**2Θ range for data collection/°**	5.372 to 53.992
a/Å	6.6190(4)	**Index ranges**	−8 ≤ h ≤ 8, −9 ≤ k ≤ 9, −19 ≤ l ≤ 19
b/Å	7.8088(5)	**Reflections collected**	19886
c/Å	15.6421(10)	**Independent reflections**	3402 [R_{int} = 0.0614, R_{sigma} = 0.0398]
α/°	75.877(2)	**Data/restraints/parameters**	3402/0/210
β/°	88.197(2)	**Goodness-of-fit on F^2**	1.170
γ/°	88.739(3)	**Final R indexes [I>=2σ (I)]**	R_1 = 0.0619, wR_2 = 0.1590
Volume/Å^3	783.57(9)	**Final R indexes [all data]**	R_1 = 0.0712, wR_2 = 0.1640
Z	2	**Largest diff. peak/hole / e Å^{-3}**	0.55/−0.37

A-1.19 – 3-((2,6-Dimethylphenyl)thio)-1,4-dimethyl-4*H*-1,2,4-triazol-1-ium tetrafluoroborate (**92o·BF$_4$**)

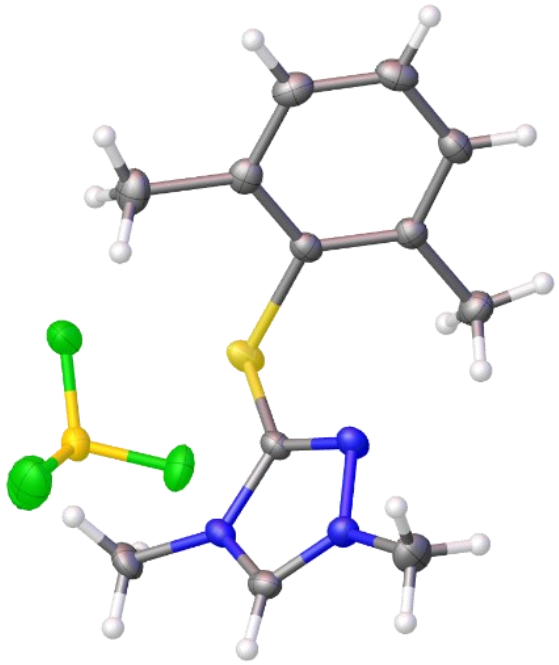
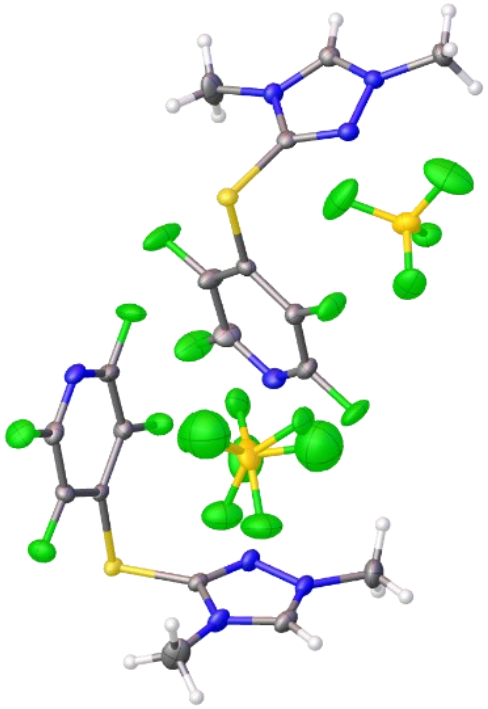


Table S19 – Crystal data and structure refinement for **92o·BF$_4$**.

Identification code	22srv086	**ρ_{calc}g/cm^3**	1.447
Empirical formula	$C_{12}H_{16}BF_4N_3S$	**μ/mm^{-1}**	0.258
Formula weight	321.15	**F(000)**	664.0
Temperature/K	120.00	**Crystal size/mm^3**	0.31 × 0.14 × 0.13
Crystal system	monoclinic	**Radiation**	Mo Kα (λ = 0.71073)
Space group	$P2_1/c$	**2Θ range for data collection/°**	5.16 to 59.992
a/Å	11.8246(3)	**Index ranges**	−16 ≤ h ≤ 16, −15 ≤ k ≤ 15, −16 ≤ l ≤ 16
b/Å	11.1872(3)	**Reflections collected**	34045
c/Å	11.7329(3)	**Independent reflections**	4274 [R_{int} = 0.0447, R_{sigma} = 0.0268]
α/°	90	**Data/restraints/parameters**	4274/0/254
β/°	108.2051(9)	**Goodness-of-fit on F^2**	1.052
γ/°	90	**Final R indexes [I>=2σ (I)]**	R_1 = 0.0369, wR_2 = 0.0901
Volume/Å^3	1474.39(7)	**Final R indexes [all data]**	R_1 = 0.0415, wR_2 = 0.0928
Z	4	**Largest diff. peak/hole / e Å^{-3}**	0.44/−0.28

A-1.20 – 1,4-Dimethyl-3-((perfluoropyridin-4-yl)thio)-4*H*-1,2,4-triazol-1-ium tetrafluoroborate (**92q·BF$_4$**)



2 crystallographically independent ionic pairs are present within the unit cell.

Table S20 – Crystal data and structure refinement for **92q·BF$_4$**.

Identification code	22srv142	**ρ_{calc}g/cm^3**	1.776
Empirical formula	$C_9H_7BF_8N_4S$	**μ/mm^{-1}**	0.332
Formula weight	366.06	**F(000)**	1456.0
Temperature/K	120.00	**Crystal size/mm^3**	0.12 × 0.04 × 0.02
Crystal system	monoclinic	**Radiation**	Mo Kα (λ = 0.71073)
Space group	$P2_1/c$	**2Θ range for data collection/°**	3.846 to 57.998
a/Å	22.1463(7)	**Index ranges**	−30 ≤ h ≤ 30, −10 ≤ k ≤ 10, −23 ≤ l ≤ 23
b/Å	7.5991(2)	**Reflections collected**	60031
c/Å	17.0137(5)	**Independent reflections**	7282 [R_{int} = 0.0713, R_{sigma} = 0.0424]
α/°	90	**Data/restraints/parameters**	7282/30/455
β/°	106.9600(11)	**Goodness-of-fit on F^2**	1.045
γ/°	90	**Final R indexes [I>=2σ (I)]**	R_1 = 0.0635, wR_2 = 0.1404
Volume/Å^3	2738.74(14)	**Final R indexes [all data]**	R_1 = 0.0811, wR_2 = 0.1498
Z	8	**Largest diff. peak/hole / e Å^{-3}**	1.02/−0.59

A-1.21 – 1-Ethyl-4-methyl-3-(phenylthio)-4*H*-1,2,4-triazol-1-ium tetrafluoroborate (**94·BF$_4$**)

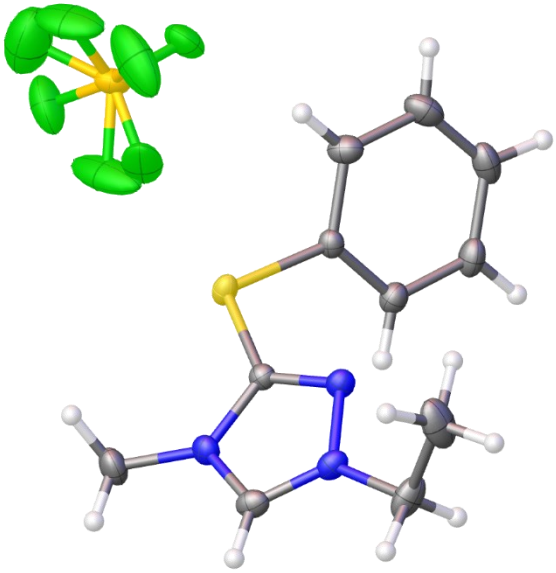


Table S21 – Crystal data and structure refinement for **94·BF$_4$**.

Identification code	22srv131	**ρ_{calc}g/cm^3**	1.502
Empirical formula	$C_{11}H_{14}BF_4N_3S$	**μ/mm^{-1}**	0.276
Formula weight	307.12	**F(000)**	1264.0
Temperature/K	120.00	**Crystal size/mm^3**	0.32 × 0.3 × 0.05
Crystal system	orthorhombic	**Radiation**	Mo Kα (λ = 0.71073)
Space group	Pbca	**2Θ range for data collection/°**	4.246 to 59.988
a/Å	17.4673(6)	**Index ranges**	−24 ≤ h ≤ 23, −11 ≤ k ≤ 11, −26 ≤ l ≤ 26
b/Å	8.1063(3)	**Reflections collected**	60877
c/Å	19.1838(7)	**Independent reflections**	3959 [R_{int} = 0.0732, R_{sigma} = 0.0283]
α/°	90	**Data/restraints/parameters**	3959/51/264
β/°	90	**Goodness-of-fit on F^2**	1.100
γ/°	90	**Final R indexes [I>=2σ (I)]**	R_1 = 0.0656, wR_2 = 0.1493
Volume/Å^3	2716.33(17)	**Final R indexes [all data]**	R_1 = 0.0701, wR_2 = 0.1521
Z	8	**Largest diff. peak/hole / e Å^{-3}**	1.25/−0.91

A-1.22 – (*S*)-(1-(4-((1-Methoxy-1-oxopropan-2-yl)carbamoyl)phenyl)-4-phenyl-4*H*-1,2,4-triazol-1-ium-3-yl)(phenyl)amide (**83H·Cl**)

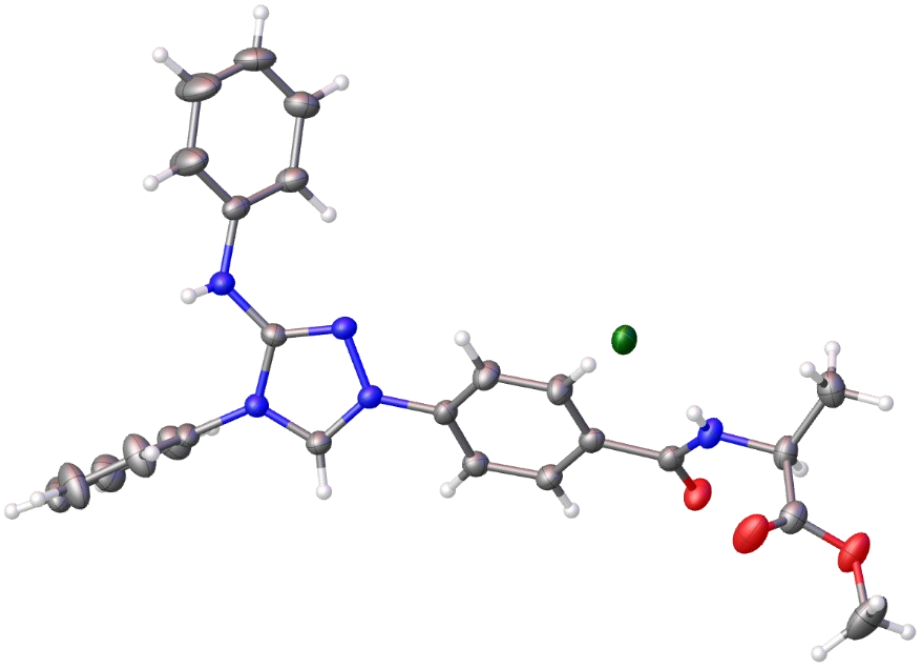


Table S22 – Crystal data and structure refinement for **83H·Cl**.

Identification code	21srv404	**μ/mm^{-1}**	1.715
Empirical formula	$C_{25}H_{24}ClN_5O_3$	**F(000)**	1000.0
Formula weight	477.94	**Crystal size/mm^3**	0.33 × 0.24 × 0.15
Temperature/K	120.0	**Radiation**	Mo Kα (λ = 1.54178)
Crystal system	orthorhombic	**2Θ range for data collection/°**	7.75 to 143.984
Space group	$P2_12_12_1$	**Index ranges**	−11 ≤ h ≤ 10, −17 ≤ k ≤ 18, −22 ≤ l ≤ 22
a/Å	9.0149(3)	**Reflections collected**	22195
b/Å	14.6828(5)	**Independent reflections**	4644 [R_{int} = 0.0321, R_{sigma} = 0.0243]
c/Å	18.1182(6)	**Data/restraints/parameters**	4644/1/403
α/°	90	**Goodness-of-fit on F^2**	1.033
β/°	90	**Final R indexes [I>=2σ (I)]**	R_1 = 0.0330, wR_2 = 0.0898
γ/°	90	**Final R indexes [all data]**	R_1 = 0.0333, wR_2 = 0.0901
Volume/Å^3	2398.20(14)	**Largest diff. peak/hole / e Å^{-3}**	0.35/−0.17
Z	4	**Flack parameter**	−0.009(5)
ρ_{calc}g/cm^3	1.324		

A-2 – XRD data from Chapter 3

A-2.1 – 1-(4-Bromophenyl)-3-(*N*-formylanilino)-1,4-dihydrobenzo[*e*][1,2,4]triazin-4-yl radical (**37f**)

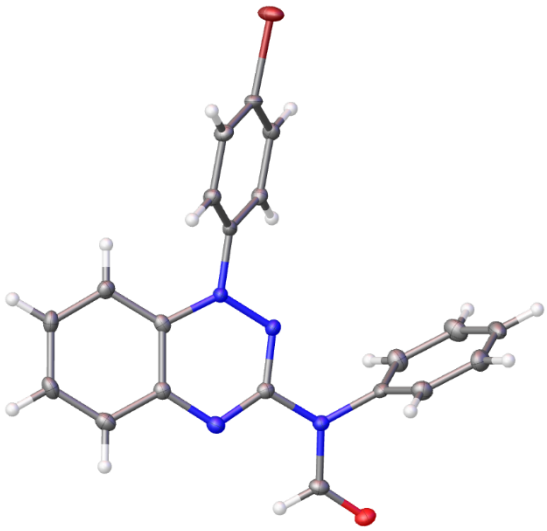


Table S23 – Crystal data and structure refinement for **37f**.

Identification code	21srv420	**ρ_{calc}g/cm^3**	1.598
Empirical formula	$C_{20}H_{14}BrN_4O$	**μ/mm^{-1}**	2.452
Formula weight	406.26	**F(000)**	3280.0
Temperature/K	120.0	**Crystal size/mm^3**	0.07 × 0.05 × 0.05
Crystal system	tetragonal	**Radiation**	MoKα (λ = 0.71073)
Space group	$I4_1/a$	**2Θ range for data collection/°**	4.638 to 58.992
a/Å	24.8354(4)	**Index ranges**	−34 ≤ h ≤ 34, −34 ≤ k ≤ 34, −15 ≤ l ≤ 15
b/Å	24.8354(4)	**Reflections collected**	42030
c/Å	10.9500(3)	**Independent reflections**	4709 [R_{int} = 0.0668, R_{sigma} = 0.0430]
α/°	90	**Data/restraints/parameters**	4709/0/235
β/°	90	**Goodness-of-fit on F^2**	1.015
γ/°	90	**Final R indexes [I>=2σ (I)]**	R_1 = 0.0344, wR_2 = 0.0648
Volume/Å^3	6753.9(3)	**Final R indexes [all data]**	R_1 = 0.0571, wR_2 = 0.0717
Z	16	**Largest diff. peak/hole / e Å^{-3}**	0.36/−0.39

A-2.2 – 1-Phenyl-3-(*N*-formyl-4-iodoanilino)-1,4-dihydrobenzo[*e*][1,2,4]triazin-4-yl radical (**181b**)

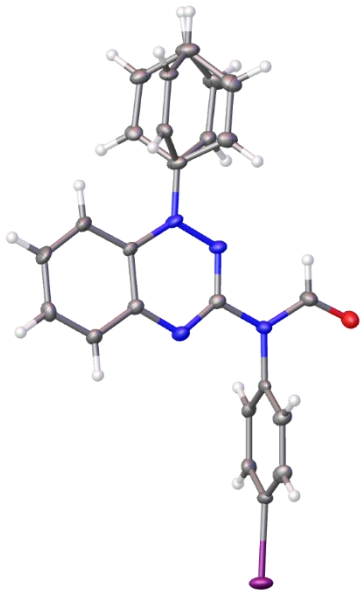


Table S24 – Crystal data and structure refinement for **181b**.

Identification code	22srv165	**ρ_{calc}g/cm^3**	1.728
Empirical formula	$C_{20}H_{14}IN_4O$	**μ/mm^{-1}**	1.855
Formula weight	453.25	**F(000)**	892.0
Temperature/K	120.00	**Crystal size/mm^3**	0.21 × 0.04 × 0.005
Crystal system	monoclinic	**Radiation**	Mo Kα (λ = 0.71073)
Space group	$P2_1/c$	**2Θ range for data collection/°**	4.304 to 59
a/Å	4.9582(2)	**Index ranges**	−6 ≤ h ≤ 6, −13 ≤ k ≤ 13, −51 ≤ l ≤ 51
b/Å	9.4633(4)	**Reflections collected**	53672
c/Å	37.1444(14)	**Independent reflections**	4905 [R_{int} = 0.0806, R_{sigma} = 0.0420]
α/°	90	**Data/restraints/parameters**	4905/66/272
β/°	91.9979(13)	**Goodness-of-fit on F^2**	1.275
γ/°	90	**Final R indexes [I>=2σ (I)]**	R_1 = 0.0735, wR_2 = 0.1222
Volume/Å^3	1741.79(12)	**Final R indexes [all data]**	R_1 = 0.0835, wR_2 = 0.1253
Z	4	**Largest diff. peak/hole / e Å^{-3}**	2.36/−2.89

A-2.3 – 1-Phenyl-3-(4-bromoanilino)-1,4-dihydrobenzo[*e*][1,2,4]triazin-4-yl radical (**182a**)

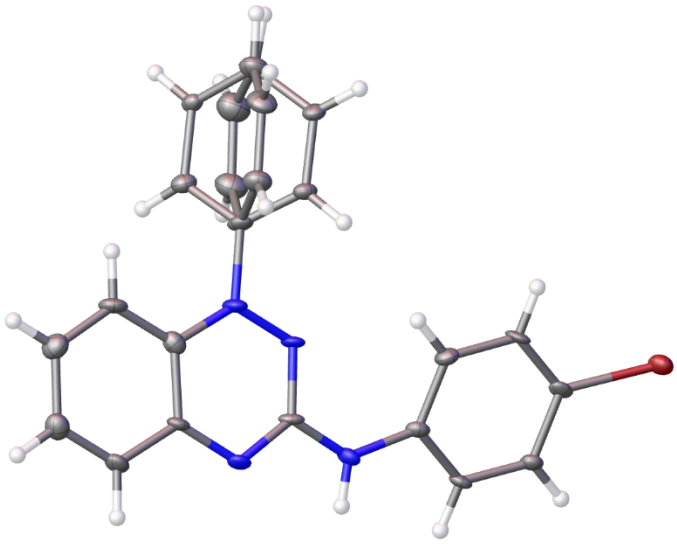


Table S25 – Crystal data and structure refinement for **182a**.

Identification code	22srv207	**ρ_{calc}g/cm^3**	1.628
Empirical formula	$C_{19}H_{14}BrN_4$	**μ/mm^{-1}**	2.671
Formula weight	378.25	**F(000)**	764.0
Temperature/K	120.00	**Crystal size/mm^3**	0.13 × 0.05 × 0.013
Crystal system	monoclinic	**Radiation**	Mo Kα (λ = 0.71073)
Space group	$P2_1/n$	**2Θ range for data collection/°**	3.956 to 54
a/Å	12.3210(17)	**Index ranges**	−17 ≤ h ≤17, −7≤ k ≤ 7, −39 ≤ l ≤ 39
b/Å	4.7921(7)	**Reflections collected**	3328
c/Å	26.587(3)	**Independent reflections**	3328 [R_{int} = 15.66, R_{sigma} = 0.1031]
α/°	90	**Data/restraints/parameters**	3328/87/253
β/°	100.555(5)	**Goodness-of-fit on F^2**	1.071
γ/°	90	**Final R indexes [I>=2σ (I)]**	R_1 = 0.0853, wR_2 = 0.1798
Volume/Å^3	1543.2(4)	**Final R indexes [all data]**	R_1 = 0.1325, wR_2 = 0.1964
Z	4	**Largest diff. peak/hole / e Å^{-3}**	1.21/−1.47

A-3 – XRD data from Chapter 4

A-3.1 – (*S*)-3-(2-((*Tert*-butoxycarbonyl)amino)propanamido)benzo[*e*][1,2,4]-triazine 1,4-dioxide (**255**)

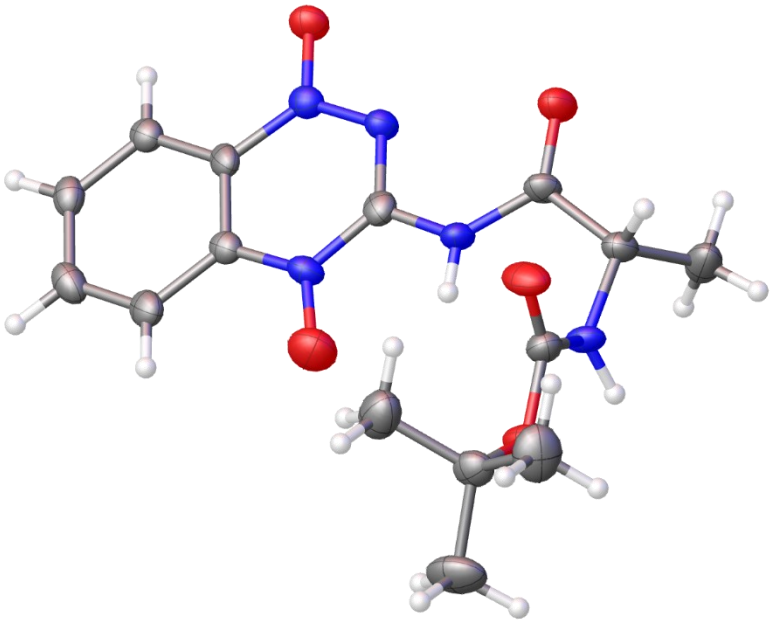


Table S26 – Crystal data and structure refinement for **255**.

Identification code	22srv123	**μ/mm^{-1}**	0.106
Empirical formula	$C_{15}H_{19}N_5O_5$	**F(000)**	1472.0
Formula weight	349.35	**Crystal size/mm^3**	0.42 × 0.02 × 0.01
Temperature/K	120.00	**Radiation**	Mo Kα (λ = 0.71073)
Crystal system	orthorhombic	**2Θ range for data collection/°**	4.202 to 52
Space group	$P2_12_12_1$	**Index ranges**	−7 ≤ h ≤ 7, −23 ≤ k ≤ 23, −34 ≤ l ≤ 34
a/Å	6.1323(5)	**Reflections collected**	43115
b/Å	19.3887(16)	**Independent reflections**	6582 [R_{int} = 0.1415, R_{sigma} = 0.1027]
c/Å	28.183(2)	**Data/restraints/parameters**	6582/0/476
α/°	90	**Goodness-of-fit on F^2**	1.026
β/°	90	**Final R indexes [I>=2σ (I)]**	R_1 = 0.0634, wR_2 = 0.1341
γ/°	90	**Final R indexes [all data]**	R_1 = 0.1219, wR_2 = 0.1608
Volume/Å^3	3350.8(5)	**Largest diff. peak/hole / e Å^{-3}**	0.28/−0.37
Z	8	**Flack parameter**	−0.7(10)
ρ_{calc}g/cm^3	1.385		

A-3.2 – N^1-phenyl-1*H*-benzo[*d*]imidazole-1,2-diamine (**257**)

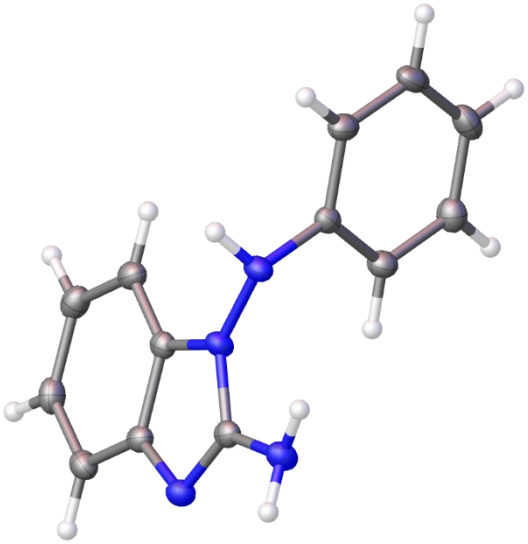
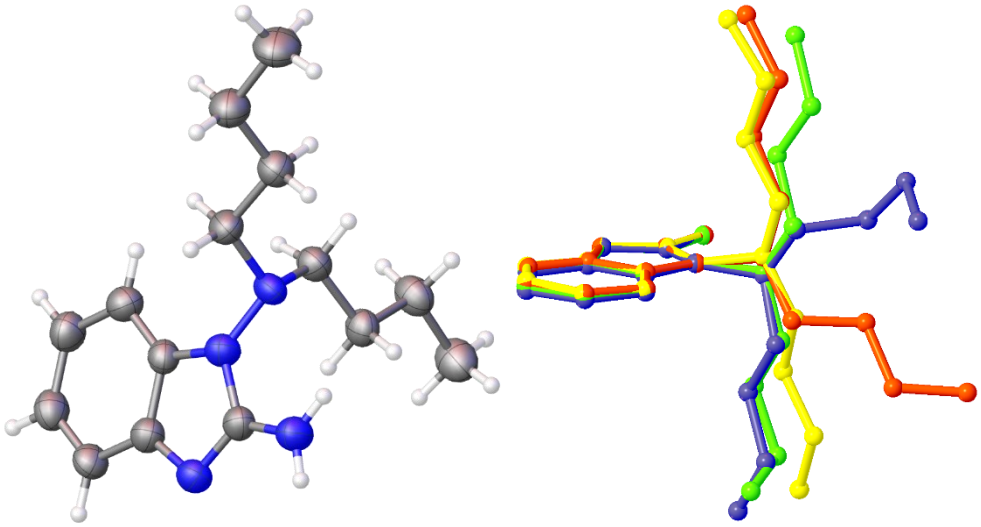


Table S27 – Crystal data and structure refinement for **257**.

Identification code	21srv470	**ρ_{calc}g/cm^3**	1.371
Empirical formula	$C_{13}H_{12}N_4$	**μ/mm^{-1}**	0.087
Formula weight	224.27	**F(000)**	472.0
Temperature/K	120.0	**Crystal size/mm^3**	0.13 × 0.07 × 0.02
Crystal system	monoclinic	**Radiation**	Mo Kα (λ = 0.71073)
Space group	$P2_1/n$	**2Θ range for data collection/°**	5.264 to 60
a/Å	12.4226(5)	**Index ranges**	−17 ≤ h ≤ 17, −7 ≤ k ≤ 7, −21 ≤ l ≤ 21
b/Å	5.6507(2)	**Reflections collected**	18718
c/Å	15.4857(6)	**Independent reflections**	3158 [R_{int} = 0.0503, R_{sigma} = 0.0373]
α/°	90	**Data/restraints/parameters**	3158/0/202
β/°	91.7558(16)	**Goodness-of-fit on F^2**	1.095
γ/°	90	**Final R indexes [I>=2σ (I)]**	R_1 = 0.0540, wR_2 = 0.1054
Volume/Å^3	1086.53(7)	**Final R indexes [all data]**	R_1 = 0.0691, wR_2 = 0.1112
Z	4	**Largest diff. peak/hole / e Å^{-3}**	0.29/−0.28

A-3.3 – N^1, N^1-dibutyl-1*H*-benzo[*d*]imidazole-1,2-diamine (**265**)



Left: 1 of the 4 crystallographically independent units within the unit cell. **Right:** Overlay of the 4 crystallographically independent units showing disorder present in *n*-butyl chains.

Table S28 – Crystal data and structure refinement for **265**.

Identification code	22srv018	**ρ_{calc}g/cm^3**	1.144
Empirical formula	$C_{15}H_{24}N_4$	**μ/mm^{-1}**	0.544
Formula weight	260.38	**F(000)**	1136.0
Temperature/K	120.00	**Crystal size/mm^3**	0.15 × 0.04 × 0.008
Crystal system	triclinic	**Radiation**	Mo Kα (λ = 1.54178)
Space group	P-1	**2Θ range for data collection/°**	6.358 to 140
a/Å	10.2636(6)	**Index ranges**	−12 ≤ h ≤ 12, −12 ≤ k ≤ 13, −34 ≤ l ≤ 34
b/Å	10.8507(8)	**Reflections collected**	33312
c/Å	27.9550(17)	**Independent reflections**	11295 [R_{int} = 0.2179, R_{sigma} = 0.2212]
α/°	95.389(5)	**Data/restraints/parameters**	11295/28/726
β/°	91.303(5)	**Goodness-of-fit on F^2**	0.930
γ/°	102.490(5)	**Final R indexes [I>=2σ (I)]**	R_1 = 0.0827, wR_2 = 0.1869
Volume/Å^3	3023.2(3)	**Final R indexes [all data]**	R_1 = 0.1979, wR_2 = 0.2653
Z	8	**Largest diff. peak/hole / e Å^{-3}**	0.29/−0.29

A-3.4 – 6-(*Tert*-butyl)benzo[*e*][1,2,4]triazin-3-amine (**268**)

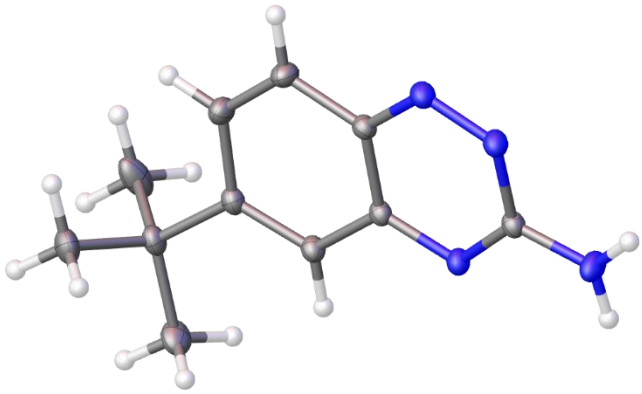


Table S29 – Crystal data and structure refinement for **268**.

Identification code	22srv229	**ρ_{calc}g/cm^3**	1.236
Empirical formula	$C_{11}H_{14}N_4$	**μ/mm^{-1}**	0.079
Formula weight	202.26	**F(000)**	432.0
Temperature/K	120.00	**Crystal size/mm^3**	0.572 × 0.466 × 0.312
Crystal system	monoclinic	**Radiation**	Mo Kα (λ = 0.71073)
Space group	$P2_1/n$	**2Θ range for data collection/°**	6.47 to 74.33
a/Å	11.0844(3)	**Index ranges**	$-18 \leq h \leq 18$, $-12 \leq k \leq 13$, $-21 \leq l \leq 20$
b/Å	7.7863(2)	**Reflections collected**	32794
c/Å	12.7996(3)	**Independent reflections**	5121 [R_{int} = 0.0579, R_{sigma} = 0.0412]
α/°	90	**Data/restraints/parameters**	5121/0/139
β/°	100.2670(10)	**Goodness-of-fit on F^2**	1.046
γ/°	90	**Final R indexes [I>=2σ (I)]**	R_1 = 0.0513, wR_2 = 0.1349
Volume/Å^3	1087.00(5)	**Final R indexes [all data]**	R_1 = 0.0681, wR_2 = 0.1445
Z	4	**Largest diff. peak/hole / e Å^{-3}**	0.50/−0.22

Appendix B - Supplementary information for Chapter 2

B-1 – XRD structural parameters for Nitron analogues

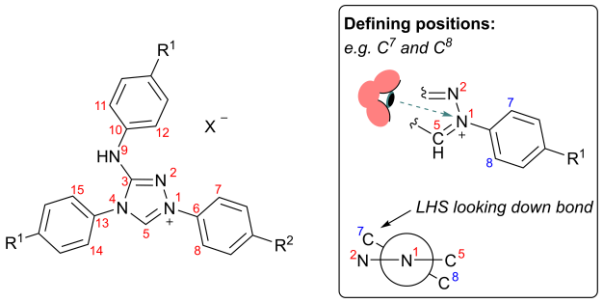


Figure S1 – General structure of Nitron analogues used in this XRD analysis. Aryl positions defined considering looking down the N-Ar bond, as shown for C^7 and C^8.

Table S30 – XRD structural parameters for **33aH·BF$_4$** to **33jH·BF$_4$** (set 1 of 2).

Parameter	33aH·BF$_4$	33eH·BF$_4$	33fH·BF$_4$	33hH·BF$_4$	33iH·BF$_4$	33jH·BF$_4$
Bond lengths (Å)						
N^1-N^2	1.380 (± 0.001)	1.375 (± 0.002)	1.381 (± 0.003)	1.378 (± 0.002)	1.378 (± 0.002)	1.379 (± 0.002)
N^1-C^5	1.311 (± 0.002)	1.316 (± 0.002)	1.312 (± 0.004)	1.314 (± 0.002)	1.312 (± 0.002)	1.318 (± 0.002)
N^1- C^6	1.433 (± 0.002)	1.432 (± 0.002)	1.434 (± 0.004)	1.433 (± 0.002)	1.427 (± 0.003)	1.431 (± 0.001)
N^2-C^3	1.320 (± 0.002)	1.313 (± 0.002)	1.321 (± 0.004)	1.316 (± 0.002)	1.319 (± 0.003)	1.316 (± 0.001)
C^3-N^4	1.390 (± 0.002)	1.385 (± 0.002)	1.395 (± 0.004)	1.391 (± 0.002)	1.389 (± 0.002)	1.391 (± 0.002)
C^3-N^9	1.347 (± 0.002)	1.355 (± 0.002)	1.342 (± 0.004)	1.347 (± 0.002)	1.345 (± 0.002)	1.343 (± 0.002)
N^4-C^5	1.342 (± 0.002)	1.343 (± 0.002)	1.339 (± 0.004)	1.344 (± 0.002)	1.341 (± 0.003)	1.342 (± 0.001)
N^4-C^{13}	1.444 (± 0.002)	1.446 (± 0.002)	1.449 (± 0.004)	1.439 (± 0.002)	1.441 (± 0.002)	1.446 (± 0.002)
C^5-H	0.97 (± 0.02)	0.93 (± 0.03)	0.950 (± 0.003)	0.91 (± 0.02)	0.950 (± 0.002)	0.94 (± 0.02)
C^6-C^7	1.384 (± 0.002)	1.388 (± 0.003)	1.373 (± 0.005)	1.393 (± 0.002)	1.387 (± 0.003)	1.391 (± 0.002)
C^6-C^8	1.389 (± 0.002)	1.380 (± 0.003)	1.370 (± 0.005)	1.381 (± 0.002)	1.389 (± 0.003)	1.387 (± 0.002)
N^9-H	0.88 (± 0.02)	0.83 (± 0.03)	0.79 (± 0.04)	0.86 (± 0.02)	0.880 (± 0.002)	0.89 (± 0.02)
N^9-C^{10}	1.417 (± 0.002)	1.417 (± 0.002)	1.419 (± 0.004)	1.415 (± 0.002)	1.412 (± 0.002)	1.417 (± 0.002)
C^{10}-C^{11}	1.399 (± 0.002)	1.389 (± 0.003)	1.394 (± 0.005)	1.398 (± 0.002)	1.397 (± 0.003)	1.398 (± 0.002)

C^{10}-C^{12}	1.393 (± 0.002)	1.395 (± 0.002)	1.388 (± 0.005)	1.388 (± 0.002)	1.391 (± 0.003)	1.394 (± 0.002)
C^{13}-C^{14}	1.383 (± 0.002)	1.385 (± 0.002)	1.365 (± 0.004)	1.386 (± 0.002)	1.383 (± 0.003)	1.384 (± 0.002)
C^{13}-C^{15}	1.384 (± 0.002)	1.383 (± 0.003)	1.374 (± 0.004)	1.385 (± 0.002)	1.384 (± 0.003)	1.384 (± 0.002)
Bond angles (°)						
N^{1}-N^{2}-C^{3}	103.9 (± 0.1)	103.8 (± 0.1)	104.0 (± 0.2)	104.0 (± 0.1)	103.5 (± 0.1)	103.8 (± 0.1)
N^{1}-C^{5}-N^{4}	107.6 (± 0.1)	107.2 (± 0.2)	107.5 (± 0.2)	107.3 (± 0.1)	107.3 (± 0.1)	107.1 (± 0.1)
N^{1}-C^{5}-H	127.3 (± 1.0)	125.9 (± 1.6)	126.3 (± 0.3)	126.7 (± 1.4)	126.3 (± 0.2)	127.6 (± 1.0)
N^{1}-C^{6}-C^{7}	118.9 (± 0.1)	118.3 (± 0.2)	119.6 (± 0.3)	118.6 (± 0.1)	119.7 (± 0.2)	117.6 (± 0.11)
N^{1}-C^{6}-C^{8}	119.4 (± 0.1)	119.9 (± 0.2)	119.1 (± 0.3)	119.9 (± 0.1)	118.4 (± 0.2)	120.0 (± 0.1)
N^{2}-N^{1}-C^{5}	111.7 (± 0.1)	111.8 (± 0.1)	111.9 (± 0.2)	111.9 (± 0.1)	112.1 (± 0.2)	112.0 (± 0.1)
N^{2}-N^{1}-C^{6}	119.9 (± 0.1)	120.2 (± 0.1)	119.9 (± 0.2)	119.3 (± 0.1)	121.1 (± 0.1)	118.5 (± 0.1)
N^{2}-C^{3}-N^{4}	110.6 (± 0.1)	111.2 (± 0.2)	110.2 (± 0.3)	110.7 (± 0.1)	110.9 (± 0.2)	110.9 (± 0.1)
N^{2}-C^{3}-N^{9}	127.7 (± 0.1)	127.9 (± 0.2)	127.9 (± 0.3)	127.8 (± 0.1)	128.1 (± 0.1)	127.9 (± 0.1)
C^{3}-N^{4}-C^{5}	106.1 (± 0.1)	106.0 (± 0.1)	106.4 (± 0.3)	106.2 (± 0.1)	106.1 (± 0.2)	106.3 (± 0.1)
C^{3}-N^{4}-C^{13}	129.2 (± 0.1)	128.7 (± 0.1)	129.2 (± 0.2)	129.0 (± 0.1)	129.2 (± 0.2)	126.6 (± 0.1)
C^{3}-N^{9}-H	115.6 (± 1.2)	114.4 (± 1.9)	116.0 (± 2.0)	114.0 (± 1.4)	116.5 (± 0.1)	116.2 (± 1.5)
C^{3}-N^{9}-C^{10}	126.6 (± 0.1)	125.0 (± 1.5)	126.6 (± 0.3)	125.9 (± 0.1)	127.0 (± 0.2)	126.6 (± 0.1)
N^{4}-C^{3}-N^{9}	121.7 (± 0.1)	120.9 (± 0.2)	121.9 (± 0.3)	121.5 (± 0.1)	120.9 (± 0.2)	121.2 (± 0.1)
N^{4}-C^{5}-H	125.1 (± 1.0)	126.9 (± 1.6)	126.3 (± 0.3)	126.0 (± 1.4)	126.3 (± 0.2)	125.3 (± 1.0)
N^{4}-C^{13}-C^{14}	118.8 (± 0.1)	118.9 (± 0.2)	119.3 (± 0.3)	118.2 (± 0.1)	118.4 (± 0.17)	119.4 (± 0.09)
N^{4}-C^{13}-C^{15}	118.9 (± 0.1)	118.6 (± 0.2)	119.1 (± 0.3)	119.5 (± 0.1)	119.4 (± 0.2)	118.3 (± 0.1)
C^{5}-N^{1}-C^{6}	128.4 (± 0.1)	127.6 (± 0.2)	128.2 (± 0.2)	128.8 (± 0.1)	126.6 (± 0.1)	129.5 (± 0.11)

C^5-N^4-C^{13}	124.7 (± 0.1)	125.1 (± 0.1)	124.4 (± 0.2)	124.9 (± 0.1)	124.6 (± 0.1)	127.1 (± 0.1)
N^9-C^{10}-C^{11}	116.8 (± 0.1)	117.5 (± 0.2)	116.7 (± 0.3)	116.4 (± 0.1)	116.4 (± 0.2)	116.0 (± 0.1)
N^9-C^{10}-C^{12}	123.5 (± 0.1)	121.8 (± 0.2)	124.0 (± 0.3)	123.9 (± 0.1)	123.9 (± 0.2)	124.1 (± 0.1)
Dihedral angles (°)						
N^1-N^2-C^3-N^4	+1.3 (± 0.1)	+0.2 (± 0.2)	−1.2 (± 0.3)	−1.2 (± 0.1)	+0.5 (± 0.2)	+0.5 (± 0.1)
N^1-N^2-C^3-N^9	−178.6 (± 0.1)	−178.6 (± 0.2)	+178.9 (± 0.3)	+178.6 (± 0.1)	−177.8 (± 0.2)	+179.6 (± 0.1)
N^1-C^5-N^4-C^3	+1.0 (± 0.1)	+1.4 (± 0.2)	−1.3 (± 0.3)	−1.0 (± 0.1)	0.2 (± 0.2)	0.4 (± 0.1)
N^1-C^5-N^4-C^{13}	−176.5 (± 0.1)	−173.9 (± 0.2)	177.6 (± 0.2)	−179.8 (± 0.1)	−176.3 (± 0.2)	−179.4 (± 0.1)
N^2-N^1-C^5-N^4	−0.2 (± 0.1)	−1.4 (± 0.2)	+0.6 (± 0.3)	+0.3 (± 0.2)	+0.1 (± 0.2)	−0.1 (± 0.1)
N^2-N^1-C^5-H	+179.4 (± 1.1)	+180.0 (± 2.0)	−179.3 (± 0.3)	+178.1 (± 1.4)	+180.0 (± 0.2)	−178.2 (± 1.1)
N^2-N^1-C^6-C^7	−5.3 (± 0.2)	−5.8 (± 0.2)	−8.1 (± 0.4)	−6.0 (± 0.2)	+21.8 (± 0.3)	−4.6 (± 0.2)
N^2-N^1-C^6-C^8	+174.3 (± 0.1)	+178.9 (± 0.2)	+171.0 (± 0.3)	+172.6 (± 0.1)	−158.9 (± 0.2)	+175.7 (± 0.1)
N^2-C^3-N^4-C^5	−1.5 (± 0.1)	−1.0 (± 0.2)	1.6 (± 0.3)	1.4 (± 0.2)	−0.4 (± 0.2)	−0.6 (± 0.1)
N^2-C^3-N^4-C^{13}	+175.9 (± 0.1)	+174.1 (± 0.2)	−177.3 (± 0.2)	−179.9 (± 0.1)	+175.8 (± 0.2)	+179.2 (± 0.1)
N^2-C^3-N^9-H	+171.2 (± 1.1)	+144.3 (± 1.9)	−165.0 (± 2.0)	−156.9 (± 1.3)	+165.3 (± 0.2)	+174.7 (± 1.5)
N^2-C^3-N^9-C^{10}	+2.1 (± 0.2)	−19.0 (± 0.3)	−2.2 (± 0.5)	0.0 (± 0.2)	−14.7 (± 0.4)	−2.0 (± 0.2)
C^3-N^2-N^1-C^5	−0.7 (± 0.1)	+0.8 (± 0.2)	+0.4 (± 0.3)	+0.6 (± 0.1)	−0.3 (± 0.2)	−0.2 (± 0.1)
C^3-N^2-N^1-C^6	+179.8 (± 0.1)	+174.1 (± 0.2)	−178.4 (± 0.2)	−177.6 (± 0.1)	+176.0 (± 0.2)	179.4 (± 0.1)
C^3-N^4-C^5-H	−178.6 (± 1.1)	+180.0 (± 2.0)	+178.7 (± 0.3)	−178.8 (± 1.4)	−179.7 (± 0.2)	+178.5 (± 1.1)
C^3-N^4-C^{13}-C^{14}	+123.9 (± 0.1)	+112.9 (± 0.2)	−118.6 (± 0.3)	−122.6 (± 0.2)	133.8 (± 0.2)	105.8 (± 0.2)
C^3-N^4-C^{13}-C^{15}	−58.5 (± 0.2)	−69.8 (± 0.2)	+64.3 (± 0.4)	+58.6 (± 0.2)	−49.8 (± 0.3)	−70.9 (± 0.2)
C^3-N^9-C^{10}-C^{11}	+176.4 (± 0.1)	+154.8 (± 0.2)	−175.6 (± 0.3)	−173.0 (± 0.1)	−179.0 (± 0.2)	+179.5 (± 0.1)

C^3-N^9-C^{10}-C^{12}	−3.9 (± 0.2)	−30.2 (± 0.3)	+5.1 (± 0.4)	+7.6 (± 0.2)	−1.3 (± 0.3)	−0.3 (± 0.2)
N^4-C^3-N^9-H	−8.7 (± 1.1)	−34.4 (± 1.9)	+15.0 (± 2.0)	+22.8 (± 0.1)	−12.8 (± 0.3)	−6.2 (± 1.5)
N^4-C^3-N^9-C^{10}	−177.8 (± 0.1)	+162.3 (± 0.2)	+178.0 (± 0.2)	+179.8 (± 0.1)	+167.3 (± 0.2)	+177.1 (± 0.1)
N^4-C^5-N^1-C^6	+179.2 (± 0.1)	−174.2 (± 0.2)	+179.2 (± 0.2)	+178.2 (± 0.1)	−176.0 (± 0.2)	−179.7 (± 0.1)
C^5-N^1-C^6-C^7	175.3 (± 0.1)	166.4 (± 0.2)	173.3 (± 0.3)	176.2 (± 0.1)	−162.4 (± 0.2)	175.0 (± 0.1)
C^5-N^1-C^6-C^8	−5.2 (± 0.2)	−8.9 (± 0.3)	−7.5 (± 0.4)	−5.2 (± 0.2)	+16.8 (± 0.3)	−4.8 (± 0.2)
C^5-N^4-C^{13}-C^{14}	−59.2 (± 0.2)	−72.9 (± 0.2)	+62.7 (± 0.4)	+55.9 (± 0.2)	−50.6 (± 0.3)	−74.4 (± 0.2)
C^5-N^4-C^{13}-C^{15}	+118.4 (± 0.1)	+104.4 (± 0.2)	−114.4 (± 0.3)	−122.9 (± 0.2)	+125.9 (± 0.2)	+108.9 (± 0.2)
C^5-N^4-C^3-N^9	+178.4 (± 0.1)	+177.9 (± 0.2)	−178.5 (± 0.3)	−178.4 (± 0.1)	177.9 (± 0.2)	−179.8 (± 0.1)
C^6-N^1-C^5-H	−1.2 (± 1.2)	+7.0 (± 2.0)	−0.7 (± 0.5)	−4.0 (± 1.4)	+3.9 (± 0.4)	+2.3 (± 1.1)
N^9-C^3-N^4-C^{13}	−4.2 (± 0.2)	−7.1 (± 0.3)	+2.6 (± 0.4)	+0.3 (± 0.2)	−5.8 (± 0.3)	0.0 (± 0.2)
C^{11}-C^{10}-N^9-H	+7.5 (± 1.2)	−8.0 (± 2.0)	−12.0 (± 2.0)	−16.5 (± 1.3)	+1.0 (± 0.3)	+2.8 (± 1.5)
C^{12}-C^{10}-N^9-H	−172.8 (± 1.2)	+167.0 (± 2.0)	+168.0 (± 2.0)	+164.1 (± 1.3)	+178.7 (± 0.2)	−177.0 (± 1.5)
C^{13}-N^4-C^5-H	+3.9 (± 1.1)	+5.0 (± 2.0)	−2.4 (± 0.5)	+2.4 (± 1.4)	+3.8 (± 0.4)	−1.3 (± 1.1)

Table S31 – XRD structural parameters for **81aH·Cl** to **33m** (set 2 of 2).

Parameter	81aH·Cl	83H·Cl	33m [a]
Bond lengths (Å)			
N^1-N^2	1.375 (± 0.002)	1.377 (± 0.003)	1.384 (± 0.003)
N^1-C^5	1.318 (± 0.002)	1.311 (± 0.003)	1.301 (± 0.004)
N^1- C^6	1.426 (± 0.002)	1.430 (± 0.003)	1.430 (± 0.004)
N^2-C^3	1.316 (± 0.002)	1.318 (± 0.003)	1.337 (± 0.004)
C^3-N^4	1.390 (± 0.002)	1.384 (± 0.003)	1.423 (± 0.003)
C^3-N^9	1.348 (± 0.002)	1.359 (± 0.003)	1.313 (± 0.004)
N^4-C^5	1.344 (± 0.002)	1.341 (± 0.003)	1.334 (± 0.003)
N^4-C^{13}	1.439 (± 0.002)	1.446 (± 0.003)	1.427 (± 0.003)
C^5-H	0.950 (± 0.001)	0.92 (± 0.03)	0.940 (± 0.003)
C^6-C^7	1.386 (± 0.002)	1.387 (± 0.004)	1.377 (± 0.004)
C^6-C^8	1.386 (± 0.002)	1.386 (± 0.003)	1.373 (± 0.004)

N^9-H	0.866 (± 0.018)	0.81 (± 0.03)	
N^9-C^{10}	1.411 (± 0.002)	1.419 (± 0.003)	1.391 (± 0.004)
C^{10}-C^{11}	1.403 (± 0.002)	1.388 (± 0.004)	1.402 (± 0.004)
C^{10}-C^{12}	1.394 (± 0.002)	1.378 (± 0.004)	1.402 (± 0.004)
C^{13}-C^{14}	1.382 (± 0.002)	1.394 (± 0.004)	1.372 (± 0.004)
C^{13}-C^{15}	1.388 (± 0.002)	1.351 (± 0.004)	1.379 (± 0.004)
Bond angles (°)			
N^1-N^2-C^3	103.8 (± 0.1)	103.7 (± 0.2)	105.2 (± 0.2)
N^1-C^5-N^4	106.7 (± 0.1)	106.8 (± 0.2)	108.8 (± 0.2)
N^1-C^5-H	126.6 (± 0.1)	126.5 (± 1.8)	125.6 (± 0.3)
N^1-C^6-C^7	118.6 (± 0.1)	119.0 (± 0.2)	118.9 (± 0.2)
N^1-C^6-C^8	119.2 (± 0.1)	119.3 (± 0.2)	120.5 (± 0.2)
N^2-N^1-C^5	112.3 (± 0.1)	112.28 (± 0.2)	111.4 (± 0.2)
N^2-N^1-C^6	119.4 (± 0.1)	121.1 (± 0.2)	119.8 (± 0.2)
N^2-C^3-N^4	110.7 (± 0.1)	110.5 (± 0.2)	108.1 (± 0.2)
N^2-C^3-N^9	127.7 (± 0.1)	128.28 (± 0.2)	132.4 (± 0.2)
C^3-N^4-C^5	106.4 (± 0.1)	106.7 (± 0.19)	106.5 (± 0.2)
C^3-N^4-C^{13}	127.8 (± 0.1)	128.91 (± 0.2)	129.4 (± 0.2)
C^3-N^9-H	115.5 (± 1.1)	112.0 (± 2.0)	- [a]
C^3-N^9-C^{10}	126.2 (± 0.1)	124.1 (± 0.2)	121.6 (± 0.2)
N^4-C^3-N^9	121.6 (± 0.1)	121.2 (± 0.2)	119.4 (± 0.2)
N^4-C^5-H	126.6 (± 0.1)	126.6 (± 1.8)	125.7 (± 0.3)
N^4-C^{13}-C^{14}	119.4 (± 0.1)	117.6 (± 0.2)	118.8 (± 0.3)
N^4-C^{13}-C^{15}	118.5 (± 0.1)	120.1 (± 0.2)	120.5 (± 0.3)
C^5-N^1-C^6	128.2 (± 0.1)	126.6 (± 0.2)	128.8 (± 0.2)
C^5-N^4-C^{13}	125.4 (± 0.1)	124.2 (± 0.2)	124.0 (± 0.2)
N^9-C^{10}-C^{11}	116.7 (± 0.1)	118.4 (± 0.3)	115.5 (± 0.2)
N^9-C^{10}-C^{12}	123.8 (± 0.1)	121.9 (± 0.2)	127.1 (± 0.2)
Dihedral angles (°)			
N^1-N^2-C^3-N^4	+0.3 (± 0.2)	−0.6 (± 0.2)	−0.1 (± 0.3)
N^1-N^2-C^3-N^9	−177.9 (± 0.1)	+179.9 (± 0.2)	+178.5 (± 0.3)
N^1-C^5-N^4-C^3	−0.2 (± 0.2)	−0.9 (± 0.2)	+0.3 (± 0.3)
N^1-C^5-N^4-C^{13}	−174.2 (± 0.1)	+174.3 (± 0.2)	+179.3 (± 0.2)
N^2-N^1-C^5-N^4	+0.4 (± 0.2)	+0.6 (± 0.3)	−0.4 (± 0.3)
N^2-N^1-C^5-H	−179.6 (± 0.1)	−176.0 (± 2.0)	+179.6 (± 0.3)
N^2-N^1-C^6-C^7	+20.2 (± 0.2)	+34.1 (± 0.3)	−3.5 (± 0.4)
N^2-N^1-C^6-C^8	−160.6 (± 0.1)	−145.8 (± 0.2)	+175.4 (± 0.3)
N^2-C^3-N^4-C^5	−0.1 (± 0.2)	+0.9 (± 0.3)	−0.1 (± 0.3)
N^2-C^3-N^4-C^{13}	+173.7 (± 0.1)	−174.0 (± 0.2)	−179.1 (± 0.3)
N^2-C^3-N^9-H	+164.5 (± 1.5)	−130.0 (± 3.0)	- [a]
N^2-C^3-N^9-C^{10}	−8.5 (± 0.2)	18.3 (± 0.4)	−5.9 (± 0.5)

C^3-N^2-N^1-C^5	−0.4 (± 0.2)	0.0 (± 0.2)	0.3 (± 0.3)
C^3-N^2-N^1-C^6	+179.7 (± 0.1)	−179.8 (± 0.2)	−178.9 (± 0.2)
C^3-N^4-C^5-H	+179.8 (± 0.1)	+175.0 (± 2.0)	−179.7 (± 0.3)
C^3-N^4-C^{13}-C^{14}	+120.9 (± 0.2)	+96.3 (± 0.3)	−145.7 (± 0.3)
C^3-N^4-C^{13}-C^{15}	−59.6 (± 0.2)	−84.3 (± 0.4)	36.2 (± 0.4)
C^3-N^9-C^{10}-C^{11}	+179.9 (± 0.1)	−152.3 (± 0.3)	+174.6 (± 0.3)
C^3-N^9-C^{10}-C^{12}	−3.2 (± 0.2)	+31.9 (± 0.4)	−7.4 (± 0.4)
N^4-C^3-N^9-H	−13.5 (± 1.5)	50.0 (± 3.0)	- [a]
N^4-C^3-N^9-C^{10}	+173.5 (± 0.1)	−161.2 (± 0.2)	+172.7 (± 0.2)
N^4-C^5-N^1-C^6	−179.7 (± 0.1)	−179.6 (± 0.2)	+178.7 (± 0.3)
C^5-N^1-C^6-C^7	−159.7 (± 0.1)	−145.7 (± 0.2)	+177.4 (± 0.3)
C^5-N^1-C^6-C^8	+19.6 (± 0.2)	+34.4 (± 0.3)	−3.7 (± 0.4)
C^5-N^4-C^{13}-C^{14}	−66.4 (± 0.2)	−77.8 (± 0.3)	+35.5 (± 0.4)
C^5-N^4-C^{13}-C^{15}	+113.1 (± 0.2)	+101.5 (± 0.3)	−142.6 (± 0.3)
C^5-N^4-C^3-N^9	+178.2 (± 0.1)	−179.5 (± 0.2)	−179.0 (± 0.3)
C^6-N^1-C^5-H	+0.3 (± 0.3)	+4.0 (± 2.0)	−1.2 (± 0.5)
N^9-C^3-N^4-C^{13}	−8.0 (± 0.2)	+5.5 (± 0.4)	+2.1 (± 0.4)
C^{11}-C^{10}-N^9-H	+7.1 (± 1.5)	−5.0 (± 3.0)	- [a]
C^{12}-C^{10}-N^9-H	−176.0 (± 1.5)	+179.0 (± 3.0)	- [a]
C^{13}-N^4-C^5-H	+5.8 (± 0.2)	−9.0 (± 2.0)	−0.7 (± 0.5)

[a] Compound crystallised as zwitterion

B-2 – Zwitterion – carbene tautomerisation calculations

B-2.1 – Overview of methods and determination of ΔG_{taut}

The energy optimised geometries of Nitron tautomers were determined using the Gaussian 16 interface with GaussView 6 software. Calculations were performed at DFT level of theory using either B3LYP or M06-2X functionals. The 6-31+G(d,p) basis set was generally used, however in some cases the ECP model LANL2DZ was used to allow consideration of the iodinated Nitron analogue **33g**. PCM solvation models, within either MeCN or H_2O, were used. Further details of each DFT method are provided in Chapter 2.3.7. **Table S32** describes each method used in this work.

Table S32 – Details of the DFT methods used in this work.

Method code	Functional	Basis set	Solvation model
M1	B3LYP	6-31+G(d,p)	PCM(MeCN)
M2	B3LYP	LANL2DZ	PCM(MeCN)
M3	B3LYP	6-31+G(d,p)	PCM(H_2O)
M4	M06-2X	6-31+G(d,p)	PCM(MeCN)
M5	M06-2X	6-31+G(d,p)	PCM(H_2O)

To determine the Gibbs free energy of tautomerisation (ΔG_{taut}), the variation in sum of electronic and thermal free-energies was determined. These values were converted into Kcal mol^{-1} and are provided in **Table S33**.

Table S33 – Summary of ΔG_{taut} values obtained from DFT optimised geometries of the corresponding zwitterionic and carbenic tautomers of Nitron analogues. Calculations in Kcal mol^{-1} were undertaken with values in Hartree of higher precision than are tabulated.

Analogue		ΔG_{Taut} (Hartree)					ΔG_{taut} (Kcal mol^{-1})				
		M1	**M2**	**M3**	**M4**	**M5**	**M1**	**M2**	**M3**	**M4**	**M5**
33a		+0.0103	+0.0081	+0.0105	+0.0059	+0.0060	+6.465	+5.060	+6.574	+3.682	+3.790
33b		+0.0070		+0.0074	+0.0039	+0.0043	+4.361		+4.627	+2.425	+2.698
33c		+0.0143		+0.0146	+0.0092	+0.0096	+8.976		+9.177	+5.761	+6.034
33d		+0.0084		+0.0089	+0.0044	+0.0045	+5.277		+5.605	+2.751	+2.848
33e		+0.0098		+0.0098	+0.0044	+0.0047	+6.178		+6.155	+2.742	+2.932
33f		+0.0094	+0.0075	+0.0096	+0.0044	+0.0047	+5.893	+4.702	+6.042	+2.764	+2.950
33g			+0.0076					+4.748			
33h		+0.0112		+0.0114	+0.0062	+0.0065	+7.019		+7.149	+3.880	+4.067
33i	Acid form	+0.0074		+0.0076	+0.0035	+0.0038	+4.614		+4.784	+2.196	+2.411
	Carboxylate form	+0.0127		+0.0142	+0.0064	+0.0079	+7.952		+8.921	+4.044	+4.935
33j		+0.0067		+0.0070	+0.0026	+0.0030	+4.187		+4.408	+1.659	+1.910
33k		+0.0109		+0.0113	+0.0073	+0.0086	+6.861		+7.073	+4.573	+5.366
33l		+0.0115		+0.0115	+0.0063	+0.0069	+6.995		+7.233	+3.963	+4.358
33m		+0.0161		+0.0164	+0.0103	+0.0105	+10.075		+10.308	+6.463	+6.568

B-2.2 – Optimised geometry coordinates

The following section provides coordinates of the optimised geometry for the zwitterionic and carbenic tautomers of Nitron analogues.

*B-2.2.1 – Nitron (**33a**) (zwitterionic form)*

M1				
Tag	**Symbol**	**X**	**Y**	**Z**
1	C	1.975666	1.999052	-0.10679
2	C	1.056281	3.079461	-0.07633
3	C	3.352989	2.327385	-0.2002
4	C	1.506413	4.403541	-0.13239
5	H	-0.00433	2.877227	-0.00832
6	C	3.789332	3.647997	-0.2577
7	C	2.867952	4.705342	-0.22342
8	H	0.775088	5.208229	-0.10528
9	H	4.854114	3.856149	-0.3292
10	H	3.205863	5.736602	-0.26748
11	N	1.675453	0.64436	-0.04603
12	C	0.460208	0.166294	0.003073
13	C	-3.07369	-0.0617	0.030241
14	C	-3.94653	-0.99269	-0.54324
15	C	-3.55253	1.116004	0.611763

16	C	-5.32041	-0.74823	-0.50557
17	H	-3.56591	-1.88384	-1.03107
18	C	-4.92835	1.352001	0.630412
19	H	-2.85499	1.82461	1.04142
20	C	-5.81529	0.421859	0.079057
21	H	-6.00056	-1.46761	-0.95032
22	H	-5.30539	2.26386	1.082756
23	H	-6.884	0.610651	0.097463
24	N	-0.76864	0.741527	-0.01837
25	N	-1.66786	-0.30711	0.021924
26	N	0.264653	-1.25638	0.069489
27	C	-1.05837	-1.47894	0.079588
28	H	-1.53279	-2.44317	0.168389
29	C	1.26803	-2.278	0.07933
30	C	1.244369	-3.26747	-0.90786
31	C	2.241578	-2.28397	1.082576
32	C	2.202196	-4.28504	-0.88044
33	H	0.492253	-3.23653	-1.68994
34	C	3.200194	-3.2984	1.093594
35	H	2.244347	-1.50545	1.83624
36	C	3.181539	-4.3003	0.116408
37	H	2.184952	-5.05697	-1.64339
38	H	3.958486	-3.30879	1.870353
39	H	3.928344	-5.08813	0.132298
40	H	4.069819	1.511117	-0.22567

M2				
Tag	**Symbol**	**X**	**Y**	**Z**
1	C	2.015117	2.015413	-0.07934
2	C	1.08191	3.096278	-0.09932
3	C	3.402834	2.338326	-0.12422
4	C	1.533812	4.429075	-0.16016
5	H	0.019918	2.883133	-0.0673
6	C	3.841822	3.66958	-0.18452
7	C	2.909304	4.731605	-0.20295
8	H	0.803111	5.236041	-0.17407
9	H	4.908553	3.88235	-0.21753
10	H	3.248295	5.763583	-0.24959
11	N	1.69991	0.64793	-0.01527
12	C	0.481115	0.158795	0.01662
13	C	-3.09943	-0.04661	0.038265

14	C	-4.02238	-1.06765	-0.26826
15	C	-3.53688	1.254246	0.35245
16	C	-5.39755	-0.7822	-0.23589
17	H	-3.69041	-2.06451	-0.54283
18	C	-4.91617	1.527483	0.373798
19	H	-2.80748	2.023653	0.57485
20	C	-5.85093	0.513912	0.084563
21	H	-6.11044	-1.56716	-0.47157
22	H	-5.25737	2.529689	0.617876
23	H	-6.91537	0.730035	0.102988
24	N	-0.76832	0.757848	-0.0003
25	N	-1.69059	-0.31705	0.025384
26	N	0.266139	-1.28339	0.058838
27	C	-1.07303	-1.50182	0.066235
28	H	-1.54418	-2.46584	0.146581
29	C	1.263978	-2.31835	0.051817
30	C	1.08014	-3.44564	-0.7755
31	C	2.397087	-2.21177	0.881768
32	C	2.030554	-4.48251	-0.75586
33	H	0.219088	-3.50909	-1.43562
34	C	3.34577	-3.24975	0.885758
35	H	2.529914	-1.33251	1.500067
36	C	3.166061	-4.38765	0.072873
37	H	1.888318	-5.35163	-1.392
38	H	4.21977	-3.17194	1.526649
39	H	3.902228	-5.18677	0.08261
40	H	4.117195	1.518942	-0.11053

M3				
Tag	**Symbol**	**X**	**Y**	**Z**
1	C	1.971998	2.001162	-0.10854
2	C	1.05155	3.080333	-0.06419
3	C	3.347986	2.332111	-0.21365
4	C	1.499367	4.405344	-0.11766
5	H	-0.00812	2.87645	0.013001
6	C	3.781976	3.653623	-0.26904
7	C	2.859565	4.709571	-0.22049
8	H	0.767234	5.20883	-0.07931
9	H	4.845739	3.863541	-0.34985
10	H	3.195648	5.741495	-0.26262
11	N	1.674285	0.645902	-0.04998

12	C	0.459353	0.165929	0.002093
13	C	-3.07403	-0.06686	0.029991
14	C	-3.94461	-0.99716	-0.54797
15	C	-3.55525	1.108317	0.614677
16	C	-5.31889	-0.75444	-0.51184
17	H	-3.56192	-1.88629	-1.03782
18	C	-4.93139	1.34265	0.631683
19	H	-2.85946	1.816305	1.048212
20	C	-5.81618	0.413191	0.075647
21	H	-5.9974	-1.47327	-0.95997
22	H	-5.31039	2.252478	1.086466
23	H	-6.88515	0.600616	0.092815
24	N	-0.7699	0.739618	-0.0185
25	N	-1.66778	-0.31039	0.022769
26	N	0.266137	-1.2564	0.069516
27	C	-1.05649	-1.4812	0.080528
28	H	-1.52928	-2.44624	0.169545
29	C	1.272003	-2.27595	0.080232
30	C	1.259657	-3.25762	-0.9148
31	C	2.236524	-2.28699	1.092104
32	C	2.220318	-4.27259	-0.88684
33	H	0.51369	-3.22313	-1.70257
34	C	3.197993	-3.29874	1.103843
35	H	2.229837	-1.51484	1.852396
36	C	3.190833	-4.29287	0.11854
37	H	2.211826	-5.03886	-1.6556
38	H	3.949144	-3.31341	1.887435
39	H	3.939546	-5.07887	0.135046
40	H	4.065984	1.517222	-0.24971

M4				
Tag	**Symbol**	**X**	**Y**	**Z**
1	C	1.923517	2.010336	-0.12024
2	C	0.979627	3.058088	-0.0221
3	C	3.282493	2.377428	-0.26134
4	C	1.392406	4.392359	-0.06032
5	H	-0.07197	2.82909	0.086437
6	C	3.680423	3.706272	-0.30197
7	C	2.735391	4.733757	-0.20085
8	H	0.642199	5.174752	0.020469
9	H	4.734633	3.945165	-0.41245

10	H	3.042786	5.774119	-0.23146
11	N	1.66736	0.647945	-0.07642
12	C	0.45942	0.157064	-0.02341
13	C	-3.05257	-0.10673	0.018916
14	C	-3.92044	-1.06232	-0.50676
15	C	-3.52281	1.084491	0.566986
16	C	-5.29178	-0.82654	-0.45217
17	H	-3.53844	-1.96517	-0.97193
18	C	-4.89664	1.309951	0.602337
19	H	-2.81778	1.809723	0.956035
20	C	-5.78265	0.356454	0.100634
21	H	-5.9746	-1.56435	-0.85943
22	H	-5.27337	2.233627	1.028655
23	H	-6.8517	0.537699	0.132385
24	N	-0.76975	0.711721	-0.04374
25	N	-1.64671	-0.3397	-0.00319
26	N	0.284788	-1.25792	0.042065
27	C	-1.03048	-1.50004	0.055141
28	H	-1.49573	-2.4701	0.147708
29	C	1.306361	-2.25428	0.069564
30	C	1.245925	-3.31423	-0.83238
31	C	2.330611	-2.15883	1.010535
32	C	2.222529	-4.3081	-0.7782
33	H	0.451825	-3.35491	-1.57166
34	C	3.306598	-3.15042	1.045771
35	H	2.355601	-1.316	1.691256
36	C	3.253165	-4.22587	0.156436
37	H	2.179867	-5.13847	-1.47498
38	H	4.108155	-3.0856	1.774041
39	H	4.01582	-4.99682	0.191729
40	H	4.016303	1.579847	-0.33738

M5				
Tag	**Symbol**	**X**	**Y**	**Z**
1	C	1.92057	2.012444	-0.12112
2	C	0.975781	3.058559	-0.01304
3	C	3.278013	2.382347	-0.27066
4	C	1.386166	4.393647	-0.05024
5	H	-0.0746	2.8277	0.103182
6	C	3.67351	3.711983	-0.31042
7	C	2.727549	4.7377	-0.19971

8	H	0.63531	5.174552	0.038491
9	H	4.726536	3.952868	-0.42762
10	H	3.033026	5.77864	-0.22956
11	N	1.66699	0.64963	-0.07856
12	C	0.459383	0.156771	-0.02342
13	C	-3.05216	-0.11046	0.018777
14	C	-3.91859	-1.06735	-0.50693
15	C	-3.52391	1.080777	0.565544
16	C	-5.2902	-0.83261	-0.45386
17	H	-3.5354	-1.97042	-0.97067
18	C	-4.898	1.305163	0.59932
19	H	-2.82004	1.806903	0.955057
20	C	-5.78265	0.350469	0.097418
21	H	-5.97198	-1.57144	-0.86101
22	H	-5.27597	2.228788	1.024644
23	H	-6.85189	0.530776	0.127985
24	N	-0.76998	0.710177	-0.04375
25	N	-1.64598	-0.34212	-0.00207
26	N	0.286582	-1.25792	0.043897
27	C	-1.0284	-1.50164	0.057396
28	H	-1.49232	-2.47227	0.150867
29	C	1.309452	-2.25323	0.070962
30	C	1.252378	-3.31073	-0.83406
31	C	2.331384	-2.15896	1.014571
32	C	2.230662	-4.30307	-0.78067
33	H	0.459284	-3.35111	-1.57442
34	C	3.309118	-3.14888	1.049011
35	H	2.352803	-1.3188	1.698771
36	C	3.259363	-4.22169	0.156214
37	H	2.19058	-5.13176	-1.47958
38	H	4.108787	-3.08511	1.779438
39	H	4.023167	-4.99153	0.190912
40	H	4.012923	1.586405	-0.3537

*B-2.2.2 – Nitron **(33a)** (carbenic form)*

M1				
Tag	**Symbol**	**X**	**Y**	**Z**
1	C	1.89693	2.048798	-0.06332
2	C	0.933617	3.070432	-0.04216
3	C	3.262722	2.386196	-0.11343

4	C	1.346837	4.406825	-0.07018
5	H	-0.11814	2.822139	-0.00544
6	C	3.65643	3.721966	-0.14094
7	C	2.700674	4.745254	-0.11918
8	H	0.591798	5.187695	-0.05341
9	H	4.714858	3.962224	-0.17964
10	H	3.008572	5.785922	-0.14078
11	N	1.576907	0.678539	-0.03398
12	C	0.353358	0.078885	0.002314
13	C	-3.10249	-0.19502	0.025604
14	C	-4.00207	-1.26011	-0.1237
15	C	-3.57855	1.112261	0.181321
16	C	-5.37428	-1.00975	-0.10827
17	H	-3.62256	-2.2668	-0.2491
18	C	-4.95646	1.348107	0.191047
19	H	-2.87791	1.929685	0.293928
20	C	-5.86113	0.293245	0.048507
21	H	-6.06509	-1.83966	-0.22439
22	H	-5.31818	2.364816	0.313126
23	H	-6.93025	0.481783	0.057297
24	N	-0.82604	0.648673	-0.0053
25	N	-1.6994	-0.44713	0.017851
26	N	0.222413	-1.31199	0.034846
27	C	-1.10834	-1.65893	0.041308
28	C	1.30705	-2.25343	0.042683
29	C	1.523687	-3.0612	-1.07776
30	C	2.128983	-2.35623	1.17
31	C	2.572426	-3.98366	-1.06548
32	H	0.87364	-2.96532	-1.94109
33	C	3.18373	-3.27368	1.168612
34	H	1.936529	-1.73584	2.039912
35	C	3.404955	-4.08811	0.053994
36	H	2.740706	-4.61627	-1.93146
37	H	3.822737	-3.35691	2.042105
38	H	4.22159	-4.80346	0.058236
39	H	4.012057	1.599044	-0.13134
40	H	2.363969	0.043161	-0.04771

M2				
Tag	**Symbol**	**X**	**Y**	**Z**
1	C	1.906465	2.085151	-0.06462
2	C	0.910194	3.088346	-0.02128
3	C	3.272253	2.456016	-0.13441
4	C	1.291639	4.443741	-0.04575
5	H	-0.13442	2.81023	0.029045
6	C	3.635566	3.811528	-0.15866
7	C	2.647164	4.817733	-0.11371
8	H	0.519618	5.208857	-0.01164
9	H	4.687346	4.080896	-0.21229
10	H	2.929792	5.866661	-0.13213
11	N	1.614371	0.696213	-0.03777
12	C	0.388016	0.087602	0.010783
13	C	-3.11293	-0.20595	0.034269
14	C	-4.0203	-1.28749	0.027274
15	C	-3.58716	1.121643	0.048765
16	C	-5.4017	-1.03294	0.0354
17	H	-3.64013	-2.30308	0.016132
18	C	-4.97416	1.362259	0.056534
19	H	-2.88095	1.943101	0.053697
20	C	-5.88833	0.29103	0.04998
21	H	-6.09742	-1.86815	0.029984
22	H	-5.33625	2.387196	0.067776
23	H	-6.95806	0.482005	0.056067
24	N	-0.81196	0.664449	0.009167
25	N	-1.70458	-0.46145	0.025527
26	N	0.252664	-1.3226	0.036194
27	C	-1.0988	-1.68943	0.037662
28	C	1.33333	-2.27642	0.036118
29	C	1.401309	-3.24206	-0.98658
30	C	2.297301	-2.24853	1.064256
31	C	2.446943	-4.18288	-0.98175
32	H	0.646566	-3.25051	-1.76682
33	C	3.34734	-3.18662	1.054731
34	H	2.216746	-1.52644	1.872564
35	C	3.424482	-4.15449	0.034086
36	H	2.500565	-4.93058	-1.76827
37	H	4.090813	-3.16732	1.84669
38	H	4.233054	-4.88031	0.032018
39	H	4.04137	1.687069	-0.1698

40	H	2.416151	0.074694	-0.07344

M3				
Tag	**Symbol**	**X**	**Y**	**Z**
1	C	1.89535	2.049876	-0.06361
2	C	0.931074	3.070703	-0.04444
3	C	3.260932	2.388573	-0.11209
4	C	1.343023	4.40753	-0.073
5	H	-0.12055	2.82171	-0.00872
6	C	3.653348	3.724726	-0.14016
7	C	2.696612	4.747199	-0.12054
8	H	0.587179	5.187654	-0.05777
9	H	4.711608	3.965912	-0.17759
10	H	3.003577	5.788135	-0.14258
11	N	1.576489	0.67934	-0.03377
12	C	0.353489	0.07889	0.001878
13	C	-3.10225	-0.19715	0.025303
14	C	-4.00124	-1.26136	-0.13343
15	C	-3.57904	1.108714	0.190739
16	C	-5.37364	-1.01177	-0.11726
17	H	-3.62141	-2.26691	-0.26678
18	C	-4.95708	1.343916	0.200873
19	H	-2.87894	1.925595	0.310511
20	C	-5.86117	0.289765	0.04928
21	H	-6.06395	-1.84101	-0.24076
22	H	-5.31935	2.359478	0.330538
23	H	-6.93037	0.477799	0.05844
24	N	-0.82645	0.647899	-0.00606
25	N	-1.69903	-0.44849	0.017294
26	N	0.223425	-1.312	0.034597
27	C	-1.10698	-1.65979	0.041258
28	C	1.308843	-2.2528	0.04304
29	C	1.5301	-3.05633	-1.07955
30	C	2.126785	-2.35871	1.172922
31	C	2.579482	-3.97809	-1.06671
32	H	0.883505	-2.95756	-1.94516
33	C	3.182145	-3.27549	1.172158
34	H	1.931279	-1.74089	2.043965
35	C	3.407911	-4.08591	0.055515
36	H	2.751562	-4.60735	-1.93436
37	H	3.818278	-3.36104	2.047509

38	H	4.225111	-4.80061	0.060189
39	H	4.011137	1.602261	-0.12814
40	H	2.364067	0.044516	-0.04682

M4				
Tag	**Symbol**	**X**	**Y**	**Z**
1	C	1.856841	2.05303	-0.0854
2	C	0.874	3.047082	-0.00764
3	C	3.208205	2.420092	-0.18223
4	C	1.257459	4.389597	-0.0254
5	H	-0.17072	2.778102	0.064885
6	C	3.570646	3.760575	-0.19931
7	C	2.596334	4.758697	-0.12049
8	H	0.48736	5.152412	0.036228
9	H	4.620636	4.025085	-0.27474
10	H	2.87966	5.805661	-0.13395
11	N	1.572723	0.678814	-0.06329
12	C	0.357001	0.069721	-0.01726
13	C	-3.07876	-0.22288	0.022066
14	C	-3.96672	-1.29096	-0.12924
15	C	-3.55416	1.077873	0.189914
16	C	-5.33656	-1.04816	-0.10218
17	H	-3.57944	-2.29353	-0.26528
18	C	-4.93003	1.304958	0.210849
19	H	-2.85373	1.89611	0.303322
20	C	-5.82663	0.24819	0.067488
21	H	-6.02426	-1.87954	-0.21956
22	H	-5.29719	2.317745	0.342725
23	H	-6.89594	0.430776	0.085481
24	N	-0.82256	0.624161	-0.02437
25	N	-1.67663	-0.4669	0.00494
26	N	0.238491	-1.31326	0.021219
27	C	-1.08565	-1.6735	0.031326
28	C	1.330945	-2.23577	0.04605
29	C	1.475114	-3.15129	-0.99442
30	C	2.229781	-2.20817	1.11219
31	C	2.534856	-4.05524	-0.96216
32	H	0.759495	-3.14866	-1.81002
33	C	3.296169	-3.10607	1.127002
34	H	2.085449	-1.50115	1.924089
35	C	3.447727	-4.02986	0.093162

36	H	2.650609	-4.77483	-1.76577
37	H	3.999307	-3.08949	1.952924
38	H	4.275124	-4.73151	0.110788
39	H	3.970935	1.64854	-0.2437
40	H	2.36917	0.057119	-0.1229

M5				
Tag	**Symbol**	**X**	**Y**	**Z**
1	C	1.855762	2.053825	-0.08714
2	C	0.872303	3.047328	-0.00942
3	C	3.206962	2.421767	-0.18378
4	C	1.254868	4.390163	-0.0272
5	H	-0.1723	2.777934	0.063246
6	C	3.568476	3.762514	-0.20091
7	C	2.593518	4.760097	-0.12226
8	H	0.484241	5.152447	0.034425
9	H	4.618318	4.027655	-0.27616
10	H	2.876207	5.807235	-0.13576
11	N	1.572489	0.679418	-0.06511
12	C	0.357234	0.069745	-0.01873
13	C	-3.07847	-0.22418	0.021838
14	C	-3.96612	-1.29066	-0.14198
15	C	-3.55414	1.074744	0.202816
16	C	-5.33607	-1.04834	-0.1137
17	H	-3.5787	-2.29167	-0.28875
18	C	-4.93007	1.301513	0.224514
19	H	-2.8539	1.891809	0.32575
20	C	-5.8264	0.246141	0.069148
21	H	-6.02357	-1.87843	-0.2409
22	H	-5.29751	2.312806	0.366605
23	H	-6.89574	0.428442	0.087814
24	N	-0.82273	0.623649	-0.02647
25	N	-1.67628	-0.46773	0.004043
26	N	0.239318	-1.31322	0.021072
27	C	-1.08462	-1.67396	0.031844
28	C	1.332168	-2.23539	0.046981
29	C	1.477392	-3.15109	-0.99322
30	C	2.230081	-2.20721	1.113859
31	C	2.537264	-4.05488	-0.95978
32	H	0.762866	-3.14855	-1.80978
33	C	3.296611	-3.10493	1.12982

34	H	2.085333	-1.49963	1.925195
35	C	3.449151	-4.02908	0.096413
36	H	2.654003	-4.77452	-1.7632
37	H	3.999227	-3.08772	1.956159
38	H	4.276742	-4.73046	0.114906
39	H	3.970306	1.650823	-0.24482
40	H	2.369385	0.058169	-0.12412

*B-2.2.3 – Di-(p-tolyl) Nitron (**33b**) (zwitterionic form)*

M1				
Tag	**Symbol**	**X**	**Y**	**Z**
1	C	0.354051	2.523969	-0.06638
2	C	-0.99112	2.963621	-0.02567
3	C	1.348085	3.53239	-0.1507
4	C	-1.30192	4.32942	-0.06549
5	H	-1.79105	2.237689	0.036582
6	C	1.022381	4.883753	-0.19065
7	C	-0.31592	5.319193	-0.1489
8	H	-2.34901	4.625316	-0.03118
9	H	1.822579	5.618841	-0.25592
10	N	0.81319	1.211541	-0.02542
11	C	0.029649	0.167564	0.01144
12	C	-2.86208	-1.87712	0.028533
13	C	-3.12029	-3.12861	-0.54156
14	C	-3.88631	-1.12226	0.608139
15	C	-4.41917	-3.63841	-0.50234
16	H	-2.33024	-3.69072	-1.02813
17	C	-5.18258	-1.64031	0.628388
18	H	-3.66168	-0.15232	1.034747
19	C	-5.45282	-2.89827	0.080517
20	H	-4.62278	-4.60838	-0.94475
21	H	-5.98066	-1.0587	1.079061
22	H	-6.46261	-3.29587	0.100018
23	N	-1.31978	0.014734	-0.00559
24	N	-1.53625	-1.35061	0.018119
25	N	0.608048	-1.14827	0.057051
26	C	-0.4024	-2.03008	0.061781
27	C	1.998258	-1.49131	0.054368
28	C	2.50397	-2.30919	-0.95719
29	C	2.835544	-1.02249	1.071765

30	C	3.854378	-2.67058	-0.93953
31	H	1.853294	-2.65565	-1.75421
32	C	4.181166	-1.38327	1.06895
33	H	2.433943	-0.38581	1.851543
34	C	4.715267	-2.21319	0.067007
35	H	4.240235	-3.31136	-1.72732
36	H	4.82752	-1.019	1.863063
37	H	2.388871	3.221009	-0.18367
38	C	6.178365	-2.58816	0.078775
39	C	-0.6625	6.790504	-0.1927
40	H	-0.30098	-3.10106	0.136161
41	H	-0.21706	7.335682	0.648679
42	H	-1.74527	6.943273	-0.15159
43	H	-0.29384	7.265236	-1.11044
44	H	6.810684	-1.7074	-0.08325
45	H	6.468084	-3.01933	1.043254
46	H	6.409404	-3.3162	-0.70319

M3				
Tag	**Symbol**	**X**	**Y**	**Z**
1	C	0.365595	2.521448	-0.06653
2	C	-0.97761	2.967327	-0.02471
3	C	1.363981	3.525707	-0.15151
4	C	-1.28236	4.334559	-0.06436
5	H	-1.78089	2.245178	0.038524
6	C	1.044258	4.878534	-0.19135
7	C	-0.29208	5.32001	-0.14872
8	H	-2.32811	4.635045	-0.02911
9	H	1.84772	5.609993	-0.2571
10	N	0.819034	1.20707	-0.02601
11	C	0.030428	0.166286	0.011442
12	C	-2.87083	-1.86456	0.028408
13	C	-3.13557	-3.11249	-0.54642
14	C	-3.89069	-1.10713	0.612397
15	C	-4.43691	-3.61615	-0.5077
16	H	-2.34868	-3.67646	-1.03587
17	C	-5.18947	-1.61894	0.632042
18	H	-3.66103	-0.14016	1.04309
19	C	-5.46632	-2.87337	0.0793
20	H	-4.64566	-4.5834	-0.95364
21	H	-5.98419	-1.03543	1.086165

22	H	-6.47797	-3.26623	0.098421
23	N	-1.31943	0.020139	-0.00548
24	N	-1.54241	-1.34436	0.018424
25	N	0.602607	-1.15164	0.057365
26	C	-0.41174	-2.02896	0.062038
27	C	1.991596	-1.50045	0.054906
28	C	2.496398	-2.31093	-0.96296
29	C	2.828139	-1.04427	1.078615
30	C	3.845526	-2.67724	-0.9457
31	H	1.845821	-2.64857	-1.76381
32	C	4.172521	-1.40979	1.075501
33	H	2.426859	-0.41416	1.863963
34	C	4.70583	-2.23224	0.066931
35	H	4.230686	-3.31253	-1.73825
36	H	4.818307	-1.05568	1.874643
37	H	2.403528	3.210117	-0.18489
38	C	6.167452	-2.61291	0.078645
39	C	-0.63218	6.792843	-0.19237
40	H	-0.31507	-3.10044	0.135797
41	H	-0.18336	7.336129	0.648412
42	H	-1.7142	6.950394	-0.15012
43	H	-0.26231	7.265797	-1.11053
44	H	6.803522	-1.73306	-0.0733
45	H	6.453042	-3.05433	1.039697
46	H	6.397605	-3.33433	-0.70967

M4				
Tag	**Symbol**	**X**	**Y**	**Z**
1	C	-0.01917	2.526304	-0.0744
2	C	-1.4092	2.74493	0.022639
3	C	0.797747	3.67373	-0.20568
4	C	-1.93109	4.042744	-0.01071
5	H	-2.08376	1.905459	0.126174
6	C	0.263604	4.952437	-0.23953
7	C	-1.12043	5.168838	-0.14276
8	H	-3.00876	4.172486	0.068493
9	H	0.931216	5.805726	-0.34318
10	N	0.646454	1.307425	-0.04095
11	C	0.019473	0.164847	-0.00067
12	C	-2.54011	-2.2562	0.021713
13	C	-2.60764	-3.54715	-0.50033

14	C	-3.66054	-1.62796	0.560866
15	C	-3.82022	-4.22981	-0.45079
16	H	-1.73915	-4.0091	-0.95838
17	C	-4.86866	-2.32031	0.59108
18	H	-3.57409	-0.61911	0.946951
19	C	-4.95124	-3.62068	0.093271
20	H	-3.88111	-5.23459	-0.85487
21	H	-5.7464	-1.84023	1.010574
22	H	-5.89494	-4.15489	0.121274
23	N	-1.28567	-0.17941	-0.01831
24	N	-1.30304	-1.54961	0.00454
25	N	0.775827	-1.04513	0.046204
26	C	-0.09218	-2.06151	0.050849
27	C	2.19666	-1.17696	0.048439
28	C	2.806355	-2.00588	-0.88747
29	C	2.953413	-0.49311	0.999753
30	C	4.191968	-2.16374	-0.85905
31	H	2.207377	-2.51642	-1.6356
32	C	4.333578	-0.65267	1.005258
33	H	2.458661	0.153921	1.715024
34	C	4.974998	-1.48921	0.080176
35	H	4.66692	-2.81521	-1.58681
36	H	4.926708	-0.12301	1.745858
37	H	1.871675	3.525515	-0.28051
38	C	6.474619	-1.63695	0.099035
39	C	-1.69222	6.564372	-0.182
40	H	0.160739	-3.10848	0.126541
41	H	-1.28699	7.183143	0.625404
42	H	-2.78008	6.545726	-0.07798
43	H	-1.45287	7.066063	-1.1255
44	H	6.958069	-0.70728	-0.21717
45	H	6.831955	-1.86519	1.107021
46	H	6.801415	-2.43401	-0.57188

M5				
Tag	**Symbol**	**X**	**Y**	**Z**
1	C	-0.02272	2.525441	-0.07615
2	C	-1.41234	2.742136	0.031908
3	C	0.791015	3.674125	-0.21683
4	C	-1.93672	4.039039	0.000071
5	H	-2.08467	1.901863	0.143341

6	C	0.254435	4.951887	-0.24929
7	C	-1.12914	5.166257	-0.1414
8	H	-3.0139	4.167093	0.08819
9	H	0.919749	5.80601	-0.36046
10	N	0.645278	1.307849	-0.04419
11	C	0.019872	0.163935	-0.00161
12	C	-2.53674	-2.25997	0.021324
13	C	-2.60249	-3.55089	-0.50099
14	C	-3.65813	-1.63296	0.559969
15	C	-3.81448	-4.2347	-0.4525
16	H	-1.73307	-4.01205	-0.95806
17	C	-4.86565	-2.32647	0.589091
18	H	-3.57312	-0.62425	0.946745
19	C	-4.94656	-3.62678	0.090791
20	H	-3.87401	-5.23952	-0.85668
21	H	-5.74414	-1.84741	1.008198
22	H	-5.88974	-4.16195	0.117986
23	N	-1.28461	-0.18164	-0.01877
24	N	-1.30037	-1.55198	0.004781
25	N	0.777668	-1.04456	0.046411
26	C	-0.08885	-2.06222	0.051414
27	C	2.198928	-1.17397	0.049151
28	C	2.811232	-1.99346	-0.89323
29	C	2.953013	-0.49695	1.007445
30	C	4.197245	-2.14835	-0.86466
31	H	2.213917	-2.49958	-1.64568
32	C	4.333553	-0.65329	1.013146
33	H	2.455894	0.141817	1.728581
34	C	4.977744	-1.48022	0.081288
35	H	4.67441	-2.7928	-1.59719
36	H	4.924695	-0.12921	1.759279
37	H	1.864631	3.527899	-0.29987
38	C	6.477626	-1.62517	0.100803
39	C	-1.70359	6.560744	-0.17895
40	H	0.16562	-3.10885	0.126909
41	H	-1.29296	7.181831	0.623912
42	H	-2.79055	6.540464	-0.06627
43	H	-1.47251	7.060912	-1.1253
44	H	6.959677	-0.69167	-0.20611
45	H	6.833955	-1.86192	1.107172
46	H	6.806818	-2.41539	-0.57698

*B-2.2.4 – Di-(p-tolyl) Nitron (**33b**) (carbenic form)*

M1				
Tag	**Symbol**	**X**	**Y**	**Z**
1	C	0.902604	2.35051	-0.0256
2	C	-0.30674	3.057553	0.018136
3	C	2.11054	3.069822	-0.0908
4	C	-0.29016	4.457539	-0.00276
5	H	-1.24625	2.524118	0.066452
6	C	2.102737	4.460849	-0.11003
7	C	0.900767	5.189273	-0.06616
8	H	-1.23974	4.985935	0.031712
9	H	3.051182	4.989995	-0.16138
10	N	0.98978	0.944494	-0.00456
11	C	-0.01052	0.020645	0.018797
12	C	-3.24213	-1.23438	0.021271
13	C	-3.79744	-2.52068	-0.04099
14	C	-4.07565	-0.11096	0.081036
15	C	-5.18391	-2.67347	-0.03931
16	H	-3.1442	-3.38317	-0.08974
17	C	-5.46345	-0.27997	0.080675
18	H	-3.64043	0.878982	0.127203
19	C	-6.02625	-1.55708	0.021538
20	H	-5.6061	-3.67293	-0.08769
21	H	-6.1027	0.596749	0.127791
22	H	-7.10458	-1.68289	0.021669
23	N	-1.30426	0.228757	0.014316
24	N	-1.82605	-1.07273	0.022104
25	N	0.26353	-1.34934	0.035852
26	C	-0.91085	-2.06375	0.033795
27	C	1.575403	-1.93421	0.030856
28	C	2.044323	-2.57492	-1.11901
29	C	2.374453	-1.86871	1.176049
30	C	3.31453	-3.15293	-1.11589
31	H	1.413808	-2.62495	-2.00084
32	C	3.648023	-2.44188	1.161082
33	H	1.998094	-1.38723	2.073566
34	C	4.140139	-3.09138	0.018447
35	H	3.669266	-3.65784	-2.01026
36	H	4.261664	-2.39207	2.056331
37	H	3.055936	2.534413	-0.12819
38	C	5.527581	-3.68807	0.001345

39	C	0.90533	6.700612	-0.08501
40	H	1.925647	0.560588	-0.0182
41	H	1.430743	7.109337	0.786302
42	H	1.412673	7.087705	-0.97634
43	H	-0.11296	7.099551	-0.07872
44	H	6.26202	-2.95391	-0.3525
45	H	5.837406	-4.00503	1.001277
46	H	5.581389	-4.55212	-0.66723

M3				
Tag	**Symbol**	**X**	**Y**	**Z**
1	C	0.899938	2.351057	-0.02583
2	C	-0.31056	3.056596	0.010804
3	C	2.107383	3.071964	-0.08338
4	C	-0.29571	4.456685	-0.00952
5	H	-1.24976	2.522096	0.053303
6	C	2.097852	4.462994	-0.10228
7	C	0.894653	5.189919	-0.06548
8	H	-1.24617	4.983817	0.019355
9	H	3.045909	4.993359	-0.14758
10	N	0.988718	0.945125	-0.00539
11	C	-0.01051	0.020327	0.017327
12	C	-3.24093	-1.23813	0.020717
13	C	-3.7951	-2.52439	-0.0522
14	C	-4.07552	-0.11612	0.091783
15	C	-5.18143	-2.67868	-0.0493
16	H	-3.14115	-3.38578	-0.11009
17	C	-5.46317	-0.28655	0.092236
18	H	-3.64135	0.873888	0.146091
19	C	-6.02478	-1.5637	0.022896
20	H	-5.6027	-3.67808	-0.106
21	H	-6.10322	0.589046	0.148209
22	H	-7.10297	-1.69062	0.023733
23	N	-1.30462	0.227004	0.012643
24	N	-1.82502	-1.07501	0.020964
25	N	0.264997	-1.34929	0.034796
26	C	-0.90852	-2.06486	0.033274
27	C	1.577827	-1.93255	0.030381
28	C	2.054935	-2.55702	-1.12506
29	C	2.369361	-1.88122	1.181453
30	C	3.325979	-3.13325	-1.12165

31	H	1.430397	-2.59562	-2.01174
32	C	3.643685	-2.45274	1.167055
33	H	1.986887	-1.41127	2.082468
34	C	4.144031	-3.08605	0.01887
35	H	3.687325	-3.62522	-2.02056
36	H	4.251649	-2.41392	2.066686
37	H	3.053683	2.537833	-0.1148
38	C	5.53246	-3.68043	0.002544
39	C	0.897455	6.701284	-0.08373
40	H	1.92507	0.562232	-0.01715
41	H	1.417834	7.110237	0.790486
42	H	1.409128	7.089337	-0.97217
43	H	-0.12134	7.098975	-0.08266
44	H	6.267347	-2.9414	-0.34002
45	H	5.837844	-4.00722	1.000666
46	H	5.591024	-4.53732	-0.6748

M4				
Tag	**Symbol**	**X**	**Y**	**Z**
1	C	0.710627	2.39407	-0.04186
2	C	-0.55484	2.983759	0.016574
3	C	1.845284	3.21629	-0.1281
4	C	-0.66441	4.37699	-0.01217
5	H	-1.44298	2.370237	0.082218
6	C	1.710846	4.596437	-0.15465
7	C	0.450726	5.208785	-0.09739
8	H	-1.65649	4.819015	0.03332
9	H	2.604138	5.212422	-0.22215
10	N	0.927881	1.006273	-0.01186
11	C	0.002186	0.011193	0.016611
12	C	-3.11379	-1.4662	0.025935
13	C	-3.57106	-2.77642	-0.13841
14	C	-4.01602	-0.41558	0.194944
15	C	-4.93941	-3.02835	-0.12469
16	H	-2.85632	-3.57917	-0.27418
17	C	-5.38453	-0.68436	0.202658
18	H	-3.64733	0.595114	0.319351
19	C	-5.85366	-1.98674	0.044948
20	H	-5.29165	-4.04697	-0.25252
21	H	-6.08389	0.13496	0.335207
22	H	-6.91937	-2.18998	0.052262

23	N	-1.29731	0.118609	0.010564
24	N	-1.71543	-1.20336	0.019382
25	N	0.37508	-1.32617	0.036685
26	C	-0.7389	-2.12679	0.033772
27	C	1.722851	-1.80423	0.040248
28	C	2.185724	-2.56048	-1.03402
29	C	2.558787	-1.51543	1.117627
30	C	3.495188	-3.03242	-1.0222
31	H	1.517772	-2.77801	-1.86129
32	C	3.871621	-1.98186	1.107666
33	H	2.179232	-0.94507	1.960799
34	C	4.35943	-2.74481	0.041115
35	H	3.853503	-3.63042	-1.85545
36	H	4.521574	-1.75955	1.949271
37	H	2.833714	2.766457	-0.1741
38	C	5.787195	-3.22674	0.025549
39	C	0.321607	6.710882	-0.12571
40	H	1.89185	0.702059	-0.06071
41	H	0.830686	7.165644	0.729833
42	H	0.771229	7.127841	-1.03214
43	H	-0.7271	7.015256	-0.09634
44	H	6.432485	-2.49654	-0.47387
45	H	6.167081	-3.36647	1.040123
46	H	5.877633	-4.17247	-0.51378

M5				
Tag	**Symbol**	**X**	**Y**	**Z**
1	C	0.709325	2.394271	-0.0447
2	C	-0.55643	2.983299	0.015098
3	C	1.843502	3.217136	-0.13178
4	C	-0.66683	4.376542	-0.01296
5	H	-1.44428	2.369439	0.081408
6	C	1.708256	4.597236	-0.15759
7	C	0.447826	5.208946	-0.09886
8	H	-1.65911	4.817977	0.03368
9	H	2.601156	5.213714	-0.22566
10	N	0.927411	1.006578	-0.01534
11	C	0.002354	0.011122	0.014196
12	C	-3.11303	-1.46769	0.025668
13	C	-3.57045	-2.77548	-0.15635
14	C	-4.01493	-0.41989	0.213309

15	C	-4.9387	-3.02825	-0.14072
16	H	-2.85612	-3.5759	-0.30729
17	C	-5.38333	-0.68926	0.222269
18	H	-3.64611	0.589066	0.351096
19	C	-5.85257	-1.98951	0.047599
20	H	-5.29113	-4.04497	-0.28229
21	H	-6.08246	0.127748	0.369377
22	H	-6.91817	-2.19324	0.056025
23	N	-1.29734	0.117869	0.007733
24	N	-1.71479	-1.20427	0.018089
25	N	0.375845	-1.32599	0.035915
26	C	-0.73774	-2.12708	0.034029
27	C	1.72393	-1.80342	0.040865
28	C	2.188158	-2.55948	-1.03295
29	C	2.558624	-1.51399	1.119039
30	C	3.497827	-3.03091	-1.01977
31	H	1.521396	-2.77695	-1.86122
32	C	3.871655	-1.97988	1.11043
33	H	2.178243	-0.94315	1.961511
34	C	4.360834	-2.74281	0.044436
35	H	3.857329	-3.62862	-1.85273
36	H	4.520774	-1.75686	1.952476
37	H	2.832092	2.76783	-0.1789
38	C	5.788896	-3.22385	0.030289
39	C	0.317956	6.711001	-0.12612
40	H	1.89166	0.702994	-0.06363
41	H	0.826378	7.16531	0.730053
42	H	0.768047	7.128854	-1.03189
43	H	-0.73092	7.014833	-0.09712
44	H	6.434402	-2.49222	-0.46673
45	H	6.167263	-3.36507	1.045223
46	H	5.8808	-4.16846	-0.51073

*B-2.2.5 – Di-(4-trifluoromethylphenyl) Nitron (**33c**) (zwitterionic form)*

M1				
Tag	**Symbol**	**X**	**Y**	**Z**
1	C	1.774009	-1.02553	-0.04721
2	C	2.941854	-0.21735	-0.00389
3	C	1.966135	-2.43202	-0.12509
4	C	4.211948	-0.79111	-0.03491

5	H	2.848158	0.858483	0.051395
6	C	3.230406	-2.99832	-0.15748
7	C	4.372802	-2.17911	-0.11602
8	H	5.084019	-0.14563	-0.00078
9	H	3.334177	-4.07722	-0.22002
10	N	0.463873	-0.59543	-0.01629
11	C	0.107122	0.66504	0.017697
12	C	0.242268	4.19965	0.029675
13	C	-0.57263	5.160256	-0.57782
14	C	1.442706	4.5539	0.651662
15	C	-0.18611	6.501021	-0.53515
16	H	-1.48171	4.87228	-1.09489
17	C	1.821067	5.897315	0.675273
18	H	2.058583	3.788416	1.107903
19	C	1.008669	6.87307	0.088937
20	H	-0.81398	7.250332	-1.00638
21	H	2.750994	6.179619	1.15857
22	H	1.308132	7.916082	0.111421
23	N	0.801032	1.825244	0.001835
24	N	-0.14899	2.825192	0.016758
25	N	-1.28821	0.998662	0.051036
26	C	-1.37756	2.340189	0.050965
27	C	-2.40019	0.102697	0.044247
28	C	-3.42557	0.295121	-0.88575
29	C	-2.46042	-0.93854	0.975783
30	C	-4.5325	-0.55305	-0.875
31	H	-3.35837	1.091811	-1.6187
32	C	-3.5622	-1.78985	0.975871
33	H	-1.65692	-1.07634	1.687714
34	C	-4.59904	-1.5943	0.054917
35	H	-5.3308	-0.4023	-1.59252
36	H	-3.61677	-2.5948	1.700223
37	H	1.085603	-3.06596	-0.16238
38	C	-5.76489	-2.54438	0.036349
39	C	5.730665	-2.79439	-0.0975
40	F	-5.51446	-3.64739	-0.72805
41	F	-6.88981	-1.97964	-0.46944
42	F	-6.07666	-3.00646	1.274413
43	F	6.709838	-1.94356	-0.50836
44	F	5.821996	-3.9027	-0.8884
45	F	6.112815	-3.21613	1.154394
46	H	-2.28985	2.9107	0.120535

M3				
Tag	**Symbol**	**X**	**Y**	**Z**
1	C	1.772366	-1.02616	-0.04954
2	C	2.940828	-0.21884	-0.00119
3	C	1.964242	-2.43266	-0.13109
4	C	4.210677	-0.79317	-0.03103
5	H	2.847741	0.856865	0.057387
6	C	3.228265	-2.99952	-0.16241
7	C	4.371088	-2.18105	-0.11608
8	H	5.082924	-0.14815	0.007196
9	H	3.331476	-4.07831	-0.22781
10	N	0.462572	-0.59566	-0.0199
11	C	0.106528	0.665561	0.016009
12	C	0.244698	4.19985	0.029741
13	C	-0.56921	5.160999	-0.57819
14	C	1.445235	4.553133	0.652124
15	C	-0.1814	6.501424	-0.53576
16	H	-1.4786	4.873707	-1.09503
17	C	1.824907	5.896213	0.675445
18	H	2.0602	3.787393	1.109186
19	C	1.013598	6.872544	0.088502
20	H	-0.80859	7.251175	-1.0072
21	H	2.754864	6.177796	1.159102
22	H	1.313989	7.915293	0.110833
23	N	0.801443	1.82477	0.000735
24	N	-0.14781	2.8257	0.016826
25	N	-1.28802	0.999968	0.05035
26	C	-1.37666	2.341486	0.051095
27	C	-2.40049	0.104318	0.044144
28	C	-3.42231	0.292357	-0.89053
29	C	-2.46428	-0.9319	0.980963
30	C	-4.52937	-0.55572	-0.87951
31	H	-3.35261	1.085851	-1.62666
32	C	-3.56604	-1.78326	0.98134
33	H	-1.66398	-1.0655	1.69734
34	C	-4.59931	-1.5923	0.055357
35	H	-5.32513	-0.40822	-1.60052
36	H	-3.62347	-2.58432	1.709767
37	H	1.083677	-3.06637	-0.17188
38	C	-5.76512	-2.54235	0.037217

39	C	5.728501	-2.79701	-0.09631
40	F	-5.51214	-3.64897	-0.72144
41	F	-6.88842	-1.98022	-0.47493
42	F	-6.08115	-2.99912	1.276204
43	F	6.70899	-1.94584	-0.50345
44	F	5.820895	-3.90369	-0.8895
45	F	6.108311	-3.2218	1.155311
46	H	-2.28875	2.912328	0.120696

M4

Tag	Symbol	X	Y	Z
1	C	1.742064	-1.03602	-0.04891
2	C	2.903581	-0.22909	-0.00015
3	C	1.93006	-2.4402	-0.12153
4	C	4.17209	-0.80516	-0.02369
5	H	2.814408	0.846863	0.054063
6	C	3.18983	-3.00647	-0.146
7	C	4.325456	-2.18615	-0.0994
8	H	5.047516	-0.16433	0.013262
9	H	3.29897	-4.08578	-0.20501
10	N	0.43189	-0.61	-0.02801
11	C	0.098723	0.655472	0.001487
12	C	0.294204	4.16911	0.025979
13	C	-0.52057	5.150026	-0.53545
14	C	1.516275	4.480801	0.616623
15	C	-0.10795	6.478697	-0.47613
16	H	-1.44938	4.886591	-1.03043
17	C	1.919362	5.813158	0.656401
18	H	2.127722	3.689615	1.034448
19	C	1.109252	6.812852	0.117604
20	H	-0.73452	7.249888	-0.91088
21	H	2.868512	6.068378	1.115342
22	H	1.428734	7.848873	0.15311
23	N	0.805557	1.798818	-0.00947
24	N	-0.12182	2.804239	-0.00081
25	N	-1.28129	1.008029	0.024305
26	C	-1.35341	2.345721	0.024588
27	C	-2.39772	0.123491	0.019301
28	C	-3.43275	0.347802	-0.88386
29	C	-2.4407	-0.93255	0.930473
30	C	-4.54519	-0.49038	-0.86842

31	H	-3.36777	1.160195	-1.59992
32	C	-3.54633	-1.7717	0.933879
33	H	-1.61739	-1.08651	1.616749
34	C	-4.59348	-1.54422	0.0381
35	H	-5.35969	-0.3229	-1.5637
36	H	-3.59854	-2.59454	1.639361
37	H	1.045779	-3.0685	-0.1608
38	C	-5.76274	-2.48661	0.045996
39	C	5.676713	-2.81586	-0.09054
40	F	-5.45262	-3.67538	-0.51267
41	F	-6.81816	-2.00473	-0.62985
42	F	-6.18184	-2.75663	1.297026
43	F	6.669633	-1.93366	-0.31208
44	F	5.801494	-3.78463	-1.02612
45	F	5.965119	-3.41875	1.090122
46	H	-2.2581	2.932234	0.086406

M5				
Tag	**Symbol**	**X**	**Y**	**Z**
1	C	1.741145	-1.03437	-0.04997
2	C	2.901467	-0.22919	0.036233
3	C	1.930832	-2.43722	-0.14897
4	C	4.170738	-0.80472	0.022259
5	H	2.811357	0.845224	0.114354
6	C	3.190802	-3.00254	-0.16439
7	C	4.325599	-2.18347	-0.07939
8	H	5.04501	-0.1651	0.089986
9	H	3.30101	-4.08069	-0.24317
10	N	0.430837	-0.609	-0.03871
11	C	0.097642	0.6569	-0.00383
12	C	0.29479	4.170126	0.024711
13	C	-0.51911	5.151934	-0.53645
14	C	1.517008	4.480564	0.615801
15	C	-0.10525	6.480222	-0.47663
16	H	-1.44822	4.889515	-1.03136
17	C	1.921335	5.812563	0.656027
18	H	2.127753	3.688898	1.03378
19	C	1.11222	6.813134	0.11731
20	H	-0.7312	7.252085	-0.91108
21	H	2.870598	6.066787	1.11529
22	H	1.432623	7.84886	0.153174

23	N	0.804935	1.799578	-0.0116
24	N	-0.12211	2.8055	-0.00327
25	N	-1.28184	1.009591	0.018156
26	C	-1.35387	2.347215	0.01978
27	C	-2.39786	0.124349	0.011625
28	C	-3.42841	0.343183	-0.89721
29	C	-2.44277	-0.92861	0.926935
30	C	-4.53922	-0.49821	-0.88488
31	H	-3.36157	1.153038	-1.61595
32	C	-3.54558	-1.77055	0.926842
33	H	-1.62246	-1.0781	1.617823
34	C	-4.58828	-1.54959	0.023442
35	H	-5.34969	-0.33643	-1.58592
36	H	-3.59852	-2.59291	1.633141
37	H	1.047621	-3.06489	-0.21432
38	C	-5.76163	-2.48629	0.050674
39	C	5.674764	-2.81743	-0.08783
40	F	-5.40043	-3.74967	-0.25398
41	F	-6.7256	-2.13537	-0.81458
42	F	-6.32903	-2.54311	1.272423
43	F	6.678555	-1.92099	-0.07214
44	F	5.873404	-3.59949	-1.17567
45	F	5.873487	-3.63222	0.977205
46	H	-2.25879	2.933514	0.080148

*B-2.2.6 – Di-(4-trifluoromethylphenyl) Nitron (**33c**) (carbenic form)*

M1				
Tag	**Symbol**	**X**	**Y**	**Z**
1	C	1.332272	2.23363	-0.04201
2	C	0.138003	2.970962	0.022624
3	C	2.562446	2.914695	-0.12446
4	C	0.185905	4.364333	0.006352
5	H	-0.81345	2.46192	0.080995
6	C	2.599654	4.302167	-0.13995
7	C	1.407782	5.03791	-0.07759
8	H	-0.74309	4.922136	0.054725
9	H	3.556102	4.809012	-0.20652
10	N	1.378906	0.833481	-0.02709
11	C	0.348514	-0.0607	0.010951
12	C	-2.91834	-1.19914	0.030522

13	C	-3.51686	-2.46525	-0.04583
14	C	-3.71092	-0.04862	0.115074
15	C	-4.90308	-2.57405	-0.0342
16	H	-2.89608	-3.34962	-0.11093
17	C	-5.10015	-0.16566	0.124653
18	H	-3.24489	0.925757	0.175327
19	C	-5.70119	-1.42539	0.053127
20	H	-5.35968	-3.55619	-0.09133
21	H	-5.70825	0.7294	0.193361
22	N	-0.93437	0.192	0.010463
23	N	-1.5025	-1.08738	0.022369
24	N	0.572987	-1.44158	0.030447
25	C	-0.62531	-2.11369	0.030179
26	C	1.852583	-2.0878	0.032643
27	C	2.21871	-2.88193	-1.05738
28	C	2.71134	-1.92923	1.124794
29	C	3.455077	-3.52512	-1.05491
30	H	1.53811	-2.99571	-1.89349
31	C	3.953469	-2.56388	1.119998
32	H	2.407301	-1.33335	1.978924
33	C	4.321033	-3.36258	0.032429
34	H	3.73962	-4.14691	-1.89609
35	H	4.619392	-2.44761	1.967501
36	H	3.48968	2.352151	-0.18008
37	C	5.678205	-4.01301	0.011858
38	C	1.449491	6.534463	-0.04397
39	F	6.626747	-3.19492	-0.53051
40	F	5.696843	-5.15414	-0.72088
41	F	6.119516	-4.33263	1.254439
42	F	0.330587	7.103514	-0.56503
43	F	2.506275	7.044945	-0.73086
44	F	1.560386	7.027829	1.228832
45	C	-7.19546	-1.54984	0.012474
46	F	-7.67762	-1.60415	-1.26666
47	F	-7.82619	-0.50408	0.606027
48	F	-7.64238	-2.67814	0.625397
49	H	2.303553	0.425814	-0.0769

M3				
Tag	**Symbol**	**X**	**Y**	**Z**
1	C	1.330803	2.234323	-0.04304
2	C	0.135748	2.970736	0.018721
3	C	2.560641	2.916507	-0.12214
4	C	0.182446	4.364148	0.002917
5	H	-0.81551	2.461053	0.074668
6	C	2.596678	4.303993	-0.13726
7	C	1.403998	5.038774	-0.07778
8	H	-0.74722	4.92101	0.049137
9	H	3.552951	4.811519	-0.20109
10	N	1.37853	0.834324	-0.02848
11	C	0.348901	-0.06049	0.009579
12	C	-2.91719	-1.20106	0.030163
13	C	-3.51518	-2.46721	-0.04986
14	C	-3.71039	-0.0512	0.118605
15	C	-4.90135	-2.57683	-0.03778
16	H	-2.89418	-3.35116	-0.1183
17	C	-5.09955	-0.16898	0.128521
18	H	-3.24497	0.923294	0.181654
19	C	-5.69998	-1.42883	0.053477
20	H	-5.35735	-3.55906	-0.09788
21	H	-5.70795	0.725637	0.200218
22	N	-0.93428	0.191282	0.009213
23	N	-1.50149	-1.08844	0.021705
24	N	0.574304	-1.44114	0.029491
25	C	-0.62341	-2.11404	0.029928
26	C	1.854513	-2.08652	0.031979
27	C	2.223238	-2.87651	-1.06017
28	C	2.710964	-1.93084	1.126276
29	C	3.459907	-3.51912	-1.0574
30	H	1.544666	-2.98732	-1.89833
31	C	3.953441	-2.56484	1.121804
32	H	2.4053	-1.33723	1.981379
33	C	4.323425	-3.35988	0.032381
34	H	3.746556	-4.13765	-1.90026
35	H	4.617774	-2.45059	1.970812
36	H	3.488505	2.354808	-0.17509
37	C	5.680678	-4.00998	0.012619
38	C	1.444336	6.5352	-0.04355
39	F	6.63061	-3.19035	-0.52494
40	F	5.701127	-5.1489	-0.72377

41	F	6.119399	-4.33384	1.255147
42	F	0.326178	7.103725	-0.56704
43	F	2.502297	7.047121	-0.72766
44	F	1.551722	7.028548	1.22976
45	C	-7.19416	-1.55385	0.013202
46	F	-7.67719	-1.60427	-1.26583
47	F	-7.82522	-0.5104	0.610502
48	F	-7.64034	-2.68441	0.62268
49	H	2.303595	0.42737	-0.07724

M4

Tag	Symbol	X	Y	Z
1	C	1.306414	2.220207	-0.05966
2	C	0.109697	2.929542	0.09408
3	C	2.517936	2.919422	-0.20521
4	C	0.135081	4.323219	0.101842
5	H	-0.82911	2.406068	0.205066
6	C	2.531405	4.302279	-0.19601
7	C	1.334669	5.009426	-0.04237
8	H	-0.79434	4.868903	0.221826
9	H	3.472439	4.831847	-0.30949
10	N	1.380476	0.824525	-0.06609
11	C	0.354103	-0.0705	-0.02816
12	C	-2.89621	-1.20335	-0.00379
13	C	-3.48775	-2.46532	-0.12372
14	C	-3.6788	-0.05797	0.134664
15	C	-4.86985	-2.57352	-0.09668
16	H	-2.86357	-3.34316	-0.23358
17	C	-5.06631	-0.17569	0.158018
18	H	-3.20708	0.91189	0.226086
19	C	-5.6583	-1.42909	0.045699
20	H	-5.3343	-3.55048	-0.1866
21	H	-5.67875	0.712075	0.269246
22	N	-0.92374	0.175271	-0.02941
23	N	-1.482	-1.09194	-0.02157
24	N	0.580608	-1.44175	-0.01241
25	C	-0.61238	-2.11829	-0.01617
26	C	1.860221	-2.07414	0.007396
27	C	2.190124	-2.96761	-1.00871
28	C	2.748602	-1.79807	1.047081
29	C	3.430565	-3.59687	-0.98566

30	H	1.477089	-3.16524	-1.80131
31	C	3.99415	-2.41714	1.059256
32	H	2.461014	-1.12244	1.846628
33	C	4.325493	-3.31379	0.044638
34	H	3.697536	-4.29959	-1.76703
35	H	4.692925	-2.21487	1.863922
36	H	3.44648	2.369769	-0.32612
37	C	5.688835	-3.94544	0.048063
38	C	1.379457	6.50483	-0.0355
39	F	6.620092	-3.12813	-0.48768
40	F	5.726173	-5.08651	-0.65932
41	F	6.109005	-4.23416	1.292845
42	F	0.165538	7.061939	0.109818
43	F	1.903788	7.00415	-1.17645
44	F	2.151788	6.986367	0.963539
45	C	-7.14968	-1.57464	0.038792
46	F	-7.62552	-1.86779	-1.19168
47	F	-7.78144	-0.45826	0.438963
48	F	-7.56474	-2.57323	0.844241
49	H	2.305155	0.428072	-0.17819

M5				
Tag	**Symbol**	**X**	**Y**	**Z**
1	C	1.306026	2.220082	-0.06162
2	C	0.108958	2.929238	0.09073
3	C	2.517723	2.919576	-0.20492
4	C	0.134071	4.322926	0.099337
5	H	-0.83003	2.405766	0.200148
6	C	2.530913	4.302427	-0.19498
7	C	1.333812	5.009362	-0.04273
8	H	-0.79568	4.868263	0.218318
9	H	3.472142	4.832034	-0.3067
10	N	1.380259	0.824501	-0.06889
11	C	0.354158	-0.07061	-0.03054
12	C	-2.89603	-1.2039	-0.00473
13	C	-3.48778	-2.46516	-0.13102
14	C	-3.67846	-0.05923	0.140631
15	C	-4.86986	-2.57353	-0.10301
16	H	-2.86393	-3.34249	-0.2467
17	C	-5.06596	-0.177	0.164688
18	H	-3.20672	0.910164	0.236924

19	C	-5.65809	-1.42981	0.04632
20	H	-5.33434	-3.55	-0.19792
21	H	-5.67817	0.710238	0.281271
22	N	-0.92384	0.174907	-0.03195
23	N	-1.48187	-1.09234	-0.02316
24	N	0.580865	-1.44178	-0.0139
25	C	-0.61193	-2.11844	-0.01687
26	C	1.860692	-2.07395	0.006665
27	C	2.191816	-2.96639	-1.00996
28	C	2.747883	-1.79835	1.047433
29	C	3.43237	-3.59539	-0.98618
30	H	1.479952	-3.16312	-1.80385
31	C	3.993566	-2.41716	1.060389
32	H	2.459608	-1.12293	1.846899
33	C	4.326076	-3.31297	0.045413
34	H	3.700361	-4.29714	-1.76806
35	H	4.691507	-2.21499	1.865782
36	H	3.446584	2.370198	-0.32442
37	C	5.689481	-3.94437	0.049655
38	C	1.378378	6.504687	-0.03497
39	F	6.621081	-3.12736	-0.48597
40	F	5.727367	-5.08581	-0.65726
41	F	6.109262	-4.23274	1.294722
42	F	0.164404	7.061719	0.110831
43	F	1.902446	7.005012	-1.17569
44	F	2.150765	6.985948	0.96423
45	C	-7.14944	-1.57531	0.040167
46	F	-7.62659	-1.86273	-1.19122
47	F	-7.78097	-0.46093	0.446194
48	F	-7.56384	-2.57773	0.841302
49	H	2.305143	0.428203	-0.18017

*B-2.2.7 – Di-(4-ethoxyphenyl) Nitron (**33d**) (zwitterionic form)*

M1				
Tag	**Symbol**	**X**	**Y**	**Z**
1	C	-1.95099	-0.89774	0.234419
2	C	-3.01501	0.030638	0.099949
3	C	-2.31735	-2.25446	0.382539
4	C	-4.34642	-0.38967	0.111694
5	H	-2.79658	1.084175	-0.0138

6	C	-3.64708	-2.6788	0.395456
7	C	-4.68113	-1.74087	0.260198
8	H	-5.14716	0.337888	0.008338
9	H	-3.85606	-3.73642	0.507369
10	N	-0.58514	-0.62158	0.225895
11	C	-0.08723	0.57986	0.126858
12	C	0.195764	4.102701	-0.12198
13	C	1.120154	5.002488	0.42049
14	C	-0.9552	4.556071	-0.77384
15	C	0.898046	6.373384	0.279802
16	H	1.989156	4.645602	0.963052
17	C	-1.16964	5.930255	-0.89548
18	H	-1.65999	3.839469	-1.17751
19	C	-0.24483	6.841779	-0.37633
20	H	1.612974	7.073335	0.700507
21	H	-2.0608	6.286354	-1.40281
22	H	-0.41687	7.908959	-0.47479
23	N	-0.64602	1.816388	0.040076
24	N	0.4186	2.698628	-0.00845
25	N	1.341043	0.755296	0.116981
26	C	1.582423	2.071291	0.029363
27	C	2.343329	-0.26073	0.224208
28	C	3.240321	-0.24156	1.298795
29	C	2.434696	-1.2595	-0.74513
30	C	4.232082	-1.21235	1.391006
31	H	3.158586	0.525434	2.062599
32	C	3.421977	-2.24206	-0.65245
33	H	1.737143	-1.27213	-1.57481
34	C	4.328649	-2.2235	0.420034
35	H	4.93397	-1.20919	2.218301
36	H	3.474831	-3.00204	-1.4215
37	H	-1.52449	-2.99028	0.48532
38	O	-6.02907	-2.03207	0.282098
39	O	5.319952	-3.13673	0.620888
40	H	2.557322	2.52672	-0.04151
41	C	5.526468	-4.21313	-0.31892
42	H	6.072505	-4.96287	0.257882
43	H	4.561749	-4.64795	-0.60156
44	C	6.337701	-3.78027	-1.5332
45	H	5.818847	-3.02276	-2.1274
46	H	7.305374	-3.37498	-1.2222
47	H	6.519871	-4.64882	-2.17511

48	C	-6.46462	-3.40038	0.337864
49	H	-7.49969	-3.33743	0.683638
50	H	-5.89484	-3.94522	1.099894
51	C	-6.40281	-4.09796	-1.0167
52	H	-7.00727	-3.55865	-1.75284
53	H	-5.3789	-4.16878	-1.39447
54	H	-6.80194	-5.11401	-0.92381

M3

Tag	Symbol	X	Y	Z
1	C	1.950919	-0.89836	-0.23549
2	C	3.014805	0.029268	-0.0943
3	C	2.317733	-2.2546	-0.38807
4	C	4.34624	-0.39123	-0.104
5	H	2.796332	1.082348	0.023502
6	C	3.647439	-2.67908	-0.39917
7	C	4.681289	-1.74185	-0.25721
8	H	5.146653	0.335919	0.004803
9	H	3.856532	-3.73627	-0.51474
10	N	0.585086	-0.62217	-0.22899
11	C	0.087286	0.579748	-0.12868
12	C	-0.19454	4.102487	0.120904
13	C	-1.11663	5.00236	-0.42526
14	C	0.95463	4.555564	0.776155
15	C	-0.89388	6.373252	-0.28512
16	H	-1.9844	4.645655	-0.96988
17	C	1.169802	5.929707	0.897173
18	H	1.657496	3.838964	1.18321
19	C	0.247325	6.841404	0.374113
20	H	-1.60706	7.073313	-0.70856
21	H	2.059506	6.285627	1.407172
22	H	0.419825	7.908545	0.472162
23	N	0.646629	1.815673	-0.04129
24	N	-0.41794	2.698367	0.007761
25	N	-1.34036	0.755302	-0.11864
26	C	-1.58176	2.071222	-0.03048
27	C	-2.34221	-0.26167	-0.22502
28	C	-3.22621	-0.25571	-1.31037
29	C	-2.44499	-1.24825	0.755562
30	C	-4.21631	-1.22823	-1.40268
31	H	-3.13616	0.502845	-2.08162

32	C	-3.43079	-2.23237	0.663232
33	H	-1.75821	-1.24981	1.594379
34	C	-4.32424	-2.22744	-0.42054
35	H	-4.90854	-1.2351	-2.23807
36	H	-3.49323	-2.98238	1.441291
37	H	1.525268	-2.99023	-0.49563
38	O	6.029211	-2.03314	-0.27675
39	O	-5.31266	-3.14358	-0.62209
40	H	-2.55669	2.526698	0.03977
41	C	-5.53194	-4.20713	0.329734
42	H	-6.07166	-4.96398	-0.24367
43	H	-4.57125	-4.63896	0.629998
44	C	-6.35749	-3.75704	1.527906
45	H	-5.8451	-2.99198	2.118011
46	H	-7.32093	-3.35527	1.199641
47	H	-6.54826	-4.61661	2.179293
48	C	6.464858	-3.40165	-0.33505
49	H	7.500914	-3.33772	-0.67758
50	H	5.897241	-3.94417	-1.10026
51	C	6.398949	-4.10286	1.017359
52	H	7.001348	-3.56578	1.756819
53	H	5.373919	-4.17488	1.391861
54	H	6.798306	-5.11863	0.9227

M4				
Tag	**Symbol**	**X**	**Y**	**Z**
1	C	1.907112	-0.93083	-0.23289
2	C	2.968555	-0.02143	-0.02332
3	C	2.264797	-2.27621	-0.44625
4	C	4.293511	-0.45239	-0.03012
5	H	2.758608	1.026042	0.147548
6	C	3.587159	-2.7104	-0.45755
7	C	4.620768	-1.79071	-0.24906
8	H	5.099413	0.257922	0.132063
9	H	3.791194	-3.76193	-0.62464
10	N	0.543888	-0.64909	-0.23396
11	C	0.079162	0.563432	-0.13442
12	C	-0.10357	4.073944	0.115362
13	C	-1.02549	4.998855	-0.37287
14	C	1.084373	4.478923	0.720087
15	C	-0.75995	6.357334	-0.22283

16	H	-1.92606	4.670984	-0.88142
17	C	1.340314	5.841795	0.851014
18	H	1.783679	3.732456	1.077893
19	C	0.420408	6.782289	0.387556
20	H	-1.47237	7.082848	-0.60057
21	H	2.262045	6.166771	1.321895
22	H	0.625615	7.842189	0.493601
23	N	0.664609	1.778096	-0.04647
24	N	-0.36761	2.679678	-0.00609
25	N	-1.33378	0.774146	-0.13122
26	C	-1.54356	2.091279	-0.04708
27	C	-2.35356	-0.21717	-0.23709
28	C	-3.32242	-0.10527	-1.23488
29	C	-2.38668	-1.27655	0.662498
30	C	-4.33479	-1.05004	-1.31747
31	H	-3.27884	0.713295	-1.94689
32	C	-3.39326	-2.23494	0.575226
33	H	-1.62332	-1.35385	1.428415
34	C	-4.37493	-2.12346	-0.41791
35	H	-5.0985	-0.98206	-2.08456
36	H	-3.40134	-3.04981	1.28813
37	H	1.466062	-2.99534	-0.60466
38	O	5.958991	-2.09174	-0.26565
39	O	-5.38788	-3.00573	-0.60536
40	H	-2.50757	2.573354	0.018734
41	C	-5.54015	-4.10295	0.29994
42	H	-6.18527	-4.80377	-0.23227
43	H	-4.57249	-4.59217	0.455091
44	C	-6.18421	-3.67626	1.608262
45	H	-5.57216	-2.94872	2.14711
46	H	-7.16323	-3.23042	1.41592
47	H	-6.32192	-4.54988	2.250913
48	C	6.353217	-3.45873	-0.34562
49	H	7.411025	-3.42351	-0.61432
50	H	5.820487	-3.95618	-1.16459
51	C	6.169068	-4.19101	0.974344
52	H	6.746491	-3.69729	1.760335
53	H	5.120219	-4.21742	1.280062
54	H	6.524381	-5.22079	0.878916

M5				
Tag	**Symbol**	**X**	**Y**	**Z**
1	C	1.905467	-0.93355	-0.23402
2	C	2.967919	-0.02555	-0.0228
3	C	2.262059	-2.2792	-0.44832
4	C	4.292458	-0.45803	-0.02894
5	H	2.759203	1.021941	0.149416
6	C	3.583951	-2.71488	-0.45896
7	C	4.618478	-1.79653	-0.24881
8	H	5.098871	0.251367	0.134784
9	H	3.78689	-3.76653	-0.62666
10	N	0.542548	-0.65037	-0.23564
11	C	0.079289	0.563148	-0.13484
12	C	-0.09749	4.073824	0.115073
13	C	-1.017	5.000073	-0.37515
14	C	1.090344	4.476912	0.721328
15	C	-0.74895	6.358167	-0.22573
16	H	-1.91765	4.673618	-0.88443
17	C	1.348828	5.839395	0.851589
18	H	1.78764	3.729491	1.08111
19	C	0.431403	6.781301	0.385995
20	H	-1.45951	7.084745	-0.6049
21	H	2.270421	6.162931	1.323731
22	H	0.63848	7.840883	0.491597
23	N	0.66681	1.776472	-0.04685
24	N	-0.36403	2.679898	-0.00583
25	N	-1.33291	0.775885	-0.13082
26	C	-1.54082	2.093296	-0.04643
27	C	-2.35374	-0.21467	-0.2364
28	C	-3.31392	-0.11032	-1.24328
29	C	-2.39543	-1.26614	0.672019
30	C	-4.32591	-1.05547	-1.32679
31	H	-3.26432	0.702982	-1.96087
32	C	-3.40159	-2.22496	0.584123
33	H	-1.63965	-1.33678	1.446157
34	C	-4.37422	-2.1215	-0.41882
35	H	-5.08319	-0.99311	-2.1007
36	H	-3.41665	-3.03339	1.304205
37	H	1.462928	-2.99771	-0.60776
38	O	5.956315	-2.09912	-0.26454
39	O	-5.38553	-3.00519	-0.60806
40	H	-2.50417	2.576788	0.01896

41	C	-5.54741	-4.09395	0.306092
42	H	-6.1881	-4.79911	-0.22572
43	H	-4.58173	-4.58247	0.474919
44	C	-6.20342	-3.65439	1.60411
45	H	-5.5958	-2.92238	2.141911
46	H	-7.1802	-3.20964	1.398342
47	H	-6.34794	-4.52187	2.253535
48	C	6.349086	-3.46693	-0.34299
49	H	7.407299	-3.43305	-0.61013
50	H	5.81695	-3.96422	-1.16238
51	C	6.162084	-4.19794	0.97721
52	H	6.738461	-3.70403	1.763868
53	H	5.112657	-4.2238	1.281017
54	H	6.517031	-5.22794	0.883105

*B-2.2.8 – Di-(4-ethoxyphenyl) Nitron (**33d**) (carbenic form)*

M1				
Tag	**Symbol**	**X**	**Y**	**Z**
1	C	-1.92119	-0.94482	0.20232
2	C	-2.98459	-0.03121	0.110471
3	C	-2.2148	-2.3129	0.294238
4	C	-4.30044	-0.49199	0.11321
5	H	-2.78449	1.029191	0.038727
6	C	-3.5328	-2.77258	0.296197
7	C	-4.59269	-1.85906	0.20724
8	H	-5.12141	0.215128	0.044724
9	H	-3.7085	-3.83899	0.364065
10	N	-0.56141	-0.56632	0.204798
11	C	-0.01696	0.677527	0.122441
12	C	0.114438	4.134501	-0.10694
13	C	1.145306	5.084514	-0.06297
14	C	-1.21584	4.547729	-0.24939
15	C	0.837572	6.441062	-0.1659
16	H	2.170807	4.755292	0.050445
17	C	-1.50889	5.911049	-0.35004
18	H	-2.00691	3.809704	-0.2814
19	C	-0.48892	6.86456	-0.30991
20	H	1.641806	7.170137	-0.1309
21	H	-2.5434	6.222532	-0.46103
22	H	-0.72176	7.922051	-0.3884

23	N	-0.6369	1.829181	0.032468
24	N	0.423629	2.747291	-0.00536
25	N	1.367654	0.867277	0.135025
26	C	1.658771	2.208213	0.054834
27	C	2.345355	-0.17932	0.238634
28	C	2.996252	-0.40887	1.45756
29	C	2.65686	-0.96162	-0.8742
30	C	3.952021	-1.413	1.555586
31	H	2.754142	0.203032	2.320462
32	C	3.611601	-1.97849	-0.78147
33	H	2.163114	-0.77349	-1.82263
34	C	4.264681	-2.20955	0.438973
35	H	4.465716	-1.60021	2.492793
36	H	3.838173	-2.56476	-1.66276
37	H	-1.40648	-3.03619	0.3623
38	O	-5.92438	-2.18782	0.221731
39	O	5.19902	-3.17691	0.654316
40	C	5.622711	-4.03993	-0.42319
41	H	6.04024	-4.91025	0.087768
42	H	4.749777	-4.37522	-0.99341
43	C	6.673304	-3.38917	-1.31343
44	H	6.285991	-2.50794	-1.83253
45	H	7.543569	-3.08922	-0.72187
46	H	7.003924	-4.10995	-2.06892
47	C	-6.32654	-3.57026	0.252791
48	H	-7.35714	-3.5379	0.61433
49	H	-5.73235	-4.11521	0.99519
50	C	-6.26671	-4.23184	-1.1189
51	H	-6.89358	-3.68897	-1.83306
52	H	-5.24714	-4.27099	-1.51269
53	H	-6.64163	-5.25842	-1.04471
54	H	0.108582	-1.32088	0.277582

M3				
Tag	**Symbol**	**X**	**Y**	**Z**
1	C	-1.92091	-0.94572	0.207287
2	C	-2.98467	-0.03236	0.116806
3	C	-2.21409	-2.31408	0.297194
4	C	-4.30044	-0.49362	0.11882
5	H	-2.7852	1.028269	0.04665
6	C	-3.5319	-2.77421	0.298462

7	C	-4.59217	-1.86093	0.210849
8	H	-5.12155	0.213461	0.051348
9	H	-3.70718	-3.84078	0.364653
10	N	-0.56124	-0.56681	0.210628
11	C	-0.01729	0.677021	0.126961
12	C	0.111893	4.133804	-0.10633
13	C	1.137258	5.086894	-0.02097
14	C	-1.21412	4.543278	-0.29292
15	C	0.828822	6.442958	-0.1291
16	H	2.1592	4.760644	0.127983
17	C	-1.50815	5.906097	-0.39732
18	H	-2.00097	3.802704	-0.35622
19	C	-0.49328	6.862684	-0.31767
20	H	1.628707	7.174536	-0.06191
21	H	-2.53917	6.214822	-0.543
22	H	-0.72689	7.919753	-0.39941
23	N	-0.63792	1.828519	0.03736
24	N	0.422055	2.74707	-0.00201
25	N	1.367186	0.86749	0.137984
26	C	1.65746	2.208525	0.056387
27	C	2.345795	-0.17861	0.23944
28	C	2.99595	-0.4109	1.458253
29	C	2.658764	-0.95752	-0.87537
30	C	3.952652	-1.41436	1.554155
31	H	2.752307	0.197953	2.322891
32	C	3.614541	-1.97357	-0.78482
33	H	2.165059	-0.76777	-1.82349
34	C	4.266957	-2.20741	0.435463
35	H	4.465523	-1.60384	2.491371
36	H	3.842045	-2.55736	-1.6675
37	H	-1.40557	-3.03722	0.364028
38	O	-5.92374	-2.19034	0.224917
39	O	5.202217	-3.17434	0.648632
40	C	5.625744	-4.03554	-0.43075
41	H	6.042947	-4.90697	0.078542
42	H	4.752665	-4.36924	-1.00156
43	C	6.676618	-3.38335	-1.31952
44	H	6.289698	-2.50095	-1.83692
45	H	7.547082	-3.08511	-0.72734
46	H	7.006852	-4.10278	-2.07644
47	C	-6.32529	-3.5733	0.253216
48	H	-7.35589	-3.5421	0.614785

49	H	-5.73079	-4.11934	0.994494
50	C	-6.26501	-4.23196	-1.11979
51	H	-6.89205	-3.68794	-1.83295
52	H	-5.24535	-4.27011	-1.51344
53	H	-6.63957	-5.2588	-1.04765
54	H	0.108966	-1.32132	0.282483

M4

Tag	Symbol	X	Y	Z
1	C	-1.86673	-0.97494	0.19641
2	C	-2.93168	-0.08951	-0.01552
3	C	-2.14559	-2.32832	0.406041
4	C	-4.23772	-0.56794	-0.01225
5	H	-2.74448	0.96287	-0.18021
6	C	-3.45358	-2.80514	0.408031
7	C	-4.51583	-1.9201	0.199532
8	H	-5.06657	0.113921	-0.17378
9	H	-3.6197	-3.86312	0.570627
10	N	-0.51444	-0.5841	0.195397
11	C	-0.00687	0.672729	0.113356
12	C	0.00923	4.113982	-0.10869
13	C	0.99713	5.095028	0.012982
14	C	-1.32114	4.471117	-0.33063
15	C	0.64409	6.436497	-0.09584
16	H	2.024391	4.800591	0.190657
17	C	-1.65903	5.820309	-0.43419
18	H	-2.07668	3.700442	-0.4209
19	C	-0.68314	6.808074	-0.31947
20	H	1.413775	7.195837	-0.00076
21	H	-2.69484	6.094363	-0.60738
22	H	-0.95171	7.856095	-0.40102
23	N	-0.65556	1.8006	0.021308
24	N	0.36444	2.740459	-0.00366
25	N	1.362208	0.903891	0.134643
26	C	1.614308	2.250523	0.063864
27	C	2.363457	-0.11108	0.23977
28	C	3.170112	-0.17167	1.377903
29	C	2.535882	-1.02931	-0.79047
30	C	4.149129	-1.14755	1.475053
31	H	3.026647	0.55109	2.174593
32	C	3.509043	-2.024	-0.69262

33	H	1.917588	-0.96482	-1.68125
34	C	4.321548	-2.08445	0.444924
35	H	4.789718	-1.21051	2.348134
36	H	3.625583	-2.72438	-1.51
37	H	-1.32975	-3.02731	0.568493
38	O	-5.83602	-2.26599	0.20555
39	O	5.287221	-3.01207	0.656691
40	C	5.58383	-3.96414	-0.36949
41	H	6.135849	-4.75172	0.145777
42	H	4.653966	-4.40167	-0.7486
43	C	6.428775	-3.36033	-1.47848
44	H	5.909661	-2.547	-1.99157
45	H	7.362957	-2.97002	-1.06726
46	H	6.670075	-4.13064	-2.21573
47	C	-6.18901	-3.6453	0.30963
48	H	-7.24649	-3.63539	0.579875
49	H	-5.63977	-4.10987	1.136444
50	C	-5.98448	-4.39031	-0.99945
51	H	-6.57776	-3.92583	-1.79116
52	H	-4.93615	-4.39175	-1.30814
53	H	-6.30935	-5.42824	-0.88708
54	H	0.166377	-1.31957	0.336141

M5				
Tag	**Symbol**	**X**	**Y**	**Z**
1	C	-1.86657	-0.97556	0.199413
2	C	-2.93176	-0.09059	-0.01324
3	C	-2.14499	-2.32912	0.408962
4	C	-4.23768	-0.56959	-0.01075
5	H	-2.74514	0.961859	-0.17815
6	C	-3.45276	-2.80646	0.410178
7	C	-4.5153	-1.92186	0.20095
8	H	-5.0666	0.112035	-0.17299
9	H	-3.61845	-3.86452	0.572643
10	N	-0.51438	-0.58428	0.199343
11	C	-0.00724	0.672435	0.115843
12	C	0.007107	4.113642	-0.10885
13	C	0.992432	5.095889	0.023601
14	C	-1.3217	4.469249	-0.34257
15	C	0.638634	6.43707	-0.087
16	H	2.018392	4.802918	0.211029

17	C	-1.6605	5.81813	-0.44742
18	H	-2.07535	3.697688	-0.44094
19	C	-0.68699	6.807079	-0.3225
20	H	1.406303	7.197351	0.016407
21	H	-2.69504	6.091004	-0.62983
22	H	-0.95623	7.854832	-0.40518
23	N	-0.65649	1.800168	0.024051
24	N	0.363098	2.740392	-0.00279
25	N	1.361748	0.904152	0.135174
26	C	1.61313	2.25078	0.063013
27	C	2.363798	-0.1102	0.239764
28	C	3.171824	-0.16927	1.377009
29	C	2.535584	-1.02906	-0.79003
30	C	4.151904	-1.14418	1.473574
31	H	3.028461	0.553528	2.173692
32	C	3.509726	-2.02281	-0.69268
33	H	1.915893	-0.96617	-1.67994
34	C	4.323829	-2.08164	0.443827
35	H	4.793393	-1.20596	2.346089
36	H	3.625449	-2.72395	-1.50951
37	H	-1.32898	-3.02777	0.571806
38	O	-5.83535	-2.26845	0.206172
39	O	5.290722	-3.00814	0.654862
40	C	5.586023	-3.96157	-0.37074
41	H	6.139295	-4.74819	0.144615
42	H	4.655711	-4.39991	-0.74763
43	C	6.4288	-3.35876	-1.48188
44	H	5.908277	-2.54664	-1.99547
45	H	7.363469	-2.96736	-1.07277
46	H	6.669324	-4.13007	-2.21831
47	C	-6.18763	-3.64833	0.308523
48	H	-7.24538	-3.63929	0.577674
49	H	-5.63892	-4.11331	1.135386
50	C	-5.98122	-4.3918	-1.00109
51	H	-6.5741	-3.92707	-1.79297
52	H	-4.93255	-4.39234	-1.30859
53	H	-6.30544	-5.43004	-0.88993
54	H	0.16665	-1.31987	0.338715

*B-2.2.9 – 4-Fluorophenyl Nitron (**33e**) (zwitterionic form)*

M1				
Tag	**Symbol**	**X**	**Y**	**Z**
1	C	2.202279	2.079723	-0.10639
2	C	1.229167	3.112042	-0.08247
3	C	3.561673	2.477286	-0.19141
4	C	1.611957	4.457204	-0.13685
5	H	0.179706	2.856707	-0.02081
6	C	3.930948	3.818296	-0.24706
7	C	2.956998	4.827526	-0.21934
8	H	0.840667	5.223819	-0.11511
9	H	4.984251	4.080039	-0.31198
10	H	3.242481	5.87456	-0.26207
11	N	1.97074	0.711273	-0.04699
12	C	0.781624	0.172075	-0.00268
13	C	-2.73369	-0.23299	0.015816
14	C	-3.56037	-1.19304	-0.57756
15	C	-3.27052	0.911228	0.614455
16	C	-4.94461	-1.02326	-0.54653
17	H	-3.13863	-2.05746	-1.07834
18	C	-4.6534	1.09131	0.635102
19	H	-2.61099	1.645938	1.059322
20	C	-5.45904	0.11638	0.059442
21	H	-5.60885	-1.75006	-0.99994
22	H	-5.09835	1.966987	1.094005
23	N	-0.47519	0.684057	-0.02786
24	N	-1.3192	-0.40967	0.009565
25	N	0.658437	-1.25889	0.061356
26	C	-0.65118	-1.54925	0.068008
27	H	-1.07653	-2.53648	0.153845
28	C	1.714643	-2.22651	0.078683
29	C	1.7667	-3.19963	-0.92335
30	C	2.664303	-2.19558	1.104016
31	C	2.778015	-4.16397	-0.88858
32	H	1.03175	-3.19692	-1.72217
33	C	3.676422	-3.15642	1.12262
34	H	2.607182	-1.4304	1.869239
35	C	3.73409	-4.14201	0.130476
36	H	2.820126	-4.92366	-1.66274
37	H	4.416495	-3.13812	1.916582
38	H	4.522129	-4.88844	0.152194

39	H	4.319267	1.698598	-0.21196
40	F	-6.81003	0.289447	0.081015

M3				
Tag	**Symbol**	**X**	**Y**	**Z**
1	C	2.200822	2.079604	-0.10816
2	C	1.227566	3.111681	-0.07456
3	C	3.559616	2.478228	-0.20007
4	C	1.609582	4.457223	-0.12593
5	H	0.178531	2.855923	-0.00745
6	C	3.928065	3.819594	-0.25307
7	C	2.953963	4.828435	-0.2154
8	H	0.83814	5.223417	-0.09635
9	H	4.980865	4.081923	-0.3235
10	H	3.238819	5.87572	-0.25582
11	N	1.970182	0.711017	-0.0513
12	C	0.780702	0.171405	-0.0048
13	C	-2.73433	-0.23479	0.014932
14	C	-3.55962	-1.19225	-0.58446
15	C	-3.27239	0.905733	0.619434
16	C	-4.94403	-1.02356	-0.55386
17	H	-3.13655	-2.05374	-1.08912
18	C	-4.65542	1.084847	0.639644
19	H	-2.61402	1.638337	1.069483
20	C	-5.45969	0.112469	0.057749
21	H	-5.60728	-1.74848	-1.01171
22	H	-5.10143	1.957573	1.103105
23	N	-0.47583	0.683319	-0.02892
24	N	-1.31968	-0.41081	0.009068
25	N	0.658164	-1.25891	0.059541
26	C	-0.6512	-1.55006	0.067039
27	H	-1.07603	-2.53762	0.152126
28	C	1.716035	-2.22518	0.079002
29	C	1.784035	-3.18532	-0.93436
30	C	2.651297	-2.2047	1.117682
31	C	2.797843	-4.14711	-0.89809
32	H	1.059084	-3.17511	-1.74216
33	C	3.665977	-3.16286	1.138049
34	H	2.581073	-1.44982	1.892159
35	C	3.739958	-4.13538	0.134085
36	H	2.852452	-4.89714	-1.68083

37	H	4.394943	-3.15297	1.942358
38	H	4.529679	-4.87998	0.157127
39	H	4.31765	1.700124	-0.22782
40	F	-6.81095	0.2846	0.07894

M4				
Tag	**Symbol**	**X**	**Y**	**Z**
1	C	2.168433	2.07571	-0.12208
2	C	1.181483	3.084539	-0.04368
3	C	3.513653	2.496566	-0.24227
4	C	1.540917	4.434278	-0.0802
5	H	0.13822	2.813786	0.048127
6	C	3.858532	3.840192	-0.28111
7	C	2.871317	4.82896	-0.19925
8	H	0.75867	5.18613	-0.01497
9	H	4.903984	4.121072	-0.37476
10	H	3.137078	5.880778	-0.22832
11	N	1.967466	0.703953	-0.07776
12	C	0.78127	0.163341	-0.02976
13	C	-2.71459	-0.24767	0.001215
14	C	-3.54027	-1.22277	-0.55566
15	C	-3.2371	0.909269	0.576006
16	C	-4.92048	-1.05374	-0.50932
17	H	-3.1206	-2.0975	-1.04081
18	C	-4.6162	1.087478	0.611204
19	H	-2.56653	1.653274	0.989249
20	C	-5.42606	0.098276	0.073725
21	H	-5.59359	-1.78972	-0.93313
22	H	-5.06021	1.972759	1.051493
23	N	-0.47052	0.665962	-0.05526
24	N	-1.30174	-0.42214	-0.01594
25	N	0.665901	-1.258	0.036589
26	C	-0.63775	-1.55545	0.046191
27	H	-1.06247	-2.54398	0.138405
28	C	1.727915	-2.21099	0.071011
29	C	1.714587	-3.27588	-0.82711
30	C	2.743626	-2.06976	1.015409
31	C	2.732142	-4.22739	-0.76635
32	H	0.925047	-3.35298	-1.56849
33	C	3.760499	-3.01909	1.057118
34	H	2.730821	-1.22472	1.693688

35	C	3.755507	-4.09855	0.171059
36	H	2.726797	-5.0613	-1.46016
37	H	4.556018	-2.9182	1.787878
38	H	4.550069	-4.8363	0.211129
39	H	4.28013	1.728925	-0.30282
40	F	-6.76398	0.268402	0.11035

M5

Tag	Symbol	X	Y	Z
1	C	2.167261	2.076194	-0.12303
2	C	1.180332	3.084422	-0.03504
3	C	3.511405	2.498417	-0.25182
4	C	1.53867	4.434516	-0.07096
5	H	0.137926	2.812984	0.064277
6	C	3.855138	3.842377	-0.29025
7	C	2.867904	4.830403	-0.19909
8	H	0.756426	5.185662	0.001977
9	H	4.899716	4.124115	-0.39078
10	H	3.132794	5.882443	-0.22776
11	N	1.967508	0.704345	-0.07975
12	C	0.781178	0.162927	-0.0297
13	C	-2.71442	-0.24881	0.001463
14	C	-3.53897	-1.22202	-0.56032
15	C	-3.23788	0.905662	0.580323
16	C	-4.91931	-1.05354	-0.51503
17	H	-3.11827	-2.09479	-1.0481
18	C	-4.61708	1.083413	0.614436
19	H	-2.56823	1.648149	0.997804
20	C	-5.42584	0.096059	0.071889
21	H	-5.59159	-1.78818	-0.94248
22	H	-5.06188	1.966727	1.057871
23	N	-0.47033	0.665429	-0.05484
24	N	-1.30147	-0.4229	-0.01493
25	N	0.666388	-1.25795	0.037495
26	C	-0.63716	-1.55596	0.047446
27	H	-1.06144	-2.54471	0.139575
28	C	1.729002	-2.21048	0.072155
29	C	1.719255	-3.27241	-0.82944
30	C	2.741524	-2.07137	1.020294
31	C	2.737819	-4.22294	-0.76875
32	H	0.931474	-3.34839	-1.57278

33	C	3.759442	-3.01959	1.061951
34	H	2.725156	-1.22914	1.702052
35	C	3.758312	-4.09599	0.172088
36	H	2.73526	-5.05481	-1.465
37	H	4.552419	-2.92057	1.79572
38	H	4.553483	-4.83309	0.212193
39	H	4.278241	1.731651	-0.31926
40	F	-6.76397	0.265752	0.107466

*B-2.2.10 – 4-Fluorophenyl Nitron (**33e**) (carbenic form)*

M1				
Tag	**Symbol**	**X**	**Y**	**Z**
1	C	2.156186	2.10244	-0.06317
2	C	1.157582	3.08937	-0.03595
3	C	3.508985	2.487672	-0.11892
4	C	1.523378	4.439536	-0.06295
5	H	0.11535	2.804368	0.004736
6	C	3.85535	3.836519	-0.1453
7	C	2.864246	4.825421	-0.11707
8	H	0.741459	5.193347	-0.04125
9	H	4.904464	4.113971	-0.18833
10	H	3.135197	5.876328	-0.13774
11	N	1.88489	0.721514	-0.03399
12	C	0.683778	0.078769	0.000355
13	C	-2.75798	-0.3187	0.017861
14	C	-3.61919	-1.41436	-0.13579
15	C	-3.28042	0.970515	0.174645
16	C	-5.00026	-1.22297	-0.12339
17	H	-3.20682	-2.40748	-0.26207
18	C	-4.66394	1.16756	0.182724
19	H	-2.61155	1.813227	0.290477
20	C	-5.49412	0.066405	0.035085
21	H	-5.6812	-2.05885	-0.24061
22	H	-5.086	2.159167	0.303749
23	N	-0.51558	0.606152	-0.00903
24	N	-1.34797	-0.52081	0.012736
25	N	0.602616	-1.31591	0.032239
26	C	-0.71465	-1.7107	0.03652
27	C	1.720652	-2.21759	0.043341
28	C	1.970681	-3.01572	-1.07701

29	C	2.541234	-2.29149	1.173858
30	C	3.052156	-3.89955	-1.06137
31	H	1.321034	-2.94258	-1.94285
32	C	3.628603	-3.17002	1.17577
33	H	2.322991	-1.67941	2.043533
34	C	3.883555	-3.97473	0.061293
35	H	3.246683	-4.52474	-1.92721
36	H	4.266835	-3.23082	2.051661
37	H	4.725663	-4.65988	0.06812
38	H	4.28536	1.727367	-0.14218
39	H	2.69398	0.11433	-0.04801
40	F	-6.84847	0.254971	0.043433

M3				
Tag	**Symbol**	**X**	**Y**	**Z**
1	C	2.155856	2.102432	-0.06369
2	C	1.156972	3.089245	-0.04009
3	C	3.508756	2.487933	-0.11641
4	C	1.522485	4.439521	-0.06782
5	H	0.11465	2.804254	-0.00148
6	C	3.854802	3.836866	-0.1436
7	C	2.86341	4.825638	-0.11911
8	H	0.740314	5.193147	-0.04894
9	H	4.90397	4.114472	-0.18424
10	H	3.134201	5.876576	-0.14039
11	N	1.884648	0.721512	-0.03387
12	C	0.683649	0.07878	0.000019
13	C	-2.75817	-0.31926	0.017361
14	C	-3.61891	-1.4128	-0.15284
15	C	-3.28106	0.967702	0.190598
16	C	-5.00008	-1.2219	-0.13993
17	H	-3.20625	-2.40403	-0.29243
18	C	-4.66461	1.164468	0.198856
19	H	-2.61257	1.808923	0.318984
20	C	-5.4943	0.06518	0.035141
21	H	-5.68064	-2.05619	-0.26994
22	H	-5.08698	2.154311	0.332528
23	N	-0.51594	0.605953	-0.0098
24	N	-1.34815	-0.52112	0.012395
25	N	0.602703	-1.31581	0.032607
26	C	-0.71443	-1.71078	0.037753

27	C	1.721216	-2.21715	0.044316
28	C	1.977526	-3.00846	-1.07946
29	C	2.535904	-2.29698	1.178641
30	C	3.05938	-3.89186	-1.0633
31	H	1.332692	-2.93029	-1.94848
32	C	3.623595	-3.17512	1.181204
33	H	2.313286	-1.68928	2.050265
34	C	3.88473	-3.97326	0.063397
35	H	3.258985	-4.51171	-1.93181
36	H	4.257476	-3.24048	2.059909
37	H	4.727196	-4.65796	0.070653
38	H	4.285487	1.727934	-0.13652
39	H	2.693734	0.114248	-0.04694
40	F	-6.84875	0.253461	0.043696

M4				
Tag	**Symbol**	**X**	**Y**	**Z**
1	C	2.123654	2.099333	-0.08163
2	C	1.111434	3.063807	-0.01117
3	C	3.46401	2.505871	-0.17324
4	C	1.455081	4.417132	-0.03093
5	H	0.074844	2.764206	0.057516
6	C	3.786684	3.856383	-0.19244
7	C	2.782828	4.825365	-0.12101
8	H	0.662478	5.15696	0.025038
9	H	4.828691	4.151743	-0.26377
10	H	3.035172	5.880198	-0.13622
11	N	1.880933	0.717139	-0.05851
12	C	0.685188	0.070508	-0.01361
13	C	-2.73803	-0.33164	0.0151
14	C	-3.59128	-1.42808	-0.13301
15	C	-3.25537	0.954242	0.17213
16	C	-4.96878	-1.23903	-0.11467
17	H	-3.17429	-2.41944	-0.26042
18	C	-4.63564	1.14803	0.185961
19	H	-2.5838	1.796214	0.283291
20	C	-5.46248	0.047335	0.04426
21	H	-5.65232	-2.07297	-0.2273
22	H	-5.06291	2.136998	0.307119
23	N	-0.51174	0.587319	-0.02309
24	N	-1.32965	-0.53098	0.004744

25	N	0.610736	-1.31541	0.025543
26	C	-0.70126	-1.718	0.032916
27	C	1.731795	-2.2031	0.048664
28	C	1.904477	-3.11012	-0.99489
29	C	2.629446	-2.15062	1.114795
30	C	2.991896	-3.9806	-0.96574
31	H	1.189225	-3.12709	-1.81061
32	C	3.723475	-3.01479	1.126412
33	H	2.463277	-1.45123	1.929152
34	C	3.903694	-3.93004	0.089588
35	H	3.130029	-4.69346	-1.77179
36	H	4.426007	-2.97872	1.952215
37	H	4.752781	-4.60532	0.104894
38	H	4.249562	1.757082	-0.22867
39	H	2.696329	0.119946	-0.11281
40	F	-6.80356	0.231818	0.058513

M5				
Tag	**Symbol**	**X**	**Y**	**Z**
1	C	2.123291	2.099606	-0.08332
2	C	1.110889	3.063987	-0.01272
3	C	3.463448	2.506387	-0.17739
4	C	1.45407	4.417426	-0.03551
5	H	0.07443	2.764465	0.058311
6	C	3.785634	3.857022	-0.19968
7	C	2.781589	4.825887	-0.12851
8	H	0.661323	5.157112	0.020431
9	H	4.827464	4.152515	-0.27307
10	H	3.033555	5.880783	-0.14609
11	N	1.881017	0.717386	-0.05659
12	C	0.685324	0.070675	-0.0131
13	C	-2.73787	-0.33186	0.015042
14	C	-3.59042	-1.42429	-0.16334
15	C	-3.25561	0.949905	0.201767
16	C	-4.96805	-1.23594	-0.14405
17	H	-3.1728	-2.41203	-0.31484
18	C	-4.6359	1.14334	0.215904
19	H	-2.58432	1.788821	0.335874
20	C	-5.46218	0.046269	0.044769
21	H	-5.6512	-2.06673	-0.27989
22	H	-5.06368	2.129026	0.359922

23	N	-0.5118	0.587343	-0.02403
24	N	-1.32949	-0.53103	0.004787
25	N	0.610986	-1.3152	0.02713
26	C	-0.70095	-1.71783	0.034886
27	C	1.732288	-2.20278	0.05119
28	C	1.906871	-3.1085	-0.99321
29	C	2.627855	-2.15146	1.119102
30	C	2.994135	-3.97918	-0.96297
31	H	1.193478	-3.12414	-1.81061
32	C	3.721801	-3.01576	1.131788
33	H	2.460561	-1.45246	1.93354
34	C	3.903815	-3.92992	0.0943
35	H	3.133966	-4.69097	-1.76966
36	H	4.422961	-2.98045	1.958776
37	H	4.752876	-4.60522	0.110411
38	H	4.249237	1.757832	-0.23233
39	H	2.696375	0.120295	-0.11317
40	F	-6.80327	0.230414	0.059294

*B-2.2.11 – 4-Bromophenyl Nitron (**33f**) (zwitterionic form)*

M1				
Tag	**Symbol**	**X**	**Y**	**Z**
1	C	3.125106	2.130447	-0.0948
2	C	2.116711	3.128433	-0.09893
3	C	4.471664	2.573977	-0.1494
4	C	2.454115	4.485754	-0.15117
5	H	1.075504	2.837087	-0.06067
6	C	4.795796	3.926731	-0.20229
7	C	3.787248	4.901747	-0.20315
8	H	1.65668	5.225429	-0.15171
9	H	5.840701	4.224486	-0.24298
10	H	4.037532	5.957821	-0.24399
11	N	2.938577	0.754871	-0.03696
12	C	1.767631	0.177504	-0.00279
13	C	-1.72977	-0.34568	-0.00297
14	C	-2.52698	-1.37113	-0.52109
15	C	-2.30229	0.820905	0.510768
16	C	-3.91457	-1.24124	-0.49561
17	H	-2.08376	-2.25825	-0.95981
18	C	-3.68977	0.958104	0.517558

19	H	-1.66728	1.607491	0.898715
20	C	-4.48262	-0.07707	0.022505
21	H	-4.5384	-2.03289	-0.89373
22	H	-4.14183	1.859847	0.914033
23	N	0.494872	0.646842	-0.03324
24	N	-0.3125	-0.47474	-0.00222
25	N	1.691775	-1.25724	0.057305
26	C	0.394303	-1.59173	0.056992
27	H	0.00346	-2.59351	0.13781
28	C	2.781721	-2.18751	0.076255
29	C	2.893132	-3.13045	-0.94926
30	C	3.705473	-2.14821	1.124489
31	C	3.939584	-4.05662	-0.9155
32	H	2.176844	-3.13386	-1.76478
33	C	4.752617	-3.0708	1.142599
34	H	3.601498	-1.40639	1.907742
35	C	4.870339	-4.02623	0.126521
36	H	4.02849	-4.79313	-1.70786
37	H	5.473158	-3.0463	1.95412
38	H	5.685516	-4.74293	0.147575
39	H	5.256026	1.821985	-0.14817
40	Br	-6.38142	0.104095	0.045003

M2				
Tag	**Symbol**	**X**	**Y**	**Z**
1	C	3.145342	2.178633	-0.05967
2	C	2.108381	3.159148	-0.10382
3	C	4.493983	2.63925	-0.07765
4	C	2.424513	4.530516	-0.1635
5	H	1.072936	2.839781	-0.09132
6	C	4.797551	4.00787	-0.13638
7	C	3.763109	4.969905	-0.18044
8	H	1.616777	5.259645	-0.19682
9	H	5.837761	4.32723	-0.14863
10	H	3.997189	6.030622	-0.22646
11	N	2.967134	0.785992	0.001614
12	C	1.804442	0.177297	0.018216
13	C	-1.73266	-0.38861	0.009462
14	C	-2.55853	-1.5156	-0.17811
15	C	-2.29403	0.889107	0.194735
16	C	-3.95427	-1.36531	-0.16447

17	H	-2.14507	-2.50509	-0.3445
18	C	-3.69124	1.041057	0.203802
19	H	-1.64534	1.745259	0.330336
20	C	-4.50705	-0.08746	0.026898
21	H	-4.58894	-2.233	-0.30898
22	H	-4.12356	2.025541	0.348328
23	N	0.500598	0.645581	-0.00832
24	N	-0.30745	-0.51903	0.007179
25	N	1.736529	-1.28064	0.053094
26	C	0.428971	-1.63503	0.047032
27	H	0.061372	-2.64407	0.112428
28	C	2.836546	-2.20728	0.046733
29	C	2.792898	-3.32024	-0.8178
30	C	3.929502	-2.00873	0.912361
31	C	3.84636	-4.25244	-0.79996
32	H	1.9605	-3.45088	-1.50428
33	C	4.98152	-2.94169	0.914842
34	H	3.951552	-1.14202	1.561716
35	C	4.943271	-4.06567	0.064321
36	H	3.813293	-5.11136	-1.4643
37	H	5.82517	-2.79392	1.583377
38	H	5.758622	-4.78381	0.07303
39	H	5.287341	1.896749	-0.04464
40	Br	-6.46597	0.122501	0.04017

M3				
Tag	**Symbol**	**X**	**Y**	**Z**
1	C	3.124792	2.129404	-0.09642
2	C	2.116935	3.128077	-0.08973
3	C	4.471223	2.572761	-0.15889
4	C	2.454661	4.48548	-0.13886
5	H	1.075821	2.837291	-0.04516
6	C	4.795634	3.92557	-0.20908
7	C	3.787597	4.901132	-0.1988
8	H	1.657579	5.225483	-0.13066
9	H	5.840379	4.222943	-0.25608
10	H	4.038109	5.957231	-0.23728
11	N	2.938141	0.753844	-0.04129
12	C	1.766587	0.176569	-0.00511
13	C	-1.7307	-0.34644	-0.00366
14	C	-2.52749	-1.37002	-0.52604

15	C	-2.3034	0.818049	0.514604
16	C	-3.91513	-1.24026	-0.50061
17	H	-2.08389	-2.25544	-0.96776
18	C	-3.69091	0.955224	0.521285
19	H	-1.66876	1.603078	0.906308
20	C	-4.48333	-0.07809	0.021719
21	H	-4.53866	-2.03051	-0.90197
22	H	-4.14313	1.855332	0.921259
23	N	0.49426	0.646222	-0.03454
24	N	-0.31334	-0.47549	-0.00298
25	N	1.69088	-1.25753	0.055226
26	C	0.393601	-1.59238	0.055671
27	H	0.003064	-2.59437	0.135688
28	C	2.782133	-2.18674	0.076449
29	C	2.908989	-3.11581	-0.9597
30	C	3.691722	-2.15896	1.13731
31	C	3.95758	-4.0396	-0.92445
32	H	2.202276	-3.11099	-1.78349
33	C	4.741075	-3.07907	1.157177
34	H	3.575095	-1.42818	1.929279
35	C	4.874614	-4.0205	0.129982
36	H	4.058531	-4.76582	-1.72481
37	H	5.450662	-3.06382	1.978508
38	H	5.691215	-4.73553	0.152378
39	H	5.255476	1.82062	-0.16575
40	Br	-6.3823	0.103055	0.043926

M4				
Tag	**Symbol**	**X**	**Y**	**Z**
1	C	3.089193	2.125205	-0.10998
2	C	2.069803	3.102078	-0.04536
3	C	4.421426	2.587816	-0.2189
4	C	2.386378	4.462434	-0.0846
5	H	1.034887	2.798387	0.037893
6	C	4.723635	3.941608	-0.26072
7	C	3.704635	4.8986	-0.19281
8	H	1.580065	5.189279	-0.03028
9	H	5.760414	4.255397	-0.34569
10	H	3.937086	5.958213	-0.2243
11	N	2.931125	0.747667	-0.06277
12	C	1.762619	0.170788	-0.02066

13	C	-1.71636	-0.35124	-0.01317
14	C	-2.50889	-1.38291	-0.512
15	C	-2.27734	0.821672	0.485214
16	C	-3.89265	-1.25176	-0.48034
17	H	-2.06426	-2.27401	-0.94173
18	C	-3.66132	0.958548	0.497563
19	H	-1.63413	1.611221	0.854976
20	C	-4.45413	-0.0821	0.023227
21	H	-4.5228	-2.04642	-0.86233
22	H	-4.11503	1.86495	0.881393
23	N	0.495987	0.633217	-0.05144
24	N	-0.30095	-0.48065	-0.01713
25	N	1.691436	-1.25443	0.045388
26	C	0.399249	-1.5929	0.04802
27	H	0.007312	-2.59496	0.138487
28	C	2.781944	-2.1749	0.074552
29	C	2.793686	-3.23961	-0.82391
30	C	3.799171	-2.00367	1.012142
31	C	3.839024	-4.16072	-0.77049
32	H	2.002274	-3.3395	-1.56059
33	C	4.843633	-2.92301	1.046546
34	H	3.766353	-1.15917	1.690328
35	C	4.864373	-4.00197	0.160196
36	H	3.853677	-4.99411	-1.46474
37	H	5.640833	-2.79881	1.771829
38	H	5.680632	-4.71593	0.194541
39	H	5.212517	1.844742	-0.26834
40	Br	-6.33347	0.098748	0.052658

M5				
Tag	**Symbol**	**X**	**Y**	**Z**
1	C	3.087815	2.125507	-0.11057
2	C	2.068283	3.101752	-0.03676
3	C	4.418997	2.589497	-0.22796
4	C	2.383666	4.462449	-0.07556
5	H	1.034163	2.797363	0.05368
6	C	4.719968	3.943594	-0.26953
7	C	3.700803	4.899822	-0.19262
8	H	1.577246	5.188581	-0.01384
9	H	5.755907	4.25824	-0.36127
10	H	3.932303	5.959643	-0.22381

11	N	2.931071	0.747889	-0.06431
12	C	1.762435	0.170225	-0.02037
13	C	-1.71625	-0.35243	-0.01243
14	C	-2.50837	-1.38361	-0.5129
15	C	-2.27749	0.819833	0.48722
16	C	-3.89217	-1.25245	-0.48189
17	H	-2.06352	-2.27435	-0.94313
18	C	-3.66149	0.956755	0.49889
19	H	-1.63472	1.60894	0.858705
20	C	-4.45389	-0.08335	0.022664
21	H	-4.52197	-2.04681	-0.86506
22	H	-4.11537	1.862632	0.883757
23	N	0.496066	0.632472	-0.05065
24	N	-0.30074	-0.48165	-0.01604
25	N	1.691889	-1.25449	0.046082
26	C	0.399876	-1.59362	0.049031
27	H	0.008583	-2.59598	0.139184
28	C	2.783198	-2.17421	0.075298
29	C	2.799705	-3.23454	-0.82814
30	C	3.796172	-2.00626	1.018072
31	C	3.846231	-4.15442	-0.77496
32	H	2.010791	-3.33235	-1.56775
33	C	4.841875	-2.92421	1.052275
34	H	3.758812	-1.16581	1.70111
35	C	4.867673	-3.9987	0.160561
36	H	3.864601	-4.9847	-1.47283
37	H	5.635716	-2.80281	1.781703
38	H	5.684661	-4.71183	0.194868
39	H	5.210489	1.847289	-0.28413
40	Br	-6.33337	0.097503	0.051179

*B-2.2.12 – 4-Bromophenyl Nitron **(33f)** (carbenic form)*

M1				
Tag	**Symbol**	**X**	**Y**	**Z**
1	C	3.096423	2.143059	-0.04126
2	C	2.072082	3.103335	-0.0218
3	C	4.439192	2.563225	-0.08282
4	C	2.402945	4.462592	-0.04354
5	H	1.037244	2.791363	0.009169
6	C	4.750587	3.920627	-0.10401

7	C	3.733779	4.88326	-0.08435
8	H	1.601578	5.195839	-0.02811
9	H	5.792474	4.225405	-0.1361
10	H	3.977436	5.940894	-0.101
11	N	2.861211	0.75526	-0.01808
12	C	1.677925	0.081306	0.008155
13	C	-1.74809	-0.41321	0.016988
14	C	-2.57793	-1.54258	0.022975
15	C	-2.30858	0.868797	0.010199
16	C	-3.96246	-1.38973	0.02187
17	H	-2.13861	-2.53224	0.028307
18	C	-3.69653	1.022969	0.008884
19	H	-1.6663	1.739692	0.005558
20	C	-4.5108	-0.10652	0.014478
21	H	-4.60209	-2.26499	0.026561
22	H	-4.1284	2.017298	0.003536
23	N	0.465055	0.575925	0.002334
24	N	-0.3361	-0.57365	0.015949
25	N	1.634747	-1.31606	0.029558
26	C	0.330549	-1.74685	0.028821
27	C	2.778058	-2.18617	0.02927
28	C	3.058325	-2.95117	-1.10684
29	C	3.592379	-2.26155	1.164065
30	C	4.164454	-3.80406	-1.10263
31	H	2.412717	-2.87705	-1.97562
32	C	4.704134	-3.10895	1.15474
33	H	3.350935	-1.6747	2.044924
34	C	4.989489	-3.88098	0.02459
35	H	4.382837	-4.40387	-1.98064
36	H	5.337839	-3.17132	2.033789
37	H	5.850614	-4.54209	0.022694
38	H	5.235314	1.823452	-0.09849
39	H	3.685899	0.169379	-0.03051
40	Br	-6.41199	0.100802	0.013168

M2				
Tag	**Symbol**	**X**	**Y**	**Z**
1	C	3.117867	2.183488	-0.06236
2	C	2.060557	3.122451	-0.03287
3	C	4.458844	2.63809	-0.11461
4	C	2.357254	4.498946	-0.05486

5	H	1.034554	2.780351	0.005208
6	C	4.737388	4.013567	-0.13685
7	C	3.687695	4.956247	-0.1067
8	H	1.538874	5.214657	-0.03165
9	H	5.770933	4.347923	-0.17705
10	H	3.904777	6.020687	-0.12358
11	N	2.912537	0.77874	-0.03877
12	C	1.727559	0.094566	0.003606
13	C	-1.74165	-0.42784	0.014158
14	C	-2.57653	-1.56573	0.007287
15	C	-2.30462	0.864083	0.024062
16	C	-3.972	-1.41204	0.01078
17	H	-2.13514	-2.55582	-0.00013
18	C	-3.70308	1.020259	0.027382
19	H	-1.65962	1.73382	0.0293
20	C	-4.5218	-0.1188	0.020743
21	H	-4.61017	-2.28973	0.005508
22	H	-4.13244	2.016902	0.03517
23	N	0.492902	0.593438	-0.00356
24	N	-0.32385	-0.58877	0.010313
25	N	1.682974	-1.3226	0.029366
26	C	0.360018	-1.77602	0.02556
27	C	2.823727	-2.20444	0.036053
28	C	2.964606	-3.1576	-0.9908
29	C	3.772428	-2.11996	1.075123
30	C	4.068541	-4.02926	-0.97877
31	H	2.220781	-3.21022	-1.77975
32	C	4.880648	-2.9886	1.072789
33	H	3.637076	-1.40858	1.885538
34	C	5.030904	-3.94375	0.048279
35	H	4.178885	-4.76745	-1.76829
36	H	5.612738	-2.92594	1.873018
37	H	5.884461	-4.61604	0.051775
38	H	5.274826	1.918405	-0.13683
39	H	3.751791	0.208691	-0.07213
40	Br	-6.48556	0.097734	0.025556

M3				
Tag	**Symbol**	**X**	**Y**	**Z**
1	C	3.096333	2.142851	-0.04081
2	C	2.071942	3.103168	-0.02327
3	C	4.439243	2.563073	-0.07896
4	C	2.402774	4.462506	-0.04359
5	H	1.036967	2.791384	0.005124
6	C	4.750573	3.920531	-0.09883
7	C	3.733707	4.883205	-0.08111
8	H	1.60132	5.195687	-0.02967
9	H	5.792541	4.225301	-0.12828
10	H	3.977424	5.940844	-0.09671
11	N	2.860932	0.755075	-0.01928
12	C	1.677711	0.081292	0.006493
13	C	-1.74833	-0.4136	0.015996
14	C	-2.57821	-1.54297	0.021429
15	C	-2.3089	0.868405	0.010074
16	C	-3.96275	-1.39019	0.02073
17	H	-2.13915	-2.53273	0.026007
18	C	-3.69687	1.022553	0.009106
19	H	-1.66681	1.739432	0.005866
20	C	-4.51109	-0.10697	0.014217
21	H	-4.60227	-2.26554	0.025005
22	H	-4.12863	2.016925	0.004443
23	N	0.464652	0.575749	0.000588
24	N	-0.33633	-0.57391	0.014716
25	N	1.634671	-1.316	0.02806
26	C	0.330717	-1.74694	0.027865
27	C	2.778523	-2.1858	0.028407
28	C	3.067959	-2.93986	-1.11271
29	C	3.584015	-2.2711	1.168724
30	C	4.174472	-3.79231	-1.10786
31	H	2.429404	-2.85757	-1.98598
32	C	4.696051	-3.11814	1.160252
33	H	3.336002	-1.69158	2.052592
34	C	4.990485	-3.87955	0.025183
35	H	4.4002	-4.38361	-1.98976
36	H	5.323147	-3.1882	2.043438
37	H	5.85192	-4.54026	0.02386
38	H	5.23553	1.823471	-0.09293
39	H	3.685539	0.169017	-0.03143

40	Br	-6.41231	0.100288	0.013481

M4				
Tag	**Symbol**	**X**	**Y**	**Z**
1	C	3.056237	2.138634	-0.05617
2	C	2.017337	3.075407	-0.00219
3	C	4.38628	2.580599	-0.13048
4	C	2.324761	4.437404	-0.02282
5	H	0.988353	2.748266	0.054424
6	C	4.67264	3.939278	-0.15078
7	C	3.64212	4.880938	-0.09695
8	H	1.511956	5.155888	0.019723
9	H	5.707168	4.262455	-0.20895
10	H	3.866108	5.942142	-0.11308
11	N	2.850642	0.750158	-0.03288
12	C	1.672542	0.07251	-0.00016
13	C	-1.73494	-0.42328	0.01385
14	C	-2.55813	-1.5518	0.018023
15	C	-2.28802	0.856737	0.011528
16	C	-3.93889	-1.39791	0.020022
17	H	-2.11565	-2.54033	0.019703
18	C	-3.67242	1.010328	0.013079
19	H	-1.64182	1.72541	0.008242
20	C	-4.48421	-0.11682	0.017063
21	H	-4.58269	-2.27022	0.023414
22	H	-4.10803	2.003082	0.011187
23	N	0.462708	0.557256	-0.00694
24	N	-0.32498	-0.58279	0.010083
25	N	1.63483	-1.31607	0.025782
26	C	0.335899	-1.75383	0.025214
27	C	2.780758	-2.17232	0.036174
28	C	2.986777	-3.04722	-1.02845
29	C	3.669314	-2.11929	1.109703
30	C	4.099247	-3.88579	-1.01292
31	H	2.277566	-3.06466	-1.84944
32	C	4.788282	-2.95104	1.107898
33	H	3.477352	-1.44453	1.939028
34	C	5.001981	-3.83466	0.050165
35	H	4.263997	-4.57384	-1.83535
36	H	5.484293	-2.91476	1.939185
37	H	5.870603	-4.4848	0.05502

38	H	5.192515	1.853087	-0.17143
39	H	3.681585	0.174822	-0.08764
40	Br	-6.36517	0.089735	0.019794

M5				
Tag	**Symbol**	**X**	**Y**	**Z**
1	C	3.055736	2.139037	-0.05628
2	C	2.01652	3.07555	-0.00259
3	C	4.38572	2.581422	-0.1301
4	C	2.323504	4.437703	-0.02307
5	H	0.987541	2.748324	0.053714
6	C	4.671615	3.940223	-0.15022
7	C	3.640777	4.881626	-0.09671
8	H	1.510442	5.155913	0.019251
9	H	5.70608	4.263682	-0.20799
10	H	3.864471	5.942898	-0.11271
11	N	2.850581	0.750488	-0.03329
12	C	1.672778	0.072584	-0.00064
13	C	-1.73476	-0.42363	0.013564
14	C	-2.558	-1.55215	0.016941
15	C	-2.28788	0.856407	0.012196
16	C	-3.93878	-1.39831	0.019169
17	H	-2.11577	-2.54078	0.01779
18	C	-3.6723	1.009992	0.013905
19	H	-1.64183	1.7252	0.00955
20	C	-4.48407	-0.1172	0.017166
21	H	-4.58248	-2.2707	0.021921
22	H	-4.10781	2.002788	0.012712
23	N	0.462741	0.557108	-0.00755
24	N	-0.32477	-0.58302	0.009694
25	N	1.635272	-1.31598	0.025541
26	C	0.33648	-1.75384	0.02517
27	C	2.781337	-2.17221	0.036109
28	C	2.988189	-3.04618	-1.02914
29	C	3.668958	-2.11997	1.110421
30	C	4.10055	-3.88492	-1.01329
31	H	2.28004	-3.06258	-1.85108
32	C	4.787845	-2.95186	1.10892
33	H	3.476702	-1.4455	1.939901
34	C	5.002297	-3.83476	0.050722
35	H	4.266105	-4.57217	-1.83622

36	H	5.483309	-2.91603	1.94067
37	H	5.87091	-4.4849	0.055775
38	H	5.192225	1.854219	-0.17078
39	H	3.681855	0.175434	-0.08667
40	Br	-6.36508	0.08934	0.019998

*B-2.2.13 – 4-Iodophenyl Nitron (**33g**) (zwitterionic form)*

M2				
Tag	**Symbol**	**X**	**Y**	**Z**
1	C	3.713912	2.190043	-0.05762
2	C	2.670262	3.163332	-0.10381
3	C	5.059407	2.659878	-0.07291
4	C	2.977063	4.53684	-0.16289
5	H	1.637051	2.836706	-0.09333
6	C	5.353634	4.03056	-0.13109
7	C	4.312642	4.985424	-0.17724
8	H	2.16441	5.260413	-0.19785
9	H	6.39162	4.357151	-0.14128
10	H	4.53949	6.047731	-0.22288
11	N	3.545305	0.796236	0.0031
12	C	2.386932	0.179218	0.017271
13	C	-1.14622	-0.41161	0.002606
14	C	-1.96465	-1.54472	-0.17785
15	C	-1.71766	0.862404	0.179239
16	C	-3.36151	-1.40293	-0.16564
17	H	-1.54491	-2.53286	-0.33721
18	C	-3.11624	1.003162	0.186537
19	H	-1.07583	1.724623	0.309786
20	C	-3.93392	-0.12904	0.017194
21	H	-3.98425	-2.27996	-0.30506
22	H	-3.54921	1.988145	0.324878
23	N	1.079898	0.638195	-0.01155
24	N	0.28	-0.53194	0.002451
25	N	2.329334	-1.27908	0.051692
26	C	1.02424	-1.64271	0.043279
27	H	0.663795	-2.65439	0.107469
28	C	3.435735	-2.19803	0.046883
29	C	3.400959	-3.31133	-0.81765
30	C	4.526005	-1.99214	0.914172
31	C	4.460734	-4.23631	-0.79825

32	H	2.570397	-3.44766	-1.50526
33	C	5.584376	-2.91788	0.918213
34	H	4.541049	-1.12544	1.563733
35	C	5.555096	-4.04205	0.067613
36	H	4.434506	-5.09546	-1.46259
37	H	6.425972	-2.76438	1.58805
38	H	6.375327	-4.7546	0.077534
39	H	5.857684	1.922694	-0.0383
40	I	-6.06441	0.084167	0.03102

*B-2.2.14 – 4-Iodophenyl Nitron (**33g**) (carbenic form)*

M2				
Tag	**Symbol**	**X**	**Y**	**Z**
1	C	3.6898	2.192527	-0.06218
2	C	2.626768	3.125115	-0.03565
3	C	5.028179	2.655089	-0.11119
4	C	2.915255	4.503363	-0.05739
5	H	1.602769	2.776766	-1.3E-05
6	C	5.298488	4.032237	-0.13327
7	C	4.243075	4.968593	-0.10612
8	H	2.092568	5.214194	-0.0365
9	H	6.330092	4.372831	-0.171
10	H	4.453816	6.034313	-0.1229
11	N	3.492783	0.786607	-0.03907
12	C	2.311847	0.095299	0.002458
13	C	-1.15418	-0.44843	0.010266
14	C	-1.98293	-1.59028	-0.0011
15	C	-1.72589	0.839204	0.023716
16	C	-3.37935	-1.44373	0.001647
17	H	-1.53651	-2.57821	-0.01127
18	C	-3.12552	0.985705	0.02625
19	H	-1.08685	1.713462	0.032396
20	C	-3.94734	-0.15497	0.01529
21	H	-4.00641	-2.32929	-0.00715
22	H	-3.55447	1.982398	0.036887
23	N	1.074229	0.586565	-0.00606
24	N	0.264583	-0.60076	0.007484
25	N	2.276042	-1.32199	0.028659
26	C	0.955963	-1.78371	0.024122
27	C	3.422449	-2.19644	0.036777
28	C	3.572191	-3.14692	-0.99128

29	C	4.367965	-2.10743	1.078367
30	C	4.681729	-4.01144	-0.97784
31	H	2.830777	-3.20304	-1.78227
32	C	5.481797	-2.96885	1.077498
33	H	4.22596	-1.39803	1.889363
34	C	5.640846	-3.92138	0.051848
35	H	4.798875	-4.7476	-1.76826
36	H	6.211476	-2.90269	1.879648
37	H	6.498751	-4.58811	0.05645
38	H	5.848553	1.940304	-0.13102
39	I	-6.08161	0.067863	0.019562
40	H	4.335401	0.221573	-0.07163

*B-2.2.15 – p-Anisyl Nitron (**33h**) (zwitterionic form)*

M1				
Tag	**Symbol**	**X**	**Y**	**Z**
1	C	2.627544	2.0272	-0.12415
2	C	1.689202	3.090973	-0.07857
3	C	3.996609	2.381492	-0.24427
4	C	2.113553	4.423037	-0.14554
5	H	0.634001	2.869515	0.009792
6	C	4.407148	3.709813	-0.31276
7	C	3.467224	4.750139	-0.26306
8	H	1.367909	5.214003	-0.10619
9	H	5.46638	3.937362	-0.40501
10	H	3.784968	5.787399	-0.3156
11	N	2.354333	0.667592	-0.05475
12	C	1.148381	0.16604	0.011876
13	C	-2.37992	-0.12313	0.079056
14	C	-3.24086	-1.02668	-0.54359
15	C	-2.88808	1.010941	0.725717
16	C	-4.62224	-0.82062	-0.50154
17	H	-2.84888	-1.88458	-1.07993
18	C	-4.25959	1.224302	0.757135
19	H	-2.20946	1.710649	1.198752
20	C	-5.1376	0.308814	0.150407
21	H	-5.27301	-1.5325	-0.9932
22	H	-4.67094	2.095845	1.255404
23	N	-0.091	0.719466	0.005042
24	N	-0.97082	-0.34468	0.060945

25	N	0.979866	-1.25823	0.082131
26	C	-0.34085	-1.50451	0.112543
27	H	-0.79814	-2.47632	0.208417
28	C	2.000589	-2.26208	0.082113
29	C	1.984705	-3.25275	-0.90412
30	C	2.983674	-2.25163	1.076068
31	C	2.95974	-4.25411	-0.8852
32	H	1.22452	-3.23523	-1.67881
33	C	3.959699	-3.24937	1.078523
34	H	2.979976	-1.47311	1.829786
35	C	3.94881	-4.25218	0.102141
36	H	2.948186	-5.02695	-1.64736
37	H	4.725279	-3.24636	1.848202
38	H	4.708896	-5.02732	0.111436
39	H	4.728214	1.578913	-0.28192
40	O	-6.463	0.607443	0.241754
41	C	-7.41234	-0.28655	-0.35024
42	H	-8.39109	0.14613	-0.14511
43	H	-7.26272	-0.35852	-1.43285
44	H	-7.34912	-1.28244	0.101292

M3				
Tag	**Symbol**	**X**	**Y**	**Z**
1	C	2.625757	2.027245	-0.12609
2	C	1.687458	3.090769	-0.07123
3	C	3.994082	2.382582	-0.25295
4	C	2.111083	4.423238	-0.13555
5	H	0.632829	2.868826	0.022618
6	C	4.403853	3.711287	-0.31905
7	C	3.463962	4.751223	-0.25991
8	H	1.365468	5.213814	-0.0887
9	H	5.462469	3.939446	-0.41663
10	H	3.781124	5.788751	-0.31039
11	N	2.353391	0.667446	-0.0591
12	C	1.147223	0.165341	0.00983
13	C	-2.38073	-0.12524	0.079353
14	C	-3.24073	-1.02664	-0.54777
15	C	-2.88975	1.0058	0.730525
16	C	-4.62218	-0.82126	-0.50596
17	H	-2.84784	-1.88226	-1.08704
18	C	-4.26142	1.218552	0.76171

19	H	-2.21192	1.703642	1.207484
20	C	-5.13848	0.305282	0.150301
21	H	-5.27227	-1.5314	-1.00101
22	H	-4.67348	2.087687	1.263605
23	N	-0.09197	0.718464	0.004196
24	N	-0.97147	-0.34619	0.061235
25	N	0.979607	-1.25836	0.080901
26	C	-0.34081	-1.50562	0.112681
27	H	-0.79745	-2.47777	0.208576
28	C	2.002316	-2.26068	0.082495
29	C	2.00139	-3.2399	-0.91505
30	C	2.972466	-2.25889	1.08909
31	C	2.979223	-4.23863	-0.89524
32	H	1.250219	-3.21605	-1.69829
33	C	3.951318	-3.25389	1.092722
34	H	2.956516	-1.48937	1.852003
35	C	3.955666	-4.24525	0.104598
36	H	2.97936	-5.00301	-1.66595
37	H	4.706837	-3.25797	1.872265
38	H	4.717649	-5.01851	0.114791
39	H	4.72596	1.58054	-0.29749
40	O	-6.46413	0.603068	0.241694
41	C	-7.41272	-0.28878	-0.35529
42	H	-8.39177	0.142675	-0.1491
43	H	-7.26202	-0.35583	-1.43801
44	H	-7.34942	-1.28659	0.091856

M4				
Tag	**Symbol**	**X**	**Y**	**Z**
1	C	2.585977	2.024529	-0.13783
2	C	1.631084	3.063488	-0.05063
3	C	3.941451	2.405222	-0.27906
4	C	2.030133	4.401661	-0.0984
5	H	0.58166	2.824556	0.056742
6	C	4.325687	3.737736	-0.32873
7	C	3.369838	4.756196	-0.23781
8	H	1.271501	5.176745	-0.02589
9	H	5.377681	3.98667	-0.43841
10	H	3.666435	5.799464	-0.27548
11	N	2.344871	0.660143	-0.0853
12	C	1.142518	0.155226	-0.01969

13	C	-2.36526	-0.14284	0.05645
14	C	-3.22786	-1.05361	-0.53942
15	C	-2.85499	1.000958	0.690684
16	C	-4.60576	-0.84524	-0.4809
17	H	-2.84081	-1.91866	-1.06835
18	C	-4.22159	1.21602	0.737421
19	H	-2.16262	1.704093	1.139327
20	C	-5.10528	0.293028	0.158638
21	H	-5.26569	-1.56301	-0.95135
22	H	-4.62973	2.094779	1.224847
23	N	-0.09286	0.697335	-0.02858
24	N	-0.958	-0.36302	0.025581
25	N	0.984041	-1.26007	0.049517
26	C	-0.33044	-1.51596	0.079564
27	H	-0.78646	-2.48977	0.178958
28	C	2.015639	-2.24565	0.071902
29	C	1.955152	-3.31355	-0.82074
30	C	3.050145	-2.1338	1.000012
31	C	2.941857	-4.29767	-0.77055
32	H	1.152634	-3.36787	-1.55
33	C	4.036144	-3.11554	1.031208
34	H	3.07501	-1.28588	1.674341
35	C	3.982796	-4.19841	0.150902
36	H	2.898856	-5.13391	-1.46028
37	H	4.845395	-3.03741	1.749629
38	H	4.753241	-4.96172	0.183052
39	H	4.68382	1.614853	-0.34736
40	O	-6.42239	0.592335	0.262131
41	C	-7.35753	-0.31338	-0.3087
42	H	-8.34111	0.107282	-0.10828
43	H	-7.20767	-0.39913	-1.38965
44	H	-7.27781	-1.30104	0.156574

M5				
Tag	**Symbol**	**X**	**Y**	**Z**
1	C	2.585177	2.024813	-0.13923
2	C	1.630729	3.063293	-0.04044
3	C	3.93939	2.406695	-0.29026
4	C	2.028878	4.401819	-0.08699
5	H	0.582369	2.823703	0.075609
6	C	4.32268	3.739558	-0.3389

7	C	3.367218	4.757406	-0.2368
8	H	1.270593	5.176322	-0.00525
9	H	5.373638	3.989246	-0.45645
10	H	3.663096	5.800897	-0.2736
11	N	2.344973	0.660315	-0.08844
12	C	1.142446	0.154805	-0.02045
13	C	-2.36515	-0.14343	0.05657
14	C	-3.22711	-1.0531	-0.54194
15	C	-2.85542	0.998786	0.693197
16	C	-4.60507	-0.84506	-0.48388
17	H	-2.83953	-1.91709	-1.07218
18	C	-4.22213	1.21358	0.739425
19	H	-2.16366	1.700899	1.144412
20	C	-5.10521	0.291698	0.157886
21	H	-5.26452	-1.56208	-0.95614
22	H	-4.63064	2.091075	1.22883
23	N	-0.09259	0.696965	-0.02909
24	N	-0.95781	-0.36348	0.026101
25	N	0.98433	-1.26003	0.05008
26	C	-0.33006	-1.51624	0.080708
27	H	-0.78573	-2.49022	0.180452
28	C	2.016346	-2.24539	0.072991
29	C	1.959737	-3.31026	-0.82347
30	C	3.047199	-2.13596	1.005438
31	C	2.9473	-4.2936	-0.77311
32	H	1.159308	-3.36326	-1.55511
33	C	4.034114	-3.11679	1.036832
34	H	3.068275	-1.29088	1.683539
35	C	3.984939	-4.1965	0.152336
36	H	2.907309	-5.12773	-1.46556
37	H	4.840466	-3.0407	1.758721
38	H	4.755867	-4.95931	0.184686
39	H	4.681836	1.617084	-0.36681
40	O	-6.42249	0.59043	0.261161
41	C	-7.35709	-0.31471	-0.31198
42	H	-8.34094	0.105072	-0.11108
43	H	-7.20667	-0.39816	-1.39298
44	H	-7.27698	-1.30323	0.151313

*B-2.2.16 – p-Anisyl Nitron (**33h**) (carbenic form)*

M1				
Tag	**Symbol**	**X**	**Y**	**Z**
1	C	2.584304	2.049644	-0.09705
2	C	1.617556	3.068346	-0.08182
3	C	3.948575	2.391746	-0.15961
4	C	2.025824	4.405815	-0.1272
5	H	0.566983	2.816634	-0.03582
6	C	4.33728	3.72849	-0.2045
7	C	3.378066	4.748688	-0.18834
8	H	1.26801	5.184106	-0.11464
9	H	5.394613	3.971977	-0.2525
10	H	3.682049	5.790143	-0.22349
11	N	2.26974	0.679083	-0.0503
12	C	1.047905	0.074646	0.000928
13	C	-2.40716	-0.2042	0.050564
14	C	-3.30366	-1.19987	-0.3429
15	C	-2.89439	1.043148	0.464294
16	C	-4.68146	-0.96614	-0.31071
17	H	-2.92661	-2.16032	-0.67387
18	C	-4.26483	1.282215	0.48749
19	H	-2.20165	1.818858	0.766811
20	C	-5.16968	0.280378	0.104769
21	H	-5.35289	-1.75712	-0.62135
22	H	-4.64937	2.245351	0.807547
23	N	-0.13382	0.641436	-0.00612
24	N	-1.00329	-0.45684	0.035108
25	N	0.921373	-1.31473	0.048118
26	C	-0.41153	-1.66543	0.070438
27	C	2.007711	-2.25324	0.063655
28	C	2.214612	-3.08346	-1.04227
29	C	2.842145	-2.33228	1.183888
30	C	3.265361	-4.00352	-1.02264
31	H	1.555355	-3.00627	-1.90047
32	C	3.899094	-3.24716	1.189684
33	H	2.657471	-1.69541	2.043511
34	C	4.110303	-4.08361	0.089536
35	H	3.425758	-4.65314	-1.87747
36	H	4.547533	-3.31131	2.057846
37	H	4.92861	-4.79701	0.09941
38	H	4.700724	1.607183	-0.17312

39	H	3.059002	0.046576	-0.06511
40	O	-6.49486	0.612815	0.166165
41	C	-7.46297	-0.37166	-0.20598
42	H	-8.43464	0.104315	-0.07448
43	H	-7.341	-0.6705	-1.25313
44	H	-7.39753	-1.25446	0.439866

M3

Tag	Symbol	X	Y	Z
1	C	2.583642	2.050056	-0.09845
2	C	1.616604	3.068552	-0.08373
3	C	3.94788	2.392618	-0.16035
4	C	2.024444	4.406217	-0.12903
5	H	0.566032	2.816815	-0.03794
6	C	4.336133	3.72951	-0.20522
7	C	3.376615	4.749493	-0.18965
8	H	1.266351	5.184242	-0.11679
9	H	5.393424	3.973271	-0.25266
10	H	3.680324	5.791029	-0.22477
11	N	2.269489	0.679378	-0.05179
12	C	1.047968	0.074694	-0.00013
13	C	-2.40708	-0.20498	0.051066
14	C	-3.30305	-1.19679	-0.35317
15	C	-2.89484	1.03839	0.47611
16	C	-4.68098	-0.96359	-0.32005
17	H	-2.92594	-2.15387	-0.69378
18	C	-4.2653	1.277174	0.500083
19	H	-2.20256	1.811323	0.786805
20	C	-5.16972	0.278823	0.107003
21	H	-5.35198	-1.75149	-0.63931
22	H	-4.65009	2.237253	0.828927
23	N	-0.13409	0.641175	-0.00746
24	N	-1.00319	-0.45731	0.035257
25	N	0.921759	-1.31461	0.048553
26	C	-0.41094	-1.66556	0.07201
27	C	2.008441	-2.25296	0.064456
28	C	2.217601	-3.08098	-1.0427
29	C	2.84075	-2.33365	1.186106
30	C	3.268519	-4.00088	-1.02275
31	H	1.560379	-3.00205	-1.90231
32	C	3.897844	-3.2484	1.192248

33	H	2.654828	-1.69784	2.04623
34	C	4.111249	-4.08286	0.090997
35	H	3.43088	-4.64872	-1.87854
36	H	4.544873	-3.31372	2.061359
37	H	4.92976	-4.79601	0.101105
38	H	4.700367	1.608418	-0.17313
39	H	3.058979	0.047081	-0.06632
40	O	-6.49487	0.610486	0.170398
41	C	-7.46284	-0.37073	-0.2118
42	H	-8.43457	0.103886	-0.07615
43	H	-7.34015	-0.65925	-1.2617
44	H	-7.3974	-1.25959	0.425569

M4				
Tag	**Symbol**	**X**	**Y**	**Z**
1	C	2.551131	2.043998	-0.11677
2	C	1.57103	3.040918	-0.03852
3	C	3.902804	2.407918	-0.22254
4	C	1.957452	4.382466	-0.06414
5	H	0.526098	2.774603	0.040454
6	C	4.268124	3.747499	-0.24765
7	C	3.296581	4.74828	-0.16813
8	H	1.189337	5.14726	-0.00192
9	H	5.318317	4.009245	-0.32984
10	H	3.582161	5.794535	-0.18788
11	N	2.264117	0.670919	-0.08679
12	C	1.046694	0.064486	-0.02639
13	C	-2.38972	-0.21203	0.034605
14	C	-3.28428	-1.21805	-0.31522
15	C	-2.86476	1.04674	0.411899
16	C	-4.65861	-0.98265	-0.27524
17	H	-2.90752	-2.18786	-0.61888
18	C	-4.23091	1.286096	0.443024
19	H	-2.16416	1.828956	0.679347
20	C	-5.13691	0.274379	0.104451
21	H	-5.33512	-1.78193	-0.55157
22	H	-4.61611	2.257554	0.734713
23	N	-0.1318	0.622793	-0.03597
24	N	-0.98837	-0.46528	0.012144
25	N	0.924285	-1.31619	0.0295
26	C	-0.40379	-1.67209	0.053472

27	C	2.013136	-2.24187	0.0645
28	C	2.145651	-3.17877	-0.95852
29	C	2.920884	-2.19745	1.12264
30	C	3.201904	-4.08638	-0.91688
31	H	1.423539	-3.18931	-1.7683
32	C	3.983891	-3.09913	1.146654
33	H	2.786184	-1.47391	1.921552
34	C	4.123528	-4.04392	0.130231
35	H	3.30826	-4.82217	-1.70704
36	H	4.693722	-3.069	1.966461
37	H	4.948318	-4.74841	0.155121
38	H	4.663606	1.634454	-0.28409
39	H	3.058615	0.047165	-0.14957
40	O	-6.45452	0.605495	0.170032
41	C	-7.40351	-0.39819	-0.15778
42	H	-8.38238	0.062162	-0.03497
43	H	-7.28174	-0.72977	-1.19436
44	H	-7.31463	-1.25679	0.516179

M5				
Tag	**Symbol**	**X**	**Y**	**Z**
1	C	2.550648	2.044292	-0.11942
2	C	1.570324	3.040952	-0.03977
3	C	3.902264	2.408644	-0.22489
4	C	1.956373	4.382684	-0.06379
5	H	0.525435	2.774486	0.039322
6	C	4.267185	3.748386	-0.24842
7	C	3.295419	4.748908	-0.16758
8	H	1.188073	5.1472	-0.00042
9	H	5.317315	4.010464	-0.33033
10	H	3.580796	5.795243	-0.18611
11	N	2.263858	0.671108	-0.09144
12	C	1.046784	0.064518	-0.02903
13	C	-2.38965	-0.21267	0.034786
14	C	-3.28404	-1.21587	-0.32354
15	C	-2.86486	1.043234	0.421432
16	C	-4.65843	-0.98082	-0.28244
17	H	-2.90744	-2.18328	-0.63511
18	C	-4.23101	1.28247	0.4535
19	H	-2.16441	1.823369	0.695444
20	C	-5.13685	0.273305	0.106698

21	H	-5.33481	-1.77781	-0.56559
22	H	-4.61616	2.251748	0.752444
23	N	-0.13198	0.622571	-0.03899
24	N	-0.98831	-0.46569	0.011614
25	N	0.924725	-1.31602	0.029211
26	C	-0.4032	-1.67208	0.054976
27	C	2.013789	-2.24158	0.065232
28	C	2.147232	-3.17856	-0.95762
29	C	2.920589	-2.19684	1.124126
30	C	3.203429	-4.08621	-0.91487
31	H	1.426231	-3.18903	-1.76841
32	C	3.983565	-3.09856	1.149247
33	H	2.785623	-1.47281	1.922545
34	C	4.124043	-4.04361	0.133166
35	H	3.310622	-4.82197	-1.70493
36	H	4.692833	-3.068	1.96951
37	H	4.948874	-4.74801	0.158889
38	H	4.663335	1.635548	-0.28724
39	H	3.058714	0.047525	-0.15208
40	O	-6.45444	0.603927	0.174111
41	C	-7.40349	-0.39732	-0.16205
42	H	-8.38234	0.062241	-0.03632
43	H	-7.28096	-0.72085	-1.20103
44	H	-7.315	-1.26095	0.50542

*B-2.2.17 – 4-Carboxyphenyl Nitron (**33i**) (carboxylate zwitterion form)*

		M1		
Tag	**Symbol**	**X**	**Y**	**Z**
1	C	2.674802	2.166904	-0.0874
2	C	1.652513	3.126337	-0.1168
3	C	4.019273	2.57485	-0.11243
4	C	1.990013	4.482969	-0.17031
5	H	0.614366	2.825582	-0.09884
6	C	4.337112	3.93013	-0.1657
7	C	3.323636	4.895024	-0.19495
8	H	1.192253	5.219391	-0.19287
9	H	5.3804	4.230101	-0.18449
10	H	3.572133	5.950718	-0.23643
11	N	2.436747	0.772776	-0.03156
12	C	1.26262	0.109024	-0.00392

13	C	-2.20758	-0.3483	-0.00148
14	C	-2.99392	-1.29669	-0.6602
15	C	-2.77801	0.745245	0.653472
16	C	-4.38072	-1.15246	-0.63572
17	H	-2.53686	-2.12013	-1.1992
18	C	-4.16604	0.877133	0.651089
19	H	-2.14648	1.469152	1.155312
20	C	-4.98465	-0.06822	0.016237
21	H	-5.01133	-1.87582	-1.1397
22	H	-4.63289	1.717311	1.152389
23	N	0.037819	0.607763	-0.02777
24	N	-0.78228	-0.499	0.009182
25	N	1.222577	-1.28461	0.046019
26	C	-0.0843	-1.61885	0.059554
27	H	-0.47171	-2.62317	0.125131
28	C	2.343834	-2.19738	0.080294
29	C	2.782114	-2.77572	-1.11349
30	C	2.957421	-2.47272	1.305098
31	C	3.864999	-3.65661	-1.07324
32	H	2.285005	-2.54007	-2.04861
33	C	4.041755	-3.35257	1.328239
34	H	2.590371	-2.01237	2.216444
35	C	4.492881	-3.94267	0.143284
36	H	4.215374	-4.1167	-1.99123
37	H	4.527706	-3.5783	2.271649
38	H	5.33462	-4.62746	0.168125
39	H	4.811487	1.831493	-0.09041
40	C	-6.51272	0.08381	0.029235
41	O	-7.17748	-0.84282	-0.5153
42	O	-6.97261	1.121655	0.584522
43	H	3.261968	0.185689	-0.01742

M3				
Tag	**Symbol**	**X**	**Y**	**Z**
1	C	2.67495	2.166522	-0.08797
2	C	1.652792	3.126231	-0.11635
3	C	4.019519	2.574476	-0.11344
4	C	1.990303	4.482915	-0.16933
5	H	0.61463	2.825554	-0.09777
6	C	4.337339	3.929796	-0.1662
7	C	3.323958	4.894901	-0.19449

8	H	1.192562	5.219407	-0.191
9	H	5.380666	4.229646	-0.18529
10	H	3.572579	5.950594	-0.23557
11	N	2.436547	0.772678	-0.0326
12	C	1.262315	0.109157	-0.00439
13	C	-2.20749	-0.34883	-0.00086
14	C	-2.99407	-1.29874	-0.65708
15	C	-2.77787	0.746299	0.651503
16	C	-4.38088	-1.15434	-0.63289
17	H	-2.53713	-2.12365	-1.19383
18	C	-4.16587	0.878392	0.64896
19	H	-2.14629	1.471211	1.151786
20	C	-4.98469	-0.06833	0.016323
21	H	-5.01092	-1.87938	-1.13514
22	H	-4.63207	1.719891	1.148602
23	N	0.037491	0.607786	-0.02849
24	N	-0.78235	-0.49924	0.009561
25	N	1.222404	-1.28448	0.046734
26	C	-0.08408	-1.61897	0.060737
27	H	-0.47129	-2.62334	0.126993
28	C	2.343769	-2.19725	0.080612
29	C	2.780823	-2.77639	-1.11321
30	C	2.958438	-2.47168	1.305018
31	C	3.863783	-3.6572	-1.07336
32	H	2.282852	-2.54138	-2.04799
33	C	4.04285	-3.35145	1.327729
34	H	2.592255	-2.01062	2.216322
35	C	4.492877	-3.94237	0.14276
36	H	4.213291	-4.11787	-1.9914
37	H	4.529771	-3.57637	2.270833
38	H	5.334752	-4.62701	0.167261
39	H	4.811813	1.831199	-0.09197
40	C	-6.51207	0.084285	0.028818
41	O	-7.17815	-0.84121	-0.51662
42	O	-6.97283	1.121874	0.584521
43	H	3.261463	0.185111	-0.01889

M4				
Tag	**Symbol**	**X**	**Y**	**Z**
1	C	2.654505	2.143621	-0.11107
2	C	1.626886	3.091336	-0.11116

3	C	3.991917	2.557914	-0.16556
4	C	1.955302	4.447352	-0.16629
5	H	0.590465	2.786997	-0.06954
6	C	4.299109	3.911377	-0.2202
7	C	3.28111	4.867192	-0.22113
8	H	1.15301	5.178274	-0.16625
9	H	5.339127	4.21804	-0.26242
10	H	3.521286	5.924014	-0.26425
11	N	2.429698	0.751485	-0.05333
12	C	1.253436	0.09674	-0.02029
13	C	-2.20157	-0.3509	-0.01407
14	C	-2.98701	-1.31497	-0.63966
15	C	-2.75457	0.759333	0.617159
16	C	-4.37042	-1.16794	-0.60389
17	H	-2.53158	-2.15042	-1.16165
18	C	-4.13964	0.891829	0.627051
19	H	-2.11015	1.492119	1.089853
20	C	-4.95779	-0.06889	0.02691
21	H	-5.01297	-1.89983	-1.0804
22	H	-4.60587	1.743099	1.110611
23	N	0.035218	0.592533	-0.05234
24	N	-0.77777	-0.50387	-0.01038
25	N	1.211317	-1.28769	0.043009
26	C	-0.09007	-1.62239	0.051955
27	H	-0.48153	-2.62626	0.126365
28	C	2.336787	-2.18484	0.09169
29	C	2.654075	-2.92888	-1.0409
30	C	3.076869	-2.26497	1.268941
31	C	3.747735	-3.78993	-0.98394
32	H	2.057561	-2.83041	-1.94186
33	C	4.174573	-3.12178	1.305425
34	H	2.792209	-1.67493	2.134521
35	C	4.505821	-3.88249	0.183563
36	H	4.008667	-4.38247	-1.85373
37	H	4.763682	-3.19887	2.212452
38	H	5.359236	-4.5512	0.219681
39	H	4.787067	1.817625	-0.16458
40	C	-6.48522	0.083523	0.055288
41	O	-7.14545	-0.83692	-0.48588
42	O	-6.93027	1.113177	0.618767
43	H	3.255337	0.163493	-0.05965

M5				
Tag	**Symbol**	**X**	**Y**	**Z**
1	C	2.65261	2.144229	-0.11214
2	C	1.624654	3.091621	-0.10233
3	C	3.989488	2.559345	-0.17537
4	C	1.952011	4.447969	-0.15647
5	H	0.5887	2.786708	-0.05348
6	C	4.295602	3.913106	-0.22892
7	C	3.277217	4.868564	-0.22006
8	H	1.149412	5.178532	-0.14852
9	H	5.335175	4.220306	-0.27795
10	H	3.516671	5.925595	-0.26233
11	N	2.42876	0.752142	-0.05544
12	C	1.253017	0.096641	-0.01977
13	C	-2.2012	-0.35373	-0.01036
14	C	-2.98645	-1.3213	-0.63078
15	C	-2.75464	0.759979	0.614384
16	C	-4.36988	-1.17387	-0.59686
17	H	-2.5309	-2.15985	-1.1476
18	C	-4.13968	0.892905	0.622398
19	H	-2.11058	1.495329	1.083531
20	C	-4.95759	-0.07083	0.026718
21	H	-5.01148	-1.90897	-1.06968
22	H	-4.60551	1.747203	1.100932
23	N	0.03442	0.591441	-0.05124
24	N	-0.77753	-0.50573	-0.0065
25	N	1.212128	-1.28772	0.045978
26	C	-0.08868	-1.62361	0.0569
27	H	-0.47906	-2.62777	0.133094
28	C	2.33847	-2.18399	0.092835
29	C	2.653782	-2.92812	-1.04024
30	C	3.081199	-2.26294	1.268455
31	C	3.748351	-3.78815	-0.98543
32	H	2.05504	-2.83057	-1.9398
33	C	4.179778	-3.11873	1.302726
34	H	2.798085	-1.6727	2.134377
35	C	4.509191	-3.87956	0.180392
36	H	4.007842	-4.38075	-1.85562
37	H	4.771098	-3.19479	2.208397
38	H	5.363382	-4.54738	0.214797
39	H	4.784987	1.819461	-0.18185
40	C	-6.48435	0.083146	0.05129

41	O	-7.14549	-0.839	-0.48639
42	O	-6.93068	1.116267	0.608001
43	H	3.254642	0.164517	-0.06498

*B-2.2.18 – 4-Carboxyphenyl Nitron (**33i**) (acid zwitterion form)*

M1				
Tag	**Symbol**	**X**	**Y**	**Z**
1	C	2.718023	2.132981	-0.10204
2	C	1.70774	3.128519	-0.09038
3	C	4.063253	2.578136	-0.16587
4	C	2.042375	4.486676	-0.13712
5	H	0.667451	2.834842	-0.04465
6	C	4.384685	3.931771	-0.21367
7	C	3.374417	4.904771	-0.19902
8	H	1.243981	5.225149	-0.12557
9	H	5.428593	4.231687	-0.26215
10	H	3.622617	5.961475	-0.23584
11	N	2.533558	0.756316	-0.04953
12	C	1.36459	0.177632	-0.01607
13	C	-2.12918	-0.35918	-0.01341
14	C	-2.93504	-1.44219	-0.39118
15	C	-2.69754	0.861531	0.366834
16	C	-4.31717	-1.30289	-0.36104
17	H	-2.49923	-2.37741	-0.72333
18	C	-4.08362	0.99202	0.384185
19	H	-2.05638	1.687316	0.646507
20	C	-4.90447	-0.08788	0.025762
21	H	-4.95199	-2.13207	-0.6518
22	H	-4.52662	1.93484	0.681903
23	N	0.090571	0.641604	-0.04971
24	N	-0.7138	-0.48326	-0.01934
25	N	1.293509	-1.25948	0.047749
26	C	0.000445	-1.59869	0.042639
27	H	-0.38254	-2.60363	0.117848
28	C	2.38801	-2.18499	0.078065
29	C	2.513447	-3.12868	-0.94488
30	C	3.300747	-2.13848	1.13548
31	C	3.564192	-4.04944	-0.89893
32	H	1.805338	-3.13688	-1.76742
33	C	4.351725	-3.05629	1.165838

34	H	3.185186	-1.39583	1.916323
35	C	4.484033	-4.01273	0.152514
36	H	3.664711	-4.78686	-1.689
37	H	5.063871	-3.02711	1.984537
38	H	5.302279	-4.72555	0.183081
39	H	4.848533	1.827212	-0.176
40	C	-6.38634	0.011595	0.033126
41	O	-7.14383	-0.8993	-0.26617
42	O	-6.83841	1.227428	0.409687
43	H	-7.81081	1.206341	0.38836

M3				
Tag	**Symbol**	**X**	**Y**	**Z**
1	C	2.717546	2.132242	-0.10307
2	C	1.70741	3.12799	-0.08462
3	C	4.062543	2.577796	-0.17234
4	C	2.041886	4.486287	-0.12977
5	H	0.66728	2.834447	-0.03455
6	C	4.383778	3.931538	-0.21882
7	C	3.373623	4.904602	-0.19712
8	H	1.243525	5.224683	-0.11264
9	H	5.427465	4.231491	-0.2716
10	H	3.621668	5.961374	-0.23272
11	N	2.533442	0.755589	-0.0519
12	C	1.363916	0.176793	-0.01726
13	C	-2.12972	-0.35963	-0.01453
14	C	-2.93497	-1.44083	-0.39834
15	C	-2.69841	0.859066	0.371735
16	C	-4.31723	-1.30191	-0.36808
17	H	-2.49869	-2.37415	-0.73518
18	C	-4.08447	0.989231	0.389101
19	H	-2.05767	1.683544	0.656249
20	C	-4.90493	-0.08907	0.024703
21	H	-4.95149	-2.12987	-0.66346
22	H	-4.52778	1.930367	0.691638
23	N	0.090366	0.641228	-0.05043
24	N	-0.71427	-0.48371	-0.02008
25	N	1.292899	-1.25962	0.046807
26	C	-8.5E-05	-1.59908	0.041824
27	H	-0.38304	-2.60411	0.116558
28	C	2.388361	-2.18438	0.07884

29	C	2.526563	-3.1162	-0.95316
30	C	3.289266	-2.14791	1.146702
31	C	3.579053	-4.03502	-0.90631
32	H	1.8263	-3.11735	-1.7824
33	C	4.342048	-3.06368	1.178162
34	H	3.163185	-1.41479	1.935025
35	C	4.487508	-4.00808	0.155323
36	H	3.689525	-4.76362	-1.70319
37	H	5.045039	-3.04256	2.004972
38	H	5.30691	-4.71952	0.186726
39	H	4.848027	1.82711	-0.18755
40	C	-6.38683	0.010223	0.032029
41	O	-7.14406	-0.89943	-0.27216
42	O	-6.83929	1.223879	0.414453
43	H	-7.81172	1.202988	0.392996

M4				
Tag	**Symbol**	**X**	**Y**	**Z**
1	C	2.69299	2.124326	-0.12185
2	C	1.674262	3.101279	-0.05246
3	C	4.024702	2.585638	-0.23924
4	C	1.990999	4.461422	-0.09636
5	H	0.639786	2.797951	0.037772
6	C	4.327116	3.939285	-0.2857
7	C	3.308789	4.896625	-0.21376
8	H	1.185397	5.188737	-0.03846
9	H	5.36342	4.252635	-0.37751
10	H	3.54143	5.956074	-0.24906
11	N	2.533993	0.746546	-0.07082
12	C	1.365456	0.171429	-0.02898
13	C	-2.1126	-0.35405	-0.02418
14	C	-2.9067	-1.41203	-0.47019
15	C	-2.67162	0.840903	0.425617
16	C	-4.28695	-1.27567	-0.43284
17	H	-2.46169	-2.31963	-0.86261
18	C	-4.05554	0.968947	0.447975
19	H	-2.02476	1.64565	0.752731
20	C	-4.86492	-0.08888	0.025752
21	H	-4.92662	-2.08217	-0.77395
22	H	-4.50598	1.890181	0.798899
23	N	0.099029	0.633181	-0.06656

24	N	-0.69821	-0.48127	-0.03125
25	N	1.294042	-1.25505	0.045058
26	C	0.004001	-1.59391	0.042257
27	H	-0.38631	-2.59636	0.134826
28	C	2.385237	-2.17482	0.086249
29	C	2.405585	-3.24138	-0.80966
30	C	3.393309	-1.99992	1.032864
31	C	3.451149	-4.16144	-0.7443
32	H	1.621032	-3.3435	-1.55333
33	C	4.437922	-2.91853	1.079292
34	H	3.353372	-1.15385	1.708758
35	C	4.467502	-3.99954	0.195664
36	H	3.47297	-4.99649	-1.43632
37	H	5.228239	-2.79214	1.811661
38	H	5.283878	-4.71283	0.23945
39	H	4.81507	1.842034	-0.29172
40	C	-6.35	0.008759	0.038384
41	O	-7.09458	-0.88034	-0.31752
42	O	-6.79534	1.189155	0.488353
43	H	-7.76601	1.178612	0.469993

M5				
Tag	**Symbol**	**X**	**Y**	**Z**
1	C	2.690728	2.125287	-0.12209
2	C	1.671379	3.101129	-0.04422
3	C	4.021171	2.588613	-0.24722
4	C	1.986274	4.461763	-0.08755
5	H	0.637831	2.796624	0.052587
6	C	4.321707	3.942719	-0.29331
7	C	3.30275	4.898805	-0.21301
8	H	1.180211	5.187986	-0.02278
9	H	5.357035	4.257416	-0.39129
10	H	3.53393	5.958578	-0.24791
11	N	2.533695	0.747335	-0.07205
12	C	1.365297	0.170906	-0.02853
13	C	-2.11227	-0.35636	-0.02313
14	C	-2.90605	-1.41533	-0.4673
15	C	-2.67162	0.839302	0.424461
16	C	-4.28633	-1.2789	-0.43081
17	H	-2.46104	-2.32394	-0.85733
18	C	-4.05555	0.967347	0.445948

19	H	-2.02521	1.644747	0.750749
20	C	-4.86467	-0.09125	0.025121
21	H	-4.92554	-2.08631	-0.7706
22	H	-4.50605	1.889204	0.795133
23	N	0.098948	0.631943	-0.06556
24	N	-0.69775	-0.48306	-0.02993
25	N	1.295087	-1.25511	0.045823
26	C	0.005364	-1.59514	0.04334
27	H	-0.38379	-2.59809	0.135461
28	C	2.387399	-2.17379	0.086705
29	C	2.412695	-3.23578	-0.81438
30	C	3.391307	-2.0021	1.038321
31	C	3.459707	-4.15433	-0.74966
32	H	1.630559	-3.33585	-1.56084
33	C	4.437416	-2.91906	1.084158
34	H	3.346713	-1.16024	1.719235
35	C	4.472235	-3.9954	0.194967
36	H	3.485385	-4.98611	-1.44546
37	H	5.224435	-2.79539	1.820531
38	H	5.289539	-4.70765	0.238415
39	H	4.812312	1.846257	-0.30595
40	C	-6.34974	0.006619	0.036647
41	O	-7.0942	-0.88321	-0.31807
42	O	-6.79523	1.18783	0.483851
43	H	-7.76594	1.177667	0.465141

*B-2.2.19 – 4-Carboxyphenyl Nitron (**33i**) (carbenic form)*

M1				
Tag	**Symbol**	**X**	**Y**	**Z**
1	C	2.690829	2.143215	-0.04628
2	C	1.666467	3.10328	-0.02923
3	C	4.033659	2.562631	-0.08678
4	C	1.997499	4.462475	-0.05175
5	H	0.631533	2.791538	0.000512
6	C	4.345294	3.920003	-0.10892
7	C	3.328527	4.882635	-0.09137
8	H	1.196367	5.19596	-0.03809
9	H	5.387231	4.224612	-0.14015
10	H	3.572431	5.940194	-0.10875
11	N	2.455161	0.754844	-0.02258

12	C	1.272443	0.082074	0.003582
13	C	-2.14905	-0.42027	0.011612
14	C	-2.97733	-1.55465	-0.02163
15	C	-2.71336	0.862577	0.046289
16	C	-4.35652	-1.39766	-0.01758
17	H	-2.53273	-2.54123	-0.04943
18	C	-4.09833	1.008203	0.049155
19	H	-2.07032	1.732218	0.071635
20	C	-4.93554	-0.11735	0.0177
21	H	-5.00029	-2.26999	-0.04312
22	H	-4.52818	2.002654	0.076674
23	N	0.05966	0.5758	-0.00468
24	N	-0.74109	-0.57524	0.009635
25	N	1.230242	-1.31729	0.028046
26	C	-0.07034	-1.75005	0.027079
27	C	2.375912	-2.18538	0.033116
28	C	2.667406	-2.94363	-1.10452
29	C	3.179756	-2.26445	1.174985
30	C	3.775201	-3.79434	-1.0946
31	H	2.029397	-2.86637	-1.97863
32	C	4.29288	-3.11	1.171427
33	H	2.929239	-1.68222	2.056343
34	C	4.58983	-3.87556	0.039818
35	H	4.002727	-4.38928	-1.97357
36	H	4.918666	-3.17587	2.055848
37	H	5.452087	-4.53517	0.042405
38	H	4.829566	1.822621	-0.10093
39	C	-6.41174	-0.00341	0.019758
40	O	-7.18598	-0.95041	-0.0078
41	O	-6.854	1.275342	0.055823
42	H	-7.82643	1.253255	0.054636
43	H	3.27977	0.168653	-0.03367

M3				
Tag	**Symbol**	**X**	**Y**	**Z**
1	C	2.69068	2.142982	-0.04571
2	C	1.666254	3.103094	-0.03179
3	C	4.033668	2.562446	-0.08209
4	C	1.997269	4.46235	-0.0534
5	H	0.631181	2.791519	-0.00506
6	C	4.345257	3.919863	-0.1034

7	C	3.328417	4.88253	-0.08904
8	H	1.196052	5.195784	-0.04219
9	H	5.38729	4.224461	-0.13141
10	H	3.572374	5.940091	-0.10575
11	N	2.454827	0.754642	-0.02318
12	C	1.272157	0.082025	0.002178
13	C	-2.14935	-0.42075	0.010287
14	C	-2.97763	-1.55505	-0.02641
15	C	-2.71382	0.861945	0.048748
16	C	-4.35685	-1.39821	-0.02175
17	H	-2.5332	-2.5416	-0.05733
18	C	-4.0988	1.00745	0.052096
19	H	-2.07099	1.731656	0.076739
20	C	-4.93599	-0.11805	0.017392
21	H	-5.00034	-2.27065	-0.04995
22	H	-4.52858	2.001837	0.082614
23	N	0.059188	0.575588	-0.00624
24	N	-0.7414	-0.57554	0.008057
25	N	1.230132	-1.31725	0.026446
26	C	-0.07023	-1.75019	0.025786
27	C	2.376402	-2.18494	0.032392
28	C	2.678792	-2.93038	-1.11086
29	C	3.169799	-2.27568	1.180623
30	C	3.787099	-3.78047	-1.10009
31	H	2.049019	-2.84367	-1.99006
32	C	4.283317	-3.12071	1.178148
33	H	2.911366	-1.70221	2.065421
34	C	4.591097	-3.87372	0.040981
35	H	4.023314	-4.36544	-1.98343
36	H	4.901241	-3.19563	2.067352
37	H	5.453772	-4.53279	0.044293
38	H	4.829739	1.822591	-0.09359
39	C	-6.4122	-0.00401	0.019971
40	O	-7.18638	-0.95117	-0.01028
41	O	-6.85436	1.27436	0.059816
42	H	-7.82683	1.252901	0.058737
43	H	3.279373	0.168283	-0.03265

M4				
Tag	**Symbol**	**X**	**Y**	**Z**
1	C	2.654058	2.139802	-0.06013
2	C	1.614563	3.075579	-0.0036
3	C	3.983701	2.582401	-0.13597
4	C	1.92092	4.437815	-0.02329
5	H	0.585886	2.747659	0.054131
6	C	4.269073	3.94134	-0.15537
7	C	3.237914	4.882126	-0.09899
8	H	1.107722	5.155705	0.021226
9	H	5.303255	4.26535	-0.21479
10	H	3.461173	5.943496	-0.1144
11	N	2.448996	0.750786	-0.03819
12	C	1.271756	0.07315	-0.00419
13	C	-2.13246	-0.43157	0.011084
14	C	-2.95233	-1.56639	-0.00185
15	C	-2.68858	0.849617	0.028103
16	C	-4.32918	-1.4089	0.004254
17	H	-2.50365	-2.55168	-0.01573
18	C	-4.07156	0.994564	0.033455
19	H	-2.04155	1.71727	0.037506
20	C	-4.89866	-0.1308	0.021874
21	H	-4.97835	-2.27804	-0.00533
22	H	-4.50707	1.987316	0.046971
23	N	0.061653	0.556246	-0.01243
24	N	-0.72504	-0.58553	0.006579
25	N	1.23593	-1.31694	0.025364
26	C	-0.0599	-1.75726	0.025718
27	C	2.384057	-2.17098	0.038448
28	C	2.594029	-3.04522	-1.02582
29	C	3.269277	-2.11626	1.114565
30	C	3.707798	-3.882	-1.00725
31	H	1.887074	-3.06372	-1.84872
32	C	4.389303	-2.94654	1.115836
33	H	3.073958	-1.4418	1.943328
34	C	4.607269	-3.82963	0.058505
35	H	3.875902	-4.56975	-1.82923
36	H	5.082876	-2.90946	1.949103
37	H	5.476774	-4.47855	0.065827
38	H	4.790313	1.85543	-0.17892
39	C	-6.37814	-0.01675	0.027012
40	O	-7.14051	-0.96218	0.016105

41	O	-6.81203	1.252962	0.045144
42	H	-7.78264	1.242172	0.047371
43	H	3.280323	0.175791	-0.09191

M5				
Tag	**Symbol**	**X**	**Y**	**Z**
1	C	2.653602	2.140196	-0.06049
2	C	1.613815	3.075741	-0.00431
3	C	3.983197	2.583172	-0.13587
4	C	1.919767	4.438124	-0.02391
5	H	0.585136	2.747763	0.053152
6	C	4.268141	3.942224	-0.15515
7	C	3.236686	4.882783	-0.09914
8	H	1.106332	5.155763	0.020345
9	H	5.302267	4.266486	-0.21419
10	H	3.459681	5.944214	-0.11448
11	N	2.448946	0.751115	-0.03877
12	C	1.271995	0.073251	-0.00479
13	C	-2.13226	-0.4319	0.010682
14	C	-2.95215	-1.5667	-0.0044
15	C	-2.68847	0.849245	0.029977
16	C	-4.32903	-1.40929	0.002016
17	H	-2.50369	-2.55204	-0.02021
18	C	-4.07148	0.994117	0.035528
19	H	-2.04164	1.717027	0.041034
20	C	-4.89858	-0.13125	0.021938
21	H	-4.97794	-2.2786	-0.00921
22	H	-4.50688	1.986886	0.050818
23	N	0.061696	0.556134	-0.01334
24	N	-0.72484	-0.58572	0.00605
25	N	1.236361	-1.31682	0.025188
26	C	-0.05933	-1.75723	0.025799
27	C	2.384599	-2.17087	0.038608
28	C	2.595356	-3.0444	-1.02611
29	C	3.268897	-2.11677	1.115485
30	C	3.708977	-3.8814	-1.00708
31	H	1.889459	-3.06198	-1.84996
32	C	4.388805	-2.94724	1.117208
33	H	3.073327	-1.44242	1.944274
34	C	4.607473	-3.82983	0.059586
35	H	3.877848	-4.5685	-1.82942

36	H	5.081842	-2.91046	1.950919
37	H	5.476944	-4.47879	0.067222
38	H	4.790057	1.856485	-0.1785
39	C	-6.37809	-0.0171	0.02726
40	O	-7.14037	-0.96272	0.01467
41	O	-6.81183	1.252371	0.047639
42	H	-7.7825	1.242233	0.049852
43	H	3.280603	0.176385	-0.09094

*B-2.2.20 – 4-Cyanophenyl Nitron **(33j)** (zwitterionic form)*

M1				
Tag	**Symbol**	**X**	**Y**	**Z**
1	C	2.361773	2.113976	-0.09078
2	C	1.366256	3.123603	-0.05919
3	C	3.712481	2.539685	-0.16643
4	C	1.720133	4.477119	-0.09778
5	H	0.322341	2.844709	-0.00425
6	C	4.053135	3.888877	-0.20645
7	C	3.057397	4.876178	-0.17145
8	H	0.932875	5.227014	-0.07062
9	H	5.100652	4.174047	-0.26461
10	H	3.320597	5.929439	-0.20198
11	N	2.15771	0.739555	-0.04661
12	C	0.981497	0.17736	-0.01179
13	C	-2.51752	-0.31119	-0.00184
14	C	-3.34121	-1.38314	-0.37122
15	C	-3.06436	0.921327	0.37422
16	C	-4.72143	-1.22791	-0.33912
17	H	-2.92245	-2.32698	-0.70006
18	C	-4.44596	1.077491	0.3977
19	H	-2.40894	1.738093	0.646577
20	C	-5.28241	0.003582	0.046465
21	H	-5.3632	-2.05337	-0.62516
22	H	-4.8766	2.027928	0.692047
23	N	-0.28636	0.658871	-0.03744
24	N	-1.10551	-0.45569	-0.01239
25	N	0.890871	-1.25977	0.04324
26	C	-0.40589	-1.58146	0.040258
27	H	-0.80167	-2.58178	0.110442
28	C	1.972738	-2.20043	0.063999

29	C	2.075472	-3.14615	-0.95964
30	C	2.895174	-2.16646	1.113419
31	C	3.113094	-4.082	-0.92223
32	H	1.360604	-3.14421	-1.77636
33	C	3.932903	-3.09943	1.135036
34	H	2.797401	-1.4218	1.894719
35	C	4.042405	-4.05821	0.121222
36	H	3.196103	-4.82104	-1.71281
37	H	4.652497	-3.08018	1.947482
38	H	4.850451	-4.78282	0.145108
39	H	4.48632	1.777376	-0.19216
40	C	-6.70602	0.164659	0.073388
41	N	-7.86313	0.295424	0.096751

M3				
Tag	**Symbol**	**X**	**Y**	**Z**
1	C	2.361093	2.113402	-0.09164
2	C	1.365705	3.123146	-0.05439
3	C	3.711585	2.53961	-0.17115
4	C	1.719438	4.476798	-0.09114
5	H	0.321947	2.844301	0.00371
6	C	4.052048	3.888917	-0.20952
7	C	3.056415	4.876178	-0.16876
8	H	0.93221	5.22654	-0.05939
9	H	5.099357	4.174207	-0.27076
10	H	3.319468	5.929507	-0.19786
11	N	2.157396	0.738965	-0.04918
12	C	0.98067	0.176567	-0.01344
13	C	-2.51817	-0.31195	-0.00336
14	C	-3.34124	-1.38239	-0.37829
15	C	-3.06538	0.918591	0.378574
16	C	-4.72154	-1.22778	-0.34575
17	H	-2.92187	-2.32434	-0.71175
18	C	-4.44702	1.074249	0.402444
19	H	-2.41048	1.734283	0.655397
20	C	-5.28288	0.001665	0.045741
21	H	-5.36288	-2.05209	-0.63599
22	H	-4.87801	2.023055	0.701456
23	N	-0.28675	0.658341	-0.03874
24	N	-1.10608	-0.45631	-0.01394
25	N	0.890229	-1.25993	0.04145

26	C	-0.40639	-1.582	0.038326
27	H	-0.80208	-2.58249	0.107344
28	C	1.973211	-2.19971	0.064276
29	C	2.0897	-3.13328	-0.96884
30	C	2.882926	-2.17597	1.124983
31	C	3.129217	-4.06708	-0.93017
32	H	1.38331	-3.12419	-1.79283
33	C	3.922629	-3.10676	1.148059
34	H	2.773781	-1.44111	1.914159
35	C	4.046292	-4.05322	0.124266
36	H	3.222933	-4.7971	-1.72789
37	H	4.632386	-3.09572	1.969258
38	H	4.855601	-4.77637	0.149274
39	H	4.485658	1.777626	-0.201
40	C	-6.70653	0.162228	0.073205
41	N	-7.86367	0.292745	0.097021

M4				
Tag	**Symbol**	**X**	**Y**	**Z**
1	C	2.332673	2.108931	-0.10736
2	C	1.32482	3.096441	-0.03266
3	C	3.669999	2.555652	-0.21485
4	C	1.657303	4.453249	-0.06139
5	H	0.286498	2.804275	0.04987
6	C	3.988223	3.906106	-0.24587
7	C	2.980571	4.874219	-0.16832
8	H	0.859907	5.189206	0.000329
9	H	5.028428	4.208432	-0.32992
10	H	3.225537	5.931216	-0.19144
11	N	2.157686	0.7323	-0.07112
12	C	0.983578	0.170133	-0.03259
13	C	-2.49802	-0.3166	-0.01405
14	C	-3.31342	-1.37996	-0.40476
15	C	-3.03417	0.90522	0.391272
16	C	-4.69124	-1.22649	-0.36113
17	H	-2.89011	-2.31242	-0.76012
18	C	-4.41356	1.05856	0.424749
19	H	-2.37249	1.713358	0.676774
20	C	-5.24125	-0.0076	0.054841
21	H	-5.33799	-2.04258	-0.66206
22	H	-4.84813	1.999982	0.741029

23	N	-0.27814	0.645064	-0.06035
24	N	-1.087	-0.46176	-0.03187
25	N	0.89727	-1.25701	0.027231
26	C	-0.3949	-1.58266	0.026876
27	H	-0.79247	-2.58307	0.108031
28	C	1.980113	-2.18745	0.062057
29	C	1.995069	-3.2444	-0.84506
30	C	2.98492	-2.03107	1.015314
31	C	3.032491	-4.17404	-0.78441
32	H	1.213009	-3.33197	-1.59318
33	C	4.021239	-2.95912	1.057065
34	H	2.94895	-1.19196	1.700076
35	C	4.045593	-4.03087	0.162079
36	H	3.050472	-5.00197	-1.48501
37	H	4.809006	-2.84745	1.794542
38	H	4.855495	-4.75172	0.20216
39	H	4.45187	1.803486	-0.2719
40	C	-6.67103	0.152047	0.093529
41	N	-7.82153	0.280166	0.125937

M5				
Tag	**Symbol**	**X**	**Y**	**Z**
1	C	2.331675	2.10903	-0.10814
2	C	1.323815	3.09609	-0.02549
3	C	3.668114	2.556904	-0.22342
4	C	1.655396	4.45316	-0.05425
5	H	0.286167	2.803425	0.06364
6	C	3.985389	3.907609	-0.25468
7	C	2.977711	4.875121	-0.16934
8	H	0.857986	5.188535	0.013914
9	H	5.02488	4.210601	-0.34494
10	H	3.221935	5.93228	-0.19254
11	N	2.157729	0.732372	-0.07223
12	C	0.983378	0.169586	-0.03204
13	C	-2.49797	-0.31727	-0.01406
14	C	-3.31243	-1.37842	-0.41244
15	C	-3.03468	0.901927	0.398338
16	C	-4.69038	-1.22557	-0.36928
17	H	-2.88817	-2.30832	-0.77335
18	C	-4.41411	1.0548	0.431242
19	H	-2.37362	1.708429	0.689919

20	C	-5.24099	-0.00938	0.053728
21	H	-5.33653	-2.03994	-0.67605
22	H	-4.84924	1.994062	0.753094
23	N	-0.27795	0.644629	-0.05979
24	N	-1.08685	-0.46227	-0.03117
25	N	0.897396	-1.25707	0.028482
26	C	-0.39473	-1.58307	0.028087
27	H	-0.79239	-2.5835	0.109324
28	C	1.980866	-2.18697	0.063506
29	C	2.00038	-3.23978	-0.84823
30	C	2.981603	-2.03376	1.021556
31	C	3.038918	-4.16829	-0.78782
32	H	1.220713	-3.32537	-1.59905
33	C	4.019095	-2.96054	1.063094
34	H	2.941328	-1.19845	1.710774
35	C	4.048284	-4.02805	0.163122
36	H	3.060442	-4.99329	-1.49177
37	H	4.803646	-2.8515	1.804385
38	H	4.858865	-4.74814	0.203134
39	H	4.450313	1.805488	-0.28623
40	C	-6.67083	0.149814	0.091865
41	N	-7.82138	0.277762	0.123806

*B-2.2.21 – 4-Cyanophenyl Nitron **(33j)** (carbenic form)*

M1				
Tag	**Symbol**	**X**	**Y**	**Z**
1	C	2.337038	2.12314	-0.04506
2	C	1.328188	3.099117	-0.01709
3	C	3.685928	2.521158	-0.09578
4	C	1.68047	4.452944	-0.03866
5	H	0.288678	2.803929	0.02029
6	C	4.018863	3.873493	-0.11666
7	C	3.017647	4.851998	-0.08793
8	H	0.891201	5.198953	-0.01641
9	H	5.065181	4.161685	-0.15582
10	H	3.278122	5.905607	-0.10435
11	N	2.079622	0.738372	-0.02186
12	C	0.886938	0.084411	0.005089
13	C	-2.53999	-0.36666	0.014989
14	C	-3.38335	-1.48949	-0.01338
15	C	-3.08461	0.925155	0.04564

16	C	-4.76077	-1.3195	-0.00888
17	H	-2.9523	-2.48201	-0.03809
18	C	-4.4654	1.094199	0.049454
19	H	-2.42896	1.785269	0.06702
20	C	-5.3152	-0.02501	0.022695
21	H	-5.41079	-2.18728	-0.03085
22	H	-4.88541	2.093767	0.073889
23	N	-0.31822	0.596939	-0.00119
24	N	-1.1359	-0.542	0.012256
25	N	0.823018	-1.31461	0.028078
26	C	-0.48331	-1.72742	0.027616
27	C	1.955211	-2.20049	0.031394
28	C	2.232646	-2.96358	-1.10648
29	C	2.759197	-2.29185	1.172176
30	C	3.326738	-3.83184	-1.09783
31	H	1.594655	-2.87643	-1.97966
32	C	3.85867	-3.15505	1.16721
33	H	2.519274	-1.70549	2.05374
34	C	4.141652	-3.9256	0.035415
35	H	3.543433	-4.43061	-1.97692
36	H	4.484644	-3.23064	2.050708
37	H	4.993288	-4.59887	0.036967
38	H	4.469756	1.768621	-0.1193
39	H	2.89504	0.139392	-0.03551
40	C	-6.7359	0.149125	0.026679
41	N	-7.89277	0.290524	0.029941

M3				
Tag	**Symbol**	**X**	**Y**	**Z**
1	C	2.336697	2.123095	-0.04458
2	C	1.327596	3.09899	-0.02046
3	C	3.685747	2.521371	-0.09051
4	C	1.679671	4.452926	-0.0412
5	H	0.287953	2.803826	0.013381
6	C	4.018437	3.873797	-0.11066
7	C	3.016957	4.852199	-0.08586
8	H	0.890162	5.198769	-0.02197
9	H	5.064853	4.162121	-0.14607
10	H	3.27733	5.905846	-0.10169
11	N	2.07927	0.73833	-0.02251
12	C	0.886697	0.08438	0.003968

13	C	-2.54021	-0.36731	0.014322
14	C	-3.38355	-1.49014	-0.01558
15	C	-3.08494	0.924455	0.046794
16	C	-4.76098	-1.32031	-0.01066
17	H	-2.95264	-2.48267	-0.04183
18	C	-4.46573	1.09343	0.050991
19	H	-2.42946	1.784662	0.069356
20	C	-5.31542	-0.02585	0.022792
21	H	-5.41086	-2.18814	-0.03381
22	H	-4.88572	2.092957	0.076882
23	N	-0.31867	0.596636	-0.00244
24	N	-1.13611	-0.54244	0.011333
25	N	0.823064	-1.3146	0.027051
26	C	-0.48304	-1.72766	0.026965
27	C	1.955784	-2.20008	0.030714
28	C	2.240982	-2.95395	-1.11139
29	C	2.752422	-2.29971	1.175907
30	C	3.335492	-3.82173	-1.10245
31	H	1.608879	-2.85999	-1.98816
32	C	3.852238	-3.16249	1.171386
33	H	2.506971	-1.71955	2.060034
34	C	4.142895	-3.92406	0.035434
35	H	3.558411	-4.41331	-1.98484
36	H	4.472728	-3.24444	2.058168
37	H	4.994899	-4.59687	0.037246
38	H	4.469925	1.769131	-0.11072
39	H	2.894662	0.139239	-0.03478
40	C	-6.73609	0.148151	0.027208
41	N	-7.893	0.289407	0.030842

M4				
Tag	**Symbol**	**X**	**Y**	**Z**
1	C	2.303098	2.119527	-0.06105
2	C	1.279831	3.072104	0.007048
3	C	3.639242	2.539956	-0.14603
4	C	1.608719	4.429096	-0.00986
5	H	0.246263	2.761382	0.071705
6	C	3.947236	3.893994	-0.1623
7	C	2.932397	4.851563	-0.09402
8	H	0.808052	5.160296	0.04389
9	H	4.98618	4.200921	-0.22873

10	H	3.173218	5.909116	-0.10694
11	N	2.075318	0.733765	-0.04127
12	C	0.887928	0.075241	-0.00585
13	C	-2.52128	-0.37993	0.013552
14	C	-3.35567	-1.50364	0.006519
15	C	-3.05917	0.909473	0.026816
16	C	-4.73074	-1.33418	0.014547
17	H	-2.92028	-2.49479	-0.00445
18	C	-4.43806	1.076084	0.034247
19	H	-2.40075	1.768407	0.031656
20	C	-5.27717	-0.04311	0.028532
21	H	-5.3838	-2.19978	0.009517
22	H	-4.86334	2.073533	0.044864
23	N	-0.31476	0.576877	-0.01232
24	N	-1.11795	-0.55337	0.007075
25	N	0.830923	-1.31472	0.023151
26	C	-0.47044	-1.73555	0.024957
27	C	1.966416	-2.18588	0.036494
28	C	2.163779	-3.06342	-1.02739
29	C	2.851496	-2.14376	1.113246
30	C	3.264947	-3.91675	-1.00761
31	H	1.457196	-3.07173	-1.85078
32	C	3.958936	-2.9907	1.115639
33	H	2.665697	-1.46613	1.9416
34	C	4.164352	-3.87732	0.058762
35	H	3.423315	-4.60728	-1.82917
36	H	4.652415	-2.96366	1.949359
37	H	5.02404	-4.53918	0.066914
38	H	4.433062	1.799764	-0.19874
39	H	2.89722	0.145387	-0.09679
40	C	-6.70431	0.130327	0.036633
41	N	-7.85464	0.269601	0.043183

M5				
Tag	**Symbol**	**X**	**Y**	**Z**
1	C	2.302676	2.119925	-0.0613
2	C	1.279092	3.072277	0.006249
3	C	3.638802	2.540752	-0.14554
4	C	1.607568	4.429423	-0.01051
5	H	0.245509	2.761478	0.070422
6	C	3.94635	3.894915	-0.16167

7	C	2.931191	4.852258	-0.09397
8	H	0.806631	5.160362	0.042821
9	H	4.98526	4.202097	-0.2275
10	H	3.171742	5.909879	-0.10677
11	N	2.075277	0.73411	-0.04178
12	C	0.888158	0.075346	-0.00636
13	C	-2.5211	-0.38027	0.013307
14	C	-3.35548	-1.50399	0.004829
15	C	-3.05904	0.909132	0.028157
16	C	-4.73056	-1.33466	0.013124
17	H	-2.9203	-2.49519	-0.0075
18	C	-4.43794	1.075703	0.035807
19	H	-2.4008	1.768195	0.03411
20	C	-5.27696	-0.04358	0.02874
21	H	-5.38351	-2.20033	0.006971
22	H	-4.86318	2.073144	0.047679
23	N	-0.31472	0.576759	-0.01305
24	N	-1.11775	-0.55358	0.006691
25	N	0.831363	-1.3146	0.022989
26	C	-0.46987	-1.73554	0.025086
27	C	1.966942	-2.18578	0.036513
28	C	2.164679	-3.06294	-1.02764
29	C	2.851477	-2.14403	1.113701
30	C	3.265661	-3.91653	-1.00753
31	H	1.458856	-3.07056	-1.8517
32	C	3.958759	-2.99121	1.11639
33	H	2.665727	-1.46631	1.941982
34	C	4.164475	-3.87764	0.059398
35	H	3.424466	-4.60669	-1.82932
36	H	4.651982	-2.96426	1.950313
37	H	5.024098	-4.53957	0.067747
38	H	4.432934	1.800878	-0.19772
39	H	2.897467	0.145964	-0.09605
40	C	-6.70407	0.129754	0.037107
41	N	-7.85443	0.268884	0.043889

*B-2.2.22 – Benzyl Nitron **(33k)** (zwitterionic form)*

M1				
Tag	**Symbol**	**X**	**Y**	**Z**
1	C	-1.19628	2.456387	0.083008
2	C	0.021232	3.083868	-0.28974
3	C	-2.22407	3.295573	0.587426
4	C	0.182607	4.46795	-0.15869
5	H	0.83295	2.48443	-0.67988
6	C	-2.05182	4.670972	0.714881
7	C	-0.842	5.275892	0.342107
8	H	1.128609	4.9163	-0.45421
9	H	-2.86503	5.276943	1.107108
10	H	-0.70496	6.348814	0.440731
11	N	-1.49822	1.104095	0.002719
12	C	-0.6549	0.189598	-0.40458
13	N	0.639352	0.229606	-0.81487
14	N	0.978474	-1.07502	-1.08533
15	N	-1.07376	-1.1819	-0.45408
16	C	-0.0202	-1.90538	-0.87562
17	H	-0.00663	-2.97289	-1.03229
18	C	-2.35145	-1.71698	-0.08851
19	C	-2.43584	-2.63357	0.963271
20	C	-3.49197	-1.32755	-0.79674
21	C	-3.67915	-3.17634	1.301073
22	H	-1.54219	-2.91274	1.512526
23	C	-4.73052	-1.86614	-0.44397
24	H	-3.40496	-0.61398	-1.60815
25	C	-4.82636	-2.79152	0.601793
26	H	-3.74819	-3.89162	2.114678
27	H	-5.61958	-1.56709	-0.99046
28	H	-5.79176	-3.20973	0.86978
29	H	-3.1632	2.831377	0.876424
30	C	2.326187	-1.40287	-1.56894
31	H	2.496951	-0.80539	-2.46744
32	H	2.301066	-2.45672	-1.85594
33	C	3.403651	-1.14174	-0.53538
34	C	4.26951	-0.05033	-0.67615
35	C	3.555451	-1.99817	0.564961
36	C	5.270351	0.187597	0.271652
37	H	4.161981	0.615538	-1.52807
38	C	4.551408	-1.76016	1.514595

39	H	2.896423	-2.85502	0.679587
40	C	5.411331	-0.66542	1.369698
41	H	5.936121	1.037085	0.151377
42	H	4.660414	-2.4306	2.361957
43	H	6.188043	-0.48221	2.106277

M3				
Tag	**Symbol**	**X**	**Y**	**Z**
1	C	-1.1821	2.459422	0.082231
2	C	0.038859	3.079664	-0.29184
3	C	-2.20448	3.305373	0.58676
4	C	0.208505	4.462923	-0.16193
5	H	0.846721	2.475393	-0.68251
6	C	-2.02402	4.679829	0.71312
7	C	-0.81087	5.27737	0.339056
8	H	1.156869	4.905412	-0.45869
9	H	-2.83342	5.290842	1.105387
10	H	-0.66743	6.34953	0.436708
11	N	-1.49234	1.108981	0.003157
12	C	-0.65398	0.189014	-0.40395
13	N	0.640376	0.221905	-0.81333
14	N	0.9726	-1.0849	-1.0831
15	N	-1.08054	-1.17953	-0.45325
16	C	-0.03096	-1.90931	-0.87372
17	H	-0.02338	-2.97704	-1.02933
18	C	-2.36172	-1.70707	-0.08806
19	C	-2.4534	-2.61325	0.972021
20	C	-3.49783	-1.32073	-0.80504
21	C	-3.70006	-3.14824	1.310025
22	H	-1.56266	-2.89095	1.526691
23	C	-4.73977	-1.85156	-0.45224
24	H	-3.40484	-0.61615	-1.62368
25	C	-4.84305	-2.76621	0.602266
26	H	-3.77493	-3.85573	2.12989
27	H	-5.62547	-1.55527	-1.00563
28	H	-5.81094	-3.17867	0.870139
29	H	-3.14637	2.847284	0.876592
30	C	2.318747	-1.42038	-1.56602
31	H	2.491395	-0.82843	-2.46781
32	H	2.289293	-2.47561	-1.84726
33	C	3.397443	-1.15758	-0.53412

34	C	4.26882	-0.0715	-0.6824
35	C	3.544696	-2.00691	0.572379
36	C	5.270639	0.168266	0.263993
37	H	4.165087	0.588613	-1.53928
38	C	4.541642	-1.76702	1.520569
39	H	2.88151	-2.85971	0.692881
40	C	5.407083	-0.6776	1.368174
41	H	5.940841	1.013389	0.137684
42	H	4.64717	-2.43204	2.372623
43	H	6.18461	-0.49313	2.103582

M4

Tag	Symbol	X	Y	Z
1	C	-1.03778	2.478419	0.06562
2	C	0.231087	3.017608	-0.24944
3	C	-2.0242	3.382128	0.527655
4	C	0.478317	4.385279	-0.10495
5	H	1.019831	2.368325	-0.60447
6	C	-1.7672	4.738662	0.666286
7	C	-0.5067	5.258656	0.349736
8	H	1.464482	4.767753	-0.35562
9	H	-2.55382	5.39754	1.023877
10	H	-0.30175	6.319024	0.45664
11	N	-1.43072	1.15232	-0.02565
12	C	-0.63362	0.204673	-0.44371
13	N	0.646304	0.188678	-0.87313
14	N	0.919099	-1.11661	-1.15686
15	N	-1.10978	-1.13802	-0.48843
16	C	-0.10126	-1.90444	-0.93227
17	H	-0.13457	-2.97178	-1.09519
18	C	-2.39337	-1.61665	-0.09023
19	C	-2.47201	-2.67405	0.813809
20	C	-3.54162	-1.03413	-0.62449
21	C	-3.72466	-3.16741	1.176703
22	H	-1.565	-3.09795	1.234081
23	C	-4.78704	-1.52627	-0.24414
24	H	-3.44836	-0.2066	-1.31796
25	C	-4.88125	-2.59292	0.652236
26	H	-3.79237	-3.99273	1.877516
27	H	-5.68642	-1.07855	-0.65378
28	H	-5.85522	-2.97322	0.942148

29	H	-3.00253	2.97893	0.774215
30	C	2.252409	-1.49051	-1.62607
31	H	2.460278	-0.89094	-2.51472
32	H	2.199966	-2.54315	-1.91252
33	C	3.291541	-1.25992	-0.55387
34	C	4.170258	-0.17966	-0.63847
35	C	3.364861	-2.12506	0.541485
36	C	5.116533	0.036033	0.364374
37	H	4.112622	0.495093	-1.48837
38	C	4.306179	-1.9094	1.545119
39	H	2.683999	-2.97054	0.608107
40	C	5.184288	-0.82733	1.456865
41	H	5.79743	0.878047	0.291852
42	H	4.358627	-2.58606	2.392012
43	H	5.91997	-0.66004	2.237101

M5				
Tag	**Symbol**	**X**	**Y**	**Z**
1	C	-1.02561	2.479408	0.066845
2	C	0.241546	3.014248	-0.26272
3	C	-2.00348	3.386981	0.539788
4	C	0.495466	4.381037	-0.12098
5	H	1.023594	2.362393	-0.62766
6	C	-1.73976	4.742499	0.675959
7	C	-0.48094	5.257927	0.345428
8	H	1.480002	4.759913	-0.38322
9	H	-2.51987	5.404202	1.042472
10	H	-0.27081	6.317464	0.450403
11	N	-1.42468	1.155033	-0.02131
12	C	-0.63247	0.202985	-0.4403
13	N	0.647591	0.180443	-0.86804
14	N	0.91424	-1.12668	-1.15072
15	N	-1.11547	-1.13669	-0.48494
16	C	-0.11055	-1.90888	-0.9268
17	H	-0.14925	-2.97632	-1.0881
18	C	-2.4035	-1.6071	-0.09054
19	C	-2.49214	-2.6541	0.824451
20	C	-3.54569	-1.02658	-0.63974
21	C	-3.74927	-3.13855	1.184186
22	H	-1.58944	-3.07729	1.254571
23	C	-4.79567	-1.50958	-0.26263

24	H	-3.44444	-0.20819	-1.34299
25	C	-4.89998	-2.56556	0.64529
26	H	-3.82503	-3.95604	1.893279
27	H	-5.69049	-1.06362	-0.68399
28	H	-5.87737	-2.93906	0.932501
29	H	-2.98084	2.987922	0.796832
30	C	2.245609	-1.50734	-1.61982
31	H	2.45459	-0.91347	-2.51204
32	H	2.189276	-2.56127	-1.9006
33	C	3.286999	-1.27408	-0.5503
34	C	4.182807	-0.20958	-0.65302
35	C	3.346195	-2.12127	0.559972
36	C	5.132546	0.008126	0.346267
37	H	4.136276	0.451239	-1.51448
38	C	4.290805	-1.90343	1.560005
39	H	2.651679	-2.95428	0.64096
40	C	5.186427	-0.83735	1.453415
41	H	5.827026	0.837587	0.259272
42	H	4.332286	-2.56615	2.418448
43	H	5.924801	-0.66871	2.230818

*B-2.2.23 – Benzyl Nitron (**33k**) (carbenic form)*

M1				
Tag	**Symbol**	**X**	**Y**	**Z**
1	C	-1.27502	2.420686	0.080224
2	C	-0.07519	3.063657	-0.2662
3	C	-2.35954	3.187008	0.548589
4	C	0.022436	4.453749	-0.14115
5	H	0.7637	2.484177	-0.62625
6	C	-2.24465	4.570014	0.66759
7	C	-1.05109	5.216628	0.323165
8	H	0.95602	4.938451	-0.41267
9	H	-3.09256	5.143252	1.030976
10	H	-0.96263	6.294499	0.416243
11	N	-1.46642	1.030758	-0.01427
12	C	-0.59693	0.064276	-0.43269
13	N	0.646768	0.208853	-0.82477
14	N	1.032344	-1.10296	-1.11048
15	N	-0.9669	-1.27957	-0.47691
16	C	0.100277	-2.04462	-0.91578

17	C	-2.25177	-1.80628	-0.11375
18	C	-2.37516	-2.58371	1.042141
19	C	-3.36468	-1.54392	-0.92031
20	C	-3.62363	-3.10491	1.389829
21	H	-1.49971	-2.77609	1.653469
22	C	-4.61291	-2.05876	-0.55819
23	H	-3.25092	-0.95439	-1.8249
24	C	-4.74326	-2.84012	0.593869
25	H	-3.72129	-3.71291	2.283877
26	H	-5.47767	-1.85698	-1.18259
27	H	-5.71292	-3.24323	0.869482
28	H	-3.29033	2.694633	0.818289
29	C	2.397314	-1.32211	-1.58117
30	H	2.564712	-0.68907	-2.4572
31	H	2.431742	-2.36573	-1.90246
32	C	3.453693	-1.04541	-0.52627
33	C	4.471312	-0.11508	-0.7695
34	C	3.443412	-1.73739	0.694352
35	C	5.464953	0.121882	0.187544
36	H	4.48826	0.428885	-1.71054
37	C	4.430228	-1.49972	1.653344
38	H	2.658131	-2.4618	0.894038
39	C	5.445561	-0.56873	1.401952
40	H	6.247492	0.847286	-0.01558
41	H	4.410064	-2.04211	2.594304
42	H	6.213748	-0.38488	2.147431
43	H	-2.37863	0.693582	0.263434

M3				
Tag	**Symbol**	**X**	**Y**	**Z**
1	C	-1.27124	2.421294	0.078656
2	C	-0.0707	3.062614	-0.26852
3	C	-2.35444	3.189185	0.547575
4	C	0.029003	4.452628	-0.14367
5	H	0.767144	2.482086	-0.62932
6	C	-2.23752	4.572052	0.666339
7	C	-1.04321	5.217021	0.321209
8	H	0.963048	4.936035	-0.41592
9	H	-3.08445	5.146494	1.030097
10	H	-0.95324	6.294782	0.414079
11	N	-1.46478	1.031673	-0.01566

12	C	-0.59655	0.063708	-0.43285
13	N	0.647684	0.205961	-0.82448
14	N	1.031167	-1.10659	-1.10961
15	N	-0.96874	-1.27942	-0.47667
16	C	0.097198	-2.04636	-0.91487
17	C	-2.25475	-1.80363	-0.11322
18	C	-2.38188	-2.5697	1.049834
19	C	-3.3647	-1.54971	-0.92649
20	C	-3.63132	-3.08835	1.397933
21	H	-1.50871	-2.75518	1.666585
22	C	-4.61389	-2.06208	-0.56417
23	H	-3.24798	-0.96806	-1.83577
24	C	-4.74801	-2.83226	0.595008
25	H	-3.73205	-3.68742	2.297645
26	H	-5.47649	-1.86676	-1.19355
27	H	-5.71846	-3.23325	0.87093
28	H	-3.28573	2.698099	0.817754
29	C	2.395904	-1.32815	-1.57991
30	H	2.564075	-0.69724	-2.45733
31	H	2.429388	-2.37247	-1.89904
32	C	3.452389	-1.05023	-0.52544
33	C	4.471836	-0.12249	-0.77117
34	C	3.440289	-1.73831	0.697403
35	C	5.465493	0.115677	0.185617
36	H	4.490321	0.418369	-1.71396
37	C	4.427164	-1.49947	1.656094
38	H	2.653602	-2.46063	0.899152
39	C	5.444321	-0.5711	1.402212
40	H	6.249483	0.838947	-0.01947
41	H	4.405589	-2.03886	2.598734
42	H	6.212542	-0.38635	2.147422
43	H	-2.37782	0.696097	0.261421

M4				
Tag	**Symbol**	**X**	**Y**	**Z**
1	C	-1.29198	2.390502	0.052534
2	C	-0.10899	3.040658	-0.31928
3	C	-2.37263	3.143168	0.539195
4	C	-0.02605	4.429501	-0.20051
5	H	0.73062	2.472029	-0.69392
6	C	-2.2713	4.523606	0.65152

7	C	-1.09476	5.180066	0.281614
8	H	0.895886	4.923333	-0.49204
9	H	-3.11743	5.088438	1.029971
10	H	-1.01602	6.258358	0.369276
11	N	-1.47349	1.002643	-0.03552
12	C	-0.58874	0.058406	-0.46296
13	N	0.641896	0.22614	-0.8656
14	N	1.047133	-1.064	-1.15474
15	N	-0.92735	-1.28538	-0.50182
16	C	0.147729	-2.02868	-0.94639
17	C	-2.19381	-1.83107	-0.127
18	C	-2.2608	-2.73137	0.934859
19	C	-3.34109	-1.45958	-0.8282
20	C	-3.49435	-3.26954	1.294833
21	H	-1.35151	-3.00159	1.461869
22	C	-4.57353	-1.99045	-0.44971
23	H	-3.26364	-0.77357	-1.66691
24	C	-4.65063	-2.89591	0.608271
25	H	-3.5526	-3.97524	2.116843
26	H	-5.46935	-1.70419	-0.99056
27	H	-5.61028	-3.31225	0.896292
28	H	-3.29112	2.638994	0.827522
29	C	2.417891	-1.25118	-1.58959
30	H	2.604062	-0.59946	-2.44775
31	H	2.48858	-2.28912	-1.92405
32	C	3.424275	-0.97259	-0.49157
33	C	4.693282	-0.49491	-0.82645
34	C	3.121573	-1.22237	0.849383
35	C	5.652829	-0.27988	0.162914
36	H	4.932036	-0.28742	-1.8666
37	C	4.077734	-1.00342	1.840127
38	H	2.132783	-1.5841	1.119844
39	C	5.34686	-0.53362	1.499722
40	H	6.635148	0.092588	-0.11048
41	H	3.830506	-1.19802	2.879153
42	H	6.090035	-0.36153	2.271839
43	H	-2.36621	0.648817	0.28352

M5				
Tag	**Symbol**	**X**	**Y**	**Z**
1	C	-1.29635	2.389027	0.052689

2	C	-0.11549	3.041933	-0.32126
3	C	-2.37808	3.139335	0.540708
4	C	-0.03563	4.431074	-0.2032
5	H	0.724859	2.475355	-0.69731
6	C	-2.27983	4.520075	0.652276
7	C	-1.10539	5.179253	0.280326
8	H	0.884613	4.927023	-0.49652
9	H	-3.12676	5.083028	1.031721
10	H	-1.02913	6.257771	0.367406
11	N	-1.47475	1.000712	-0.03439
12	C	-0.58857	0.058369	-0.46262
13	N	0.641849	0.228419	-0.86543
14	N	1.049178	-1.06082	-1.15566
15	N	-0.92485	-1.28591	-0.5023
16	C	0.151312	-2.02695	-0.94763
17	C	-2.19028	-1.8341	-0.12719
18	C	-2.25551	-2.73247	0.936437
19	C	-3.33796	-1.46678	-0.82988
20	C	-3.48791	-3.27328	1.296553
21	H	-1.346	-2.99885	1.465028
22	C	-4.56926	-2.00026	-0.45125
23	H	-3.26186	-0.78161	-1.66939
24	C	-4.64465	-2.90405	0.608322
25	H	-3.54493	-3.97736	2.120026
26	H	-5.46549	-1.71711	-0.99301
27	H	-5.60341	-3.32231	0.89651
28	H	-3.29491	2.633064	0.830525
29	C	2.420351	-1.24549	-1.5902
30	H	2.606097	-0.59239	-2.44738
31	H	2.492872	-2.28277	-1.9263
32	C	3.425918	-0.96727	-0.49127
33	C	4.697648	-0.49664	-0.82618
34	C	3.120092	-1.2103	0.850238
35	C	5.656747	-0.28217	0.163724
36	H	4.93885	-0.29442	-1.8668
37	C	4.075943	-0.99188	1.841553
38	H	2.129294	-1.56627	1.120999
39	C	5.347706	-0.52928	1.501157
40	H	6.641164	0.084664	-0.10973
41	H	3.826273	-1.18125	2.880955
42	H	6.090591	-0.35763	2.273648
43	H	-2.36706	0.645289	0.2842

*B-2.2.24 – Tri-(trifluoromethylphenyl) Nitron (**33l**) (zwitterionic form)*

M1				
Tag	**Symbol**	**X**	**Y**	**Z**
1	C	1.337409	2.246845	-0.03259
2	C	0.144998	3.018287	-0.01329
3	C	2.565987	2.958625	-0.09021
4	C	0.19242	4.411033	-0.0493
5	H	-0.81509	2.522471	0.026208
6	C	2.609054	4.34339	-0.12668
7	C	1.416031	5.087532	-0.11038
8	H	-0.73697	4.971648	-0.03495
9	H	3.56815	4.849967	-0.17313
10	N	1.436962	0.870495	0.001793
11	C	0.407105	0.063466	0.027279
12	C	-2.90725	-1.15577	0.020687
13	C	-3.48444	-2.32115	-0.49386
14	C	-3.69756	-0.12548	0.538029
15	C	-4.86916	-2.46475	-0.46578
16	H	-2.87483	-3.10398	-0.93016
17	C	-5.08243	-0.27267	0.552348
18	H	-3.22992	0.77051	0.925509
19	C	-5.6686	-1.44266	0.057545
20	H	-5.31921	-3.36734	-0.8628
21	H	-5.69888	0.521522	0.957996
22	N	-0.92986	0.262464	0.007036
23	N	-1.49159	-0.99819	0.015408
24	N	0.629619	-1.3563	0.058305
25	C	-0.57261	-1.95034	0.051004
26	C	1.884891	-2.03939	0.049055
27	C	2.114828	-3.03086	-0.90801
28	C	2.855758	-1.71805	1.002439
29	C	3.325958	-3.72275	-0.90279
30	H	1.36292	-3.25535	-1.65691
31	C	4.06732	-2.40383	0.997305
32	H	2.662422	-0.94509	1.735034
33	C	4.299899	-3.40764	0.04845
34	H	3.505403	-4.49551	-1.64121
35	H	4.821773	-2.16342	1.738072
36	H	3.487616	2.385223	-0.10888
37	C	5.629491	-4.11137	0.027752
38	C	1.466427	6.577974	-0.09699

39	F	6.572621	-3.40164	-0.65743
40	F	5.566396	-5.33022	-0.56297
41	F	6.13296	-4.30149	1.274667
42	F	0.31779	7.15604	-0.54192
43	F	2.476894	7.081323	-0.86304
44	F	1.675788	7.096908	1.158715
45	H	-0.75072	-3.01196	0.116759
46	C	-7.16641	-1.57513	0.031395
47	F	-7.70589	-1.06094	-1.11241
48	F	-7.76299	-0.91932	1.058879
49	F	-7.57505	-2.8673	0.095527

M3

Tag	Symbol	X	Y	Z
1	C	1.336575	2.245474	-0.03342
2	C	0.143823	3.016589	-0.00949
3	C	2.5646	2.958252	-0.09522
4	C	0.190398	4.409356	-0.04511
5	H	-0.81594	2.520443	0.033456
6	C	2.606805	4.343023	-0.1314
7	C	1.413423	5.086628	-0.11054
8	H	-0.73932	4.969338	-0.02695
9	H	3.565535	4.849997	-0.18106
10	N	1.436988	0.869415	0.000372
11	C	0.406833	0.061867	0.027812
12	C	-2.90721	-1.15754	0.022175
13	C	-3.48403	-2.32146	-0.49597
14	C	-3.69769	-0.1288	0.542384
15	C	-4.86878	-2.46519	-0.46875
16	H	-2.8742	-3.103	-0.93422
17	C	-5.08256	-0.27597	0.555673
18	H	-3.23038	0.766016	0.932984
19	C	-5.66841	-1.44457	0.05711
20	H	-5.31852	-3.36673	-0.86849
21	H	-5.69913	0.517034	0.963445
22	N	-0.92976	0.260994	0.008021
23	N	-1.49153	-0.99984	0.017501
24	N	0.629571	-1.35726	0.060153
25	C	-0.57237	-1.95174	0.053553
26	C	1.885484	-2.03967	0.050901
27	C	2.120797	-3.02181	-0.9143

28	C	2.851144	-1.72644	1.012148
29	C	3.332879	-3.71213	-0.91003
30	H	1.372025	-3.2406	-1.66798
31	C	4.063728	-2.41043	1.00619
32	H	2.652968	-0.96157	1.751995
33	C	4.302035	-3.40459	0.048564
34	H	3.516524	-4.47787	-1.65468
35	H	4.814204	-2.17646	1.753004
36	H	3.486684	2.385645	-0.11723
37	C	5.6328	-4.10599	0.026902
38	C	1.463048	6.576946	-0.09696
39	F	6.57725	-3.38902	-0.64931
40	F	5.574153	-5.32004	-0.57395
41	F	6.132521	-4.30534	1.273896
42	F	0.312569	7.154652	-0.53765
43	F	2.470573	7.081187	-0.86644
44	F	1.67662	7.096012	1.158146
45	H	-0.75009	-3.01344	0.119441
46	C	-7.16611	-1.57684	0.029756
47	F	-7.70512	-1.05886	-1.11279
48	F	-7.76344	-0.92419	1.058888
49	F	-7.57519	-2.86905	0.089444

M4				
Tag	**Symbol**	**X**	**Y**	**Z**
1	C	1.284987	2.24564	-0.05256
2	C	0.077882	2.975471	0.048245
3	C	2.487797	2.989376	-0.16055
4	C	0.086175	4.369228	0.041397
5	H	-0.86594	2.455033	0.13263
6	C	2.490861	4.37054	-0.16941
7	C	1.281482	5.072325	-0.06741
8	H	-0.85319	4.906924	0.121802
9	H	3.429868	4.910717	-0.25481
10	N	1.430553	0.8745	-0.04454
11	C	0.412513	0.055384	-0.0119
12	C	-2.86884	-1.20152	-0.0004
13	C	-3.42788	-2.37192	-0.50969
14	C	-3.65728	-0.17955	0.52402
15	C	-4.80777	-2.53181	-0.46756
16	H	-2.80814	-3.14348	-0.95244

17	C	-5.03711	-0.34371	0.551363
18	H	-3.18961	0.720266	0.904375
19	C	-5.60505	-1.51896	0.062274
20	H	-5.25689	-3.43821	-0.85791
21	H	-5.66514	0.439674	0.961478
22	N	-0.91989	0.23218	-0.0247
23	N	-1.45673	-1.02663	-0.01742
24	N	0.655325	-1.35053	0.014322
25	C	-0.5325	-1.96369	0.012657
26	C	1.921605	-2.00421	0.013983
27	C	2.147127	-3.04168	-0.88581
28	C	2.898435	-1.60223	0.92587
29	C	3.370754	-3.70719	-0.86457
30	H	1.38388	-3.32162	-1.60434
31	C	4.119853	-2.26104	0.934331
32	H	2.696509	-0.78555	1.607601
33	C	4.347878	-3.31162	0.042604
34	H	3.557724	-4.5198	-1.557
35	H	4.889665	-1.96453	1.639407
36	H	3.419488	2.437751	-0.23756
37	C	5.689784	-3.98605	0.058062
38	C	1.30998	6.563137	-0.07899
39	F	6.653045	-3.19683	-0.46159
40	F	5.70132	-5.12835	-0.6469
41	F	6.08537	-4.28773	1.309716
42	F	0.08788	7.11459	0.036778
43	F	1.850474	7.063108	-1.21619
44	F	2.059592	7.074725	0.926795
45	H	-0.69643	-3.02926	0.078495
46	C	-7.09956	-1.66681	0.04915
47	F	-7.64503	-1.14743	-1.07118
48	F	-7.68098	-1.03514	1.083786
49	F	-7.48427	-2.95355	0.100347

M5				
Tag	**Symbol**	**X**	**Y**	**Z**
1	C	1.282164	2.246675	-0.04934
2	C	0.073894	2.974898	0.051861
3	C	2.483588	2.992605	-0.15968
4	C	0.079792	4.368633	0.042962
5	H	-0.869	2.453164	0.138537

6	C	2.484256	4.373777	-0.17062
7	C	1.273766	5.073709	-0.06841
8	H	-0.86047	4.904705	0.123859
9	H	3.422367	4.915251	-0.25774
10	N	1.430087	0.876013	-0.03932
11	C	0.41291	0.055082	-0.00518
12	C	-2.86694	-1.2053	0.003884
13	C	-3.42334	-2.3766	-0.50611
14	C	-3.65765	-0.18385	0.525949
15	C	-4.80321	-2.53787	-0.46725
16	H	-2.80168	-3.1478	-0.94677
17	C	-5.03736	-0.34931	0.549866
18	H	-3.19195	0.716607	0.907247
19	C	-5.60281	-1.52547	0.059887
20	H	-5.25029	-3.44503	-0.85815
21	H	-5.66719	0.43368	0.957991
22	N	-0.91935	0.230556	-0.02008
23	N	-1.45494	-1.02884	-0.0103
24	N	0.657373	-1.3501	0.025027
25	C	-0.52972	-1.96473	0.023357
26	C	1.9245	-2.0024	0.026176
27	C	2.151511	-3.04045	-0.87355
28	C	2.899898	-1.59971	0.938179
29	C	3.375416	-3.70375	-0.85122
30	H	1.388246	-3.32256	-1.5912
31	C	4.123278	-2.25664	0.947517
32	H	2.696322	-0.78436	1.621029
33	C	4.352624	-3.30674	0.05675
34	H	3.56278	-4.51765	-1.54242
35	H	4.891371	-1.95973	1.653707
36	H	3.416446	2.442891	-0.23667
37	C	5.696456	-3.97767	0.051683
38	C	1.299645	6.56448	-0.08233
39	F	6.601676	-3.28206	-0.66889
40	F	5.650942	-5.21163	-0.4777
41	F	6.208017	-4.09476	1.290572
42	F	0.076767	7.114044	0.035338
43	F	1.83653	7.063838	-1.2216
44	F	2.050678	7.079113	0.920802
45	H	-0.69261	-3.03034	0.091176
46	C	-7.0971	-1.6745	0.043113
47	F	-7.64072	-1.15276	-1.07719

48	F	-7.68146	-1.04556	1.077914
49	F	-7.48131	-2.96151	0.090433

*B-2.2.25 – Tri-(trifluoromethylphenyl) Nitron (**33l**) (carbenic form)*

M1				
Tag	**Symbol**	**X**	**Y**	**Z**
1	C	1.332272	2.23363	-0.04201
2	C	0.138003	2.970962	0.022624
3	C	2.562446	2.914695	-0.12446
4	C	0.185905	4.364333	0.006352
5	H	-0.81345	2.46192	0.080995
6	C	2.599654	4.302167	-0.13995
7	C	1.407782	5.03791	-0.07759
8	H	-0.74309	4.922136	0.054725
9	H	3.556102	4.809012	-0.20652
10	N	1.378906	0.833481	-0.02709
11	C	0.348514	-0.0607	0.010951
12	C	-2.91834	-1.19914	0.030522
13	C	-3.51686	-2.46525	-0.04583
14	C	-3.71092	-0.04862	0.115074
15	C	-4.90308	-2.57405	-0.0342
16	H	-2.89608	-3.34962	-0.11093
17	C	-5.10015	-0.16566	0.124653
18	H	-3.24489	0.925757	0.175327
19	C	-5.70119	-1.42539	0.053127
20	H	-5.35968	-3.55619	-0.09133
21	H	-5.70825	0.7294	0.193361
22	N	-0.93437	0.192	0.010463
23	N	-1.5025	-1.08738	0.022369
24	N	0.572987	-1.44158	0.030447
25	C	-0.62531	-2.11369	0.030179
26	C	1.852583	-2.0878	0.032643
27	C	2.21871	-2.88193	-1.05738
28	C	2.71134	-1.92923	1.124794
29	C	3.455077	-3.52512	-1.05491
30	H	1.53811	-2.99571	-1.89349
31	C	3.953469	-2.56388	1.119998
32	H	2.407301	-1.33335	1.978924
33	C	4.321033	-3.36258	0.032429
34	H	3.73962	-4.14691	-1.89609

35	H	4.619392	-2.44761	1.967501
36	H	3.48968	2.352151	-0.18008
37	C	5.678205	-4.01301	0.011858
38	C	1.449491	6.534463	-0.04397
39	F	6.626747	-3.19492	-0.53051
40	F	5.696843	-5.15414	-0.72088
41	F	6.119516	-4.33263	1.254439
42	F	0.330587	7.103514	-0.56503
43	F	2.506275	7.044945	-0.73086
44	F	1.560386	7.027829	1.228832
45	C	-7.19546	-1.54984	0.012474
46	F	-7.67762	-1.60415	-1.26666
47	F	-7.82619	-0.50408	0.606027
48	F	-7.64238	-2.67814	0.625397
49	H	2.303553	0.425814	-0.0769

M3				
Tag	**Symbol**	**X**	**Y**	**Z**
1	C	1.330803	2.234323	-0.04304
2	C	0.135748	2.970736	0.018721
3	C	2.560641	2.916507	-0.12214
4	C	0.182446	4.364148	0.002917
5	H	-0.81551	2.461053	0.074668
6	C	2.596678	4.303993	-0.13726
7	C	1.403998	5.038774	-0.07778
8	H	-0.74722	4.92101	0.049137
9	H	3.552951	4.811519	-0.20109
10	N	1.37853	0.834324	-0.02848
11	C	0.348901	-0.06049	0.009579
12	C	-2.91719	-1.20106	0.030163
13	C	-3.51518	-2.46721	-0.04986
14	C	-3.71039	-0.0512	0.118605
15	C	-4.90135	-2.57683	-0.03778
16	H	-2.89418	-3.35116	-0.1183
17	C	-5.09955	-0.16898	0.128521
18	H	-3.24497	0.923294	0.181654
19	C	-5.69998	-1.42883	0.053477
20	H	-5.35735	-3.55906	-0.09788
21	H	-5.70795	0.725637	0.200218
22	N	-0.93428	0.191282	0.009213
23	N	-1.50149	-1.08844	0.021705

24	N	0.574304	-1.44114	0.029491
25	C	-0.62341	-2.11404	0.029928
26	C	1.854513	-2.08652	0.031979
27	C	2.223238	-2.87651	-1.06017
28	C	2.710964	-1.93084	1.126276
29	C	3.459907	-3.51912	-1.0574
30	H	1.544666	-2.98732	-1.89833
31	C	3.953441	-2.56484	1.121804
32	H	2.4053	-1.33723	1.981379
33	C	4.323425	-3.35988	0.032381
34	H	3.746556	-4.13765	-1.90026
35	H	4.617774	-2.45059	1.970812
36	H	3.488505	2.354808	-0.17509
37	C	5.680678	-4.00998	0.012619
38	C	1.444336	6.5352	-0.04355
39	F	6.63061	-3.19035	-0.52494
40	F	5.701127	-5.1489	-0.72377
41	F	6.119399	-4.33384	1.255147
42	F	0.326178	7.103725	-0.56704
43	F	2.502297	7.047121	-0.72766
44	F	1.551722	7.028548	1.22976
45	C	-7.19416	-1.55385	0.013202
46	F	-7.67719	-1.60427	-1.26583
47	F	-7.82522	-0.5104	0.610502
48	F	-7.64034	-2.68441	0.62268
49	H	2.303595	0.42737	-0.07724

M4				
Tag	**Symbol**	**X**	**Y**	**Z**
1	C	1.306414	2.220207	-0.05966
2	C	0.109697	2.929542	0.09408
3	C	2.517936	2.919422	-0.20521
4	C	0.135081	4.323219	0.101842
5	H	-0.82911	2.406068	0.205066
6	C	2.531405	4.302279	-0.19601
7	C	1.334669	5.009426	-0.04237
8	H	-0.79434	4.868903	0.221826
9	H	3.472439	4.831847	-0.30949
10	N	1.380476	0.824525	-0.06609
11	C	0.354103	-0.0705	-0.02816
12	C	-2.89621	-1.20335	-0.00379

13	C	-3.48775	-2.46532	-0.12372
14	C	-3.6788	-0.05797	0.134664
15	C	-4.86985	-2.57352	-0.09668
16	H	-2.86357	-3.34316	-0.23358
17	C	-5.06631	-0.17569	0.158018
18	H	-3.20708	0.91189	0.226086
19	C	-5.6583	-1.42909	0.045699
20	H	-5.3343	-3.55048	-0.1866
21	H	-5.67875	0.712075	0.269246
22	N	-0.92374	0.175271	-0.02941
23	N	-1.482	-1.09194	-0.02157
24	N	0.580608	-1.44175	-0.01241
25	C	-0.61238	-2.11829	-0.01617
26	C	1.860221	-2.07414	0.007396
27	C	2.190124	-2.96761	-1.00871
28	C	2.748602	-1.79807	1.047081
29	C	3.430565	-3.59687	-0.98566
30	H	1.477089	-3.16524	-1.80131
31	C	3.99415	-2.41714	1.059256
32	H	2.461014	-1.12244	1.846628
33	C	4.325493	-3.31379	0.044638
34	H	3.697536	-4.29959	-1.76703
35	H	4.692925	-2.21487	1.863922
36	H	3.44648	2.369769	-0.32612
37	C	5.688835	-3.94544	0.048063
38	C	1.379457	6.50483	-0.0355
39	F	6.620092	-3.12813	-0.48768
40	F	5.726173	-5.08651	-0.65932
41	F	6.109005	-4.23416	1.292845
42	F	0.165538	7.061939	0.109818
43	F	1.903788	7.00415	-1.17645
44	F	2.151788	6.986367	0.963539
45	C	-7.14968	-1.57464	0.038792
46	F	-7.62552	-1.86779	-1.19168
47	F	-7.78144	-0.45826	0.438963
48	F	-7.56474	-2.57323	0.844241
49	H	2.305155	0.428072	-0.17819

M5				
Tag	**Symbol**	**X**	**Y**	**Z**
1	C	1.306026	2.220082	-0.06162
2	C	0.108958	2.929238	0.09073
3	C	2.517723	2.919576	-0.20492
4	C	0.134071	4.322926	0.099337
5	H	-0.83003	2.405766	0.200148
6	C	2.530913	4.302427	-0.19498
7	C	1.333812	5.009362	-0.04273
8	H	-0.79568	4.868263	0.218318
9	H	3.472142	4.832034	-0.3067
10	N	1.380259	0.824501	-0.06889
11	C	0.354158	-0.07061	-0.03054
12	C	-2.89603	-1.2039	-0.00473
13	C	-3.48778	-2.46516	-0.13102
14	C	-3.67846	-0.05923	0.140631
15	C	-4.86986	-2.57353	-0.10301
16	H	-2.86393	-3.34249	-0.2467
17	C	-5.06596	-0.177	0.164688
18	H	-3.20672	0.910164	0.236924
19	C	-5.65809	-1.42981	0.04632
20	H	-5.33434	-3.55	-0.19792
21	H	-5.67817	0.710238	0.281271
22	N	-0.92384	0.174907	-0.03195
23	N	-1.48187	-1.09234	-0.02316
24	N	0.580865	-1.44178	-0.0139
25	C	-0.61193	-2.11844	-0.01687
26	C	1.860692	-2.07395	0.006665
27	C	2.191816	-2.96639	-1.00996
28	C	2.747883	-1.79835	1.047433
29	C	3.43237	-3.59539	-0.98618
30	H	1.479952	-3.16312	-1.80385
31	C	3.993566	-2.41716	1.060389
32	H	2.459608	-1.12293	1.846899
33	C	4.326076	-3.31297	0.045413
34	H	3.700361	-4.29714	-1.76806
35	H	4.691507	-2.21499	1.865782
36	H	3.446584	2.370198	-0.32442
37	C	5.689481	-3.94437	0.049655
38	C	1.378378	6.504687	-0.03497
39	F	6.621081	-3.12736	-0.48597
40	F	5.727367	-5.08581	-0.65726

41	F	6.109262	-4.23274	1.294722
42	F	0.164404	7.061719	0.110831
43	F	1.902446	7.005012	-1.17569
44	F	2.150765	6.985948	0.96423
45	C	-7.14944	-1.57531	0.040167
46	F	-7.62659	-1.86273	-1.19122
47	F	-7.78097	-0.46093	0.446194
48	F	-7.56384	-2.57773	0.841302
49	H	2.305143	0.428203	-0.18017

*B-2.2.26 – 4-Methoxyphenyl di-(trifluoromethylphenyl) Nitron (**33m**) (zwitterionic form)*

M1				
Tag	**Symbol**	**X**	**Y**	**Z**
1	C	-0.52503	2.282985	-0.04914
2	C	-1.94449	2.263252	0.013602
3	C	0.097469	3.557293	-0.15288
4	C	-2.6803	3.446763	-0.02293
5	H	-2.46464	1.318242	0.088298
6	C	-0.63765	4.731065	-0.19136
7	C	-2.04226	4.687901	-0.12964
8	H	-3.76346	3.396879	0.027043
9	H	-0.12378	5.683974	-0.27413
10	N	0.323977	1.197166	-0.01441
11	C	-0.08098	-0.04899	0.036693
12	C	-2.16287	-2.90778	0.08181
13	C	-2.06284	-4.12361	-0.5938
14	C	-3.32769	-2.57678	0.785586
15	C	-3.11993	-5.03593	-0.54937
16	H	-1.17719	-4.36435	-1.17279
17	C	-4.38371	-3.47692	0.820105
18	H	-3.39556	-1.62579	1.300429
19	C	-4.28689	-4.71448	0.159031
20	H	-3.02514	-5.97353	-1.08197
21	H	-5.29299	-3.2404	1.362421
22	N	-1.30457	-0.62505	0.034827
23	N	-1.07349	-1.98471	0.061698
24	N	0.891123	-1.10258	0.072306
25	C	0.215617	-2.26733	0.089826
26	C	2.313028	-0.98069	0.056139
27	C	3.052919	-1.73339	-0.85991

28	C	2.94917	-0.12933	0.965747
29	C	4.444986	-1.64554	-0.85888
30	H	2.550497	-2.37452	-1.57602
31	C	4.338038	-0.03626	0.956053
32	H	2.362504	0.448713	1.667828
33	C	5.085511	-0.7966	0.047477
34	H	5.020053	-2.23133	-1.56652
35	H	4.835392	0.618235	1.663318
36	H	1.181359	3.592588	-0.20515
37	C	6.582182	-0.65298	0.021129
38	C	-2.8247	5.956727	-0.11909
39	F	6.978906	0.440262	-0.69384
40	F	7.200896	-1.72053	-0.54111
41	F	7.108777	-0.50017	1.264193
42	F	-4.12808	5.786063	-0.46938
43	F	-2.31614	6.900863	-0.96408
44	F	-2.85181	6.561446	1.115622
45	H	0.651904	-3.2504	0.166646
46	O	-5.37506	-5.52536	0.257795
47	C	-5.34541	-6.80243	-0.39076
48	H	-6.30616	-7.26624	-0.16926
49	H	-5.23316	-6.69044	-1.47442
50	H	-4.53652	-7.42548	0.005596

M3				
Tag	**Symbol**	**X**	**Y**	**Z**
1	C	-0.50419	2.285634	-0.0523
2	C	-1.92352	2.279255	0.018457
3	C	0.129196	3.554266	-0.16275
4	C	-2.6487	3.46941	-0.01628
5	H	-2.45204	1.339334	0.098465
6	C	-0.59535	4.734554	-0.19951
7	C	-2.00005	4.704446	-0.12931
8	H	-3.73193	3.429411	0.040353
9	H	-0.07318	5.682511	-0.28736
10	N	0.334983	1.192539	-0.01894
11	C	-0.08151	-0.05027	0.035126
12	C	-2.1891	-2.88974	0.083186
13	C	-2.10052	-4.10492	-0.59504
14	C	-3.3505	-2.54975	0.788433
15	C	-3.16582	-5.0077	-0.552

16	H	-1.21705	-4.35277	-1.17434
17	C	-4.41466	-3.4403	0.821491
18	H	-3.4096	-1.59952	1.305818
19	C	-4.32946	-4.67739	0.157726
20	H	-3.07973	-5.94501	-1.08658
21	H	-5.3214	-3.19651	1.364891
22	N	-1.31016	-0.61471	0.03429
23	N	-1.09142	-1.97664	0.063928
24	N	0.880662	-1.11197	0.073024
25	C	0.1951	-2.27066	0.092789
26	C	2.303846	-1.00169	0.057243
27	C	3.037029	-1.75166	-0.86628
28	C	2.94684	-0.16395	0.9745
29	C	4.429767	-1.67453	-0.86525
30	H	2.528896	-2.3827	-1.5873
31	C	4.336408	-0.08131	0.964883
32	H	2.365079	0.411445	1.682937
33	C	5.077238	-0.83889	0.048577
34	H	4.999905	-2.25843	-1.57841
35	H	4.839204	0.562451	1.678082
36	H	1.213068	3.579682	-0.22134
37	C	6.57496	-0.70678	0.021672
38	C	-2.77003	5.980704	-0.11775
39	F	6.979787	0.383134	-0.69425
40	F	7.185279	-1.77915	-0.54063
41	F	7.103583	-0.5574	1.264176
42	F	-4.08014	5.820059	-0.44651
43	F	-2.26549	6.912875	-0.97874
44	F	-2.77189	6.596533	1.111829
45	H	0.622932	-3.25737	0.170636
46	O	-5.42459	-5.47902	0.255496
47	C	-5.40457	-6.75638	-0.39319
48	H	-6.36896	-7.2127	-0.17224
49	H	-5.29073	-6.64503	-1.47671
50	H	-4.60079	-7.38566	0.003452

M4				
Tag	**Symbol**	**X**	**Y**	**Z**
1	C	-0.60836	2.244061	-0.04035
2	C	-2.01783	2.147199	0.037593
3	C	-0.05275	3.545739	-0.14575

4	C	-2.81349	3.291115	0.011655
5	H	-2.4906	1.178552	0.118253
6	C	-0.84569	4.676172	-0.17242
7	C	-2.24045	4.55406	-0.09445
8	H	-3.8924	3.189536	0.073738
9	H	-0.38795	5.658214	-0.25539
10	N	0.299012	1.207811	-0.0185
11	C	-0.06213	-0.05033	0.023672
12	C	-2.03254	-2.96443	0.071621
13	C	-1.88421	-4.18211	-0.57885
14	C	-3.2075	-2.65264	0.758488
15	C	-2.91029	-5.1248	-0.52617
16	H	-0.9855	-4.40155	-1.14657
17	C	-4.23156	-3.58274	0.800784
18	H	-3.30435	-1.69173	1.250925
19	C	-4.08785	-4.82542	0.16537
20	H	-2.7824	-6.06932	-1.03939
21	H	-5.15475	-3.36924	1.328386
22	N	-1.25635	-0.66866	0.024697
23	N	-0.97621	-2.00706	0.044187
24	N	0.941335	-1.05995	0.047801
25	C	0.314393	-2.24618	0.065454
26	C	2.353163	-0.87842	0.026578
27	C	3.118751	-1.63816	-0.85336
28	C	2.943005	0.035926	0.901582
29	C	4.5049	-1.49705	-0.85099
30	H	2.640854	-2.32525	-1.54361
31	C	4.322802	0.181527	0.890623
32	H	2.322455	0.618889	1.570366
33	C	5.09676	-0.58723	0.017681
34	H	5.110962	-2.08636	-1.5292
35	H	4.797343	0.885057	1.567309
36	H	1.027615	3.632373	-0.2068
37	C	6.586084	-0.39709	0.032476
38	C	-3.07461	5.789201	-0.11502
39	F	6.937245	0.845325	-0.35804
40	F	7.225774	-1.25653	-0.77565
41	F	7.099083	-0.56021	1.268693
42	F	-4.39547	5.532699	-0.10129
43	F	-2.84166	6.554632	-1.20781
44	F	-2.83166	6.599017	0.944943
45	H	0.785865	-3.21499	0.137451

46	O	-5.14303	-5.66691	0.269079
47	C	-5.04257	-6.94004	-0.3562
48	H	-5.98071	-7.45016	-0.14633
49	H	-4.91536	-6.83395	-1.43819
50	H	-4.20955	-7.51445	0.061376

M5				
Tag	**Symbol**	**X**	**Y**	**Z**
1	C	-0.53026	2.258103	-0.05256
2	C	-1.94149	2.213617	0.042143
3	C	0.071888	3.538145	-0.16813
4	C	-2.69418	3.386326	0.022371
5	H	-2.44877	1.263214	0.131361
6	C	-0.67862	4.697221	-0.18953
7	C	-2.07583	4.627154	-0.0945
8	H	-3.77523	3.325054	0.097638
9	H	-0.18542	5.661213	-0.28086
10	N	0.339004	1.190218	-0.03536
11	C	-0.06662	-0.05455	0.014102
12	C	-2.13539	-2.89987	0.066385
13	C	-2.02337	-4.12693	-0.57368
14	C	-3.30319	-2.54432	0.744177
15	C	-3.07916	-5.03599	-0.5179
16	H	-1.1292	-4.38002	-1.1343
17	C	-4.35701	-3.44062	0.788485
18	H	-3.37149	-1.57683	1.22842
19	C	-4.25015	-4.69283	0.164638
20	H	-2.97868	-5.98846	-1.02232
21	H	-5.27558	-3.19293	1.309203
22	N	-1.2814	-0.63089	0.016471
23	N	-1.04746	-1.97849	0.037514
24	N	0.900924	-1.09774	0.041474
25	C	0.23442	-2.26182	0.059021
26	C	2.31817	-0.96219	0.027061
27	C	3.061415	-1.73289	-0.86199
28	C	2.932933	-0.0779	0.915478
29	C	4.451071	-1.63191	-0.8567
30	H	2.563715	-2.3967	-1.56091
31	C	4.316421	0.027879	0.907851
32	H	2.328417	0.514026	1.59124
33	C	5.068105	-0.75097	0.024487

34	H	5.040628	-2.22904	-1.54254
35	H	4.810356	0.708856	1.593646
36	H	1.154013	3.584204	-0.24117
37	C	6.562043	-0.601	0.037649
38	C	-2.86497	5.891662	-0.10789
39	F	6.945288	0.633158	-0.3498
40	F	7.177558	-1.47412	-0.77497
41	F	7.073354	-0.78151	1.271895
42	F	-4.19459	5.683456	-0.08561
43	F	-2.612	6.649692	-1.20145
44	F	-2.58615	6.690863	0.951085
45	H	0.673158	-3.24616	0.128729
46	O	-5.33284	-5.4988	0.270149
47	C	-5.27127	-6.78069	-0.34235
48	H	-6.22648	-7.2579	-0.13197
49	H	-5.13597	-6.6896	-1.42472
50	H	-4.45929	-7.37789	0.084558

*B-2.2.27 – 4-Methoxyphenyl di-(trifluoromethylphenyl) Nitron (**33m**) (carbenic form)*

M1				
Tag	**Symbol**	**X**	**Y**	**Z**
1	C	-0.25684	2.311113	0.043936
2	C	-1.65356	2.415	-0.07141
3	C	0.515624	3.484391	0.158867
4	C	-2.25535	3.673118	-0.07192
5	H	-2.2591	1.524167	-0.15906
6	C	-0.09271	4.731469	0.157745
7	C	-1.48647	4.834729	0.038855
8	H	-3.3339	3.739412	-0.16419
9	H	0.519404	5.622712	0.245107
10	N	0.430683	1.091978	0.042063
11	C	-0.07204	-0.17892	-0.00868
12	C	-2.46877	-2.68246	-0.05404
13	C	-2.49031	-4.00344	0.396424
14	C	-3.64644	-2.09009	-0.52911
15	C	-3.67543	-4.74373	0.360791
16	H	-1.58197	-4.45697	0.775211
17	C	-4.8297	-2.82088	-0.55582
18	H	-3.6329	-1.06403	-0.87609
19	C	-4.85421	-4.15334	-0.11547

20	H	-3.66354	-5.76656	0.71644
21	H	-5.74615	-2.37017	-0.92286
22	N	-1.32908	-0.54214	-0.012
23	N	-1.24994	-1.93909	-0.03414
24	N	0.758103	-1.30075	-0.03181
25	C	-0.00635	-2.4509	-0.04513
26	C	2.189337	-1.29612	-0.04044
27	C	2.881691	-0.69412	-1.09583
28	C	2.880717	-1.91501	1.005801
29	C	4.277115	-0.70011	-1.0975
30	H	2.339547	-0.24295	-1.9202
31	C	4.273428	-1.93286	0.995246
32	H	2.328036	-2.38016	1.814014
33	C	4.969864	-1.32246	-0.0551
34	H	4.815092	-0.23823	-1.91728
35	H	4.810928	-2.4178	1.802602
36	H	1.595841	3.414793	0.24654
37	C	6.474078	-1.30207	-0.0317
38	C	-2.13974	6.180819	0.086025
39	F	6.9587	-0.27639	0.727748
40	F	7.013999	-1.14982	-1.26604
41	F	6.998609	-2.43955	0.492284
42	F	-3.36756	6.192554	-0.49451
43	F	-1.40252	7.142019	-0.5352
44	F	-2.32602	6.629961	1.366568
45	O	-6.06394	-4.78557	-0.18474
46	C	-6.14857	-6.14718	0.245047
47	H	-7.18787	-6.43992	0.096648
48	H	-5.49725	-6.79223	-0.35522
49	H	-5.88907	-6.24403	1.305174
50	H	1.436878	1.155786	0.12483

M3				
Tag	**Symbol**	**X**	**Y**	**Z**
1	C	-0.25878	2.310746	0.04845
2	C	-1.65519	2.413372	-0.0725
3	C	0.512095	3.484757	0.166812
4	C	-2.25824	3.670868	-0.07514
5	H	-2.25963	1.522089	-0.16306
6	C	-0.09748	4.731243	0.163608
7	C	-1.49088	4.833195	0.039123

8	H	-3.33647	3.736064	-0.17186
9	H	0.513495	5.622985	0.253691
10	N	0.429849	1.092309	0.048754
11	C	-0.07162	-0.17886	-0.00399
12	C	-2.46607	-2.68454	-0.05363
13	C	-2.4886	-4.00325	0.403468
14	C	-3.64215	-2.09538	-0.53663
15	C	-3.67295	-4.74475	0.366321
16	H	-1.58172	-4.45411	0.788948
17	C	-4.82475	-2.8272	-0.56477
18	H	-3.62792	-1.071	-0.88865
19	C	-4.85007	-4.15758	-0.11803
20	H	-3.6619	-5.7657	0.727336
21	H	-5.73991	-2.37891	-0.93798
22	N	-1.32842	-0.54336	-0.00734
23	N	-1.24797	-1.94013	-0.03245
24	N	0.759518	-1.29983	-0.02962
25	C	-0.00385	-2.45058	-0.04521
26	C	2.190848	-1.29379	-0.03929
27	C	2.881696	-0.69078	-1.09504
28	C	2.883559	-1.91225	1.006336
29	C	4.277115	-0.69564	-1.09791
30	H	2.338551	-0.23916	-1.91847
31	C	4.27627	-1.929	0.99459
32	H	2.332076	-2.37757	1.815273
33	C	4.971227	-1.3179	-0.05634
34	H	4.813889	-0.23271	-1.91786
35	H	4.814776	-2.41348	1.801545
36	H	1.591998	3.416176	0.258563
37	C	6.475398	-1.2967	-0.03441
38	C	-2.14589	6.17841	0.084151
39	F	6.960564	-0.27176	0.725679
40	F	7.01423	-1.14299	-1.2691
41	F	7.001143	-2.43458	0.487825
42	F	-3.36976	6.189956	-0.5049
43	F	-1.40563	7.141764	-0.53004
44	F	-2.34193	6.625172	1.364218
45	O	-6.05896	-4.79111	-0.18951
46	C	-6.14454	-6.15083	0.246719
47	H	-7.18292	-6.44507	0.095011
48	H	-5.48998	-6.79825	-0.34736
49	H	-5.88981	-6.24209	1.308444

50	H	1.435844	1.157048	0.133808

M4				
Tag	**Symbol**	**X**	**Y**	**Z**
1	C	-0.2774	2.285295	0.074002
2	C	-1.66298	2.357499	-0.11647
3	C	0.463233	3.46787	0.249754
4	C	-2.28962	3.602022	-0.1297
5	H	-2.2457	1.457492	-0.25176
6	C	-0.16935	4.697969	0.234671
7	C	-1.55252	4.767829	0.04321
8	H	-3.36253	3.65256	-0.28022
9	H	0.413182	5.603987	0.369494
10	N	0.437002	1.085523	0.084652
11	C	-0.0561	-0.18585	0.027028
12	C	-2.42632	-2.68921	-0.03281
13	C	-2.42053	-4.03366	0.322775
14	C	-3.61772	-2.07121	-0.42053
15	C	-3.60015	-4.77653	0.280049
16	H	-1.49414	-4.50286	0.63308
17	C	-4.79383	-2.80595	-0.45475
18	H	-3.61826	-1.02246	-0.69316
19	C	-4.79387	-4.16231	-0.10883
20	H	-3.57084	-5.82201	0.560985
21	H	-5.72775	-2.34178	-0.75373
22	N	-1.30325	-0.55974	0.025277
23	N	-1.21358	-1.94043	-0.00481
24	N	0.777358	-1.29379	-0.00427
25	C	0.026854	-2.44859	-0.02051
26	C	2.202966	-1.26762	-0.02707
27	C	2.866472	-0.57776	-1.04059
28	C	2.908222	-1.95148	0.962821
29	C	4.258892	-0.55843	-1.05557
30	H	2.301792	-0.07756	-1.82118
31	C	4.297283	-1.94481	0.935842
32	H	2.365323	-2.48271	1.736558
33	C	4.963996	-1.24432	-0.07035
34	H	4.785663	-0.02805	-1.84078
35	H	4.85802	-2.47849	1.696093
36	H	1.537811	3.414585	0.39568
37	C	6.465519	-1.20653	-0.05347

38	C	-2.21926	6.106702	0.062978
39	F	6.934	-0.30864	0.839134
40	F	6.984493	-0.87084	-1.24585
41	F	6.995862	-2.39418	0.291473
42	F	-3.48843	6.062195	-0.3778
43	F	-1.56913	7.010311	-0.70032
44	F	-2.26283	6.639196	1.305831
45	O	-5.99467	-4.79626	-0.17693
46	C	-6.03401	-6.1735	0.166273
47	H	-7.06992	-6.48439	0.042358
48	H	-5.39236	-6.7616	-0.49827
49	H	-5.72679	-6.32728	1.206049
50	H	1.436729	1.162782	0.223455

M5				
Tag	**Symbol**	**X**	**Y**	**Z**
1	C	-0.27911	2.28471	0.07722
2	C	-1.66444	2.355651	-0.1158
3	C	0.460123	3.468028	0.254323
4	C	-2.29232	3.599559	-0.13005
5	H	-2.2462	1.45525	-0.25259
6	C	-0.17366	4.697489	0.238209
7	C	-1.55662	4.766035	0.044358
8	H	-3.36499	3.648952	-0.28263
9	H	0.407888	5.603984	0.374065
10	N	0.43636	1.085645	0.089168
11	C	-0.05554	-0.18598	0.029997
12	C	-2.42376	-2.69109	-0.03356
13	C	-2.4208	-4.03125	0.337728
14	C	-3.61188	-2.07777	-0.4385
15	C	-3.59983	-4.77508	0.293023
16	H	-1.49729	-4.49657	0.662256
17	C	-4.78754	-2.8131	-0.47436
18	H	-3.61011	-1.03218	-0.7232
19	C	-4.79019	-4.16556	-0.11313
20	H	-3.5728	-5.81723	0.586266
21	H	-5.7189	-2.35254	-0.78664
22	N	-1.30252	-0.56096	0.028111
23	N	-1.21161	-1.94154	-0.00419
24	N	0.778785	-1.29316	-0.00309
25	C	0.029271	-2.4485	-0.02128

26	C	2.204459	-1.26567	-0.02651
27	C	2.866753	-0.57524	-1.04038
28	C	2.910697	-1.94878	0.963209
29	C	4.259153	-0.55487	-1.05614
30	H	2.301343	-0.07492	-1.82034
31	C	4.299732	-1.94117	0.935414
32	H	2.368766	-2.47987	1.73773
33	C	4.965273	-1.24039	-0.07139
34	H	4.784956	-0.02374	-1.84147
35	H	4.861217	-2.47419	1.695572
36	H	1.534498	3.415793	0.4019
37	C	6.466752	-1.20196	-0.0556
38	C	-2.22471	6.104168	0.063001
39	F	6.935815	-0.30405	0.836684
40	F	6.984911	-0.8662	-1.24835
41	F	6.997905	-2.38953	0.288834
42	F	-3.49312	6.058552	-0.37999
43	F	-1.57425	7.008664	-0.69903
44	F	-2.27118	6.63669	1.305857
45	O	-5.99022	-4.80052	-0.18444
46	C	-6.03248	-6.17393	0.174304
47	H	-7.06738	-6.48617	0.045561
48	H	-5.38553	-6.76951	-0.47828
49	H	-5.7337	-6.31567	1.218195
50	H	1.436022	1.163821	0.228306

B-3 – Calculation of $F_{carbene}$

B-3.1 – Conversion of ΔG_{taut} to K_{eq}

Equation S1 was used to convert the Gibbs free energy change of tautomerisation (ΔG_{taut}) into the equilibrium constant between the two tautomers. Values of ΔG_{taut} were obtained by calculating the difference in the sum of electronic and thermal free energies between zwitterion and carbene.

$$\Delta G_{taut}(cal\ mol^{-1}) = -RTln(K_{eq}) \qquad \textbf{Equation S1}$$

B-3.2 – Fraction of Carbene from K_{eq}

The ratio of carbene was calculated from combining **Equation S2** and **Equation S3** to give **Equation S4**, which can be simplified to **Equation 1**.

$$K_{eq} = \frac{[Carbene]}{[Zwitterion]} \qquad \textbf{Equation S2}$$

$$F_{Carbene} = \frac{[Carbene]}{[Zwitterion] + [Carbene]} \qquad \textbf{Equation S3}$$

$$F_{Carbene} = \frac{K_{eq}[Zwitterion]}{[Zwitterion] + K_{eq}[Zwitterion]} \qquad \textbf{Equation S4}$$

$$F_{Carbene} = \frac{K_{eq}}{1 + K_{eq}} \qquad \textbf{Equation 1}$$

B-3.2.1 – For acid-functionalised triazolium

When dealing with **33i**, three species are in existence within the mixture when formally neutral: the carboxylate zwitterion (CZ), acid zwitterion (ZA) and the carbene (C). For this description, K_1 describes the equilibrium of carboxylate zwitterion to acid zwitterion, whilst K_2 describes acid zwitterion equilibrium to carbene (c.f. normal zwitterion-carbene tautomerisation).The fraction of carbene and of the acid zwitterion can therefore be defined by **Equation S5** and **Equation S6**, respectively.

$$F_C{}^{rel.\ AZ} = \frac{K_2}{1 + K_2} \qquad \textbf{Equation S5}$$

$$F_{AZ}{}^{rel.\ CZ} = \frac{K_1}{1 + K_1} \qquad \textbf{Equation S6}$$

Thus, the ratio of carbene *versus* acid zwitterion and carboxylate zwitterion can be defined by **Equation S7**. This can then be used to determine the fraction of carbene (**Equation S8**) in terms of the relative fraction of acid zwitterion and carboxylate zwitterion. Finally, by using **Equation S5** and

Equation S6, the fraction of carbene can be described in terms of the equilibrium constants of the two processes (**Equation S9**, simplified to give **Equation S10**).

$$1\ C : \frac{1}{{F_C}^{rel.\ AZ}}\ AZ : \left(\frac{1}{{F_{AZ}}^{rel.\ CZ}} \times \frac{1}{{F_C}^{rel.\ AZ}}\right) CZ \qquad \textbf{Equation S7}$$

$$F_{carbene} = \frac{1}{1 + \frac{1}{{F_C}^{rel.\ AZ}} + \left(\frac{1}{{F_{AZ}}^{rel.\ CZ}} \times \frac{1}{{F_C}^{rel.\ AZ}}\right)} \qquad \textbf{Equation S8}$$

$$F_{carbene} = \frac{1}{1 + \frac{1 + K_2}{K_2} + \left(\frac{1 + K_1}{K_1} \times \frac{1 + K_2}{K_2}\right)} \qquad \textbf{Equation S9}$$

$$F_{carbene} = \frac{1}{1 + \frac{1 + K_2}{K_2} + \frac{(1 + K_1)(1 + K_2)}{K_1 K_2}} \qquad \textbf{Equation S10}$$

B-4 – Attempted *S*-triazole arylation by Cu-diamine catalysis

Run N°	Cat. (mol%)	Ligand (mol%)	Base (equiv.)	Solv.	Temp. (°C)	Result
1	CuI (5)	DMEDA (10)	K_3PO_4 (2)	DMF	110	Trace
2	CuI (5)	DMEDA (10)	K_3PO_4 (2)	DMF	250, MW	Partial conversion, NI
3	CuI (5)	DMEDA (10)	TEA (2)	MeCN	150, MW	NC
4	CuI (5)	DMEDA (10)	none	MeCN	150, MW	Trace
5	CuI (5)	DMEDA (10)	K_3PO_4 (2)	DMF	150, MW	Trace
6	CuI (10)	DMEDA (20)	K_3PO_4 (2)	DMF	110	Partial conversion, NI
7	CuI (10)	**Ligand A** (20)	none	DMF	110	NC
8	CuO (5)	none	K_2CO_3 (1)	DMF	RT	NC
9	CuO (10)	none	K_2CO_3 (1)	DMF	RT	NC
10	$(Ph_3P)_2PdCl_2$ (5)	none	none	DMF	150, MW	NC
11	CuI (5)	DMEDA (20)	K_2CO_3 (2)	toluene	110	NC
12	CuI (10)	DMEDA (20)	K_3PO_4 (2)	DMF (diluted *versus* **6**)	110	Partial conversion, NI
13	CuI (10)	DMEDA (20)	none	DMF	150	NC
14	CuI (10)	TMEDA (20)	none	DMF	110	NC
15	CuI (10)	**Ligand B** (20)	none	DMF	110	NC
16	CuI (10)	**Ligand C** (20)	none	DMF	110	Partial conversion, NI
17	CuI (10)	DMEDA (20)	K_3PO_4 (2)	Dioxane	80	Good conversion, NI
18	CuI (10)	DMEDA (20)	K_3PO_4 (2)	Dioxane	RT	NC
19	CuI (10)	**Ligand D** (20)	K_3PO_4 (2)	DMF	110	Partial conversion, NI
20	CuI (10)	**Ligand E** (20)	K_3PO_4 (2)	DMF	110	Complete, highly impure, NI
21	CuI (10)	1,10-phen (20)	K_3PO_4 (2)	DMF	110	Complete, reasonable purity, NI
22	CuI (10)	DMEDA (20)	K_3PO_4 (2)	DMF	200	Partial conversion, NI
23	CuI (10)	2,2'-bipy (20)	K_3PO_4 (2)	DMF	110	Good conversion, NI
24	CuI (10)	DEEDA (20)	K_3PO_4 (2)	DMF	110	Trace
25	CuI (20)	1,10-phen (40)	K_3PO_4 (2)	DMF	110	Trace
26	CuI (10)	1,10-phen (20)	K_3PO_4 (2)	Dioxane	110	Partial conversion, NI

Ligand A = *Trans*-1,2-diaminocyclohexane. **Ligand B** = *N,N'*-diisopropylethylenediamine. **Ligand C** = *N,N'*-dibenzylethylenediamine. **Ligand D** = 1,2-diphenylethylenediamine. **Ligand E** = *Trans-N,N'*-dimethyl-cyclohexane-1,2-diamine. NI = not isolated. NC = no conversion (observed by LC-MS)

Appendix C - Supplementary information for Chapter 3

C-1 – Potential isomerisation of 181b during hydrolysis

LC-MS of Blatter radicals characteristically show 2 peaks for the same *m/z* corresponding to product, which is proposed to arise from the separation of the radical from the protonated form. However, when **181b** was hydrolysed the observation of 4 *m/z* peaks corresponding to **182b** were observed (**Figure S2A**). Looking at the LC-MS of **181b** only two corresponding *m/z* peaks were observed (**Figure S2B**), LC-MS of the isomer **38g** also only shows two corresponding peaks (**Figure S2C**). The doubling of peaks seen in the starting material to the crude product points towards an isomerisation, and comparing data with that for **37g** indicates it is a result of the iodine atom location.

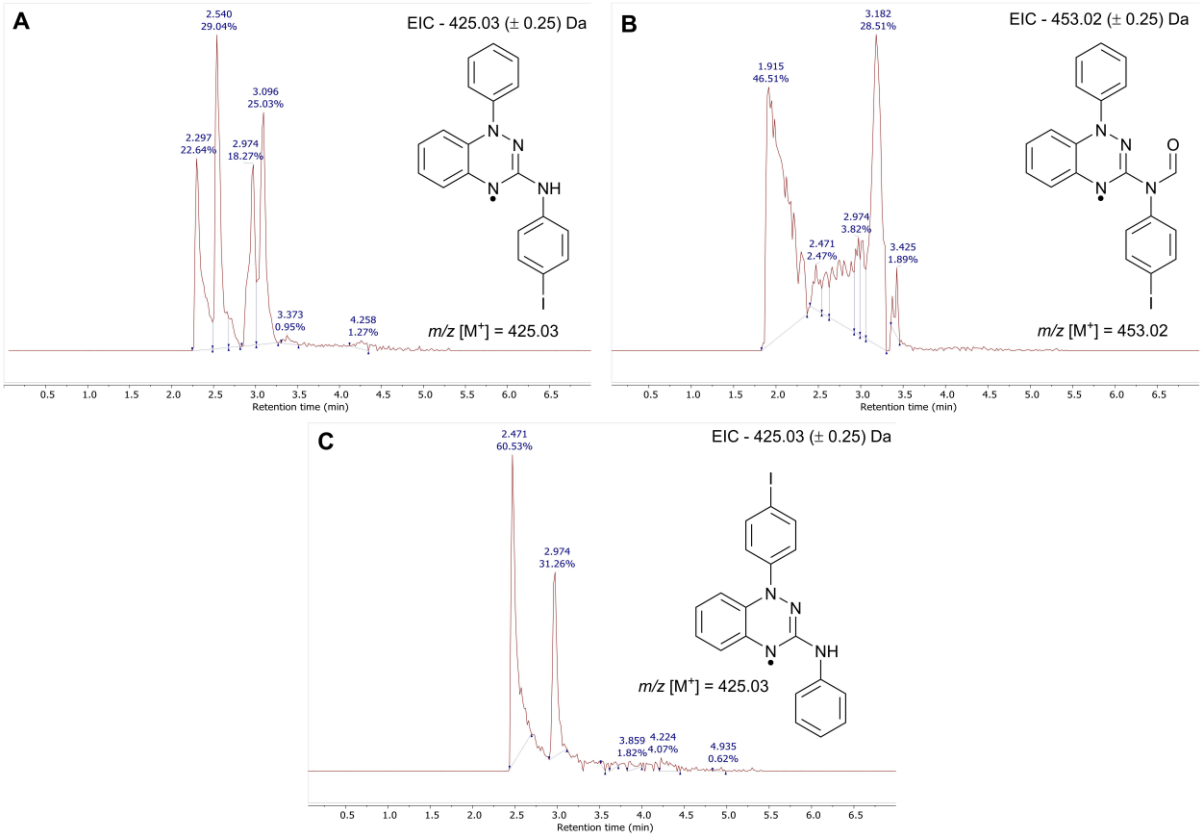
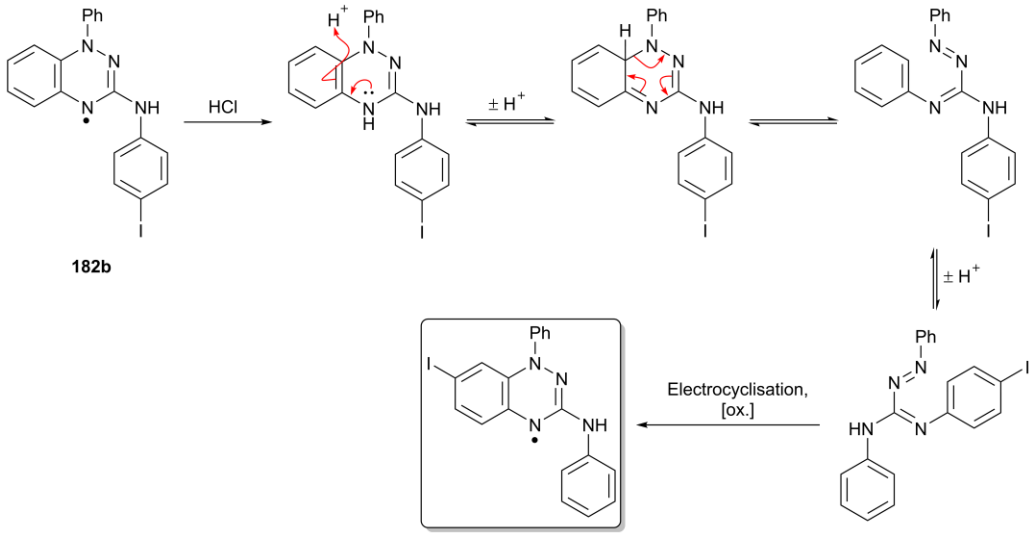


Figure S2 – LC-MS EIC analysis of iodinated Blatter radicals. **A**) The formation of iodo anilino radical **182b** after 19 h stirring, showing 4 corresponding *m/z* peaks; **B**) The formation of iodo amido radical **181b** after 7 d stirring, with 2 corresponding *m/z* peaks; **C**) The formation of iodo anilino radical **38g** after 18 h stirring, which also shows 2 corresponding *m/z* peaks.

It is therefore proposed that under acidic conditions the ring opening of Blatter radical may occur in a reverse of the mechanism proposed to lead to Blatter radical – electrocyclic ring opening to the triazabutadiene (**Scheme S1**). This triazabutadiene can then undergo electrocyclization to the Blatter radical, and give rise to the other peaks observed by LC-MS.



Scheme S1 – The proposed pathway for acid-catalysed isomerisation of anilino radicals. Under acidic conditions, the radical centre of **182b** is reduced to the benzotriazine. This protonation enables the tautomerisation and electrocyclic ring opening to the C(3)-anilinoamidrazone, followed by electrocyclization to the regioisomer.

C-2 – NMR spectroscopy of Blatter radicals

As initial evidence of the paramagnetic nature of Blatter radicals, attempts to characterise the species by ^{1}H NMR spectroscopy showed broadened signals (**Figure S3**). This prompted further studies to provide evidence of radical character (CV, EPR, XRD).

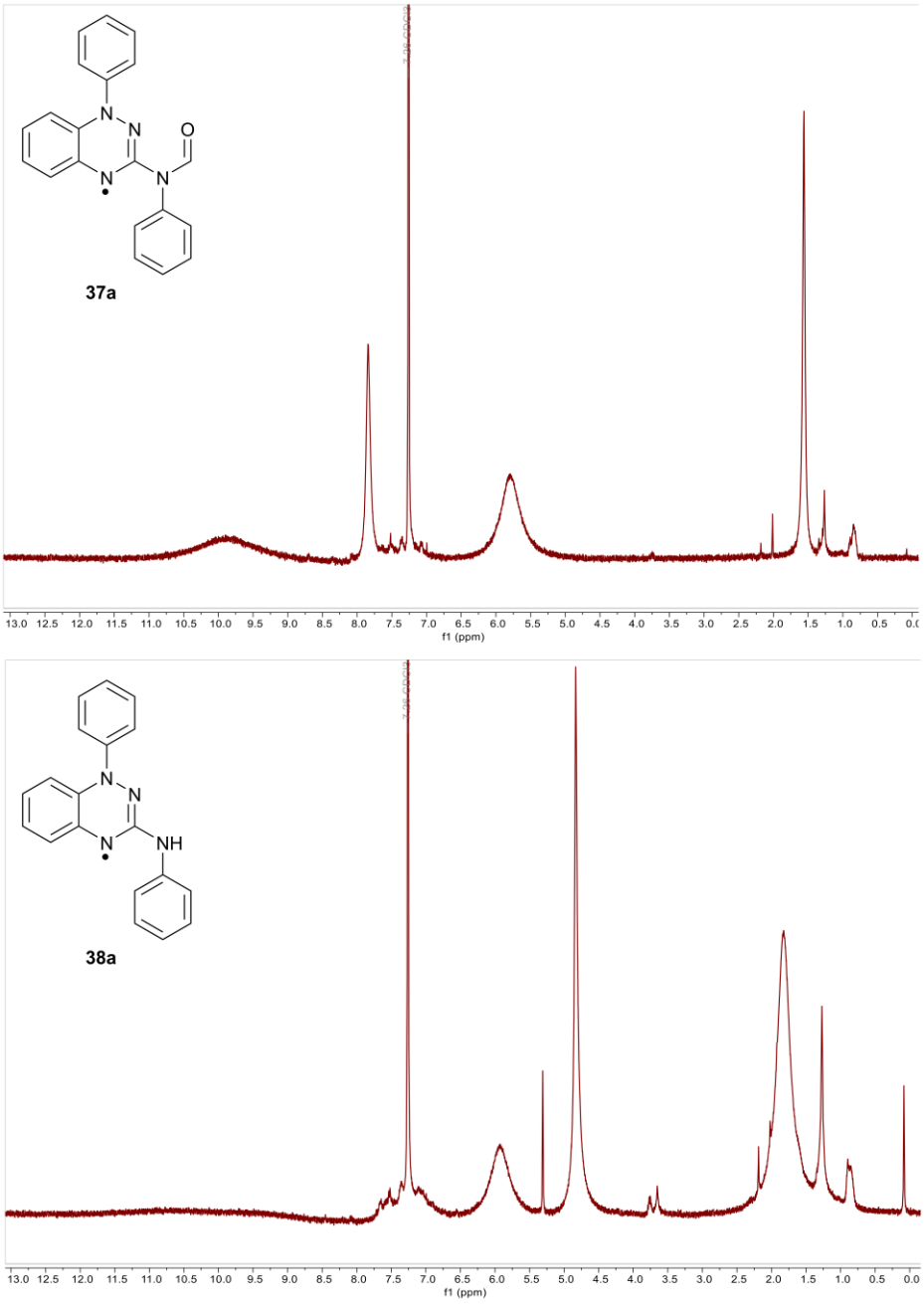


Figure S3 – NMR spectroscopy of Blatter radicals **37a** and **38a**. $CDCl_3$ solvent, 400 MHz, B4 instrument.

C-3 – Blatter radical formation studies by ^{1}H NMR

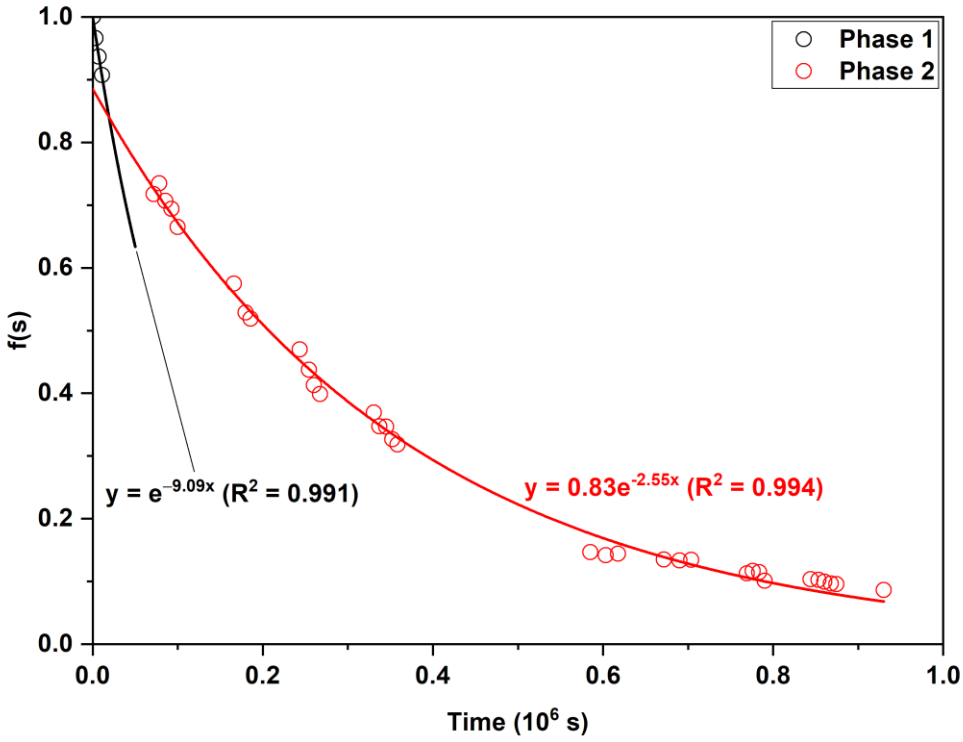


Figure S4 – Plot of the fraction of remaining starting material as a function of time for Nitron **33a**.

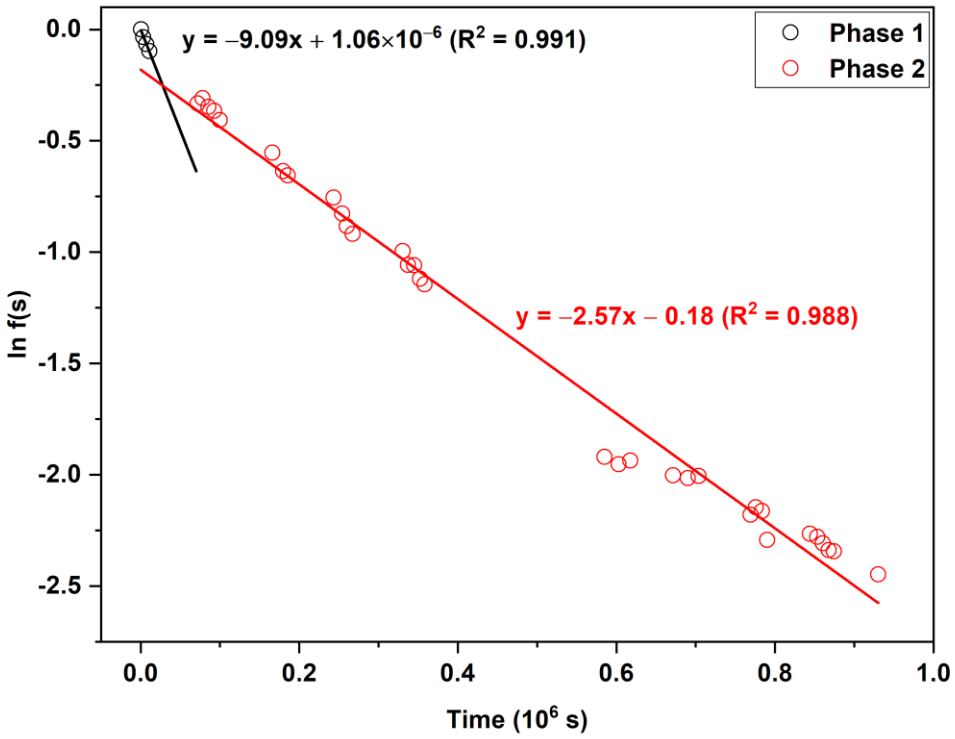


Figure S5 – Semilogarithmic plot of the fraction of remaining starting material as a function of time for Nitron **33a**.

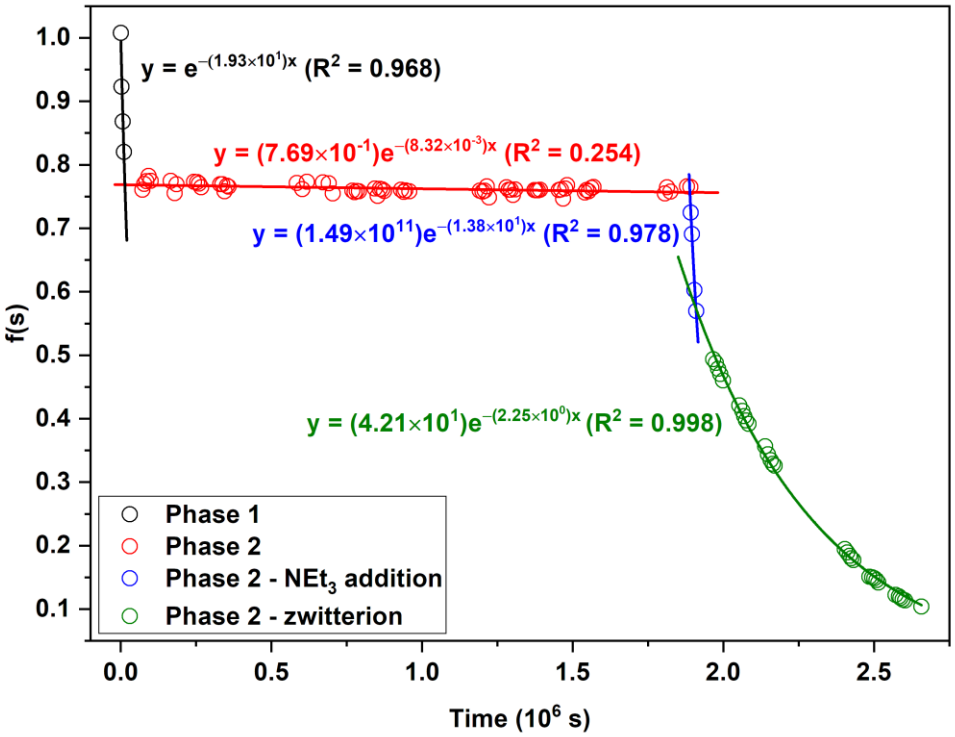


Figure S6 – Plot of the fraction of remaining starting material as a function of time for the hydrochloride salt of Nitron **33aH·Cl**.

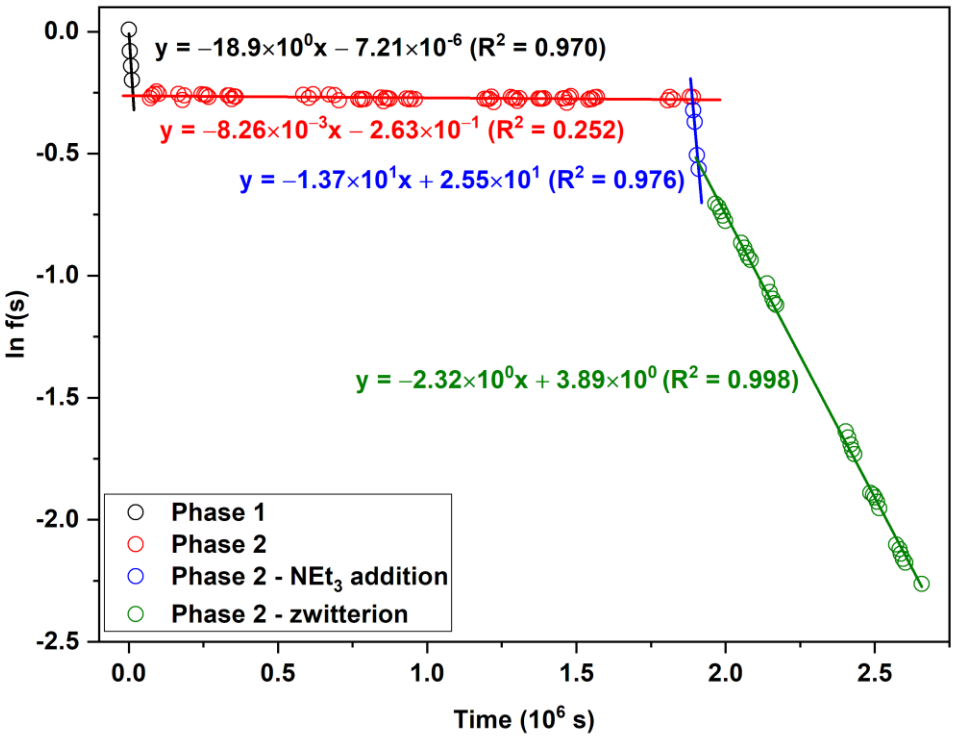


Figure S7 – Semilogarithmic plot of the fraction of remaining starting material as a function of time for the hydrochloride salt of Nitron **33aH·Cl**

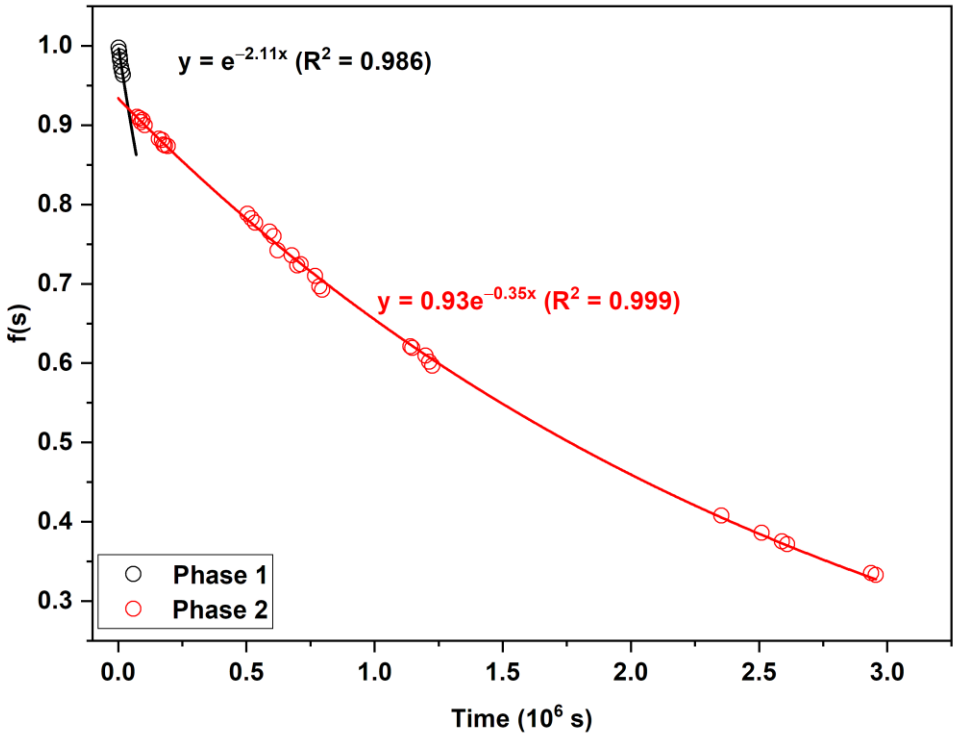


Figure S8 – Plot of the fraction of remaining starting material as a function of time for CF_3 Nitron **33c**.

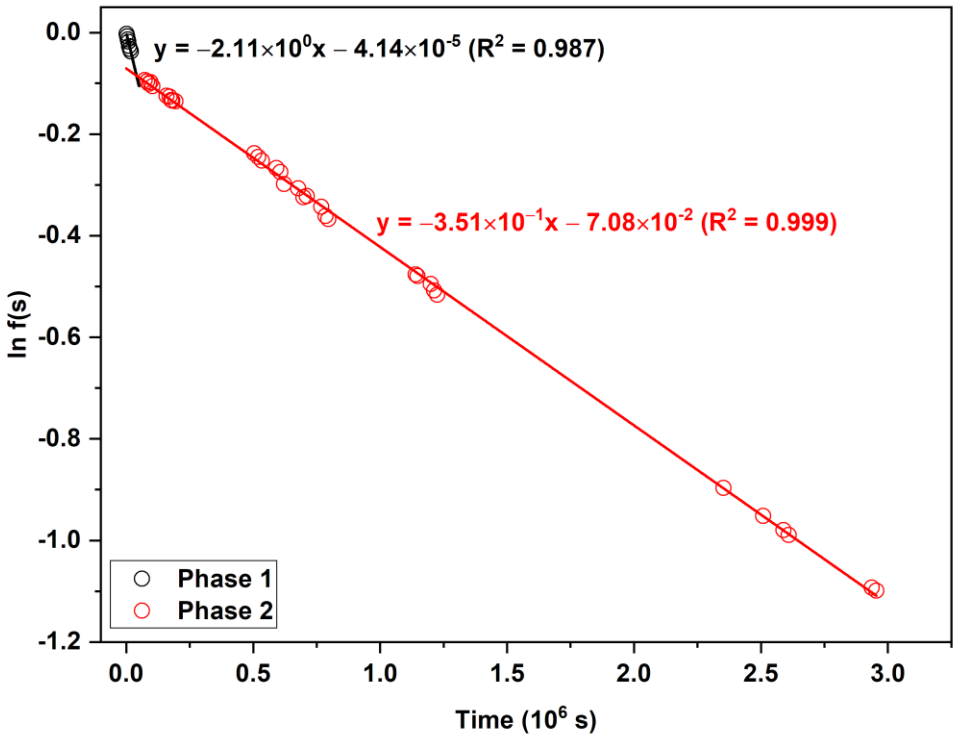


Figure S9 – Semilogarithmic plot of the fraction of remaining starting material as a function of time for CF_3 Nitron **33c**.

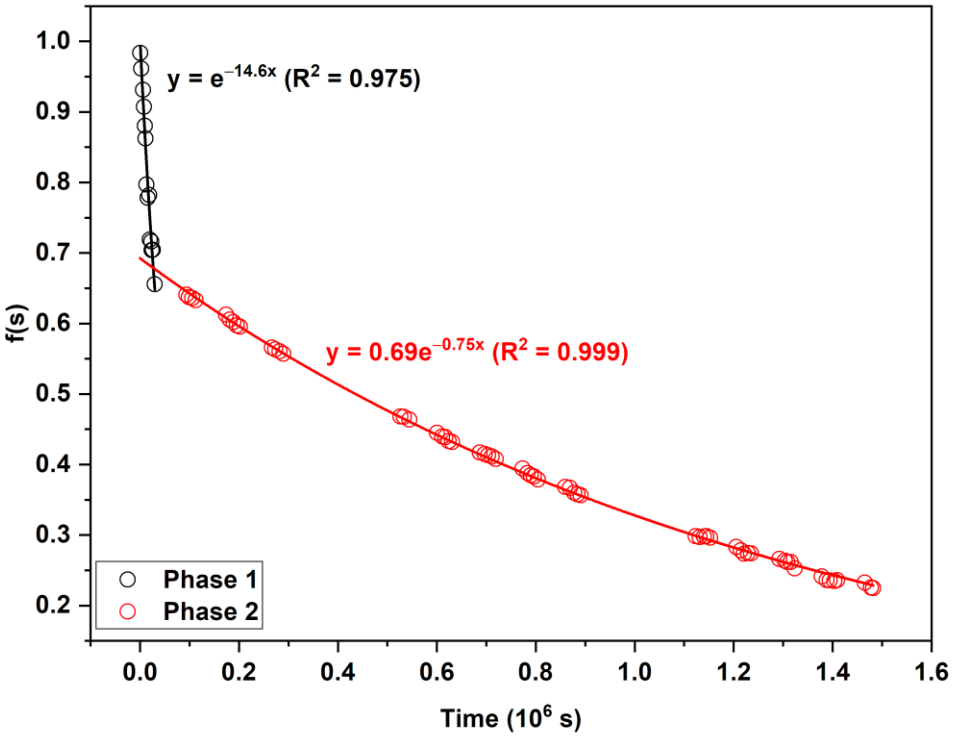


Figure S10 – Plot of the fraction of remaining starting material as a function of time for *p*-Br substituted Nitron **33f**.

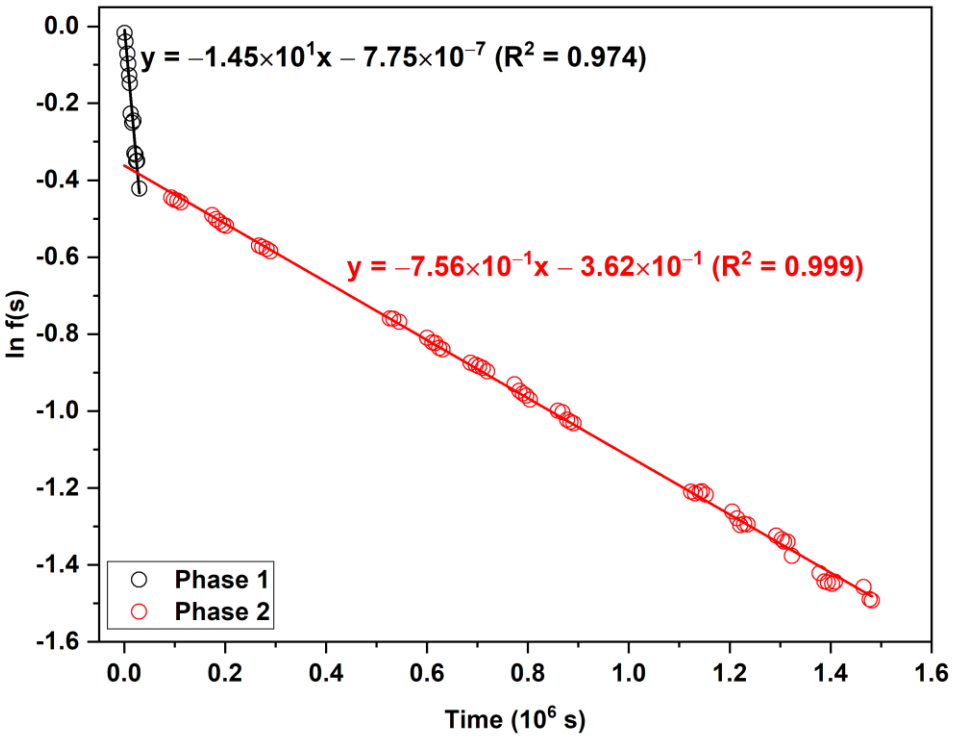


Figure S11 – Semilogarithmic plot of the fraction of remaining starting material as a function of time for *p*-Br Nitron **33f**.

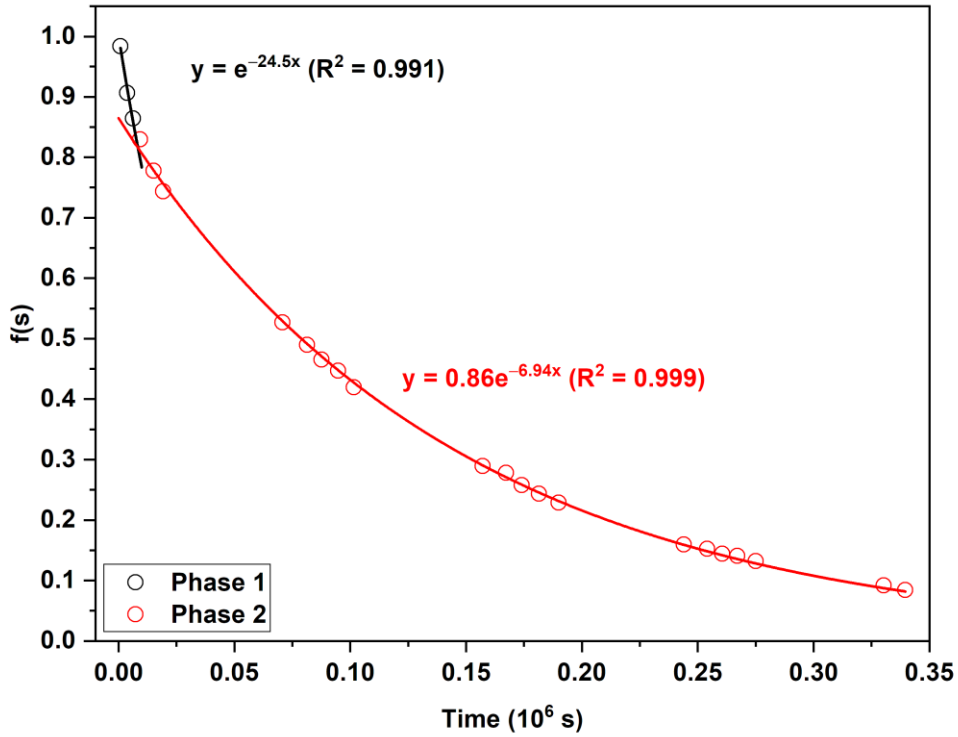


Figure S12 – Plot of the fraction of remaining starting material as a function of time for *p*-I substituted Nitron **33g**.

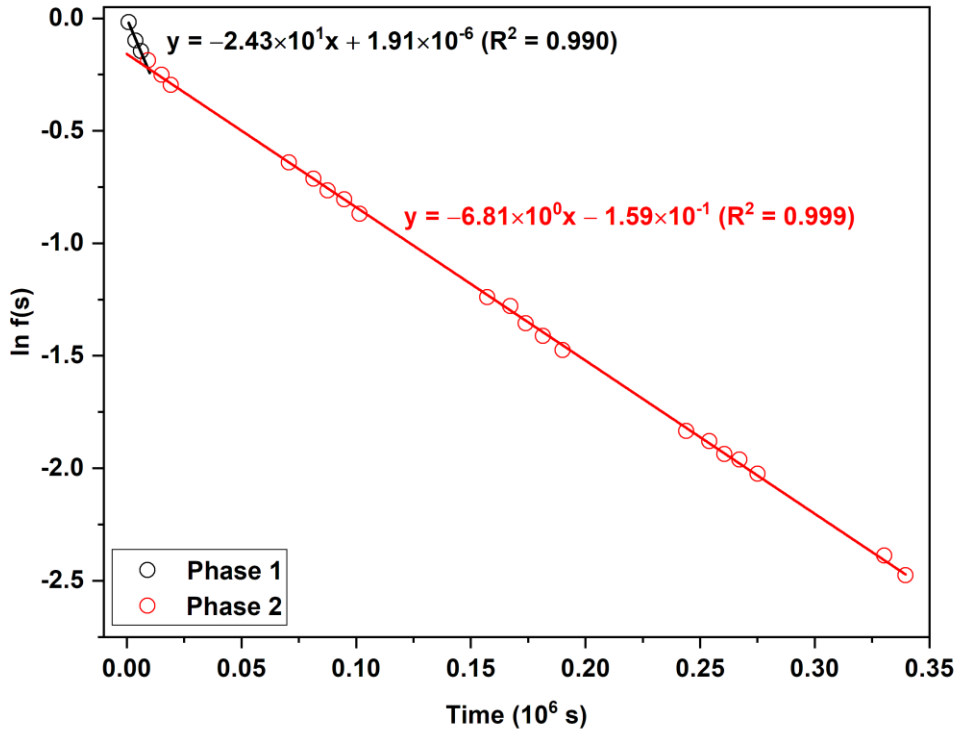


Figure S13 – Semilogarithmic plot of the fraction of remaining starting material as a function of time for *p*-I substituted Nitron **33g**.

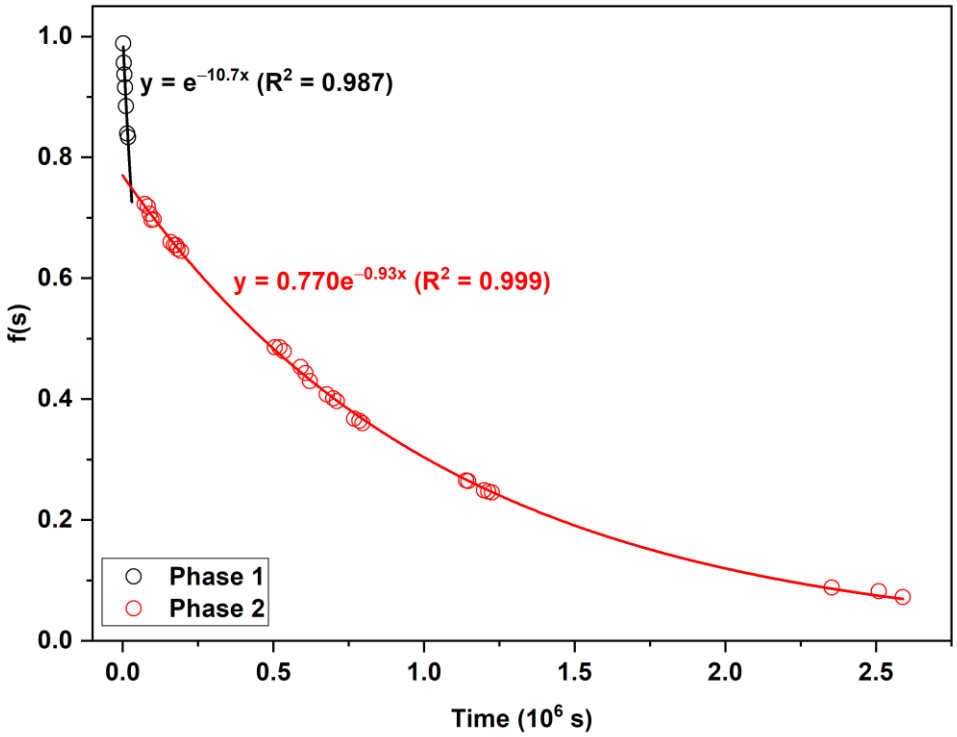


Figure S14 – Plot of the fraction of remaining starting material as a function of time for *p*-CN substituted Nitron **33j**.

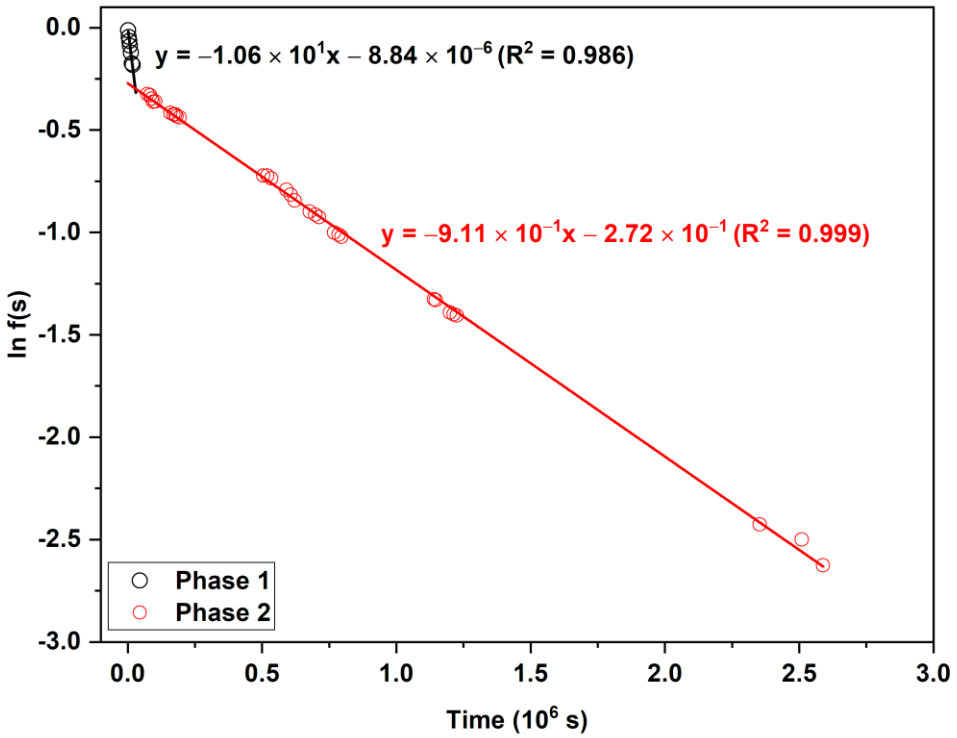


Figure S15 – Semilogarithmic plot of the fraction of remaining starting material as a function of time for *p*-CN substituted Nitron **33j**.

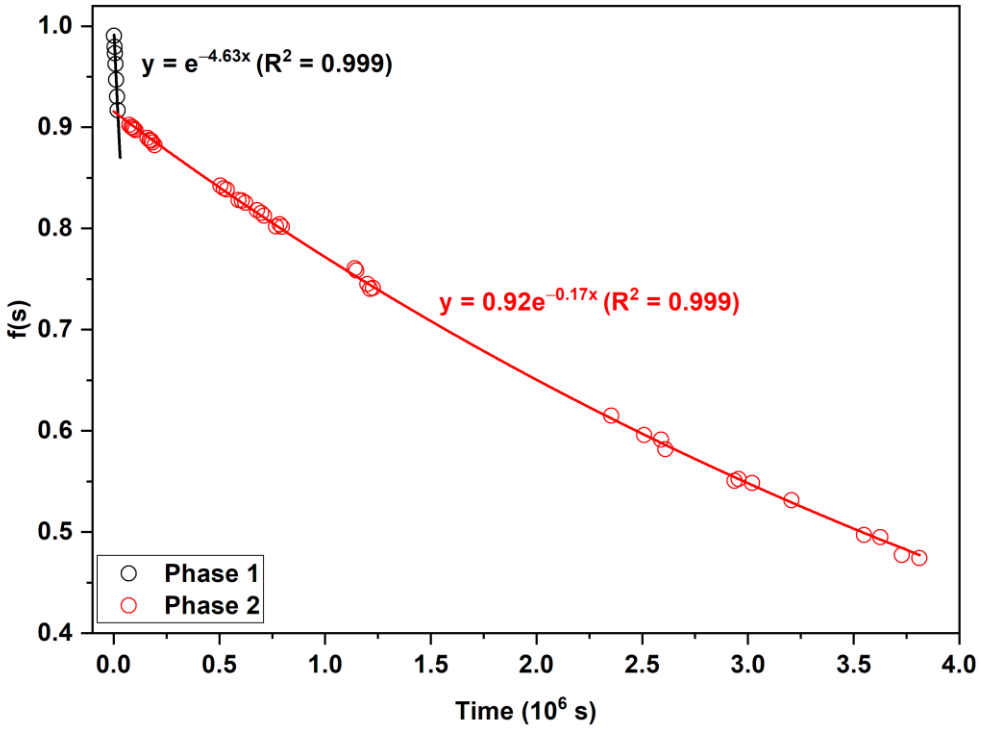


Figure S16 – Plot of the fraction of remaining starting material as a function of time for the *p*-CF_3 substituted CF_3 Nitron **33l**.

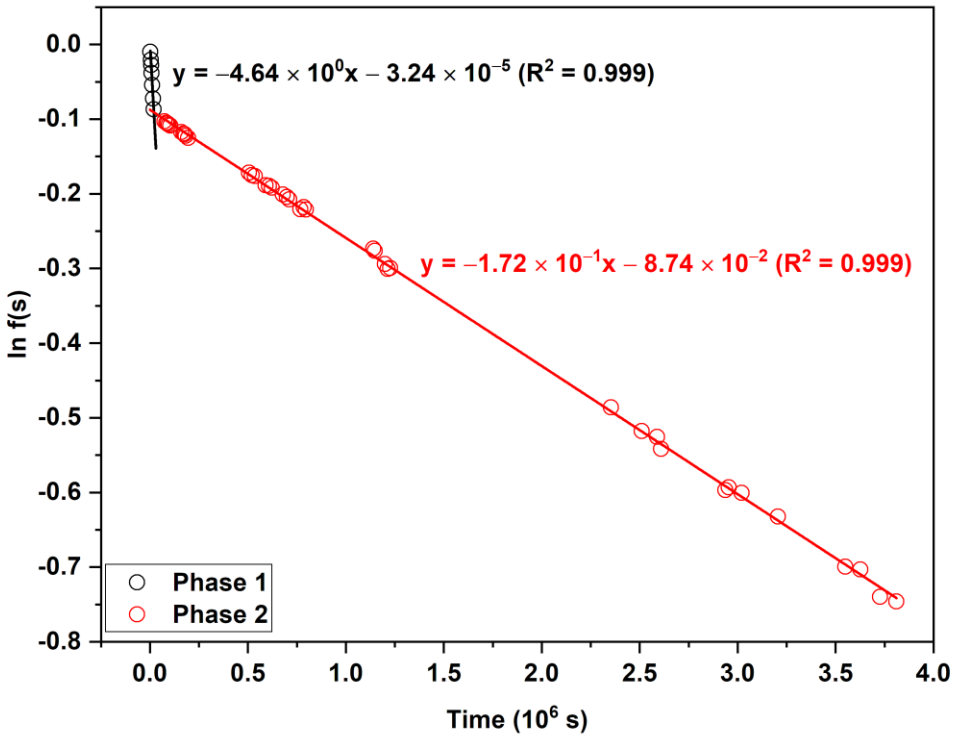


Figure S17 – Semilogarithmic plot of the fraction of remaining starting material as a function of time for the *p*-CF_3 substituted CF_3 Nitron **33l**.

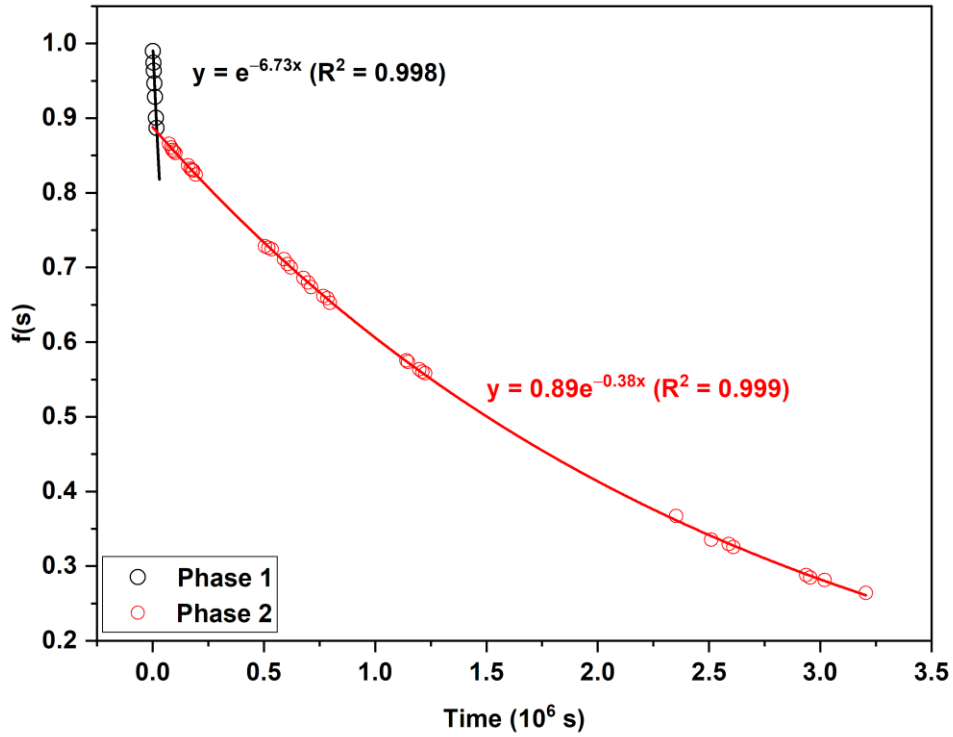


Figure S18 – Plot of the fraction of remaining starting material as a function of time for the *p*-OMe substituted CF_3 Nitron **33m**.

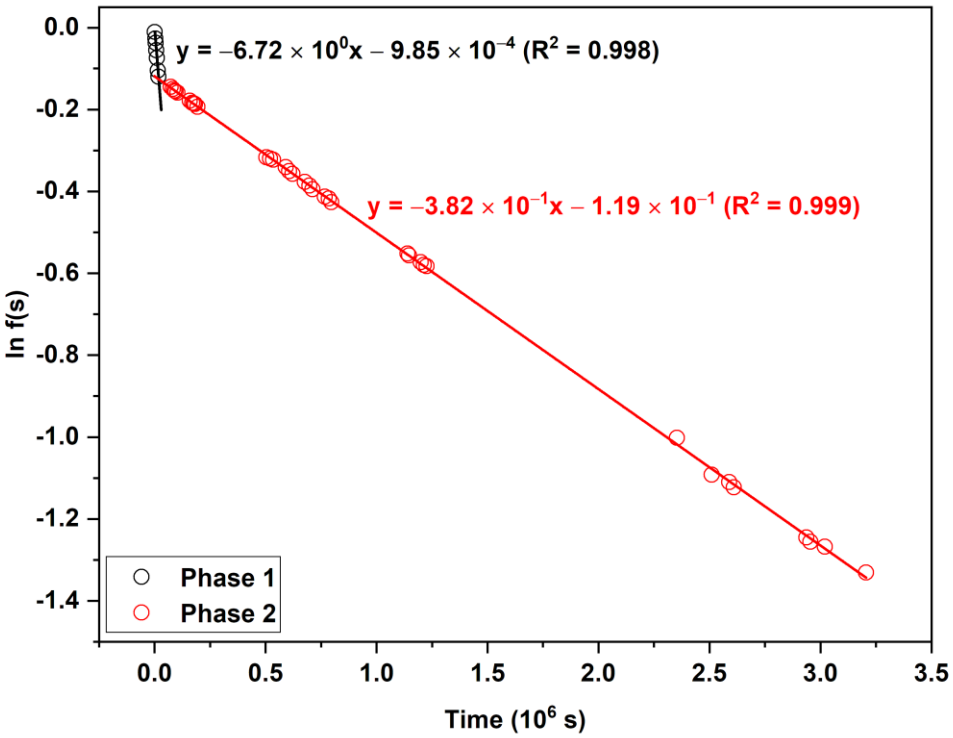


Figure S19 – Semilogarithmic plot of the fraction of remaining starting material as a function of time for the *p*-OMe substituted CF_3 Nitron **33m**.

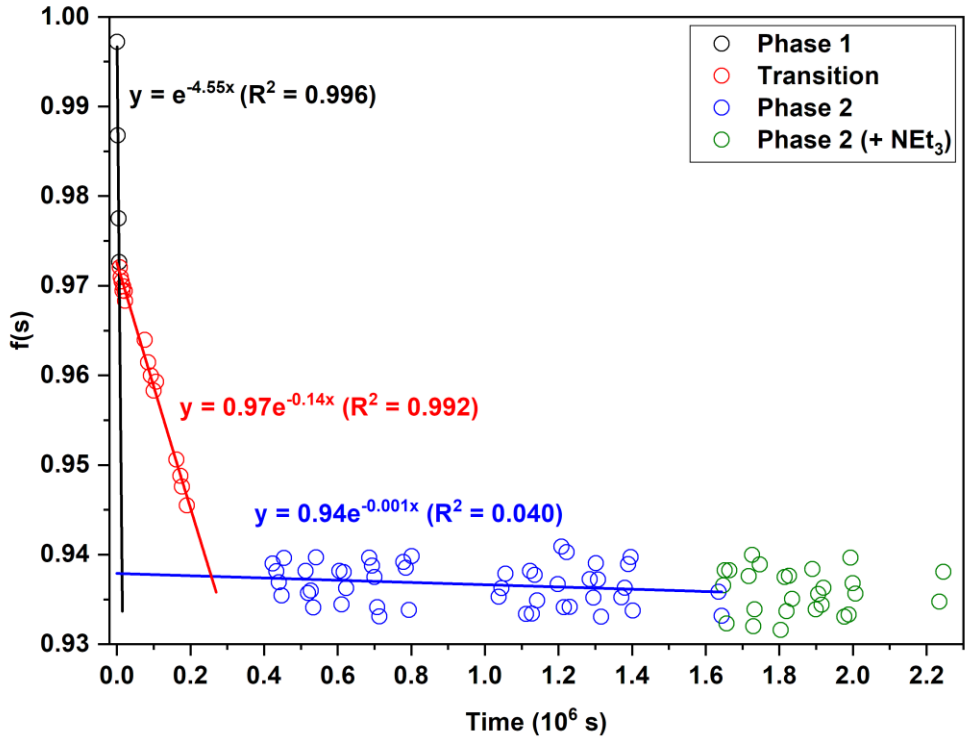


Figure S20 – Plot of the fraction of remaining starting material as a function of time for the *N*-methylated Nitron **192**.

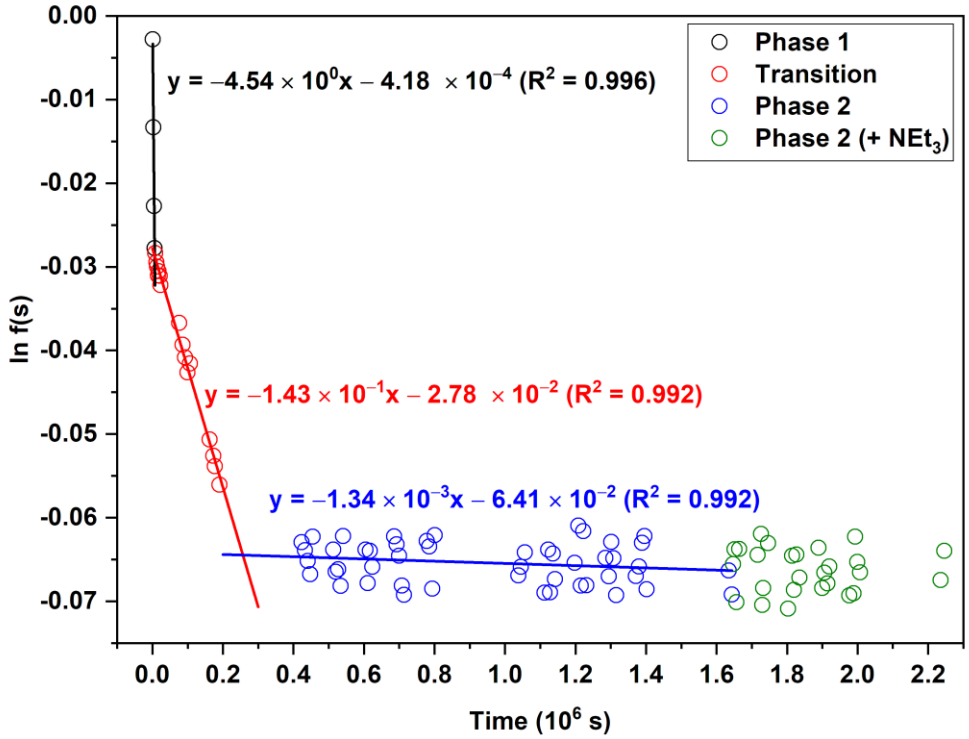


Figure S21 – Semilogarithmic plot of the fraction of remaining starting material as a function of time for the *N*-methylated Nitron **192**.

Appendix D - Supplementary information for Chapter 5

D-1 – Detailed description of H/D-exchange experiments

First and second order rate constants for exchange of the C(5)-H of *S*-triazolium salts for deuterium were determined in solutions of DCl in D_2O, and in formate buffer, at 25 °C and I = 1.0 (KCl). Compounds tested are all triazolium tetrafluoroborate salts unless otherwise stated. Reactions undertaken within fully aqueous media containing 10 mmol triazolium salt and 2 mmol tetramethylammonium chloride as the internal standard unless otherwise stated. Kinetic data obtained using the C5 instrument unless otherwise stated. Data collected and plotted for at least 5 half-lives unless otherwise stated.

D-1.1 – Spectrometer parameters and data processing

For A4 kinetics, which were preliminary investigations not used in the determination of k_{DO} values, samples were kept in 25.00 °C water bath and removed for the minimum time required for analysis.

For C5 kinetics, samples were kept within spectrometer determined to be thermostatted at 25.5 ± 0.2 °C using the difference in chemical shifts between the CH_2 and OH peaks of an ethylene glycol standard. The standard was analysed every hour over a 24-hour period and temperature values obtained from the 'tempcal' command on Vnmrj.

All spectra were subject to automatic phase correction and a sixth order Berstein polynomial fit before analysis.

Experiment parameters are provided in **Table S34** for each spectrometer:

Table S34 – Experiment parameters for the instruments used in kinetic measurements.

Parameter	A4	C5
Spectrometer model	Bruker Avance III-HD-400	Varian DD2-500
Spectrometer frequency for ^{1}H NMR (Hz)	399.95	499.44
Number of scans	4	32
Relaxation delay (s)	50.000	35.000
Pulse width (s)	10.000	11.400
Acquisition time (s)	4.0894	4.0894

D-1.2 – Determination of p*D* values in pure aqueous buffers

In pure aqueous buffers, p*D* values were calculated from the p*H* values by adding 0.4 to the observed reading on the p*H* probe based on literature values, according to **Equation S11**.[349] Deuteroxide concentration was determined using **Equation S12**, using the p*D* value at the start of the reaction for consistency.

$$pD(corr) = pH\ meter\ reading + 0.4 \qquad \textbf{Equation S11}$$

$$[DO^-] = \left(10^{pD(corr) - pK_w}\right) / \gamma_{DO} \qquad \textbf{Equation S12}$$

Where $K_W = 10^{-14.87}$ M^2 is the ion product of D_2O[350] at 25 °C and γ_{DO} is the apparent activity coefficient of deuteroxide ion under our experimental conditions. The apparent activity coefficient of deuteroxide ion, $\gamma_{DO} = 0.696 \pm 0.005$, was determined from the measured p*H* of solutions of known [HO^-] in water at I = 1.0 (KCl) and 25 °C, with the assumption that $\gamma_{DO} = \gamma_{HO}$.

D-1.3 – Determination of p*D* values in 2:8 d_3-MeCN / D_2O buffer

In 2:8 d_3-MeCN / D_2O, corrected p*D* values were calculated by adding 0.4 to the observed reading on the p*H* probe and the subtraction of $\delta = 0.067$, a constant based on values calculated in the literature, according to **Equation S13** and **Equation S14** respectively.[350, 351] This δ value accounts for p*D* variation arising from the use of pure aqueous standards for calibration with subsequent p*D* measurements in 2:8 d_3-MeCN / D_2O.

$$pD(obs) = pH\ meter\ reading + 0.4 \qquad \textbf{Equation S13}$$

$$pD(corr) = pD(obs) - \delta \qquad \textbf{Equation S14}$$

The deuteroxide concentration (M) was calculated from **Equation S15** where pK_{AP}(MeCN-D_2O) = 15.36 for a mixture of 2:8 MeCN / D_2O. This value is calculated from the equivalent value in 2:8 MeCN / H_2O (K_{AP}(MeCN-H_2O) = $10^{-14.49}$ M^2 for $\chi_{MeCN} = 0.2$), which is determined from the autoionization constant of a 1:2 solution of acetonitrile : water at 25 °C (K_{AP}(MeCN-H_2O) = $10^{-14.82}$ M^2 for $\chi_{MeCN} = 0.333$).[443] Literature autoprotolysis values[445] illustrate a linear relationship between K_{AP}(MeCN-H_2O) and χ_{MeCN} and so K_{AP}(MeCN-H_2O) for 2:8 MeCN / H_2O was calculated from comparing the values of K_w of pure water and K_{AP}(MeCN-H_2O) for $\chi_{MeCN} = 0.333$. In determining pK_{AP}(MeCN-D_2O) it is assumed that the same ratio K_{AP}(H_2O) / K_{AP}(D_2O) = 7.4 applies to K_{AP}(MeCN-H_2O) / K_{AP}(MeCN-D_2O).[350] The apparent activity coefficient of deuteroxide ion at 2:8 d_3-MeCN / D_2O, $\gamma_{DO} = 0.893$, was calculated based on previous work undertaken in 1:2 d_3-MeCN / D_2O.[65] It is assumed that the same ratio $\gamma_{DO(D2O)}$ / $\gamma_{DO(1:2\ MeCN\ /\ D2O)} = 0.468$ applies to the setup used within this work on electrodes provided from the same manufacturer, and that there exists a linear relationship between γ_{DO} and χ_{D_2O} moving from pure aqueous solutions to 1:2 d_3-MeCN / D_2O.

$$[DO^-] = \left(10^{pD(corr) - pK_{AP}(MeCN-D_2O)}\right) / \gamma_{DO} \qquad \textbf{Equation S15}$$

D-1.4 – Determination of k_{ex} and k_{DO}

k_{ex} values were determined from the slope of a plot of ln[f(s)] against time, fitted using the least squares method. Errors in the value of k_{ex} stated are the standard error values obtained from the linear fit. To determine the fraction of remaining substrate, f(s), the peak integral corresponding to the C(5)-H position was compared to the peak of the internal standard that was set to an arbitrary figure of 1000. The integral of the C(5)-H position from the first spectrum of the array was taken as I(0) and f(s) values at time 't' determined using **Equation S16**.

$$f(s) = \frac{I(t)}{I(0)} \qquad \textbf{Equation S16}$$

The second order rate constant, k_{DO}, was obtained for each triazolium salt from the slope of the plot of k_{ex} against [DO^-] according to **Equation S17**. A plot of log(k_{ex}) against p*D* was also used to calculate k_{DO}, alongside verifying a deuteroxide-catalysed exchange mechanism shown by a slope of the plot equal to 1, according to **Equation S18**. **Equation S18** is derived from **Equation S17** by consideration of the relationship of [DO^-] to p*D* and pK_W.

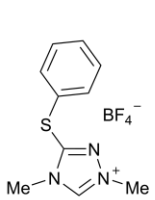
$$k_{ex} = k_{DO}[DO^-] \qquad \textbf{Equation S17}$$

$$\log(k_{ex}) = \log\left(\frac{k_{DO}K_w}{\gamma_{DO}}\right) + pD \qquad \textbf{Equation S18}$$

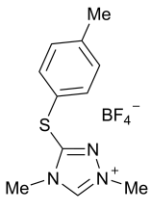
Where $K_w = 10^{-14.87}$ is the ion product of D_2O at 25 °C and $\gamma_{DO} = 0.696 \pm 0.005$ in pure aqueous solution, or 0.893 in 2:8 d_3-MeCN / D_2O, as defined earlier.[350]

D-2 – H/D-exchange results

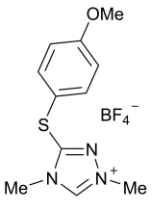
D-2.1 – Structures of all *S*-triazolium salts analysed



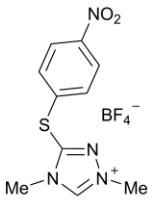
92a·BF$_4$



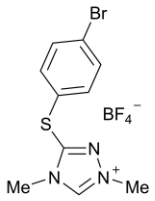
92b·BF$_4$



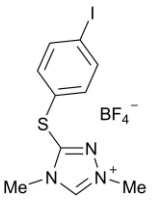
92d·BF$_4$



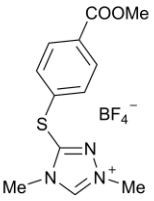
92e·BF$_4$



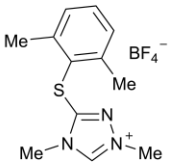
92h·BF$_4$



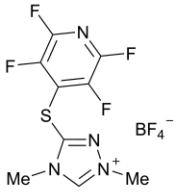
92i·BF$_4$



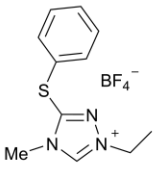
92n·BF$_4$



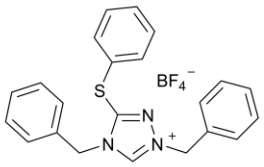
92o·BF$_4$



92q·BF$_4$



94·BF$_4$



99·Br

D-2.2 – 1,4-Dimethyl-3-(phenylthio)-4*H*-1,2,4-triazol-1-ium tetrafluoroborate (**92a·BF$_4$**)

Table S35 – Summary of the results from all H/D-exchange experiments relating to **92a·BF$_4$**.

Buffer / [DCl]	p*D*(Corr)	[DO$^-$] (M)	k_{ex} (s^{-1})	$t_{1/2}$ (h)	k_{DO} (M^{-1}s^{-1})
1.00 × 10^{-2} M DCl	2.07 → 2.10	2.28 × 10^{-13}	9.42 (± 0.01) × 10^{-6}	20.43	
1.00 × 10^{-2} M DCl (20% v/v MeCN)[c]	2.20 → 2.17	7.75 × 10^{-14}	9.48 (± 0.03) × 10^{-6}	20.30	
5.00 × 10^{-3} M DCl	2.42 → 2.45	5.10 × 10^{-13}	2.04 (± 0.003) × 10^{-5}	9.42	**Equation S17** 4.25 (± 0.03) × 10^7
2.00 × 10^{-3} M DCl	2.87 → 2.88	1.44 × 10^{-12}	5.19 (± 0.01) × 10^{-5}	3.71	**Equation S18** 3.74 (± 0.03) × 10^7
10% fb formate	3.20 → 3.19	3.07 × 10^{-12}	1.22 (± 0.01) × 10^{-4}	1.58	
30% fb formate	3.59 → 3.59	7.54 × 10^{-12}	3.18 (± 0.03) × 10^{-4}	0.61 (36 min)	
50% fb formate	3.85 → 3.84	1.37 × 10^{-11}	5.79 (± 0.02) × 10^{-4}	0.33 (20 min)	

[a] Data collected on A4 instrument. Reaction also undertaken with 20% v/v MeCN, using the quintet arising from MeCN as the internal standard.

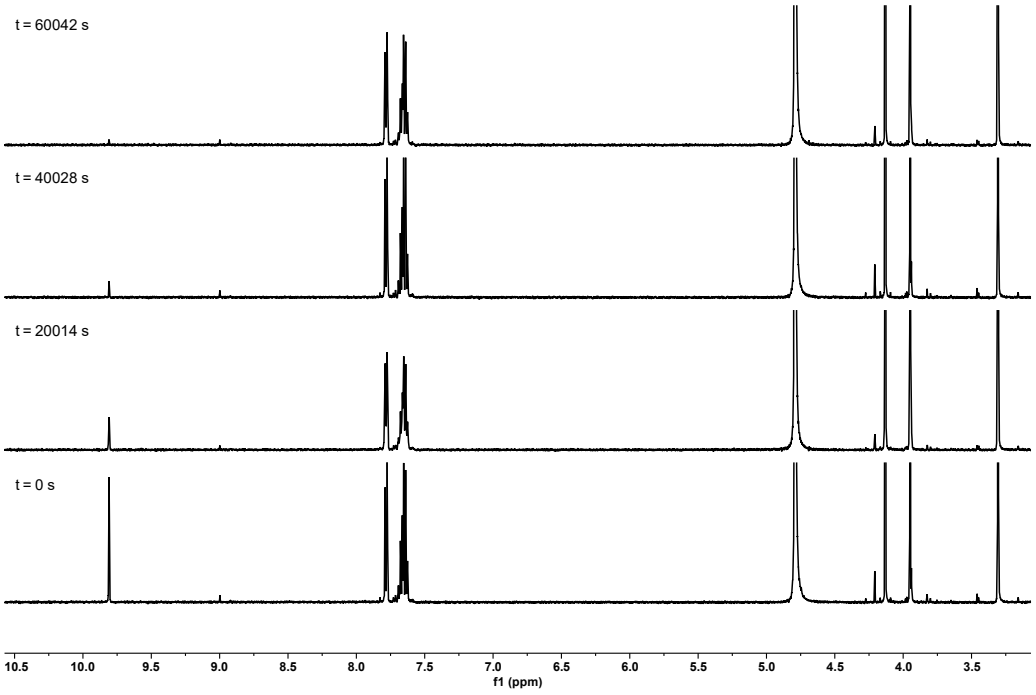


Figure S22 – Representative NMR overlay at 500 MHz for **92a·BF$_4$** at 2.00 × 10^{-3} M DCl (10 mM, p*D*(corr) 2.87), obtained during exchange of the C(5)-H (s, 9.81 ppm) for deuterium in D_2O at 25 °C and I = 1.0 (KCl). Tetramethylammonium chloride internal standard (s, 3.31 ppm).

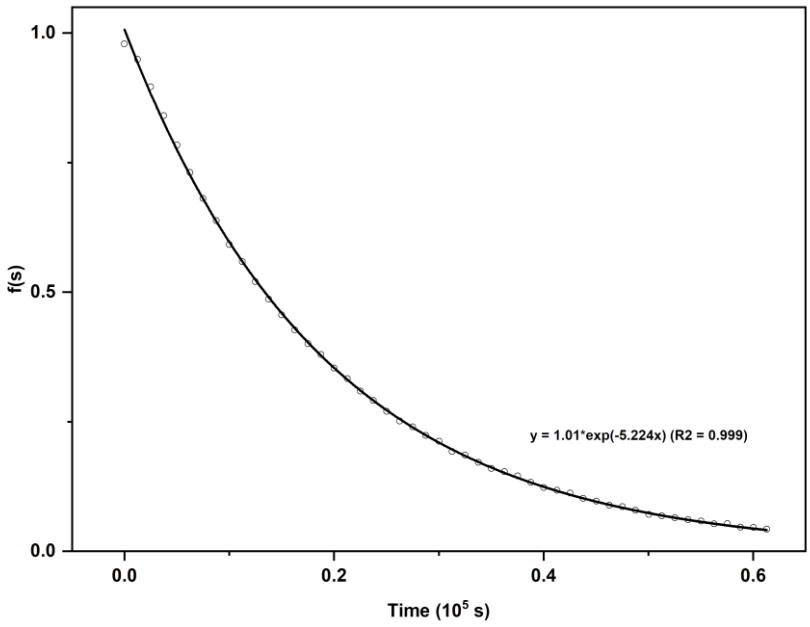


Figure S23 – Representative plot of the fraction of unexchanged substrate against time for the deuterium exchange reaction of **92a**·BF_4 at 2.00×10^{-3} DCl (10 mM, p*D*(corr) = 2.87) in D_2O at 25 °C and I = 1.0 (KCl). The line through the data shows the non-linear least squares fit for a 1st order decay process.

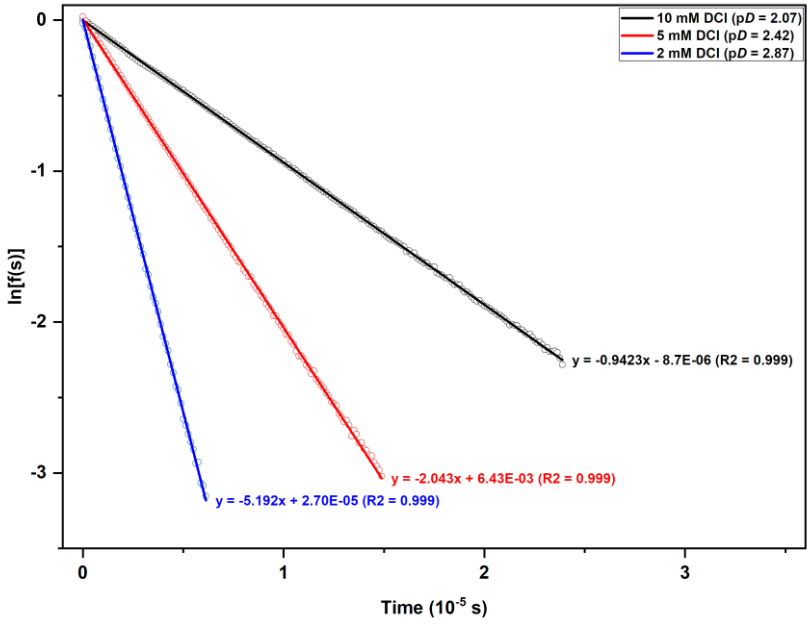


Figure S24 – Semilogarithmic plots of the fraction of unexchanged substrate against time for the deuterium exchange reaction of **92a**·BF_4 in solutions of DCl within D_2O at 25 °C and I = 1.0 (KCl).

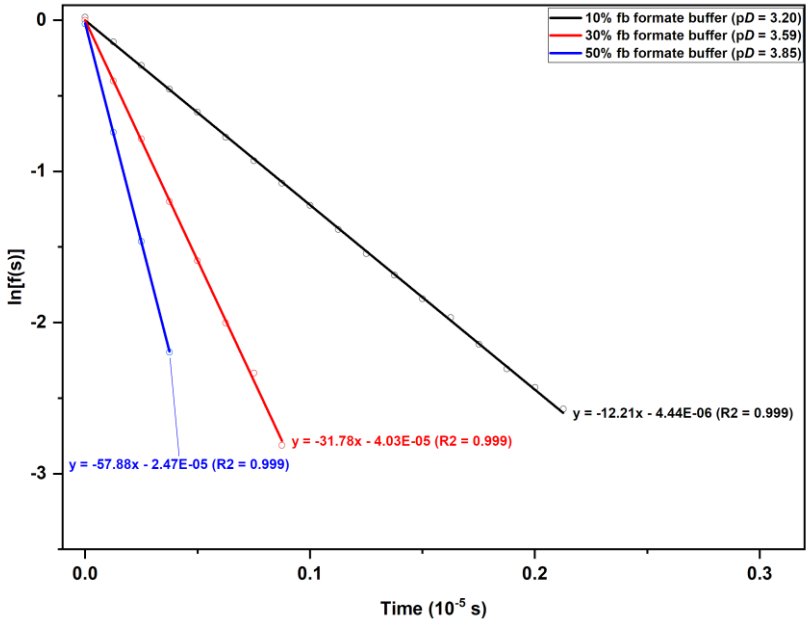


Figure S25 – Semilogarithmic plots of the fraction of unexchanged substrate against time for the deuterium exchange reaction of **92a·BF$_4$** in formate buffer within D_2O at 25 °C and I = 1.0 (KCl).

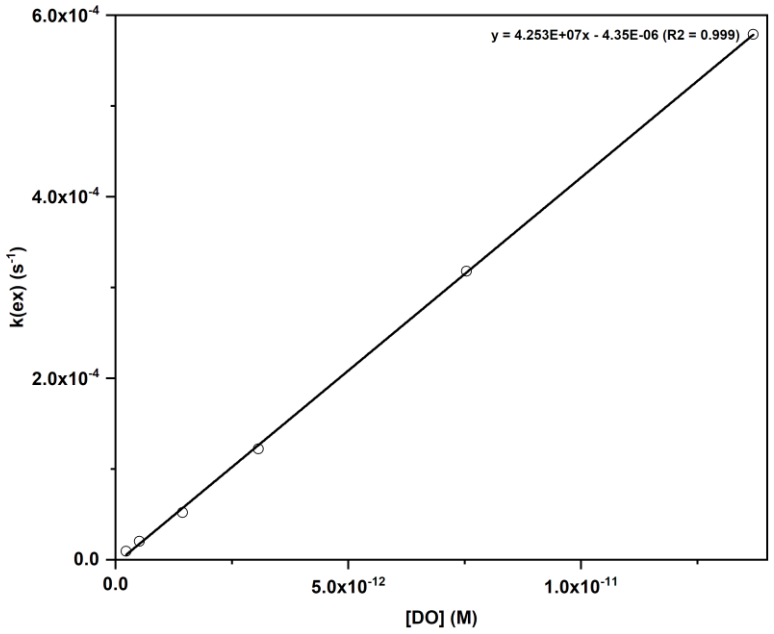


Figure S26 – Plot of k_{ex} against [DO^-] for **92a·BF$_4$** in solutions of DCl and formate buffer in D_2O at p*D*s 2.07 – 3.85, 25 °C and I = 1.0 (KCl). The line through the data shows the fit of k_{ex} – [DO^-] to **Equation S17**.

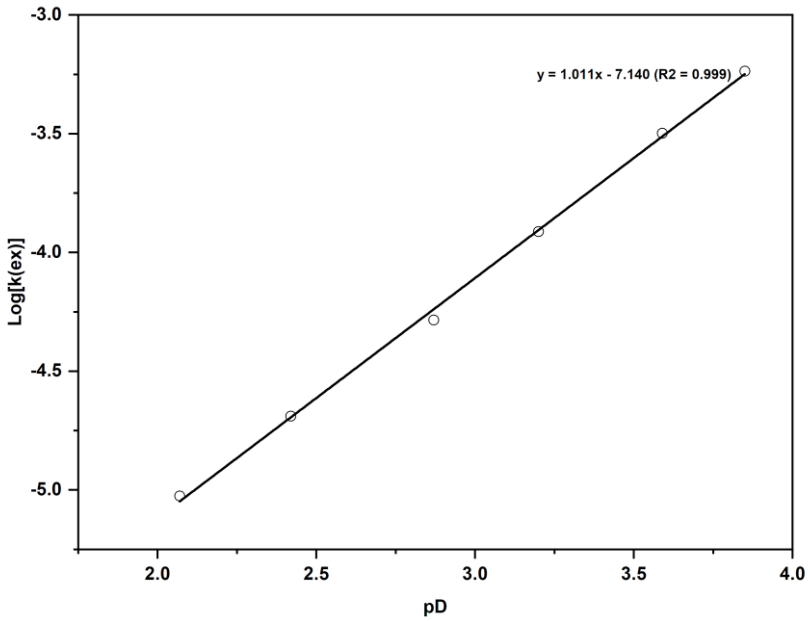


Figure S27 – Plot of log(k_{ex}) against p*D* for **92a·BF$_4$** in solutions of DCl and formate buffer in D_2O at 25 °C and I = 1.0 (KCl). The line through the data shows the fit of log(k_{ex}) – p*D* data to **Equation S18**.

D-2.3 – 1,4-Dimethyl-3-(*p*-tolylthio)-4*H*-1,2,4-triazol-1-ium tetrafluoroborate (**92b·BF$_4$**)

Table S36 – Summary of the results from all H/D-exchange experiments relating to **92b·BF$_4$**

Buffer / [DCl]	p*D*	[DO$^-$] (M)	k_{ex} (s^{-1})	$t_{1/2}$ (h)	k_{DO} (M^{-1}s^{-1})
5.00 × 10^{-3} M DCl [a]	2.49 → 2.46	5.99 × 10^{-13}	1.79 (± 0.003) × 10^{-5}	10.77	
2.00 × 10^{-3} M DCl	2.78 → 2.76	1.17 × 10^{-12}	3.76 (± 0.01) × 10^{-5}	5.12	**Equation S17** 3.27 (± 0.03) × 10^7
10% fb formate	3.20 → 3.20	3.07 × 10^{-12}	1.04 (± 0.003) × 10^{-4}	1.85	
30% fb formate	3.62 → 3.60	8.08 × 10^{-12}	2.69 (± 0.02) × 10^{-4}	0.72 (43 min)	**Equation S18** 2.67 (± 0.05) × 10^7
50% fb formate	3.87 → 3.86	1.44 × 10^{-11}	4.69 (± 0.04) × 10^{-4}	0.41 (25 min)	

[a] Values obtained after tracking reaction for 2 half-lives.

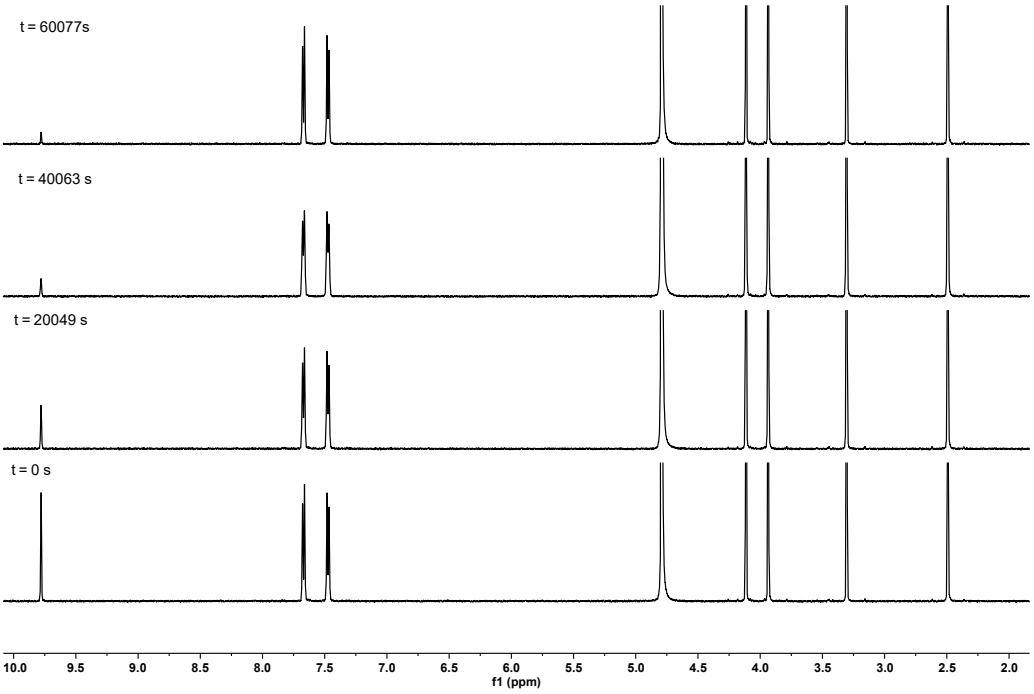


Figure S28 – Representative NMR overlay at 500 MHz for **92b·BF$_4$** at 2.00 × 10^{-3} M DCl (10 mM, p*D*(corr) 2.78), obtained during exchange of the C(5)-H (s, 9.78 ppm) for deuterium in D_2O at 25 °C and I = 1.0 (KCl). Tetramethylammonium chloride internal standard (s, 3.30 ppm).

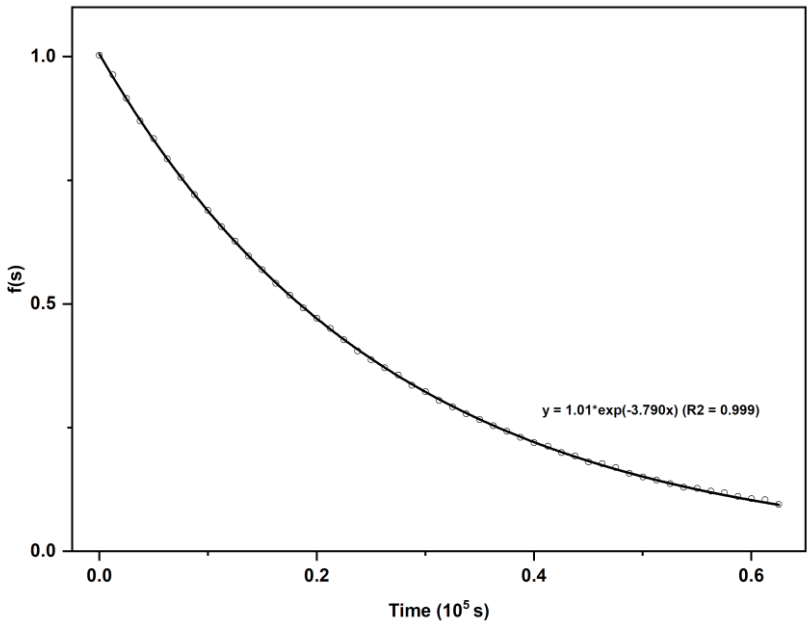


Figure S29 – Representative plot of the fraction of unexchanged substrate against time for the deuterium exchange reaction of **92b·BF$_4$** at 2.00 × 10^{-3} DCl (10 mM, p*D*(corr) = 2.78) in D_2O at 25 °C and I = 1.0 (KCl). The line through the data shows the non-linear least squares fit for a 1st order decay process.

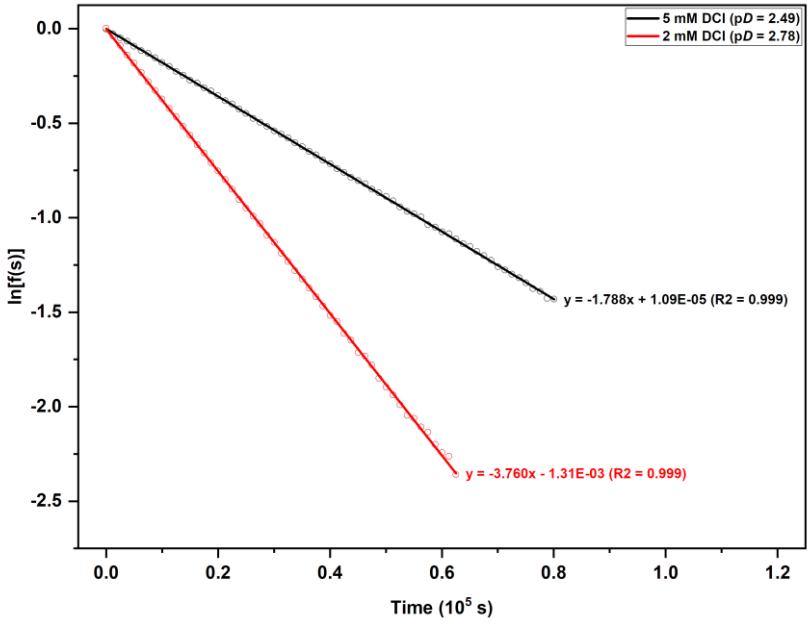


Figure S30 – Semilogarithmic plots of the fraction of unexchanged substrate against time for the deuterium exchange reaction of **92b·BF$_4$** in solutions of DCl within D_2O at 25 °C and I = 1.0 (KCl).

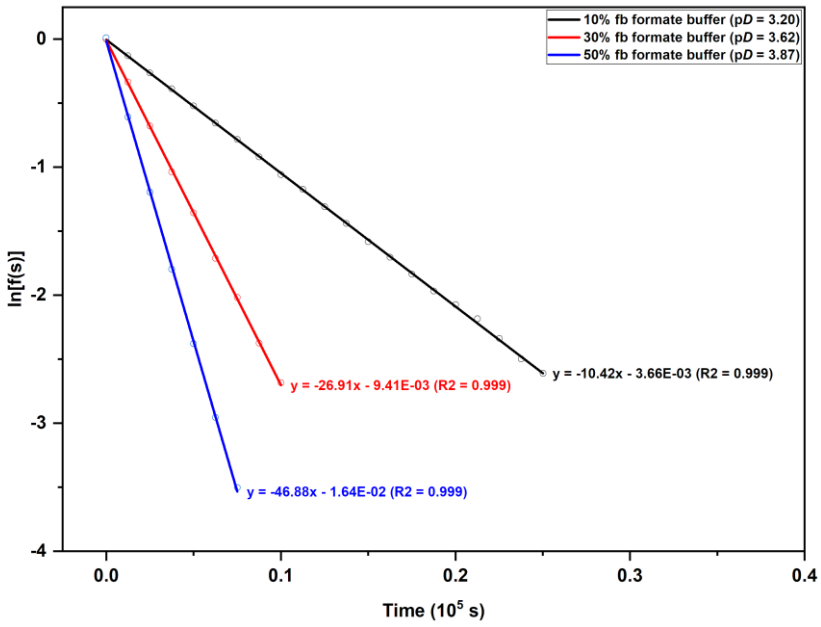


Figure S31 – Semilogarithmic plots of the fraction of unexchanged substrate against time for the deuterium exchange reaction of **92b·BF$_4$** in formate buffer within D_2O at 25 °C and I = 1.0 (KCl).

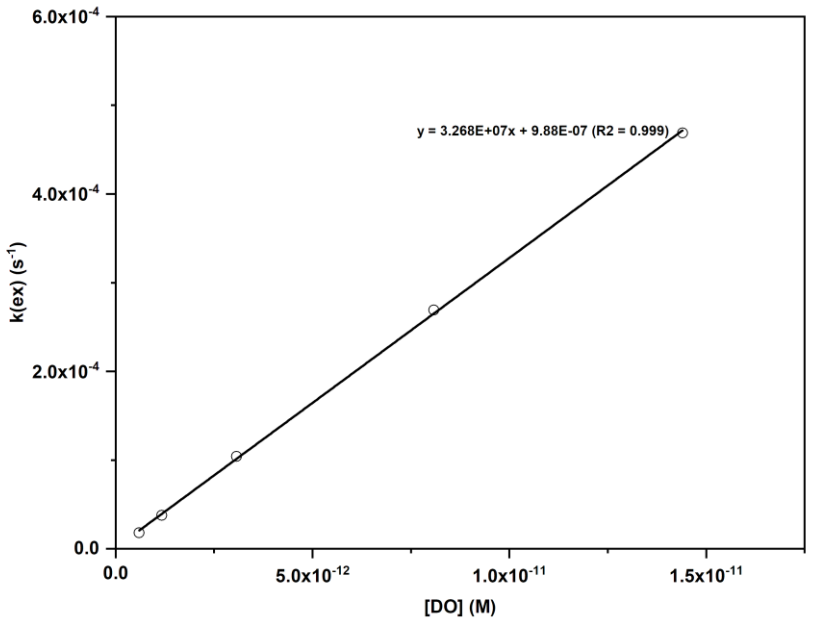


Figure S32 – Plot of k_{ex} against [DO^-] for **92b·BF$_4$** in solutions of DCl and formate buffer in D_2O at p*D*s 2.49 – 3.87, 25 °C and I = 1.0 (KCl). The line through the data shows the fit of k_{ex} – [DO^-] to **Equation S17**.

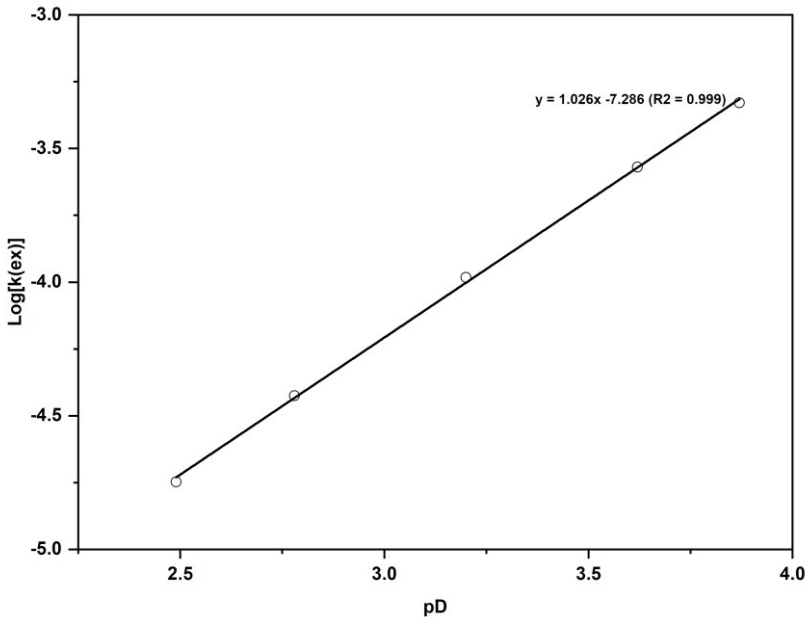


Figure S33 – Plot of log(k_{ex}) against p*D* for **92b·BF$_4$** in solutions of DCl and formate buffer in D_2O at 25 °C and I = 1.0 (KCl). The line through the data shows the fit of log(k_{ex}) – p*D* data to **Equation S18**.

D-2.4 – 3-((4-Methoxyphenyl)thio)-1,4-dimethyl-4*H*-1,2,4-triazol-1-ium tetrafluoroborate (**92d·BF$_4$**)

Table S37 – Summary of the results from all H/D-exchange experiments relating to **92d·BF$_4$**

Buffer / [DCl]	p*D*	[DO$^-$] (M)	k_{ex} (s^{-1})	$t_{1/2}$ (h)	k_{DO} (M^{-1}s^{-1})
5.00 × 10^{-3} M DCl [a]	2.44 → 2.44	5.34 × 10^{-13}	1.49 (± 0.002) × 10^{-5}	12.91	
2.00 × 10^{-3} M DCl	2.93 → 2.91	1.65 × 10^{-12}	4.48 (± 0.01) × 10^{-5}	4.30	**Equation S17** 2.70 (± 0.07) × 10^7 [d]
10% fb formate	3.19 → 3.20	3.00 × 10^{-12}	8.90 (± 0.03) × 10^{-5}	2.16	
30% fb formate	3.62 → 3.61	8.08 × 10^{-12}	2.33 (± 0.02) × 10^{-4}	0.83 (50 min)	**Equation S18** 2.84 (± 0.06) × 10^7 [e]
50% fb formate	3.90 → 3.86	1.54 × 10^{-11}	4.14 (± 0.01) × 10^{-4}	0.47 (28 min)	

[a] Values obtained after tracking the reaction for 2 half-lives.

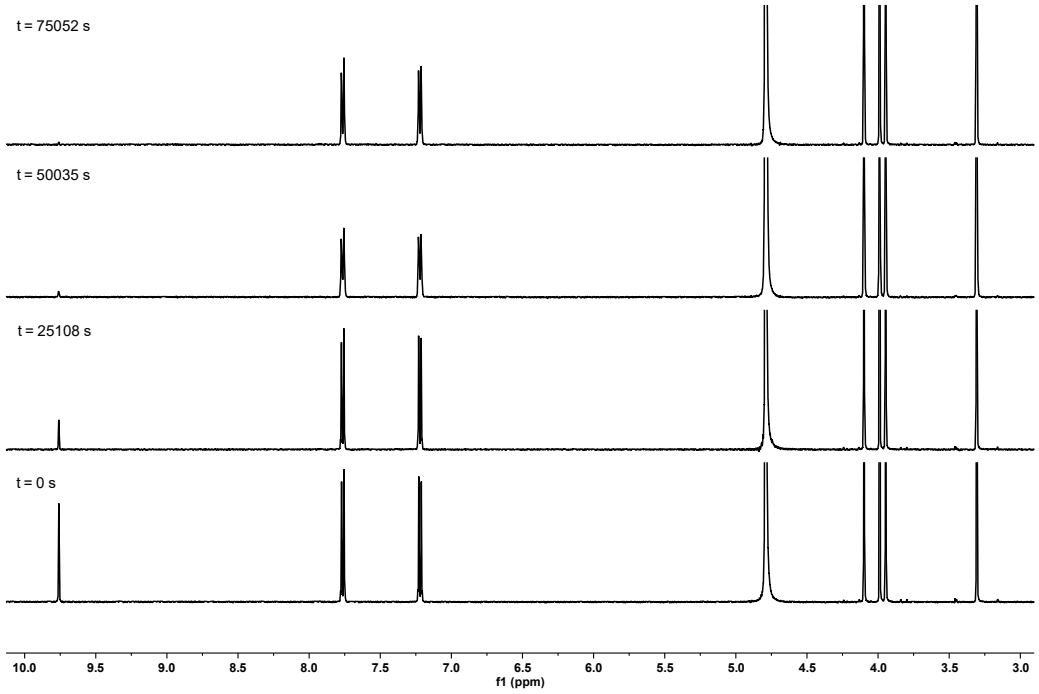


Figure S34 – Representative NMR overlay at 500 MHz for **92d·BF$_4$** at 2.00 × 10^{-3} M DCl (10 mM, p*D*(corr) 2.93), obtained during exchange of the C(5)-H (s, 9.76 ppm) for deuterium in D_2O at 25 °C and I = 1.0 (KCl). Tetramethylammonium chloride internal standard (s, 3.31 ppm).

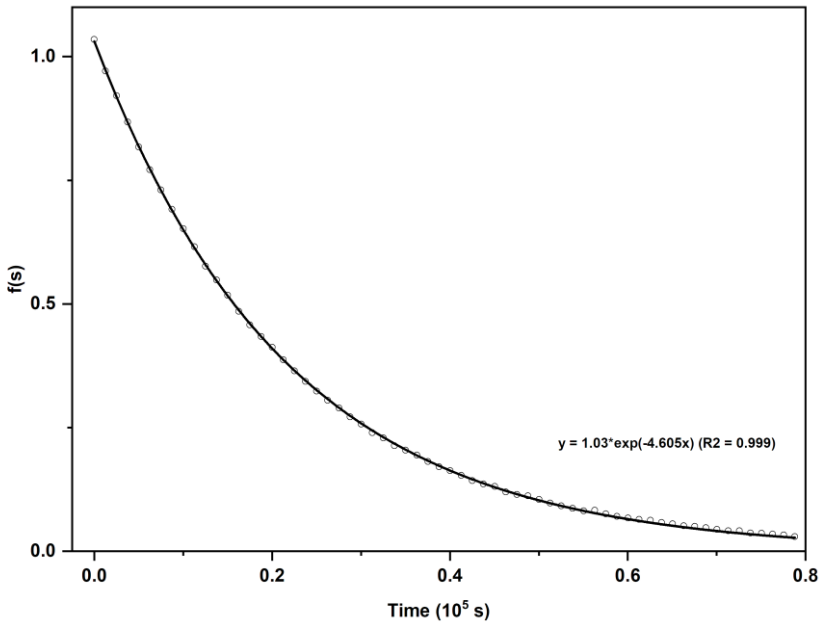


Figure S35 – Representative plot of the fraction of unexchanged substrate against time for the deuterium exchange reaction of **92d·BF$_4$** at 2.00 × 10^{-3} DCl (10 mM, p*D*(corr) = 2.93) in D_2O at 25 °C and I = 1.0 (KCl). The line through the data shows the non-linear least squares fit for a 1st order decay process.

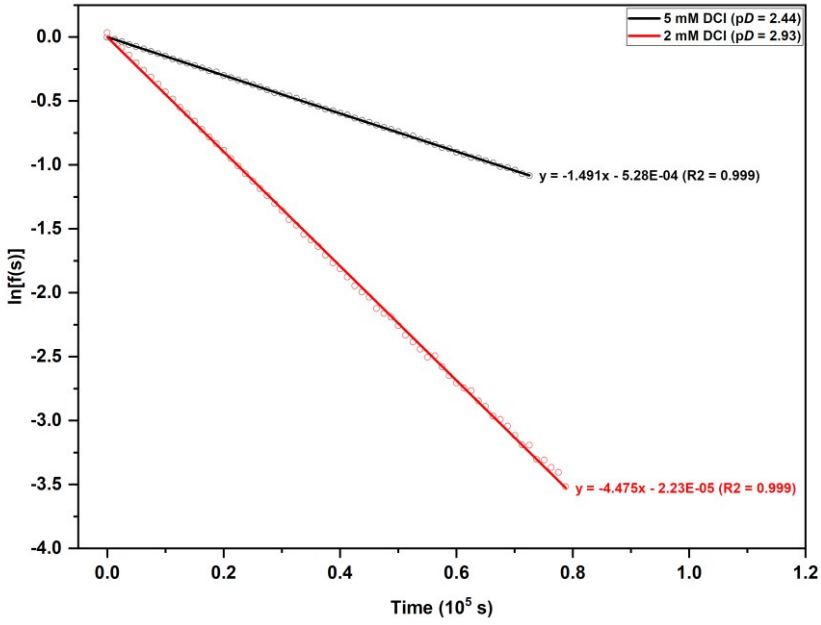


Figure S36 – Semilogarithmic plots of the fraction of unexchanged substrate against time for the deuterium exchange reaction of **92d·BF$_4$** in solutions of DCl within D_2O at 25 °C and I = 1.0 (KCl).

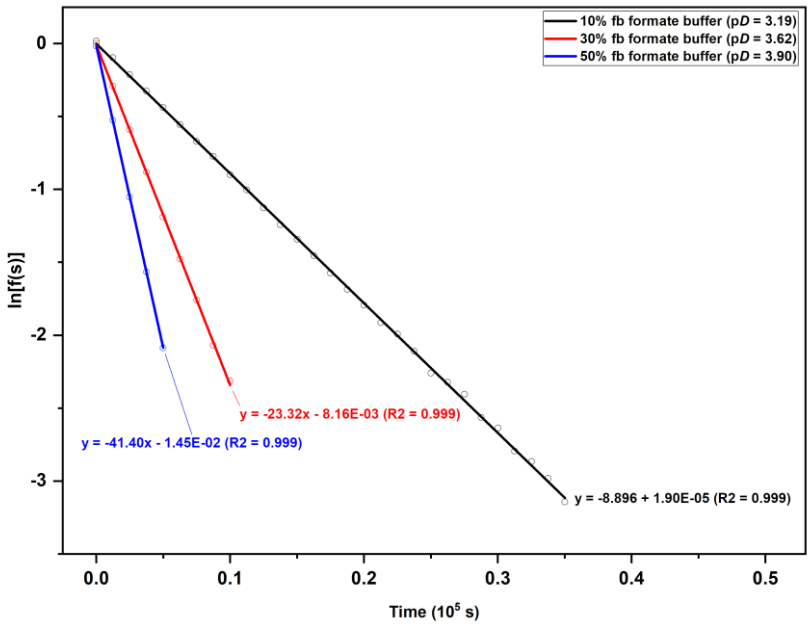


Figure S37 – Semilogarithmic plots of the fraction of unexchanged substrate against time for the deuterium exchange reaction of **92d·BF$_4$** in formate buffer within D_2O at 25 °C and I = 1.0 (KCl).

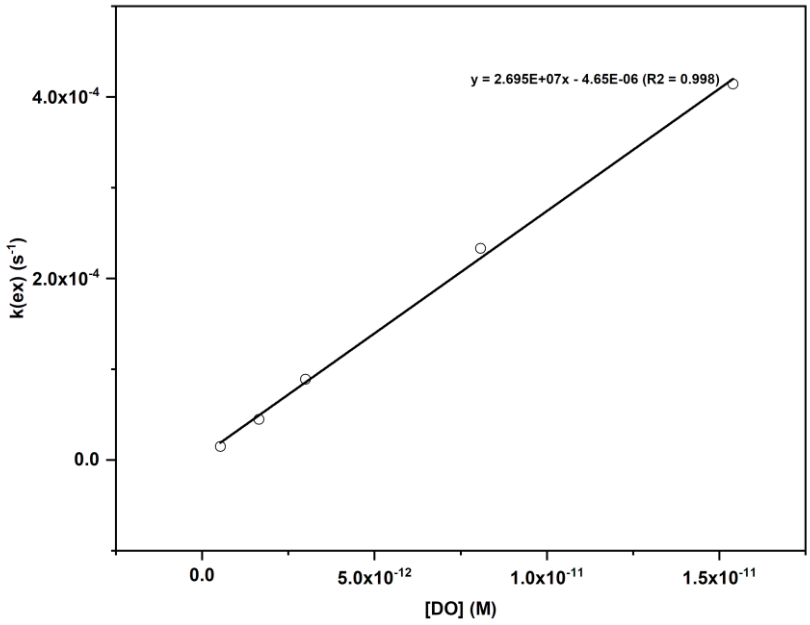


Figure S38 – Plot of k_{ex} against [DO^-] for **92d·BF$_4$** in solutions of DCl and formate buffer in D_2O at p*D*s 2.44 – 3.90, 25 °C and I = 1.0 (KCl). The line through the data shows the fit of k_{ex} – [DO^-] to **Equation S17**.

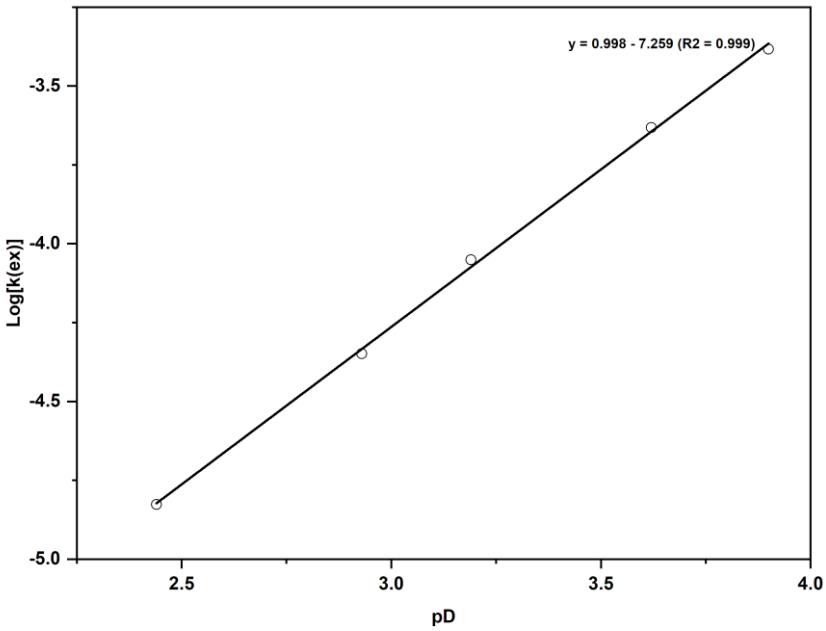


Figure S39 – Plot of log(k_{ex}) against p*D* for **92d·BF$_4$** in solutions of DCl and formate buffer in D_2O at 25 °C and I = 1.0 (KCl). The line through the data shows the fit of log(k_{ex}) – p*D* data to **Equation S18**.

D-2.5 – 1,4-Dimethyl-3-((4-nitrophenyl)thio)-4*H*-1,2,4-triazol-1-ium tetrafluoroborate (**92e·BF$_4$**)

Table S38 – Summary of the results from all H/D-exchange experiments relating to **92e·BF$_4$**

Buffer / [DCl]	p*D*	[DO$^-$] (M)	k_{ex} (s^{-1})	$t_{1/2}$ (h)	k_{DO} (M^{-1}s^{-1})
1.00 × 10^{-2} M DCl	2.12 → 2.10	2.55 × 10^{-13}	2.20 (± 0.003) × 10^{-5}	8.74	**Equation S17** 9.20 (± 0.36) × 10^7
5.00 × 10^{-3} M DCl	2.42 → 2.41	5.08 × 10^{-13}	4.63 (± 0.01) × 10^{-5}	4.24	
2.00 × 10^{-3} M DCl	2.99 → 2.99	1.89 × 10^{-12}	1.61 (± 0.01) × 10^{-4}	1.20	**Equation S18** 8.29 (± 0.08) × 10^7
10% fb formate	3.21 → 3.20	3.14 × 10^{-12}	2.91 (± 0.02) × 10^{-4}	0.66 (40 min)	

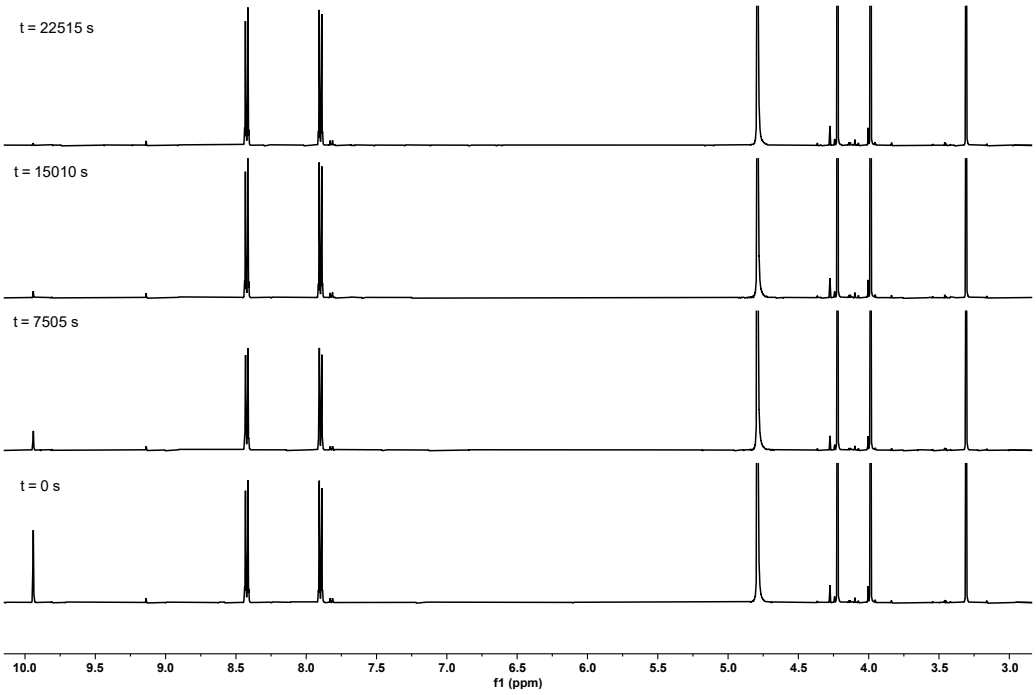


Figure S40 – Representative NMR overlay at 500 MHz for **92e·BF$_4$** at 2.00 × 10^{-3} M DCl (10 mM, p*D*(corr) 2.99), obtained during exchange of the C(5)-H (s, 9.94 ppm) for deuterium in D_2O at 25 °C and I = 1.0 (KCl). Tetramethylammonium chloride internal standard (s, 3.31 ppm).

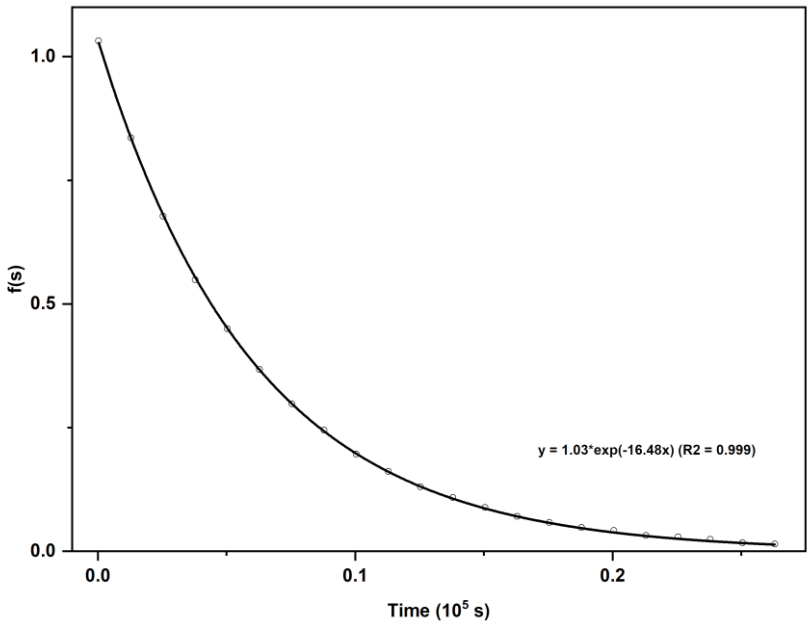


Figure S41 – Representative plot of the fraction of unexchanged substrate against time for the deuterium exchange reaction of **92e·BF$_4$** at 2.00 × 10^{-3} DCl (10 mM, p*D*(corr) = 2.99) in D_2O at 25 °C and I = 1.0 (KCl). The line through the data shows the non-linear least squares fit for a 1st order decay process.

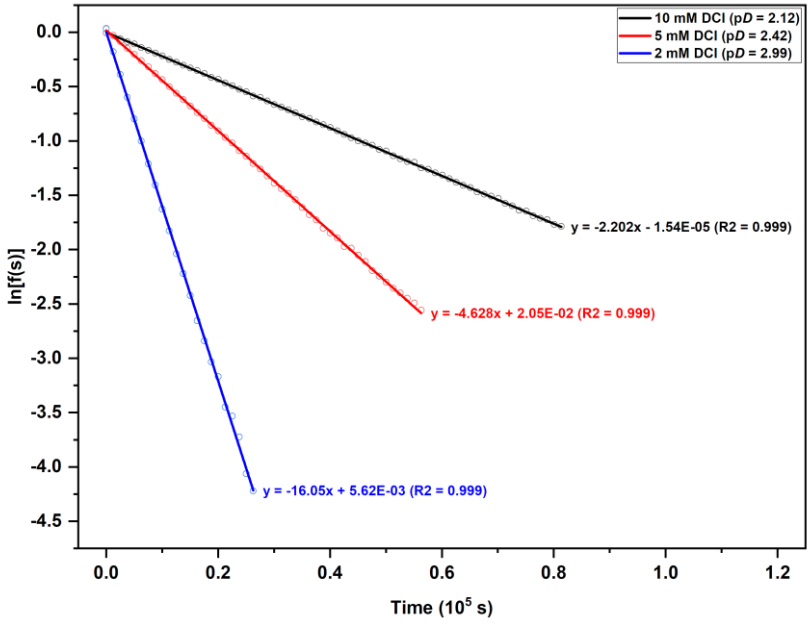


Figure S42 – Semilogarithmic plots of the fraction of unexchanged substrate against time for the deuterium exchange reaction of **92e·BF$_4$** in solutions of DCl within D_2O at 25 °C and I = 1.0 (KCl).

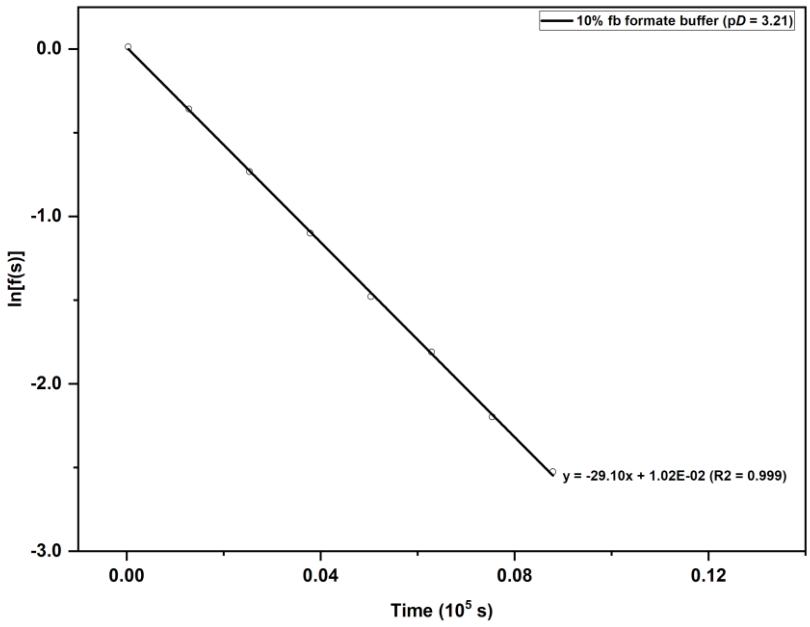


Figure S43 – Semilogarithmic plots of the fraction of unexchanged substrate against time for the deuterium exchange reaction of **92e·BF$_4$** in formate buffer within D_2O at 25 °C and I = 1.0 (KCl).

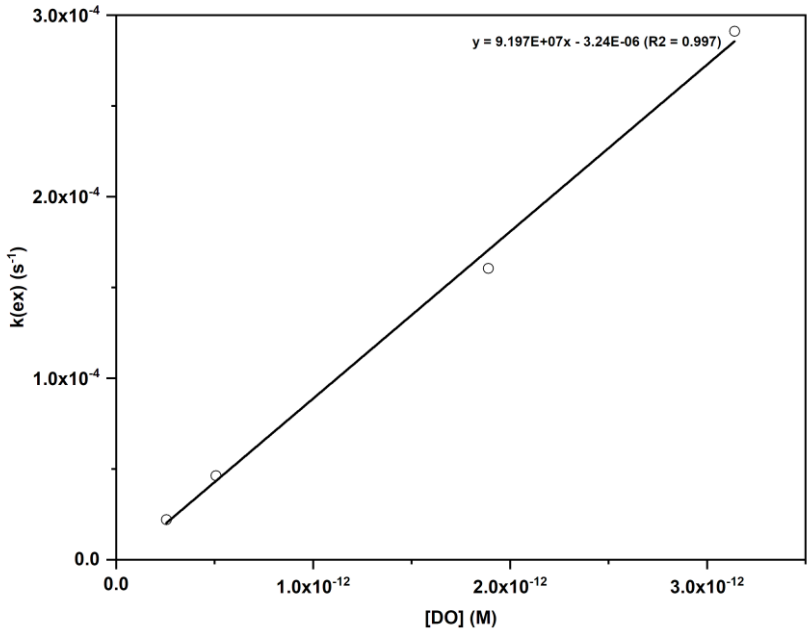


Figure S44 – Plot of k_{ex} against [DO^-] for **92e·BF$_4$** in solutions of DCl and formate buffer in D_2O at p*D*s 2.12 – 3.21, 25 °C and I = 1.0 (KCl). The line through the data shows the fit of k_{ex} – [DO^-] to **Equation S17**.

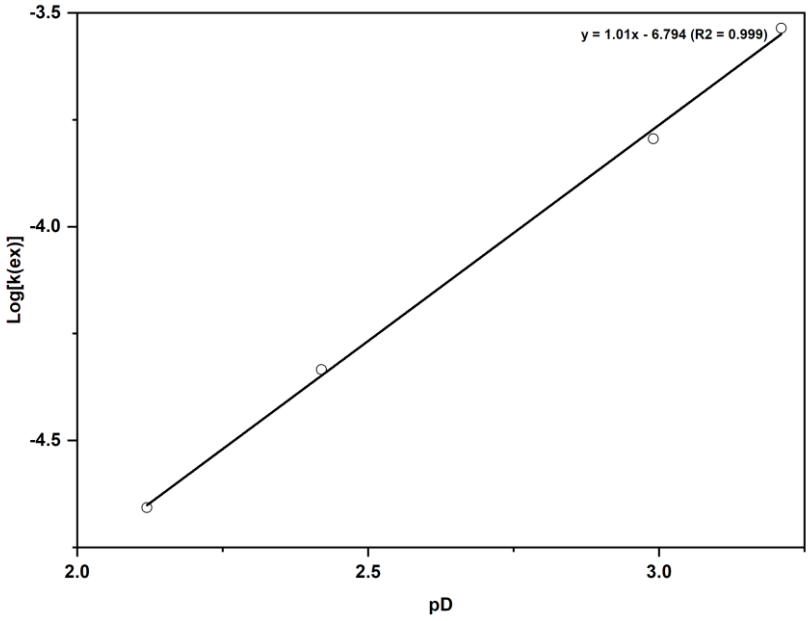


Figure S45 – Plot of log(k_{ex}) against p*D* for **92e·BF₄** in solutions of DCl and formate buffer in D_2O at 25 °C and I = 1.0 (KCl). The line through the data shows the fit of log(k_{ex}) – p*D* data to **Equation S18**.

D-2.6 – 3-((4-Bromophenyl)thio)-1,4-dimethyl-4*H*-1,2,4-triazol-1-ium tetrafluoroborate (**92h·BF$_4$**)

Table S39 – Summary of the results from all H/D-exchange experiments relating to **92h·BF$_4$**

Buffer / [DCl]	p*D*	[DO$^-$] (M)	k_{ex} (s^{-1})	$t_{1/2}$ (h)	k_{DO} (M^{-1}s^{-1})
1.00 × 10^{-2} M DCl	2.09 → 2.11	2.38 × 10^{-13}	1.13 (± 0.001) × 10^{-5}	17.08	**Equation S17** 4.43 (± 0.02) × 10^7
5.00 × 10^{-3} M DCl	2.44 → 2.45	5.34 × 10^{-13}	2.42 (± 0.003) × 10^{-5}	7.97	
2.00 × 10^{-3} M DCl	2.88 → 2.86	1.47 × 10^{-12}	6.58 (± 0.03) × 10^{-5}	2.93	**Equation S18** 5.42 (± 0.03) × 10^7

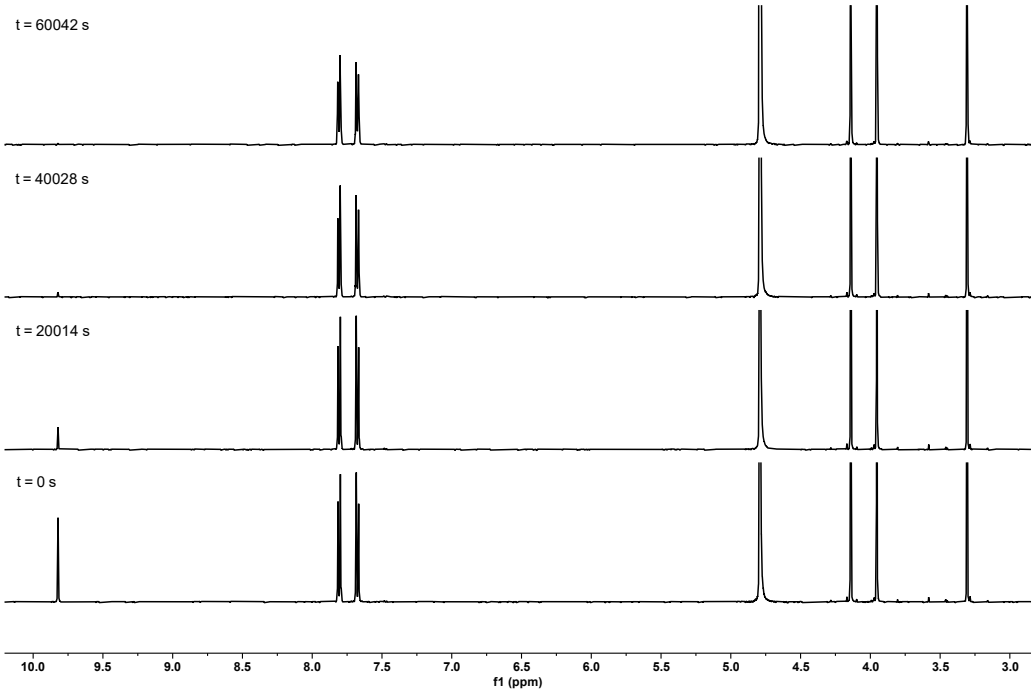


Figure S46 – Representative NMR overlay at 500 MHz for **92h·BF$_4$** at 2.00 × 10^{-3} M DCl (10 mM, p*D*(corr) 2.88), obtained during exchange of the C(5)-H (s, 9.82 ppm) for deuterium in D_2O at 25 °C and I = 1.0 (KCl). Tetramethylammonium chloride internal standard (s, 3.31 ppm).

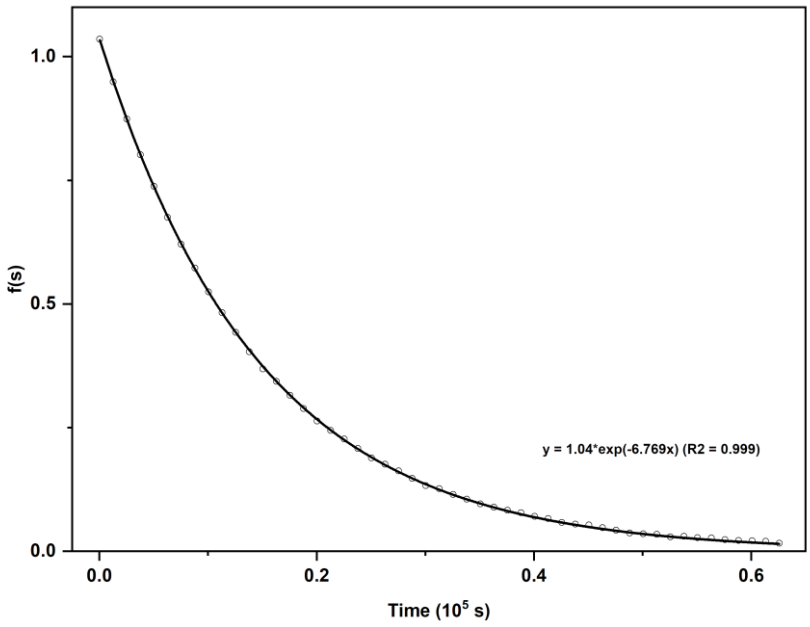


Figure S47 – Representative plot of the fraction of unexchanged substrate against time for the deuterium exchange reaction of **92h·BF$_4$** at 2.00 × 10^{-3} DCl (10 mM, p*D*(corr) = 2.88) in D_2O at 25 °C and I = 1.0 (KCl). The line through the data shows the non-linear least squares fit for a 1st order exponential decay process.

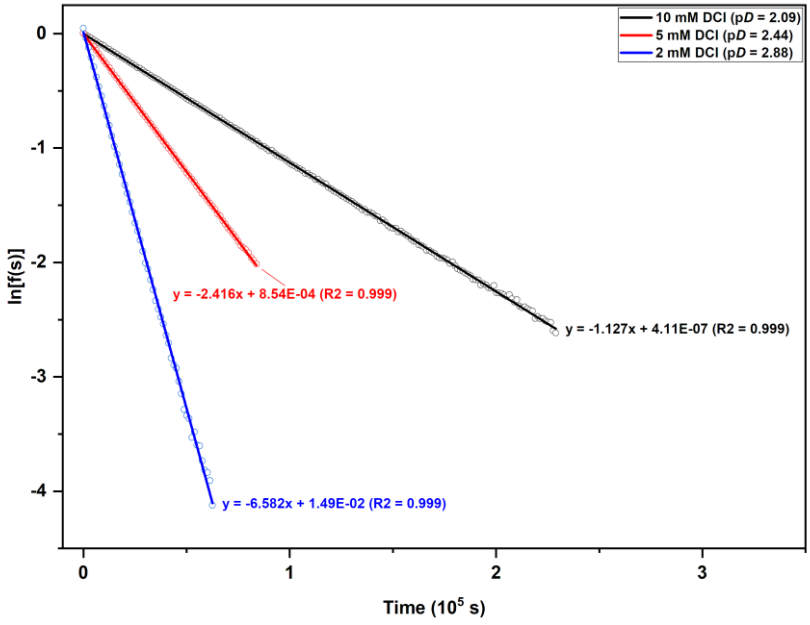


Figure S48 – Semilogarithmic plot of the fraction of unexchanged substrate against time for the deuterium exchange reaction of **92h·BF$_4$** in solutions of DCl in D_2O at 25 °C and I = 1.0 (KCl).

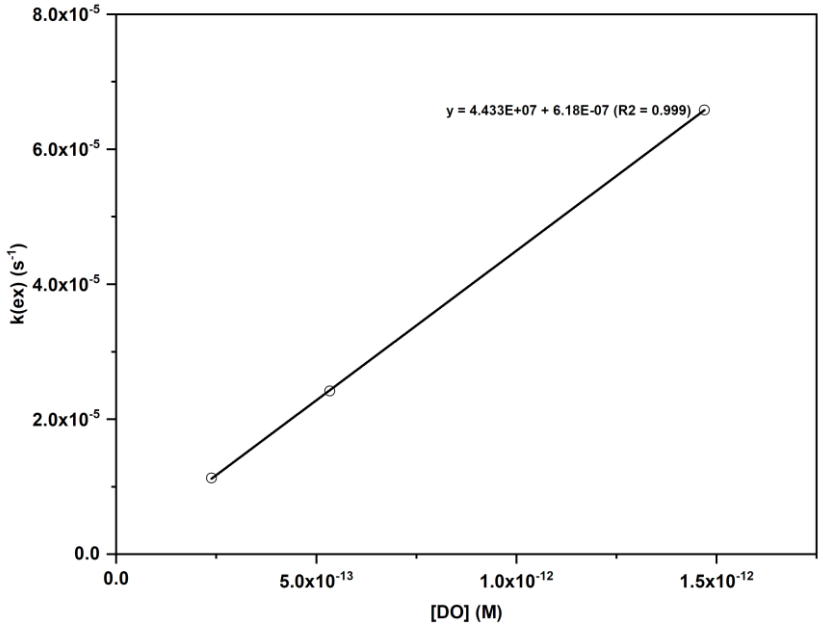


Figure S49 – Plot of k_{ex} against [DO^-] for **92h·BF$_4$** in solutions of DCl in D_2O at p*D*s 2.09 – 2.88, 25 °C and I = 1.0 (KCl). The line through the data shows the fit of k_{ex} – [DO^-] to **Equation S17**.

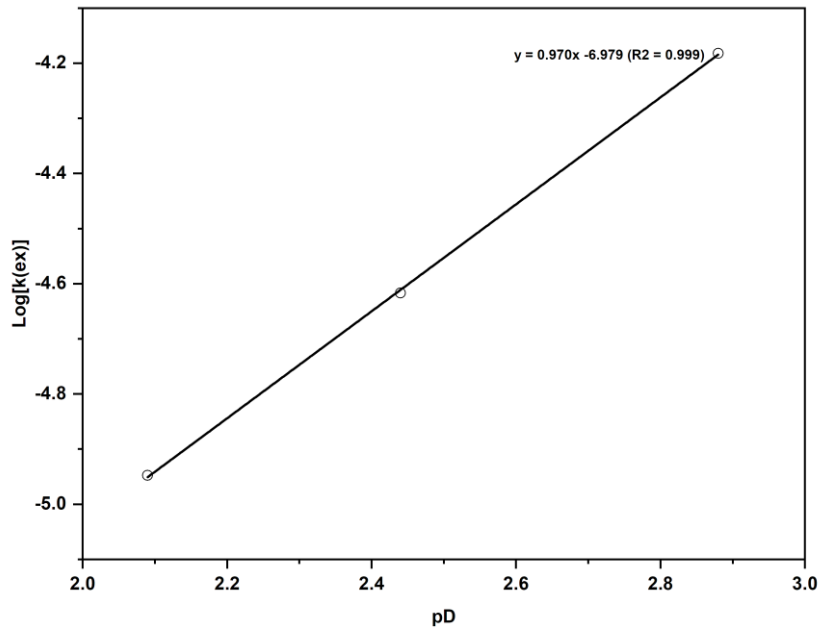


Figure S50 – Plot of log(k_{ex}) against p*D* for **92h·BF$_4$** in solutions of DCl in D_2O at 25 °C and I = 1.0 (KCl). The line through the data shows the fit of log(k_{ex}) – p*D* data to **Equation S18**.

D-2.7 – 3-((4-Iodophenyl)thio)-1,4-dimethyl-4*H*-1,2,4-triazol-1-ium tetrafluoroborate (**92i·BF$_4$**)

Table S40 – Summary of the results from all H/D-exchange experiments relating to **92i·BF$_4$**

Buffer / [DCl]	p*D*	[DO$^-$] (M)	k_{ex} (s^{-1})	$t_{1/2}$ (h)	k_{DO} (M^{-1}s^{-1})
5.00 × 10^{-3} M DCl	2.43 → 2.44	5.22 × 10^{-13}	2.40 (± 0.01) × 10^{-5}	8.03	**Equation S17** 4.60 (± 0.05) × 10^7
2.00 × 10^{-3} M DCl	2.89 → 2.86	1.50 × 10^{-12}	6.76 (± 0.04) × 10^{-5}	2.84	
10% fb formate	3.24 → 3.22	3.37 × 10^{-12}	1.55 (± 0.004) × 10^{-4}	1.24	**Equation S18** 4.63 (± 0.04) × 10^7

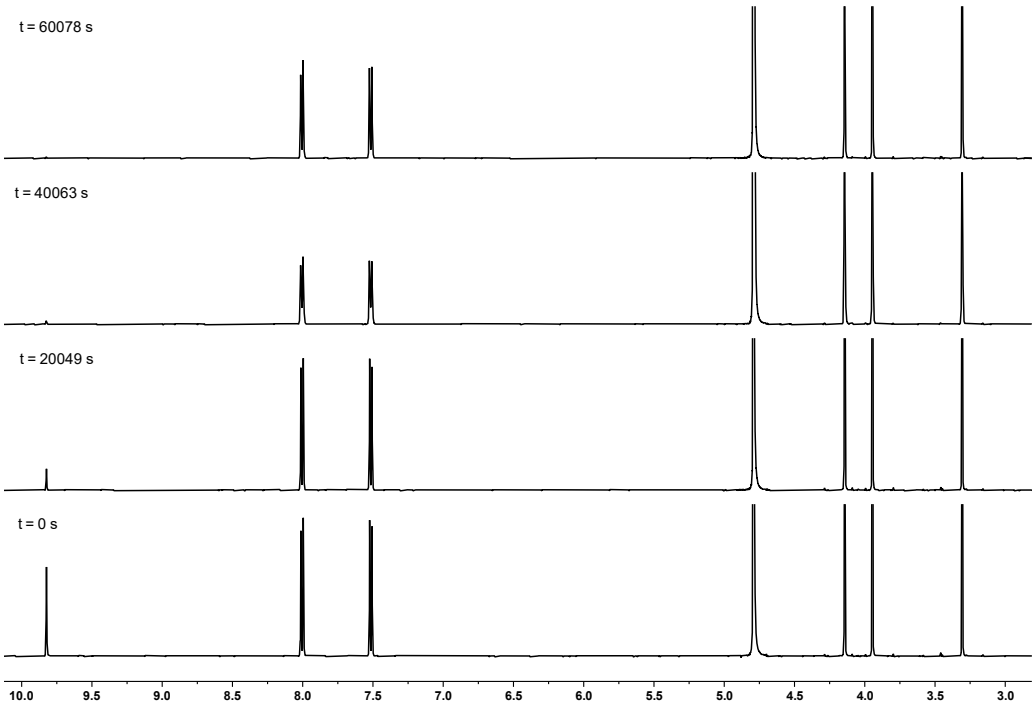


Figure S51 – Representative NMR overlay at 500 MHz for **92i·BF$_4$** at 2.00 × 10^{-3} M DCl (10 mM, p*D*(corr) 2.89), obtained during exchange of the C(5)-H (s, 9.82 ppm) for deuterium in D_2O at 25 °C and I = 1.0 (KCl). Tetramethylammonium chloride internal standard (s, 3.31 ppm).

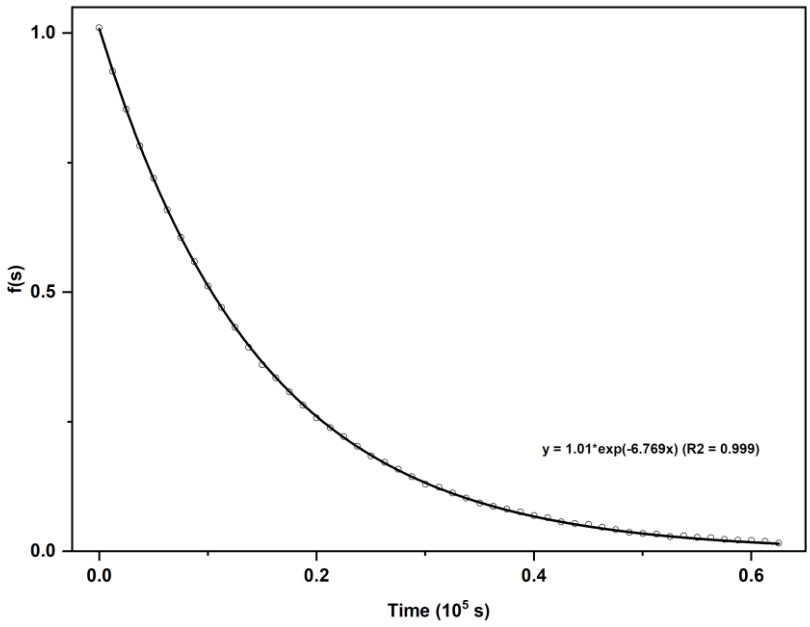


Figure S52 – Representative plot of the fraction of unexchanged substrate against time for the deuterium exchange reaction of **92i·BF$_4$** at 2.00 × 10^{-3} DCl (10 mM, p*D*(corr) = 2.89) in D_2O at 25 °C and I = 1.0 (KCl). The line through the data shows the non-linear least squares fit for a 1st order decay process.

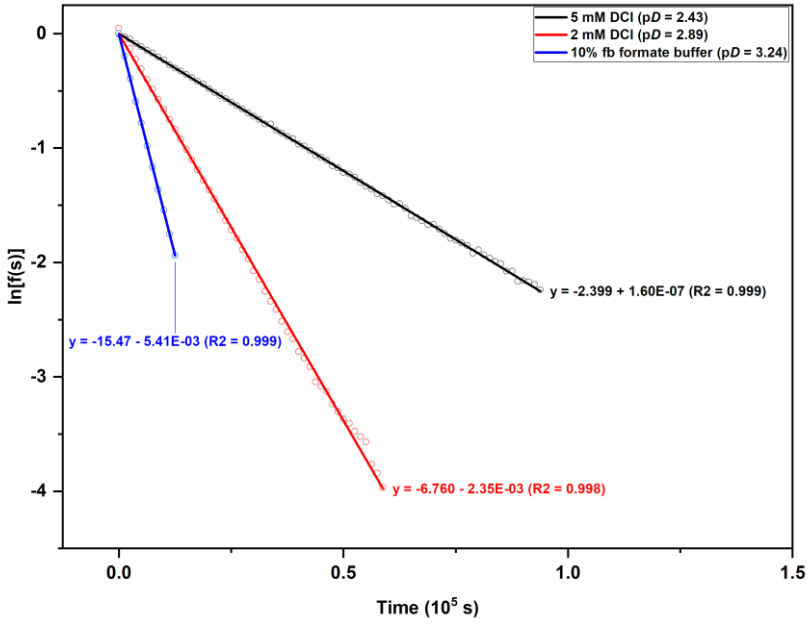


Figure S53 – Semilogarithmic plots of the fraction of unexchanged substrate against time for the deuterium exchange reaction of **92i·BF$_4$** in solutions of DCl and formate buffer in D_2O at 25 °C and I = 1.0 (KCl).

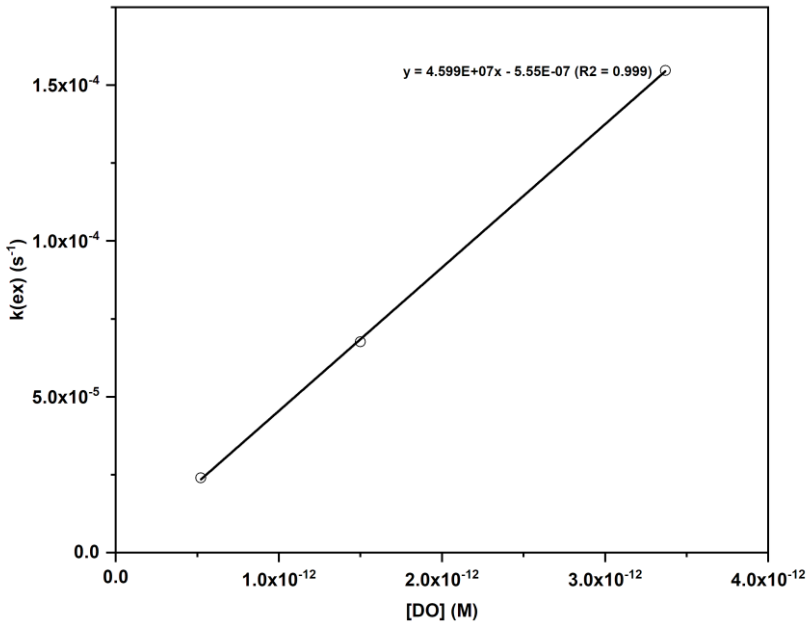


Figure S54 – Plot of k_{ex} against [DO^-] for **92i·BF$_4$** in solutions of DCl and formate buffer in D_2O at p*D*s 2.43 – 3.24, 25 °C and I = 1.0 (KCl). The line through the data shows the fit of k_{ex} – [DO^-] to **Equation S17**.

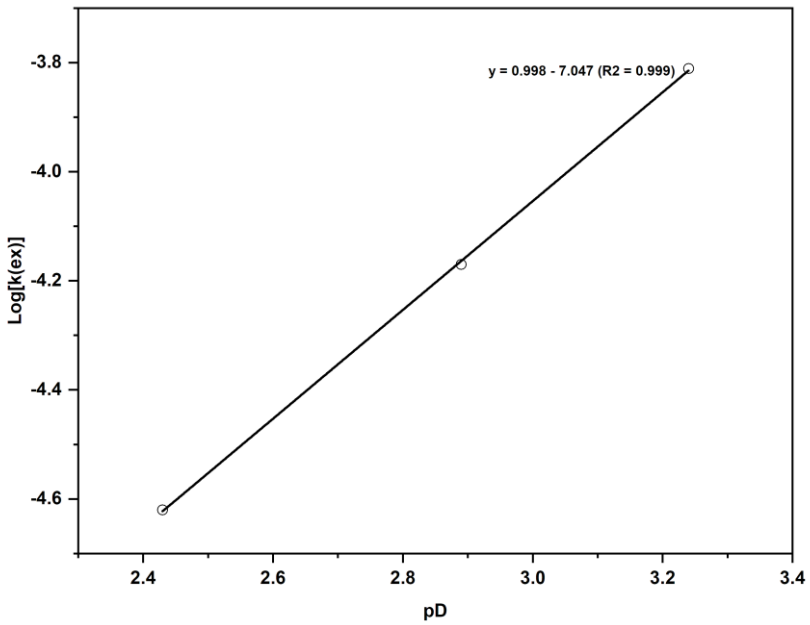


Figure S55 – Plot of log(k_{ex}) against p*D* for **92i·BF$_4$** in solutions of DCl and formate buffer in D_2O at 25 °C and I = 1.0 (KCl). The line through the data shows the fit of log(k_{ex}) – p*D* data to **Equation S18**.

D-2.8 – 3-((4-(Methoxycarbonyl)phenyl)thio)-1,4-dimethyl-4*H*-1,2,4-triazol-1-ium tetrafluoroborate (**92n·BF$_4$**)

Table S41 – Summary of the results from all H/D-exchange experiments relating to **92n·BF$_4$**.

Buffer / [DCl]	p*D*	[DO$^-$] (M)	k_{ex} (s^{-1})	$t_{1/2}$ (h)	k_{DO} ($M^{-1}s^{-1}$)
5.00×10^{-3} M DCl	2.41 → 2.43	4.98×10^{-13}	3.42 (± 0.01) $\times 10^{-5}$	5.64	**Equation S17** $6.61 (\pm 0.13) \times 10^7$
2.00×10^{-3} M DCl	2.77 → 2.75	1.14×10^{-12}	7.29 (± 0.03) $\times 10^{-5}$	2.64	
10% fb formate	3.22 → 3.20	3.21×10^{-12}	2.12 (± 0.03) $\times 10^{-4}$	0.91 (54 min)	**Equation S18** $7.46 (\pm 0.10) \times 10^7$

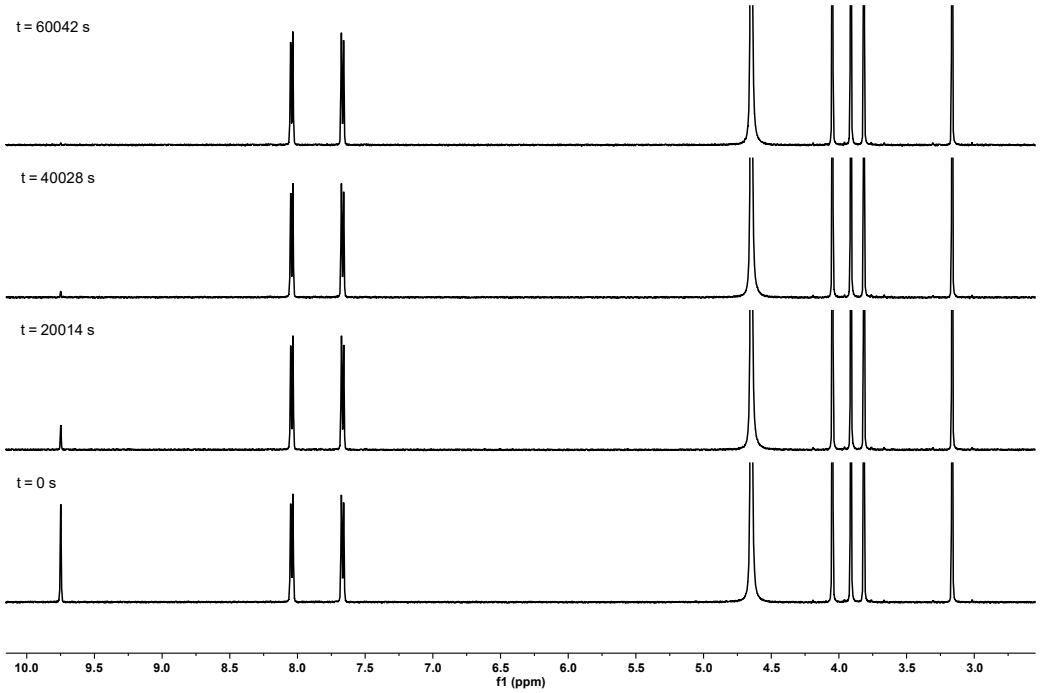


Figure S56 – Representative NMR overlay at 500 MHz for **92n·BF$_4$** at 2.00×10^{-3} M DCl (10 mM, p*D*(corr) 2.77), obtained during exchange of the C(5)-H (s, 9.89 ppm) for deuterium in D_2O at 25 °C and I = 1.0 (KCl). Tetramethylammonium chloride internal standard (s, 3.31 ppm).

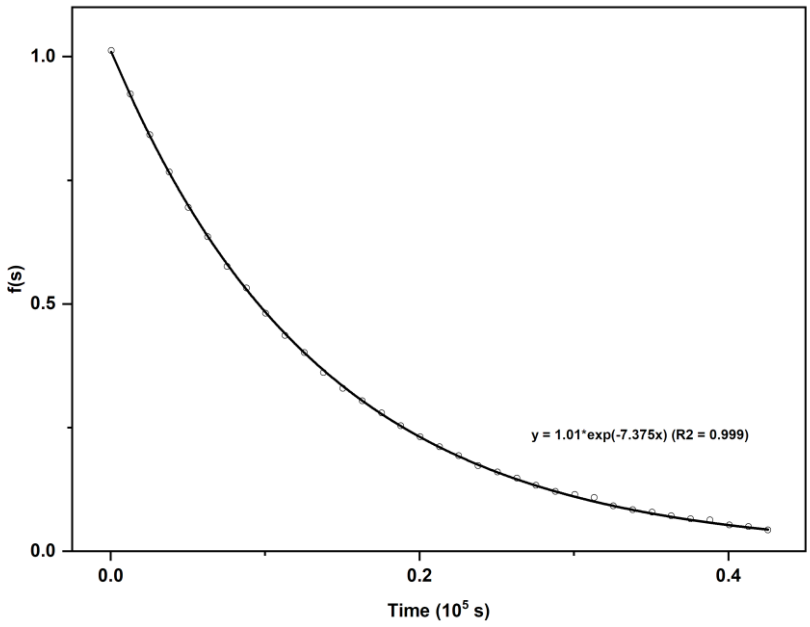


Figure S57 – Representative plot of the fraction of unexchanged substrate against time for the deuterium exchange reaction of **92n·BF$_4$** at 2.00 × 10^{-3} DCl (10 mM, p*D*(corr) = 2.77) in D_2O at 25 °C and I = 1.0 (KCl). The line through the data shows the non-linear least squares fit for a 1st order decay process.

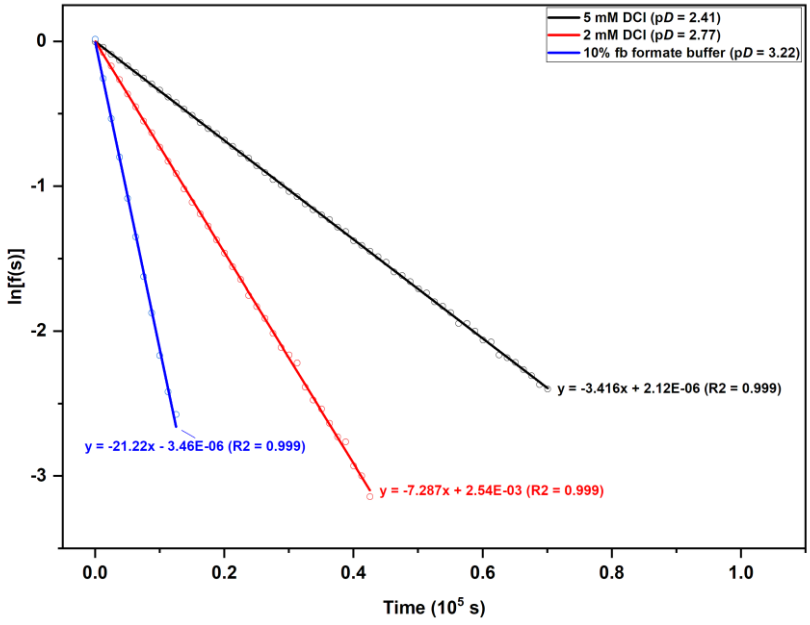


Figure S58 – Semilogarithmic plots of the fraction of unexchanged substrate against time for the deuterium exchange reaction of **92n·BF$_4$** in solutions of DCl and formate buffer in D_2O at 25 °C and I = 1.0 (KCl).

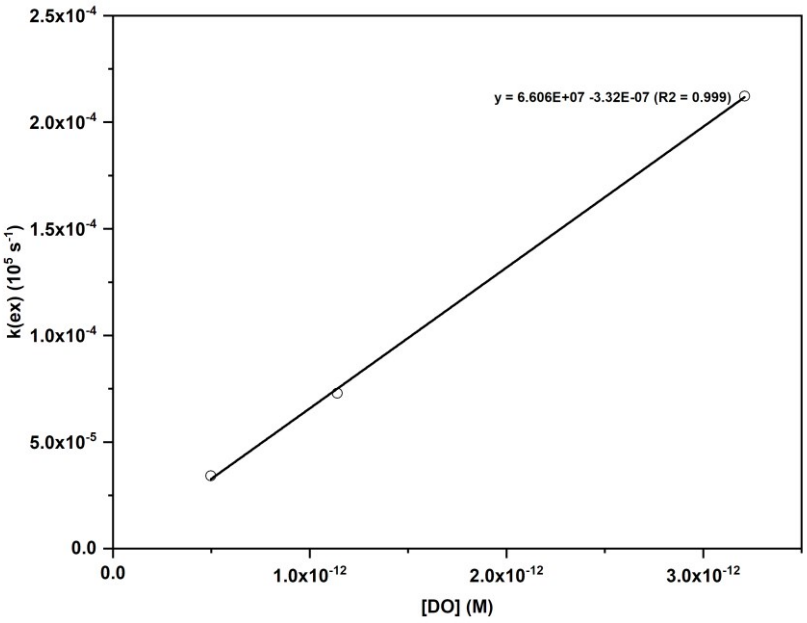


Figure S59 – Plot of k_{ex} against [DO^-] for **92n·BF₄** in solutions of DCl and formate buffer in D_2O at p*D*s 2.12 – 3.21, 25 °C and I = 1.0 (KCl). The line through the data shows the fit of k_{ex} – [DO^-] to **Equation S17**.

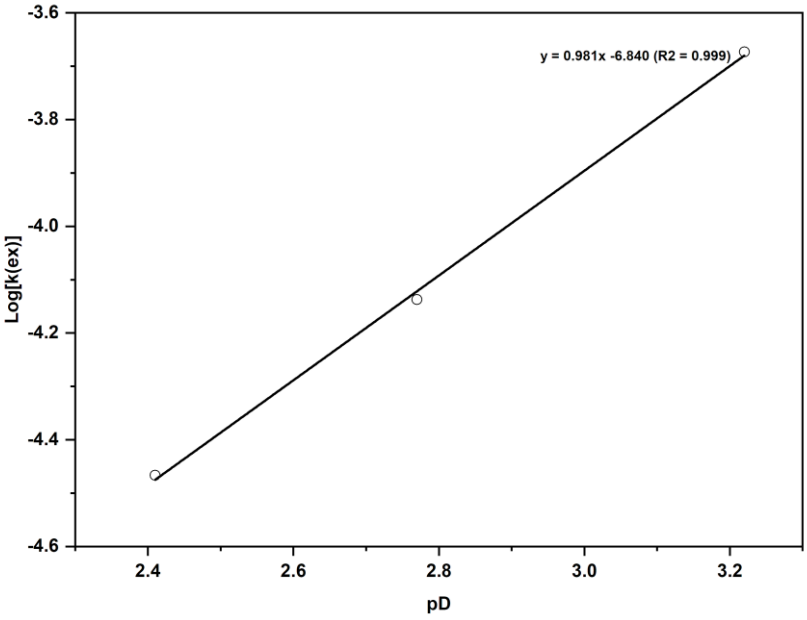


Figure S60 – Plot of log(k_{ex}) against p*D* for **92n·BF₄** in solutions of DCl and formate buffer in D_2O at 25 °C and I = 1.0 (KCl). The line through the data shows the fit of log(k_{ex}) – p*D* data to **Equation S18**.

D-2.9 – 3-((2,6-Dimethylphenyl)thio)-1,4-dimethyl-4*H*-1,2,4-triazol-1-ium tetrafluoroborate (**92o·BF$_4$**)

Table S42 – Summary of the results from all H/D-exchange exchange experiments relating to **92o·BF$_4$**

Buffer / [DCl]	p*D*	[DO$^-$] (M)	k_{ex} (s^{-1})	$t_{1/2}$ (h)	k_{DO} (M^{-1}s^{-1})
5.00 × 10^{-3} M DCl	2.63 → 2.63	8.27 × 10^{-13}	1.33 (± 0.002) × 10^{-5}	14.52	**Equation S17** 2.16 (± 0.13) × 10^7 [c]
2.00 × 10^{-3} M DCl	2.93 → 2.88	1.65 × 10^{-12}	2.82 (± 0.01) × 10^{-5}	6.82	**Equation S18**
10% fb formate	3.21 → 3.20	3.14 × 10^{-12}	6.28 (± 0.02) × 10^{-5}	3.06	5.84 (± 0.09) × 10^6 [d]

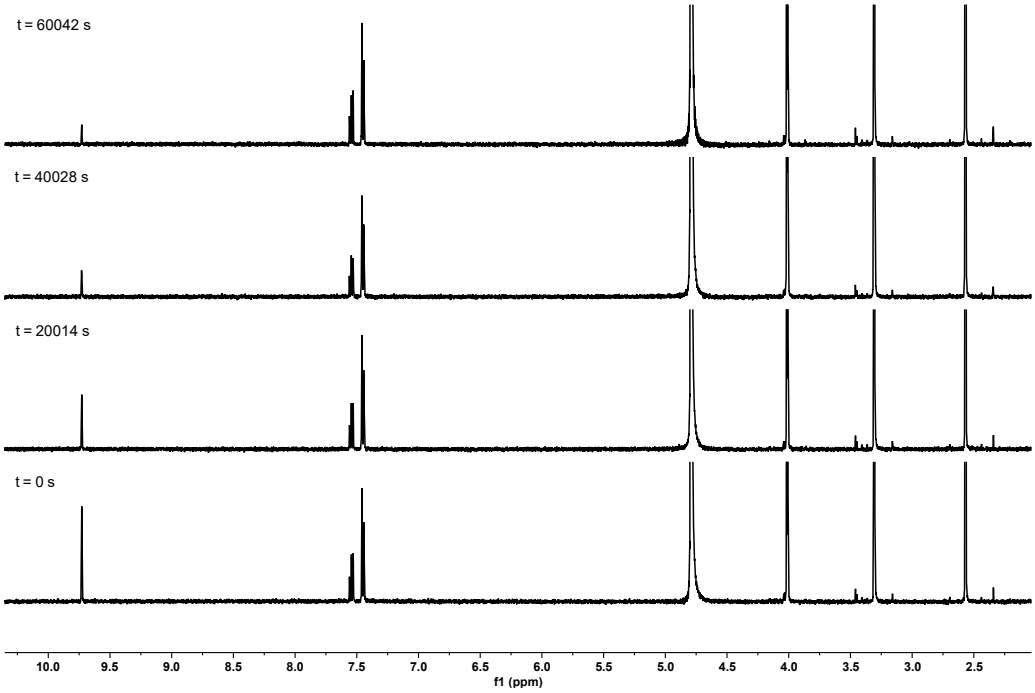


Figure S61 – Representative NMR overlay at 500 MHz for **92o·BF$_4$** at 2.00 × 10^{-3} M DCl (10 mM, p*D*(corr) 2.93), obtained during exchange of the C(5)-H (s, 9.73 ppm) for deuterium in D_2O at 25 °C and I = 1.0 (KCl). Tetramethylammonium chloride internal standard (s, 3.31 ppm).

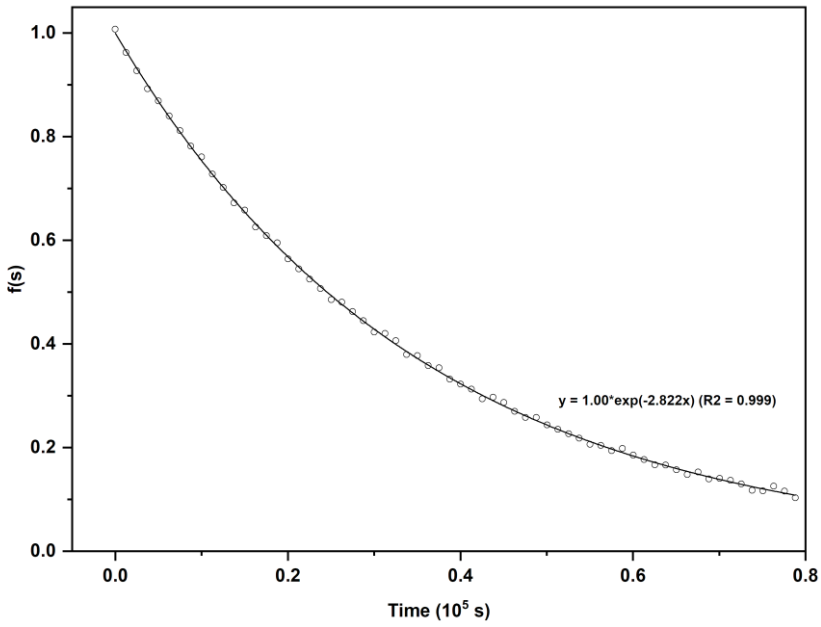


Figure S62 – Representative plot of the fraction of unexchanged substrate against time for the deuterium exchange reaction of **92o·BF$_4$** at 2.00 × 10^{-3} DCl (10 mM, p*D*(corr) = 2.93) in D_2O at 25 °C and I = 1.0 (KCl). The line through the data shows the non-linear least squares fit for a 1st order decay process.

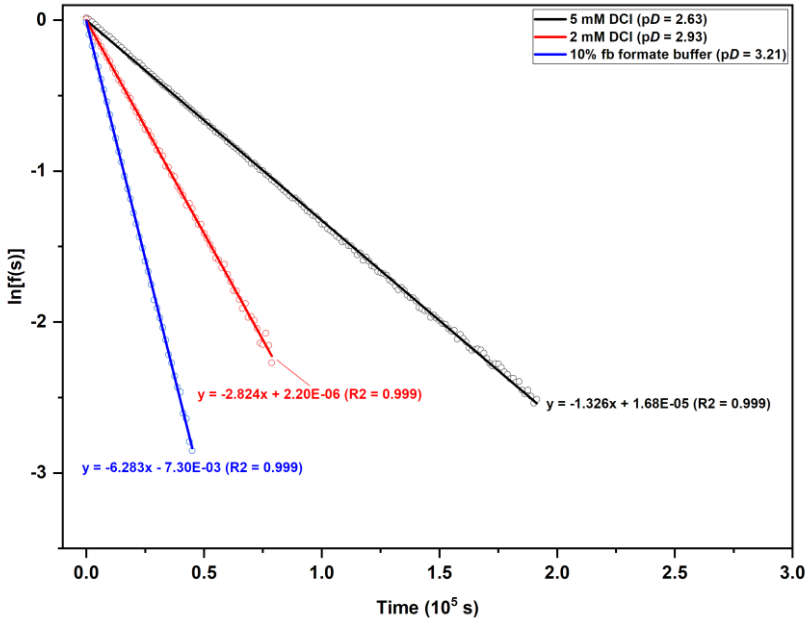


Figure S63 – Semilogarithmic plots of the fraction of unexchanged substrate against time for the deuterium exchange reaction of **92o·BF$_4$** in solutions of DCl and formate buffer in D_2O at 25 °C and I = 1.0 (KCl).

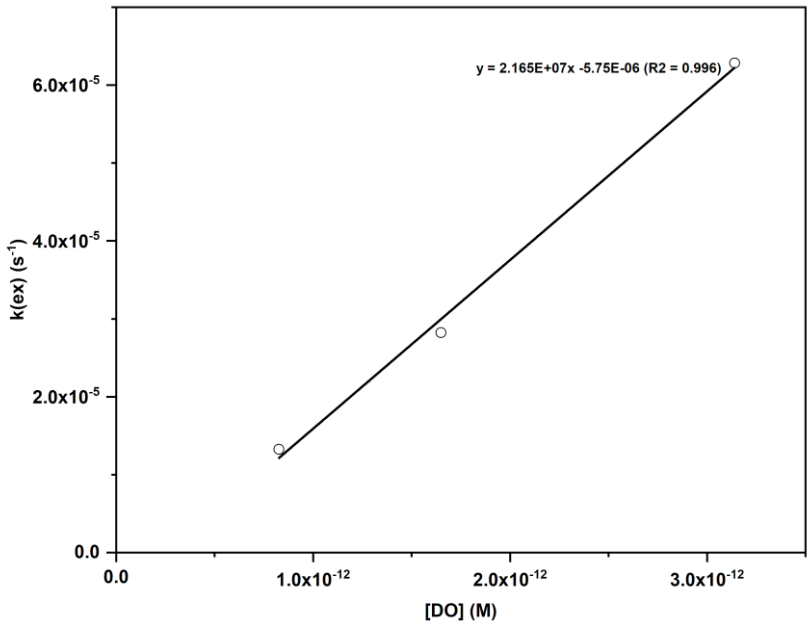


Figure S64 – Plot of k_{ex} against [DO^-] for **92o·BF₄** in solutions of DCl and formate buffer in D_2O at p*D*s 2.63 – 3.21, 25 °C and I = 1.0 (KCl). The line through the data shows the fit of k_{ex} – [DO^-] to **Equation S17**.

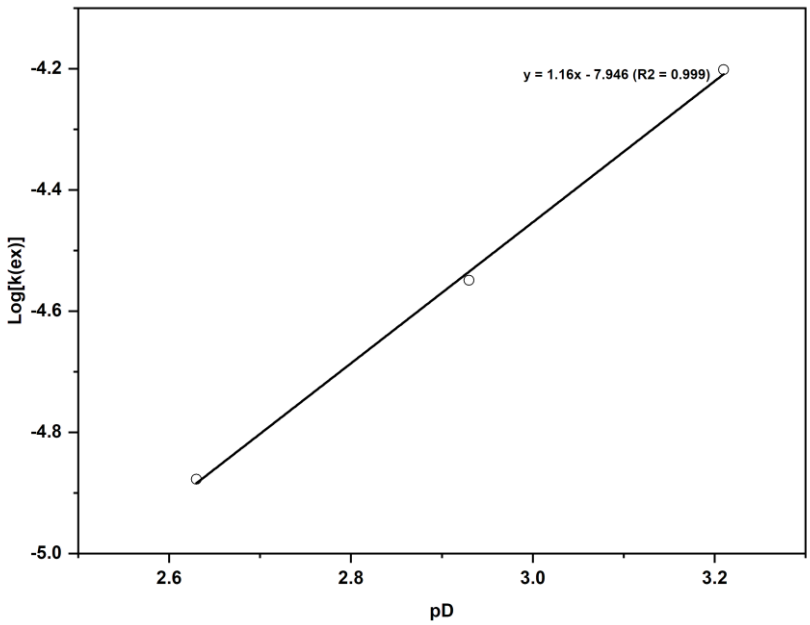


Figure S65 – Plot of log(k_{ex}) against p*D* for **92o·BF₄** in solutions of DCl and formate buffer in D_2O at 25 °C and I = 1.0 (KCl). The line through the data shows the fit of log(k_{ex}) – p*D* data to **Equation S18**.

D-2.10 – 1,4-Dimethyl-3-((perfluoropyridin-4-yl)thio)-4*H*-1,2,4-triazol-1-ium tetrafluoroborate (**92q·BF$_4$**)

Table S43 – Summary of the results from all H/D-exchange experiments relating to **92q·BF$_4$**.

Buffer / [DCl]	p*D*	[DO$^-$] (M)	k_{ex} (s^{-1})	$t_{1/2}$ (h)	k_{DO} (M^{-1}s^{-1})
1.00 × 10^{-2} M DCl	2.12 → 2.10	2.55 × 10^{-13}	4.12 (± 0.01) × 10^{-5}	4.67	**Equation S17** 1.62 (± 0.04) × 10^8 [c]
5.00 × 10^{-3} M DCl	2.42 → 2.42	5.10 × 10^{-13}	8.27 (± 0.03) × 10^{-5}	2.33	
2.00 × 10^{-3} M DCl	2.84 → 2.84	1.34 × 10^{-12}	2.29 (± 0.02) × 10^{-4}	0.84 (50 min)	**Equation S18** 1.45 (± 0.02) × 10^8 [d]
10% fb formate	3.22 → 3.19	3.22 × 10^{-12}	5.19 (± 0.04) × 10^{-4}	0.37 (22 min)	

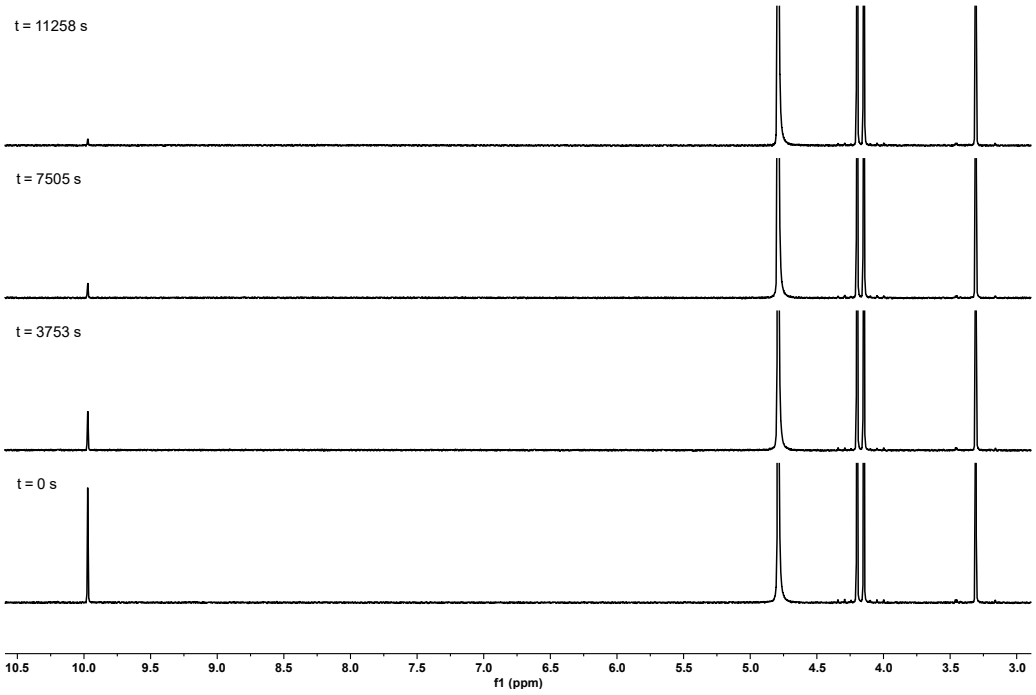


Figure S66 – Representative NMR overlay at 500 MHz for **92q·BF$_4$** at 2.00 × 10^{-3} M DCl (10 mM, p*D*(corr) 2.84), obtained during exchange of the C(5)-H (s, 9.97 ppm) for deuterium in D_2O at 25 °C and I = 1.0 (KCl). Tetramethylammonium chloride internal standard (s, 3.31 ppm).

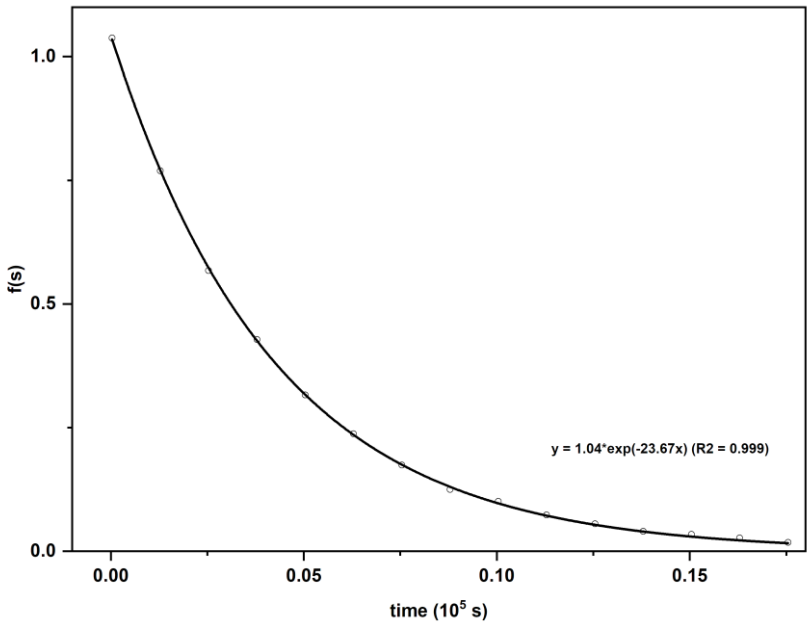


Figure S67 – Representative plot of the fraction of unexchanged substrate against time for the deuterium exchange reaction of **92q·BF$_4$** at 2.00 × 10^{-3} DCl (10 mM, p*D*(corr) = 2.84) in D_2O at 25 °C and I = 1.0 (KCl). The line through the data shows the non-linear least squares fit for a 1st order decay process.

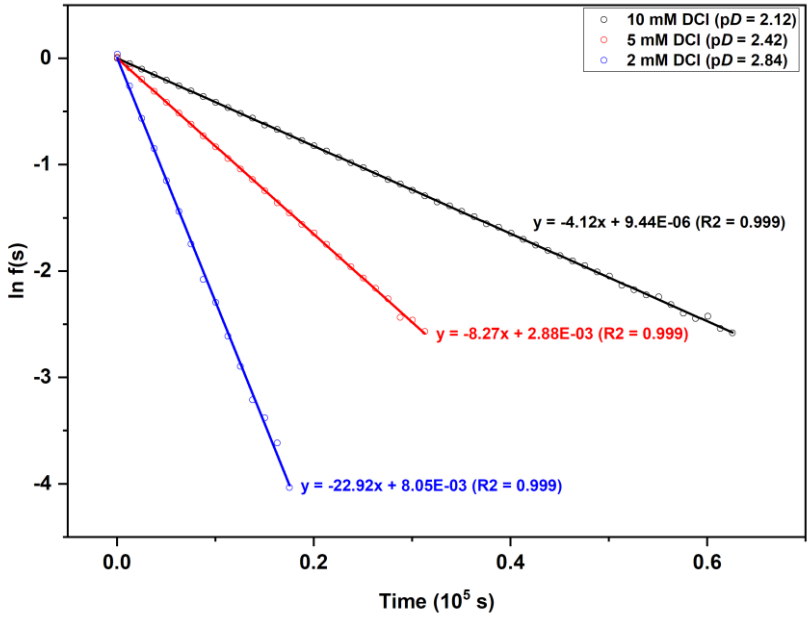


Figure S68 – Semilogarithmic plots of the fraction of unexchanged substrate against time for the deuterium exchange reaction of **92q·BF$_4$** 1,4-dimethyl in solutions of DCl within D_2O at 25 °C and I = 1.0 (KCl).

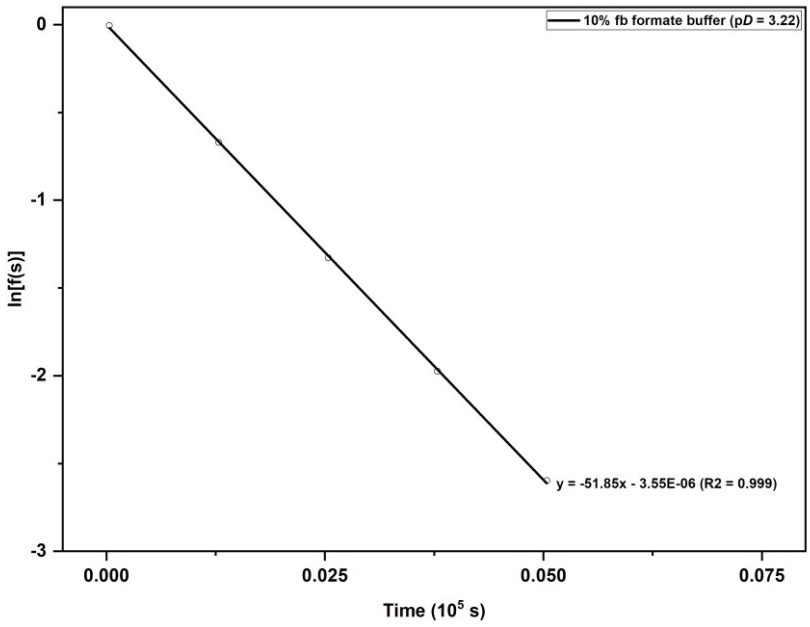


Figure S69 – Semilogarithmic plots of the fraction of unexchanged substrate against time for the deuterium exchange reaction of **92q·BF$_4$** 1,4-dimethyl in formate buffer within D_2O at 25 °C and I = 1.0 (KCl).

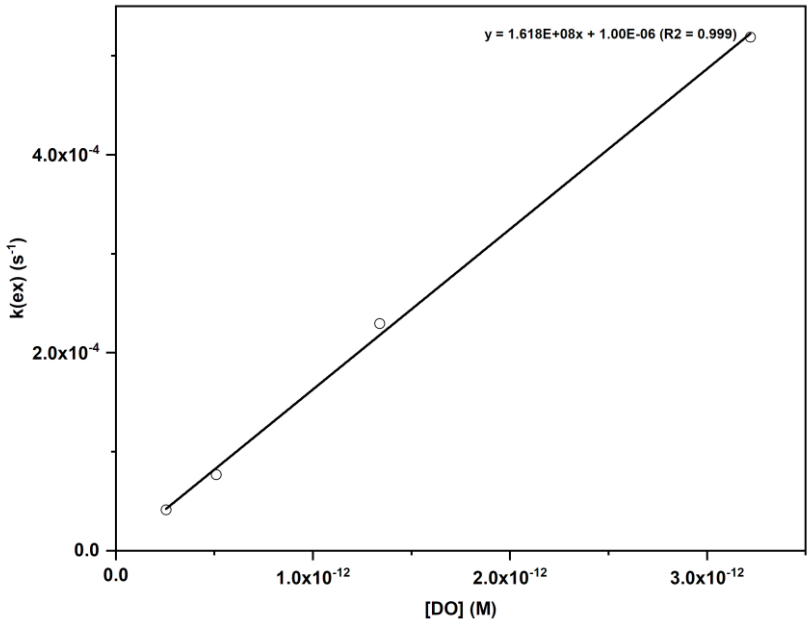


Figure S70 – Plot of k_{ex} against [DO$^-$] for **92q·BF$_4$** in solutions of DCl and formate buffer in D_2O at p*D*s 2.12 – 3.22, 25 °C and I = 1.0 (KCl). The line through the data shows the fit of k_{ex} – [DO$^-$] to **Equation S17**.

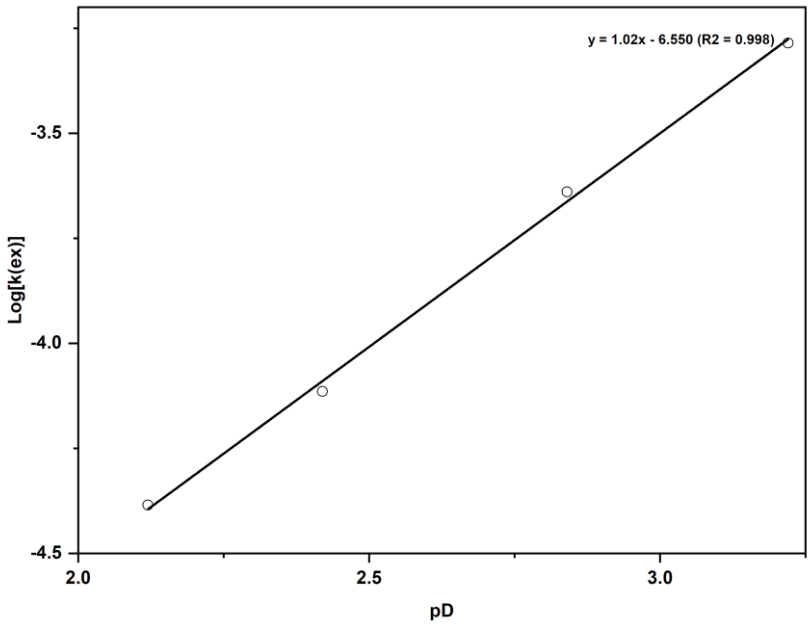


Figure S71 – Plot of log(k_{ex}) against p*D* for **92q·BF$_4$** in solutions of DCl and formate buffer in D_2O at 25 °C and I = 1.0 (KCl). The line through the data shows the fit of log(k_{ex}) – p*D* data to **Equation S18**.

D-2.11 – 1-Ethyl-4-methyl-3-(phenylthio)-4*H*-1,2,4-triazol-1-ium tetrafluoroborate (**94·BF$_4$**)

Table S44 – Summary of the results from all H/D-exchange experiments relating to **94·BF$_4$**

Buffer / [DCl]	p*D*	[DO$^-$] (M)	k_{ex} (s^{-1})	$t_{1/2}$ (h)	k_{DO} (M^{-1}s^{-1})
5.00 × 10^{-3} M DCl	2.42 → 2.44	5.10 × 10^{-13}	1.62 (± 0.01) × 10^{-5}	11.89	
2.00 × 10^{-3} M DCl	2.90 → 2.88	1.54 × 10^{-12}	4.91 (± 0.01) × 10^{-5}	3.92	**Equation S17** 3.38 (± 0.03) × 10^7
10% fb formate	3.21 → 3.21	3.14 × 10^{-12}	1.04 (± 0.01) × 10^{-4}	1.85	
30% fb formate	3.61 → 3.61	7.90 × 10^{-12}	2.60 (± 0.01) × 10^{-4}	0.74 (45 min)	**Equation S18** 2.88 (± 0.01) × 10^7
50% fb formate	3.85 → 3.85	1.37 × 10^{-11}	4.63 (± 0.07) × 10^{-4}	0.42 (25 min)	

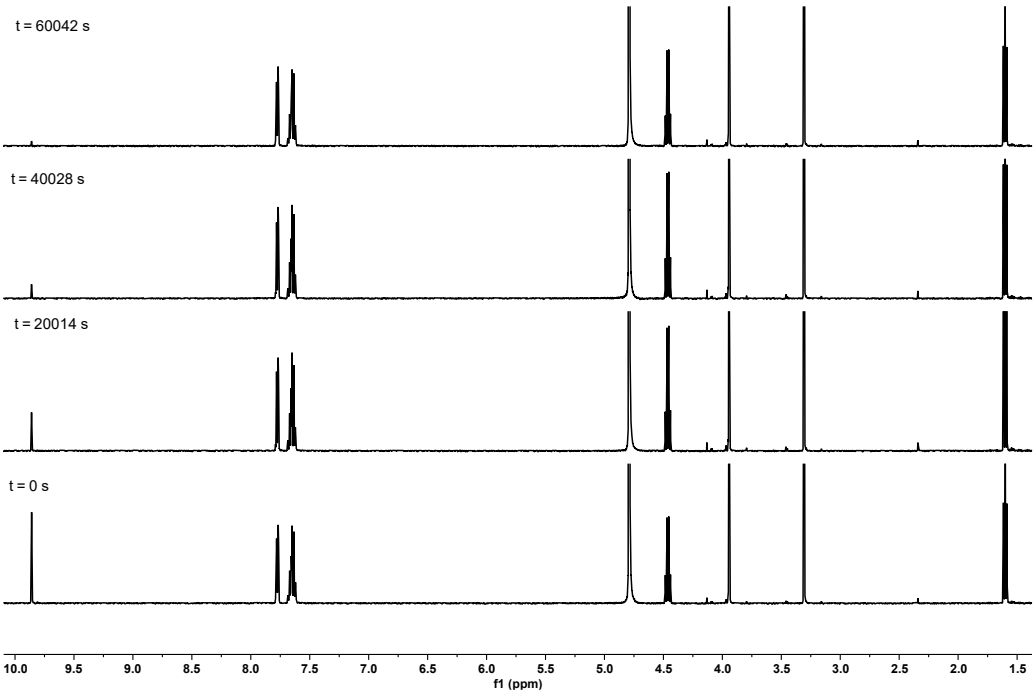


Figure S72 – Representative NMR overlay at 500 MHz for **94·BF$_4$** at 2.00 × 10^{-3} M DCl (10 mM, p*D*(corr) 2.90), obtained during exchange of the C(5)-H (s, 9.86 ppm) for deuterium in D_2O at 25 °C and I = 1.0 (KCl). Tetramethylammonium chloride internal standard (s, 3.31 ppm).

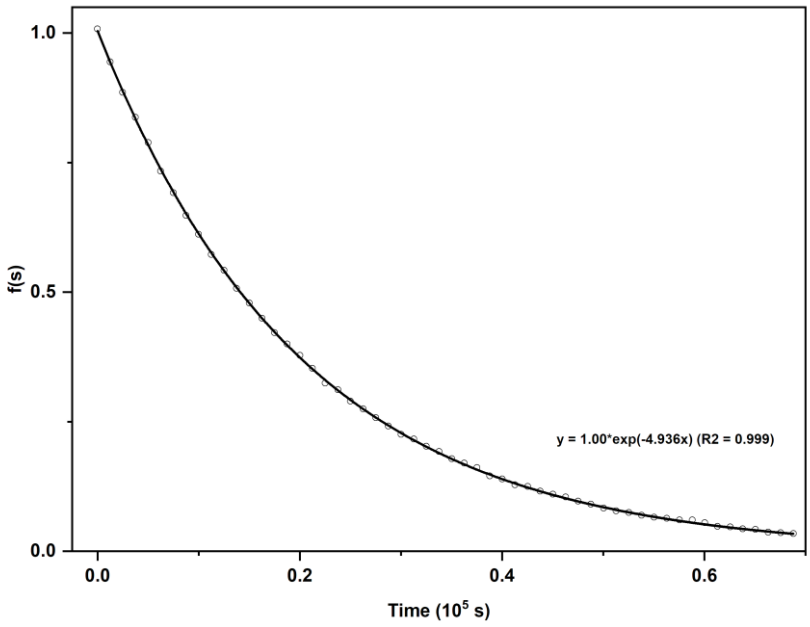


Figure S73 – Representative plot of the fraction of unexchanged substrate against time for the deuterium exchange reaction of **94·BF$_4$** at 2.00 × 10^{-3} DCl (10 mM, p*D*(corr) = 2.90) in D_2O at 25 °C and I = 1.0 (KCl). The line through the data shows the non-linear least squares fit for a 1st order decay process.

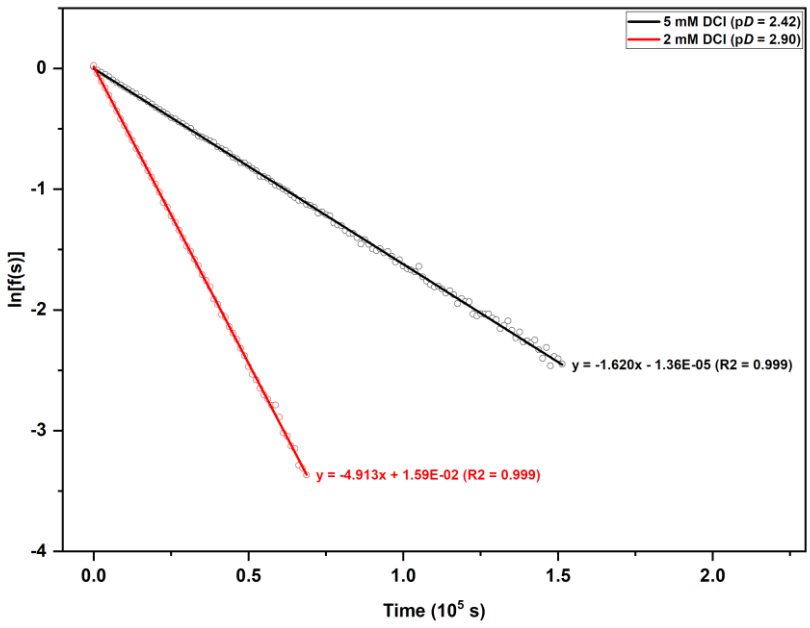


Figure S74 – Semilogarithmic plots of the fraction of unexchanged substrate against time for the deuterium exchange reaction of **94·BF$_4$** in solutions of DCl within D_2O at 25 °C and I = 1.0 (KCl).

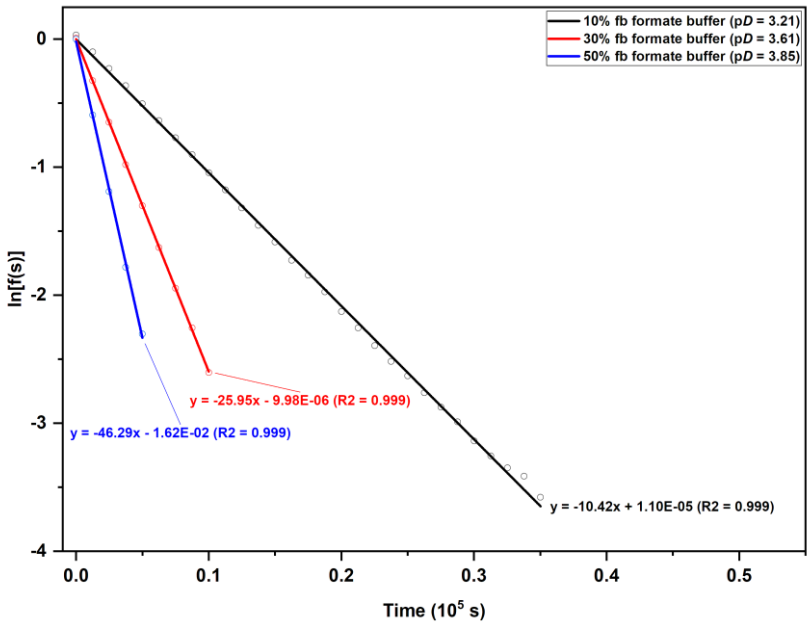


Figure S75 – Semilogarithmic plots of the fraction of unexchanged substrate against time for the deuterium exchange reaction of **94·BF$_4$** in formate buffer within D_2O at 25 °C and I = 1.0 (KCl).

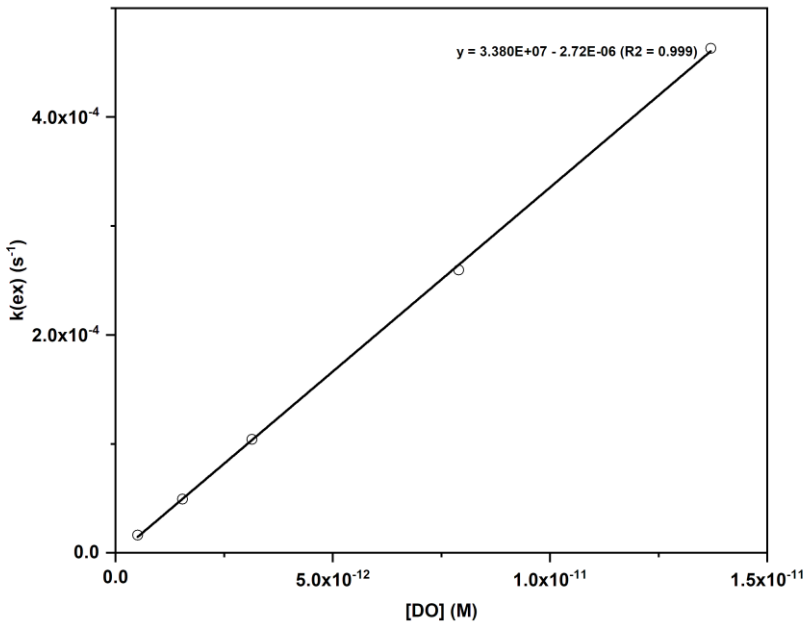


Figure S76 – Plot of k_{ex} against [DO^-] for **94·BF$_4$** in solutions of DCl and formate buffer in D_2O at p*D*s 2.42 – 3.85, 25 °C and I = 1.0 (KCl). The line through the data shows the fit of k_{ex} – [DO^-] to **Equation S17**.

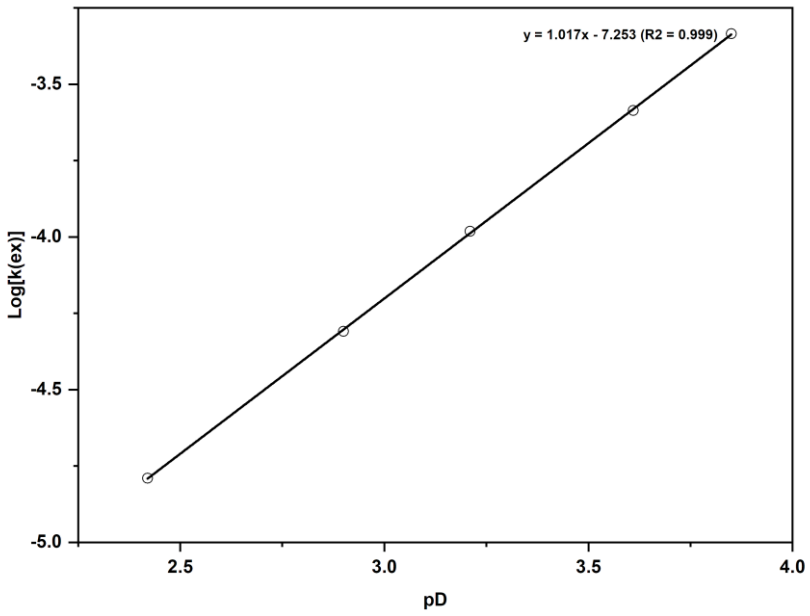


Figure S77 – Plot of log(k_{ex}) against p*D* for **94·BF$_4$** in solutions of DCl and formate buffer in D_2O at 25 °C and I = 1.0 (KCl). The line through the data shows the fit of log(k_{ex}) – p*D* data to **Equation S18**.

D-2.12 – 1,4-Dibenzyl-3-(phenylthio)-4*H*-1,2,4-triazol-1-ium bromide (**99·Br**)

Due to poor solubility, most experiments undertaken with 20 %v MeCN. It is assumed that the counterion does not affect k_{ex} in the mostly aqueous buffer solutions used in the fit due to solvation, and thus no correction is made for the counterion.

Table S45 – Summary of the results from all H/D-exchange experiments relating to **99·Br**.

Buffer / [DCl]	**p*D***	**[DO$^-$] (M)**	**k_{ex} (s^{-1})**	**$t_{1/2}$ (h)**	**k_{DO} ($M^{-1}s^{-1}$)**
1.00×10^{-2} M DCl (20% v/v MeCN)	2.05 → 2.07	5.48×10^{-14}	$3.58 (\pm 0.01) \times 10^{-5}$	5.38	**Equation S17** $4.51 (\pm 0.10) \times 10^8$ **Equation S18** $3.29 (\pm 0.06) \times 10^8$
5.00×10^{-3} M DCl (20% v/v MeCN)	2.38 → 2.40	1.17×10^{-13}	$6.31 (\pm 0.05) \times 10^{-5}$	3.05	
2.00×10^{-3} M DCl	3.27 [a]	3.61×10^{-12}	$9.85 (\pm 0.38) \times 10^{-4}$	0.20 (12 min)	
2.00×10^{-3} M DCl (20% v/v MeCN)	3.00 → 2.99	4.89×10^{-13}	$2.11 (\pm 0.06) \times 10^{-4}$	0.91 (55 min)	
10% fb formate (20% v/v MeCN)	3.51 → 3.50	1.58×10^{-12}	$7.22 (\pm 0.06) \times 10^{-4}$	0.27 (16 min)	

[a] Due to the speed of the reaction, the p*H* at the start and end of the reaction were not obtained. The value quoted was obtained after the reaction was complete and is used in the determination of deuteroxide concentration. Value not included in fit to determine k_{DO}.

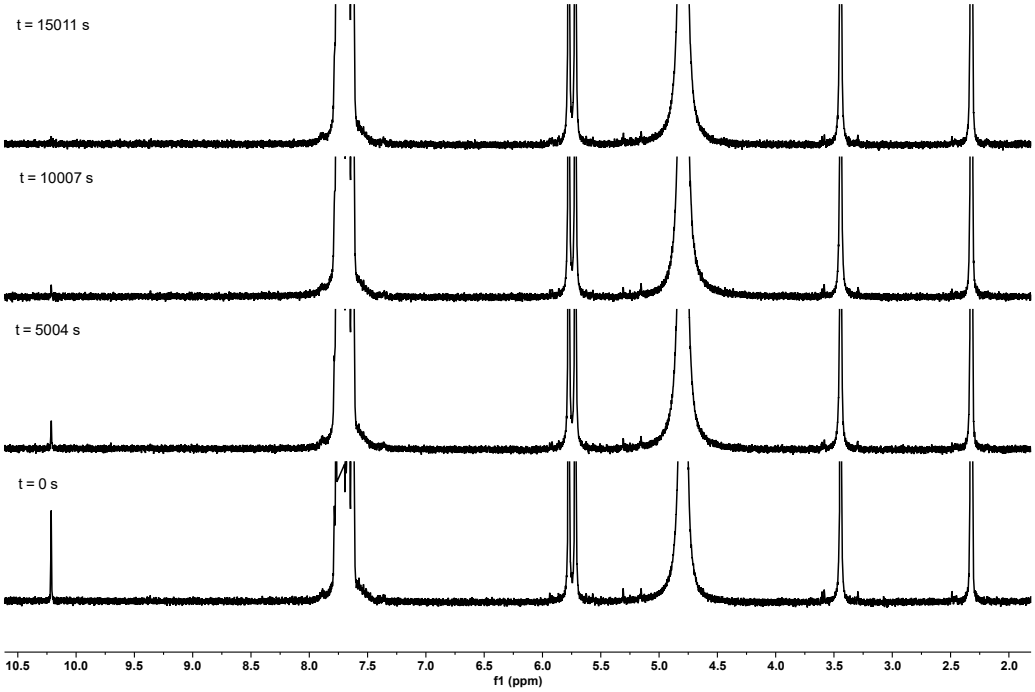


Figure S78 – Representative NMR overlay at 500 MHz for **99·Br** at 2.00 × 10^{-3} M DCl (10 mM, p*D*(corr) 3.00), obtained during exchange of the C(5)-H (s, 10.21 ppm) for deuterium in 2:8 d_3-MeCN / D_2O at 25 °C and I = 1.0 (KCl). Tetramethylammonium chloride internal standard (s, 3.44 ppm).

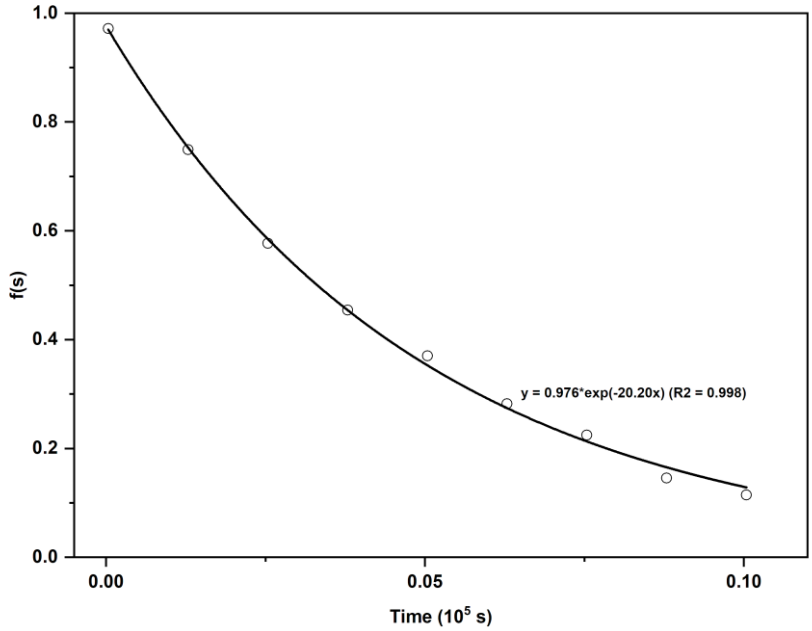


Figure S79 – Representative plot of the fraction of unexchanged substrate against time for the deuterium exchange reaction of **99·Br** at 2.00 × 10^{-3} DCl (10 mM, p*D*(corr) = 3.00) in 2:8 d_3-MeCN / D_2O at 25 °C and I = 1.0 (KCl). The line through the data shows the non-linear least squares fit for a 1st order exponential decay process.

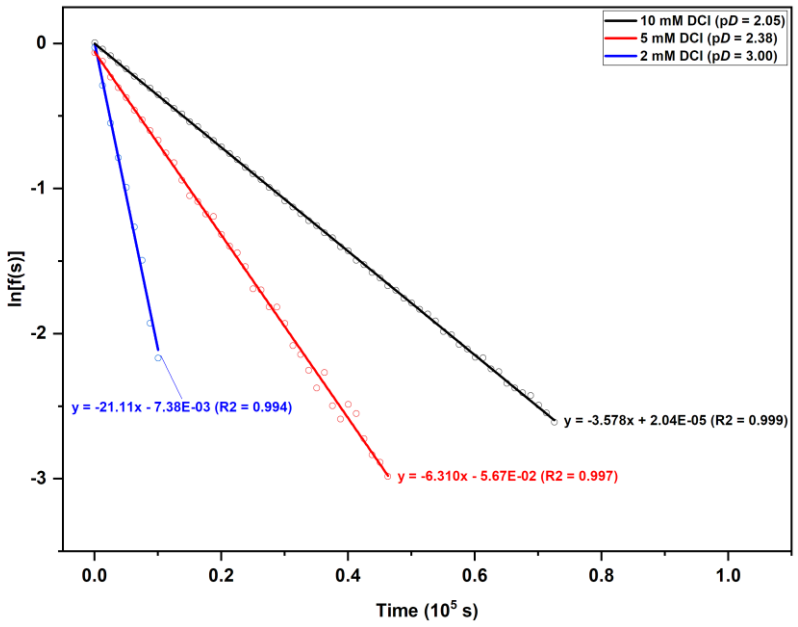


Figure S80 – Semilogarithmic plots of the fraction of unexchanged substrate against time for the deuterium exchange reaction of **99·Br** in solutions of DCl within 2:8 d_3-MeCN / D_2O at 25 °C and I = 1.0 (KCl).

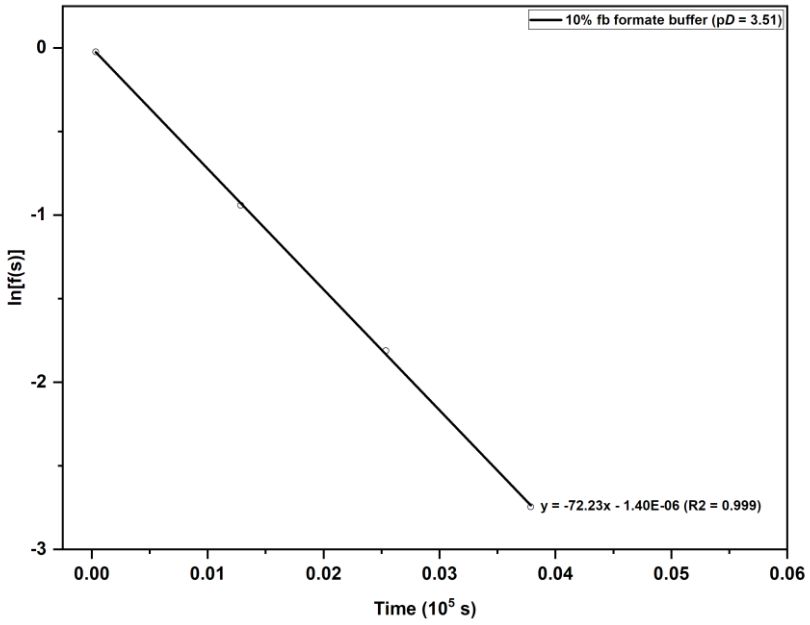


Figure S81 – Semilogarithmic plots of the fraction of unexchanged substrate against time for the deuterium exchange reaction of **99·Br** in formate buffer within 2:8 d_3-MeCN / D_2O at 25 °C and I = 1.0 (KCl).

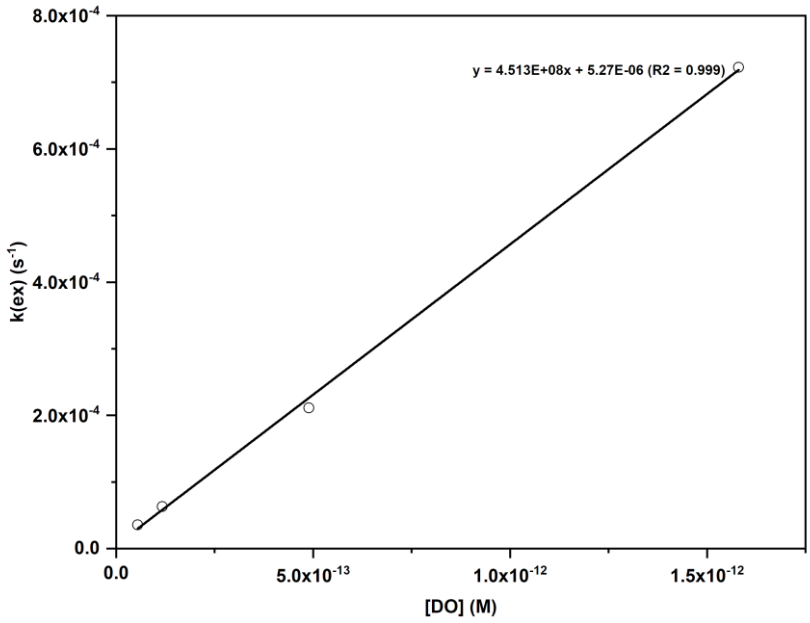


Figure S82 – Plot of k_{ex} against [DO^-] for **99·Br** in solutions of DCl and formate buffer in 2:8 d_3-MeCN / D_2O at p*D*s 2.05 – 3.51, 25 °C and I = 1.0 (KCl). The line through the data shows the fit of k_{ex} – [DO^-] to **Equation S17**.

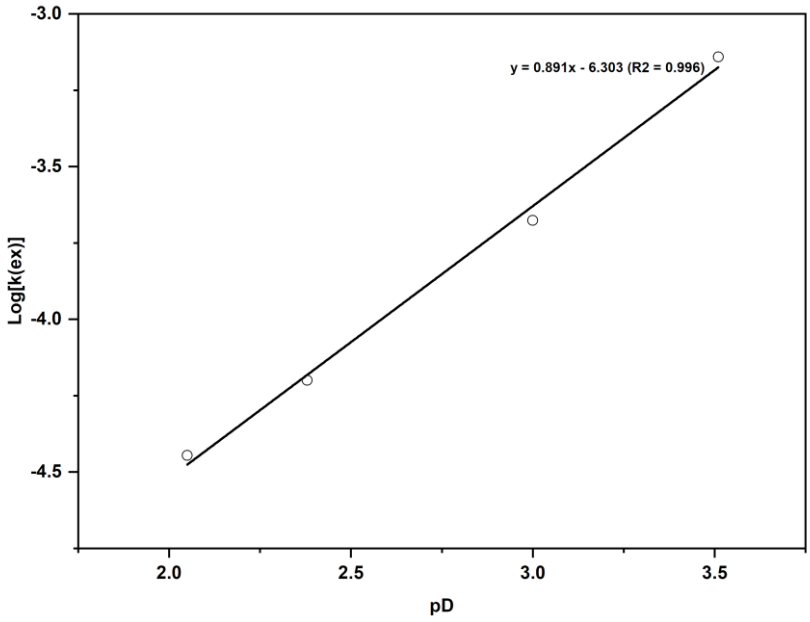


Figure S83 – Plot of log(k_{ex}) against p*D* for **99·Br** in solutions of DCl and formate buffer in 2:8 d_3-MeCN / D_2O at 25 °C and I = 1.0 (KCl). The line through the data shows the fit of log(k_{ex}) – p*D* data to **Equation S18**.

D-3 – *S*-triazolium organocatalytic activity

The following data was collected using 10 μmol of the *S*-triazolium catalyst of interest within a triethylamine buffer. When considering the benzoin condensation, benzaldehyde (2 equiv.) was added to the buffered solution. When considering the Stetter reaction, Ethyl (*E*)-4-(2-formylphenoxy)but-2-enoate (**323**) (1 equiv.) was added to the buffered solution. Reaction monitoring by ^{1}H NMR spectroscopy involved observing the appearance of either the α-proton of benzoin (s, 6.12 ppm) or the ethyl group of chromanone **324** (q, 3.62 ppm), for the benzoin condensation or Stetter reaction respectively. Further experimental details can be found in Chapter 8.1.2.

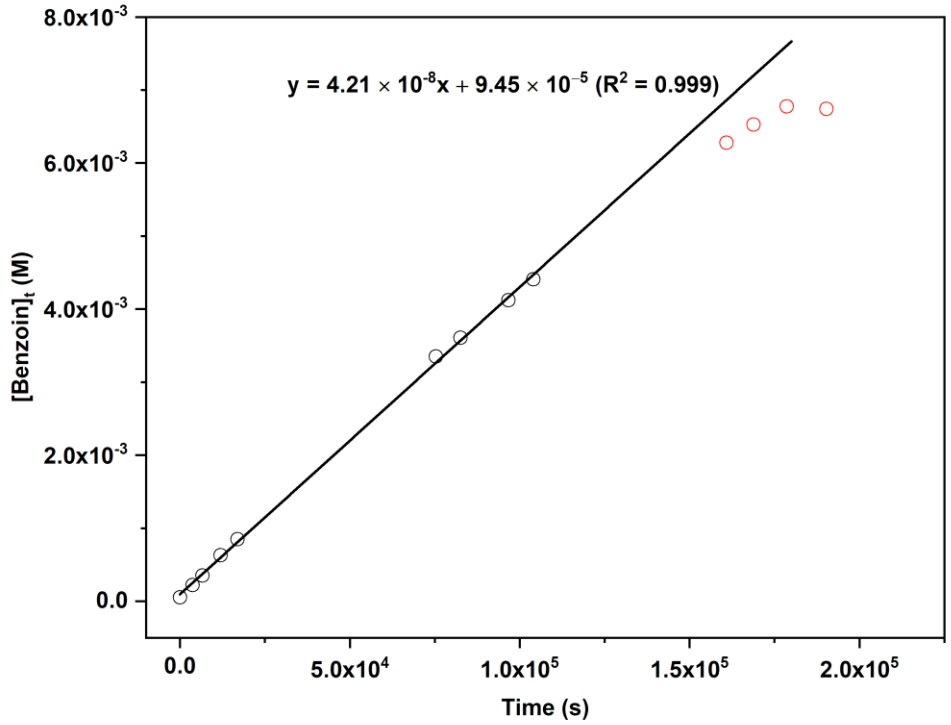


Figure S84 – Plot of [Benzoin], corrected *versus* TMACl standard, as a function of time catalysed by **92a**·BF_4.

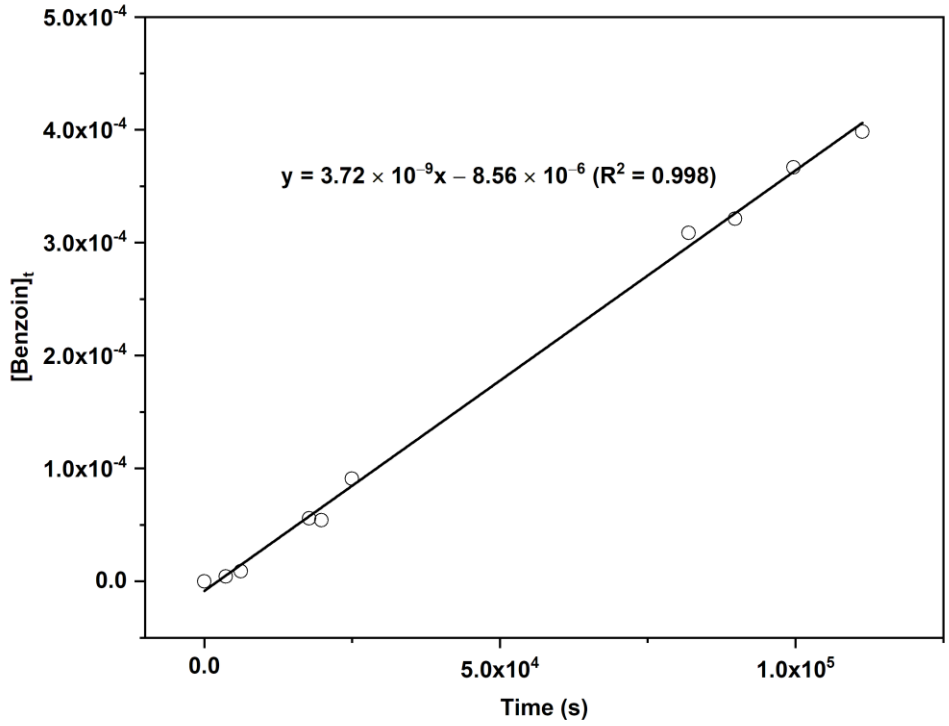


Figure S85 – Plot of [Benzoin], corrected *versus* TMACl standard, as a function of time catalysed by **99·Br**.

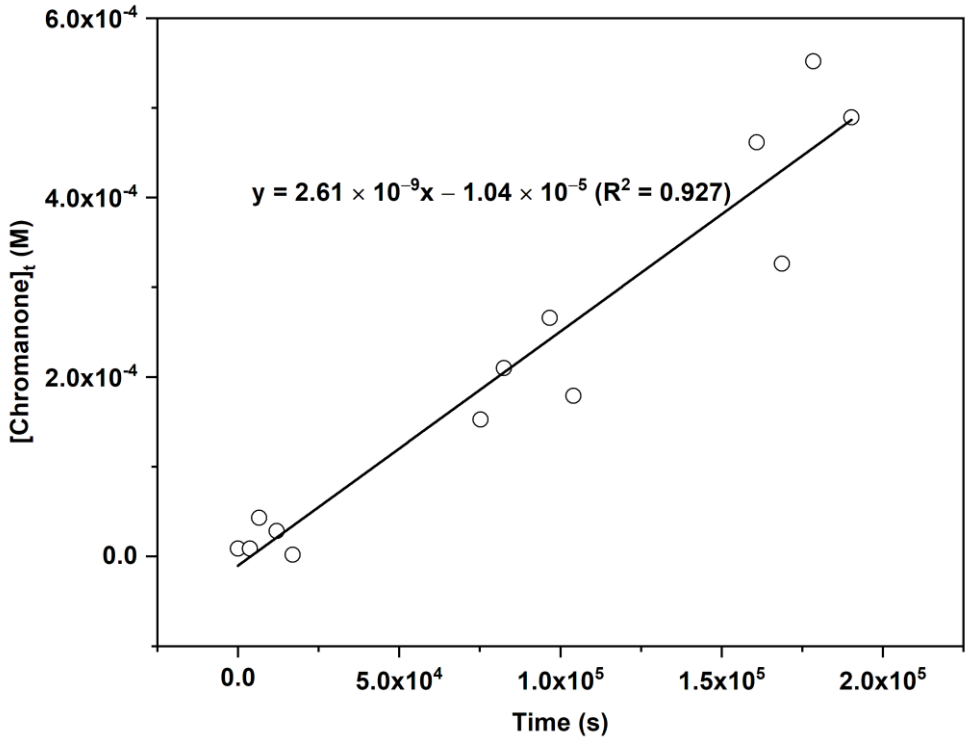


Figure S86 – plot of [Chromanone], corrected *versus* TMACl standard, as a function of time catalysed by **92a·BF$_4$**.

Appendix E - Supplementary information for Chapter 6

E-1 – SRB assay results overview

Table S46 and **Table S47** provide the experiment numbers where each compound was investigated, and relevant GI_{50} values that were averaged to obtain the values provided in Chapter 6. Note that reported GI_{50} values beyond the scale of the experiment, denoted by the use of inequality symbols, were not included in obtaining the average GI_{50} value.

Table S46 – List of experiment numbers and GI_{50} values (in brackets) for all compounds analysed by the SRB assay against the SJSA-1 cell line. IT = incubation time.

	IT (d)	SJSA-1 (bone)	
37a	3	Exp. 01 (6.58)	Exp. 01 (6.63)
38a	3	Exp. 01 (29.27)	Exp. 01 (31.49)

Table S47 – List of experiment numbers and GI_{50} values (in brackets) for all compounds analysed by the SRB assay against the MCF-7 and GB-1 cell lines. IT = incubation time.

	IT (d)	GB-1 (brain)			MCF-7 (breast)		
33a	3	Exp. 15 (32.41)	Exp. 16 (49.07)	Exp. 16 (50.48)	Exp. 15 (16.01)	Exp. 16 (34.26)	Exp. 16 (28.75)
	7	Exp. 32 (21.20)	Exp. 33 (5.45)	Exp. 34 (5.74)	Exp. 32 (9.52)	Exp. 33 (6.17)	Exp. 34 (5.53)
33dH·BF4	3	Exp. 30 (9.47)			Exp. 30 (6.80)		
33f	3	Exp. 23 (19.82)	Exp. 24 (17.32)	Exp. 25 (18.79)	Exp. 23 (12.88)	Exp. 24 (13.64)	Exp. 25 (17.82)
33fH·BF_4	3	Exp. 23 (22.64)	Exp. 24 (15.82)	Exp. 25 (16.58)	Exp. 23 (11.42)	Exp. 24 (13.06)	Exp. 25 (13.42)
33g	3	Exp. 30 (14.53)			Exp. 30 (8.07)		
33h	3	Exp. 30 (23.46)			Exp. 30 (19.50)		
	7	Exp. 31 (13.81)			Exp. 31 (4.16)		
33i	3	Exp. 23 (> 300)	Exp. 24 (111.02)	Exp. 25 (108.77)	Exp. 23 (> 300)	Exp. 24 (58.88)	Exp. 25 (42.31)
33iH·Cl	3	Exp. 17 (> 300)	Exp. 18 (> 300)	Exp. 19 (> 300)	Exp. 17 (>300)	Exp. 18 (> 300)	Exp. 19 (> 300)
37a	3	Exp. 04 (4.86)	Exp. 05 (5.88)	Exp. 13 (5.71)	Exp. 04 (4.60)	Exp. 05 (5.43)	Exp. 13 (3.74)
	7	Exp. 34 (3.17)	Exp. 32 (3.01)	Exp. 33 (3.14)	Exp. 34 (3.19)	Exp. 32 (< 3)	Exp. 33 (5.00)
37d	3	Exp. 13 (2.64)	Exp. 11 (13.19)	Exp. 16 (> 10)	Exp. 11 (7.45)	Exp. 13 (0.94)	

37e	3	Exp. 08 (5.50)	Exp. 09 (5.58)	Exp. 11 (7.71)	Exp. 08 (3.52)	Exp. 09 (3.70)	Exp. 11 (4.85)
37f	3	Exp. 03 (22.77)	Exp. 03 (25.62)	Exp. 10 (26.39)	Exp. 03 (14.02)	Exp. 10 (13.53)	Exp. 13 (26.18)
37g	3	Exp. 07 (6.18)	Exp. 12 (17.80)	Exp. 13 (8.63)	Exp. 06 (< 3)	Exp. 07 (25.53)	Exp. 14 (7.30)
37h	3	Exp. 08 (3.34)	Exp. 09 (4.10)	Exp. 11 (4.69)	Exp. 12 (4.61)	Exp. 13 (1.95)	Exp. 14 (3.49)
37j	3	Exp. 08 (4.59)	Exp. 09 (6.61)	Exp. 11 (13.60)	Exp. 08 (4.14)	Exp. 09 (4.95)	Exp. 11 (8.66)
38a	3	Exp. 04 (7.17)	Exp. 05 (6.39)	Exp. 13 (11.39)	Exp. 04 (6.96)	Exp. 05 (7.00)	Exp. 13 (9.03)
	7	Exp. 34 (5.01)	Exp. 32 (3.72)	Exp. 33 (3.64)	Exp. 34 (8.09)	Exp. 32 (4.18)	Exp. 33 (5.45)
38e	3	Exp. 12 (7.69)	Exp. 13 (8.02)	Exp. 13 (6.52)	Exp. 12 (8.81)	Exp. 13 (3.34)	Exp. 14 (7.73)
38f	3	Exp. 03 (16.69)	Exp. 03 (17.61)	Exp. 10 (14.49)	Exp. 03 (14.26)	Exp. 10 (11.03)	Exp. 13 (10.17)
38g	3	Exp. 07 (6.97)	Exp. 12 (27.93)	Exp. 13 (15.01)	Exp. 06 (6.52)	Exp. 07 (43.91)	Exp. 14 (21.32)
38h	3	Exp. 13 (3.01)	Exp. 09 (4.02)	Exp. 11 (4.66)	Exp. 12 (2.78)	Exp. 13 (0.87)	Exp. 14 (1.81)
	7	Exp. 34 (2.30)	Exp. 32 (2.10)	Exp. 33 (2.06)	Exp. 31 (1.14)	Exp. 32 (2.42)	Exp. 34 (2.94)
38i	3	Exp. 20 (58.22)	Exp. 21 (58.75)	Exp. 22 (55.55)	Exp. 20 (51.97)	Exp. 21 (51.17)	Exp. 22 (46.33)
38j	3	Exp. 10 (7.99)	Exp. 11 (13.54)	Exp. 16 (13.16)	Exp. 10 (5.22)	Exp. 11 (7.99)	Exp. 14 (7.24)
39	3	Exp. 08 (24.73)	Exp. 09 (22.46)	Exp. 12 (29.38)	Exp. 08 (18.22)	Exp. 09 (25.31)	Exp. 12 (55.31)
72a	3	Exp. 27 (15.43)	Exp. 28 (14.72)	Exp. 29 (16.76)	Exp. 27 (17.49)	Exp. 28 (25.70)	Exp. 29 (15.30)
	7	Exp. 34 (6.72)	Exp. 32 (5.42)	Exp. 33 (4.50)	Exp. 31 (5.46)	Exp. 32 (7.74)	Exp. 34 (10.18)
75a	3	Exp. 30 (130.06)			Exp. 30 (23.75)		
75f	3	Exp. 30 (70.96)			Exp. 30 (20.40)		
80b	3	Exp. 23 (5.91)	Exp. 24 (15.74)	Exp. 25 (13.43)	Exp. 23 (5.34)	Exp. 24 (9.76)	Exp. 25 (7.82)
80b·TFAc	3	Exp. 23 (5.23)	Exp. 24 (5.74)	Exp. 25 (6.12)	Exp. 23 (4.71)	Exp. 24 (5.59)	Exp. 25 (5.13)
81aH·Cl	3	Exp. 17 (29.71)	Exp. 18 (20.64)	Exp. 19 (20.86)	Exp. 17 (36.97)	Exp. 18 (20.98)	Exp. 19 (25.09)
81bH·Cl	3	Exp. 17 (44.52)	Exp. 18 (22.15)	Exp. 19 (21.26)	Exp. 17 (39.98)	Exp. 18 (23.68)	Exp. 19 (15.97)

83H·Cl	3	Exp. 27 (187.78)	Exp. 28 (188.12)	Exp. 29 (177.77)	Exp. 27 (115.75)	Exp. 28 (147.89)	Exp. 29 (83.06)
86a	3	Exp. 15 (> 300)	Exp. 16 (> 300)	Exp. 20 (> 300)	Exp. 15 (> 300)	Exp. 16 (> 300)	Exp. 20 (> 300)
86b	3	Exp. 22 (> 300)	Exp. 23 (> 300)	Exp. 24 (> 300)	Exp. 22 (> 300)	Exp. 23 (> 300)	Exp. 24 (> 300)
86d	3	Exp. 15 (> 300)	Exp. 21 (> 300)	Exp. 22 (> 300)	Exp. 15 (> 300)	Exp. 21 (> 300)	Exp. 22 (> 300)
86e	3	Exp. 15 (> 300)	Exp. 20 (> 300)		Exp. 15 (> 300)	Exp. 16 (> 300)	Exp. 20 (> 300)
86f	3	Exp. 26 (> 300)			Exp. 26 (> 300)		
86h	3	Exp. 26 (> 300)			Exp. 26 (> 300)		
86o	3	Exp. 26 (> 300)			Exp. 26 (> 300)		
86p	3	Exp. 26 (> 300)			Exp. 26 (> 300)		
89	3	Exp. 15 (> 300)	Exp. 21 (> 300)	Exp. 22 (> 300)	Exp. 15 (> 300)	Exp. 21 (> 300)	Exp. 22 (>300)
92a·BF_4	3	Exp. 15 (> 300)	Exp. 20 (> 300)		Exp. 15 (> 300)	Exp. 16 (298.70)	Exp. 20 (> 300)
92d·BF_4	3	Exp. 26 (> 300)			Exp. 26 (100.31)		
92e·BF_4	3	Exp. 15 (66.79)	Exp. 21 (91.42)		Exp. 15 (143.97)	Exp. 16 (131.54)	Exp. 21 (120.82)
98·Br	3	Exp. 25 (> 300)	Exp. 26 (> 300)		Exp. 25 (68.40)	Exp. 26 (77.96)	
117	3	Exp. 17 (78.20)	Exp. 18 (67.64)	Exp. 19 (106.67)	Exp. 17 (66.20)	Exp. 18 (40.92)	Exp. 19 (61.80)
118	3	Exp. 17 (194.67)	Exp. 18 (70.77)	Exp. 19 (158.02)	Exp. 17 (96.40)	Exp. 18 (165.65)	Exp. 19 (77.38)
137	3	Exp. 27 (4.69)	Exp. 28 (4.47)	Exp. 29 (3.94)	Exp. 27 (4.34)	Exp. 28 (4.43)	Exp. 29 (< 3)
158	3	Exp. 30 (0.76)	Exp. 28 (< 3)	Exp. 29 (< 3)	Exp. 30 (0.68)	Exp. 28 (< 3)	Exp. 29 (< 3)
181b	3	Exp. 03 (23.10)	Exp. 10 (10.26)	Exp. 12 (8.10)	Exp. 03 (14.07)	Exp. 10 (5.46)	Exp. 12 (6.98)
182a	3	Exp. 06 (3.63)	Exp. 07 (5.58)	Exp. 16 (6.19)	Exp. 06 (4.39)	Exp. 07 (11.08)	Exp. 14 (7.04)
182b	3	Exp. 03 (18.06)	Exp. 03 (19.12)	Exp. 10 (15.91)	Exp. 03 (13.89)	Exp. 10 (7.07)	Exp. 12 (9.86)
183b	3	Exp. 17 (24.18)	Exp. 18 (10.28)	Exp. 19 (32.71)	Exp. 17 (14.33)	Exp. 18 (17.81)	Exp. 19 (7.60)
184a	3	Exp. 06 (43.10)	Exp. 07 (69.94)		Exp. 06 (57.00)	Exp. 07 (279.63)	Exp. 11 (83.72)

192	3	Exp. 27 (88.74)	Exp. 28 (70.19)	Exp. 29 (69.12)	Exp. 27 (30.38)	Exp. 28 (29.07)	Exp. 29 (27.69)
	7	Exp. 34 (39.60)	Exp. 32 (53.51)	Exp. 33 (32.83)	Exp. 31 (9.24)	Exp. 32 (11.58)	Exp. 34 (18.04)
208	3	Exp. 27 (9.55)	Exp. 28 (9.48)	Exp. 29 (8.82)	Exp. 27 (4.42)	Exp. 28 (5.20)	Exp. 29 (3.80)
210b	3	Exp. 20 (14.86)	Exp. 21 (24.05)	Exp. 22 (10.08)	Exp. 20 (19.62)	Exp. 21 (25.71)	Exp. 22 (14.43)
210c	3	Exp. 20 (5.96)	Exp. 21 (7.12)	Exp. 22 (5.34)	Exp. 20 (10.95)	Exp. 21 (9.95)	Exp. 22 (10.22)
214	3	Exp. 04 (286.01)	Exp. 05 (230.93)	Exp. 12 (> 300)	Exp. 04 (255.09)	Exp. 05 (> 300)	Exp. 12 (> 300)
222	3	Exp. 04 (> 300)	Exp. 05 (247.01)	Exp. 12 (> 300)	Exp. 04 (170.54)	Exp. 05 (237.94)	Exp. 12 (> 300)
TEMPO	3	Exp. 15 (> 300)	Exp. 16 (> 300)	Exp. 16 (> 300)	Exp. 15 (> 300)	Exp. 16 (> 300)	Exp. 16 (296.55)

E-2 – SRB assay graphs

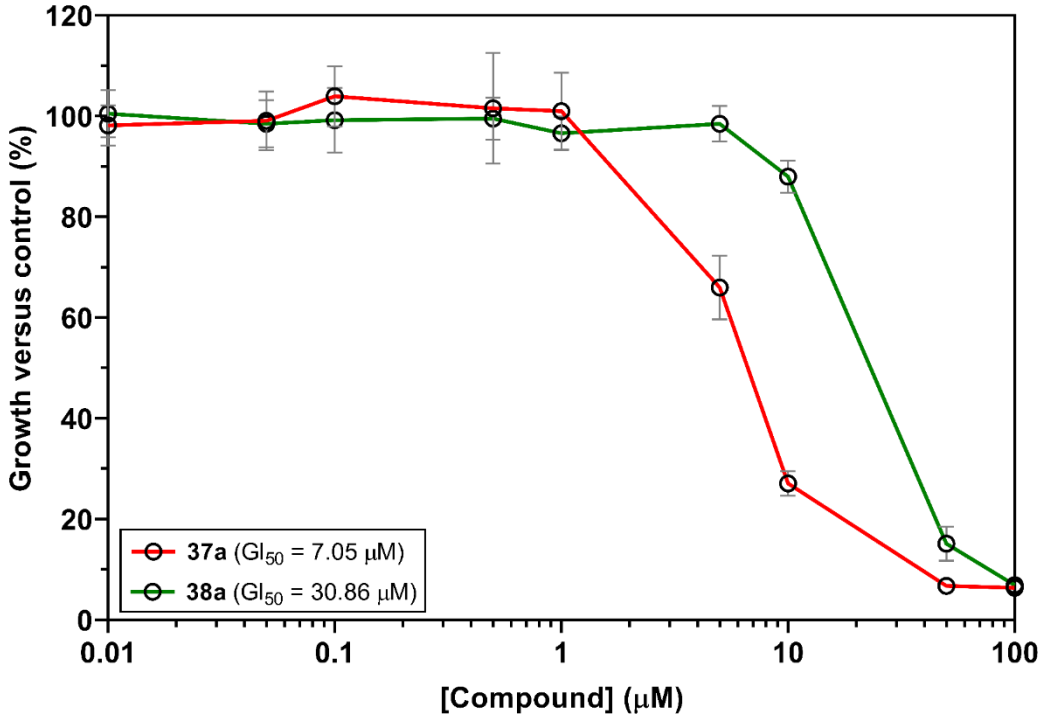


Figure S87 – Experiment 1, SJSA-1 cell line.

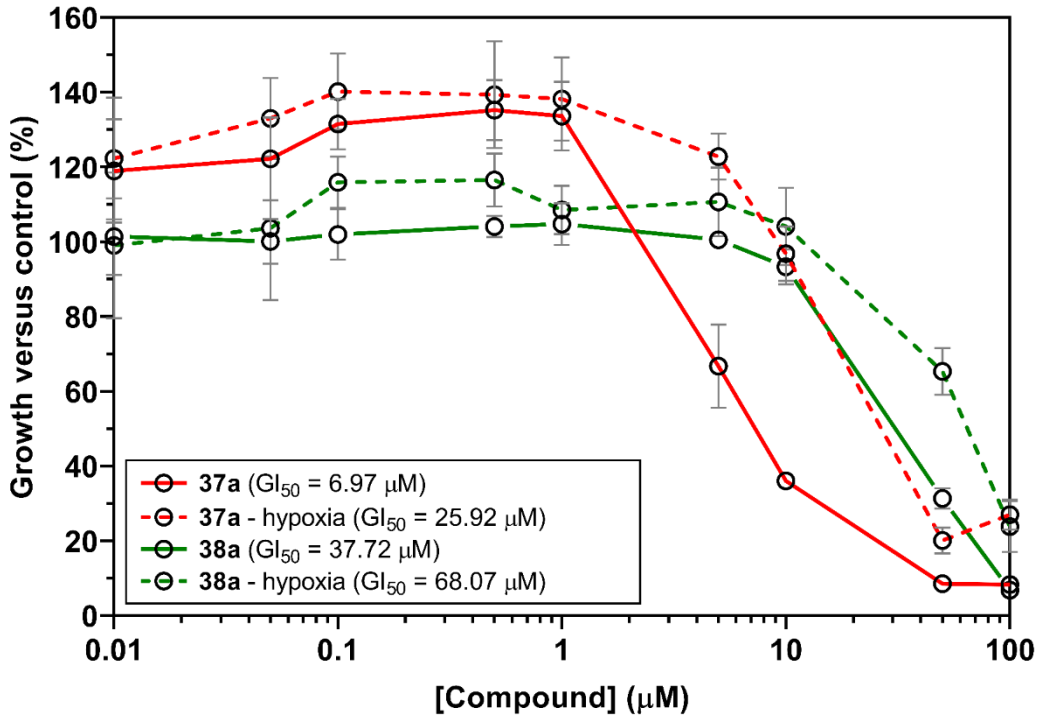


Figure S88 – Experiment 2, SJSA-1 cell line.

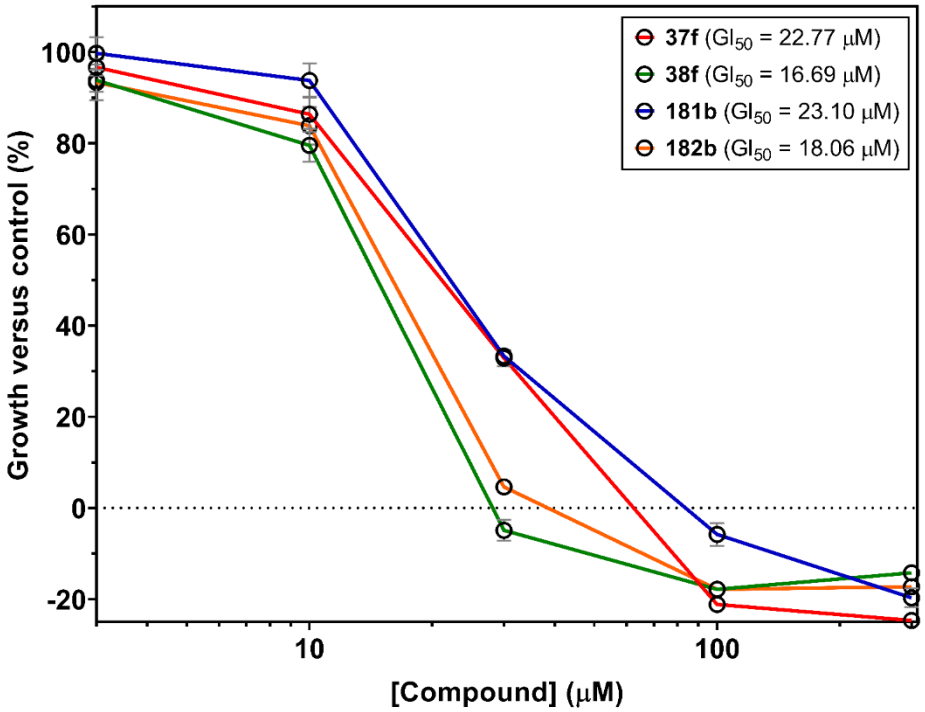


Figure S89 – Experiment 3, GB-1 cell line, set 1.

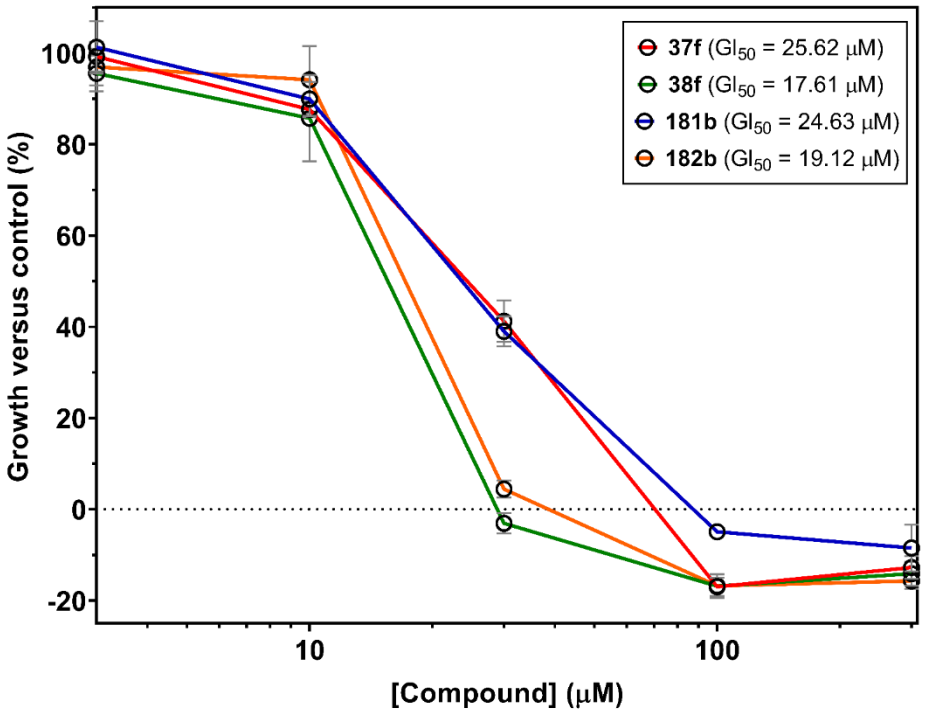


Figure S90 – Experiment 3, GB-1 cell line, set 2.

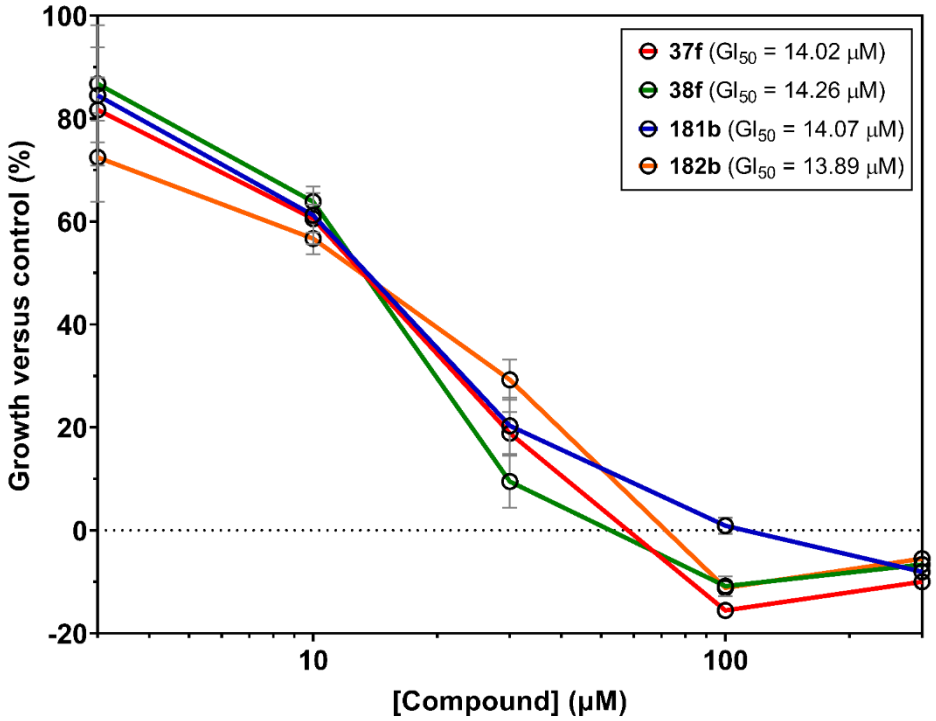


Figure S91 – Experiment 3, MCF-7 cell line.

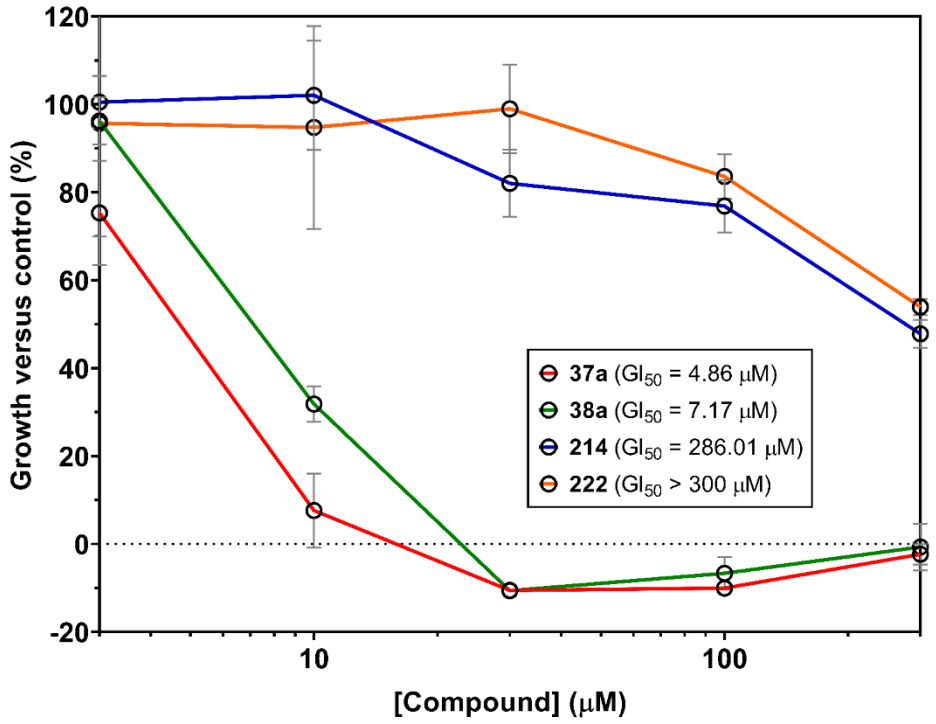


Figure S92 – Experiment 4, GB-1 cell line.

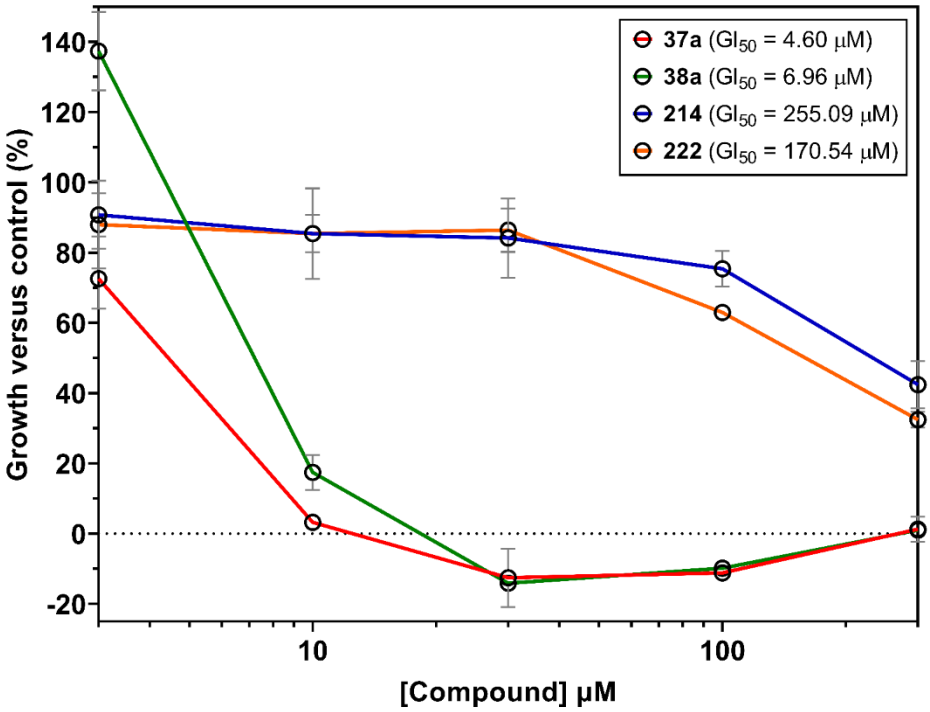


Figure S93 – Experiment 4, MCF-7 cell line.

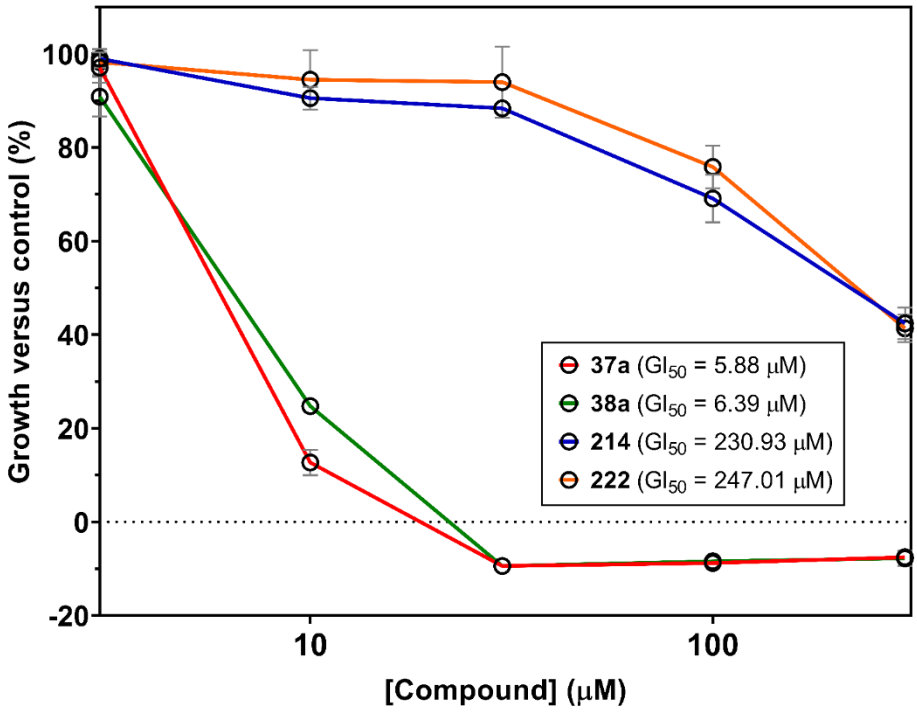


Figure S94 – Experiment 5, GB-1 cell line.

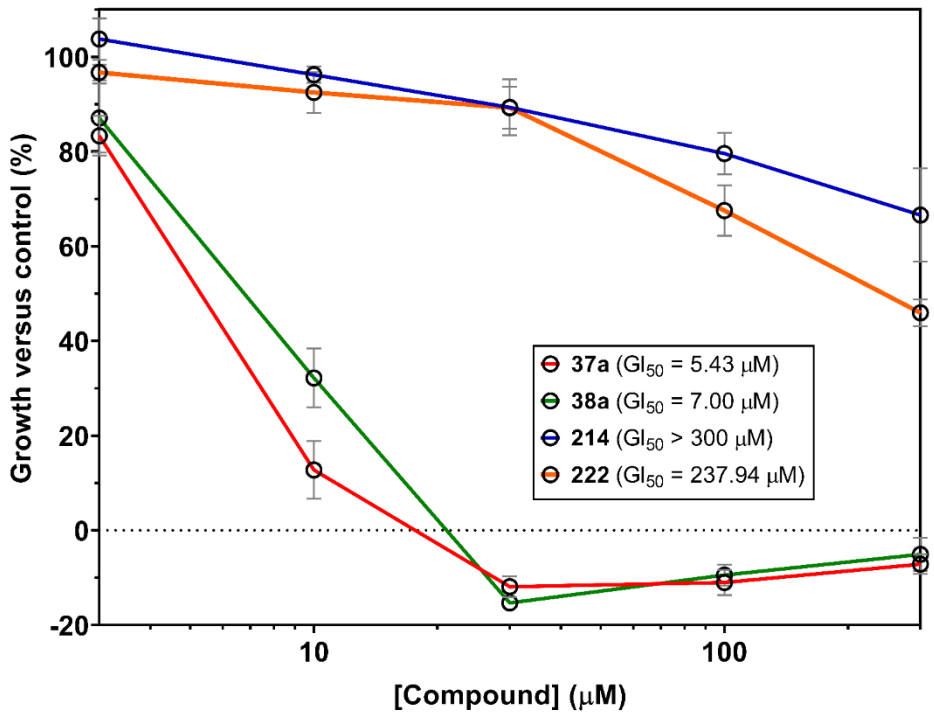


Figure S95 – Experiment 5, MCF-7 cell line.

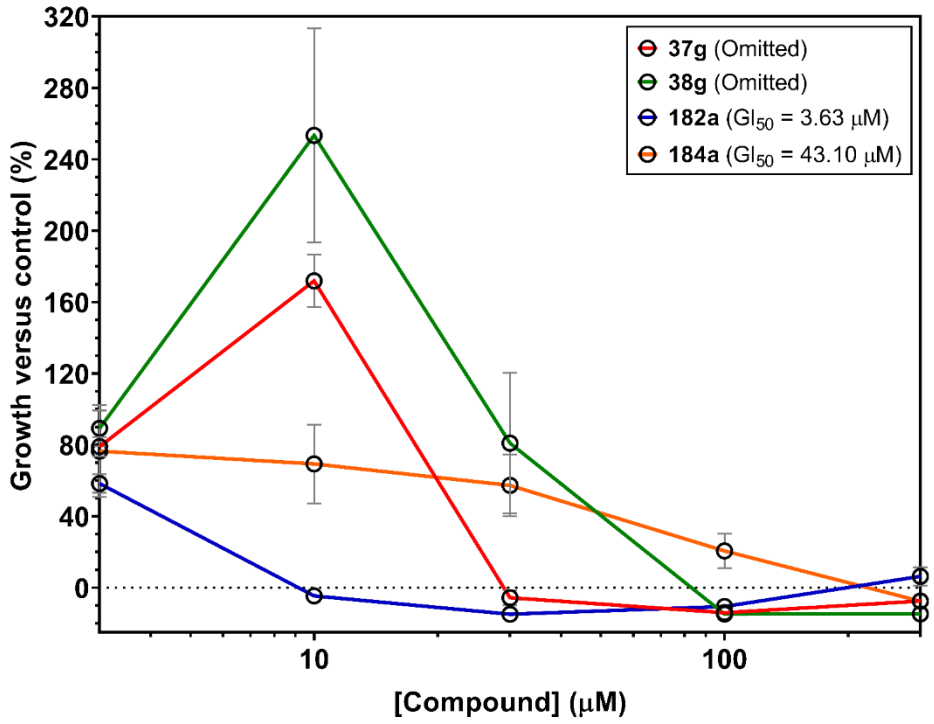


Figure S96 – Experiment 6, GB-1 cell line.

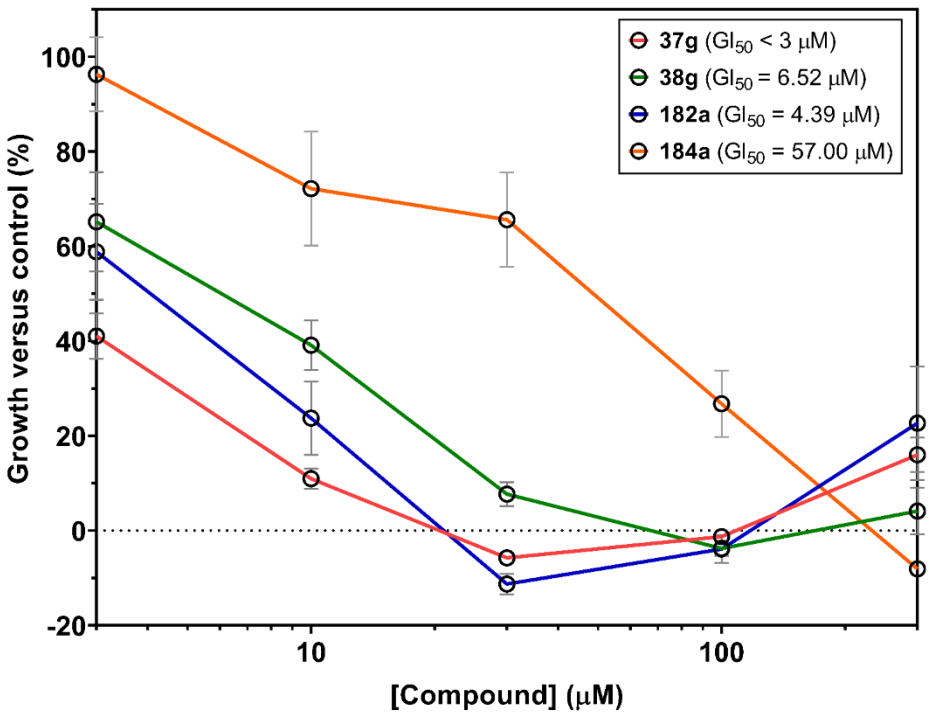


Figure S97 – Experiment 6, MCF-7 cell line.

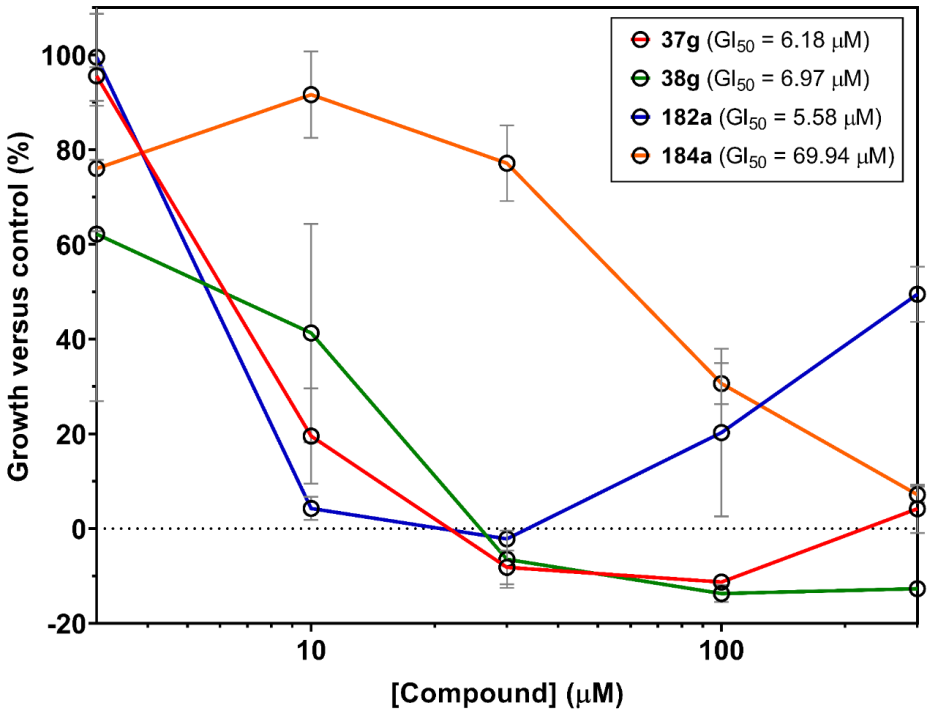


Figure S98 – Experiment 7, GB-1 cell line.

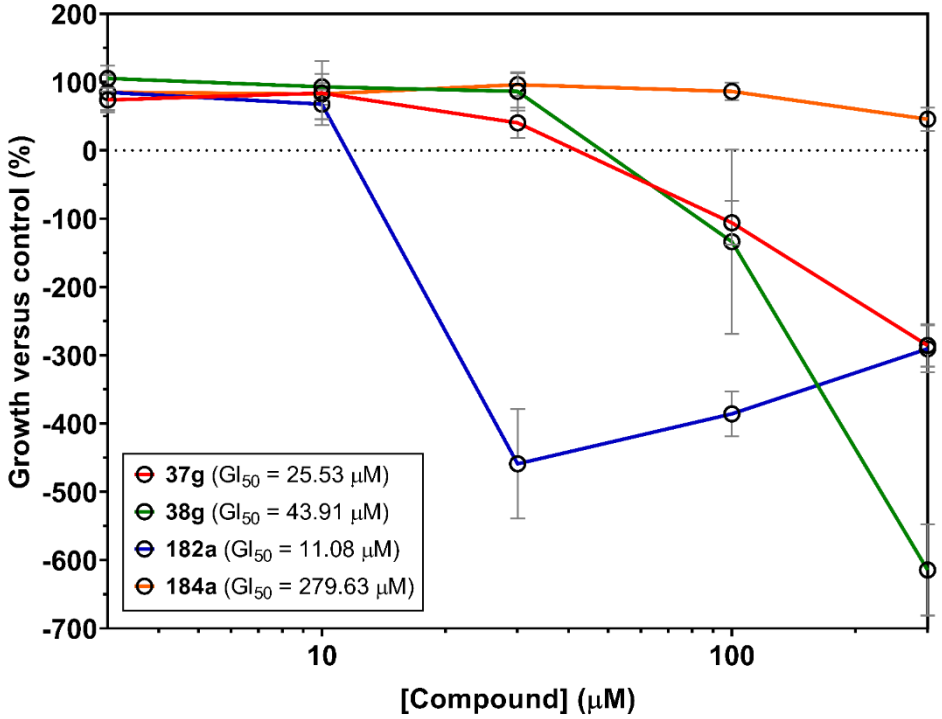


Figure S99 – Experiment 7, MCF-7 cell line.

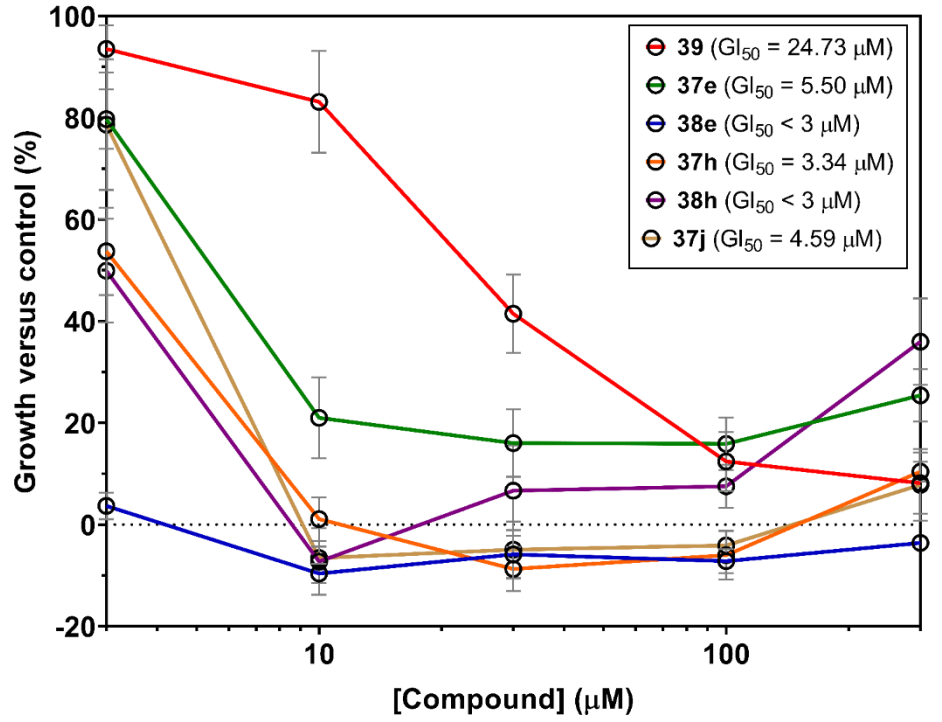


Figure S100 – Experiment 8, GB-1 cell line.

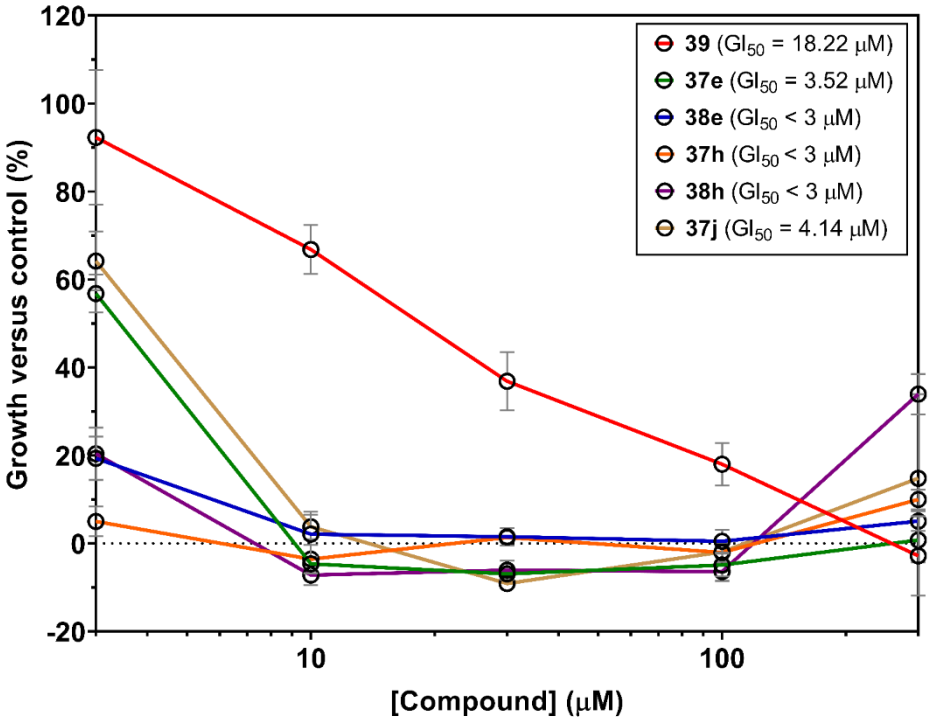


Figure S101 – Experiment 8, MCF-7 cell line.

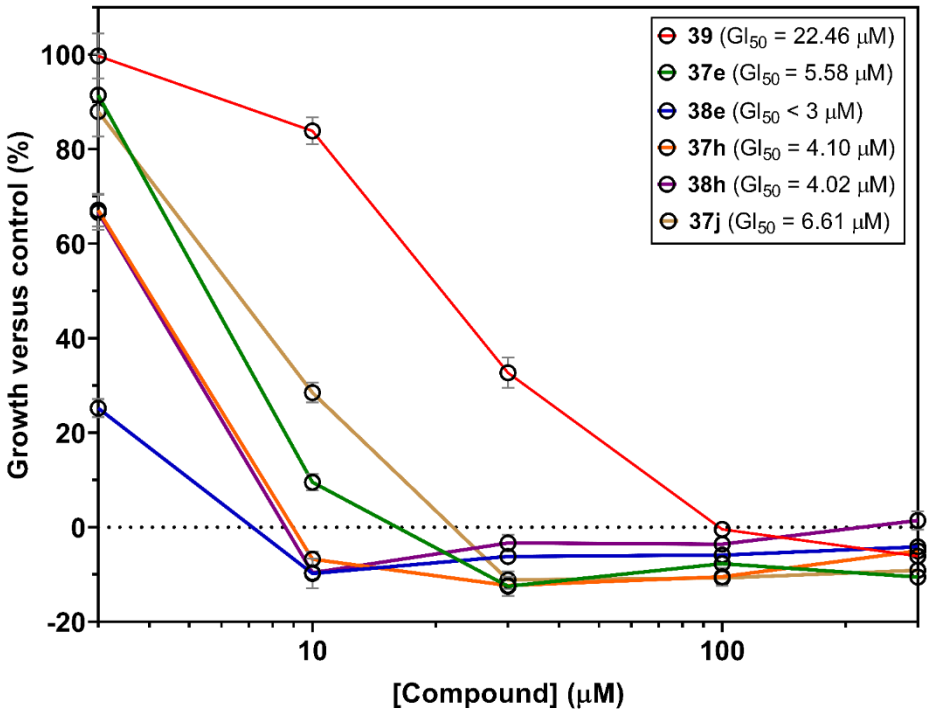


Figure S102 – Experiment 9, GB-1 cell line.

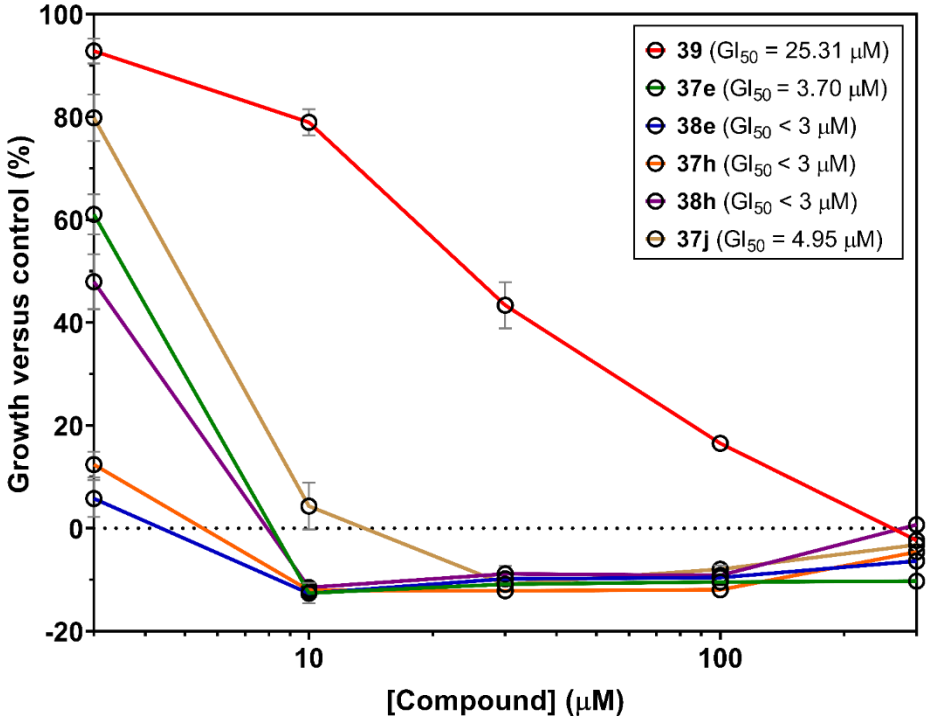


Figure S103 – Experiment 9, MCF-7 cell line.

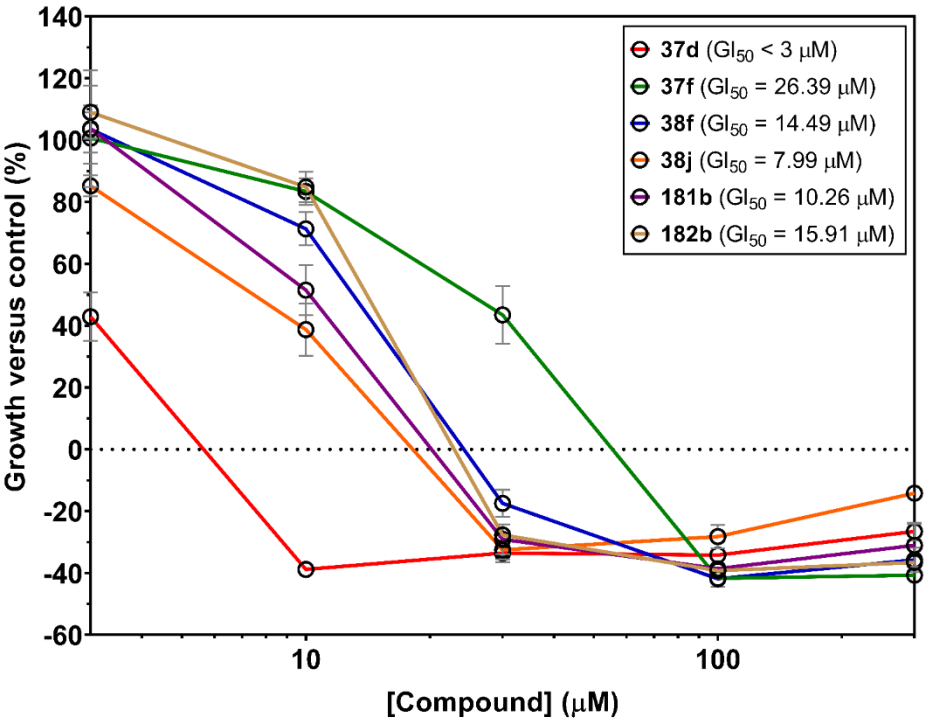


Figure S104 – Experiment 10, GB-1 cell line.

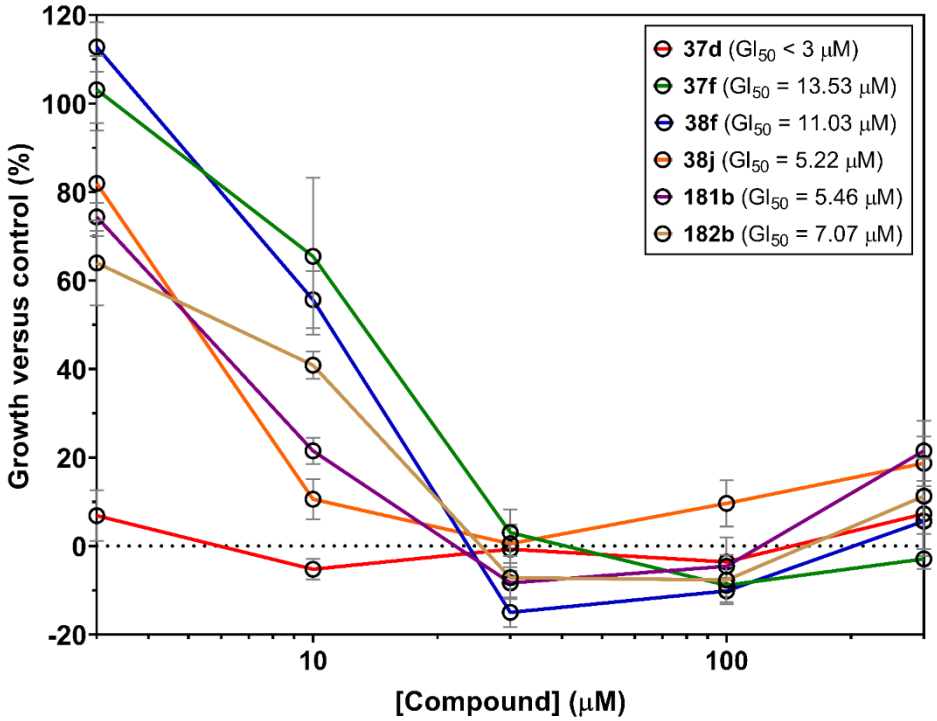


Figure S105 – Experiment 10, MCF-7 cell line.

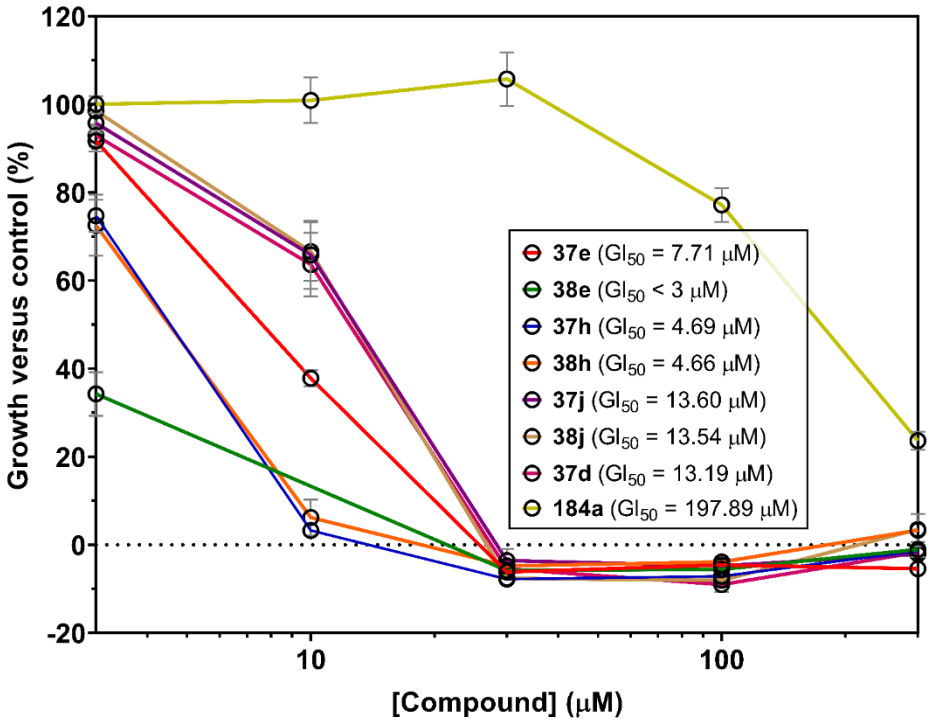


Figure S106 – Experiment 11, GB-1 cell line.

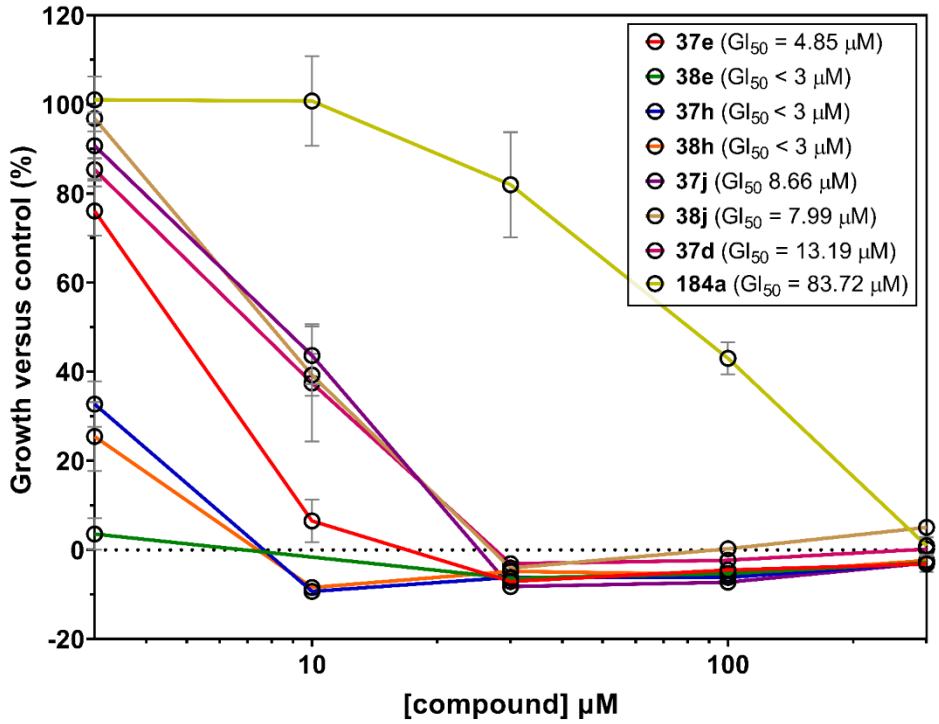


Figure S107 – Experiment 11, MCF-7 cell line.

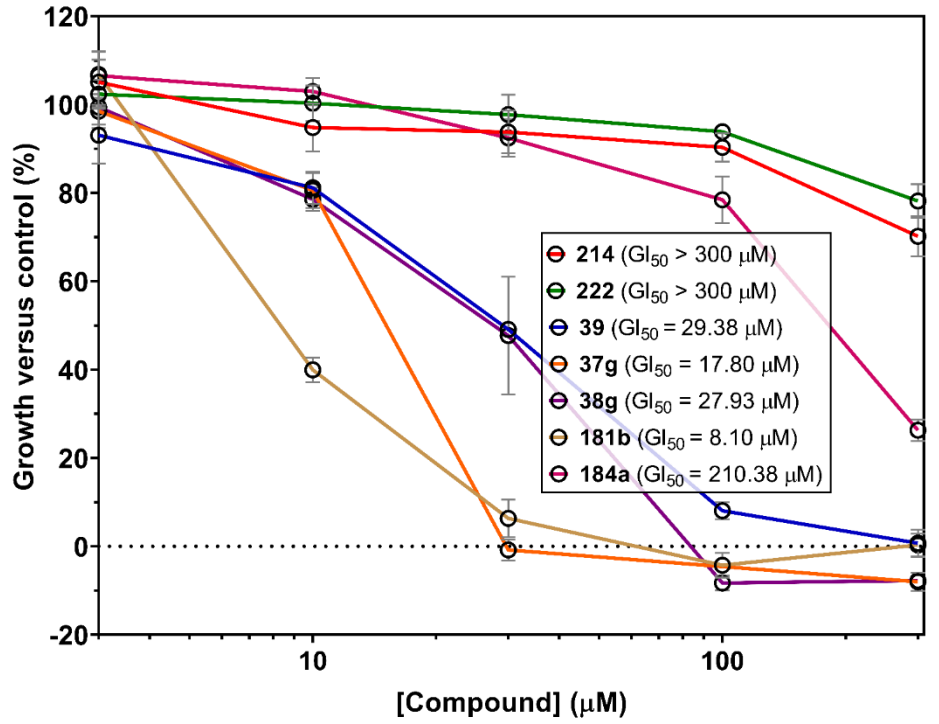


Figure S108 – Experiment 12, GB-1 cell line, high concentration.

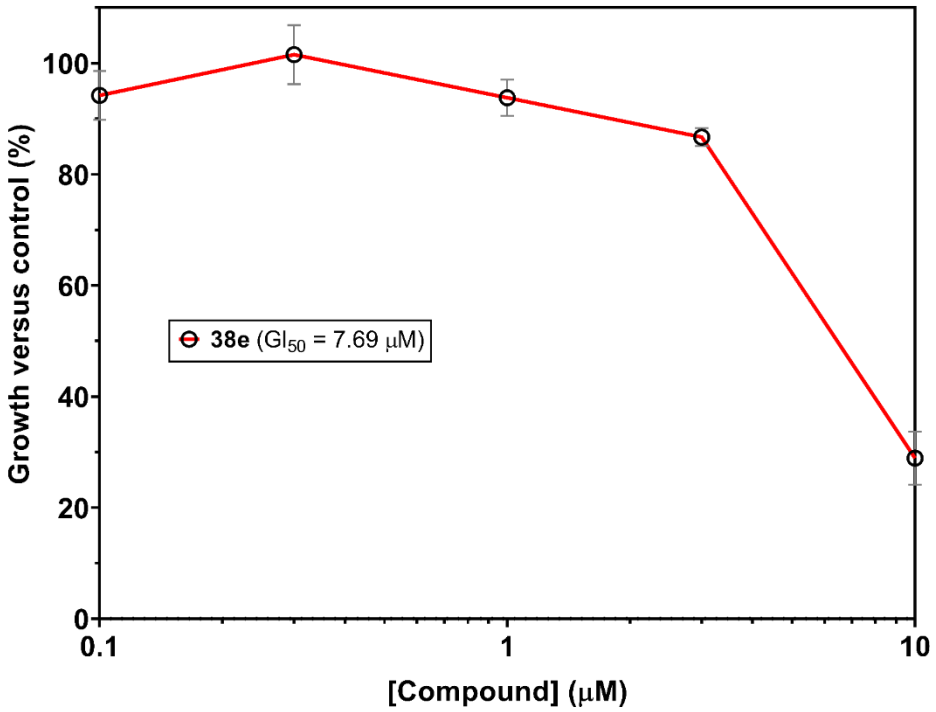


Figure S109 – Experiment 12, GB-1 cell line, low concentration.

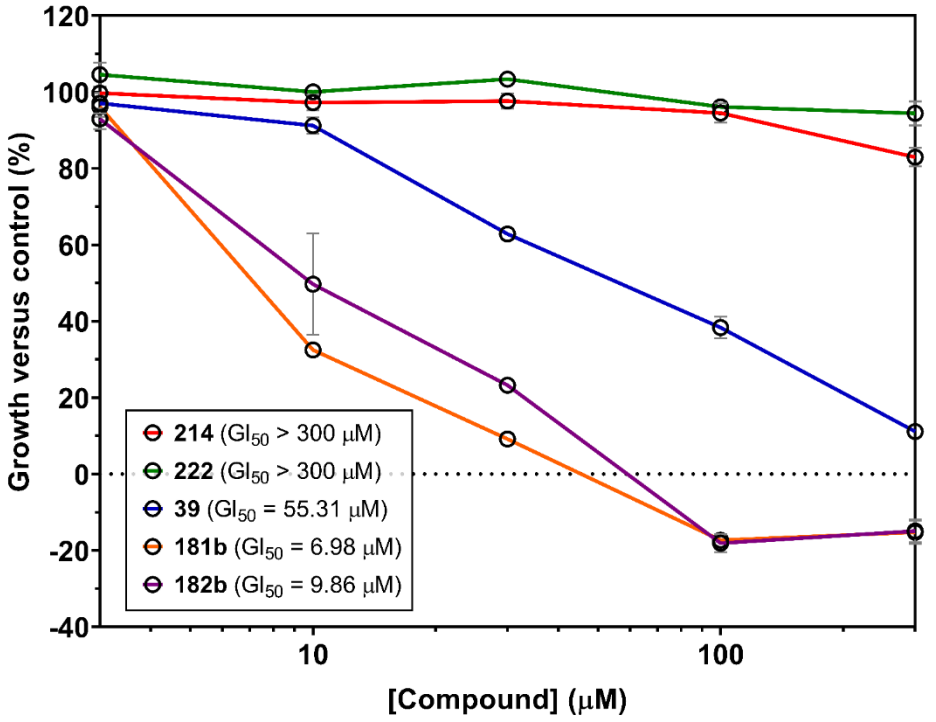


Figure S110 – Experiment 12, MCF-7 cell line, high concentration.

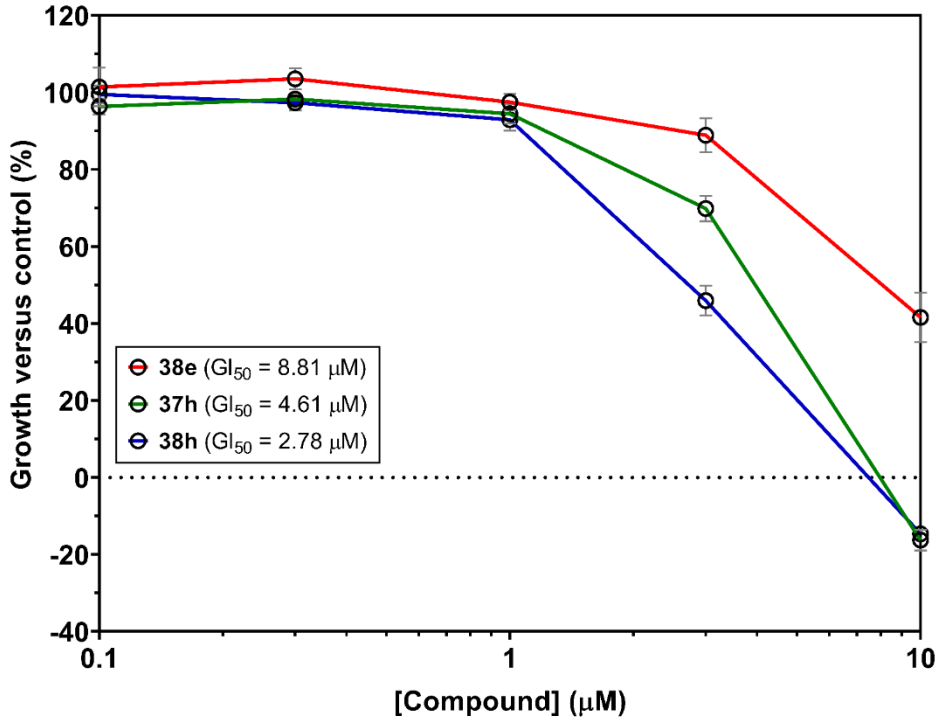


Figure S111 – Experiment 12, MCF-7 cell line, low concentration.

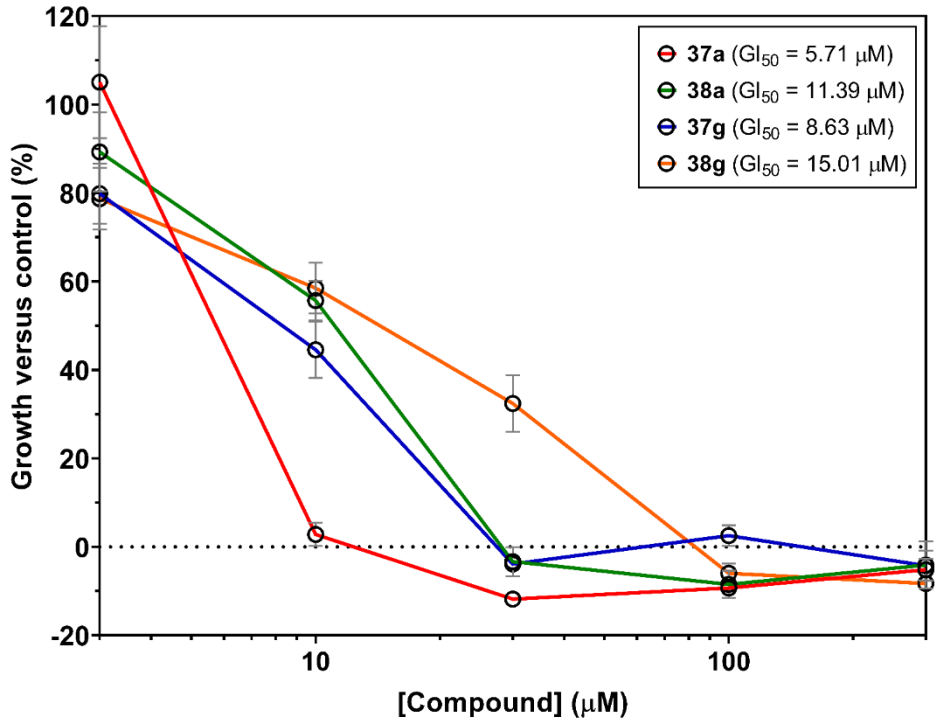


Figure S112 – Experiment 13, GB-1 cell line, high concentration.

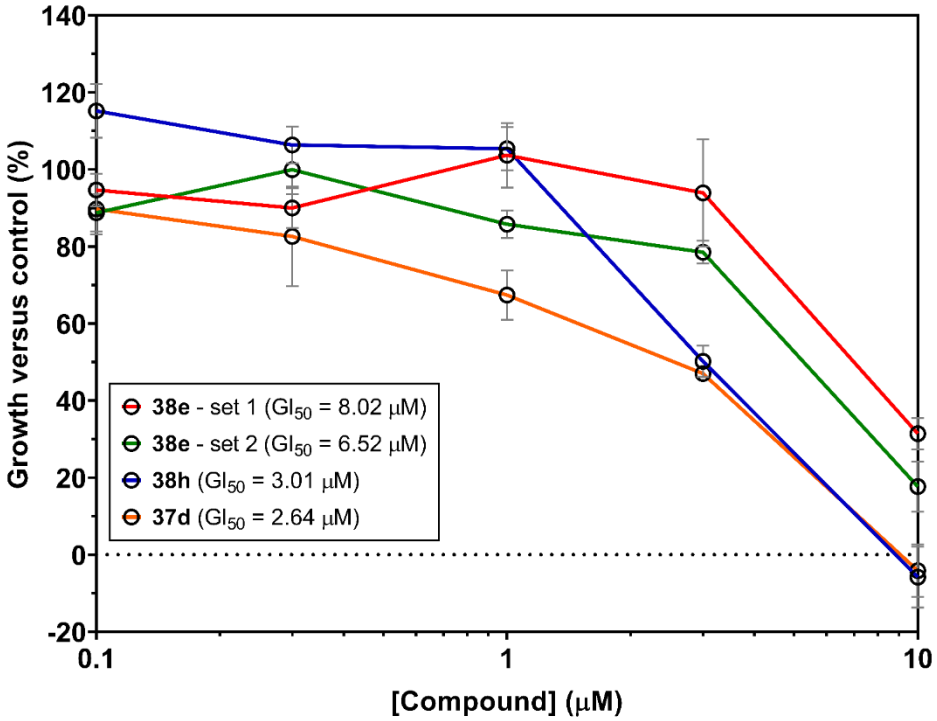


Figure S113 – Experiment 13, GB-1 cell line, low concentration.

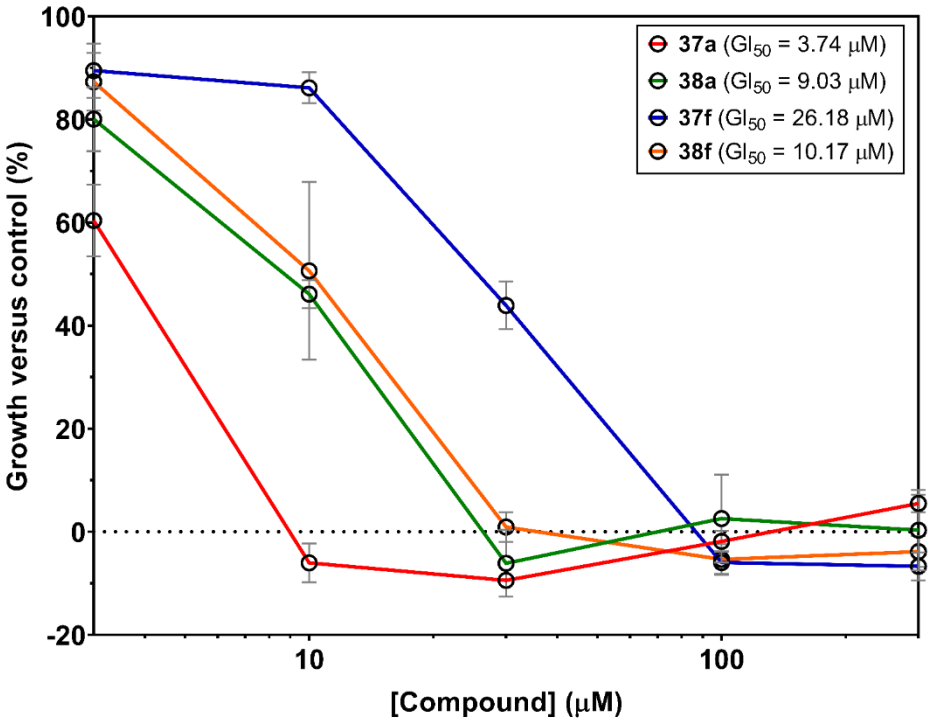


Figure S114 – Experiment 13, MCF-7 cell line, high concentration.

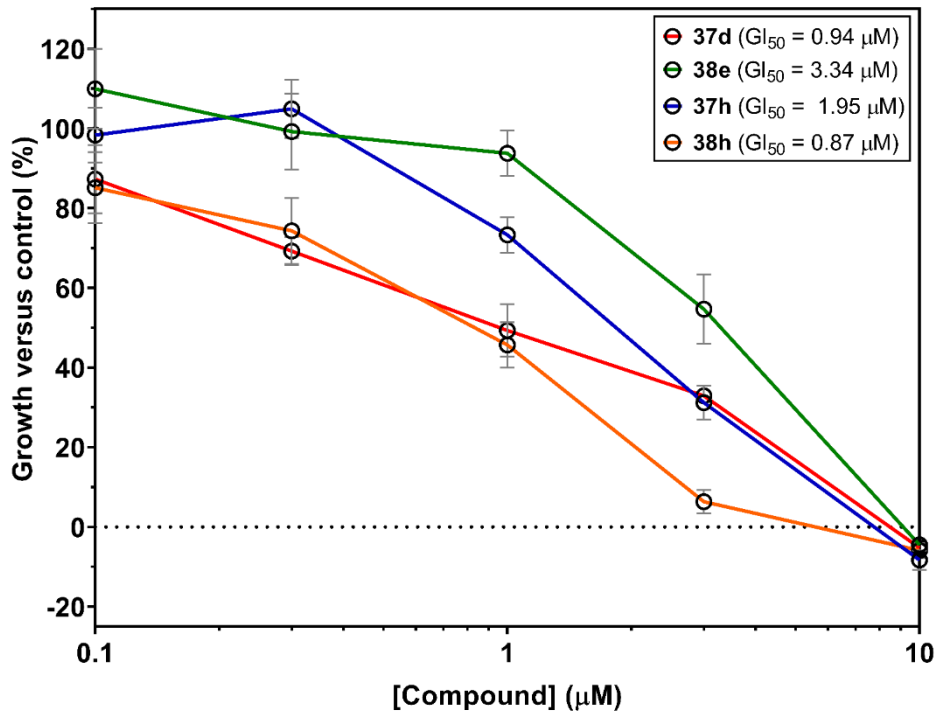


Figure S115 – Experiment 13, MCF-7 cell line, low concentration.

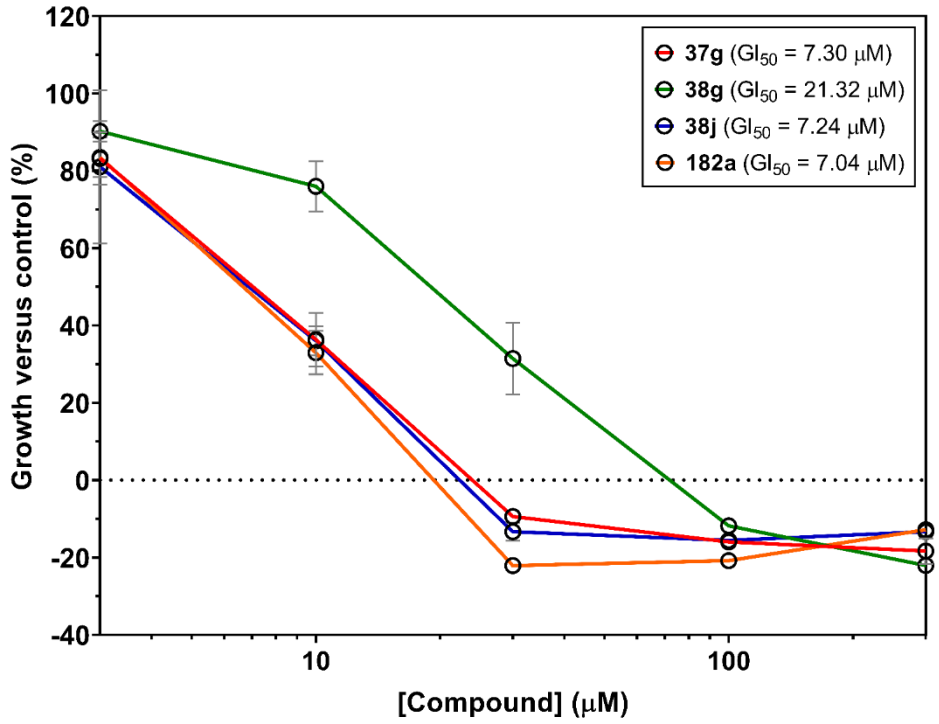


Figure S116 – Experiment 14, MCF-7 cell line, high concentration.

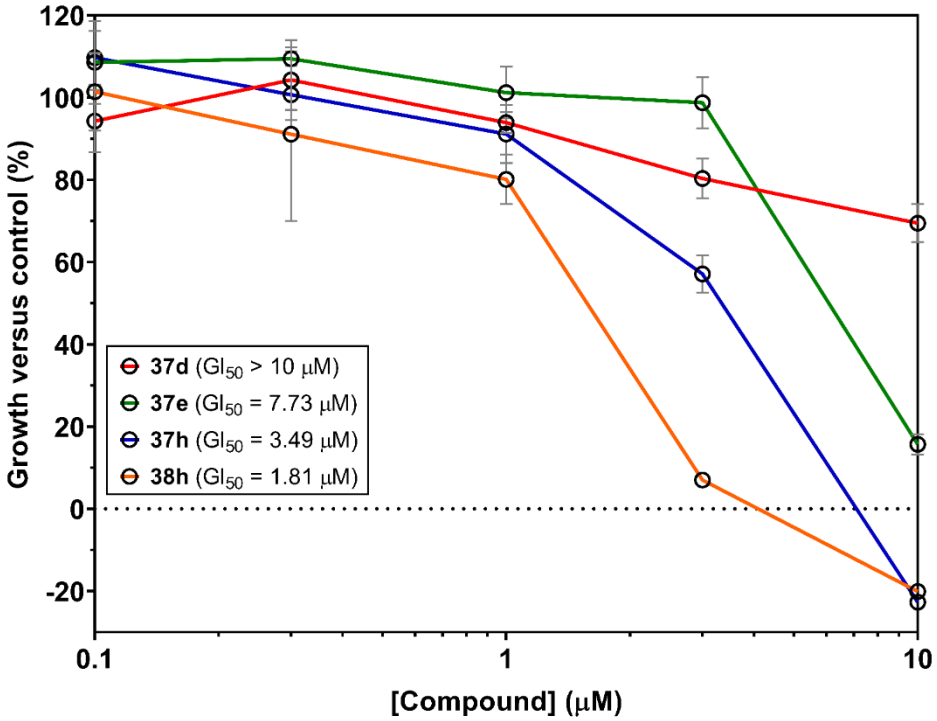


Figure S117 – Experiment 14, MCF-7 cell line, low concentration.

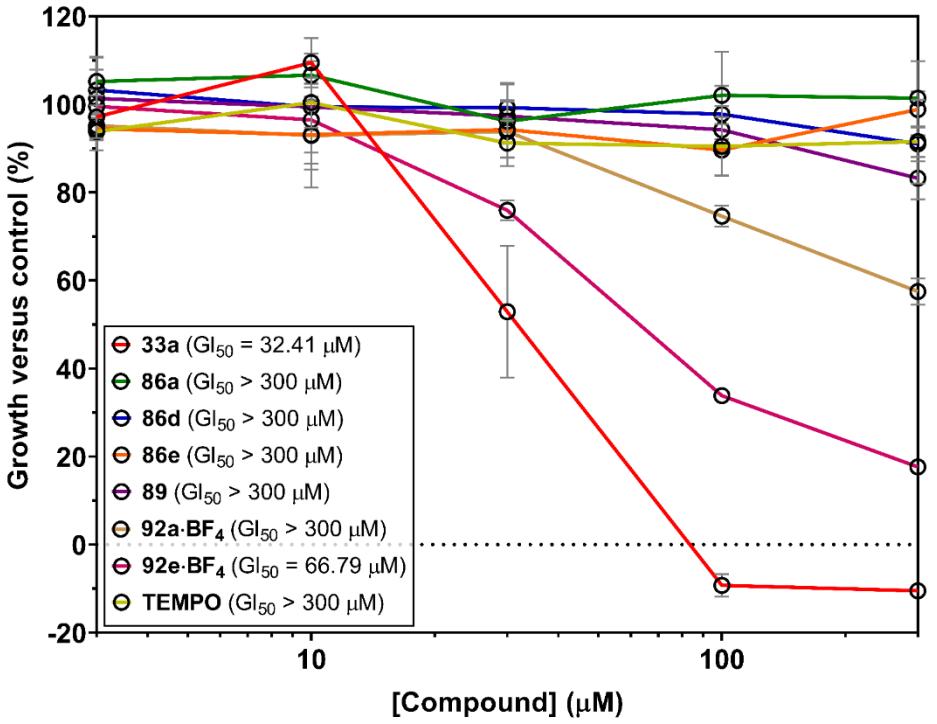


Figure S118 – Experiment 15, GB-1 cell line.

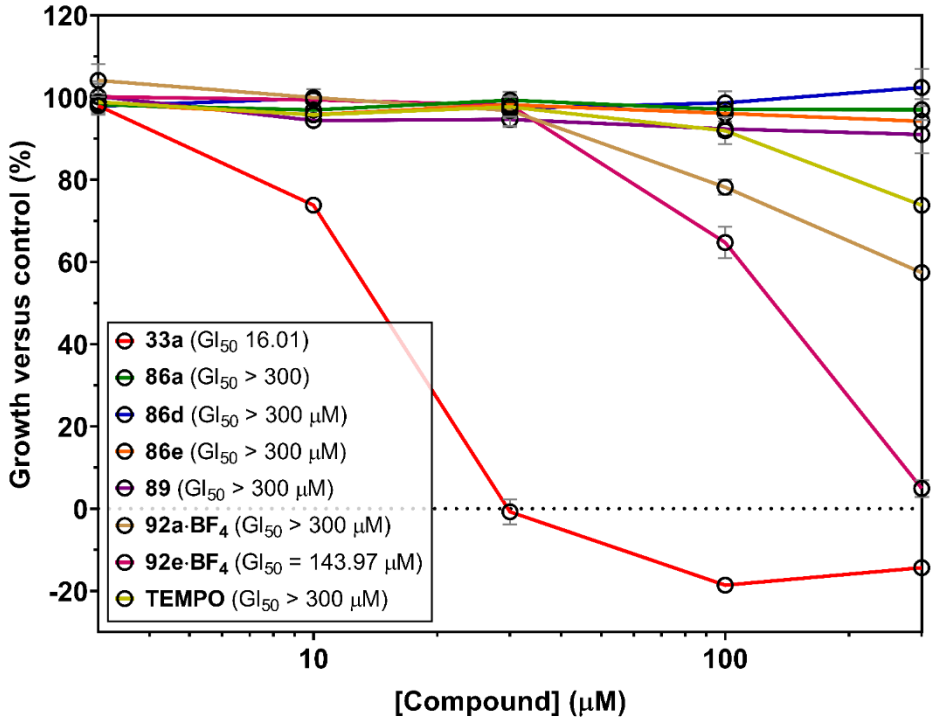


Figure S119 – Experiment 15, MCF-7 cell line.

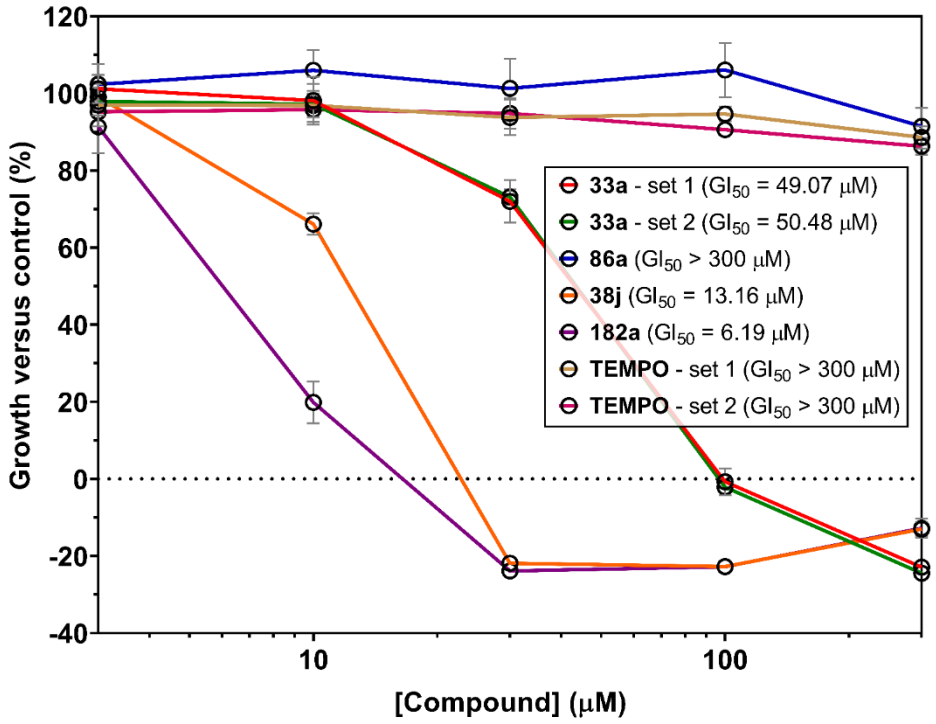


Figure S120 – Experiment 16, GB-1 cell line, high concentration.

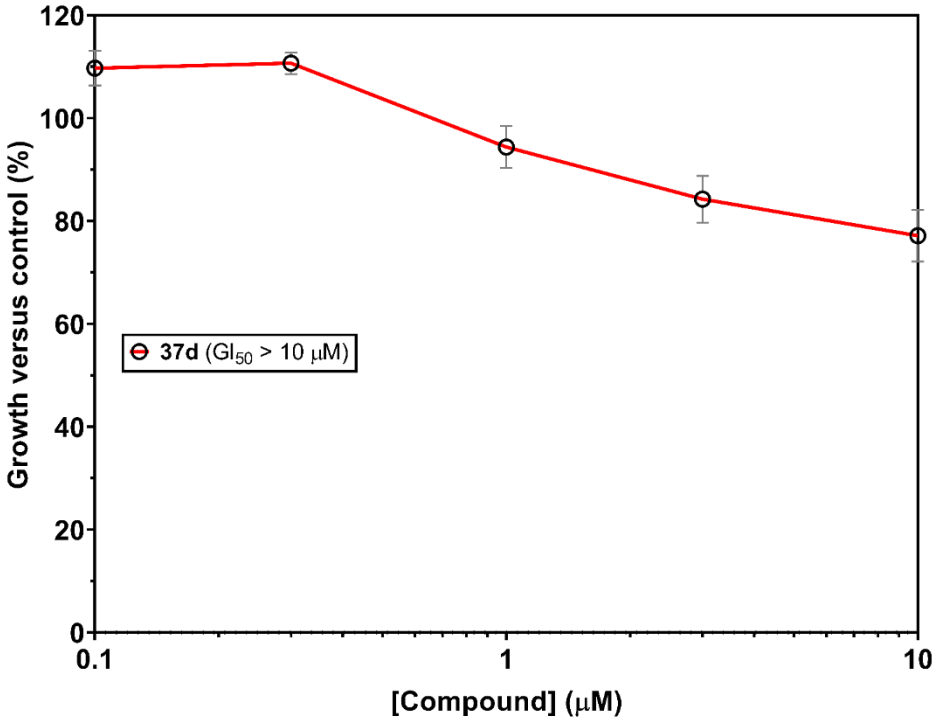


Figure S121 – Experiment 16, GB-1 cell line, low concentration.

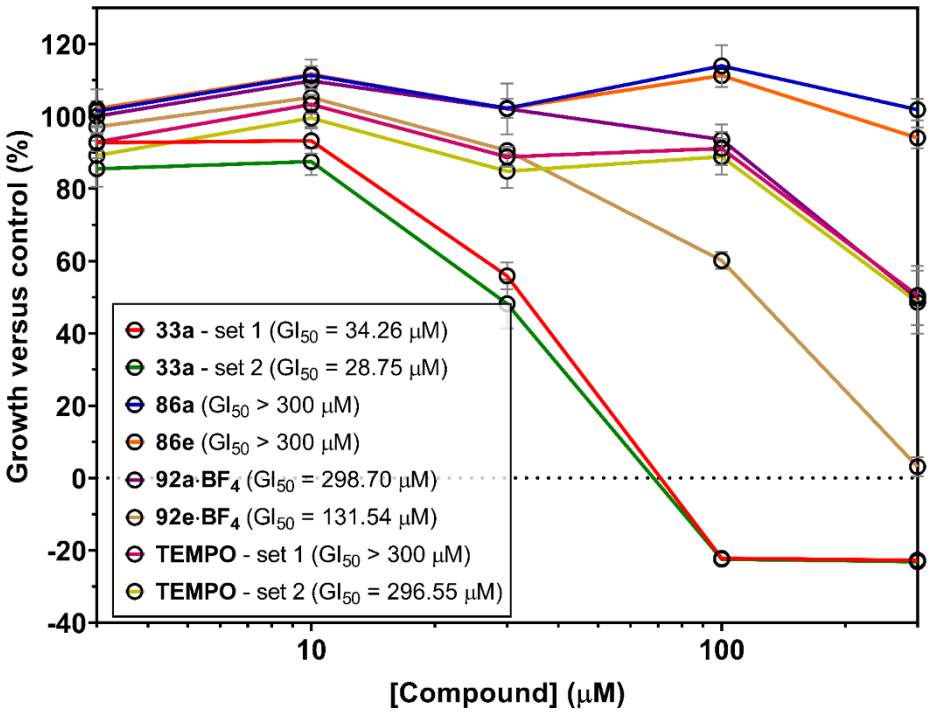


Figure S122 – Experiment 16, MCF-7 cell line.

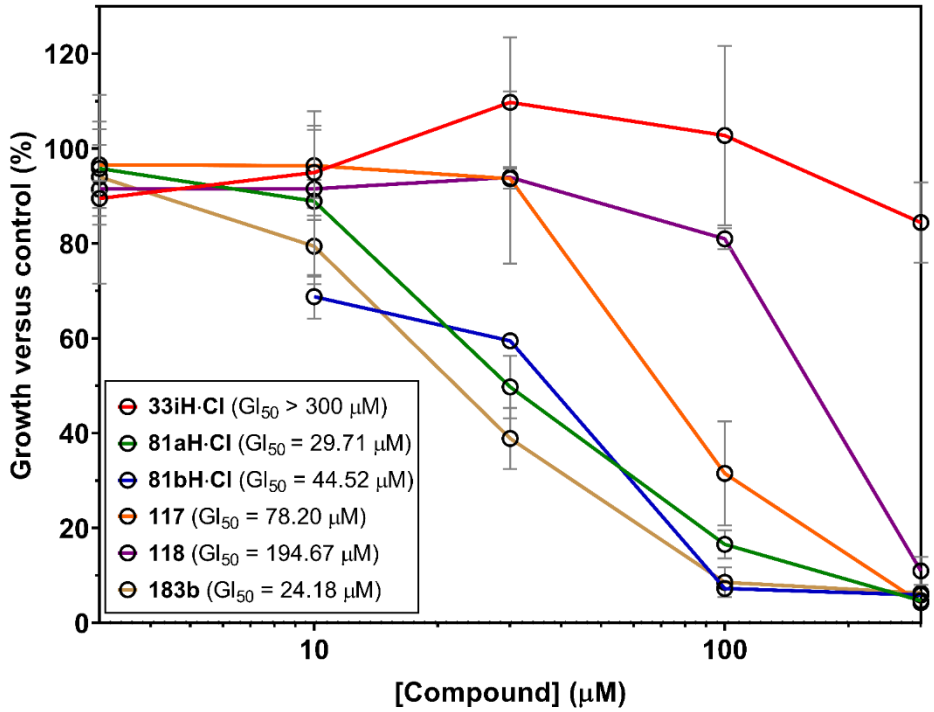


Figure S123 – Experiment 17, GB-1 cell line.

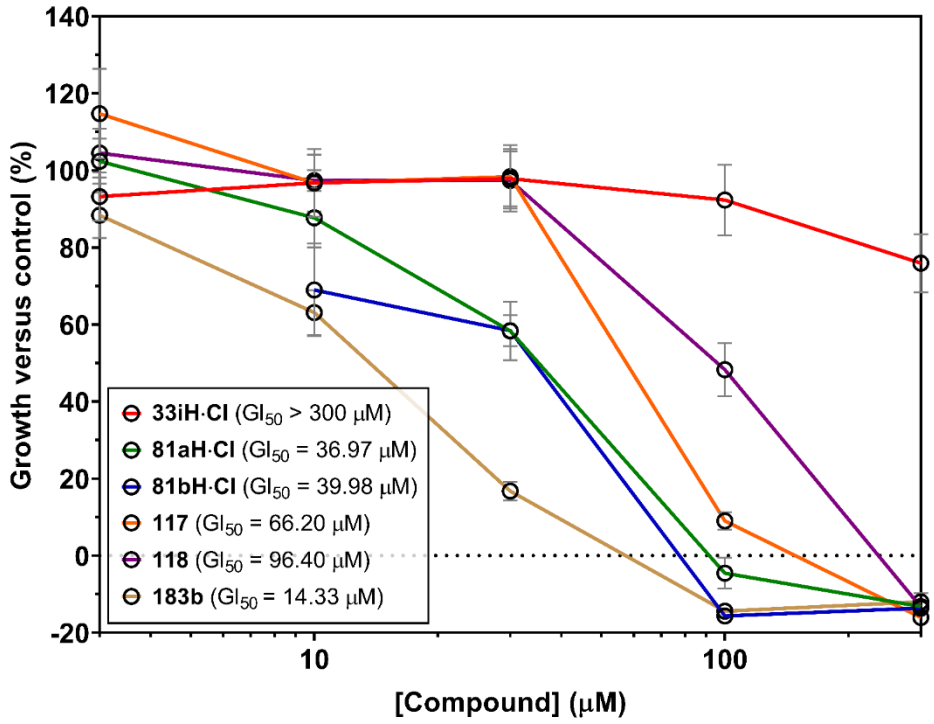


Figure S124 – Experiment 17, MCF-7 cell line.

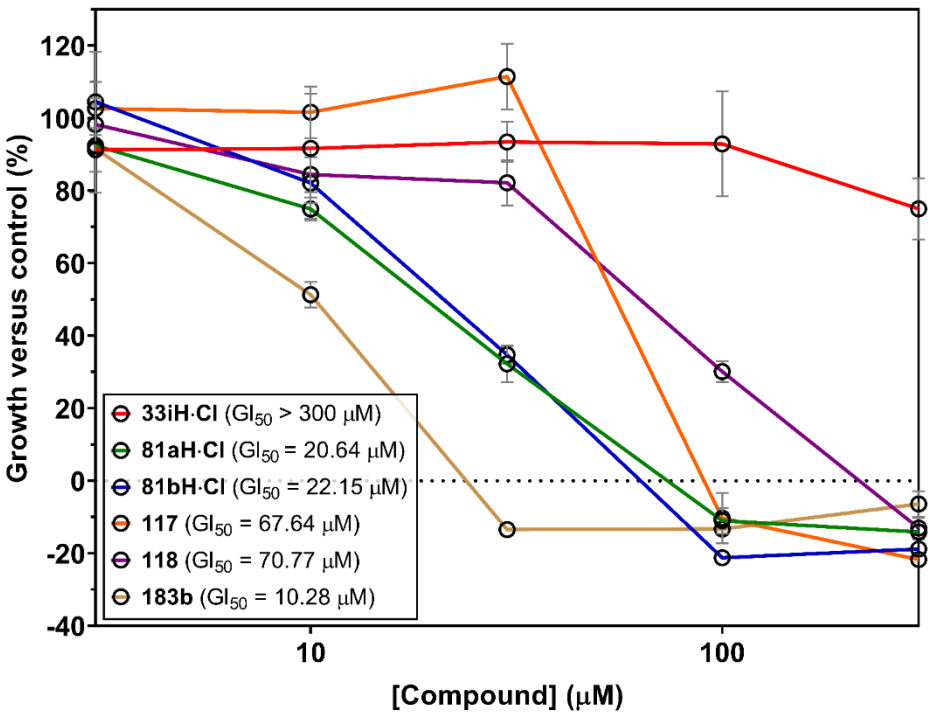


Figure S125 – Experiment 18, GB-1 cell line.

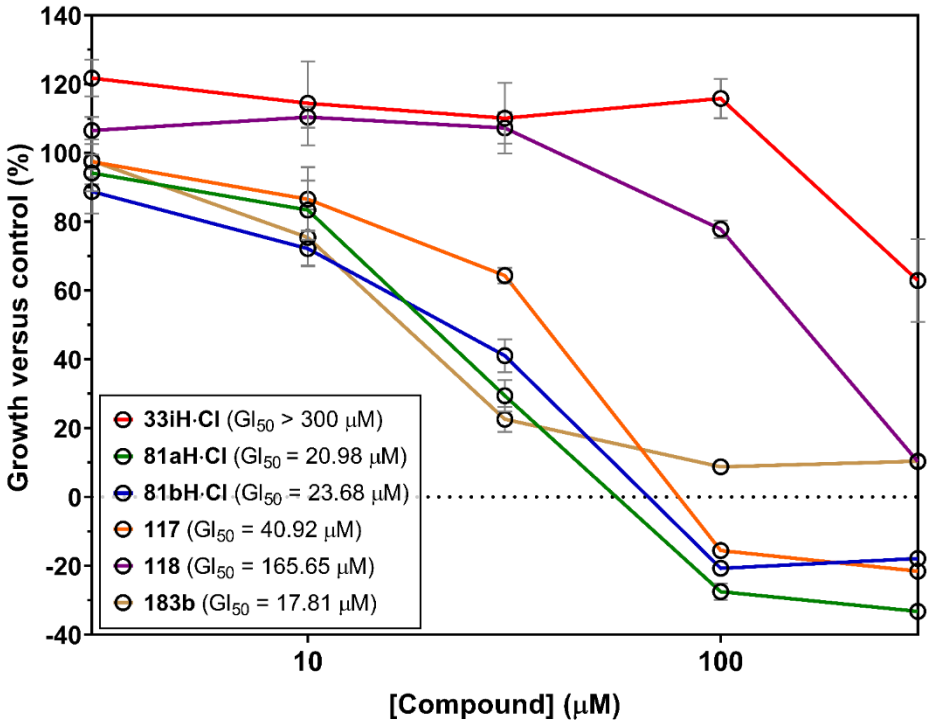


Figure S126 – Experiment 18, MCF-7 cell line.

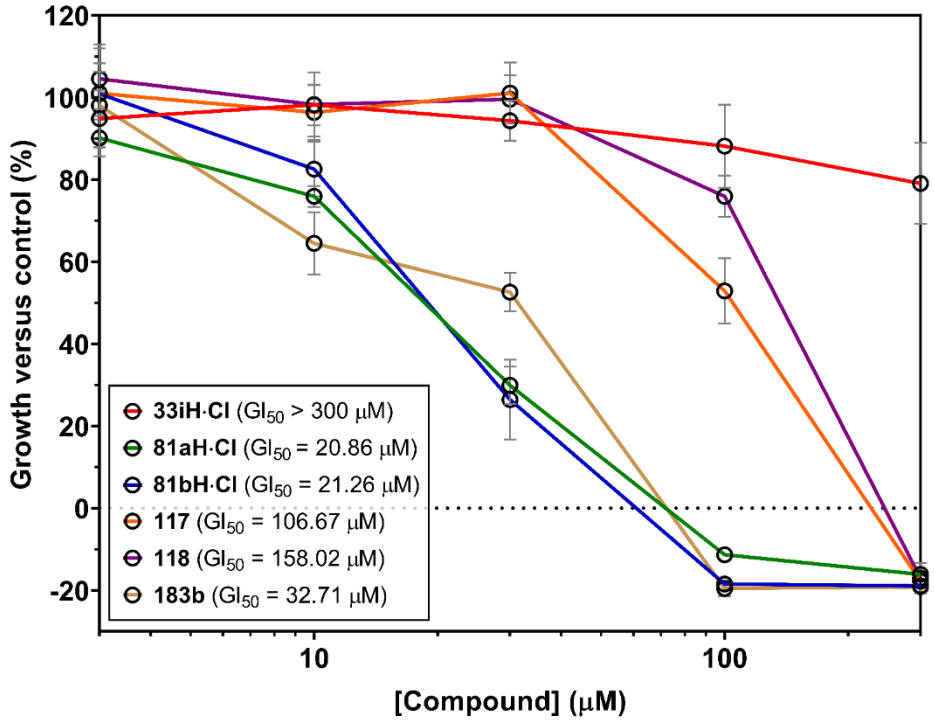


Figure S127 – Experiment 19, GB-1 cell line.

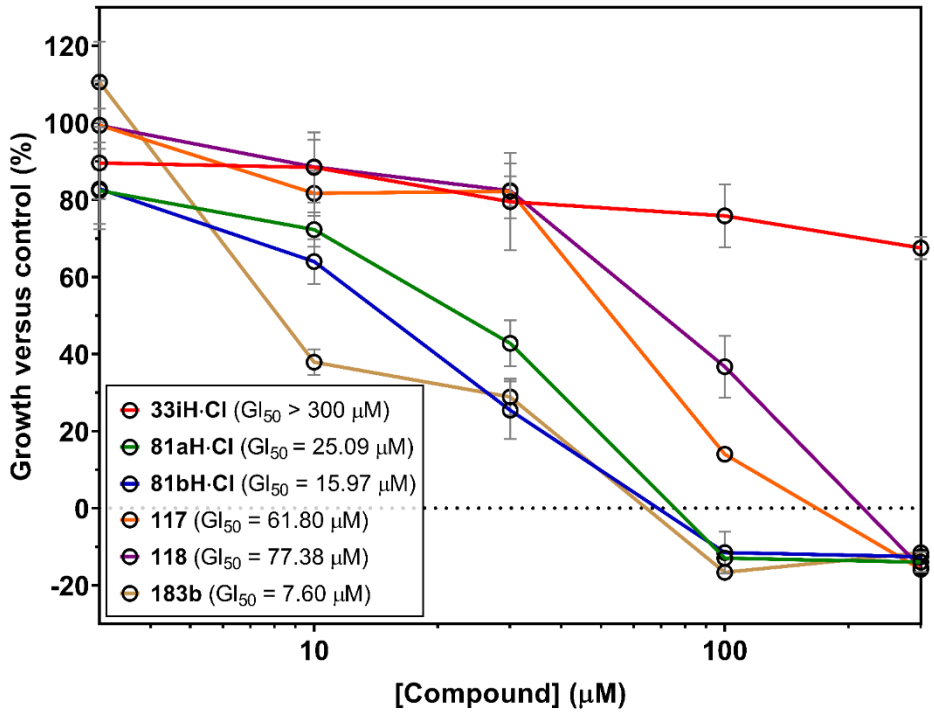


Figure S128 – Experiment 19, MCF-7 cell line.

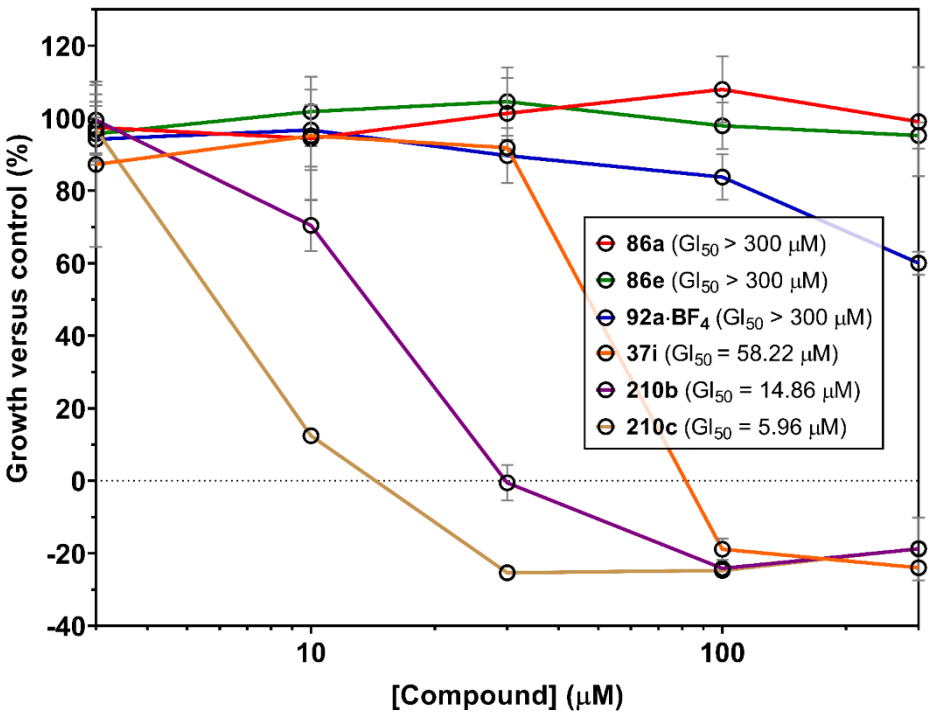


Figure S129 – Experiment 20, GB-1 cell line.

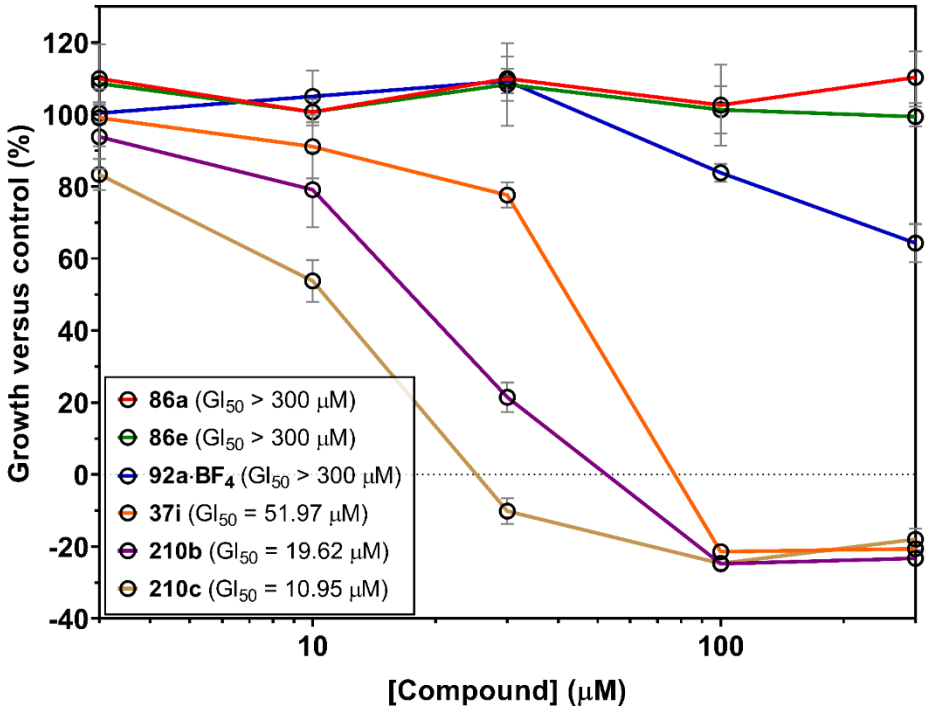


Figure S130 – Experiment 20, MCF-7 cell line.

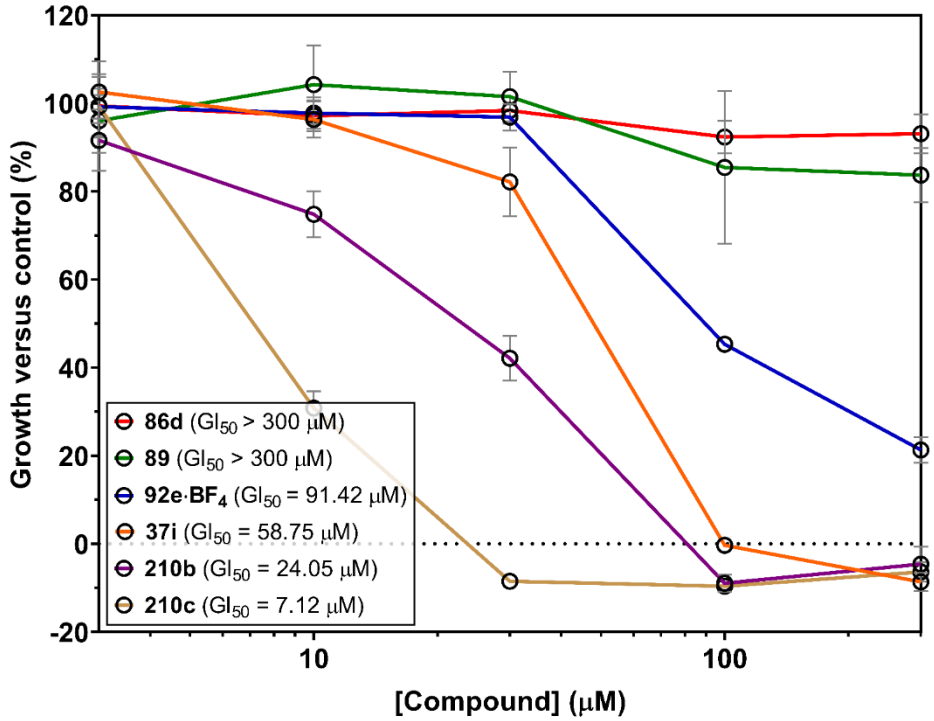


Figure S131 – Experiment 21, GB-1 cell line.

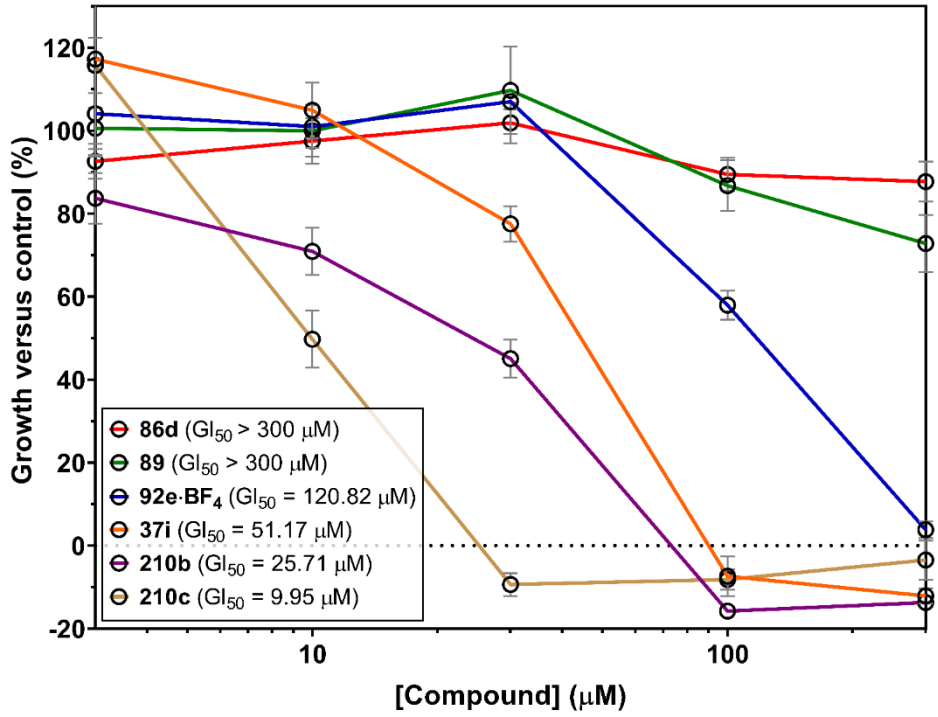


Figure S132 – Experiment 21, MCF-7 cell line.

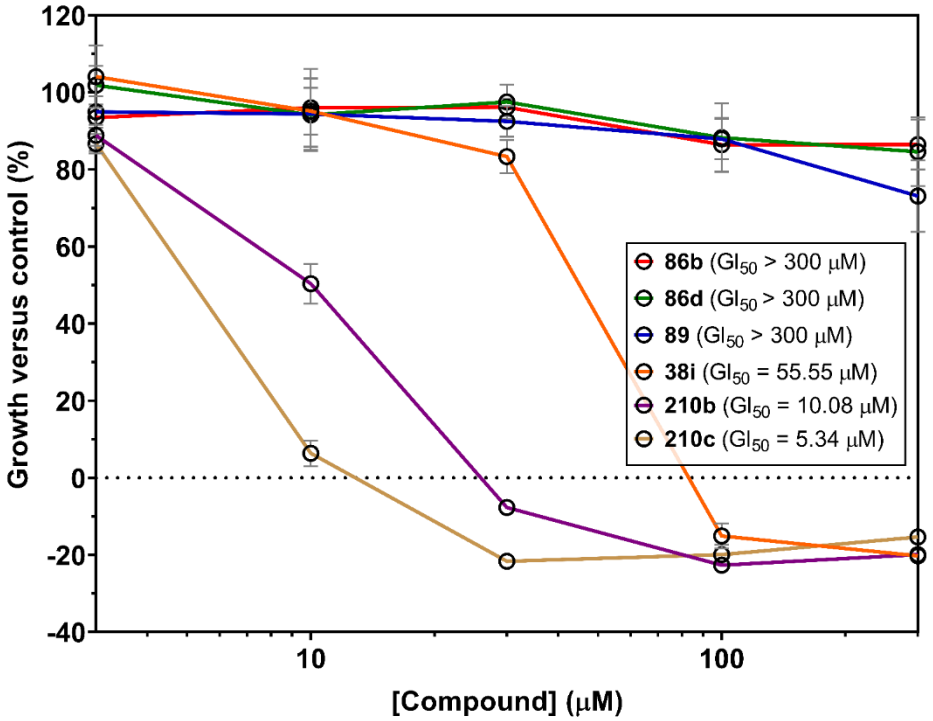


Figure S133 – Experiment 22, GB-1 cell line.

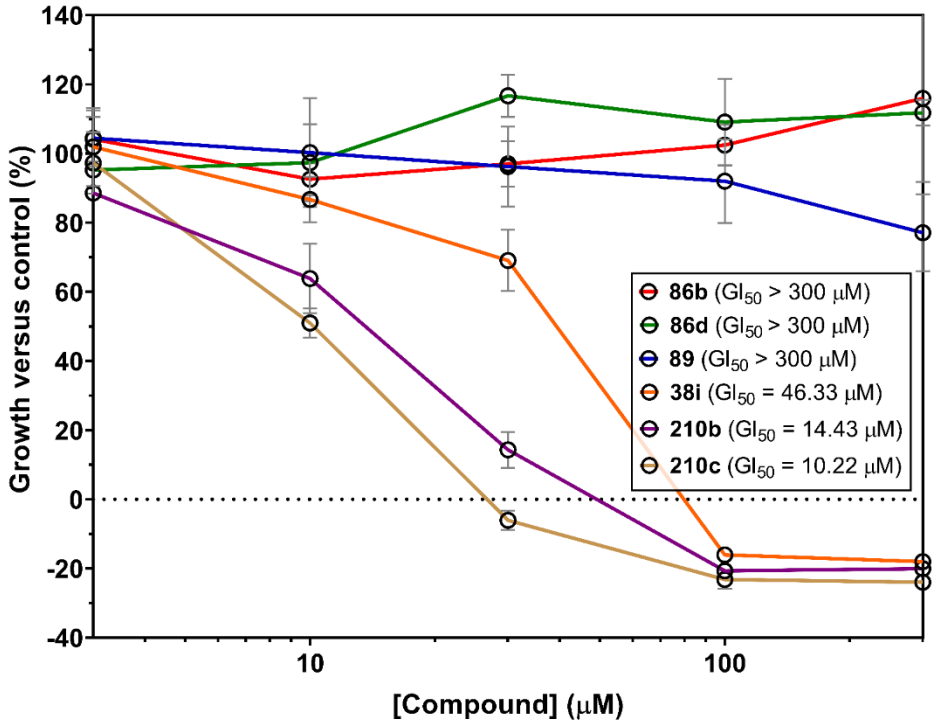


Figure S134 – Experiment 22, MCF-7 cell line.

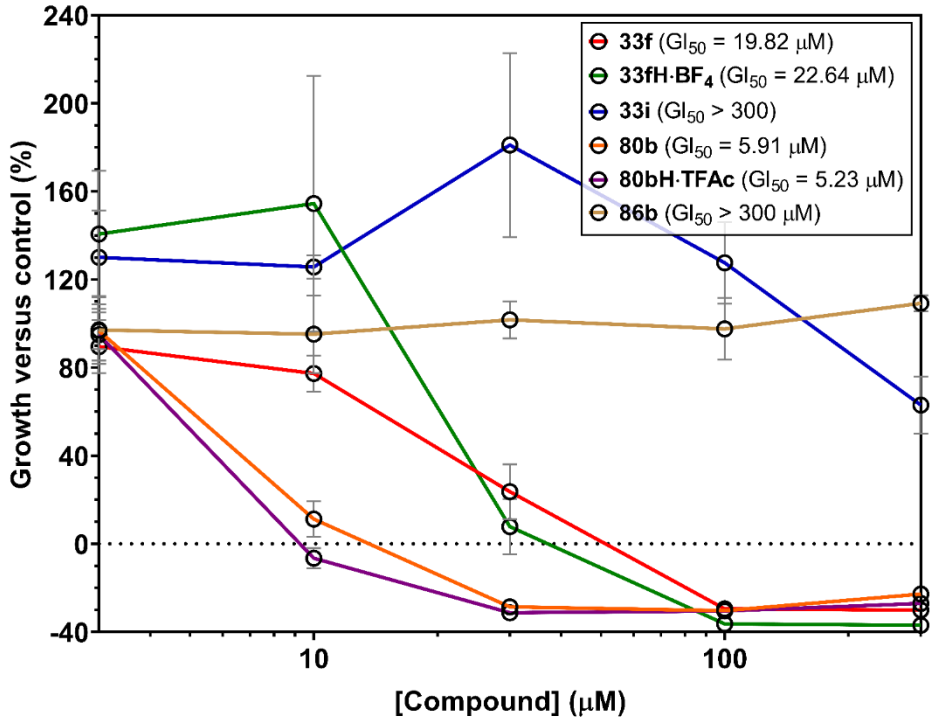


Figure S135 – Experiment 23, GB-1 cell line.

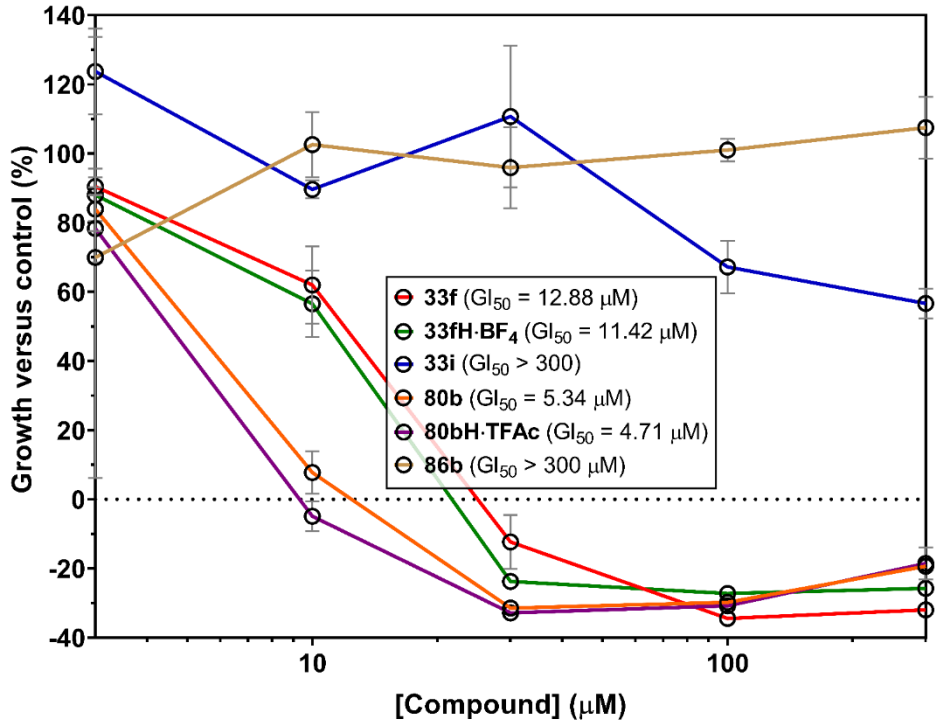


Figure S136 – Experiment 23, MCF-7 cell line.

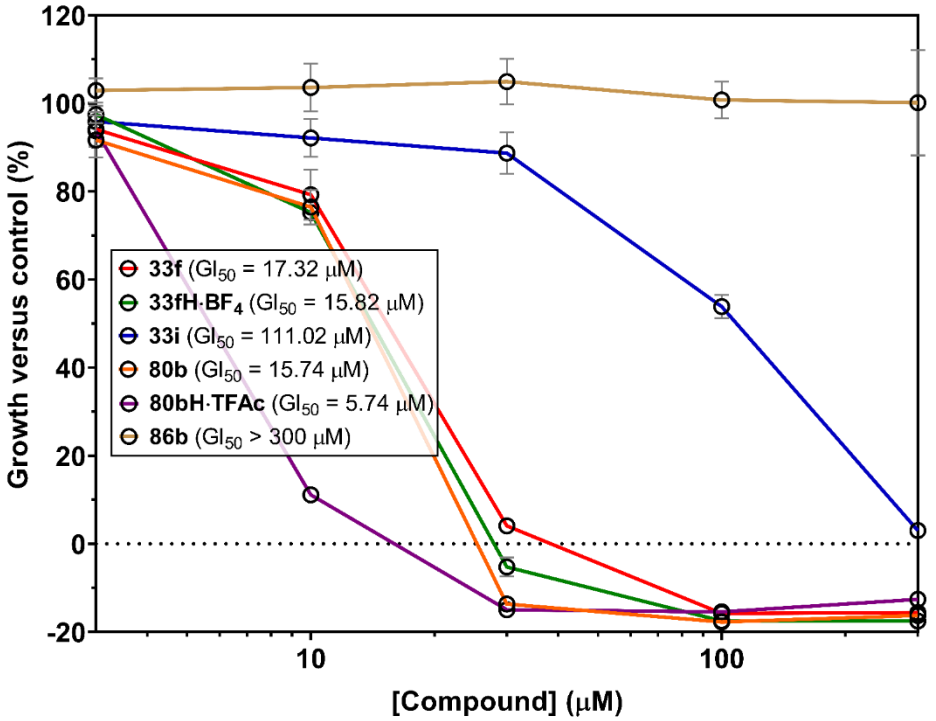


Figure S137 – Experiment 24, GB-1 cell line.

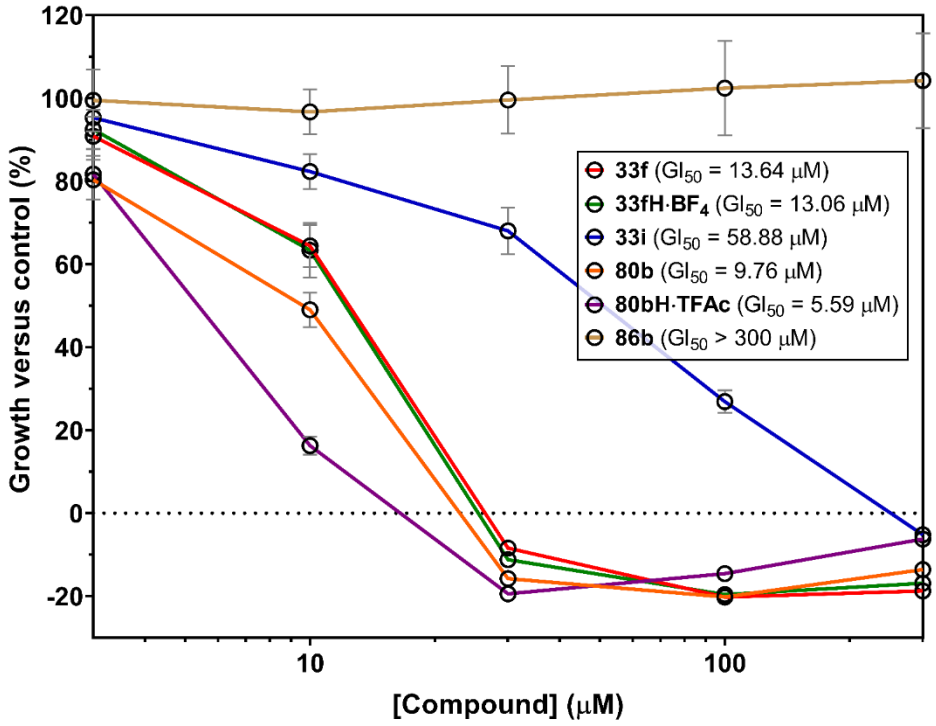


Figure S138 – Experiment 24, MCF-7 cell line.

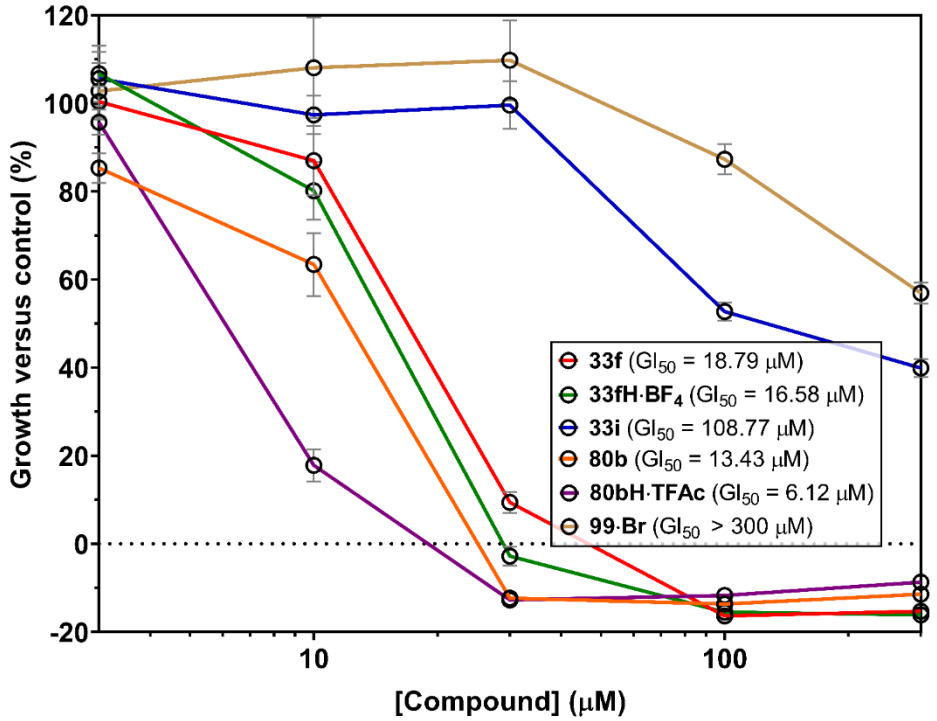


Figure S139 – Experiment 25, GB-1 cell line.

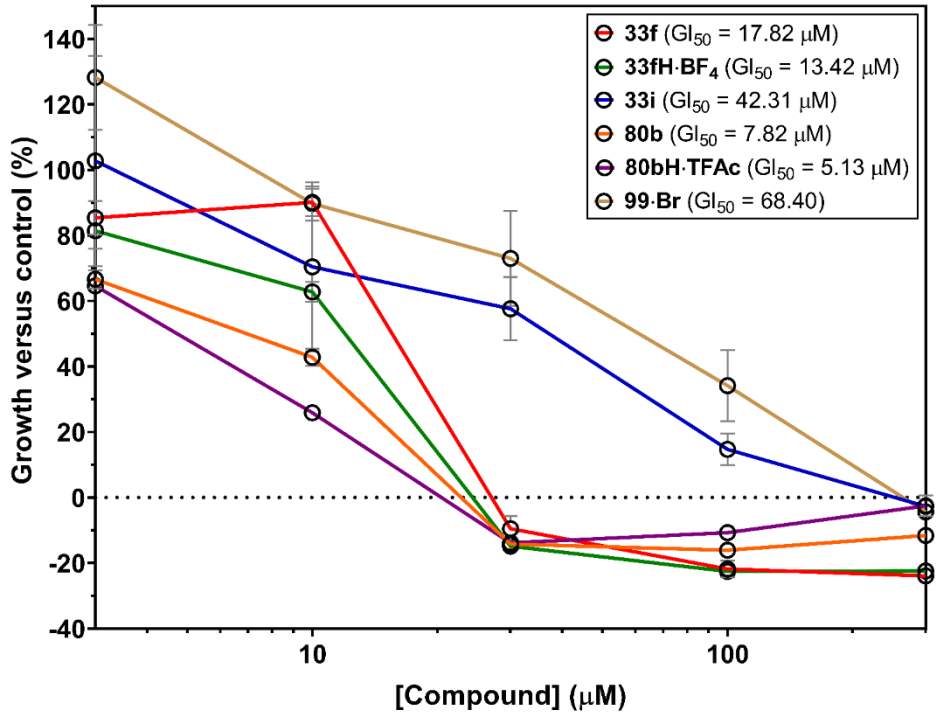


Figure S140 – Experiment 25, MCF-7 cell line.

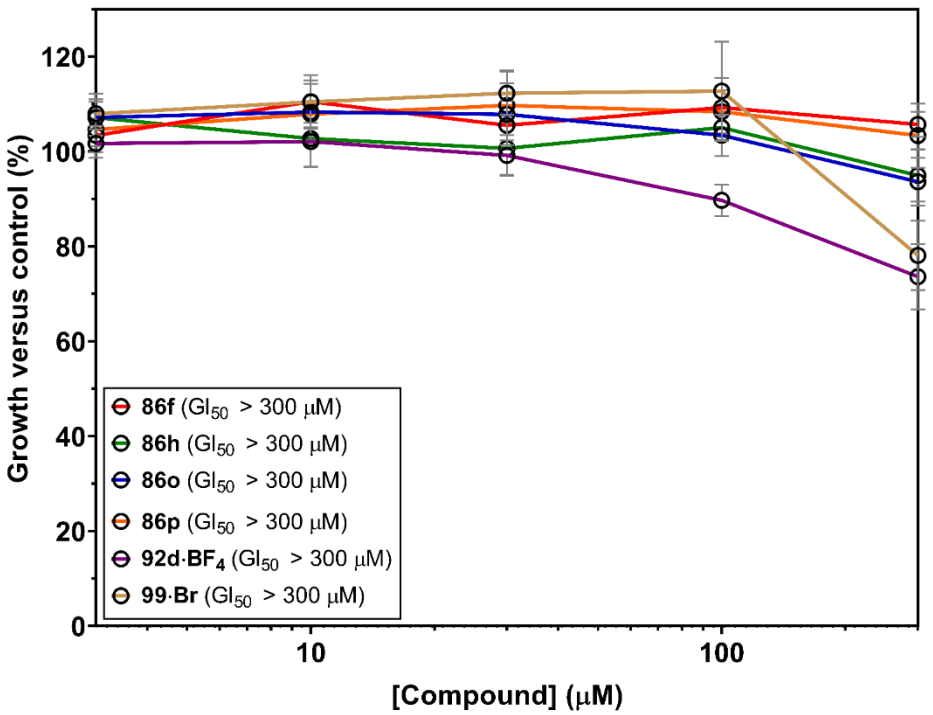


Figure S141 – Experiment 26, GB-1 cell line.

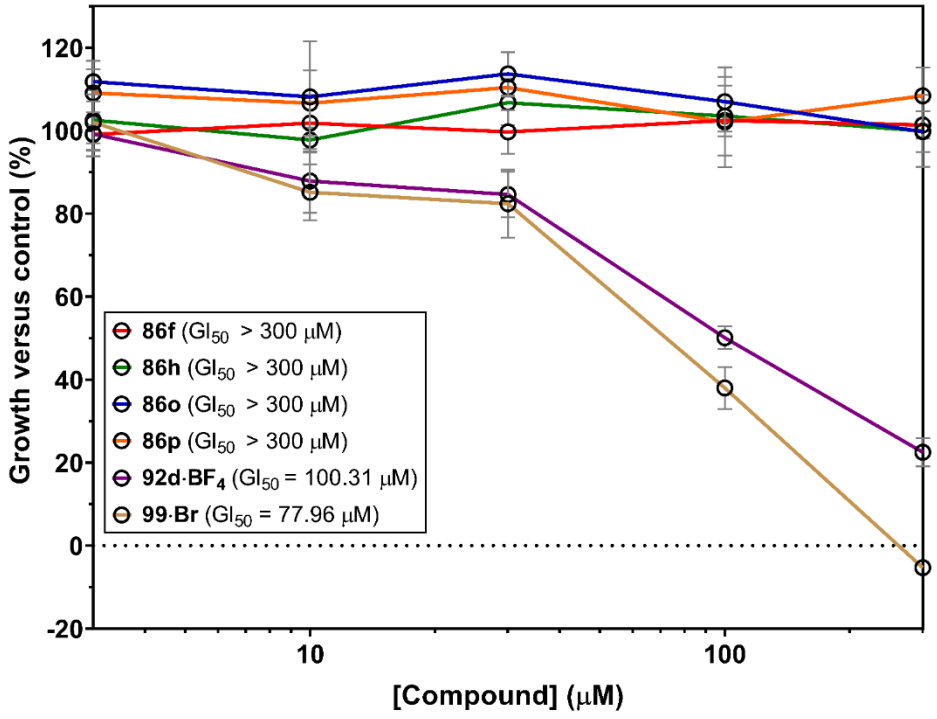


Figure S142 – Experiment 26, MCF-7 cell line.

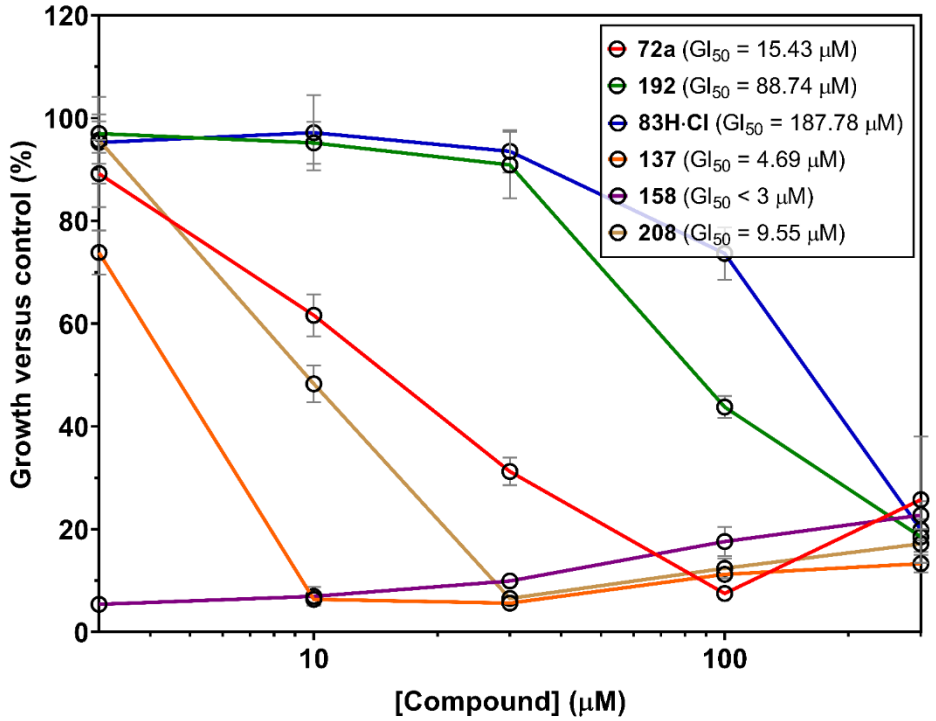


Figure S143 – Experiment 27, GB-1 cell line.

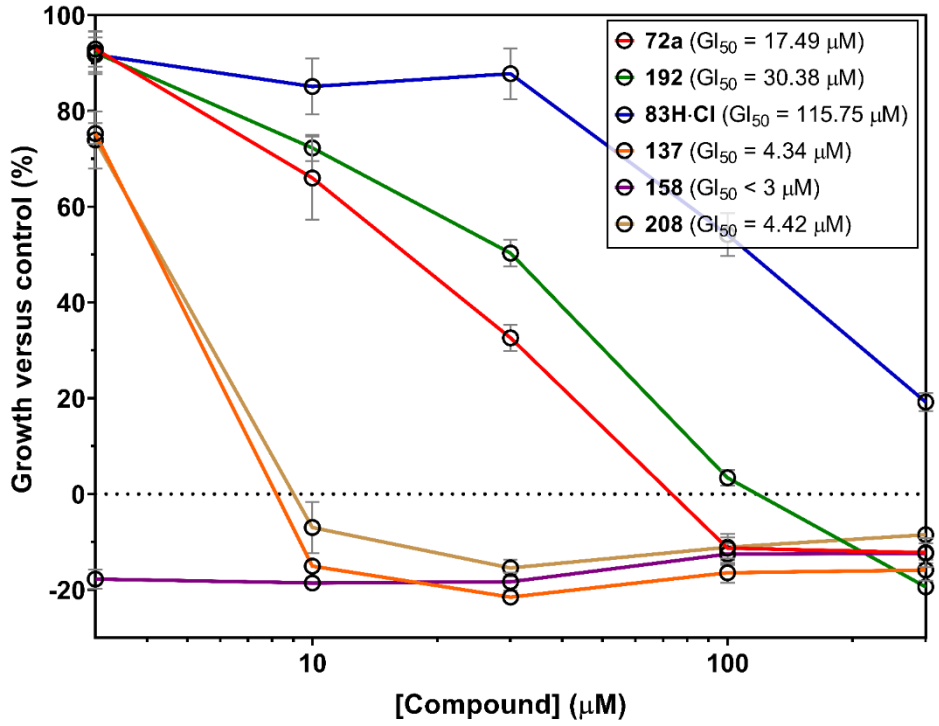


Figure S144 – Experiment 27, MCF-7 cell line.

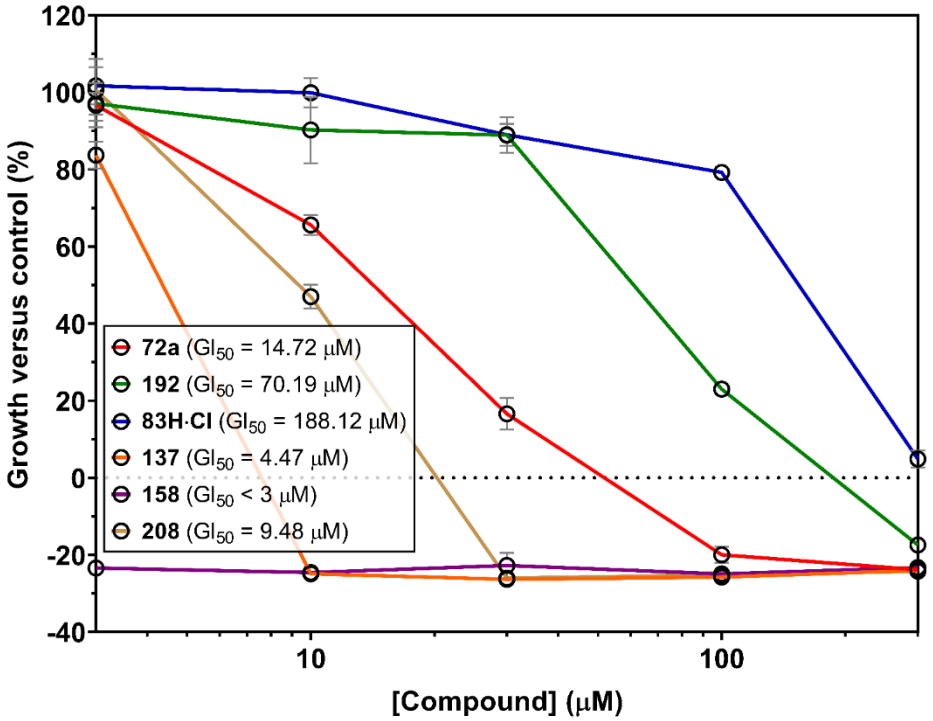


Figure S145 – Experiment 28, GB-1 cell line.

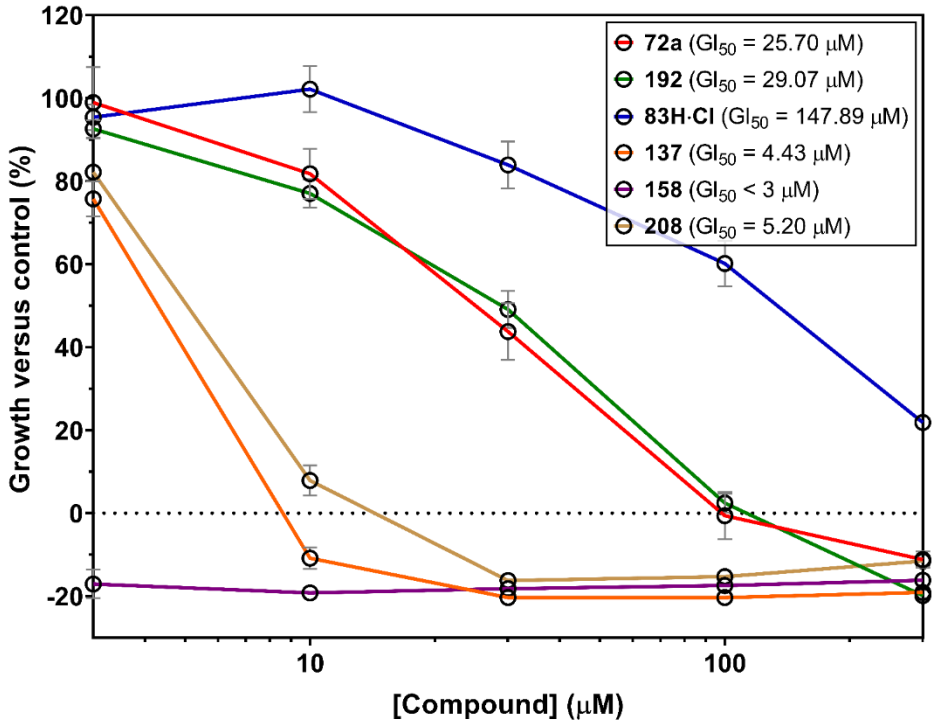


Figure S146 – Experiment 28, MCF-7 cell line.

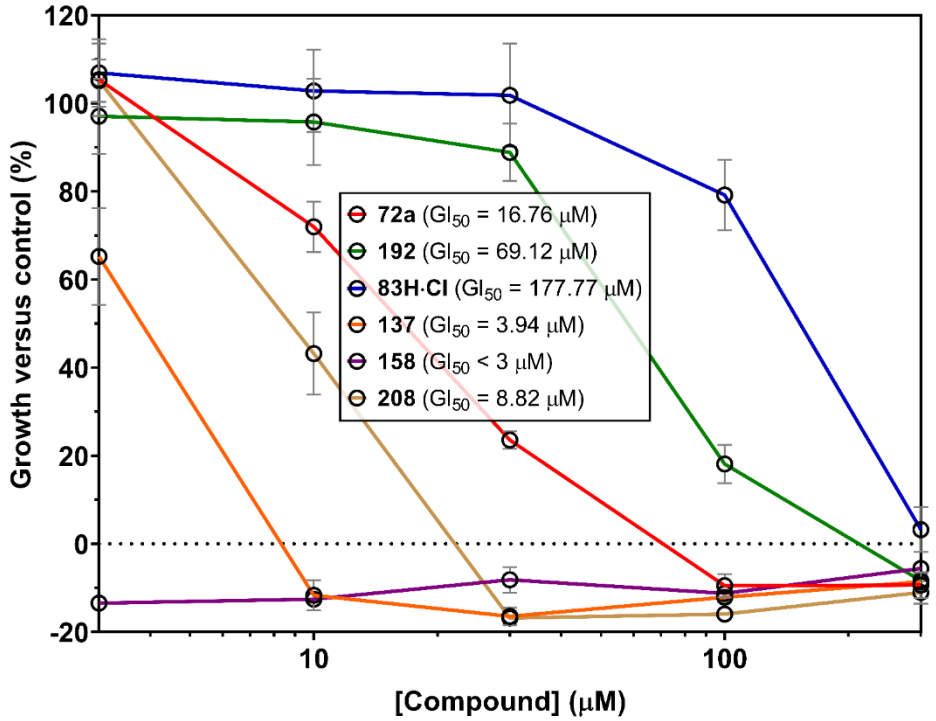


Figure S147 – Experiment 29, GB-1 cell line.

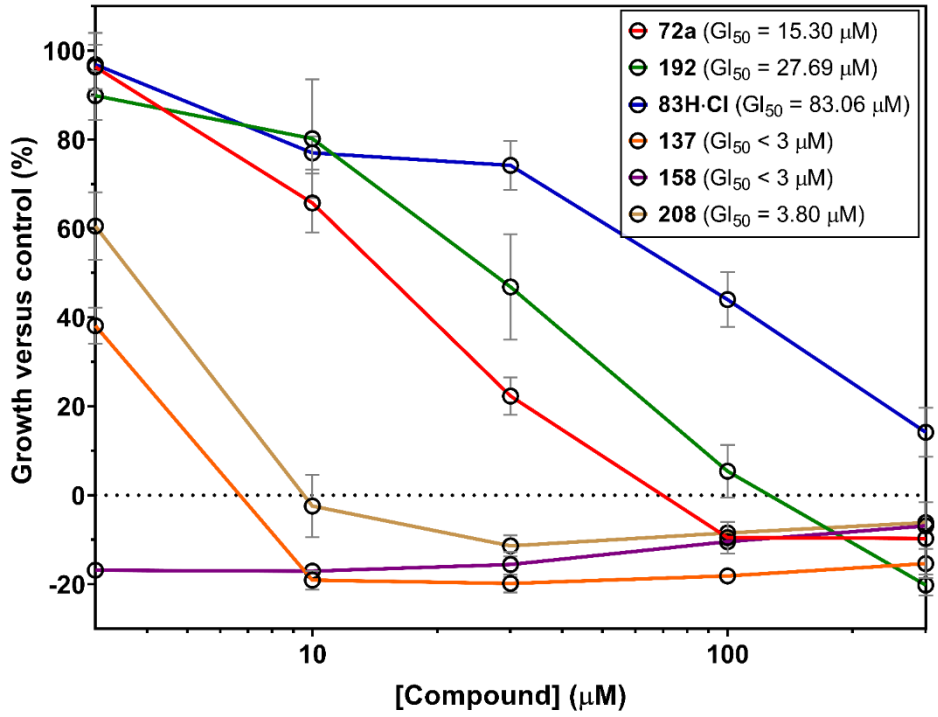


Figure S148 – Experiment 29, MCF-7 cell line.

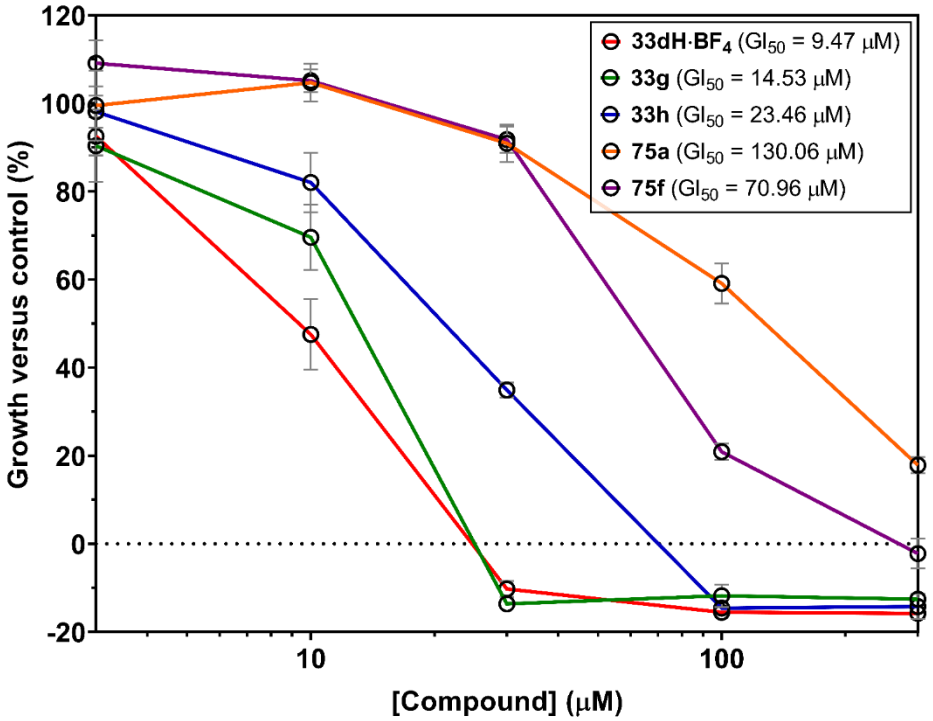


Figure S149 – Experiment 30, GB-1 cell line, high concentration.

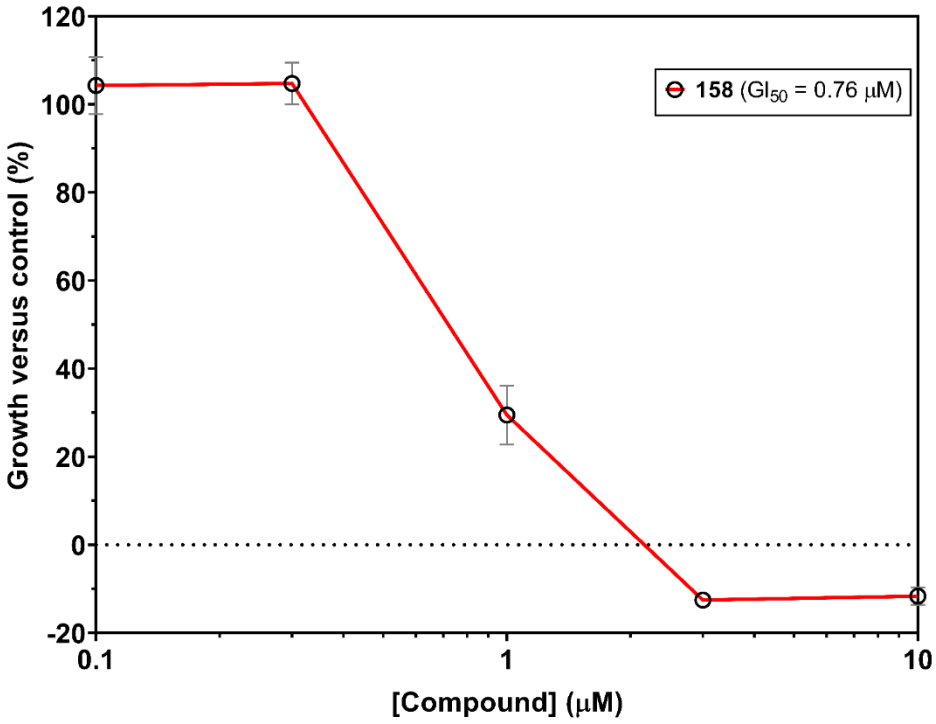


Figure S150 – Experiment 30, GB-1 cell line, low concentration.

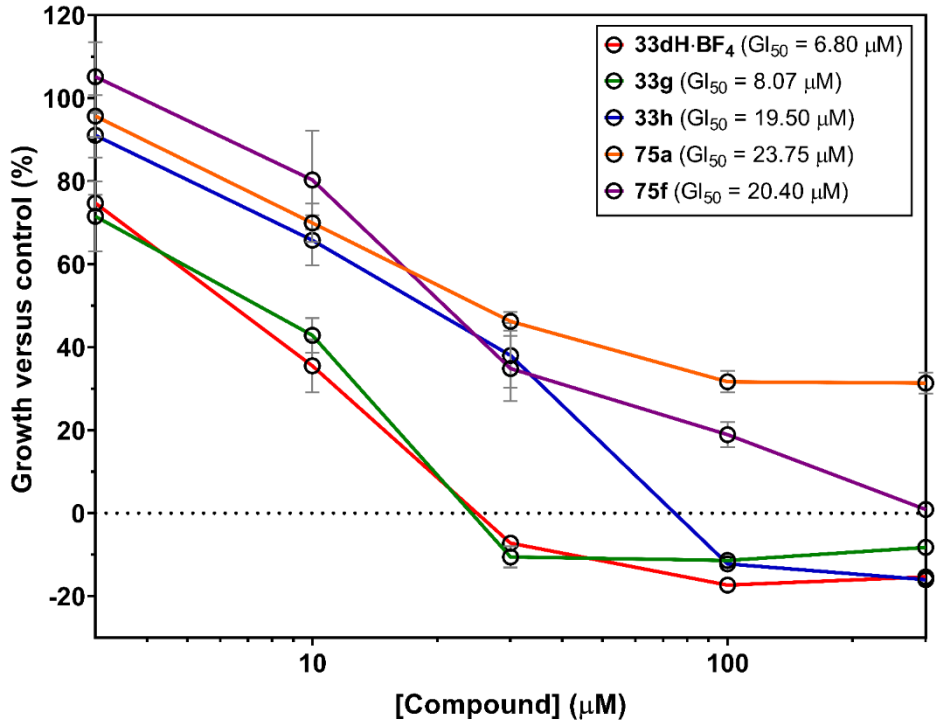


Figure S151 – Experiment 30, MCF-7 cell line, high concentration.

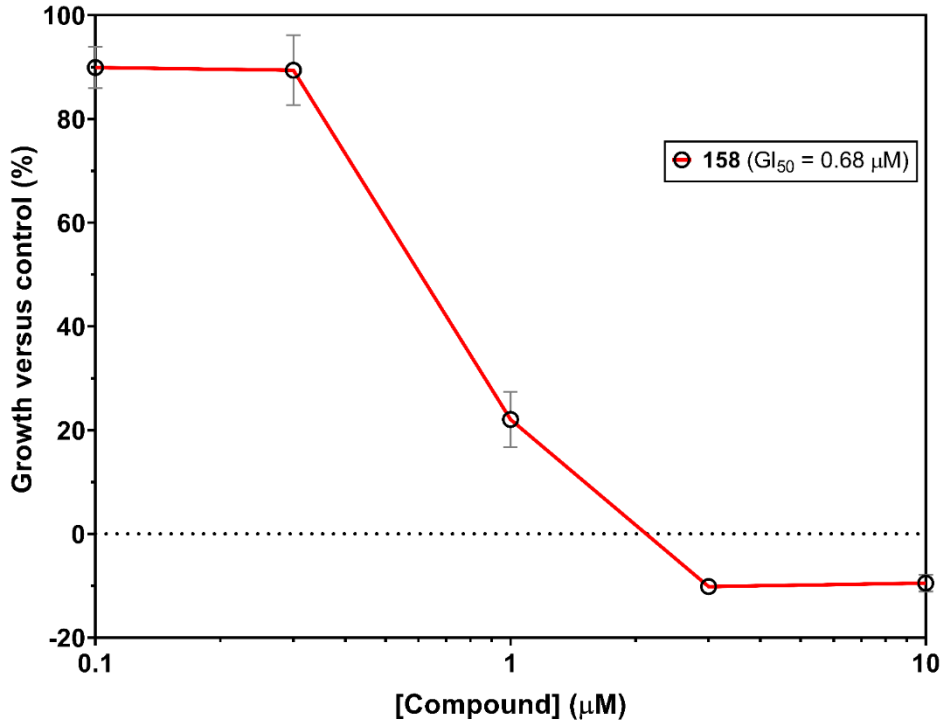


Figure S152 – Experiment 30, MCF-7 cell line, low concentration.

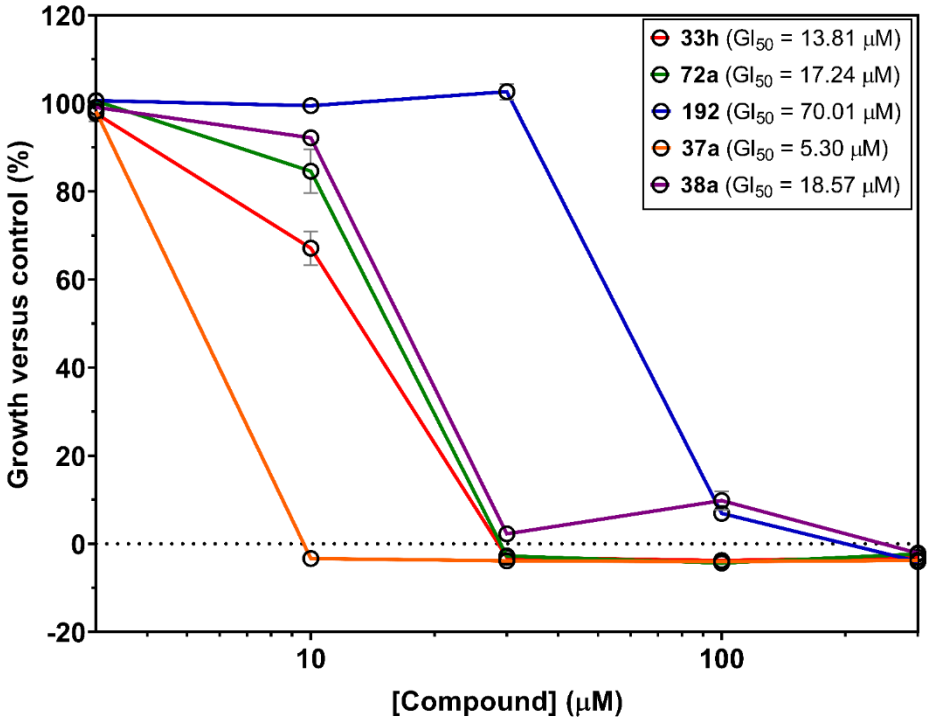


Figure S153 – Experiment 31, GB-1 cell line, high concentration.

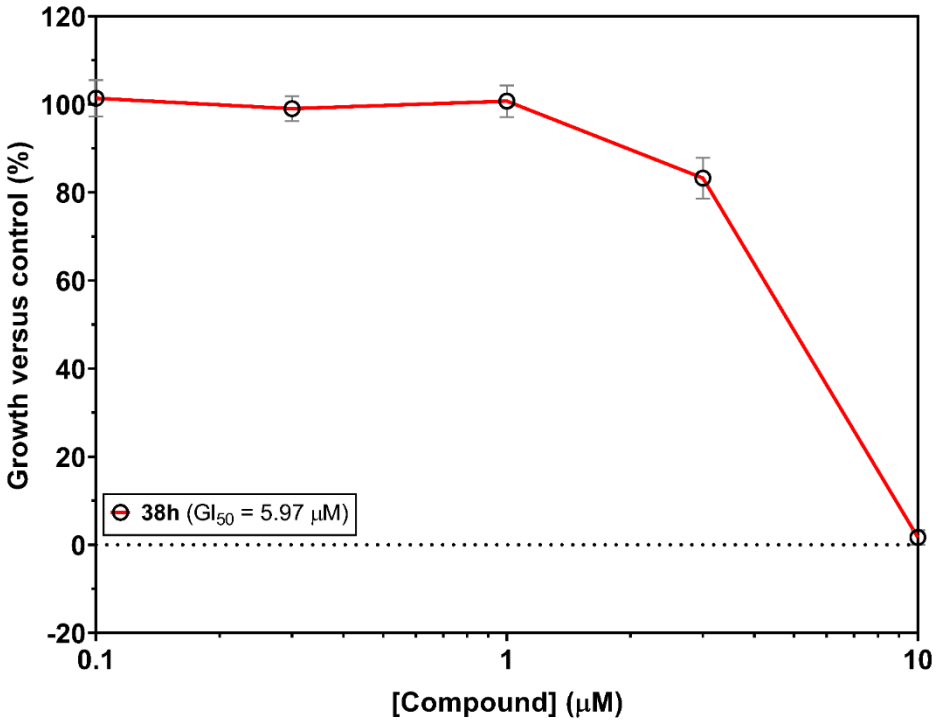


Figure S154 – Experiment 31, GB-1 cell line, low concentration.

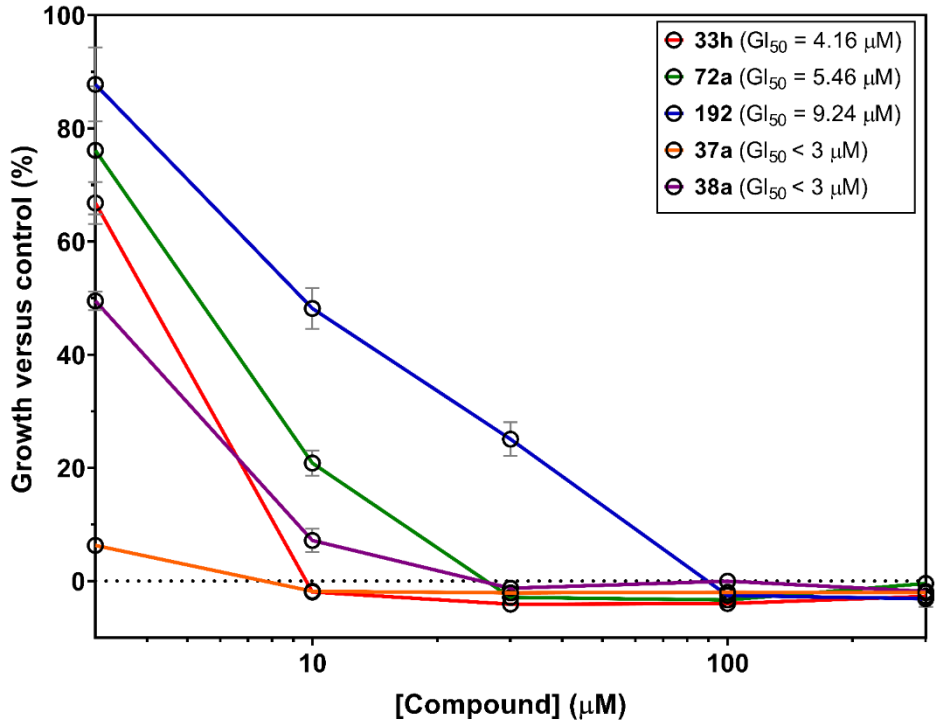


Figure S155 – Experiment 31, MCF-7 cell line, high concentration.

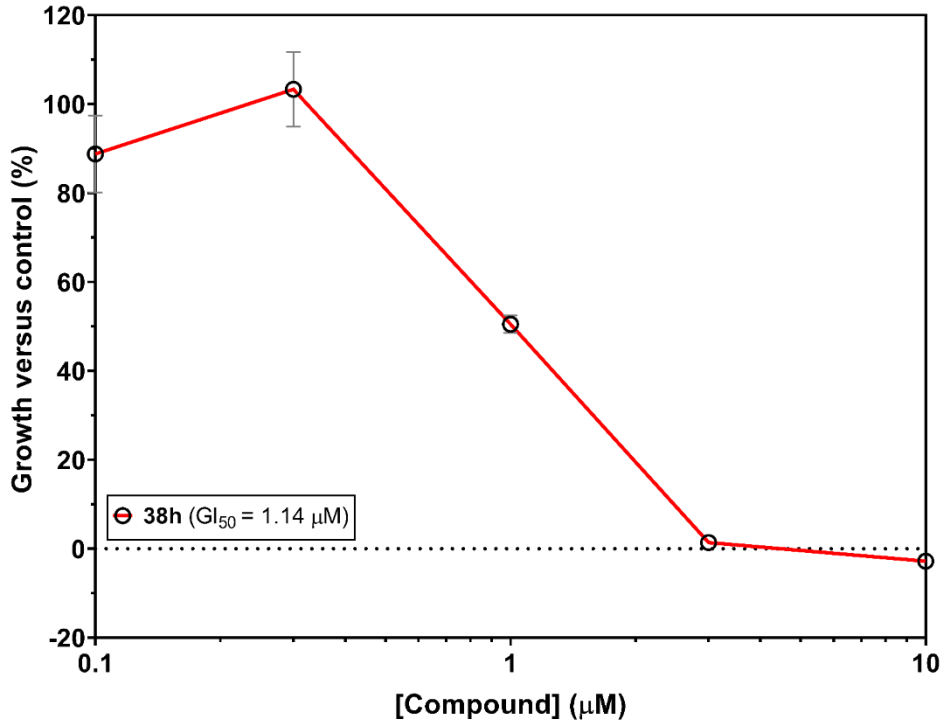


Figure S156 – Experiment 31, MCF-7 cell line, low concentration.

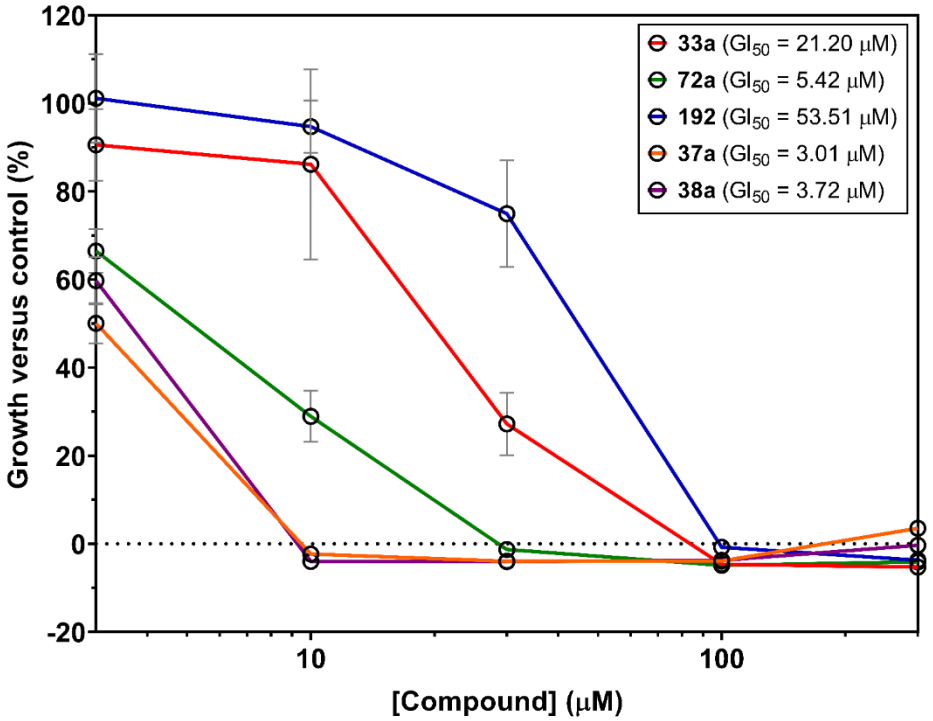


Figure S157 – Experiment 32, GB-1 cell line, high concentration.

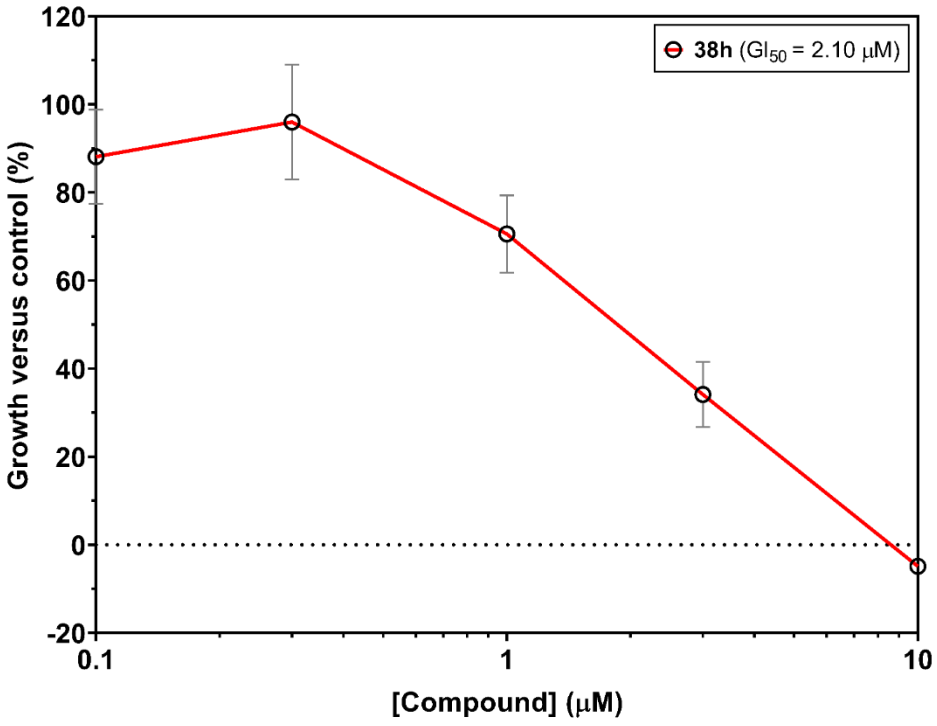


Figure S158 – Experiment 32, GB-1 cell line, low concentration.

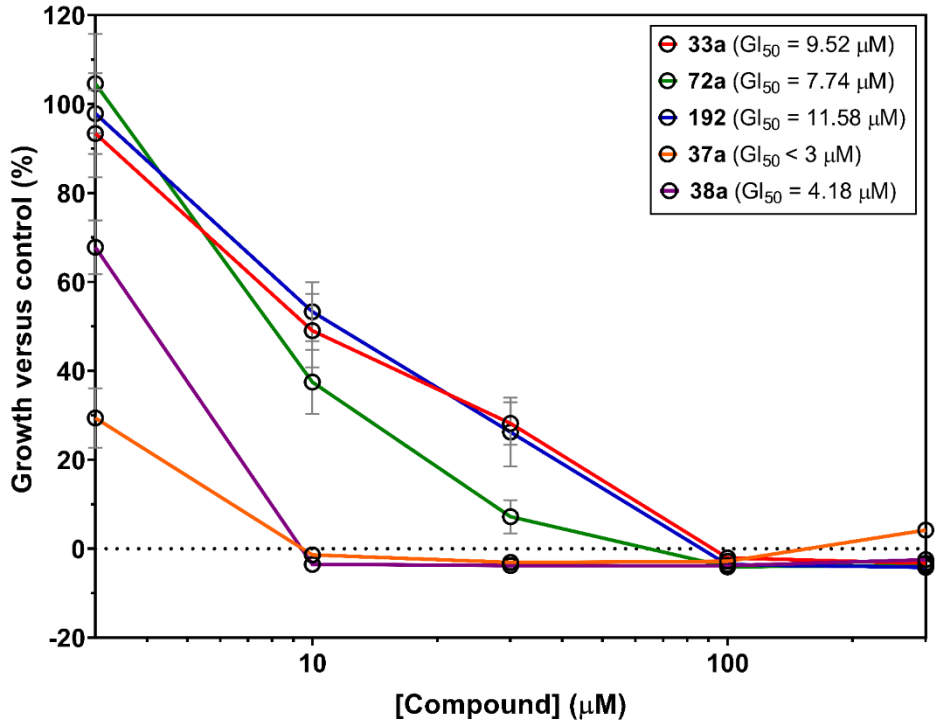


Figure S159 – Experiment 32, MCF-7 cell line, high concentration.

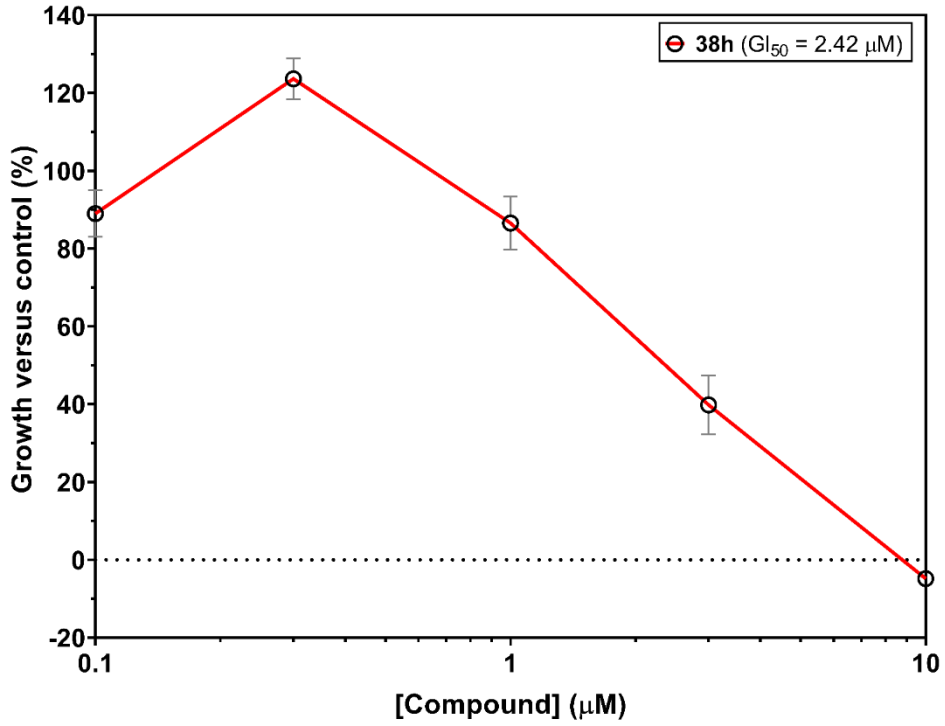


Figure S160 – Experiment 32, MCF-7 cell line, low concentration.

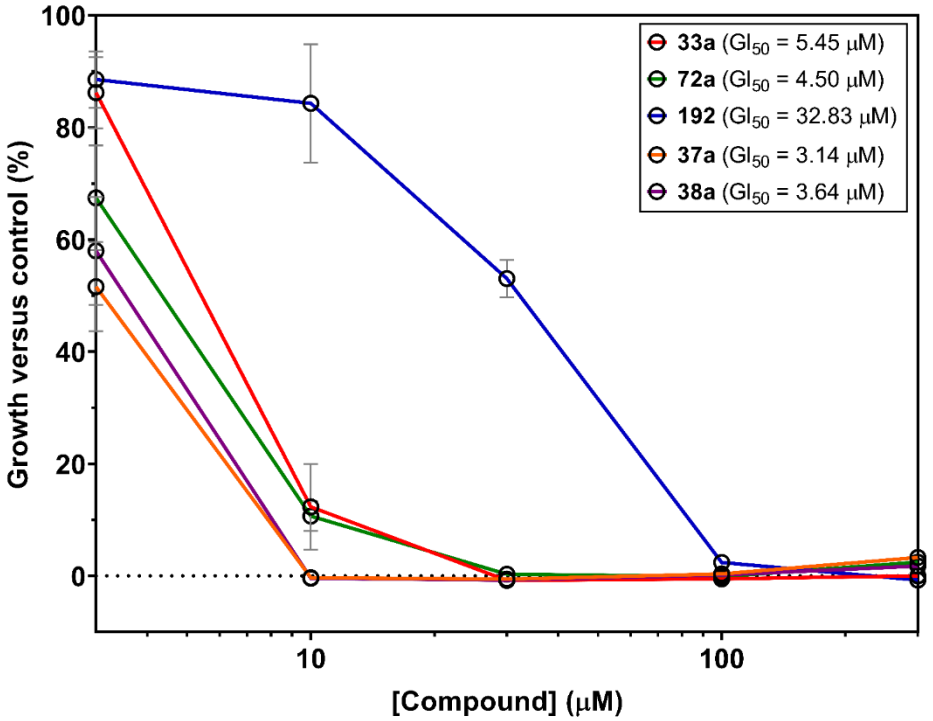


Figure S161 – Experiment 33, GB-1 cell line, high concentration.

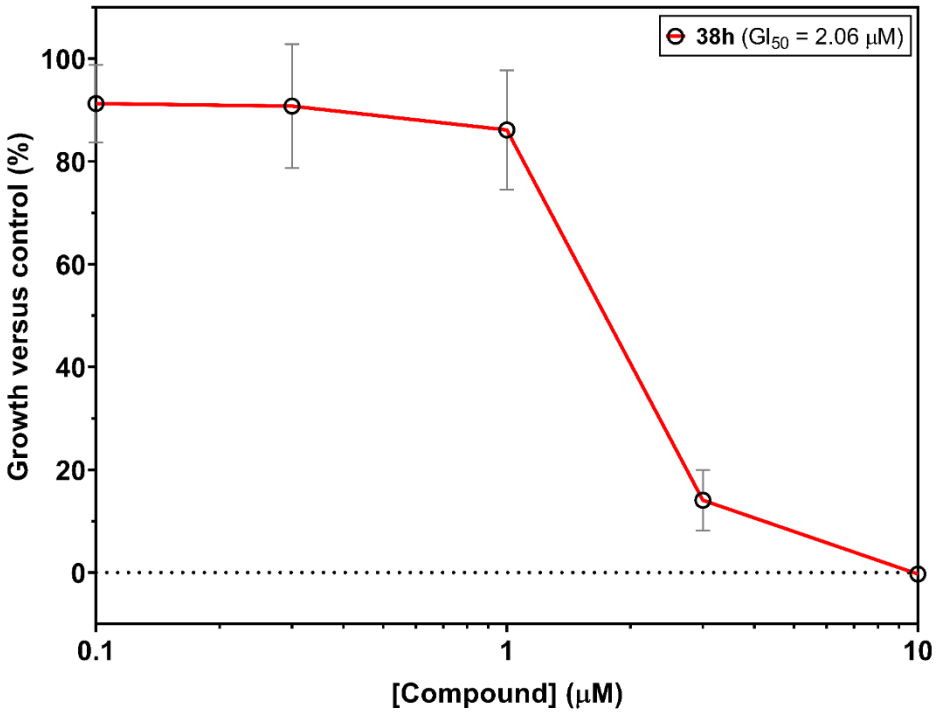


Figure S162 – Experiment 33, GB-1 cell line, low concentration.

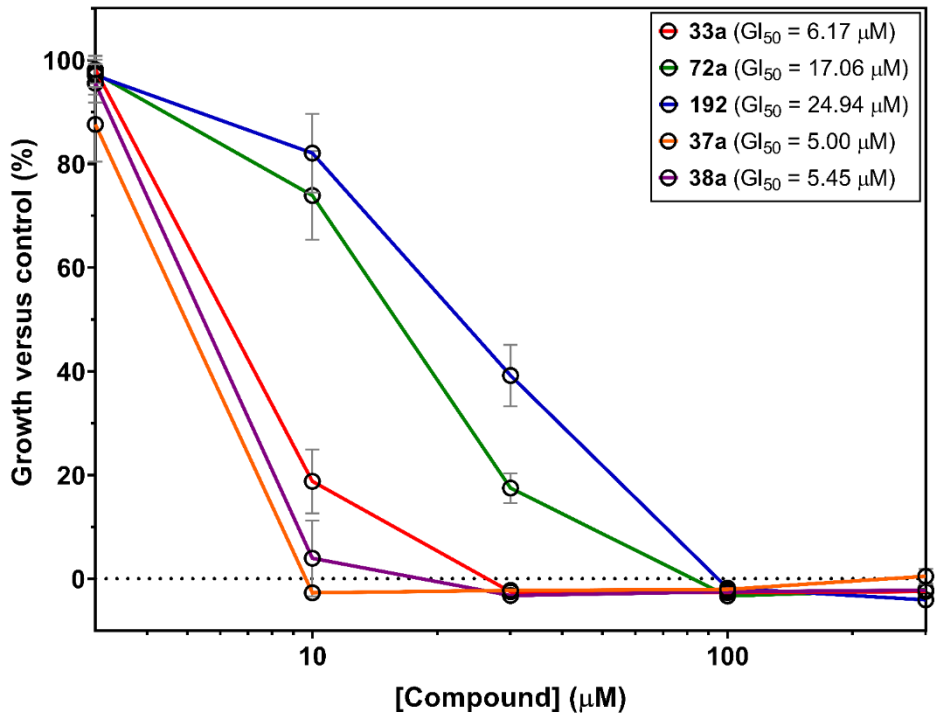


Figure S163 – Experiment 33, MCF-7 cell line, high concentration.

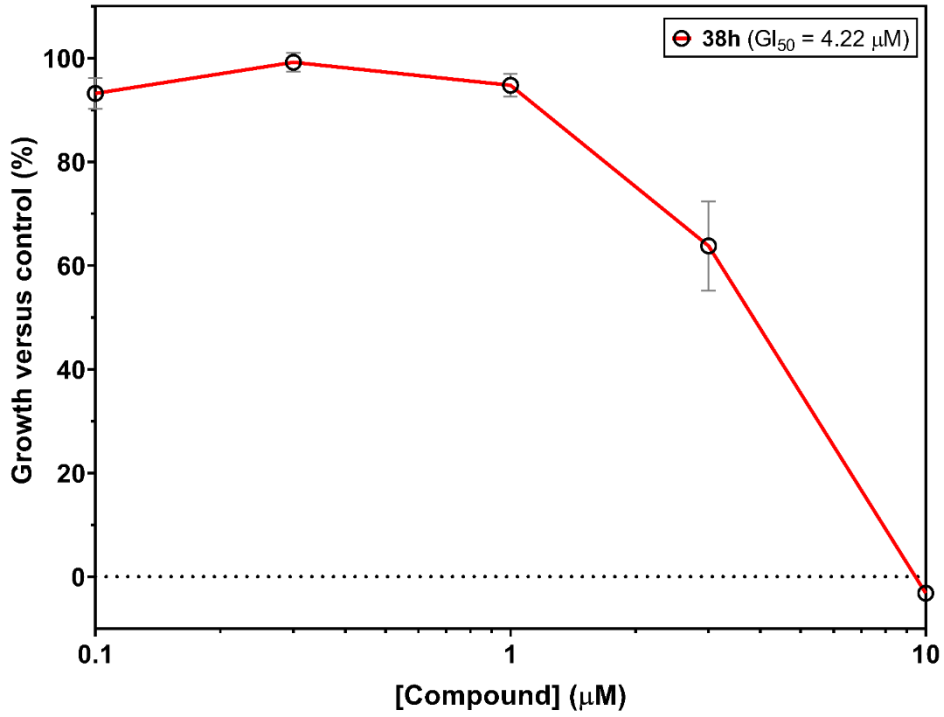


Figure S164 – Experiment 33, MCF-7 cell line, low concentration.

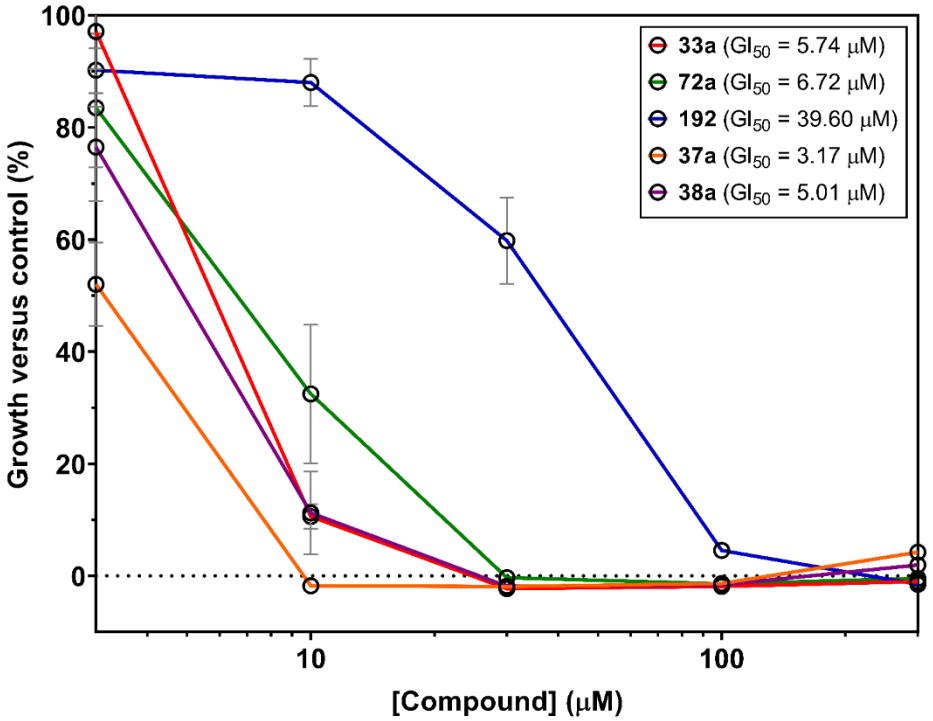


Figure S165 – Experiment 34, GB-1 cell line, high concentration.

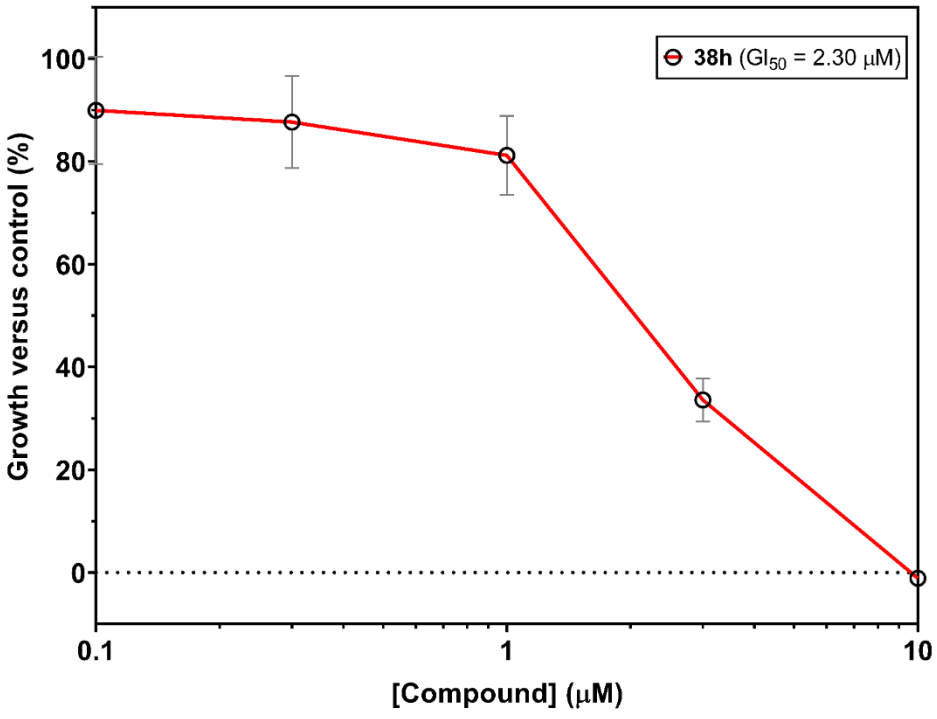


Figure S166 – Experiment 34, GB-1 cell line, low concentration.

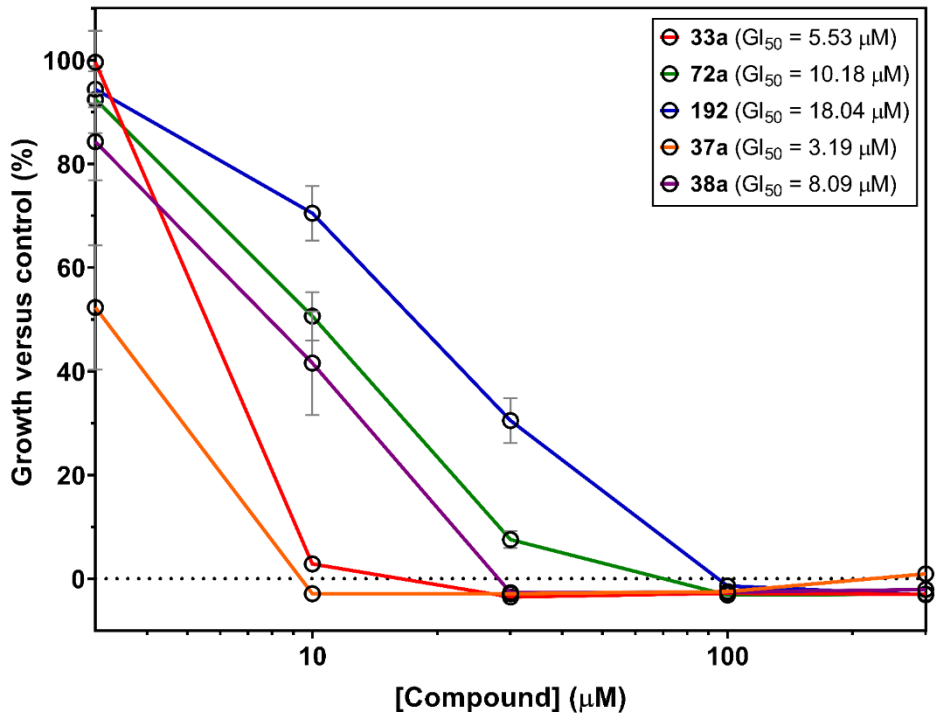


Figure S167 – Experiment 34, MCF-7 cell line, high concentration.

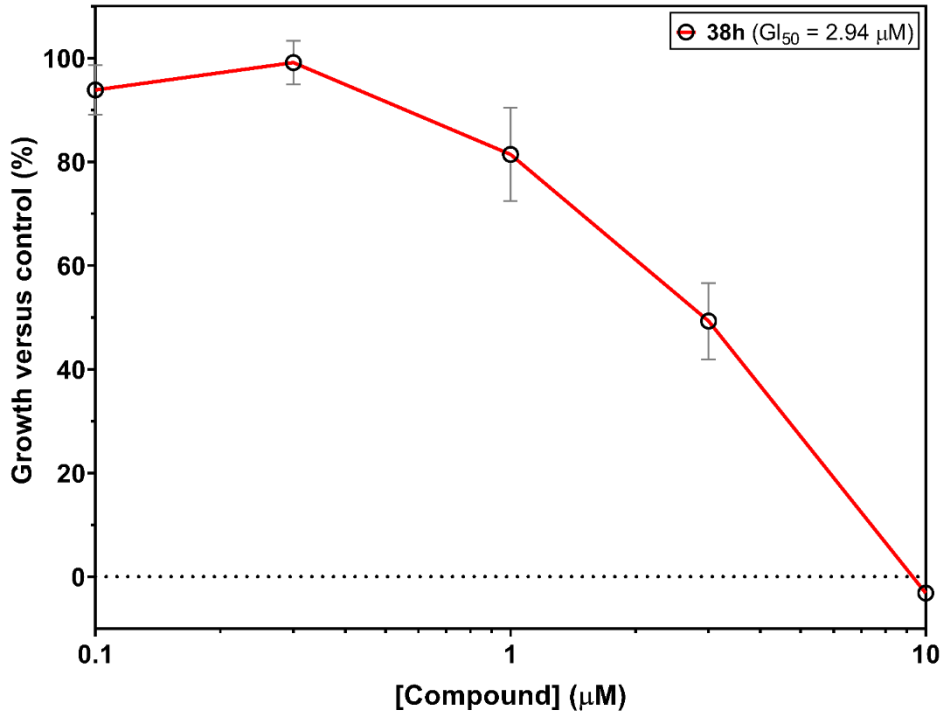


Figure S168 – Experiment 34, MCF-7 cell line, low concentration.

Bibliography

1. M. Gomberg, *Ber. Dtsch. Chem. Ges.*, 1900, **33**, 3150-3163.
2. Z. X. Chen, Y. Li and F. Huang, *Chem*, 2021, **7**, 288-332.
3. L. Ji, J. Shi, J. Wei, T. Yu and W. Huang, *Adv. Mater.*, 2020, **32**, 1908015.
4. I. Ratera and J. Veciana, *Chem. Soc. Rev.*, 2012, **41**, 303-349.
5. B. Tang, J. Zhao, J. F. Xu and X. Zhang, *Chem. Sci*, 2020, **11**, 1192-1204.
6. T. H. Colle, P. S. Glaspie and E. S. Lewis, *J. Org. Chem*, 1978, **43**, 2722-2725.
7. I. Ratera, J. Vidal-Gancedo, D. Maspoch, S. T. Bromley, N. Crivillers and M. Mas-Torrent, *J. Mater. Chem. C*, 2021, **9**, 10610-10623.
8. *United States Pat.,* 5530140, 1996.
9. *International Pat.,* WO 97/09633, 1997.
10. *United States Pat.,* 5728370, 1998.
11. *International Pat.,* WO 98/39277, 1998.
12. U. Sanzhaeva, M. Poncelet, O. Tseytlin, M. Tseytlin, M. Gencheva, T. D. Eubank, V. V. Khramtsov and B. Driesschaert, *J. Org. Chem*, 2020, **85**, 10388-10398.
13. X. Tan, L. Chen, Y. Song, A. Rockenbauer, F. A. Villamena, J. L. Zweier and Y. Liu, *Chem. Res. Toxicol.*, 2017, **30**, 1664-1672.
14. H. G. Viehe, Z. Janousek, R. Merenyi and L. Stella, *Acc. Chem. Res.*, 1985, **18**, 148-154.
15. J. P. Peterson and A. H. Winter, *J. Am. Chem. Soc.*, 2019, **141**, 12901-12906.
16. D. Griller and K. U. Ingold, *Acc. Chem. Res.*, 1976, **9**, 13-19.
17. J. Hioe, D. Šakić, V. Vrček and H. Zipse, *Org. Biomol. Chem*, 2015, **13**, 157-169.
18. J. Hioe and H. Zipse, *Org. Biomol. Chem*, 2010, **8**, 3609-3617.
19. A. A. Zavitsas, *J. Chem. Educ.*, 2001, **78**, 417.
20. H. Douroudgari, M. Vahedpour and F. Khouini, *Sci. Rep*, 2021, **11**, 13220.
21. F. Rastrelli and A. Bagno, *Chem. Eur. J*, 2009, **15**, 7990-8004.
22. A. J. Pell, G. Pintacuda and C. P. Grey, *Prog. Nucl. Magn. Reson. Spectrosc.*, 2019, **111**, 1-271.
23. M. M. Roessler and E. Salvadori, *Chem. Soc. Rev.*, 2018, **47**, 2534-2553.
24. D. Matuschek, S. Eusterwiemann, L. Stegemann, C. Doerenkamp, B. Wibbeling, C. G. Daniliuc, N. L. Doltsinis, C. A. Strassert, H. Eckert and A. Studer, *Chem. Sci*, 2015, **6**, 4712-4716.
25. V. Chechik, E. Carter and D. Murphy, *Electron Paramagnetic Resonance*, Oxford University Press, Oxford, United Kingdom, 2016.
26. N. m. Elgrishi, K. J. Rountree, B. D. Mccarthy, E. S. Rountree, T. T. Eisenhart and J. L. Dempsey, *J. Chem. Educ.*, 2017, DOI: 10.1021/acs.jchemed.7b00361.
27. P. Puthongkham and B. J. Venton, *Analyst*, 2020, **145**, 1087-1102.
28. P. A. Southorn and G. Powis, *Mayo Clin. Proc*, 1988, **63**, 381-389.
29. J. Stubbe and D. G. Nocera, *J. Am. Chem. Soc.*, 2021, **143**, 13463-13472.
30. P. A. Southorn and G. Powis, *Mayo Clin. Proc*, 1988, **63**, 390-408.
31. M. A. Marletta, *Biochem.*, 2021, **60**, 3491-3496.
32. B. M. Sjöberg, P. Reichard, A. Gräslund and A. Ehrenberg, *J. Biol. Chem.*, 1978, **253**, 6863-6865.
33. S. S. Shinde, A. Maroz, M. P. Hay, A. V. Patterson, W. A. Denny and R. F. Anderson, *J. Am. Chem. Soc.*, 2010, **132**, 2591-2599.
34. C. M. Gooley, H. Keyzer and F. Setchell, *Nature*, 1969, **223**, 80-81.
35. L. H. Piette and I. S. Forrest, *Biochim. Biophys. Acta*, 1962, **57**, 419-420.
36. L. H. Piette, G. Bulow and I. Yamazaki, *Biochim. Biophys. Acta, Spec. Sect. Biophys. Subj.*, 1964, **88**, 120-129.
37. O. Yoshio and H. M. Mehendale, *Biochem. Pharmacol.*, 1982, **31**, 157-162.
38. F. C. Peter and W. W. Westerfeld, *J. Pharmacol. Exp. Ther.*, 1967, **157**, 446.
39. R. Knoll, W. Christ, B. Müller-Oerlinghausen and H. Coper, *Naunyn-Schmiedeberg's Arch. Pharmacol.*, 1977, **297**, 195-200.
40. D. Bourissou, O. Guerret, F. P. Gabbaï and G. Bertrand, *Chem. Rev.*, 2000, **100**, 39-92.
41. R. Gleiter and R. Hoffmann, *J. Am. Chem. Soc.*, 1968, **90**, 5457-5460.
42. L. Pauling, *J. Chem. Soc., Chem. Commun.*, 1980, DOI: 10.1039/C39800000688, 688-689.
43. J. B. Dumas and E. Péligot, *Ann. Chim. Phys*, 1835, **58**.

44. A. J. Arduengo and G. Bertrand, *Chem. Rev.*, 2009, **109**, 3209-3210.
45. A. Geuther, *Justus Liebigs Ann. Chem.*, 1862, **123**, 113-121.
46. A. J. Arduengo III and R. Krafczyk, *Chem. unserer Zeit*, 1998, **32**, 6-14.
47. W. von E. Doering and A. K. Hoffmann, *J. Am. Chem. Soc.*, 1954, **76**, 6162-6165.
48. H. E. Zimmerman and D. H. Paskovich, *J. Am. Chem. Soc.*, 1964, **86**, 2149-2160.
49. H. Tomioka, E. Iwamoto, H. Itakura and K. Hirai, *Nature*, 2001, **412**, 626-628.
50. T. Nakajo, J. Kumagai, S. Kusaka, A. Hori, Y. Hijikata, J. Pirillo, Y. Ma and R. Matsuda, *J. Am. Chem. Soc.*, 2021, **143**, 8129-8136.
51. H.-W. Wanzlick, *Angew. Chem. Int. Ed.*, 1962, **1**, 75-80.
52. H.-W. Wanzlick and H.-J. Kleiner, *Angew. Chem.*, 1961, **73**, 493.
53. H.-W. Wanzlick and E. Schikora, *Chem. Ber.*, 1961, **94**, 2389-2393.
54. H.-W. Wanzlick and H.-J. Schönherr, *Angew. Chem. Int. Ed.*, 1968, **7**, 141-142.
55. A. Igau, H. Grutzmacher, A. Baceiredo and G. Bertrand, *J. Am. Chem. Soc.*, 1988, **110**, 6463-6466.
56. H.-J. Schönherr and H.-W. Wanzlick, *Justus Liebigs Ann. Chem.*, 1970, **731**, 176-179.
57. A. J. Arduengo III, R. L. Harlow and M. Kline, *J. Am. Chem. Soc.*, 1991, **113**, 361-363.
58. C. Färber, M. Leibold, C. Bruhn, M. Maurer and U. Siemeling, *Chem. Commun.*, 2012, **48**, 227-229.
59. J. A. Grant, Z. Lu, D. E. Tucker, B. M. Hockin, D. S. Yufit, M. A. Fox, R. Kataky, V. Chechik and A. C. O'Donoghue, *Nat. Commun.*, 2017, **8**, 6-11.
60. R. M. Wilson and T. H. Lambert, *Acc. Chem. Res.*, 2022, **55**, 3057-3069.
61. J. P. Moerdyk, D. Schilter and C. W. Bielawski, *Acc. Chem. Res.*, 2016, **49**, 1458-1468.
62. S. C. Sau, P. K. Hota, S. K. Mandal, M. Soleilhavoup and G. Bertrand, *Chem. Soc. Rev.*, 2020, **49**, 1233-1252.
63. C. J. Collett, R. S. Massey, O. R. Maguire, A. S. Batsanov, A. C. O'Donoghue and A. D. Smith, *Chem. Sci*, 2013, **4**, 1514-1522.
64. E. M. Higgins, J. A. Sherwood, A. G. Lindsay, J. Armstrong, R. S. Massey, R. W. Alder and A. C. O'Donoghue, *Chem. Commun.*, 2011, **47**, 1559-1561.
65. R. S. Massey, C. J. Collett, A. G. Lindsay, A. D. Smith and A. C. O'Donoghue, *J. Am. Chem. Soc.*, 2012, **134**, 20421-20432.
66. C. J. Collett, R. S. Massey, J. E. Taylor, O. R. Maguire, A. C. O'Donoghue and A. D. Smith, *Angew. Chem. Int. Ed.*, 2015, **54**, 6887-6892.
67. A. P. Kriven'ko and N. A. Morozova, *Russ. J. Appl. Chem.*, 2006, **79**, 506-507.
68. M. S. S. Palanki, J. Cao, C. P. Chow, E. Dneprovskaia, C. C. Mak, A. McPherson, V. P. Pathak, J. Renick, R. Soll, B. Zeng and G. Noronha, *Expert Opin. Drug Discov.*, 2009, **4**, 33-49.
69. D. Pomikło, A. Bodzioch, A. Pietrzak and P. Kaszyński, *Org. Lett.*, 2019, **21**, 6995-6999.
70. D. Pomikło, A. Bodzioch and P. Kaszyński, *J. Org. Chem*, 2023, DOI: 10.1021/acs.joc.2c02703.
71. L. Qu, H. Chen, H. Chen, C. Shi, H. Li, W. Lian, M. Mao, Y. Hou, Q. Ai, H. Yang, X. Yan, X. Liu and X. Hu, *ACS Appl. Nano Mater*, 2023, **6**, 5781-5788.
72. W. C. Cope and J. Barab, *J. Am. Chem. Soc.*, 1917, **39**, 504-514.
73. *Analyst*, 1909, **34**, 114-119.
74. T. Akira and M. Hiroko, *Bull. Chem. Soc. Jpn.*, 1974, **47**, 2885-2886.
75. K. Meadows, C. K. Wright, S. C. Sims and V. R. Morris, presented in part at the The First National Student Conference: NASA University Research Centers at Minority Institutions, Greensboro, NC, United States, 31st March - 2nd April, 1996.
76. E. Amit, I. Berg and E. Gross, *Chem. Eur. J*, 2020, **26**, 13046-13052.
77. *United States Pat.,* US2005/0003114A1, 2005.
78. *United States Pat.,* US2006/0024454A1, 2006.
79. Y.-Y. Zhang, J.-L. Mi, C.-H. Zhou and X.-D. Zhou, *Eur. J. Med. Chem*, 2011, **46**, 4391-4402.
80. A. Savateev, C. Liedel, S. Tröger-Müller, A. S. de León, M. Antonietti and D. Dontsova, *Chem. Commun.*, 2017, **53**, 10192-10195.
81. Y. Zhang, X. Chen, J. Lan, J. You and L. Chen, *Chem. Biol. Drug Des.*, 2009, **74**, 282-288.

82. *Ionic Liquids in Organic Synthesis*, American Chemical Society, Washington DC, 2007.
83. *Electrochemistry in Ionic Liquids*, Springer International Publishing, Switzerland, 1st edn., 2015.
84. S.-h. Liu, H. Wang, J.-k. Sun, M. Antonietti and J. Yuan, *Acc. Chem. Res.*, 2022, **55**, 3675-3687.
85. W. Cao, L. Tan, H. Wang and J. Yuan, *ACS Macro Lett*, 2021, **10**, 161-166.
86. J. Song, J. Zou, J. Jin, J. Lv, C. Mou and Y. R. Chi, *Chem. Eur. J*, 2023, **29**, e202203661.
87. D. A. DiRocco, K. M. Oberg, D. M. Dalton and T. Rovis, *J. Am. Chem. Soc.*, 2009, **131**, 10872-10874.
88. Q. Y. Toh, A. McNally, S. Vera, N. Erdmann and M. J. Gaunt, *J. Am. Chem. Soc.*, 2013, **135**, 3772-3775.
89. X. Bugaut, F. Liu and F. Glorius, *J. Am. Chem. Soc.*, 2011, **133**, 8130-8133.
90. I. Piel, M. Steinmetz, K. Hirano, R. Fröhlich, S. Grimme and F. Glorius, *Angew. Chem. Int. Ed.*, 2011, **50**, 4983-4987.
91. M. P. van der Helm, B. Klemm and R. Eelkema, *Nat. Rev. Chem.*, 2019, **3**, 491-508.
92. J. Yan, R. Sun, K. Shi, K. Li, L. Yang and G. Zhong, *J. Org. Chem*, 2018, **83**, 7547-7552.
93. M. Debiais, A. Hamoud, R. Drain, P. Barthélémy and V. Desvergnes, *RSC Adv*, 2020, **10**, 40709-40718.
94. M. Hong, X. Tang, L. Falivene, L. Caporaso, L. Cavallo and E. Y. X. Chen, *J. Am. Chem. Soc.*, 2016, **138**, 2021-2035.
95. M. Monticelli, S. Bellemin-Laponnaz, C. Tubaro and M. Rancan, *Eur. J. Inorg. Chem.*, 2017, **2017**, 2488-2495.
96. E. Peris, *Chem. Rev.*, 2018, **118**, 9988-10031.
97. V. K. Singh, S. N. R. Donthireddy, P. M. Illam and A. Rit, *Dalton Trans*, 2020, **49**, 11958-11970.
98. K. Stęsik, A. Franczyk, A. Czapik, I. Kownacki and J. Walkowiak, *ChemCatChem*, 2023, **15**, e202201510.
99. L. Oehninger, R. Rubbiani and I. Ott, *Dalton Trans*, 2013, **42**, 3269-3284.
100. N. A. Johnson, M. R. Southerland and W. J. Youngs, *Molecules*, 2017, **22**.
101. K. M. Hindi, M. J. Panzner, C. A. Tessier, C. L. Cannon and W. J. Youngs, *Chem. Rev.*, 2009, **109**, 3859-3884.
102. S. Nayak and S. L. Gaonkar, *ChemMedChem*, 2021, **16**, 1360-1390.
103. J. Dai, S. Tian, X. Yang and Z. Liu, *Front. Chem.*, 2022, **10**.
104. L. Gonnet, M. Baron and M. Baltas, *Molecules*, 2021, **26**.
105. A. Kashyap and O. Silakari, in *Key Heterocycle Cores for Designing Multitargeting Molecules*, ed. O. Silakari, Elsevier, 2018, DOI: https://doi.org/10.1016/B978-0-08-102083-8.00009-1, pp. 323-342.
106. G. T. Sukhanov, A. G. Sukhanova and Y. V. Sheikov, *Chem. Heterocycl. Compd.*, 2007, **43**, 786-792.
107. Odd R. Gautun and Per H. J. Carlsen, *Eur. J. Org. Chem.*, 2000, **2000**, 3745-3748.
108. J. Turek, I. Panov, M. Semler, P. Štěpnička, F. De Proft, Z. Padělková and A. Růžička, *Organometallics*, 2014, **33**, 3108-3118.
109. L. D. Funt, O. A. Tomashenko, A. F. Khlebnikov, M. S. Novikov and A. Y. Ivanov, *J. Org. Chem*, 2016, **81**, 11210-11221.
110. S. M. Hutchinson, L. G. Ardón-Muñoz, M. L. Ratliff and J. L. Bolliger, *ACS Omega*, 2019, **4**, 17923-17933.
111. D. Enders, K. Breuer, J. Runsink and J. Henrique Teles, *Liebigs Annalen*, 1996, **1996**, 2019-2028.
112. D. G. Neilson, R. Roger, J. W. M. Heatlie and L. R. Newlands, *Chem. Rev.*, 1970, **70**, 151-170.
113. W. Marckwald and P. Wolff, *Ber. Dtsch. Chem. Ges.*, 1892, **25**, 3116-3119.
114. A. I. Eliseeva, O. O. Nesterenko, P. A. Slepukhin, E. Benassi and N. P. Belskaya, *J. Org. Chem*, 2017, **82**, 86-100.
115. M. A. Epishina, A. S. Kulikov and L. L. Fershtat, *Molecules*, 2022, **27**, 2575.

116. N. N. Makhova, A. N. Mikhajluk, G. A. Kaprov, N. V. Protopopova, B. N. Khasapov, L. I. Khmelnitski and S. S. Novikov, *Tetrahedron*, 1978, **34**, 413-418.
117. P. Frohberg, G. Drutkowski and C. Wagner, *Eur. J. Org. Chem.*, 2002, **2002**, 1654-1663.
118. P. Langer, A. Bodtke, N. N. R. Saleh, H. Görls and P. R. Schreiner, *Angew. Chem. Int. Ed.*, 2005, **44**, 5255-5259.
119. W. M. Basyouni, S. Y. Abbas, K. A. M. El-Bayouki, E. A. Younis, S. A. Ali and H. F. Aly, *Bioorg. Chem.*, 2021, **117**, 105418.
120. K. M. Watson and D. G. Neilson, in *Amidines and Imidates (1975)*, 1975, DOI: https://doi.org/10.1002/9780470771495.ch10, pp. 491-545.
121. P. Frohberg, C. Kupfer, P. Stenger, U. Baumeister and P. Nuhn, *Arch. Pharm.*, 1995, **328**, 505-516.
122. V. R. Yatham, W. Harnying, D. Kootz, J.-M. Neudörfl, N. E. Schlörer and A. Berkessel, *J. Am. Chem. Soc.*, 2016, **138**, 2670-2677.
123. T. M. Trnka, J. P. Morgan, M. S. Sanford, T. E. Wilhelm, M. Scholl, T.-L. Choi, S. Ding, M. W. Day and R. H. Grubbs, *J. Am. Chem. Soc.*, 2003, **125**, 2546-2558.
124. M. Busch, *Ber. Dtsch. Chem. Ges.*, 1905, **38**, 856-860.
125. W. E. Motzer, *Environ. Forensics*, 2001, **2**, 301-311.
126. C. S. Marvel and V. d. Vigneaud, *J. Am. Chem. Soc.*, 1924, **46**, 2661-2663.
127. J. Murray, PhD, Durham University, 2022.
128. P. J. Quinlivan, A. Loo, D. G. Shlian, J. Martinez and G. Parkin, *Organometallics*, 2021, **40**, 166-183.
129. European Chemicals Agency, *Orange lead*, European Union, https://echa.europa.eu, 2022.
130. K. Deibler and P. Basu, *Eur. J. Inorg. Chem.*, 2013, **2013**, 1086-1096.
131. P. Navasumrit, S. Chanvaivit, P. Intarasunanont, M. Arayasiri, N. Lauhareungpanya, V. Parnlob, D. Settachan and M. Ruchirawat, *Chem. Biol. Interact.*, 2005, **153-154**, 75-83.
132. Public Health England, Benzene: general information, https://www.gov.uk/government/publications/benzene-general-information-incident-management-and-toxicology/benzene-general-information, (accessed 13th December, 2023).
133. L. Benhamou, E. Chardon, G. Lavigne, S. Bellemin-Laponnaz and V. César, *Chem. Rev.*, 2011, **111**, 2705-2733.
134. C. Fliedel and P. Braunstein, *J. Organomet. Chem.*, 2014, **751**, 286-300.
135. G. Doleschall, *Tetrahedron*, 1976, **32**, 2549-2558.
136. A. Nasr, A. Winkler and M. Tamm, *Coord. Chem. Rev.*, 2016, **316**, 68-124.
137. D. J. Nelson and S. P. Nolan, *Chem. Soc. Rev.*, 2013, **42**, 6723-6753.
138. G. Doleschall, *Tetrahedron Lett.*, 1975, **16**, 1889-1892.
139. G. Doleschall, *Tetrahedron Lett.*, 1977, **18**, 381-382.
140. G. Doleschall, *Tetrahedron Lett.*, 1975, **16**, 681-682.
141. G. Doleschall and G. Tóth, *Tetrahedron*, 1980, **36**, 1649-1665.
142. M. Numata, M. Yamaoka, I. Minamida, M. Kuritani and Y. Imashiro, *J Antibiot*, 1978, **31**, 1245-1251.
143. D. V. Pasyukov, A. Y. Chernenko, I. V. Lavrentev, V. A. Baydikova, M. E. Minyaev, O. A. Starovoytova and V. M. Chernyshev, *Russ. Chem. Bull.*, 2022, **71**, 993-1008.
144. K. T. Potts, *Chem. Rev.*, 1961, **61**, 87-127.
145. J. R. Miecznikowski, W. Lo, M. A. Lynn, S. Jain, L. C. Keilich, N. F. Kloczko, B. E. O'Loughlin, A. P. DiMarzio, K. M. Foley, G. P. Lisi, D. J. Kwiecien, E. E. Butrick, E. Powers and R. Al-Abbasee, *Inorg. Chim. Acta*, 2012, **387**, 25-36.
146. M. Liu, M. Nieger and A. Schmidt, *Chem. Commun.*, 2015, **51**, 477-479.
147. O. Koniev and A. Wagner, *Chem. Soc. Rev.*, 2015, **44**, 5495-5551.
148. M. S. Kang, T. W. S. Kong, J. Y. X. Khoo and T.-P. Loh, *Chem. Sci*, 2021, **12**, 13613-13647.
149. P. Elzahhar, A. S. F. Belal, F. Elamrawy, N. A. Helal and M. I. Nounou, in *Pharmaceutical Nanotechnology: Basic Protocols*, eds. V. Weissig and T. Elbayoumi, Springer New York, New York, NY, 2019, DOI: 10.1007/978-1-4939-9516-5_11, pp. 125-182.
150. V. Agouridas, O. El Mahdi, V. Diemer, M. Cargoët, J.-C. M. Monbaliu and O. Melnyk, *Chem. Rev.*, 2019, **119**, 7328-7443.

151. S. Hanreich, E. Bonandi and I. Drienovská, *ChemBioChem*, 2023, **24**, e202200566.
152. H. Osseili, D. F. Sauer, K. Beckerle, M. Arlt, T. Himiyama, T. Polen, A. Onoda, U. Schwaneberg, T. Hayashi and J. Okuda, *Beilstein J. Org. Chem.*, 2016, **12**, 1314-1321.
153. H. U. Vora and T. Rovis, *J. Am. Chem. Soc.*, 2010, **132**, 2860-2861.
154. E. G. Delany, C.-L. Fagan, S. Gundala, K. Zeitler and S. J. Connon, *Chem. Commun.*, 2013, **49**, 6513-6515.
155. D. Enders and T. Balensiefer, *Acc. Chem. Res.*, 2004, **37**, 534-541.
156. M. S. Kerr, J. Read de Alaniz and T. Rovis, *J. Org. Chem*, 2005, **70**, 5725-5728.
157. D. Enders, K. Breuer, U. Kallfass and T. Balensiefer, *Synthesis*, 2003, **2003**, 1292-1295.
158. A. R. Ali, H. Ghosh and B. K. Patel, *Tetrahedron Lett.*, 2010, **51**, 1019-1021.
159. H. G. Khorana, *Chem. Rev.*, 1953, **53**, 145-166.
160. E. Lieber and G. B. L. Smith, *Chem. Rev.*, 1939, **25**, 213-271.
161. R. Wessel, *Ber. Dtsch. Chem. Ges.*, 1888, **21**, 2272-2278.
162. C. Schall, *Journal für Praktische Chemie*, 1901, **64**, 261-273.
163. S. C. Holm and B. F. Straub, *Org. Prep. Proced. Int.*, 2011, **43**, 319-347.
164. C. Hansch, A. Leo and R. W. Taft, *Chem. Rev.*, 1991, **91**, 165-195.
165. W. D. G. Brittain and S. L. Cobb, *J. Org. Chem*, 2020, **85**, 6862-6871.
166. J. Zhu, I. Moreno, P. Quinn, D. S. Yufit, L. Song, C. M. Young, Z. Duan, A. R. Tyler, P. G. Waddell, M. J. Hall, M. R. Probert, A. D. Smith and A. C. O'Donoghue, *J. Org. Chem*, 2022, **87**, 4241-4253.
167. Y. Zhao and D. G. Truhlar, *Theor. Chem. Acc.*, 2008, **120**, 215-241.
168. M. Walker, A. J. A. Harvey, A. Sen and C. E. H. Dessent, *J. Phys. Chem. A*, 2013, **117**, 12590-12600.
169. D. F. d. S. Paschoal, M. d. S. Gomes, L. P. N. Machado and H. F. Dos Santos, in *Basis Sets in Computational Chemistry*, ed. E. Perlt, Springer International Publishing, Cham, 2021, DOI: 10.1007/978-3-030-67262-1_7, pp. 183-214.
170. B. P. Pritchard, D. Altarawy, B. Didier, T. D. Gibson and T. L. Windus, *J. Chem. Inf. Model*, 2019, **59**, 4814-4820.
171. R. Sunderdiek and G. Zinner, *Arch. Pharm.*, 1974, **307**, 509-516.
172. V. Borek, L. R. Elberson, J. P. McCaffrey and M. J. Morra, *J. Agric. Food. Chem.*, 1998, **46**, 5318-5323.
173. N. Masutomi, K. Toyoda, M. Shibutani, N. Niho, C. Uneyama, N. Takahashi and M. Hirose, *Toxicol. Pathol.*, 2001, **29**, 617-622.
174. J. R. Williams, J. R. Rayburn, G. R. Cline, R. Sauterer and M. Friedman, *Toxicol. Rep.*, 2015, **2**, 222-227.
175. C. Tao, A. Lv, N. Zhao, S. Yang, X. Liu, J. Zhou, W. Liu and J. Zhao, *Synlett*, 2011, **2011**, 134-138.
176. P. Buranaprasertsuk, J. W. W. Chang, W. Chavasiri and P. W. H. Chan, *Tetrahedron Lett.*, 2008, **49**, 2023-2025.
177. C. G. Bates, R. K. Gujadhur and D. Venkataraman, *Org. Lett.*, 2002, **4**, 2803-2806.
178. W. D. G. Brittain and S. L. Cobb, *Org. Lett.*, 2021, **23**, 5793-5798.
179. L. N. D. Beardmore, S. L. Cobb and W. D. G. Brittain, *Org. Biomol. Chem*, 2022, **20**, 8059-8064.
180. J. C. Antilla, J. M. Baskin, T. E. Barder and S. L. Buchwald, *J. Org. Chem*, 2004, **69**, 5578-5587.
181. K. S. Sindhu and G. Anilkumar, *RSC Adv*, 2014, **4**, 27867-27887.
182. D. E. Tucker, Doctor of Philosophy, Durham University, 2018.
183. G. Hilgetag and H. Teichmann, *Chem. Ber.*, 1963, **96**, 1446-1453.
184. F. Klages and H. Meuresch, *Chem. Ber.*, 1953, **86**, 1322-1326.
185. N. Ree, A. H. Göller and J. H. Jensen, *Digital Discovery*, 2024, DOI: 10.1039/D3DD00224A.
186. J. Magano, *Org. Process Res. Dev.*, 2022, **26**, 1562-1689.
187. H.-A. Christ, Y. Bourgat and H. Menzel, *Polymers*, 2021, **13**, 2702.
188. B. M. Trost and M. T. Rudd, *Org. Lett.*, 2003, **5**, 4599-4602.
189. M. Meldal and C. W. Tornøe, *Chem. Rev.*, 2008, **108**, 2952-3015.

190. W. D. G. Brittain, Doctor of Philosophy, University of Birmingham, 2017.
191. W. D. G. Brittain and S. L. Cobb, *Org. Biomol. Chem*, 2019, **17**, 2110-2115.
192. F. Firooznia, C. Gude, K. Chan, N. Marcopulos and Y. Satoh, *Tetrahedron Lett.*, 1999, **40**, 213-216.
193. Y. Zhang, Y. Zheng, H. Zhou, M.-S. Miao, F. Wudl and T.-Q. Nguyen, *Adv. Mater.*, 2015, **27**, 7412-7419.
194. S. Kapuściński, A. Gardias, D. Pociecha, M. Jasiński, J. Szczytko and P. Kaszyński, *J. Mater. Chem. C*, 2018, **6**, 3079-3088.
195. M. Jasiński, S. Kapuściński and P. Kaszyński, *J. Mol. Liq.*, 2019, **277**, 1054-1059.
196. M. Jasiński, K. Szymańska, A. Gardias, D. Pociecha, H. Monobe, J. Szczytko and P. Kaszyński, *ChemPhysChem*, 2019, **20**, 636-644.
197. K. I. Shivakumar, D. Pociecha, J. Szczytko, S. Kapuściński, H. Monobe and P. Kaszyński, *J. Mater. Chem. C*, 2020, **8**, 1083-1088.
198. M. Jasiński, J. Szczytko, D. Pociecha, H. Monobe and P. Kaszyński, *J. Am. Chem. Soc.*, 2016, **138**, 9421-9424.
199. M. Cigl, D. Pociecha, R. Jakubowski, S. Kapuściński and P. Kaszyński, *Chem. Eur. J*, 2023, **29**, e202203288.
200. S. Zhang, M. Pink, T. Junghoefer, W. Zhao, S.-N. Hsu, S. Rajca, A. Calzolari, B. W. Boudouris, M. B. Casu and A. Rajca, *J. Am. Chem. Soc.*, 2022, **144**, 6059-6070.
201. Y. Zheng, M.-s. Miao, G. Dantelle, N. D. Eisenmenger, G. Wu, I. Yavuz, M. L. Chabinyc, K. N. Houk and F. Wudl, *Adv. Mater.*, 2015, **27**, 1718-1723.
202. J. S. Steen, J. L. Nuismer, V. Eiva, A. E. T. Wiglema, N. Daub, J. Hjelm and E. Otten, *J. Am. Chem. Soc.*, 2022, **144**, 5051-5058.
203. *Germany Pat.,* DE102017005924A1, 2017.
204. R. F. Anderson, S. S. Shinde, M. P. Hay, S. A. Gamage and W. A. Denny, *J. Am. Chem. Soc.*, 2003, **125**, 748-756.
205. H. M. Blatter and H. Lukaszewski, *Tetrahedron Lett.*, 1968, **9**, 2701-2705.
206. F. J. M. Rogers, P. L. Norcott and M. L. Coote, *Org. Biomol. Chem*, 2020, **18**, 8255-8277.
207. Y. Ji, L. Long and Y. Zheng, *Mater. Chem. Front.*, 2020, **4**, 3433-3443.
208. A. Calzolari, A. Rajca and M. B. Casu, *J. Mater. Chem. C*, 2021, **9**, 10787-10793.
209. E. M. Nowik-Boltyk, T. Junghoefer, M. Glaser, E. Giangrisostomi, R. Ovsyannikov, S. Zhang, C. Shu, A. Rajca, A. Calzolari and M. B. Casu, *ACS Appl. Mater. Interfaces*, 2023, DOI: 10.1021/acsami.3c02057.
210. A. A. Berezin, C. P. Constantinides, S. I. Mirallai, M. Manoli, L. L. Cao, J. M. Rawson and P. A. Koutentis, *Org. Biomol. Chem*, 2013, **11**, 6780-6795.
211. A. Bodzioch, M. Zheng, P. Kaszyński and G. Utecht, *J. Org. Chem.*, 2014, **79**, 7294-7310.
212. Y. Zheng, M.-s. Miao, M. C. Kemei, R. Seshadri and F. Wudl, *Isr. J. Chem.*, 2014, **54**, 774-778.
213. C. P. Constantinides, G. A. Zissimou, A. A. Berezin, T. A. Ioannou, M. Manoli, D. Tsokkou, E. Theodorou, S. C. Hayes and P. A. Koutentis, *Org. Lett.*, 2015, **17**, 4026-4029.
214. P. Kaszyński, C. P. Constantinides and V. G. Young, *Angew. Chem. Int. Ed.*, 2016, **55**, 11149-11152.
215. C. P. Constantinides, D. B. Lawson, G. A. Zissimou, A. A. Berezin, A. Mailman, M. Manoli, A. Kourtellaris, G. M. Leitus, R. Clérac, H. M. Tuononen and P. A. Koutentis, *CrystEngComm*, 2020, **22**, 5453-5463.
216. P. Bartos, V. G. Young, Jr. and P. Kaszyński, *Org. Lett.*, 2020, **22**, 3835-3840.
217. A. Saal, C. Friebe and U. S. Schubert, *Macromol. Chem. Phys.*, 2021, DOI: https://doi.org/10.1002/macp.202100194, 2100194.
218. M. Demetriou, A. A. Berezin, P. A. Koutentis and T. Krasia-Christoforou, *Polym. Int.*, 2014, **63**, 674-679.
219. Y. L. Kuznetsova, A. S. Vavilova, Y. B. Malysheva, M. A. Lopatin, I. D. Grishin, T. O. Burdyukova, E. A. Zaburdaeva, E. Y. Polozov and A. Y. Fedorov, *Russ. Chem. Bull.*, 2020, **69**, 1470-1477.
220. F. Saenz, M. Tamski, J. Milani, C. Roussel, H. Frauenrath and J.-P. Ansermet, *Chem. Commun.*, 2022, **58**, 689-692.

221. F. Miao, Y. Ji, B. Han, S. M. Quintero, H. Chen, G. Xue, L. Cai, J. Casado and Y. Zheng, *Chem. Sci*, 2023, DOI: 10.1039/D3SC00367A.
222. I. S. Morgan, A. Peuronen, M. M. Hänninen, R. W. Reed, R. Clérac and H. M. Tuononen, *Inorg. Chem.*, 2014, **53**, 33-35.
223. I. S. Morgan, A. Mansikkamäki, G. A. Zissimou, P. A. Koutentis, M. Rouzières, R. Clérac and H. M. Tuononen, *Chem. Eur. J*, 2015, **21**, 15843-15853.
224. B. Yan, J. Cramen, R. McDonald and N. L. Frank, *Chem. Commun.*, 2011, **47**, 3201-3203.
225. F. Ciccullo, N. M. Gallagher, O. Geladari, T. Chassé, A. Rajca and M. B. Casu, *ACS Appl. Mater. Interfaces*, 2016, **8**, 1805-1812.
226. M. Catto, A. A. Berezin, D. Lo Re, G. Loizou, M. Demetriades, A. De Stradis, F. Campagna, P. A. Koutentis and A. Carotti, *Eur. J. Med. Chem*, 2012, DOI: 10.1016/j.ejmech.2012.10.003.
227. S. Chopra, G. A. Koolpe, A. A. Tambo-Ong, K. N. Matsuyama, K. J. Ryan, T. B. Tran, R. S. Doppalapudi, E. S. Riccio, L. V. Iyer, C. E. Green, B. Wan, S. G. Franzblau and P. B. Madrid, *J. Med. Chem.*, 2012, **55**, 6047-6060.
228. M. Birincioglu, P. Jaruga, G. Chowdhury, H. Rodriguez, M. Dizdaroglu and K. S. Gates, *J. Am. Chem. Soc.*, 2003, **125**, 11607-11615.
229. L.-A. J. Keane, S. I. Mirallai, M. Sweeney, M. P. Carty, G. A. Zissimou, A. A. Berezin, P. A. Koutentis and F. Aldabbagh, *Molecules*, 2018, **23**, 574.
230. Y. Ji, S. Moles Quintero, Y. Dai, J. M. Marín-Beloqui, H. Zhang, Q. Zhan, F. Sun, D. Wang, X. Li, Z. Wang, X. Gu, F. Negri, J. Casado and Y. Zheng, *Angew. Chem. Int. Ed.*, 2023, **62**, e202311387.
231. C. P. Constantinides, E. Carter, D. M. Murphy, M. Manoli, G. M. Leitus, M. Bendikov, J. M. Rawson and P. A. Koutentis, *Chem. Commun.*, 2013, **49**, 8662-8664.
232. X. Hu, L. Zhao, H. Chen, Y. Ding, Y.-Z. Zheng, M.-s. Miao and Y. Zheng, *J. Mater. Chem. C*, 2019, **7**, 6559-6563.
233. C. P. Constantinides, E. Obijalska and P. Kaszyński, *Org. Lett.*, 2016, **18**, 916-919.
234. A. A. Berezin, G. Zissimou, C. P. Constantinides, Y. Beldjoudi, J. M. Rawson and P. A. Koutentis, *J. Org. Chem.*, 2014, **79**, 314-327.
235. P. A. Koutentis and D. Lo Re, *Synthesis*, 2010, DOI: 10.1055/s-0029-1218782, 2075-2079.
236. C. P. Constantinides, P. A. Koutentis and G. Loizou, *Org. Biomol. Chem*, 2011, **9**, 3122-3125.
237. C. P. Constantinides, P. A. Koutentis and J. M. Rawson, *Chem. Eur. J*, 2012, **18**, 15433-15438.
238. F. A. Neugebauer and I. Umminger, *Chem. Ber.*, 1980, **113**, 1205-1225.
239. M. Z. Al-Noaimi, R. J. Abdel-Jalil, M. M. El-Abadelah, S. F. Haddad, Y. N. H. Baqi and W. Voelter, *Monatsh. Chem.*, 2006, **137**, 745-750.
240. A. C. Savva, S. I. Mirallai, G. A. Zissimou, A. A. Berezin, M. Demetriades, A. Kourtellaris, C. P. Constantinides, C. Nicolaides, T. Trypiniotis and P. A. Koutentis, *J. Org. Chem.*, 2017, **82**, 7564-7575.
241. M. K. Kadirov, B. I. Buzykin and N. G. Gazetdinova, *Russ. Chem. Bull.*, 2002, **51**, 1796-1799.
242. F. Arndt and B. Eistert, *Ber. Dtsch. Chem. Ges.*, 1927, **60**, 2598-2602.
243. G. A. Zissimou, A. A. Berezin, M. Manoli, C. Nicolaides, T. Trypiniotis and P. A. Koutentis, *Tetrahedron*, 2020, **76**, 131077.
244. F. Arndt, *Ber. Dtsch. Chem. Ges.*, 1913, **46**, 3522-3530.
245. A. Bodzioch, D. Pomikło, M. Celeda, A. Pietrzak and P. Kaszyński, *J. Org. Chem.*, 2019, **84**, 6377-6394.
246. Y. Takahashi, Y. Miura and N. Yoshioka, *Chem. Lett.*, 2014, **43**, 1236-1238.
247. M. Sweeney, R. Coyle, P. Kavanagh, A. A. Berezin, D. Lo Re, G. A. Zissimou, P. A. Koutentis, M. P. Carty and F. Aldabbagh, *Bioorg. Med. Chem.*, 2016, **24**, 3565-3570.
248. P. A. Koutentis, G. Loizou and D. Lo Re, *J. Org. Chem*, 2011, **76**, 5793-5802.
249. A. A. Berezin, C. P. Constantinides, C. Drouza, M. Manoli and P. A. Koutentis, *Org. Lett.*, 2012, **14**, 5586-5589.
250. A. A. Berezin and P. A. Koutentis, *Org. Biomol. Chem*, 2014, **12**, 1641-1648.

251. C. P. Constantinides, P. A. Koutentis, H. Krassos, J. M. Rawson and A. J. Tasiopoulos, *J. Org. Chem*, 2011, **76**, 2798-2806.
252. P. A. Koutentis, H. Krassos and D. Lo Re, *Org. Biomol. Chem*, 2011, **9**, 5228-5237.
253. D. M. Walsh, I. Klyubin, J. V. Fadeeva, W. K. Cullen, R. Anwyl, M. S. Wolfe, M. J. Rowan and D. J. Selkoe, *Nature*, 2002, **416**, 535-539.
254. G. A. Zissimou, A. Kourtellaris, M. Manoli and P. A. Koutentis, *J. Org. Chem*, 2018, **83**, 9391-9402.
255. J. Areephong, K. M. Mattson, N. J. Treat, S. O. Poelma, J. W. Kramer, H. A. Sprafke, A. A. Latimer, J. Read de Alaniz and C. J. Hawker, *Polym. Chem*, 2016, **7**, 370-374.
256. G. Archer, K. Song, M. Médebielle and J. Merad, *ChemPhotoChem*, 2023, **7**, e202300096.
257. C. Pratley, S. Fenner and J. A. Murphy, *Chem. Rev.*, 2022, **122**, 8181-8260.
258. K. Kwon, R. T. Simons, M. Nandakumar and J. L. Roizen, *Chem. Rev.*, 2022, **122**, 2353-2428.
259. M. M. Haugland, J. E. Lovett and E. A. Anderson, *Chem. Soc. Rev.*, 2018, **47**, 668-680.
260. D. Abdullin, N. Florin, G. Hagelueken and O. Schiemann, *Angew. Chem. Int. Ed.*, 2015, **54**, 1827-1831.
261. P. Roser, M. J. Schmidt, M. Drescher and D. Summerer, *Org. Biomol. Chem*, 2016, **14**, 5468-5476.
262. C. Altenbach, S. L. Flitsch, H. G. Khorana and W. L. Hubbell, *Biochem.*, 1989, **28**, 7806-7812.
263. M. R. Fleissner, E. M. Brustad, T. Kálai, C. Altenbach, D. Cascio, F. B. Peters, K. Hideg, S. Peuker, P. G. Schultz and W. L. Hubbell, *Proc Natl Acad Sci U S A*, 2009, **106**, 21637-21642.
264. M. J. Schmidt, J. Borbas, M. Drescher and D. Summerer, *J. Am. Chem. Soc.*, 2014, **136**, 1238-1241.
265. J. M. Isas, R. Langen, H. T. Haigler and W. L. Hubbell, *Biochem.*, 2002, **41**, 1464-1473.
266. R. D. Astronomo and D. R. Burton, *Nat. Rev. Drug Discov*, 2010, **9**, 308-324.
267. P. H. Seeberger, *Chem. Rev.*, 2021, **121**, 3598-3626.
268. K. O. Hicks, B. G. Siim, J. K. Jaiswal, F. B. Pruijn, A. M. Fraser, R. Patel, A. Hogg, H. D. S. Liyanage, M. J. Dorie, J. M. Brown, W. A. Denny, M. P. Hay and W. R. Wilson, *Clin. Cancer Res*, 2010, **16**, 4946-4957.
269. S. Mattsson, M. Dahlström and S. Karlsson, *Tetrahedron Lett.*, 2007, **48**, 2497-2499.
270. I. T. Barnish and M. S. Gibson, *J. Chem. Soc. C*, 1970, DOI: 10.1039/J39700000854, 854-859.
271. Y. Ben-Tal, P. J. Boaler, H. J. A. Dale, R. E. Dooley, N. A. Fohn, Y. Gao, A. García-Domínguez, K. M. Grant, A. M. R. Hall, H. L. D. Hayes, M. M. Kucharski, R. Wei and G. C. Lloyd-Jones, *Prog. Nucl. Magn. Reson. Spectrosc.*, 2022, **129**, 28-106.
272. R. Wei, C. L. Dickson, D. Uhrín and G. C. Lloyd-Jones, *J. Org. Chem*, 2021, **86**, 9023-9029.
273. A. A. Berezin, G. Zissimou, C. P. Constantinides, Y. Beldjoudi, J. M. Rawson and P. A. Koutentis, *J. Org. Chem*, 2015, **80**, 8943-8944.
274. F. Yang, T. Huang, Y.-M. Lin and L. Gong, *Chem. Catal.*, 2023, DOI: https://doi.org/10.1016/j.checat.2023.100812, 100812.
275. M. Sankar, E. Nowicka, E. Carter, D. M. Murphy, D. W. Knight, D. Bethell and G. J. Hutchings, *Nat. Commun.*, 2014, **5**, 3332.
276. S. K. Vaish, A. Singh, A. K. Singh and N. K. Mehrotra, *Indian J. Pure Appl. Phys.*, 2005, **43**.
277. Y. Stamatin and G. Maayan, *Eur. J. Org. Chem.*, 2020, **2020**, 3147-3152.
278. Z. Shah, R. Mahbuba and B. Turcotte, *FEMS Microbiol. Lett.*, 2013, **347**, 61-69.
279. T. Moriwaki, S. Okamoto, H. Sasanuma, H. Nagasawa, S. Takeda, S.-i. Masunaga and K. Tano, *Chem. Res. Toxicol.*, 2017, **30**, 699-704.
280. G. Noronha, K. Barrett, J. Cao, E. Dneprovskaia, R. Fine, X. Gong, C. Gritzen, J. Hood, X. Kang, B. Klebansky, G. Li, W. Liao, D. Lohse, C. C. Mak, A. McPherson, M. S. S. Palanki, V. P. Pathak, J. Renick, R. Soll, U. Splittgerber, W. Wrasidlo, B. Zeng, N. Zhao and Y. Zhou, *Bioorg. Med. Chem. Lett.*, 2006, **16**, 5546-5550.

281. J. Cao, R. Fine, C. Gritzen, J. Hood, X. Kang, B. Klebansky, D. Lohse, C. C. Mak, A. McPherson, G. Noronha, M. S. S. Palanki, V. P. Pathak, J. Renick, R. Soll, B. Zeng and H. Zhu, *Bioorg. Med. Chem. Lett.*, 2007, **17**, 5812-5818.
282. G. Noronha, K. Barrett, A. Boccia, T. Brodhag, J. Cao, C. P. Chow, E. Dneprovskaia, J. Doukas, R. Fine, X. Gong, C. Gritzen, H. Gu, E. Hanna, J. D. Hood, S. Hu, X. Kang, J. Key, B. Klebansky, A. Kousba, G. Li, D. Lohse, C. C. Mak, A. McPherson, M. S. S. Palanki, V. P. Pathak, J. Renick, F. Shi, R. Soll, U. Splittgerber, S. Stoughton, S. Tang, S. Yee, B. Zeng, N. Zhao and H. Zhu, *Bioorg. Med. Chem. Lett.*, 2007, **17**, 602-608.
283. J. K. Horner and D. W. Henry, *J. Med. Chem.*, 1968, **11**, 946-949.
284. E. Obijalska and M. K. Kowalski, *Chem. Heterocycl. Compd.*, 2017, **53**, 846-848.
285. G. M. Ziarani, M. Mostofi, P. Gholamzadeh, M. Mohammadi-Khanaposhtani and H. Yavari, *Arkivoc*, 2019, DOI: 10.24820/ark.5550190.p010.791, 0-0.
286. F. J. Wolf, K. Pfister, R. M. Wilson and C. A. Robinson, *J. Am. Chem. Soc.*, 1954, **76**, 3551-3553.
287. M. Boyd, M. P. Hay and P. D. W. Boyd, *Magn. Reson. Chem.*, 2006, **44**, 948-954.
288. J. C. Mason and G. Tennant, *J., Chem. Soc. B*, 1970, DOI: 10.1039/j29700000911, 911.
289. A. Messmer, G. Hajós, P. Benkó and L. Pallos, *Acta Chim. Acad. Sci. Hung.*, 1980, **103**, 123-133.
290. F. Arndt and B. Rosenau, *Ber. Dtsch. Chem. Ges.*, 1917, **50**, 1248-1261.
291. R. F. Robbins and K. Schofield, *J. Chem. Soc.*, 1957, DOI: 10.1039/JR9570003186, 3186-3194.
292. E. M. Zeman, M. A. Baker, M. J. Lemmon, C. I. Pearson, J. A. Adams, J. M. Brown, W. W. Lee and M. Tracy, *Int. J. Radiat. Oncol. Biol. Phys.*, 1989, **16**, 977-981.
293. Q. Xia, L. Zhang, J. Zhang, R. Sheng, B. Yang, Q. He and Y. Hu, *Eur. J. Med. Chem*, 2011, **46**, 919-926.
294. J. Gatenyo, K. Johnson, A. Rajapakse, K. S. Gates and S. Rozen, *Tetrahedron*, 2012, **68**, 8942-8944.
295. International Labour Organization and World Health Organization, *Thiocyanic acid*, International Labour Organization, ILO.org, 2021.
296. E. M. Zeman, J. M. Brown, M. J. Lemmon, V. K. Hirst and W. W. Lee, *Int. J. Radiat. Oncol. Biol. Phys.*, 1986, **12**, 1239-1242.
297. S. B. Reddy and S. K. Williamson, *Expert Opin. Investig. Drugs*, 2009, **18**, 77-87.
298. D. Lee, S.-y. Jang, S. Kwon, Y. Lee, E. Park and H. Koo, *ACS Appl. Mater. Interfaces*, 2021, **13**, 10812-10821.
299. G. Ajnai, C.-C. Cheng, T.-C. Kan, J.-W. Lu, S. Rahayu, A. Chiu and J. Chang, *Pharmaceutics*, 2022, **14**, 847.
300. X. Yuan, K. Tabassi and J. A. Williams, *Radiat. Oncol. Investig.*, 1999, **7**, 218-230.
301. Z. Ma, Y. Zhang, X. Dai, W. Zhang, M. F. Foda, J. Zhang, Y. Zhao and H. Han, *Adv. Mater.*, 2021, **33**, 2104504.
302. P. Hamley and A. C. Tinker, *Bioorg. Med. Chem. Lett.*, 1995, **5**, 1573-1576.
303. F. Humphries, L. Shmuel-Galia, Z. Jiang, R. Wilson, P. Landis, S.-L. Ng, K. M. Parsi, R. Maehr, J. Cruz, A. Morales, J. M. Ramanjulu, J. Bertin, G. S. Pesiridis and K. A. Fitzgerald, *Sci. Immunol.*, 2021, **6**, eabi9002.
304. A. Kumar, M. Parshad, R. K. Gupta and D. Kumar, *Synthesis*, 2009, **2009**, 1663-1666.
305. R. B. Bates, L. M. Kroposki and D. E. Potter, *J. Org. Chem*, 1972, **37**, 560-562.
306. D. F. Aycock, *Org. Process Res. Dev.*, 2007, **11**, 156-159.
307. P. de Frémont, N. Marion and S. P. Nolan, *Coord. Chem. Rev.*, 2009, **253**, 862-892.
308. M. Mora, M. C. Gimeno and R. Visbal, *Chem. Soc. Rev.*, 2019, **48**, 447-462.
309. D. M. Flanigan, F. Romanov-Michailidis, N. A. White and T. Rovis, *Chem. Rev.*, 2015, **115**, 9307-9387.
310. Wöhler and Liebig, *Annalen der Pharmacie*, 1832, **3**, 249-282.
311. T. Ukai, R. Tanaka and S. Dokawa, *J J. Pharm. Soc. Jpn.*, 1943, **63**, 296-304.
312. R. Breslow, *J. Am. Chem. Soc.*, 1958, **80**, 3719-3726.
313. J. Rehbein, S.-M. Ruser and J. Phan, *Chem. Sci*, 2015, **6**, 6013-6018.

314. R. C. Cookson and R. M. Lane, *J. Chem. Soc., Chem. Commun.*, 1976, DOI: 10.1039/C39760000804, 804-805.
315. M. Y. Jin, S. M. Kim, H. Han, D. H. Ryu and J. W. Yang, *Org. Lett.*, 2011, **13**, 880-883.
316. M. Y. Jin, S. M. Kim, H. Mao, D. H. Ryu, C. E. Song and J. W. Yang, *Org. Biomol. Chem*, 2014, **12**, 1547-1550.
317. S. M. Langdon, M. M. D. Wilde, K. Thai and M. Gravel, *J. Am. Chem. Soc.*, 2014, **136**, 7539-7542.
318. J. C. Sheehan and D. H. Hunneman, *J. Am. Chem. Soc.*, 1966, **88**, 3666-3667.
319. D. Enders, O. Niemeier and A. Henseler, *Chem. Rev.*, 2007, **107**, 5606-5655.
320. D. Enders and J. Han, *Tetrahedron: Asymmetry*, 2008, **19**, 1367-1371.
321. Y. Ma, S. Wei, J. Wu, F. Yang, B. Liu, J. Lan, S. Yang and J. You, *Adv. Synth. Catal.*, 2008, **350**, 2645-2651.
322. J. P. Brand, J. I. O. Siles and J. Waser, *Synlett*, 2010, **2010**, 881-884.
323. T. Soeta, Y. Tabatake, K. Inomata and Y. Ukaji, *Tetrahedron*, 2012, **68**, 894-899.
324. L. Baragwanath, C. A. Rose, K. Zeitler and S. J. Connon, *J. Org. Chem*, 2009, **74**, 9214-9217.
325. H. Stetter, *Angew. Chem. Int. Ed.*, 1976, **15**, 639-647.
326. H. Stetter and H. Kuhlmann, in *Organic Reactions*, John Wiley & Sons, Inc., Hoboken, NJ, USA, 1991, DOI: 10.1002/0471264180.or040.04, ch. 4, pp. 407-496.
327. B. M. Trost, C. D. Shuey and F. DiNinno, Jr., *J. Am. Chem. Soc.*, 1979, **101**, 1284-1285.
328. E. Ciganek, *Synthesis*, 1995, DOI: 10.1055/s-1995-4100, 1311-1314.
329. J. R. de Alaniz, M. S. Kerr, J. L. Moore and T. Rovis, *J. Org. Chem*, 2008, **73**, 2033-2040.
330. S. C. Cullen and T. Rovis, *Org. Lett.*, 2008, **10**, 3141-3144.
331. K. R. Law and C. S. P. McErlean, *Chem. Eur. J*, 2013, **19**, 15852-15855.
332. K. Zeitler and I. Mager, *Adv. Synth. Catal.*, 2007, **349**, 1851-1857.
333. S. Vedachalam, S. M. Tan, H. P. Teo, S. Cai and X.-W. Liu, *Org. Lett.*, 2012, **14**, 174-177.
334. D. Enders, Berlin, Heidelberg, 1993.
335. Q. Liu and T. Rovis, *Org. Lett.*, 2009, **11**, 2856-2859.
336. Q. Liu, S. Perreault and T. Rovis, *J. Am. Chem. Soc.*, 2008, **130**, 14066-14067.
337. D. Enders and J. Han, *Synthesis*, 2008, **2008**, 3864-3868.
338. D. Enders, J. Han and A. Henseler, *Chem. Commun.*, 2008, DOI: 10.1039/B809913H, 3989-3991.
339. C. De Risi, A. Brandolese, G. Di Carmine, D. Ragno, A. Massi and O. Bortolini, *Chem. Eur. J*, 2023, **29**, e202202467.
340. H. Mayr and A. R. Ofial, *Acc. Chem. Res.*, 2016, **49**, 952-965.
341. F. G. Bordwell, W. S. Matthews and N. R. Vanier, *J. Am. Chem. Soc.*, 1975, **97**, 442-443.
342. M. W. Washabaugh and W. P. Jencks, *Biochem.*, 1988, **27**, 5044-5053.
343. J. Peon, D. Polshakov and B. Kohler, *J. Am. Chem. Soc.*, 2002, **124**, 6428-6438.
344. T. L. Amyes, S. T. Diver, J. P. Richard, F. M. Rivas and K. Toth, *J. Am. Chem. Soc.*, 2004, **126**, 4366-4374.
345. D. E. Tucker, P. Quinn, R. S. Massey, C. J. Collett, D. J. Jasiewicz, C. R. Bramley, A. D. Smith and A. C. O'Donoghue, *J. Phys. Org. Chem.*, 2015, **28**, 108-115.
346. R. S. Massey, P. Quinn, S. Zhou, J. A. Murphy and A. C. O'Donoghue, *J. Phys. Org. Chem.*, 2016, **29**, 735-740.
347. P. Quinn, M. S. Smith, J. Zhu, D. R. W. Hodgson and A. C. O'Donoghue, *Catalysts*, 2021, **11**, 1055.
348. J. Reijenga, A. van Hoof, A. van Loon and B. Teunissen, *Anal Chem Insights*, 2013, **8**, 53-71.
349. P. K. Glasoe and F. A. Long, *J. Phys. Chem.*, 1960, **64**, 188-190.
350. A. K. Covington, R. A. Robinson and R. G. Bates, *J. Phys. Chem.*, 1966, **70**, 3820-3824.
351. L. G. Gagliardi, C. B. Castells, C. Ràfols, M. Rosés and E. Bosch, *Anal. Chem.*, 2007, **79**, 3180-3187.
352. R. L. Vold, J. S. Waugh, M. P. Klein and D. E. Phelps, *J. Chem. Phys.*, 2003, **48**, 3831-3832.
353. R. Freeman and H. D. W. Hill, *J. Chem. Phys.*, 2003, **51**, 3140-3141.
354. P. W. Percival and J. S. Hyde, *J. Magn. Reson.*, 1976, **23**, 249-257.

355. M. Huisjen and J. S. Hyde, *J. Chem. Phys.*, 2003, **60**, 1682-1683.
356. R. Freeman and H. D. W. Hill, *J. Chem. Phys.*, 2003, **54**, 3367-3377.
357. K. Maduka, Doctor of Philiosophy, Durham University, 2019.
358. R. S. Massey, J. Murray, C. J. Collett, J. Zhu, A. D. Smith and A. C. O'Donoghue, *Org. Biomol. Chem*, 2021, **19**, 387-393.
359. C. J. Collett, C. M. Young, R. S. Massey, A. C. O'Donoghue and A. D. Smith, *Eur. J. Org. Chem.*, 2021, **2021**, 3670-3675.
360. M. Charton, *Can. J. Chem.*, 1960, **38**, 2493-2499.
361. A. J. Kresge, R. A. M. O'Ferrall and M. F. Powell, in *Isotopes in organic chemistry*, eds. E. Buncel and C. C. Lee, Elsevier, New York, 1977.
362. V. Vichai and K. Kirtikara, *Nature Protocols*, 2006, **1**, 1112-1116.
363. D. C. Singleton, A. Macann and W. R. Wilson, *Nat Rev. Clin. Oncol.*, 2021, **18**, 751-772.
364. R. H. Thomlinson and L. H. Gray, *Br J Cancer*, 1955, **9**, 539-549.
365. J. M. Brown and W. R. Wilson, *Nat. Rev. Cancer*, 2004, **4**, 437-447.
366. G. C. Rice, C. Hoy and R. T. Schimke, *Proc Natl Acad Sci U S A*, 1986, **83**, 5978-5982.
367. Ç. Tosun, A. L. D. Wallabregue, M. Mallerman, S. E. Phillips, C. M. Edwards, S. J. Conway and E. M. Hammond, *JACS Au*, 2023, DOI: 10.1021/jacsau.3c00562.
368. N. Campillo, B. Falcones, J. Otero, R. Colina, D. Gozal, D. Navajas, R. Farré and I. Almendros, *Front. Oncol.*, 2019, **9**.
369. V. Bhandari, C. Hoey, L. Y. Liu, E. Lalonde, J. Ray, J. Livingstone, R. Lesurf, Y.-J. Shiah, T. Vujcic, X. Huang, S. M. G. Espiritu, L. E. Heisler, F. Yousif, V. Huang, T. N. Yamaguchi, C. Q. Yao, V. Y. Sabelnykova, M. Fraser, M. L. K. Chua, T. van der Kwast, S. K. Liu, P. C. Boutros and R. G. Bristow, *Nat. Genet.*, 2019, **51**, 308-318.
370. V. Bhandari, C. H. Li, R. G. Bristow, P. C. Boutros and PCAWG Consortium, *Nat. Commun.*, 2020, **11**, 737.
371. J. E. Ziello, I. S. Jovin and Y. Huang, *Yale J Biol Med*, 2007, **80**, 51-60.
372. P. Vaupel, K. Schlenger, C. Knoop and M. Höckel, *Cancer Res.*, 1991, **51**, 3316-3322.
373. R. A. Gatenby, L. R. Coia, M. P. Richter, H. Katz, P. J. Moldofsky, P. Engstrom, D. Q. Brown, R. Brookland and G. J. Broder, *Radiology*, 1985, **156**, 211-214.
374. R. A. Gatenby, H. B. Kessler, J. S. Rosenblum, L. R. Coia, P. J. Moldofsky, W. H. Hartz and G. J. Broder, *Int J Radiat Oncol Biol Phys*, 1988, **14**, 831-838.
375. I. F. Tannock, *The Lancet*, 1998, **351**, SII9-SII16.
376. I. F. Tannock, *Br J Cancer*, 1968, **22**, 258-273.
377. B. A. Teicher, J. S. Lazo and A. C. Sartorelli, *Cancer Res*, 1981, **41**, 73-81.
378. R. M. Batchelder, W. R. Wilson, M. P. Hay and W. A. Denny, *Br J Cancer Suppl*, 1996, **27**, S52-56.
379. R. Xu, F. Wang, H. Yang and Z. Wang, *Molecules*, 2022, **27**.
380. G. Beale, E. J. Haagensen, H. D. Thomas, L.-Z. Wang, C. H. Revill, S. L. Payne, B. T. Golding, I. R. Hardcastle, D. R. Newell, R. J. Griffin and C. Cano, *Br. J. Cancer*, 2016, **115**, 682-690.
381. K. M. Comerford, T. J. Wallace, J. Karhausen, N. A. Louis, M. C. Montalto and S. P. Colgan, *Cancer Res*, 2002, **62**, 3387-3394.
382. J. M. Brown, *Drug. Resist. Updat.*, 2000, **3**, 7-13.
383. R. J. Riley, S. A. Hemingway, M. A. Graham and P. Workman, *Biochem. Pharmacol.*, 1993, **45**, 1065-1077.
384. A. V. Patterson, M. P. Saunders, E. C. Chinje, D. C. Talbot, A. L. Harris and I. J. Strafford, *Br J Cancer*, 1997, **76**, 1338-1347.
385. R. J. Riley and P. Workman, *Biochem. Pharmacol.*, 1992, **43**, 167-174.
386. P. Karihtala and Y. Soini, *APMIS*, 2007, **115**, 81-103.
387. B. G. Wouters, Y. M. Delahoussaye, J. W. Evans, G. W. Birrell, M. J. Dorie, J. Wang, D. MacDermed, R. K. Chiu and J. M. Brown, *Cancer Res.*, 2001, **61**, 145-152.
388. V. N. Iyer and W. Szybalski, *Science*, 1964, **145**, 55-58.
389. C. Avendaño and J. C. Menéndez, in *Medicinal Chemistry of Anticancer Drugs*, eds. C. Avendaño and J. C. Menéndez, Elsevier, Amsterdam, The Netherlands, 1st edn., 2008, ch. 6.

390. C. Avendaño and J. C. Menéndez, in *Medicinal Chemistry of Anticancer Drugs (Third Edition)*, eds. C. Avendaño and J. C. Menéndez, Elsevier, Boston, 2023, DOI: https://doi.org/10.1016/B978-0-12-818549-0.00020-0, pp. 291-323.
391. S. Rockwell, K. A. Kennedy and A. C. Sartorelli, *Int. J. Radiat. Oncol. Biol. Phys.*, 1982, **8**, 753-755.
392. M. M. Paz, X. Zhang, J. Lu and A. Holmgren, *Chem. Res. Toxicol.*, 2012, **25**, 1502-1511.
393. J. M. Brown, *Br. J. Cancer*, 1993, **67**, 1163-1170.
394. Y. M. Delahoussaye, J. W. Evans and J. M. Brown, *Biochem. Pharmacol.*, 2001, **62**, 1201-1209.
395. K. B. Peters and J. M. Brown, *Cancer Res.*, 2002, **62**, 5248-5253.
396. C. Avendaño and J. C. Menéndez, in *Medicinal Chemistry of Anticancer Drugs*, Elsevier, 2008, DOI: 10.1016/b978-0-444-52824-7.00004-4, ch. 4, pp. 93-138.
397. G. Chowdhury, V. Junnotula, J. S. Daniels, M. M. Greenberg and K. S. Gates, *J. Am. Chem. Soc.*, 2007, **129**, 12870-12877.
398. E. Polmickaitė-Smirnova, J. Šarlauskas, K. Krikštopaitis, Ž. Lukšienė, Z. Staniulytė and Ž. Anusevičius, *Appl. Sci.*, 2020, **10**, 4062.
399. K. Hellauer, G. Lesage, A.-M. Sdicu and B. Turcotte, *Mol. Pharmacol.*, 2005, **68**, 1365-1375.
400. G. Cheng, W. Sa, C. Cao, L. Guo, H. Hao, Z. Liu, X. Wang and Z. Yuan, *Front Pharmacol*, 2016, **7**, 64-64.
401. B. Ganley, G. Chowdhury, J. Bhansali, J. S. Daniels and K. S. Gates, *Bioorg. Med. Chem.*, 2001, **9**, 2395-2401.
402. L. H. Patterson, *Cancer Metastasis Rev*, 1993, **12**, 119-134.
403. L. H. Patterson, *Drug Metab Rev*, 2002, **34**, 581-592.
404. L. H. Patterson and G. I. Murray, *Curr Pharm Des*, 2002, **8**, 1335-1347.
405. M. V. Papadopoulou, W. D. Bloomer, A. P. Taylor, M. Hernandez, R. D. Blumenthal and M. G. Hollingshead, *Radiat. Res.*, 2007, **168**, 65-71, 67.
406. S. J. Lunt, C. Cawthorne, M. Ali, B. A. Telfer, M. Babur, A. Smigova, P. J. Julyan, P. M. Price, I. J. Stratford, W. D. Bloomer, M. V. Papadopoulou and K. J. Williams, *Br. J. Cancer*, 2010, **103**, 201-208.
407. M. V. Papadopoulou, W. D. Bloomer and M. R. McNeil, *Int J Antimicrob Agents*, 2007, **29**, 724-727.
408. P. Kestell, F. B. Pruijn, B. G. Siim, B. D. Palmer and W. R. Wilson, *Cancer Chemother. Pharmacol.*, 2000, **46**, 365-374.
409. N. A. Helsby, D. M. Ferry, A. V. Patterson, S. M. Pullen and W. R. Wilson, *Br. J. Cancer*, 2004, **90**, 1084-1092.
410. W. Chen, X.-Y. Deng, Y. Li, L.-J. Yang, W.-C. Wan, X.-Q. Wang, H.-B. Zhang and X.-D. Yang, *Bioorg. Med. Chem. Lett.*, 2013, **23**, 4297-4302.
411. X. Chen, Y. M. Shi, C. Huang, S. Xia, L. J. Yang and X. D. Yang, *Anticancer Agents Med Chem*, 2016, **16**, 377-386.
412. Z. J. Lin, J. Bies, S. S. Johnson, J. D. Gorden, J. F. Strickland, M. Frazier, J. M. Meyers and K. L. Shelton, *J. Heterocycl. Chem.*, 2019, **56**, 533-538.
413. P. L. McCormack, *Drugs*, 2015, **75**, 817-822.
414. I. Pahuja, A. Verma, A. Ghoshal, S. Mukhopadhyay, A. Kumari, A. Shaji, S. Chaturvedi, V. P. Dwivedi and A. Bhaskar, *Microbiol. Spectr.*, 2023, **11**, e00858-00823.
415. W. Lee, M.-C. Baek, K.-M. Kim and J.-S. Bae, *Int. J. Mol. Sci.*, 2020, **21**, 1462.
416. B. M. Geetha, J. G. Małecki, M. Alwarsamy, R. S. Keri, V. S. Betageri and S. Budagumpi, *J. Mol. Liq.*, 2020, **316**, 113809.
417. W. J. Youngs, A. R. Knapp, P. O. Wagers and C. A. Tessier, *Dalton Trans*, 2012, **41**, 327-336.
418. A. Kascatan-Nebioglu, A. Melaiye, K. Hindi, S. Durmus, M. J. Panzner, L. A. Hogue, R. J. Mallett, C. E. Hovis, M. Coughenour, S. D. Crosby, A. Milsted, D. L. Ely, C. A. Tessier, C. L. Cannon and W. J. Youngs, *J. Med. Chem.*, 2006, **49**, 6811-6818.
419. M. Pellei, V. Gandin, M. Marinelli, A. Orsetti, F. Del Bello, C. Santini and C. Marzano, *Dalton Trans*, 2015, **44**, 21041-21052.

420. P. Skehan, R. Storeng, D. Scudiero, A. Monks, J. Mcmahon, D. Vistica, J. T. Warren, H. Bokesch, S. Kenney and M. R. Boyd, *J. Natl. Cancer Inst.*, 1990, **82**, 1107-1112.
421. A. L. Kasinski, K. Kelnar, C. Stahlhut, E. Orellana, J. Zhao, E. Shimer, S. Dysart, X. Chen, A. G. Bader and F. J. Slack, *Oncogene*, 2015, **34**, 3547-3555.
422. E. Orellana and A. Kasinski, *Bio Protoc.*, 2016, **6**.
423. L. Koontz, *Methods Enzymol.*, 2014, **541**, 3-10.
424. M. Domènech, A. Hernández, A. Plaja, E. Martínez-Balibrea and C. Balañà, *Int J Mol Sci*, 2021, **22**.
425. F. Jiang, X. L. Miao, X. T. Zhang, F. Yan, Y. Mao, C. Y. Wu and G. P. Zhou, *J Immunol Res*, 2021, **2021**, 5523832.
426. D. Liu, Z. Hu, J. Jiang, J. Zhang, C. Hu, J. Huang and Q. Wei, *Sci Rep*, 2022, **12**, 1617.
427. A. L. Chédeville and P. A. Madureira, *Cancers (Basel)*, 2021, **13**.
428. Y. Chen, T. Zou, G. Xin, X. Liu, Y. Yang, L. Wei, B. Zhang, P. Yu, Y. Ren, Y. Feng, R. Chen, F. Cao, X. Chen and Y. Cheng, *Adv. Mater.*, 2024, **36**, 2307929.
429. D. Guo, S. Xu, W. Yasen, C. Zhang, J. Shen, Y. Huang, D. Chen and X. Zhu, *Biomater. Sci.*, 2020, **8**, 694-701.
430. S. Suy, J. B. Mitchell, D. Ehleiter, A. Haimovitz-Friedman and U. Kasid, *J. Biol. Chem.*, 1998, **273**, 17871-17878.
431. S. Ye, P. Xu, M. Huang, X. Chen, S. Zeng, Q. Wang, J. Chen, K. Li, W. Gao, R. Liu, J. Liu, Y. Shao, H. Zhang, Y. Xu, Q. Zhang, Z. Zhong, Z. Wei, J. Wang, B. Hao, W. Huang and Q. Liu, *Cell Death Dis.*, 2020, **11**, 312.
432. S. Suy, J. B. Mitchell, A. Samuni, S. Mueller and U. Kasid, *Cancer*, 2005, **103**, 1302-1313.
433. C. Nathan and A. Cunningham-Bussel, *Nat. Rev. Immunol.*, 2013, **13**, 349-361.
434. X. Shen and K. S. Gates, *Chem. Res. Toxicol.*, 2019, **32**, 348 - 361.
435. D. Pomikło, A. Pietrzak, R. Kishi and P. Kaszyński, *Mater. Chem. Front.*, 2023, **7**, 4928-4943.
436. S. Cong, Q. Shen, M. Shan, J. Wang, J. Liu and Y. Zhang, *Chem. Eng. J.*, 2020, **383**, 123137.
437. I. E. Tolpygin, T. A. Kuz'menko, A. Y. Fedyanina, S. Y. Pluzhnikova, O. S. Popova, Y. V. Revinskii, A. D. Dubonosov and V. A. Bren', *Russ. J. Org. Chem.*, 2014, **50**, 911-912.
438. X. Feng, D. Liu, Z. Li and J. Bian, *Drug Discov. Today*, 2020, **25**, 230-237.
439. A. R. Collins, *Appl. Biochem. Biotechnol B*, 2004, **26**, 249-261.
440. O. V. Dolomanov, L. J. Bourhis, R. J. Gildea, J. A. K. Howard and H. Puschmann, *J. Appl. Crystallogr.*, 2009, **42**, 339-341.
441. G. M. Sheldrick, *Acta Crystallogr. Sect. A: Found. Crystallogr.*, 2015, **71**, 3-8.
442. J. K. Barral, E. Gudmundson, N. Stikov, M. Etezadi-Amoli, P. Stoica and D. G. Nishimura, *Magn. Reson. Med.*, 2010, **64**, 1057-1067.
443. H. S. Harned and R. A. Robinson, *Trans. Faraday Soc.*, 1940, **36**, 973-978.
444. U. Kaatze, *J. Chem. Eng. Data*, 1989, **34**, 371-374.
445. M. Roses, C. Rafols and E. Bosch, *Anal. Chem.*, 1993, **65**, 2294-2299.